THE
PHYSICAL REVIEW

A journal of experimental and theoretical physics established by E. L. Nichols in 1893

SECOND SERIES, VOL. 99, NO. 3 AUGUST 1, 1955

Perturbed Gamma-Gamma Directional Correlation in Cd^{114}†

SCOTT C. DAUBIN* AND DONALD R. HAMILTON
Palmer Physical Laboratory, Princeton University, Princeton, New Jersey
(Received March 21, 1955)

The directional correlation of the 722–556 kev gamma-gamma cascade in Cd^{114} following K-capture in In^{114} has been observed as a function of physical and chemical state of the source. Dry $InCl_3$ and frozen solutions thereof are consistent in giving an attenuation factor 0.77 ± 0.08 in the anisotropy. The lifetime of the intermediate state is found to be $\lesssim 2.3\times10^{-10}$ sec. Assuming that the perturbing interaction is electric and making a crude estimate of an upper limit in the electric field gradient at the nucleus, one obtains a quadrupole moment $|Q| \gtrsim 0.4\times10^{-24}$ cm² for the intermediate state of the cascade.

THE perturbation of gamma-gamma directional correlations by extranuclear fields acting during the lifetime of the intermediate state of the cascade has been used in several instances to obtain information about nuclear moments in the intermediate state; excellent summaries with references are available.[1,2] We report here measurements of the perturbing effect, on the Cd^{114} 722–556 kev cascade which follows K-capture in In^{114}, of change of physical state of the medium involved. Such an effect has been reported by Steffen and Zobel[3] but not subsequently reproduced in the same laboratory.

The apparatus used was conventional in most respects, with the functions of energy discrimination and time selection separated. From each of two detecting units consisting of a sodium iodide crystal and DuMont 6292 photomultiplier, one channel leads via a differential discriminator to a slow (10^{-6} sec) triple coincidence circuit, and a second channel leads via a fast amplifier to a fast (2×10^{-8} sec) double coincidence circuit; the output of the fast double also goes to the slow triple circuit. The differential discriminator "window" in each channel was set to accept pulse heights corresponding to a gamma energy range 430 kev to 1 Mev, care being taken in the final analysis, as noted below, to compensate for the anisotropy introduced by the decay of In^{114} positrons.

In the taking of data, particular attention was given to checking the constancy of resolving time and discriminator channel limits, and the accuracy of geometrical line-up, and to interleaving runs with the source in various physical conditions. The entire apparatus was enclosed in a large dry box to minimize the formation of frost on the source during runs at low source temperature; in any case, the scattering effect of such frost was observed by using a Na^{22} point source in both the frosted and unfrosted states and was found to be negligible.

For a dilute aqueous solution in $InCl_3$ in HCl (and for this case only), the relative probability $W(\theta)$ of cascade coincidences at an angle θ was measured at five values of $\cos\theta$, thus giving the coefficients A_2 and A_4 in the expected relation:

$$W(\theta)=1+A_2P_2(\cos\theta)+A_4P_4(\cos\theta).$$

It is consistent with the perturbations found with other Cd^{114} sources to call the dilute aqueous source unperturbed. After making corrections for detector size (based upon a modification of the annihilation-quanta method[4]), for source size (based upon geometrical calculations) and for the presence of the positron component (based upon coincidence rates at 90° and 180° with the positron emitter Na^{22} in point and extended sources),

† This work was supported by the U. S. Atomic Energy Commission and The Higgins Scientific Trust Fund.
* Lieutenant, U. S. Navy, on leave from U. S. Navy Postgraduate School, Monterey, California; now with Office of Naval Research, Washington, D. C.
[1] R. M. Steffen, Am. J. Phys. (to be published).
[2] H. Frauenfelder, Chapter "Angular Correlation" in K. Siegbahn, *Beta and Gamma Spectroscopy* (to be published) and in Ann. Rev. Nuc. Sci. **2**, 129 (1953).
[3] R. M. Steffen and W. Zobel, Phys. Rev. **88**, 170 (1952).
[4] E. L. Church and J. J. Kraushaar, Phys. Rev. **88**, 419 (1952).

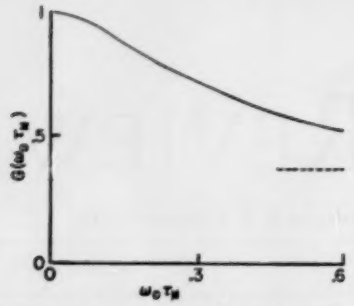

FIG. 1. Attenuation factor $G(\omega_0\tau_N)$ for electric quadrupole interaction, $I=2$, $\tau_N \ll$ resolving time, and observed A_2 and A_4; $G \approx G_2$ since in case under discussion $A_2 \ll A_4$. Dotted line indicates "hard core" asymptote for axial symmetry.

the unperturbed correlation was found to be given by

$$A_2=0.090\pm0.011, \quad A_4=0.022\pm0.016,$$

which is consistent with the results of previous workers.[5-7] From the gamma-gamma correlation and the details of the K-capture which feeds the second excited state, the Cd^{114} levels have been thought[5-7] to be 0-2-2-0; our data fit this well with the 2-2 transition an $E2$-$M1$ mixture, (4.2 ± 0.6) percent of the intensity being in the quadrupole. We have not carried out more detailed measurements of other quantities to verify this assignment.

Further measurements, on the perturbation of the correlation, were confined to the anisotropy

$$A=[W(180°)/W(90°)]-1.$$

Correction of observed A for the effect of positron annihilation gammas in increasing $W(180°)$ consists of subtracting from the observed anisotropy a constant (0.015 ± 0.004) measured, as already noted, by auxiliary experiments. In principle the correction of A for finite-source and finite-detector effects requires a measurement of A_2 and A_4 separately, since these coefficients have separate correction factors and separate perturbations; but the fortunate circumstance that $A_2 \gg A_4$ makes it possible to apply to all observed A the same correction factor 1.25 as applies to the unperturbed case. The results of the anisotropy measurements, thus corrected, are summarized in Table I.

In the liquid sources there is no decrease in A at least for the range 1–4000 centipoises in viscosity. At high viscosities at which there appears to be a fall-off, the theory of correlation attenuation in liquids[5] in any case does not apply since the conventionally estimated liquid correlation time is orders of magnitudes longer than the nuclear lifetime; the fall-off here may well represent an onset of microcrystal formation.

[5] R. M. Steffen, Phys. Rev. **83**, 166 (1951).
[6] E. D. Klema and F. K. McGowan, Phys. Rev. **87**, 524 (1952).
[7] Johns, McMullen, Donnely, and Nablo, Can. J. Phys. **32**, 35 (1954).
[8] A. Abragam and R. V. Pound, Phys. Rev. **92**, 943 (1953).

In the several solid environments of $InCl_3$ there appears to be a small but real attenuation of A; the three cases are not significantly different and, if combined, yield an average anisotropy attenuation factor, denoted by G, with the value

$$G=0.77\pm0.08; \qquad (1)$$

the indicated variation is the statistical standard deviation.

After completing the experimental work here reported, we received a preprint of reference 1, in which are reported, among other results, measurements on Cd^{114} in an ionic crystal, in dilute aqueous solution, and in room temperature glycerin solution; calculating a value of G for the ionic crystal as compared to dilute aqueous solution, we obtain from Steffen's data $G=0.95\pm0.08$. More generally, Steffen's data are consistent and ours inconsistent with absence of perturbation. Our variations in A, obtained with interleaved runs with sources in different physical states, include variations (liquid *versus* frozen solutions) associated with a change of state produced without mechanical motion of or near the source. In general, absence of anisotropies in the single-channel rates indicated that the observed changes in anisotropy of the coincidence rates did not result from inadvertent mechanical eccentricity at the source. We therefore consider the variations to be real ones, to the extent indicated by statistics, and proceed to discuss the result stated in Eq. (1).

To make use of this result, one also needs knowledge of the lifetime τ_N of the intermediate state of the cascade. Measurements of τ_N, made by the method of delayed coincidences and with the aid of Dr. W. F. Hornyak, gave the result

$$\tau_N \leqslant 2.3\times10^{-10} \text{ sec.} \qquad (2)$$

Since this gives a limit on τ_N, the ultimate deductions from Eq. (1) take the form of limits.

Theoretical calculations[8] have been made for time-dependent attenuation factors $G_k(t)$, and for G_k, the average of $G(t)$ over the nuclear lifetime τ_N; since in our case $A_4 \ll A_2$, $G \approx G_2$. The calculations refer to an axially symmetric and classically describable electric field such as that in a crystal and may be easily applied to classical and similarly symmetric magnetic fields. However, the quenching of orbital electron moments in solids suggests[2] that the interaction is electric in nature. Thus, although the magnetic analog to Eq. (5) below is consistent with the interaction of a nuclear magneton with a classical field of 10^5 gauss, a magnitude associated in many cases with the nonclassical fields in free atoms, we shall assume an electric interaction for purposes of further discussion.

Figure 1 shows the resulting dependence of G on the parameter $\omega_0\tau_N$ for $I=2$; ω_0, as defined by Abragam and Pound[8] has for $I=2$ the value

$$\omega_0=e|Q|V''/8\hbar. \qquad (3)$$

From Fig. 1 and Eq. (1),

$$\omega_0\tau_N = 0.25 \pm 0.08; \tag{4}$$

hence, from Eq. (2),

$$e|Q|V''/\hbar \geq (0.87 \pm 0.30) \times 10^{10} \text{ sec}^{-1}, \tag{5}$$

which has been so written as to make apparent the effect of the separate uncertainties in G and τ_N.

The theory upon which Fig. 1 and hence Eqs. (4) and (5) are based may well be inappropriate for detailed application to the case under consideration; nevertheless, Eqs. (4) and (5) should represent useful estimates.

Various methods may be used to estimate V'' or to set limits upon it. Thus, applying Eqs. (2) and (3) to a compilation[9] of data for cases in which Q and ω_0 are independently known, we find values of V'' in solids ranging from 8×10^{15} to 4×10^{16} statvolts/cm^2. These are, however, static fields whereas the fields acting on Cd^{114} after K-capture in In^{114} (or on Cd^{111} after K-capture in In^{111}) depend on time during the rearrangement of the atomic electrons after the beta process. As noted by Frauenfelder,[2,10] these rearrangements take place very rapidly in the inner shells (times of the order of 10^{-16} sec); in a metal the process goes quickly to completion in the outer shells (10^{-12} sec); but in an insulator the active atom acts as an impurity center and the final de-excitation may go as slowly or more slowly than would an optical transition in a free atom (e.g., 10^{-6}–10^{-8} second[1,2]). Thus it seems likely that in $InCl_3$ or In_2O_3 or in frozen solutions thereof, the V'' effective during the lifetime of Cd^{114} ($\leq 2\times10^{-10}$ sec) and part or all of the lifetime of Cd^{111} (10^{-7} second) would be the field of an excited Cd atom, that is, the field of the original indium p-electron. For a p-electron in iodine (one p-electron hole in the same shell as is the indium p-electron), Townes and Dailey[11] give $V''=4.5\times10^{16}$ statvolts/cm^2.

Since we are forced by our uncertainty about the Cd^{114} lifetime to deal only with lower limits to Q_{114}, we adopt as the upper limit for V'' the largest of the above values,

$$V'' \leq 4.5\times10^{16} \text{ statvolts/cm}^2,$$

which in turn gives, with Eq. (5), the limit

$$|Q_{114}| \geq (4\pm1)\times10^{-25} \text{ cm}^2.$$

The above upper limit on V'', if combined with the Zurich determination[12] of 5×10^{-25} cm^2 for Q_{111}, yields for Cd^{111} the value $\omega_0=1.5\times10^9$ sec^{-1} which then may be compared with the measurement of $G(t)$ for Cd^{111} as made by Fraser and Milton.[13] The measured $G(t)$ does not have a detailed time-dependence which corresponds to the theory of Abragam and Pound and hence does not yield a specific value of ω_0; but the observed exponential decay has a time constant of the order of 10^{-8} sec, which is an order of magnitude larger than one would expect from an ω_0 of the order of 10^9 sec^{-1}. This implies that, at least in Cd^{111}, V'' is an order of magnitude smaller than 4.5×10^{16} statvolts/cm^2 within a time somewhat less than 10^{-9} second. Conceivably V'' could be high for times comparable to the $\leq 2\times10^{-10}$ second lifetime of Cd^{114} and then, by a rapid electronic de-excitation, reduce to a lower value within 10^{-9} second; or it could be that the same V'' is effective for Cd^{111} and Cd^{114}, in which case the above lower limit on Q_{114} would be an order of magnitude too small. The present data are insufficient to decide between these possibilities.

TABLE I. Anisotropy observed for various states of the source.

Liquid sources	Temp (°C)	Viscosity (centipoises)	A
Dilute aqueous $InCl_3$ in HCl	20	1	0.155 ± 0.009
$InCl_3$ in 0.4N HCl in >99% glycerin	20	$(8.0\pm2.6)\times10^3$	0.148 ± 0.014
	4	$(4.0\pm0.8)\times10^5$	0.148 ± 0.014
	−14	$(3.3\pm1.0)\times10^6$	0.092 ± 0.009
	−28	$(6.0\pm2.0)\times10^6$	0.106 ± 0.011
Solid sources	**Temp (°C)**		**A**
$InCl_3$ dry	20		0.121 ± 0.016
Dilute aqueous $InCl_3$ frozen	−104		0.128 ± 0.014
$InCl_3$ in glycerin, as above	−104		0.109 ± 0.013

From Ford's analysis[14] of the relation of nuclear distortion and energy of the first excited state including the empirical correction factor 1.7 (see his Fig. 4), we deduce an expected Q of 5×10^{-24} cm^2 for Cd^{114}. It is thus apparent that more exact knowledge of the lifetime of the excited state of Cd^{114} and of the fields acting upon the nucleus during the lifetime would allow an interesting comparison of the collective nuclear model with experiment. (*Note added in proof.*—At the April, 1955 meeting of the American Physical Society, paper CA9 reported, on the basis of Coulomb excitation measurement, values for Cd^{114}. $\tau_N=1.1\times10^{-11}$ sec, $Q=2.7\times10^{-24}$ cm^2. This is consistent with our measurements; it gives additional evidence that the quadrupole interaction is responsible for the correlation perturbation and indicates that the value of V'' upon which we based our estimate of Q is high by a factor of 3.)

More generally, it would appear that small partial perturbations of angular correlations with a very short-lived intermediate state provide a method of investigating moments of excited states which is complementary to the method of Fraser and Milton and other methods.

[9] Gordy, Smith, and Trambarulo, *Microwave Spectroscopy* (John Wiley and Sons, Inc., New York, 1953), Appendix A6.
[10] H. Frauenfelder, Phys. Rev. **82**, 549 (1951).
[11] C. H. Townes and B. P. Dailey, J. Chem. Phys. **17**, 782 (1949).
[12] Albers-Schönberg, Alder, Braun, Heer, and Novey, Phys. Rev. **91**, 1287 (1953).
[13] J. S. Fraser and J. C. D. Milton, Phys. Rev. **94**, 795 (1954), and private communication.
[14] K. W. Ford, Phys. Rev. **90**, 29 (1953).

Proton Bremsstrahlung*

S. D. DRELL AND KERSON HUANG
Department of Physics and Laboratory for Nuclear Science, Massachusetts Institute of Technology, Cambridge Massachusetts

(Received March 16, 1955)

The cross section for proton bremsstrahlung is calculated from Sommerfeld's work and expressed as the classical orbit result plus a first quantum correction. This correction is due to the energy loss of the proton to radiation. For 150-kev x-rays emitted at 90° to a beam of 2-Mev protons incident on a tin ($Z=50$) target, this correction decreases the classical prediction by 25 percent and serves to establish theoretical agreement with experimental results of Mark, McClelland, and Goodman.

I. INTRODUCTION

THE bremsstrahlung emitted when low-energy protons are scattered by nuclei has been studied in recent experiments by Zupančič and Huus[1] and by Mark, McClelland, and Goodman.[2] The latter observe x-rays in a 3-kev energy interval about 150 kev which are emitted at 90° to a beam of 2-Mev protons incident on a tin ($Z=50$) target.[2] As reported by Mark, the differential cross section for this process is

$$\sigma(90°)=(1.3\pm0.5)\times10^{-31}\ \text{cm}^2/\text{sterad}. \quad (1)$$

We present here a theoretical analysis of the above result. Since the proton radiates only 7.5 percent of its energy and has a deBroglie wavelength, $\lambda_D=3.3\times10^{-13}$ cm, which is quite small on an atomic scale, we turn to a classical orbit picture of the process as a convenient starting point. We expect that the effects of retardation, electronic shielding, and finite nuclear size can be neglected, since the x-ray wavelength, $\lambda=1.3\times10^{-10}$ cm, is 36 times greater than the distance of closest approach (r_m) of the proton to the tin nucleus ($r_m=3.6\times10^{-12}$ cm); and r_m is 28 times smaller than the K-shell Bohr orbit for tin, $a_s=a_0/Z=10^{-10}$ cm, and six times larger than the nuclear radius $R_N=6\times10^{-13}$ cm.

We consider then first of all the dipole radiation emitted classically by a beam of particles scattered in a Coulomb field as discussed, for example, by Landau and Lifschitz.[3] The cross section derived on this basis in the following section (II) is found to be

$$\sigma_{\text{classical}}(90°)=2.1\times10^{-31}\ \text{cm}^2/\text{sterad}, \quad (2)$$

in disagreement with the experimental result, Eq. (1).

We are thus led to perform a more complete quantum-mechanical calculation, taking into account the not inconsiderable energy loss of the proton to radiation. Sommerfeld and his co-workers have investigated at length the quantum-mechanical problem of bremsstrahlung from charged particles moving in Coulomb fields.[4] In particular, Sommerfeld has derived the differential cross section for dipole bremsstrahlung emission in a given direction, with the particle recoiling at fixed angle (Fig. 1). Integration of this result over all proton recoil angles was possible only in special limiting cases which do not apply here (e.g., hard x-rays, which slow down the particle considerably). Sommerfeld also achieved the integration over both x-rays and recoil angles for the total cross section.

The contribution of the present paper is a deduction from Sommerfeld's work of the cross section for dipole x-ray emission as a function of x-ray direction and energy and of incident particle energy only. Our work is valid for parameter choices such as discussed above which permit an expansion in powers of $(\hbar\omega/E)\ll1$ about the classical result ($\hbar\omega$ is the x-ray energy, and E the proton energy). Essentially then we reduce the bremsstrahlung cross section to the classical result plus the first-order quantum correction. The quantum correction arises from the decrease in proton energy after it radiates. This damping effect of the bremsstrahlung on the motion of the proton is not included in the classical orbit calculation. We expect it to decrease the cross section from the classical value of Eq. (2) since the proton is slowed down and repelled further away from the Coulomb field source as it loses energy. The effective dipole moment is thereby reduced. Quantum mechanically, there is a decrease in wave function overlap. We calculate this decrease in Sec. III and show that it suffices to establish agreement with experiment. It is also of interest in this calculation to exhibit explicitly a parameter in terms of which to expand the cross section about its classical value. The Coulomb field (in the absence of any shielding length) has the well-known property of giving rise to elastic scattering cross sections which do not involve $\hbar$ and which are essentially classical in nature. This point has been analyzed in great detail by Williams[5] and is a consequence of the large effective impact parameters in Coulomb scattering. However, the quantum corrections to the classical orbit treatment of bremsstrahlung arise from the damping of the orbit and can be ex-

* This work was supported in part by the Office of Naval Research and the U. S. Atomic Energy Commission.

[1] C. Zupančič and T. Huus, Phys. Rev. **94**, 205 (1954).

[2] Mark, McClelland, and Goodman (private communication to be published).

[3] L. Landau and E. Lifshitz, *The Classical Theory of Fields* (Addison-Wesley Publishing Company, Cambridge, 1951), Chap. 9.

[4] A. Sommerfeld, *Wellenmechanik* (Frederick Ungar, New York, 1950), Chap. 7.

[5] E. J. Williams, Revs. Modern Phys. **17**, 217 (1945).

pressed in the form $(\hbar\omega/E)$, the measure of the inelasticity.

II. CLASSICAL CALCULATION

We outline in this section the classical calculation of the dipole radiation from a beam of protons scattered by nuclei of charge Z and mass number A. In particular, we investigate the intensity and angular distribution of the radiation emitted by the scattered protons.

First, we briefly consider the scattering of a single proton by such a nucleus. At a large distance R_0 from the radiating system, in the wave zone of the radiation, the ωth Fourier component of the vector potential of the radiation field is given (through $l=2$ multipoles) by

$$\mathbf{A}_\omega = e^{ikR_0+i\mathbf{k}\cdot\mathbf{R}_0} \times\left[\frac{d\mathbf{d}_\omega/dt}{cR_0}+\frac{(d^2\mathbf{Q}_\omega/dt^2)\cdot\mathbf{n}}{6c^2R_0}+\frac{(d\mathbf{m}_\omega/dt)\times\mathbf{n}}{cR_0}\right], \quad (3)$$

where $\mathbf{n}$ is the radial unit vector at the observation point, and $\mathbf{k}=\mathbf{n}\omega/c$. The quantities $\mathbf{d}_\omega$, $\mathbf{Q}_\omega$, $\mathbf{n}_\omega$ are respectively the ωth Fourier components of the electric dipole moment, the electric quadrupole moment, and the magnetic dipole moment of the radiating systems. These moments are given by

$$\begin{aligned}\mathbf{d}&=e\left[\left(1-\frac{Z}{A}\right)\Big/\left(1+\frac{1}{A}\right)\right]\mathbf{r},\\ \mathbf{Q}&=e\left[\left(1+\frac{Z}{A^2}\right)\Big/\left(1+\frac{1}{A}\right)^2\right](3\mathbf{r}\mathbf{r}-r^2), \quad (4)\\ \mathbf{m}&=e\left[\left(1+\frac{Z}{A^2}\right)\Big/\left(1+\frac{1}{A}\right)^2\right]\frac{1}{2c}(\mathbf{r}\times\dot{\mathbf{r}}),\end{aligned}$$

where $\mathbf{r}$ is the vector pointing from the nucleus to the proton. The intensity of radiation emitted into the solid angle $d\Omega$, with frequency between ω and $\omega+\Delta\omega$ is, to the multipole orders considered, given by

$$\begin{aligned}d\mathcal{E}_\omega&=(\omega^2/c)\,|\mathbf{n}\times\mathbf{A}_\omega|^2R_0^2d\Omega\Delta\omega\\ &=(\omega^4/c^3)\{|\mathbf{d}_\omega\times\mathbf{n}|^2-(\omega/3c)\,\mathrm{Im}(\mathbf{d}_\omega\cdot\mathbf{Q}_\omega^*\cdot\mathbf{n})\\ &\quad+2\,\mathrm{Re}[\mathbf{d}_\omega\cdot(\mathbf{m}_\omega^*\times\mathbf{n}]\}d\Omega\Delta\omega, \quad (5)\end{aligned}$$

where an asterisk indicates complex conjugate, and $|\mathbf{d}_\omega|^2=(\mathbf{d}_\omega^*\cdot\mathbf{d}_\omega)$. If we now consider the actual problem of the scattering of a uniform monoenergetic proton beam, we must average $d\mathcal{E}_\omega$ over the different orientations of the moments in the beam; i.e., we must average over the different azimuths of the planes of the proton orbit. We are mainly interested in the electric dipole term, because eventually we compare with experiments in which the radiation is emitted at 90° to the direction of the incident beam, and it can be easily shown that at 90°, the cross terms between it and the quadrupole and the magnetic dipole terms vanish, upon averaging over the incident proton beam. The higher moments will contribute at angles other than 90°, but their contribution is expected to be small compared to the dipole term $((r_n/\lambda)<0.1)$. After averaging over the incident protons in the beam, we have for the intensity of dipole radiation:

$$d\mathcal{E}_\omega=(\omega^4/c^3)[\tfrac{2}{3}|\mathbf{d}_\omega|^2+\tfrac{1}{2}(3\cos^2\theta-1) \times(\tfrac{1}{3}|\mathbf{d}_\omega|^2-|d_{\omega z}|^2)]d\Omega\Delta\omega, \quad (6)$$

where θ denotes the angle between $\mathbf{n}$ and the incident direction, and $d_{\omega z}$ is the component of $\mathbf{d}_\omega$ along the incident direction. Integrating over proton impact parameters[8] and dividing by $\hbar\omega$, we obtain for the differential cross section for bremsstrahlung in frequency interval $(\omega, \omega+\Delta\omega)$ emitted into the solid angle $d\Omega$:

$$\sigma_\omega d\Omega=(\omega^4/c^3)(\Delta\omega/\hbar\omega)d\Omega\int_0^\infty 2\pi\rho d\rho \times[\tfrac{2}{3}|\mathbf{d}_\omega|^2+\tfrac{1}{2}(3\cos^2\theta-1)(\tfrac{1}{3}|\mathbf{d}_\omega|^2-|d_{\omega z}|^2)], \quad (7)$$

where ρ is the impact parameter of an incident proton.

We present several steps here in the evaluation of Eq. (7) in order to exhibit the impact parameters and eccentricities of the orbits which contribute most of the radiation. To express $\mathbf{d}_\omega$ as a function of the impact parameter, ρ, we parametrize the hyperbolic orbit of the proton as follows[3]:

$$\begin{aligned}x&=-a(\cosh\xi+\epsilon),\\ y&=a(\epsilon^2-1)^{\frac{1}{2}}\sinh\xi, \quad (8)\\ t&=(\xi+\epsilon\sinh\xi)/\omega_0,\end{aligned}$$

where

$$\begin{aligned}&\omega_0=(Ze^2/ma^2)^{\frac{1}{2}}, \quad m=\text{proton mass},\\ &a=Ze^2/2E \quad (E=\text{incident proton energy}),\end{aligned} \quad (9)$$

and

$$\epsilon=[1+(\rho/a)^2]^{\frac{1}{2}} \quad (10)$$

is the eccentricity of the orbit. The geometric significance of these quantities are illustrated in Fig. 2. The angle ϕ between one asymptote and the x-axis is given by

$$\cos\phi=1/\epsilon. \quad (11)$$

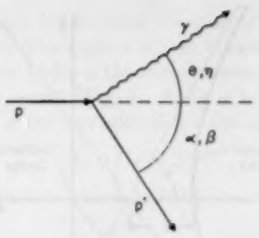

FIG. 1. Definition of angles. The proton is scattered through polar angle α and azimuthal angle β, emitting bremsstrahlung at polar angle θ and azimuthal angle η.

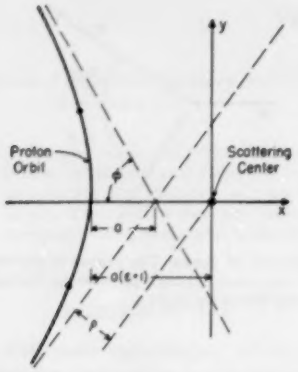

FIG. 2. Classical orbit for a proton in the Coulomb field of a fixed positively charged scattering center, showing impact parameter ρ, distance of closest approach $a(1+\epsilon)$, and asymptote angle ϕ.

From Eq. (4) we see that $\mathbf{d}_\omega = e'\mathbf{r}_\omega$, where we introduce the reduced charge:

$$e' = e\left(1-\frac{Z}{A}\right)\Big/\left(1+\frac{1}{A}\right), \tag{12}$$

and the Fourier transform of $\mathbf{r}$:

$$\mathbf{r}_\omega = \frac{1}{2\pi}\int_{-\infty}^{+\infty} \mathbf{r}e^{i\omega t}dt. \tag{13}$$

To conform to the coordinate system used in Eq. (7), the orbit as given by Eq. (8) must be rotated through an angle ϕ so that the proton is incident along the x-direction. We therefore get

$$\begin{aligned} d_{\omega x} &= d_{\omega x}'\sin\phi - d_{\omega y}'\cos\phi, \\ d_{\omega y} &= d_{\omega x}'\cos\phi + d_{\omega y}'\sin\phi, \end{aligned} \tag{14}$$

where $\sin\phi = (\epsilon^2-1)^{\frac{1}{2}}/\epsilon$, $\cos\phi = 1/\epsilon$, and

$$\begin{aligned} d_{\omega x}' &= (e'/2\pi)\int_{-\infty}^{+\infty} xe^{i\omega t}dt, \\ d_{\omega y}' &= (e'/2\pi)\int_{-\infty}^{+\infty} ye^{i\omega t}dt, \end{aligned} \tag{15}$$

and x, y, t are given by Eq. (8). These integrals can be evaluated to give

$$\begin{aligned} d_{\omega y}' &= \frac{e'a}{i\pi\omega}\frac{(\epsilon^2-1)^{\frac{1}{2}}}{\epsilon}\exp\left(-\frac{\pi}{2}\frac{\omega}{\omega_0}\right)K_{i\omega/\omega_0}(\epsilon\omega/\omega_0), \\ d_{\omega x}' &= -\frac{e'a}{i\pi\omega}\exp\left(-\frac{\pi}{2}\frac{\omega}{\omega_0}\right)K_{i\omega/\omega_0}'(\epsilon\omega/\omega_0), \end{aligned} \tag{16}$$

where $K_n(x)$ is related to the Hankel function of the first kind,[6] of imaginary argument, and $K_n'(x)$, its derivative with respect to x. We thus obtain, by substituting Eq. (16) into Eq. (14):

$$\begin{aligned} d_{\omega x} &= \frac{e'a}{\pi\omega}e^{-\frac{1}{2}\pi p}\frac{(\epsilon^2-1)^{\frac{1}{2}}}{\epsilon}\left[-K_{ip}'(p\epsilon)+\frac{i}{\epsilon}K_{ip}(p\epsilon)\right], \\ d_{\omega y} &= \frac{e'a}{\pi\omega}e^{-\frac{1}{2}\pi p}\frac{1}{\epsilon}\left[-K_{ip}'(p\epsilon)-\frac{i(\epsilon^2-1)}{\epsilon}K_{ip}(p\epsilon)\right], \\ |\mathbf{d}_\omega|^2 &= \frac{e'^2a^2}{\pi^2\omega^2}e^{-\pi p}\left\{[K_{ip}'(p\epsilon)]^2+\frac{\epsilon^2-1}{\epsilon^2}[K_{ip}(p\epsilon)]^2\right\}, \end{aligned} \tag{17}$$

where $p = \omega/\omega_0$. To obtain the cross section, Eq. (17) must be substituted into Eq. (7). The integration in Eq. (7) over the impact parameter ρ can be converted into an integral over the eccentricity ϵ by the relation $\epsilon = [1+(\rho/a)^2]^{\frac{1}{2}}$. Thus we obtain

$$\sigma_\omega d\Omega = \left[A(\omega)+B(\omega)\frac{3\cos^2\theta-1}{2}\right]\frac{\Delta\omega}{\hbar\omega}d\Omega, \tag{18}$$

where

$$\begin{aligned} A(\omega) &= \frac{4}{3\pi}\frac{e'^2\omega^2a^4}{c^3}e^{-\pi p}\int_1^\infty\left\{[K_{ip}'(p\epsilon)]^2\right. \\ &\qquad \left.+\frac{\epsilon^2-1}{\epsilon^2}[K_{ip}(p\epsilon)]^2\right\}\epsilon d\epsilon, \\ B(\omega) &= \tfrac{1}{2}A(\omega)-\frac{2}{\pi}\frac{e'^2\omega^2a^4}{c^3}e^{-\pi p}\int_1^\infty\left\{[K_{ip}'(p\epsilon)]^2\right. \\ &\qquad \left.+\left(\frac{\epsilon^2-1}{\epsilon}\right)^2[K_{ip}(p\epsilon)]^2\right\}\frac{d\epsilon}{\epsilon}. \end{aligned}$$

At $\theta = 90°$, we obtain

$$\sigma_\omega(90°) = A_0p^2\int_1^\infty\frac{d\epsilon}{\epsilon}\left\{(\epsilon^2+1)K_{ip}'^2+\frac{(\epsilon^2-1)(2\epsilon^2-1)}{\epsilon^2}K_{ip}^2\right\}, \tag{19}$$

where

$$A_0 = e^{-\pi p}\left(\frac{\Delta(\hbar\omega)}{\pi\hbar\omega}\right)\left[\left(1-\frac{Z}{A}\right)\Big/\left(1+\frac{1}{A}\right)\right]^2 \times\left(\frac{e^2}{\hbar c}\right)\left(\frac{2E}{mc^2}\right)\left(\frac{Ze^2}{2E}\right)^2. \tag{20}$$

Substituting the values

$$Z = 50, \quad E = 2 \text{ Mev}, \quad \hbar\omega = 150 \text{ kev}, \quad \Delta\hbar\omega = 3 \text{ kev}, \tag{21}$$

we find

$$\begin{aligned} &p = \omega/\omega_0 = 0.206, \quad a = 1.80\times10^{-12} \text{ cm}, \\ &\omega_0 = 1.10\times10^{21} \text{ sec}^{-1}, \quad A_0 = 1.09\times10^{-31} \text{ cm}^2. \end{aligned} \tag{22}$$

[6] G. N. Watson, *Theory of Bessel Functions* (Cambridge University Press, 1948), Sec. 3.7.

Numerically integrating Eq. (19), we obtain the cross section result quoted in Eq. (2). For smaller values of $p \cong 0.1$ it is possible to simplify Eq. (19) to the approximate form

$$\sigma_\omega(90°) \cong A_0[\log(2/\gamma p)+1],$$

with $\gamma = 1.781\cdots$, the Euler constant.

In concluding this discussion of the classical problem, we note that in the integration of Eq. (19), most of the contributions to the cross section results from orbits of eccentricities $1 \leq \epsilon \lesssim 2$. Protons moving in such parabolic or nearly parabolic orbits approach to within $(3.6\text{–}6.2)\times 10^{-12}$ cm of the nucleus. This is well within the K-shell radius, (10^{-10} cm) of the tin atom. For this reason, we turn to quantum-mechanical rather than shielding corrections as the source of the discrepancy between Eqs. (2) and (1).[7]

III. QUANTUM-MECHANICAL CALCULATION

The quantum-mechanical calculation of the differential cross section for the dipole emission of a quantum of frequency ω into the solid angle $d\Omega$ has been carried out by Sommerfeld.[4] The matrix element which induces dipole transition between the continuum Coulomb states of the proton with emission of bremsstrahlung has the familiar form $\mathbf{M} = \int \psi_2^* \mathbf{r} \psi_1 d\tau$.

The cross section for the emission of a quantum of polarization $\mathbf{e}$ in the frequency interval $(\omega, \omega+\Delta\omega)$ into a solid angle element $d\Omega$, with the proton recoiling into solid angle element $d\Omega_k$, is directly:

$$\sigma(k_1,k_2,\omega,\mathbf{e}_k) = \left(\frac{e^2}{\hbar c}\right)\left[\left(1-\frac{Z}{A}\right)\Big/\left(1+\frac{1}{A}\right)\right]^2 \frac{1}{16\pi^4}\left(\frac{k_2}{k_1}\right)\frac{m^2\omega^3}{\hbar^2 c^2} \times |\mathbf{e}_k\cdot\mathbf{M}|^2 \Delta\omega d\Omega_k d\Omega, \quad (23)$$

where k_1 and k_2 are the incident and final proton wave numbers, and the continuum wave functions in $\mathbf{M}$ are taken to be normalized in a unit volume. Integrating over the recoil proton solid angle and summing over photon polarizations, we obtain the differential cross section in dipole bremsstrahlung in the frequency interval $(\omega, \omega+\Delta\omega)$:

$$\sigma(\theta)d\Omega = \left(\frac{e^2}{\hbar c}\right)\left[\left(1-\frac{Z}{A}\right)\Big/\left(1+\frac{1}{A}\right)\right]^2 \times \frac{1}{8\pi^3}\left(\frac{k_2}{k_1}\right)\frac{m^2\omega^4}{\hbar^2 c^2}\left(\frac{\Delta\hbar\omega}{\hbar\omega}\right)d\Omega \int_0^\pi d\alpha \sin\alpha \times \{\tfrac{2}{3}|\mathbf{M}|^2 + \tfrac{1}{2}(3\cos^2\theta - 1)[\tfrac{1}{3}|\mathbf{M}|^2 - |M_x|^2]\}. \quad (24)$$

[7] A classical calculation of the screening correction which treats the difference between a shielded and an unshielded Coulomb potential as a small perturbation has been carried through. For a shielding length as given by the Fermi-Thomas model, the correction is quite negligible (<0.1 percent).

We have taken the incident direction of the proton to be the x-axis. The angle θ is that between the photon and the x-axis, and α is the angle between the final proton and the x-axis, (Fig. 1). Angle α is related to the eccentricity of the corresponding classical orbit by

$$\sin\alpha = 2(\epsilon^2-1)^{\frac{1}{2}}/\epsilon^2. \quad (25)$$

The dipole matrix elements have been evaluated by Sommerfeld:

$$M_x = C[(n_2-n_1\cos\alpha)F + (1-\cos\alpha)(1-x)F'](1-x)^{-n_1-n_2-1},$$

$$\left.\begin{matrix} M_y \\ M_z \end{matrix}\right\} = C\left\{\begin{matrix} \cos\beta \\ \sin\beta \end{matrix}\right\}\sin\alpha[n_1 F + (1-x)F'] \times (1-x)^{-n_1-n_2-1}, \quad (26)$$

where F is the hypergeometric function and F' is the derivative of F with respect to its argument:

$$F = F(-n_1, -n_2, 1; x)$$
$$F' = dF/dx = n_1 n_2 F(1-n_1, 1-n_2, 2; x), \quad (27)$$

with

$$n_1 = Ze^2m^2/ik_1\hbar^2,$$
$$n_2 = Ze^2m^2/ik_2\hbar^2,$$
$$x = -(4k_1k_2\sin^2\alpha/2)/(k_1-k_2)^2, \quad (28)$$

and

$$C = -16\pi e^{-i\pi n_1}\frac{k_1k_2}{(k_1+k_2)^2(k_1-k_2)^4}\left(\frac{k_1+k_2}{k_1-k_2}\right)^{n_1+n_2}. \quad (29)$$

The integration of Eq. (24) cannot be effected in closed form. Sommerfeld,[4] Scherzer,[8] Weinstock[9] (and others) have given approximate expressions, valid for conditions that do not prevail in the experiments under consideration here.

The problem here reduces to one of finding a suitable representation for the hypergeometric function, F, that permits a series expansion in powers of $\hbar$. We achieve this by transforming the independent variable from x to $1/x$ with the formula for the analytic continuation of the hypergeometric function:

$$F(a,b,c;x) = \frac{\Gamma(c)\Gamma(b-a)}{\Gamma(b)\Gamma(c-a)}(-x)^{-a} \times F(a, 1-c+a, 1-b+a; x^{-1}) + \frac{\Gamma(c)\Gamma(a-b)}{\Gamma(a)\Gamma(c-b)}(-x)^{-b} \times F(b, 1-c+b, 1-a+b; x^{-1}). \quad (30)$$

Noting that both n_1 and $n_2 \to \infty$ as $\hbar \to 0$,

$$F(a,b,c;x) \xrightarrow[\substack{|a|\to\infty \\ |b|\to\infty}]{} \Gamma(c)\left(\frac{x}{ab}\right)^{\frac{1}{2}(c-1)}\left\{I_{c-1}(2(ab/x)^{\frac{1}{2}}) + \frac{1}{2}\left(\frac{1}{a}+\frac{1}{b}\right)\left(\frac{ab}{x}\right)^{\frac{1}{2}}I_{c+1}(2(ab/x)^{\frac{1}{2}}) + O\left(\frac{1}{a^2},\frac{1}{b^2}\right)\right\}, \quad (31)$$

[8] O. Scherzer, Ann. Physik **13**, 137 (1932).
[9] R. Weinstock, Phys. Rev. **61**, 584 (1946).

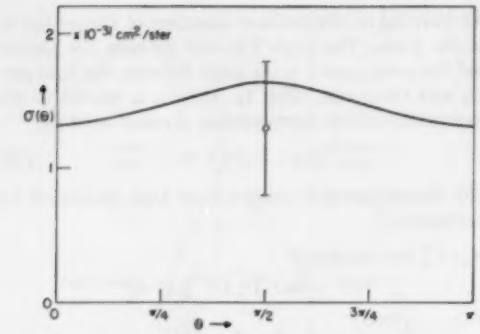

FIG. 3. Angular distribution of x-rays in a 3-kev interval about 150 kev for 2-Mev protons incident on a tin nucleus. The experimental point is that of Mark *et al.* (reference 2).

where

$$I_\nu(x)=\exp\left(\frac{\pi\nu}{2i}\right)J_\nu(e^{\frac{1}{2}i\pi}x)$$
$$=\left(\frac{x}{2}\right)^\nu\sum_{m=0}^{\infty}\frac{(x/2)^{2m}}{m!\Gamma(\nu+m+1)}. \quad (32)$$

Note that the new independent variable has a classical limit:

$$\left(\frac{ab}{x}\right)^{\frac{1}{2}}=\left(\frac{n_1n_2}{x}\right)^{\frac{1}{2}}\xrightarrow[\hbar\to 0]{}\tfrac{1}{2}p\epsilon\left(1-\frac{\hbar\omega}{4E}\right)+O(\hbar^2).$$

Here ϵ is the eccentricity of the classical orbit as defined in Eq. (10), and $p=\omega/\omega_0$ is the same as that defined earlier in Eq. (22).

Carrying out this expansion in powers of $\hbar$ we obtain, for example,

$$F(1+in, in, 2-ip; x^{-1})\xrightarrow[\hbar\to 0]{}\Gamma(2-ip)(\tfrac{1}{2}p\epsilon)^{-1+ip}$$
$$\times\left\{I_{1-ip}(p\epsilon)-\frac{i}{n}\frac{p\epsilon}{2}[\tfrac{1}{2}p\epsilon I_{1-ip}(p\epsilon)-I_{2-ip}(p\epsilon)]\right\} \quad (33)$$
$$F(i\lambda n, -1+i\lambda n, ip; x^{-1})\xrightarrow[\hbar\to 0]{}\Gamma(ip)(\tfrac{1}{2}p\epsilon)^{1-ip}$$
$$\times\left\{I_{ip-1}(p\epsilon)-\frac{i}{n}\frac{p\epsilon}{2}[\tfrac{1}{2}p\epsilon I_{ip-1}(p\epsilon)-I_{ip}(p\epsilon)]\right\},$$

where $n=-in_1$, $\lambda n=-in_2$, $\lambda=(k_1/k_2)$.

The expansion parameter is seen to be

$$p/n=\hbar\omega/2E. \quad (34)$$

Making use of the identity[6]

$$[I_{-\nu}(x)-I_\nu(x)]=(2/\pi)(\sin\pi\nu)K_\nu(x),$$

we now obtain

$$F(1+in, i\lambda n, 2; x)\xrightarrow[\hbar\to 0]{}\frac{2x^{-1-in}(\frac{1}{2}p\epsilon)^{-1+ip}}{\Gamma(i\lambda n)\Gamma(1-in)}\left\{K_{ip-1}(p\epsilon)\right.$$
$$\left.-\frac{i}{n}\frac{p\epsilon}{2}[\tfrac{1}{2}p\epsilon K_{ip-1}(p\epsilon)+K_{ip-2}(p\epsilon)]\right\}. \quad (35)$$

Finally, we have

$$\left.\begin{matrix}|M_y|^2\\|M_x|^2\end{matrix}\right\}=\left\{\begin{matrix}\cos^2\beta\\\sin^2\beta\end{matrix}\right\}\frac{e^{-\pi p}}{p^2}\frac{(2\pi)^2(\epsilon^2-1)}{n^2}\left(\frac{n}{k_1}\right)^5\left(1-\frac{4p}{n}\right)\epsilon^2$$
$$\times\left[\left(K_{ip}'^2+\frac{1}{\epsilon^2}K_{ip}^2\right)-\frac{2p}{n}\left(K_{ip}'^2+\frac{2-\epsilon^2}{2\epsilon^2}K_{ip}^2\right)\right], \quad (36)$$

$$|M_x|^2=\frac{e^{-\pi p}}{n^2p^2}\left(\frac{n}{k_1}\right)^5\left(1-\frac{4p}{n}\right)(2\pi)^2\epsilon^2$$
$$\times\left\{K_{ip}'^2+\left(\frac{\epsilon^2-1}{\epsilon}\right)^2K_{ip}^2-\frac{p\epsilon}{n}\left(\frac{2-\epsilon^2}{\epsilon}K_{ip}'^2\right.\right.$$
$$\left.\left.+\frac{2(\epsilon^2-1)^2}{\epsilon^3}K_{ip}^2\right)\right\}, \quad (37)$$

$$|\mathbf{M}|^2=\frac{(2\pi)^2e^{-\pi p}}{n^2p^2}\left(\frac{n}{k_1}\right)^5\left(1-\frac{5p}{n}\right)$$
$$\times\epsilon^4\left[K_{ip}'^2+\frac{\epsilon^2-1}{\epsilon^2}K_{ip}^2\right]. \quad (38)$$

The differential cross section is thereby

$$\sigma(\theta)=A_0\left(1-\frac{5\hbar\omega}{2E}\right)\left\{\frac{4}{3}\left(1-\frac{\hbar\omega}{2E}\right)J_1\right.$$
$$\left.+(3\cos^2\theta-1)\left(J_2+\frac{\hbar\omega}{2E}J_3\right)\right\}, \quad (39)$$

where

$$J_1=\int_p^\infty\left[K_{ip}'^2(x)+\frac{x^2-p^2}{x^2}K_{ip}^2(x)\right]xdx,$$
$$J_2=\int_p^\infty\left[\left(\frac{x^2}{3}-p^2\right)K_{ip}'^2(x)\right.$$
$$\left.+\frac{(x^2-p^2)(\frac{2}{3}x^2-p^2)}{x^2}K_{ip}^2(x)\right]\frac{dx}{x}, \quad (40)$$
$$J_2=\int_p^\infty\left[\left(2p^2-\frac{4}{3}x^2\right)K_{ip}'^2(x)\right.$$
$$\left.+\frac{(x^2-p^2)(5x^2-6p^2)}{3x^2}K_{ip}^2(x)\right]\frac{dx}{x}.$$

We see that Eqs. (39) and (40) reduce to the classical formulas of the preceding section in the limit $(\hbar\omega/E)\to 0$. Numerical integration of these formulas for the parameter values given in Eqs. (21) and (22) gives a differential cross section at 90° of

$$\sigma(90°)=1.65\times10^{-31}\text{ cm}^2/\text{sterad},$$

in satisfactory agreement with the experimental result in Eq. (1). We have also computed an angular distribu-

tion curve for the emission of x-rays in a 3-kev energy interval about 150 kev for 2 Mev protons incident on a tin target. The result given in Fig. 3 is nearly isotropic in agreement with preliminary[2] results. For angles other than 90° there will be corrections to this curve due to the dipole-quadrupole cross terms in Eq. (5), but these are expected to alter the results by less than 10 percent. The total cross section is, from Eqs. (39) and (40),

$$\sigma_{\omega\sigma}(k_1,k_2,\omega)=(16\pi/3)A_0(1-3\hbar\omega/E)J_1$$
$$=18\cdot9\times10^{-31}\ \text{cm}^2.$$

IV. CONCLUSION

The quantum correction to the classical orbit treatment of dipole radiation emitted by a beam of protons scattered in a coulomb field has been calculated and found to agree with experiments of Mark *et al.*[2] This correction has been expressed in terms of the inelasticity of the scattered proton, $(\hbar\omega/E)$. It serves to decrease the classical prediction by ~25 percent for the experiments under discussion here. This reduction seems at first to be surprisingly large in view of the fact that the proton radiates only $\hbar\omega/E=7.5$ percent of its energy. However, we can make it reasonable by recalling that the important orbits in the classical picture are parabolic or nearly parabolic. The damping effect of the bremsstrahlung on the motion of the proton, which is neglected in the classical treatment, causes it to be slowed down and repelled further away from the Coulomb field source, thereby reducing the effective dipole moment by an appreciable amount.

Other corrections due to retardation effects, electronic shielding, and finite nuclear size can be neglected for the energies studied in this work.

We wish to thank Dr. Hans Mark for informing us of his experimental results prior to publication and thereby arousing our interest in this problem.

Note added in proof.—We have learned (private communication) that Professor L. C. Biedenharn of The Rice Institute has made the reduction to the classical orbit calculation expressed in Eq. (35) in connection with his studies on the electric excitation problem.

PHYSICAL REVIEW VOLUME 99, NUMBER 3 AUGUST 1, 1955

Angular Correlation of the Gamma Rays of Ba^{134}

M. G. Stewart, R. P. Scharenberg, and M. L. Wiedenbeck
Department of Physics, University of Michigan, Ann Arbor, Michigan
(Received April 11, 1955)

The angular correlations have been measured between the following pairs of gamma rays from Ba^{134}: 605 kev–797 kev, 1368 kev–605 kev, and 570 kev–605 kev. These measurements indicate that the spins of the states associated with these gamma rays are 4, 4, 2, 0. The 605, 797, and 1368-kev gamma rays are pure quadrupole while the 570-kev gamma ray is a mixture of 94 percent quadrupole and 6 percent dipole.

I. INTRODUCTION

THE angular correlation of the gamma rays following the beta decay of the 2.3-year isomer of Cs^{134} has been investigated by a number of authors.[1–4] While the complete decay scheme is very complex,[5,6] the main features are shown in Fig. 1. The gamma-ray spectrum as observed is shown in Fig. 2. It should be noted that the remaining lines are too weak to be observed. The first investigators noted the similarity between the shape of the curve obtained from their measurements of the overall angular correlation and the shape of the angular correlation function obtained from the gamma rays following the beta decay of Co^{60}. The cases differed in that the asymmetry for the Ba^{134} was approximately 12 percent while that of Co^{60} was 17 percent. Since the majority of the coincidence counts were due to the 797-kev and 605-kev gamma rays, it was proposed that these two gamma rays gave rise to a basic quadrupole-quadrupole correlation. Since Ba^{134} is an even-even nucleus (56 protons-78 neutrons) the ground state is assumed to have a spin of 0 with even parity. Thus, as is in the case of Co^{60}, spins of 2 and 4 were assigned to the first and second excited states respectively with both radiations quadrupole. Robinson and Madansky[3] measured the correlation of the lower two gamma rays by demanding that they also be in coincidence with the high-energy beta ray. From this measurement and from a measurement of the over-all correlation, spins of 5, 4, 2, 0 were assigned to the important states with the radiation being dipole, quadrupole, quadrupole respectively. However because of the discrepancies between the over-all correlation and the above assignment, it was decided to reinvestigate the angular correlations in greater detail.

[1] E. L. Brady and M. Deutsch, Phys. Rev. **78**, 558 (1950).
[2] J. R. Beyster and M. L. Wiedenbeck, Phys. Rev. **79**, 411 (1950).
[3] B. L. Robinson and L. Madansky, Phys. Rev. **84**, 604 (1951).
[4] Kloepper, Lennox, and Wiedenbeck, Phys. Rev. **88**, 695 (1952).
[5] Cork, LeBlanc, Nester, Martin, and Brice, Phys. Rev. **90** 444 (1953).
[6] Keister, Lee, and Schmidt, Phys. Rev. **97**, 451 (1955).

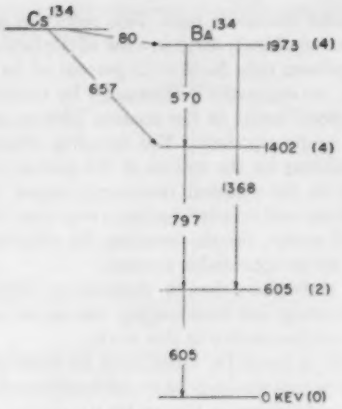

FIG. 1. Simplified decay scheme of Cs^{134}. The numbers in parenthesis are the spins of the nuclear levels.

II. APPARATUS

Scintillation counters were used as the gamma-ray detectors. They consisted of NaI(Tl) crystals mounted on RCA type 5819 photomultiplier tubes. The crystals were 1.5 in. in diameter and 1 in. thick. The source was mounted at the intersection of the axes of the cylindrical crystals and was about 5 in. above the table. The crystals were covered with $\frac{1}{16}$ in. aluminum to stop the beta rays.

Figure 3 is a block diagram of the coincidence spectrometer. It consists of two fast channels which have a resolving time of about 8 millimicroseconds in parallel with slower energy selection channels. The fast coincidence output is placed in slow triple coincidence with the two energy selection outputs. The resolving time of the slow triple coincidence circuit is about 200 millimicroseconds.

From the phototube the pulse was fed into a fast and slow channel. The fast channel consisted of Hewlett-Packard distributed amplifiers (types 460A and 460B) and a 6AU6 limiter. The resulting fast rising pulse was used to trigger a fast blocking oscillator which gave a positive output pulse of about 40 volts amplitude, 0.06 microsecond duration, and with a 0.01 microsecond rise. This was inverted and then clipped with a shorted delay line to give a fast negative pulse suitable for triggering a Garwin-type coincidence circuit.[7,8] The slow channel consisted of a Bell-Jordan A-1 type amplifier[9] and a single-channel discriminator. The output pulses from the fast coincidence circuit and the two differential discriminators were used to trigger slow blocking oscillators which in turn activated the slow coincidence circuit.

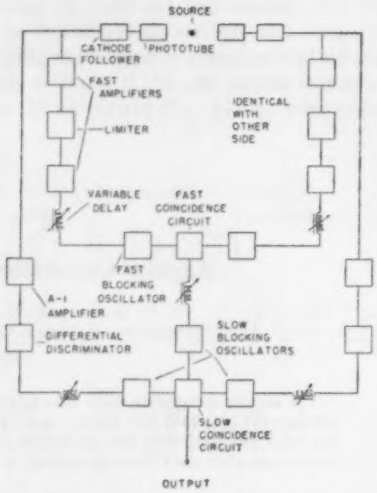

FIG. 3. Block diagram of the coincidence spectrometer.

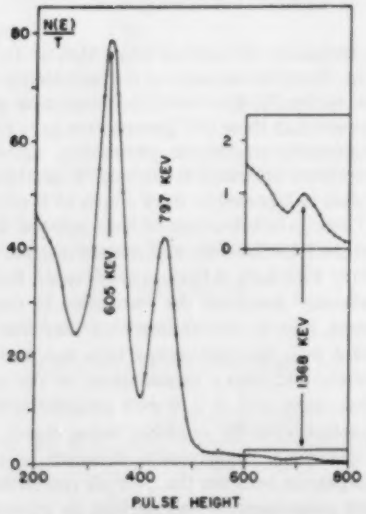

FIG. 2. Gamma-ray spectrum of Ba^{134}.

III. RESULTS

The over-all angular correlation was measured using both a solid and a liquid source. The solid source was Cs_2CO_3 and the liquid source was Cs_2CO_3 dissolved in water. The identical results of these two measurements indicate there are no perturbations of the nucleus while it is in the intermediate states. The results of the over-all correlation are shown in Fig. 4 and are in agreement with those of the previous investigators. The measured correlation will depend somewhat on the discrimination level since this will change the relative intensities of the three cascade gamma rays. A least-squares fit of

[7] R. L. Garwin, Rev. Sci. Instr. **21**, 569 (1950).
[8] R. L. Garwin, Rev. Sci. Instr. **24**, 618 (1953).
[9] W. H. Jordan and P. R. Bell, Rev. Sci. Instr. **18**, 703 (1947).

the data to the curve

$$W(\theta)=1+A_2P_2(\cos\theta)+A_4P_4(\cos\theta)$$

was made where $P_k(\cos\theta)$ are the Legendre polynomials of degree k. Table I shows the experimental values for A_2 and A_4 along with the theoretical values for the basic quadrupole-quadrupole correlation and the basic dipole-quadrupole correlation. For the proposed assignment[3] $5(D)4(Q)2(Q)0$, the over-all correlation would be compounded from a combination of the 2^2-2^2 and 2^1-2^2 correlations. It is seen that an arbitrary combination of these correlations cannot give the observed results. Hence, it must be concluded that the assignment $5(D)4(Q)2(Q)0$ is in disagreement with the observed results.

The 797 kev–605 kev correlation was measured by setting both counters integrally on the high side of the 600-kev line. For an energy resolution of 13 percent, the 570-kev line would extend to a maximum of about 645 kev. Thus if the counters were set above 645 kev the only coincidences recorded would be between the 797 kev and the 605 kev and between the 1368-kev and the 605-kev lines. However since the 1368-kev line is very weak, this latter coincidence can be neglected. Figure 5 shows the results of this measurement. The solid curve is the theoretical curve for the basic 2^2-2^2 correlation and the dashed curve is the least squares fit to the experimental points, corrected for the finite geometry. The experimental coefficients are $A_2=0.101\pm0.008$ and $A_4=-0.002\pm0.012$. Since Ba^{134} is an even-even nucleus the ground state is assumed to have spin 0. Thus spins of 2 and 4 are assigned to the 605-kev and the 1402-kev states, respectively. Both transitions are quadrupole radiation.

TABLE I. Coefficients for the theoretical curves for the basic 2^2-2^2 correlation, the basic 2^1-2^2 correlation, and the experimental over-all correlation of Ba^{134}. The experimental coefficients have been corrected for the finite geometry.

Correlation	A_2	A_4
Experimental	0.076 ± 0.002	0.017 ± 0.003
2^2-2^2	0.102	0.009
2^1-2^2	−0.071	0

The spin of the ground state of Cs^{134} has been measured as 4[10,11] and the ΔI for the 80-kev beta transition has been measured as 0, ±1.[12] Thus the 1973-kev level in Ba^{134} must have a spin of either 3, 4, or 5.

The correlation between the 1368-kev–605-kev gamma rays was measured by setting one counter integrally at 1200 kev and the other counter integrally at about 500 kev. The results of this measurement are shown in Fig. 6. Curves 1, 2, and 3 are the theoretical curves for the basic 2^1-2^2, 2^2-2^2, and 2^3-2^2 correlations, respectively. The dashed curve is the least-squares fit to the experimental points corrected for the finite geometry. The experimental coefficients are $A_2=0.094\pm0.007$ and $A_4=-0.024\pm0.009$. It is seen that the observed correlation is in best agreement with a 2^2-2^2 correlation. If mixtures are considered, the experimental curve can be fitted with an assignment $3(D,Q)2(Q)0$. However with this assignment the 570 kev–797 kev and the 570 kev–605 kev correlations have an A_4 coefficient which is zero or negative. This is again in disagreement with the large A_4 coefficient observed in the over-all correlation. An assignment of 5 for the upper state with a mixture of 2^3–2^4 pole radiation can be ruled out on lifetime considerations. Thus the experimental data are compatible with a spin assignment of 4 for the 1973-kev level, but are not compatible with either a 3 or a 5. The 1368-kev transition is quadrupole radiation.

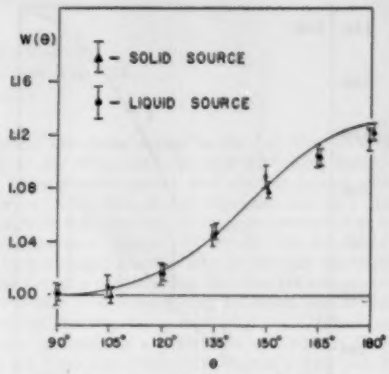

FIG. 4. Over-all angular correlation of Ba^{134}. This is composed mainly of three separate correlations; the 797–605, 570–797, and 570–605 kev correlations.

A measurement of the one-three angular correlation between the 570 kev and the 605-kev gamma-rays

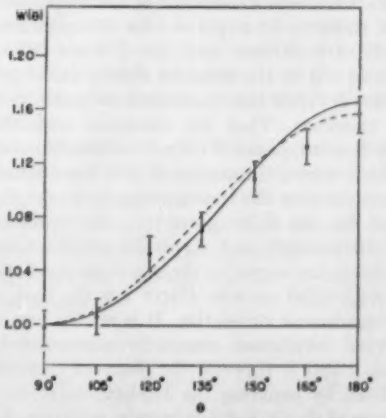

FIG. 5. Angular correlation of the 605–797 kev gamma rays. The dashed curve is the least-squares fit to the experimental points and has been corrected for finite geometry. The solid curve is the theoretical curve for a basic 2^2-2^2 correlation.

[10] M. Goldhaber and R. D. Hill, Revs. Modern Phys. **24**, 179 (1952).
[11] Jaccarino, Bederson, and Stroke, Phys. Rev. **87**, 676 (1952).
[12] Alonzo E. Stoddard, thesis, University of Michigan, 1953 (unpublished).

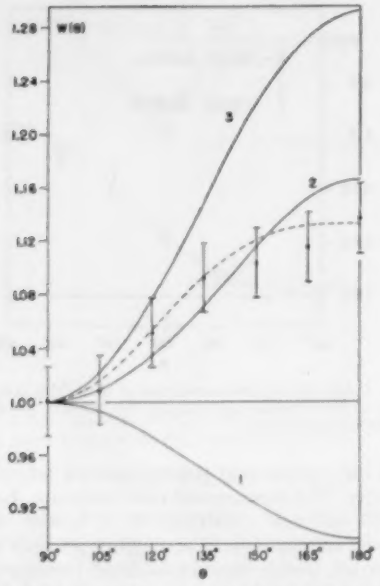

FIG. 6. Angular correlation of the 1368–605 kev gamma rays. The dashed curve is the least-squares fit to the experimental points and has been corrected for finite geometry. Curves 1, 2, and 3 are the theoretical curves for the basic 2^1-2^0, 2^2-2^0, and 2^3-2^0 correlations, respectively. The experimental curve contains a small admixture of a triple correlation due to the summing of the 570-kev and 797-kev gamma rays.

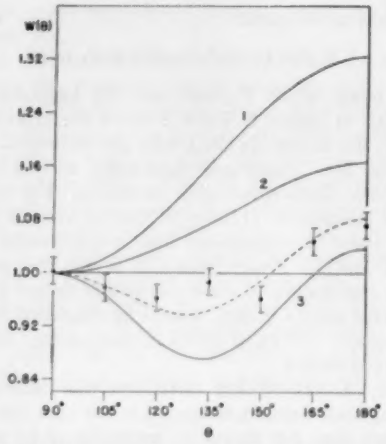

FIG. 7. Angular correlation of the 570–605 kev gamma rays. The dashed curve is the least squares fit to the experimental points and has been corrected for finite geometry. Curve 1 is the theoretical curve for the one-three correlation for a $4(D)4(Q)2(Q)0$ cascade. Curve 2 is the theoretical curve for a basic 2^2-2^0 correlation. Curve 3 is the theoretical curve for the one-three correlation for a $4(D,Q)4(Q)2(Q)0$ cascade with the first transition 94 percent quadrupole to 6 percent dipole radiation. The experimental curve is composed of 38 percent curve 2 plus 62 percent curve 3.

with the 797-kev transition unobserved allows a determination of the multipole order of the 570-kev gamma ray.[13,14] For this work, each counter was set at 570-kev (i.e., on the lower edge of the 605-kev line) with a 60-kev window width. In addition to the 570-kev–605-kev coincidences there will be 570-kev—797-kev and 605-kev–797-kev coincidences due to the Compton background from the 797-kev line. Hence the measured correlation will be a composite of three separate correlations. However for a spin of 4 for the uppermost state, the 570-kev–797-kev and the 570-kev–605-kev correlations will be the same for dipole, quadrupole, or a mixture of dipole and quadrupole radiation in the 570-kev transition. Thus the measured correlation will really be a composite of only two different correlations. Figure 7 shows the results of this measurement. The dashed curve is the least-squares fit to the data, corrected for the finite geometry. The coefficients are $A_2=0.019\pm0.019$ and $A_4=0.092\pm0.029$. Curve 1 is the theoretical curve for the one-three correlation for a $4(D)4(Q)2(Q)0$ cascade. Curve 2 is the basic quadrupole-quadrupole correlation. It is readily seen that the observed correlation cannot be compounded out of curves 1 and 2. However the observed correlation can be fitted by requiring the 570-kev transition to be a mixture of dipole and quadrupole radiation. Equating the observed coefficients A_2 and A_4 to the theoretical ones gives two equations with two parameters to be determined; the ratio δ of the quadrupole to the dipole nuclear matrix elements[15] and the fraction f of the basic 2^2-2^2 correlation that must be present. δ^2 gives the ratio of the intensities of the quadrupole to the dipole radiation. The required mixture is 94 percent quadrupole to 6 percent dipole with 0° phase difference. The fraction f is 0.38. Curve 3 is the correlation function for the 570-kev–605-kev cascade with the 2^2-2^2 correlation subtracted out.

IV. SUMMARY

The angular correlations of the gamma rays of Ba^{134} following the beta decay of the 2.3 year isomer of Cs^{134} were reinvestigated. The 797-kev–605-kev cascade is in agreement with a $4(Q)2(Q)0$ assignment and the 1368-kev–605-kev cascade is also best fitted by a $4(Q)2(Q)0$ assignment. The one-three correlation for the 570-kev–(797-kev)–605-kev cascade requires a mixture of 94 percent quadrupole and 6 percent dipole radiation for the 570-kev transition. For a reasonable branching ratio between the 650-kev and 80-kev beta rays, the theoretical over-all correlation is in agreement with the observed results. The large percentage of quadrupole radiation in the 4 to 4 transition may be compared to the similar cases of 2 to 2 transitions in which there are also large admixtures of quadrupole radiation.[16]

[13] Arfken, Biedenharn, and Rose, Phys. Rev. **86**, 761 (1952).
[14] L. C. Biedenharn and M. E. Rose, Revs. Modern Phys. **25**, 729 (1953).
[15] The notation of reference 14 is used.
[16] J. J. Kraushaar and M. Goldhaber, Phys. Rev. **89**, 1081 (1953).

Decay of Bi^{207}

D. E. Alburger and A. W. Sunyar
Brookhaven National Laboratory, Upton, New York*

(Received April 26, 1955)

Bi^{207} has been found to decay by electron capture accompanied by gamma rays of energies 0.569±0.0015, 0.894±0.007, 1.0639, 1.43±0.01, and 1.771±0.005 Mev having transition intensities of 100:0.16:87:0.16:8 percent per disintegration, respectively. K-conversion electron intensities are 1.7, 0.0039, 8.2, 0.0009, and 0.022 electrons per 100 disintegrations respectively. The 0.894, 1.43 and 1.771-Mev transitions have K-conversion coefficients of $(2.4\pm1)\times10^{-3}$, $(5\pm2)\times10^{-3}$ and $(2.5\pm0.5)\times10^{-3}$. The first of these is in agreement with $M1$ radiation and the latter two with $E2$ or $E2+M1$ radiations. Electron capture branches are 87 percent to the $i_{13/2}$ state at 1.633 Mev, 5±2 percent to the 0.57-Mev first excited state and 8±2 percent to a level at 2.35 Mev. Branching to the 2.35-Mev level proceeds only by L-capture as shown from the x-ray spectrum in coincidence with 1.78+0.57 Mev photopeak sum pulses. The decay energy to the 2.35-Mev level thus lies between 15 and 90 kev and the total Bi^{207} decay energy is 2.40 ±0.04 Mev. Gamma-gamma and electron-gamma correlation experiments confirm the 1.06–0.57 Mev cascade as $13/2\rightarrow5/2\rightarrow1/2$ while the 1.78–0.57 Mev gamma-gamma correlation is isotropic to within 5 percent. A spin $\geq7/2$ for the 2.35 Mev state is supported by a crossover intensity of $<6\times10^{-6}$ per disintegration as determined with a photoneutron detector. An assignment of $f_{7/2}$ to the 2.35 Mev level is compatible with all of the data including the 1.78–0.57 Mev angular correlation, if the 1.78-Mev transition is assumed to consist of a mixture of ~94 percent $E2$ and ~6 percent $M1$. Fast-coincidence techniques have been used to show that the 0.57-Mev level has a lifetime of $<4\times10^{-10}$ sec.

INTRODUCTION

THE energy levels of Pb^{207}, a nucleus having one neutron less than a closed shell, should be describable[1,2] according to the shell model in the same way as for a system with one nucleon outside of a closed shell. On the basis of a Pb^{207} level arrangement similar to the one proposed in this paper except for the configuration assignment of the state at 2.35 Mev (formerly assumed to be $h_{9/2}$), theoretical calculations were made by Pryce[1] on the levels expected in the "two-hole" nucleus Pb^{206}. These calculations were correlated successfully with the experimentally observed states. We shall describe a number of recent results according to which the probable assignment to the 2.35-Mev level in Pb^{207} is $f_{7/2}$ and which reveal other interesting features of the Bi^{207} decay. The effect of the $f_{7/2}$ assignment on the predicted levels in Pb^{206} will be discussed later.

Bi^{207} was discovered[3] by Neumann and Perlman who found that it decays by electron capture to Pb^{207} with a half-life of approximately 50 years. They reported that the decay is accompanied by eight gamma rays, four of which lie above 2 Mev, as observed from the internal conversion electron spectrum. A much shorter Bi^{207} half-life, 8.0±0.6 years, has been published[4] recently by Cheng *et al.* Wapstra[5] and McGowan and Campbell[6] confirmed the presence of only two transitions of energies 0.56 and 1.06 Mev. Wapstra also proposed that the electron capture of Bi^{207} branches 80 percent to a level at 1.625 Mev in Pb^{207} and 20 percent to a level at 0.565 Mev.

Earlier it had been found[7] that a 0.8-sec isomeric state is excited in Bi^{207} decay. This was identified as resulting from the 1.06-Mev transition by Goldhaber and Sunyar,[8] who gave it an $M4$ assignment on the basis of lifetime and energy. The high energy and large conversion coefficient has made this transition useful[9] as an energy standard in beta spectroscopy.

That the 1.06–0.57 Mev main cascade is probably an $M4-E2$ cascade was confirmed by the conversion coefficients measured by Wapstra[5] and by McGowan and Campbell.[6] The angular correlation experiments of McGowan and Campbell[6] established the spin sequence as $13/2\rightarrow5/2\rightarrow1/2$, the shell-model assignments being $i_{13/2}\rightarrow f_{5/2}\rightarrow p_{1/2}$. The latter workers also observed a 1.76-Mev gamma ray in their scintillation spectrum, but did not assign this to Bi^{207}, and placed a very low limit on the intensity of any higher-energy gamma rays.

Prescott has reported[7] Bi^{207} gamma rays of 0.57, 1.07, 1.76, and 2.47 Mev with evidence for a prompt gamma ray of 1.46 Mev. From coincidence data he suggests that the 1.07-Mev line may actually be double, 6 percent of it being in prompt coincidence with electron capture.

Other evidence on the Pb^{207} levels comes from the beta decay[10] of Tl^{207} which excites a level at 0.87 Mev and from the alpha decay[11] of Po^{211} to levels at 0.56, 0.87, and 1.63 Mev. (d,p) and (d,t) nuclear reaction experiments by Harvey[12] are also consistent with Pb^{207} levels at 0.56, 0.89, 1.63, and 2.33 Mev as well as others at higher energies.

* Under contract with the U. S. Atomic Energy Commission.

[1] D. E. Alburger and M. H. L. Pryce, Phys. Rev. **95**, 1482 (1954).
[2] M. H. L. Pryce, Proc. Phys. Soc. (London) **A65**, 773 (1952).
[3] H. M. Neumann and I. Perlman, Phys. Rev. **81**, 958 (1951).
[4] Cheng, Ridolfo, Pool, and Kundu, Phys. Rev. **98**, 231(A) (1955).
[5] A. H. Wapstra, Arkiv Fysik **7**, 279 (1954).
[6] F. K. McGowan and E. C. Campbell, Phys. Rev. **92**, 523 (1953); F. K. McGowan, Phys. Rev. **92**, 524 (1953).
[7] J. R. Prescott [Proc. Phys. Soc. (London) **A67**, 540 (1954)] gives a more complete review of previous evidence on Bi^{207} decay.
[8] M. Goldhaber and A. W. Sunyar, Phys. Rev. **83**, 906 (1951).
[9] D. E. Alburger, Phys. Rev. **92**, 1257 (1953).
[10] J. Surugue, J. phys. radium **7**, 145 (1946).
[11] Jentschke, Juveland, and Kinsey, Phys. Rev. **96**, 231 (1954).
[12] J. Harvey, Can. J. Phys. **31**, 278 (1953).

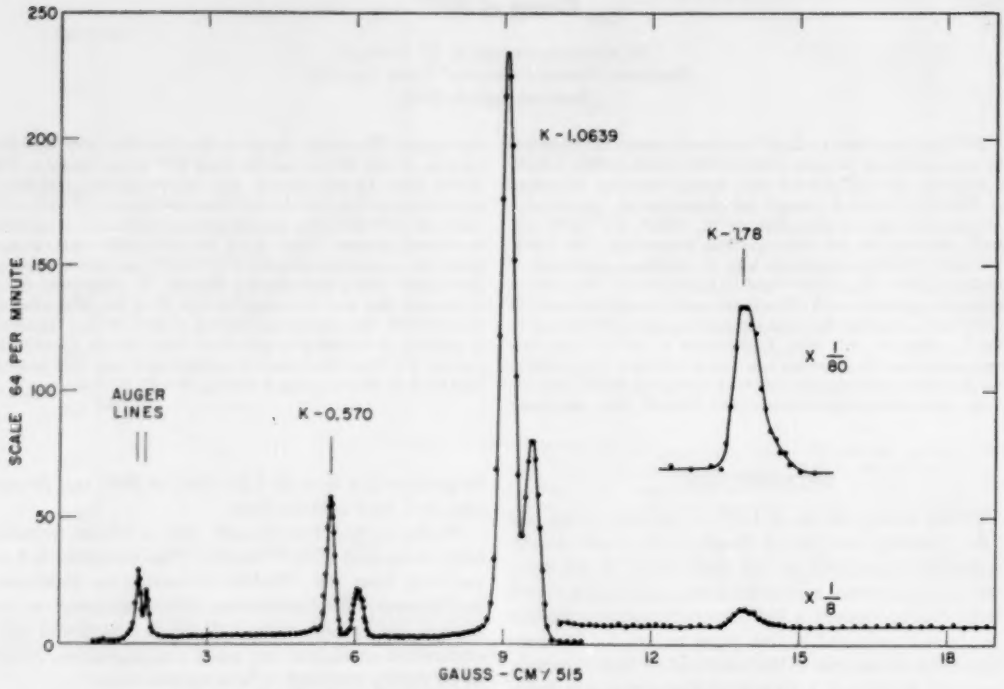

FIG. 1. Internal conversion spectrum of Bi^{207} using a 36-μC source at 3.7 percent resolution.

CONVERSION ELECTRON AND GAMMA RAY SPECTRA†

Most of the experiments to be described were made on sources taken from 2.5 mC of Bi^{207} activity which had been prepared by a 9000 μa-hour 22-Mev deuteron bombardment of ordinary lead in the Oak Ridge cyclotron, carried out in July, 1953. Subsequent chemical separations[18] were made at Brookhaven. Since all of the experiments were performed at least 8 months after bombardment, 6-day Bi^{204} and 14-day Bi^{205} had decayed to negligible proportions.

The conversion electron spectrum from a 36-μC source of Bi^{207} electroplated on a 10-mg/cm^2 Cu backing was examined in the Brookhaven lens spectrometer with the results shown in Fig. 1. Auger lines and conversion electrons corresponding to transitions of 0.57, 1.06, and 1.78 Mev are indicated. Of the conversion lines above 1.8 Mev reported[3] by Neumann and Perlman, the weakest would have been 6 times the probable errors of the points in the corresponding region of Fig. 1 and their K-1.46 line would have been 10 times as large as the K-1.78 line. Relative conversion intensities were checked 9 months after the data of Fig. 1 with the same results.

A more thorough search for weak conversion electrons between L-0.57 and K-1.06 and between L-1.06 and K-1.78 was carried out with a 150-μC source at a resolution of 4 percent. In the lower of these two energy regions the scattered tail of the K-1.06 line hindered the measurements. However, there seemed to be slight evidence of a line corresponding to a transition of about 0.9 Mev. If such a line is present its intensity is $\leq$0.1 percent of K-1.06. Figure 2 shows the higher-energy region obtained for one of two different source geometries, both of which gave comparable results. A line is observed which, if it is real, corresponds to a transition of 1.44 Mev and has a K-conversion intensity 4 ± 1 percent as strong as K-1.78. Since its intensity is a factor of 10^4 weaker than K-1.06 there is a possibility that the line is a ghost arising from scattering effects. In any case, the quoted intensity can be considered as an upper limit.

If the K-conversion intensities are normalized on the assumption that the 0.57-Mev transition is pure $E2$ and occurs once per disintegration, then the 0.57, 1.0639, 1.44, and 1.78-Mev transitions have K-line intensities of 1.7, 8.2, 0.0009, and 0.022 electrons per 100 disintegrations. A correction of 10 percent in the K-1.78 peak height has been made because of the unresolved L-electron contribution.

Energy values for the 1.44 ± 0.015 and 1.78 ± 0.01 Mev gamma rays were obtained from the data of

† See note added in proof on page 702.

[18] D. E. Alburger and G. Friedlander, Phys. Rev. **81**, 523 (1951).

Fig. 2. The 569±1.5 kev gamma-ray energy[14] was determined at 1.2 percent resolution with a 13-microcurie source 3 mm in diameter by comparing its K-conversion peak and extrapolated edge positions with those of the 1.0639-Mev gamma ray.

A K/L ratio measurement on the 0.57-Mev gamma ray was carried out at 1.4 percent resolution. The M line is then sufficiently well resolved to make a negligible contribution to the L peak height. A ratio 3.4±0.4 is obtained which agrees well with the theoretical $K/L_{I+II+III}$ ratio of 3.2 calculated for a 0.57-Mev $E2$ transition at $Z=85$ from L-shell conversion tables privately distributed by Rose, Goertzel, and Swift. In a previous report[9] the K/L ratio of the 1.06-Mev transition was given as 3.95±0.25. Since the L_{II} conversion coefficient at 2.0 mc^2 is not yet available it is only possible to estimate by extrapolation that the $K/L_{I+II+III}$ ratio at $Z=85$ and 2.0 mc^2 (1.022 Mev) for an $M4$ transition is between 3.5 and 4. Hence both K/L ratios are consistent with the $E2$ and $M4$ assignments to the 0.57- and 1.06-Mev gamma rays, respectively.

The unconverted gamma-ray spectrum, measured with 1 in.×1½ in. and 2 in.×2 in. NaI crystals, showed prominent Compton and photo distributions for the 0.57-, 1.06-, and 1.78-Mev gamma rays. With a 36-μC source 10 in. from the 1 in.×1½ in. crystal the yield at high energies dropped off by a factor of 500 below the 1.78-Mev peak intensity. From the full-energy peak efficiency as a function of gamma-ray energy, calculated with the total efficiency tables[15] of McGowan and the peak-to-total curve[16] of Heath, Bell, and Davis, the maximum possible intensity of any gamma ray between 2 and 2.5 Mev is 1 per 2000 disintegrations. Correcting for efficiency and internal conversion it is found that the 1.06- and 1.78-Mev transitions have intensities of 88 percent and 9 percent of the 0.57-Mev line, respectively.

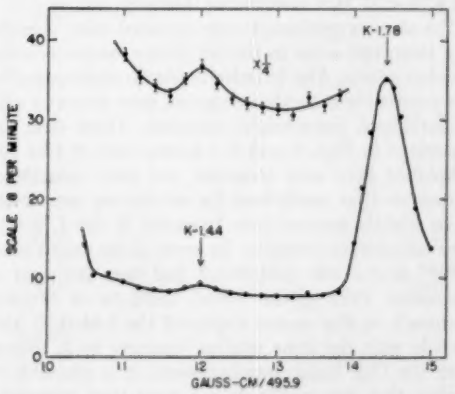

Fig. 2. Conversion electrons above 1.1 Mev measured at 4 percent resolution, showing the presence of a weak K-1.44 line.

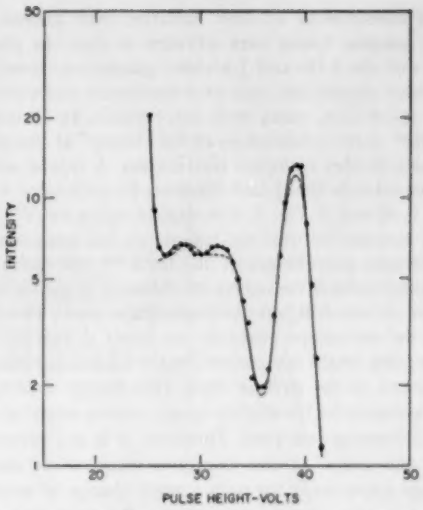

Fig. 3. Singles scintillation spectrum above 1 Mev of Bi^{207} (solid curve) and Y^{88} (dashed curve).

A more detailed study of the scintillation spectrum above 1 Mev was carried out with an Atomic Instruments Company 20-channel pulse-height analyzer. In order to establish the pulse-height distribution for a gamma ray of about 1.8 Mev, a source of Y^{88} was prepared by deuteron bombardment of Sr followed by chemical separation. This activity has been reported[17] as emitting gamma rays of 0.908 and 1.853 Mev of equal intensity and a 2.76-Mev gamma ray of 1 percent intensity. Comparisons of the energies of the Y^{88} and Bi^{207} lines were made both with a gray-wedge analyzer, using microscope reading of Polaroid photographs, and with the 20-channel analyzer. The same total counting rates were maintained in the Dumont 6292 phototube output. These precautions were taken because of studies of peak shifts with counting rate made recently[18] by Bernstein. It was found that the Y^{88} gamma is 2.8 percent higher in energy than the 1.78-Mev Bi^{207} line. This places it at 1.83 Mev based on the Bi^{207} energy. The region above 1.8 Mev did not show a well-defined line of 2.76 Mev which could be distinguished from pulse pile-up. Our work suggests that the 2.76-Mev Y^{88} gamma ray, if present, is ≤0.5 percent as intense as the 1.83-Mev gamma ray. Hence the effect of its pulse-height distribution on that of the 1.83-Mev gamma ray is negligible.

Comparisons of the Bi^{207} and Y^{88} scintillation spectrum shapes were made using liquid sources of equal volume in identical weighing bottles. Approximately

[14] P. Marmier and F. Boehm of the California Institute of Technology have determined the energy of this transition to be 569.7±0.2 kev (private communication).

[15] F. K. McGowan (privately circulated tables); see Phys. Rev. **93**, 163 (1954).

[16] Heath, Bell, and Davis, Oak Ridge National Laboratory Report ORNL 1415 (unpublished).

[17] Hollander, Perlman, and Seaborg, Revs. Modern Phys. **25**, 469 (1953).

[18] W. Bernstein (unpublished).

equal strengths of 1.8-Mev radiation were present in both samples. Gains were adjusted so that the photo peaks of the 1.78- and 1.83-Mev gammas occurred in the same channel and runs were made with and without lead collimation, using both size crystals. In all cases, the Bi^{207} curve exhibited an excess "hump" at the peak of the 1.78-Mev Compton distribution. A typical set of curves taken with a $\frac{3}{4}$-inch diameter Pb collimator 8 cm long is shown in Fig. 3. The dashed curve for Y^{88} has been matched so that the full-energy-loss peak occurs at the same pulse height as that for Bi^{207}, and such that the amplitudes of the curves are the same in the vicinity of the one-annihilation-quantum escape peak. The fact that the one-escape peaks do not occur at exactly the same pulse height is explained by the 2.8 percent energy difference of the gamma rays. This energy difference also accounts for the slightly lower relative height of the Y^{88} full-energy-loss peak. However, it is not expected that the shape of the Compton distribution would change appreciably for such a small change of energy. Based on the normalization shown, the extra hump in the Bi^{207} curve corresponds to the full-energy-loss peak of a 1.44-Mev gamma ray whose intensity is 2.5 percent of the 1.78-Mev gamma-ray intensity.

Pile-up of the relatively stronger 0.57- and 1.06-Mev gamma-ray distributions of Bi^{207} were considered for their effect on the 1–1.8 Mev region. The sum energy of 1.63 Mev occurs at the trough of the 1.78-Mev pulse-height distribution and this point would be expected to be most sensitive to pile-up. For a variation of a factor of 6 in counting rate as used in the various runs, there was no essential change in the peak-to-trough ratio for the 1.78-Mev gamma ray. It is concluded that pile-up could not account for the difference between the Bi^{207} and Y^{88} curves in the neighborhood of the 1.44-Mev photoline. Pulse addition can also be neglected since the peak-to-trough ratio of the 1.78-Mev gamma ray remained constant for source-to-crystal distances as great as 25 inches. The trough of the 1.63-Mev pulse addition distribution occurs near 1.4 Mev and cannot appreciably influence the 1.44-Mev photopeak intensity.

The lens spectrometer and 1 in.$\times 1\frac{1}{2}$ in. NaI crystal data, together with the known conversion coefficients of the 0.57- and 1.06-Mev transitions, can be used to derive the K-conversion coefficients of the 1.44- and 1.78-Mev gamma rays. These are found to be $(5\pm 2)\times 10^{-4}$ and $(2.5\pm 0.5)\times 10^{-4}$, respectively. If the adopted branching of 8 percent to the 2.35-Mev level (see Fig. 7) is used rather than the gamma ray data alone both of these coefficients are 10 percent higher. As a check on the 0.57- and 1.06-Mev K conversion and gamma-ray intensity data, the ratio of K-conversion coefficients of 1.06/0.57 can be calculated from the ratio K-1.06/K-0.57 = 4.8 derived from Fig. 1 and the gamma-ray intensity ratio from the NaI crystal data. The result is 5.98 compared with a theoretical[19] conversion coefficient ratio of 6.03 if the transitions are assumed to be pure $M4$ and $E2$ respectively. Independently of the NaI gamma-ray measurements, the relative transition intensities of 1.06/0.57 can be calculated from the ratio 4.8 of the K-conversion line intensities, again based on the assumed multipolarities $M4$ and $E2$. The result is that the 1.06/0.57 transition ratio is 0.89 ± 0.04.

COINCIDENCE MEASUREMENTS

Gamma-gamma coincidence experiments were carried out using two 2 in.$\times$2 in. NaI crystal detectors and Bi^{207} sources of 0.18, 0.44, and 1.0 microcurie. In the first tests one counter was channeled on either the 0.57- or 1.06-Mev line and the coincidence spectrum was scanned in the other detector by using a single-channel pulse-height analyzer. It was found that the 0.57-Mev transition is in coincidence with both the 1.06- and 1.78-Mev gamma rays but that the latter two are not in coincidence with each other.

A search was then made with a coincidence gray-wedge analyzer[20] for possible gamma rays of 1.44 and 0.9 Mev. The same detectors as above were used except that a Pb absorber sandwiched with brass was included between the crystals in order to reduce spurious effects arising from addition of back-scattered Compton gamma rays in the display crystal. With the channel in the 900-kev region the photo peak of a gamma ray of 1.44 Mev was observed to be in coincidence. When the channel was set for pulses greater than 1.3 Mev a photopeak of about 0.9 Mev was found. From the calibration of the gray wedge the 1.44–0.9 Mev coincidence intensity was estimated to be 2 ± 1 percent as strong as the 1.78–0.57 Mev coincidence intensity.

The above experiments were repeated using a geometry improved so as to further reduce back-scattering addition effects. Also in order to obtain more quantitative results the coincidence spectra were recorded with a 20-channel pulse-height analyzer. These data are illustrated in Figs. 4 and 5. Gamma rays of 1.44 and 0.90 ± 0.02 Mev were observed, and their coincidence intensities after corrections for efficiencies were found to be slightly greater than 2 percent of the 1.78–0.57 Mev coincidence intensity. In some of the experiments a Bi^{207} source was used which had been prepared in December, 1952 at the Nobel Institute of Physics. Inasmuch as this source displayed the 1.44–0.90 Mev cascade with the same relative intensity as in sources from the Oak Ridge bombardment, it is plausible to assume that the results do not arise from impurities and that the 1.44–0.90 Mev cascade actually belongs to Bi^{207}. On the basis of the singles and coincidence

[19] Rose, Goertzel, Spinrad, Harr, and Strong, Phys. Rev. **83**, 79 (1951).

[20] Bernstein, Chase, and Schardt, Rev. Sci. Instr. **24**, 437 (1953); R. L. Chase, Brookhaven National Laboratory Report 263 (1954) (unpublished); A. W. Schardt, Brookhaven National Laboratory Report 237 (1954) (unpublished).

data, we adopt for the 1.44-Mev gamma ray an intensity 2.0±0.6 percent of the 1.78-Mev transition intensity, or 0.16 percent per disintegration.

The capture process to the 2.35-Mev level was studied by observing the x-ray spectrum in coincidence with the (1.78+0.57)-Mev photo sum peak, thereby avoiding all x-rays associated with internal conversion. For detection of the x-rays a NaI crystal 2 mm thick and 1 inch square was used. It was necessary to channel the gamma-ray counter on the 2.35-Mev full-energy peak and not to include any of the sum Compton distribution since the latter has associated with it back scattered gamma rays which can be detected in coincidence by the x-ray crystal. This experiment showed that only L x-rays are in coincidence with the sum peak and that there is at most a 2 percent K x-ray coincidence intensity. If one assumes an L fluorescent yield of 0.40, the maximum number of K-shell vacancies is 1 percent of the total capture to the 2.35-Mev state.

Possible electron capture to the 0.57-Mev level of Pb^{207} was investigated by measuring the 0.57- and 1.06-Mev gamma-ray spectra in coincidence with K x-rays. Since the 1.06-Mev gamma ray follows an 0.8-sec isomeric state, the only possible K x-ray coincidences arise from internal conversion of the 0.57-Mev gamma ray. On the other hand, the 0.57-Mev state can be fed in three ways, i.e., by the 1.78- and 1.06-Mev transitions and by possible electron capture. It has already been shown that the 2.35-Mev level is formed only by L capture and furthermore that the conversion of the 1.78-Mev gamma ray is very small. Hence the feeding of the 0.57-Mev level by the 1.78-Mev transition will result in a negligible number of coincidences between K x-rays and 0.57-Mev gamma rays.

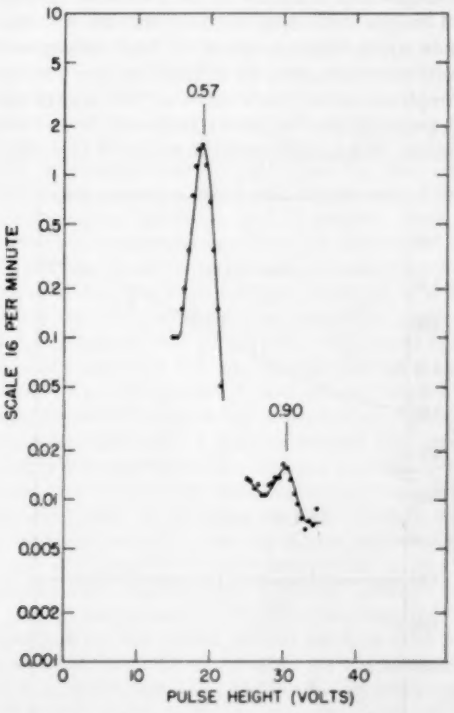

FIG. 4. Pulse-height spectrum in coincidence with a channel set for >1.3 Mev. The 0.57-Mev peak arises from coincidences with 1.78-Mev gamma rays and the 0.90-Mev peak is associated with 1.44-Mev gamma rays.

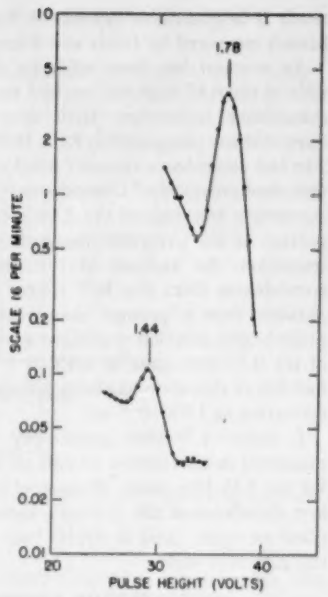

FIG. 5. Upper curve — coincidences with a channel set on 0.57 Mev. Lower curve — coincidence yield when the channel is centered at 0.90 Mev, showing a 1.44-Mev photo line.

The magnitude of the net K x-ray—0.57-Mev gamma-ray coincidence yield can be deduced from the coincidence measurements listed in Table I. In deducing the net K x-ray—0.57-Mev gamma-ray coincidence yield, a small correction has to be made for the difference between the Compton distribution under the photopeak from that measured just above the photopeak. A similar set of experiments involving K x-rays and the 1.06-Mev photopeak gives the net K x-ray—1.06-Mev gamma-ray coincidence yield. The ratio of 570-kev to 1.06-Mev photopeak yields within the channels is measured in the same experiment and must be corrected for the Bi^{207} decays branching to the 2.35-Mev state. From the above measurements the K-branch to the 0.57-Mev state may be derived. We find the K-branch to be 5±2 percent per disintegration. This

TABLE I. Channel settings for deriving the net K x-ray 0.57-Mev gamma-ray coincidence intensity.

Channel 1	Channel 2
K x-ray	0.57-Mev photopeak
K x-ray	just above 0.57-Mev photopeak
just above K x-ray	0.57-Mev photopeak
just above K x-ray	just above 0.57-Mev photopeak

result is in reasonable agreement with the 2.8 percent branch measured by Lazar and Klema.[21]

An attempt has been made to determine the lifetime of the 0.57-Mev first excited state of Pb^{207} by fast coincidence techniques. Both detectors consisted of *trans*-stilbene phosphors on RCA 5819 photomultipliers. The fast coincidence system ($2\tau \simeq 3\times10^{-9}$ sec) has been described previously.[22] Coincidences were taken between conversion electrons of the 1.06-Mev transition and a portion of the Compton distribution of the 0.57-Mev transition. An analysis of the time distribution of coincidences from the Bi^{207} source compared to that obtained from a "prompt" source taken under identical pulse-height selection conditions shows that the half-life of the 0.57-Mev state is $<4\times10^{-10}$ sec. Recently, the half-life of this state has been deduced[23] from Coulomb excitation as 1.0×10^{-10} sec.

L x-ray—1.78-Mev gamma-ray coincidences were measured in an attempt to find an observable lifetime for the 2.35-Mev state. Because of the low energy and low abundance of the *L* x-rays, it was only possible to place an upper limit of 3×10^{-8} sec on the half-life of the 2.35-Mev state.

PHOTONEUTRON EXPERIMENTS

In order to place a limit on the intensity of energetic gamma rays in the Bi^{207} decay lower than that obtained from the scintillation spectrum, photoneutron measurements have been made. The detector[24] consisted of four BF_3 counters immersed in a large box of paraffin (approximately 15 cu ft) having a central cavity into which a source could be inserted and surrounded with either Be blocks or heavy water.

With 1 mC of Bi^{207} surrounded by 9.7 kg of Be, the yield resulting from the 1.78-Mev gamma ray was 4000 counts per minute. The Be photoneutron cross section at this energy is 9×10^{-28} cm^2 according[25] to Guth and Mullin and at 2.35 Mev, the energy of the possible crossover transition, the deuterium photoneutron cross section has nearly the same value.[26] Thus the absolute detection efficiency need not be known if it is assumed that the geometries and absorption effects are the same using Be or D_2O and that the efficiency for detecting 100-kev neutrons from Be+1.78 Mev is the same as that for detecting 60-kev neutrons from D+2.35 Mev. The yields then depend only on the relative numbers of Be or D atoms present and on the relative gamma-ray intensities.

With 4 liters of D_2O surrounding the source, there was no net photoneutron yield greater than the statistical error of the background (±0.5 counts per min). If the maximum possible yield is taken to be twice the background statistical error and if the Be+1.78-Mev yield is used as a reference, then the intensity of a possible 2.35-Mev gamma ray is $<7\times10^{-4}$ of the 1.78-Mev gamma-ray intensity or $<6\times10^{-5}$ per disintegration. This figure is about 10 times lower than the limit obtained from the scintillation spectrometer measurements.

ANGULAR CORRELATION MEASUREMENTS

The gamma-gamma directional correlations of the 1.06–0.57 Mev and 1.78–0.57 Mev cascades were investigated, with the results shown in Fig. 6. For these measurements the channel windows were set to include the full-energy peaks detected by 2 in.×2 in. NaI phosphors. Similar distributions were obtained for two sources. The first source contained 50 μC of Bi^{207} and consisted of $BiSO_4$ in dilute H_2SO_4 held in a Lucite cup of 2.5-mm inside diameter and 5-mm height. The second source was 36 μC in strength and was an electroplated deposit 1 cm in diameter on a 10 mg/cm^2 Cu backing. The 1.06–0.57 Mev correlation shows a positive anisotropy of about 36 percent in agreement with the results[6] of McGowan and Campbell. The 1.78–0.57 Mev correlation is isotropic to within 5 percent.

A rough check was made on the correlation between the 1.06-Mev conversion electrons and the 0.57-Mev gamma ray by replacing one of the NaI counters with an anthracene beta detector and making runs with the electroplated source. Data taken at 180 degrees and 90 degrees indicated a positive anisotropy in excess of 30 percent, in agreement with the results[6] of McGowan.

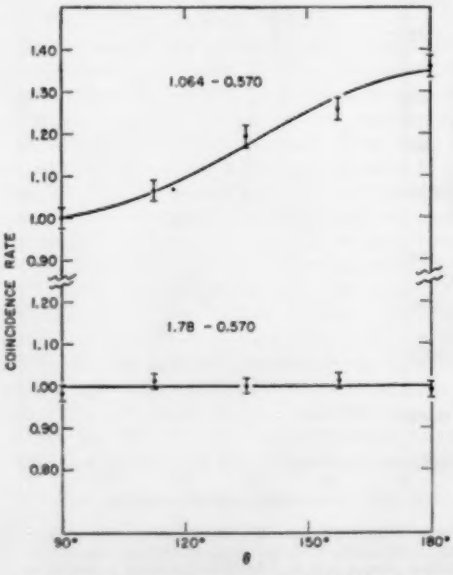

FIG. 6. Bi^{207} gamma-gamma angular correlation results.

[21] N. H. Lazar and E. D. Klema, Bull. Am. Phys. Soc. **30**, No. 1, 47 (1955) and private communication.
[22] A. W. Sunyar, Phys. Rev. **93**, 1122 (1954).
[23] P. H. Stelson and F. K. McGowan, Phys. Rev. **99**, 112 (1955).
[24] E. der Mateosian and M. Goldhaber, Phys. Rev. **78**, 326 (1950).
[25] E. Guth and C. J. Mullin, Phys. Rev. **76**, 234 (1949).
[26] A. Wattenburg, National Research Council Preliminary Report No. 6 July, 1949 (unpublished).

DISCUSSION

All of the results presented in the foregoing are consistent with the level diagram given in Fig. 7. While many features of the Pb^{207} levels up to and including the $i_{13/2}$ state at 1.63 Mev had already been established by previous research, these experiments have shown that the 0.90- and 2.35-Mev levels are excited in Bi^{207} decay.

The state at 2.35 Mev is not likely to have a spin of $\leq 5/2$ as can be seen from the following observations:

(1) The small upper limit on the intensity of a 2.35-Mev transition to the $p_{1/2}$ ground state as found in the photoneutron experiments.

(2) The low intensity of the 1.44-Mev transition to the $p_{3/2}$ level at 0.90 Mev.

(3) The comparable intensities of electron capture branching to the states at 2.35 Mev and 0.57 Mev (spin $5/2-$) in spite of the very great difference in available energy.

The measured conversion coefficient for the 1.78-Mev transition limits the spin change involved in the transition to ≤ 2. Hence the spin of the 2.35-Mev state cannot be greater than 9/2.

Agreement of the 1.06–0.57 Mev electron-gamma angular correlation with the theoretical correlation shows that there are no disturbing effects in our sources as suggested earlier[27] resulting from the filling of electron shells following either electron capture or internal conversion. Hence the isotropy of the 1.78–0.57-Mev gamma-gamma correlation can be considered as real. If the 2.35-Mev state were $h_{9/2}$ the 1.78-Mev transition must necessarily be an $E2+M3$ transition, since a pure quadrupole transition would lead to a correlation showing a positive anisotropy of 16.7 percent. From the theoretical correlation functions[28] of Biedenharn and Rose it can be shown that for the $h_{9/2}$ assignment one can achieve approximate isotropy and at the same time satisfy the 1.78-Mev gamma-ray conversion coefficient with a mixture of $\sim$97 percent $E2+\sim$3 percent $M3$.

In the case of a 7/2 spin for the 2.35-Mev state, a mixture of $\sim$94 percent $E2$ and $\sim$6 percent $M1$ is a compatible with both the conversion and angular correlation measurements. A decision between the possible shell model assignments $f_{7/2}$ and $h_{9/2}$ to the 2.35-Mev state cannot be made from our angular correlation measurements. On the basis of more accurate correlation measurements, Lazar and Klema have assigned[21] a spin of $h_{9/2}$ to the 2.35-Mev state, with the $E2+M3$ mixture stated above for the 1.78-Mev transition.

An $h_{9/2}$ assignment would mean that the 1.44-Mev transition to the second excited state at 0.90 Mev must be at least $M3$, if the latter state is assumed to be $p_{3/2}$. In this case, the 1.44-Mev K-conversion coefficient would be 2.7×10^{-3} for pure $M3$ radiation. Our value of $(5\pm2)\times10^{-3}$ for the K-conversion coefficient of this transition is lower than that of a pure $M3$ by a factor of 5. No $E4$ admixture can lower the K-conversion coefficient below $\sim$1 percent. We feel that this argues most strongly against an $h_{9/2}$ assignment. In the event that the K-1.44 line of Fig. 2 were actually a ghost, the real conversion coefficient would be even lower and the discrepancy with $M3$ or $M3+E4$ would be still greater. An assignment of $h_{9/2}$ to the 2.35-Mev state implies a lower limit for the lifetime of $M3$ radiation from this state, if one considers the transition within the framework of the single-particle model. Our value of 3×10^{-8} sec as the upper limit of the lifetime of the 2.35-Mev state is not by itself short enough to rule out the $h_{9/2}$ assignment.

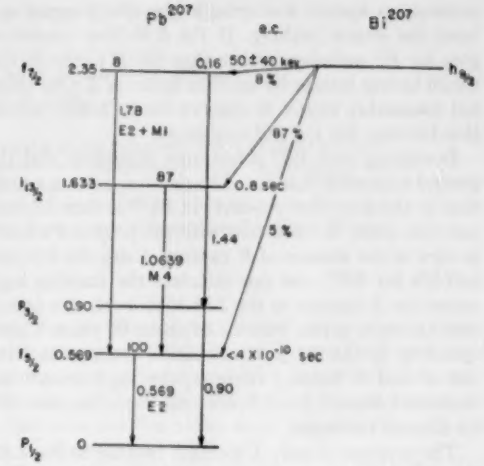

FIG. 7. Proposed decay scheme of Bi^{207}. Branching and transition intensities are adopted as being the most probable from several sets of data.

On the other hand, an assignment of $f_{7/2}$ to the 2.35-Mev state fits all of our observations. The measured 1.44-Mev K-conversion coefficient is consistent with $E2$ radiation to the $p_{3/2}$ state. When the E^5 energy dependence is removed from the transition intensity ratio, the ratio of 1.44-Mev to 1.78-Mev $E2$ matrix elements is about 1/20 which may not be unreasonable. Prescott's observation[7] of a weak gamma ray of 1.46 Mev in coincidence with K x-rays is not compatible with the scheme proposed here since it has been found that the 2.35-Mev state is formed by L capture only. The only coincident K x-rays in this case would then arise from internal conversion of the 0.90-Mev transition and this coincidence effect would be 100 times smaller than the 1.78 K x-ray coincidence intensity.

If the 0.90-Mev gamma ray is an $M1$ transition, its K line would have an intensity 1/1500 of K-1.06 or just below the limit placed by the data. This line might become observable with a strong source and greater

[27] D. E. Alburger and A. W. Sunyar, Phys. Rev. **98**, 276(A) (1955).
[28] L. C. Biedenharn and M. E. Rose, Revs. Modern Phys. **25**, 729 (1953).

precautions against scattering in the spectrometer and from the source backing. If the 0.90-Mev transition goes by $E2$ radiation rather than by $M1$, the K line would be less intense by another factor of 4. One could not reasonably expect to observe the 0.72-Mev transition between the $f_{7/2}$ and $i_{13/2}$ states.

In analogy with Bi^{209} it has been suggested[2] that the ground state of Bi^{207} is $h_{9/2}$. The electron capture transition to the 2.35-Mev $f_{7/2}$ level of Pb^{207} is then allowed and this could be consistent with the proposed scheme in view of the absence of K capture. Using the 8.0-year half-life for Bi^{207}, one can calculate the limiting logft values for L capture to the 2.35-Mev level, this transition having a partial half-life of about 90 years. Corresponding to the range of transition energies between the K and L binding energies, the logft value[29] lies between 5.6 and 7.8 and hence could be consistent with an allowed transition.

The presence of only L electron capture to the 2.35-Mev level leads to a value of 2.40±0.04 Mev for the total decay energy of Bi^{207}. The error implies allowable limits and the value 2.40 Mev is not necessarily the most probable decay energy. If the decay energy had been as much as 10 kev above the K-capture threshold, then the K x-ray yield in coincidence with the 2.35-Mev sum photo line would be 1/10 of the L x-ray yield according to the formula of Marshak[30] and this would have been easily observable.

Logft values may also be calculated for the main capture branch to the 1.633-Mev level and for capture to the 0.57-Mev level based on the level scheme of Fig. 7. If one uses the graphs[31] of Moszkowski, the main branch has a logft of 9.6 while the branch to the 0.57-Mev level has a logft of 11.5. These values are consistent with first and second forbidden transitions respectively as would be expected from the level assignments.

The reasonably firm assignment of $f_{7/2}$ to the 2.35-Mev level in Pb^{207} requires a reconsideration of the predicted levels in Pb^{206}. $h_{9/2}$ was assumed for the 2.35-Mev level in making these calculations. According to a private communication from M. H. L. Pryce, the only serious effect of this change is to remove the predicted 5+ level at 3124.7 kev (see Figs. 7 and 8 in reference 1), a level which was already considered as doubtful. In place of this, a 3+ level at approximately this energy is expected but it is not likely that the 739.9-kev transition or the doubtful 107.2-kev transition could be associated with it. Hence the positions of these two transitions in the Pb^{206} scheme are now uncertain. Other Pb^{206} configurations affected are numbers 11 and 12 in Table IX of reference 1 but the energies of these are so high that they are not relevant to the interpretation of the gamma-ray spectrum.

The lifetime[32] of 1.0×10^{-10} sec for the 0.57-Mev $E2$ transition is much shorter than could be expected on the single particle model for an $E2$ transition involving a neutron jump and is close to that expected for a single proton transition with unit matrix element. The transition follows the general trend[32] exhibited by $E2$'s in this region of the periodic table, most of which show a speed-up which can be interpreted in terms of collective effects.

We are indebted to J. Hudis and E. Baker for chemical preparation of the Bi^{207} electroplating solution and to J. Hudis for separation of the Y^{88} sample. We also wish to thank M. Goldhaber for helpful discussions and suggestions.

Note added in proof.—The internal conversion spectrum of Bi^{207} has been reinvestigated at 2.0 percent resolution using an intermediate-image beta spectrometer recently constructed at Brookhaven and a 15-μC source deposited on 0.5 mg/cm² Nylon. A line, which we believe is real, has been observed corresponding to K conversion of a 0.894±0.007 Mev transition. Its intensity is 0.0039 K electrons per 100 disintegrations (1/2100 as strong as K-1.06). The K-conversion coefficient based on this observation and on the gamma-ray measurements is $(2.4\pm1)\times10^{-3}$ suggesting $M1$ radiation (theoretical $\alpha_K=2.8\times10^{-3}$) with possible admixture of $E2$ radiation ($\alpha_K=6.9\times10^{-3}$).

The 1.44-Mev K-conversion line has been observed again and its intensity has been found to be 4.8±1 percent as strong as K-1.78 in agreement with previous measurements. The $K/(L+M)$ ratio of the 1.78-Mev transition is 4.4±0.4. Improved values for the two highest energy gamma rays are 1.43±0.01 Mev and 1.771±0.005 Mev corresponding to a most probable energy of 2.338±0.005 Mev for the Pb^{207} level.

An upper limit of 0.0015 electron per 100 disintegrations has been placed on the K-conversion line of a possible 0.324-Mev $M1$ transition between the 0.894- and 0.570-Mev states. If this transition were not l forbidden its K line might have been expected to have approximately the same intensity as K-0.894.

Upper limits of 0.002 electron per 100 disintegrations have been placed on the K-conversion lines of either a possible 0.704-Mev transition between the 2.338- and 1.634-Mev levels or a possible 0.740-Mev transition between the 1.634- and 0.894-Mev levels. If the 2.338-Mev state were $h_{9/2}$, one can calculate on the basis of single-particle estimates that a 0.704-Mev $M2$ would win out over a 1.43-Mev $M3$ by a factor of ~500. Their relative K-conversion intensities would then be in the ratio of ~2000 in favor of the 0.704-Mev line whereas our upper limit is a factor of 2. We could not rule out the $h_{9/2}$ assignment to the 2.338-Mev level from conversion intensities if the 1.43-Mev transition were predominantly $E4$. However, in that case the lifetime of the 2.338-Mev level would probably be $>10^{-9}$ sec as compared with our upper limit of 3×10^{-9} sec. These new results further confirm the $f_{7/2}$ assignment to the 2.338-Mev level.

A measurement of the half-life of Bi^{207} is now in progress by G. Harbottle of this Laboratory. Using a balanced double ion chamber standardized with radium he has obtained a preliminary value of 27±3 years for Bi^{207} based on data taken over a three-month period

[29] The authors are indebted to Dr. M. E. Rose for making these calculations.
[30] R. E. Marshak, Phys. Rev. **61**, 431 (1942).
[31] S. A. Moszkowski, Phys. Rev. **82**, 35 (1951).
[32] A. W. Sunyar, Phys. Rev. **98**, 653 (1955).

Energies of the Radiations from Co^{57} and Co^{58}†

J. M. Cork, M. K. Brice, and L. C. Schmid
Department of Physics, University of Michigan, Ann Arbor, Michigan

(Received March 28, 1955)

Using magnetic and scintillation spectrometers the energies of the radiations from Co^{57} and Co^{58} have been evaluated. Several gamma rays not previously reported have been observed. Co^{57} decays mainly by K capture but also to a slight extent by positron emission with an upper energy limit of about 300 kev, followed by gamma rays with energies 14.6, 29, 99.8, 122.8, 137.4, and 700 kev. Co^{58} decays by K capture and with positron emission of upper energy 485 ± 10 kev. Gamma rays with energies of 814 and 500 and possibly 1300 kev accompany the decay.

As early as 1937 it was found[1] that iron bombarded with deuterons in the cyclotron yielded several long-lived cobalt radioactivities. Subsequent investigations[2] resulted in the assignment of activities with half-lives of 270 and 72 days to Co^{57} and Co^{58}, respectively. The reports on the energies of the radiations show considerable disagreement indicating a need for further study.

In the present investigation magnetic photographic, and scintillation spectrometers were employed to study gamma rays, and the double-focusing, magnetic spectrometer was used to observe the positron spectrum of Co^{58}. In addition to the gamma energies previously recorded certain gamma transitions not previously reported are observed. The Co^{57} source was obtained from the Oak Ridge National Laboratory and was produced by a $p,2n$ reaction on Ni^{58} in a target of ordinary nickel. The resulting Cu^{57} in turn decays by positron emission through Ni^{57} to Co^{57} and thence to Fe^{57}. The Co^{58} specimen was from the same source but produced in the reactor by the (n,p) reaction on Ni^{58}. It decays mainly by K capture but also by weak positron emission to Fe^{58}.

COBALT-57

Some of the previously reported energies for the three well-known gamma rays, together with the results of the present investigation, are shown in Table I. In addition to these three gamma rays, others appear with energies of 700, 99.8, and 29 kev. These additional gamma rays are observed with the scintillation spectrometer. Of them, only the 99.8-kev gamma appears by conversion and this with a single line assumed to be due to Fe K-electrons.

For the three gamma rays shown in Table I, many electron lines are observed whose energies and relative intensities are shown in Table II. The relative intensities for the lines due to the 14.6-kev gamma ray are from visual estimates of the photographic densities, corrected for variation in radius and sensitivity of the emulsion with energy. The intensities for the other two gamma rays were obtained both by microphotometer traces of the photographic plates and by comparing the resolved peaks obtained with the source in the double-focusing spectrometer. The 14.6-kev in Fe^{57} has been reported[3] to have a half-life of 1.1×10^{-7} sec and the transition to the ground state was assumed[4] to be $M1$. The Z^2/W for this radiation is 46.2. From the empirical summary of Goldhaber and Sunyar, the observed K/L ratio of 3 appears to be somewhat lower than expected for an $M1$ transition. It would seem to be more compatible with an $E1$ or an $M2$ transition. The lifetime for the $M2$ transition at this energy would be of the order of seconds and this designation is thus improbable.

The large values of the K/L ratios for the 122.8- and 137.4-kev gamma rays suggest $E1$, $E2$, $M1$, or $M2$ transitions. The half-life of the $M2$ transition would

Table I. Gamma energies of Co^{57} as reported, in kev.

Observer	P[a]	ED[b]	DW[c]	AG[d]	CM[e]	Present work
γ_1	117	119		122.8	119	122.8
γ_2	130	131		137.6	133	137.4
γ_3			14			14.6

[a] E. H. Plesset, Phys. Rev. **62**, 181 (1942).
[b] E. Elliott and M. Deutsch, Phys. Rev. **64**, 321 (1943).
[c] M. Deutsch and W. Wright, Phys. Rev. **77**, 139 (1950).
[d] D. Alburger and M. Grace, Proc. Phys. Soc. (London) **A67**, 280 (1954).
[e] B. Craseman and D. Manley, Phys. Rev. **98**, 279 (A) (1955).

Table II. Energy and relative intensity of electron conversion lines from Co^{57}.

Designation	Electron energy, kev	Relative intensity	Energy sum, kev
K_1	7.3	3	14.4
L_1	13.7	1	14.6
M_1	14.5	0.25	14.6
K	92.7		99.8
K_2	115.7	10	122.8
L_2	121.8	0.9	122.7
M_2	122.7	0.15	122.8
K_3	130.3	8	137.4
L_3	136.6	0.8	137.5

† This investigation received the joint support of the U. S. Atomic Energy Commission and the Office of Naval Research.
[1] Livingood, Seaborg, and Fairbrother, Phys. Rev. **52**, 135 (1937).
[2] Hollander, Perlman, and Seaborg, "Table of Isotopes," Berkeley (1952).
[3] M. Deutsch and W. Wright, Phys. Rev. **77**, 139 (1950).
[4] M. Goldhaber and A. Sunyar, Phys. Rev. **83**, 906 (1951).

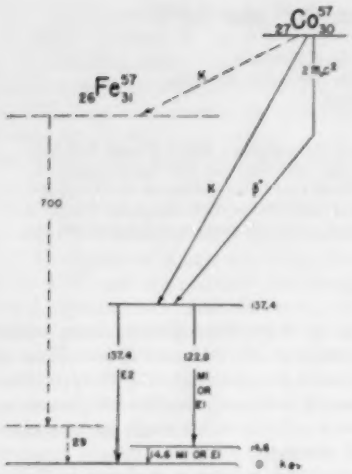

FIG. 1. Nuclear level scheme for Fe^{57}.

still be of the order of a thousandth of a second and hence should probably be excluded. While the K-conversion lines for the two gamma rays are of the same order of darkness and their K/L ratios are about the same, it is observed that the unconverted peak at 122.8 kev is many times[5] stronger than the peak at 137.4 kev. Hence, if the absolute conversion coefficient for the 137-kev gamma ray is ten times that for the 123-kev gamma ray, then the former is probably due to an $E2$ and the latter to an $E1$ or $M1$ transition. The positron spectrum was found to be extremely weak, with an upper limit of about 300 kev. It was not resolved into the two components reported.[6]

The 29-kev peak was found to be in coincidence with both the 100- and 700-kev radiations but not with the 123- or 137-kev gammas. No coincidences could be observed between the 700- and the 100-, 123-, or 137-kev radiations. It should be noted that coincidences as observed might result from the iodine x-ray (28 kev) escaping from one crystal back to the opposite crystal, resulting in an apparent peak due to the true peak energy minus the x-ray energy. Evidence that the low-energy peak is a gamma ray comes from the fact that it appears in the "singles" curve when there is no idoine or other scatterer back of the source. When iodine is intentionally placed directly back of the source the peak shifts slightly toward lower energy. Moreover, the 100-kev gamma ray yields a conversion line. The weak 700-kev transition probably follows K capture, and from the coincidence observation it might be concluded that it terminates at a level other than the ground state although this evidence is not incontrovertible. The escape peak is less likely to be significant at this high energy. The well-established transitions are shown as heavy lines in the nuclear level scheme of Fig. 1. The 99.8-kev transition is not included.

The half-life of the Co^{57} sample observed over a period of 8 months appears to be 267 days.

COBALT-58

Co^{58} decays by both K capture and positron emission to Fe^{58}. A single gamma ray of energy 0.81 Mev had been reported.[2] In the present investigation this gamma ray is observed both by electron conversion and by the scintillation spectrometer. The K-conversion line has an energy of 807 kev, indicating a gamma energy of 814 kev. The L line is very weak so that the K/L ratio is exceedingly large. It is impossible to infer from this ratio the type of multipole radiation, since at this small Z^2/W (0.8), the K/L ratio is large for all types of radiation. However, the ground state for the even-even $_{26}Fe^{58}$ nucleus is undoubtedly a level of even parity and zero spin. In such nuclei the first excited state is usually one of even parity and spin 2, so that an $E2$ transition is expected.

The Co^{58} source also contains some Co^{60} with its long-lived radiation at 1.17 and 1.33 Mev. With the scintillation spectrometer, strong peaks are obtained at 500 and 800 kev, and a weaker peak at 1.3 Mev. The 500-kev peak was at first assumed to be annihilation radiation. On observing coincidences between all betas in an anthracene crystal, and the gamma distribution in a NaI crystal, the 500- and 800-kev peaks were present in about the same relative intensity. On observing gamma-gamma coincidences with one crystal

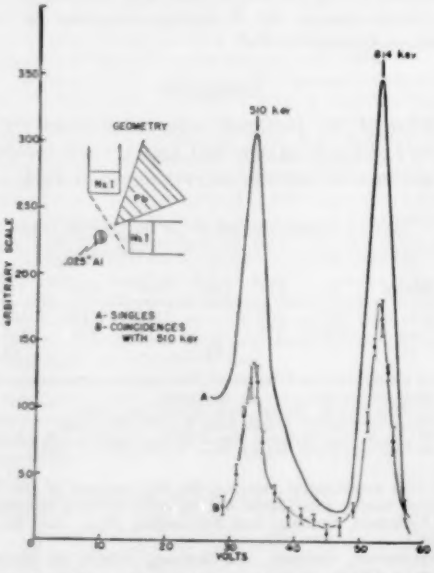

FIG. 2. Coincidence data for Co^{58}, with crystals at right angles.

[5] D. Alburger and M. Grace, Proc. Phys. Soc. (London) **A67**, 280 (1954).

[6] B. Craseman and D. Manley, Phys. Rev. **98**, 279 (1955).

set to receive the 500-kev peak, again the other crystal noted the two peaks in the same relative intensity. Since the annihilation photons travel in opposite directions and could yield 500–500 kev coincidences, the crystals were arranged at right angles with the source as shown in Fig. 2. The singles and coincidence curves are represented by solid and dotted lines, respectively, strongly indicating the existence of a gamma ray of about 500-kev energy. The peak at 1.3 Mev could be a summation peak for the other gamma rays or represent a crossover transition, or be in part due to the slight amount of Co^{60} that is known to be present. On inserting about 2 cm of lead between source and crystal the intensity is reduced much more than would be the case if it were all 1.3-Mev radiation, with its absorption coefficient of 0.66 cm^{-1}. This indicates that it is largely

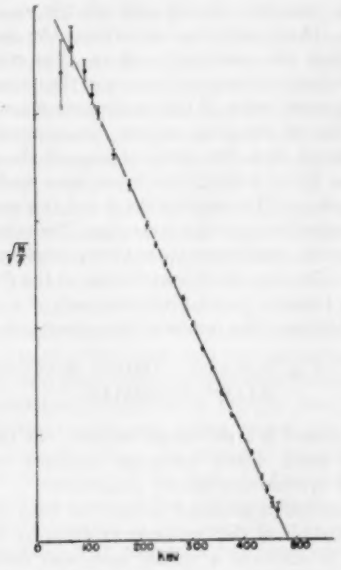

FIG. 3. The Fermi plot for the positron spectrum of Co^{58}.

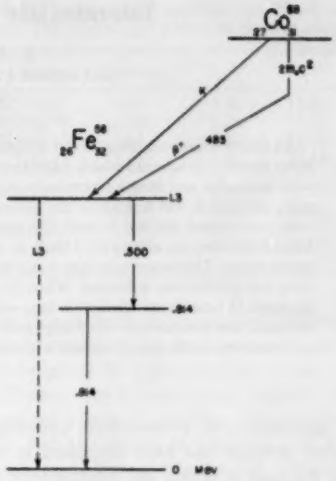

FIG. 4. Nuclear level scheme for Fe^{58}.

a summation peak, but in part it may be due to a cross-over transition.

The positron spectrum was investigated in the double-focusing spectrometer and was found to have only one component. The almost massless source consisted of a line of the carrier-free material ruled on a conducting zapon film. The spectrometer window, also of zapon, was of minimum thickness (about 15 micrograms per cm^2) to withstand a pressure difference of 6 or 7 cm of Hg. The linearity of the Fermi plot, shown in Fig. 3, down to very low energies, indicates the very small stopping power of the film. The upper energy limit is 485 ± 10 kev. If the positron decay occurs for about 15 percent of the decays, then the log ft value is about 6.5, which indicates a first forbidden transition. The simple decay scheme is shown in Fig. 4. The half-life of the Co^{58} source corrected for the presence of a slight amount of longer-lived activity is found to be 71.0 days.

Intermediate Coupling in Odd-Odd Nuclei

R. ADKINS AND J. G. BRENNAN
The Catholic University of America, Washington, D. C.
(Received March 10, 1955)

An intermediate-coupling model is applied to the structure of lithium-6 and nitrogen-14. A ground-state wave function is selected which reproduces the observed ground-state moment data. A two-body potential, with spin-orbit and tensor forces included, is sought which will have the proper wave function as its lowest state and which will reproduce the observed level splitting of the lower excited states of the nucleus. The usual variational method is used, the potential is assumed to have a Yukawa radial dependence, and the wave functions are assumed to have an harmonic oscillator radial dependence. Only the p-shell nucleons are included. This procedure leads to a consistent, but not unique, result for lithium requiring a strong tensor force for satisfactory solutions. When the additional requirement of the near vanishing of the carbon-14–nitrogen-14 beta-decay element is imposed, and the procedure repeated for the nitrogen nucleus, the results are much less satisfactory. Very large and physically unmeaningful values of the potential parameters appear to be needed to obtain agreement with experimental data.

THE application of intermediate coupling to the p-shell polyads has been discussed in detail by Inglis[1] for the case in which the internucleon potential is central. Elliott[2] and Regge[3] have investigated intermediate coupling in lithium-6 for the case in which a small amount of tensor force is included in the internucleon potential. Their results indicate that in this case one cannot simultaneously produce the energy level scheme and the ground-state data. Jancovici and Talmi[4] have shown that a very strong tensor force can account for the observed carbon-14–nitrogen-14 beta decay. The present investigation shows that an internucleon potential with a strong tensor force provides a reasonably consistent scheme for describing lithium-6, within the scope of the intermediate coupling model with configuration mixing neglected.

The approach usually followed in applying the model is to start from a specific two-body potential and to obtain from it the level structure and the ground-state wave function. This investigation has proceeded in the reverse order. A wave function is obtained from the ground-state data. A potential is then sought which will produce this wave function for its lowest state, and which will also give the low-lying level structure for lithium-6.

A. LITHIUM

The ground state of lithium-6 is a $J=1$, even parity state with a magnetic moment of 0.822 nm and a static electric quadrupole moment less than $\frac{1}{2}$ millibarn in absolute value. The sign of the quadrupole moment is uncertain. The most general wave function which can be formed for this state from the p nucleons is

$$\Psi = a\,{}^3S_1 + b\,{}^3D_1 + c\,{}^1P_1. \tag{1}$$

Three conditions including normalization are available to fix the coefficients: the wave function must reproduce the static magnetic dipole and electric quadrupole moments. These conditions determine the limits between which the coefficients will lie. The coefficients are not uniquely determined because of the uncertainties in the observed value of the quadrupole moment, and in the value of the mean square displacement of the p-shell proton from the center-of-mass of the nucleus. The value $\frac{3}{4}(1.42\times10^{-13}A^{\frac{1}{3}}\text{ cm})^2$ has been used for the latter quantity. This requires the S and D states of the wave function to have the same sign. The calculations show that the coefficients are not very sensitive to this quantity. The sign of the contribution of the P state to the wave function is not fixed since only c^2 appears in these conditions. The results of the calculations are

$$0.8515 \leqslant |a|^2 \leqslant 0.8557; \quad 0.0030 \leqslant |b|^2 \leqslant 0.0113; \quad 0.1330 \leqslant |c|^2 \leqslant 0.1455. \tag{2}$$

Since lithium-6 is a self-mirror nucleus, one can argue that the usual meson exchange magnetic moments which are symmetrical cannot contribute.[5]

The potential is assumed to have the form suggested by the analysis of the two-body problem by Hall and Powell.[6] In addition, a specific spin-orbit force is assumed in which the spin-other-orbit forces are neglected. Thus,

$$V_{np} = -V_0\left[(1-g+gP^\sigma)\frac{e^{-r/\alpha_c}}{r/\alpha_c} + \gamma\frac{e^{-r/\alpha_t}}{r/\alpha_t}S_{np}\right] \times (1-\epsilon+\epsilon P^\sigma) - V_{0\zeta}\sum_i \mathbf{l}_i\cdot\mathbf{s}_i, \tag{3}$$

where ζ and γ are dimensionless parameters for the spin-orbit coupling and for the tensor coupling respectively, g and ϵ are the fractions of spin exchange and space exchange, respectively, α_c and α_t are the central and tensor ranges respectively, and V_0 is the depth of the potential. P^r is the Majorana space exchange operator and P^σ is the spin exchange operator.

[1] D. R. Inglis, Phys. Rev. **87**, 915 (1952); Revs. Modern Phys. **25**, 390 (1953).
[2] J. P. Elliott, Proc. Roy. Soc. (London) **A218**, 345 (1953).
[3] T. Regge, Nuovo cimento **11**, 285, (1954).
[4] B. Jancovici and I. Talmi, Phys. Rev. **95**, 289 (1954).
[5] R. G. Sachs, *Nuclear Theory* (Addison-Wesley Press, Cambridge, 1953).
[6] H. H. Hall and J. L. Powell, Phys. Rev. **90**, 912 (1953).

A standard variation method is used, in which the coefficients of the L-S states of the wave function are used as variation parameters. This method gives the usual sets of secular equations and determinants. The matrix elements for the spin-orbit force are given by Condon and Shortely.[7] The matrix elements for the internucleon potential can be evaluated by methods given by Talmi[8] or Elliott.[2]

Only one $J=3$ state can be formed from the two p nucleons, hence the matrix of this state has only one element and the energy is given in terms of the parameters of the potential. This energy is then combined with the observed splitting between the $J=3$ state and the other levels of the nucleus to eliminate the eigenvalues from the remaining matrices. The matrices then become relations among the potential parameters. The secular equations for the ground state become a set of equations in the potential parameters, when the coefficients Eq. (2) are used in place of the variation parameters. These relations have been numerically solved for the case when the central potential has a range of 1.18×10^{-13} cm.

It is possible to match the observed splitting between the $J=3$ state and the ground state only when the P state has the same sign as the S and D states. For the parameters used in this calculation, it is possible to retain the form of the Hall and Powell potential only when the potential is a Serber type, if the observed level splitting between the ground state and the $J=0$ state is to be matched. The requirement to maintain the form of the Hall and Powell potential is not a rigid one, and hence calculations have been performed also for a potential having the same exchange properties as the Christian and Hart[9] potential but with the addition of a spin-orbit force exactly as in Eq. (3). This potential has a Serber central part and a tensor part with 63 percent space exchange. The results of the calculations are given in Table I for the Hall and Powell form, and in Table II for the Christian and Hart form.

The electromagnetic transitions within lithium-6 have been examined with the wave functions which result from these potentials. Qualitative agreement with the results of Day and Walker,[10] that the $M1$ transition from the $J=0$ state to ground is overwhelming in comparison with the $E2$ transition from the $J=3$ state to ground, is obtained. The ft value for the helium-6–lithium-6 beta decay has also been calculated with these wave functions. The Christian and Hart form of the potential gives $\log ft=2.99$ in reasonable agreement with the observed $\log ft=2.94\pm0.04$. The value of the $\log ft$ for the Hall and Powell form of the potential is somewhat higher.

These calculations show that the intermediate-coupling model of the nucleus can provide a consistent, but not unique, scheme for describing lithium-6 if the interaction potential has a strong tensor contribution. It should be noted that the position of the $J=2$ level is unsatisfactory for its calculated position, is always lower than its observed position. This tendency is in agreement with the results of Jancovici and Talmi, and Regge, and probably is due to the neglect of configuration interaction.

TABLE I. Parameters of the modified Hall-Powell potential for lithium. The symbols are defined in the text after Eq. (3).

	V_0(Mev)	a_0(10^{-13} cm)	ξ	γ	δ
$a^2=0.8515$	71.35	1.18	−9.80	11.92	0.28
$b^2=0.0030$	43.98	1.355	−6.04	11.72	0.38
$c=0.3815$	25.13	1.53	−3.47	16.62	0.45
	13.24	1.705	−1.83	23.12	0.73
$a^2=0.8557$	44.18	1.18	−6.41	17.29	0.37
$b^2=0.0113$	26.01	1.355	−3.80	18.22	0.58
$c=0.3647$	13.26	1.53	−1.97	24.25	1.25
	4.80	1.705	−0.76	49.09	1.23

B. NITROGEN-14

Since nitrogen-14 has a neutron and a proton hole in the p shell, it may be treated in a manner quite similar to that used for lithium-6. However the sign of the spin-orbit coupling parameter and the sign of the electric quadrupole moment operator must be reversed for the p-shell holes.

One would expect that the intermediate-coupling model would be less successful in describing nitrogen, since the higher configurations should mix more strongly with the p-shell configuration in nitrogen than they apparently do in lithium-6. Certainly the presence of low-lying states of odd parity in nitrogen gives qualitative evidence of this increased importance of higher configurations. Therefore, by considering both nuclei to be described by the same two-body p-shell interaction, one may hope to obtain information about the relative importance of configuration mixing for the two nuclei.

Inglis[1] has pointed out that the strength of the spin-orbit coupling appears to increase as one goes from the beginning of the first p shell to the end beyond it. Beyond O^{16}, a fully developed j-j coupling appears to have set in. This increase in the spin-orbit force will

TABLE. II. Parameters of the modified Christian and Hart potential for lithium. The symbols are defined in the text after Eq. (3).

	V_0(Mev)	a_0(10^{-13} cm)	ξ	γ	δ
$a^2=0.8515$	71.35	1.18	−9.80	11.92	0.19
$b^2=0.0030$	43.98	1.355	−6.04	11.72	0.26
$c=0.3815$	25.13	1.53	−3.47	16.62	0.31
	13.24	1.705	−1.83	23.12	0.47
$a^2=0.8557$	44.18	1.18	−6.41	17.29	0.25
$b^2=0.0113$	26.01	1.355	−3.80	18.22	0.37
$c=0.3647$	13.26	1.53	−1.97	24.25	0.66
	4.80	1.705	−0.76	49.09	1.74

[7] E. U. Condon and G. H. Shortley, *Theory of Atomic Spectra* (Cambridge University Press, Cambridge, 1951), p. 268.
[8] I. Talmi, Helv. Phys. Acta **25**, 185 (1953); Phys. Rev. **89**, 1065 (1953).
[9] R. S. Christian and E. W. Hart, Phys. Rev. **77**, 441 (1950).
[10] R. B. Day and R. L. Walker, Phys. Rev. **85**, 582 (1952).

necessitate an increase in the tensor force also as these two forces tend to oppose each other.

As in lithium, the ground state is a positive parity, $J=1$ state, so the most general wave function that can be constructed is given by Eq. (1). Once again the Russell-Saunders components are normalized functions formed out of the single p holes. The coefficients can be determined from normalization and from the experimental value of the magnetic moment, 0.404 nm and the experimental value of the electric quadrupole moment, 0.01 barn.

The very long half-life of the carbon-14–nitrogen-14 beta decay provides additional information about the structure of the ground state and the first excited state of nitrogen-14. Upon the assumption of charge independence of forces the first excited state of nitrogen-14 is a member of the same supermultiplet as the ground state of carbon-14, and so it should have the same wave function apart from a small Coulomb effect. Since this state has $J=0$, the general wave function can be written

$$\Psi = x\,{}^1S_0 + y\,{}^3P_0. \tag{4}$$

The ft value of the beta decay between carbon and nitrogen is given by

$$ft = \frac{K}{\left|\int \sigma\right|^2} = \frac{K}{6(xa - yc/\sqrt{3})^2}, \tag{5}$$

where K is an average beta-decay coupling strength. Now the denominator of this expression must be very small to give a lifetime in agreement with experiment. For convenience, it will be set equal to zero, and the coefficients of the carbon-14 ground state and the first excited state of nitrogen-14 will be taken to be

$$x = y \cong 0.71. \tag{6}$$

This also fixes the sign of the P-state coefficient for the ground state of nitrogen-14 to be positive. Using a value of the mean square displacement of the p proton hole from the center of the nucleus of $(2.79\times10^{-13}\ \text{cm})^2$, one obtains for the coefficients of the ground-state wave function of nitrogen-14, the values

$$a=0.2872;\quad b=0.8190;\quad c=0.4974. \tag{7}$$

These values are more sensitive to the value of the mean square displacement than were the values for lithium. However, the experimental quadrupole moment is more certain for nitrogen. As has been shown by Jancovici and Talmi,[4] this choice of the carbon-14 wave function is consistent with the oxygen-14–nitrogen-14 positron decay because the Coulomb repulsion will cause a slight change in the ground state of oxygen-14.

The near vanishing of the carbon-14–nitrogen-14 beta-decay matrix element might seem to imply a near vanishing of the gamma-ray element between the first excited level of nitrogen and the ground state. Experimentally this gamma transition has been observed to to be quite strong.[11] But for an allowed beta decay as this one is,[12] there is a selection rule which prevents the orbital angular momentum from changing. The gamma transition which proceeds by magnetic dipole radiation, on the other hand, will have contributions from states differing by one unit of orbital angular momentum. Thus, when the wave functions which have been obtained above, are used to calculate the gamma transition probability for this process, one obtains a result in qualitative agreement with experiment.

One can proceed to determine the parameters of potential assumed to be of the same form as Eq. (3) by an analogous procedure to that described for lithium. One inserts the coefficients of the ground state and first excited state wave function into the matrices for the $J=1$ and $J=0$ levels. When the observed splitting between the first excited state and the ground state of nitrogen is inserted, one obtains relationships among the parameters of the potential. When these relationships are satisfied, the static moment data of the ground state of nitrogen-14, the observed splitting between the first excited state and the ground state, and the observed half-life of the beta decay will be reproduced. An auxiliary condition, that the observed splitting between the first excited $J=1$ level and the ground level be reproduced, can also be imposed.

Preliminary numerical solutions of these equations have been performed, with reasonable values for the ranges and depth of the potential. These indicate that the condition imposed from the beta-decay half-life severely limits the freedom of choice of parameters compared with the lithium situation. For reasonable values of the ranges and depth of the potential, the numerical values of the spin-orbit parameter and of the tensor parameter which have been found necessary to satisfy the relationships are so large as to make difficult any physical interpretation of the results. This tends to confirm the difficulties that Jancovici and Talmi[4] experienced in fitting the level structure.

Although the calculations performed so far have not exhausted the possibility that a reasonable solution exists, one can speculate that neglecting the interactions among the other particles in the p shell and neglecting higher configuration interactions may be entirely unjustified in nitrogen. The severe requirements imposed by observation may require a more realistic model, for even qualitative agreement.

[11] T. Lauritsen and F. Ajzenberg, Revs. Modern Phys. (to be published).

[12] Pohm, Waddell, Powers, and Jensen, Phys. Rev. **97**, 432 (1955).

Masses of Light Nuclei. A Method for Correcting a Table of Masses for New Data

J. E. DRUMMOND
Department of Scientific and Industrial Research, Wellington, New Zealand

(Received March 5, 1955)

A formula is derived for correcting a set of least-squares solutions for new data. Two examples are given to show how this method can be easily applied to correct the author's own table of masses.

ANY table of masses will become outdated by new, more accurate experimental data and will require complete recalculation when sufficient new data are available, but in the meantime it is possible to correct a table as follows.

Suppose the old and new data are in the form of a set of equations,

$$\sum_{r=1}^{n} a_{rs}x_r=y_s,$$

where the y_s are Q-values or spectroscopic doublet differences; x_r are a set of n unknown masses; a_{rs} are the scaled multiples of the masses occurring in the reactions, scaled so that all the probable errors are brought to the same magnitude; and s runs from 1 to N for an initial set of equations and $N+1$ to $N+N'$ for a new set of equations. Then the least-squares equations for the masses will be

$$\sum_{r=1}^{n} \alpha_{ir}x_r=\beta_i, \quad i=1\cdots n,$$

where

$$\alpha_{ir}=\sum_{s=1}^{N} a_{is}a_{rs}, \quad \beta_i=\sum_{s=1}^{N} a_{is}y_s.$$

When one uses the old and new data together, the new equations for masses will be

$$\sum_{i=1}^{n}(\alpha_{ir}+\alpha_{ir}')(x_r+x_r')=\beta_i+\beta_i', \quad r=1\cdots n,$$

where

$$\alpha_{ir}'=\sum_{s=N+1}^{N+N'} a_{is}a_{rs}, \quad \beta_i'=\sum_{s=N+1}^{N+N'} a_{is}y_s.$$

On multiplying these equations by A_{ji} (the element of the reciprocal matrix of α_{ji}) and summing over i, then cancelling $x_j=\sum_{i=1}^{n} A_{ji}\beta_i$, we have

$$x_j'=\sum_{i=1}^{n} A_{ji}\left[\beta_i'-\sum_{r=1}^{n}\alpha_{ir}'(x_r+x_r')\right]$$

$$=\sum_{i=1}^{n} A_{ji}\left\{\sum_{s=N+1}^{N+N'} a_{is}\left[y_s-\sum_{r=1}^{n} a_{rs}(x_r+x_r')\right]\right\}, \quad j=1\cdots n,$$

where x_j' is the correction to be applied to the jth mass value.

If the new data are less accurate than the old data, an approximate solution may be found by omitting x_r' from the right side of these equations. For more accurate new data this approximation overcorrects the mass values, so x_r' must be retained and the equations solved by successive approximations.

In the case of one new mass result, the equations to be solved reduce to

$$x_j'=\sum_{i=1}^{n} A_{ji}a_i k,$$

where

$$k=y-\sum_{r=1}^{n} a_r(x_r+x_r');$$

and using the result that the Q-value of the $Al^{27}(p,\alpha)Mg^{24}$ reaction is 1.594 ± 0.002 Mev[1] and the author's set of masses,[2] we have

$$20p-20\alpha-20\ Mg^{24}+20\ Al^{27}=31.88\pm0.04\ \text{Mev}.$$

The four equations involving the corrections to these masses can easily be solved exactly by using the fact that the corrections are all proportional to $\sum_i A_{ji}a_i$, giving $k=-0.050$ Mev. The remaining mass corrections may then be determined from the equation

$$x_j'=\textstyle\sum_i A_{ji}a_i k,$$

which is simply (row α)+(row Mg^{24})−(row p)−(row Al^{27}) multiplied by $(-20k)$, which is near enough to 1 Mev in this case. The most important corrections to masses resulting from this reaction measurement are +0.004 Mev for Na^{24}, +0.005 Mev for Mg^{24}, and −0.005 Mev for Al^{27} and in the subsidiary results Si^{27} is tied to Al^{27} by an (n,p) reaction. As the more distant off-diagonal elements are less reliable, it is not advisable to carry these corrections very far from the diagonal. The correction to masses due to the other reaction $Na^{23}(p,\alpha)Ne^{20}$ in the same paper[1] whose Q-value is 2.379 ± 0.003 Mev is

$$0.147\{(\text{row } p)-(\text{row } \alpha)-(\text{row } Ne^{20})+(\text{row } Na^{23})\}\ \text{Mev}.$$

There seems to be no satisfactory simple way for correcting the inverse matrix when the new data are more accurate than the old data. When the new data

[1] Donahue, Jones, McEllistrem, and Richards, Phys. Rev. **89**, 824 (1953).
[2] J. E. Drummond, Phys. Rev. **97**, 1004 (1955).

are less accurate, the correction to the inverse matrix is

$$A_{ij}' = -A_{ik}a_{kl}'A_{lj} + A_{ik}a_{kl}'A_{lr}a_{rs}'A_{sj} - \cdots,$$

where A_{ik} is the old inverse matrix and a_{kl}' is the new contribution to the matrix from the new data and summation is carried out over repeated suffixes. It is believed that this series oscillates infinitely in the only useful case, i.e., when the new data are more accurate. However the first term points the direction for corrections to the inverse matrix though it overcorrects.

PHYSICAL REVIEW VOLUME 99, NUMBER 3 AUGUST 1, 1955

Gamma Rays from the Deuteron Bombardment of Be^9, B^{10}, N^{14}, and F^{19}†

R. D. Bent, T. W. Bonner, J. H. McCrary, W. A. Ranken, and R. F. Sippel
The Rice Institute, Houston, Texas

(Received April 18, 1955)

A magnetic lens pair spectrometer has been used to study the radiations produced by the bombardment of certain light nuclei with deuterons from a Van de Graaff accelerator. Gamma rays from the bombardment of Be^9 with 2.5-Mev deuterons were observed at 6.00±0.06, 5.10±0.1, and 4.52±0.1 Mev. At 3.85-Mev bombarding energy no lines were observed between 6.5 and 8.0 Mev with an intensity as great as 5 percent of that of the 6.0-Mev line. Gamma rays from the bombardment of B^{10} with 2.0-Mev deuterons were observed at 8.93±0.04, 8.57±0.04, 7.30±0.03, 6.75±0.03, 6.50±0.03, 5.03±0.03, 4.73±0.03, and 4.49±0.05 Mev. Gamma rays from the bombardment of N^{14} with 4.0-Mev deuterons were observed at 10.73±0.08, 10.04±0.04, 9.13±0.06, 8.33±0.04, 7.31±0.04, 6.81±0.04, 6.33±0.05, 6.12±0.06, and 5.26±0.04 Mev. Gamma rays from the bombardment of F^{19} with 3.6-Mev deuterons were observed at 11.51±0.2, 10.61±0.1, 9.97±0.1, and 9.34±0.1 Mev. All the energies of gamma rays given above are corrected for Doppler shifts.

A comparison is made for some of the reactions of the relative (d,p) and (d,n) cross sections.

I. INTRODUCTION

In an earlier paper,[1] a report was given on the radiations from the Li^7+d, $B^{11}+p$, $C^{12}+d$, $C^{13}+d$, and $F^{19}+p$ reactions as observed with a lens-type pair spectrometer. As a continuation of this work, the present paper gives the results of measurements of the gamma rays from the Be^9+d, $B^{10}+d$, $N^{14}+d$, and $F^{19}+d$ reactions. The apparatus and experimental procedures used to make these measurements have been previously described.[1] Most of the experiments have been carried out with either 2.5 or 3.6 percent energy resolution, but in the case of the complicated gamma-spectra from $B^{10}+d$ a resolution of 1.8 percent was used. Plastic scintillators are currently being used for detection of the positrons and electrons instead of stilbene crystals, since larger clipped pulses are obtained from the plastic and it can be more easily machined to the desired shapes.

II. SPECTROMETER EFFICIENCY

The gamma-ray energies and yields were obtained in most of the experiments from measurements of the internal pair spectra. The number of internal pairs which are transmitted by the spectrometer and detected in coincidence, per quantum, is a function of the gamma-ray energy and multipolarity. In order for a pair to be detected in coincidence, the positron and electron must have nearly the same energy, and they must both be emitted within the acceptance solid angle of the spectrometer. The angular correlation of the positrons and electrons, i.e., the number of pairs per quantum, per $d\theta$, per unit energy interval where the positron and electron have nearly the same energy, was calculated from the expressions given by Rose[2] for gamma rays of different energies and multipolarities. The peak number of pairs transmitted by the spectrometer, per quantum, was then calculated numerically with an acceptance solid angle equal to 8.7 percent of the total sphere (maximum acceptance half-angle = 47°, minimum acceptance half-angle = 31°, energy resolution = 2.5 percent), assuming that the gamma-ray angular distributions were isotropic with respect to the beam. The results are shown in Fig. 1.

The efficiency of the spectrometer for detecting gamma rays of different energies was determined experimentally by comparing the pair yields obtained with the spectrometer from the $C^{13}+d$ reaction with the absolute gamma-ray yields given for this reaction by Baggett and Bame,[3] and Thomas and Lauritsen.[4] The experimentally determined peak number of coincidence counts per quantum was less than the calculated number of transmitted pairs per quantum by about a factor of 3 at 9 Mev, and a factor of 10 at 4 Mev. This can be explained in the following ways. (1) Half of the transmitted pairs are not detected in coincidence since in half of the cases the positron and electron both strike the same scintillator. (2) The alignment of the spec-

† Supported in part by the U. S. Atomic Energy Commission.
[1] Bent, Bonner, and Sippel, Phys. Rev. **98**, 1237 (1955).
[2] M. E. Rose, Phys. Rev. **76**, 678 (1949).
[3] L. M. Baggett and S. J. Bame, Phys. Rev. **84**, 154 (1951).
[4] R. G. Thomas and T. Lauritsen, Phys. Rev. **88**, 969 (1952).

trometer and choice of baffle widths are not exactly optimum, so that some of the electrons emitted within the acceptance solid angle do not pass through the intermediate baffle. (3) In order to minimize background effects due to the scattering of high-energy gamma rays and neutrons from the walls and coils of the spectrometer, the detectors were chosen to be somewhat smaller than the spot size at the exit end of the spectrometer. (4) At the fastest resolving times (2×10^{-9} sec) some of the true coincidences are missed because of random delays in the photomultipliers and associated electronics. (5) In order to bias out as much background as possible, only the largest coincidence pulses are counted. Thus coincidences due to electrons and positrons passing through the edges of the crystals are missed. It is hoped to minimize this loss by the proper shaping of the detecting scintillators. Losses due to the use of too large a bias are probably more important at low gamma-ray energies.

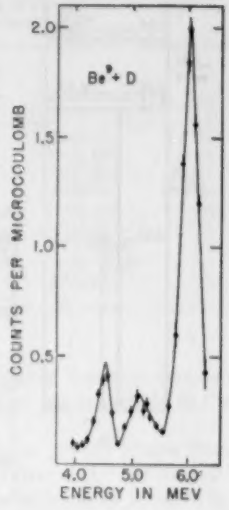

FIG. 2. Internal pair spectrum from the bombardment of a 25-mg/cm² metallic beryllium target with 2.5-Mev deuterons. Spectrometer resolution = 5.5 percent.

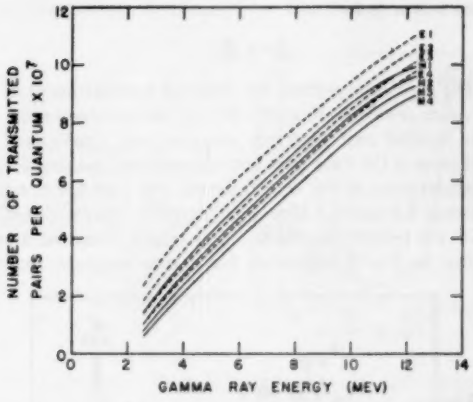

FIG. 1. Spectrometer efficiency.

III. RESULTS AND DISCUSSION

A. Be^9+H^2

The internal pairs from the bombardment of a 25-mg/cm² metallic beryllium target with 2.50- and 3.85-Mev deuterons were observed with 5.5 percent resolution. The results obtained at 2.5-Mev bombarding energy are shown in Fig. 2. They have been corrected for a background observed with zero magnetic field, which is due to true coincidences from scattered gamma radiation and neutrons, equal to about 35 percent of the 4.54-Mev peak and for an accidental coincidence rate equal to about 4 percent of this peak. At 3.85-Mev bombarding energy, the internal pair spectrum was observed up to 8.0-Mev gamma-ray energy, but no lines were observed between 6.5 and 8.0 Mev with an intensity as great as 5 percent of that of the 6.00-Mev line. The gamma-ray energies and yields are given in Table I.[5–7] An attempt was made to observe the internal pair spectrum below 6 Mev with 2.5 percent resolution. However, the transmission of the spectrometer for pairs is reduced by about a factor of 10 in going from 5.5 percent to 2.5 percent resolution, whereas the background with no magnetic field is not affected. Hence at 2.5 percent resolution this background was five times larger than the 4.5-Mev pair peak. This background was worse for the Be^9+d reaction than for any of the other reactions studied.

When Be^9 is bombarded with deuterons the following reactions, which could account for the gamma rays, occur:

$$Be^9(d,p)Be^{10}, \quad Q=4.59 \text{ Mev},$$
$$Be^9(d,n)B^{10}, \quad Q=4.36 \text{ Mev}.$$

Energy levels of Be^{10} have been reported at 3.37, 5.96, 6.18, 6.26, 7.37, and 7.54 Mev by Jung and Bockelman,[5] and Bockelman *et al.*[6] from measurements

TABLE I. Energies and yields of the gamma rays from the deuteron bombardment of Be^9.

Uncorrected energy (Mev)	Doppler corrected energy (Mev)	Yield (γ/deut. ×10⁶)	Total cross section[a] (mb)	Assignment	Reference
6.03±0.05	6.00±0.06	0.70	1.4	Be^{10}(5.96)	5, 6
5.13±0.09	5.10±0.1	0.13	0.2	B^{10}(5.16)	7
4.54±0.09	4.52±0.1	0.23	0.4	B^{10} cascade (5.16 to 0.72)	7

[a] Average value, E_d = 0 to 2.5 Mev.

[5] J. J. Jung and C. K. Bockelman, Phys. Rev. **96**, 1353 (1954).
[6] Bockelman, Browne, and Buechner, Massachusetts Institute of Technology Progress Report, May, 1954 (unpublished).
[7] F. Ajzenberg, Phys. Rev. **82**, 43 (1951); Phys. Rev. **88**, 298 (1952); A. J. Dyer and J. A. Bird, Australian J. Phys. **6**, 45 (1951); Bockelman, Browne, Sperduto, and Buechner, Phys. Rev. **90**, 340 (1953); Phys. Rev. **92**, 665 (1953); Pruitt, Swartz, and Hanna, Phys. Rev. **92**, 1456 (1953); T. W. Bonner and C. F. Cook, Phys. Rev. **96**, 122 (1954).

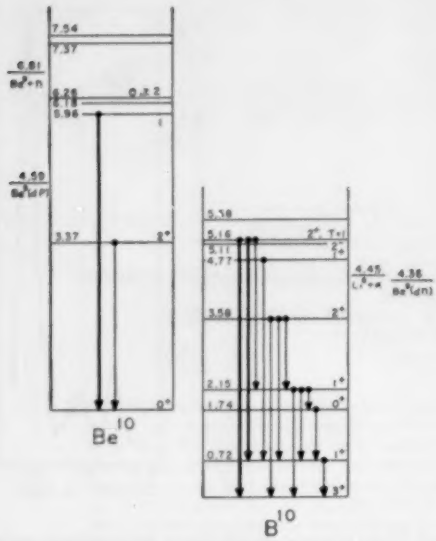

FIG. 3. Energy levels and decay schemes of Be^{10} and B^{10}. Gamma rays observed in the present experiment are represented by heavy vertical lines.

of the proton groups from the $Be^9(d,p)Be^{10}$ reaction. B^{10} has known levels at 0.72, 1.74, 2.15, 3.58, 4.77, 5.11, 5.16, 5.58, 5.93, 6.06, 6.16, 6.40, 6.58 Mev,[7] and higher levels.

Previous measurements of the gamma rays from the Be^9+d reaction have been made by Rasmussen, Hornyak, and Lauritsen[8]; Chao, Lauritsen, and Rasmussen[9]; Shafroth and Hanna[10]; and Mackin.[11] Gamma rays from the $Li^6(\alpha,\gamma)B^{10}$ reaction have been studied by Jones and Wilkinson.[12] The 6.00-, 5.10-, and 4.52-Mev gamma rays observed in the present experiment probably correspond to the gamma rays reported at 4.47 and 5.20 Mev by Chao *et al.*,[9] and at 4.44 and 5.98 Mev by Mackin.[11]

The 6.00-Mev gamma ray is assigned to a ground-state transition from the 5.96-Mev state in Be^9 since states in this energy region in B^{10} probably break up by alpha emission much faster than by gamma emission. The 5.10- and 4.52-Mev gamma rays are assigned to transitions from the 5.11- or 5.16-Mev state in B^{10} to the ground and 0.72-Mev states, respectively. Within the experimental errors of the present experiment, it is not possible to tell which member of the pair of states at 5.1 Mev is involved. However, according to the arguments of Jones and Wilkinson[12] the 5.16-Mev state is a 2^+, $T=1$ state, and the 5.11-Mev state is 2^-, $T=0$, and so these two lines probably are due to transitions from the 5.16-Mev state, the breakup into $Li^6+\alpha$ being slowed down by the isotopic spin selection rule.

Energy-level diagrams and decay schemes of Be^{10} and B^{10} are shown in Fig. 3. Spin and parity assignments of B^{10} are given which are consistent with the neutron angular distributions of Ajzenberg[7] and the gamma-ray measurements.[8–12] The spin and parity of the 3.37-Mev state of Be^{10} have been shown to be 2^+.[13] The fact that the 5.96-Mev state in Be^{10} decays predominantly to the 0^+ ground state rather than to the 2^+, 3.37-Mev state, suggests that the angular momentum of this state is 1. Measurements of the proton groups from the $Be^9(d,p)Be^{10}$ reaction by Bockelman *et al.*[7] at 5.4- to 7.4-Mev bombarding energies and by Phillips and Windham[14] at 3.85-Mev bombarding energy have shown that the proton group leaving Be^{10} in the 6.26-Mev level has about the same intensity as the proton group leading to the excitation of the 5.96-Mev level. The absence of a ground-state transition from the 6.26-Mev state suggests that the angular momentum of this state is 0 or ≥ 2.

$B^{10}+H^2$

The gamma rays from the deuteron bombardment of B^{10} were first investigated with 2.5 percent resolution. The internal pair spectrum obtained was complicated and most of the lines were not well resolved, making the interpretation of the data difficult. The pair spectrum between 5.8 and 9.2 Mev was therefore reinvestigated with 1.8 percent resolution. The results obtained are shown in Fig. 4, corrected for a zero magnetic field

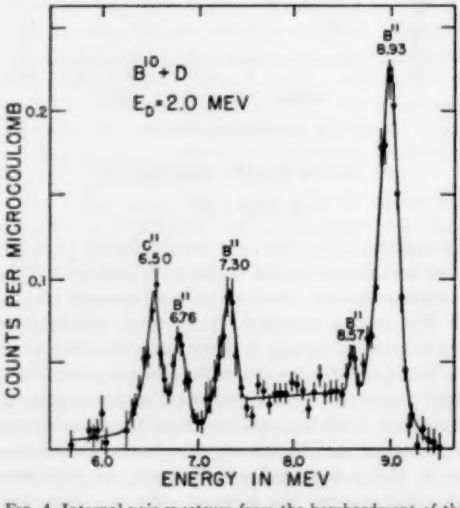

FIG. 4. Internal pair spectrum from the bombardment of thick B^{10} targets with 2.0-Mev deuterons. Spectrometer resolution = 1.8 percent.

[8] Rasmussen, Hornyak, and Lauritsen, Phys. Rev. **76**, 581 (1949).
[9] Chao, Lauritsen, and Rasmussen, Phys. Rev. **76**, 582 (1949).
[10] J. M. Shafroth and S. S. Hanna, Phys. Rev. **95**, 86 (1954).
[11] R. J. Mackin (private communication).
[12] G. A. Jones and D. H. Wilkinson, Phys. Rev. **90**, 722 (1953); Phys. Rev. **91**, 1575 (1953).
[13] Cohen, Hanna, and Class, Phys. Rev. **94**, 419 (1954).
[14] G. C. Phillips and P. M. Windham (private communication).

background which was equal to about 20 percent of the 7.3-Mev peak and for an accidental rate equal to about 8 percent of the 7.3-Mev peak. A 45 mg/cm² 96 percent B^{10} target pressed onto a 21 mg/cm² copper foil was used for the region between 7.5- and 9.3-Mev gamma-ray energy and a 99.5 percent B^{10} target about 6 mg/cm² thick was used for the region between 6 and 7.5 Mev. The 99.5 percent B^{10} was used to minimize the accidental rate due to the beta rays from B^{12} resulting from the $B^{11}(d,p)B^{12}$ reaction. The internal pair spectrum of the low-energy gamma rays taken at 2.5 percent resolution is shown in Fig. 5, corrected for a zero magnetic field background equal to about 7 percent of the 4.73-Mev peak and an accidental rate equal to about 20 percent of this peak. The lower energy gamma rays were not investigated with 1.8 percent resolution because of the low yields in this region.

Because of uncertainties in determining the thicknesses of the boron targets, this spectrum was calibrated on the lines which were identified as being from the $B^{10}(d,p)B^{11}$ reaction, since the energy levels of B^{11} have been accurately determined by Van Patter, Buechner, and Sperduto[15] from measurements of the proton groups. In doing this it was assumed that each pair line experienced the maximum possible Doppler shift. The gamma-ray yields and Doppler corrected energies are listed in Table II.[15,16]

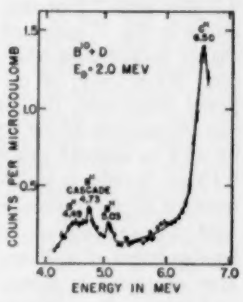

FIG. 5. Internal pair spectrum from the bombardment of a 45-mg/cm², 96 percent B^{10} target with 2.0-Mev deuterons. Spectrometer resolution = 2.5 percent.

The main features of the present results are in agreement with earlier pair spectrometer measurements of the gamma rays from the deuteron bombardment of B^{10} which were carried out with poorer resolution.[17]

When B^{10} is bombarded with deuterons, the following reactions, which could account for the gamma rays, occur:

$$B^{10}(d,p)B^{11}, \quad Q = 9.23 \text{ Mev},$$
$$B^{10}(d,n)C^{11}, \quad Q = 6.47 \text{ Mev},$$
$$B^{10}(d,\alpha)Be^{8}, \quad Q = 17.81 \text{ Mev}.$$

TABLE II. Energies and yields of the gamma rays from deuteron bombardment of B^{10}.

Doppler corrected energy (Mev)	Yield (γ/deut. ×10⁵)	Total cross section[a] (mb)	Assignment	References
8.93±0.04	2.6	8.1	B^{11}(8.93)	15
8.57±0.04	0.6	1.8	B^{11}(8.57)	15
7.30±0.03	1.9	6.0	B^{11}(7.30)	15
6.75±0.03	1.7	5.4	B^{11}(6.76)	15
6.50±0.03	2.6	8.0	C^{11}(6.40)	16
5.03±0.03	0.9	3.0	B^{11}(5.03)	15
4.73±0.03	2.0	6.3	B^{11} cascade (9.19→4.46)	15
4.49±0.05	1.6	5.0	B^{11}(4.46)	15

[a] Average value E_d = 0 to 2.0 Mev.

The excited states of Be^8 probably break up into two alpha particles and hence would not contribute to the pair spectrum.

Accurate measurements of the proton groups from the $B^{10}(d,p)$ reaction by Van Patter *et al.*[15] and Elkind[18] have established the existence of levels in B^{11} at 9.28, 9.19, 8.92, 8.57, 7.99, 7.30, 6.81, 6.76, 5.03, 4.46, and 2.14 Mev. A comparison of the gamma-ray energies and intensities with these results leads to the assignment of the 8.93-, 8.57-, 7.30-, 6.75-, 5.03-, and 4.49-Mev lines to ground state transitions in B^{11}. The 4.73-Mev line is assigned to a transition between the 9.19- and 4.46-Mev levels of B^{11}. The 6.50-Mev line is assigned to a ground state transition in C^{11} corresponding to the level at 6.40 in C^{11} reported by Johnson[16] from measurements of the neutron groups from the $B^{10}(d,n)C^{11}$ reaction.

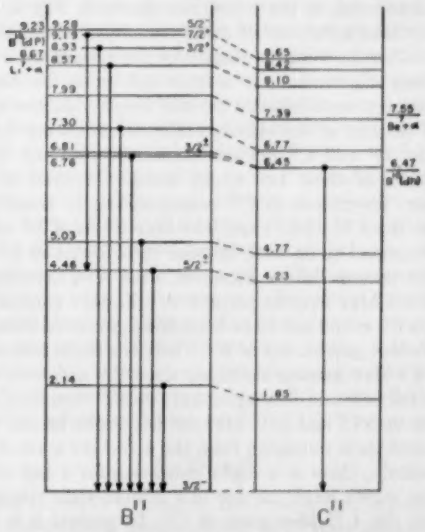

FIG. 6. Energy levels of B^{11} and C^{11} and the gamma rays from $B^{10}+d$.

[15] Van Patter, Buechner, and Sperduto, Phys. Rev. **82**, 248 (1951).
[16] V. R. Johnson, Phys. Rev. **86**, 302 (1952).
[17] J. Terrell and G. C. Phillips, Phys. Rev. **83**, 703 (1951); S. J. Bame and L. M. Baggett, Phys. Rev. **84**, 891 (1951); Ruthergien, Rae, and Smith, Proc. Phys. Soc. (London) **A64**, 906 (1951).
[18] M. M. Elkind, Phys. Rev. **92**, 127 (1953).

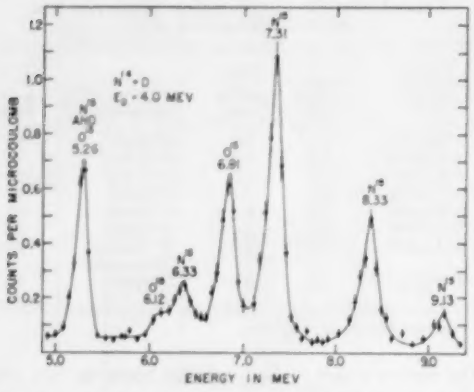

FIG. 7. Internal pair spectrum from the bombardment of an 18-mg/cm² CrN target with 4.0-Mev deuterons. Spectrometer resolution = 2.5 percent.

Energy level diagrams of B^{11} and C^{11} showing the gamma rays from $B^{10}+d$ are given in Fig. 6. The energies of the B^{11} levels are due to the proton group measurements.[15,18] The 1.85, 4.23, 4.77, 6.77, and 7.39 energies for C^{11} are due to Johnson.[16] The 6.45-Mev value is an average of the gamma-ray and neutron group measurements. The 8.10-, 8.42-, and 8.65-Mev values are from the neutron threshold measurements of Marion, Cook, and Bonner.[19] Spin and parity assignments have been given which are consistent with the present gamma-ray measurements, the angular distributions of Evans and Parkinson,[20] and the $\alpha-\gamma$ and $\gamma-\gamma$ angular correlations of Jones and Wilkinson.[21]

In addition to the transitions shown in Fig. 6, it is likely that a number of other transitions occur which are either too weak to observe or are unresolved in the present experiment. It is expected from the charge symmetry hypothesis of nuclear forces that the spins and parities of the corresponding levels of the mirror nuclei B^{11} and C^{11} are the same, and that the decay schemes of these two nuclei should therefore be the same. Transitions in C^{11} corresponding to transitions from the 8.57-, 8.93-, and 9.19-Mev levels of B^{11} would be expected to be weak because these states in C^{11} can break up into $Be^7+\alpha$. However, weak lines between 7.5 and 8.5 Mev may be present. A 6.77-Mev gamma ray from C^{11} would not have been distinguishable from the 6.76-Mev gamma ray of B^{11}. There is a slight indication of 4.9-Mev gamma radiation since the spectrum does not fall as low in this region as it should were there only lines at 4.73 and 5.03 Mev, which might be due to a ground state transition from the 4.77-Mev state of C^{11}. Similarly, there is a slight indication for a line at 4.3 Mev, which might be due to a ground-state transition from the 4.23-Mev state of C^{11}. In general it is seen that at 2.0-Mev bombarding energy the lines from the $B^{10}(d,n)C^{11*}$ reaction are weaker than the lines from the $B^{10}(d,p)B^{11*}$ reaction. The only exception is the 6.50-Mev line from C^{11} which is stronger than the 6.75-Mev line from the mirror level in B^{11}. In an attempt to explain this exception, the spectrum between 6 and 7.5 Mev was also observed at 4.0-Mev bombarding energy. It was found that the relative intensities of the 6.50-, 6.76-, and 7.30-Mev gamma rays are about the same at 4.0 Mev as at 2.0-Mev bombarding energy. This point is discussed further in Sec. IV.

There is indirect evidence that the 4.46-Mev state of B^{11} cascades partly to the 2.14-Mev level, since if the 4.73-Mev line is due to a transition from the 9.19 to the 4.46-Mev level, then the 4.46-Mev line should be at least as intense as the 4.73-Mev line if the 4.46-Mev state decayed 100 percent to the ground state.

C. $N^{14}+H^2$

An 18-mg/cm² CrN target pressed onto a 20-mg/cm² copper foil was bombarded with 4.0-Mev deuterons and the internal pair spectrum was observed between 5 and 9.2 Mev with 2.5 percent resolution. The results are shown in Fig. 7, corrected for zero magnetic field and chance backgrounds which were about 10 and 40 percent, respectively, of the lowest points. Because of power limitations, the intermediate image spectrometer arrangement giving 2.5 percent resolution could not be used to measure gamma-ray energies greater than 9.3 Mev. In order to look for higher energy gamma rays from the $N^{14}+d$ reaction, a ring focus arrangement was used. The internal pair spectrum obtained from the bombardment of a 25-mg/cm² ZrN target with 4.25-Mev deuterons is shown in Fig. 8, uncorrected for background effects. The instrument resolution for this experiment was 3.6 percent. ZrN was found to be a more stable target than CrN. The gamma-ray energies and yields are given in Table III.[22,23]

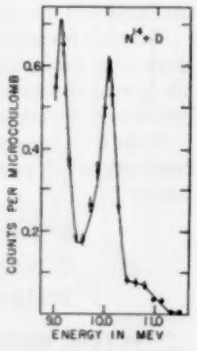

FIG. 8. Internal pair spectrum from the bombardment of a 25-mg/cm² ZrN target with 4.25-Mev deuterons. Spectrometer resolution = 3.6 percent.

[19] Marion, Cook, and Bonner (private communication).
[20] N. T. S. Evans and W. C. Parkinson, Proc. Phys. Soc. (London) **A78**, 684 (1954).
[21] G. A. Jones and D. H. Wilkinson, Phys. Rev. **88**, 423 (1952).
[22] Sperduto, Buechner, Bockelman, and Browne, Phys. Rev. **96**, 1316 (1954).
[23] Evans, Greene, and Middleton, Proc. Phys. Soc. (London) **A66**, 108 (1953).

When N^{14} is bombarded with deuterons the following reactions, which could account for the gamma rays, occur:

$$N^{14}(d,p)N^{15}, \quad Q = 8.61 \text{ Mev},$$
$$N^{14}(d,n)O^{15}, \quad Q = 5.12 \text{ Mev},$$
$$N^{14}(d,\alpha)C^{12}, \quad Q = 13.57 \text{ Mev}.$$

The 10.73-, 10.04-, 9.13-, 8.33-, 7.31-, and 6.33-Mev lines are all assigned to N^{15} since they correspond to ground-state transitions from known excited states of N^{15}.[22] Similarly, the 6.81- and 6.12-Mev lines are assigned to O^{15}. The 5.26-Mev peak is too broad for a single line indicating that gamma rays from both N^{15} and O^{15} contribute to this peak. There is no evidence for a nuclear pair line from the $N^{14}(d,\alpha\pi)C^{12}$ reaction at 7.65 Mev.

These results are in agreement with other measurements of the gamma rays from the $N^{14}+d$ reaction by Terrell and Phillips[17] who observed lines at 4.4, 5.33, 6.4, 7.40, and 8.46 Mev, and with the neutron capture gamma-ray measurements of Kinsey, Bartholomew, and Walker[24] who reported gamma rays from N^{15} at 4.48, 5.29, 5.55, 6.32, 7.16, 7.36, 8.28, 9.15, and 10.82 Mev. The gamma rays reported at 5.55 and 7.16 Mev by Kinsey *et al.* were not observed in the present experiment. The 7.31- and 8.33-Mev values from the present experiment disagree with the corresponding values given by Kinsey *et al.* by amounts larger than the estimated experimental errors, but agree with the proton group values of Sperduto *et al.*[22] Within the experimental errors, the 10.82-Mev line observed by Kinsey *et al.* and the 10.73-Mev line observed in the present experiment may be due to the same gamma ray.

Energy level diagrams of N^{15} and O^{15} showing the gamma rays from $N^{14}+d$ are given in Fig. 9. The energies of the levels of N^{15} have been accurately determined by Sperduto *et al.*[22] from measurements of the proton groups from the $N^{14}(d,p)N^{15}$ reaction. The 6.12- and 6.81-Mev values of O^{15} are from the present gamma-ray measurements and are 70 and 30 kev, respectively, lower than the values given for these levels by Evans, Greene, and Middelton.[23] The 5.29-Mev value is from Evans *et al.* In view of the proton group intensities of Sperduto *et al.*,[22] the absence of ground-state transitions from the 7.16- and 7.57-Mev levels of N^{15} suggests that these levels decay by cascades to lower levels. A 1.88-Mev gamma ray reported by Thompson[25] from the $N^{14}+d$ reaction has been interpreted as being the result of a transition from the 7.16-Mev state to the 5.28- or 5.30-Mev state of N^{15}. Spin and parity assignments are given which are consistent with the gamma-ray measurements together with the angular distributions of Gibson and Thomas[26] and Evans, Greene, and Middleton.[23]

TABLE III. Energies and yields of the gamma rays from the deuteron bombardment of N^{14}.

Uncorrected energy (Mev)	Doppler corrected energy (Mev)	Yield (γ/deut. $\times 10^6$)	Total cross section[a] (mb)	Assignment	Reference
10.77 ±0.07	10.73 ±0.08	0.02	0.1	N^{15}(10.70)	22
10.08 ±0.03	10.04 ±0.04	0.14	0.8	N^{15}(10.07)	22
9.17 ±0.05	9.13 ±0.06	0.15	0.9	N^{15}(9.16)	22
8.37 ±0.03	8.33 ±0.04	0.71	4.3	N^{15}(8.32)	22
7.34 ±0.03	7.31 ±0.04	2.3	14	N^{15}(7.31)	22
6.84 ±0.03	6.81 ±0.04	1.6	9.7	O^{15}(6.84)	23
6.36 ±0.04	6.33 ±0.05	0.75	4.5	N^{15}(6.33)	22
6.15 ±0.05	6.12 ±0.06	0.50	3.0	O^{15}(6.19)	23
5.29 ±0.03	5.26 ±0.04	3.3	20	N^{15}(5.29) and O^{15}(5.29)	22 23

[a] Average value $E_d = 0$ to 4 Mev.

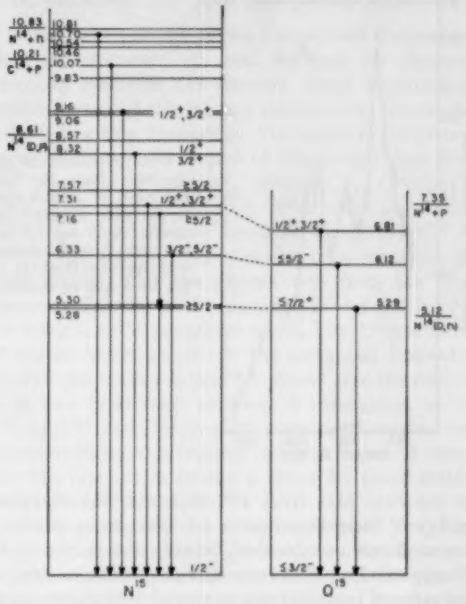

FIG. 9. Energy levels of N^{15} and O^{15} and gamma rays from $N^{14}+d$.

The decay schemes of the two mirror nuclei N^{15} and O^{15} appear to be the same where comparisons can be made. Levels above 7.4 Mev in O^{15} can break up into $N^{14}+p$ and hence would be expected to give only weak gamma rays. Also, the spin and parity measurements which have been made seem to indicate that the spins and parities of the corresponding levels are the same.

A comparison of the gamma-ray yields from the corresponding levels shows that the gamma rays from the $N^{14}(d,p)N^{15*}$ reaction are about 1.5 times stronger than the gamma rays from the $N^{14}(d,n)O^{15*}$ reaction.

D. $F^{19}+H^2$

First attempts to measure the internal pair spectrum from the deuteron bombardment of F^{19} were unsuccessful because of the large accidental coincidence rate due

[24] Kinsey, Bartholomew, and Walker, Can. J. Phys. **29**, 1 (1951).

[25] L. C. Thompson, Phys. Rev. **96**, 369 (1954).

[26] W. M. Gibson and E. E. Thomas, Proc. Roy. Soc. (London) **A210**, 543 (1952).

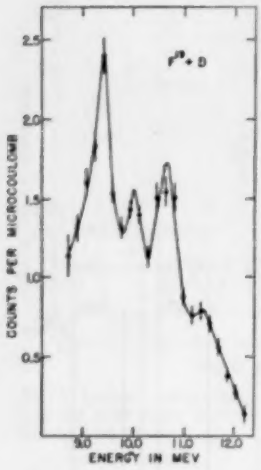

FIG. 10. External pair spectrum from the bombardment of a thick CaF_2 target with 3.6-Mev deuterons. A 77-mg/cm² lead converter 9 mm in diameter was separated from the target by 5 mm of aluminum absorber.

to the beta rays from F^{20}. However, the maximum energy of these beta-rays is 5.4 Mev, so by placing a 5-mm aluminum absorber between the target and a 77-mg/cm² lead converter it was possible to look at the external pair spectrum down to 8.5-Mev gamma-ray energy. The results obtained from the bombardment of a thick CaF_2 target with 3.6-Mev deuterons are shown in Fig. 10, uncorrected for background effects. A ring focus spectrometer arrangement giving 3.6 percent resolution was used. The energies of the lines were calculated from the peak positions using the 6.05-Mev nuclear pair line from the $F^{19}(p,\alpha\pi)O^{16}$ reaction for calibration assuming that each external pair peak was shifted down by an amount equal to the most probable energy lost by a single electron in passing through the 77-mg/cm² lead converter. This shift was calculated to be 0.154 Mev. The gamma-ray energies and yields are summarized in Table IV.

When F^{19} is bombarded with deuterons the following reactions occur:

$$F^{19}(d,n)Ne^{20}, \quad Q=10.65 \text{ Mev},$$
$$F^{19}(d,p)F^{20}, \quad Q=4.37 \text{ Mev},$$
$$F^{19}(d,\alpha)O^{17}, \quad Q=10.04 \text{ Mev}.$$

States above 4.2 Mev in O^{17} can break up into $O^{16}+n$ and hence would not be expected to give rise to intense gamma radiation. Because of the low Q value for the $F^{19}(d,p)F^{20}$ reaction, F^{20} cannot give rise to gamma rays with energies greater than 7.7 Mev. The gamma rays that are observed between 8 and 12 Mev must therefore be from Ne^{20}.

The 9.34- and 9.97-Mev gamma rays are assigned to ground-state transitions from the levels reported at 9.0 and 10.1 Mev from measurements of the neutron groups from the $F^{19}(d,n)Ne^{20}$ reaction.[27] The 11.51-Mev gamma ray is also assigned to a ground-state transition from an excited state in Ne^{20} at this energy since this line was also observed by Terrell and Phillips[17] at 1.56-Mev bombarding energy where it is energetically impossible that it could be due to a transition from a higher level in Ne^{20} to the 1.63-Mev level. The 10.61-Mev gamma ray is assigned to a ground-state transition from a level in Ne^{20} at this energy although this line could also be due to a transition to the 1.63-Mev level from a level at 12.28 Mev in Ne^{20}. A gamma-ray line has been reported at 8.1 Mev by Terrell and Phillips,[17] which may correspond to a ground-state transition from the level reported at 7.3 Mev by Bonner,[27] or to a cascade transition from the 9.97-Mev level to the 1.63-Mev level.

The 9.34-Mev state must have odd angular momentum and even parity, or *vice versa*, since otherwise it could break up into $O^{16}+\alpha$ much faster than it could emit a gamma ray. Since this state decays predominantly to the ground state rather than to the 2^+, 1.63-Mev[28] state, the spin and parity are probably either 1^+ or 2^-. A 2^- assignment is possible because of the isotopic spin selection rule discouraging an $E1$ transition to the 1.63-Mev level. The same arguments may be applied to the 9.97- and 10.61-Mev gamma emitting states; however, since the difference in energies of these two states is very nearly the same as the excitation energy of the first excited state of F^{20}, and since the first $T=1$ state of Ne^{20} is expected to be at about 10.2 Mev,[29] the 9.97- and 10.61-Mev levels might be $T=1$ states corresponding to the ground and first excited states of F^{20}. The spins and parities of these two states in Ne^{20} would then have to be 1^+ to be consistent with the decay scheme. This assignment is in agreement with the 1^+ ground state of F^{20} and the first excited state of F^{20}, which has been reported to have even parity and a spin of 1, 2, or 3.[30] Similar arguments suggest that the spin and parity of the 11.51-Mev state of Ne^{20} are 1^+ or 2^-. The fact that the 11.51-Mev gamma radiation is weaker than the other lines may be due to the competition with alpha emission, since states above 10.9 Mev in Ne^{20} can break up into $O^{16}+\alpha$ leaving O^{16} excited in the 3^- state at 6.14 Mev.

An energy level diagram of Ne^{20} showing the gamma rays from $F^{19}+d$ is given in Fig. 11. The energies, spins,

TABLE IV. Energies and yields of the gamma rays from the deuteron bombardment of F^{19}.

Uncorrected energy (Mev)	Doppler corrected energy (Mev)	Yield (γ/deut. $\times 10^6$)	Total cross section[a] (mb)	Assignment
9.38±0.09	9.34±0.1	0.48	1.7	Ne^{20}
10.01±0.09	9.97±0.1	0.29	1.0	Ne^{20}
10.65±0.09	10.61±0.1	0.32	1.1	Ne^{20}
11.56±0.19	11.51±0.2	0.14	0.5	Ne^{20}

[a] Average value $E_d=0$ to 3.6 Mev.

[27] T. W. Bonner, Proc. Roy. Soc. (London) **A174**, 339 (1940); C. F. Powell, Proc. Roy. Soc. (London) **A181**, 344 (1942).

[28] J. Seed, Phil. Mag. **44**, 921 (1953).

[29] F. Ajzenberg and T. Lauritsen, Boston University Progress Report, September, 1954 (unpublished).

[30] Bromley, Bruner, and Fulbright, Phys. Rev. **89**, 396 (1953).

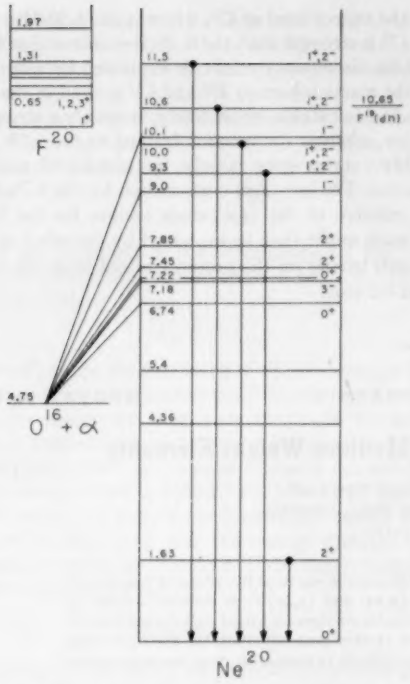

FIG. 11. Energy levels of Ne^{20} and gamma rays from $F^{19}+d$.

and parities of the levels at 6.74, 7.18, 7.22, 7.45, and 7.85 Mev have been reported by Cameron[31] from measurements of resonances in the scattering of alpha particles from O^{16}. The energies, spins, and parities of the 9.0- and 10.1-Mev levels are due to Ferguson and Walker[32] from measurements of the $O^{16}(\alpha,\alpha')$ reaction. The 9.3- and 10.0-Mev values are from the present gamma-ray measurements. Within the experimental errors the energies of these gamma-emitting states are the same as the energies of the alpha-emitting states at 9.0 and 10.1 Mev. However, the states observed from resonances in the scattering of alpha particles from O^{16} cannot be the same as the states giving rise to the strong gamma rays since gamma emission is much less probable than particle emission. Since the energies of the two levels near 9 Mev and the two levels near 10 Mev are only known to within a few hundred kilovolts, the energy separation and relative positions of the levels may not be significant. The existence of pairs of levels with very nearly the same energies but different parities might result from an alpha particle model of Ne^{20} due to the tunneling motion.[33] The similar case of O^{16} has been worked out in some detail by Dennison.[33]

[31] J. R. Cameron, Phys. Rev. **90**, 839 (1953).
[32] A. J. Ferguson and L. R. Walker, Phys. Rev. **58**, 666 (1940).
[33] J. A. Wheeler, Phys. Rev. **52**, 1083 (1937); D. M. Dennison, Phys. Rev. **96**, 378 (1954).

IV. RELATIVE (d,p) AND (d,n) CROSS SECTIONS

It has been pointed out by Cooper and Tobocman[34] that measurements of cross sections for deuteron stripping reactions can provide direct experimental measurements of the relative neutron and proton distributions within the nucleus. The results of the present paper and an earlier paper[1] of the gamma rays from the reactions $B^{10}(d,p)B^{11}$, $B^{10}(d,n)C^{11}$, $C^{13}(d,p)C^{14}$, $C^{13}(d,n)N^{14}$, and $N^{14}(d,p)N^{15}$, $N^{14}(d,n)O^{15}$ show that, except for the 6.50-Mev line from the $B^{10}(d,n)C^{11}$ reaction, the gamma rays from the (d,p) reactions are more intense than the gamma rays from the (d,n) reactions. For two of the reactions, $B^{10}+d$ and $N^{14}+d$, the residual nuclei are mirror nuclei. The decay schemes of mirror nuclei should be the same and hence the relative gamma-ray intensities should give the relative (d,p) and (d,n) cross sections. A comparison of the $N^{14}(d,p)N^{15}$ and $N^{14}(d,n)O^{15}$ cross sections for two corresponding states is given in Table V, which shows that the (d,p) cross section is about 1.5 times greater than the (d,n) cross section.

A comparison of the cross sections of the Mg^{24} $(d,p)Mg^{25}$ and $Mg^{24}(d,n)Al^{25}$ reactions for the three lowest states has been made by Goldberg[35] which shows that the (d,p) cross sections at 8.0-Mev bombarding energy are 4 to 6 times larger than the (d,n) cross sections at 4.0-Mev bombarding energy. Using these data Fujimoto, Kikuchi, and Yoshida[36] calculated the reduced widths for three corresponding levels in the mirror nuclei Mg^{25} and Al^{25} neglecting Coulomb effects, and found that the reduced widths for Mg^{25} were about 10 times greater than the reduced widths for Al^{25}. It is expected from the charge symmetry of nuclear forces that the reduced widths of corresponding levels in mirror nuclei should be the same; however, a difference of a factor of 10 seems to be too large to be accounted for by the fact that Coulomb effects were neglected in these calculations, and it was suggested that it might be due to the protons occupying a smaller volume than neutrons in the nucleus.[34,36] Part of this discrepancy may also be due to uncertainties in the absolute (d,p) and (d,n) cross sections.

The $N^{14}(d,p)N^{15}$ and $N^{14}(d,n)O^{15}$ cross sections were

TABLE V. Cross sections of the $N^{14}(d,p)N^{15}$ and $N^{14}(d,n)O^{15}$ reactions.

$N^{14}(d,p)N^{15}$		$N^{14}(d,n)O^{15}$	
E_d (Mev)	Total cross section[a] (mb)	E_d (Mev)	Total cross section[a] (mb)
6.33	4.5	6.12	3.0
7.31	14	6.81	9.7

[a] Average values $E_d = 1.6$ to 4.0 Mev. Accuracy of relative values is about 15 percent. Absolute values are accurate to within about a factor of 4.

[34] L. N. Cooper and W. Tobocman, Phys. Rev. **97**, 243 (1955).
[35] E. Goldberg, Phys. Rev. **89**, 760 (1955).
[36] Fujimoto, Kikuchi, and Yoshida, Progr. Theoret. Phys. (Japan) **11**, 264 (1954).

measured in the present experiment under exactly the same experimental conditions, and the relative values are accurate to within about 15 percent. It seems reasonable that the difference of a factor of 1.5 in the relative (d,p) and (d,n) cross sections may be accounted for by Coulomb effects,[17] without indicating a larger spatial extension in the nucleus for neutrons than for protons.

The gamma-ray yields from the $B^{10}(d,p)B^{11}$ and $B^{10}(d,n)C^{11}$ reactions show a strange result. The 7.30-Mev line from B^{11} is stronger than the 6.77-Mev line from the mirror level of C^{11}, whereas the 6.50-Mev line from C^{11} is stronger than the 6.75-Mev mirror line from B^{11}. This discrepancy might be explained by assuming that the reaction leaving B^{11} and C^{11} excited in the 7.3- and 6.77-Mev states, respectively, is mainly a stripping reaction, whereas the reaction leading to the 6.75- and 6.50-Mev states goes mainly by compound nucleus formation. The low (d,p) cross section for the 6.75-Mev state relative to the (d,n) cross section for the 6.50-Mev state might then be explained by the effect of the Coulomb barrier on the proton emitted from the compound nucleus.

[17] D. C. Peaslee, Phys. Rev. **74**, 1001 (1948).

PHYSICAL REVIEW VOLUME 99, NUMBER 3 AUGUST 1, 1955

(p,pn) and $(p,2n)$ Cross Sections in Medium Weight Elements

BERNARD L. COHEN AND EUGENE NEWMAN*
Oak Ridge National Laboratory, Oak Ridge, Tennessee
(Received March 7, 1955)

The quantity F_p/F_n, the ratio of probabilities for proton and neutron emission from nuclear reactions in the statistical region, is determined from measurements of (p,pn) and $(p,2n)$ cross sections induced by 21.5-Mev protons bombarding nuclei of masses 48 to 71. The results are then compared with determinations of F_p/F_n from reactions induced by lower-energy protons and 14-Mev neutrons. Both the absolute values of F_p/F_n and their variation with bombarding energy are very difficult to explain by usual nuclear reaction theories.

INTRODUCTION AND THEORY

IN studies of nuclear reactions in the statistical region, considerable attention has been given to the quantity F_p/F_n, the relative probability of proton and neutron emission from nuclear reactions.[1] In particular, interest was aroused by the fact that the experimental determinations[2] were in disagreement with the theoretical estimates[1] from the statistical theory of nuclear reactions, and several attempts have been made to revise the theoretical estimates by modifying the statistical theory,[3] or by introducing direct interactions.[4]

In the experiments described in this paper, a much more serious difficulty with the behavior of F_p/F_n seems to be uncovered. Measurements are reported of F_p/F_n from 21.5-Mev proton-induced reactions in the iron-copper mass region, and these are then compared with determinations at lower incident proton and neutron energies. It is found that F_p/F_n increases by well over an order of magnitude within a few Mev, and attains values considerably larger than unity.

In order to demonstrate how difficult these facts are to reconcile, a simple but quite general treatment of the theory is given. Since a compound nucleus model is the most familiar and the most easily handled, it is used here, but other possibilities will be discussed later. It is further assumed that equal energies are available for both proton and neutron emission; while this is not the usual case, the experimental results for various differences in these energies may be extrapolated to it.

A straightforward application of the reciprocity theorem to the decay of the compound nucleus gives[5]

$$\frac{F_p}{F_n}=\frac{\int_0^{E_0}\sigma_p\eta_p E\omega_p(E_0-E)dE}{\int_0^{E_0}\sigma_n\eta_n E\omega_n(E_0-E)dE}, \tag{1}$$

where E_0 is the maximum energy available for neutron or proton emission, σ_p is the cross section for capture of a proton of energy E, assuming unit sticking probability (tables of σ_p are given in reference 1), $\omega_p(E_0-E)$ is the density of states of the residual nucleus after proton emission [it is a function of (E_0-E), its excitation energy], η_p is a quantity that takes into account selection rules in the nuclear transitions from compound nucleus to residual nucleus plus proton, and the corresponding quantities with subscript n refer to neutrons. While ω_p and ω_n may be different in any particular case,

* Present address: U. S. Army.
[1] J. M. Blatt and V. F. Weisskopf, *Theoretical Nuclear Physics* (John Wiley and Sons, Inc., New York, 1952).
[2] E. B. Paul and R. L. Clarke, Can. J. Physics **31**, 267 (1953).
[3] D. B. Beard, Phys. Rev. **94**, 738 (1954); V. F. Weisskopf (private communication).
[4] H. McManus and W. T. Sharp, Phys. Rev. **87**, 188 (1952); R. M. Eisberg, Phys. Rev. **94**, 739 (1954).
[5] B. L. Cohen, Phys. Rev. **92**, 1245 (1953).

on a statistical basis there clearly can be no consistent difference between them. There is evidence[5] that η may be a function of E and E_0, but a consistent difference between η_p and η_n would be a clear violation of charge independence of nuclear forces (charge independence is well substantiated at these energies). σ_p differs from σ_n only by a Coulomb factor, so let us define such a factor, P_c, as

$$P_c=\sigma_p/\sigma_n. \tag{2}$$

Since the integrand in the denominator of Eq. (1) is just the energy spectrum of emitted neutrons, Eq. (1) may be written

$$F_p/F_n=\bar{P}_c, \tag{3}$$

where $\bar{P}_c$ is the average value of P_c, the average being taken over the energy spectrum of the emitted neutrons.

If this energy spectrum is assumed to be Maxwellian with a temperature of 2 Mev, application of Eq. (3) gives $F_p/F_n=0.07$ in the mass region of interest here; if the temperature is raised to 5 Mev, Eq. (3) gives $F_p/F_n=0.2$, and even if the Maxwellian energy distribution is abandoned and the energy distribution is chosen to maximize F_p/F_n in these experiments, the result would only yield $F_p/F_n=0.4$.

EXPERIMENTAL

The quantities directly measured in these experiments were ratios between pairs of activation cross sections; by combining these, the relative cross sections of all reactions were obtained, and these were made absolute by use of known absolute cross sections as has been described previously.[6] Most cross sections were determined by ratios to at least two others independently, and many cross checks were made.

The procedure most generally used for measuring the ratio between two cross sections was to bombard a finely ground chemical compound (or, in a few cases, a mixture) of the two elements, and count the induced beta activities under an end-window Geiger counter. Bombardments were sufficiently intense that it was necessary to count only a very small mass of material, thus eliminating beta self-absorption and self-scattering corrections. Corrections for backscattering, window and air absorption, etc., were made by the methods of Zumwalt.[7] In the few cases where the materials were available as foils, foil combinations were bombarded behind a "window frame"[6] instead of using chemical compounds. Corrections for self-absorption and self-scattering were then applied.

The activation cross sections for the long-lived gamma-emitting isotopes Cr^{51}, Mn^{54}, and Co^{58} were obtained relative to the $Fe^{56}(p,2n)Co^{55}$ cross section by bombarding mixtures containing iron oxide and counting both these activities and the Co^{55} activity on their respective gamma-ray peaks with a scintillation spectrometer. The spectrometer efficiencies for the long-lived isotopes were obtained by use of accurately assayed standards.[8] The Co^{55} spectrometer efficiency was measured by determining absolute disintegration rates by beta counting, with a phosphorous-32 standard[8] for the Geiger counter calibration. As a check on the entire method, the cross section for production of Na^{22} from Na^{22} was measured by both this method and the usual beta-counting-ratio method; the agreement was excellent.

The cross section for $Fe^{56}(p,pn)Fe^{55}$ relative to that of $Fe^{56}(p,2n)Co^{55}$ was obtained by absolute beta counting one aliquot for the Co^{55} activity, and then determining the absolute disintegration rate in another of the pure electron-capturing isotope Fe^{55} by counting the x-rays under an end-window Geiger counter calibrated with a standard Fe^{55} source.[9] Chemical purification of the iron was carried out, and the fact that the samples were free of betas (which are counted with very much higher efficiency) was checked by comparing their absorption characteristics with those of the standard by the use of thin silver foils. (The inverse mass absorption coefficient of silver for the manganese x-ray is about 1.5 mg/cm^2.)

The cross section for $Zn^{65}(p,2n)Ga^{67}$ relative to that of $Zn^{64}(p,pn)Zn^{63}$ was obtained by absolute beta counting an aliquot for the Zn^{63} activity, and then determining the Ga^{67} disintegration rate by comparing its counting rate with that of a Ga^{67} standard[8] on a scintillation spectrometer set on the 110-kev gamma-ray peak.

Every cross-section ratio was measured independently at least five times. (Those used most frequently in combining ratios were measured at least ten times.) The general reproducibility of the data and the consistency of the cross checks indicates an uncertainty in the raw data of about 7%; considering errors due to beta counting corrections, the relative cross sections may be uncertain by as much as 15%. In addition, the absolute calibration of all cross sections[6] may be in error by about 15%, but this has little effect on the theoretical interpretation, since only cross-section ratios are used.

RESULTS

The measured (p,pn) and $(p,2n)$ cross sections are listed in Table I, along with the energetic thresholds of the pertinent reactions and the character of the final nuclei involved. Table I also lists ratios of (p,pn) to $(p,2n)$ cross sections, although both cross sections were measured in only four of the twelve cases. In the other eight cases, the estimates were arrived at by using our recent measurements of $(p,pn)+(p,2n)$ cross sections.[9]

[6] Cohen, Newman, Charpie, and Handley, Phys. Rev. **94**, 620 (1954); G. H. McCormick and B. L. Cohen, Phys. Rev. **96**, 722 (1954).

[7] L. R. Zumwalt, U. S. Atomic Energy Commission Report, MDDC 1346 (unpublished).

[8] We are greatly indebted to Mr. W. S. Lyon of the Analytical Chemistry Division, Oak Ridge National Laboratory for supplying and assaying these standards.

[9] Cohen, Newman, and Handley, following paper [Phys. Rev. **99**, 723 (1955)].

TABLE I. (p,pn) and $(p,2n)$ cross sections and related information.

Initial nucleus	Thresholds (Mev) (p,n)	(p,pn)	$(p,2n)$	Cross sections (mb) (p,pn)	$(p,2n)$	$\sigma(p,pn)/\sigma(p,2n)$	Favoring by $\sigma \to \sigma$ as $\epsilon \to \epsilon$ $(p,n)/(p,p)$	$(p,np)/(p,2n)$
$_{22}Ti^{49}$	4.7	11.7	15.3	···	120	5.8	x	
$_{24}Cr^{53}$	5.4	12.6	16.0	425	155	2.8	x	
$_{25}Mn^{55}$	0.9	10.3	10.4	620	···	3.5		x
$_{26}Fe^{56}$	5.3	11.5	15.7	760	105	7.2	x	
$_{27}Co^{59}$	1.0	10.9	10.8	540	···	2.7		x
$_{28}Ni^{61}$	5	10.6	13.5	···	385	1.4	x	
$_{29}Cu^{63}$	4.2	11.0	13.4	590	100	5.9		x
$_{29}Cu^{65}$	2.1	10.4	10.5	500	···	1.7		x
$_{30}Zn^{68}$	3.6	8.9	10.7	···	780	0.20[a]	x	
$_{32}Ge^{70}$	4.1	10.4	11.0	360	360	1.0		x
$_{31}Ga^{71}$	1.0	9.0	8.0	260	···	0.37		x
$_{33}As^{75}$	1.6	10.3	10.9	350	···	0.70		x

[a] See reference 10.

In no case do these estimates introduce sufficient uncertainty to qualitatively affect the ensuing discussion.

The most striking observation from Table I is that (p,pn) cross sections are considerably larger than $(p,2n)$ cross sections in eight of the twelve cases, and about equal to them in two of the other four. On the other hand, there is one anomalous case, Zn^{68}, where the $(p,2n)$ cross section is by far the larger.[10] The ratio of (p,pn) to $(p,2n)$ cross sections is very much less in all of the four heaviest isotopes studied than in any of the eight lighter ones. Data for the heavier isotopes are therefore indicated by open symbols in the figures and are considered separately.

Before proceeding with a detailed analysis of the data, it is important to establish that (p,pn) reactions consist principally of (p,p) reactions followed by neutron "boil off." The most important alternative process to be considered is (p,n) reactions followed by proton emission.

In such a process, the energy available for proton emission is in the region 0–10 Mev, with about 7 Mev representing a fair average. These excitations are exactly the same as those encountered in measurements of (p,n) cross sections by Blaser *et al.* and by Blosser.[11] In those experiments it was found that neutron emission even predominates over proton emission when the former is energetically possible by only 1 Mev while the latter is energetically possible by as much as 5 Mev. Proton emission following a (p,n) reaction is therefore very unlikely so long as neutron emission is energetically possible. There are cases, of course, where the emission of the first neutron leaves the nucleus with too little excitation for neutron emission but still with enough for proton emission, so that the latter should take place with high probability. However, calculations based on measured neutron energy spectra[12] indicate that such situations arise relatively seldom.

Another approach to this problem is to compare these data with data on the relative probability for (x,np) and $(x,2n)$ reactions in cases where x is a neutron rather than a proton. Assume, temporarily, that the observed (p,pn) cross sections are entirely due to (p,n) reactions followed by proton emission, and consider the ratio $\sigma(x,np)/\sigma(x,2n)$. This ratio may be estimated[13] for 14-Mev neutron-induced reactions from the ratio of observed to calculated $(n,2n)$ cross sections from the data of Paul and Clarke.[8] Figure 1 shows it plotted against the difference between the energetic thresholds of (x,np) and $(x,2n)$. It is quite evident that $\sigma(x,np)/\sigma(x,2n)$ is greater by at least an order of magnitude in the proton-induced reactions. Actually, this method of comparison grossly underestimates the discrepancy; the proton-induced reactions are carried out with bombarding energies much further above threshold so that situations where emission of a second neutron is energetically forbidden arise much less frequently. In the only neutron-induced reaction where $\sigma(n,np)$ is apparently quite large, the bombarding energy is only 2 Mev above the $(n,2n)$ threshold, but 6 Mev above the (n,np) threshold. It thus seems quite evident that (p,n) reactions followed by proton "boil off" cannot explain the large observed (p,pn) cross sections.[14]

Another process that would lead to the same residual nucleus as a (p,pn) reaction is the simultaneous emission of a proton and a neutron, or "three-body breakup."[15] However, all the arguments about the ratio F_p/F_n apply equally to F_{pn}/F_{2n}, and in fact even more strongly since there is less energy available for the latter processes.

A final possibility is the (p,d) reaction which is essentially a special case of three-body breakup except

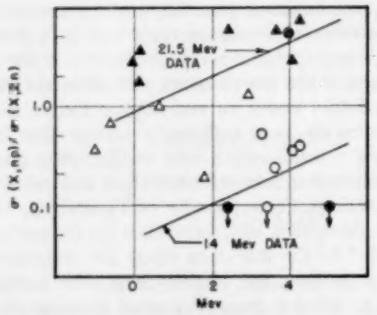

FIG. 1. $\sigma(x,np)/\sigma(x,2n)$ *vs* difference in the energetic thresholds for (x,np) and $(x,2n)$. Triangles are from 21.5-Mev proton data and circles are from 14.5-Mev neutron data. Open points are for $30 \lesssim Z \lesssim 33$, and solid points are for $22 \lesssim Z \lesssim 29$.

[10] There is evidence from the lower-energy work (reference 11) that the reaction cross section from Zn^{68} is abnormally large. This would increase the $(p,pn)/(p,2n)$ ratio to about 0.5.

[11] Blaser, Boehm, Marmier, and Peaslee, Helv. Phys. Acta **24**, 3, 441 (1951); H. G. Blosser (to be published).

[12] P. C. Gugelot, Phys. Rev. **81**, 51 (1951).

[13] This method is very inaccurate for large values of observed-to-calculated $(n,2n)$ cross sections. When such values occur, it is assumed here that the ratio is greater than 0.9. These points are designated with a vertical arrow in Fig. 1.

[14] In the three cases with high $(p,2n)$ thresholds, as much as 25% of the (p,n) reactions may lead to (p,np) reactions. This would decrease F_p/F_n by only about 35%, which is quite negligible.

[15] Good, Kunz, and Moak, Phys. Rev. **94**, 87 (1954).

that an additional 2.2-Mev energy is available from the binding energy of the deuteron. However, it is difficult to see how that amount of energy can materially affect matters. Furthermore, experiments to detect deuterons directly[6,16] have shown that they are not common reaction products in proton-induced reactions in this energy region.

It therefore seems probable that the predominant reaction contributing to the (p,pn) cross section is inelastic scattering followed by neutron emission. Calculations based on the energy spectra of the emitted particles,[12,17] indicate[9] that actually somewhat less than 75% of all (p,p) reactions become (p,pn), whereas a considerably greater fraction of all (p,n) reactions in the elements considered here become $(p,2n)$; but these corrections will be neglected since they are difficult to apply and only accentuate an effect which is already overwhelmingly large. We therefore assume that $\sigma(p,pn)/\sigma(p,2n)$ is an experimental determination of F_p/F_n.

Figure 2 shows F_p/F_n plotted *vs* the difference in energy available for emission of protons and neutrons. It appears that there is little dependence on the abscissa (in agreement with the Hurwitz-Bethe proposal[18]), and that the average value of F_p/F_n is about 2.5 for the lighter elements and 0.5 for the heavier ones.

In accordance with usual nuclear reaction theories,[1] F_p/F_n should depend on the nature of the nuclei involved. If the residual nuclei after proton and neutron emission are even-even and odd-odd, respectively, neutron emission should be favored by about a factor of four; then, in such cases, observed values of F_p/F_n should be multiplied by four to put them on an equal basis with reactions where the residual nuclei are odd-even or even-odd. This has been done in Fig. 3. A noticeable dependence on the abscissa is introduced, and a line through the data crosses zero abscissa at about

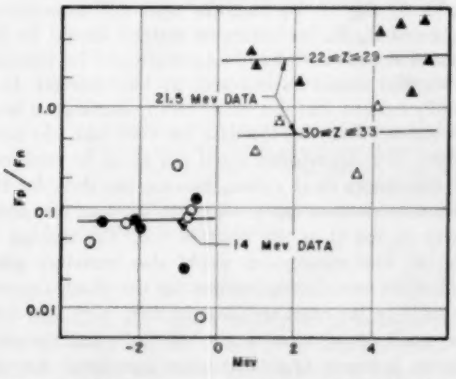

FIG. 2. F_p/F_n *vs* difference in energies available for proton and neutron emission. See caption for Fig. 1.

[16] R. M. Eisberg and G. Igo, Phys. Rev. **93**, 1039 (1954); J. B. Reynolds and K. G. Standing, Phys. Rev. **95**, 639 (1954).
[17] P. C. Gugelot, Phys. Rev. **93**, 425 (1954).
[18] H. Hurwitz and H. A. Bethe, Phys. Rev. **81**, 898 (1951).

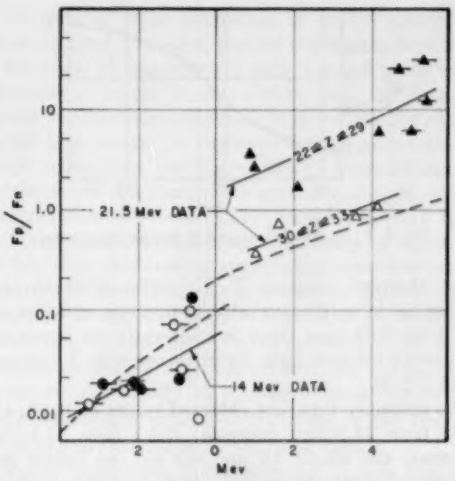

FIG. 3. F_p/F_n *vs* difference in energies available for proton and neutron emission. Data has been corrected for odd-odd *vs* even-even level density differences. Points so corrected are crossed with horizontal lines. See caption for Fig. 1. Dashed lines are predictions of statistical theory (reference 1).

F_p/F_n equal 1.5 for the lighter elements and 0.4 for the heavier ones. The difference between the two methods of extrapolation is thus relatively minor.

For purposes of reference, the theoretical curves calculated from statistical theory are shown as dashed lines in Fig. 3. However, the authors feel that much more can be learned by comparing these data with other data rather than with the very adjustable predictions of statistical theory.

CONCLUSIONS AND DISCUSSION

At least two other experiments give estimations of F_p/F_n at lower energies. The most directly comparable work is the measurements of (p,n) cross sections at 11.5 Mev by Blosser.[11] He finds that they account for essentially the complete reaction cross section, and in fact, uses the data to determine the nuclear radius. It is estimated that the upper limit to F_p/F_n from his work is ~0.2. It includes many cases where the energy available for neutron emission is considerably less than that available for proton emission.

Another experiment that may be compared with this is the measurements of (n,p) cross sections by Paul and Clarke.[2] This comparison has the disadvantage that, since the target nuclei must be beta stable, neutron emission is always energetically favored in neutron-induced reactions whereas proton emission is always energetically favored in proton-induced reactions, so that the two sets of data must be extrapolated in opposite directions. However, this could hardly cause a very large discrepancy. The data from reference 2 are shown in Figs. 2 and 3 where in each case the data are plotted in the same way as the 21.5-Mev proton data.

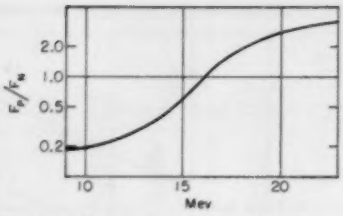

FIG. 4. F_p/F_n for Cu^{63} vs proton bombarding energy.

The observed value of F_p/F_n extrapolated to zero difference in energy available to neutrons and protons is about 0.05, and there is apparently no important difference between data for elements with $Z<30$ and with $Z\geqslant 30$.

In summary then, the observed values of F_p/F_n are 0.05 from 14.5-Mev neutrons, <0.2 from 11.5-Mev protons, and about 2.0 and 0.5 for the lighter and heavier elements respectively from 21.5-Mev protons. The manner in which F_p/F_n increases with incident proton energy for Cu^{63} can be determined from the excitation function measurements of Ghoshal[19]; this is shown in Fig. 4. The low-energy portion is calculated by subtracting two large and nearly equal numbers, each of which is quite uncertain, so that the values plotted are roughly upper limits for energies below 15 Mev.

These results are somewhat unique in two ways—in the large absolute values of F_p/F_n, and in its rather strange energy dependence. Other experiments[2] have found unexpectedly large values for F_p/F_n, but it has always been possible to explain them consistently with Eq. (3) by introducing distortions in the energy spectra of emitted particles.[3,4] The values of F_p/F_n from this experiment, however, are very much too large to be explained by any such distortions. The dependence of F_p/F_n on bombarding energy is also completely unexplainable by Eq. (3).

Before considering alternative theories, account must be taken of the measurements of energy distributions of inelastically scattered protons carried out by Gugelot[16] with 18.3-Mev incident protons. They indicate that the energy distributions are approximately Maxwellian with temperatures of about 2 Mev, and that for protons below 10 Mev (the highest energy that could lead to a (p,pn) reaction in these experiments), the angular distributions are not strongly anisotropic ($\sim$20% higher at 60 deg than at 150 deg). Figure 4 indicates that there is no drastic change in F_p/F_n between 18.3-Mev and 21.5-Mev, and this is further supported by measurements of (p,pn) and $(p,2n)$ excitation functions.[6,20]

The fact that most of the protons are emitted with relatively low energy [as evidenced by Gugelot's measurements and the very fact that (p,pn) reactions are observed] would seem, at first thought, to exclude the possibility that the effect observed here is due to reemission of the incident proton. Weisskopf has pointed out,[21] however, that in considering collisions within the nucleus, the binding energy of the incident particle should be added before the collision, and subtracted when a particle emerges from the nucleus. Furthermore, refraction effects occur at the nuclear boundary. Thus, the low energy and relatively isotropic angular distributions of the emitted protons are not inconsistent with reemission of the incident particle. The question can best be settled by investigating the quantity F_p/F_n in reactions induced by other bombarding particles. In the two cases of alpha-particle-induced reactions that have been reported,[19,22] very large values of F_p/F_n were found. In the single neutron-induced reaction that has been investigated in this mass region,[23] the observed value of F_p/F_n was relatively small. Further investigations would be very desirable.

Wigner has suggested[24] that proton emission in this mass region may be favored by a "giant resonance" of the type introduced by his "intermediate coupling" theory. However, it is his opinion that this could not explain so large an effect.

The most difficult to explain of the large observed (p,pn) cross sections are the cases of Mn^{55}, Co^{59}, and Cu^{65} where the energetics of neutron and proton emission are quite equivalent. If these could be explained, the extrapolations in Figs. 2 and 3 might be sufficiently altered to remove the other discrepancies. One possibility for explaining them lies in the fact that (p,np) reactions in these cases lead to odd-odd residual nuclei. The data could be reasonably explained, for example, if level densities in odd-odd nuclei were assumed to be larger than those in even-even nuclei by a factor of 20.

In order to investigate this possibility, horizontal lines are drawn through the data points for even-even nuclei in Fig. 3. To conform with our assumption, values of F_p/F_n for circles so marked should be decreased at least an order of magnitude, and for triangles so marked should be increased by that amount. It is readily evident that this would clearly introduce a large discrepancy between the data for even and odd mass nuclei. This discrepancy could not easily be explained by differences in Q values, because the data for the various even-mass nuclei does not show such a sensitivity to the Q of the reaction (i.e., the abscissa in Fig. 3). Our assumption would also introduce great difficulties into the explanation for the small observed $(p,pn)+(p,2n)$ cross sections[9] in Zn^{64}, Ni^{58}, and Ti^{46}, the small $(p,\alpha n)$ cross section[6] in Zn^{64}, and the similarities between (p,n) excitation functions[11] for the copper isotopes and the isotopes of nickel and zinc,

[19] S. N. Ghoshal, Phys. Rev. **80**, 939 (1950).
[20] Rough measurements of several (p,pn) and $(p,2n)$ excitation functions have been made by the authors and by R. A. Charpie.
[21] V. F. Weisskopf (private communication).
[22] Miller, Friedlander, and Markowitz, Phys. Rev. **98**, 1197(A) (1955).
[23] Brolley, Fowler, and Schlacks, Phys. Rev. **88**, 618 (1953).
[24] E. P. Wigner (private communication).

and between the (p,pn) excitation functions[6,19] for Cu^{63} and Cu^{65}.

We might note two other indications that the reactions observed are probably not proton emission following (p,n) reactions. Firstly, Gugelot's measurements[16] indicate that the energy spectra of emitted protons are the same in copper as in nickel and iron. Measurements at higher energies[9] clearly show that the first particle emitted in nickel is a proton, and it seems relatively certain from the preceding discussion that the same is true for iron.

Secondly, a remeasurement was made of the excitation functions in Cu^{63}, and it was found that $[\sigma(p,n)+\sigma(p,2n)+\sigma(p,pn)]/\sigma_R$ decreases by 15% as the energy is increased from 11 to 15 Mev. This indicates that the (p,n) cross section probably drops off from competition with the unobserved (p,p') reaction rather than from competition with (p,np).

The conclusions of this paper that F_p/F_n is abnormally large is also supported by two other experiments:

(1) Meadows,[25] in measuring excitation functions in copper with high-energy protons, found that not only are the (p,pn) cross sections much larger than the $(p,2n)$'s, but $(p,p2n)$ and $(p,p3n)$ cross sections are much larger than the $(p,3n)$'s and $(p,4n)$'s.

(2) In the following paper,[11] it is shown that $(p,2p)$ cross sections are very large in this mass region, and in slightly lighter nuclei, commonly are the most probable of all reactions.

[25] W. Meadows, Phys. Rev. **91**, 885 (1953).

In spite of these arguments, it should always be borne in mind, of course, that we are dealing here with a statistical phenomenon; as such, it is subject to wide fluctuations, as can be seen directly from the data. It would be essentially impossible to prove that the effects found here cannot be explained by a combination of these fluctuations, the Wigner effect,[24] large differences between level densities in even-even and odd-odd nuclei, and contributions from (p,d) "pickup" reactions. Certainly any isolated piece of data can easily be explained in that way. However, after prolonged consideration of the various aspects of the problem, the authors have reached the opinion that the large ratio of proton to neutron emission cannot be explained by the usual nuclear reaction theories. Experiments are being undertaken to further study the problem by observing energy distributions and angular distributions of the emitted protons as a function of bombarding energy.

Before concluding, it is interesting to note that the large (p,pn) cross sections indicate that the neutron energy spectra measured by Gugelot[12] are greatly distorted by neutrons from those reactions.

ACKNOWLEDGMENTS

The authors are greatly indebted to Professor E. P. Wigner and Professor V. F. Weisskopf for their very valuable suggestions, to R. S. Livingston for his continual encouragement, and to J. A. Martin for his stimulating discussions. The $As(p,pn)$ cross section was measured by A. Timnick.

PHYSICAL REVIEW VOLUME 99, NUMBER 3 AUGUST 1, 1955

$(p,pn)+(p,2n)$ and $(p,2p)$ Cross Sections in Medium Weight Elements*

B. L. Cohen, E. Newman,† and T. H. Handley
Oak Ridge National Laboratory, Oak Ridge, Tennessee

(Received March 7, 1955)

Several $(p,pn)+(p,2n)$ and $(p,2p)$ cross sections of nuclei of mass 19 to 69 were measured with 21.5-Mev incident protons. For all elements with mass less than 55 and for Ni^{58}, the $(p,pn)+(p,2n)$ cross section is very much less than the total reaction cross section. Detailed analysis of the data indicates that this is largely due to competition from $(p,2p)$ reactions. The conclusion from the previous paper that the ratio of probabilities for proton and neutron emission is much larger than expected seems to be confirmed and extended to lighter nuclei.

INTRODUCTION

IN planning our recent survey of activation cross sections for various types of nuclear reactions in medium weight elements, little attention was at first given to the relatively large number of cases where the sum of the $(p,pn)+(p,2n)$ cross sections can be conveniently measured. It was assumed that, apart from small corrections, these would add up to the total reaction cross section (σ_R).[1] It was soon found, however, that this was not by any means the case. In many of the early measurements, values very much less than σ_R were obtained, and as the data were extended, it turned

* The "$(p,pn)+(p,2n)$ cross section" is used here to mean the sum of the $(p,2n)$, (p,pn), (p,np) and (p,d) cross sections, all of which lead to the same radioactive nucleus (after a beta decay in the first case).

† Present address: U. S. Army.

[1] J. M. Blatt and V. F. Weisskopf, *Theoretical Nuclear Physics* (John Wiley and Sons, Inc., New York, 1952).

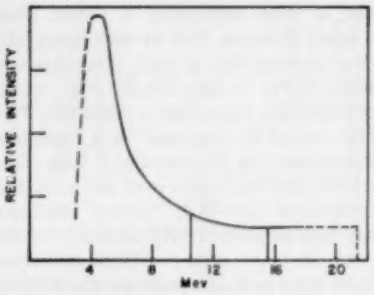

FIG. 1. Assumed energy distribution for 21.5-Mev protons inelastically scattered by copper. This was obtained from reference 3 by assuming the low-energy portion to be unchanged when the incident proton energy is raised from 18 to 21.5 Mev, and smoothly extrapolating the high-energy portion after averaging over resonances. In reference 3, similar results were obtained for iron and nickel.

out that this was true in general for every measurable case of mass less than 55, and for Ni^{58}. A detailed theoretical analysis revealed that competition from $(p,2p)$ reactions might be an important factor in the problem, so that the experiments were extended to include cross section measurements for those reactions wherever possible.

THEORY

In accordance with nuclear reaction theory,[1] a (p,p) reaction generally becomes a (p,pn) reaction when the proton is emitted with low enough energy to leave neutron emission energetically possible. In cases where the residual energy is such that emission of a second proton is possible but neutron emission is not, a $(p,2p)$ reaction should result. When either can be emitted, the Coulomb barrier should suppress proton emission leaving neutron emission more probable, unless this effect is compensated by the extra energy available for proton emission. In order to understand these cross sections we must therefore have some knowledge of the energy distribution with which neutrons and protons are emitted from (p,n) and (p,p) reactions. Measurements of these have been reported by Gugelot[2,3] for 16- and 18-Mev protons. It is assumed here that the low-energy portions of the spectra are not changed by increasing the incident proton energy to 21.5 Mev, and that the high-energy portions extrapolate smoothly to 21.5 Mev after averaging over resonances (and, of course, neglecting the elastic peak in the proton spectra). The proton spectra for copper and aluminum obtained in this way are shown in Figs. 1 and 2. Figure 2 will be used in the analyses for the light elements ($A \lesssim 39$), and Fig. 1 will be used for the heavier elements.

The probabilities for secondary reactions can be seen from Fig. 1. The thresholds for (p,pn) and $(p,2p)$ reactions in copper are about 11 Mev and 6 Mev, respectively. Emission of a neutron following a (p,p) reaction will then be energetically possible if the proton is emitted with an energy less than 11 Mev below the maximum energy, or 10.5 Mev. The probability for this is therefore nearly equal to the area under the curve to the left of 10.5 Mev, divided by the total area under the curve; this is about 72%. If the proton is emitted with an energy between 10.5 and 15.5 Mev, emission of a second proton is energetically possible while emission of a neutron is not, so that a $(p,2p)$ reaction will occur (neglecting competition with alpha emission and electromagnetic de-excitation). The area under the curve between 10.5 and 15.5 Mev is about 13% of the total area, so that at least 13% of (p,p) reactions become $(p,2p)$. However, among the 72% where neutron emission is possible, proton emission will be energetically favored by 5 Mev and may therefore still compete effectively. Thus, of the total number of original (p,p) reactions, somewhat more than 13% become $(p,2p)$, somewhat less than 72% become (p,pn), and 15% remain (p,p). These results are, of course, sensitive to the energetic thresholds for the various reactions. For example, if the $(p,2p)$ threshold is higher than the (p,pn), the former reaction should occur only very rarely.

If the original reaction is a (p,n), an analysis similar to that above reveals that over 90% of the time, a $(p,2n)$ or a (p,np) reaction occurs A measurement of $(p,pn)+(p,2n)$ cross sections should therefore give the sum of nearly all of the original (p,n) cross section, plus much of the (p,p) cross section.

The only other reaction which can occur with appreciable probability is the (p,α) which at this energy is largely $(p,\alpha n)$ and $(p,\alpha p)$. This has been found[4] to have a cross section of about 150 mb or less in this mass region. Therefore, the sum of the $(p,pn)+(p,2n)$ and the $(p,2p)$ cross sections should add up to a large fraction of the total reaction cross section. If the predominant original reaction is (p,n), this must be true of the $(p,pn)+(p,2n)$ alone.

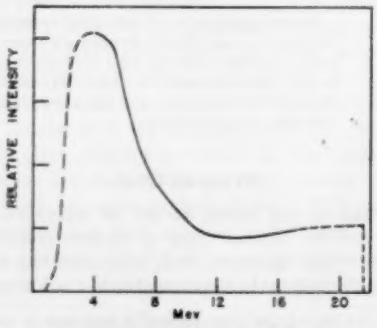

FIG. 2. Assumed energy distribution for 21.5-Mev protons inelastically scattered by aluminum. See caption for Fig. 1.

[1] P. C. Gugelot, Phys. Rev. **81**, 51 (1951).
[2] P. C. Gugelot, Phys. Rev. **93**, 425 (1954).
[4] D. J. Coombe (private communication).

For the lighter elements, the situation is somewhat different. Figure 2 indicates that an especially large number of high-energy protons are emitted, so that about 25% of the (p,p) reactions are not followed by further particle emission. In addition, the area where $(p,2p)$ reactions occur while (p,pn)'s are energetically forbidden is quite appreciable, making up about 25% of the total. Furthermore, Coulomb effects are not as strong here, so that $(p,2p)$ also competes effectively with (p,pn) in the remaining 50% of the cases where (p,pn) reactions are energetically possible. Thus, we might expect the total reaction cross sections, after the (p,α) and (p,n) contributions have been subtracted, to consist of about 25% (p,p), considerably more than 25% $(p,2p)$, and considerably less than 50% (p,pn).

EXPERIMENTAL

Cross sections for several $(p,pn)+(p,2n)$ and $(p,2p)$ reactions were measured with the internal, circulating 22-Mev proton beam from the ORNL 86-inch cyclotron. The methods have been described previously.[5] In all of the $(p,2p)$ reactions except those on Mg^{25} and Si^{29}, chemical separations were used. For $Zn^{68}(p,2p)Cu^{67}$ and for $Si^{29}(p,2p)Al^{28}$, it was found necessary to use separated isotopes.[6] The absorption corrections for the Cu^{67} activity were found to be very large—in fact, much larger than expected even from the very low beta energies involved—so that the uncertainty in that cross section is much larger than in the others. The end product of the reaction $Ca^{43}(p,2p)K^{42}$ can also be produced by a (p,He^3) reaction on the fifteen times more abundant isotope Ca^{44}, but the cross section for that has been measured[7] and found to be very small. A small correction has been applied.

The cross section for $Ni^{58}(p,2p)Co^{57}$ was measured relative to that for $Ni^{58}\{(p,pn)+(p,2n)\}Ni^{57}$ by radiochemically separating the nickel and cobalt fractions shortly after the bombardment and allowing 36-hour Ni^{57} to decay into Co^{57}. The relative amounts of Co^{57} in the two fractions was then determined by counting on the 130-kev gamma peak with a scintillation spectrometer.

The average error in these cross sections is about 7% as judged by reproducibility, but if one includes beta counting corrections, is probably about 20%. This does not include a possible error of about 15% in the absolute calibration of all cross sections.

RESULTS

The measured cross sections are listed in Table I. The Cr^{52}, Mn^{55}, Fe^{56}, Co^{59}, Cu^{63}, Cu^{65}, Zn^{64}, and Ga^{69} cross sections were taken from reference 5. In all other cases, the end product of the $(p,2n)$ reaction was allowed to decay into the same isotope as is produced by the (p,pn) reaction, and only the cross section for production of that isotope was measured. Table I also lists the energetic thresholds for the various reactions.

TABLE I. Summary of measured cross sections and energetic thresholds for various reactions.

Elements	Measured cross sections (mb) $(p,pn)+(p,2n)$	$(p,2p)$	Thresholds (Mev) (p,pn)	$(p,2p)$	$(p,2n)$	(p,n)
$_9F^{19}$	175	···	10.4	8.0	15.3	3.9
$_{11}Na^{23}$	225	···	12.7	9.1	17.8	4.8
$_{12}Mg^{25}$	···	54	7.6	12.6	~12	5.0
$_{14}Si^{29}$	···	110	8.7	11.8	~17	5.3
$_{15}P^{31}$	240	···	12.8	7.4	17.8	6.0
$_{17}Cl^{35}$	120[a]	···	13.6	6.6	18.6	6.3
$_{19}K^{39}$	105[a]	···	13.5	6.6	20.1	7.0
$_{20}Ca^{43}$	···	15	8.0	10.9	~13	3.8
$_{20}Ca^{44}$	···	5.0	11.6	12.7	14.5	4.4
$_{22}Ti^{48}$	<500[b]	···	15.2	11.4	22.6	~5
$_{24}Cr^{52}$	580	···	12.0	10.9	16.0	5.4
$_{25}Mn^{55}$	>620	···	10.3	8.2	10.4	0.9
$_{26}Fe^{54}$	165	···	14.1	9.7	22.4	~7.5
$_{26}Fe^{56}$	870	···	11.5	10.6	15.7	5.3
$_{26}Fe^{57}$	···	12.5	7.6	10.5	13.0	2.1
$_{27}Co^{59}$	>540	···	10.9	7.9	10.8	~1.0
$_{28}Ni^{58}$	240	680	11.9	8.0	20.6	~9
$_{29}Cu^{63}$	700	···	11.0	5.3	13.4	4.2
$_{29}Cu^{65}$	>500	···	10.4	6.9	10.5	2.1
$_{30}Zn^{64}$	675	···	12.0	7.7	~18	~6
$_{30}Zn^{66}$	920	···	10.8	8.7	~15	5.9
$_{30}Zn^{68}$	>780	3.8	8.9	8.7	10.7	3.6
$_{31}Ga^{69}$	730	···	10.4	6.8	11.0	4.1

[a] The cross sections observed were for the 34-minute and 7-minute activities for Cl^{34} and K^{38}, respectively. Recently, short-lived positron emitting isomers of these nuclei have been discovered, so that the values listed should be considered minima. The actual cross sections are probably about twice as large.

[b] The observed cross section on Ti^{48} includes the cross section for (p,α) reactions on two equally abundant isotopes and a $(p,\alpha n)$ reaction on a much more abundant isotope. They produce activities with about the half-life as that produced by $(p,pn)+(p,2n)$ on Ti^{46}.

In several cases, the activity of the end product of the $(p,2n)$ reaction has never been detected, so that there exists the possibility that its half-life may be very long rather than very short. In all of these cases but one (Zn^{64}), the ground-state mass can be calculated by assuming that the difference in mass between a nucleus with n protons and $(n+2)$ neutrons, and a nucleus with $(n+2)$ protons and n neutrons is due only to the Coulomb repulsion energy of the two additional protons in the latter. This method has been found to be accurate in explaining known masses, and successfully predicted the maximum beta energy of Ne^{18} before that isotope was discovered.[8] The results of this calculation indicate that in every case, the unobserved activity should be short lived. As a check, a search was made for possible long-lived activities in several of these isotopes. If the half-lives are assumed to be longer than two minutes and to be produced with cross sections equal to the (p,pn) cross sections, the following minimum half-lives are established[9]: Mg^{22}—10^7 years, A^{34}—10^5 years, Ca^{38}—

[5] B. L. Cohen and E. Newman, preceding paper [Phys. Rev. 99, 718 (1955)].

[6] Separated stable isotopes were obtained from the Stable Isotopes Division, Oak Ridge National Laboratory.

[7] H. G. Blosser (private communication).

[8] J. D. Gow and L. Alvarez, Phys. Rev. 94, 365 (1954).

[9] This work was done in collaboration with W. H. Jones, Oak Ridge Institute for Nuclear Studies research participant from Emory University.

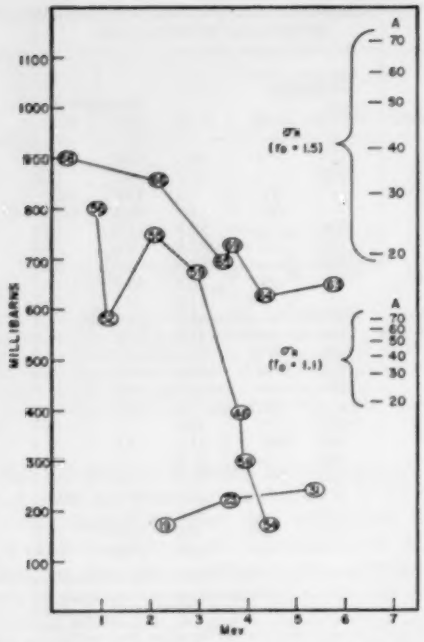

FIG. 3. $(p,pn)+(p,2n)$ cross sections *vs* excess energy available for $(p,2p)$ over (p,pn) reactions. Figures are mass numbers of target nuclei. Lines on right margin are theoretical total reaction cross sections for various masses and constants in the nuclear radius formula.

10^4 years. It therefore seems quite certain that the unknown activities actually are short lived.

CONCLUSIONS

In all six cases where the $(p,2p)$ threshold is higher than the (p,pn), the $(p,2p)$ cross sections from Table I are found to be relatively small, in agreement with the theory. The $(p,2p)$ cross section for Ni^{58} will be discussed below.

Figure 3 shows the $(p,pn)+(p,2n)$ cross sections from Table I plotted *vs* the energy by which the $(p,2p)$ energetic threshold is lower than that for (p,pn). In cases where only minimum values are listed in Table I, the extrapolation is based on the results of reference 5. In no case does this introduce an uncertainty greater than about 15 percent in the points on Fig. 3; this cannot affect the qualitative conclusions. Lines are shown connecting points with mass less than 40, with mass between 40 and 60, and with mass larger than 60. Figure 3 also shows σ_R for various masses and nuclear radii.

When one considers that the observed cross sections should be considerably smaller than σ_R, it is quite apparent (and will become more so when the $(p,2p)$ cross sections are considered below) that nuclear radii corresponding to r_0 equal to at least 1.5 are suggested from the heavy element data. Some of the advantages of determining the nuclear radius by the total reaction cross section have been discussed in a previous paper.[10]

It has been shown previously[5] that for most of the elements heavier than mass 52, (p,n) reactions [ordinarily detected as $(p,2n)$] are only minor contributors to the total reaction cross sections. It is immediately obvious from Fig. 3 that this is also true of all elements lighter than mass 52, and for masses 54 and 58 which were not covered in reference 5. This will be discussed further below.

In view of this result from reference 5, the data for the elements of mass 63–69 in Fig. 3 are in general agreement with the theoretical predictions. Some estimate of the effectiveness of competition from $(p,2p)$ reactions can be made by assuming that it is this competition which causes the lines through the data to slope downward to the right. By extrapolating the lines to zero abscissa, the value for the $(p,pn)+(p,2n)$ cross section, free of competition from $(p,2p)$, is obtained. For masses between 63 and 69, this is between 900 and 1000 mb. It therefore seems that the $(p,2p)$ cross sections for Cu^{63}, Cu^{65}, Zn^{64}, and Ga^{69} are about 200–300 mb. This represents about 20% of $\sigma_R-\sigma(p,\alpha)$, which is in agreement with the prediction of somewhat more than 13%.

The data for the elements of mass 19–39 are not as simple to analyze. The (p,α) cross sections make up an

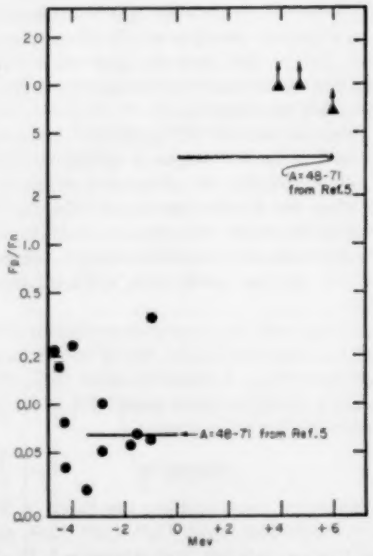

FIG. 4. Ratio of probabilities for emission of protons and neutrons *vs* difference in maximum energy available to them. Triangles are from 21.5-Mev proton data and circles are from 14-Mev neutron data, all in the mass range 16 to 41. Lines are from similar data in the mass range 48 to 71 from Fig. 2 of reference 5.

[10] G. H. McCormick and B. L. Cohen, Phys. Rev. **96**, 722 (1954).

appreciable fraction of σ_R, and they probably vary considerably from element to element. They should be especially large for F^{19} and Na^{23} because they lead to very high energy releases for these isotopes. It is, therefore, difficult to extrapolate the line through the data to zero abscissa. The data certainly agree, however, with the theoretical prediction that $\sigma(p,pn)$ is considerably less than 50% of $\sigma_R-\sigma(p,\alpha)$. For F^{19}, Na^{23}, and P^{31}, it may be estimated as about 30% of this difference.

This data for the light elements can be used to extend the thesis of reference 5 that proton emission is much more probable in 21-Mev proton-induced reactions than in 14-Mev neutron-induced reactions. In view of the very large $(p,2p)$ cross sections, a considerable fraction ($\gtrsim\frac{1}{3}$) of the activity produced by $(p,pn)+(p,2n)$ reactions must be due to (p,pn) rather than to (p,np) or $(p,2n)$. Figure 4 shows a plot of F_p/F_n, the relative probabilities for emission of protons and neutrons, in the original reaction, plotted *vs* the difference in energy available for proton and neutron emission. The 14-Mev neutron data from the (n,p) cross section measurements of Paul and Clarke[11] are also shown. Figure 2 of reference 5 is a similar plot of data for the region of masses 48–71; the lines through the data from that figure are also shown in Fig. 4. It seems quite clear that the conclusion of reference 5—that even after correcting for energetic differences, F_p/F_n is considerably larger at 21.5 Mev than at 14 Mev—is also valid in the lighter mass region.

It should be noted that the very small $(p,pn)+(p,2n)$ cross sections found in the light elements are in agreement with neutron yield measurements.[12] For 23-Mev protons bombarding thick targets of both magnesium and aluminum, only about one neutron was observed for every four nuclear reactions.

For the elements between mass 46 and 59, one would expect cross sections similar to those found in the heavier elements since the Coulomb barriers and energy distributions of emitted particles[2,3] are about the same for the two groups. This expectation is reasonably well fulfilled for Cr^{52}, Mn^{55}, Fe^{56}, and Co^{59}, and the somewhat lower value for Ti^{46} might be explained by the facts that it is the lightest isotope of the group and has a very high (p,pn) threshold. For Fe^{54} and Ni^{58}, on the other hand, the observed cross sections are very much lower than can be easily explained. Fortunately, the $(p,2p)$ cross section in Ni^{58} is measurable (see Table I),[13] so that it is definitely established that the low value of the $(p,pn)+(p,2n)$ cross section is due to competition with the $(p,2p)$. This cannot be explained by a difference in the energy spectrum of the emitted particles (these were measured in references 2 and 3). One possibility that perhaps should not be overlooked is that Ni^{57} and Fe^{53} may have short-lived isomers which decay by positron emission. This could also explain why the activation cross section for $Ni^{58}(n,2n)Ni^{57}$ was also found[11] to be very much smaller than expected.

The two most important conclusions of this paper may be summarized as follows:

1. The conclusion of reference 5, that even after correcting for energetic differences, F_p/F_n is many times larger in 21.5-Mev proton-induced reactions than in 14-Mev neutron-induced reactions, is apparently verified and extended to the mass region 19 to 39. It should be noted, however, that this verification is based wholly on cases where proton emission is strongly favored energetically. Such was not the case in reference 5.

2. $(p,2p)$ cross sections are apparently very much larger than might have been expected from elementary barrier penetration considerations. For some of the heavier nuclei (mass 59–69) they are about 200–300 mb, for all of the lighter nuclei (mass 19–52) they are at least that large and in some cases much larger, for Fe^{54} the cross section is probably well over 500 mb, and for Ni^{58} it has been measured to be 680 mb. In general, these large cross sections are explained by more or less conventional methods if conclusion 1 above and Gugelot's measurements[3] of energy distributions of inelastically scattered protons are assumed; but the two most extreme cases, Fe^{54} and Ni^{58} are still very difficult to explain.

ACKNOWLEDGMENTS

The authors would like to acknowledge some very helpful discussions with J. D. Gow (University of California Radiation Laboratory) and J. A. Martin, and the continuous encouragement of R. S. Livingston.

[11] E. B. Paul and R. L. Clarke, Can. J. Phys. **31**, 267 (1953).
[12] B. L. Cohen, Phys. Rev. **98**, 49 (1955).
[13] The large $(p,2p)$ cross section in Ni^{58} was previously found by Martin, Green, and Lyon (private communication).

Decay of Sc^{47}

W. S. Lyon and Bernd Kahn*
Oak Ridge National Laboratory, Oak Ridge, Tennessee
(Received April 18, 1955)

Sc^{47} was milked from Ca^{47}, prepared by proton irradiation of CaO, and its radiations were studied by coincidence and gamma-ray spectrometry. Sc^{47} was found to decay with the emission of beta rays of 0.46 ±0.02 and 0.62±0.03 Mev maximum energy. 66±3% of the decay is accompanied by a 0.157±0.007 Mev gamma ray in coincidence with the 0.46-Mev beta rays.

THE radioisotope Sc^{47} was studied to determine its decay scheme, since recent published values (see Table I) show considerable disagreement in the energy values of the beta and gamma components.[1–4] Knowledge of the decay scheme is of special interest because the radioisotope appears to have a relatively simple decay scheme, an almost unconverted gamma ray, beta-gamma coincidences permitting determination of its activity, and a half-life of several days. When the gamma/beta ratio is known, it may be used in the calibration of gamma detectors for the elucidation of decay schemes involving gamma rays of low energy.

PROCEDURE AND DISCUSSION

Calcium oxide was irradiated with 14-Mev protons in the ORNL 86-inch cyclotron. Following irradiation, the CaO was dissolved in nitric acid and the *p*H of the solution adjusted to between 1 and 2 by the addition of dilute sodium hydroxide. The product scandium, and the trivalent radioisotopes which resulted from the irradiation of strontium and barium impurities, were removed by repeated extractions with 0.5*M* thenoyltrifluoroacetone (TTA) in xylene.[5] Identified in the organic fraction were Sc^{43}, Sc^{44}, Sc^{46}, Sc^{47}, and Sc^{48}, which are known to be produced by proton bombardment of calcium.

The aqueous solution was made slightly acid and heated, saturated oxalic acid added, and the solution cooled. The precipitated calcium oxalate was filtered, washed, dissolved in dilute HCl, and the calcium oxalate reprecipitated. The calcium oxalate was then ignited to calcium oxide in a furnace. A portion of this precipitate was examined daily with a 3 in.×3 in. NaI(Tl) gamma-ray spectrometer to follow the growth of the 157-kev photopeak from Sc^{47}.

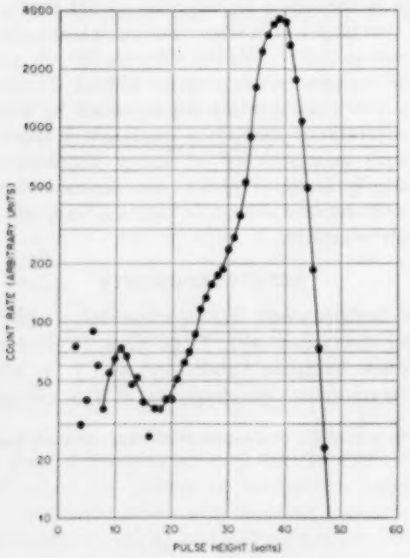

FIG. 1. Gamma-ray spectrum of Sc^{47}.

TABLE I. Previously reported decay data for Sc^{47}.

Beta energy (Mev)	γ energy (Mev)	Comments	Ref.
0.622 (34±4%)[a]	0.185±0.007[b,c]	(0.434β–0.185γ) Coinc.	1
0.434 (66±4%)[a]			
0.64±0.03 (100%)[d]	0.159.5[b,c,e]	(0.64 β–0.160γ) Coinc.	2
0.286 (28%)[d]	0.218[e]		3
0.490 (72%)			
0.52[f]	0.16[b]	γ/β=5/4	4

[a] Lens spectrometer.
[b] Scintillation spectrometer.
[c] Conv. e^--spectrometer.
[d] Double-focusing magnetic spectrometer.
[e] Photoelectron spectrometer.
[f] Al absorption data.

After one week, the precipitate was dissolved, its *p*H adjusted to between 1 and 2, and the Sc^{47} extracted with 0.5*M* TTA in xylene. The organic fraction was washed three times with water at *p*H 1.5, and the Sc^{47} was extracted from the organic phase with 2*M* nitric acid. Aliquots of this solution were used in the subsequent measurements.

The decay of Sc^{47} was followed for 20 days with an end-window Geiger-Müller beta counter, with a well-type gamma scintillation counter, and with a gamma

* Robert A. Taft Sanitary Engineering Center, U. S. Public Health Service, on assignment to Health Physics Division, Oak Ridge National Laboratory.
[1] L. S. Cheng and M. L. Pool, Phys. Rev. **90**, 886 (1953).
[2] Cork, Leblanc, Brice, and Nester, Phys. Rev. **92**, 367 (1953).
[3] Luis Marquez, Phys. Rev. **92**, 1511 (1953).
[4] Aten, Greuell, and Van Dijk, Physica **19**, 1049 (1953).
[5] A. Broido, U. S. Atomic Energy Commission Report AECD-2616, 1947 (unpublished).

spectrometer adjusted to count only the photoelectric peak from the 0.157-Mev gamma ray. A 3.45±0.10 day half-life was obtained by these counting methods.

Beta-gamma coincidence measurements, using a proportional counter for beta detection and a 3 in. ×3 in. NaI(Tl) crystal spectrometer as the gamma detector, indicated that a gamma ray was in coincidence with a beta group. The slope of the absorption curve, using aluminum before the beta detector, yielded a maximum beta energy of 0.46±0.02 Mev for this group. From range measurements, a maximum energy of 0.62±0.03 Mev was obtained for the non-coincident beta group. The energy of the gamma ray was found to be 12 kev higher than that of Ce^{141},

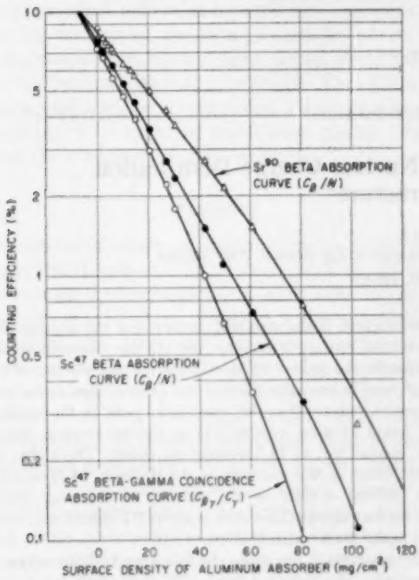

FIG. 2. Variation of β counting efficiency of Sc^{47} and Sr^{90} as a function of aluminum absorber.

indicating an energy of 0.157±0.007 Mev. No other gamma ray was found.

The number of gamma rays per disintegration was obtained in two ways. One method consisted of determining the number of gamma rays by absorption in the 3 in.×3 in. NaI(Tl) crystal, and determining the total disintegrations by 4π-coincidence counting. Using attentuation coefficients for 0.15-Mev gamma rays,[6] and integrating graphically, the total absorption was computed to be 92%, and the photoelectric absorption 88%. Since the total area under the curve in Fig. 1 includes counts contributed by degraded radiation scattered into the crystal from the surroundings, only the area under the photoelectric peak was measured.

[6] G. R. White, National Bureau of Standards Report 1003, 1952 (unpublished).

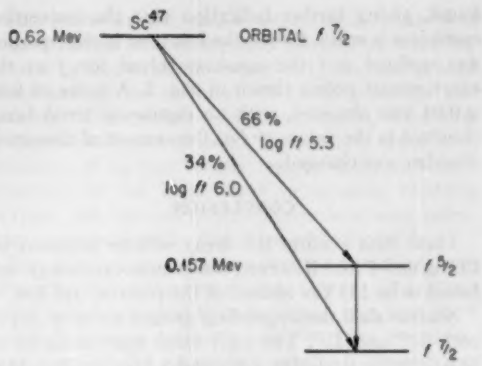

FIG. 3. Decay scheme of Sc^{47}.

The gamma disintegration rate, N_γ, was found by

$$N_\gamma = C_\gamma/[\epsilon\omega(1-m_I)(1-m_a)], \quad (1)$$

where C_γ is the gamma count rate calculated from the area under the photoelectric peak, ϵ is the fraction of gamma rays entering the crystal which are completely absorbed by photoelectric absorption (0.88) and by multiple processes (assumed to be 0.01), ω is the fraction of the angle subtended at the source by the crystal (0.262), m_I is the fraction of escaping iodine x-rays (0.014), and m_a is the fraction of gamma rays absorbed in the beryllium beta absorber, the aluminum container, and the magnesium oxide reflector (0.041). The ratio of gamma rays to total activity was thus found to be 0.66±0.03.

In the second method, the gamma/beta ratio, f, was calculated from $\beta-\gamma$ coincidence data, by using the equation

$$\frac{C_{\text{beta}}C_{\text{gamma}}}{C_{\beta-\gamma}N} = f\left(1-\frac{e_{\beta 2}}{e_{\beta 1}}\right)+\frac{e_{\beta 2}}{e_{\beta 1}}+c\left(\frac{e_e}{e_{\beta 1}}-e_e\right), \quad (2)$$

where the C's are count rates, N is the disintegration rate, c is the ratio of conversion electrons to total activity, and e is the counting efficiency for the two beta groups and the conversion electrons. The efficiency of the weak beta group, $e_{\beta 1}$, is the ratio of coincidence to gamma counts shown in Fig. 2. In evaluating $e_{\beta 2}$, the efficiency of the strong beta group, the counting efficiency of Sr^{90} (maximum beta energy 0.6 Mev), was used. The Sr^{90} was separated from its Y^{90} daughter and its activity determined by absolute beta counting. An approximate value of c can be found by extrapolating the values of C to zero absorber, in which case $e_{\beta 1}$ equals $e_{\beta 2}$, and the first term on the right-hand side in Eq. (2) is eliminated, while the second equals unity. In repeated determinations, the value of the left-hand side of the equation is 1.00, indicating that c is very small. A search for titanium x-rays was made with an argon-methane filled proportional counter spectrometer, but none were

found, giving further indication that the conversion coefficient is small. Hence, the last term in the equation was omitted and the equation solved for f at the experimental points shown in Fig. 2. A value of 0.68 $\pm$0.04 was obtained, with no significant trend being observed in the values of f as the amount of aluminum absorber was changed.

CONCLUSION

These data confirm the decay scheme proposed by Cheng and Pool.[1] However, the gamma-ray energy was found to be 157 kev instead of the reported 185 kev.

Nuclear shell theory predicts ground states of $f_{7/2}$ in both Sc^{47} and Ti^{47}. The logft value was calculated to be 6.0 for the 0.62-Mev β ray and 5.3 for the 0.46-Mev β ray. These logft values indicate[7] that both beta groups fall in the $\Delta I=0$, 1 (no) allowed classification. A level scheme consistent with these data is shown in Fig. 3. The assignment of $f_{5/2}$ to the excited state in Ti^{47} would thus make the 157-kev gamma a magnetic dipole transition. The only reported conversion coefficient,[1] 3.6×10^{-3}, falls within the range predicted for either electric or magnetic dipole.[8]

ACKNOWLEDGMENTS

The authors are indebted to Farno Green, who suggested the problem and supervised the irradiations.

[7] Mayer, Moszkowski, and Nordheim, Revs. Modern Phys. **23**, 315 (1951).

[8] M. E. Rose *et al.*, Phys. Rev. **83**, 79 (1951).

PHYSICAL REVIEW VOLUME 99, NUMBER 3 AUGUST 1, 1955

Fission of U^{235} by 14-Mev Neutrons: Nuclear Charge Distribution and Yield Fine Structure*

ARTHUR C. WAHL†
University of California, Los Alamos Scientific Laboratory, Los Alamos, New Mexico

(Received December 20, 1954)

The following results were derived from experiments in which iodine was quickly separated from irradiated uranium metal at a known time after irradiation. The fractional chain yields are based on the cumulative chain yields at iodine.

	Ratio of cumulative yields, 14-Mev/thermal neutron fission	Fractional chain yield 14-Mev	Thermal
I^{131}	1.48 $\pm$0.07	<0.08	<0.01
Te^{131m}	5.5 $\pm$1.5	0.35 $\pm$0.05	<0.05
Te^{131}	...	<0.30	<0.03
I^{132}	1.12 $\pm$0.02	0.16 $\pm$0.01	<0.01
Te^{132}	0.97 $\pm$0.02	...	...
I^{133}	0.81 $\pm$0.03	<0.40	<0.05
Te^{133m}	0.64 $\pm$0.15	...	...
Te^{133}	...	<0.40	<0.1
I^{134}	0.65 $\pm$0.02	0.43 $\pm$0.02	0.11 $\pm$0.02
I^{135}	0.69 $\pm$0.02	...	...

The error given is the standard deviation of the average of the experimental results; it does not include the 4 percent standard deviation for the ratio of 14-Mev to thermal neutron fission yields of Mo^{99} used in the calculation of the ratio of cumulative yields. The results indicate that the pronounced peak in the mass-yield curve found at mass number 134 in thermal-neutron fission is nearly washed out in 14-Mev-neutron fission. The higher independent yields of late members of the chains in 14-Mev-neutron fission indicate a shift toward stability of the most probable initial nuclear charge. This shift is about 0.7 charge unit for the chains in the mass region studied.

As by-products of the work, the following half-life values were determined: I^{133}, 20.9$\pm$0.3 hour; I^{132}, 2.30$\pm$0.05 hour; fission precursor of I^{135}, <0.4 minute.

INTRODUCTION

THIS paper presents the results of experiments carried out during the summer of 1951. Prior to the start of this work, Ford and Gilmore[1] had measured the relative cumulative 14-Mev and thermal-neutron yields of I^{131}, and Glendenin[2] had reported values for the independent yields of I^{134} and I^{133} formed in thermal-neutron fission. Pappas,[3,4] in determining the thermal-neutron fission yields of the antimony, tellurium, and iodine isotopes, also obtained a value for the independent yield I^{132}(+2-min Te^{132}).

The general procedure followed was to irradiate for a short time a stack of two or more pieces of uranium metal in a flux of 14-Mev or thermal neutrons. One piece was dissolved immediately after the irradiation, and the iodine quickly separated. The iodine activities in this sample, corrected for the small growth from

* This work was performed under the auspices of the U. S. Atomic Energy Commission.

† Department of Chemistry, Washington University, St. Louis, Missouri.

[1] G. P. Ford and J. S. Gilmore (private communication from the Los Alamos Scientific Laboratory).

[2] L. E. Glendenin, Technical Report No. 35, Laboratory for Nuclear Science, Massachusetts Institute of Technology, 1949 (unpublished).

[3] A. C. Pappas, Technical Report No. 63, Laboratory for Nuclear Science, Massachusetts Institute of Technology, 1953 (unpublished).

[4] A. C. Pappas, Progress Report, Laboratory for Nuclear Science, Massachustetts Institute of Technology, May, 1951 (unpublished).

antimony and tellurium precursors, gave a measure of the independent yields of the iodine isotopes. A second sample was dissolved and the iodine separated after the bulk of the antimony and tellurium precursors had decayed. The activities in this sample, after application of appropriate growth and decay corrections, gave a measure of the cumulative yields of the iodine isotopes.

EXPERIMENTAL METHODS

Irradiations

Thermal-neutron irradiations were carried out in the Los Alamos Homogeneous and Fast Reactors. For irradiations of less than one minute duration, the stacked uranium foils were injected into and out of an operating reactor by use of a pneumatic rabbit. The 14-Mev neutron irradiations were carried out in the Los Alamos Cockcroft-Walton accelerator. The $T(d,n)He^4$ reaction produced the fast neutrons. Two approximately 3-gram pieces of uranium metal were placed directly behind the tritium-zirconium target.

Chemistry

An irradiated piece of uranium metal (~0.3 g or ~3 g) was dissolved in a mixture of 5 or 10 ml of concentrated hydrochloric acid and 2.00 ml of KI carrier solution (20.0 mg of iodine). (The larger volume of hydrochloric acid, and of water and hydrogen peroxide used later, was for the ~3-gram samples.) The dissolving took place in an open-top separatory funnel fitted with a centrifugal stirrer. After solution was complete, 5 or 10 ml of water and 25 ml of carbon tetrachloride were added, the stirrer started, and 1.5 or 7 ml of 1 *f* H_2O_2 was added in a slow stream. The hydrogen peroxide oxidized the U^{+3}, formed on solution of the metal, to a mixture of U^{+4} and UO_2^{++} and most of the I^- to I_2, which was extracted into the carbon tetrachloride. The stirrer was stopped, and as the phases separated the carbon tetrachloride phase was drained into another separatory funnel.

The time the stirrer was stopped was taken as the time of separation of the iodine isotopes from their tellurium precursors. This time is in error by no more than 30 seconds since the stirrer was stopped within 30 seconds after the start of the hydrogen peroxide addition, and the phase separation was completed within 30 seconds after the stirrer was stopped. For the ~0.3-gram samples, these times were about 15 seconds.

The aqueous phase containing the uranium and the bulk of the fission products was treated with excess hydrogen peroxide and with bromine. The resulting solution was used for the Mo^{99} determination,[5] which gave a measure of the number of fissions.

[5] I wish to thank C. O. Minkkinen and J. S. Gilmore for running the Mo^{99} determinations.

The iodine in the carbon tetrachloride phase was back-extracted into an aqueous solution of $NaHSO_3$, purified by two oxidation-reduction cycles, and precipitated as AgI for chemical yield determination and counting. The oxidation-reduction cycles, consisting of $NaNO_2$ oxidation of iodide ion in dilute nitric acid, extraction of I_2 into carbon tetrachloride, and back extraction of the iodine into an aqueous $NaHSO_3$ solution, and the precipitation procedure were essentially those outlined by Glendenin and Metcalf.[6]

The decay of the gamma activity of a sample was followed on a scintillation counter through 11.7 g/cm² of lead, which absorbed the soft gamma rays from Xe^{133} and Xe^{135} growing from I^{133} and I^{135}. After five days, when most of the xenon had grown, a sample was dissolved by digesting it along with the filter paper and Scotch tape cover for about 15 minutes in concentrated ammonium hydroxide containing metallic zinc. After reduction of silver iodide to silver was complete, the solution was acidified and boiled to remove any remaining xenon, and the iodine carried through another oxidation-reduction cycle. It was precipitated as AgI as before, the chemical yield determined, and the precipitate mounted for counting under 5 mils of aluminum. This aluminum cover plus the 0.7-mil aluminum window on the beta-proportional counter absorbed most of the soft beta particles and electrons from Xe^{133} and Xe^{131m} so that the beta-decay curve was easily resolved into its I^{133} and I^{131} components. It is estimated that <5 percent of the long-lived activity attributed to I^{131} could have been due to xenon.

A coincidence correction of 1 percent per 10^5 counts/min was applied to the counting data.

Uranium metal was used with the expectation[7] that radioactive iodine isotopes formed in the uranium metal would exchange readily and completely with the iodide ion carrier present during the solution process. This point was checked experimentally. A stack of four uranium metal foils were irradiated with thermal neutrons. Two of the foils were worked up for iodine by the method described in the previous paragraphs; two were carried through additional steps designed to further exchange. Oxidation in alkaline solution of I^- to IO_4^- by ClO^- was carried out as recommended by Glendenin and Metcalf,[6] and reduction in acid of the IO_4^- to I^- by H_2SO_3 and precipitation of PdI_2 was included as recommended by Ford and Gilmore.[1] The decays of the four samples mounted as AgI were followed under lead on the scintillation counter, and the decay curves were resolved into their I^{131}, I^{133}, and I^{135} components. The results summarized in Table I

[6] L. E. Glendenin and R. P. Metcalf in *Radiochemical Studies: The Fission Products*, edited by C. D. Coryell and N. Sugarman (McGraw-Hill Book Company, Inc., New York, 1951), Paper No. 278, National Nuclear Energy Series, Plutonium Project Record, Vol. 9, Div. IV, p. 1625.

[7] Katcoff, Dillard, Finston, Finkle, Seiler, and Sugarman, Paper No. 280, p. 1635 of reference 6.

TABLE I. Exchange tests.

	Counts/min per mg U		
	From metal solution only	From alkaline oxidation	Ratio
I^{135}	1068, 1065	1072, 1083	0.99
I^{134}	243, 242	244, 248	0.99
I^{131}	3.34, 3.39	3.45, 3.50	0.97

show that, as expected, exchange is essentially complete during the solution process.

Resolution of Decay Curves

Decay curves were resolved by fitting the experimental points with lines of the correct slope. The half-life values[1,3,9–12] used are given in the second column of Table II. They and the values obtained by drawing the best line through the points agree within the ~1 percent error estimated for the latter. The 20.9-hour value for I^{133} was determined by following the decay over about 10 half-lives on the beta-proportional counter through 145 mg/cm² of aluminum to minimize the I^{131} component. The value agrees well with the 20.8-hour value reported by Katcoff and Rubinson.[13]

The beta-decay curves were easily resolved into their 8.07-day I^{131} and 20.9-hour I^{133} components. In order to subtract the I^{131} and I^{133} components from the gamma-decay curves, the relative counting efficiencies of these nuclides on the beta-proportional and scintillation counters were determined by following the decay of four remounted samples on both counters. In calculating the curves to be subtracted, the different chemical yields of the original and remounted samples had to be considered.

The 2.3-hour I^{132} activity which had grown from 77.7-hour Te^{132} before the tellurium-iodine separation was also subtracted from the gamma-decay curve. This activity was calculated from the I^{132} activity in equilibrium with Te^{132} 113 hours after the irradiation (samples *F3-A* and *B*, *T3-A* and *B*).

The residual gamma-decay curve consisted of the 52.5-minute I^{134}, the independently formed 2.3-hour I^{132}, and the 6.7-hour I^{135} activities. The I^{135} component was easily resolved and subtracted, but the remaining mixture of I^{134} and independently formed I^{132} activities was difficult to resolve by the usual method of drawing a line with a 2.3-hour half-life through the oldest points. Therefore, a method suggested by Ford[14] was employed, in which the activity at time t, $A(t)$, multiplied by $e^{\lambda_{132}t}$ is plotted against $e^{-(\lambda_{134}-\lambda_{132})t}$ as shown in Fig. 1. As seen from Eq. (2), the slope of the straight line gives the value of A^0_{134}, and the intercept gives the value of A^0_{132}.

$$A(t)=A^0_{134}e^{-\lambda_{134}t}+A^0_{132}e^{-\lambda_{132}t}. \quad (1)$$

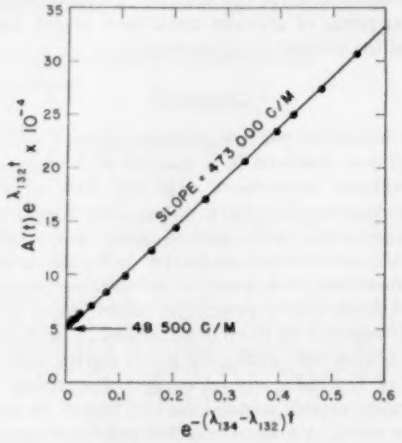

FIG. 1. Resolution of 52.5-min I^{134} and 2.3-hr I^{132} (independently formed) activities in sample *F2-A*. t is the time interval after the mean time of irradiation.

Division by $e^{-\lambda_{132}t}$ gives

$$A(t)e^{\lambda_{132}t}=A^0_{134}e^{-(\lambda_{134}-\lambda_{132})t}+A^0_{132}. \quad (2)$$

For thermal-neutron fission, there was no measurable amount of I^{132} formed independently, as was shown by the small positive and negative values of the intercepts. A^0_{134} for the samples from thermal-neutron fission was therefore determined from the slope of the best line passing through zero.

Typical resolved gamma- and beta-decay curves are reproduced in Figs. 2 and 3. A count was taken every 15 minutes for the first six hours, but due to space limitations, only the points at 30-minute intervals are shown in Fig. 2.

TABLE II. Half-life values.

Isotope	Used in resolution	Obtained from data
I^{135}	6.7 hr[a,b]	6.75 hr
I^{134}	52.5 min[c]	52.4 min
I^{133}	20.9 hr	20.9 hr
I^{132}	2.3 hr[d,e]	2.30 hr
I^{131}	8.07 days[f,g]	8.0 days

[a] See reference 8.
[b] See reference 9.
[c] See reference 3.
[d] See reference 10.
[e] See reference 11.
[f] See reference 1.
[g] See reference 12.

[8] L. E. Glendenin and R. P. Metcalf, Paper No. 140, p. 992 of reference 6.
[9] S. Katcoff, Dillard, Finston, Finkle, Seiler, and Sugarman, Paper No. 141, p. 1005 of reference 6.
[10] J. S. Gilmore (private communication from the Los Alamos Scientific Laboratory).
[11] O. Hahn and F. Strassmann, Naturwiss. **27**, 451 (1939).
[12] Selger, Cavallo, and Culpepper, Phys. Rev. **90**, 443 (1953).
[13] S. Katcoff and W. Rubinson, Phys. Rev. **91**, 1458 (1953).
[14] G. P. Ford (private communication from the Los Alamos Scientific Laboratory).

Data

The activity, corrected for chemical yield, of each iodine isotope at the time of the tellurium-iodine separation was divided by the Mo^{99} activity at the mean irradiation time.[15] This ratio, D, is proportional to the number of iodine atoms per fission that were present at the time of the tellurium-iodine separation. The proportionality constant is of course different for each iodine isotope because of different counting efficiencies and decay constants; it also is different for fission by thermal and 14-Mev neutrons since the Mo^{99} yield is different.[16] For independently formed I^{132} and for I^{134}, for which there is no precursor of measurable half-life, it was more convenient to extrapolate the activity to the mean time of irradiation[15] and divide by the Mo^{99} activity to give a ratio denoted by d.

The data are summarized in Table III. Uranium containing >90 percent U^{235} was used in all of the 14-Mev runs and in thermal run $T6$. Normal uranium was used in the other thermal-neutron runs. Approximately 3 g samples were used in runs $T1$ and $T3$ so that the chemistry would be the same as for the 14-Mev runs. Also these runs were timed to match approximately the 14-Mev runs.

It was not possible to maintain a constant flux of 14-Mev neutrons. For runs $F1$ and $F2$ the average flux over one-minute intervals deviated as much as 30 percent from the six-minute average, the mean deviation being 10 and 15 percent, respectively. For run $T1$ the power of the Fast Reactor was varied at one-minute intervals to match the fluctuation of flux in run $F1$. The matching of runs $F1$ and $T1$ was done to maximize the cancellation of errors in comparison of 14-Mev and thermal-neutron fission yields.

The assumption is made in the calculations that follow that the neutron flux was constant. Although this is only approximately true for the 14-Mev irradiations, the approximation causes no apprecialbe error. All of the iodine isotopes studied and most of their precursors have half-lives long compared to the irradiation times. For these the uniformity of the flux is not important. Since a large fraction of the two short-lived precursors, 4.4-m Sb^{133} and 2-m Te^{133}, decayed during the time interval between the end of the irradiation and the tellurium-iodine separation, it is not highly important when during the irradiation they were formed.

CALCULATIONS AND RESULTS

Equations and Definitions

The equations developed below are adopted from the standard equations of radioactive transformation. A

[15] When the irradiation time T is short compared to the half-life of a product, the simplifying approximation can be made that $(1-e^{-\lambda T})/\lambda T = e^{-\lambda T/2}$, which corresponds physically to an infinitely short irradiation occurring at time $T/2$. If the irradiation time is $\frac{1}{4}$ of a half-life, the approximation is in error by less than 0.1 percent.

[16] Terrell, Scott, Gilmore, and Minkkinen, Los Alamos Scientific Report LADC-1463 (1953).

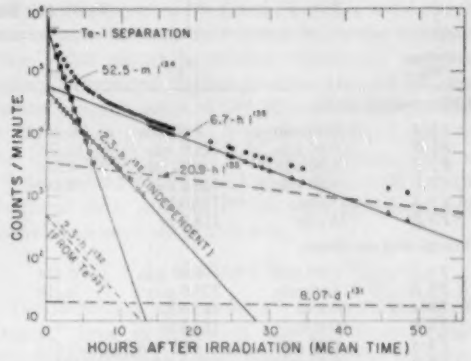

FIG. 2. Gamma-decay curve of sample $F2$-A followed on the scintillation counter through 11.7 g/cm² of Pb.

useful general equation given by Rubinson[17] for the nth member of decay chain whose first member is formed at a constant rate, r, for time, T, is

$$\lambda_n N_n = r\sum_{i=1}^{n} b_i(1-e^{-\lambda_i T})(e^{-\lambda_i t}),$$
$$b_i = \prod_{j\neq i} \frac{\lambda_j}{\lambda_j-\lambda_i} \quad (j=1,2,\cdots,n), \tag{4}$$

where t = time after end of irradiation, N = number of atoms, and λ = decay constant.

Consider the following fission-product chain in which member C has a cumulative yield of Y_C, and x, y, and z are the fractional chain yields based on Y_C ($x+y+z=1$).

$$\begin{array}{ccccc} & x & & y & & z & \\ & \downarrow\lambda_A & & \downarrow\lambda_B & & \downarrow\lambda_C & \\ A & \rightarrow & B & \rightarrow & C & \rightarrow. \end{array}$$

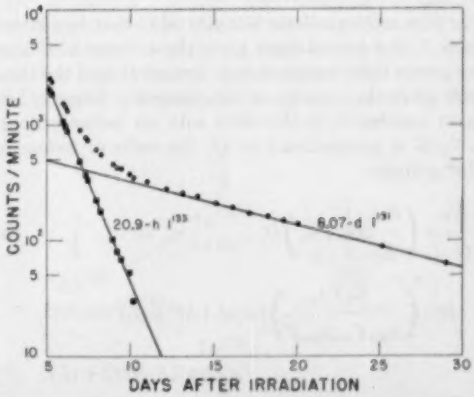

FIG. 3. Beta-decay curve of sample $F2$-A followed on the beta-proportional counter through 40 mg/cm² of Al.

[17] W. Rubinson, J. Chem. Phys. 17, 542 (1949).

TABLE III. Summary of data.*

Sample No.	T	t	$d_{I^{131}}$	$D_{I^{131}}$	$D_{I^{131}}$	$D_{I^{131}}$ (from Te^{131m})	$d_{I^{131}}$ (independent)	$D_{I^{131}}$
14-Mev-neutron fission								
F1-A	6.00 min	8.60 min	0.332	2.457	0.840	(0.0026)	0.284	0.0053
F1-B	6.00 min	125.0 min	(0.335)	1.394	1.722	(0.0221)	0.316	0.0290
F2-A	6.00 min	9.10 min	0.333	2.384	0.895	(0.0028)	0.287	0.0056
F2-B	6.00 min	125.3 min	0.339	1.372	1.804	(0.0222)	0.283	0.0302
F3-A	75 min	112.8 hr	···	···	0.0532	0.01711	···	0.0379
F3-B	75 min	112.8 hr	···	···	0.0513	0.01683	···	0.0341
Thermal-neutron fission								
T1-A	6.00 min	8.60 min	0.414	1.619	0.581	(0.0023)	0.016	0.00142
T1-B	6.00 min	125.0 min	0.412	2.137	1.799	(0.0193)	−0.014	0.0236
T3-A	60 min	112.5 hr	···	···	0.0548	0.01484	···	0.0207
T3-B	60 min	112.5 hr	···	···	0.0542	0.01485	···	0.0200
T4-A	0.17 min	1.83 min	0.413	0.837	0.109	(0.0004)	0.013	<0.0005
T4-B	0.17 min	120.6 min	0.417	2.245	1.811	(0.0185)	−0.012	0.0237
T5-A	0.42 min	2.20 min	0.411	0.896	0.139	(0.0005)	0.012	<0.0003
T5-B	0.42 min	4.45 min	0.404	1.044	0.250	(0.0009)	0.005	<0.0006
T5-C	0.42 min	181.8 min	0.400	1.244	1.846	(0.0244)	−0.016	0.0271
T6-A	0.25 min	8.50 min	···	···	0.457	···	···	0.00096
T6-B	0.25 min	15.75 min	···	···	0.726	···	···	0.00249

* T = duration of irradiation. t = time interval between end of irradiation and tellurium-iodine separation. d = ratio of iodine to Mo^{99} activity at mean irradiation time, activities corrected for chemical yield. D = ratio of iodine activity at time of tellurium-iodine separation to Mo^{99} activity at mean irradiation time, activities corrected for chemical yield. ( ) = value calculated from other data and used in resolution of the decay curve.

If a total of G fissions occur at a uniform rate during irradiation time T, the activity of C at time t after the irradiation is given by Eq. (5).[13]

$$\lambda_C N_C = (GY_C/T)\{x(aJ+bK+cL) + y(\mathfrak{b}K+\mathfrak{c}L)+zL\}, \quad (5)$$

$$J=(1-e^{-\lambda_A T})(e^{-\lambda_A t}),$$
$$K=(1-e^{-\lambda_B T})(e^{-\lambda_B t}),$$
$$L=(1-e^{-\lambda_C T})(e^{-\lambda_C t}),$$
$$a=\lambda_B\lambda_C/(\lambda_B-\lambda_A)(\lambda_C-\lambda_A),$$
$$b=\lambda_A\lambda_C/(\lambda_A-\lambda_B)(\lambda_C-\lambda_B),$$
$$c=\lambda_A\lambda_B/(\lambda_A-\lambda_C)(\lambda_B-\lambda_C),$$
$$\mathfrak{b}=\lambda_C/(\lambda_C-\lambda_B),$$
$$\mathfrak{c}=\lambda_B/(\lambda_B-\lambda_C).$$

The first term gives the activity of C that has grown from A, the second term gives the activity of C that has grown from independently formed B, and the third term gives the activity of independently formed C. If chain member C is identified with an iodine isotope, $\lambda_C N_C/G$ is proportional to D, the ratio of iodine to Mo^{99} activity.

$$\frac{\lambda_C N_C}{G}=\left(\frac{E_{Mo}}{E_C}\lambda_{Mo}Y_{Mo}\right)D, \quad (6)$$

$$D=\left(\frac{E_C Y_C}{E_{Mo}Y_{Mo}\lambda_{Mo}T}\right)\{x(aJ+bK+cL) + y(\mathfrak{b}K+\mathfrak{c}L)+zL\}, \quad (7)$$

where E represents the counting efficiency.

For two samples irradiated together, so that T is the same for both, but separated at different times t and t', the ratio of the activities of the samples at their respective separation times and normalized to the same number of fissions is

$$M=\frac{D'}{D}=\frac{\lambda_C N_C'/G'}{\lambda_C N_C/G} =\frac{x(aJ'+bK'+cL')+y(\mathfrak{b}K'+\mathfrak{c}L')+zL'}{x(aJ+bK+cL)+y(\mathfrak{b}K+\mathfrak{c}L)+zL}. \quad (8)$$

Solution of Eq. (8) for z gives

$$z=-\frac{(y\mathfrak{c}+xc)(ML-L') +(y\mathfrak{b}+xb)(MK-K')+ax(MJ-J')}{(ML-L')}. \quad (9)$$

For the purpose of calculating the relative cumulative yields of an iodine isotope from 14-Mev and thermal-neutron fission it is convenient to define a function D^p.

$$D^p=\left(\frac{E_C\lambda_C}{E_{Mo}\lambda_{Mo}}\right)\left(\frac{Y_C}{Y_{Mo}}\right) =\frac{DT\lambda_C}{x(aJ+bK+cL)+y(\mathfrak{b}K+\mathfrak{c}L)+zL}, \quad (10)$$

$$R=\frac{D^p{}_{14\text{-Mev}}}{D^p{}_{\text{thermal}}}=\frac{(Y_C/Y_{Mo})_{14\text{-Mev}}}{(Y_C/Y_{Mo})_{\text{thermal}}}. \quad (11)$$

An error listed for an average value obtained in the following calculations is the standard deviation of the average value. Where there is uncertainty in the mode of formation of a nuclide, e.g., an unknown branching ratio of a precursor, calculations using limiting values

have been made, and the error has been increased to include this uncertainty.

Iodine-135

As can be seen in Table III, there is no detectable dependence of d on the separation time, showing that the half-life of the precursor of I^{135} is short compared to the separation times. For the d values of samples *T4-A* and *T5-A* to be within 2 percent of the other d values, as they are, more than 98 percent of a precursor must have decayed before the separation 2 minutes after the irradiation. The half-life of a precursor would have to be <0.4 minute for this to occur. Previous work[8,9,18] had shown that if Te^{135} is the precursor of I^{135} its half-life is less than 1 or 2 minutes. The ~0.8-minute antimony activity found in fission by Pappas[3,4] and assigned by him to mass number 134 or 135 must either not be Sb^{135}, or if it is, less than about one tenth of the I^{135} formed in fission comes from it.

An R value of 0.815 ± 0.020 is obtained as the ratio of the average d values for 14-Mev and thermal-neutron fission.

Iodine-134

$$\begin{array}{ccccccc} & x & & y & & z & \\ & \downarrow & & \downarrow & & \downarrow & \\ Sb^{134} & \rightarrow & Te^{134} & \rightarrow & I^{134} & \rightarrow & \\ (\sim 0.8\ \text{min?})^3 & & (44.5\ \text{min})^4 & & (52.5\ \text{min})^3 & & \end{array}$$

The results of the calculations for I^{134} are summarized in Table IV. Since it is not certain that the ~0.8-minute antimony is the parent of Te^{134} and since the fraction of the 134 chain formed at antimony and at tellurium is not known, calculations were made using Eq. (9) for the two extreme conditions, $y=0$ and $x=0$. As seen, the difference between the results of the two calculations is not large. A D^0 value listed for a pair of samples was calculated by using the z value calculated for the pair and the data for the sample with the greater time before separation.

In the samples that were separated soon after the irradiation, a large fraction of the I^{134} activity was due to independent formation of I^{134}. This fraction varied from 43 percent in *T1-A* to 87 percent in *T4-A*, and was 80 percent in *F1-A* and *F2-A*. Since the correction for growth from Te^{134} is not large, the fractional chain yields should be reliable. Glendenin[2] had previously determined the independent yield of I^{134} from thermal-neutron fission of U^{235}. His value as recalculated by Pappas[3] is (0.94 ± 0.13) percent. This, divided by the (8.00 ± 0.21) percent cumulative fission yield of I^{134} determined by Pappas,[3] gives 0.12 ± 0.02 for the fractional chain yield of I^{134}, in good agreement with the value determined in this work.

TABLE IV. Relative yields of I^{134}.

Neutron energy	Samples	z_{max} ($y=0$)	z_{min} ($x=0$)	Selected z	D^0	R
14-Mev	*F1-A* and *B*	0.44	0.43	0.43 ±0.02	5.36 | 5.31 ±0.06	0.77 ±0.22
	F2-A and *B*	0.43	0.42		5.27	
Thermal	*T1-A* and *B*	0.125	0.104	0.11 ±0.02	7.06 | 6.91 ±0.19	
	T4-A and *B*	0.110	0.093		7.04	
	T5-A or *B* and *C*	0.127	0.111		6.38[a]	

[a] Given only half-weight in the average because t was an hour greater than for the other samples, so that growth and decay corrections were quite different. Therefore, less cancellation of half-life errors in the calculation of R was to be expected.

[18] R. W. Dodson and R. D. Fowler, Phys. Rev. **57**, 966 (1940).

Iodine-133

The formation scheme for I^{133} is shown in Fig. 4. Pappas,[3] from estimates of absolute fission yields, gives $0.92/0.08=(1)/(2)$ for the value of the branching ratio of Sb^{133}. This ratio is too high as will be shown in this section. Pappas[3] also determined for thermal-neutron fission the sum of the independent yields of I^{133} and the 2-min Te^{132}. His value and the values he recalculated from the data of Glendenin[2] and Katcoff *et al.*[9] are in the range of 20 to 30 percent of the total chain yield. These values are also too large because the fraction of Sb^{133} decaying by path 2 is larger than Pappas estimated.

The paths shown in Fig. 5 are considered. For the purpose of the calculations all paths through Te^{133m} are lumped into path 1 as an average. Equation (10) modified to include path 1 is given below.

$$D^0=\frac{D T\lambda_C}{(x_1+y')(a'J+b'K'+c'L)+x_2(aJ+bK+cL)+y(bK+cL)+zL}. \quad (12)$$

The terms a', b', c', and K' are the same as a, b, c, and K with $\lambda_{B'}$ substituted for λ_B.

The D values of the samples *F3-A* and *B* and *T3-A* and *B* separated after all the precursors of I^{133} had decayed can be used to calculate the values of D^0. There is about a 5 percent uncertainty in the results, depending on whether the I^{133} was formed rapidly via the short-lived paths 2, 3, and 4 or was held up at Te^{133m}. As a first approximation it was assumed that half was held up and half was not ($x_1+y'=0.5$, $z=0.5$). The

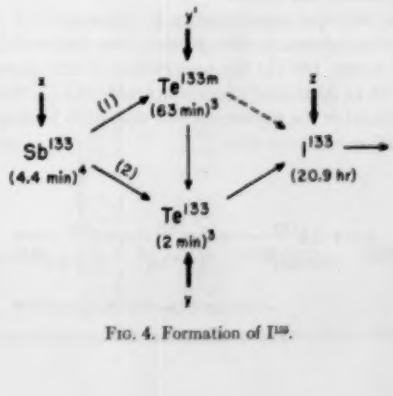

FIG. 4. Formation of I^{133}.

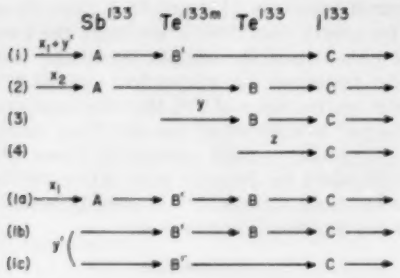

FIG. 5. Paths leading to the formation of I^{133}.

average D^0 values so obtained (2.19 and 2.25 for 14-Mev and thermal-neutron fission, respectively) were then used with the D values of the samples separated as soon as possible after the irradiation to calculate upper limits for $y+z$ ($x_1+x_2+y'=0$ assumed). These limits were 0.40 and 0.10 for 14-Mev and thermal-neutron fission, respectively.

The above information was then used to calculate the fraction of I^{132} formed from Te^{132m} (path 1). Data were used from samples separated 8 to 16 minutes after the end of the irradiation when most of the 4.4-min Sb^{132} and 2-min Te^{132}, but little of the 63-min Te^{132m}, had decayed. Two calculations were made for each sample, one for $y+z=0$ and one for $y+z$ equal to the upper limit calculated above. The average of the calculated limits are listed in Table V; the error for each value shows the spread of the limits.

The limits of 0.70 to 0.74 for the fraction of I^{133} formed from Te^{133m} in thermal-neutron fission were used in Eq. (12) to recalculate the limits on y and z. The results of these calculations are summarized in Table VI.

Finally, the values of D^0 were recalculated by using the determined limits on x_1+y'. The data used were from samples separated two hours or more after the irradiation; paths 2, 3, and 4 were therefore essentially equivalent. Two calculations were made for each sample, one for each x_1+y' limit. The average of the two limiting values are listed in Table VII; the errors show the spread of the limits.

The principal uncertainties in the reliability of the values calculated in this section, not included in the listed errors, are (1) the uncertainty in the separation time, 15 to 30 second maximum error, and (2) the error introduced in the approximation that path 1 adequately

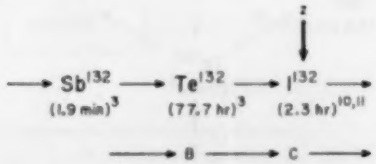

FIG. 6. Formation of I^{132}.

TABLE V. Fraction of I^{132} formed from Te^{132m}.

Neutron energy	Sample	x_1+y'
14-Mev	F1-A	0.59±0.08
	F2-A	0.56±0.08
		0.57±0.11
Thermal	T1-A	0.72±0.02
	T6-A	0.73±0.04
	T6-B	0.71±0.01
		0.72±0.02

represent all possible paths, 1, 1a, 1b, and 1c, through Te^{132m}. A 30 second error in the separation time would change the value of x_1+y' by about 0.02, z_{max} by about 0.01, $(y+z)_{max}$ by about 0.03, $(y+z)_{min}$ by about 0.01, and D^0 not at all. If path 1a is the only important path through Te^{132m}, limits on x_1 would be 0.03 to 0.04 lower than those calculated for x_1+y'. If path 1c is the important path, y' limits would be 0.04 to 0.07 higher than those calculated for x_1+y'. The values of D^0 and the upper limits on z and $(y+z)$ would be affected very little by use of path 1a or 1c instead of path 1 in the calculations. The minimum value of $(y+z)$ would be reduced to ~0 if path 1c were the important one. The calculated minimum value for $(y+z)$ of 0.02 may be due entirely to uncertainties in timing and chain path.

Iodine-132

The formation scheme for I^{132} is shown in Fig. 6.

In the samples that were allowed to stand 113 hours after irradiation before the tellurium-iodine separation, the I^{132} was in transient equilibrium with Te^{132}.

$$\lambda_C N_C = (\lambda_B N_B^0)\frac{\lambda_C}{\lambda_C-\lambda_B}e^{-\lambda_B\tau}, \tag{13}$$

where $\tau=t+T/2$. Division of both sides of Eq. (13) by the Mo^{99} activity at irradiation time gives

$$D=D_B^0\frac{\lambda_C}{\lambda_C-\lambda_B}e^{-\lambda_B\tau}. \tag{14}$$

D_B^0 is proportional to the ratio of Te^{132} and Mo^{99} cumulative fission yields.

$$D_B^0=\left(\frac{E_C}{E_{Mo}}\frac{\lambda_B}{\lambda_{Mo}}\right)\left(\frac{Y_B}{Y_{Mo}}\right). \tag{15}$$

TABLE VI. Independent formation of I^{132} and 2-min Te^{132} in thermal neutron-fission.

Sample	z_{max}	$(y+z)_{max}$	$(y+z)_{min}$
T4-A	0.03	0.07	0.03
T5-A	0.04	0.07	0.03
T5-B	0.04	0.05	0.02
	0.04	0.07	0.02

TABLE VII. Relative yields of I^{130}.

Neutron energy	Sample	D^0		R
14-Mev	F1-B	2.14±0.07	2.19±0.04	0.96±0.03
	F2-B	2.25±0.07		
	F3-A	2.21±0.01		
	F3-B	2.14±0.01		
Thermal	T1-B	2.33±0.22	2.28±0.05	
	T4-B	2.40±0.02		
	T5-C	2.22±0.01		
	T3-A	2.24±0.00		
	T3-B	2.21±0.00		

It has the same form as D^0, except that the decay constant and yield of tellurium replace those of iodine; the counting efficiency of the iodine radiation, which is measured, is retained.

The relative yields of Te^{132} are shown in Table VIII. The R value for Te^{132} is in agreement with the value of 1.13±0.03 obtained by Gilmore.[10]

For the other samples, which were separated a few hours or less after the irradiation, the activity of the I^{132} that had grown from Te^{132} was calculated from the D_B^0 values given above and subtracted from the gross decay curves. Any 2.3-hour period remaining was attributed to independently formed I^{132}. The independent yield of I^{132} relative to the cumulative yield of Te^{132} is given by

$$\frac{z}{1-z}=\left(\frac{d}{D_B^0}\right)\left(\frac{2.3\text{ hr}}{77.7\text{ hr}}\right), \tag{16}$$

and the results are listed in Table IX.

From 14-Mev-neutron fission, the activity of independently formed I^{132} was as a maximum between 15 and 20 percent of the total iodine activity; from thermal-neutron fission it was <1.5 percent of the total. If, as seems reasonable, the reliability of a resolved component of a decay curve is taken to be about 1 percent of the total activity, the ±0.01 error placed on the independent yields of I^{132} is a good indication of the reliability of the values.

An R value for I^{132} of 1.33±0.03 is obtained by multiplying the R value for Te^{132} by 1.16.

Iodine-131

The formation scheme for I^{131} is shown in Fig. 7. The paths shown in Fig. 8 are considered. For the purpose of the calculation all paths through Te^{131m} are lumped into path 1 as an average.

TABLE VIII. Relative yields of Te^{132}.

Neutron energy	Sample	D_B^0		R
14-Mev	F3-A	0.0457	0.0453±0.006	1.15±0.02
	F3-B	0.0449		
Thermal	T3-A	0.0395	0.0395	
	T3-B	0.0395		

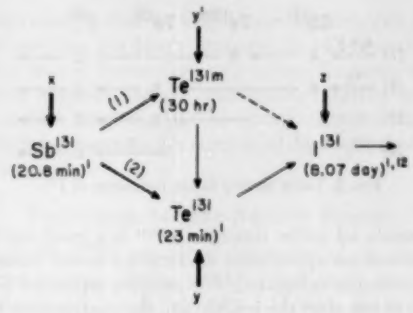

FIG. 7. Formation of I^{131}.

Calculations were made using Eq. (12) by two series of approximations similar to the method used for the 133-chain. In the first approximation, D^0 was calculated from the data of the samples separated 113 hours after the irradiation, with the use of the assumption that $x_1+y'=0.5$, which introduced a 3 percent uncertainty in the calculations. The values obtained, 0.0527 and 0.0297 for 14-Mev and thermal-neutron fission, respectively, were then used with the data from the samples separated shortly after irradiation to calculate upper limits for y and z. These limits, $z<0.10$ and <0.01, and $(y+z)<0.35$ and <0.15 for 14-Mev and thermal neutron fission, respectively, were then used to calculate the fraction of I^{131} formed from Te^{131m}. The results were $x_1+y'=0.41\pm0.03$ and 0.11 ± 0.04 for 14-Mev and thermal-neutron fission, respectively.

The results of the second series of calculations are summarized in Tables X, XI, and XII. For D^0 and x_1+y' two calculations were made for each sample, one for each of the possible limiting values for the other fractional chain yields. The average of the two calculations are listed along with an error indicating the spread.

For the 131 chain, whose members have half-lives of >20 minutes, the <0.5-minute timing error is not significant. The approximation that path 1 adequately

TABLE IX. Independent yield of I^{132}.

Neutron energy	Sample	$\frac{z}{1-z}$		z
14-Mev	F1-A	0.186	0.191±0.006	0.16±0.01
	F1-B	0.206		
	F2-A	0.188		
	F2-B	0.185		
Thermal	T1-A	0.012	0.001±0.004	<0.01
	T1-B	−0.010		
	T4-A	0.010		
	T4-B	−0.009		
	T5-A	0.009		
	T5-B	0.004		
	T5-C	−0.012		

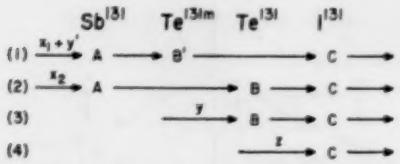

FIG. 8. Paths leading to the formation of I^{131}.

represents all paths through Te^{131m} is a good one and introduces no appreciable uncertainty in the values of the constants calculated. For samples separated a few hours or less after the irradiation, the contribution from any path through Te^{131m} is small, and it makes little difference which is used; for the samples separated 113 hours after an irradiation all paths through Te^{131m} lead to equivalent results.

There is reasonable agreement between the R value for I^{131} determined in this work and the value of 1.70 $\pm$0.03 determined by Ford and Gilmore.[1] However, Ford and Gilmore assumed that the same fraction of I^{131} was formed from Te^{131m} in 14-Mev and thermal-neutron fission. This is not the case, and if a correction is made, Ford and Gilmore's value is lowered to 1.61.

There is also reasonable agreement between the value of 0.11$\pm$0.03 for the fraction of I^{131} formed from Te^{131m} in thermal-neutron fission and the value of 0.14 reported by Pappas.[8] The branching ratio of Sb^{131} of 0.15/0.85 = (1)/(2), also reported by Pappas, more than accounts for all of the Te^{131m} formed in thermal neutron fission, so the independent yield of Te^{131m} must be small, probably <5 percent of the total chain yield. However, in 14-Mev-neutron fission the yield of Te^{131m} is high, 41$\pm$2 percent of the cumulative I^{131} yield. Since only 15 percent of Sb^{131} decays to Te^{131m}, the independent yield of Te^{131m} in 14-Mev-neutron fission must be large.

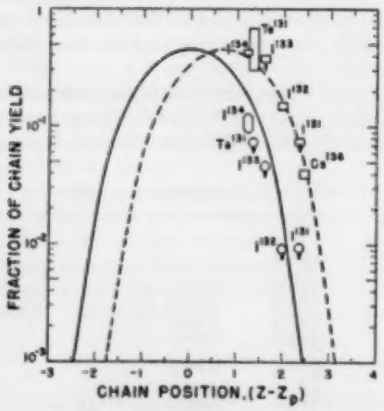

FIG. 9. Variation of yield with nuclear charge. The circles and ovals refer to thermal-neutron fission, the rectangles to 14-Mev neutron fission. The vertical arrows indicate upper limits. Except for Cs^{134} (reference 24), fractional chain yields are based on cumulative yields at iodine.

TABLE X. Relative yields of I^{131}.

Neutron energy	Sample	D^a		R
14-Mev	*F1-B*	51.8±3.5	52.9±2.1	1.76±0.08
	F2-B	53.9±3.7		
	F3-A	55.6±0.1		
	F3-B	50.1±0.1		
Thermal	*T1-B*	29.0±1.5	30.1±0.7	
	T4-B	29.6±1.5		
	T5-C	31.2±1.4		
	T3-A	30.8±0.1		
	T3-B	29.8±0.1		

The calculated value is 35$\pm$5 percent of the cumulative I^{131} yield.

DISCUSSION

Independent Fission Yields

The fractional chain yields determined in this research are plotted in Fig. 9 as a function of their chain position. The function used is $(Z-Z_P)$ in which Z_P is the most probable initial charge of the chain calculated according to the postulate[19] that the most probable mode of nuclear charge division is one that leads to equal idealized chain lengths (Z_A-Z_P) for both primary fragments.

$$Z_P=Z_A-[Z_A+Z_{(236-A)}-92]/2. \qquad (17)$$

The Z_P values were taken from the tabulation of Pappas,[8] who assumed that one neutron was emitted from each fragment. He obtained the Z_A values from the lines of maximum stability given by Coryell, Brightsen, and Pappas.[20] Those lines are discontinuous at shell edges.

The solid curve is the one that has been found[3] to best fit other thermal-neutron data. The thermal-neutron points reported in this paper generally fall below this line. The I^{134} and I^{132} points might be expected to fall low because of the abnormally large 134- and 133-chain yields, presumably due to a preference for

TABLE XI. Independent yields of I^{131} and 23-min Te^{131}.

Neutron energy	Sample	g_{max}	$(\gamma+g)_{max}$	$(\gamma+g)_{min}$
14-Mev	*F1-A*	0.08	0.29	0.07
	F2-A	0.08	0.30	0.08
		0.08	0.30	0.07
Thermal	*T1-A*	0.02	0.07	0.00
	T4-A	<0.02	<0.31	···
	T5-A	<0.01	<0.13	···
	T5-B	<0.01	<0.07	···
	T6-A	0.01	0.03	0.00
	T6-B	0.01	0.02	0.00
		0.01	0.03	0.00

[19] Glendenin, Coryell, and Edwards, Paper No. 52, p. 489, of reference 6.

[20] Coryell, Brightsen, and Pappas, Phys. Rev. 85, 732 (1952).

TABLE XII. Fraction of I^{131} formed from Te^{131m}.

Neutron energy	Sample	x_1+y'	
14-Mev	*F1-B*	0.42±0.02	0.41±0.02
	F2-B	0.40±0.01	
Thermal	*T1-B*	0.14	0.11±0.03
	T4-B	0.12	
	T5-B	0.08	

closed-shell configuration in fission[21,22] and the excessive evaporation from primary fission fragments of the loosely bound neutrons just outside closed shells.[2,3,23] If the fractional chain yields are calculated on the basis of the smooth mass-yield curve, the I^{134} and I^{133} points would be raised 40 and 30 percent, respectively, to bring them near the line. In addition, the independent formation of I^{134} may be less than that predicted from charge-displacement considerations because I^{135}, which has 82 neutrons, may emit fewer prompt neutrons than most other primary fragments.

No such explanation exists for Te^{131}. To bring it up to the line would require that most of the 0.11±0.03 cumulative fractional chain yield of Te^{131m} be attributed to independent formation, which in turn would require the branching ratio of Sb^{131} to be much less than the 0.15/0.85 reported by Pappas.[3]

The independent yields from 14-Mev-neutron fission, including the yield of Cs^{136} determined by Comstock,[24] all fall considerably above the solid curve. The dashed curve, which is the solid curve displaced by 0.7 charge units, fits the points well. The I^{134} point is a little high, but it would be brought onto the dashed curve if the fractional yield were based on the total chain yield rather than the cumulative yield at iodine, since, as estimated from the dashed curve, about 12 percent of the 134 chain is formed at Xe^{134}.

A possible explanation for the apparent shift in Z_P toward stability in 14-Mev neutron fission is that more neutrons are boiled off. Since in the mass region 130 to 138 the slope[3] of Z_P/A is 0.37, the ~0.7 shift in Z_P would correspond to the loss of approximately two more neutrons from the heavy fragment in 14-Mev-neutron fission than in thermal-neutron fission. However, there is little evidence for the assumption inherent in the explanation that the nuclear charge distribution for primary fragments is the same in 14-Mev and thermal-neutron fission.

TABLE XIII. Yields from 14-Mev neutron fission.

Isotope	$R\left(\frac{5.17}{6.14}\right)$	Thermal yield,[a] %	14-Mev yield, %	Estimated fraction of total chain yield	Estimated total chain yield, %
I^{131}	1.48	3.02	4.47	1.00	4.5
I^{132}	1.12	4.49	5.03	1.00	5.0
I^{133}	0.81	6.62	5.36	0.97	5.5
I^{134}	0.65	8.00	5.20	0.90	5.8
I^{135}	0.69	6.31	4.35	0.79	5.5

[a] See reference 3.

Yields from 14-Mev-Neutron Fission

In Table XIII are given the ratios of 14-Mev to thermal-neutron fission yields. These were obtained by multiplying the R values by 5.17/6.14, the ratio of Mo^{99} yields in 14-Mev and thermal-neutron fission determined by Terrell, Scott, Gilmore, and Minkkinen.[16] This allowed calculation of absolute 14-Mev-neutron fission yields from known thermal-neutron fission yields. The total chain yields were estimated from the charge distribution curve for 14-Mev-neutron fission (dashed curve in Fig. 9).

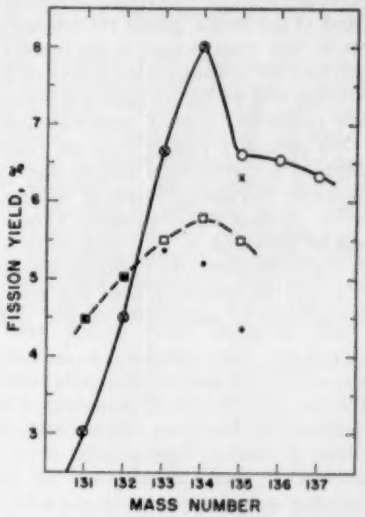

FIG. 10. Mass-yield curves. 14-Mev-neutron fission: ● iodine cumulative yield, □ total chain yield (estimated). Thermal-neutron fission: × iodine cumulative yield,[3] ○ total chain yield.[3]

In Fig. 10 are plotted both the 14-Mev and thermal neutron yields *vs* mass number. It may be seen that the prominent fine structure in thermal neutron fission is pretty well washed out at the higher energy.

ACKNOWLEDGMENTS

It is a pleasure to thank Dr. R. W. Spence and the members of his group for their hospitality and their interest and assistance in this work. I also wish to thank the groups responsible for the operation of the Cockcroft-Walton accelerator and the homogeneous and fast reactors for the irradiations they provided.

[21] Wiles, Smith, Horsley, and Thode, Can. J. Phys. **31**, 419 (1953).
[22] Glendenin, Steinberg, Ingram, and Hess, Phys. Rev. **84**, 860 (1951).
[23] L. E. Glendenin, Phys. Rev. **75**, 337 (1949).
[24] A. Comstock, reported by G. P. Ford in U. S. Atomic Energy Commission Report AECD-3597, 1953 (unpublished).

Total Cross Sections for High-Energy Neutrons*

VAUGHN CULLER AND R. W. WANIEK
Cyclotron Laboratory, Harvard University, Cambridge, Massachusetts
(Received April 4, 1955)

The total cross sections for high-energy neutrons have been determined for 12 elements (H, D, C, O, Al, Si, Cl, Ti, Fe, Cu, Hg, and Pb) for several points in the range between 60 and 110 Mev. The good-geometry attenuation experiment was conducted in the neutron beam produced by the bombardment of a beryllium target by the internal proton beam of the Harvard 95-in. synchrocyclotron. The angular and energy resolution permitted by the use of scintillation counter telescope techniques is discussed. Results are analyzed by using the optical model of the nucleus.

I. INTRODUCTION

THE values and the variations of total neutron cross sections as a function of incident neutron energy serve as a basis for comparison of various nuclear models, and, to this extent, permit the determination of nuclear radii. The cross sections in the region between 50 and 100 Mev are of special interest because the more rapid variation with energy indicates a transition effect in nuclear properties. From a phenomenological approach, this denotes a change from an opaque to a transparent nucleus. Additional interest is provided by the presence in this energy region of maxima in the cross section curves of high-Z elements. Thus, a precise knowledge of the values of total cross sections in this region is highly desirable. We therefore felt that cross sections should be examined with the good energy resolution afforded by scintillation counter techniques.

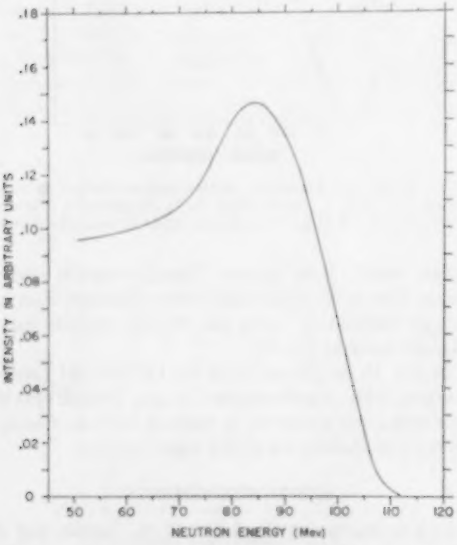

FIG. 1. Neutron spectrum produced in forward direction by internal proton beam bombardment of $\frac{1}{4}$-in. Be target in the Harvard 95-in. synchrocyclotron.

II. GEOMETRY AND APPARATUS

(A) Source of Neutrons and Experimental Lay-Out

The high-energy neutron beam used in this experiment (Fig. 1) was produced in charge exchange collisions by an internal proton beam bombardment of a $\frac{1}{4}$ in. thick, 1.5 in. high beryllium target. The neutrons emitted in the forward direction were collimated by brass tubing of rectangular cross section (1.37 in. by 2.87 in.) placed in a 6-ft water tank in the cyclotron shielding (Fig. 2). The beam intensity was constantly monitored at the exit of this pipe by a coincidence counter telescope. Approximately 150 cm from the monitor scatterer the beam passed through the appropriate attenuators and continued then through a second collimator consisting of a pipe, similar to the first one, encased in a water jacket 4 feet long permanently cemented in a concrete cube 7 feet thick. At the exit of this second collimator a scintillation counter telescope was used to determine the neutron beam intensity for various energy bands.

(B) Monitor Telescope System

Originally[1,2] a triple-coincidence scintillation counter telescope served to monitor the neutron beam by counting recoil protons from a polyethylene scatterer. The telescope, composed of plastic scintillators mounted on 1P21 photomultipliers, was placed at an angle of 15° to the neutron beam. By comparison of its counting rate with the rates of the various channels of the counter telescope described in the next section, two things were noted. The first was that the telescope had a constant efficiency; the second was that there were shifts in the high energy region of the neutron spectrum. It was found that results with good internal consistency could be obtained if the beam intensity was steady and if no controls of the cyclotron were manipulated. In order to minimize the effects of any steady drift in the neutron beam spectrum data were taken in symmetric cycles. At least five such cycles were made for each energy band, cross sections being determined for each cycle and resultant values appropriately weighted and averaged.

* Supported by the joint program of the Office of Naval Research and the U. S. Atomic Energy Commission.

[1] V. Culler and R. W. Waniek, Phys. Rev. **87**, 221 (1952).
[2] V. Culler and R. W. Waniek, Phys. Rev. **95**, 585 (1954).

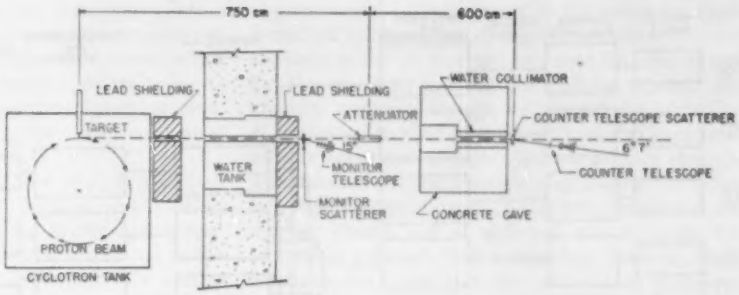

FIG. 2. Top view of experimental lay-out.

Later, in order to save running time as well as to get even more reliable data, a new monitor telescope with an added fourth counter was used. With this telescope suitable polyethylene absorbers were placed between the third and fourth counters so that the threshold energy for a recoil proton producing quadruple coincidence was about 85 Mev. The ratio of triple to quadruple coincidences then gave an indication of spectral changes. Any dubious counting cycles were rejected, the criterion for rejection being either beam intensity changes beyond about 15 percent or inconsistencies with the "empty-polyethylene" counts (no sample and a polyethylene scatterer in the counter telescope system) made at the beginning and at the end of each cycle. Rejections were made of the entire cycle in doubt before final results were calculated.

(C) Attenuators and Attenuator Changer

The solid attenuators were machined to four inches in diameter. The liquid and powder (silicon) attenuators were in containers machined to the same diameter. The containers had foil windows retained by "O" rings at each end. Whenever possible, lengths were chosen to be approximately two mean free paths, this length yielding about the best counting statistics in a given counting time.[3] The cross section of hydrogen was determined by a CH_2-C subtraction. In the measurement of the deuterium cross section which was determined by a D_2O-H_2O difference, the lengths of the containers were matched so that the oxygen components were nearly the same. During this rather long run intensity measurements were made also with no attenuator, thus permitting the determination of the cross section of oxygen by a H_2O-2H subtraction. The cross section of chlorine was determined by a CCl_4-C subtraction.

The areal densities of the solid samples were determined by measurements with micrometer calipers and analytical balances. Volume densities were also measured to ascertain the homogeneity of the samples. The areal density of the silicon was determined by measuring the inner diameter of the machined container and finding the difference between its "gross" and "tare" weights. The areal densities of the liquids were found by the use of hydrometers and the lengths of the containers. A recording thermometer was used to monitor the temperature in the area in which the attenuator changer was placed. Only negligible temperature changes existed. All samples, with the exception of titanium were pure to better than 99.5%. The titanium[4] was found to contain 3.2% Al, 3.3% Mg, and 0.10% C. The attenuator changer permitted the accurate alignment of three samples, and included a position for measuring the unattenuated beam. It was remotely operated from the control room with a reproducibility in each position of $\pm\frac{1}{16}$ in. from the central point.

(D) Counter Telescope System

The counter telescope system is composed of two sections and is pictured in Fig. 3. One section is the

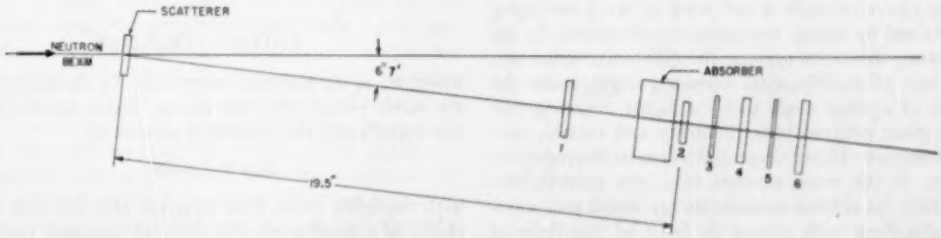

FIG. 3. Counter telescope system.

[3] M. E. Rose and M. M. Shapiro, Phys. Rev. **74**, 1853 (1948).
[4] The titanium sample was loaned by Rem-Cru Titanium Inc., Midland, Pennsylvania, through the auspices of Mr. A. E. Sylvester of Hawkridge Bros. Company, Boston, Massachusetts.

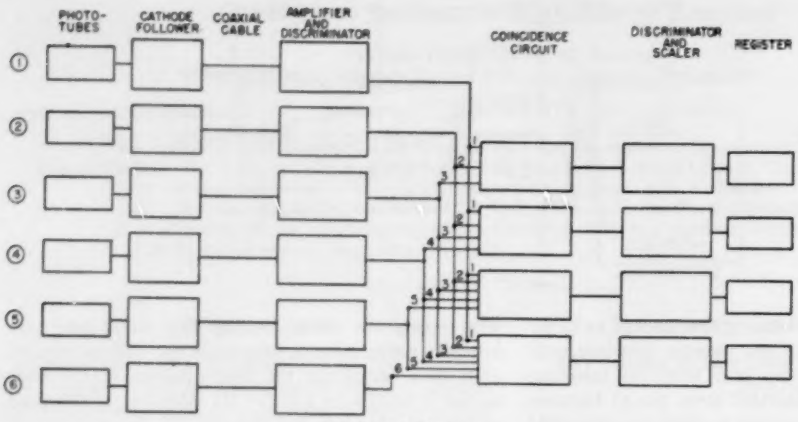

(a) Absorber telescope.

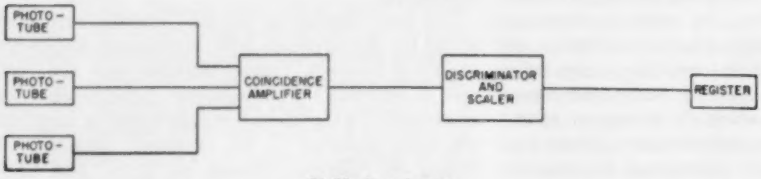

(b) Monitor telescope.

FIG. 4. Block diagram of electronic system.

counter telescope itself which is made up of 6 scintillation counters at a design angle of 6° 7′ to the neutron beam. The other section is a scatterer changer, operated remotely from the control room, which places a polyethylene or a carbon scatterer in the beam. In addition, a background or no-scatterer position is used.

The telescope consists of six plastic scintillators mounted on 1P21 multiplier phototubes. An aluminum stand supports the counters rigidly and permits careful alignment of the centers of the plastic scintillators so that the axis of the telescope can be made to fall at any given angle to the neutron beam. This angle is chosen as small as possible consistent with the necessity of keeping all counters out of the direct neutron beam, thus keeping the singles rate of every counter at a reasonable value. We estimate an error of less than $\frac{1}{4}°$ in positioning the telescope.

The choice of angle is indicated by $n-p$ scattering results and by energy resolution considerations. In the laboratory reference system, the differential cross section falls off rapidly with increasing angle, hence the choice of a small angle yields a higher counting rate for a given neutron beam intensity and counter size. The telescope utilized range differences to determine the energy of the recoil protons from the polyethylene scatterer. To achieve suitable energy bands polyethylene absorbers were placed in front of the defining crystal. In order to take advantage of the two-body scattering component due to the hydrogen in the scatterer, and thus uniquely determine the energy of the incident neutrons producing the recoils, it was necessary to subtract out the contribution due to carbon. This was done statistically by placing in the beam a carbon scatterer whose stopping power for the protons matched that of the polyethylene scatterer. Since this meant putting more carbon atoms per square centimeter in the neutron beam than did the polyethylene scatterer, only the proper fraction, f, of the proton intensity recoiling from the carbon scatterer was subtracted. This subtraction simultaneously removed the same fraction, f, of the background (no-scatterer) intensity. In order to account completely for this background a contribution $(1-f)$ of the intensity with no scatterer was also subtracted, thus getting only that portion of scattered protons for which the related neutron energy could be determined exactly, according to the relativistically correct formula:

$$E_p=\frac{E_n}{1+(1+E_n/2Mc^2)\tan^2\theta}, \tag{1}$$

where E_n is the neutron energy and E_p the energy of the recoil proton. For the energy region involved in this experiment, the expression reduces to

$$E_n=E_p/\cos^2\theta \tag{2}$$

with negligible error. This equation also indicates the choice of a small angle θ in order to minimize the dependence of energy on angular variation.

Pulses from each phototube are fed into a cathode follower and then through about 300 feet of RG62U coaxial cable (terminated by its characteristic im-

pedance) to a linear amplifier and then passed into a discriminator. The discriminator outputs are then fed into standard diode-type coincidence circuits which permit any combination of coinciding pulses to be recorded by conventional scalers and mechanical register. This equipment (Fig. 4) is in the cyclotron control room.

Coincidences from the first three, four, five, and all six counters are recorded, the difference counts yielding the number of protons stopping in the appropriate counter. The resolution of the entire system, up to the scalers, is better than one microsecond. The scalers have a resolution of about five microseconds, hence are sufficiently fast to cause no trouble since the coincidence rates are relatively low. Losses due to deadtime, multiple scattering of protons out of the telescope, and nuclear absorption were negligible. The efficiency of every counter was found to be essentially 100%. The entire system was frequently checked for stability and for over-all efficiency.

(E) Angular and Energy Resolution

In this type of experiment, angular resolution *per se* is only of slight importance since we are measuring a total rather than a differential cross section. The effect, however, of the angular resolution on the energy resolution must be taken into account as indicated by Eq. (2). Having decided on an angular resolution commensurate with the energy resolution requirements a few practical points in the design of this telescope may now be considered. The choice of small angles is dictated for best energy resolution consistent with the necessity of keeping the counters out of the direct neutron beam. This avoids both inordinately high singles counting rates and the high background coincidence rate caused by proton recoils produced by neutrons in the first counter. Therefore a preliminary experiment was made to determine just how well the beam could be collimated.

By using both photographic plates and counters as detectors, it was found possible to build a collimation system such that the beam spread at the exit of the system was essentially the one geometrically predicted by the size of the source and aperture system.

An arbitrary minimum distance was chosen for the defining crystal to clear the beam. In a plane perpendicular to the beam axis let us now visualize the projections of an arbitrarily shaped defining scatterer and defining crystal, one on each side of a band of width equal to our minimum separation distance. If both the scatterer and the crystal lie in planes orthogonal to the incident beam, then the tangent of the angle through which a particle is scattered is proportional to the distance between the two corresponding points in our projection. Some reflection will indicate that the optimum counting rate consistent with the angular resolution requirements is determined by the circle shown in Fig. 5. The diameter (D_θ) of this circle is proportional to the tangent of the maximum angle permitted by the criteria of angular resolution. The two segments in the circle would represent the ideal shapes for the scatterer and for the defining crystal. For practical purposes, though, we selected the rectangles of maximum inscribed area. The extension to a scatterer and crystal system of finite thickness is fairly obvious. The remainder of the telescope would appear to follow in a logical sequence, each crystal being parallel to the defining crystal and of sufficient size to cover the acceptance pyramid. Such a telescope, however, has a drawback due to the fact that two protons of a given energy but scattered at angular extremes would have sizeably different projected ranges, very possibly stopping in different crystals. The solution of this problem lies in a rotation of the scatterer and defining crystal so that the line through their centers is perpendicular to their faces. This is followed by either a graphical or an analytical determination of the sizes of the remaining crystals. In our specific case we felt it advisable to choose the collimating system rather than the scatterer as the defining source. We found that 1.5 in. by 3 in. o.d. wave guide of 0.064 in. wall thickness was sufficiently near the optimum rectangular shape. The scatterers were made somewhat larger in each dimension thus obviating the complication of precise positioning apparatus. We now have a defining system which satisfies two requirements: (1) it gives us definite minimum and maximum angles through which a particle may be scattered; (2) it gives us an optimized counting rate.

Especially if the angular acceptance interval is large we may wish to know more about what we may term the angular resolution function of the counter telescope. In other words, we may inquire as to the relative probability of seeing a particle scattered through some angle θ, and, since we know only that the origin of the

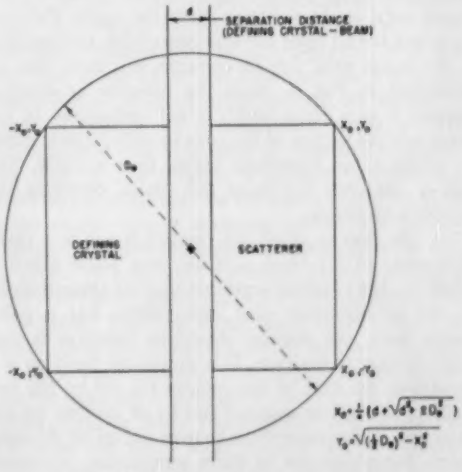

FIG. 5. Defining crystal-scatterer system.

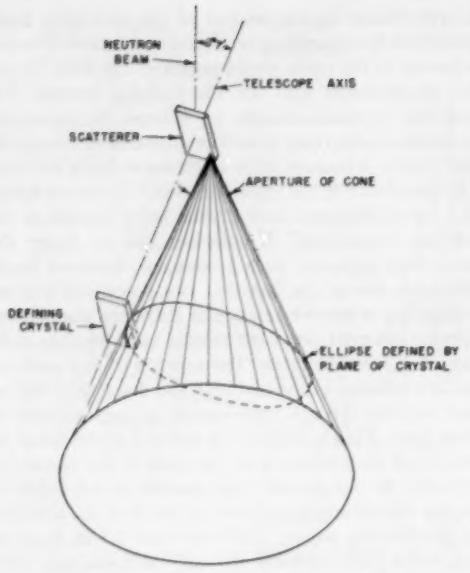

FIG. 6. Geometry for angular resolution calculations.

particle is somewhere in the scatterer, we must state this probability for the case of any two points in the scatterer being equally probable origins. We thus may define the angular resolution function of the telescope as being the function of scattering angle which states the relative probability of detection of the particle, in the case in which the particle has equal likelihood of being scattered in any angular interval θ to $\theta+d\theta$, θ being the angle between the trajectory of the scattered particle and the axis of the incoming beam.

In this case, then, we may think of the scattered flux from any point in the scatterer as being made up of cones with equal flux for equal angular intervals, the source point in the scatterer being the origin. Further, the cones are all right circular cones with axes parallel to the beam axis. Let us consider one such cone as illustrated in Fig. 6. Since the detector or defining counter is in a plane which is not orthogonal to the beam axis the section of the cone by this plane is either an ellipse or an hyperbola rather than a circle. The axis of the cone intersects this plane, therefore the section is an ellipse.

For the case in which the counter is not in a plane orthogonal to the beam axis but in a plane which is nearly so, the elliptical segments may be approximated as circular segments with small error. For a point source then, the angular resolution function is particularly easy to evaluate. It is simply the function of θ expressing the area of the counter cut off by the two cones of semivertex angles θ and $\theta+d\theta$ divided by the total area in the plane of the counter cut off by the same cones. Generalization to finite source (i.e., scatterer) may be approximated by subdividing the scatterer into sections of equal area, each of which is assumed characterized by a point source.

In the more general case in which the ellipses cannot be approximated as circles, we are faced with an alternative approach which is, of course, applicable to the simple case and which may actually be somewhat easier to use in practice. For a point source let us consider the circular sections made by the various cones in a plane perpendicular to the beam axis. Let us for convenience take this reference plane as being farther from the source than any similar plane through the defining counter: the angles of scattering are then uniquely related to the radius of the various circles. The angular resolution function is then the arc length "removed" by the defining counter divided by the circumference of the circle as a function of radius (i.e., scattering angle). Even more simply, by choosing the projected source point as the origin of a polar diagram the angular resolution function is then the polar angle subtended by the defining crystal as a function of radius (i.e., scattering angle). Since we know the exact intersection of the scattering cone with the counter, we may take the extreme points of intersection as reference points for the determination of this angle.

The actual mechanical procedure used may make this process more understandable. For a given source point we find the intersection with the defining counter of the cone of semivertex angle θ. This section or curve is

TABLE I. Total cross sections in units of 10^{-27} cm².

Neutron energy (Mev)	High-energy bands 93.4±0.5	97.2±1.0	101.1±0.5	106.8±2
H	77± 5	76± 3	80± 7	59± 16
D	110± 7	108± 5	81± 10	62± 22
C	518± 6	494± 4	466± 7	508± 18
O	721± 13	675± 9	649± 14	668± 42
Al	1067± 29	1046± 23	920± 50	1064±130
Si	1136± 52	1067± 42	1040± 90	925±220
Cl	1382± 58	1336± 40	1380± 75	1260± 90
Ti	1650± 41	1565± 29	1574± 54	1490± 80
Fe	1947± 48	1874± 37	1735± 80	1940±185
Cu	2204± 56	2023± 39	1880± 70	1935±110
Hg	4315±150	4450±105	4525±180	4540±255
Pb	4630± 90	4595± 65	4410±120	4740±210

Neutron energy (Mev)	Medium-energy bands 76.7±0.5	81.2±1.0	85.5±0.5	99.4±4
C	614± 31	585± 17	602± 19	518± 7
Cl	1420± 85	1597± 59	1371± 59	1332± 19
Ti	1760± 90	1900± 57	1772± 59	1628± 20
Cu	2150±100	2335± 65	2225± 70	2118± 23
Hg	4310±200	4985±150	4680±150	4697± 50
Pb	4590±225	4450±160	4650±195	4605±120

Neutron energy (Mev)	Low-energy bands 61.0±0.5	66.1±1.0	71.2±0.5	92.3±7
C	674± 62	671± 42	601± 41	520± 80
Ti	1905± 90	2210± 80	1880± 80	1737± 15
Cu	2440± 20	2495± 80	2450±103	2139± 18
Hg	3770±490	5000±400	5320±575	4765±120
Pb	4590±225	4550±160	4650±195	4605±120

elliptical. This ellipse intersects the counter in an even number of points. Each of these points determines a definite ray of the cone since the origin of the cone is fixed. The intersection of each of these rays with the reference plane is found. These new points necessarily lie on a circle. The appropriate arc lengths or angles subtended may then be easily measured to give the value of the angular resolution function for this value of the scattering angle θ.

The angular resolution function is weighted by the value of $\sin\theta$ at each point to give a new angular resolution function in terms of solid angle. The final angular resolution function is the appropriate sum of the "point source" angular resolution functions. We are now in a position to consider the effects of angular resolution on energy. The angular resolution function is first weighted by the differential $n-p$ cross section, modified because it is the proton and not the neutron which is seen by the telescope. A mean proton energy derived from range energy relations for the telescope is used to find the equivalent neutron energy for each angle, the angular resolution function as a result being transformed into an energy resolution function. Finally, this function is weighted by the spectrum of the incident neutron beam and a mean or effective neutron energy determined. In order to estimate the error in this mean neutron energy deliberate discrepancies may be introduced at any point. It was found that practically any step in this derivation could be dropped without shifting the effective neutron energy by more than about 0.2 Mev. On this basis the errors in the effective energies were calculated not to exceed those indicated in Table I. It should be pointed out that this procedure must be used carefully. If there are any very large fluctuations of any component with angle or energy the effective energy as well as resultant energy resolution could be affected.

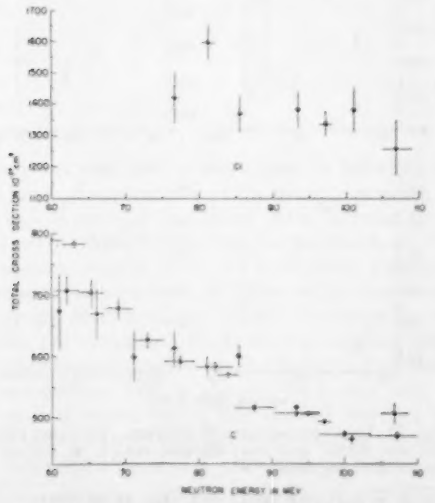

FIG. 7. Total cross sections of carbon and chlorine; Harvard results: ●, Harwell results: ○, Berkeley results: ×.

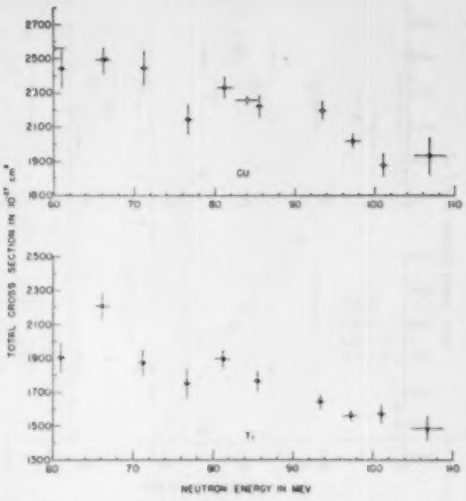

FIG. 8. Total cross sections of copper and titanium; Harvard results: ●, Harwell results: ○.

III. EXPERIMENTAL PROCEDURES

The procedure of a typical measurement consisted in carefully aligning collimators, monitor and counter telescopes and the attenuator samples by means of a cathetometer aimed at the internal beryllium target. The monitor telescope was then checked for constant efficiency and the absolute efficiency of each of the counters in the counter telescope was determined. The requirements for the counter and for the related electronics were essentially 100% efficiency and phototube voltage near the center of an efficiency *versus* phototube voltage plateau. The runs were carried out in symmetric cycles, each being started and finished with a no-attenuator measurement of the intensity. A typical cycle was made up of the following beam intensity measurements: no-attenuator, sample A, sample B, sample B, sample A, no-attenuator. Each of these determinations was composed of measurements made with each of the possible scatterers (polyethylene, carbon and no-scatterer) for the reasons outlined in the section on the counter telescope system. The purpose of the symmetric cycles was to counterbalance partially the effects of long term cyclotron beam fluctuations which could have possibly affected the energy spectrum of the beam. The time apportioned to each measurement in the cycle was such as to yield optimum statistics for a given counting time. This required a preliminary cycle for each set of samples in order to ascertain the relative counting rates. The length of time allowed for each cycle was never more than 3 hours for several considerations. The most obvious one was the prevention of the loss of much data in the event of machine or

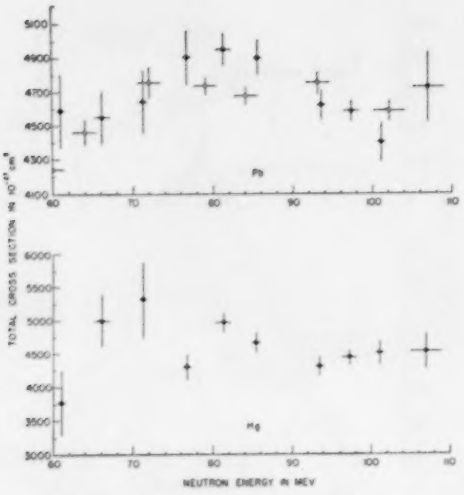

FIG. 9. Total cross sections of mercury and lead; Harvard results: ●, Harwell results: ○.

equipment failure, the second was the beam drift possibility mentioned before and the third was to permit an easy check of the internal consistency of the data. In general, the cycles were repeated until a cross section with about 2.5% standard deviation was obtained.

IV. RESULTS AND ANALYSIS

The values of the cross sections are listed in Table I and are graphically presented in Figs. 7–10. Diffraction corrections were calculated either according to the theoretical procedure given by McMillan and Sewell[5] and outlined by Cook *et al.*[6] or, in the cases where experimental data was available, from the value of the differential elastic scattering cross section extrapolated to 0°.[7] The correction was about 1% for the heaviest elements, lead and mercury, and smaller for all others.

Corrections for impurities were negligible in every case, including that of titanium.

The cross sections of carbon and lead were taken with different thicknesses of sample material to check the exponential dependence of the absorption. This indicates the absence of beam degradation effects (increases in beam transmission due to in-scattered neutrons) other than those predicted by the diffraction correction.

The values at 106.8 Mev were taken at the extreme tail of the neutron spectrum where beam energy fluctuation effects and low counting rates impair the accuracy of the results. In this case the maximum energy of the neutrons (Fig. 1) defined the upper limit of the energy band, since this data was taken with the last counter of the telescope. This is also the case for the data at 92.3 and 99.4 Mev with the exception that wider energy ranges were used with a corresponding increase in counting rates.

The apparently low value in the cross section of deuterium at 101.1 Mev may possibly be attributed to counting errors.

For purposes of comparison, contemporaneous measurements made at Harwell[8] and at Berkeley[9] have been indicated in Figs. 7–10. This is the only data in this energy range, to our knowledge, taken with energy resolution comparable to ours, and the agreement is good. The maximum in the lead cross section falling at about 82 Mev appears to be defined more sharply than in the Harwell data. Comments on the significance of these peaks have been made by Lawson[10] although the situation is not completely understood.

It seems that future experiments with better absolute energy resolution and smaller counting errors are required to investigate the possibility of a more detailed structure. The total cross sections obtained in this

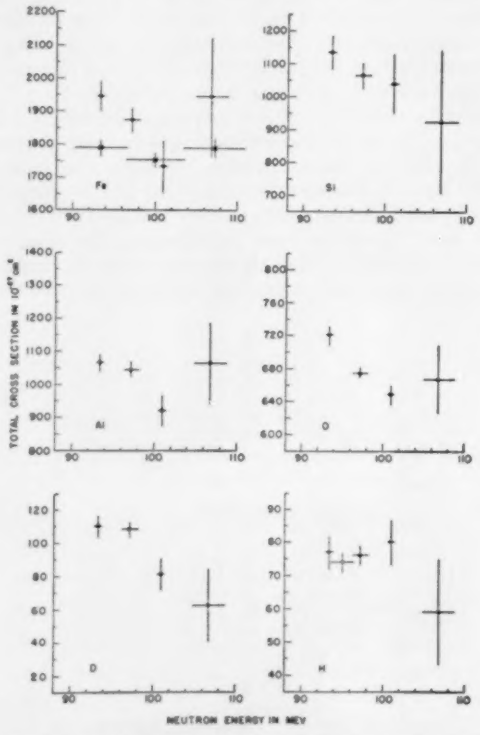

FIG. 10. Total cross sections of hydrogen, deuterium, oxygen, aluminum, silicon, and iron; Harvard results: ●, Harwell results: ○, Berkeley results: ×.

[5] E. M. McMillan and D. C. Sewell, U. S. Atomic Energy Commission Report MDDC-1558, November, 1947 (unpublished).
[6] Cook, McMillan, Peterson, Sewell, Phys. Rev. **75**, 7 (1949).
[7] Bratenahl, Fernbach, Hildebrand, Leith, and Moyer, Phys. Rev. **77**, 597 (1950).
[8] A. E. Taylor and E. Wood, Phil. Mag. **44**, 95 (1953).
[9] B. Ragent, Phys. Rev. (to be published).
[10] J. D. Lawson, Phil. Mag. **44**, 102 (1953).

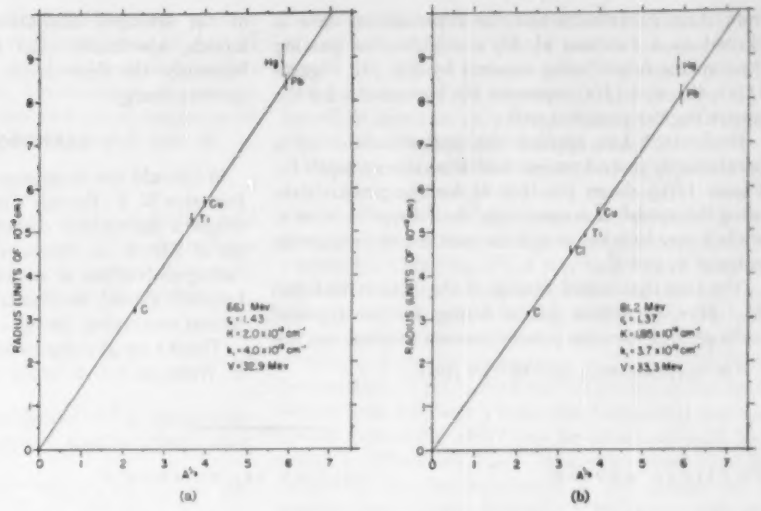

FIG. 11. Analysis of the experimental data at (a) 66.1 Mev, (b) 81.2 Mev, using the optical model of reference 11.

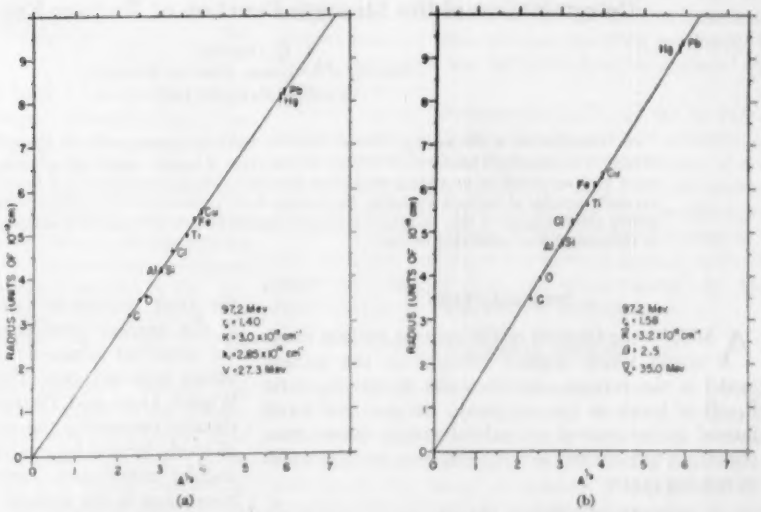

FIG. 12. Analysis of the experimental data at 97.2 Mev using (a) the optical model of reference 11, (b) that of reference 13.

experiment were used to investigate the reliability and the range of applicability of the theory describing the nucleus in terms of an analogy out of physical optics. The optical model[11,12] describes the nucleus as a sphere of uniform density, with an appropriate absorption coefficient and an index of refraction for the Schrödinger-de-Broglie neutron waves. The main limitation imposed is that the wavelength of the incident neutron should be much smaller than the nuclear radius, a high-energy approximation. This is already nearly the case for neutrons of several tens of Mev and will therefore hold even better around 100 Mev. This concept represents an oversimplification of a more realistic picture as it does not investigate any structural effects nor does it take care of interfacial reflections. The values of the propagation vectors outside and inside the nucleus, k and $k+k_1$, respectively, are calculated (the change in the phase velocity upon entering nuclear matter is related to the nuclear potential well of depth determined from the Fermi gas model of the nucleus). An absorption coefficient, K, is determined from the knowledge of $p-p$ and $n-p$ cross sections, the Pauli principle being taken into account. If we retain the expression,

$$R = r_0 A^{\frac{1}{3}} \times 10^{-13} \text{ cm}, \tag{3}$$

for the radius of a nucleus, it is necessary to use other than the predicted k_1 and K.

Best fitting values of k_1 and K are determined by an iteration procedure in which the nuclear radius obtained

[11] Fernbach, Serber, and Taylor, Phys. Rev. **75**, 1352 (1949).
[12] S. Fernbach, University of California Radiation Laboratory Report UCRL 1382, 1951 (unpublished).

from these parameters and the experimental data is plotted as a function of $A^{\frac{1}{3}}$, a straight line passing through the origin being required by Eq. (3). Figures 11(a), (b), and 12(a) represent the best results for the square nuclear potential well.

Heckrotte[12] has applied the optical model to a parabolically shaped nuclear well of maximum depth V_0. Figure 12(b) shows the best fit for the present data using this model. $\bar{K}$ is essentially the average value of K while β may be taken as 4/3 the quotient of the average value of k_1 and $\bar{K}$.

The fact that forced fittings of the data at 66.1 and 81.2 Mev, as well as similar fittings by two types of wells at 97.2 Mev are possible, serves to point out one of the strongest limitations of the present optical models, specifically that they do not yield unambiguously the dependence of total cross sections on neutron energy.

[12] W. Heckrotte, Phys. Rev. **95**, 1279 (1954).

V. ACKNOWLEDGMENTS

We should like to express our sincere appreciation to Professor N. F. Ramsey for his continued support and frequent discussions concerning the experiment. The aid of Mr. R. L. Smith was particularly valuable in curing all troubles of electronic nature, and Mr. R. H. Lambert should be thanked for the numerical calculations concerning the optical model.

Thanks are also due to Mr. M. J. Hurley and Mr. G. P. Weiss, as well as to the cyclotron staff.

PHYSICAL REVIEW VOLUME 99, NUMBER 3 AUGUST 1, 1955

Determination of the Strength Function of Nuclear Energy Levels*

S. E. DARDEN†
University of Wisconsin, Madison, Wisconsin
(Received March 28, 1955)

An investigation of the average reduced neutron width to spacing ratio, or strength function, $\langle\gamma_0^2\rangle/\bar{D}$, of nuclear energy levels has been carried out as a function of atomic weight and neutron energy. The experiment was performed by measuring deviations from exponential attenuation of a beam of neutrons passing through samples of various elements. Deviations from exponential attenuation were observed by comparing transmissions of thin samples for neutron beams filtered through thick samples with transmissions of thin samples for unfiltered beams.

1. INTRODUCTION

AMONG the features of the neutron-nucleus interaction which depend strongly on the nuclear model is the average neutron width to spacing ratio $\Gamma_{nl}/\bar{D}$ of levels of the compound nucleus. For levels formed by neutrons of zero orbital angular momentum, the strong interaction model[1] predicts an average width to spacing ratio:

$$\Gamma_{n0}/\bar{D}=2k\langle\gamma_0^2\rangle/\bar{D}\simeq 2k/\pi K, \qquad (1)$$

where k is the wave number of the emitted neutron and K is the wave number corresponding to the average kinetic energy of the neutron inside the nucleus. $\langle\gamma_0^2\rangle/\bar{D}$ is the average reduced neutron width to spacing ratio or strength function[2] for levels formed by S-wave neutrons. The complex square well model of Feshbach, Porter, and Weisskopf,[3] on the other hand, predicts sharp maxima in $\Gamma_{n0}/\bar{D}$ as a function of atomic weight and energy. These maxima occur near the positions of the giant resonances attributed to S-wave neutrons in the average total cross sections.[4] Between peaks the predicted values of $\Gamma_{n0}/\bar{D}$ fall to a fraction of the values expected from the strong interaction theory. Wigner, Lane, and Thomas[5] have come to similar conclusions concerning the reduced width density $\langle\gamma_l^2\rangle/\bar{D}$ of levels formed by neutrons having l units of orbital angular momentum. They have interpreted the giant resonances in the average total cross sections in terms of oscillations, over wide energy and atomic weight intervals, of $\langle\gamma_l^2\rangle/\bar{D}$.

Carter *et al.*[6] have performed a survey of slow neutron resonance parameters for nuclei having atomic weights between 100 and 200 in an attempt to investigate the dependence of $\langle\gamma_0^2\rangle/\bar{D}$ on atomic weight. Their results show a maximum in $\langle\gamma_0^2\rangle/\bar{D}$ for values of A near 160, in agreement with the predictions of the complex square well model. A similar collection of data which show a maximum in $\langle\gamma_0^2\rangle/\bar{D}$ for elements having atomic weight near 55 has been reported.[7] However, the in-

* Work supported by the U. S. Atomic Energy Commission and the Wisconsin Alumni Research Foundation.
† National Science Foundation Predoctoral Fellow.
[1] Feshbach, Peaslee, and Weisskopf, Phys. Rev. **71**, 145 (1947); V. F. Weisskopf, Helv. Phys. Acta **23**, 187 (1950).
[2] R. G. Thomas, Phys. Rev. **97**, 224 (1955).
[3] Feshbach, Porter, and Weisskopf, Phys. Rev. **96**, 448 (1954).
[4] H. H. Barschall, Phys. Rev. **86**, 431 (1952); R. K. Adair, Phys. Rev. **94**, 737 (1954).
[5] Wigner, Lane, and Thomas, Phys. Rev. **98**, 693 (1955).
[6] Carter, Harvey, Hughes, and Pilcher, Phys. Rev. **96**, 113 (1954).
[7] R. Cote and L. M. Bollinger, Phys. Rev. **98**, 1162(A) (1955).

vestigations using this method are confined to slow neutrons, so that the energy dependence of $\langle\gamma_0^2\rangle/\bar{D}$ cannot be determined. Total cross-section measurements[8] performed at Duke University in the energy region from 2 to 100 kev also indicate a maximum in $\langle\gamma_0^2\rangle/\bar{D}$ for elements having atomic weight near 50.

2. METHOD

If neutrons having an energy spectrum $f(E)$, where $\int f(E)dE=1$, pass through a sample of thickness t the transmission is related to the total cross section $\sigma(E)$ of the nucleus under investigation by the expression

$$T=\int f(E)\exp[-n\sigma(E)t]dE, \tag{2}$$

where n is the number of nuclei per cm³ in the sample. If the sample is made thin enough that $n\sigma(E)t\ll 1$, then

$$T\simeq\exp(-n\bar{\sigma}t), \tag{3}$$

where

$$\bar{\sigma}=\int f(E)\sigma(E)dE. \tag{4}$$

Equation (3) is ordinarily used to compute average cross sections from measured transmissions. The average computed in this way is the same as the average defined by Eq. (4) only for thin samples. If $n\sigma(E)t$ is not small compared to one and the cross section varies rapidly with energy over the neutron spectrum $f(E)$, the attenuation will not be exponential and the average cross sections computed using formula (3) will be lower than the average defined by Eq. (4). The effect will be particularly pronounced if the neutron spectrum extends over an energy interval which includes resonances.

Thomas[9] has derived an expression relating the deviation from exponential attenuation to the properties of the cross section averaged over the incident neutron spectrum. He has shown that when only S-wave neutrons interact with nuclei of a sample containing a single isotope of zero spin, the measured transmission of a sample of thickness t is given by

$$T=[1+\alpha(t)]\exp(-n\bar{\sigma}t), \tag{5}$$

where $\alpha(t)$ is a measure of the deviation from exponential attenuation and is proportional to

$$(1-|\langle U(E)\rangle_{Av}|^2).$$

$U(E)$ is the collision function for neutrons of zero orbital angular momentum. If $\Gamma/D\ll 1$ and the neutron energy is low,[2]

$$1-|\langle U(E)\rangle_{Av}|^2\simeq\frac{2\pi\Gamma_{n0}}{\bar{D}}\left(1-\frac{\pi\Gamma_{n0}}{\bar{D}}\right). \tag{6}$$

Equation (5) has been generalized[9] for elements containing more than one isotope and for cases where the sample nuclei have nonzero spin. The observed deviation from exponential attenuation can then be interpreted in terms of an average value of $\Gamma_{n0}/\bar{D}$ for all the contributing isotopes and spin states.

Equation (5) and the corresponding equation for more than one isotope and spin state can be used to obtain $\alpha(t)$ and $\Gamma_{n0}/\bar{D}$ from measured values of T, the transmission of a thick sample of thickness t, providing $\bar{\sigma}$ is known. Using Eq. (3), $\bar{\sigma}$ may be obtained from the transmission T_d of a thin sample of thickness d. Equation (5) is then solved for $\alpha(t)$ and $\Gamma_{n0}/\bar{D}$. This procedure is sometimes subject to a large statistical uncertainty, since the uncertainty in $T_d^{t/d}$ is t/d times the uncertainty in T_d, and the thickness t of the thick sample must be about 7 times the thickness of the thin sample before the effect can be measured with any accuracy. Therefore $\Gamma_{n0}/\bar{D}$ was determined also by comparing the transmission of a thin sample for a neutron beam filtered through a thick sample with the transmission of the thin sample alone. This procedure is more accurate than the one described previously if $\Gamma_{n0}/\bar{D}$, and hence the deviation from exponential attenuation, is small.

Errors in the determination of $\Gamma_{n0}/\bar{D}$ can be introduced by the fact that deviations from exponential attenuation will occur because of the variation of the nonresonant cross section with energy over the neutron spectrum. The magnitude of this effect can be calculated if the energy dependence of the nonresonant cross section is known, and turns out to be at least an order of magnitude smaller than the effect caused by the resonances in the cross section in most cases.

3. EXPERIMENTAL PROCEDURE

The choice of sample elements was based on several considerations. It would be best to have separated isotopes of spin-zero nuclei since the deviations from exponential attenuation are largest in this case. A restriction on the choice of elements is imposed by the Doppler effect[9,10] which broadens resonances in the cross section and reduces their maximum heights. If the Doppler broadening is as large as the level spacing, the resonances overlap, the cross section becomes constant, and there is no deviation from exponential attenutation. Another criterion that must be considered is that the level density must be sufficiently high so that many resonances are included in the energy spread of the neutrons.

Transmission measurements were performed in the conventional manner.[11] Neutrons were produced by bombarding lithium targets with 2-Mev protons from the electrostatic accelerator. Neutrons emitted in the forward direction with respect to the proton beam were

[8] H. Marshak and H. W. Newson, Phys. Rev. **98**, 1162(A) (1955).
[9] R. G. Thomas, Phys. Rev. **98**, 77 (1955).
[10] J. M. Blatt and V. F. Weisskopf, *Theoretical Nuclear Physics* (John Wiley and Sons, Inc., New York, 1952), p. 473.
[11] H. H. Barschall, Revs. Modern Phys. **24**, 120 (1952).

detected by a propane recoil counter 2.5 cm in diameter and 25 cm long. Cylindrical scattering samples 2.5 cm in diameter were supported approximately half-way between the neutron source and the effective center of the counter. The distance from source to center of counter was 45 cm. Background counts caused by neutrons scattered from the floor and other surrounding objects were measured by inserting a 25-cm long paraffin cone between the neutron source and detector. Counting rates obtained in this way were about one percent of the counting rates in the direct beam. All the transmissions were measured to about one-half percent statistical accuracy.

The average neutron energies used in evaluating the data were obtained by considering the energy sensitivity of the counter, the neutron energy spectrum from the $Li^7(p,n)$ reaction and the variation with energy of the quantity $\lambda^2\Gamma_{n0}$. The last mentioned quantity is a measure of the magnitude of the effect being investigated.

Measurements were performed on carbon, nickel, zinc, selenium, strontium, silver, indium, cerium, tantalum, radio lead, and bismuth. Carbon, which has no known resonance levels in the energy region used in this investigation, was used as a check, since no appreciable effect was expected. The level spacing in tantalum is about 6 ev,[6] and consequently the Doppler broadening should prevent the appearance of any effect beyond that caused by the variation of the average cross section.

For many of the sample elements only two or three isotopes were present in any appreciable abundance, and the remaining isotopes had abundances of only a few percent. Since approximations were already involved in the interpretation of the data, in some cases rounded off values of the fractional abundances were used in evaluating the experiments.

4. RESULTS

Table I contains the values of $\Gamma_{n0}/\bar{D}$ and $\langle\gamma_0^2\rangle/\bar{D}$ computed from the data. The second column lists the average neutron energies at which measurements were carried out, and the third column gives the observed increase in transmission of the thin samples when the neutron beam was filtered through the thick samples. Averages of $\Gamma_{n0}/\bar{D}$ computed in the two ways discussed in Sec. II are presented in the fourth column. The last column contains values of $\langle\gamma_0^2\rangle/\bar{D}$ calculated by dividing the values of $\Gamma_{n0}/\bar{D}$ in the fourth column by $2k$. The uncertainties quoted in Table I are statistical uncertainties only.

In some cases, the 120-kev and 160-kev results for the same element disagree considerably. These fluctuations may be caused by large level spacings in the nuclei concerned. For example, good resolution total cross-section measurements[12,13] on nickel and bismuth indicate

TABLE I. Summary of experimental results.

Element	$\bar{E}_n$ (kev)	T_2-T_1 (all ±0.006)	Average $\bar{\Gamma}_{n0}/\bar{D}$	$\langle\gamma_0^2\rangle/\bar{D}$ in 10^{-13} cm
Nickel	120	0.043	0.067±0.011	0.44 ±0.072
	160	0.048	0.123±0.015	0.70 ±0.085
Zinc	80	0.026	0.033±0.008	0.265±0.064
	120	0.032	0.065±0.012	0.427±0.079
	160	0.031	0.097±0.018	0.55 ±0.10
	230	0.012	0.072±0.036	0.34 ±0.17
Selenium	80	0.017	0.08 ±0.02	0.642±0.16
	120	0.030	0.22 ±0.05	1.45 ±0.33
	230	0.020	0.30 ±0.10	1.42 ±0.48
Strontium	120	0.033	0.081±0.014	0.53 ±0.09
	160	0.004	0.012±0.018	0.068±0.102
Silver	120	0.014	0.046±0.018	0.30 ±0.12
Cerium	80	0.047	0.038±0.005	0.305±0.040
	120	0.026	0.021±0.005	0.138±0.033
	160	0.042	0.049±0.007	0.278±0.040
	230	0.044	0.072±0.011	0.34 ±0.05
Bismuth	80	0.016	0.022±0.009	0.177±0.072
	120	0.016	0.040±0.016	0.263±0.105
	160	0.003	0.012±0.024	0.068±0.136
Radio-lead	160	0.024	0.070±0.02	0.40 ±0.11

average level spacings from 10 to 20 kev in these elements. The total cross section of strontium[14] measured with 20-kev resolution shows a large resonance or group of resonances near 100 kev, as well as similar peaks at 330, 440, and 530 kev. If these results are indicative of the level spacing in Sr^{89}, an energy spread of 100 kev may not produce a good average over levels.

Transmission measurements with carbon were taken at average neutron energies of 120 kev and 160 kev. At both energies T_2-T_1 was found to be 0.007 ± 0.006. This is to be compared with a value of $T_2-T_1\simeq0.001$ calculated using the known variation of the carbon total cross section with energy. Similarly, the fact that the level spacing in tantalum is less than the Doppler broadening above 100 kev leads one to expect no resonance effects in this energy region. For tantalum, values of T_2-T_1 of 0.006 ± 0.006 and -0.007 ± 0.006 were found at average neutron energies of 120 kev and 160 kev, respectively. These results on carbon and tantalum indicate that no unexpected deviations from exponential absorption comparable with the expected effects occur. (See Table I.)

Measurements taken on silver showed a slightly increased effect when the sample was cooled to liquid air temperatures, although the change was within the experimental error.

In Fig. 1, values of $\langle\gamma_0^2\rangle/\bar{D}$ are plotted as a function of energy for five of the elements listed in Table I. The vertical lines give the magnitude of statistical uncertainties and the horizontal lines indicate the neutron energy spread in each case. According to the strong interaction theory $\langle\gamma_0^2\rangle/\bar{D}$ is independent of energy and atomic weight and is about 0.23×10^{-13} cm if the kinetic energy of the neutron inside the nucleus is taken to be 40 Mev. On the complex square well model,

[12] C. T. Hibdon and A. Langsdorf, Jr., Phys. Rev. **98**, 223 (1955).
[13] R. C. Block and H. W. Newson, Phys. Rev. **98**, 1162(A) (1955).
[14] Miller, Adair, Bockelman, and Darden, Phys. Rev. **88**, 83 (1952).

$\langle\gamma_0^2\rangle/\bar{D}$ is not expected to vary rapidly with energy except for elements having a giant S-wave resonance in this energy region. For elements such as selenium and bismuth, whose atomic weights are not in the region of a low-energy S-wave giant resonance,[4] the complex square-well model predicts a $\langle\gamma_0^2\rangle/\bar{D}$ of the order of 0.05×10^{-12} cm. For nickel, zinc and cerium values of $\langle\gamma_0^2\rangle/\bar{D}$ several times larger than this are predicted.[3]

The selenium results exhibit an unexpected behavior. Even after taking into account the uncertainties inherent in this method, the values of $\langle\gamma_0^2\rangle/\bar{D}$ at 160 kev and 230 kev are much higher than those expected on the basis of either the strong interaction theory or the complex square-well potential. The values of $\langle\gamma_0^2\rangle/\bar{D}$ for 160 and 230 kev are so large that Eq. (6) cannot be expected to be valid. The quantity of significance is $Q=(1-|\langle U(E)\rangle_{Av}|^2)$, the cross section for formation of the compound nucleus by S-wave neutrons divided by $\pi\lambda^2$, and cannot be more than unity. The fact that the values of Q corresponding to the 160-kev and 230-kev data are 0.9 and 1.2, respectively suggests that at these energies an appreciable amount of P-wave interaction is taking place. Furthermore, there is a peak, presumably produced by P-wave neutrons,[3] in the measured total cross section[15] of selenium at an energy of about 200 kev. It is possible[6] that $\langle\gamma_1^2\rangle/\bar{D}$ is sufficiently large at these energies to account for the high values of Q. The observed level spacing in selenium is of the order of 1 kev, a fact which makes it unlikely that the large values of Q at 160 and 230 kev are due to statistical fluctuations in $\langle\gamma_0^2\rangle/\bar{D}$.

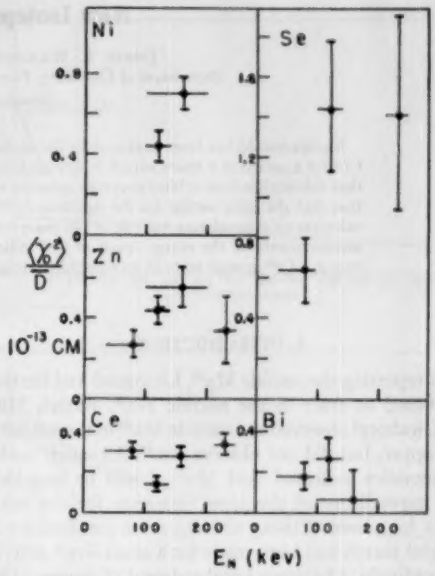

FIG. 1. Strength function $\langle\gamma_0^2\rangle/\bar{D}$ vs energy. The values were computed from the data by assuming that only S-wave neutrons interacted appreciably.

5. DISCUSSION

The results presented have shown the feasibility of obtaining average reduced neutron width densities by observing deviations from exponential attenuation of fast neutrons. However there are not enough data to provide definite conclusions about the behavior of $\langle\gamma_0^2\rangle/\bar{D}$ as a function of atomic weight, and consequently one could not make a choice between the complex square well and strong interaction models on the basis of these data alone. The values of $\langle\gamma_0^2\rangle/\bar{D}$ for nickel and zinc might be evidence for the peak in $\langle\gamma_0^2\rangle/\bar{D}$ as a function of atomic weight predicted by the complex square-well and intermediate[5] nuclear models. The fact that $\langle\gamma_0^2\rangle/\bar{D}$ does not change much over an energy range of nearly 200 kev for zinc, cerium, and bismuth seems to indicate only S-wave neutrons interact appreciably with these elements below 200 kev. The selenium data, on the other hand, suggest a contribution by P-waves.

Deviations from exponential attenuation will affect measured average total cross sections. As has been pointed out, average cross sections computed from Eq. (3) will in general be too low unless the sample used in the transmission experiment is thin. This effect is pronounced in the case of selenium, where average total cross sections[15] measured with samples giving about 45 percent transmission are about ten percent lower than the values obtained in the present experiment with samples of about 85 percent transmission. For all of the other elements used in this investigation, previously published[14] average total cross sections agree with the values found in this experiment within five percent.

[15] Walt, Becker, Okazaki, and Fields, Phys. Rev. **89**, 1271 (1953).

New Isotope Manganese-53†*

JOSEPH R. WILKINSON AND RAYMOND K. SHELINE
Department of Chemistry, Florida State University, Tallahassee, Florida
(Received April 18, 1955)

Manganese-53 has been produced by the nuclear reaction $Cr^{50}(p,n)Mn^{53}$ in the bombardment of enriched Cr^{50} for a period of 8 hours with 9.5-Mev protons. Measurements of the decay and absorption data indicate that this nuclide is an orbital electron capturing activity without gamma rays or positrons. With the assumption that the cross section for the reactions $Cr^{53}(p,n)Mn^{53}$ and $Cr^{54}(p,n)Mn^{54}$ are the same, it is possible to calculate an approximate half-life of 140 years for this nuclide. These data together with those from previous measurements on the energy levels of Cr^{53} indicate that Mn^{53} probably decays from an $F_{5/2}$ ground state to a $p_{3/2}$ Cr^{53} ground state in an *l*-forbidden transition with a relatively high log*ft* value.

I. INTRODUCTION

IN reporting the nuclide Mn^{54}, Livingood and Seaborg[1] found no trace of the nuclide Mn^{53}. Batzel, Miller and Seaborg[2] observed the nuclide Mn^{54} in the spallation of copper, but did not observe Mn^{53}. Although nuclear systematics indicated that Mn^{53} should be long-lived, the expenditure of the time necessary for the search for a long-lived activity did not seem justified until a careful search had been made for a short-lived activity. Accordingly, a betatron bombardment of elemental iron was undertaken at the University of Chicago betatron. The nuclear reaction expected was $Fe^{54}(\gamma,p)Mn^{53}$. The sample in cylindrical form was mounted directly in the beam of the betatron in such a way that the axis of the cylinder was the axis of the beam. A Geiger tube, shielded from the beam with six inches of lead, was placed parallel to the beam and two inches from the beam center. The entire apparatus has been previously described.[3]

If a Mn^{53} activity in the half-life region from 0.02 second to several minutes were to be produced in this bombardment, it should have been observed. Only the half-life region in the vicinity of 9 minutes and 2 minutes is obscured by other activities. A similar type of bombardment with chemical separation of the manganese was undertaken by Marquez[4] to look for an activity in the intermediate half-life range. All of these results were negative.

In view of these experiments and because shell closure occurs at 28 neutrons, it seemed probable that Mn^{53} would have a very long half-life, probably considerably longer than the half-life of Mn^{54}. The need for a high cross section for the production of Mn^{53} because of its probable long half-life and the necessity of keeping the contaminating Mn^{54} activity at a minimum, seemed to dictate low-energy proton bombardment of the enriched isotope Cr^{53}.

II. EXPERIMENTAL

A sample of Cr_2O_3 containing 92.1% Cr^{53}, 5.7% Cr^{52}, 1.7% Cr^{54}, and 0.5% Cr^{50} was obtained from the Stable Isotopes Research and Production Division of the Oak Ridge National Laboratory. This sample was bombarded in the 60-inch cyclotron at the University of California for a period of 8 hours with 9.5-Mev protons. The total beam current for the bombardment was 29.03 microampere hours. The sample was dissolved in concentrated nitric acid to which a few drops of 30% hydrogen peroxide had been added. The solution was boiled to destroy the excess H_2O_2 and 10 mg of manganese as $Mn(NO_3)_2$ was added as carrier. The solution was brought to boiling and solid $KClO_3$ added to precipitate the manganese as MnO_2. The precipitate was filtered, washed with concentrated HNO_3, then with distilled water and redissolved in concentrated HNO_3 to which a few drops of 30% H_2O_2 had been added. The resulting solution was boiled to destroy the excess H_2O_2 and holdback carriers of chromium, cobalt, and iron were added. The manganese was again precipitated from the boiling solution with solid $KClO_3$. The precipitate was filtered, washed, and dissolved as before. Holdback carriers were again added and the manganese precipitated as before. This step was repeated twice more with the holdback carriers present and a final time without the holdback carriers. The final precipitate of MnO_2 was evaporated nearly to dryness on a hot plate and then placed in a plastic planchet and dried

TABLE I. Analysis of the long-lived components of manganese activity resulting from the proton bombardment of Cr^{53}.

Case No.	Constant amounts of activity subtracted (in counts/minute)	Half-time of remaining straight line (in days)	Mean deviation [log activity/day]
1	10	360	0.02341
2	20	312	0.02328
3	30	260	0.02392
4	40	210	0.02707

† This work was supported in part by the U. S. Atomic Energy Commission.
* This paper was taken from a portion of a thesis submitted by J. R. Wilkinson to the Graduate Faculty of Florida State University in partial fulfillment of the requirements for the Ph.D. degree.
[1] J. J. Livingood and G. T. Seaborg, Phys. Rev. **54**, 391 (1943).
[2] Batzel, Miller, and Seaborg, Phys. Rev. **84**, 671 (1951).
[3] R. K. Sheline, Phys. Rev. **87**, 557 (1952).
[4] L. Marquez (private communication).

under an infrared light. The activity was then measured by means of an ordinary Geiger counter.

III. RESULTS AND DISCUSSION

The activity of the sample was very high at first due to the presence of 5.8-day Mn^{52}. After the Mn^{52} activity had completely died away, there were at least two longer-lived activities present. These long-lived activities have now been followed for a period of 29 months.

In order to insure the purity of the sample after the observation of the long-lived activities, a second series of chemical separations similar to those already described were made. These chemical separations in no way affected the absorption characteristics or gross activity of the sample showing that the activities were manganese.

To eliminate any chance of the longer-lived activities being influenced by the relatively large amount of the 5.8-day Mn^{52} activity, that portion of the decay curve resulting from the 100 days immediately following the bombardment was discarded and only the last 26 months of the decay used in the analysis. This analysis indicates that there were only two long-lived activities present. One of these long-lived components was 310-day Mn^{54} as indicated by decay and absorption characteristics. The other component was a much longer-lived manganese activity than Mn^{54}.

Simple inspection of the decay curve also indicated that this long-lived activity is present in relatively small amounts. Accordingly, small constant amounts of activity were subtracted from the over-all decay curve and the best straight line, as determined by the method of least squares, drawn through the resulting points. A plot of these straight lines gave the results shown in Table I.

As indicated in Table I, the mean deviation of the plotted points from the straight line was least for case 2 and greatest for case 4. The half-time of the remaining straight line of 312 days in case 2 agrees most closely with the half-life of Mn^{54} of 310 days as determined by Livingood and Seaborg[4] and the most recent determination of the half-life of Mn^{54} as 291 days by Backofen and Herber.[5] The fact that the mean deviation in case 2 was the smallest precisely when the Mn^{54} half-life agrees most closely with previous experimental results gave some credulence to the belief that we were actually observing a new manganese activity which was very long-lived in comparison to Mn^{54}. In particular, it would seem to be justified to assume no decay of this activity over a period of 26 months if it is formed with a cross section even remotely close to that with which Mn^{54} is formed. However, the potential accidental coincidence between the best Mn^{54} half-life and the mean deviation of the straight lines made it imperative

[5] E. W. Backofen and R. H. Herber, Phys. Rev. 97, 743 (1955).

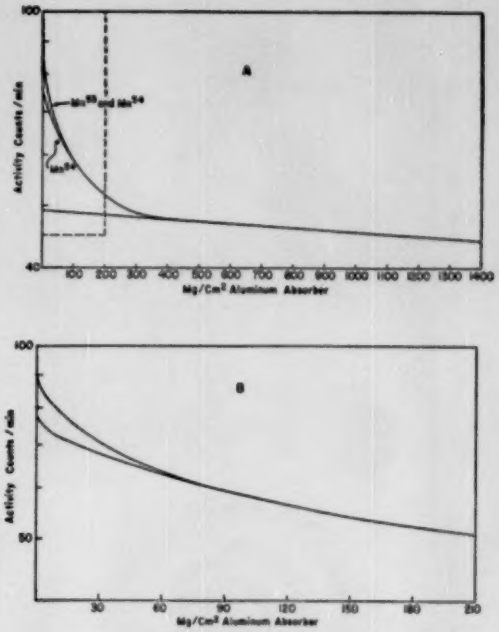

FIG. 1. Absorption curve of Mn^{53} and Mn^{54}. Curve *B* is an expanded plot of the dotted area in curve *A*.

to justify the existence of a small number of long-lived manganese counts in some independent way. In order to attain this end as well as obtain a better value of the amount of activity of the longer-lived component, the absorption curve of the sample was compared with the absorption curve of Mn^{54} which contained less than 1% Mn^{53}.

This sample of Mn^{54} was obtained from the Oak Ridge National Laboratory and a portion of the sample chosen to give approximately the same specific activity as that of the bombarded sample. The Mn^{54} was precipitated as MnO_2 in the same manner as the original sample and mounted in the same type planchet. The experimental conditions for the precipitations duplicated as closely as possible those of the precipitations of the original bombarded sample. The absorption curves of this Mn^{54} and that of the original bombarded sample were taken and compared by normalizing their gamma ray components as shown in Fig. 1. The difference between the activities of the two absorption curves when normalized is 19 counts/minute.

The close agreement of the activity of 19 counts/minute as obtained from the comparison of the absorption curves with that calculated from the decay data justified the assignment of this amount of activity to a long-lived isotope of manganese.

The difference between the absorption curve of Mn^{54} and that of the bombarded sample is the absorption curve of Mn^{53}. This absorption curve is shown in Fig. 2.

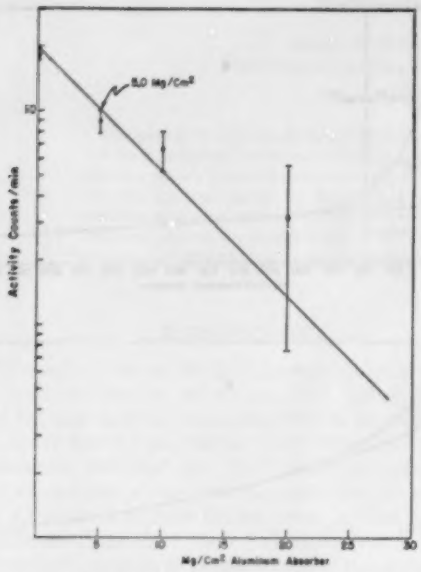

FIG. 2. Absorption curve of Mn^{52}.

The half-thickness from this plot was found to be 5.0 mg/cm². This half-thickness is within the error of our experiments of the calculated value of the chromium K_α x-ray of 4.8 mg/cm². Not only is the half-thickness 5.0 mg/cm², but there is a single component in the absorption plot. This indicates that there are no gamma rays present in the decay of the new long-lived manganese activity.

It is established then that we have a long-lived gammaless orbital electron capturing isotope of manganese. In view of the isotopic composition of the enriched Cr^{52} isotope used in the proton bombardment, the presence of an unassigned position in the nuclear periodic table at 25 protons and 28 neutrons, the unusual stability expected because of shell closure at 28 neutrons, and finally, the fact that this is a proton excess nucleus since it is an orbital electron capturer, the only reasonable assignment of this long-lived manganese activity is Mn^{52}.

From the Mn^{52} activity of 19 counts/minute, the Mn^{54} activity remaining after the gamma-ray component has been subtracted, the isotopic composition of the enriched Cr^{52} used in the bombardment, and the cross section for the production of Mn^{52} (assuming it is the same as that for Mn^{54} in the reactions $Cr^{54}(p,n)Mn^{54}$ and $Cr^{52}(p,n)Mn^{52}$) it is estimated that the half-life of Mn^{52} is 140 years.

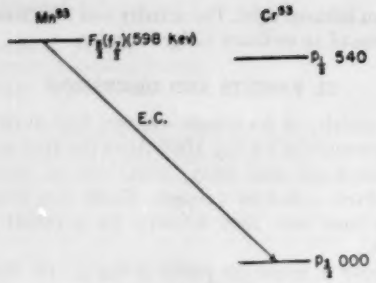

FIG. 3. A decay scheme for Mn^{52}.

The data of McClelland *et al.*[6] and Stelson and Preston[7] in studying the $Cr^{52}(p,n)Mn^{52}$ threshold indicate that Mn^{52} should decay with an energy of 598-kev. The ground state of Cr^{52} is known to be a $p_{3/2}$ state, whereas the relative intensities of the Cr^{52} neutron-capture gamma rays[8] indicates that the first excited state of Cr^{52} is probably $p_{1/2}$.[9] Therefore, Mn^{52} should decay into the ground state of Cr^{52} only, whether the ground state of Mn^{52} is $F_{5/2}$ or $f_{7/2}$. On the other hand, other experimental indications point fairly strongly to the correct spin and parity assignment for the ground state of Mn^{52}. If the ground state of Mn^{52} is $F_{5/2}$, then a $5/2- \rightarrow 3/2-$ l-forbidden transition with logft value from 5.0–9.0 would result in a half-life for a 598-kev orbital electron capture of 70 days to 500 years. However, the second forbidden transition (logft value = 13.0) expected if the ground state of Mn^{52} is $f_{7/2}$ would result in a half-life of $\sim 10^6$ years. In spite of the uncertainties involved in the half-life determination of Mn^{52} as 140 years and the assignment of logft values, it seems probable that the half-life is known sufficiently accurately to discriminate rather strongly against the $f_{7/2}$ assignment as the ground state of Mn^{52}.

On the basis of all of these considerations the decay scheme for Mn^{52} shown in Fig. 3 is proposed.

ACKNOWLEDGMENTS

The authors wish to express their appreciation to the Stable Isotopes Research and Production Division of the Oak Ridge National Laboratory for the loan of the enriched Cr^{52} used in these experiments and to Dr. G. Bernard Rossi and the crew of the 60-inch cyclotron at the University of California for their help and cooperation in arranging the necessary bombardments.

[6] McClelland, Goodman, and Stelson, Phys. Rev. **86**, 631 (1952).
[7] P. H. Stelson and W. M. Preston, Phys. Rev. **86**, 807 (1952).
[8] B. B. Kinsey and G. A. Bartholomew, Phys. Rev. **89**, 375 (1953).
[9] R. H. Nussbaum, thesis, University of Amsterdam, December, 1954 (unpublished).

Long-Lived Isomer of Al^{26}†

T. H. Handley and W. S. Lyon
Oak Ridge National Laboratory, Oak Ridge, Tennessee
(Received April 13, 1955)

Long-lived Al^{26} has been chemically purified from aluminum targets used in the 86-in. cyclotron. The main decay observed is through a 1.30±0.15 Mev positron in coincidence with a 1.82-Mev gamma ray. In addition, gamma rays of 0.717 Mev and 2.91 Mev have been found.

INTRODUCTION

FROM experimental as well as theoretical considerations, it has been suggested [Kavanagh *et al.*[1] give an excellent summary of these data] that the 6-second β^+-emitting Al^{26} is not the ground state. Recently, Simanton, Rightmire, Long, and Kohman[2] have isolated a small amount of a long-lived aluminum activity from a target of magnesium bombarded with 15-Mev deuterons at the University of Pittsburgh cyclotron. From their very low intensity source, they were able to identify gamma peaks from the 0.51-Mev annihilation radiation, and evidence was found for a gamma ray at ~1.9 Mev. In addition, aluminum absorption data showed the presence of ~1-Mev electron. These data were consistent with the postulated positron decay from the 5^+ level in Al^{26} to the known 1.8-Mev excited level in Mg^{26}. The half-life of such isomer should then be 10^4–10^6 years.

At the Oak Ridge National Laboratory, there are available several old aluminum targets which have received many hours of proton irradiation. Al^{26} could be produced by the (p,pn) reaction or $(p,2n)$ to short-lived Si^{26} with decay to Al^{26}, and these targets should be a source of a considerable amount of Al^{26}. Several targets were obtained and were processed as described below.

PREPARATION OF THE SOURCE

These old aluminum test targets used in the ORNL 86-in. cyclotron had received an unrecorded number of hours bombardment with 22.4-Mev protons. The target of solid aluminum, 6 in.×10 in., which was cooled by circulating water and slightly concave, was flattened and placed in a tray with the face in contact with concentrated hydrochloric acid. Approximately 25 g of aluminum were removed from the face. Holdback carriers of suspected possible contaminants were added, i.e., Co, Fe, Mn, and Zn. Purification of the aluminum was accomplished by taking the hydrochloric acid solution of aluminum and saturating it with gaseous hydrochloric acid while cooling to a temperature of 15°C.[3] A volume of ether equal to the volume of the liquid was added and gaseous hydrochloric acid passed through until the solution was saturated; this was noted by a disappearance of the two layers. After standing approximately one hour, the supernate was discarded by decanting. The precipitate of $AlCl_3$ was washed with a solution composed of equal parts of hydrochloric acid and ether and saturated with hydrochloric acid gas at 15°C. The precipitate of $AlCl_3$ was dissolved in approximately 10*N* HCl, by warming, if necessary. Reprecipitation of $AlCl_3$ was repeated eight times. After a study of the gamma spectrum and coincidence measurements, the purification was repeated with eight additional $AlCl_3$ precipitations followed by an acid sulfide pre-

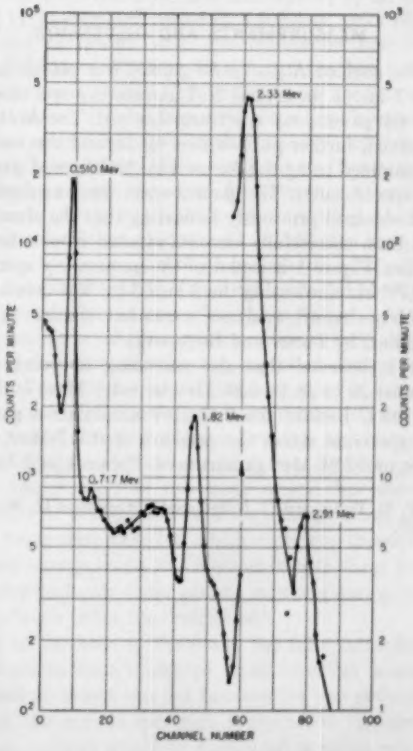

FIG. 1. Gamma-ray spectrum of Al^{26}.

† Work performed under contract to the U. S. Atomic Energy Commission.

[1] Kavanagh, Mills, and Sherr, Phys. Rev. **97**, 248 (1955).

[2] Simanton, Rightmire, Long, and Kohman, Phys. Rev. **96**, 1711 (1954).

[3] W. F. Hillebrand and G. E. F. Lundell, *Applied Inorganic Chemistry* (John Wiley and Sons, Inc., New York, 1929), p. 392.

TABLE I. Radiation from Al^{26g}.

Type	E (Mev)	Absolute γ intensity relative to total β^+	Remarks
Annihil. gamma	0.51	2	Coinc. with 1.82-Mev γ-ray
Gamma 1	0.717	0.01	
Gamma 2	1.82	1	
Gamma 3	2.91	0.004	
Beta	1.30±0.15	1	Coinc. with 1.82-Mev γ-ray

cipitation using Cu as a scavenger. The solution was then evaporated just to dryness and further studies made.

The supernate containing the impurities was collected and boiled just to dryness. A qualitative scheme separation of these impurities followed by a gamma-ray spectrum of the separated groups showed the presence of Na, Mn, Fe, Co, and Zn radioactivities. These activities were produced from impurities in the original aluminum target, or the target was contaminated with them during the various test runs. However, since a gamma spectrum of the final product did not show the presence of these impurities either before or after the final repurification, it is felt the final product is pure.

MEASUREMENTS AND DISCUSSION

The purified Al_2O_3 (~50 grams) was placed on top of a 3 in.×3 in. crystal NaI gamma-ray spectrometer and the gamma-ray spectrum obtained. The Al_2O_3 was dissolved, further purifications made, and the material re-examined using the 3 in.×3 in. NaI crystal gamma-ray spectrometer. The gamma spectrum was similar to that obtained previously indicating that the aluminum had been successfully decontaminated from other activities. Figure 1 is a plot of the gamma-ray spectrum of Al^{26g} obtained using the 3 in.×3 in. NaI crystal and a thirty-channel analyzer somewhat similar to that described by Porter and Borkowski.[4]

It is believed that the scattering of points from channel 20 to 38 (~0.86 Mev to ~1.5 Mev) is due to statistics. Besides the 0.51-Mev annihilation gamma, the spectrum shows the presence of 0.717-Mev, 1.82-Mev, and 2.91-Mev gamma rays. The peak at 2.33 Mev is believed to be mainly due to summing of the coincident positron and 1.82-Mev gamma ray. The peak at 2.91 Mev is believed to represent a real gamma ray of this energy and not a scattering pile up phenomena. A source of Na^{22} (β^+ and 1.28-Mev γ ray) of about twice the intensity of the Al^{26} was examined for a peak at (1.02+1.28) Mev; such a peak would result from a pile-up scattering also if the Al^{26} 2.91-Mev γ ray was produced in this manner. There was no peak observed in this region with the Na^{22} source. The approximate relative intensities of the gamma rays was obtained by dividing by the photopeak efficiency obtained from known standards in the usual manner. These data are shown in Table I.

Aluminum absorption data were obtained by using a source containing ~100 mg of the Al_2O_3 and an end-window Geiger-Muller counter as detector. Comparison of the slope of the activity *vs* absorber thickness plot with plots made of known energy beta emitters mounted in a similar manner indicated the positron energy to be 1.30±0.15 Mev.

Gamma-gamma coincidence measurements were made by using a 1 in.×1.5 in. NaI crystal spectrometer set to accept only 0.51-Mev photoelectrons from the annihilation gamma as one detector, and the 3 in.×3 in. NaI crystal set to accept only 1.82-Mev gamma-ray photoelectrons as the other detector. These data indicated the positron decay is to the 1.82-Mev level. No significant coincidence data were obtained between any of the other gamma rays.

From the approximate intensity measurements, it appears that the number of β^+ and 1.82-Mev gamma rays are about the same; this is confirmed by ion chamber measurements.

From the known energy difference, $Al^{26g}-Mg^{26g}=4.01\pm0.02$ Mev,[5] it appears that the positron energy must be $4.01-1.83-1.02=1.16$ Mev which agrees with the observed value noted above. The 1.83-Mev and 2.9-Mev levels in Mg^{26} are known,[6] but no level at 0.7 Mev has been reported; because of the exhaustive chemical treatment, however, it is felt that this level does occur in the decay of Al^{26g}.

The authors are indebted to F. M. Porter and C. J. Borkowski for permission to use the thirty-channel analyzer.

[4] F. M. Porter and C. J. Borkowski, Nucleonics **12**, No. 3, 53 (1952).

[5] C. P. Browne, Phys. Rev. **95**, 860 (1954).

[6] P. M. Endt and J. C. Kluyver, Revs. Modern Phys. **26**, 95 (1954).

Cascade Gamma Rays from $_{84}Po^{214}$ (RaC′)†

R. E. ROWLAND
Radiological Physics Division, Argonne National Laboratory, Lemont, Illinois
(Received April 21, 1955)

Seven gamma cascades of $_{84}Po^{214}$ have been identified by means of coincidence scintillation spectrometry: gamma rays of energy 0.77, 0.93, 1.12, 1.24, 1.38, 1.52, and 1.85 Mev appear in coincidence with the 0.607-Mev photon transition to the ground state. The existence of a weak beta transition to the 0.607-Mev level was also verified.

Four other gamma rays, of energy 0.85, 1.77, 2.20, and 2.40 Mev, appear as direct transitions to the ground state. Both gamma-gamma and beta-gamma coincidences were employed to verify the suggested energy level scheme.

I. INTRODUCTION

ALTHOUGH many reports[1–5] have appeared on the gamma-ray spectrum following the beta decay of $_{83}Bi^{214}$(RaC), the decay scheme has not yet been satisfactorily described. In view of the somewhat discordant reports,[6] an attempt has been made to clarify the problem by means of gamma-gamma and beta-gamma coincidence scintillation spectrometry.

II. APPARATUS AND EXPERIMENTAL PROCEDURES

Approximately 5×10^{-6} curie of RaCl in equilibrium with its daughters was used as the source of RaC′ gamma rays. This source was dried and sealed between two Mylar films (0.88 mg/cm²) to prevent escape of radon and to insure detection of most of the beta radiation in the beta-gamma coincidence experiments.

Gamma-gamma coincidence spectrometry was performed with two NaI(Tl) crystals, each $2\frac{1}{2}$ in. in diameter and $2\frac{1}{8}$ in. high. Their resolution was approximately 8 percent at 661 kev, and the height of the Compton distribution was 20 percent of the photopeak height in the absence of any collimation.

The pulse-height spectrum in coincidence with any one gamma ray was obtained by accepting from one crystal and its single-channel analyzer a narrow band of pulse heights corresponding to the gamma-ray photopeak and by gating with it the multichannel analyzer. The second crystal fed directly a 24-channel Marconi pulse-height analyzer, which had been modified by the addition of a coincidence gating circuit.

The source was placed directly between the two NaI crystals, and a portion of the RaC′ gamma spectrum was recorded on the multichannel analyzer. Beta-ray detection was eliminated by shielding the source with 1 mm of Pb. The gating crystal was then adjusted to cover each photopeak in turn, and the resulting coincidence spectrum obtained. Its interpretation was carried out by keeping in mind that the counts in the peak, as seen by the gating analyzer, were due to both the desired gamma rays undergoing full energy loss in the crystal and to those gamma rays of greater energy that lost in the crystal energies falling within the band under consideration.

For beta-gamma coincidence spectrometry, one of the $2\frac{1}{2}$ in.$\times2\frac{1}{8}$ in. NaI crystals was retained to record the gamma spectrum on the multichannel analyzer in coincidence with the beta rays of the source, as detected by a suitable scintillator. For beta energies below 0.8 Mev the latter consisted of a NaI crystal, $\frac{1}{32}$ in. thick and $\frac{1}{2}$ in. in diameter, sealed by a 0.001 in. thick nickel foil, and calibrated with the conversion line from Cs^{137} (0.63 Mev). For beta energies greater than 1 Mev, a $\frac{7}{16}$-in. thick plastic scintillator, $1\frac{1}{8}$ in. in diameter, was employed. In both instances, corrections were made for the gamma response of the beta-ray detector by interposing sufficient thickness of Al to filter out the hardest beta rays. If the residual response to gamma rays was at all appreciable, the resulting gamma-gamma coincidence spectrum was subtracted from the observed beta-gamma coincidence spectrum. The purpose of the beta analysis was to determine which of two gamma rays (not in coincidence) originated from the higher energy level and to thus provide an independent method of verification for the suggested energy level scheme. The beta-ray scintillator, connected to a single-channel analyzer, opened the coincidence gate on the multichannel analyzer when a beta ray was detected in the energy band under consideration. By setting the lower energy limit of this band above the beta-ray end point of a transition to a high-energy level, only those betas were detected which represent transitions to lower energy levels. In coincidence with these betas were detected only those gamma rays originating from energy levels below the limit chosen.

For all methods of detection, the false coincidence contributions were evaluated in an identical manner. The radium source was left between the two detectors, so that the gamma spectrum presented to the multichannel analyzer would be unchanged in either rate or shape. The gating analyzer was turned off, after the

† Work performed under the auspices of the U. S. Atomic Energy Commission.

[1] C. D. Ellis and G. H. Aston, Proc. Roy. Soc. (London) **A129**, 180 (1930).
[2] C. D. Ellis, Proc. Roy. Soc. (London) **A143**, 350 (1935).
[3] R. M. Pearce and K. C. Mann, Can. J. Phys. **31**, 592 (1953).
[4] M. Mladjanovic and A. Hedgran, Arkiv Fysik **8**, 49 (1954).
[5] G. D. Latyshev, Revs. Modern Phys. **19**, 132 (1947).
[6] F. Demichelis and R. Malvano, Nuovo cimento **9**, 1106 (1952); **10**, 405 and 1359 (1953); **12**, 358 (1954).

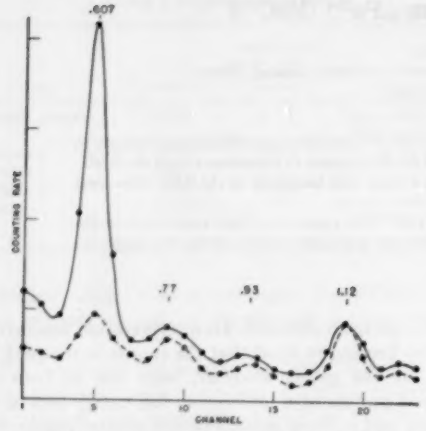

FIG. 1. The solid curve shows the pulse-height spectrum of the RaC′ gammas between the 0.607- and the 1.12-Mev photopeaks as seen by the large NaI crystal. The dashed curve is obtained by gating the multichannel analyzer with the 0.607-Mev photopeak. Both curves are normalized at the 1.12-Mev photopeak.

gating rate had been determined. An independent source of pulses was then applied to the gating circuit of the multichannel analyzer at the same rate obtained in the coincidence experiment. These random pulses originated from a weak radioactive source placed in a remote location.

III. EXPERIMENTAL RESULTS

A. Gamma-Gamma Coincidences

The pulse-height spectra were investigated in three consecutive portions of the 0.5–2.5-Mev energy band, and typical results are shown in Figs. 1 to 3. The solid and broken lines denote respectively the ungated spectrum and the spectrum gated by the 0.607-Mev line; in Figs. 1 and 2 the two curves have been normalized on the 1.12-Mev photopeak in order to estimate roughly the intensities involved. It is evident from these data that of the ten gamma rays resolved by the crystal in the ungated spectra, six are in coincidence with the 0.607-Mev line. Their energies are 0.77, 0.93, 1.12, 1.24, 1.38, and 1.52 Mev. In addition, the previously reported weak photon of 1.85 Mev,[3,4] overshadowed by the 1.77-Mev peak in the ungated spectrum, is clearly detected in coincidence analogous to the others. The small peak at 0.607 Mev, in Fig. 1, that occurs when the analyzer is gated by the 0.607 photopeak, is due to the fact that the coincidence gate may be opened by Compton scattered components of gammas harder than 0.607 Mev, and that the 0.607-Mev gamma is in coincidence with some of these.

By repeating this technique with each of the other photopeaks in turn, no other coincidence peak was revealed outside the 0.607-Mev line.

The photopeaks of 1.77, 2.20, and 2.4 Mev do not appear to be in coincidence with either the 0.607-Mev gamma or any other gamma. From these data we have constructed the decay scheme as shown in Fig. 4.

B. Beta-Gamma Coincidence

Beta-gamma coincidences offered the possibility of confirming the existence of at least some of the energy levels assumed in Fig. 4.

Thus, for the 0.77-Mev gamma to be in coincidence with the 0.607-Mev gamma, it must originate from an energy level at least 1.38 Mev above the ground state. Since the beta energy to the ground state is 3.17 Mev,[7]

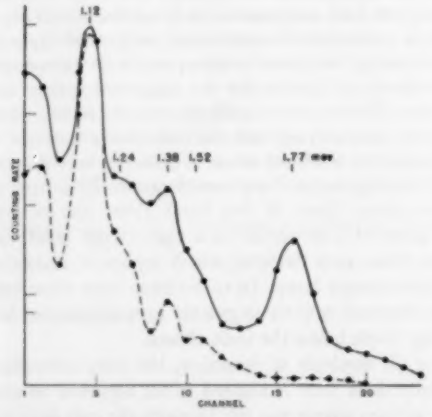

FIG. 2. The solid curve shows the pulse-height spectrum of the RaC′ gammas between the 1.12- and the 1.77-Mev photopeaks. The dashed curve is obtained by gating the multichannel analyzer with the 0.607-Mev photopeak. Both curves are normalized at the 1.12-Mev photopeak.

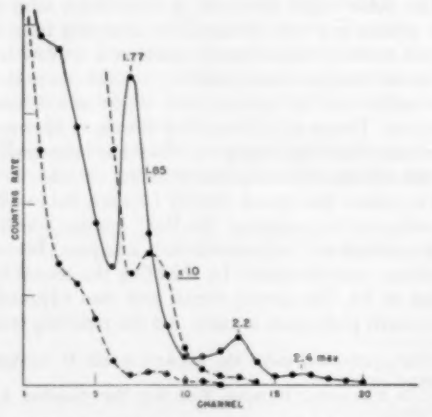

FIG. 3. The solid curve shows the pulse-height spectrum of the RaC′ gammas between the 1.77- and the 2.4-Mev photopeaks. The dashed curve is obtained by gating the multichannel analyzer with the 0.607-Mev photopeak.

[7] A. H. Wapstra, Physica **18**, 1247 (1952).

the beta ray decaying to the level in question must have an end point of 1.79 Mev. When the plastic scintillator is biased to look at beta energies greater than 1.8 Mev, no coincidences with the 0.77-Mev gamma ray should appear if our decay scheme is correct. When this test was made, the beta-gamma coincidence spectrum showed two peaks, corresponding to the expected 0.607-Mev gamma and to one at 0.85 Mev, as shown in Fig. 5. Hence, the assumption that the 0.77-Mev gamma originated from a level at least as high as the 1.38-Mev level is correct. The appearance of the gamma ray at 0.85 Mev confirms the findings of Pearce and Mann,[3] and the other at 0.607 Mev verifies the existence of a weak beta transition to this level as suggested by Wapstra[7] and others,[8] since residual gamma-gamma coincidences were duly taken into account.

In a similar manner, each of the gamma rays appearing in coincidence with the 0.607-Mev line was verified to come from an energy level as indicated by the decay scheme. The beta-gamma coincidence technique was admittedly not as decisive as the gamma-gamma coincidence technique, but it appeared adequate to determine that the photons of 1.12, 1.24, and 1.77 Mev all came from nearly the same level; that those of 0.77 and 0.93 Mev originated from below this level; and that those of 1.38, 1.52, 2.2, and 2.4 Mev came from above this level.

Some of the 1.38-Mev gammas have been shown to be in cascade with the 0.607-Mev gamma by both gamma-gamma and beta-gamma techniques. The latter, however, were not rigorous enough to exclude the possibility that some of the 1.38-Mev photons originate as an alternative to the 0.77–0.607-Mev cascade.

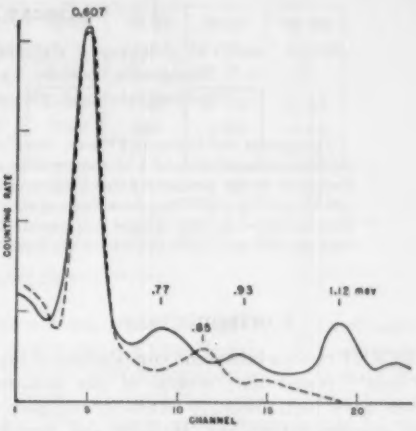

FIG. 5. The solid curve shows the pulse-height spectrum of the RaC′ gammas between the 0.607- and the 1.12-Mev photopeaks. The dashed curve is obtained by gating the multichannel analyzer with betas of energy greater than 1.8 Mev.

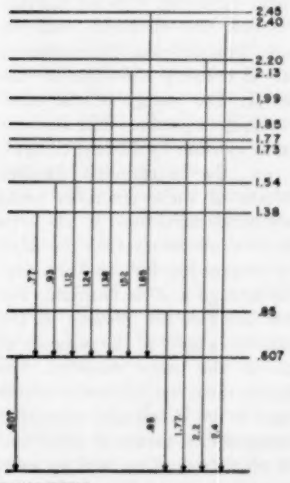

FIG. 4. The energy level system of $_{84}Po^{214}$, as determined by NaI coincidence scintillation spectrometry. Only those gamma rays actually detected in this work are included in this level scheme.

IV. CONCLUSION

The decay scheme as determined by gamma-gamma coincidences, and in a sense verified by the beta-gamma coincidences, describes satisfactorily the cascades and energy level origins of the more intense gammas from $_{84}Po^{214}$. Pearce and Mann,[3] and others,[9] have reported some gammas below 600 kev. These were not seen in coincidence with the 0.607-Mev line but were not looked for in coincidence with the other gammas. It is assumed that they must be very weak.

We were unable to confirm the coincidences between 0.76-Mev and 1.29-Mev gammas, as reported by Demichelis and Malvano.[6] We have, however, verified the other three pairs reported by them, namely those of 1.12, 1.38, and 1.52 Mev with the 0.607-Mev gamma.

ACKNOWLEDGMENTS

I would like to thank Mr. L. D. Marinelli for valuable suggestions and discussions concerning this work. The modification of the Marconi multichannel analyzer to coincidence-anticoincidence spectrometry was designed and engineered by Dr. C. E. Miller of this Laboratory.

[6] R. A. Ricci and G. Trivero, Atti accad. nazl. Lincei **17**, 44–46 (1954).

[9] K. C. Mann and M. J. Ozeroff, Can. J. Research **A27**, 164 (1949).

Decay Scheme of Y^{92}†

WAYNE A. CASSATT, JR.,* AND W. WAYNE MEINKE
Department of Chemistry, University of Michigan, Ann Arbor, Michigan
(Received February 7, 1955; revised manuscript received April 21, 1955)

The gamma radiations of Y^{92} have been investigated with a scintillation spectrometer. The Y^{92} was produced in a cyclotron by a (d,α) reaction on zirconium and was not contaminated with Y^{91} or Y^{93} isotopes present in fission product solutions. Gamma rays of 0.21±0.01, 0.475±0.02, 0.94±0.03, 1.45±0.10, 1.9 ±0.10, and 2.4±0.10 Mev have been observed and both β-γ and γ-γ coincidences of the lower-energy lines tabulated. A decay scheme is proposed which is consistent with the experimental data and with recent data on Nb^{92} and Nb^{92m} reported in the literature.

I. INTRODUCTION

RECENT isotope tables and compilations of nuclear data[1,2] reveal that several of the isotopes of yttrium have been carefully characterized and their decay schemes determined. Half-life and beta-decay data for Y^{92} are also reported in these tables but no attempt has yet been made to formulate a decay scheme. This nuclide was previously observed by several workers as a fission product and also as a product of the (n,p) reaction on zirconium. Work in this laboratory[3] verified the mass assignment of this 3.6-hr activity to mass 92 by comparison of relative (d,α) reaction yields on the stable zirconium isotopes.

The half-life of Y^{92} was determined as 3.60±0.05 hours by Ames and his co-workers.[4] Values of 3.4, 3.5, and 3.6 Mev[1] have been reported for the maximum β-ray energy of this nuclide obtained by absorption methods. Ames *et al.*[4] studied this β-ray spectrum with a magnetic spectrometer and from their data postulated the presence of three β rays having maximum energies of 1.3, 2.7, and 3.60 Mev but do not give information regarding the relative intensities of these radiations. The γ-ray energies for this isotope were estimated by Hoagland and Katcoff[5] to be between 0.7 and 1.1 Mev by lead absorption. A search of the literature up to January, 1955 has revealed no additional work on this isotope. A chart showing the isotopes of niobium, zirconium, and yttrium given in Fig. 1 indicates the relationship of the various isotopes which might be found in low-energy deuteron bombardments of zirconium. Further information[1] on the radiations of the yttrium isotopes is given in Table I.

TABLE I. Nuclear characteristics for yttrium isotopes.

Isotope	Percent abundance	Type of decay[a]	Half-life	Energy of radiation in Mev: Particles	Energy of radiation in Mev: Gamma transitions
Y^{87m}		IT, no β^+	14 hr		0.384
Y^{87}		EC 99+% β^+ ~0.3%	80.0 hr	0.7	0.485, 0.390 (with Sr^{87m})
Y^{88}		EC 99+% β^+ 0.19%	104 day	0.83	0.908 (~99%) 1.853 (~99%) 2.76 (~1%)
Y^{89m}		IT	~14 sec		0.913
Y^{89}	100				
Y^{90}		β^-	61 hr	2.18	No γ
Y^{91m}		IT	51.0 min		0.551
Y^{91}		β^-	61 day	1.537	1.2, 0.2 (both 0.1%)
Y^{92}		β^-	3.60 hr	3.60, 2.7, 1.3	0.7–1.1
Y^{93}		β^-	10.0 hr	3.1	0.7
Y^{94}		β^-	16.5 min	5.4	1.4
Y^{95}		β^-	10.5 min		

[a] IT = isomeric transition; EC = electron capture.

II. EXPERIMENTAL METHODS[6,7]

The yttrium was produced by bombardment of high-purity zirconium metal foil with 7.8-Mev deuterons in the University of Michigan cyclotron. This foil (having natural isotopic abundances) was obtained from the Foote Mineral Company, Philadelphia, Pennsylvania and spectrographic analysis revealed the chemical impurities listed in Table II. The energy of the bombarding deuterons was such as to produce only isotopes of niobium, zirconium, and yttrium by (d,xn), (d,xnp), and (d,α) reactions on the zirconium. Smaller amounts of other products of these reactions could be expected from the chemical impurities. It has been found experimentally in this laboratory that the (d,α) reaction is energetically impossible for 7.8-Mev deuterons on an element of as high a Z as hafnium. For this reason no lutetium isotopes are present in the chemically separated samples in spite of the presence of several percent hafnium in the target material. For satisfactory characterization then, the yttrium products of the (d,α) reaction had to be chemically separated from a hundred- or thousand-fold excess of (d,n) and (d,p) reaction products of zirconium as well as from products of these reactions on the impurity elements.

* Present address: Phillips Petroleum Company, Bartlesville, Oklahoma.
† This work was partially supported by the U. S. Atomic Energy Commission.
[1] Hollander, Perlman, and Seaborg, Revs. Modern Phys. **25**, 469 (1953).
[2] *Nuclear Data*, National Bureau of Standards Circular No. 499 (U. S. Government Printing Office, Washington, D. C., 1950), including supplements and cards bringing table up to date.
[3] G. L. Schott and W. W. Meinke, Phys. Rev. **89**, 1156 (1953).
[4] Ames, Bunker, and Starner as given by reference 1.
[5] E. J. Hoagland and S. Katcoff, *Radiochemical Studies: The Fission Products* (McGraw-Hill Book Company, Inc., New York, 1950), Paper 73, p. 660, National Nuclear Energy Series, Plutonium Project Record, Vol. **9**, Div. IV.
[6] The equipment and techniques mentioned in this section are described in more detail in the doctoral thesis of W. A. Cassatt, Jr. (reference 7).
[7] Wayne A. Cassatt, Jr., Ph.D. Thesis, University of Michigan, September, 1954 (unpublished).

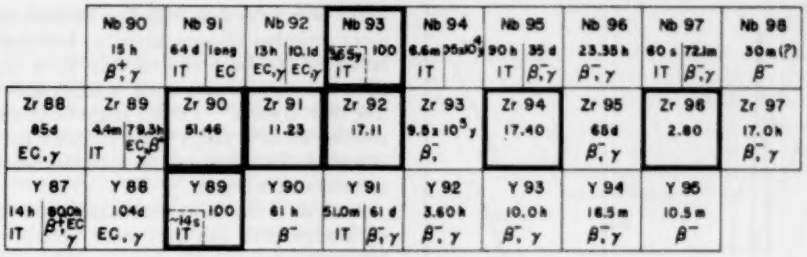

FIG. 1. Chart of niobium, zirconium, and yttrium isotopes.

The zirconium target was dissolved in hydrofluoric acid containing niobium and yttrium carriers, the precipitates digested, centrifuged, and washed. The yttrium fluoride precipitate was metathesized with concentrated potassium hydroxide solution, the hydroxide precipitate washed three times with water to remove the fluoride ion, and then redissolved in a minimum amount of HCl. More zirconium and niobium carriers were added, the zirconium and niobium precipitated by the addition of concentrated phosphoric acid and these phosphate precipitates centrifuged out, leaving the yttrium in the supernatant solution. This solution of yttrium was then recycled twice through the above procedure, the final hydroxide precipitate dissolved in a minimum amount of concentrated nitric acid, and an aliquot of the purified yttrium mounted for decay measurements.

The gross decay of the yttrium fraction was followed on both a scintillation well-type counter (Nuclear-Chicago Model DS-3) and a 4π proportional flow counter similar to that described by Borkowski.[8] These detectors were used in conjunction with a scale of 128 counting circuit. High-purity methane (99 mole percent minimum from Phillips Petroleum Company) was used as a counting gas.

A γ-ray scintillation spectrometer was used to study the γ-ray spectrum of a purified yttrium fluoride sample which was taken before the final hydroxide precipitation. This instrument utilizes as a detector a sealed 1-in. cube of NaI(Tl) coupled to a DuMont 6992 photomultiplier tube. The scintillation pulse is amplified by an Atomic Instrument Company Model 204B linear amplifier and fed into a Tektronix 514D oscilloscope, where the lines are recorded by a Polaroid Land camera. Pictures were taken of the spectrum appearing on the oscilloscope at various times after bombardment. An alternate system fed the pulses from the linear amplifier into an Atomic Instrument Company Model 510 single-channel pulse-height analyzer. The pulses selected by this analyzer trigger a counting rate meter whose output is plotted on a Leeds and Northrup Speedomax strip chart recorder.

For other data, the β-ray spectrum of an yttrium sample was measured with a survey β-ray spectrometer.[9] This instrument is a variable-field, 180° magnetic-type spectrometer with a four-centimeter focusing radius and utilizes a thin-window Geiger-Mueller tube as a detector. The yttrium sample was prepared by evaporating an aliquot of purified yttrium nitrate solution on a thin (0.00025-in.) Teflon film with the aid of an infrared heat lamp. The dry sample was then covered with another thin Teflon film which was held in place with rubber cement.

β-γ and γ-γ coincidence studies were also carried out on the 3.6-hr yttrium activity. The coincidence counter consists of two scintillation detectors feeding through linear amplifiers (Atomic Model 204B) into twin single-channel differential pulse-height analyzers (Atomic Model 510) which in turn trigger a coincidence analyzer (Atomic Model 502A). This setup makes possible the study of the coincidences occuring between various parts of the γ-ray spectrum of a sample, or between parts of the γ-ray spectrum in coincidence with portions of the β-ray spectrum when suitable scintillation crystals and/or absorbers are used.

In the β-γ coincidence measurements, a $\frac{3}{16}$-in. thick by $1\frac{1}{2}$-in. diameter *trans*-stilbene crystal was used in one scintillation detector to detect β rays and a 1 in. $\times 1\frac{1}{2}$ in. NaI(Tl) crystal was used in the other scintillation detector to count the γ rays. A beryllium absorber (2430 mg/cm²), thick enough to stop the most energetic (3.6-Mev) β rays from the yttrium, was used between the sample and the NaI(Tl) crystal. No absorber was

TABLE II. Chemical impurities in zirconium target foil as determined by spectrographic analysis.

Element	Percent	Element	Percent
Al	0.04–0.08	Mo	0.001
Ca	0.003	N	0.004–0.04
Cr	0.001	Pb	0.001
Cu	0.007	Si	0.02
Fe	0.01–0.20	Sn	0.001
Hf	2.5–3.0	Ti	0.04
Mg	0.003	W	0.001
Mn	0.001		

[8] C. J. Borkowski and T. H. Handley, Oak Ridge National Laboratory Progress Report ORNL-1056, April, 1951 (unpublished), p. 1.

[9] Meinke, Cassatt, and Hall, "A Variable Field Survey Beta-Ray Spectrometer," AEC Nuclear Chemistry Project Report, University of Michigan, June 1954. Also Atomic Energy Commission Unclassified Document AECU-2944 (unpublished).

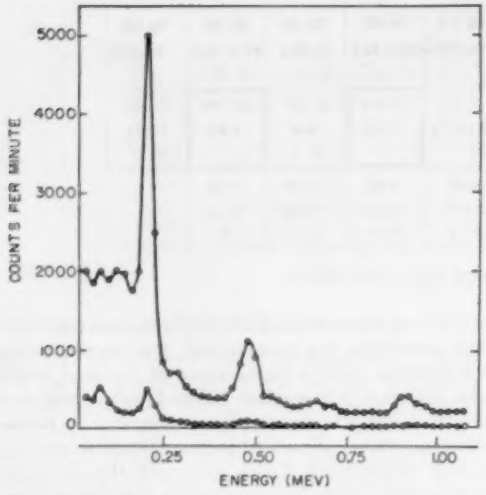

FIG. 2. Yttrium-92 γ-ray spectra. Top curve was taken three and one-half hours after the end of bombardment and ten and one-half hours before the lower curve.

used between the stilbene crystal and the sample. The base line and channel width of the single-channel pulse-height analyzer connected to the NaI(Tl) crystal were adjusted so that this analyzer passed on to the coincidence counter only those pulses lying within the energy region of one of the photoelectric peaks. The β-ray spectrum was then scanned in discrete steps with the single-channel pulse-height analyzer connected to the stilbene crystal. At each step the coincidence count rate and the gross count rate in each detector were recorded. This scanning was repeated for each of the four γ rays.

For γ-γ coincidence studies the stilbene crystal was replaced by a 1 in.$\times$1½ in. NaI(Tl) crystal and a beryllium absorber (2640 mg/cm^2) was placed between this crystal and the yttrium sample. One of the single-channel pulse-height analyzers was set to count only those pulses under a given γ-ray photoelectric-peak. The γ-ray spectrum was then scanned with the other pulse-height analyzer. The gross counts and coincidence counts were recorded for each setting of the latter pulse-height analyzer. To reduce false coincidences arising from 180° Compton scattering from one crystal to another, a ½-in. lead absorber was placed midway between the crystals with a ¾-in. hole in the center so that the sample could "see" both crystals.

III. RESULTS

Resolution of the decay curves taken with thin samples on the 4π proportional counter showed clearly that only three components, 3.6-hr, 61-hr, and 105-day, were present. Curves taken with the scintillation well counter showed a definite 3.6-hour component but were less conclusive for components of several days because of interference from the bremsstrahlung of the β-ray emitting 61-hour activity. Isotopes with these half-lives can be produced only by a (d,α) reaction upon the natural zirconium isotopes shown in Fig. 1. The short-lived Y^{89m} [which might be formed by a (d,α) reaction on Zr^{91}] and Y^{94} isotopes were not observed in this work since they had decayed out before the measurements were begun.

Analysis of the decay curves indicated that activities of intermediate half-lives were present in amounts less than a few percent as compared with the amount of the 3.6-hr activity. The absence of any 51-min, 10-hr, 14-hr, 80-hr or 61-day components in the decay curve indicates that the $(d,\alpha n)$ reaction does not occur to an appreciable extent at this deuteron energy. It also insures that the Y^{92} can be characterized without interference from radiations of these intermediate half-life isotopes, some of which would be present in good yields in fission product solutions and which could be discriminated against only by careful "milkings" of the strontium fission product parents. The absence of other components in the decay curve is further taken as proof that the yttrium was satisfactorily separated from the contaminating bombardment products of other elements in the target and also that no lutetium was formed as the result of a (d,α) reaction on the hafnium present in the target (the chemical procedure would not differentiate between yttrium and lutetium).

The γ-ray spectra[10] taken during the first few hours after bombardment show three strong peaks at 0.21, 0.475, and 0.94 Mev. Three weaker photolines were also observed at 1.45, 1.9, and 2.4 Mev. Spectra taken several days after bombardment show only a 0.90-Mev line and 1.8-Mev line, corresponding to lines reported for the 105-day Y^{88} isotope. These same two lines still persisted in the sample three months after bombard-

TABLE III. Energies, intensities and γ-γ coincidences of Y^{91} γ rays observed with scintillation spectrometers. (Errors are standard deviations.)

	Energy (Mev)	Rel. intensity (corrected)	γ rays in "coincidence" (Mev)
γ_1	0.21 ±0.01	1	0.48, 0.94
γ_2	0.475±0.02	1.1±0.1	0.21, 0.475, 0.94 (weak)
γ_3	0.94 ±0.03	1.9±0.4	...
γ_4	1.45 ±0.10	~1	0.21, 0.475, 0.94
γ_5	1.9 ±0.10	~0.1	...
γ_6	2.4 ±0.10	~0.02	...
	Other reported values		
From Nb^{89} [a]:			
γ_a	0.930	0.98	0.900, Zr x-rays
γ_b	0.900	0.01	0.930, Zr x-rays
γ_c	1.83	0.02	Zr x-rays
From Nb^{89m} [b]:			
γ_d	2.35		

[a] See reference 12.
[b] See reference 13.

[10] Pictures of these spectra and coincidence spectra referred to later in the paper can be found in reference 7.

ment and had decreased in intensity by a factor of approximately two.

Graphs of the lower-energy lines of the γ-ray spectrum of Y^{92} are shown in Fig. 2. A comparison of the original curves which are redrawn for Fig. 2 showed that the three γ-ray peaks at 0.21-, 0.475-, and 0.94-Mev decay with the same half-life. Oscilloscope pictures of these lines also show that the lower-intensity lines at 1.45(?), 1.9(?), and 2.4(?) Mev decay with roughly the same half-life as the three lower-energy lines. As further proof, intensity measurements on the 1.9-Mev line show it to be at least twenty times more intense than the 1.8-Mev line ascribed to the 105-day Y^{88} present in the sample. These six γ rays in the chemically purified sample were thus assigned to Y^{92} because they all appeared to decay with a half-life estimated to be between 3 and 4 hours.

The experimental energy and relative intensity values for the lines of Y^{92} are listed in Table III. Estimated errors are reported as standard deviations. The relative intensities of γ_1, γ_2, and γ_3 were obtained by integration of the area under the photoelectric peaks after subtraction of the background and the Compton distribution of the higher-energy γ rays. These areas were then corrected for the "photoelectric yield" of the crystal by use of the curves of McLaughlin and O'Kelley.[11] Relative intensities for γ_4, γ_5, and γ_6 were estimated from oscilloscope pictures and the same corrections applied.

The negative β-ray spectrum obtained approximately twelve hours after bombardment of the zirconium gave an end point of 3.6±0.2 Mev, while two days after bombardment it gave an endpoint of 2.2±0.1 Mev, characteristic of Y^{90}. The counting rate at 2.3 Mev of this two-component β-ray spectrum was followed down, giving a half-life of 3.4±0.1 hours. Next, the counting rate at the peak of the longer-lived β-ray spectrum remaining was followed down to background, giving a single half-life of 61±0.5 hours. These half-life and energy data were taken as adequate proof for assigning the 61-hour β ray to Y^{90} and the 3.4-hour β ray to Y^{92}.

A sweep of the positive β-ray spectrum showed no detectable amount of activity. This is to be expected since the only positron emitter produced in yttrium by a (d,α) reaction on zirconium would be the 105-day Y^{88} isotope which decays only 0.19% by β^+. The small number of disintegrations of this isotope would not have been detected by our equipment.

Curves were taken of β-γ and γ-γ coincidences covering the entire β-ray spectrum and including all γ rays except the weak ones at 1.9 and 2.4 Mev. All the observed coincidence data were corrected by standard methods for random or chance coincidences and background coincidences due to cosmic-ray showers. These curves show the 0.475-, 0.94-, and 1.45-Mev γ rays to be

[11] P. W. McLaughlin and G. D. O'Kelley, California Research and Development Company Report MTA-40, September, 1953 (unpublished), p. 11.

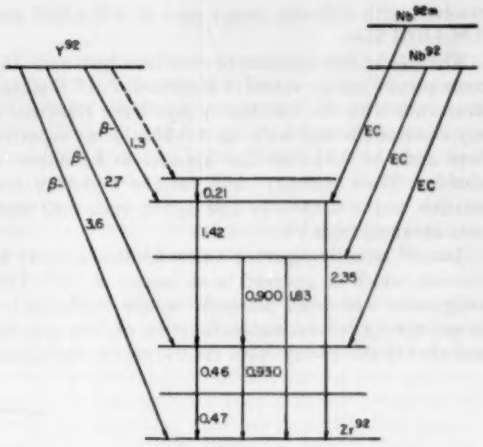

FIG. 3. Proposed decay scheme for yttrium-92.

in coincidence with β rays beyond 1.3 Mev, while the 1.45-Mev γ ray is in coincidence only with β rays up to 1.3 Mev. Data on the 0.21-Mev γ ray were inconclusive.

The results of the γ-γ coincidence experiments are shown in Table III. No curves were taken for the 0.94-, 1.9-, and 2.4-Mev γ rays.

IV. DISCUSSION

The γ-ray energy and coincidence data obtained in this work should correlate with levels of Zr^{92} reported in the work of other laboratories. Hayward, Hoppes, and Ernst[12] have recently reported the energies and abundances of three γ rays of Nb^{92} as shown in Table III. In addition, James[13] has reported a 2.35-Mev γ ray associated with what he considers to be an isomer of Nb^{92m}.

The decay scheme shown in Fig. 3 is consistent with most of these experimental data. The β-ray energies are those listed by Ames *et al.*[4] since their instrument apparently gave better resolution of the individual β rays than did the instrument used in this work. The 1.1-Mev β-ray transition suggested in this decay scheme was not observed. The large relative intensity of the 0.94-Mev photopeak, however, precludes the possibility of placing the 0.21-Mev γ ray in cascade with the 3.6-Mev β ray. It would undoubtedly have been difficult for Ames *et al.* to completely resolve two such low-energy β rays (1.0 and 1.3 Mev) in this complex spectrum.

The width of the γ_2 and γ_3 lines in the γ-ray spectrometer curves would seem to indicate that they might actually consist of two γ rays each. From γ_2, there can be readily resolved two γ rays of 0.46±0.02 and 0.49±0.02 Mev energy. Similarly, from γ_3 there can be

[12] Hayward, Hoppes, and Ernst, Phys. Rev. **98**, 231 (A) (1955).
[13] R. A. James, Phys. Rev. **93**, 288 (1954).

resolved with difficulty two γ rays of 0.92±0.03 and 0.96±0.03 Mev.

The γ_3 doublet appears to correlate best with the more precise energy values of Hayward *et al.*[12] if placed in cascade with the 1.45-Mev γ ray. Their 1.83-Mev γ ray corresponds well with the 1.9-Mev γ ray reported here and the 0.94-Mev line appears to be indeed a doublet. Their intensity ratio for the 1.83-Mev line relative to the 0.930-Mev line agrees quite well with that obtained from Y^{92}.

James[13] recently reported a new 13-hour activity in niobium which he assigned to an isomer of Nb^{92}. This assignment was based primarily on the similarity between the (p,pn) excitation function of this activity and that of the 10-day Nb^{92}. He states that the isomer emits K x-rays of zirconium and a γ ray whose energy was determined to be 2.35 Mev by a scintillation spectrometer. This γ-ray energy fits well into the level scheme proposed in Fig. 3 and would seem to substantiate the assignment of the 13-hour activity to Nb^{92m}. While one might expect that the 1.42- and 0.47-Mev γ rays would have been also reported as present, they may have been obscured by the 0.93- and 1.83-Mev γ rays of the more abundant 10-day Nb^{92}.

ACKNOWLEDGMENTS

The authors wish to express their thanks to Professor W. C. Parkinson, Professor P. V. C. Hough, and the crew of the University of Michigan cyclotron for their cooperation.

PHYSICAL REVIEW VOLUME 99, NUMBER 3 AUGUST 1, 1955

Metastable States of Re^{180}, Ir^{191}, Au^{193}, Pb^{201}, and Pb^{203}†*

VERA KISTIAKOWSKY FISCHER
Radiation Laboratory, University of California, Berkeley, California, and Columbia University, New York, New York

(Received April 25, 1955)

Ten elements of atomic number between 60 and 82 have been bombarded with 31.5-Mev protons and examined for activities with half-lives between 0.5 and 200 seconds. None were observed in Sm, Ho, Tm, Lu, and Ta. Those produced in W, Ir, Pt, Au, and Tl were investigated with scintillation and proportional counters. Isotope assignments were made on the basis of excitation function studies. Observed were Re^{180m} (145 seconds), Ir^{191m} (4.9 seconds), Au^{193m} (3.9 seconds), Au^{194m} (31 seconds), Au^{197m} (7.4 seconds), Pb^{201m} (60 seconds), and Pb^{203m} (6.7 seconds). Decay schemes are proposed and some regularities are discussed.

INTRODUCTION

IN agreement with considerations based on the shell model it has been observed that many isotopes in the region between atomic number 60 and 82 have low-lying metastable states. It has further been pointed out[1,2] that there is a grouping within this region defined by closed nucleon shells: the density of cases of nuclear isomerism increases sharply at the upper end of the region, there being seven observed cases with $Z=60$ to 72 and twenty-four, with $Z=72$ to 82. In order to determine whether this effect is due solely to insufficient study of the lower end of the region, a search for new cases of isomerism was undertaken.

Ten elements have been bombarded with 31.5-Mev protons and examined for activities with half-life between 0.5 and 200 seconds. These experimentally set limits include the expected half-lives of $M3$ and $E3$ transitions of energy <200 kev, $M4$ and $E4$ transitions of energy >500 kev and energetic beta-decay transitions. Since a number of nuclear reactions are possible at the maximum bombarding energy, excitation function studies were performed to permit isotopic assignment of the observed activities.

EXPERIMENTAL

I. Bombardment and Counting Arrangement

The ten targets which were bombarded are $_{62}$Sm (>98%),[3] $_{67}$Ho (>99%),[3] $_{69}$Tm (>96%),[3] $_{71}$Lu (>98%),[3] $_{73}$Ta (>99%), $_{74}$W (>99%), $_{77}$Ir (99.5%), $_{78}$Pt (>99%), $_{79}$Au (>99%), and $_{81}$Tl (99.8%). All of these were in the form of the metal and the numbers in the brackets indicate their elemental purity excluding oxygen contaminations from the formation of oxide coatings.

The bombardments were performed at the University of California Radiation Laboratory linear accelerator. The beam was focused into a spot $\frac{3}{16}$ inch by $\frac{5}{8}$ inch by a strong-focusing magnet consisting of four quadrupole lenses. In addition, to make certain that the beam did not strike the target holder, a collimator was placed immediately before the target position. The energy of the protons from the linear accelerator is 31.5±0.5 Mev; for excitation function studies the desired energies

† This work was sponsored in part by the U. S. Atomic Energy Commission.
* This work was made possible by the Sarah Berliner Fellowship (1953–54) of the American Association of University Women.
[1] M. Goldhaber and R. D. Hill, Revs. Modern Phys. **24**, 179 (1952).
[2] J. W. Mihelich and A. de-Shalit, Phys. Rev. **93**, 135 (1954).
[3] On loan from Dr. F. H. Spedding, Ames Laboratory, Ames, Iowa.

were obtained by the use of appropriate absorbers placed directly in front of the collimator. The beam current was measured by a gas scintillation beam monitor designed and built by Kitchen,[4] the output of which was connected to a standard integrating electrometer-recorder. This monitor was placed in the beam path in front of the absorbers and calibrated against a Faraday cup placed in the target position for all absorbers used.

Shielding, consisting of eight inches of paraffin and $\frac{1}{16}$ inch of cadmium, proved sufficient to minimize neutron activation of the NaI(Tl) scintillation crystal used for gamma-ray studies. In addition two inches of lead were used to reduce the external gamma-ray background. During bombardment, the target holder, centered on the beam spot, rested between two vertical rails on a catch. At the end of bombardment the catch was solenoidally withdrawn and the target holder fell, guided by the rails, through a slot in the shielding to a position between a scintillation and a gas counter. Thus the lower limit on the half-lives observable was set by the time of fall, ~0.5 second, while the upper limit was set to minimize accelerator idle time.

II. Counters; Electronics

The scintillation counter was of conventional design consisting of a one-inch by 1½-inch diameter NaI(Tl) crystal and a DuMont 6292 photomultiplier packaged in an aluminum housing and protected by a magnetic shielding and lead shield. Under standard operating conditions, the photopeak of the Cs^{137} 0.66-Mev gamma ray was observed with 8% resolution.

The gas counter was a continuous flow type employing a 90% argon-10% carbon-dioxide mixture. It was operated in the proportional region and used to detect electrons. Energy determinations were made by absorption studies.

A two-pen, three-speed Brush Company recorder was used to record the data. Pulses from the scintillation counter, amplified by a standard University of California Radiation Laboratory nonoverloading linear amplifier, were placed into a scaler connected to one pen of the recorder. The other pen was used to record either the pulses from the gas counter followed by a preamplifier, linear amplifier and scaler, or the pulses from a second output of the scintillation counter linear amplifier followed by an A.I. Model 510 single-channel pulse-height analyzer and a scaler. All the scalers were gated off for the duration of the linear accelerator radio-frequency pulse.

Gamma-ray spectroscopy was performed by using a grey-wedge pulse-height analyzer which has been described previously.[5]

III. Method

The control used to end bombardment by shutting a flip gate or dephasing the Van de Graaff and linear accelerator, simultaneously started the recorder chart drive. Thus the starting points of the recorder traces correspond to end of bombardment. At the same time the target was dropped. The decay after each bombardment was followed until the counting rate due to longer-lived activities and external background became constant enough to permit resolution of the decay curves.

The spectra of gamma-ray energies were studied with the grey-wedge pulse-height analyzer by exposing a given negative for a time interval after bombardment in which pulses from the desired activity were predominant. This was repeated until sufficient pulses for an intelligible spectrum were accumulated. The general method has been previously described.[5] Energy calibrations were made at intervals throughout each series of bombardments. The relative intensities of observed gamma rays were determined with the single-channel pulse-height analyzer. Decay curves simultaneously recorded on the differential and integral counting rates were resolved and the components were extrapolated to the time at end of bombardment. The ratio of these extrapolated counting rates were plotted as a function of pulse-height analyzer setting. The heights of the photopeaks corrected by empirical counting efficiency factors and calculated absorption corrections gave the relative intensities. The K x-ray values were corrected for the Auger effect.[6]

Absorption curve determinations were made of the electron energies associated with each activity. Ratios of gas counter to scintillation counter counting rates at end of bombardment were plotted as a function of absorber thickness, and these curves were resolved. Electron to gamma-ray intensity ratios were corrected by the factors mentioned for gamma rays, by electron absorption corrections, and for the geometries of the two counters.

Relative cross sections for the excitation functions were calculated from the counting rates of components of the resolved scintillation counter decay curves extrapolated to the end of bombardment. These were corrected as previously discussed and also by a saturation factor calculated from the length of bombardment. Absolute cross-section values were obtained by applying additional corrections for geometry, isotopic abundance, and branching ratio and conversion considerations.

IV. Results

Bombardment of Sm, Ho, Lu, Tm, and Ta yielded only very weak traces of short-lived activities. The amounts corresponded to cross sections of at least a factor of 10^5 smaller than the compound nucleus

[4] S. W. Kitchen, Rev. Sci. Instr. **26**, 234 (1955).
[5] Vera Kistiakowsky Fischer, Phys. Rev. **96**, 1549 (1954).
[6] H. S. W. Massey and E. H. S. Burhop, Proc. Roy. Soc. (London) **153**, 661 (1935–36).

TABLE I. Summary of results.

Target Z	Element	Observed half-life (seconds)	Gamma-ray energies (kev)		Electron energies (Mev)	Assignment
74	W	145±4[38]	880±40	510±20	1.1±0.1	Re^{180m}
			106±10	65±10	<0.3	
77	Ir	4.91±0.14[55]	135±10	65±10	<0.3	Ir^{191m}
		3.88±0.25[69]	255±20	70±10	<0.3	Au^{190m}
78	Pt	30.6±0.19[65]	260±20	70±10	<0.3	Au^{193m}
		7.23±0.28[40]	270±20	130±10	<0.3	Au^{197m}
79	Au			70±10		
		30.0±1.74[24]	260±20	70±10	<0.3	Au^{193m}
81	Tl	6.73±0.44[68]	860±40	75±10	<1.0	Pb^{203m}
		60.1±4.4[42]	650±30	75±10	<1.0	Pb^{201m}

formation cross sections for the given target and energy. The characteristics of the activities in so far as they could be determined indicated that they probably arose from oxygen and other low-Z elements.

Table I summarizes the results with the other five targets. The half-lives quoted represent averages of those determinations which satisfied certain statistical criteria; the errors are their standard deviations. The number of determinations represented by each value is given in the brackets. No quantitative attempt to estimate systematic errors was made. However, the internal consistency between different runs under varying conditions indicates that they are not more than a few percent. In the fourth column, listing the observed gamma-ray energies, the 65–75-kev radiations observed in all cases are probably K x-rays. The errors given are estimated experimental errors. The electron energies as measured by the absorption studies are given in the fifth column. The only case where a good end-point determination was possible was wolfram. In all other cases only upper limits could be set.

The last column of Table I gives the assignments which were made for the observed activities on the basis of the excitation functions given in Figs. 1 and 2. In these the ratio of the experimentally determined cross section to the compound nucleus formation cross section[7] ($r_0=1.3\times10^{-13}$ cm) is given as a function of the energy of the bombarding proton in the center of mass system. The uncertainties in energy of the points include the uncertainty concerning the energy of the initial beam and the spread due to target thickness. The uncertainties in cross section include an estimate of the experimental errors but do not include uncertainties in some of the factors involved in calculating the absolute cross sections. A downward pointing arrow indicates that the activity was not observed and only an upper limit could be set.

[7] J. M. Blatt and V. F. Weisskopf, *Theoretical Nuclear Physics* (John Wiley and Sons, Inc., New York, 1952).

INTERPRETATION OF RESULTS

I. Gold

Two short half-life activities were observed in the gold bombardments. One has a half-life of 7.2 seconds with which are associated 130- and 270-kev gamma rays, K x-rays and electrons. This is readily identified with the well-known metastable state of Au^{197}.[8] The second activity has a half-life of 30 seconds with which is associated a 260-kev gamma ray, K x-rays and electrons. These values agree with those previously found for a metastable state of Au^{195} [9,10] which emits 56.5- and 261.6-kev gamma rays. The 56.5-kev gamma ray is very highly converted and therefore would not have been observed in the present study. The experimentally determined intensity ratios for both isotopes agree very well with the known conversion coefficients. Previously proposed [9–10] decay schemes for both isomers are given in Fig. 3.

The observed excitation functions are given in Fig. 1(a). Curve A corresponds to the reaction, $Au^{197}(p,p')Au^{197m}$, and curve B, to the reaction, $Au^{197}(p,p2n)Au^{195m}$. The values of the ratio σ_{exp}/σ_c are small at all energies, the experimental cross section, σ_{exp} being only a few percent of the compound nucleus formation cross section, σ_c. The total inelastic scattering cross section for 31.5-Mev protons in gold has been shown[11] to be 0.29 barn, giving $\sigma_{exp}/\sigma_c=0.26$, and and the cross section for the reaction $Ta^{181}(p,pn)Ta^{180}$ with 23.4-Mev protons gives $\sigma_{exp}/\sigma_c=0.1$.[12] Both of these values represent upper limits for the formation probability of any excited state in the product nucleus and thus a σ_{exp}/σ_c of a few percent would be expected for such a reaction. The (p,p') curve, curve A, rises with increasing bombardment energy to 15 Mev, the height of the potential barrier in gold. Then it drops off due to the increasing probability that the residual

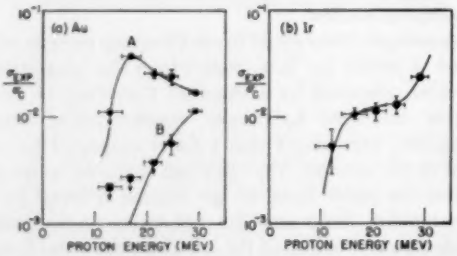

FIG. 1. Excitation functions. (a) Activities produced by bombardment of gold with protons; A: 7.4-second half-life; B: 30-second half-life. (b) 4.9-second half-life activity produced by bombardment of iridium with protons.

[8] J. W. Mihelich and A. de-Shalit, Phys. Rev. **91**, 781 (1953).
[9] Huber, Halter, Joly, Maeder, and Brunner, Helv. Phys. Acta **26**, 591 (1953).
[10] Grillon, Gopalakrishnan, de-Shalit, and Mihelich, Phys. Rev. **93**, 124 (1954).
[11] R. M. Eisberg and G. Igo, Phys. Rev. **93**, 1039 (1954).
[12] Cohen, Newman, Charpie, and Handley, Phys. Rev. **93**, 1039 (1954).

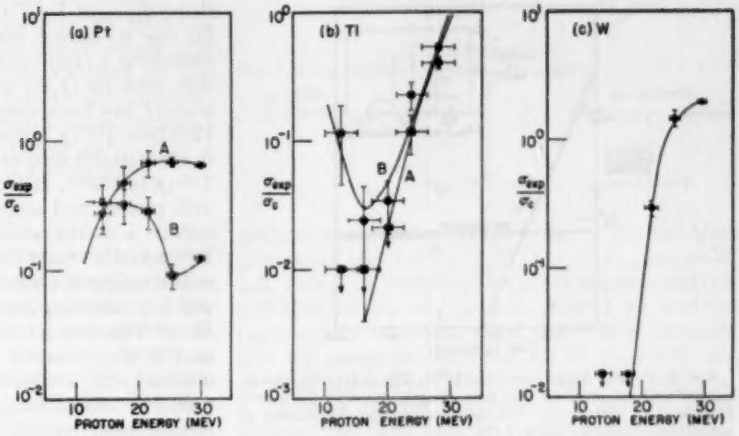

FIG. 2. Excitation functions. (a) Activities produced by bombardment of platinum with protons; A: 3.9-second half-life; B: 31-second half-life. (b) Activities produced by bombardment of thallium with protons; A: 60-second half-life; B: 6.7-second half-life. (c) 145-second half-life activity produced by bombardment of wolfram with protons.

nucleus will still have sufficient excitation energy to emit another particle. The $(p,p2n)$ curve, curve A, rises sharply above 20 Mev which is approximately the threshold for emission of three particles from the compound nucleus.

II. Platinum

Of the two activities observed after the bombardment of platinum, the one with 30.6-second half-life can be immediately assigned to Au^{195m} on the basis of half-life, gamma-ray energy and K conversion coefficient. Furthermore, the excitation function for this activity, Fig. 2(a) curve B, is what would be expected from the sum of the reactions $Pt^{195}(p,n)Au^{195m}$, $Pt^{196}(p,2n)Au^{195m}$, and $Pt^{198}(p,4n)Au^{195m}$. Both curves in this figure have not been corrected for isotopic abundance and σ_{exp}/σ_c would be approximately one at lower energies if this correction were made. In this atomic number region such a value indicates that the decay mode of the compound nucleus leading to the isotope in question does not involve charged particle emission. The shape, first constant and then falling off after 20 Mev, indicates that (p,n) and $(p,2n)$ but not $(p,3n)$ contribute, while the upward turn at 30 Mev can be explained by a $(p,4n)$ contribution.

Curve A is the excitation function for the production of the 3.88 second activity. On the basis of similar arguments it is assigned to Au^{193m} produced by the reactions $Pt^{194}(p,2n)Au^{193m}$, $Pt^{195}(p,3n)Au^{193m}$, and $Pt^{196}(p,4n)Au^{193m}$. The initial rise in the curve indicates the absence of (p,n) contribution. This isomer was observed to emit a 255-kev gamma ray with $\alpha_K=0.4\pm0.1$ and $K/L\sim2$. Comparing these numbers with the theoretical α_K values given by Rose *et al.*[13] and the empirical K/L curves given by Goldhaber and Sunyar,[14] the transition is found to be $M1$ with possible $E2$ admixture. Thus the multipole order of the gamma ray is definitely too low to account for the half-life and some other transition must be rate-determining.

Grillon *et al.*[10] have discovered a metastable state in Au^{193} following the electron capture decay of Hg^{193m} whose half-life they were not able to determine. They observed conversion electrons corresponding to 31.9-kev ($E3$), 257.9-kev ($M1$) and 291-kev (weak) gamma rays. The 257.9-kev gamma ray and the 260-kev gamma ray observed in the present study are presumably identical. The other two would not have been observed. Thus the decay scheme given by Grillon *et al.*,[10] Fig. 3(c), is assigned to the 3.88-second Au^{193m}.

III. Iridium

Figure 1(b) shows the excitation function obtained for the production of the 4.91-second half-life activity in iridium. The σ_{exp}/σ_c values are of the order of magnitude expected for reactions involving emission of charged particles from the compound nucleus. The shape of the curve indicates contributions from (p,p') and $(p,p2n)$ but not (p,pn). Therefore this activity is assigned to a metastable state in Ir^{191} produced by $Ir^{191}(p,p')Ir^{191m}$ and $Ir^{193}(p,p2n)Ir^{191m}$. Assuming all K

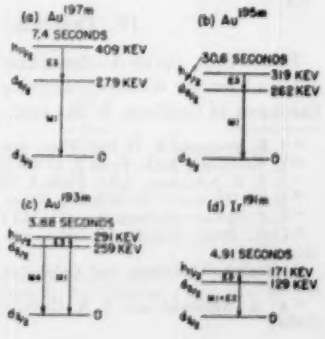

FIG. 3. Decay schemes.
(a) Au^{197m},
(b) Au^{195m},
(c) Au^{193m},
(d) Ir^{191m}.

[13] Rose, Goertzel, Spinrad, Harr, and Strong, Phys. Rev. **84**, 1056 (1951).
[14] M. Goldhaber and A. W. Sunyar, Phys. Rev. **83**, 906 (1951).

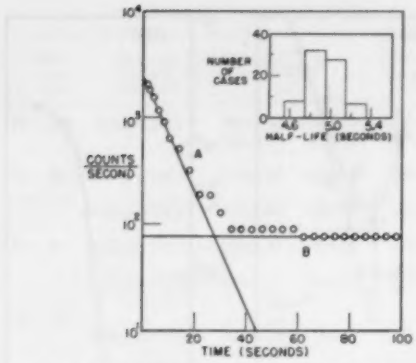

FIG. 4. Typical decay curve for Ir^{191m}. The points are experimental and are resolved into two components, (A) 4.9-second half-life, (B) background. The insert gives the distribution of values determined for the half-life.

x-rays and electrons to arise from the conversion of the observed 135-kev gamma ray it is found that $\alpha_K = 2.7 \pm 0.5$ and $K/L \sim 0.08$.

A 129.1-kev gamma ray going to the ground state of Ir^{191} has been observed both from the decay of Os^{191} [15–19] and of Pt^{191} [10,20] The gamma ray has $\alpha_K = 2.1$ and $K/L = 2.2$ and thus the transition is a mixture of $M1$ and $E2$. Identifying this with the observed gamma ray, the discrepancy in K/L ratios would be explained by a highly L-converted gamma ray corresponding to the rate determining transition. A reasonable choice for this would be the 41.7-kev gamma ray observed preceding the 129.1-kev gamma ray in the decay of Os^{191}.[15–19] Its $L_{II}:L_{III}$ ratio is compatible with assignment to an $E3$ transition.

In two recent papers, experiments are reported in which half-lives of 6.8 ± 1.0 seconds[21] and 5.6 ± 0.4 seconds[22] have been observed for a metastable state of Ir^{191} which emits a 130-kev gamma ray. In one of them, Mihelich, McKeown, and Goldhaber[21] give a very convincing argument for the same decay scheme suggested here and illustrated in Fig. 3(d). Figure 4 shows a typical decay curve and, in the insert, the distribution of values obtained for the half-life in this experiment.

IV. Thallium

Figure 2(b), curve A, shows the excitation function obtained for the 60-second activity produced by bombardment of thallium. It has both the magnitude and shape expected for a $(p,3n)$ reaction. Curve B, that for the 6.7-second activity observed, has a shape resembling a (p,n) curve at low energies and $(p,3n)$ at high, with no $(p,2n)$ component. Thus the 60-second activity has been assigned to a metastable state of Pb^{201} from $Tl^{203}(p,3n)Pb^{201m}$ and the 6.7-second activity to a metastable state of Pb^{203} from $Tl^{203}(p,n)Pb^{203m}$ and $Tl^{205}(p,3n)Pb^{203m}$. Hopkins[23] also bombarded thallium with protons and observed 50-second and 5.6-second half-life activities which he identified as Pb^{201m} from $Tl^{203}(p,3n)Pb^{201m}$ and Pb^{202m} from $Tl^{203}(p,2n)Pb^{202m}$. The second assignment was based on observing the activity with a bombarding energy of 22 Mev but not with 17 Mev.[24] This was not the case in the present work, as seen in Fig 5 which shows a typical decay curve obtained with bombarding energy ≤ 15.2 Mev. Figure 6 shows a typical decay curve from maximum energy bombardment, with an insert which gives the observed distribution of half-life values. An explanation for the discrepancy between the 6.73-second half-life observed in this experiment and the 5.6-second value previously obtained has not been found.

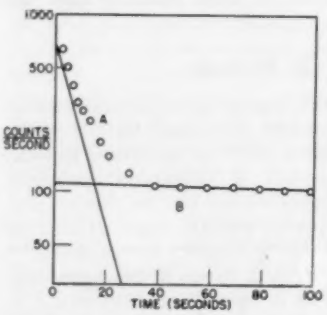

FIG. 5. Typical decay curve for Pb^{203m} produced by bombardment of thallium with protons of energy ≤ 15.2 Mev. The points are experimental and are resolved into two components: A, 6.7-second half-life; B, background.

It was found in the present study that a 0.86-Mev gamma ray with $\alpha_K = 0.13 \pm 0.06$ is emitted by Pb^{203m}. This is in best agreement with the theoretical value of an $M4$ transition.[13] The ground state of Pb^{203} has been found to be $f_{5/2}$ from its electron capture decay scheme.[25] This and the shell model suggest that the state is $i_{13/2}$ as illustrated in Fig. 7(a). Using the semiempirical formula given by Goldhaber and Sunyar[14] for the mean life, τ_γ, of an $M4$ transition:

$$\tau_\gamma = 1 \times 10^4 (2i+1)/A^2 E^9,$$

where i is the spin of the initial state and E, the energy of the transition in Mev, an expected half-life of 7.2 seconds is calculated for Pb^{203m}, in excellent agreement with the experimental value.

In the present work, Pb^{201m} was observed to decay with a 60.1-second half-life emitting a 0.65-Mev gamma with $\alpha_K = 0.75 \pm 0.25$. This is in best agreement with the theoretical value for an $M4$ transition.[13] Hopkins[23]

[15] J. B. Swan and R. D. Hill, Phys. Rev. **88**, 831 (1952).
[16] E. Kondaiah, Arkiv Fysik **3**, 47 (1952).
[17] S. A. E. Johansson, Arkiv Fysik **3**, 533 (1952).
[18] R. D. Hill and J. W. Mihelich, Phys. Rev. **89**, 323 (1953).
[19] F. F. McGowan, Phys. Rev. **93**, 163 (1954).
[20] Cork, Brice, Schmid, Hickman, and Nine, Phys. Rev. **94**, 1218 (1954).
[21] Mihelich, McKeown, and Goldhaber, Phys. Rev. **96**, 1450 (1954).
[22] R. A. Naumann and J. B. Gerhart, Phys. Rev. **96**, 1452 (1954).
[23] N. J. Hopkins, Phys. Rev. **88**, 680 (1952).
[24] N. J. Hopkins (private communication, 1955).
[25] J. Varma, Phys. Rev. **94**, 1688 (1954).

reported a 56-second half-life and 0.67-, 0.42-, and 0.25-Mev gamma rays. More recently his work has been repeated and the two lower-energy gamma rays were not observed.[24] The half-life calculated for this transition using the Goldhaber-Sunyar equation[14] is 61 seconds, again in good agreement with the experimental value. Thus the decay scheme shown in Fig. 7(b) is proposed for Pb^{201m} in analogy to that for Pb^{203m}.

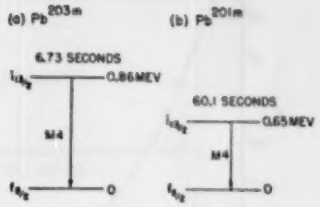

FIG. 7. Decay schemes.
(a) Pb^{203m}
(b) Pb^{201m}

V. Wolfram

Figure 2(c) shows the excitation function obtained for the 145-second activity produced in wolfram. The order of magnitude of the maximum value and the shape of the curve assign the activity to the product of a $(p,3n)$ reaction alone. Thus it must be Re^{180} from $W^{182}(p,3n)Re^{180}$. The contribution from $W^{180}(p,n)Re^{180}$ is not seen because of the 0.135% abundance of W^{180}.

Gamma rays with energies of 880 kev, 510 kev, and

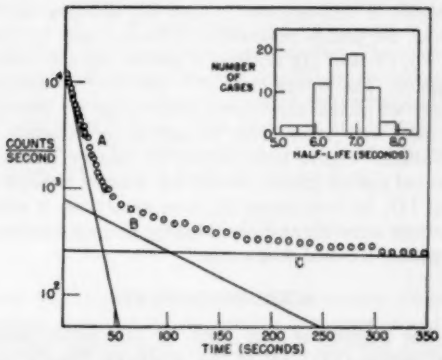

FIG. 6. Typical decay curve for Pb^{201m} and Pb^{203m}. The points are experimental and are resolved into three components: A, 6.7-second half-life; B, 60-second half-life; C, background. The insert gives the distribution of values determined for the shorter half-life.

106 kev; K x-rays; electrons and a beta-particle group of maximum energy 1.1 Mev were observed from the decay of this isotope. It is calculated from the semi-empirical mass equation[25] that the ground state of Re^{180} is unstable by 2.8 Mev with respect to the ground of W^{180}, suggesting that the 1.1-Mev beta particle is a positron. That this is the case and that the 0.51-Mev gamma ray is annihilation radiation is confirmed by the ratio of their intensities, $N_{\beta\,1.1\text{ Mev}}/N_{\gamma\,0.51\text{ Mev}}=0.7\pm0.4$. The theoretical ratio of K electron capture to positron emission is found to be $f_K/f_+=50$ from the curves of Feenberg and Trigg[27] and it is calculated that $\log ft_{\beta^+,K}=4.0$. A correction for L electron capture[28] raises this to $\log ft_{\beta^+,K}=4.1$.

The ratio of the intensity of the 1.1-Mev positron-electron capture decay branch to that of the 0.88-Mev gamma ray is $[(f_++f_K)/f_+]N_{\beta\,1.1\text{ Mev}}/N_{\gamma\,0.88\text{ Mev}}=10\pm4$. Thus these transitions are not in sequence and the 0.88-Mev gamma ray probably follows an electron capture decay to an excited level in W^{180}. If one assumes that the energy of this transition is $(E_{\beta^+}+1.0)-E_\gamma=1.2$ Mev, it is found that $\log ft=4.6$. When $\log ft_{\beta^+,K}$ is corrected for this branching, it is still 4.1. This suggests that there must be a third competing decay mode and an obvious choice, in view of the radiations observed, is that electron capture and positron decays proceed from a metastable state of Re^{180}. The 106-kev gamma ray is possibly emitted in this suggested isomeric transition. However, Brown *et al.*[29] observed a level of W^{180} 102 kev above the ground state. By analogy to Hf^{180} and all other stable even-A wolfram isotopes which have 2+ rotational states at about 100 kev,[30] this is probably an $E2$ transition. The observed 106-kev gamma ray may also be partially or completely due to this transition and a number of decay schemes are possible as indicated in Fig. 8.

CONCLUDING REMARKS

Of the ten targets studied, only those at the upper end of the atomic number region gave observable activities. In view of the limitations of the experiment, this is not conclusive but it does substantiate the previously mentioned effect. There are now seven known cases of isomerism between $Z=60$ and 72, and twenty-seven between $Z=72$ and 82. Goldhaber and Hill[1] and Mihelich and de-Shalit[2] have suggested that the absence of odd-proton isomers in the lower region can be

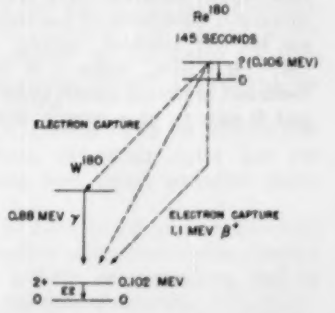

FIG. 8. Decay scheme proposed for Re^{180m}.

[25] N. Metropolis and G. Reitwiesner, "Table of Atomic Masses," Atomic Energy Commission Report NP-180, 1950 (unpublished).
[27] E. Feenberg and G. Trigg, Revs. Modern Phys. **22**, 399 (1950).
[28] M. E. Rose and J. L. Jackson, Phys. Rev. **76**, 1540 (1949).
[29] Brown, Bendel, Shore, and Becker, Phys. Rev. **84**, 292 (1951).
[30] N. P. Heydenburg and G. M. Temmer, Phys. Rev. **93**, 906 (1952).

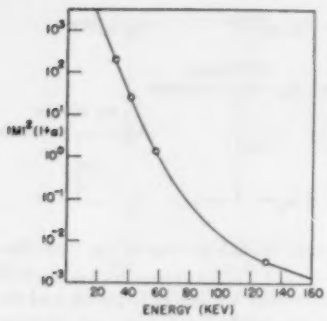

FIG. 9. $|M|^2(1+\alpha)$ as a function of transition energy for $E3$ transitions between $h_{11/2}$ and $d_{3/2}$ levels in odd-neutron Au and Ir isotopes.

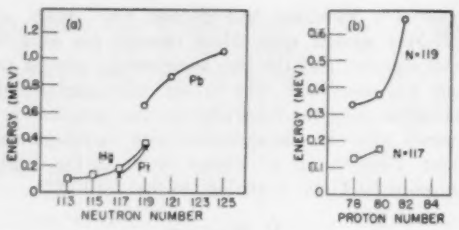

FIG. 10. Energy separation of $i_{13/2}$ and $f_{5/2}$ levels in odd-A Pt, Hg, and Pb isotopes (a) as a function of neutron number, (b) as a function of proton number.

explained by the destruction of the metastability of the expected single-particle levels through the intervention of low-lying levels of the coupled system.

Mihelich and de-Shalit[2] have pointed out that the transition matrix elements, $|M|^2$, for the $M4$ transitions between $i_{13/2}$ and $f_{5/2}$ states in odd-neutron Pb, Hg, and Pt isotopes show a dependence on nucleon number. $|M|^2$ is defined as the ratio of the mean life for the transition calculated as in Blatt and Weisskopf[7] to the experimental value corrected for conversion. Table II

TABLE II. Values of $|M|^2$ for $M4$ transitions.

N	115	117	119	120	123	125
Pb			1.02	1.18		1.54
Hg	0.88	1.02	1.00			
Pt		0.77	0.98			

combines the values for Pb^{201m} and Pb^{203m} observed in the present study with those previously given.[2] It again emphasizes that $|M|^2$ increases as the nucleon numbers of the isomers approach closed shells. The observation however, that this increase is less than a factor of two accounts for the success of Goldhaber and Sunyar[16] in fitting an expression to the observed half-lives without considering closed shell effects.

The $E3$ transitions between $h_{11/2}$ and $d_{3/2}$ levels in the odd-neutron Au and Ir isomers might be expected to show similar behavior. Since accurate values for the conversion coefficients of low-energy $E3$ gamma rays are not yet available, nothing can be said about $|M|^2 \cdot |M|^2(1+\alpha)$, where α is the total conversion coefficient, is plotted against transition energy in Fig. 9 and is seen to be a smooth and rapidly decreasing function. If one assumes that $|M|^2$ does not vary by large factors as is the case in the $M4$ transitions discussed above, then the curve is essentially the energy dependence of $(1+\alpha)$.

It has been shown[2] that the energy separation of the $i_{13/2}$, $f_{5/2}$, and $p_{1/2}$ levels changes smoothly with neutron number in odd-neutron Pt and Hg isotopes. In Fig. 10(a), the energy separation of the $i_{13/2}$ and $f_{5/2}$ levels in Pb, Pt, and Hg isotopes is plotted against neutron number. The values for Pb^{201m} and Pb^{203m} were those observed in this experiment while those for the other isomers were taken from the article by Mihelich and de-Shalit.[2] Figure 10(b) shows the energy separation plotted against proton number for neutron number 119 and 117. In both cases the level separation is seen to increase smoothly as expected as the nucleon number approaches a closed shell value.

ACKNOWLEDGMENTS

The support of this work by the Sarah Berliner Fellowship (1953–54) of the American Association of University Women is acknowledged with great pleasure. Professor L. W. Alvarez is gratefully thanked for his encouragement and sponsorship of this research. Many thanks are also due to Mr. R. Watt and all the members of the linear accelerator crew for their patient assistance and to the members of Mr. Farnsworth's group for their help in assembling and maintaining the electronics. The author is much indebted to Dr. F. H. Spedding for loaning her the rare earth samples and to Professor J. M. Miller for making possible the completion of the work at Columbia University. Several helpful discussions with Dr. L. J. Lidofsky are gratefully acknowledged.

K^{40} Branching Ratio

A. McNair, R. N. Glover, and H. W. Wilson
Department of Natural Philosophy, The University, Glasgow, Scotland

(Received April 11, 1955)

The ratio of gamma to beta transitions occurring in the decay of K^{40} has been accurately determined by two different counting methods, yielding the ratios 0.124 ± 0.002 and 0.121 ± 0.004, respectively.

IT is generally accepted that the isotope K^{40} decays to A^{40} by electron capture followed by a gamma ray and to Ca^{40} by beta emission.[1,2] Two methods have been used to measure the branching ratio for the decay: (a) The ratio of gamma (or electron capture) to beta transitions, with suitable corrections, is determined by counting methods. (b) The ratio is inferred from the quantity of argon, or calcium, or both in a potassium-mineral of known age. Disagreement between the results obtained by the two methods[3] justified another careful study of the branching ratio by method (a).

Two different procedures were followed. The ratio of the number of gamma to beta transitions occurring in the decay of Co^{60} was compared with the corresponding ratio for the K^{40} decay, thus avoiding, to a first order, calculations of the efficiencies of the beta and gamma detectors. The ratio is given by the expression

$$R=2\frac{\gamma_K}{\gamma_{Co}}\cdot\frac{\beta_{Co}}{\beta_K},$$

where γ_K, γ_{Co} are the directly measured gamma counting rates and β_K, β_{Co} are the beta rates. Had the two beta spectra been identical and had the gamma transitions been of equal energy, a very precise value of R would have followed directly. As it was, various corrections, mentioned later, had to be made.

The gamma detector consisted of a cylindrical NaI crystal (2 in. long$\times\frac{3}{4}$ in. diam.) placed coaxially within a vessel of approximately 200 cc capacity into which could be poured the solutions under test. There was sufficient absorber to prevent the detection of the beta particles. The vessel and crystal were mounted on an E.M.I. type 6262 photomultiplier and the whole surrounded by a 4-in. lead screen. The solutions were water containing $Co^{60}Cl_2$ and KOH ($\sim$493 g K/liter) the latter giving $\sim$700 cpm above background ($\sim$80 cpm). Calibration was effected with the 46.7-kev gamma rays of RaD. A cylindrical proportional counter was used as a beta detector, and large source areas ($\sim$1000 cm^2) yielded reasonable counting rates even with thin sources of K^{40}.

The measurement had to be corrected for (i) coincident detection in the crystal of both Co^{60} gamma rays, (ii) absorption and scattering of K^{40} gammas by the potassium hydroxide solution, (iii) slight difference in the crystal detection efficiency for K^{40} and Co^{60} gamma rays, (iv) counts due to bremsstrahlung in the gamma-detector especially in the case of K^{40}. The fraction of electrons reflected at the source support in the proportional counter was found by a separate experiment to be the same for Co^{60} and K^{40} beta particles. These corrections will be discussed more fully elsewhere. The observed value of γ_K/β_K was 0.124 ± 0.002, or

$$\gamma_K/(\beta_K+\gamma_K)=0.110\pm0.002.$$

The second method eliminated many of the correction factors involved in the first. The gamma-ray spectra of Na^{24} (1.38 Mev and 2.76 Mev) and of K^{40} (1.46 Mev) were measured by using a large (2 in. long$\times$2 in. diam.) NaI crystal mounted on a DuMont type 6292 multiplier associated with a kick-sorter. By measuring the areas under the peaks of the 1.46-Mev and the 1.38-Mev gamma rays and comparing the beta counting rates, an estimation of the ratio may be made. No correction for the scattering and absorption of gammas by the KOH solution is required if the Na^{24} is added to the potassium source. Also there is no correction for bremsstrahlung since the beta energies (1.36 Mev and 1.39 Mev for K^{40} and Na^{24}, respectively) are close to the gamma-ray energies. Allowance is made for (i) the effect of coincident detection of the 1.38-Mev and 2.76-Mev gammas of Na^{24} and (ii) the slight difference in gamma detection efficiency. The relative source intensities are determined by comparing the beta activities in the proportional counter. The ratio γ_K/β_K observed was 0.121 ± 0.004.

These results are in agreement with the previous best physical measurements, but rather higher than the value (0.09) reported from recent geological determinations.

Fuller details of the methods will be given elsewhere together with the results of coincidence studies, absolute counting-rate and half-life determinations, and of experiments on the reflection of electrons.

We wish to thank Dr. S. C. Curran for frequent helpful discussions during this investigation.

[1] H. E. Suess, Phys. Rev. **73**, 1209 (1948).
[2] W. H. Johnson, Phys. Rev. **88**, 1213 (1952).
[3] G. A. Sawyer and M. L. Wiedenbeck, Phys. Rev. **79**, 490 (1950); Inghram, Brown, Patterson, and Hess, Phys. Rev. **80**, 916 (1950); Russell, Shillibeer, Farquhar, and Mousuf, Phys. Rev. **91**, 1223 (1953); G. J. Wasserburg and R. J. Hayden, Phys. Rev. **93**, 645 (1954); Shillibeer, Russell, Farquhar, and Jones, Phys. Rev. **94**, 1793 (1954); H. A. Shillibeer and R. D. Russell, Can. J. Phys. **32**, 681 (1954).

Energy Eigenvalues for a Spherical Well with an Exponentially Diffuse Boundary*

ALEX E. S. GREEN AND KIUCK LEE†
Department of Physics, The Florida State University, Tallahassee, Florida
(Received March 23, 1955)

The discrete energy eigenvalues of a spherical well with an exponentially diffuse boundary are obtained to a good approximation for a range of well parameters of interest in nuclear physics. The method used involves replacing the centrifugal energy in the exponentially diffuse region by an approximate expression which leads to analytic solutions of the wave equation. The matching of the internal and external wave functions is then accomplished by the use of specially prepared graphs and tables. The eigenvalues and eigenfunctions are thought to be of interest in connection with studies of the independent particle model of the nucleus.

1. INTRODUCTION

A NUMBER of recent studies[1-3] have stimulated interest in the problem of a single particle in a central field with a diffuse boundary. While most of this interest has been in connection with the positive energy states of the continuum, nevertheless the bound states are also of considerable importance. In this paper, an approximate method is developed which appears to be adequate for the range of well parameters encountered in nuclear physics.

The solution of the square spherical well eigenvalue problem is an essential preliminary phase of the approximate method of solution of the diffuse boundary problem. Accordingly, this older problem, which has been solved earlier in the literature,[4] will be considered briefly first.

2. EIGENVALUES FOR THE SQUARE SPHERICAL WELL

The radial wave equation for the lth state of orbital angular momentum for a central field characterized by the potential $V(r)$ may be placed in the form

$$d^2G/dr^2+(2m/\hbar^2)[W-V(r)-\hbar^2l(l+1)/2mr^2]G=0, \quad (1)$$

where $G=rR$ and R is the radial wave function. For the study of the spherical well of depth V_0 and radius a, it is convenient to let a serve as a unit of length, $E_0=\hbar^2/2ma^2$ serve as a unit of energy and to define the dimensionless parameters:

$$\epsilon_w^2=-W/E_0, \quad (2)$$

$$\epsilon_0^2=V_0/E_0, \quad (3)$$

and

$$\epsilon'^2=\epsilon_0^2-\epsilon_w^2. \quad (4)$$

Letting $\rho=r/a$, the radial wave equation becomes

$$G''+[\epsilon'^2-l(l+1)\rho^{-2}]G=0, \quad \rho<1 \quad (5)$$

and

$$G''-[\epsilon_w^2+l(l+1)\rho^{-2}]G=0, \quad \rho>1, \quad (6)$$

where prime denotes differentiation relative to ρ. The internal solution which is well-behaved at $\rho=0$ is

$$G_i=A_i\rho^{\frac{1}{2}}J_{l+\frac{1}{2}}(\epsilon'\rho), \quad (7)$$

where J denotes the usual Bessel function and A_i denotes a normalization constant. The external solution which is well-behaved as $\rho\to\infty$ may be expressed in terms of modified Hankel functions. Denoting these functions by $K_{l+\frac{1}{2}}$ the external solution may be written as

$$G_e=A_e\rho^{\frac{1}{2}}K_{l+\frac{1}{2}}(\epsilon_w\rho). \quad (8)$$

The ϵ_w eigenvalues are obtained without consideration of the normalization constants by imposing the requirement that at the boundary,

$$\rho=1, \quad -G_i'/G_i=-G_e'/G_e \quad \text{or} \quad I_l(\epsilon')=E_l(\epsilon_w), \quad (9)$$

where $I_l(\epsilon')$ and $E_l(\epsilon_w)$ are defined as the negatives of the logarithmic derivatives of the internal and external radial wave functions.

To facilitate the solution of this transcendental equation subject to the condition imposed by Eq. (4), tables and graphs of I_l and E_l have been prepared. In this effort, use was made of the recurrence relations:

$$I_l(x)=l-(x^2/I_{l-1}+l), \quad (10)$$

$$E_l(x)=l+(x^2/E_{l-1}+l), \quad (11)$$

which follow from the usual recurrence relations between Bessel functions. Using Eq. (11) and

$$E_0(x)=x, \quad (12)$$

the higher integral order $E_l(x)$ were generated. To obtain higher order $I_l(x)$ including nonintegral orders which are needed in Sec. 3, tabulated Bessel functions for orders between $-\frac{1}{2}$ and $+\frac{1}{2}$ were first used to generate the corresponding I_l functions. Then Eq. (10) was used to generate the higher order functions. In Fig. 1 and Fig. 2 the values of various $I_l(x)$ and $E_l(x)$ are plotted at abscissas corresponding to x^2. These graphs

* This investigation was supported by grants from the U. S. Atomic Energy Commission and Florida State University Research Council.

† On leave from the Seoul University, Seoul, Korea. This work will serve as a portion of a dissertation to be submitted by Kiuck Lee in partial fulfillment of the requirements for a Ph.D. degree at the Florida State University.

[1] R. D. Woods, dissertation, University of California, August, 1954 (unpublished).
[2] D. M. Chase and F. Rohrlich, Phys. Rev. **94**, 81 (1954).
[3] Feshbach, Porter, and Weisskopf, Phys. Rev. **96**, 448 (1954).
[4] H. Margenau, Phys. Rev. **46**, 613 (1934).

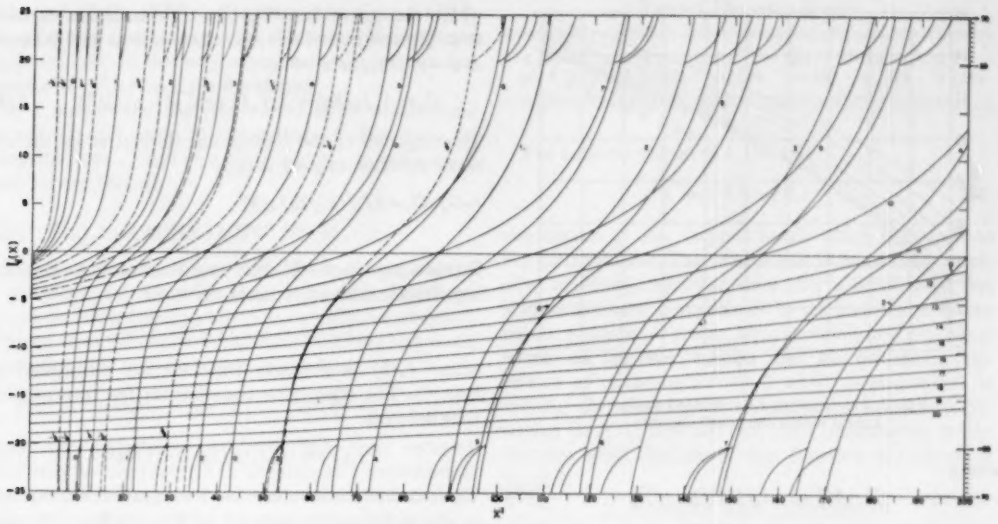

FIG. 1. The function $I_l(x)$ plotted against x^2. Labels within the graph denote l. The second set of curves which start at $I=\pm 20$ correspond to the right scales.

greatly facilitate the task of obtaining functional relations between ϵ_w^2 and ϵ_0^2 for various l's which simultaneously satisfy Eq. (4) and Eq. (9).

Figure 3 contains the results of the work with the square well potential. The form of presentation of the eigenvalues follows that of Moszkowski[5] who has prepared a similar graph for a somewhat narrower range of the well range parameter. Essentially, Fig. 3 represents the energy eigenvalue in units of E_0 measured relative to the bottom of the well. For a given state this parameter has a far smaller range of variation as ϵ_0^2 is changed than ϵ_w^2 which corresponds to the actual energy. Furthermore, these ϵ'^2 values go over to the results of the infinite spherical well as ϵ_0^2 goes to infinity. The ϵ'^2 eigenvalues for the infinite spherical well case are obtained simply by imposing the requirement that $J_{l+\frac{1}{2}}(\epsilon')=0$. These ϵ'^2 eigenvalues for the infinite case results are shown on the right side of Fig. 3. Some noteworthy points which are apparent in Fig. 3 are the $3s-1h$ and $1j-2g$ cross-overs as well as the fact that the approximate equality in spacing of the low-lying levels breaks down above the $1g$ state.

3. SPHERICAL WELL WITH AN EXPONENTIALLY DIFFUSE BOUNDARY

In this section, a continuous central potential is assumed which changes at $r=a$ from a constant $-V_0$ to

$$V(r)=-V_0\exp[(a-r)/\delta a]. \tag{13}$$

The dimensionless parameter δ characterizes the "shortness" of the exponential "tail". The case $\delta=0$ is simply the case discussed in the previous section. The form of the interior radial wave equation and its solutions are, of course, unaltered from those developed in the previous section; however, the dimensionless radial equation for $\rho>1$ in this case is

$$G''+[\epsilon_0^2\exp(1-\rho/\delta)-l(l+1)\rho^{-2}-\epsilon_w^2]G=0. \tag{14}$$

Because of the presence of both the exponential and ρ^{-2} terms, Eq. (14) cannot be reduced to any of the well-studied differential equations. It is, however, known that for s states, i.e., when the ρ^{-2} term vanishes, Eq. (14) can be transformed into Bessel's equation.[6] One approximate procedure which has been used[7] to overcome the difficulty for other than s states is equivalent to replacing ρ^{-2} by 1. The centrifugal energy can then be taken together with ϵ_w^2 and solutions can be obtained in terms of Bessel functions. This approximation, however, is fairly crude and the chief concern here shall be to improve upon it. The improvement considered here is based upon the assumption that

$$\rho^{-2}\approx\alpha^2+(1-\alpha^2)\exp[(1-\rho)/\delta], \tag{15}$$

where the constant α^2 is chosen to accomplish the best match of the function on the right to the function on the left over the external region of importance. Thus, the "centrifugal" energy in the external region is absorbed into the exponential tail and the total energy. The external radial wave equation now becomes

$$4\delta^2G''+\{k^2\exp[(1-\rho)/\delta]-n^2\}G=0, \tag{16}$$

[5] S. A. Moszkowski, Phys. Rev. **89**, 482 (1953).

[6] P. M. Morse and H. Feshbach, *Methods of Theoretical Physics* (McGraw-Hill Book Company, Inc., New York, 1953), Part II, Chap. 12.

[7] B. J. Malenka, Phys. Rev. **86**, 68 (1952).

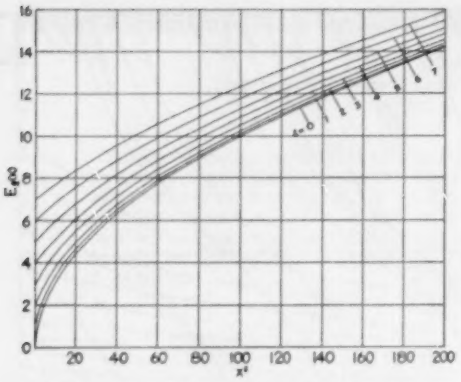

FIG. 2. The function $E_l(x)$ plotted against x^2. Labels within the graph denote l.

where

$$k^2=4\delta^2[\epsilon_0^2-l(l+1)(1-\alpha^2)], \tag{17}$$

$$n^2=4\delta^2[\epsilon_w^2+l(l+1)\alpha^2]. \tag{18}$$

Letting

$$x=\exp((1-\rho)/2\delta), \tag{19}$$

the radial equation becomes

$$x^2G''+xG'+(k^2x^2-n^2)G=0, \tag{20}$$

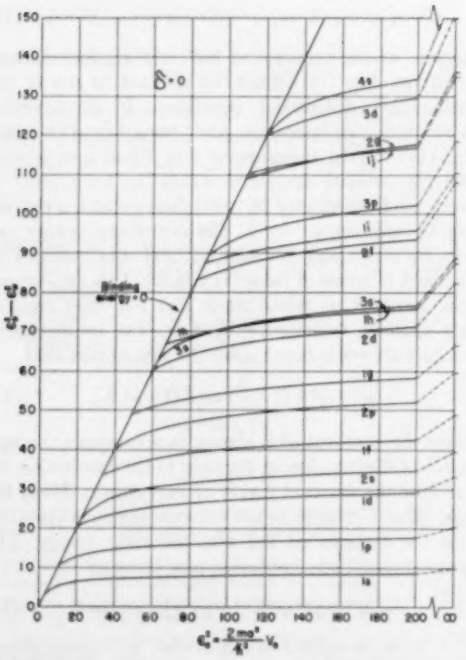

FIG. 3. Energy eigenvalues for the square spherical well (i.e., $\delta=0$). The right scale gives the infinite spherical well eigenvalues.

where the prime here denotes differentiation relative to x. The solution of this equation which is well behaved as $\rho\to\infty$, i.e., as $x\to 0$ is

$$G_e=A_eJ_n(kx)=A_eJ_n\{k\exp[(1-\rho)/2\delta]\}. \tag{21}$$

The negative of the logarithmic derivative of the exterior function at $\rho=1$ is thus

$$-G_e'/G_e=kJ_n'(k)/2\delta J_n(k)$$
$$=\tfrac{1}{2}[n-kJ_{n+1}(k)/J_n(k)]. \tag{22}$$

Introducing $\nu=n-\frac{1}{2}$, the negative of the external logarithmic derivative takes the form

$$E_\nu(k,\delta)=-I_\nu(k)/2\delta-1/4\delta, \tag{23}$$

where $I_\nu(k)$ is precisely the function introduced in Eq. (9). The eigenvalue equation for the present case thus becomes

$$I_l(\epsilon')=-[I_\nu(k)/2\delta]-(1/4\delta). \tag{24}$$

The parameters involved in this equation are subject to the requirements imposed by Eq. (4), Eq. (17), and Eq. (18). These may be combined into

$$\epsilon'^2=[k^2-(\nu+\tfrac{1}{2})^2]/4\delta^2+l(l+1). \tag{25}$$

For a given δ, l, and k^2, Eq. (24) and Eq. (25) may be regarded as two simultaneous equations for the determination of ϵ' and ν. Actually, for the application to which these solutions have been applied, δ and l are first chosen in accord with the states under study and ν is taken in accord with the orders of tabulated or graphed I functions. Then, Eq. (24) and Eq. (25) are solved simultaneously for ϵ'^2 and k^2. Since ν^2 fixes ϵ_w^2, and ϵ'^2 in conjunction with ϵ_w^2 determines ϵ_0^2, it is possible to generate the curves relating ϵ'^2 to ϵ_0^2 throughout the range of interest.

For the purposes of solving Eq. (24) and Eq. (25) for ϵ'^2 and k^2, the graph of the values of I functions may be utilized in the following way. According to Eq. (25), ϵ'^2 is a linear function of k^2 with the slope $(1/4\delta^2)$. If a compressed scale is prepared such that one unit on the ϵ'^2 scale corresponds to $(1/4\delta^2)$ units of ϵ'^2 on the compressed scale, then for chosen values of ν and l the compressed scale may be positioned so that any ϵ'^2 on the compressed scale corresponds directly to k^2 on the basic scale. This may be accomplished simply by aligning the value of $(\nu+\frac{1}{2})^2$ on the regular scale next to $l(l+1)$ on the compressed scale. Next, a compressed vertical scale is prepared with an offset index so that as the index point is slid along the center axis of the horizontal scale the readings of the curve correspond directly to $E_\nu(k,\delta)$ given by Eq. (23). Now to solve simultaneously for the values of ϵ'^2 and k^2 the special vertical scale is moved in relation to ϵ'^2 values listed on the horizontal scale and readings of the νth curve are taken. At the same time, values of $I_l(\epsilon')$ are read at the corresponding ϵ'^2 of the basic scale. Proceeding in this way, one finds readily the ϵ'^2 eigenvalues. Having

generated all the ϵ'^2 (and k^2) values for a given ν and l, one advances to the next ν for the same l and repeats the procedure. In this way, a series of relationships between ϵ'^2 *vs* ν^2 for each l is developed.

It is noteworthy that the values of ϵ'^2 so obtained do not depend upon the constant α^2. However, to translate from ϵ'^2 and k^2 into ϵ_0^2 and ϵ_w^2, a value of α^2 must be established.

4. ADJUSTMENT OF α^2

The form chosen for Eq. (15) insures the agreement of the right and left sides at $\rho=1$. Clearly, therefore, α^2 may be related to a second point at which agreement between these functions is imposed. Denoting this point by ρ_1, Eq. (15) may be placed in the form

$$\alpha^2=[\rho_1^{-2}-\exp(1-\rho_1/\delta)]/[1-\exp(1-\rho_1/\delta)]. \quad (26)$$

Thus, the adjustment problem has been reduced essentially to the problem of arriving at a prescription for the second cross over point between the functions characterized in Eq. (15).

The procedure used in this study takes advantage of the fact that the case $\delta=0$ can be solved exactly, as well as by the approximation method. Therefore, this case was studied carefully in an effort to find how best to accomplish the adjustment of α^2 for the small values of δ which may be of interest in nuclear physics.

Equation (17) and Eq. (18) indicate that as $\delta\to 0$ both the order, n, and the argument, k, of the external radial function vanish. Since $J_1(0)=0$ and $J_0(0)=1$, it follows immediately from Eq. (22) that

$$-G_e'/G_e=[\epsilon_w^2+l(l+1)\alpha^2]^{\frac{1}{2}}. \quad (27)$$

To obtain a reasonable value for α^2, the right side of this equation was equated to the function $E_l(\epsilon_w)$ derived in Sec. 2. When solved for α^2, Eq. (27) then becomes

$$\alpha^2=[E_l^2(\epsilon_w)-\epsilon_w^2]/l(l+1). \quad (28)$$

Substituting into this for a range of values for ϵ_w^2 and l it became clear that the values of α^2 so obtained varied only slightly (in the range from 0.8 to 0.9). The final constant,

$$\alpha^2=0.82645 \quad \text{for} \quad \delta=0, \quad (29)$$

was chosen as an appropriate one. This corresponds to a second cross-over point at

$$\rho=1.1=1+0.1 \quad \text{for} \quad \delta=0. \quad (30)$$

This choice was made not only because of its convenience but also because it works particularly well for small values of ϵ_w^2, the region for which Eq. (27) is most sensitive to α^2. This region of ϵ_w^2 values is particularly of interest in applications of these results to the study of particle binding energies and nuclear transitions. Accordingly, it would seem best to favor this region in an adjustment.

TABLE I. The values of $\alpha^2(\delta)$.

δ	0	0.1	0.2	0.3	0.4	0.5
α^2	0.8264	0.6466	0.4744	0.3349	0.2214	0.1280

For nonzero values of δ, the rule

$$\rho_1=1+\delta+0.1 \quad (31)$$

was chosen as the simplest result which goes over to Eq. (30) for $\delta=0$. This simple rule is admittedly somewhat arbitrary; however, since only a small correction is involved here, it is difficult to see how Eq. (31) can lead to appreciable errors. Most certainly this procedure represents an improvement over the usual approximation of replacing ρ^{-2} by 1 which is equivalent to making the second point of agreement at infinity. Inserting Eq. (31) into Eq. (26) leads immediately to the function $\alpha^2(\delta)$. Values of this function are given in Table I.

5. RESULTS AND DISCUSSION

The ϵ'^2 *vs* ν and l, and k^2 *vs* ν and l relationships arrived at by the procedure described in Sec. 3 may now be translated into ϵ'^2 *vs* ϵ_0^2 relationships for comparison with Fig. 3. These are shown in Figs. 4, 5, 6, and 7 for $\delta=0.1$, 0.2, 0.3 and 0.4, respectively. For case $\delta=0$, the eigenvalues arrived at by the approximate method rarely deviate by more than a line width from

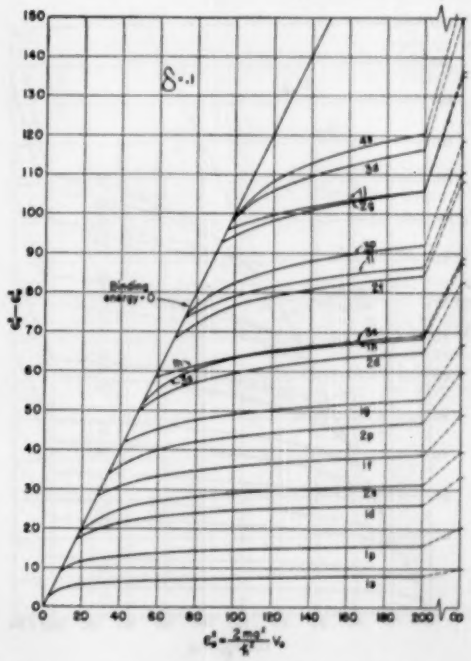

FIG. 4. Eigenvalues for $\delta=0.1$.

the curves shown in Fig. 3 It must be remembered that the results for $\delta \neq 0$ are exact for s states but are approximate for $p, d, \ldots f$. By first-order perturbation theory the error of the energy eigenvalue in natural units may be estimated to be

$$\Delta\epsilon_n^2 = l(l+1)\frac{\int_1^\infty G_\epsilon^2[\rho^{-2}-\alpha^2-(1-\alpha^2)\exp(1-\rho/\delta)]d\rho}{\int_0^1 G_\epsilon^2 d\rho+\int_1^\infty G_\epsilon^2 d\rho}. \tag{32}$$

By virtue of the vanishing of the perturbation at $\rho=1$ and $\rho=1+\delta+0.1$, the factor in the bracket is less than 0.05 in the intermediate region, which is the region within which the external wave function is significantly large. Accordingly the error is expected to be less than $0.05l(l+1)f$, where f is the probability for the particle being found beyond $\rho=1$. Since f is expected to be considerably less than 1, the error in ϵ_n^2 due to the method of approximation is expected to be considerably less than unity. Quantitative estimates using numerical integration substantiate this statement. At the present stage of our knowledge of the nucleus the approximate eigenvalues given in Figs. 3–7 should be sufficiently accurate so that their further refinement at this time is unnecessary. If these approximate eigenvalues and the corresponding analytical eigenfunctions prove helpful in resolving nuclear problems, further efforts toward refining them would certainly be warranted. In many instances refinements may be accomplished by the direct use of available tables of Bessel functions.[8,9] As an illustration of such a calculation it can be shown that the critical ϵ_0 values at which various s states of binding set in, satisfy

$$j_1(\epsilon_0)/j_0(\epsilon_0)=\epsilon_0^{-1}-J_1(2\delta\epsilon_0)/J_0(2\delta\epsilon_0), \tag{33}$$

where j_1 and j_0 are spherical Bessel functions and J_1 and J_0 are ordinary Bessel functions. Using the graphical results to locate the approximate ϵ_0 values, it is relatively simple to refine them to four or even five significant figures by interpolation. The results of this particular calculation are given in Table II. These ϵ_0 values are listed because of their possible usefulness in connection with the interpretation of the low velocity maxima in the Barschall neutron cross section surface.[10] On the "diffuse-cloudy crystal ball" model of neutron scattering the observed low velocity maxima at $A=11$, 55 and 150 would be expected to correspond to the $2s$, $3s$, and $4s$ critical ϵ_0 values for the appropriate diffuseness parameters, hence the "well strengths" in

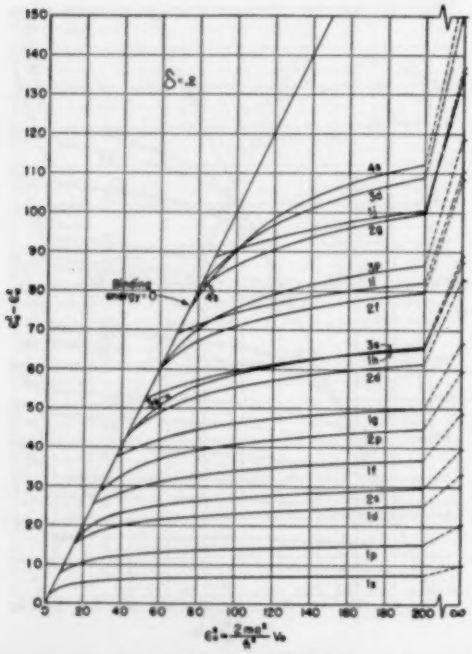

FIG. 5. Eigenvalues for $\delta=0.2$.

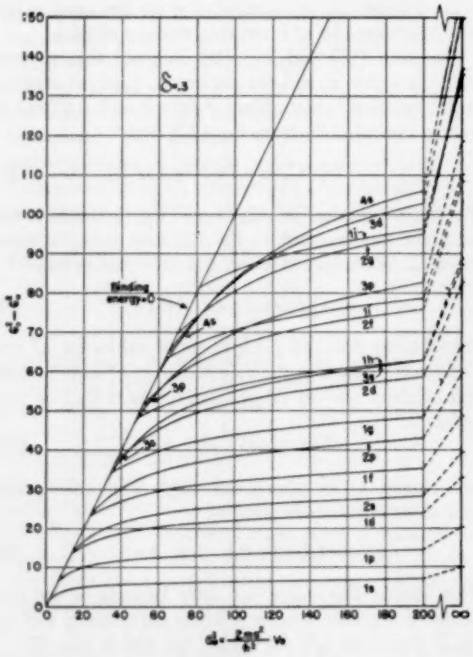

FIG. 6. Eigenvalues for $\delta=0.3$.

[8] *Tables of Spherical Bessel Functions* (Columbia University Press, New York, 1947), Vols. 1 and 2.
[9] E. Cambi, *Bessel Functions* (Dover Publications, Inc., New York, 1948).
[10] H. H. Barschall, Phys. Rev. **86**, 431 (1952).

TABLE II. The critical ϵ_0 values for the s states.

δ	$\epsilon_0(1s)$	$\epsilon_0(2s)$	$\epsilon_0(3s)$	$\epsilon_0(4s)$
0	1.571	4.712	7.854	10.996
0.1	1.428	4.272	7.084	9.825
0.2	1.307	3.855	6.204	8.370
0.3	1.202	3.454	5.371	7.324
0.4	1.111	3.081	4.747	6.554
0.5	1.031	2.761	4.280	5.896

any one column are effectively equivalent from the standpoint of these observations.

In a number of other instances, it is possible to arrange the calculations to take advantage of existing tables of Bessel functions for the refinement of the approximate eigenvalues presented in Figs. 3–7. However, with the advent of high-speed digital computers, the best way of refining the eigenvalues would probably be to solve the exact radial wave equation directly by numerical methods. Here again, the eigenvalues shown in Figs. 3–7 should be helpful by providing starting points which will greatly speed up the calculations.[11] Indeed one might expect that this family of eigenvalues and their analytical eigenfunctions might provide good initial approximations for the investigation of any other potential functions similar in general shape to the exponentially diffuse spherical well cases treated here.

In conclusion, it is important to note that the infinite spherical well eigenvalues provide a poor representation of the finite spherical well eigenvalues in the range of ϵ_0^2 values of interest in nuclear physics (certainly less than 200). When the boundary is made diffuse to a moderate degree the infinite spherical well eigenvalues are hopelessly inaccurate. Thus the numerous theoretical results in the nuclear literature which are based upon the infinite spherical or cubic well approximations must clearly be treated with great care. Even the finite square spherical well eigenvalues differ considerably from the diffuse boundary eigenvalues, particularly in the region of small energies, which is the region of greatest interest in nuclear physics.[12] Accordingly, one might

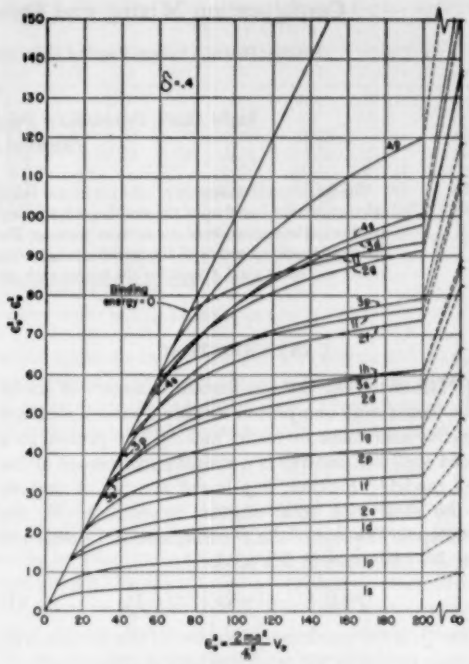

FIG. 7. Eigenvalues for $\delta=0.4$.

hope that some of the well-known difficulties of the independent-particle model based upon square well eigenvalues and eigenfunctions might be removed by the use of the diffuse boundary eigenvalues and eigenfunctions.

ACKNOWLEDGMENTS

The authors would like to express their thanks to Julius Salacz-Dohnanyi, Richard Gentry, Dane A. McNeill, and Kenneth L. Zankel for assistance with the computations.

[11] The writer is indebted to Dr. Ward C. Sangren of the Oak Ridge National Laboratory Mathematics Panel for an illuminating discussion relative to this point.

[12] In examining the influence of an increase in the diffuseness parameter δ one must, of course, reduce the radius parameter a (hence increase the natural energy unit E_0) and the well strength parameter ϵ_0 in order to preserve an effective radius and an effective well strength defined by a particular set of experimental observations. Similar considerations are applied in the so-called shape-independent treatment of two-nucleon systems in which the critical $1s$ well strengths of various types of potentials are placed in correspondence. In the study of complex nuclei, the best prescriptions for $a(\delta)$ and $\epsilon_0(\delta)$ will depend upon the intended application.

Configuration Mixing and Quadrupole Moments of Odd Nuclei

HISASHI HORIE,* *Palmer Physical Laboratory, Princeton University, Princeton, New Jersey*

AND

AKITO ARIMA, *Department of Physics, University of Tokyo, Tokyo, Japan*

(Received April 18, 1955)

The quadrupole moments of odd nuclei are calculated from the standpoint of configuration mixing. The calculations are based upon the simple perturbation theory. The quadrupole moments of odd-neutron nuclei are due to the excitation of one or more protons. The quadrupole moments of odd-proton nuclei also contain the quadrupole moments of the initial configuration. The agreement between the calculated and observed values are fairly good except for the nuclei with very large quadrupole moments.

I. INTRODUCTION

THE fact that the quadrupole moments of nuclei containing one proton outside a closed shell are negative and those of nuclei lacking one proton to a closed shell are positive is a simple consequence of the shell model.[1,2] Further, if p is the number of protons in the shell with total angular momentum $j\hbar$, the quadrupole moment of the j^p configuration (p odd) and spin $J=j$ becomes in this model[3,4]:

$$Q=Q_j(2j+1-2p)/(2j-1), \tag{1}$$

where Q_j is the quadrupole moment of the nucleus with a single proton in the orbit j outside a closed shell:

$$Q_j=-(2j-1)/(2j+2)\cdot\langle r^2\rangle_j. \tag{2}$$

$\langle r^2\rangle_j$ is the expectation value of r^2 for the proton in the outermost orbit j. Thus, quadrupole moments are negative for less than half-filled shells and positive for more than half-filled shells. The observed signs of quadrupole moments are, in general, in agreement with this rule.

The quadrupole moments of some nuclei with an odd number of protons lying between the magic numbers 50 and 82 are so large that one cannot expect to explain them by the shell model. The collective model ascribes these very large quadrupole moments to core deformation.[5,6] According to this model, the magnitude of the quadrupole moments of closed shell ± one proton nuclei should also be very large—considerably larger than the observed values.[6,7] These are usually two or three times larger than the values given by the simple shell model.

Quadrupole moments of several odd-neutron nuclei show a similar variation with the number of neutrons in the not-closed shell to that shown by odd-proton nuclei with respect to the number of protons. This might be explained by the collective model. Again this model gives too large quadrupole moments for nuclei with a closed shell ± one neutron. On the other hand, the usual shell model gives zero quadrupole moments for odd-neutron nuclei, since the neutrons carry no charge and since the effect of the recoil of the core is negligibly small except for extremely light nuclei.

We consider the effect of configuration mixing which explains the deviations of magnetic moments of odd nuclei from the Schmidt lines in a reasonable way.[8] As the starting configuration, we adopt again the configuration given by the single-particle model, i.e., assume that the even particles couple to angular momentum zero and the state of the odd particles is that of lowest seniority consistent with the observed spin. Thus, for some of our wave functions the isotopic spin is not a good quantum number. However, introduction of the isotopic spin does not improve the agreement with respect to quadrupole moments[9] and its use does not change the wave function for medium heavy and heavy nuclei.

II. THE QUADRUPOLE MOMENTS DUE TO THE EXCITATION OF PROTONS

In the shell model with strong spin-orbit interaction, even and odd numbers of nucleons in the same orbit j couple in such a way that the resultant angular momenta are $J=0$ and $J=j$, respectively.[1] Although there are a few exceptions under this rule for an odd number of nucleons, it does hold in most cases and will be adopted as the starting point for our considerations. As was mentioned before, if one disregards the intermixing of configurations, the quadrupole moments of odd-proton nuclei in the j^p configuration is given by (1). The quadrupole moments of odd-neutron nuclei are zero in this model.

Let us consider the effects of configuration mixing on quadrupole moments of odd nuclei. If we assume

* On leave of absence from Department of Physics, University of Tokyo, Tokyo, Japan.

[1] M. G. Mayer, Phys. Rev. **78**, 16, 22 (1950).

[2] E. P. Wigner, Lecture note at Wisconsin University, 1951 (unpublished).

[3] R. G. Sachs, *Nuclear Theory* (Addison-Wesley Press, Cambridge, 1953).

[4] S. A. Moszkowski and C. H. Townes, Phys. Rev. **93**, 306 (1954).

[5] J. Rainwater, Phys. Rev. **79**, 432 (1950).

[6] A. Bohr and B. R. Mottelson, Kgl. Danske. Videnskab. Selskab Mat.-fys. Medd. **27**, No. 16 (1953).

[7] F. J. Milford, Phys. Rev. **93**, 1297 (1954).

[8] A. Arima and H. Horie, Progr. Theoret. Phys. **12**, 623 (1954).

[9] M. Umezawa, Progr. Theoret. Phys. **10**, 505 (1953).

that the admixture of excited configurations to the original one is so small that the effects proportional to the square of the admixture coefficients can be neglected, only the contributions from the nondiagonal elements of the quadrupole moment operator between the excited and ground configurations need be considered. Let us denote the ground configuration given by the shell model by $\Psi_0(jm)$. Let $\Psi_n(jm)$ be a typical excited configuration; j and m are the angular momentum and its z-component, respectively, for these states. Then the whole wave function is given by

$$\Psi_{\text{mixed}}(jm)=\Psi_0(jm)+\sum_n \alpha_n\Psi_n(jm), \tag{3}$$

where the α are the coefficients of mixing. The expectation value of the quadrupole moment operator for the state represented by the first term of (3) with $m=j$ gives the value (1) of the single-particle model, while the main correction caused by the addition of the other terms is given by the cross terms between the first and later terms with $m=j$. Thus, the quadrupole moment caused by the configuration mixing is given by expressions of the form

$$\delta Q=2\alpha_1(\Psi_0(jj), Q_{\text{op}}\Psi_1(jj)), \tag{4}$$

where Q_{op} represents the quadrupole moment operator

$$Q_{\text{op}}=\sum_{i=1}^{Z} er_i^2(3\cos^2\theta_i-1). \tag{5}$$

r_i and θ_i are radial and angular variables of the ith proton. The excited configuration $\Psi_1(jm)$ must not differ from the original one $\Psi_0(jm)$ by more than one orbit in order to have a nonvanishing δQ in (4) because the quadrupole operator Q_{op} is a one-particle operator. It is also evident that either the orbital angular momenta of the orbits in which Ψ_0 and Ψ_1 differ must be equal, or their difference must be ± 2. The coefficient of mixing, α, is given by perturbation theory in terms of the nondiagonal element of energy matrix:

$$\alpha_1=-(\Psi_0(jm), \sum_{i<k} V_{ik}\Psi_1(jm))/\Delta E, \tag{6}$$

where V_{ik} is the interaction between the ith and kth nucleons and ΔE is the energy difference between the first and second configuration. We assume, for the sake of simplicity, that the radial dependence of the interaction has delta-function character.

There are several modes of excitation of the proton group which will give rise to quadrupole moments. First of all, we consider the excitation of a proton from one of the orbits filled with an even number of protons to another orbit which is not filled, due to the interaction with the odd nucleons[10] in the outermost orbit. We represent the zeroth-order state of the nucleus given by the single-particle model as

$$\Psi_0(jm)=\Psi(j_1^n(0)j^p(j); jm),$$

where nucleons in the orbit j_1 are protons and n is an even number not larger than $2j_1+1$; p is the number of nucleons in the outermost orbit. Then a sequence of excited states in which one proton in j_1 orbit jumps to j_2,

$$\Psi_1(jm)=\Psi([j_1^{n-1}(j_1)j_2](J)j^p(j); jm),$$

can interact with the above state.[11] J is restricted by the condition $|j_1-j_2|\leq J\leq j_1+j_2$. However, it can easily be seen that only the state with $J=2$ gives nonvanishing δQ by (4) and the orbital angular momentum of j_2 must be equal to that of j_1 or differ from it by two units. Hence, the mixed configuration which can give rise to the quadrupole moment is expressed as

$$\Psi(j_1^n(0)j^p(j); jm)+\alpha\Psi([j_1^{n-1}(j_1)j_2](2)j^p(j); jm). \tag{I}$$

After a straightforward calculation following the procedure (4) and (6) which is given in Appendix I, δQ is obtained as

$$\delta Q_1=-n[(2j+1-2p)/(2j+2)](j_1\,\tfrac{1}{2}\,20|\,j_1\,2j_2\,\tfrac{1}{2})^2 \times\langle j_1|r^2|j_2\rangle\begin{cases}(-V_sI)/\Delta E & \text{for odd-proton nuclei}\\ (-\frac{1}{2}V_s-\frac{3}{2}V_t)I/\Delta E & \text{for odd-neutron nuclei,}\end{cases} \tag{7}$$

where $(j_1\,\frac{1}{2}\,20|\,j_1\,2j_2\,\frac{1}{2})^2$ is the square of the Clebsch-Gordan coefficient, the values of which are shown in Table I, and V_s and V_t are interaction strengths in the singlet and triplet states, respectively. $\langle j_1|r^2|j_2\rangle$ is a matrix element of r^2 between the radial wave functions of j_1 and j_2 orbits:

$$\langle j_1|r^2|j_2\rangle=\int_0^\infty R(j_1)r^2R(j_2)r^2dr, \tag{8}$$

and I is a Slater integral for a delta-function interaction

$$I=\tfrac{1}{2}\int_0^\infty R^2(j)R(j_1)R(j_2)r^2dr. \tag{9}$$

The R are radial wave functions; their phases do not affect the signs of δQ since each radial wave function appears necessarily an even number of times in Eq. (7).

TABLE I. The values of the square of Clebsch-Gordan coefficient $(j_1\,\frac{1}{2}\,20|\,j_1\,2j_2\,\frac{1}{2})^2$.

$j_1\backslash j_2$	1/2	3/2	5/2	7/2	9/2	11/2	13/2
1/2	...	2/5	3/5	...	...	...	...
3/2	1/5	1/5	3/35	18/35	...	...	...
5/2	1/5	2/35	8/35	4/105	10/21	...	...
7/2	...	9/35	1/35	5/21	5/231	5/11	...
9/2	...	...	2/7	4/231	8/33	2/143	64/143
11/2	...	...	...	28/65	7/715	35/143	5/429
13/2	...	...	...	...	36/85	8/1105	16/65

[10] In an odd nucleus which has an odd number of protons, the protons are the "odd nucleons." Similarly, the neutrons will be called "odd nucleons" if their number is odd. This notation facilitates the discussion.

[11] The case that j_2 coincides with j in odd proton nuclei will be considered later in the excitation (II).

Although it was assumed that the zeroth-order state contained no proton in the orbit j_2, (7) will be valid also when there are m protons in the orbit j_2 (m even) and if they couple to an angular momentum zero, except that the right side must be multiplied by $(2j_2+1-m)/(2j_2+1)$. Equation (7) and the equation modified in this way are applicable for both odd-proton and odd-neutron nuclei and they correspond to Table I of reference 8 for the case of magnetic moments.

For odd-proton nuclei, there are two other configurations which give a quadrupole moment. In one of these, j_2 coincides with j in (I) and the corresponding mixed configuration is

$$\Psi(j_1^n(0)j^p(j);\,jm) + \sum_J \beta_J \Psi(j_1^{n-1}(j_1)j^{p+1}(J);\,jm), \quad \text{(II)}$$

where β_J is the coefficient of mixing for each J and $J=2, 4, \cdots, 2j-1$ so that $j^{p+1}(J)$ represent the states of seniority two.[12,13] The derivation of the quadrupole moment caused by the configuration mixing (II) is somewhat more complicated than that of (I). However, by making use of the average value of the reciprocals of the zeroth order energy differences between the first and each of the second configurations as $\langle 1/\Delta E\rangle$, we obtain a formula for δQ which is similar to (7) (see Appendix B):

$$\delta Q_{\text{II}} = -n[(2j-p)/(2j+2)] \times (j_1\,\tfrac{1}{2}\,20|\,j_1\,2j_2\,\tfrac{1}{2})^2\langle j_1|r^2|\,j_2\rangle(-V_s I)\langle 1/\Delta E\rangle. \quad (10)$$

The integral I is obtained by putting $j_2=j$ in (9). The factor $(2j-p)$ in (10) reflects the fact that this mode of excitation cannot take place in those odd-proton nuclei in which a single proton is missing from the outermost orbit.

In the other configuration which must be considered for the quadrupole moments of odd-proton nuclei the number of protons in the outermost orbit j is larger than 1. It corresponds to the inverse case of the excitation mode (II) and is expressed as

$$\Psi(j_1^n(0)j^p(j);\,jm) + \sum_J \gamma_J \Psi(j_1^{n+1}(j_1)j^{p-1}(J);\,jm), \quad \text{(III)}$$

where the even number n may be equal to zero, and γ_J is the coefficient of mixing. The quadrupole moment caused by the excitation (III) is

$$\delta Q_{\text{III}} = (p-1)[(2j_1+1-n)/(2j_1+2)] \times (j_1\,\tfrac{1}{2}\,20|\,j_1\,2j\,\tfrac{1}{2})^2\langle j_1|r^2|\,j\rangle(-V_s I)\langle 1/\Delta E\rangle, \quad (11)$$

where I is similar to the corresponding integral in (10). Equations (10) and (11) correspond to (11) and (14) of reference 8, respectively.

In addition to the three modes of excitation which were described above, the state $j_1^n(0)$ (n even) of protons can be excited into a state $j_1^n(J)$. The lowest excited states $j_1^n(J)$ are usually assumed to be those of seniority two. Again only the state with $J=2$ can contribute to the quadrupole moment in our approximation.[14] This type of excitation may be taken as a degenerate case of (I) in which j_2 coincides with j_1, so that the result is obtained at once by putting $j_2=j_1$ in (7) and multiplying a factor $(2j_1+1-n)/(2j_1-1)$ which comes from the coefficient of fractional parentage. Hence, the excitation

$$\Psi(j_1^n(0)j^p(j)jm)+\alpha'\Psi(j_1^n(2)j^p(j)jm), \quad \text{(IV)}$$

gives

$$\delta Q_{\text{IV}} = -n[(2j_1+1-n)(2j+1-2p)/(2j_1-1)(2j+2)] \times (j_1\,\tfrac{1}{2}\,20|\,j_1\,2j_1\,\tfrac{1}{2})^2\langle j_1|r^2|\,j_1\rangle \times \begin{cases} (-V_s I)/\Delta E_2 & \text{for odd-proton nuclei} \\ (-\tfrac{1}{2}V_s - \tfrac{3}{2}V_t)I/\Delta E_2) & \text{for odd-neutron nuclei.} \end{cases} \quad (12)$$

Thus, the corrections to the quadrupole moments in the approximation here considered are given by the sum of (7) and (12) for odd-neutron nuclei, and the sum of (7), (10), (11), and (12) for odd-proton nuclei. They depend on the number p of nucleons in the outermost orbit linearly. Furthermore, the contributions given by (7) and (12) depend on p in the same way as the single-particle model's expression (1). This applies also for odd-neutron nuclei. The other corrections to the odd-proton nuclei, given in (10) and (11), have a different dependence upon p. The former vanishes at the end of the subshell while the latter vanishes at the beginning of the subshell.

III. COMPARISON WITH THE OBSERVED VALUES

(i) Determination of the Parameters

In order to compare the theoretical values for the quadrupole moment, obtained in the preceding section, with the observed values it is necessary to estimate the quantities which appear in (7), (10), (11), and (12). First of all, we assume that the interactions between nucleons are attractive and the attractive force in the triplet state is stronger than in the singlet state so that $|V_t|=1.5|V_s|$. Although this agrees with the experimental data of two-nucleon systems at low energy, it remains an assumption since the interactions in larger nuclei might differ from those in two-nucleon systems. It is possible, in fact, that the integrals I and the matrix elements of r^2 become negative in some cases. It is necessary, therefore, to obtain a somewhat more accurate estimate of these quantities than was necessary for the calculation of the magnetic moments. We assume that the wave functions for nucleons are those of a harmonic oscillator[15]:

$$R_{nl}(r) = N_{nl}\exp(-\nu r^2/2)r^l v_{nl}(r).$$

[12] G. Racah, Phys. Rev. **63**, 367 (1943).
[13] B. H. Flowers, Proc. Roy. Soc. (London) **A212**, 248 (1952).
[14] This type of excitation does not contribute to the magnetic moment in the approximation of reference 8, since there is no low excited state with $J=1$.
[15] For example, I. Talmi, Helv. Phys. Acta **25**, 185 (1952).

N_{nl} is a normalization constant and $v_{nl}(r)$ is an associated Laguerre polynomial

$$v_{nl}(r)=L_{n+l-1/2}^{l+1/2}(\nu r^2).$$

The constant ν is determined by evaluating the diagonal elements of r^2. For $n=1$, these are $\langle 1l|r^2|1l\rangle=(2l+3)/2\nu$. If one assumes a uniform nuclear density, the average value of r^2 is $\langle r^2\rangle=(3/5)(1.45A^{1/3})^2\times10^{-26}$ cm^2, A being the mass number. Thus, putting $1/2\nu=c_1A^{2/3}$, the order of magnitude of c_1 becomes 1 to 1.8 times 10^{-27} cm^2 (assuming $l=2\sim5$). Furthermore, the matrix elements of r^2 become

$$\langle j_1|r^2|j_2\rangle=f(j_1;j_2)/(2\nu)=c_1f(j_1;j_2)A^{2/3},$$

where $f(j_1;j_2)$ does not depend on the mass number, and they can be obtained by straightforward integration.

The integrals I are inversely proportional to the mass number A since they involve four wave functions. For harmonic oscillator wave functions, they have the form

$$I(jj_1;jj_2)=\tfrac{1}{2}F(jj_1;jj_2)(\nu^3/\pi)^{1/2},$$

where $F(jj_1;jj_2)$ does not depend upon ν or A, while the factor $\nu^{3/2}$ provides an A^{-1} dependence because of the proportionality of ν to $A^{-2/3}$. The average value of V_sI can be estimated from the difference of binding energies of odd and even nuclei[1,8] to be $-25/A$ Mev. Hence, we obtain from

$$V_sI(jj_1;jj_2)=-c_2F(jj_1;jj_2)/2A,$$

200 to 300 Mev for the order of magnitude of c_2 at $A\sim200$ because the values of F for $2d$, $1g$, and $1h$ orbits are 0.260, 0.213, and 0.176, respectively. This gives the estimate $c_1c_2=(0.3$ to $0.6)\times10^{-24}$ cm^3 Mev. Actually, the value $c_1c_2=0.5\times10^{-24}$ cm^3 Mev was used in the calculations.

(ii) Determination of the Energy Denominators

The energy difference ΔE consists of two parts. One is the difference between the single-particle levels in which the ground and excited configurations differ, and the other is that between the energies caused by the interaction between nucleons in each configuration. The estimate of the latter is complicated and it will be ignored in the actual calculation. Even if we restrict ourselves only to the energy differences of the single-particle levels, it is not easy to determine completely on the basis of conventional potentials, spin-orbit interactions, and the observed values of nuclear spins. The oscillator potential gives strongly degenerate states with different principal and azimuthal quantum numbers, and the square well potential with finite or infinite well depth does not always provide the order of levels which, together with plausible doublet splittings, would yield the observed values of the nuclear spins. Therefore, we attempted to construct a level scheme by using both empirical data and theoretical information.

TABLE II. Doublet splitting assumed in the calculation. The splitting $1d_{3/2}-1d_{5/2}$ is taken from the experimental data on O^{17}.[17] The others are estimated by the formula by determining the proportionality constant by the doublet splitting of O^{17}.

	$\Delta E_{\text{doublet}}$ in Mev	$\bar{A}$
$1p_{1/2}-p_{3/2}$	3	17
$1d_{3/2}-d_{5/2}$	5	...
$1f_{5/2}-f_{7/2}$	3	60
$2p_{1/2}-p_{3/2}$	1.5	60
$1g_{7/2}-g_{9/2}$	2.5	105
$2d_{3/2}-d_{5/2}$	1.5	120
$1h_{9/2}-h_{11/2}$	2	200
$2f_{5/2}-f_{7/2}$	1.5	200
$3p_{1/2}-p_{3/2}$	0.5	200
$1i_{11/2}-i_{13/2}$	2	260

First of all, the doublet splittings are estimated by the simple formula of Inglis[16]: $\Delta E_{\text{doublet}}=K(2l+1)A^{-2/3}$, where A and K are the mass number and a proportionality constant with the dimension of energy. If we employ the observed value[17] of the splitting $1d_{5/2}-1d_{3/2}$ in O^{17}, we obtain $K=6.6$ Mev. However, the doublet splitting was assumed to be constant for a subshell and the mass number A adopted for calculating it was the average A of those nuclei the observed spins of which indicate that they contain this subshell partially filled. The assumed doublet splittings obtained in this way are given in Table II and the above-mentioned mass numbers are shown under $\bar{A}$. The values adopted will be seen to be considerably in excess of the excitation energy of isomeric levels. This was not considered to be an inconsistency because the isomeric levels are probably not single-particle levels but result from many-body effects.

The position of the $1s$ level relative to the $1p$ levels cannot be obtained directly from the experimental data. However, as the contribution from the excitation of a $1s$ proton can be seen to be small, the estimate obtained from the square well potential[2] was considered to be sufficiently accurate. The spacing is given as 15.5 Mev and 9.2 Mev by the potential with infinite depth if one assumes a mass number 17 and 37, respectively (and corresponding nuclear radii). These figures are the two extreme mass numbers in which the $1s$ level plays a role in our calculation. Therefore, we assume the $1s-1p$ energy difference to be 12 Mev. Then the $1p_{3/2}$ level is assumed to be lower than the center of gravity of the $1p$ levels by 1 Mev and the $1p_{1/2}$ higher by 2 Mev. These numbers were obtained by dividing the doublet splitting 3 Mev in the ratio 1 to 2.

The observed levels of C^{13} and N^{13} give the spacings between $1p_{1/2}$ and $1d_{5/2}$ as 3.86 Mev and 3.56 Mev, respectively.[17] We assume the $1d_{5/2}-1p_{1/2}$ spacing to be 3 Mev for nuclei, the mass number of which are larger than 20. The position of the $2s_{1/2}$ level relative to the $1d_{5/2}$ is assumed in accordance with the observed levels

[16] D. R. Inglis, Revs. Modern Phys. **25**, 390 (1953).
[17] F. Ajzenberg and T. Lauritsen, Revs. Modern Phys. **27**, 77 (1955).

TABLE III(a). Spacing of even-parity levels which was used in our calculation.

	$1d_{5/2}$	$2s$	$1d_{3/2}$	$1g_{7/2}$	$1g_{9/2}$	$2d_{5/2}$	$2d_{3/2}$	$3s$	$1i_{13/2}$	$1i_{11/2}$
$1s$	17	···	22	···	···	32	33.5	···	···	···
$1d_{5/2}$		1	5	12	14.5	15	16.5	16.75	···	···
$2s$			4	···	···	14	15.5	···	···	···
$1d_{3/2}$				7	9.5	10	11.5	11.75	···	···
$1g_{9/2}$					2.5	3	4.5	4.75	8.5	10.5
$1g_{7/2}$						0.5	2	2.25	6	8
$2d_{5/2}$							1.5	1.75	···	···
$2d_{3/2}$								0.25	···	···
$3s$									···	···
$1i_{13/2}$										2

TABLE III(b). Spacing of odd-parity levels which was used in our calculation.

	$1p_{1/2}$	$1f_{7/2}$	$2p_{3/2}$	$1f_{5/2}$	$2p_{1/2}$	$1h_{11/2}$	$1h_{9/2}$	$2f_{7/2}$	$2f_{5/2}$	$2p_{3/2}$	$2p_{1/2}$
$1p_{3/2}$	3	13	15.5	16	17	···	···	24.5	26	26.75	27.25
$1p_{1/2}$		···	12.5	13	···	···	···	···	23	23.75	···
$1f_{7/2}$			2.5	3	···	9	11	11.5	13	13.75	···
$2p_{3/2}$				0.5	1.5	···	···	9	10.5	11.25	11.75
$1f_{5/2}$					1	6	8	8.5	10	10.75	11.25
$2p_{1/2}$						···	···	···	9	9.75	···
$1h_{11/2}$							2	2.5	4	4.75	5.25
$1h_{9/2}$								0.5	2	2.75	3.25
$2f_{7/2}$									1.5	2.25	2.75
$2f_{5/2}$										0.75	1.25
$3p_{3/2}$											0.5

for O^{17} so that the $2s$ level is higher than the $1d_{5/2}$ by 1 Mev.[17] The spacing between $1f_{7/2}$ and $1d_{3/2}$ is assumed to be 2 Mev, since the corresponding spacings of S^{33} and K^{41} appear to be 2.85 Mev and 1.37 Mev, respectively.[18] Although the spacing between the $2p_{3/2}$ and $1f_{7/2}$ levels seems to be 2 Mev from the observed data on Ca^{41}, we use the value of 2.5 Mev for this spacing in order to bring the $2p_{3/2}$ level close to $1f_{5/2}$. It is known that $2p_{3/2}$ and $1f_{5/2}$ are close to each other from the change of spins in Rb isotopes.

The pair of levels $2p_{1/2}$ and $1g_{9/2}$ often change position in isomeric nuclei. However, the inversion seems to take place on account of the large pairing energy of the $1g_{9/2}$ nucleons. Hence we adopt the energy difference observed in $_{39}Y^{89}$ which might be free from this effect. The observed data indicate that the $1g_{9/2}$ is higher than $2p_{1/2}$ by 0.913 Mev,[19] and we assume the spacing as 1 Mev. The situation is similar with respect to the $1g_{7/2}$ and $2d_{5/2}$ levels. Fortunately, as the contribution to the quadrupole moment from the jump of a proton between these levels is much smaller than the contribution from other excitations (see Table I), the relative position of these levels does not influence the calculated results critically. We assume on the basis of the observed energy differences of 0.66, 0.15 and 0.33 Mev for Mo^{99}, Sb^{125} and Sb^{123}, respectively,[19] that the $2d_{5/2}$ level lies 0.5 Mev above the $1g_{7/2}$ level.

[18] P. M. Endt and J. C. Kluyver, Revs. Modern Phys. **26**, 95 (1954).

[19] M. Goldhaber and R. D. Hill, Revs. Modern Phys. **24**, 179 (1952).

The spacings between $1h_{11/2}$, $2d_{3/2}$, and $3s$ are known to be small from isomeric transitions. It was pointed out by Mihelich and de-Shalit[20] that it is uncertain whether the isomeric transitions between these states are "particle transitions" or "hole transitions." Fortunately, the energy differences $2d_{3/2}-1h_{11/2}$ and $3s-1h_{11/2}$ do not affect the calculated values of the quadrupole moments. We assume that the $1h_{11/2}$ level is lowest, the $2d_{3/2}$ second, and the $3s_{1/2}$ level highest, and that the spacing $2d_{3/2}-1h_{11/2}$ is 0.5 Mev and $3s-2d_{3/2}$ is 0.25 Mev. The order of magnitude of the former is inferred from the level of Ba^{137} at 0.66 Mev and the latter is taken from the 0.26-Mev level[19] in Au^{197}.

The spacing between $1h_{9/2}$ and $2f_{7/2}$ levels is expected to be small but no experimental data are available. Since the spin of $_{83}Bi^{209}$ is $9/2$, we assume that $h_{9/2}$ is slightly lower than $2f_{7/2}$; the spacing is tentatively assumed to be 0.5 Mev. We note in passing that no case is known in which a $h_{9/2}$ proton jumps to the $2f_{7/2}$ level.

The position of the $2f_{5/2}$, $1i_{13/2}$ and $3p_{3/2}$ levels must be determined for estimating the contribution of the excitation of protons from lower levels even though these levels appear only as the neutron levels in actual nuclei. Therefore, we obtain their relative positions from the levels of odd-neutron nuclei. The analysis of isomeric states[20] of Hg, Au, and Pt indicates that $1i_{13/2}$ is higher than $2f_{5/2}$ by about 0.5 Mev and that $3p_{3/2}$ is higher than $2f_{5/2}$ by almost the same amount; the spacing $3p_{3/2}-1i_{13/2}$ is assumed as 0.25 Mev. It might be mentioned that this level scheme is somewhat different from that obtained recently[21] for Pb^{207}. However, our results are not seriously affected by our assumptions concerning the positions of these levels.

The assumed position of all the levels is summarized in Tables III(a) and (b). The former gives the spacings between levels with even parity and the latter of those with odd parity. The values given in these tables are assumed to give the energy differences between levels for all nuclei, regardless of their masses. This might seem to be a crude approximation because the level spacings decrease with increasing A. However, only limited numbers of level spacings affect the calculated values and most level spacings have very little effect on our results. The uncertainties which appeared in the determination of high levels might give rise to some ambiguities in the calculated quadrupole moments of heavier nuclei, but it is not likely that our results could be changed substantially by assuming different level spacings.

For the excitation modes (II) and (III) the average value $\langle 1/\Delta E\rangle$ would be needed. These are assumed to be equal to $1/\Delta E$ for the sake of simplicity. On the other hand, the ΔE_2 in the excitation mode (IV) is the

[20] J. H. Mihelich and A. de-Shalit, Phys. Rev. **93**, 135 (1954).

[21] D. E. Alburger and M. H. L. Pryce, Phys. Rev. **95**, 1482 (1954).

energy difference between $J=0$ and $J=2$ states of the j_1^n configuration (n=even, $0<n<2j_1+1$). Theoretically, this energy difference does not depend upon the numbers n of nucleons[22] and we estimate it from the experimental data near the closed shell. It decreases from 2 to 0.5 Mev as the mass number increases.[23,24]

(iii) Comparison with the Observed Values

The calculation of the quadrupole moments was carried out only for the nuclei with normal coupling; the quadrupole moments of Na^{23}, Mn^{55}, Se^{79}, and Eu^{153} were not calculated.[4] Those nuclei with mass numbers less than 16 were also omitted because the approximation adopted might break down. The observed values for the quadrupole moments were obtained from the compilations of Klinkenberg[25] and Murakawa and Kamei[26] and the configurations adopted are based upon the tables of Klinkenberg,[25] unless otherwise stated. The results for odd-neutron nuclei are given in the fourth column of Table IV. The fifth column of this table gives the hydrodynamic estimates of the collective model (reference 6, Table IX). Our calculated values are for odd neutron nuclei (except for Er^{167}) in general somewhat larger than the observed values. For O^{17}, the assumption that the interaction has delta-function character might not be valid. Two zeroth-order configurations are tried for Ge^{73} because there is a competition between the $p_{1/2}$ and $g_{9/2}$ neutron levels. The calculated values of the magnetic moment following the treatment of reference 8, are -1.72 and -0.76 nm for the configurations $(p_{1/2})^2\, g_{9/2}$ and $(g_{9/2})^3$, respectively. The observed value is -0.88 nm. Hence, the latter configuration gives better agreement both for magnetic and quadrupole moments. The large quadrupole moment of Er^{167} cannot be explained by the present calculation. Some remarks concerning such large quadrupole moments which appear also in odd-proton nuclei will be given in the next section. The detailed contribution of each type of configuration mixing is shown in Table V for S^{33} as an example. The largest contribution comes from the excitation mode $(1d_{5/2})^6 \rightarrow (1d_{5/2})^5\, 1g_{9/2}$ for protons and the probability of this excited configuration is 2.8%. This justifies the use of the first order perturbation theory; the reduction of the zeroth order configuration is negligible at least in most cases.

TABLE IV. Calculated and observed values of quadrupole moments of odd-neutron nuclei. $c_1c_2=0.5\times10^{-24}$ cm² Mev. The $Q_{H.M.}$'s are the hydrodynamical estimate of the collective model (reference 6).

Nucleus	Configuration proton	neutron	Q_{obs}	Q_{calc}	$Q_{H.M.}$
$_8O^{17}$	···	$d_{5/2}$	−0.004	−0.04	−0.16
$_{16}S^{33}$	···	$d_{3/2}$	−0.064	−0.09	−0.22
$_{16}S^{35}$	···	$(d_{3/2})^3$	0.045	0.09	0.22
$_{32}Ge^{73}$	···	$(p_{1/2})^2\, g_{9/2}$	−0.2±0.1	−0.43	−1.2
	···	$(g_{9/2})^3$		−0.27	···
$_{36}Kr^{83}$	$(f_{5/2})^4$	$(g_{9/2})^7$	0.15	0.28	···
$_{54}Xe^{131}$	$(g_{7/2})^4$	$d_{3/2}$	−0.12	−0.26	···
$_{68}Er^{167}$	$(h_{11/2})^4$	$(f_{7/2})^7$	10.2	0.70	···

For odd-proton nuclei, we obtain the values listed in Table VI. The value of the parameter c_1 was assumed to be 1.2×10^{-27} cm² for the calculation of the quadrupole moment (1) due to the normal configuration. The only nucleus for which the calculation gives a quadrupole moment with the wrong sign is V^{51}. However, if the normal configuration is assumed to be $(d_{3/2})^{-2}(f_{7/2})^5$ in this case, the calculated value becomes positive in agreement with the observed value. It might be recalled that the $(d_{3/2})^{-2}(f_{7/2})^3$ proton configuration gives a much better value than the $(f_{7/2})^1$ configuration for magnetic moment of Sc^{45}. However, this configuration assignment is difficult to reconcile with the magic character of nuclei with 20 protons. For Tc^{99}, the value calculated for the configuration $(g_{9/2})^5$ is much smaller than the observed value. The experimental moment is, however, somewhat ambiguous. Two configurations are examined for Pr^{141}. One of these gives a large negative, the other a small positive quadrupole moment. Therefore, it is likely that the zeroth-order wave function is a mixture of both. The observed value is obtained by assuming that the main configuration is $(d_{5/2})^2$ with a small admixture of $(g_{7/2})^2 d_{5/2}$. This is consistent with the value of the magnetic moment $\mu_{obs}=4.0$, since the $(d_{5/2})^2$ and $(g_{7/2})^2\, d_{5/2}$ configurations give 3.95 nm and 4.53 nm, respectively. From Eu^{153} to Re^{187}, the observed values are much larger than the calculated values, just as in the case of Er^{167}. The values given by the collective model are in general much larger than the observed values for the shell ± one nuclei for both odd-proton and odd-neutron nuclei.

TABLE V. Contributions from the individual mode of excitation of protons for the quadrupole moment of S^{33}. The zeroth-order proton configuration is $(1s)^2(1p_{3/2})^4(1p_{1/2})^2(1d_{5/2})^6(2s)^2$.

Excitation modes of protons		Q
$(1s)^2 \rightarrow (1s)\ 1d_{5/2}$		−0.004
$(1p_{3/2})^4 \rightarrow (1p_{3/2})^3\ 1f_{7/2}$		−0.007
$(1p_{3/2})^4 \rightarrow (1p_{3/2})^3\ 1f_{5/2}$		−0.001
$(1p_{3/2})^4 \rightarrow (1p_{3/2})^3\ 2p_{3/2}$		0.001
$(1p_{3/2})^4 \rightarrow (1p_{3/2})^3\ 2p_{1/2}$		0.001
$(1p_{1/2})^2 \rightarrow (1p_{1/2})\ 1f_{5/2}$		−0.005
$(1p_{1/2})^2 \rightarrow (1p_{1/2})\ 2p_{1/2}$		0.001
$(1d_{5/2})^6 \rightarrow (1d_{5/2})^4\ 1d_{3/2}$		−0.015
$(1d_{5/2})^6 \rightarrow (1d_{5/2})^5\ 1g_{9/2}$		−0.042
$(1d_{5/2})^6 \rightarrow (1d_{5/2})^5\ 1g_{7/2}$		−0.003
$(1d_{5/2})^6 \rightarrow (1d_{5/2})^4\ 2d_{5/2}$		0.004
$(1d_{5/2})^6 \rightarrow (1d_{5/2})^4\ 2d_{3/2}$		0.001
$(2s)^2 \rightarrow (2s)\ 1d_{5/2}$		−0.021
	Sum	−0.090

[22] C. Schwartz and A. de-Shalit, Phys. Rev. **94**, 1257 (1954).
[23] G. Scharff-Goldhaber, Phys. Rev. **87**, 218 (1952).
[24] P. Stähelin and P. Presiwek, Nuovo cimento **10**, 1219 (1953).
[25] P. F. A. Klinkenberg, Revs. Modern Phys. **24**, 63 (1952).
[26] K. Murakawa and T. Kamei, Rept. Inst. Sci. and Technol., Univ. Tokyo **7**, 219 (1953).

TABLE VI. Calculated and observed values of quadrupole moments of odd proton nuclei. $c_1=1.2\times10^{-27}$ cm^2 and $c_1c_2=0.5\times10^{-24}$ cm^2 Mev. $Q_{s.p.}$ and $Q_{h.m.}$ are the values given by the single-particle model and the hydrodynamic estimates of the collective model (reference 6), respectively.

Nucleus	Proton configuration	Q_{obs}	Q_{calc}	$Q_{s.p.}$	$Q_{h.m.}$
$_{13}Al^{27}$	$(d_{5/2})^5$	0.156 ± 3	0.16	0.04	0.30
$_{17}Cl^{35}$	$d_{3/2}$	−0.07894 ± 2	−0.08	−0.04	−0.26
$_{17}Cl^{37}$	$d_{3/2}$	−0.06213 ± 2	−0.08	−0.04	−0.26
$_{23}V^{51}$	$(f_{7/2})^3$	0.3 ±2	−0.03	−0.03	···
$_{27}Co^{59}$	$(f_{7/2})^7$	0.5 ±2	0.19	0.11	···
$_{29}Cu^{63}$	$p_{3/2}$	−0.157	−0.11	−0.07	−0.48
$_{29}Cu^{65}$	$p_{3/2}$	−0.147	−0.11	−0.07	−0.48
$_{31}Ga^{69}$	$(p_{3/2})^3$	0.2318 ± 23	0.15	0.07	0.53
$_{31}Ga^{71}$	$(p_{3/2})^3$	0.1461 ± 15	0.15	0.07	0.53
$_{33}As^{75}$	$(f_{5/2})^3(p_{3/2})^3$	0.32 ± 5	0.18	0.08	···
$_{35}Br^{79}$	$(f_{5/2})^4(p_{3/2})^3$	0.26 ± 8	0.19	0.08	···
$_{35}Br^{81}$	$(f_{5/2})^4(p_{3/2})^3$	0.21 ± 7	0.19	0.08	···
$_{41}Nb^{93}$	$g_{9/2}$	−0.4	−0.33	−0.20	···
$_{43}Tc^{99}$	$(g_{9/2})^5$	0.34 ±17	0.03	0.00	···
$_{49}In^{113}$	$(g_{9/2})^9$	1.144	0.41	0.22	2.4
$_{49}In^{115}$	$(g_{9/2})^9$	1.161	0.42	0.23	2.4
$_{51}Sb^{121}$	$d_{5/2}$	−0.52 ±10	−0.26	−0.18	−1.5
$_{51}Sb^{123}$	$g_{7/2}$	−0.67 ±10	−0.39	−0.22	−2.1
$_{53}I^{127}$	$(g_{7/2})^8d_{5/2}$	−0.72 ± 2	−0.31	−0.19	···
$_{53}I^{129}$	$(g_{7/2})(d_{5/2})^3$	−0.43 ±15	−0.42	−0.22	···
$_{57}La^{139}$	$(g_{7/2})^7$	0.9 ±1	0.44	0.24	···
$_{59}Pr^{141}$	$d_{5/2}$	−0.05	−0.30	−0.20	···
	$(g_{7/2})^{-2}(d_{5/2})^3$		0.02	0.00	···
$_{63}Eu^{151}$	$(d_{5/2})^5$	1.2	0.36	0.21	···
$_{71}Lu^{175}$	$(h_{11/2})^8(g_{7/2})^7$	5.9	0.74	0.28	···
$_{73}Ta^{181}$	$(h_{11/2})^{10}(g_{7/2})^7$	6	0.65	0.28	···
$_{75}Re^{185}$	$(d_{5/2})^5$	2.8	0.39	0.24	···
$_{75}Re^{187}$	$(d_{5/2})^5$	2.6	0.40	0.25	···
$_{77}Ir^{191}$	$(h_{11/2})^{10}(d_{3/2})^3$	1.0 ±5	0.40	0.18	···
$_{77}Ir^{193}$	$(h_{11/2})^{10}(d_{3/2})^3$	1.0 ±5	0.40	0.18	···
$_{79}Au^{197}$	$(d_{3/2})^3$	0.56	0.29	0.18	···
$_{83}Bi^{209}$	$h_{9/2}$	−0.4	−0.53	−0.39	−5.6

IV. DISCUSSION AND CONCLUSION

There are isotopes with equal spins but somewhat different quadrupole moments. These will not be discussed in detail; one can explain such a situation by assuming a mixture for the zeroth-order wave function. This was shown for Pr^{141} in the preceding section. The configuration interaction of this kind has been discussed concerning beta transitions with anomalous *ft* values and the first excited states of even-even nuclei by other authors.[26,27]

The harmonic oscillator wave functions might not be the appropriate nucleon wave functions in the heavy nuclei. The wave functions for potentials similar to the square well will presumably give larger quadrupole moments for heavier nuclei by virtue of the increased matrix element of r^2. In general, our calculated values for odd-neutron nuclei are somewhat larger, those for odd-proton nuclei somewhat smaller, than the observed values. This holds even for closed shell ± one nuclei. It is likely that this discrepancy is due to our assumption concerning the interaction between nucleons. The quadrupole moments due to the excitation of the proton group of odd-neutron and odd-proton nuclei are proportional to $\frac{1}{2}(V_\sigma+3V_t)$ and V_σ, respectively, if a delta-function interaction is assumed. Hence, a better agreement could be obtained by decreasing V_t/V_σ. However, one cannot determine this ratio exactly, although some indications have been obtained from the ground-state spins of odd-odd nuclei.[28]

The treatment by first-order perturbation theory appears justified, at least in most cases. This was shown in the example of S^{32}. However, it should be noted that the estimate of the energy denominators is not sufficiently accurate. The observed level spacing between $J=0$ and $J=2$ states of even-even nuclei decreases to as little as 0.1 Mev in heavy nuclei between the magic numbers. If this is true also for the states of the even groups of odd nuclei, the treatment by perturbation theory will break down. The large quadrupole moments in the rare earth region, which cannot be explained by the present treatment, may be caused by such a mechanism. In order to interpret the large quadrupole moments in this way, it will be necessary to investigate the level spacings given by the model underlying the present article.

It follows from the calculations here presented that the quadrupole moments of odd-neutron nuclei can be explained as resulting from the excitation of the proton group and that the additional quadrupole moments of odd-proton nuclei due to the same cause are rather large. The agreement between the calculated and observed values of the quadrupole moments of odd nuclei is fairly good except for nuclei with very large quadrupole moments.

The authors wish to express their sincere thanks to Professor T. Yamanouchi at University of Tokyo and to Professor E. P. Wigner at Princetion University for their kind interest and valuable discussion. They would like also thank Professor S. Nakamura at University of Tokyo and Professor A. S. Wightman at Princeton University for their continual encouragement. One of the authors (A. Arima) is indebted to the Yomiuri Yukawa Fellowship for the financial aid. The senior author is a Higgins Research Fellow at Princeton University.

[27] A. de-Shalit and M. Goldhaber, Phys. Rev. **92**, 1211 (1953).

[28] C. Schwartz, Phys. Rev. **94**, 95 (1954).

APPENDIX A. DERIVATION OF EQ. (7)

The derivation of (7) is given only briefly since the derivation of a similar equation for magnetic moments has been given before.[8] The methods of Racah[12,29] are employed for the calculation of the various matrix elements.

The matrix element in (4) can be expressed in terms of the double-barred element

$$(j_1^n(0)j^p(j);\,jj|Q_{op}|[j_1^{n-1}(j_1)j_2](2)j^p(j);\,jj)$$
$$=[j(2j-1)/(j+1)(2j+1)(2j+3)]^{\frac{1}{2}}$$
$$\times(j_1^n(0)j^p(j);\,j\|Q_{op}\|[j^{n_1-1}(j_1)j_2](2)j^p(j);\,j).$$

The double-barred element is reduced to that of the single particle by making use of the coefficients of fractional parentage and Racah coefficients:

$$(j_1^n(0)j^p(j);\,j\|Q_{op}\|[j_1^{n-1}(j_1)j_2](2)j^p(j);\,j)$$
$$=[n(2j+1)/5(2j_1+1)]^{\frac{1}{2}}(j_1\|r^2(3\cos^2\theta-1)\|j).$$

One can show in general that

$$(j'\|C^{(k)}\|j)=(-1)^{j-\frac{1}{2}}[(2j+1)(2j'+1)/(2k+1)]^{\frac{1}{2}}$$
$$\times(j'\tfrac{1}{2}\;j-\tfrac{1}{2}|\,j'jk0),$$

where $C_q^{(k)}$ is an unnormalized spherical harmonic: $C_q^{(k)}=[4\pi/(2k+1)]^{\frac{1}{2}}\Theta(kq)\Phi(q)$, and the difference of the orbital angular momenta of j and j' must have the same parity as k. In our case, because of $3\cos^2\theta-1=2C_0^{(2)}$, the double-barred matrix element of the last equation can be given in terms of a Clebsch-Gordan coefficient with $k=2$.

The calculation of the nondiagonal matrix element of the interaction in (6) is somewhat lengthy. The matrix element between many-particle configurations can be expressed in terms of matrix elements for two-particle configurations:

$$(j_1^n(0)j^p(j);\,jm|\sum_{i<k}V_{ik}|[j_1^{n-1}(j_1)j_2](2)j^p(j);\,jm)$$
$$=[(2j+1-2p)/(2j-1)]\times[5n/(2j+1)(2j_1+1)]^{\frac{1}{2}}$$
$$\times\sum_J(2J+1)W(Jjj_22;\,j_1j)(j_1jJ|V|j_2jJ).$$

The summation over J extends herein over the possible angular momenta of the j_1j and j_2j configurations. The matrix elements of the interaction between two-particle configurations can then be obtained in a usual way. The assumption of the delta-function interaction makes the calculation relatively simple and the summation over J can be carried out without difficulty. If the particles in the orbits j and j_1 are both protons, the exclusion principle must be taken into account.

APPENDIX B. DERIVATION OF EQ. (10)

For the wave function (II), the matrix element of the quadrupole moment operator becomes

$$(j_1^n(0)j^p(j);\,jj|Q_{op}|\,j_1^{n-1}(j_1)j^{p+1}(J);\,jj)$$
$$=[2nj(2j-p)(2J+1)/(j+1)(2j+3)(2j_1+1)]^{\frac{1}{2}}$$
$$\times(j_1\|r^2(3\cos^2\theta-1)\|j)\times W(j_1jjj;\,J2).$$

The explicit formulas for the coefficients of fractional parentage were used when deriving this equation. The phase factors are cancelled by the phase factors in the following formula. The nondiagonal energy matrix element for the delta-function interaction is[8]

$$(j_1^n(0)j^p(j);\,jm|\sum_{i<k}V_{ik}|\,j_1^{n-1}(j_1)j^{p+1}(J);\,jm)$$
$$=(-1)^{j+j_1}[2n(2j-p)(2J+1)/(2j-1)$$
$$\times(2j+1)(2j_1+1)]^{\frac{1}{2}}(j_1jJ|V|jjJ).$$

If the energy denominators are replaced by their average value and factored out, the summation with respect to J in (II) can be carried out by means of the property of Racah coefficient and the delta-function character of the interaction:

$$\sum_J(2J+1)W(j_1jjj;\,J2)(j_1jJ|V|jjJ)$$
$$=V_aJ[(2j_1+1)(2j+1)^3]^{\frac{1}{2}}$$
$$\times(j_1-\tfrac{1}{2}\,j\tfrac{1}{2}|\,j_1j20)(j\tfrac{1}{2}j-\tfrac{1}{2}|\,jj20)/20.$$

The J in this formula run over the allowed states of j^{p+1} configuration with seniority two and restricted by $|j_1-j|\leq J\leq j_1+j$. The derivation of (11) is quite similar.

[29] G. Racah, Phys. Rev. **62**, 438 (1942).

Resonant Capture of Protons by Fluorine in the Energy Range 0.5 to 2.2 Mev

S. E. Hunt and K. Firth
Research Laboratory, Associated Electrical Industries Ltd., Aldermaston, Berkshire, England
(Received April 1, 1955)

The energy of a proton beam from a pressurized electrostatic generator was measured absolutely by means of an electrostatic analyzer, and used to irradiate thin targets containing fluorine. The γ-ray yield was observed as a function of proton energy and the energies for resonant proton capture were determined to an accuracy of one part in a thousand in most cases. The width of each resonance at half-maximum yield was also measured.

1. INTRODUCTION

THE γ-ray yield from a F^{19} target irradiated by protons has been observed by several workers previously, using nonabsolute methods of beam energy measurement. An absolute determination of the lowest very strong resonance was made by Herb, Snowden, and Sala,[1] using an electrostatic analyzer, and Ajzenberg and Lauritsen[2] have corrected the values obtained by earlier workers, using this determination as a calibration point. Their values were drawn from several sources, and it seemed possible that experimental errors involved were to some extent cumulative when intermediate standards were used. The values also depend on the linearity of the energy measurements.

It was therefore decided to make a survey of the γ-ray yield in the energy range 0.5 to 2.2 Mev by using an absolute electrostatic analyzer. It was also hoped that the high-energy resolution would enable more accurate determinations to be made of the half-width of the resonance, and that the high target currents available would enable a search to be made for previously undetected weak resonances.

2. BEAM ENERGY MEASUREMENT

The energy of the proton beam from a pressurized electrostatic generator[3] was determined by an absolute electrostatic analyzer of deflecting angle 63.2° which has been described in detail elsewhere.[4] The energy resolution of the instrument was one part in 1200, and the uncertainty in the estimation of the mean proton beam energy is estimated to be about $5/10^4$. The linearity of the voltage scale determined by this instrument has been checked by observing the 874.5-kev resonance using mass 1, mass 2, and mass 3 components of the beam. The signals from the exit-slit jaws of the analyzer were used to stabilize the voltage of the electrostatic generator by controlling the magnitude of an electron beam up the accelerator tube.[5]

The electrostatic analyzer was followed by a magnetic deflector of angle 26.8°, which separated out ions of unwanted mass. The distance between the exit-slit jaws of the electrostatic analyzer and the deflecting magnet was equal to the focal length of the magnet so that a parallel horizontal beam was obtained at the exit of the magnet. This beam was used to irradiate the target.

Currents of up to 25 μa were obtained immediately after the electrostatic analyzer, and proton currents of up to 10 μa were recorded on the target after the magnet. These currents proved to be excessive for much of the present experiment and were reduced by the deliberate misalignment of the analyzer and magnetic deflector.

These high target currents (with high-energy resolution) were due in part to the angle of deflection of the analyzer which focused a parallel incident beam in the plane of the exit slits, and in part to the high speed of the machine voltage stabilizing circuits.

3. EXPERIMENTAL PROCEDURE

The targets were evaporated "*in vacuo*" on to carefully cleaned and polished copper backings. Those most used had a thickness in energy units of 1 kev for a 1-Mev incident proton beam. Some determinations were also made by using targets of thickness 2 and 3 kev. The targets were heated to 200°C during irradiation and a liquid nitrogen trap was installed immediately in front of them to prevent the deposition of carbon. By repeated determinations of one of the strongest and narrowest resonances, it was shown that less than 1 kev of carbon had been deposited on the target surface after twenty hours of irradiation.

The γ-rays were detected by means of a Geiger-Müller counter with a lead radiator placed immediately behind the flange supporting the target. The current falling on the target was fed into a beam current integrator[6] which, in conjunction with a standard timer, was arranged to switch off the scaler recording γ-ray counts when a charge of 10 μcoul had fallen on the targets. Over regions of special interest and for weak resonance observations higher target charges were used (Figs. 2 and 3). For most of the irradiations

[1] Herb, Snowden, and Sala, Phys. Rev. **75**, 246 (1949).
[2] F. Ajzenberg and T. Lauritsen, Revs. Modern Phys. **24**, 321 (1952).
[3] D. R. Chick and D. P. R. Petrie, Proc. Inst. Elec. Engrs. (to be published).
[4] Hunt, Petrie, Firth, and Trott, Proc. Inst. Elec. Engrs. (to be published).
[5] B. Millar and R. Bailey (to be published).
[6] J. L. W. Churchill and W. W. Evans, Electronic Eng. (to be published, 1955).

target currents of between 1 and 5 μa were adequate. Higher currents produced overheating of the target and very high counting rates at the peak of the stronger resonances. The consequent counting losses would have led to errors in the estimation of the half-widths of the resonances.

In general, the beam energy was varied in steps of 2 kev, but in order to estimate the peak and half-widths of narrow resonances, these steps were reduced to 200 ev. Each of the resonances was determined several times, and the determinations quoted are the mean values after correction for target thickness, relativity effects and the small angle of inclination of the incident beam to the normal to the entrance plane of the analyzer. This latter correction was determined by rotating the analyzer through an angle of 180° about a vertical axis and redetermining several of the stronger resonances throughout the energy range.[4]

In order to check that the resonances were due to fluorine they were observed on both calcium fluoride and lithium fluoride targets, and an additional irradiation was made of a clean copper backing. Radiation from the copper backing became detectable at about 1 Mev and increased to 5000 counts/10 μcoul at 2.2 Mev. This background is shown in Fig. 1 and has been subtracted from the resonance curves.

The background of the Geiger-Müller counter due to cosmic radiation and x-radiation from the machine was determined by intercepting the beam some distance from the target. This proved to be negligible compared with the true counting rate for all machine energies up to 2.2 Mev.

4. RESULTS

The resonances observed are shown in Fig. 1. To show the weaker resonances clearly, additional plots have been made on which the vertical scale is divided by the factor indicated, and to accommodate four of the stronger resonances the vertical scale has been multiplied by a factor of two.

The mean resonance determination and half-width measurements are shown in Table I; the values of

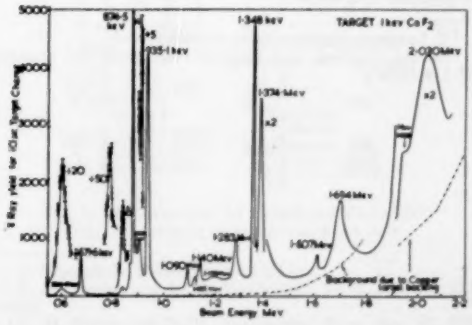

FIG. 1. γ-ray yield curve for the $F^{19}+p$ reaction (10-μcoul target charge).

TABLE I. Resonant energies and half-widths.

Values listed by Ajzenberg and Lauritsen				Values in present work	
Resonant energy kev	Half-width kev	Observer	Method of energy measurement	Resonant energy kev	Half-width kev
224.2	1.0	Hunt and Jones	Absolute electrostatic analyzer		
340.4	2.8	Hunt	Absolute electrostatic analyzer		
483.1	2.2	Hunt	Absolute electrostatic analyzer		
598	37	Bonner and Evans[a]	Magnetic analyzer	596.8 ±1.0	30.0± 3
669	7.5	Bonner and Evans[a]	Magnetic analyzer	671.6 ±0.7	6.0± 0.7
				780.3 ±0.8	7.6± 1.0
831	8.3	Bonner and Evans	Magnetic analyzer	834.8 ±0.9	6.5± 1.0
873.5	5.2	Herb *et al.*	Absolute electrostatic analyzer	874.5 ±0.9	5.4± 0.3
900	4.8	Chao *et al.*	Electrostatic analyzer	902.3 ±0.9	5.1± 1.0
935.3	8.0	Chao *et al.*	Electrostatic analyzer	935.1 ±0.9	8.6± 0.5
1092	<1.2	Bonner and Evans	Magnetic analyzer	1090 ±1.0	0.7± 0.3
				1123 ±2.0	22 ± 5
1137	4.1	Bonner and Evans	Magnetic analyzer	1140 ±1.0	2.5± 5
1176	~130	Bonner and Evans	Magnetic analyzer	1189 ±7.0	110±20
1290	19.2	Chao *et al.*	Electrostatic analyzer	1283 ±1.4	18.6± 1.0
1355	8.6	Chao *et al.*	Electrostatic analyzer	1348 ±1.3	5.6± 0.5
1381	15.0	Chao *et al.*	Electrostatic analyzer	1375 ±1.4	11.0± 1.0
				1607 ±1.6	6.0± 1.0
1690	30.0	Willard *et al.*	Magnetic analyzer	1694 ±1.7	35.0± 3.0
1940	15	Willard *et al.*	Magnetic analyzer	1949 ±2.5	40 ±10
2030	60	Willard *et al.*	Magnetic analyzer	2030 ±3.0	120±20

[a] All values obtained by Bonner and Evans were multiplied by 873.5/862 in order to agree with Herb's absolute determination.

Ajzenberg and Lauritsen are also shown for comparison. For completeness, three resonances in the lower-energy scale measured at this laboratory using a smaller generator and absolute analyzer are included. Resonances observed at 780.3 kev and 1.607 Mev are shown separately on Fig. 2. The yield in the energy range 1 Mev to 1.35 Mev appeared to be of particular interest and has been shown separately in Fig. 3.

The standard deviations of several determinations of each of the resonances were less than five parts in 10^4 of the mean values, except for the very broad peaks. These variations are produced by random errors, one of which is the uncertainty in determining the peak from an observed resonance curve. This uncertainty is proportional to the half-widths of the resonances and inversely proportional to the yield, and becomes the

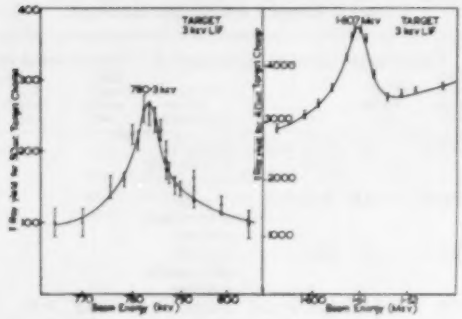

FIG. 2. The 780.3-kev and 1.607-Mev resonances.

main source of error for extremely broad resonances such as that at 1.189 Mev.

The errors quoted in Table I were obtained by adding the standard deviation of the results obtained to the estimated systematic errors in the measurements of the beam energy.[4]

5. DISCUSSION OF RESULTS

On irradiating fluorine with protons, γ rays are produced by three processes, $F^{19}(p,\alpha\gamma)O^{16}$, $F^{19}(p,p'\gamma)F^{19}$ and $F^{19}(p,\gamma)Ne^{20}$. No attempt was made in this work to distinguish between the γ rays from each of these reactions.

The present absolute determination of the lowest strong resonance at 874.5 ± 0.9 kev is in good agreement with Herb's value of 873.5 ± 0.9 kev. Except for the 1.189-Mev resonance, for which uncertainties are large because of the large half-width, the agreement with values based on the determinations of Bonner and Evans is in general better than three parts in a thousand.

Our determinations are about five parts in a thousand lower than those obtained by Chao *et al.* for the higher resonances, but the agreement is better in the lower voltage range.

Comparison with the results of Willard *et al.* is only possible over a limited energy range, but the discrepancy is not greater than the limits of accuracy to which Willard quotes his results. Our estimates of the half-width of the two higher resonances, however, are appreciably greater than those of Willard. They were made by fitting two Breit-Wigner curves to the observed yield curve, the errors are comparatively large because of uncertainty in estimating the contribution from higher resonances.

Resonances at 780.3 and 1607 kev were not observed by earlier workers, but were observed independently by Barnes[7] in the $F^{19}(p,p'\gamma)F^{19}$ reaction while the present work was in progress.

A resonance at about 1120 kev has previously been observed by Devons *et al.*[8] for the emission of electron-positron pairs from the 6.06-Mev excited state of O^{16} formed by the $F^{19}(p,\alpha)O^{16*}$ reaction. Annihilation radiation from these pairs may account for the resonance

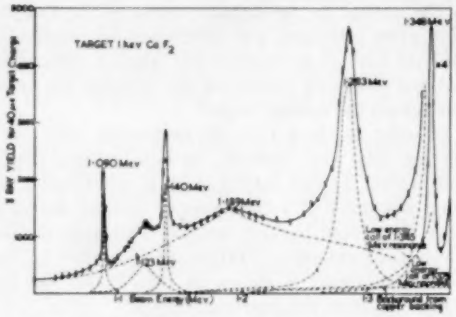

FIG. 3. γ-ray yield curve between 1 Mev and 1.3 Mev (40-μcoul target charge).

peak in the present measurements, Devons also observed a slight pair peak at about 780 kev.

ACKNOWLEDGMENTS

The authors would like to thank their colleagues for many helpful suggestions and in particular D. R. Chick and D. P. R. Petrie who suggested the program of research and made initial calculations on the design of the analyzer, and Professor J. Rotblat with whom the results have been discussed. We should also like to thank Mr. F. Verdaguer who worked with us during part of the time in which these results were obtained.

Thanks are also due Dr. T. E. Allibone for permission to publish this work.

[7] T. Lauritsen (private communication).
[8] Devons, Goldring, and Lindsey, Proc. Phys. Soc. (London) **67**, 134 (1954).

Quadrupole Moments of Ta^{181} and Lu^{175}

TOHRU KAMEI
Institute of Science and Technology, Komaba-machi, Meguro-ku, Tokyo, Japan
(Received April 15, 1955)

The hyperfine structure of the spectrum of Ta I was studied by means of a hollow-cathode discharge tube and a Fabry-Pérot étalon, in order to determine the quadrupole moment of Ta^{181}. The calculation was carried out for the quadrupole coupling constants of the levels $^4F_{3/2}$, $^4P_{3/2}$, $^4F_{5/2}$, $^4F_{7/2}$ and $^4F_{9/2}$ of the configuration $5d^3\,6s^2$, in which the three $5d$-electrons are combined by an intermediate coupling. This yielded the result that $Q(Ta^{181}) = (+4.3\pm0.4)\times10^{-24}$ cm^2, in which the polarization correction (due to Sternheimer) is taken into account. The value of $Q(Lu^{175})$ was calculated from the data given in the literature, and was found to be $(+5.7\pm0.3)\times10^{-24}$ cm^2.

I. INTRODUCTION

THE quadrupole moment (Q) of Ta^{181} was estimated by Schmidt[1] from the hyperfine structure (hfs) of some Ta I lines. The values of Q obtained from various levels were, however, not so consistent. Brown and Tomboulian[2] tried to determine $Q(Ta^{181})$ by studying the hfs of some Ta II lines. However, it subsequently turned out that the level from which they deduced the value of Q was perturbed and therefore their Q had to be withdrawn.[3]

In the present work, the hfs of the spectrum of Ta I was measured more accurately than in the previous work and the value of Q was calculated with wave functions that are more accurate than those of Schmidt.[1]

II. EXPERIMENTAL PROCEDURE

A hollow-cathode discharge tube was used as a light source and a Fabry-Pérot étalon was used in order to resolve the hfs.

Schmidt[1] determined the hfs of the ground level $^4F_{3/2}$ from the line λ4280. This line is, however, weak and has strong neighboring lines which disturb the measurement. In the present work, the hfs of the same level was deduced from the strong green line λ5403 that can be measured easily.

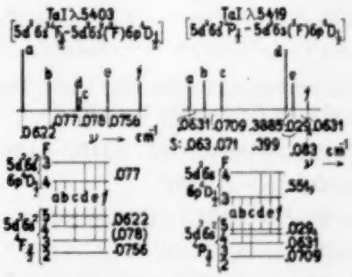

FIG. 1. Hfs of the lines Ta I λ5403 and Ta I λ5419. The measurement of Schmidt is shown as S.

[1] T. Schmidt, Z. Physik **121**, 63 (1943).
[2] B. M. Brown and D. H. Tomboulian, Phys. Rev. **88**, 1158 (1952).
[3] B. M. Brown and D. H. Tomboulian, Phys. Rev. **91**, 1580 (1953).

III. RESULTS

The observed hfs is shown schematically in Figs. 1–4. From the measured hfs the interval factors A and the quadrupole coupling constants B of the final levels were deduced as shown in Table I. The nuclear spin of Ta^{181} is known to be 7/2.[4–6] The value of Q can be calculated by the fundamental formula

$$Q=-B\frac{Z^*H}{\zeta\sum\langle 3\cos^2\theta-1\rangle_{\omega}}I(2I-1)J(2J-1)\times(1+\Delta)1.988\times10^{-21}\ \text{cm}^2,$$

in which the symbols have their usual meanings. Δ is the polarization correction factor introduced by Sternheimer.[7] We will put $\omega=3\cos^2\theta-1$ for brevity.

Published term tables[8] of Ta I show that the configuration $5d^3\,6s^2$ is not of LS-coupling.[9] In order to calculate $\sum\tilde{\omega}$, we have to express the intermediate coupling wave function in terms of LS-coupling wave functions. For that purpose, we need the solution of

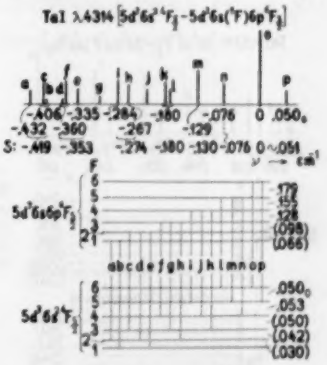

FIG. 2. Hfs of the line Ta I λ4314. The measurement of Schmidt is shown as S.

[4] J. H. Gisolf and P. O. Zeeman, Nature **132**, 566 (1933).
[5] N. S. Grace and E. McMillan, Phys. Rev. **44**, 949 (1933).
[6] J. H. Gisolf, dissertation, University of Amsterdam, 1935 (unpublished).
[7] R. M. Sternheimer, Phys. Rev. **80**, 102 (1950); **84**, 244 (1951); **86**, 316 (1952).
[8] Van den Berg, Klinkenberg, and Van den Bosch, Physica **16**, 861 (1950); **18**, 221 (1952).
[9] This fact was also pointed out by R. E. Trees, Phys. Rev. **92**, 308 (1953).

TABLE I. The hfs constants A and B of the configuration $5d^3\,6s^3$ and the values of $Q(Ta^{181})$ derived from each B.

		$^4P_{5/2}$	$^4F_{3/2}$	$^4F_{5/2}$	$^4F_{7/2}$	$^4F_{9/2}$
$A(10^{-3}\ cm^{-1})$	K[a]	12.49	17.23	10.8	9.2_2	8.79
	S[b]	12.4	16.7	10.4	···	8.6
$B(10^{-3}\ cm^{-1})$	K[a]	−0.279	−0.199	-0.05_2	−0.030	-0.013_5
	S[b]	−0.28	−0.20	−0.06	···	−0.01
$Q(10^{-24}\ cm^2)$	K[a]	+4.4 ±0.4	+4.2 ±0.4	+4.4 ±0.8	+5.0 ±1.0	+4.0 ±1.0

[a] Our measurement.
[b] Schmidt's measurement, see reference 1.

the energy matrix of $5d^3$. The energy matrix of d^3 in LS-coupling published by Marvin[10] was used. The parameter ζ, F_2 and F_4 were determined so that the solutions fit the observed positions of the levels[8] as accurately as possible (least squares method), and the following values were obtained: $\zeta=1650$, $F_2=578$ and $F_4=60$.

A wave function in intermediate coupling will be denoted with a prime. Putting the above-mentioned values of ζ, F_2, and F_4 in the energy matrix of d^3 and using the usual procedure, we get

$$^4F_{3/2}'=K_1\,^4F_{3/2}+K_2\,^2D_{3/2}{}^a+K_3\,^2D_{3/2}{}^b+K_4\,^4P_{3/2}+K_5\,^2P_{3/2},$$
$$K_1=0.9561,\quad K_2=0.1576,\quad K_3=-0.2272,\quad K_4=0.05398,\quad K_5=0.08103.$$

$$^4P_{3/2}'=K_1\,^4F_{3/2}+K_2\,^2D_{3/2}{}^a+K_3\,^2D_{3/2}{}^b+K_4\,^4P_{3/2}+K_5\,^2P_{3/2},$$
$$K_1=-0.1479,\quad K_2=0.1242,\quad K_3=-0.1710,\quad K_4=0.8516,\quad K_5=0.4563.$$

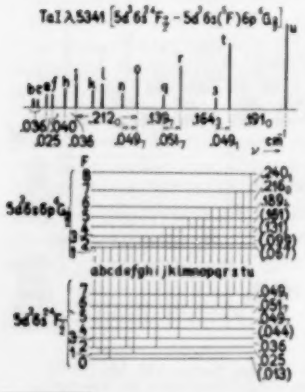

FIG. 3. Hfs of the line Ta I λ5341. The components k and l were masked by the line Ne I λ5341 and could not be measured.

$$^4F_{5/2}'=K_1\,^4F_{5/2}+K_2\,^2F_{5/2}+K_3\,^2D_{5/2}{}^a+K_4\,^2D_{5/2}{}^b+K_5\,^4P_{5/2},$$
$$K_1=0.9848,\quad K_2=0.04646,\quad K_3=0.07904,\quad K_4=-0.1450,\quad K_5=0.02751.$$

$$^4F_{7/2}'=K_1\,^2G_{7/2}+K_2\,^4F_{7/2}+K_3\,^2F_{7/2},$$
$$K_1=-0.2175,\quad K_2=0.9705,\quad K_3=0.1025.$$

$$^4F_{9/2}'=K_1\,^2H_{9/2}+K_2\,^2G_{9/2}+K_3\,^4F_{9/2},$$
$$K_1=0.1637,\quad K_2=-0.3956,\quad K_3=0.9038.$$

$\sum\tilde{\omega}$ can be calculated by using the wave functions in the M_SM_L-scheme and the fundamental formulas for d-electrons that were given by Schmidt[1] and corrected

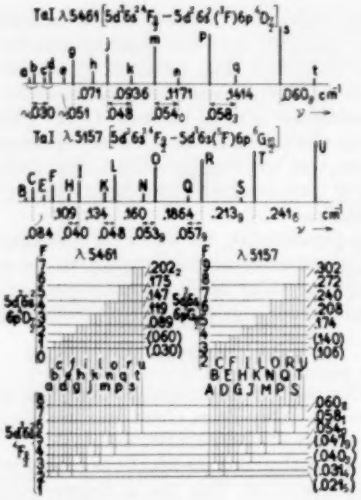

FIG. 4. Hfs of the lines Ta I λ5461 and Ta I λ5157.

by Murakawa.[11] Then we have

$$(^4F_{3/2}'|\omega|^4F_{3/2}')=K_1^2(^4F_{3/2}|\omega|^4F_{3/2})+K_2^2(^2D_{3/2}{}^a|\omega|^2D_{3/2}{}^a)+\cdots+K_5^2(^2P_{3/2}|\omega|^2P_{3/2})+2K_1K_2(^4F_{3/2}|\omega|^2D_{3/2}{}^a)+\cdots+2K_4K_5(^2P_{3/2}|\omega|^4P_{3/2}),$$

and similar expressions for the other levels. The matrix elements of ω for LS-coupling levels for $J=3/2$ are[12,13]

$$(^4F_{3/2}|\omega|^4F_{3/2})=(8/875)(13R_2'+14R_2''-12S_2),$$
$$(^2D_{3/2}{}^a|\omega|^2D_{3/2}{}^a)=-(1/5)R_2'',$$
$$(^2D_{3/2}{}^b|\omega|^2D_{3/2}{}^b)=(1/875)(-112R_2'+133R_2''-96S_2),$$
$$(^4P_{3/2}|\omega|^4P_{3/2})=(8/375)(4R_2'+5R_2''+6S_2),$$
$$(^2P_{3/2}|\omega|^2P_{3/2})=(4/525)(-4R_2'+7R_2''+12S_2),$$
$$(^4F_{3/2}|\omega|^2D_{3/2}{}^a)=(210)^{\frac{1}{2}}(2/875)(-4R_2'+7R_2''-3S_2),$$

[10] H. H. Marvin, Phys. Rev. 47, 521 (1935). G. J. van den Berg [dissertation, University of Amsterdam, 1951 (unpublished)] modified the energy matrix given by Marvin, but this modification is apparently incorrect, owing to his misinterpretation of the article of G. Racah [Phys. Rev. 63, 367 (1943)]. The table of the composition of the states of Ta I $5d^3\,6s^3$ given in reference 8 is based on Van den Berg's calculation, and is, therefore, invalid. Marvin's a is our ζ.

[11] K. Murakawa, J. Phys. Soc. (Japan) 9, 391 (1954).
[12] The expression for $(^4F_{3/2}|\omega|^4F_{3/2})$ was published by Schmidt (reference 1).
[13] The wave function for $d^3\,^4P_{3/2}$ published by Schmidt is erroneous, and therefore his $(^4P_{3/2}|\omega|^4P_{3/2})$ is invalid.

$$(^4F_{3/2}|\omega|^2D_{3/2}{}^b)=(10)^{\frac{1}{2}}(2/625)(4R_2'-R_2''-3S_2),$$
$$(^4F_{3/2}|\omega|^4P_{3/2})=(21)^{\frac{1}{2}}(8/2625)(6R_2'+7R_2''+2S_2),$$
$$(^4F_{3/2}|\omega|^2P_{3/2})=(15)^{\frac{1}{2}}(16/13125)\times(-3R_2'+7R_2''-4S_2),$$
$$(^2D_{3/2}{}^a|\omega|^2D_{3/2}{}^b)=(21)^{\frac{1}{2}}(1/175)(-8R_2'-7R_2''),$$
$$(^2D_{3/2}{}^a|\omega|^4P_{3/2})=(10)^{\frac{1}{2}}(4/125)(-2R_2'+R_2''+S_2),$$
$$(^2D_{3/2}{}^a|\omega|^2P_{3/2})=(14)^{\frac{1}{2}}(1/175)(4R_2'+7R_2''+4S_2),$$
$$(^2D_{3/2}{}^b|\omega|^4P_{3/2})=(210)^{\frac{1}{2}}(2/18375)\times(-12R_2'+35R_2''-23S_2),$$
$$(^2D_{3/2}{}^b|\omega|^2P_{3/2})=(6)^{\frac{1}{2}}(1/2625)(84R_2'-91R_2''-68S_2),$$
$$(^4P_{3/2}|\omega|^2P_{3/2})=(35)^{\frac{1}{2}}(4/1875)(4R_2'-R_2''-3S_2).$$

R_2', R_2'' and S_2 are the relativity correction factors for d-electrons given by Casimir.[14] The matrix elements of ω for other levels can be calculated similarly.

The numerical value of Q was calculated, putting[15] $R_2'=1.05$, $R_2''=1.17$, $H=1.02$, $\zeta_d=1650$, $Z_d^*=73-20=53$, and $\Delta=0.103$.[7] The value of Q calculated in this way for each value of B is shown in Table I.

In Table I, the values of B for the levels $^4F_{3/2}$ and $^4P_{3/2}$ have the greatest accuracy and therefore the values of Q deduced from these levels have the greatest accuracy.

In the above calculation, it was assumed that the effect of the perturbation of the configuration $5d^3\,6s^2$ by $5d^4\,6s$ is negligible. The error caused by neglecting this effect was estimated to be about one percent.

The weighted mean value of $Q(Ta^{181})$ is

$$Q=(+4.3\pm0.4)\times10^{-24}\text{ cm}^2.$$

Schmidt[1] obtained $Q\approx6\times10^{-24}$ cm^2 without the polarization correction.

Huus and Zupančič[16] obtained the intrinsic quadrupole moment[17] $Q_0(Ta^{181})\approx7\times10^{-24}$ cm^2 from the Coulomb excitation experiment for tantalum. If we assume a strong coupling between the unbalanced nucleon and the nuclear surface, our spectroscopic quadrupole moment yields (according to the formula given by Bohr[17]): $Q_0(Ta^{181})=9\times10^{-24}$ cm^2. This value is in good agreement with that obtained by the aforementioned Coulomb excitation experiment.

IV. QUADRUPOLE MOMENT OF Lu^{175}

Gollnow[18] studied the hfs of Lu I lines and deduced $A=+4.62\times10^{-3}$ cm^{-1}, $B=+0.114\times10^{-3}$ cm^{-1} for the level $5d\,6s^2\,{}^2D_{3/2}$ of the isotope Lu^{175} ($I=7/2$). He assumed that the screening correction for the d-electron is 11 ($Z_d^*=71-11=60$), and got $Q(Lu^{175})=+5.98\times10^{-24}$ cm^2 without the polarization correction. In the present work we use a more accurate value[15] $Z_d^*=71-20=51$, and take into account the polarization correction ($\Delta=0.107$), and get

$$Q(Lu^{175})=+5.7\times10^{-24}\text{ cm}^2,$$

which is probably accurate to 5 percent. This is definitely larger than $Q(Ta^{181})$.

ACKNOWLEDGMENTS

The author wishes to express his sincere thanks to Professor Murakawa for his kind guidance and encouragement throughout this work.

[14] H. B. G. Casimir, Verhandel. Teylers Tweede Genootschap, Haarlem, 1936.

[15] The screening correction was calculated by the method of K. Murakawa [Phys. Rev. **98**, 1285 (1955)].

[16] T. Huus and C. Zupančič, Kgl. Danske Videnskab. Selskab, Mat.-fys. Medd. **28**, No. 1 (1953).

[17] A. Bohr, Phys. Rev. **81**, 134 (1951); A. Bohr and B. R. Mottelson, Kgl. Danske Videnskab. Selskab, Mat.-fys. Medd. **27**, No. 16 (1953).

[18] H. Gollnow, Z. Physik **103**, 443 (1936).

Independent Particle Model of the Nucleus. I. Interparticle Forces and Configuration Mixing*

CARL LEVINSON AND KENNETH W. FORD†
Indiana University, Bloomington, Indiana
(Received March 7, 1955)

A simplified method of obtaining the direct interaction between two identical nucleons in the nuclear shell model is given for the special case of singlet forces. Configuration interaction is included in the method. A semi-empirical analysis of simple two and three particle nuclear spectra is outlined which enables one to determine properties of the two-body perturbing interaction provided many body forces are negligible and coupling to the nuclear surface is weak. Corrections to the singlet force formalism due to triplet central and tensor forces are discussed. Formulas are given for magnetic dipole and quadrupole moments and magnetic dipole transition rates for mixed three-particle configurations. The effect of weak surface coupling on multi-particle configuration is given in paper II of this series. A detailed discussion of the spectra of two isotopes of calcium is given in paper III.

I. INTRODUCTION

ACCORDING to the simplest picture of the nuclear shell model, nucleons move independently within the nucleus subject only to the force of a common central potential and to a spin-orbit force.[1] When the degeneracies of this idealized model have been removed by an assumed "pairing energy,"[2] then the model has surprisingly great success in affording a qualitative explanation for most of the low-energy properties of nuclei[3] (with some notable exceptions associated with collective nuclear motion).[4] This qualitative success has led to efforts to refine the shell model to the point where it may yield quantitative agreement with experiment. This refinement has at first taken the form of adding to the independent particle Hamiltonian a direct two-body interaction among the nucleons outside of closed shells. Kurath,[5] Talmi,[6] Flowers and Edmonds,[7] and Pryce[8] have studied the effects of various assumed forms of this perturbing interaction on the energy levels of two-, three-, and four-particle configurations. Although configuration interaction was neglected in their work, the predicted level ordering was in accord with experiment where comparison could be made.

As one might expect from the strength of the nuclear forces, the inclusion of perturbing inter-particle forces in the shell model leads to the prediction that configuration interaction is of substantial importance. de-Shalit and Goldhaber[9] have emphasized some important consequences of configuration interaction, and Redlich[10] has shown that a mixture of configurations considerably improves the calculated ft value of the transition $F^{18}(\beta^+)O^{18}$, as compared to any single configuration calculation. Among the many efforts to explain the deviations of nuclear magnetic moments from the Schmidt lines, one of the simplest and most unforced is embodied in the work of Blin-Stoyle and Perks,[11] who find that the direction and order of magnitude of the deviations can be accounted for in terms of simple interconfigurational mixing. Collective effects may also play an important role in the magnetic moment deviations,[4] but a general survey of this question[12] has led to the conclusion that in addition to surface effects, there must be another and at least as large an effect producing an inward deviation of the moments from the Schmidt lines. This extra effect was first interpreted in terms of a quenching of the anomalous moment of the nucleon, but now appears to be more reasonably attributed to the Blin-Stoyle and Perks effect of configuration mixing. Other recent attempts have been made to take into account both collective and configuration mixing effects[4,13] on nuclear magnetic moments. More recently Elliott and Flowers[14] have had detailed quantitative success in the analysis of simple configurations just beyond the O^{16} core, using a Rosenfeld exchange type force and including configuration interaction. Volkov[15] has carried out calculations with the "statistical shell model" based on very great configuration mixing, but this limit does not appear to be justified by more detailed shell-model calculations.

A detailed treatment of two-body interactions among nucleons outside of closed shells need not, of course,

* Supported in part by a grant from the National Science Foundation.

† The authors wish to acknowledge the hospitality of the Brookhaven National Laboratory where one of us (C.L.) spent the summer of 1954 as a visiting scientist.

[1] M. G. Mayer, Phys. Rev. **75**, 1969 (1949); **78**, 16 (1950); Haxel, Jensen, and Suess, Phys. Rev. **75**, 1766 (1949).

[2] M. G. Mayer, Phys. Rev. **78**, 22 (1950); G. Racah and I. Talmi, Phys. Rev. **89**, 913 (1953).

[3] M. H. L. Pryce, Repts. Progr. Phys. **17**, 7 (1954); M. G. Mayer, Proceedings of the International Conference on Theoretical Physics Kyoto and Tokyo, September, 1953 (unpublished).

[4] A. Bohr and B. Mottelson, Kgl. Danske Videnskab. Selskab, Mat.-fys. Medd. **27**, No. 16 (1953).

[5] Dieter Kurath, Phys. Rev. **91**, 1430 (1953).

[6] I. Talmi, Helv. Phys. Acta **25**, 185 (1952).

[7] B. H. Flowers, Proc. Roy. Soc. (London) **A212**, 248 (1952). A. R. Edmonds and B. H. Flowers, Proc. Roy. Soc. (London) **A214**, 515 (1952); **A215**, 120 (1952).

[8] M. H. L. Pryce, Proc. Phys. Soc. (London) **A65**, 773 (1952).

[9] A. de-Shalit and M. Goldhaber, Phys. Rev. **92**, 1211 (1953).

[10] Martin G. Redlich, Phys. Rev. **95**, 448 (1954).

[11] R. J. Blin-Stoyle and M. A. Perks, Proc. Phys. Soc. (London) **A67**, 885 (1954).

[12] K. W. Ford, Phys. Rev. **92**, 1094 (1953).

[13] J. G. Brennan and A. B. Volkov, Phys. Rev. **97**, 1380 (1955).

[14] J. P. Elliott and B. H. Flowers (to be published).

[15] A. B. Volkov, Phys. Rev. **94**, 1664 (1954).

lead to a quantitatively correct nuclear model. Either many-body forces or collective nuclear motions, for example, could require large corrections. Indeed the comprehensive work of Bohr and Mottelson[4] and others[16] has shown that at least in certain regions of the periodic table, coupling of nucleons to the nuclear surface and the contribution of the nuclear core to the motion are of dominant importance. These collective effects can be taken account of, however, as a further refinement of the shell model, and indeed the form of the particle-to-surface interaction used by Bohr[17] depends essentially on the zero-order assumption of independent particle motion in the nucleus.

Possible many-body forces cannot be taken into account with equal ease, but the "pair damping" postulated by Drell and Henley,[18] and Brueckner and Watson,[19] in the pseudoscalar meson theory would tend to make many-body forces in the nucleus much less important than two-body forces. At the present stage of understanding of the nuclear forces, however, the role of many-body forces in determining low-energy nuclear properties must be deduced primarily from the indirect evidence of the validity of calculations which ignore such forces. The work of Brueckner, Levinson, and Mahmoud[20] on nuclear saturation with two-body forces, for example, provides indirect evidence of this kind. The shell model calculations of Elliott and Flowers[14] and our calculations on the isotopes of calcium (paper III of this series[21]) further strengthen the conclusion that many-body forces are not of much importance for the low-energy properties of nuclei.

The theoretical[22] and experimental evidence accumulated to date favors the idea that the independent-particle model is a good starting point for any attempted quantitative theory of nuclei in the ground state and low excited states. The work reported in this and the succeeding two papers was motivated by a desire to see to what extent the independent particle model, modified by spin-orbit coupling, by direct interparticle coupling, and by particle-to-surface coupling, could be made to yield quantitative results. These three added interactions have previously been shown separately to be necessary in special cases. Altogether, the model to be tested is represented by the Hamiltonian

$$H=H_p+\sum_{i>j} V_{ij}(p)+H_s(\alpha)+\sum_i V_i(s),$$

in which H_p represents the average central field together with a one-body spin-orbit coupling, $V_{ij}(p)$ represents the direct two-body interactions among particles outside closed shells, $H_s(\alpha)$ represents the energy of collective motion (restricted in practice to the five degrees of freedom of ellipsoidal deformations), and $V_i(s)$ represents the particle-to-surface interaction derived from the linear dependence of particle kinetic energy on the deformation of the average potential well.

The primary interest in this work was divided between the nature of the interparticle forces themselves within condensed nuclear matter and the general validity of the independent-particle model as a basis for quantitative calculations.

Some important questions that naturally arise are:

(1) To what extent can interparticle forces in nuclear matter be treated as two-body forces?

(2) What is the relative importance of surface corrections and interparticle force corrections to the independent-particle model states?

(3) What is the magnitude of the energy shifts due to configuration interaction?

(4) Are the "interparticle forces" that act between particles in a nucleus equivalent to the nuclear force between two nucleons in a vacuum?

In this paper (I), a general discussion is presented of the shell-model assumptions and the nature of the particle and core forces neglecting the surface forces. In paper II,[23] there is included a discussion of weak surface coupling and idealized calculations of the effect of one and two excited phonons on two- and three-particle configurations. In paper III,[21] the techniques developed in the previous papers are applied to the energy levels of Ca^{42} and Ca^{43} and to the magnetic moment of Ca^{43}. On the basis of this limited calculation one can give tentative answers to the above-listed questions.

In this paper, we discuss properties of the shell model modified by direct two-body forces only. Previous applications of such a model have utilized specific assumptions about the two-body forces which in general do not accord with current ideas about the nature of the nuclear force as deduced from theory[24,19] or from nucleon-nucleon scattering experiments.[25] In any case, the question whether the forces in the nucleus are the same as those in the "vacuum" is not answered for certain. Consequently we emphasize a semiempirical approach in which very few details of the nuclear forces are assumed. But the model discussed in this paper does assume the following: (a) A double closed-shell nucleus, or nuclear core, may be replaced by a one-particle potential well plus spin-orbit coupling. The levels in this well are determined empirically by the nucleus containing only one nucleon beyond the closed-shell core. (b) Extra-core nucleons moving in this well interact with each other via two-body forces. (c) These

[16] D. L. Hill and J. A. Wheeler, Phys. Rev. **89**, 1102 (1953).
[17] A. Bohr, Kgl. Danske Videnskab. Selskab, Mat.-fys. Medd. **26**, No. 14 (1954).
[18] S. D. Drell and E. M. Henley, Phys. Rev. **88**, 1053 (1952).
[19] K. A. Brueckner and K. M. Watson, Phys. Rev. **92**, 1023 (1953).
[20] Brueckner, Levinson, and Mahmoud, Phys. Rev. **95**, 217 (1954).
[21] C. A. Levinson and K. W. Ford (to be published).
[22] Brueckner, Eden, and Francis, Phys. Rev. (to be published).
[23] K. W. Ford and C. A. Levinson (to be published).
[24] M. M. Levy, Phys. Rev. **88**, 725 (1952); Abraham Klein, Phys. Rev. **91**, 740 (1953); **92**, 1017 (1953).
[25] See references 35, 36, and 37.

interactions mix configurations as well as split configurations, and this mixing must be taken into account. (d) For configurations of identical particles (all neutrons or all protons) the forces are predominantly singlet. This assumption can be tested since the nucleon-nucleon interaction is sufficiently well known from analysis of scattering experiments at the energies important in a nucleus. Of course, in applying such a test one must verify that question four has an affirmative answer.

The calculation of the matrix elements of the interparticle interaction is considerably simplified if one uses methods developed by Bacher and Goudsmit,[26] Racah,[27] and others. It can be shown that the matrix elements involving n particles can be computed from those involving $n-1$ particles, where $n \geqslant 3$. Therefore, the main physical problem is the determination of the two-particle matrix elements. If the two particles are both neutrons or protons, then two simplifying features enter the calculation: (1) the forces are approximately singlet, and (2) the Pauli principle restricts the number of possible states. In order to treat the effect of various two-particle configurations of identical particles, the Schrödinger equation is algebraically manipulated so that the calculation can be done simply. This avoids the more clumsy matrix approach, and makes it possible to determine the matrix elements of the interaction from the empirical two-particle level structure including the effects of configuration interaction.

The three-particle problem is then set up as a matrix diagonalization problem, the matrix elements being derived from the two-particle elements. Hence the three-particle energy levels and wave functions are logically tied to the two-particle matrix elements. This enables one to make an empirical analysis of a two-particle configuration, and then make predictions for the three-particle problem. In this manner, one does not have to know the exact nature of the interparticle forces in order to test the model under consideration. If the model can be verified in this way, one can then test various possible interparticle potentials to see if they give the correct matrix elements. The theory in the present paper is therefore directly applicable only to special configurations of identical particles, and is not explicitly carried beyond the point required for the applications discussed in paper III.[21]

II. HAMILTONIAN WITH PARTICLE FORCES

To zero order one assumes that the particles move independently in the potential of the double closed-shell core in states given by the independent-particle model. The "particle" can in fact be a neutron, a proton, a neutron hole, or a proton hole. The levels of these particles are given by the core-plus-one-particle nuclei. The nuclei are listed in Table I, and are not very numerous. Without experimental data on these nuclei one cannot analyze in a completely empirical way the effects of configuration interaction, since these nuclei give the relative spacing of the various configurations. It is possible, of course, to make reasonable guesses in some cases of the zero-order level spacings. Also it should be mentioned that there may exist closed subshells which to a fair approximation may be incorporated in the cores. For example, Zr^{90} with 40 protons and 50 neutrons shows some of the properties of a double closed-shell nucleus.

The zero-order assumption certainly is not rigorously true. For instance, as pointed out by Blin-Stoyle and Perks,[11] the explanation of the deviation of the magnetic moment of Bi^{209} from the Schmidt value ($\Delta\mu = 1.4$ n.m.) is that the odd proton is not in a pure $h_{9/2}$ state, but other configurations involving the $h_{11/2}$ protons in the core are admixed. This effect should be most significant when there are orbital states in the core identical to orbital states of the extra core particles, i.e., when the core is "j–j magic" but not "L–S magic." Single-particle levels in the core field are not quite the pure single-particle states predicted by the independent-particle model. This effect of admixed states of core excitation is not ruled out even for L–S magic nuclei, but if its effect on the one-particle energy spacing is small, then its effect on the two- and three-particle analysis will be small, independent of its effect on the one-particle wave function.

The coherent nuclear model[20,22] has provided a theoretical justification for the concept of the effective core field. Calculations of this average potential are now being performed.

Interparticle Forces

There are two fundamental difficulties concerned with the choice of the two-body forces acting between the particles moving in the core field. (1) It is uncertain how much these forces within the nucleus differ from the vacuum nuclear forces. Some difference is predicted by the coherent nuclear model,[22] but details about the difference are still under study. (2) If the effective forces within nucleus possess repulsive cores as indicated by theory[19,24] and experiment[25] for free nucleons, then perturbation theory with independent particle wave functions is not appropriate. The first difficulty we avoid by not specifying the forces in advance, but letting matrix elements of the interaction potential appear as parameters in the theory. Only through the simplifying assumption of singlet forces between iden-

TABLE I. Double magic cores and single-particle or single-hole configuration nuclei.

	Particle	Hole	Particle	Hole	Particle	Hole	Particle	Hole
Proton	$_9F^{17}$	$_7N^{13}$	$_{21}Sc^{41}$	$_{19}K^{39}$	$_{21}Sc^{49}$	$_{19}K^{47}$	$_{81}Bi^{209}$	$_{81}Tl^{207}$
Neutron	$_8O^{17}$	$_8O^{13}$	$_{21}Ca^{41}$	$_{20}Ca^{39}$	$_{20}Ca^{49}$	$_{20}Ca^{47}$	$_{81}Pb^{209}$	$_{81}Pb^{207}$
Cores	$_8O^{16}$		$_{20}Ca^{40}$		$_{20}Ca^{48}$		$_{81}Pb^{208}$	

[26] R. F. Bacher and S. Goudsmit, Phys. Rev. **46**, 948 (1934).
[27] G. Racah, Phys. Rev. **62**, 438 (1942); **63**, 367 (1943); **76**, 1352 (1949).

tical particles are the forces in nuclei and in vacuum assumed to be similar. The second difficulty we do not strictly avoid, but rather ignore. The effect of a repulsive core on the radial parts of the wave function and short range correlations of nucleon positions is not taken into account. There is theoretical evidence[22] that the independent particle picture is approximately correct at low energies in spite of such correlations, but the final test of this approximation must come through the success or failure of calculations which start with the independent particle assumption.

Most workers have assumed a Gaussian radial dependence for the interparticle potential for convenience, but have assumed a variety of exchange mixtures. Based on a comparison of the Gaussian and Yukawa radial dependence, Talmi[6] has stressed the fact that predicted relative energy spacings are sufficiently sensitive to the shape of the potential that detailed conclusions, such as the point of crossing of two levels, should not be drawn for any specific assumed shape.

For identical particles, there are only two independent central force exchange mixtures, which can be conveniently taken to be of singlet and triplet character. In Figs. 1 through 3 we give the diagonal matrix elements of the energies of the two-particle configuration $(f_{7/2})^2$ as a function of the range of the forces for three different assumptions about the shape of the potential and for the singlet and triplet exchange character, in order to give a qualitative illustration of the roles of range, shape, and exchange character in the relative level spacings. Figure 1 is based on the Gaussian potential, $V=V_0\exp(-r^2/r_0^2)$. Energies are calculated by the method of Talmi[6] with oscillator wave functions, which contain the factor $\exp(-r^2/r_n^2)$. The relative range is defined by $\lambda=r_0/r_n$, and the abscissa is taken as $\eta=\lambda^2/(1+\lambda^2)$, which varies between 0 and 1 as the range, r_0, varies from 0 to ∞. The "correct" range can be found by fitting the Gaussian potential to an effective

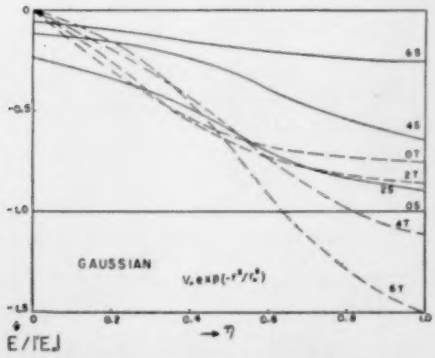

FIG. 1. Diagonal energy matrix elements for an $(f_{7/2})^2$ configuration ($J=0$, 2, 4, 6) for a singlet central (S) and triplet central (T) Gaussian well in units of the singlet spin zero matrix element. η, the range parameter is defined in the text. $\eta=0$ corresponds to a zero range interparticle force and $\eta=1$ corresponds to an infinite range interparticle force.

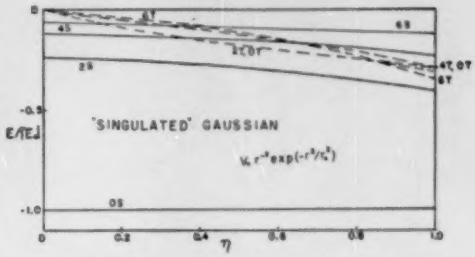

FIG. 2. Diagonal energy matrix elements for a modified Gaussian well plotted as in Fig. 1.

range of 3×10^{-13} cm and to a bound state at zero energy in order to approximate the low-energy singlet well. One finds $V_0=25.8$ Mev and $r_0=2.09\times10^{-13}$ cm. For calcium, Kurath gives as a reasonable value of r_n, 2.9×10^{-13} cm, which leads to $\lambda=0.72$. All energies on the vertical scale are normalized to a value of -1 for the energy of the spin-zero state with an attractive singlet force, and are plotted relative to the configuration energy in the absence of the perturbing forces. The short-range limit shows the characteristic large depression of the spin-zero state (seniority zero) relative to the state of spin 2, 4, and 6 (seniority two) for singlet forces, with of course no energy shifts for triplet forces. In the long-range limit, the singlet energies are proportional to $[\text{const}+J(J+1)]$, while the triplet spacings are equal and opposite to the singlet spacings. For a "reasonable" range, $\lambda\cong0.72$ $\eta\cong0.34$, the singlet 0–2 spacing is larger than the 2–4 spacing, and the triplet splittings are small compared to the singlet splittings. One is therefore qualitatively closer to the short-range than to the long-range limit.

In Fig. 2, the effect of a sharp attractive singularity in the potential is demonstrated. The potential is chosen (for convenience) to have the form,

$$V=V_0r^{-2}\exp(-r^2/r_0^2).$$

The result is that the level splittings remain for all ranges qualitatively very similar to the short range limit, with the singlet spin zero energy depression being large compared to all other energy shifts. As will be brought out in Paper III,[23] this behavior associated with the strong singularity at the origin is inconsistent with the experimental evidence.

Although a repulsive core potential cannot be taken account of properly with independent-particle wave functions, the central repulsion can be simulated by cutting off the potential to zero value at the origin. In Fig. 3, energies are plotted, as in Figs. 1 and 2, for such a potential, chosen to be,

$$V=V_0r^2\exp(-r^2/r_0^2).$$

The short- and long-range limits agree with those of the Gaussian potential, but the intermediate region of "reasonable" ranges is substantially different. The 0–2

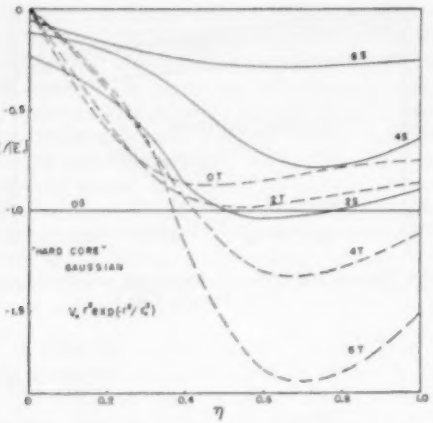

FIG. 3. Diagonal energy matrix elements for a modified Gaussian well plotted as in Fig. 1.

spacing, due to singlet forces, decreases rapidly as the range is increased from zero: the 0–2 and 2–4 spacings become equal at $\eta \cong 0.33$ ($\lambda \cong 0.71$), and the 0–2 singlet spacing becomes zero at $\eta \cong 0.5$ ($\lambda \cong 1.0$). As with the Gaussian (Fig. 1), the triplet energies show cross-over and small splittings in the neighborhood of equal 0–2 and 2–4 singlet splittings. But with this "hard core" potential the triplet splittings become inverted and quite appreciable for $\lambda \gtrsim 0.9$.

The qualitative differences among the diagonal energy spacings of Figs. 1–3 are sufficient to make desirable the kind of empirical approach to the diagonal matrix elements which is outlined in the next section. The figures also suggest that a sufficiently refined treatment of the spectra of some simple nuclear configurations may provide evidence on the shape of the interparticle potential.

It should be stressed that these figures are plotted for equal range and strength of the singlet and triplet potentials. Differences in range and strength may easily be taken account of by reading singlet and triplet splittings from different abcissas, and by multiplying the singlet or triplet energies by a suitable scale factor.

Coulomb Forces

In case one has to deal with proton configurations or to compare the level structure of similar neutron and proton configurations, the contribution of Coulomb forces to the level splitting must be calculated. This may be done readily following the method of Talmi[6] for oscillator wave functions of the nucleons. The Talmi radial integrals for the Coulomb force are

$$I_l = (l!2^{l+1}/(2l+1)!!)\epsilon_0,$$

where $(2l+1)!! = 1 \cdot 3 \cdots (2l+1)$, and the energy unit is

$$\epsilon_0 = \pi^{-\frac{1}{2}} e^2/r_n.$$

The nuclear size parameter, r_n, enters only in the energy unit. For a particular configuration, it is necessary to express the Slater integrals, F^k, in terms of the Talmi integrals, I_l, and then to express the energies E_J in terms of the F^k. Coulomb energies obtained in this way for the configurations $(f_{7/2})^2$ and $(f_{7/2})^3$ are given in Table II. The long range Coulomb force splits the levels by a lesser amount than it shifts the center of gravity. For both $(f_{7/2})^2$ and $(f_{7/2})^3$, the total level splitting is about $0.3\epsilon_0$. For $A=40$, $\epsilon_0 \cong 0.3$ Mev; therefore, the total level splitting due to Coulomb forces in about 0.1 Mev; an amount small compared to the splitting produced by the nuclear forces.

III. TWO-BODY PROBLEM WITH SINGLET FORCES

Let H_0 be the zero-order Hamiltonian of average central core field plus spin-orbit force; V, the sum of two-body interactions among particles outside the core; E, the correct nuclear energy; and $|\psi)$, the "correct" nuclear state vector.

The Schrödinger equation can be written

$$(E-H_0)\,|\psi) = V\,|\psi). \tag{1}$$

Now introduce a representation $|\alpha)$ such that H_0 is diagonal, in this case a jj coupling representation:

$$H_0\,|\alpha) = H_0(\alpha)\,|\alpha). \tag{2}$$

The energies $H_0(\alpha)$ are given empirically by the levels of the nucleus with a single nucleon outside the closed-shell core.

In the $|\alpha)$ representation, (1) can be written:

$$(\alpha|\psi) = \frac{1}{E-H_0(\alpha)}(\alpha|\,V\,|\psi). \tag{3}$$

One now introduces a representation $|\beta)$ convenient for expressing the matrix elements of V. Multiplying both sides by $(\beta|\alpha')$ and summing, we get

$$\sum_{\alpha'}(\beta|\alpha')(\alpha'|\psi) = (\beta|\psi) = \sum_{\alpha'} \frac{(\beta|\alpha')(\alpha'|\,V\,|\psi)}{E-H_0(\alpha')}$$

$$= \sum_{\alpha',\beta'} \frac{(\beta|\alpha')(\alpha'|\,V\,|\beta')(\beta'|\psi)}{E-H_0(\alpha')}. \tag{4}$$

TABLE II. Coulomb energies for configuration $(f_{7/2})^n$ of protons. $\epsilon_0 \cong 0.3$ Mev for calcium.

	$n=2$		$n=3$
J	E/ϵ_0	J	E/ϵ_0
0	1.357	3/2	3.236
2	1.160	5/2	3.336
4	1.067	7/2	3.410
6	1.033	9/2	3.176
		11/2	3.216
		15/2	3.112

We now specifically choose a singlet potential and let $|\beta)$ be the LS representation. For two particles the α and β labels become

$$|\alpha)=|JM_J j_1 j_2 l_1 l_2), \quad |\beta)=|JM_J LS l_1 l_2). \tag{5}$$

For shortness in notation we shall write $|\alpha)=|j_1 j_2 l_1 l_2)$ and $|\beta)=|l_1 l_2 L)$. The value of J, M_J will be the same throughout and since V is a pure singlet potential we shall only need $S=0$, $L=J$. Hence the above labels will be sufficient. Setting $|\beta)=|l_1 l_2 J)$, Eq. (4) becomes

$$(l_1 l_2 J|\psi) = \sum_{\substack{j_1' j_2' \\ l_1' l_2' \\ l_1'' l_2''}} \frac{(l_1 l_2 J|j_1' j_2' l_1' l_2')(j_1' j_2' l_1' l_2'|V|l_1'' l_2'' J)(l_1'' l_2'' J|\psi)}{E-H_0(j_1' j_2' l_1' l_2')}. \tag{6}$$

Now

$$\begin{aligned}(j_1' j_2' l_1' l_2'|V|l_1'' l_2'' J) &= \sum_{l_1''' l_2'''} (j_1' j_2' l_1' l_2'|l_1''' l_2''' J)(l_1''' l_2''' J|V|l_1'' l_2'' J) \\ &= (j_1' j_2' l_1' l_2'|l_1' l_2' J)(l_1' l_2' J|V|l_1'' l_2'' J),\end{aligned} \tag{7}$$

i.e., the LS to jj transformation coefficient is diagonal in $l_1' l_2'$. The fact that one can factor out the $j_1' j_2'$ dependence in Eq. (7) leads to a great simplification. Equation (6) may now be written:

$$(l_1 l_2 J|\psi) = \sum_{\substack{l_1' l_2' \\ j_1' j_2'}} \frac{|(l_1 l_2 J|j_1' j_2' l_1 l_2)|^2}{E-H_0(l_1 l_2 j_1' j_2')} \times (l_1 l_2 J|V|l_1' l_2' J)(l_1' l_2' J|\psi). \tag{8}$$

We define a new coefficient

$$\alpha(J l_1 l_2) = \sum_{j_1' j_2'} \frac{|(l_1 l_2 J|j_1' j_2' l_1 l_2)|^2}{E-H_0(l_1 l_2 j_1' j_2')}. \tag{9}$$

Then Eq. (8), which defines the expansion coefficients of $|\psi)$ in the LS representation, may be written;

$$\sum_{l_1' l_2'} \{\alpha(J l_1 l_2)(l_1 l_2 J|V|l_1' l_2' J) - \delta(l_1', l_1)\delta(l_2', l_2)\}(l_1' l_2' J|\psi) = 0. \tag{10}$$

The condition that Eq. (10) have nonzero solutions is that for each J the coefficient determinant of Eq. (10) vanish:

$$\det[\alpha(J l_1 l_2)(l_1 l_2 J|V|l_1' l_2') - \delta(l_1', l_1)\delta(l_2' l_2)] = 0, \tag{11}$$

where the rows are labeled by $l_1 l_2$ and the columns by $l_1' l_2'$.

The number of configurations included in Eq. (11) is, of course, arbitrarily great, but in order that the number of unknowns be only as great as the number of equations (equal to the number of levels of the two-particle configuration), it is necessary to make assumptions about the relative magnitudes of the radial integrals (the Slater integrals) for different l values. Near-lying levels of different l but with the same number of radial nodes have clearly similar wave functions, and may to good approximation be regarded as perfectly overlapping. If the number of radial nodes in the admixed wave function is different, one may reduce the interconfiguration matrix elements by an arbitrary factor or one may again assume a perfect overlap in order to obtain an upper limit to the configuration interaction. In either case, all required matrix elements will be expressible in terms of the diagonal matrix elements of V for the zero-order configuration. These assumptions lead to errors, so to speak, only in second order, i.e., in the effect of configuration interaction, not in the diagonal contribution to the energy. The method outlined here will then be appropriate either when configuration interaction is small, or when all important configurations have nearly the same radial dependence of their wave functions.

An especially simple situation results if the only important configurations have the same l value. Then the matrix elements are determined, according to Eq. (11), by

$$(llJ|V|llJ) = [\alpha(Jll)]^{-1}. \tag{12}$$

Using the techniques of matrix diagonalization, one would be confronted instead with a set of third-order matrices to diagonalize, corresponding to the three configurations $(l+\frac{1}{2})^2$, $(l+\frac{1}{2}, l-\frac{1}{2})$, and $(l-\frac{1}{2})^2$.

Equation (4) might be useful for three-body configurations also. One must then introduce extra quantum numbers in the $|\alpha)$ and $|\beta)$ representations. The usefulness of this approach again depends on how one can factor $(\alpha|V|\beta)$.

IV. THREE-BODY CONFIGURATION MATRIX ELEMENTS

In order to evaluate three-body matrix elements in terms of two-body matrix elements, it is necessary to use fractional parentage coefficients, which were introduced by Racah[26] for configurations containing equivalent particles. The extension of Racah's discussion of fractional parentage coefficients to apply to groups of inequivalent particles has been carried out by Redlich[28] and Meshkov.[29] A discussion and tabulation of fractional parentage coefficients for equivalent particles in jj coupling has been given by Flowers and Edmonds.[7] We shall give here Redlich's definition of fractional parentage coefficients for nonequivalent or equivalent particles with jj wave functions and his statement of the matrix element theorems.

Let $\psi_a(j_1 \cdots j_n, \alpha J)$ be an antisymmetrized n-particle wave function made up of states $j_1 \cdots j_n$ coupled together to make a total J. Let α be the other quantum numbers not explicitly written down. One can expand

[28] M. Redlich, thesis, Princeton University, January, 1954 (unpublished).
[29] S. Meshkov, Phys. Rev. **91**, 871 (1953).

ψ_a in terms of functions $\phi[(j_1\cdots j_{r-1}j_{r+1}\cdots j_n\alpha'J')_a \times j_r(n);\alpha J]$ which are constructed by combining functions $\psi_a(j_1\cdots j_{r-1}j_{r+1}\cdots j_n\alpha'J')$ with $\psi(j_r(n))$ by means of the vector coupling coefficients to make a state of angular momentum J. The notation $j_r(n)$ means that the added wave function $\psi(j_r(n))$ be written as a function of the variables $x_n\sigma_n$. ψ_a may be expanded as

$$\psi_a(j_1\cdots j_n\alpha J)=\sum_{r,\alpha',J'}(\alpha'J';j_r]\alpha J) \times\phi[(j_1\cdots j_{r-1}j_{r+1}\cdots j_n\alpha'J')_a j_r(n);\alpha J], \quad (13)$$

where the sum over r is taken only over distinct j_r. The coefficient of ϕ is called a fractional parentage coefficient. Redlich gives formulas for these coefficients for three-particle configurations with two equivalent particles in terms of Racah coefficients [see, e.g., Eq. (30)]. This definition of fractional parentage coefficient reduces to Racah's for the case of equivalent particles.

The formulas for computing matrix elements of one- and two-body operators will be given here: Let $F=\sum_{i=1}^{n}f(i)$, where $f(i)$ operates only on particle i. Then

$$(\psi_a(j_1\cdots j_n\alpha J_1)|F|\psi_a(j_1\cdots j_n\beta J_2)) =n\sum_{\alpha'J'r}(\alpha J_1[\alpha'J';j_r)(\alpha'J';j_rJ_1|f(n)|\alpha'J';j_rJ_2) \times(\alpha'J';j_r]\beta J_2), \quad (14)$$

where $(A[B)=(B]A)^*$. Let $G_n=\sum_{i>k}g(i,k)$ where $g(i,k)$ operates only on particles i and k, and $g(i,k)$ is a scalar operator.

$$(\psi_a(j_1\cdots j_n\alpha J)|G_n|\psi_a(j_1'\cdots j_n'\beta J)) =\frac{n}{n-2}\sum_{r,\alpha',\beta',J'}(\alpha J[\alpha'J';j_r)\delta(j_rj_r') \times(\psi_a(j_1\cdots j_{r-1}j_{r+1}\cdots j_n\alpha'J')|G_{n-1}|\psi_a \times(j_1'\cdots j_{r-1}'j_{r+1}'\cdots j_n'\beta'J'))(\beta'J';j_r]\beta J). \quad (15)$$

Equation (15) provides a relation between diagonal elements of n-particle and $(n-1)$-particle configurations which makes it possible to test observed nuclear spectra to find out whether or not configuration interaction is important. If configuration interaction is unimportant, then, *independent* of the potential involved (it must be a G-type two-body operator, however), Eq. (15) relates the energies of the n-particle and $(n-1)$-particle configurations. Hence if the observed energies are not related by (15), one knows either that configuration interaction is important, or that forces other than two-body forces are acting, e.g., direct many-body forces, or surface forces. (It is to be noted, however, that the *weak* coupling of particles via the surface can also be represented as two-body forces of type G.)

V. NUCLEAR MOMENTS AND TRANSITION RATES

Nuclear moments and transition rates depend more strongly on configuration admixtures than do energy spacings and hence are a better indication of the amount present. For magnetic moments the admixtures of states with the same l values are most important since they give contributions to the magnetic moments linear in the mixture amplitudes. Blin-Stoyle and Perks,[11] have analyzed the magnetic moments of nuclei from this viewpoint and have shown that, if the configuration interaction is due to attractive central forces, the predicted sign and order of magnitude of the shifts of the magnetic moments away from the Schmidt line are correct. Consider, for example, the magnetic moment of a nucleus with three identical particles beyond closed shells. Let the ground-state wave function be approximated as a three-particle shell-model function:

$$\psi=|IM\rangle=\sum_a a_a|\alpha IM\rangle, \quad (16)$$

where I is the total spin, a_a is a mixture amplitude, and α designates the jj coupling particle configuration. Configurations of three kinds are possible, according as 1, 2, or 3 single-particle states enter: $\alpha_1=[j^3]$, $\alpha_2=[j_1^2(J)j_2]$, and $\alpha_3=[j_1j_2(J)j_3]$, where J labels the intermediate angular momentum. (Antisymmetized functions are assumed.) The magnetic moment of the state is

$$\mu=\langle I,M=I|\mu_z|I,M=I\rangle=\sum_{\alpha,\alpha'}a_\alpha^*a_{\alpha'}\mu(\alpha\alpha'), \quad (17)$$

where

$$\mu(\alpha\alpha')=\langle\alpha I,M=I|\mu_z|\alpha' I,M=I\rangle, \quad (18)$$

and

$$\mu_z=\sum_i g_l l_z(i)+g_s S_z(i). \quad (19)$$

We list here formulas for the components $\mu(\alpha\alpha')$ required in (17) only for configurations of type α_1 and α_2, but components involving α_3 configurations are equally readily derived, by using fractional parentage expansions and the general methods of Racah:

$$\mu(\alpha_1\alpha_1)=\langle j^3I|\mu_z|j^3I\rangle=g_jI, \quad (20)$$

the well-known result that a group of equivalent particles has the same g factor as a single particle in the group,

$$g_j=g_l\pm(g_s-g_l)(2j+1\mp1)^{-1},\quad j=l\pm\tfrac{1}{2}; \quad (21)$$

$$\mu(\alpha_2\alpha_2)=\langle j_1^2(J)j_2I|\mu_z|j_1^2(J)j_2I\rangle =[2(I+1)]^{-1}\{g_l[I(I+1)+J(J+1)-j_2(j_2+1)] +g_s[I(I+1)-J(J+1)+j_2(j_2+1)]\}; \quad (22)$$

and

$$\mu(\alpha_1\alpha_2)=\langle j_1^3I|\mu_z|j_1^2(J)j_2I\rangle =-(J]I)(g_l-g_s)[2(2l+1)(I+1)]^{-1}\delta(l_1,l_2) \times[3(J+I+l+\tfrac{1}{2})(J+I-l+\tfrac{1}{2}) \times(J-I+l+\tfrac{1}{2})(I-J+l+\tfrac{1}{2})]^{\frac{1}{2}}, \quad (23)$$

where $(J]I)$ is shorthand for the fractional parentage

coefficient $(j^2(J)jI\}j^3I)$. The last formula gives the important off-diagonal contribution to the magnetic moment emphasized by Blin-Stoyle and Perks.

Quadrupole moments are sensitive to effects of collective nuclear deformation, and provide a better measure of the strength of surface coupling than does the energy level spectrum. By the same token, however, quadrupole moments are less useful as a measure of the degree of configuration interaction than are magnetic moments. Contributions of weak surface coupling to magnetic and quadrupole moments are discussed briefly in the following paper. In certain nuclei, however (e.g., ${}_8O^{17}$), the direct particle contribution to the quadrupole moment is dominant,[3] and it is therefore of interest to give formulas for the quadrupole moment of mixed configuration analogous to Eqs. (17) through (23) above for magnetic moments. Again let the nuclear ground state wave function be approximated by (16), but with the assumption now that the extra particles are all protons. The quadrupole moment operator is

$$Q=4e\sum_i r_i^2\mathcal{Y}_{20}(\theta_i\phi_i) \tag{24}$$

and $\mathcal{Y}_{20}=(\pi/5)^{\frac{1}{2}}Y_{20}$, Y_{20} being the normalized spherical harmonic. Analogous to Eq. (17), the quadrupole moment of the mixed state is given by

$$Q=\sum_{\alpha,\alpha'} a_\alpha^* a_{\alpha'} Q_{\alpha\alpha'}, \tag{25}$$

where

$$Q_{\alpha\alpha'}=4e\langle r^2\rangle_{\alpha\alpha'}[I(2I-1 \quad 1)(2I+1)(2I+3)]^{\frac{1}{2}} \times(\alpha I\|\textstyle\sum_i \mathcal{Y}_2(i)\|\alpha' I), \tag{26}$$

and $\langle r^2\rangle_{\alpha\alpha'}$ is the radial integral of r_i^2 of the ith proton (any i) between the antisymmetrized states α and α'. This factor is the order of magnitude of the mean square nuclear radius. Equation (26) holds for an arbitrary number of particles, but we list formulas for the reduced matrix elements appearing in (26) only for the special case of the three-particle configurations α_1 and α_2 defined below Eq. (16). For $\alpha=\alpha'=\alpha_1$,

$$(\alpha_1 I\|\textstyle\sum_i \mathcal{Y}_2(i)\|\alpha_1 I)=3(-1)^{j-I-1}(2I+1)(j\|\mathcal{Y}_2\|j) \times\sum_{J_1}(-1)^{J_1}|(j^2(J_1)jI\}j^3I)|^2W(jIjI;J_12). \tag{27}$$

Equation (27) is also somewhat more general, holding for the configuration $(j)^n$. For the special case that $I=j$, and seniority, $v=1$, a result of Racah[26] may be applied to yield,

$$(j^n\, v=1\, I=j\|\textstyle\sum_i \mathcal{Y}_2(i)\|j^n\, v=1\, I=j) =[(2j+1-2n)/(2j-1)](j\|\mathcal{Y}_2\|j), \tag{28}$$

a formula already given by Goeppert-Mayer[3] in a discussion of shell-model quadrupole moments. It is to be noted that the absolute value of the quadrupole moment found from Eq. (28) is never greater than the one-particle moment. For the quadrupole moment component diagonal with respect to configuration α_2, one gets

$$(\alpha_2 I\|\textstyle\sum_i \mathcal{Y}_2(i)\|\alpha_2 I) =(2I+1)\{(-1)^{J-i'-I}(j'\|\mathcal{Y}_2\|j')W(j'Ij'I;J2) +(j\|\mathcal{Y}_2\|j)\textstyle\sum_{J_1}|(jj'(J_1)jI\}j^2(J)j'I)|^2 \times(-1)^{J_1-i-I}W(jIjI;J_12)\}, \tag{29}$$

in which the fractional parentage coefficients may be given explicitly[28]:

$$(jj'(J_1)jI\}j^2(J)j'I) =-[\tfrac{3}{2}(2J+1)(2J_1+1)]^{\frac{1}{2}}W(Jj'jJ_1;Ij). \tag{30}$$

For the quadrupole moment component connecting configurations α_1 and α_2 one obtains,

$$(\alpha_1 I\|\textstyle\sum_i \mathcal{Y}_2(i)\|\alpha_2 I)=3^{\frac{1}{2}}(j^2(J)jI\}j^3I)(-1)^{J-i-I} \times(j\|\mathcal{Y}_2\|j')(2I+1)W(jIj'I;J2). \tag{31}$$

The one-particle reduced matrix elements appearing in (27)–(31) are

$$(lj\|\mathcal{Y}_2\|l'j')=\tfrac{1}{2}(2j+1)^{\frac{1}{2}}(j2-\tfrac{1}{2}0|\,j2j-\tfrac{1}{2}) \times|l-l'|=0,\ 2, \tag{32}$$

where $(j2-\frac{1}{2}0|\,j2j-\frac{1}{2})$ is a Clebsch-Gordon coefficient.

The predominant gamma-ray transitions among the low states of nuclei—especially if these states arise primarily from a single multiparticle configuration—are of magnetic dipole or electric quadrupole type. The general remarks above about magnetic and quadrupole moments apply also to $M1$ and $E2$ transition rates. That is, $M1$ transition rates are sensitive to configuration mixing, while $E2$ rates, although also substantially affected by mixing, are more sensitive to collective effects. $E2$ rates are discussed in the following paper.

Magnetic dipole transitions are in fact forbidden between pure states of the configuration $(j)^n$, and therefore occur only through configuration mixing or collective motion when the dominant configuration is of this simple type. Consider, for example, the matrix element,

$$(j^nJ|g_lL_z+g_sS_z|j^nJ')=(j^nJ|g_lJ_z+(g_s-g_l)S_z|j^nJ')$$

which governs magnetic dipole transitions. The part g_lJ_z does not connect states of different J. The part $(g_s-g_l)S_z$ is an F-type operator and its matrix elements are given by Eq. (14). $f(n)$ now becomes $(g_s-g_l)S_z(n)$, the single particle spin operator for the nth particle multiplied by (g_s-g_l). The matrix elements of $(g_s-g_l)S_z(n)$ which one needs in order to evaluate $(\alpha'J';j(n)J_1|S_z(n)|\alpha'J';j(n)J_2)$ are all of the form $(jm_j|S_z|jm_j')$. But as pointed out by Racah and others,[29] $(jm_j|S_z|jm_j')=\mu(j)(jm_j|j_z|jm_j')$ where $\mu(j)$ is the ratio of the reduced matrix elements of S_z and j_z and only depends on j. Hence the magnetic dipole transition operator can be written as $[g_l+(g_s-g_l)\mu(j)]J_z$ for equivalent particles of spin j. This operator is

[29] E. U. Condon and G. H. Shortley, *The Theory of Atomic Spectra* (Cambridge University Press, Cambridge, 1951).

diagonal with respect to the states of the configuration j^n. It does not connect states of different J, nor does it connect orthogonal states with the same J, e.g., states of different seniority.

We consider now the magnetic dipole transition rate between mixed configurations of three identical nucleons. Let the nuclear wave function be approximated by (16) for the final state and by the analogous expression,

$$\psi_i = |I'M'\rangle = \sum_{\alpha'} b_{\alpha'} |\alpha' I' M'\rangle \tag{33}$$

for the initial state. Then, because the magnetic dipole operator, M_1, is a vector, the methods of Racah may be applied to yield the expression for the reduced transition probability, $B_m(1)$, defined, for example, in reference 4:

$$B_m(1) = (2I'+1)|\mathfrak{M}|^2. \tag{34}$$

(The change of I' to I in this formula gives the reduced probability for the inverse transition $I \to I'$.) $\mathfrak{M}$ is a weighted mean reduced matrix element,

$$\mathfrak{M} = \sum_{\alpha,\alpha'} a_\alpha^* b_{\alpha'} \mathfrak{M}_{\alpha\alpha'}, \tag{35}$$

where

$$\mathfrak{M}_{\alpha\alpha'} = \langle \alpha I \| M_1 \| \alpha' I' \rangle, \tag{36}$$

and the double-bar matrix element is defined as by Racah.[26] The general selection rules, which apply to (36) are $\Delta I = 0, \pm 1$, and configurations α and α' differ by at most the quantum numbers of one particle. For $\alpha = \alpha' = (j)^3$, $\mathfrak{M}_{\alpha\alpha'} = 0$, as shown above. We consider three nonvanishing matrix elements which may contribute to the sum (35).

(a) $\alpha = [j^3]$, $\alpha' = [j^2(J)j']$:

$$\mathfrak{M}_{\alpha\alpha'} = (j^2(J)jI\,\|\,j^3I)(-1)^{J+I-j-I'}[3(2I+1)(2I'+1)]^{\frac{1}{2}} \times W(jIj'I'; J1)(j\|M_1\|j'), \tag{37}$$

where $(j^2(J)jI\,\|\,j^3I)$ is the fractional parentage coefficient of the state α, W is a Racah coefficient, and $(j\|M_1\|j')$ is a reduced one-particle magnetic dipole matrix element.

(b) $\alpha = [j^2(J)j']$, $\alpha' = [j^2(J')j']$:

$$\begin{aligned}\mathfrak{M}_{\alpha\alpha'} = 3(-1)^{I-I'}&[(2I+1)(2I'+1)]^{\frac{1}{2}} \times \{\tfrac{1}{2}(-1)^{J-J'}\delta JJ' W(j^2Ij^2I'; J1)(j'\|M_1\|j') \\ &+ \textstyle\sum_{J_1}(j^2(J_1)jI\,\|\,j^3Jj^2I')(j^2(J_1)jI'\,\|\,j^3J'j^2I') \\ &\times (-1)^{J-J}W(jIj'I'; J_1 1)(j\|M_1\|j)\},\end{aligned} \tag{38}$$

in which the sum over J_1 includes the fractional parentage coefficients of the states α and α'.

(c) $\alpha = [j^3(J)j']$, $\alpha' = [j'^3(J')j]$:

$$\begin{aligned}\mathfrak{M}_{\alpha\alpha'} = 3&[(2I+1)(2I'+1)]^{\frac{1}{2}}(j\|M_1\|j') \\ &\times \textstyle\sum_{J_1}(-1)^{J_1-j-I'}(jj'(J_1)jI'\,\|\,j^2(J)j'I) \\ &\times (j'j(J_1)j'I'\,\|\,j'^2(J')jI')W(jIj'I'; J_1 1).\end{aligned} \tag{39}$$

The reduced one-particle matrix elements appearing in Eqs. (37)–(39) are

$$(j\|M_1\|j) = g_j[(3/4\pi)j(j+1)(2j+1)]^{\frac{1}{2}} \tag{40}$$

and

$$\begin{aligned}(j\|M_1\|j') &= (g_s - g_l)\{(3/4\pi)[2l(l+1)/(2l+1)]\}^{\frac{1}{2}}\delta(l,l'). \\ &= (g_s-g_l)\{(3/4\pi)[2l(l+1)/(2l+1)]\}^{\frac{1}{2}}\delta(l,l').\end{aligned} \tag{41}$$

The matrix elements $\mathfrak{M}_{\alpha\alpha'}$ are of the same order of magnitude as the magnetic moments of the states involved. A substantial inhibition of the transition rate (as compared with the one-particle rate) is therefore to be expected only if the dominant configurations of initial and final states are not connected by M_1—e.g., if both are $(j)^3$ or if they differ in the quantum numbers of more than one particle. In either such case, the averaged matrix element, $\mathfrak{M}$, will be smaller than the one-particle matrix element by the order of the mixture amplitudes of configurations which are connected to the dominant configurations, and the transition rate will be smaller by the order of the square of these mixture amplitudes. It is to be noted that these effects could lead to a large inhibition of an $M1$ transition rate, but would not be expected ever to lead to an appreciable enhancement. This fact coupled with the known enhancement of $E2$ radiation due to collective effects might account for the observed $E2$–$M1$ competition in a number of cases where the one-particle transition rate formulas predict that the $M1$ rate should be much greater than the $E2$ rate. An example of such a case, the isotope $_{20}Ca^{42}$, is discussed in paper III.

Consider the following idealized example of the possible utility of transition rate measurements in determining nuclear configurations. Suppose a nucleus has ground state 5/2+ and first excited state 3/2+, and the shell-model assignment of the ground state is $d_{5/2}$. One wishes to know whether the one-particle assignments $d_{5/2}$ and $d_{3/2}$ for the two states or the multiparticle assignments $(d_{5/2})^3$ for both states are more nearly correct. If the absolute $E2$ rate between the states is, for example, determined by a Coulomb excitation process, and the $M1/E2$ ratio is inferred, or limited, by internal conversion or angular correlation experiments, then the $M1$ rate is in principal determined. It may be compared with the known $d_{3/2} \to d_{5/2}$ prediction: if the same order of magnitude, the one particle configurations are preferred; if much smaller, the $(d_{5/2})^3$ configuration is preferred. Factors of difference of 100 or more are to be expected.

Beta-decay matrix elements are especially sensitive to details of nuclear structure—the more so since states of two different nuclei are involved—and quantitative agreement between theoretical and experimental transition rates has been obtained only for mirror nuclei. Fermi matrix elements, and one-particle Gamow-Teller matrix elements are well known; they have been summarized, for example, by Bohr and Mottelson,[4]

whose notation we follow. Talmi[31] has considered three-particle Gamow-Teller matrix elements in jj coupling and shown that the distinction between favored and unfavored transitions does not exist for pure jj configurations. From his work, the reduced transition probability for $[j^3J'T']\rightarrow[j^3JT]$ follows easily:

$$D_{GT}=27(2J+1)(2T'+1)|(l_j\|B^{(1)}\|l_j)|^2 \times(T'1T_z'T_z-T_z'|T'1TT_z)^2S^2, \quad (42)$$

where $(T_1T_2T_{1z}T_{2z}|T_1T_2TT_z)$ is a Clebsch-Gordon coefficient; $(l_j\|B^{(1)}\|l_j)$ is the reduced Gamow-Teller matrix element, sometimes denoted by $\int\sigma$,

$$(l_j\|B^{(1)}\|l_j)=[(j+1)(2j+1)/j]^{\frac{1}{2}}, \quad j=l+\tfrac{1}{2}$$
$$=[j(2j+1)/(j+1)]^{\frac{1}{2}}, \quad j=l-\tfrac{1}{2} \quad (43)$$

and S is a sum over fractional parentage coefficients,

$$S=\sum_{\alpha_1,J_1,T_1}(-1)^{J_1+T_1}W(jJjJ';J_11)W(\tfrac{1}{2}T_1\tfrac{1}{2}T';T_11) \times(j^3\alpha TJ\{j^2(\alpha_1T_1J_1)jTJ) \times(j^3(\alpha_1T_1J_1)jT'J'\}j^3\alpha'T'J'). \quad (44)$$

This result could readily be generalized to other three-particle configurations by expanding them also in terms of fractional parentage coefficients. Applicable selection rules are $\Delta T=0,\ \pm1,\ \Delta J=0,\ \pm1$ and configurations differ at most in the quantum numbers of one particle.

For beta decay (nonmirror transitions), the most important configuration mixing is that between particle states of the same l value. Small deviations from either pure jj or pure LS coupling can cause large changes in the beta decay rate. This can easily be understood, since an "unfavored" transition has zero probability for pure LS coupling and goes at a "favored" rate for pure jj coupling. Mirror transitions are not so sensitive to configuration mixing.

This relative sensitivity to mixing has been shown in calculations by Redlich.[32] Starting with a zero order jj scheme, and computing mixing in the $2s-3d$ shell, he finds that the mirror transition $_{10}Ne^{19}\rightarrow{}_9F^{19}$ goes at a rate greater by a factor of 230 than the nonmirror transition $_8O^{19}\rightarrow{}_9F^{19}$, in accord with experiment, and in disagreement with theory for pure jj states. A similarly important distinction between the mirror transition $_{22}Ti^{43}\rightarrow{}_{21}Sc^{43}$ and the nonmirror transition $_{21}Sc^{43}\rightarrow{}_{20}Ca^{43}$ has been pointed out by Peaslee.[33] The mirror transition goes at a superallowed rate, while the nonmirror transition is slower by a factor of 10 than for pure configurations. As Peaslee and Talmi point out, these unfavored decays are conclusive proof against pure jj configurations. They need not, however, imply that the true coupling scheme is much closer to LS. The particular decay $Sc^{43}\rightarrow Ca^{43}$ is discussed further in paper III, where it is shown that the calculated configuration mixing is sufficient to explain the order of magnitude of the observed slowdown. This calculated mixing results in a coupling scheme about equally removed from both jj and LS coupling.

[31] I. Talmi, Phys. Rev. **91**, 122 (1953).
[32] M. Redlich (to be published)
[33] D. C. Peaslee (private communication).

VI. TRIPLET FORCES AND SCATTERING DATA

It is expected that the nuclear forces derived from scattering data will approximate those acting between the extra-core particles in nuclei. One objection to this point has been that the potentials adjusted to give correct scattering results do not lead to saturation of nuclear forces. However, it has been shown that if one uses repulsive core potentials a fit to both scattering and saturation requirements can be made.[34] For our purposes it is most important to fix the spin and exchange properties of the nuclear force since our approach is independent of the shape of the well. The spin and exchange properties of nuclear potentials adjusted to fit scattering are nearly independent of whether cores were used in the wells or not. We therefore argue that it is sufficient to examine potentials which fit nuclear scattering data but do not necessarily have repulsive cores.

Analysis of n-p and p-p scattering up to 100 Mev has been carried out by Christian and Hart,[35] Christian and Noyes,[36] and Jastrow.[37] They have concluded that:

(a) There is no appreciable central force in odd states.

(b) There is a weak odd-state tensor force present in addition to the even-state tensor force which is needed to give the deuteron quadrupole moment. In their analysis of p-p scattering at 32 Mev, Christian and Noyes fit the differential cross section with a singlet central force and an odd-state tensor force. Using wells of the form $V_0\exp(-r/0.75\times10^{-13}$ cm), these authors find that well depths

$$V_0 \text{ (singlet-central)} = -100 \text{ Mev},$$
$$V_0 \text{ (odd state tensor)} = 50 \text{ Mev},$$

gives a reasonably good fit to the data. Jastrow uses the same odd-state tensor potential as given above, but uses a singlet central potential with a repulsive core, in his discussion of p-p scattering. In addition he takes an even state tensor force with $V_0=127$ Mev and a triplet central force with $V_0=69$ Mev:

For an n-n or p-p system we need to consider only the following possibilities for the forces: (a) singlet-even, central; (b) triplet-odd, central; (c) triplet-odd, tensor; other forces being excluded by the Pauli principle. Force (a) is the largest and its range and depth are given above for an exponential well. Force (b) has not manifested itself in nucleon-nucleon scattering. Even if it were present between extra core particles its effect on level splitting would be diminished because, as shown in Figs. 1–3, the level depressions

[34] K. A. Brueckner, Phys. Rev. **96**, 508 (1954).
[35] R. S. Christian and E. W. Hart, Phys. Rev. **77**, 441 (1950).
[36] R. S. Christian and H. P. Noyes, Phys. Rev. **79**, 85 (1950).
[37] R. Jastrow, Phys. Rev. **81**, 165 (1951).

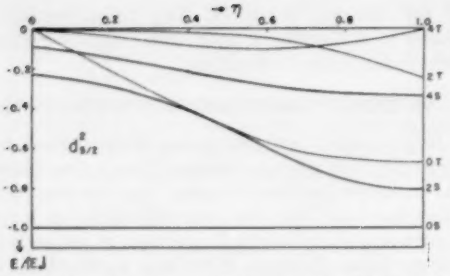

FIG. 4. Diagonal energy matrix elements for a $(d_{5/2})^2$ configuration ($J=0, 2, 4$) for a singlet central Gaussian well (S) and a tensor force with a Gaussian well (T). The tensor force well is half as deep as the singlet well. Elements plotted as in Fig. 1.

due to central triplet interactions are almost independent of J for assumed reasonable force ranges. Force (c), however, is about one-half as large as force (a) in nucleon-nucleon scattering. In order to show qualitatively the effect of such a tensor force on level structure, we plot in Fig. 4 the diagonal energy matrix elements of an attractive central singlet force and of an attractive odd-state tensor force for the configuration $(d_{5/2})^2$. (This calculation utilizes results derived by Talmi[18] for tensor forces.) Gaussian radial dependence is assumed for both potentials with singlet to tensor well depths in the ratio 2:1. The effect of the tensor force on the spin zero state is quite appreciable, as shown in Fig. 4. Because the odd-state tensor force is in fact repulsive,[19,37] the perturbation method of calculation with independent particle wave functions overestimates the effect of the tensor force relative to the singlet force. In addition calculations based on meson theory[19] indicate that the tensor well shape is quite different from the central well shape. Therefore, the results shown in Fig. 4 are at best qualitative. It seems probable that the assumption of pure singlet forces between identical particles is a good first approximation, but the magnitude of the corrections due to odd-state tensor forces may be important.

In the discussion of the Schrödinger equation in Sec. II it was important that one could factor the matrix in Eq. (7). This matrix can also be factored if V is a central triplet force. Then

$$\langle j_1 j_2 l_1 l_2 | V | LSl_1' l_2' \rangle = \langle j_1 j_2 l_1 l_2 | L1 l_1 l_2 \rangle \langle L1 l_1 l_2 | V | L1 l_1' l_2' \rangle \delta(s,1). \quad (45)$$

If V is a triplet tensor force $\mathbf{L}^2$ no longer commutes with V and the factorization cannot be carried out. However, even in this case it may be possible to write a tensor force as an effective central force.

If the semiempirical approach to nuclear spectra outlined here proves to be fruitful, it would appear best first to fix the singlet parameters of the potential by analyzing configurations of identical particles, then to analyze mixed neutron-proton configurations with only the triplet matrix elements regarded as unknowns. In paper III of this series, explicit application of these techniques will be made to the nuclei Ca^{42} and Ca^{43}.

ACKNOWLEDGMENTS

The authors would like to acknowledge many helpful discussions with Professor K. A. Brueckner, Dr. R. J. Eden, and Dr. N. C. Francis.

[18] I. Talmi, Phys. Rev. 89, 1065 (1952).

Particle States in Spheroidal Nuclei*

STEVEN A. MOSZKOWSKI
University of California, Los Angeles, California
(Received April 25, 1955)

Particle motion in a spheroidal box has been studied by making an appropriate coordinate transformation so that the potential appears as spherically symmetric. The effect of the nonsphericity then appears as a change in kinetic energy for which the perturbation matrix elements can be evaluated. Matrix elements between states in different major shells are small. The energy levels and wave functions (defined in the transformed coordinate system) can then be calculated by the customary techniques of matrix diagonalization.

This method was used to obtain energy levels of a spheroidal box both without and with an additional spin-orbit term of the magnitude suggested by nuclear shell systematics.

Corresponding results for distorted wells of finite depths appear to be rather simply related to those for a box.

Nuclear deformations predicted by this picture are in qualitative agreement with experimental values, and are, in general, considerably smaller than the values implied by a hydrodynamical model.

I. INTRODUCTION

THE striking success of the collective model in accounting for many features of nuclear structure[1,2] has stimulated interest in some of the underlying problems. One of these is the study of the properties of particle states in nonspherical potentials. The strong-coupling version of the collective model applies best for mass numbers between 155 and 185 and above 225.[1,3] For these cases, the nucleus, under the deforming influence of the particles outside of closed shells, acquires a semipermanently deformed shape, which to a good degree of approximation is a spheroid of revolution. As is well known, the collective motion of such nuclei gives rise to rotational and vibrational states and the nonsphericity results in large electric quadrupole moments, both static and dynamic. For lighter nuclei, the strong-coupling approximation is not realized, but collective effects resulting from deviation of the nuclear shape from sphericity are still important. One of the important problems in this connection is to calculate the magnitude of nuclear deformations. Previously some estimates have been made on the basis of a simple hydrodynamical model.[4-7] In general the hydrodynamical model gives deformations considerably larger than empirical values, sometimes by an order of magnitude. However any model which considers particles moving independently in a deformed potential, gives much smaller deformations.[8-12] At least part of this difference is a consequence of the inherent shell-structure regularities in spacings between particle levels for a spherical well. The opposite limit would be a strictly statistical distribution of particle states, for which hydrodynamical estimates would be more nearly valid.[1,2]

The basic assumptions made in the present paper are very extreme. The particles are assumed to move independently in a box ($V=0$ inside, $V=\infty$ outside) whose wall is elastic and deformable into a spheroid of fixed volume. As far as the particle motion is concerned, the wall is considered as static. Dynamic effects, such as rotational motion of the wall, are thus not taken into account. The results depend on the position of particle states in a spherical well. The order of particle levels in nuclei is approximately that for a spherical well of finite depth, with rounded edges and a spin-orbit coupling. The order of levels for such a well is nearly the same as for a box with an additional spin orbit term. The effect of making the well finite and rounding it can, of course, be taken into account. However, the general features of the results probably will not depend very much on the detailed potential. In any case, other effects not considered here are probably of far greater significance. Thus direct interactions between particles outside of closed shells are very important. Furthermore, the nuclear distortion is time-dependent and it must be treated as a quantum variable. Nevertheless, one might hope that the present calculations reproduce at least the qualitative trends of nuclear deformations as function of nucleon number.

In the following discussion, it is shown how wave functions and energy levels in a static nonspherical well may be found to a reasonable degree of accuracy.

* This work was partially supported by the Office of Naval Research, and the Office of Ordnance Research.

[1] A. Bohr, Kgl. Danske Videnskab. Selskab, Mat.-fys. Medd. **26**, No. 14 (1952); A. Bohr and B. R. Mottelson, Kgl. Danske Videnskab. Selskab, Mat.-fys. Medd. **27**, No. 16 (1953).

[2] D. L. Hill and J. A. Wheeler, Phys. Rev. **89**, 1102 (1953).

[3] A. Bohr and B. R. Mottelson, *Beta and Gamma Spectroscopy*, edited by K. Siegbahn (North Holland Publishing Company, Amsterdam, 1955), Chap. 17.

[4] J. Rainwater, Phys. Rev. **79**, 432 (1950).

[5] E. Feenberg and K. C. Hammack, Phys. Rev. **81**, 285 (1951).

[6] K. W. Ford, Phys. Rev. **90**, 29 (1953).

[7] R. van Wageningen and J. De Boer, Physica **18**, 369 (1952).

[8] D. Pfirsch, Z. Physik **132**, 409 (1952).

[9] R. van Wageningen, Physica **19**, 1004 (1953).

[10] S. Gallone and C. Salvetti, Nuovo cimento **10**, 145 (1953).

[11] J. P. Davidson and E. Feenberg, Phys. Rev. **89**, 856 (1953).

[12] S. G. Nilsson, Kgl. Danske Videnskab. Selskab, Mat.-fys. Medd. (to be published).

[13] D. L. Hill and J. A. Wheeler (private communication).

Section II of this paper deals with calculations of the wavefunctions and energy levels for particles in a spheroidal box. The effect of a spin orbit term is discussed in Sec. III. In Sec. IV, some estimates are made for energy levels in a distorted well of more general shape. The deformations calculated in this way and their relation to empirical values are discussed in Sec. V.

II. ENERGY LEVELS AND WAVE FUNCTIONS OF A PARTICLE IN A SPHEROIDAL BOX

Particle states in a spheroidal well do not have a well-defined angular momentum because of the absence of spherical symmetry. However, the parity is a good quantum number, and so is the component of angular momentum about the axis of deformation, denoted here by m. The spatial $(2l+1)$-fold degeneracy of levels in a spherical well is broken up in such a way that only twofold degeneracies remain, those for levels differing solely with respect to their sign of m.

The solution of the wave equation for a spheroidal box can, in principle, be carried through in several ways.

First, one can solve the wave equation by separation into spheroidal coordinates. Such calculations, which have been performed by several authors,[4,13,14] are extremely complicated, and it may be difficult to adapt them to take into account interparticle forces and the time dependence of the nuclear distortion. The spheroidal coordinates ξ and η have no apparent direct significance for problems which involve wavefunctions *inside* the nucleus, since no special distinction attaches to the focal points of a spheroidal nucleus. On the other hand, the separation into spheroidal coordinates may be extremely useful for the study of particle motion *outside* the nucleus; e.g., for α decay. Another promising approach consists of expanding the wave functions for a deformed box in terms of wave functions for a spherical box. The coefficients of this expansion, as well as the wave number, are determined by the requirement that the wave function must vanish at the wall of the box. Such calculations have been made for deformations of arbitrary shape.[2,13]

The basis of the method described in the present paper is that a spheroid (and more generally any ellipsoid) can be transformed into a sphere in a very simple way. The coordinates are merely multiplied by a strain tensor. By use of this transformation, one can calculate energy levels and wave functions for a spheroidal box to any desired degree of accuracy. It is also possible to get results quite simply without losing much precision.

Consider a box whose wall is defined by the following spheroid:

$$R_0^2 = Dx^2 + Dy^2 + D^{-2}z^2. \tag{1}$$

This spheroid has one axis of length DR_0 and two axes of length $D^{-1}R_0$. The volume is, of course, independent of D. The deformation d is defined[15] as

$$d = D - 1. \tag{2}$$

Now introduce "primed" coordinates as follows:

$$x = D^{-\frac{1}{2}}x', \quad y = D^{-\frac{1}{2}}y', \quad z = Dz'. \tag{3}$$

Then the potential is given by

$$\begin{aligned} V(\mathbf{r}') &= 0 \quad \text{for} \quad r' < R_0 \\ &= \infty \quad \text{for} \quad r' > R_0. \end{aligned} \tag{4}$$

It is seen that the spheroidal box (and in fact any spheroidal potential), is central in $\mathbf{r}'$ space. This suggests that a formulation of the wave equation in $\mathbf{r}'$ space might be of value. Thus, in the primed coordinate system, the Schrödinger equation reads:

$$\begin{aligned} (2m)^{-1}(Dp_{x'}^2 + Dp_{y'}^2 + D^{-2}p_{z'}^2)\psi(\mathbf{r}') \\ + V(r')\psi(\mathbf{r}') = E\psi(\mathbf{r}'). \end{aligned} \tag{5}$$

This equation is, apart from the coefficients of the kinetic energy terms, the same as the wave equation for a particle in a spherical potential, but with all quantities defined in $\mathbf{r}'$ space. The energy levels and wave functions can then be found by constructing the secular determinant of Eq. (5) using as zero-order functions the wave functions $\psi_i(\mathbf{r}')$ for the Hamiltonian when $D=1$ (the spherical case). For a spheriodal box, the boundary conditions require that $\psi(\mathbf{r}')$ vanish for $r' = R_0$.

The zero-order functions for a box are given as follows:

$$\psi_i(\mathbf{r}') = j_l(\omega_{nl} r'/R_0) Y_{l,m}(\theta', \phi'). \tag{6}$$

Here $\omega_i = \omega_{nl}$ denotes the nth root of the spherical Bessel function of order l. Since both the Hamiltonian and the zero-order wave functions are expressed in terms of primed coordinates, it may avoid confusion to drop the primes for calculations of matrix elements.

The secular determinant reads:

$$\textstyle\sum_k (H_{ik} - E_i\delta_{ik})\psi_k(\mathbf{r}') = 0, \tag{7}$$

where

$$H_{ik} = \tfrac{1}{3}(2D + D^{-2})\frac{p^2}{2m}\Big|_{ik} - \tfrac{2}{3}(D - D^{-2})\frac{T_{20}(\mathbf{p})}{2m}\Big|_{ik}, \tag{8}$$

and

$$T_{20}(\mathbf{p}) = (3p_z^2 - p^2)/2. \tag{9}$$

Since the potential is zero throughout the box, all matrix elements of V vanish.

For small deformations, Eq. (7) becomes

$$2mH_{ik} = (1 + d^2)p^2\big|_{ik} - 2(d - d^2)T_{20}(\mathbf{p})\big|_{ik}. \tag{10}$$

The matrix elements H_{ik} can be easily evaluated by reference to the well-known properties of spherical Bessel functions.[16]

[14] R. D. Spence, Phys. Rev. **83**, 460 (1951).

[15] The relation of d to some other quantities used to define degrees of distortion is, for small deformations: $d = \frac{3}{2}\epsilon = (5/4\pi)^{\frac{1}{2}}\beta$, where ϵ is defined (see reference 3) as the difference between axes in units of R_0, and β is defined (see reference 1) by:

$$R = R_0[1 + \beta Y_2^0(\theta, \phi)].$$

[16] P. M. Morse and H. Feshbach, *Methods of Theoretical Physics* (McGraw-Hill Book Company, Inc., New York, 1953), Vol. 2, p. 1573.

The results are:

$$\left.\frac{p^2}{2m}\right|_{ik}=E_i\delta_{ik}=\frac{\hbar^2}{2mR_0^2}\omega_i^2\delta_{ik}, \tag{11}$$

$$\left.\frac{T_{20}(\mathbf{p})}{2m}\right|_{ik}=\frac{\hbar^2}{2mR_0^2}\omega_i^2\delta_{n_in_k}\delta_{m_im_k}\frac{l_i(l_i+1)-3m_i^2}{(2l_i-1)(2l_i+3)}$$

$$=\frac{\hbar^2}{2mR_0^2}\omega_i^2P_2(\theta)|_{ik}\quad\text{for}\quad l_k=l_i, \tag{12a}$$

$$\left.\frac{T_{20}(\mathbf{p})}{2m}\right|_{ik}=\frac{\hbar^2}{2mR_0^2}\frac{\omega_i\omega_k}{\omega_k^2-\omega_i^2}\delta_{m_im_k}\times 3\left[\frac{(l_i+1+m_i)(l_i+2+m_i)\times(l_i+1-m_i)(l_i+2-m_i)}{(2l_i+1)(2l_i+5)}\right]^{\frac{1}{2}}$$

$$=\frac{\hbar^2}{2mR_0^2}\frac{\omega_i\omega_k}{\omega_k^2-\omega_i^2}2(2l_i+3)P_2(\theta)|_{ik}\quad\text{for}\quad l_k=l_i+2, \tag{12b}$$

where the subscripts i and k denote integration over angles only.

Of course, only states of the same m and of the same parity can be coupled by a spheroidal distortion. It should be noted that the matrix elements between states in different major shells vanish if the orbital angular momenta are the same and they are small for l's different by two, because of the large energy denominator.

On the other hand, the interaction strongly couples states of the same major shell. The energy differences between two states of the same major shell are given approximately by

$$\omega_k^2-\omega_i^2\simeq 2(2l_i+3)\quad\text{for}\quad l_k=l_i+2. \tag{13}$$

It follows from Eqs. (8), (11), (12), (13) that matrix elements of H between states in the same shell are given to a good degree of approximation by

$$H_{ik}=(\tfrac{2}{3}D+\tfrac{1}{3}D^{-2})(E_i\delta_{ik})-(\tfrac{2}{3}D-\tfrac{2}{3}D^{-2})(E_iE_k)^{\frac{1}{2}}P_2(\theta)|_{ik}. \tag{14}$$

To calculate energy levels and wave functions to a fair degree of accuracy it is sufficient to diagonalize only the part of the infinite secular determinant (7) between states in the major shell under consideration. This approach neglects the small interactions between different major shells and yields the following average energy for the states in each shell:

$$E_i'=E_i(\tfrac{2}{3}D+\tfrac{1}{3}D^{-2})\xrightarrow[\text{small }d]{}E_i(1+d^2). \tag{15}$$

The perturbation matrix elements $3\mathcal{C}_{ik}$ are then given by

$$3\mathcal{C}_{ik}=-(\tfrac{2}{3}D-\tfrac{2}{3}D^{-2})(E_iE_k)^{\frac{1}{2}}P_2(\theta)|_{ik}. \tag{16}$$

The secular determinant now reads as follows:

$$\sum_k[3\mathcal{C}_{ik}-E_i'\delta_{ik}]\psi_k(\mathbf{r}')=0,$$

where the sum now extends only over states k of the same major shell as state i. The smallness of the coupling term between different major shells shows that on the "average," the $\psi(\mathbf{r}')$ are good zero-order functions to use for this problem. On the average, the spheroidal distortion of a box causes the wave functions to "follow" it apart from (a) the strong mixing within a given shell, and (b) the weak coupling between different shells. It should be noted here that for boxes whose walls are rectangular parallelipipeds or right circular cylinders, the wave equation can be solved exactly. For these cases the wave functions follow the distortion exactly without any mixing.

Slightly more accurate values for the energy levels may be obtained by taking into account the small coupling between different shells. Thus, the energy can be expressed as a power series in d, and values of the coefficients up to d^2 obtained exactly from Eqs. (10)–(12) by use of second order perturbation theory.

The sums over intermediate states can be evaluated in terms of the expression

$$\sum_{\omega_l}\frac{1}{\omega_l^2-x^2}=\frac{1}{2x^2}\left[l-\frac{xj_l'(x)}{j_l(x)}\right], \tag{18}$$

and the two other sums which are obtained by differentiation of (18) with respect to x once and twice. Here x is any number and the sum extends over all positive roots of the spherical Bessel function of order l.

The energy of a given state can then be written as follows:

$$E_{nlm}=E_{nlm}^{(0)}+dE_{nlm}^{(1)}+d^2E_{nlm}^{(2)}\cdots, \tag{19}$$

where the coefficients in the power series are:

$$E_{nlm}^{(0)}=(\omega_i^2\hbar^2)/(2mR_0^2), \tag{20a}$$

$$E_{nlm}^{(1)}=E_{nlm}^{(0)}[-2P_2(\theta)|_{ii}], \tag{20b}$$

$$E_{nlm}^{(2)}=E_{nlm}^{(0)}\{1+2P_2(\theta)|_{ii}-[(2l+7)-2\omega_i^2(2l+3)^{-1}]P_2(\theta)|_{i,l+2}^2+[(2l-5)-2\omega_i^2(2l-1)^{-1}]P_2(\theta)|_{i,l-2}^2\}. \tag{20c}$$

Values of the coefficients are given in Table I.

It is evident that the power series expansion does not converge well for states which are strongly coupled to other states in the same shell; e.g., $1d0$ and $2s0$. Such an expansion by itself can therefore not be used for these states and a matrix diagonalization must be carried out.

For the numerical calculations of this paper, only matrix elements between states of the same shell were considered using Eqs. (15) to (17). However, rather than neglecting intershell contributions entirely, the

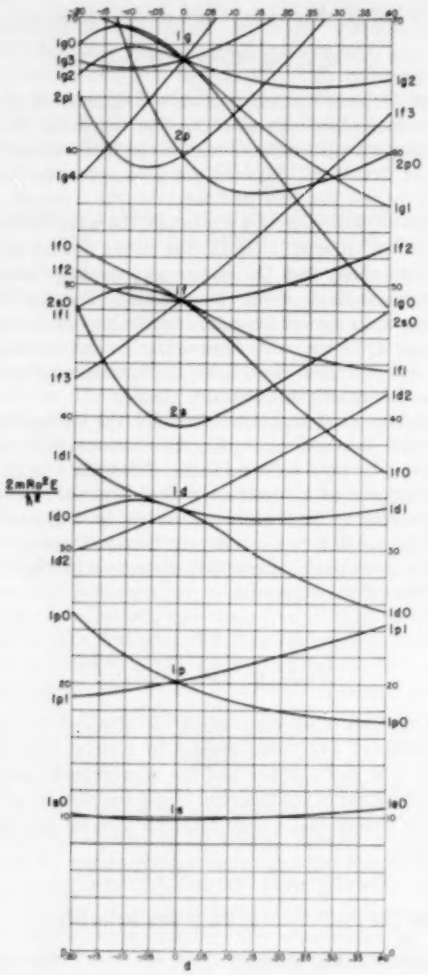

FIG. 1. Energy levels of a spheroidal box as function of deformation. No spin-orbit coupling. Length of symmetry axis $=R_0(1+d)$.

coefficients of $p^2/2m$ were altered slightly from unity to

$$1+(\eta/3)(2D+D^{-2}-3)\xrightarrow[\text{small } d]{}1+\eta d^2, \qquad (21)$$

where η is an adjustable parameter whose values are slightly smaller than unity. Values of η were picked for each state in such a way that the energy would agree exactly with the power series expansion (20) as far as terms in d^2. According to the numbers of Table I, η ranges from 0.92 for the 1s0 state to 0.66 for the 1g0 state. Terms of order d^3, d^4, etc., also appear to be quite accurately given with this approximation.

The matrices were diagonalized on the SWAC at the UCLA campus. The Jacobi method of successive rotations was used. Results for states up to the $1g$ shell are shown in Fig. 1. The numerical values obtained agree very well with calculations of Spence[14] and of Hill and Wheeler[13] who used spheroidal coordinates.

III. EFFECT OF A SPIN-ORBIT TERM ON THE ENERGY LEVELS

The above method can be extended to include a spin-orbit coupling term in the Hamiltonian. Strictly speaking, there can be no spin-orbit coupling of the Thomas type $(\boldsymbol{\sigma}\cdot\nabla V\times\mathbf{p})$ for any well with infinitely high walls. However, by adding instead a constant spin-orbit term, it is possible to reproduce the approximate order of single-particle levels in light and medium nuclei.

The particular spin-orbit term used in the present calculations is a constant with an attempted correction for the deformation:

$$H_{s.o.}=-k[(\mathbf{l}'\cdot\boldsymbol{\sigma})+d(\tfrac{3}{2}l_z'\sigma_z-\tfrac{1}{2}\mathbf{l}'\cdot\boldsymbol{\sigma})], \qquad (22)$$

where all coordinates and operators are defined in $\mathbf{r}'$ space.

The constant k was taken equal to one in units of $\hbar^2/2mR_0^2$ to give approximately the correct doublet splitting in nuclei. The zero-order states were taken as $\psi(\mathbf{r}')\chi(\text{spin})$, where $\chi(\text{spin})$ can be $\uparrow$ or $\downarrow$.

In this approximation only states of the same shell and with the same values of l and m_j are coupled by the spin-orbit term.

The rest of the Hamiltonian was not altered from the form used in the calculations of Sec. 2. The results of including this spin-orbit term are shown in Fig. 2. It is seen that for small deformations, the energy levels agree with the previous calculations using first order perturbation theory.[4–9] For example, the first-order

TABLE I. Energy levels in spheroidal box [in units of $\hbar^2/2mR_0^2$] as function of deformation. First three terms in power series expansion

$$E=E^{(0)}+E^{(1)}d+E^{(2)}d^2+\cdots.$$

n l m	$E^{(0)}$	$E^{(1)}$	$E^{(2)}$
1 s 0	9.870	0	9.041
1 p 0	20.191	−16.153	33.467
1 p 1	20.191	8.076	10.196
1 d 0	33.217	−18.981	−108.935
1 d 1	33.217	−9.491	36.570
1 d 2	33.217	18.981	11.168
2 s 0	39.479	0	192.014
1 f 0	48.831	−26.042	−79.892
1 f 1	48.831	−19.532	−38.347
1 f 2	48.831	0	39.294
1 f 3	48.831	32.554	12.042
2 p 0	59.679	−47.743	244.350
2 p 1	59.679	23.872	127.098
1 g 0	66.955	−34.782	−84.022
1 g 1	66.955	−29.565	−60.983
1 g 2	66.955	−13.913	−5.464
1 g 3	66.955	12.174	41.787
1 g 4	66.955	48.694	12.842

energy shift is given by:

$$E_{nljm}^{(1)} = -2E_{nljm}^{(0)} \frac{j(j+1)-3m^2}{2j(2j+2)}. \quad (23)$$

IV. SOME RESULTS FOR OTHER FORMS OF THE POTENTIAL

The problem of finding the energy levels in a realistic nuclear potential (e.g., square well with rounded edges) which has been deformed into spheroidal shape is a very formidable one. Moreover, it is not clear that such calculations would yield significant improvements over the results obtained with the spheroidal box. Surely the relation of the effective one-particle potential to the two-body forces must be correctly taken into account. Thus, the well depth is expected to decrease when the well is deformed into spheroidal shape,[17] which results in an additional restoring force of potential origin. Some simple approximate results may, however, be of interest.

One interesting form of the potential which has proven extremely useful for many calculations is that of the harmonic oscillator. It is well known that the energy levels and wave functions for particles in an anisotropic oscillator potential can be obtained exactly.[8–12,18]

The potential can be written as follows:

$$V = \tfrac{1}{2}m\omega^2 r'^2, \quad (24)$$

where the components of $\mathbf{r}'$ are defined in [Eq. (3)].

The average energy over a closed shell is given by

$$E' = E^{(0)}(\tfrac{2}{3}D^{1}+\tfrac{1}{3}D^{-1}) \xrightarrow[\text{small } d]{} E^{(0)}(1+\tfrac{1}{4}d^2), \quad (25)$$

and the average effect of the deformation on the wave functions is to replace $\psi(\mathbf{r})$ by $\psi(\mathbf{r}'')$, where now

$$x = x''D^{-1}, \quad y = y''D^{-1}, \quad z = z''D^{1}. \quad (26)$$

Thus the wave functions "follow" the deformation to half its extent.

The first-order shift of energy levels in a deformed well of any shape has been calculated previously by several authors.[5,7,9] It can be written as follows:

$$E_{nljm}^{(1)} = -E_{nljm}^{(0)} 2P_2(\theta)\,|_{ii} f, \quad (27)$$

where E is the total energy measured from the bottom the bottom of the well. f is the ratio of kinetic energy (expectation value) to the total energy.

For all states of a harmonic oscillator potential $f=\frac{1}{2}$. A comparison of these results with those obtained in Sec. 2 for a box ($f=1$) suggests that perhaps for an arbitrary rounded well, the effect of changing $V(\mathbf{r})$ to $V(\mathbf{r}')$ might be, at least on the average, to distort $\psi(\mathbf{r})$ to $\psi(\mathbf{r}'')$, where

$$z = D^{f}z'', \quad x = D^{-f/2}x'', \quad y = D^{-f/2}y'', \quad (28)$$

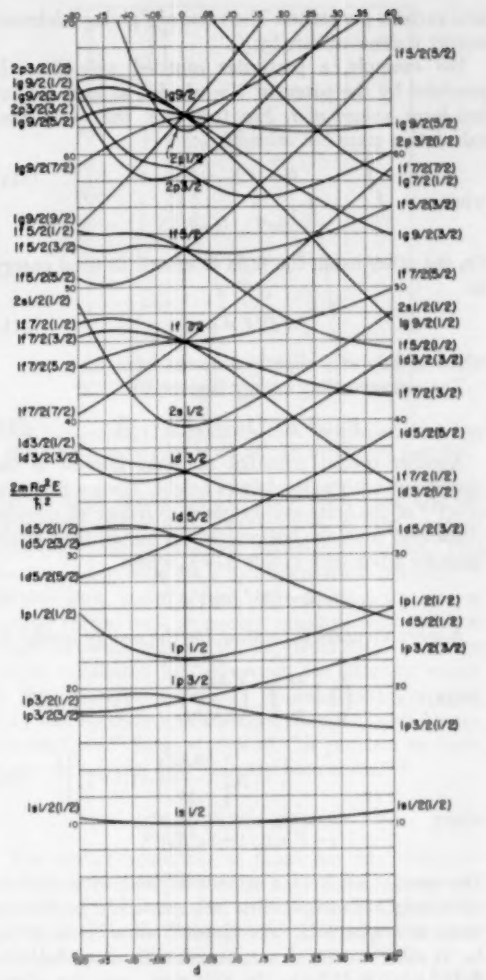

FIG. 2. Energy levels of a spheroidal box as function of deformation A reasonable spin-orbit term has been included.

and that the average energy over a closed shell is:

$$E' = E^{(0)}(\tfrac{2}{3}D^{f}+\tfrac{1}{3}D^{-2f}) \xrightarrow[\text{small } d]{} E^{(0)}(1+f^2d^2). \quad (29)$$

The residual interaction would then only mix states in the same shell. Thus [see Eq. (16)],

$$\mathcal{H}_{ik} \cong -(E_iE_k)^{\frac{1}{2}} 2fdP_2(\theta)\,|_{ik} \quad (30)$$

where f is now a reasonable average value for the shell in question.

The plausibility of this conjecture has been investigated by a variational calculation of the lowest energy level $E_{\min}$ and corresponding wave function. The wave function was assumed to be of the form $\psi(\mathbf{r}'')$ with $\mathbf{r}''$ defined in terms of $\mathbf{r}$ by Eq. (28); however f was taken

[17] K. Brueckner, Phys. Rev. **97**, 1353 (1955).
[18] M. L. Gursky, Phys. Rev. **98**, 1205(A) (1955).

as a variable parameter. The value of f giving minimum energy is denoted here by f_0.

For example, a particular rounded well shape is provided by the potential $V=ar^2-br^4$, at least for not too large values of r. For this case, the variational calculation gives the value of f_0:

$$f_0=1/2-\gamma/5, \tag{31a}$$

where

$$\gamma=(br^4|_{ii})/(ar^2|_{ii}).$$

On the other hand, the ratio of kinetic to total energy is:

$$f=T/E=\tfrac{1}{2}-\tfrac{1}{4}\gamma \tag{31b}$$

which is only very slightly different from f_0.

The corresponding energy is given by

$$E_{\min}=E^{(0)}[1+ff_0d^2+\cdots]. \tag{32}$$

Another special potential of great interest is the square well with walls of finite height. The approximate effect[2,5] of the finite wall height is to reduce all energies (measured from the bottom) to the values they would have for a box with radius $R_0+\lambda_0$ where

$$\lambda_0=[\hbar^2/(2mV_0)]^{\frac{1}{2}}. \tag{33}$$

A more accurate expression for the energy levels[10] is:

$$E_{V_0,R_0}=\epsilon\left\{1-\left(1+\frac{\lambda_0}{R_0}\right)^{-1}\left(\frac{\lambda_0^2}{3R_0^2}\right)\times\left[\frac{2mR_0^2\epsilon}{\hbar^2}-l(l+1)\right]\right\}, \tag{34}$$

where

$$\epsilon=E_{\infty,R_0}(1+\lambda_0/R_0)^{-2}.$$

The energy levels of a spheroidal well with walls of finite height V_0 might then be expected to be close to those of a spheroidal box whose "radius" is larger by λ_0, in other words, of a spheroid with axes: $R_0D+\lambda_0$, $R_0D^{-\frac{1}{2}}+\lambda_0$, $R_0D^{-\frac{1}{2}}+\lambda_0$. In this way, one can obtain approximately the same results as those resulting from application of Eqs. (28)–(30), particularly for tightly bound states.

For a square well, a good approximation to the ratio f is given by

$$f=\frac{\alpha R_0}{\alpha R_0+1}+\frac{l(l+1)}{2(\alpha R_0+1)^3}, \tag{35}$$

where

$$\alpha=[2m(V_0-E)/\hbar^2]^{\frac{1}{2}}.$$

V. SOME APPLICATIONS TO NUCLEAR STRUCTURE AND CONCLUSIONS

The results of the above calculations can be used to estimate the total relative energy of a given number of particles in an elastic well as function of deformation. Although the approximations made here are extreme, it is hoped that some qualitative trends are given correctly. Considering for simplicity only identical nucleons, Fig. 3 shows the total energies as function of deformation for the energetically most favored configuration of 20, 22, 24, 26, and 28 particles. The results are in general agreement with previous calculations[1,2,6] except for the favoring of a prolate shape for the half-filled shell at 24 particles. This is a consequence of the repulsion of the $1f\,7/2(1/2)$ state [the $m=\pm\frac{1}{2}$ substate of the $1f_{7/2}$ shell] by higher-lying states, such as $2p\,3/2(1/2)$ while the $1f\,7/2(7/2)$ state is not pushed downward.

The calculated restoring energies depend somewhat on the model chosen, but are much larger, even by as much as an order of magnitude, than the values calculated with the hydrodynamical model. One important reason for this is that for light and medium nuclei crossing of particle levels is not very extensive.

Consider, for example, the nucleus $_{22}\mathrm{Ti}^{44}$. According to the "box model," the most favored deformation $d_{\min}$ is -0.05 corresponding to the complete filling of the $m=\pm 7/2$ substates of $1f_{7/2}$ shell. For a more realistic well of finite depth, $d_{\min}\approx-0.07(f\approx 0.8)$. On the other hand, the hydrodynamical model gives $d_{\min}\approx-0.4$. To make this estimate, the hydrodynamical

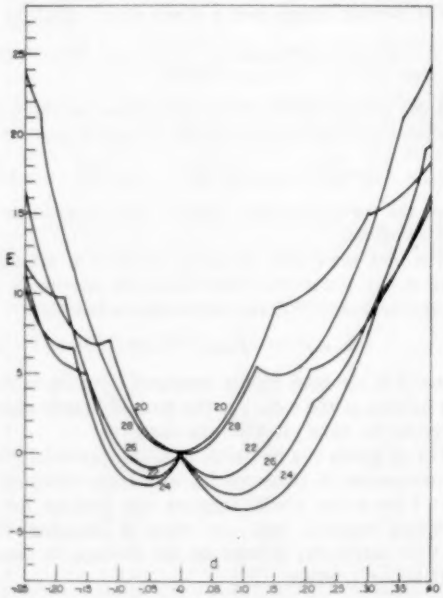

FIG. 3. Total energy as function of deformation for various numbers of identical $f_{7/2}$ particles (plus core of 20 particles) in a spheroidal box. For odd-particle numbers the energies can be obtained by linear interpolation.

[10] For loosely bound states ($V_0-E<0.25V_0$) the "3" in the denominator of Eq. (34) should be replaced by a "2." Equation (34), with this modification when appropriate, gives values of E within 0.1 to 1% of the exact values.

restoring energy was assumed to be given by[20]:

$$19A^{\frac{1}{3}}\times 0.4\delta^2 - 0.76Z^2A^{-\frac{1}{3}}\times 0.2\delta^2, \qquad (36)$$

and $2E^{(0)}f$ in Eq. (27) was taken as equal 45 Mev.

When much level crossing occurs, the effective restoring energy is reduced considerably[1,2] and large deformations can occur. This situation is very probably realized for nuclei with A between 155 and 185 and above 225.

Figure 4 shows calculated equilibrium deformations plotted against numbers of particles. The magnitudes and general trends of deformations calculated with this model seem to agree at least qualitatively with experimental values. The tendency for positive quadrupole moments indicated by Fig. 4 may be significant. Such a trend exists throughout the range of nuclei.[21] For the lighter nuclei, for which the order of particle levels predicted by a box potential is essentially correct, this trend results from the lowering of the $1d\ 5/2(1/2)$, $1f\ 7/2(1/2)$, and $1f\ 7/2(3/2)$ states due to the strong interaction with other states of the same m.

For heavier nuclei, the order of particle levels is significantly different from that in a box, so that no definite conclusions can be drawn on basis of a box model. However, in the hydrodynamical limit, part of the restoring energy is proportional to the surface area[1,2] and this tends to favor positive quadrupole moments.[21] In addition, the Coulomb effect, which also favors positive quadrupole moments, becomes important.

The above calculations show the effect of one important feature of nuclear structure, the deviation of the nuclear potential from sphericity. To obtain detailed agreement with nuclear data; e.g., ground state spins, one must, of course, consider also the direct interactions between extra-core particles. Even if these are treated by themselves, without any core deformation, it is possible to obtain remarkable agreement with experimental data[22–26] for some of the light nuclei near

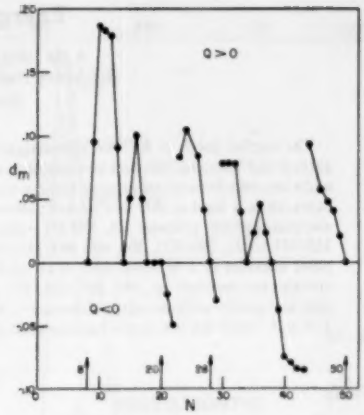

FIG. 4. Energetically favored deformations of a spheroidal box with elastic walls, as function of the number of identical particles.

double magic nuclei He^4, O^{16}, and Ca^{40}. Then also the time dependence and quantization of the nuclear distortion must be properly taken into account. This can be readily done for a hydrodynamical model.[1,27–30] In this way, some of the most striking features of nuclear states, such as energy spacings between rotational states for nuclei far away from magic numbers can be accounted for.[1] However, the absolute values of these energies appear to be considerably smaller than the hydrodynamic values deduced from known deformations.[31] Some studies of this problem on basis of the shell model have recently been made.[32,33]

ACKNOWLEDGMENTS

The author would like to thank Dr. M. Melkanoff for his untiring help with the matrix diagonalizations and Mr. J. Winocur for numerical calculations. He would also like to thank Dr. B. H. Flowers for some stimulating discussions.

[20] See A. Green, *Nuclear Physics* (McGraw-Hill Book Company, Inc., New York, 1955), Chaps. 8 and 9.
[21] S. A. Moszkowski and C. H. Townes, Phys. Rev. **93**, 306 (1954).
[22] D. Inglis, Revs. Modern Phys. **25**, 390 (1953).
[23] A. M. Lane, Phys. Rev. **92**, 839 (1953).
[24] J. P. Elliott and B. H. Flowers, Proc. Roy. Soc. (London) (to be published).
[25] M. Redlich, Phys. Rev. **98**, 199 (1955).
[26] 26. C. Levinson and K. Ford, Phys. Rev. (to be published).
[27] A. Bohr, *Rotational States of Atomic Nuclei* (Munksgaards Forlag, Copenhagen, 1954).
[28] A. K. Kerman, Phys. Rev. **92**, 1176 (1953).
[29] F. J. Milford, Phys. Rev. **93**, 1297 (1954).
[30] D. C. Choudhury, Kgl. Danske Videnskab. Selskab, Mat.-fys. Medd. **28**, No. 4 (1954).
[31] K. W. Ford, Phys. Rev. **95**, 1250 (1954).
[32] D. R. Inglis, Phys. Rev. **96**, 1059 (1954); **97**, 701 (1955).
[33] R. J. Blin-Stoyle (to be published).

Energy Levels of As^{75}†*

A. W. SCHARDT‡ AND JOAN P. WELKER
Brookhaven National Laboratory, Upton, New York

(Received April 12, 1955)

The excited levels of As^{75} were investigated by studying the decay schemes of Se^{75} and Ge^{75}. Beta- and gamma-ray energies, internal conversion coefficients and relative transition intensities were measured. In addition, coincidence and gamma-gamma directional correlation experiments were performed. Se^{75} electron-captures to a level at 402 kev in As^{75}; eleven transitions of indicated energy and multipolarity follow the electron-capture process: 25, 66($M1+E2$), 81, 97($E2$), 121($M1+E2$), 136($M1+E2$), 199($M1+E2$), 265($M1+E2$), 280($E2$), 305, and 402($M1$) kev. Ge^{75} decays by emission of negative beta groups with end-point energies of 1.19, 0.98, 0.92, 0.72, and 0.55 Mev. Subsequently, six gamma rays with the following energies are emitted: 66, 199, 265, 427, 477, and 628 kev. A level scheme for As^{75} is proposed and plausible spin and parity assignments are discussed. The evidence indicates that most of the levels of As^{75} have spin 1/2 or 3/2 and are not single-particle shell-model states.

INTRODUCTION

A NUMBER of levels of As^{75} have been found at rather low excitation energies.[1] For instance, Jensen *et al.*[2] postulate the existence of six levels below 402 kev in order to account for the gamma spectrum of a Se^{75} source. Since such close level spacing cannot be explained in terms of the single-particle shell model, core deformation has to be assumed. At arsenic the $3p_{3/2}$ and $4f_{5/2}$ proton subshells and the $3p_{1/2}$ and $5g_{9/2}$ neutron subshells are being filled.[3] In each case the energy difference between the subshells is very small; therefore, conditions are favorable for the existence of close low-lying levels due to core excitation. The purpose of this investigation is to establish, as far as possible, a definite level scheme with spin and parity assignments and thus gain information as to the neutron-proton configurations of these levels. The disintegration schemes of Se^{75} and Ge^{75} have been investigated repeatedly[1] and a brief summary of some of the published results follows. An attempt is made to emphasize existing discrepancies and deficiencies.

Se^{75} (127 days)[1] decays by electron-capture to one or several excited states of As^{75}. The internal conversion-electron spectrum and the photoelectron spectrum have been measured several times[1] and good agreement exists as to the gamma-ray energies (66, 97, 121, 136, 199, 265, 280, 305, and 402 kev). However, Cork *et al.*[4] observed internal conversion-electron lines from gamma rays of energies 24.7 and 80.8 kev though no evidence for these transitions was found by other investigators.[2,5] On the other hand, a strong 76.6-kev gamma ray, which was not seen by Cork *et al.*, has been reported.[2,5] Jensen and co-workers[2] have proposed a decay scheme for Se^{75} based on gamma-ray energies, approximate transition intensities and some preliminary coincidence observations with G.M. tubes. The level scheme proposed by Cork *et al.* on the basis of gamma-ray energies differs from that of Jensen and co-workers because the 24.7- and 80.8-kev transitions are included. Temmer and Heydenburg[6] induced by Coulomb excitation transitions of 68, 199, and 283 kev with relative yields of 0.02, 0.4, and 0.3, respectively. Only Cork's disintegration scheme is consistent with the Coulomb excitation results.[7]

To date no decay scheme has been proposed for Ge^{75} (80 min).[1] Smith *et al.*[8] found two negative beta groups having end-point energies and relative abundances of 1.137 Mev (85 percent) and 0.614 Mev (15 percent). The 1.137-Mev beta group decays to the ground state of As^{75} since no 1.137-Mev beta, gamma coincidences could be found. Internal conversion-electron lines at 408 and ~520 kev were seen superimposed on the beta spectra. The electron spectrum from a uranium converter was investigated and a photoelectric line from a 265-kev gamma ray, together with Compton electrons from a transition at ~600 kev, were observed. Weak gamma rays at 418 and 572 kev, in addition to the 265-kev line, were seen on a scintillation spectrometer. A 250-kev gamma ray, approximately 10 percent abundant, was observed by Reynolds.[9] This gamma-ray energy was obtained by aluminum absorption measurements and therefore it is not surprising that weaker lines were missed. The

† Work performed under the auspices of the U. S. Atomic Energy Commission.

* A preliminary report of this work was presented to the American Physical Society at the Chicago Meeting, November, 1953 and appears in Phys. Rev. **93**, 916 (1954).

‡ Now at Los Alamos Scientific Laboratory, Los Alamos, New Mexico.

[1] See Hollander, Perlman, and Seaborg, "Table of Isotopes," Revs. Modern Phys. **25**, 469 (1953).

[2] Jensen, Laslett, Martin, Hughes, and Pratt, Phys. Rev. **90**, 557 (1953).

[3] P. F. A. Klinkenberg, Revs. Modern Phys. **24**, 63 (1952).

[4] Cork, Rutledge, Branyan, Stoddard, and LeBlanc, Phys. Rev. **79**, 889 (1950).

[5] Ter-Pogossian, Robinson, and Cook, Phys. Rev. **75**, 995 (1949).

[6] G. M. Temmer and N. P. Heydenburg, Phys. Rev. **93**, 351 (1954).

[7] Since the completion of this manuscript Lu, Kelly, and Wiedenbeck published [Phys. Rev. **97**, 139 (1955)] a decay scheme for Se^{75} based on an investigation of the normal and "summed" gamma-ray spectra. The scheme proposed by these authors is a compromise between the schemes of Jensen *et al.* and Cork *et al.* and includes a 77-kev transition of appreciable intensity.

[8] Smith, Caird, and Mitchell, Phys. Rev. **88**, 150 (1952).

[9] S. A. Reynolds (private communication).

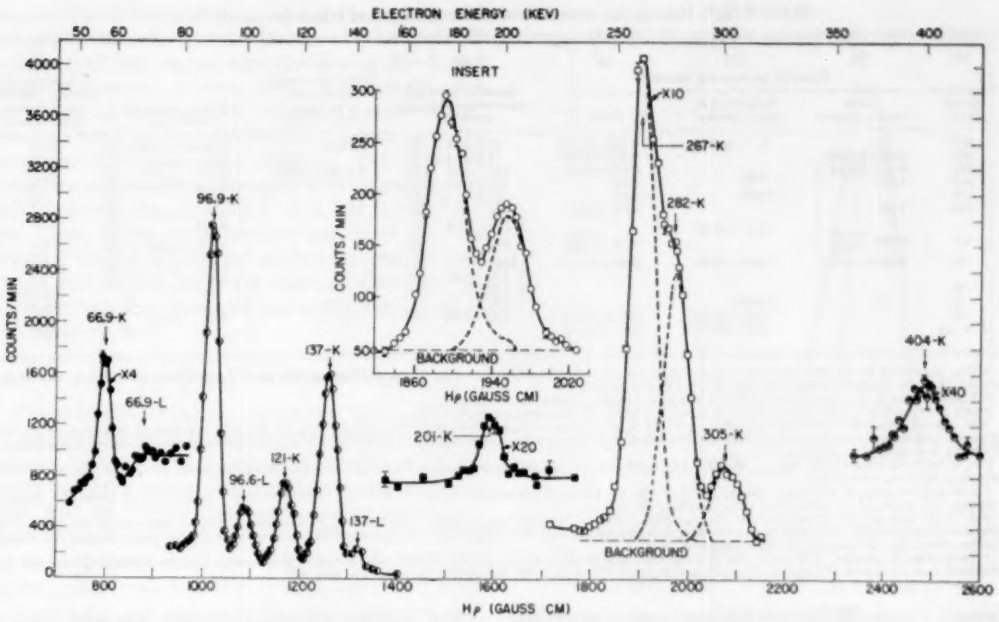

FIG. 1. Internal conversion-electron spectrum from a 0.5-mg/cm² Se^{75} source. Both G.M. counters were used and the data internormalized. Different scale factors are used for various portions of the curve. Dashed curves represent Gaussian distributions fitted to individual photopeaks. The Insert was obtained using 2.4 percent resolution.

difference in end-point energies of the two beta groups observed by Smith *et al.* points to the existence of an As^{75} level at 523 kev. No single gamma ray or gamma-gamma cascade of sufficient intensity to account for the decay of this level has been reported.

EXPERIMENTAL PROCEDURES AND RESULTS

Source Preparation

The Se^{75} sources were prepared by irradiating natural metallic selenium[10] with slow neutrons.[11] The other selenium activities made on slow-neutron irradiation are short-lived[1] with the exception of Se^{79}; a negligible amount of this activity is produced because of the relatively small capture cross section of Se^{78} and the long half-life ($\lesssim 6.5\times10^4$ years)[1] of Se^{79}. No radiochemical purification of the irradiated material from nonisotopic activities was necessary. When thin, uniform sources were required the activity was distilled in vacuum onto a cold finger covered with an aluminum foil of suitable thickness.

An additional Se^{75} source was made by bombardment of germanium with 40-Mev α particles. The selenium plus arsenic activities were isolated by a distillation procedure,[12] several milligrams of selenium carrier were added and metallic selenium was precipitated several times in the presence of arsenic hold-back carrier. The gamma-ray spectrum of this Se^{75} source, as seen on a scintillation counter, was identical with that of the pile-irradiated sources.

The Ge^{75} sources were prepared by irradiating germanium dioxide powder[13] with slow neutrons. Irradiation times were of the order of minutes and the sources were used only during the first half-life of Ge^{75}. When the radiations from sources enriched and nonenriched in Ge^{74} were compared on a scintillation spectrometer no significant differences were observed. Small amounts of nonisotopic activities such as Na^{24} were present in all sources used. When beta sources were required, the germanium dioxide powder was spread onto a thin cellophane backing and covered with 1 percent Zapon.

Conversion-Electron Spectra of Se^{75}

In order to obtain conversion-coefficient data on which to base multipolarity assignments, the relative intensities of both the internal and external conversion-electron lines from a Se^{75} source were determined. The measurements were made on a conventional magnetic lens spectrometer set for a momentum resolution of 3.2

[10] The selenium metal was purchased from the Johnson Matthey Company.

[11] The authors are indebted to the Metals Testing Reactor group for producing a sample of high specific activity.

[12] J. Irvine, J. Phys. Chem. **46**, 910 (1942).

[13] The nonenriched germanium dioxide was purchased from the Johnson Matthey Company. Germanium dioxide enriched in Ge^{74} (95.8 percent) was supplied by the Y-12 plant, Carbide and Carbon Corporation, through the Isotopes Division, U. S. Atomic Energy Commission, Oak Ridge, Tennessee.

TABLE I. Se^{75}: Gamma-ray, internal conversion-electron and transition intensities.

(1) Transition energy (kev)	(2) Relative gamma-ray intensity: Lens spectrometer[a]	(3) Relative gamma-ray intensity: Scintillation spectrometer	(4) Relative gamma-ray intensity: Final	(5) Relative internal conversion-electron intensity[c]	(6) Total conversion coefficient, scintillation spectrometer	(7) Final conversion coefficient[e,c]	(8) Transition intensity, percent of Se^{75} disintegrations[f]
402		0.17 ±0.02	0.248 ±0.025	13.3 ± 1.5 (*K*)	0.00243	0.0024 ±0.0005 (*K*)	14.0
305	0.020 ±0.005		0.020 ±0.005	14.5 ± 1.2 (*K*)		0.03 ±0.01 (*K*)	1.2
280	0.457 ±0.04	1.00	0.457 ±0.04	197 ±20 (*K*)	0.0186 ±0.005	0.019 ±0.005 (*K*)	26.2
265	1.00		1.00	369 ±30 (*K*)		0.016 ±0.005 (*K*)	57.0
199		~0.02	~0.03	23.5 ± 2.5 (*K*)		~0.03 (*K*)	1.8
136	1.00	0.84 ±0.09	0.94 ±0.12	1550 (*K*)		0.07 ±0.02 (*K*)	56.7
				190 ±20 (*L*)		0.009 (*L*)	
121	0.301 $^{+0.08}_{-0.02}$		0.28 $^{+0.06}_{-0.03}$	640 (*K*)		0.10 ±0.03 (*K*)	17.3
97	0.052 ±0.016	0.045 ±0.01	0.066 ±0.015	2640 (*K*)		1.8 ±0.8 (*K*)	11.5
				430 ±50 (*L*)		0.3 (*L*)	
81				~30[d] (*K*)			~0.13[d]
77		≤0.002		<30			≤0.2[g]
66		0.012 ±0.007	0.018 ±0.01	250 ±30 (*K*)		0.6 ±0.3 (*K*)	1.6
K x-ray		0.55 ±0.08[b]	0.81 ±0.12				80[h]

[a] The intensities of the 305- and 280-kev gamma rays are reported relative to that of the 265-kev gamma ray; the intensities of the 121- and 97-kev gamma rays are reported relative to that of the 136-kev gamma ray.
[b] The intensity of *K* x-rays relative to 121-kev plus 136-kev quanta was measured.
[c] (*K*) or (*L*) refers to the electron shell of arsenic in which the conversion occurs.
[d] It was estimated from the photographic record of a permanent magnet spectrograph experiment that 81(*K*)/66(*L*) is slightly less than unity. The intensity values were then calculated using the theoretical *K*/*L* value of the 66-kev transition (reference 39) and the theoretical *E*2 *K*-conversion coefficient of the 81-kev transition (reference 21).
[e] In order to calculate these final coefficients, the total conversion coefficients measured with the scintillation spectrometer were corrected for the contribution due to *L* conversion.
[f] Taking into account the decay scheme given in Fig. 11, the total disintegration rate of Se^{75} was calculated from the gamma-ray intensities [data of column (4)] corrected for conversion using column (7).
[g] A 77 (*K*) line was not present in the photographic record of the permanent magnet spectrograph experiment. Using a conservative estimate of the minimum line intensity detectable above the film background and the theoretical *E*1 *K*-conversion coefficient (reference 21), an upper limit of 0.6 percent can be placed on the intensity of this transition.
[h] To obtain the number of *K* holes, the *K* x-ray intensity has been corrected for the fluorescence yield (57 percent). This fluorescence-yield value was obtained from the curve of Broyles, Thomas, and Haynes, Phys. Rev. **89**, 715 (1953). See also reference 32.

percent. Geiger-Müller counters were used as detectors; one counter had a 0.5-mg/cm² nylon window, the other an approximately 2.0-mg/cm² mica window. Over the range, ~250 to ~400 kev, counter-efficiency corrections for the mica-window counter were measured relative to the thin-window counter. Absorption corrections taken from the curves of Saxon[14] for the 0.5-mg/cm² window were applied; nevertheless, the intensity data for energies below 50 kev are inaccurate. Coincidence loss corrections were made in the usual manner.[15]

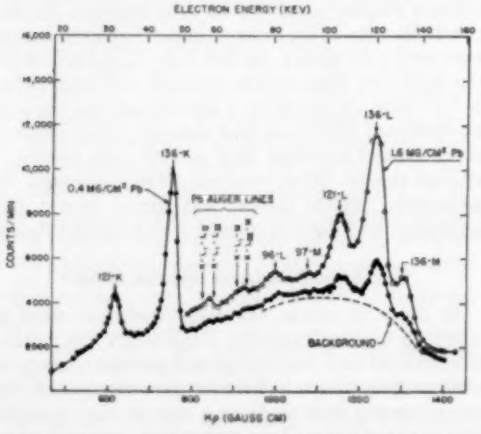

FIG. 2. Photoelectron spectra of Se^{75} obtained with the nylon-window counter. ○ 1.6-mg/cm² lead converter. ● 0.4-mg/cm² lead converter.

[14] D. Saxon, Phys. Rev. **81**, 639 (1951).
[15] G. Friedlander and J. W. Kennedy, *Introduction to Radiochemistry* (John Wiley and Sons, Inc., New York, 1949), p. 213.

The internal conversion-electron spectrum from a 0.5-mg/cm² thick Se^{75} source is shown in Fig. 1 and the relative intensity data are summarized in Table I, column (5). The photoelectron spectra from a Se^{75} source (Figs. 2 and 3) were obtained by using lead converters of suitable thickness. The Compton background curve shown in Fig. 2 was calculated on the assumption that the background is not increased by the presence of the lead converter; in this way, a lower limit for the background was obtained. Maximum values of the background at various points were estimated by interpolation between the count rates on either side of a photopeak. The errors listed in Table I, column (2) were arrived at by considering these extreme background values. The relative intensities of the 265-, 280-, and 305-kev gamma rays were calculated from the ratio of the peak heights of the *K*-conversion lines. Similarly, the relative intensities of the 136-, 121-, and 97-kev gamma rays were obtained from the ratio of the peak heights of the *L*-conversion lines.

Conversion electrons from the 76.7-kev gamma ray found by other investigators[2,5] should appear in the region of the lead Auger lines (Fig. 2). According to the intensities quoted by Jensen *et al.*,[2] the 76.7-kev gamma ray is two-thirds as intense as the 136-kev gamma ray. Therefore, the 76.7−*L* photoelectric line should be more intense than the 136−*L* line. However, the conversion-electron line intensities in this region are completely accounted for by the Auger lines of the lead *K* x-ray series.

The internal conversion spectrum of Se^{75} was also investigated with a 100-gauss permanent magnet spectrograph. Both the *K*-, *L*-, and *M*-conversion lines of a

24.4-kev transition were observed and the experimental energy differences ($K-L=10.23\pm0.15$ kev, $L-M=1.31\pm0.15$ kev) agree with the arsenic $K-L$ and $L-M$ differences. A very weak K-conversion line corresponding to an 81.2-kev transition was also found, but the identification of this line is not definite since the L-conversion line was not observed. The following transition energies were measured with an accuracy of ±0.3 percent: 24.4, 66.3, 81.2, 96.9, 121.1, and 136.1 kev. These results are in excellent agreement with the values of Cork *et al.*[4] The Se^{75} gamma-ray energies used in the rest of this paper are those of Cork and coworkers since they measured accurately the energy of every gamma ray.

Relative Transition Intensities

The relative gamma-ray intensities were measured with a scintillation spectrometer consisting of NaI(Tl) crystals, DuMont 6292 photomultipliers, a Beva 1.5-kev power supply, a nonoverload amplifier[16] with a gain of 1000, and an Atomic Instrument single-channel analyzer. Most of the measurements were made with a 1.5-inch diameter by 1-inch high crystal. The area under a photopeak corrected by a photopeak-efficiency factor is taken as a measure of the gamma-ray intensity. The photopeak efficiency is equal to the product of an intrinsic efficiency factor[17] and a peak-to-total term. The latter was evaluated from measurements of the ratios of the photopeak to Compton-plus-photopeak count rates for sources which emit one gamma ray.[18] The relative intensities of nuclear gamma rays of energy less than 150 kev were measured with a 0.2-cm thick, 2-cm diameter NaI(Tl) crystal. The necessary efficiency factors were calculated for this size crystal. In order to evaluate the count rate in each photopeak, the background due to higher energy transitions has to be subtracted. The intensity of the continuous spectrum accompanying each major transition was evaluated by normalization of the observed pulse-height distribution of a gamma ray of essentially the same energy.[19] Figure 4 serves to illustrate the procedure used. Curve (a) represents the summed Compton contributions from the 402-, 280-, and 265-kev Se^{75} gamma rays. Curves (b) and (c) represent the contributions of the 136- and 121-kev gamma rays, respectively. The latter two curves were obtained by normalization of the Tc^{99m} pulse-height distribution to the 136- and 121-kev photopeaks, respectively. The ratio of the 121- to 136-kev gamma-ray intensities was taken from the lens-spectrometer results. The sum of curves (a), (b), and (c)

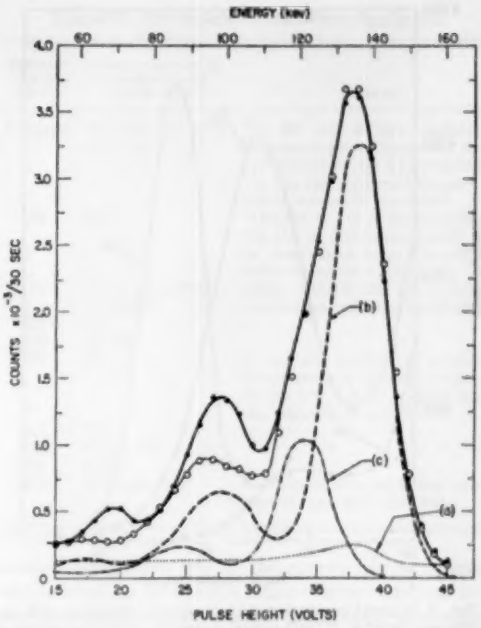

FIG. 4. Gamma-ray pulse-height spectrum from a Se^{75} source 2 cm above a 1.9-mm thick NaI(Tl) crystal. ● Se^{75} source, experimental points; ○ Sum of curves (a), (b), and (c). Curve: (a) Sum of Compton contributions from the 402-, 280-, 265-kev transitions. (b) Contribution of the 136-kev transition. (c) Contribution of the 121-kev transition.

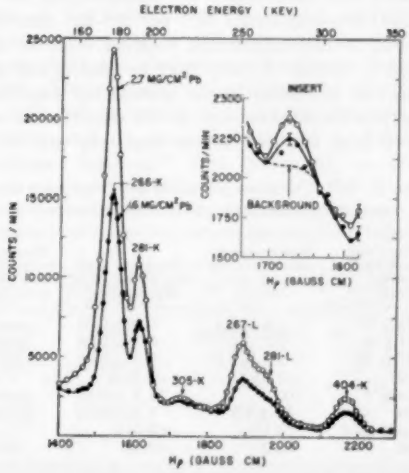

FIG. 3. Photoelectron spectra of Se^{75} obtained with the mica-window counter. ○ 2.7-mg/cm² lead converter. ● 1.6-mg/cm² lead converter. The 305—K line is shown on an enlarged scale in the Insert.

[16] W. A. Higinbotham, Brookhaven National Laboratory Report BNL 234 (T-36) (unpublished).

[17] The authors are greatly indebted to P. R. Bell for making available to them his graphs of intrinsic efficiency *vs* gamma-ray energy for a 1.5-inch diameter by 1-inch high crystal.

[18] The following gamma-ray sources were used: Tc^{99m} (140 kev), Hg^{203} (279 kev), Cr^{51} (320 kev), Au^{198} (411 kev), Cs^{137} (661 kev).

[19] The pulse-height spectra of the following sources were used: Cs^{137} for the 628-kev Ge^{73} transition; Au^{198} for the 402-kev Se^{75} transition; Hg^{203} for the 280-kev Se^{75}, 265-kev Se^{75} and 265-kev Ge^{73} transitions; Tc^{99m} for the 136- and 121-kev Se^{75} transitions.

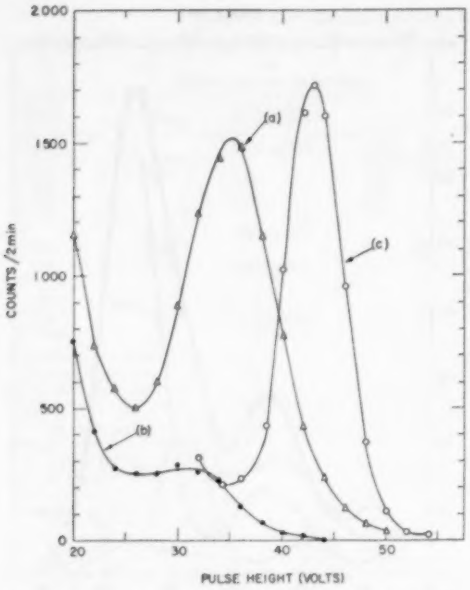

FIG. 5. Internal conversion-electron spectra obtained with an anthracene detector. (a) Se^{75} source, composite conversion-electron line of the 265- plus 280- plus 305-kev transitions. (b) Background to (a) obtained by insertion of an aluminum absorber. (c) Cs^{137} source, conversion-electron line of the 661-kev transition.

then matches the observed Se^{75} spectrum except at the photopeaks of the 97- and 66-kev gamma rays. An additional background at ~64 kev, not shown in Fig. 4, is due to the escape peak of the 98-kev transition; a correction for this effect[20] was applied.

The scintillation-spectrometer measurements of the relative intensities of the Se^{75} gamma rays are summarized in Table I, column (3). The gamma-ray intensities [column (2)] obtained from the lead *L*-conversion lines were normalized to those obtained from the lead *K*-conversion lines by use of the scintillation-spectrometer intensity measurements [column (3)]. The final gamma-ray intensities reported in column (4) are given relative to the 265-kev gamma-ray intensity.

The total conversion coefficient of the 402-kev Se^{75} gamma ray and the average of the total conversion coefficients of the 265-, 280-, and 305-kev Se^{75} gamma rays were measured relative to the total conversion coefficient ($\alpha=0.118$)[21] of the 661-kev Cs^{137} transition. The relative intensities of the gamma rays emitted by the two sources were measured with a 1.5-inch diameter by 1-inch high NaI(Tl) crystal. The relative yields of the internal conversion-electron lines (Fig. 5) were obtained using an anthracene scintillator. Unfortunately, some of the conversion electrons are scattered back out of the anthracene crystal and thus do not contribute to the full-energy peak. The fraction of scattered electrons increases with decreasing energy, thus the data of Table I, column (6) may be low. The final conversion coefficients for the Se^{75} gamma rays reported in Table I, column (7) were obtained from the data of columns (4), (5), and (6).

The energies[22] and relative intensities of the gamma rays associated with the decay of Ge^{75} are given in Table II, columns (1) and (2). Positive identification of these gamma rays with the Ge^{75} decay was made on the basis of their half-life together with the results of coincidence experiments described in the next section. Even though some of the Ge^{75} gamma rays are very weak (0.2 percent transition intensity), it was possible to measure their relative intensities. For example, a 10:1 ratio of photopeak to background count rate was obtained for the 628-kev gamma ray. A further difficulty arose because the photolines of the 427- and 477-kev gamma rays are only partially resolved from each other. The relative yields of these two transitions were estimated by fitting Gaussian distributions of the correct peak heights and resolution to the experimental pulse-height distribution. Unfortunately, this analysis is subject to errors due to the possible presence at the same pulse height of other weak photopeaks which may or may not be associated with Ge^{75}. Since a 402-kev photoline can also not be resolved from the 427-kev photopeak, an upper limit on the branching to the 402-kev level was determined by measurement of the (136, 265)-kev coincidence rate per 265-kev quantum. The result of this experiment, together with the data of Table I, column (3), may then be used to calculate the relative intensities of the gamma-ray transitions arising from the 402-kev level. So few coincidences were observed from the Ge^{75} source that they can be ac-

TABLE II. Ge^{75}: Transition intensities and coincidence data.

(1) Selected event, transition energy (kev)	(2) Gamma-ray intensity relative to 265-kev quanta	(3) Transition intensity, percent of Ge^{75} disintegrations[c,d]	(4) Gamma ray in coincidence with selected event (kev)
628± 5	1.8 ±0.3	0.20±0.03	none
477±10	2.3 ±0.7	0.26±0.08	none
427± 5[a]	2.5 ±0.7	0.28±0.08	199
402[b]	<0.03	<0.0034	···
264± 5	100	11.2 ±0.12	none
199	12 ±1.2	1.35±0.14	427, 66
121 and 136[b]	<0.15	<0.017	···
66	~2.2	~0.38	199

[a] This is the energy of the gamma ray observed in coincidence with the 199-kev transition.
[b] These gamma rays were not observed in the Ge^{75} decay; see text.
[c] The gamma-ray intensity of the 66-kev transition was corrected for the amount of internal conversion. The internal conversion coefficients for the other gamma transitions are at most a few percent.
[d] The results given in this column were obtained by normalizing the data of column (2) by means of the result, 11.2 percent, for the intensity of the 265-kev transition.

[20] P. Axel, Brookhaven National Laboratory Report BNL 271 (T-44) (unpublished).
[21] Rose, Goertzel, Harr, Spinrad, and Strong, Phys. Rev. **83**, 79 (1951); Rose, Goertzel, and Swift, *Low Energy K-Shell Coefficients* (privately circulated tables).

[22] Cs^{137}, Na^{22}, Se^{75}, and Hg^{203} were used as gamma-ray energy standards.

counted for by the presence of a small amount of Na^{24} activity.

The beta-branching ratio to the 265-kev level in As^{75} was determined by measurement of the number of beta, 265-kev gamma coincidences per beta particle. An anthracene scintillator was used to detect the negative beta particles and the bias setting was such that virtually all betas were counted. The absolute detection efficiency of the NaI(Tl) crystal for 265-kev quanta was obtained by means of a coincidence experiment in which the prominent Se^{75} gamma-gamma cascades were employed. The channel widths were sufficiently wide to include the somewhat broad photopeaks of these cascades and it was assumed that the detection efficiencies are the same for the 265- and 280-kev quanta. The fact that the 280-kev level is also populated by the 25-kev transition has no effect on the result. The solid angles subtended by the detectors were large, thus directional correlation effects could be neglected. The beta branching to the 265-kev level is 11.4 ± 1.1 percent of the Ge^{75} disintegrations. The beta-branching ratios to the other levels [Table III, column (4)] were determined from the decay scheme (Fig. 11) and the relative gamma-ray transition intensities.

Identification of Gamma-Gamma and Beta-Gamma Cascades

Coincidence studies were undertaken with both Se^{75} and Ge^{75} sources in order to establish the existence of various gamma-gamma cascades; in addition, the endpoints of the beta groups in coincidence with the different gamma rays of Ge^{75} were measured in order to help establish the level scheme for the excited states of As^{75}. The coincidence investigations were carried out with the previously described scintillation spectrometer used in conjunction with a gray-wedge coincidence analyzer.[23] The photopeak or internal conversion-electron line of the gamma ray of interest was selected by means of a single-channel analyzer and the spectra of electromagnetic radiations, conversion electrons or beta particles in coincidence with it were displayed on the gray-wedge screen. A coincidence resolution time of 10^{-7} sec was used. The geometrical arrangement of the detectors and sources and the nature of the absorbers used were varied to suit the individual experiments. The results obtained for the Ge^{75} and Se^{75} sources are summarized in Table II, column (4) and in Table IV, respectively.

Considerable care has to be taken in interpreting the coincidence results because, in general, pulses due to other gamma rays than the one of interest also fall in the channel of the pulse-selecting detector. For example, with a Se^{75} source it was observed that a broad channel centered at 66 kev (Fig. 4) includes approximately equal numbers of counts due to 66-kev quanta and due to the continuous pulse-height spectra from the 121-, 136-, 265-, and 280-kev quanta. The 136- and 265-kev photopeaks, present in the Se^{75} gamma-ray spectrum (Fig. 6), appear also in the coincidence spectrum obtained by channeling at 66 kev (Fig. 7). The presence of these photopeaks in Fig. 7 is to be expected because of the existence of the (121, 280)-kev and (136, 265)-kev cascades. In addition to the true coincidence peak at 199 kev, peaks at ~30 and ~50 kev were observed (Fig. 7). The ~30-kev peak is attributable to iodine K x-rays which escape from the pulse-selecting detector into the display crystal; the line at ~50 kev is due to a scattering process. In all cases where the possibility of scattering between the de-

TABLE III. Ge^{75}: Beta groups and logft values.

(1) Beta group (kev)	(2) Gamma ray in coincidence with β^- group (kev)	(3) Level in As^{75} (kev)	(4) Fraction of Ge^{75} activity (percent)[b]	(5) logft[d]
1188 ± 20	none	ground state	87	5.2
975 ± 20	199	199	0.69	7.0
919 ± 20	265	265	11.4	5.6
784	···	402	<0.022[c]	>8.1
720^{+20}_{-60}	477	477	0.26	6.9
553[a]	199, 427, 628	628	0.48	6.2

[a] This beta group was not observed directly; however, its existence can be deduced with certainty from the results of experiments involving the 199-, 427-, and 628-kev gamma rays (see Table II).
[b] The results given in this column were calculated using the decay scheme of Fig. 11 and the transition intensities of Table II, column (3).
[c] As beta branching to the 402-kev level was not observed, only an upper limit can be given for the intensity of the 784-kev beta group.
[d] The comparative half-lives were calculated with the aid of the graphs given by S. A. Moszkowski, Phys. Rev. **82**, 35 (1951).

TABLE IV. Se^{75}: Results of coincidence experiments.

Selected event (kev)	Events observed in coincidence with selected event	Remarks
K x-rays	402, 280, 265, 199, 136, 121, 97, 66	The 81- and 305-kev radiations were not observed because of their low intensities; the 25-kev gamma ray was not observed because it is highly internally converted.
66	199	Whether or not other transitions are also in coincidence could not be determined from this coincidence experiment (see text).
97	either 280 or 305, or both(?)	These coincidences are probably real but not positively established.
121	280	
136	66, 265	
199	66	It was not possible to establish the presence or absence of coincidences with 136-kev quanta from this coincidence experiment.
265	136	
280	97(?), 121	
305	97(?)	
402	K x-rays only	No coincidences with any other gamma rays were observed.

[23] The gray-wedge analyzer is described by Bernstein, Chase, and Schardt, Rev. Sci. Instr. **24**, 437 (1953). The specific equipment used in this experiment is described by R. L. Chase, Brookhaven National Laboratory Report BNL 263 (T-42) and by A. W. Schardt, Brookhaven National Laboratory Report BNL 237 (T-37).

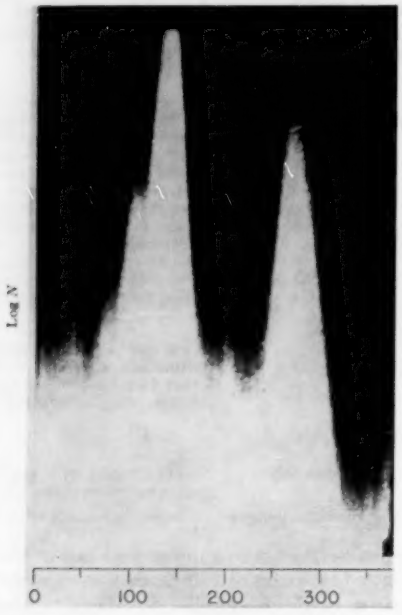

FIG. 6. Gray-wedge analyzer picture of Se^{75} gamma-ray spectrum (0 to 350 kev) as detected by a 3-cm diameter by 2-cm high NaI(Tl) crystal.

tectors existed, great care was taken to identify any spurious peaks produced in this way.

It was readily proven that coincidences exist between Se^{75} quanta included in the 97- plus 121- plus 136-kev composite photopeak and quanta included in the 265- plus 280- plus 305-kev composite photopeak. The existence of the (121, 280)-kev and (136, 265)-kev cascades could also be established since the coincidence rate per channel count depends markedly on which of the gamma rays predominated in the narrow channels used. On the other hand, the results of coincidence experiments involving the 97- and 305-kev radiations were inconclusive because of the low intensities of these transitions. Coincidences between K x-rays and 97-kev quanta were also observed but it was not determined whether these x-rays had their origin in the electron-capture process or whether they resulted from internal conversion of other gamma rays.

The spectra of the beta groups emitted by Ge^{75} were investigated with an anthracene detector. The energy response of anthracene was taken to be linear[24] and the pulse-height scale was calibrated with the 624-kev Cs^{137} and 976-kev Bi^{207} internal conversion-electron lines. The Au^{198} beta spectrum was measured; the experimental beta-endpoint energy, 0.972 Mev, is in good agreement with the accepted value, 0.963 Mev.[1]

[24] J. I. Hopkins, Rev. Sci. Instr. **22**, 29 (1951).

In order to correct the Ge^{75} beta spectra for the effects of crystal resolution and backscattering, correction factors, which were necessary to linearize the Au^{198} Fermi plot, were computed as a function of energy below the endpoint. Figure 8 shows corrected Fermi plots of the composite Ge^{75} spectrum and of the beta spectra in coincidence with the 199-, 265-, and 477-kev gamma rays, respectively. The approximate nature of the applied corrections could account for the fact that the composite beta spectrum [curve (a)] cannot be resolved into its components. Since a considerable fraction of the count rate at the photopeak of the 477-kev gamma ray was due to the Compton background from Na^{24} radiations, spectrum (d) is undoubtedly perturbed by the presence of Na^{24} betas. As no correction could be made for this effect, it is impossible to determine the exact endpoint of spectrum (d). On the other hand, Fermi plots (b) and (c) are not perturbed by the presence of a background spectrum; thus, the difference in endpoint energies, 56 kev, is accurate to ± 20 kev. The beta-group energies and intensities are summarized in Table III.

Lifetime Measurements

The theoretical half-life of the 280-kev transition, which is characterized as $E2$ from the conversion-coefficient (Table VII), is 10^{-8} sec.[25] Similarly, a lifetime might be expected for the decay of the 305-kev level. A knowledge of the actual half-lives of the 265-

FIG. 7. Gray-wedge photograph of the Se^{75} pulse-height spectrum in coincidence with pulses which fall in a channel centered at 66 kev. The photopeak at 265 kev and at least part of the photopeak at 136 kev are due to coincidences with the background pulses on which the 66-kev photoline is superimposed. Different gain settings were used for Figs. 6 and 7.

[25] J. Blatt and V. Weisskopf, *Theoretical Nuclear Physics* (John Wiley and Sons, Inc., New York, 1952), Chap. XII, p. 627.

and 280-kev levels is also desirable in order to decide whether or not the directional correlations of the (136, 265)-kev and (121, 280)-kev Se^{75} cascades can be perturbed by local fields.[26] Previous investigations[27,28] searched for isomeric transitions from a Se^{75} source and found none in the time range, 10^{-5} to 10^{-8} sec.

In the present experiments a fast coincidence circuit[29] of resolving time, $\tau = 2\times10^{-9}$ sec, was used in conjunction with 5819 photomultipliers and stilbene crystals. The coincidence rate between the internal conversion electrons of the 121- plus 136-kev Se^{75} transitions and the internal conversion electrons of the 265- plus 280-kev transitions was measured as a function of time delay over a two-hundred-fold diminution in count rate. It was concluded that both the 265- and 280-kev levels have a half-life which is less than 8×10^{-10} sec. An experiment was also performed in which the pulse-height selectors were set so that an appreciable fraction of the observed coincidence rate was due to coincidences between the internal conversion electrons of the 97-kev gamma ray and those of the 280- plus 305-kev transitions. The results indicate that the half-life of the 305-kev level is either shorter than 10^{-9} sec or longer than 5×10^{-8} sec; a half-life greater than the latter figure would not have been observed because of the presence of other coincidences. The multipolarity of the 305-kev gamma ray is therefore not greater than $E2$ unless a half-life longer than 5×10^{-8} sec was missed in the earlier investigations.[27,28]

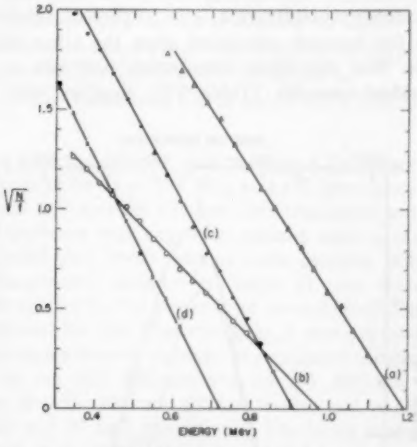

FIG. 8. Corrected Fermi plots of Ge^{75} beta spectra. (a) △ Composite beta spectrum. (b) ○ Beta spectrum in coincidence with 199-kev gamma rays. (c) ● Beta spectrum in coincidence with 265-kev gamma rays. (d) × Beta spectrum in coincidence with 477-kev gamma rays.

[26] H. Frauenfelder, Ann. Rev. Nuc. Sci. **2**, 129 (1953).
[27] S. DeBenedetti and F. K. McGowan, Phys. Rev. **74**, 728 (1948).
[28] F. K. McGowan, Oak Ridge National Laboratory Report ORNL 952 (unpublished).
[29] The authors are greatly indebted to Mr. R. L. Chase for designing and testing this circuit.

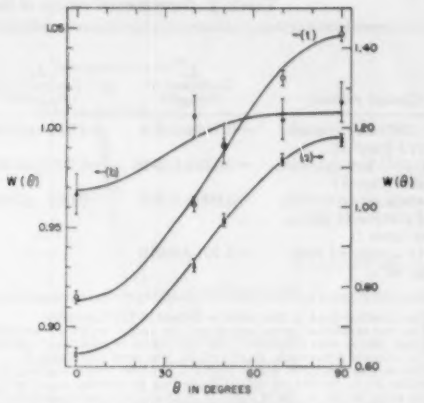

FIG. 9. Experimental directional distributions. The experimental values were normalized by dividing by a_0 (Table V). Each curve represents a least-squares fit to the data. Curve (a) and the × points refer to case *a*, Table V. Curve (b) and the ● points refer to case *b*. Curve (t) and the ○ points refer to case *t*. The arrows refer to the ordinate scale.

Gamma-Gamma Directional Correlation Studies

The directional correlations of the (121, 280)-kev and (136, 265)-kev Se^{75} cascades were investigated in order to obtain further information about the multipolarities of these gamma-ray transitions and the spins of the levels involved. The apparatus used for measuring the directional correlations has been described previously.[30] The gamma rays were detected with NaI(Tl) crystals placed in lead collimators and Atomic Instrument single-channel pulse-height analyzers were used to select the photopeak of the desired gamma ray. A fast (0.1-μsec) coincidence requirement was imposed on the unselected pulses; subsequently, a 5-μsec triple coincidence requirement was imposed on the output pulses of the fast coincidence circuit and the two single-channel analyzers. The sources, which consisted of from 2 to 10 milligrams of irradiated selenium-metal powder, were placed in an aluminum holder. The dimensions of the source holder were minimized in order to reduce perturbations due to scattering effects[26]; the holder had an outside diameter of 0.085 inch and a $\frac{1}{16}$-inch hole, $\frac{3}{8}$ inch deep. Measurements were made at the detector-to-detector angles of θ and 360° minus θ, where θ was given the following values, 90°, 110°, 130°, 140°, and 180°. An equal number of measurements was made at each angle and the results for angles symmetrical with respect to 180° were then averaged. The order of angle coverage was random.

Directional correlation data were obtained using wide channels centered on the composite photopeaks of the 121- plus 136-kev and 265- plus 280-kev gamma rays, respectively. In addition, data were taken with narrow channels set so that either the (121, 280)-kev

[30] J. J. Kraushaar and M. Goldhaber, Phys. Rev. **89**, 1081 (1953).

TABLE V. Experimental results of the directional correlation measurements with Se^{76}.[a]

Channel position	A_2 Coefficient of $P_2(\cos\theta)$[b]	A_4 Coefficient of $P_4(\cos\theta)$[b]	Gamma-ray mixing ratio in channel Detector A 121 kev a_{01}	Detector A 136 kev a_{02}	Detector B 280 kev a_{13}	Detector B 265 kev a_{23}	β[d]	a_0 sec/count $\times 10^{-5}$	(N_1+N_2)[f] counts/sec $\times 10^{-5}$
(121, 280)-kev cascade favored (case *a*)	-0.359 ± 0.014	-0.011 ± 0.014	0.84	0.16	0.68	0.32	25	0.365 ± 0.003[e]	2.31[g]
			0.66[c]	0.34[c]	0.61[c]	0.39[c]	6.7[c]	0.365 ± 0.003[e]	1.79[c,g]
(136, 265)-kev cascade favored (case *b*)	-0.022 ± 0.0095	-0.0095 ± 0.0095	0.044	0.96	0.10	0.90	0.0113	0.485 ± 0.003	2.60
Channels set to include all of composite photopeaks (case *t*)	-0.090 ± 0.003	0.003 ± 0.003	0.23	0.77	0.32	0.68	0.31	0.440 ± 0.001	2.26
Case *t* computed from Table VI	-0.101 ± 0.019	...	0.23	0.77	0.32	0.68	0.31		

[a] The notation used in this table is defined in the Appendix.
[b] The rms statistical errors are given; the actual errors are somewhat larger. No correction has been applied for the finite resolution of the detectors.
[c] These values were computed from the results of additional coincidence experiments at 180° (refer to Appendix).
[d] To compute β the ratio, $N_2/N_1=2.20$, was used (see Table I).
[e] This a_0 was measured with a source 2.27 ± 0.05 times as strong as the one used for the other experiments.
[f] Either N_1 or N_2 was computed depending on whether $a_{01}a_{13}$ or $a_{02}a_{23}$ is larger; the source strength (N_1+N_2) was then obtained by use of the experimental ratio, $N_2/N_1=2.20$. A value of $(2.57\pm0.26)\times10^{-5}$ counts/sec for (N_1+N_2) was computed from the results of experiments in which the (136, 265)-kev cascade was favored more strongly than in case *b* (see Appendix).
[g] In order to facilitate comparison with the other entries in this column, the actual source strength was divided by 2.27.

or the (136, 265)-kev cascade predominated. The discrimination between cascades was accomplished by channeling on the sloping portions of the composite photolines; as a result the count rate in the channel was very sensitive to small shifts in pulse height. Slow drifts, such as those resulting from variations in room temperature, were compensated for by manually changing the channel position. In order to minimize the effects of erratic, uncompensated drifts, the coincidence rate (after subtraction of the accidental rate) was divided by the product of the channel-count rates (refer Appendix). A complete compensation for these effects is not obtained since a shift in channel position is also accompanied by a change in detection sensitivity for the gamma rays of the two cascades.

In several instances, the rms error was computed from the deviations as a check on the consistency of the data. For example, for the fourteen measurements made at 180° with the channels set to favor the (136, 265)-kev cascade, the rms error computed from the deviations is 7 percent while the statistical rms error on each measurement is 4 percent. These errors are 6.6 and 5.6 percent, respectively, for the same measurements with the channels set to favor the (121, 280)-kev cascade. The results, that the rms error computed from the deviations is always greater than the statistical rms error, is undoubtedly due to uncompensated drift errors.

The curves fitted to the experimental points are shown in Fig. 9 and the coefficients of the Legendre polynomials are given in Table V. The formulas needed to calculate the directional distribution functions of the individual cascades from these coefficients are derived in the Appendix. The ratio of the number of 121- to 136-kev pulses and the ratio of 280- to 265-kev pulses at each channel setting also enter into the calculations. (In future these ratios will be referred to as gamma-ray mixing ratios.) The mixing ratio of two gamma rays in a channel of known width and position can be determined from an analysis of the composite photopeak. For example, Fig. 10 shows the contributions of the 265- and 280-kev gamma-ray pulses; the relative intensities of the individual gamma rays were taken from Table I, column (2). In the case of the distribution measured with the channels set to favor the (121, 280)-kev cascade, the gamma-ray mixing ratios could also be evaluated from the results of some additional coincidence experiments (see Appendix). The directional correlation function for the (121, 280)-kev cascade, computed with the mixing ratios obtained from the coincidence measurements, is in 10 percent agreement with the function calculated using the other mixing ratios. The directional distribution functions of the individual cascades (Table VI), together with the

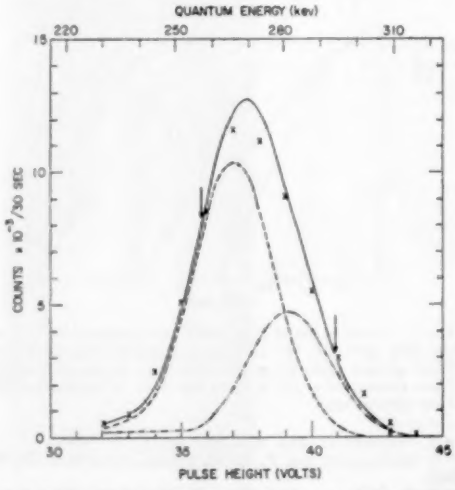

FIG. 10. Composite photopeak of the 265- plus 280-kev gamma rays. × represent experimental points, ↓ designate centers of two-volt channels.

gamma-ray intensity ratios obtained with the lens spectrometer, can be used to calculate the directional correlation to be expected if the entire composite photopeaks are included in the channels. The agreement with the experimental distribution is satisfactory (Table V).

It should be noted that the final directional correlation coefficients listed in Table VI have been corrected for the finite angular resolution of the detectors.[21] The solid angle subtended by the detectors was determined by measuring the coincidence rate of annihilation quanta as a function of angle; the resulting angular resolution curve exhibited a half-width at half-maximum of 10.5°.

DISCUSSION AND INTERPRETATION OF RESULTS

A level scheme (Fig. 11) for As^{75} can be constructed on the basis of the data presented. The level arrangement is identical with that proposed by Cork and co-workers[4] except for the addition of levels at 477 and 628 kev. The endpoints of the beta groups in coincidence with the different gamma rays of Ge^{75} show the existence of levels at 199, 265, and 477 kev. Since the 402-kev Se^{75} and the 628-kev Ge^{75} transitions are not in coincidence with any other gamma rays, it can be concluded that levels exist at these energies. All the gamma-gamma cascades of Table IV can then be accounted for by the presence of two additional levels at 280 and 305 kev. Unfortunately, it was not possible to determine directly the order of emission of the gamma rays of the (121, 280)-kev and the (97, 305)-kev cascades, thus the 280- and 305-kev levels could be placed at 121 and 97 kev, respectively. The latter scheme is unlikely since neither the 121- nor 97-kev gamma rays are excited by Coulomb excitation.[6] If the 121- and 97-kev transitions are not Coulomb excited and represent transitions to the ground state of As^{75}, then they would have to be pure magnetic multipoles. However, the conversion coefficient of the 121-kev gamma ray (Table VII) shows that this transition has a large $E2$ component. The 97-kev gamma ray, on the basis of its conversion coefficient, could be designated as a pure $M2$ with an expected half-life of $\sim 10^{-4}$ sec[35] but the fact that K x-ray, 97-kev coincidences were observed is incompatible with such an assignment. The 81-kev transition can also be included in the proposed scheme without postulating the existence of a new level. It should be noted that the measured transition intensities are consistent with the assumption that Se^{75} decays only to the 402-kev level. However, electron capture to other excited levels, amounting to as much as 10 percent of the Se^{75} decay, cannot be ruled out on the basis of the results presented in Table I. Similarly, an upper limit of 20 percent[22] can be placed on the electron-capture branching to the ground state of As^{75}.§

Plausible spins and parities can be assigned to the excited levels of As^{75} by means of logft evidence and gamma-ray multipolarities provided the ground-state spins and parities of As^{75}, Se^{75}, and Ge^{75} are known. The As^{75} ground-state configuration is $p_{3/2}$.[3] A spin of 5/2 has been measured for Se^{75},[33] but the parity has not as yet been determined. This 5/2 spin would not be expected from the shell model since the Ge^{75} nucleus,

TABLE VI. Directional correlation coefficients of the (121, 280)-kev and (136, 265)-kev cascades.

Cascade	A_2[a]	A_4[a]
(121, 280)-kev	-0.40 ± 0.03 -0.44[b]	-0.014 ± 0.017
(136, 265)-kev	$-0.019^{+0.01}_{-0.02}$[c]	-0.012 ± 0.012

[a] A correction of 7 percent to A_2 and 21 percent to A_4 has been made to take into account the finite angular resolution of the detectors. The indicated errors represent an attempt at estimating the accuracy of the coefficients.
[b] This value was obtained by use of the mixing ratios computed from the results of additional coincidence measurements made at 180°. These mixing-ratio values are given in Table V [see reference (c)].
[c] In subtracting the contribution of the (121, 280)-kev cascade its effect may have been underestimated; thus, the negative error is larger than the positive.

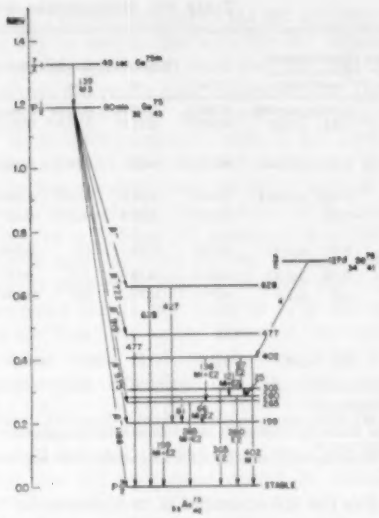

FIG. 11. Level scheme of As^{75}. Level and transition energies are given in kev.

[21] E. L. Church and J. J. Kraushaar, Phys. Rev. **88**, 419 (1952).

[22] The K-hole yield of Table I must be corrected for the number of K holes (~23 percent) produced by internal conversion of the gamma rays. A correction for the amount of L-electron capture is also necessary; the L/K electron-capture probability is 10 percent according to M. E. Rose and J. L. Jackson, Phys. Rev. **76**, 1540 (1949). The K x-ray yield is, however, insufficient to account for the transition intensities

§ *Note added in proof.*—The presence of a 280-kev photopeak in the "summed" spectrum[7] is compatible with the decay scheme of Fig. 11 since both the 97- and 25-kev transitions are highly converted. The pronounced 97-kev photopeak in the "summed" spectrum can be explained if the 305-kev level is an isomeric state. Unfortunately, this interpretation is in disagreement with the experimental results of De Benedetti and McGowan.[37]

[33] Aamodt, Fletcher, Silvey, and Townes, Phys. Rev. **94**, 789 (1954); L. C. Aamodt and P. C. Fletcher, Phys. Rev. **98**, 1224 (1955).

TABLE VII. Multipolarities of the gamma rays associated with the decay of Se^{75}.

Transition energy (kev)	Experimental K-conversion coefficient	Theoretical K-conversion coefficients[a] α_1	α_2	α_3	β_1	β_2	β_3	Multipolarity[b]	$\lvert\delta\rvert = (E2/M1)^{\frac{1}{2}}$	Remarks
402	0.0024 ±0.0005	0.0012	0.0044	0.015	0.0023	0.0084	0.028	$M1$		
305	0.03 ±0.01	0.0025	0.0115	0.045	0.0045	0.019	0.077	$E2$		Higher order transition improbable because of competition with 25-kev transition.
280	0.019 ±0.005	0.00334	0.016	0.067	0.0057	0.026	0.11	$E2$	≥ 2	$M3$ admixture impossible since $t_{\frac{1}{2}} < 8\times10^{-10}$ sec.
265	0.016 ±0.005	0.0037	0.019	0.080	0.0064	0.030	0.13	$M1+E2$	$2.0^{+\infty}_{-1.2}$	This transition can be Coulomb excited.[c]
199	~0.03	0.0079	0.050	0.25	0.13	0.072	0.39	$M1+E2$		This transition can be Coulomb excited.[c]
136	0.07 ±0.02	0.026	0.23	1.5	0.036	0.27	2.1	$M1+E2$	$0.49^{+0.18}_{-0.21}$	
121	0.10 ±0.03	0.034	0.35	2.3	0.048	0.42	3.5	$M1+E2$	$0.45^{+0.14}_{-0.17}$	
97	1.8 ±0.8	0.073	0.77	6.4	0.090	0.97	9.4	$E2$		Higher order admixture or $M2$ impossible because of competition with 402-, 136-, 121-kev gamma rays. K/L ratio compatible with $E2$.[d]
66	0.6 ±0.3	0.21	2.8	40	0.27	3.7	50	$M1$ or $M1+E2$		

[a] See reference 21.
[b] $E1+M2$ admixtures were not considered because such transitions are highly improbable. The multipolarity assignments given are based on the K-conversion coefficient evidence in conjunction with the arguments listed under "Remarks."
[c] See reference 6.
[d] The theoretical K/L ratio for $E2$ is 4.5 (reference 39) and the experimental value is 6 (Table I).

which has the same number of neutrons as Se^{75}, has a $g_{9/2}$ ground-state configuration.[3] However, the 13.5-kev first excited level of Ge^{73} is probably a $(g_{9/2})^3$ state with a spin and parity of $5/2+$.[34] It is conceivable that the addition of two protons to the Ge^{73} nucleus stabilizes the $(g_{9/2})^3$ over the $g_{9/2}$ configuration. The even-parity assignment to the ground state of Se^{75} is also supported by logft evidence. A lower limit of the logft value for the decay of Se^{75} to the As^{75} ground state was calculated on the basis of an energy-difference figure of 894±5 kev [35] and a maximum transition intensity of 20 percent. The logft value, ≥ 7.3, is consistent with a parity forbidden transition.[36] The ground-state configuration of Ge^{75} is expected to be $p_{1/2}$ from shell theory considerations[3] as this nucleus contains the same number of neutrons as Se^{77}. Other evidence also supports this $p_{1/2}$ assignment. The existence of an isomeric state of Ge^{75} at 139 kev has been reported.[8,37,38] The K-conversion coefficient value for the 139-kev gamma ray (~ 2)[37] is only consistent with an $E3$ or $M3$ transition.[21] However, the K/L ratio (~ 3)[38] and the half-life (49 sec) are only compatible with an $E3$ assignment.[25,39] Again by analogy with Se^{77},[40] an $E3$ transition between a $7/2+$ and a $p_{1/2}$ level is to be expected. The logft value, 5.2, for the Ge^{75} beta decay to the $p_{3/2}$ ground state of As^{75} supports the fact that $p_{1/2}$ and not $7/2+$, is the ground-state configuration of Ge^{75}.

The logft value [Table III, column (5)] and the gamma-ray multipolarities assigned with the aid of K-conversion coefficients (Table VII) form a basis for the following discussion of spins and parities. The logft values for the Ge^{75} beta transitions indicate that the 199-, 265-, 477-, and 628-kev levels have spins of either $1/2$ or $3/2$. In addition, the logft value (6.2) for the electron-capture decay of Se^{75} to the 402-kev level shows that this level must have either a $7/2$, $5/2$ or $3/2$ spin. However, the choice is limited to $5/2-$ or $3/2-$ since the 402-kev gamma ray proceeds to the $p_{3/2}$ ground state of As^{75} by means of an $M1$-type transition. The $M1+E2$ character of the 199- and 265-kev ground-state radiations indicates that these levels also have negative parity. The spin and parity assignments made so far are consistent with the multipolarities given in Table VII for the 66- and 136-kev transitions. An $E2$ rather than an $M2$ multipolarity was chosen for the 97-kev transition because the theoretical 97-kev $M2$-transition probability is too small[25] to explain the competition with the other gamma rays which proceed from the 402-kev level.[41] Since the 305- and 97-kev gamma rays are in cascade, the 305-kev level must have negative parity if the 97-kev radiation is $E2$. Therefore, $E2$ is the most likely multipolarity for the 305-kev gamma ray. The experimental K-conversion coefficients for the 97- and 305-kev transitions are, however, considerably larger then the theoretical $E2$ values. Unfortunately, the conversion-coefficient measurements for the 97- and 305-kev radiations are the least accurate and the errors given in Table I may be too optimistic.

It is difficult without additional evidence to arrive at more definite spin and parity assignments since detailed arguments based on logft values and relative transition probabilities are of doubtful value when

[34] Welker, Schardt, Friedlander, and Howland, Phys. Rev. **92**, 401 (1953).
[35] C. C. Trail and C. H. Johnson, Phys. Rev. **91**, 474 (1953).
[36] Mayer, Moszkowski, and Nordheim, Revs. Modern Phys. **23**, 315 (1951); L. W. Nordheim, Revs. Modern Phys. **23**, 322 (1951).
[37] A. Flammersfeld, Z. Naturforsch. **7a**, 295 (1952).
[38] Burson, Jordan, and LeBlanc, Phys. Rev. **96**, 1555 (1954).
[39] M. Goldhaber and A. W. Sunyar, Phys. Rev. **83**, 906 (1951).
[40] M. Goldhaber and R. D. Hill, Revs. Modern Phys. **24**, 179 (1952).

[41] A less plausible interpretation would be that the 97-kev transition is pure $M2$ or an $M2+E3$ mixture and proceeds from a level the energy of which is within 1.5 kev of 402 kev. The observed K x-ray, 97-kev coincidences may be due to K x-rays which arise from internal conversion of the 25-kev transition (see Fig. 11).

many of the levels involved are not single-particle states. The directional correlation functions for the (121, 280)-kev and (136, 265)-kev cascades provide a further basis for spin assignments. However, since the K-conversion coefficient results show that the 121-, 136-, and 265-kev gamma rays are $M1+E2$ mixtures, the interpretation of the directional distribution results is in itself complicated.

Theoretical directional correlation distributions can be computed by use of Rose's[42] equations for mixed-gamma, mixed-gamma correlations. For the case where both gamma rays of a cascade are $M1+E2$ mixtures, the general equations can be simplified to give

$$A_2=\frac{(a+b\delta_1+c\delta_1^2)(d+e\delta_2+f\delta_2^2)}{(1+\delta_1^2)(1+\delta_2^2)}, \qquad \text{(I)}$$

$$A_4=\frac{g\delta_1^2\delta_2^2}{(1+\delta_1^2)(1+\delta_2^2)}. \qquad \text{(II)}$$

The capital letters, A_2 and A_4, are the $P_2(\cos\theta)$ and $P_4(\cos\theta)$ coefficients, respectively. The intensity ratio, $E2/M1$, is given by δ^2; subscripts 1 and 2 on δ refer to the first and second gamma rays of a cascade. The lower case letters represent numerical coefficients which are a function of the spin assignments; these coefficients can be evaluated by use of the papers by Rose and Biedenharn.[42,43] Equation (I) can be solved for δ_1 *vs* δ_2 for a given spin sequence and experimental value of A_2. Figures 12 and 13 show plots of δ_1 *vs* δ_2 for spin sequences consistent with the results and assignments discussed earlier in this section.

Since the 265-kev level has a spin of either 3/2 or 1/2, the theoretical value of A_4 from Eq. (II) is zero, in good agreement with the experimental result for the (136, 265)-kev cascade (Table VI). Since the experimental value of A_2 for this cascade is very nearly zero, a 1/2 assignment for the 265-kev level is indicated. However, a spin of 3/2 for this level is also consistent with the experimental correlation data (Fig. 12). Spin assignments of 7/2, 5/2, or 3/2 are possible for the 280-kev level; the existence of an A_2 coefficient eliminates a 1/2 spin. Figure 13 shows plots of δ_1 *vs* δ_2 for the 5/2 and 3/2 cases for both possible spins of the 402-kev level, 5/2 and 3/2. The theoretical directional correlation for the spin sequence, $5/2(M1+E2)7/2(E2)3/2$, is also in agreement with the experimental values for δ_1 (Table VII) and A_2. An $E2+M3$ admixture for the 280-kev transition was not considered, as the measured half-life, $<8\times10^{-10}$ sec, of the 280-kev level is not compatible with such multipole mixing.[25]

A spin assignment of 5/2 for the 402-kev level appears improbable on the basis of the following argument. An examination of the δ_1 *vs* δ_2 plots for sequences in which a 5/2 spin is assigned to the 402-kev level (Figs. 12 and 13), in conjunction with the $|\delta_1|$ values given in Table VII, shows that both the 280- and 265-kev gamma rays are rather pure $E2$ transitions. The theoretical $E2$ K-conversion coefficient ratio ($\alpha_{280}/\alpha_{265}$) is 0.84,[21] while the experimental ratio is 1.17 ± 0.1. (The measured absolute K-conversion coefficients are considerably less accurate than the ratios because a normalization is involved.) The theoretical K-conversion coefficient of a 280-kev $E2$ transition is 0.016,[21] thus $\alpha_{265}=0.014$ and $|\delta_2|\approx1.2$ for the 265-kev radiation. It may be seen from Fig. 12 that for the 5/2, 3/2, 3/2 sequence such a low value of δ_2 is not reached within the limits set on δ_1. However, by combining the extreme values of A_2 and δ_1, it is barely possible to satisfy this condition for the spin sequence, $3/2(M1+E2)3/2(M1+E2)3/2$ (Insert, Fig. 12). Therefore, one may conclude that the spin of the 402-kev level is 3/2 and that the 265-kev level is probably 1/2 although the 3/2 assignment cannot be excluded. A choice of either 5/2 or 3/2 remains for the spin of the

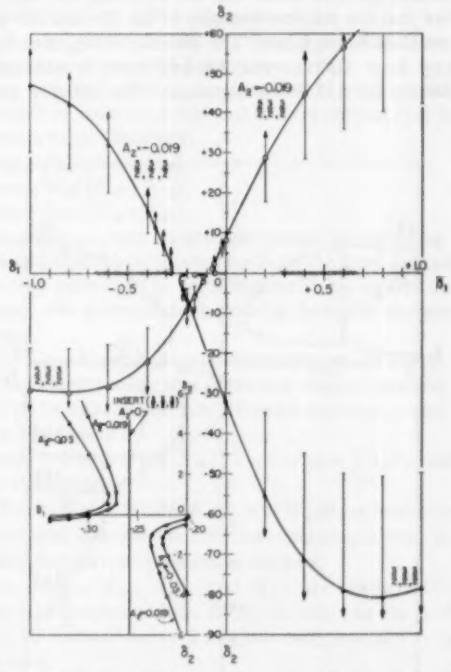

FIG. 12. Effect of $M1+E2$ mixing on the directional distribution of the (136, 265)-kev cascade. Values of δ_1 *vs* δ_2 are plotted for $A_2=-0.019$. The indicated errors are due to the errors assigned to A_2 (see Table VI). The arrows on the error symbols mean that δ_2 values up to infinity are consistent with the experimental correlation results. The shaded abscissa regions denote the values of δ_1 which are consistent with the measured K-conversion coefficient of the 136-kev gamma ray. The ○ points refer to a 5/2, 3/2, 3/2 spin sequence for the 402-, 265-kev levels and the ground state of As^{75}, respectively; the ● points refer to a 3/2, 3/2, 3/2 spin sequence. The Insert shows detail in the region of $\delta_1=-0.258$ for the 3/2, 3/2, 3/2 spin sequence.

[42] M. E. Rose, Phys. Rev. **93**, 477 (1954).
[43] L. C. Biedenharn and M. E. Rose, Revs. Modern Phys. **25**, 729 (1953).

280-kev level. In the former case $A_4 \approx -0.005$ ($|\delta_1| = 0.45$, $|\delta_2| = 2.5$), in the latter case A_4 vanishes. Both these values for A_4 are in agreement with the experimental result, $-(0.014 \pm 0.017)$.

All the spin and parity assignments which are consistent with the logft values, the gamma-ray multipolarities, and the above interpretation of the directional correlation results are given in Fig. 14. The spins not enclosed in brackets are those which are most compatible with the relative gamma-ray transition probabilities. For example, with a 7/2− assignment for the 305-kev level the competition between the 25-kev (probably $M1$) and 305-kev ($E2$) gamma rays is readily understood. On the other hand, if the 305-kev level has a spin of 5/2−, 3/2− or 1/2−, then the 305-kev transition would be a $M1$ with a very large admixture of $E2$. It is difficult to understand how a 25-kev transition involving no parity change could be ten times as intense as a 305-kev transition of such multipole order. A 5/2− assignment is preferred for the 280-kev level since the spin difference between the 305- and 280-kev levels can be, at most, one unit in order that the relative intensity of the 25- and 305-kev transitions be explained. The absence of negative beta decay from Ge^{75} to the 280-kev level is additional evidence for a 5/2− assignment. The 280-kev level

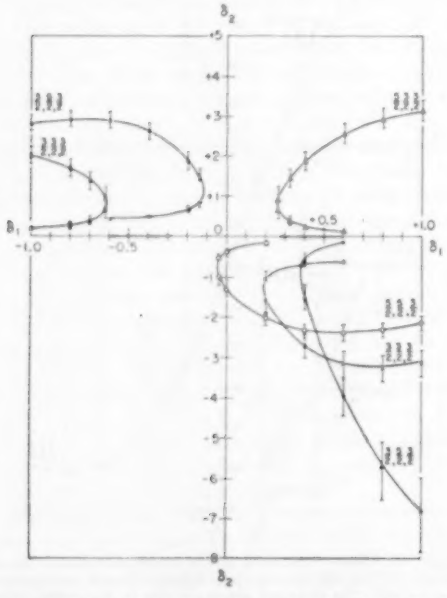

FIG. 13. Effect of $M1+E2$ mixing on the directional distribution of the (121, 280)-kev cascade. Values of δ_1 vs δ_2 are plotted for $A_2 = -0.40$. The indicated errors are due to the errors assigned to A_2. The shaded abscissa regions denote the values of δ_1 which are consistent with the measured K-conversion coefficient of the 121-kev gamma ray. The ○ points refer to a 5/2, 5/2, 3/2 spin sequence for the 402-, 280-kev levels and the ground state of As^{75}, respectively. Similarly, the △ points refer to 5/2, 3/2, 3/2, the ● points to 3/2, 5/2, 3/2 and the × points to 3/2, 3/2, 3/2.

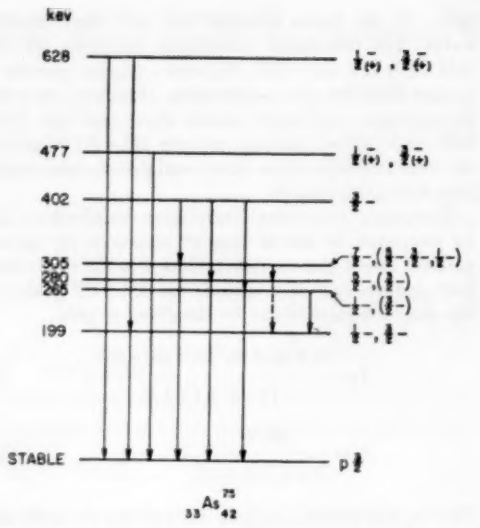

FIG. 14. Spin and parity assignments for levels of As^{75}. On the basis of transition-probability arguments, the bracketed assignments are less probable.

could very well have an $f_{5/2}$ configuration since from shell-model considerations[3] one would expect the $f_{5/2}$ state to occur at a low excitation energy. For example, in As^{77} the $f_{5/2}$ level occurs at 263 kev.[40]

The logft values for the Ge^{75} beta transitions to the 199- and 402-kev levels (7.0 and ≥ 8.1, respectively) indicate that these transitions are either l-forbidden[26] or that the configurations of the levels involved are unusually pure. An argument similar to that suggested by de-Shalit and Goldhaber[44] to explain the case of Kr^{85} may be applied here. The neutron configuration of the Ge^{75} ground state is $(p_{1/2})^1 (g_{9/2})^4$. The As^{75} ground-state neutron configuration may be either $(p_{1/2})^2 (g_{9/2})^2$ or $(p_{1/2})^0 (g_{9/2})^4$; the proton configuration could be $(p_{3/2})^1 (f_{5/2})^4$, $(p_{3/2})^3 (f_{5/2})^2$ or any other combination which gives a 3/2− spin. Since the nuclear magnetic moment of As^{75} falls between the Schmidt lines,[3] a large amount of configuration mixing in the ground state is indicated. Thus it is not surprising that the stabilizing effect of the odd $p_{3/2}$ proton on the $(p_{1/2})^2$ neutrons is insufficient in the ground-state configuration to produce an anomalously high logft value. On the other hand, if the 199-kev level is a fairly pure $p_{1/2}$ or $p_{3/2}$ proton state, then the $(p_{1/2})^2 (g_{9/2})^2$ neutron configuration may be stabilized sufficiently so that the logft value for the beta decay to this level is increased. Similarly, the configuration of the 402-kev level may also be unusually pure. Such configuration purity may be the reason for the absence of a gamma-ray transition between the 199- and 402-kev levels even though such a transition should compete favorably

[44] A. de-Shalit and M. Goldhaber, Phys. Rev. 92, 1211 (1953).

with the observed gamma-ray transitions from the 402-kev level (Fig. 11). A similar argument may be used to explain the fact that Se^{75}, which has a 5/2 ground-state spin, decays primarily to the 402-kev level, although the unobserved electron-capture transitions of Se^{75} to the other levels of As^{75} should be allowed or forbidden to the same degree.

The 477- and 628-kev levels decay primarily to the ground state of As^{75}. A possible explanation is that these levels are formed by coupling the odd As^{75} proton to an even-even core which has been excited to a level comparable to the 2+ level in an even-even nucleus. The amount of excitation energy is approximately correct as, in this region of the periodic table the 2+ level of even-even nuclei is at ~600 kev;[45] in fact, it is 596 kev in the case of Ge^{74}. One can consider that the 477- and 628-kev levels are negative parity states and that they correspond to the ground and first excited states, respectively, of the odd As^{75} proton coupled to the excited even-even core.

The surprising feature of the As^{75} level structure is the occurrence of five excited levels within 402 kev, most of which have a spin of 1/2 or 3/2. Only two single-particle states, $f_{5/2}$ and $p_{1/2}$, are available.[3] However, in the case of arsenic, there is very little energy difference between the $p_{3/2}$ and $f_{5/2}$ proton subshells and between the $p_{1/2}$ and $g_{9/2}$ neutron subshells. The energy required to transfer a proton or neutron pair from one subshell to another may, therefore, be quite small. A confirmation of this process would be the occurrence of low-lying 0+ levels in neighboring even-even nuclei. Such levels have been found in Ge^{70} at 1.21 Mev[46] and in Ge^{72} at 0.68 Mev.[40] It would not be surprising if even less energy is required in the case of As^{75} as the energy needed to transfer a nucleon pair undoubtedly depends critically on the nuclear configuration. On the other hand, it is possible that the existence of so many low-lying levels is a result of different configuration-mixing ratios since a considerable amount of configuration mixing is to be expected for As^{75}.

ACKNOWLEDGMENTS

The authors wish to thank Mr. R. L. Chase for his help with the electronic problems and Dr. D. E. Alburger for his assistance with the lens-spectrometer measurements. We are also indebted to Mr. Alfred Weinstein for making the lead converters and to Dr. Max Goldstein of the Los Alamos Scientific Laboratory for calculating the multipole-order mixing data graphed in Figs. 12 and 13. It is a pleasure to acknowledge helpful suggestions arising from discussions with Dr. G. Friedlander, Dr. M. Goldhaber, Mr. W. Bernstein, Dr. J. W. Mihelich, and Dr. A. W. Sunyar. A great encouragement was Dr. J. B. H. Kuper's continued interest in the problem.

[45] G. Scharff-Goldhaber, Phys. Rev. **90**, 587 (1953).
[46] Merle E. Bunker (private communication).

APPENDIX. TREATMENT OF DIRECTIONAL CORRELATION DATA WHEN TWO UNRESOLVED GAMMA-GAMMA CASCADES ARE PRESENT

Definitions

Subscripts: 0 refers to 402-kev level; 1 refers to 280-kev level; 2 refers to 265-kev level; 3 refers to ground state of As^{75}; a refers to channel positions set to favor cascade through level 1; b refers to channel positions set to favor cascade through level 2; t refers to wide channels set to include composite photopeaks at 121 plus 136 kev and 280 plus 265 kev, respectively.

N_1 denotes disintegrations per second from level 1 (280-kev gamma rays).

N_2 denotes disintegrations per second from level 2 (265-kev gamma rays).

N_{01} denotes count rate in channel of detector A due to transitions proceeding from level 0 to 1 (count rate of 121-kev gamma rays).

N_{02} denotes count rate in detector A channel due to 0 to 2 transitions (136-kev gamma rays).

N_{13} denotes count rate in detector B channel due to 1 to 3 trasitions (280-kev gamma rays).

N_{23} denotes count rate in detector B channel due to 2 to 3 transitions (265-kev gamma rays).

$\alpha_{01}=N_{01}/(N_{01}+N_{02})$, i.e., fraction of total counts in channel of detector A due to 0 to 1 transitions (121-kev gamma rays). Similarly,

$\alpha_{02}=N_{02}/(N_{01}+N_{02})$,
$\alpha_{13}=N_{13}/(N_{13}+N_{23})$,
$\alpha_{23}=N_{23}/(N_{13}+N_{23})$.

ϵ_{01}, ϵ_{02}, ϵ_{13}, and ϵ_{23} are efficiencies for detecting in channel transitions proceeding from the level indicated by first subscript to level indicated by second subscript; the appropriate branching factor is contained in ϵ_{01}.

$\beta=\alpha_{01}\alpha_{13}N_2/\alpha_{02}\alpha_{23}N_1$; a subscript on β refers to measurements made at a particular channel position.

$C(\theta)$ is coincidence rate between detector A and B as a function of θ.

$W(\theta)=C(\theta)/(N_{01}+N_{02})(N_{13}+N_{23})=\sum_{i=0} a_i P_i(\cos\theta)$, $a_i=0$ if i is odd.

$W_a(\theta)$, $W_b(\theta)$, $W_t(\theta)$, $W_1(\theta)$, and $W_2(\theta)$ are normalized directional distribution functions; subscripts refer to a particular channel position or cascade.

$A_{i,a}$, $A_{i,b}$, $A_{i,t}$, $A_{i,1}$, and $A_{i,2}$ are coefficients of Legendre polynomials in $W(\theta)$; A_i refers to the coefficient of $P_2(\cos\theta)$ for $i=2$ and the coefficient of $P_4(\cos\theta)$ for $i=4$.

Derivations of Equations

It follows from the definitions that

$$N_{01}=\epsilon_{01}N_1, \quad N_{02}=\epsilon_{02}N_2, \quad N_{13}=\epsilon_{13}N_1, \quad N_{23}=\epsilon_{23}N_2,$$

and that

$$C(\theta)=\epsilon_{01}\epsilon_{13}N_1\cdot W_1(\theta)+\epsilon_{02}\epsilon_{23}N_2\cdot W_2(\theta).$$

Hence,

$$w(\theta)=C(\theta)/(N_{01}+N_{02})(N_{13}+N_{23}),$$
$$=[\alpha_{01}\alpha_{13}/N_1]W_1(\theta)+[\alpha_{02}\alpha_{23}/N_2]W_2(\theta), \quad (1)$$
$$=[\alpha_{02}\alpha_{23}/N_2][\beta\cdot W_1(\theta)+W_2(\theta)]. \quad (1a)$$

Equate coefficients of corresponding Legendre polynomials to obtain the expression,

$$a_i=(\alpha_{02}\alpha_{23}/N_2)(\beta A_{i,1}+A_{i,2}), \quad \text{for} \quad i=0,\ 2 \text{ or } 4. \quad (2)$$

If $i=0$, $A_{0,1}=A_{0,2}=1$, and N_2 is given by the equation,

$$N_2=\alpha_{02}\alpha_{23}(1+\beta)/a_0. \quad (3)$$

Then,

$$A_{i,x}=a_i/a_0=(1+\beta_x)^{-1}(\beta_x A_{i,1}+A_{i,2})$$
$$\text{for} \quad i=0,\ 2 \text{ or } 4; \quad (4)$$

subscript x refers to channel positions a, b or t. Solve (4) for $A_{i,1}$ and $A_{i,2}$ using cases a and b.

$$A_{i,1}=[(1+\beta_a)A_{i,a}-(1+\beta_b)A_{i,b}]/(\beta_a-\beta_b)$$
$$\text{for} \quad i=2 \text{ or } 4, \quad (5)$$

$$A_{i,2}=[\beta_b(1+\beta_a)A_{i,a}-\beta_a(1+\beta_b)A_{i,b}]/(\beta_b-\beta_a)$$
$$\text{for} \quad i=2 \text{ or } 4. \quad (6)$$

The coefficients of the individual cascades may be obtained from the experimental directional correlation distributions with the aid of Eqs. (5) and (6) provided the mixing ratios of the gamma rays in the detectors are known. The source strength may be calculated from Eq. (3) and the value of N_2 should be independent of whether the channels were set to favor the (121, 280)-kev or the (136, 265)-kev cascade. Thus one may obtain an overall check on the mixing ratios used.

The mixing ratios for case a can be determined from the results of additional coincidence experiments. Solve Eq. (1) for α_{23}.

$$\alpha_{23}=[w(\theta)N_2]/[\alpha_{02}W_2(\theta)]$$
$$-[\alpha_{01}\alpha_{13}N_2W_1(\theta)]/[\alpha_{02}N_1W_2(\theta)]. \quad (7)$$

At one angle, 180°, $w(\theta)$ was measured with the detector channel for the 265- plus 280-kev radiations set as in case a and the other channel set so that α_{02} is large compared to α_{01}. Under these experimental conditions the first term of Eq. (7) is dominant; in fact, the magnitude of the ratio, α_{01}/α_{02}, is such that only a few percent error is incurred in the evaluation of α_{23} even if the second term of (7) is crudely estimated. The value of N_2 substituted into the first term of (7) was measured with the detector channels set to maximize α_{02} and α_{23}. This value of N_2 is more accurate than that obtained under the conditions of case b. Since $W_2(\theta)$ is almost isotropic, it does not have to be known accurately. Similarly, α_{02} for case a was determined. Equation (1) was solved for α_{02}, then $W(\theta)$ at 180° was measured with the detector channel for the 121- plus 136-kev gamma rays set as in case a and the other channel set so that α_{23} is large.

Elastic Scattering of 40-Mev Alpha Particles from Heavy Elements*

H. E. WEGNER, R. M. EISBERG, AND G. IGO
Brookhaven National Laboratory, Upton, Long Island, New York

(Received April 8, 1955)

Angular distributions have been measured for the elastic scattering of 40-Mev alpha particles from Ta, Au, Pb, and Th in the angular range 21° to 155°. If the ratios of the measured cross sections to the Coulomb cross section are assumed equal to 1.0 at small angles, they increase slightly with increasing angle, and in the vicinity of 30° decrease exponentially with increasing angle to values less than 0.001. These data are compared with the semiclassical, strong absorption model of Blair and with the recent model of Ford and Wheeler.

1. INTRODUCTION

THE elastic scattering of alpha particles is one of the oldest subjects of investigation in nuclear physics. Rutherford and others,[1] using alpha particles from naturally radioactive sources, demonstrated that the scattering from nuclei could be explained by a theoretical description employing classical trajectories in a Coulomb field. However, the theory could not account for the scattering from H and He, or for the scattering at large angles from Mg and Al. It is of interest to investigate the deviations from Coulomb scattering, since such a study could be expected to yield information about the size of the nucleus, the size of the alpha particle, and about the interaction of the alpha particle with the nucleus. These experiments require more energetic alpha particles than are available from radioactive sources.

Recently, several experiments have been performed using high-energy alpha-particle beams from cyclotrons. These experiments include: the energy dependence, from 13 to 42 Mev, of the cross section for the elastic scattering of alpha particles,[2] angular distributions for elastic scattering of 22-Mev alpha particles from heavy elements,[3] and the angular distribution for elastic scattering of 28-Mev alpha particles from Au.[4]

When measured as a function of energy, the cross section is observed to agree with the energy dependence predicted by the Coulomb formula for energies below a certain critical energy, E_c. For energies greater than E_c, the cross section decreases exponentially to values less than 0.1 of the Coulomb cross section. In the heaviest elements, the cross section increases slightly above the Coulomb cross section before suddenly decreasing. The angular distributions also show an exponential decrease in cross section at angles greater than a certain critical angle, and in the heavier elements, a similar increase before the decrease.

Blair has interpreted the energy dependence of the elastic scattering cross section by using a semiclassical, strong absorption model.[5] The outgoing lth partial wave is assumed to vanish if the apsidal distance of the corresponding classical trajectory is less than the sum of the radius of the nucleus plus the radius of the alpha particle. Partial waves, corresponding to classical trajectories with larger apsidal distances, have phases characteristic of Coulomb scattering. This model can be made to fit the small increase in the cross section and part of the subsequent exponential decrease by assuming the radius of the alpha particle to be 2×10^{-13} cm and the radius of the nucleus to be $1.5\times10^{-13}A^{\frac{1}{3}}$ cm.

The angular distribution data has been interpreted by Wall, Rees, and Ford by using a modification of Blair's semiclassical strong absorption model.[3] These authors have smoothed out the abrupt spatial transition between complete absorption and no absorption by allowing the outgoing partial wave, corresponding to a grazing classical trajectory, to have the Coulomb phase and an amplitude of 0.5 times the Coulomb amplitude. This modification reduces the diffraction oscillations in the differential cross section which are not found experimentally.

Another interpretation of the energy dependence of the cross section has been advanced by Izumo.[6] He has calculated the elastic scattering cross section using the Montroll-Greenberg variational method[7] and a potential that consists of a complex square well plus a Coulomb potential. The calculation can be made to fit the experimental results if the imaginary part of the square well has a strong dependence on both the energy of the alpha particle and the scattering angle.

The region of poorest agreement between the Blair model and experiment is the region where the measured cross section is small compared to the Coulomb cross section. (In this region the model would not be expected to give quantitative agreements.) In the energy-dependence experiments, at cross sections less than about 0.1 of the Coulomb cross section, the

* Research performed under the auspices of the U. S. Atomic Energy Commission.

[1] An excellent survey of the early work of Rutherford and others with a complete index of references is contained in the book by Rutherford, Chadwick, and Ellis, *Radiations from Radioactive Substances* (MacMillan Company, Cambridge, 1930).

[2] G. W. Farwell and H. E. Wegner, Phys. Rev. **93**, 356 (1954); **95**, 1212 (1954).

[3] Wall, Rees, and Ford, Phys. Rev. **97**, 726 (1955).

[4] H. E. Gove, Massachusetts Institute of Technology (LNSE) Progress Report, May, 1951 (unpublished).

[5] J. S. Blair, Phys. Rev. **95**, 1218 (1954).

[6] K. Izumo, Progr. Theoret. Phys. (Japan) **12**, 549 (1954).

[7] E. W. Montroll and J. M. Greenberg, Phys. Rev. **86**, 889 (1952).

strong absorption model predicts that the cross section should begin to decrease less rapidly than the observed exponential decrease. However, the experimental cross section continues to decrease in this region until, at the highest energies measured, it has a value several times smaller than the theoretical prediction. A similar situation exists in the case of the angular distributions. The experimental cross section decreases exponentially with increasing angle to values less than 0.1 times the Coulomb cross section. In the case of Ag, the lightest element investigated, the experimental cross section decreases to approximately 0.01 times the Coulomb cross section. In contrast, the cross section, predicted by either the Blair model or the modified Blair model, decreases to values of the order of 0.1 times the Coulomb cross section and then oscillates violently, finally increasing towards the Coulomb cross section at 180°.

The purpose of this experiment is to extend the measurements on the angular distribution for elastic scattering from heavy nuclei to higher alpha-particle energies in order to determine whether or not the cross section continues to decrease rapidly.

The results of the experiment show that the cross section does continue to decrease rapidly to values less than three orders of magnitude smaller than the Coulomb cross section. There is no evidence for an increase in the cross section at very large angles. These data are compared with the predictions of the Blair models and are shown to be in striking disagreement in the region where the measured cross section is small compared to the Coulomb cross section. In view of the approximations in the theory this disagreement is not surprising.

After the experiment was completed, the authors were informed of some unpublished calculations by Ford and Wheeler on the elastic scattering of alpha particles.[8] These calculations are based on a model in which the surface of the nucleus is transparent to the alpha particle. The assumptions which enter into the theory are best satisfied for large alpha-particle energy and large scattering angles. At these angles the theory predicts that the cross section drops monotonically to very small values, which is in qualitative agreement with the results of this experiment.

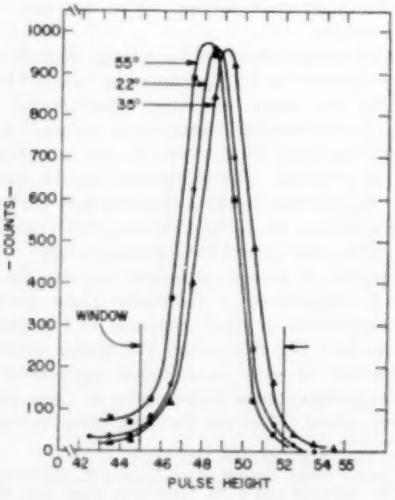

FIG. 1. Pulse-height distributions at 22°, 35°, and 55°.

2. EXPERIMENTAL PROCEDURE

For these experiments, the external alpha-particle beam of the Brookhaven 60-inch cyclotron is directed into an evacuated beam pipe. The beam pipe follows the trajectory of the alpha particles through the fringing field of the cyclotron magnet and then passes through a two-element magnetic strong-focusing lens of 2-inch aperture,[9] located 4 feet from the cyclotron vacuum chamber. The beam pipe then passes through a channel in a shielding wall and terminates at a scattering chamber located 30 feet from the cyclotron. The alpha-particle beam travels through the evacuated pipe and is brought to a focus on a thin target at the center of the scattering chamber. The focused beam forms an approximately circular spot $\frac{1}{4}$ inch in diameter. The current in the beam is 10% to 20% of the total deflected cyclotron beam and 1% to 2% of the circulating beam. Focused alpha-particle beams in excess of 5 microamperes have been obtained. In this experiment, the beam is further defined by a $\frac{1}{2}$-inch tantalum diaphragm located 10 inches in front of the target.

Particles which are scattered from the target foil into the horizontal plane of the one-foot diameter evacuated scattering chamber pass through exit windows of low areal density and are detected. The windows are arranged so that measurements can be made at any angle from 20° to 160°. A movable frame holding three targets is supported at the center of the chamber. The chamber is positioned so that the alpha-particle beam is accurately aligned with respect to the axis of the chamber and with respect to a graduated circle engraved on the outside of the chamber, used to measure the scattering angle.

After traversing the scattering chamber, the beam is stopped in a Faraday cup. The Faraday cup current is used by the operator to tune the cyclotron. The beam monitor used in the experiment is a NaI scintillation counter which detects alpha particles elastically scattered from the target at a fixed angle of 26°. This monitor provided a linear and reproducible measure of the integrated beam.

The energy of the beam is determined by measuring the range in aluminum of alpha particles elastically scattered from a target of high atomic weight. The energy is 41 ± 0.3 Mev.

[8] K. W. Ford and J. A. Wheeler (to be published).
[9] B. Cork and E. Zajec, University of California Radiation Laboratory Report No. 2182 (unpublished).

A second NaI scintillation counter, mounted on an arm which rotates about the center of the scattering chamber, is used to measure the angular distribution of the alpha particles elastically scattered from the target foil. Pulses from the detector pass through a cathode follower and into a linear amplifier. The output of the linear amplifier passes into a pulse-height analyzer.

The pulse-height distribution from the detector consists of a continuum and a sharp peak. The sharp peak contains the elastically scattered alpha particles. The continuum contains inelastically scattered alpha particles and other particles, such as protons, which result from alpha-induced reactions. The continuum extends to pulse heights greater than the pulse height of the elastic alpha-particle peak because protons lose less energy traversing the target and the scattering chamber window, and because of the nonlinear responses of NaI for alpha particles. The ratio of the area under the elastic alpha particle peak to the area under the continuum depends upon the scattering angle. At forward angles, the continuum is negligible; as the scattering angle increases, the elastic alpha-particle peak decreases relative to the continuum, until it vanishes into the continuum at large angles.

Due to the rapid change of the character of pulse-height distribution with increasing scattering angle, two methods were used to separate the elastically scattered alpha particles from the continuum. For scattering angles less than 55°, where the continuum is very small, an Atomic Instrument Company single-channel pulse-height analyzer was adjusted so that the acceptance window encompassed the elastic alpha-particle peak. Figure 1 shows pulse-height distributions, for particles scattered from a thin Au target at three forward angles. The slight shift in the location of the peak with scattering angle is due to the change, with angle, in the amount of material which the alpha particles must penetrate in traversing the scattering chamber window. The vertical lines drawn at 45 and 52 volts show the acceptance window of the single-channel pulse-height analyzer.

Figure 2 shows pulse-height distributions for alpha particles scattered from a thin Ta target at three large angles. These curves show that at these angles it is necessary to measure the differential pulse-height distribution at each scattering angle in order to correctly subtract the continuum from the elastic alpha-particle peak. Data were obtained at scattering angles greater than 55° with an Atomic Instrument Company 20-channel pulse-height analyzer. The elastic scattering cross section was assumed to be proportional to the area between the elastic peak and the continuum. The straight lines shown in Fig. 2 indicate this subtraction.

The elastic scattering cross section decreases rapidly with increasing scattering angle; the cross section drops by approximately six orders of magnitude over the range measured. In order to maintain a reasonable

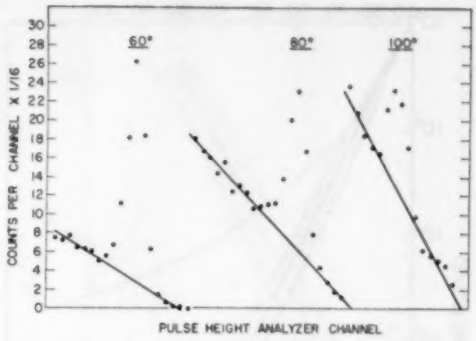

FIG. 2. Pulse-height distributions at 60°, 80°, and 100°.

counting rate in the detector as the scattering angle is changed, it is necessary to vary the intensity of the incident alpha-particle beam and the solid angle subtended by the detector. A variation of nearly two orders of magnitude can be made in the beam intensity by adjusting the strong focusing lens. The solid angle subtended by the detector is varied over a range of two orders of magnitude by changing the size of a diaphragm placed in front of the detector.

The data for each element investigated were obtained in five groups, each group spanning a restricted range of angle. The experimental conditions differed from one range to another, i.e., the single-channel pulse-height analyzer was used in some ranges while the 20-channel pulse-height analyzer was used in others, and also the diaphragm in front of the detector was changed from range to range. The angular ranges were overlapped at their extremes, and the cross sections measured in a particular range were normalized at the overlapping points to the data obtained in the adjacent ranges.

3. EXPERIMENTAL RESULTS

Figure 3 shows the measured differential cross section for the elastic scattering of 40-Mev alpha particles from Ta, Au, Pb, and Th. The abscissa is the laboratory scattering angle. The ordinate is the relative differential cross section. The heavy curve represents the angular dependence of the Coulomb scattering differential cross section. Figure 4 shows an expanded view of the data of Fig. 3 in the region 21° to 40°. Typical statistical errors are shown on the Ta data. At angles less than 40° the statistical errors are smaller than the size of the points.

At sufficiently small scattering angles, the elastic scattering cross section should be equal to the Coulomb scattering cross section. It is observed that, for the first few points, the slope of the measured cross-section curves coincides with the slope of the Coulomb scattering cross-section curve. Consequently, the measured differential cross sections were assumed equal to the Coulomb differential cross section at the 21° and the

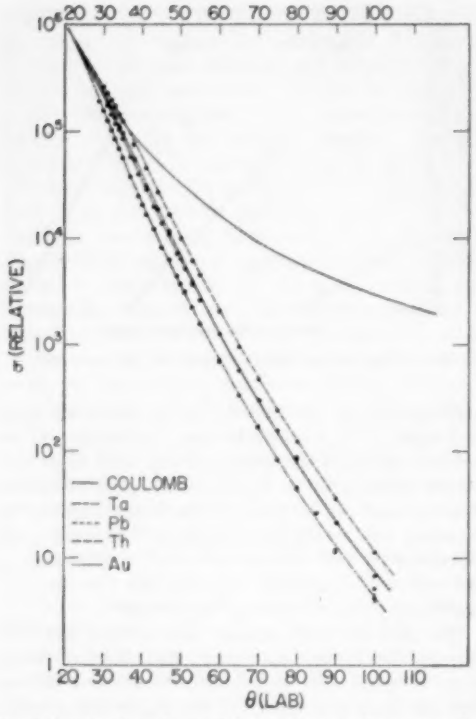

FIG. 3. Angular dependence of the elastic scattering cross section for alpha particles scattered from Ta, Pb, Th, and Au.

22° points, and the data presented in Figs. 3 and 4 have been normalized accordingly. The earlier experiments on the elastic scattering of alpha particles from heavy elements[2,3] have shown that the cross sections have an angular dependence which justifies this normalization procedure. The geometry of the scattering chamber limited the measurements to a minimum angle of 21°.

As the scattering angle increased, the measured cross sections departed from the Coulomb cross section. In the heavier elements, Au, Pb, and Th, the cross section first increased above the Coulomb cross section and then decreased rapidly. The magnitude of the increase was greater for greater atomic weights. In the case of Ta, the cross section does not initially increase as observed in the heavier elements. However, there could be an increase at angles smaller than those investigated. The observed increase, before the decrease in the cross section for the heavier elements, is in qualitative agreement with earlier experiments.

Figure 5 shows the ratio of the measured elastic scattering cross section to the Coulomb scattering cross section, σ/σ_c, plotted as a function of laboratory scattering angle. These ratios have been normalized to unity at the 21° and 22° points as discussed above. It should be noted that any errors arising from the normalization procedure will shift the curves vertically on the semilogarithmic plot but will not change their shape. Typical statistical errors are shown on the Ta data. In order to show clearly the angular dependence of σ/σ_c from 21° to 40°, the experimental points are not shown. In this region the statistical errors are less than the size of the points shown at greater angles.

In order to carry the cross-section measurements to angles larger than 100°, it is necessary to use a very thin scattering target. Such targets were available for Au. Measurements were made at 90°, 105°, 130°, and 155°. At 130° and 155°, the elastic alpha-particle peak was not distinguishable from the continuum and it was only possible to set an upper limit on the cross section. The cross section for Au continues to decrease with increasing angle; the ratio, σ/σ_c, is less than 0.0003 at 130° and 155°.

4. EXPERIMENTAL ERRORS

The alpha-particle beam passed through the axis of the scattering chamber to within 0.030 in. and was aligned with respect to the graduated circle to within 0.2°. The alignment was checked by determining the alpha-particle elastic scattering cross section at some measured angle on the left side of the chamber and then at the same measured angle on the right side of the chamber. The cross sections observed in these two cases were equal within counting statistics. This indicated that the error involved in measuring the scattering angles was less than 0.25°.

The size of the diaphragm placed in front of the detector varied from 0.040 to 0.375 in. in diameter. The width of the beam at the target foil was 0.125 in. At forward angles, where the smallest diaphragm was used, the angular resolution of the detector was limited by the width of the beam and was ±0.5°. At backward angles, where the largest diaphragm was used, the

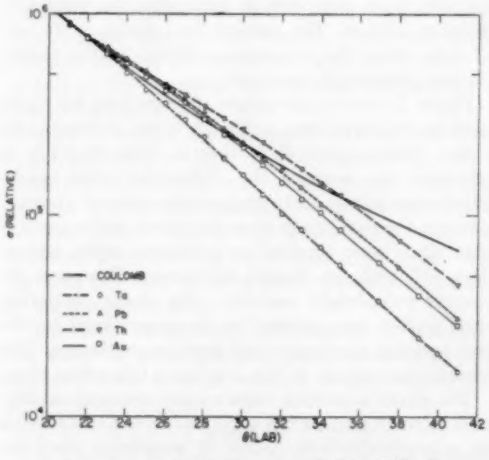

FIG. 4. Expanded view of small angle data of Fig. 3.

angular resolution was limited by the diaphragm and was ±1.5°. Since the counting rate increased rapidly with decreasing angle, a detector of finite angular resolution would measure the cross section at a somewhat smaller angle than the angle measured to the center of the diaphragm. However, a calculation showed the effect to be negligible in this experiment.

The incident alpha-particle beam lost approximately two Mev in passing through the target foils. The spread which this introduced in the energy of the alpha particles when scattering could erase very small diffraction effects. However, earlier experiments which utilized thinner targets showed no evidence of diffraction effects.[2,3] The initial energy of the beam was 41±0.3 Mev, but the scattering energy should be quoted as 40±1 Mev.

The counting rate of the detector, in the region of the elastic alpha-particle peak, was zero with the scattering target removed.

The error involved in monitoring the beam was determined by the counting statistics of the monitor detector, which were always less than 1%.

The data from 21° to 55° were obtained with a single-channel pulse-height analyzer. This procedure contributed error to the cross-section measurement because the continuum was not subtracted from the elastic alpha-particle peak. For the three heaviest elements, in the pulse-height region covered by the window of the pulse-height analyzer, the ratio of the counting rate due to the continuum to the counting rate due to the elastic alpha-particle peak varied from 3% at 21° to 6% at 55°. (See Fig. 1.) For Ta, the ratio was 6% at 21° and 12% at 55°. The effect of neglecting the angular variation in the relative contribution of the continuum was to gradually increase the measured cross section with increasing scattering angle. For the three heaviest elements, the cross section measured at 55° was approximately 3% too large, relative to the cross section measured at 21°. In the case of Ta, this effect increased the cross section at 55° approximately 6%, relative to the cross section at 21°. No correction was made for this effect since it was very small compared to the three orders of magnitude change in the cross section over this angular range.

At angles larger than 55°, a twenty-channel pulse-height analysis was made at each angle of observation. The contribution of the continuum was subtracted from the elastic alpha-particle peak by drawing a straight line through the points in the continuum on each side of the peak. The elastic scattering cross section was then assumed to be proportional to the area between the peak and the straight line. (See Fig. 2.) By placing a thin Al absorber between the target foil and the detector, it was possible to stop the scattered alpha particles while only slightly reducing the energy of the lighter particles which comprised the continuum. In this fashion, the shape of the continuum under the elastic alpha-particle peak was examined. It was shown

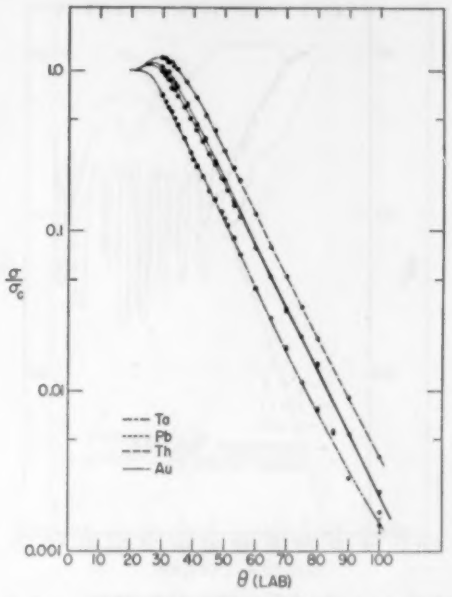

FIG. 5. Angular dependence of the ratio of the elastic scattering cross section to the Coulomb cross section, σ/σ_c, for Ta, Au, Pb, and Th.

that the continuum approximately followed the straight line interpolation. Therefore, this interpolation contributed little error.

Another possible source of error could be the presence of groups of inelastically scattered alpha particles which, within the 5% energy resolution of the detector, could not be separated from the elastically scattered alpha-particle peak. Again, comparing the continuum distribution with and without the thin Al absorber, it was possible to show, that in the region near the peak, the continuum contained few inelastically scattered alpha particles. From this it was assumed that there was a negligible number of inelastically scattered alpha particles which were not resolved from the elastic alpha-particle peak.

The statistical errors indicated for the experimental points at angles greater than 55° were determined by compounding the statistical error of the total counting rate in the peak with the statistical error involved in fitting a straight line to the continuum.

The error in normalizing the data obtained in one range of angle to the data obtained in the adjacent ranges was small compared to the statistical error of the individual points. This was a result of measuring with increased accuracy the cross section at overlapping points.

5. DISCUSSION

Under the assumptions of the Blair model[5] described in Sec. 1, the amplitude of the outgoing wave is $e^{2i\sigma l}$

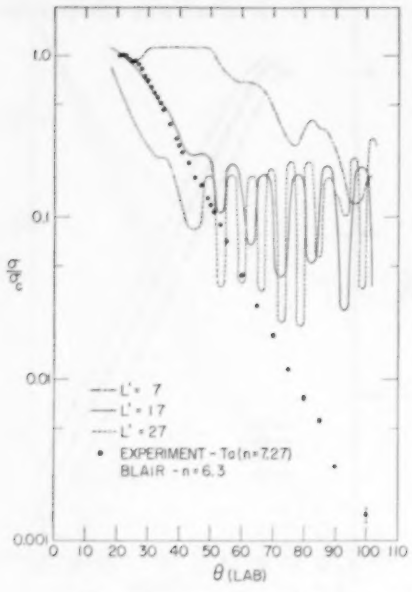

FIG. 6. Comparison of the Blair model with σ/σ_c for Ta.

for $l>l'$ and is zero for $l\leq l'$, where σ_l is the Coulomb phase. l' satisfies the equation

$$l'(l'+1)=2mR^2\hbar^{-2}(E-E_c),$$

with

$$E_c=Zze^2R^{-1}.$$

R is set equal to the radius of the nucleus plus the radius of the alpha particle; E_c is the Coulomb potential energy of a particle of charge ze at a distance R from a nucleus of charge Ze; l' is the orbital angular momentum of a particle of mass m and initial energy E.

Under the above assumptions,

$$\frac{d\sigma}{d\Omega}=\left|\frac{e^{2i\sigma_0}}{2ik}\left\{\frac{-in}{\sin^2(\theta/2)}\exp[-in\ln\sin^2(\theta/2)]-\sum_{l=0}^{l'}(2l+1)e^{2i(\sigma_l-\sigma_0)}P_l(\cos\theta)\right\}\right|^2. \quad (1)$$

The Coulomb phases are given by

$$e^{2i\sigma_l}=\Gamma(l+1+in)/\Gamma(l+1-in),$$

and

$$n=Zze^2/\hbar v.$$

The first term in Eq. (1) is the scattering due to the Coulomb potential, and the second term is due to the interaction between the nucleus and the alpha particles with $l\leq l'$. At small angles, $(\sin\frac{1}{2}\theta)^{-4}$ is large and the scattering is predominately Coulomb scattering unless l' is very large.

The modified Blair model[3] is developed in a similar manner, except that the amplitude of the outgoing wave is $0.5e^{2i\sigma_l}$ for $l=l'$.

For the calculation of σ/σ_c, n is determined by the experimental conditions and l' is adjusted to fit the experimental data. The values of σ/σ_c, as a function of the scattering angle, have been tabulated for $n=6.3$, 10.6, and 11.0; and for $l'=0$ to 35 assuming the Blair model. They have also been tabulated for $n=6.3$, and 10.6; and for $l'=0$ to 23 assuming the modified Blair model. The lightest and heaviest elements investigated in this work were Ta and Th. Their respective values of n are 7.27 and 8.95. It has been shown that the theoretical predictions for the angular distribution are not strongly dependent on n.[3] Since the values of n used in the above tabulations bracket the extreme values of n in this experiment, the theoretical predictions for the angular dependence of σ/σ_c may be employed to show whether the models are capable of qualitative agreement with the experimental data.

In Fig. 6, the experimental σ/σ_c for Ta is compared with the predictions of the Blair model for $n=6.3$ and for $l'=7$, 17, and 27. In Fig. 7 the experimental σ/σ_c for Th is compared with the predictions of the Blair model for $n=10.6$ and for $l'=12$, 22, and 32. In Fig. 8 the experimental σ/σ_c for Ta is compared with predictions of the modified Blair model for $n=6.3$ and for $l'=13$ and 23. The parameter l' which fits the data best is selected by trial and error from the tabulated values, and the effect of increasing and decreasing l' is demonstrated. Because of the limited range of l' values tabulated for the modified model, it was not

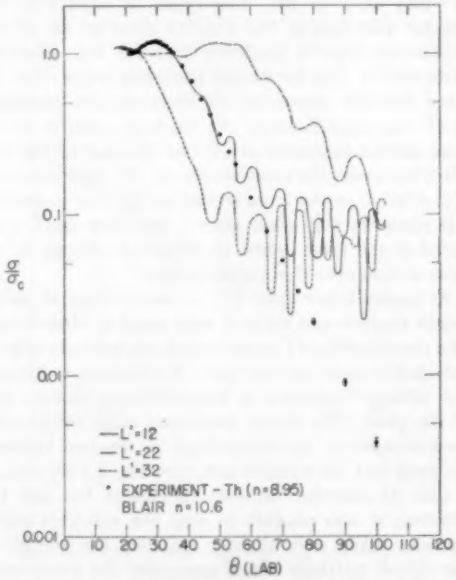

FIG. 7. Comparison of the Blair model with σ/σ_c for Th.

possible to fit the theory to the Th data or to show the effect of increasing l' to values greater than 23 for the Ta data. The l' value corresponding to the best fit for the Ta data, assuming the modified Blair model, is considerably larger than that corresponding to the best fit with the Blair model. This effect was also noted in the work of Wall, Rees, and Ford.[8]

Qualitatively, the Blair models agree with the experimental behavior of σ/σ_c for values greater than approximately 0.1. However, the experimental curve continues to decrease exponentially with increasing angle to values of σ/σ_c of the order 0.001. The theoretical curves show marked oscillations and, on the average, a gradual increase in value of σ/σ_c contrary to experiment. For Au, at angles of 130° and 155° σ/σ_c was shown to be less than 0.0003. This limit indicates that σ/σ_c does not increase in the backward direction as might be expected according to the Blair models.

The model of Ford and Wheeler[8] supposes that the potential changes gradually at the nuclear surface from strongly repulsive to strongly attractive over a number of partial waves large compared to one, and through this region the JWKB-approximate phase shift,[10] η_l, may be used:

$$\eta_l = \tfrac{1}{2}\int \theta(l)dl + \text{const.},$$

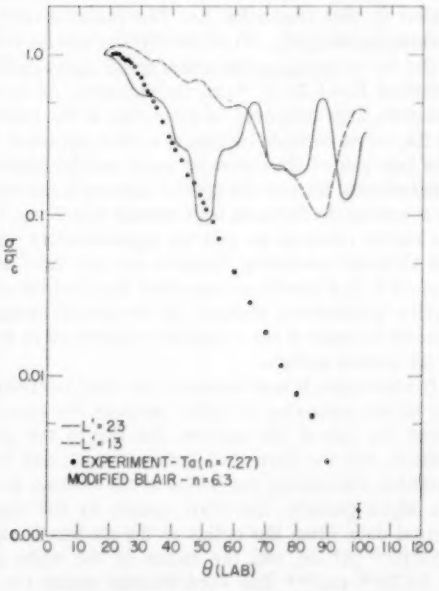

FIG. 8. Comparison of the modified Blair model with σ/σ_c for Ta.

[10] N. F. Mott and H. S. W. Massey, *The Theory of Atomic Collisions*, second edition (Clarendon Press, Oxford, 1949), p. 122.

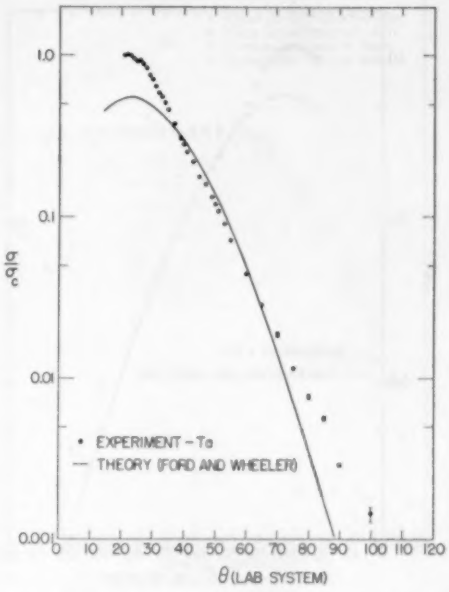

FIG. 9. Comparison of the Ford-Wheeler model with σ/σ_c for Ta.

where $\theta(l)$ is the classical deflection angle for a trajectory with angular momentum $l\hbar$. Furthermore, they suppose that the absorption may be ignored in this transition region. The form of the potential near the nuclear surface will cause the classical deflection to have a maximum, θ_1, at some critical angular momentum, l_1, near which θ will vary parabolically with l,

$$\theta \cong \theta_1 - q(l-l_1)^2.$$

The JWKB cross section may then be evaluated for angles in the neighborhood of θ in terms of the adjustable parameters θ_1 and q. There is also a weak dependence on l_1, but l_1 and θ_1 will be approximately related by the Coulomb formula,

$$l_1 = n\cot(\theta_1/2).$$

The result is

$$\sigma \cong \lambda^2\left[2\pi(l+\tfrac{1}{2})/\sin\theta_1\right]q^{-\frac{1}{2}}\,\mathrm{Ai}^2\left(\frac{\theta-\theta_1}{q^{\frac{1}{2}}}\right),$$

where $\mathrm{Ai}(x)$ is the Airy integral.[11] The Coulomb cross section is evaluated at θ_1 and the relative cross section becomes

$$\sigma/\sigma_c = \left[2\sin^2(\tfrac{1}{2}\theta_1)/nq^{\frac{1}{2}}\right]2\pi\,\mathrm{Ai}^2\left(\frac{\theta-\theta_1}{q^{\frac{1}{2}}}\right).$$

This simple formula was used to fit the observed cross sections at 40 Mev for Ta($Z=73$, $n=7.27$) and for Th($Z=90$, $n=8.95$). The Ta fit is shown in Fig. 9 and

[11] H. Jeffries and B. S. Jeffries, *Methods of Mathematical Physics* (Cambridge University Press, Cambridge, 1946).

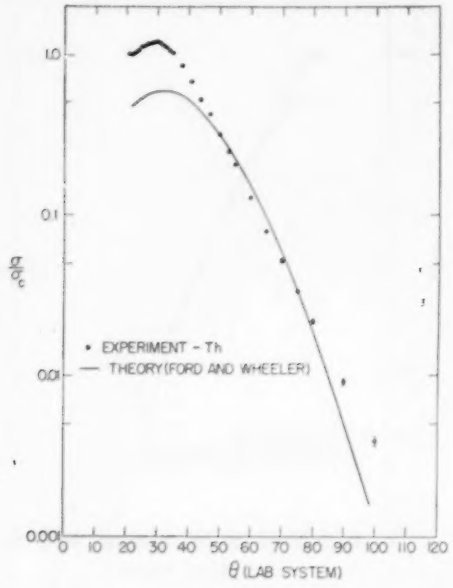

FIG. 10. Comparison of the Ford-Wheeler model with σ/σ_c for Th.

the Th fit is shown in Fig. 10. The fit is only qualitative but has the required features of a smooth and rapid decrease at angles greater than θ_1. Moreover, the determined parameters, θ_1 and q, are physically reasonable.

For Ta, the angle $\theta_1=43°$ and $l_1=18.5$. The "interaction radius", R_{int}, is defined as the point of closest approach at this angular momentum; $R_{int}=1.74\times10^{-13}A^{\frac{1}{3}}$ cm. If 2.5×10^{-13} cm is arbitrarily subtracted for the alpha particle radius, the radial constant is reduced from 1.74 to 1.30. As a measure of the surface thickness, Δl, one may define

$$\Delta l=[\theta_1/q].$$

For Ta, $q=0.0425$ radian, $\Delta l=4.2$. For Th, the fit is obtained with $\theta_1=53°$, $l_1=17.9$, and $R_{int}=1.71\times10^{-13}A^{\frac{1}{3}}$ cm. In this case, the subtraction of 2.5×10^{-13} cm from R_{int} reduces the radial constant from 1.71 to 1.30. The "surface thickness" parameter, q, is 0.0494 for Th and $\Delta l=4.3$ or about 1.3×10^{-13} cm.

The physical idea of this model is that the scattering in the region of rapid decrease of the cross section is governed by the nuclear surface region, and that this region may be "thick" ($\Delta l\gg1$) and almost nonabsorbing. The mathematical approximations are: the JWKB phase shift may be used; the classical deflection angle as a function of l is parabolic in the region of interest; the scattering amplitude sum may be replaced by an integral; the Legendre polynomials may be replaced by their asymptotic forms; and the integral may be evaluated approximately because of the condition $l_1\gg\Delta l\gg1$. These approximations lead to a very simple result. However, for the energies and angles in this experiment, it is not expected to have quantitative validity.

Previous experiments on the elastic scattering of alpha particles discussed in Sec. 1 may be compared with each other and with the results of this experiment by plotting σ/σ_c as a function of a parameter common to the various experiments. The change in linear momentum of the alpha particle upon scattering and the apsidal distance corresponding to a classical trajectory of the alpha particle are two such parameters. The change in linear momentum, Δp, is a reasonable parameter to consider because of its importance in the Born approximation. However, the results of the various experiments when plotted as a function of Δp show that σ/σ_c is not a function of Δp alone.

The results of the various experiments were plotted as a function of apsidal distance, that is, the point of nearest approach of the classical trajectory corresponding to a given energy and scattering angle. This comparison is shown in Fig. 11. The points were obtained from the following experiments on the elastic scattering of alpha particles from Au: the energy dependence in the range 13–42 Mev of the cross section for scattering at 60° and at 95°,[2] the angular dependence in the range 20–60° of the cross section for scattering at 22 Mev,[3] and the angular dependence in the range 21–100° of the cross section for scattering at 40 Mev. Plots of the various data for elastic alpha particle scattering from Th, Pb, and Ta also show agreement similar to that shown for Au. The radius of the Au nucleus, assuming $R_{Au}=1.5\times10^{-13}A^{\frac{1}{3}}$ cm, and the radius of the Au nucleus plus the radius of the alpha particle, assuming $R_\alpha=1.2\times10^{-13}$ cm, are indicated. At apsidal distances large compared to the radius of the nucleus, all the curves coincide because σ/σ_c must approach 1.0. The behavior of the curves at small apsidal distances is paradoxical because the apsidal distance is calculated by assuming the formulas for Coulomb scattering. Yet, the curves continue to coincide approximately where the Coulomb scattering formulas are not valid since $\sigma/\sigma_c<1.0$. It is clearly an important fact that the cross section qualitatively depends on the apsidal distance, but this behavior is not completely understood in terms of the present models.

In conclusion, it is of interest to see what information the elastic scattering of alpha particles has provided about the size of the nucleus, the size of the alpha particle, and the interaction between nuclei and alpha particles. Concerning the radius of the nucleus and of the alpha particle: the Blair models fit the experimental data when the radius of the nucleus is about 1.5×10^{-13} $A^{\frac{1}{3}}$ cm and the radius of the alpha par- is 2×10^{-13} cm.[2,3,5] The Ford-Wheeler model fits the experimental data when the nuclear radius is $1.3\times10^{-13}A^{\frac{1}{3}}$ cm and the alpha-particle radius is about 2.5×10^{-13} cm. Either of these sets of values is in agreement with the currently accepted range of values.

The situation concerning the interaction between the alpha particle and the nucleus is not as clear. The exact form of the nuclear potential corresponding to the Blair model is not apparent but it does imply in some sense an opaque nucleus. On the other hand, the Ford-Wheeler model is based on the assumption that the rim of the nucleus is transparent. (No assumption need be made about the interior of the nucleus.) The predictions of the former model fit the data at small scattering angles. The predictions of the latter model fit the data at large scattering angles.

Information about the interaction of the alpha particle and the nucleus may also be derived from other experiments. For instance, the cross section for the production of neutrons from heavy elements bombarded by 40-Mev alpha particles is of the order of the geometrical area of the nucleus.[12] This implies that the nucleus is reasonably opaque to the alpha particle, but is not in disagreement with the existence of a transparent rim.

In order to obtain more exact information on the sizes of the nucleus and the alpha particle, and the interaction between the nucleus and the alpha particle, it will probably be necessary to compare the experiments with an exact calculation utilizing Coulomb wave functions and a complex nuclear potential with a diffuse edge.

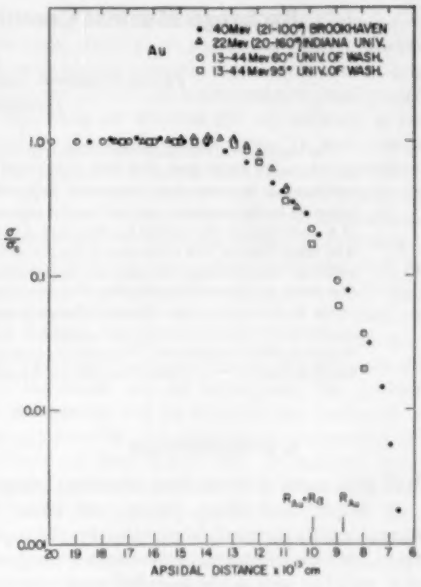

FIG. 11. σ/σ_c for Au as a function of apsidal distance.

6. ACKNOWLEDGMENTS

The authors would like to express their appreciation to the Brookhaven 60-inch cyclotron group. We would like to thank Professor K. W. Ford for generously supplying the results of computer calculations for the strong absorption models, for providing a summary of the unpublished Ford-Wheeler model, and for fitting the curves calculated from the latter model to the data of this experiment. We are indebted to Dr. C. E. Porter and Professor V. F. Weisskopf for many informative and stimulating discussions.

[12] Eisberg, Igo, and Wegner (to be published).

Exchange Moment Contributions to a Modified Shell Model

A. Russek
Physics Department, University of Buffalo, Buffalo, New York
(Received February 9, 1955)

The longitudinal exchange contribution to the nuclear magnetic moment that follows from a rather general modified shell model is studied. It is shown that for a heavy nucleus whose state can be expanded as a linear combination of certain very reasonable independent particle configurations, the longitudinal exchange contribution to the magnetic moment can be expressed, independent of the amplitudes of these states, in terms of a correction to the orbital Landé g-factor that appears in the single particle ordinary moment operator. The magnitude of this correction is simply given in terms of the fraction of the neutron-proton two-body potential that is charge exchange and spin-independent. Being independent of the configuration amplitudes, this result is expected to hold even if the core behaves as a liquid drop. Calculations assuming roughly half of the nuclear force to be charge exchange in nature reasonably account for the deviations from the values predicted by the shell model of the magnetic moments of those nuclei which consist of a single odd nucleon outside a doubly magic core. The exchange contributions generally improve the moment agreement of other nuclei in the $j=l-1/2$ cases, but make the agreement in the $f_{7/2}$ and $g_{9/2}$ cases poorer.

1. INTRODUCTION

THE shell model of the nucleus, when first advanced by Mayer[1] and Haxel, Jensen, and Suess,[2] enjoyed considerable success in accounting for the angular momenta, parities, and magnetic moments of the ground states of nuclei as well as the so-called magic numbers. It was then felt that the rather small deviations of the observed magnetic moments from the Schmidt values, predicted by this model, could be explained in terms of the contribution of the charged mesons responsible for charge exchange forces. This contribution, it was believed, acts essentially to quench the anomalous spin magnetic moments possessed by isolated nucleons when they are in the proximity of other nucleons, as in a nucleus.[3]

However, later evidence from quadrupole moments, isomeric transition rates, etc., has indicated that substantial corrections must be made to the shell model. Moreover, Kerman[4] has shown that when the sizes of the terms constituting the exchange moment contribution are adjusted to fit the parameters of a reasonable two-body force, the spin quenching effect is too small by a factor of about 10.

As a consequence of these developments, recent work has been mainly directed toward a modification of the nuclear model, but in the comparison of the observed values of the magnetic dipole moments with the values implied by a given model, exchange effects have thus far been entirely ignored despite the fact that there exists evidence for a sizeable longitudinal exchange moment contribution. This contribution, as was shown by Sachs[5] and Osborn and Foldy,[6] can be unambiguously determined in terms of the charge exchange part of the nuclear potential. Calculations were made by Spruch[7] for light nuclei and Ross[8] and Russek and Spruch[9] for heavy nuclei. The latter calculations were based on the shell model, and these are here extended to investigate the contribution of the longitudinal exchange moment to a prototype of a modified shell model. In Sec. 2, the model employed in the calculation is described and an intuitive justification for its use is given. In Sec. 3, the ordinary magnetic moments are calculated and in Sec. 4, the longitudinal exchange moment contribution is obtained.

The main result achieved in this paper is that so long as the $J=2$ part of the core can be expressed as a linear combination of certain very reasonable modified shell model states, the longitudinal exchange moment contribution to the moment of a heavy nucleus can be expressed, independent of the precise values of the amplitudes of these states, as a correction to the orbital Landé g-factor that appears in the single particle ordinary moment operator. If the $J=2$ part of the core consists of both neutron and protons, the exchange moment contributions of these to the over-all core magnetic moment effectively cancel each other, leaving a residual exchange moment due to the odd nucleon. This has the effect of raising the calculated moments of all odd-proton nuclei and lowering the moments of all odd-neutron nuclei. By the addition of the longitudinal exchange contribution, the strength of which is determined by the assumption that the charge exchange potential is about 50 percent of the total neutron-proton potential, the magnetic moments of the two odd-proton nuclei K^{39} and Bi^{209} are reasonably accounted for. (Both have a doubly magic core which should have no appreciable $J=2$ component.) The odd-neutron nucleus with a doubly magic core Pb^{207} has spin 1/2, the shell model state being $p_{1/2}$. The exchange moment contribution to this nucleus is small, thus retaining the

[1] M. G. Mayer, Phys. Rev. **75**, 16 (1950); M. G. Mayer, Phys. Rev. **78**, 22 (1950).
[2] Haxel, Jensen, and Suess, Z. Physik **128**, 295 (1950).
[3] H. Miyazawa, Progr. Theoret. Phys. (Japan) **6**, 801 (1951); F. Villars and V. F. Weisskopf (unpublished).
[4] A. K. Kerman, Phys. Rev. **92**, 1176 (1953).
[5] R. G. Sachs, Phys. Rev. **74**, 433 (1948).
[6] R. K. Osborn and L. L. Foldy, Phys. Rev. **79**, 795 (1950).
[7] L. Spruch, Phys. Rev. **80**, 372 (1950).
[8] M. Ross, Phys. Rev. **88**, 935 (1952).
[9] A. Russek and L. Spruch, Phys. Rev. **87**, 1111 (1952).

good agreement between the observed and the shell model moments.

2. THE MODEL

Among the proposed modifications of the "Mayer" state for odd-A nuclei,[10] nearly all include, in addition, states in which the odd nucleon interacts with a $J=2$ core. Of the two main types, the first assumes a liquid drop core coupled to the odd nucleon,[11] while the second admixes individual particle states in which the odd nucleon is coupled to the core nucleons by the addition of perturbations to the shell model Hamiltonian.[12] Inasmuch as the states obtained on the former are not suited to exchange moment calculations, the latter viewpoint will here be adopted. Although some detailed results have already been obtained in this direction, the states of heavy nuclei have not yet been fully worked out. For this reason, and because the results to be obtained do not warrant so fine a model, the nuclear ψ functions here employed for the moment calculations are rough prototypes of those which might be expected to result from a modified shell model. They can be used in this connection only because the magnetic moments are relatively insensitive to the finer details of the core structure.

The state Ψ of a heavy odd-A nucleus which is not an exception to the shell model and which has total angular momentum J and maximum projection $M_J=J$ is taken to be

$$\Psi=\alpha\Psi_s+\beta\sum_{nlj}a_{nlj}\Psi_a(nlj;2),$$
$$\sum_{nlj}|a_{nlj}|^2=1,\quad |\alpha|^2+|\beta|^2=1, \tag{1}$$

where Ψ_s is the shell-model state and the symbol $\Psi_a(nlj;2)$ represents the alternative state formed by a single nucleon or hole in the subshell of odd-type nucleons with total quantum number n, and orbital and total angular momentum quantum numbers l and j being coupled to a core with total angular momentum 2 so as to give a state with the same total angular momentum as the shell model state with maximum projection. Thus,

$$\Psi_a(nlj;2)=\sum_{m=-2}^{+2}\langle j2J-mm|j2JJ\rangle\psi_{nlj}{}^{J-m}\Phi_2{}^m, \tag{2}$$

where $\Phi_2{}^m$ represents the angular-momentum-2 core wave function in the state with projection m and $\langle j2J-mm|j2JJ\rangle$ are the appropriate Clebsch-Gordon coefficients, while $\psi_{nlj}{}^{j_z}$ represents either a nucleon or hole with major quantum number n, orbital angular momentum l, total angular momentum j and projection j_z, depending on whether the nlj subshell is full or empty in the shell model state. In most magnetic moment calculations, however, it is not necessary to distinguish between nucleons and holes. The summation over n, l, and j extends over all those subshells in the incomplete shell of odd-type nucleons for which l has the same parity as that predicted by the shell model (since all core states have even parity, odd nucleon states must have the same parity as the shell model state) and for which $J-2\leq j\leq J+2$, while a_{nlj} denotes the relative amplitudes of the alternate states. Since the states are all orthogonal, the probability that the nucleus will be found in any particular state is proportional to the absolute value squared of the amplitude of that state. The probability that the nucleus is in the shell model state is thus taken to be $|\alpha|^2$, while the sum of the probabilities of the odd nucleon being in any one of the allowed alternate states must then be equal to the remaining $1-|\alpha|^2=|\beta|^2$.

The core wave function is taken to be

$$\Phi_2{}^m=\sum_{nlj\tau}b_{nlj\tau}\varphi_2{}^m(nlj\tau)\chi_0{}^0, \tag{3}$$

where $\varphi_2{}^m(nlj\tau)$ is formed when either two nucleons or two holes in the n, l, j, τ subshell (τ is the isotopic spin, here used merely to distinguish neutron from proton subshells) couple to give a state with angular momentum 2:

$$\varphi_2{}^m(nlj\tau)=\sum_{m'}\langle jjm-m'm'|jj2m\rangle\psi_{nlj\tau}{}^{m-m'}\psi_{nlj\tau}{}^{m'}, \tag{4}$$

the coefficients $\langle jjm-m'm'|jj2m\rangle$ being the appropriate Clebsch-Gordon coefficients. $\chi_0{}^0$ is the zero angular momentum state describing the remaining core nucleons. The detailed structure of this part of the core is irrelevent in ordinary moment calculations and has no appreciable effect on the exchange contribution. $|b_{nlj\tau}|^2$ gives the probability that the $J=2$ part of the core consists of a pair of nucleons or holes in the n, l, j, τ subshell. $b_{nlj\tau}$ is assumed to differ appreciably from zero only for neutron and proton subshells in the respective incomplete shells, and the summation in Eq. (3) is, in general, extended over those subshells, with the exception of s-subshells, which are complete with two nucleons. However, if a nucleus contains a magic number of even-type nucleons, then even-type nucleons are not allowed to contribute to the $J=2$ core; similarly, if a nucleus contains one more or less than a magic number of odd-type nucleons, then these are not allowed to contribute to the $J=2$ core. It should be noted that the incomplete neutron and proton shells may be different. This is often the case in heavy nuclei.

Except for the fact that the core, in general, contains

[10] The term "Mayer" state is here used loosely to denote an odd nucleon outside a zero angular momentum core without necessarily assuming a shell structure to the core.

[11] L. L. Foldy and F. J. Milford, Phys. Rev. **80**, 751 (1950); A. Bohr, Phys. Rev. **81**, 134 (1951); A. Bohr and B. R. Mottelson, Kgl. Danske Videnskab. Selskab, Mat.-fys. Medd. **27**, (1953); A. K. Kerman (reference 4).

[12] D. Kurath, Phys. Rev. **80**, 98 (1950); B. H. Flowers, Phys. Rev. **86**, 254 (1952); B. H. Flowers, Proc. Roy. Soc. **A215**, 398 (1952); I. Talmi, Helv. Phys. Acta **25**, 185 (1952); D. Kurath, Phys. Rev. **91**, 1430 (1953).

both neutrons and protons, the nuclear wave function (1) is quite similar to that which follows from the statistical model proposed by Volkov.[13] However, in the intuitive justification to follow, more complicated couplings are indicated, which, although not affecting the magnetic moments profoundly affect the quadrupole moments.

The intuitive justification for the use of the nuclear wave function (1)–(4) can be based upon an argument advanced by Weisskopf[14,15] to explain the apparent weak interaction between individual nucleons required by the shell model. Weisskopf holds that it is possible for a nucleon to make several revolutions in a given orbit, being unable to suffer changes in momentum in collisions with other nucleons, inasmuch as the possible states into which it could be scattered are already occupied. To the extent that there are, in the partially filled neutron and proton shells, available empty states, there should appear, in addition to the predominant shell-model state, a small admixture of states which appear to be formed by the odd nucleon interacting with a $J=2$ core. It seems reasonable to assume that:

(I) The state of the nucleus is predominantly the shell model state.

(II) As a result of momentum transfers due to collisions, the nucleus spends part of the time in alternate states, the percentage of time decreasing exponentially with increasing energy calculated on the basis of the shell model with a small nucleon-nucleon potential added as a perturbation to the shell model Hamiltonian. Since the nucleus spends most of the time in the shell-model state, only collisions in which this is the initial state need be considered, and these can be divided into two classes.

(A) States formed when nucleons in filled j-subshells collide, sending some of them into empty subshells. The outer nucleon is unaffected and any alteration in the state of the core cannot affect the electric or ordinary magnetic moments, since, by conservation of angular momentum, the core must still have zero total angular momentum and, therefore, cannot contribute to the moments. The exchange contribution to the odd-nucleon moment, which results from an interaction with core nucleons, could, in principle, be affected, but the difference turns out to be negligible.

(B) States formed by the collision of nucleons in a filled subshell with nucleons in the subshell of the odd nucleon. The length of time spent by the nucleus in any resulting configuration decreases exponentially with the energy of that configuration due to the small mutual interaction of individual nucleons. Inasmuch as the lowest energy configurations have the least number of unpaired nucleons on account of the pairing energy[1,16] it will be assumed that the only configurations with appreciable half-lives have an odd number of nucleons in only one subshell. These couple to give a state of half-odd-integral angular momentum, which, in general, is different from the angular momemtum of the nucleus as a whole. In order for the latter to be conserved, this state must be coupled to a core with nonzero angular momentum, $J=2$ presumably being energetically favored. Since the energy gap between subshells on closing a shell is large, the probability is small that any of the alternate states are formed by the coupling of neutron and proton states other than those in the respective partially filled shells.

For the present discussion, a simple nucleus will be considered, in which, in the shell-model state, all subshells are filled up to the subshell containing the odd nucleon, the latter containing but a single nucleon. Starting from such a state, all alternate states which satisfy the above conditions, which affect the nuclear moments and which arise from two-nucleon collisions must, of necessity, be the result of a collision between a pair of odd-type nucleons; i.e., the odd nucleon and one from a filled subshell. Both must be scattered into the same subshell (either that of the odd nucleon or an empty one) and couple to $J=2$; the hole that remains behind in the previously filled subshell now becomes the "odd nucleon." Three-nucleon collisions would involve the odd nucleon and a pair of nucleons from a filled subshell of either protons or neutrons. Two of the three would be scattered into an available subshell of of the proper type where they would couple to $J=2$ or $J=0$. Inasmuch as the pair of holes left behind could also couple to $J=2$ or $J=0$, there are three possibilities: either a pair of nucleons in a normally empty subshell or a pair of holes in a normally full subshell could constitute the $J=2$ part of the core or, less probably, on the basis of energy considerations, both could couple simultaneously to $J=2$, the two then coupling together to give the required $J=2$ core. It is not even excluded that the two individual components of this core each couple to $J=1$. However, the more complicated multiple core couplings are not included in the core wave function (3), since, as will be shown in the following section, it is reasonable to expect that the inclusion of such states will not greatly affect the magnetic moment.

Only a simple nucleus was considered in this analysis, and, of course, additional configurations could arise if the subshell of the odd nucleon contained more than one nucleon, or if, in the basic state, two subshells are partially filled. These possibilities are ignored in the rough model considered here, and to this extent, the alternative configurations to be admixed with the shell-model state consist of the "odd" nucleon in any one of the subshells in the incomplete odd-nucleon shell (consistent with parity requirements) coupled to a $J=2$ core which consists of pairs of either protons or neutrons in normally empty subshells, or pairs of holes in normally filled subshells of the respective incomplete shells coupled to $J=2$. The so-called "odd nucleon"

[13] A. B. Volkov, Phys. Rev. **94**, 1664 (1954).
[14] V. F. Weisskopf, Science **113**, 101 (1951).
[15] V. F. Weisskopf, Physica **18**, 1083 (1952).
[16] A. de-Shalit and M. Goldhaber, Phys. Rev. **92**, 1211 (1953).

consists of either a single nucleon in an otherwise empty subshell or a single hole in an otherwise filled subshell. The nuclear state described by Eqs. (1) to (4) neither includes alternative configurations of the $J=0$ core nor more complicated configurations of the $J=2$ core, since these considerations do not affect the magnetic moments.

3. NONEXCHANGE MOMENT

The ordinary magnetic moment M_z^{ord} is defined as the expectation value of the magnetic moment operator μ_z^{ord}, where

$$\mu_z^{\text{ord}}=\sum_{\nu=1}^{Z}[g_{lp}l_{z\nu}+g_{sp}s_{z\nu}]+\sum_{\nu=Z+1}^{A}[g_{ln}l_{z\nu}+g_{sn}s_{z\nu}] \quad (5)$$

for that state in which the z-component of angular momentum is maximum. Here g_{lp}, g_{sp}, g_{ln}, and g_{sn} are, respectively, the orbital and spin gyromagnetic ratios of the proton and neutron. The summation is extended over all protons and neutrons in the nucleus. Letting Ψ represent the unsymmetrized state (1), which has angular momentum J and $M_J=J$ understood, then

$$M_z^{\text{ord}}=\left(\frac{1}{(Z!(A-Z)!)^{\frac{1}{2}}}P\Psi,\ \mu_z^{\text{ord}}\frac{1}{(Z!(A-Z)!)^{\frac{1}{2}}}P\Psi\right), \quad (6)$$

where the antisymmetrization operator P is the sum over all $Z!(A-Z)!$ permutations of the A particles in the nucleus which do not interchange neutrons and protons, the odd permutations being multiplied by -1, the even permutations by $+1$. Since all permutation operators commute with μ_z^{ord} and are self-adjoint, they can be transposed to the left-hand side of the inner product to give

$$M_z^{\text{ord}}=(P\Psi,\mu_z^{\text{ord}}\Psi), \quad (7)$$

owing to identity

$$P^2=Z!(A-Z)!P. \quad (8)$$

Substitution of (1) and (2) into (7) yields

$$M_z^{\text{ord}}=|\alpha|^2(P\Psi_s,\mu_z^{\text{ord}}\Psi_s)+\sum_{nljm}\sum_{n'l'j'm'}\{|\beta|^2\bar{a}_{nlj}a_{n'l'j'}\langle j2J-mm|j2JJ\rangle^*\langle j'2J-m'm'|j'2JJ\rangle$$
$$\times(P\psi_{nlj}{}^{J-m}(o)\Phi_2{}^m(c)\chi_0{}^0(c'),\mu_z^{\text{ord}}\psi_{n'l'j'}{}^{J-m'}(o)\Phi_2{}^{m'}(c)\chi_0{}^0(c'))+\alpha\bar{\beta}\bar{a}_{nlj}\langle j2J-mm|j2JJ\rangle^*$$
$$\times(P\psi_{nlj}{}^{J-m}(o)\Phi_2{}^m(c)\chi_0{}^0(c'),\mu_z^{\text{ord}}\Psi_s)+\bar{\alpha}\beta a_{n'l'j'}\langle j'2J-m'm'|j'2JJ\rangle(P\Psi_s,\mu_z^{\text{ord}}\psi_{n'l'j'}{}^{J-m'}(o)\Phi_2{}^{m'}(c)\chi_0{}^0(c'))\}, \quad (9)$$

where o stands for the space and spin coordinates of the nucleon, or nucleons in the subshell containing the odd number of nucleons, while c and c' stand for the space and spin coordinates of the $J=2$ and $J=0$ parts of the core, respectively. In this connection, it should be noted that for the unsymmetrized ψ function it is immaterial which nucleons are assigned to the core and which are assigned to the odd subshell in each term.

A detailed investigation shows that all cross terms between the shell model state Ψ_s and the alternate states vanish, as do most of the cross-terms between the different alternate states. As a matter of fact, the only nonvanishing cross terms occur between states in which a single nucleon or hole is shifted from a $j=l+1/2$ subshell to the $j=l-1/2$ subshell with the same orbital quantum number, or *vice versa*. No conclusions can be drawn regarding the actual cross-term contributions, except to indicate the maximum size, since these contributions to the moment depend, in magnitude and sign, on the relative phases of the amplitudes of the shell model and alternate states. These phases cannot be guessed at from the physical arguments presented in the previous section, and it is for this reason that free use was made of the words "time spent in" and "probability" instead of "amplitude" in that section. The latter implies more information than the two former. Therefore, the third and fourth expressions of Eq. (9) vanish identically, and the only terms which survive from the second expression are those for which $l=l'$ and $j=j'$ or $j=j'\pm1$. Finally, orthogonality relations require that $m=m'$. Making use of the relations,

$$\langle JM_J|\mathfrak{y}|JM_J\rangle=(M_J/J)\langle JJ|\mathfrak{y}|JJ\rangle, \quad (10)$$

that hold between the expectation values of the moment operator in the states of different projection of the total angular momentum quantum number,[17] and remembering that the $J=0$ part of the core cannot contribute to the moment, the nonvanishing terms of (9) can be written, more simply, as

$$M_z^{\text{ord}}=|\alpha|^2(M_s)_{lsjs\tau_z}+|\beta|^2$$
$$\times\left\{\sum_{nlj}|a_{nlj}|^2\sum_{m=-2}^{+2}|\langle j2J-mm|j2JJ\rangle|^2\right.$$
$$\times\left[\frac{J-m}{j}(M_s)_{lj\tau}+\frac{m}{2}(M_s)_{c\tau}\right]$$
$$\left.+2\ \text{Re}\sum_{nl}{}'\bar{a}_{nll+\frac{1}{2}}a_{nll-\frac{1}{2}}A_{lJ}(g_{l\tau}-g_{s\tau})\right\}, \quad (11)$$

where

$$A_{lJ}=\sum_m\langle l+\tfrac{1}{2}2J-mm|l+\tfrac{1}{2}2JJ\rangle^*$$
$$\times\langle l-\tfrac{1}{2}2J-mm|l-\tfrac{1}{2}2JJ\rangle\frac{[(l+\frac{1}{2})^2-(J-m)^2]^{\frac{1}{2}}}{2l+1}, \quad (12)$$

$$(M_s)_{lj\tau}=g_{l\tau}\langle l_s\rangle_{lj}+g_{s\tau}\langle s_z\rangle_{lj}.$$

[17] E. V. Condon and G. H. Shortley, *The Theory of Atomic Spectra* (The Macmillan Company, New York, 1935), pp. 59–64.

$(M_z)_{lj\tau}$ is the ordinary moment of a single nucleon or hole in the l, j, τ subshell (τ differentiating proton from neutron) with $m_j=j$ and $l_z j_z \tau_z$ are the quantum numbers describing the odd-nucleon subshell in the shell-model state, while $(M_z)_{c2}$ is the ordinary moment of the $J=2$ part of the core, also in the state of maximum projection. The summation $\sum_{nlj}$ is taken over all odd-type nucleon subshells which are allowed, in a given nucleus, to participate in the alternate states, whereas the summation $\sum_{nl}'$ over the cross terms extends over those allowed values of n, l for which both the $j=l+1/2$ and $j=l-1/2$ subshells are in the same shell and are either full or empty in the shell-model state. (A subshell with only one occupant in the shell-model state should here be considered as empty, while one with a single hole should be considered as full.)

Making use of the core wave function (3), the moment of the core is given by

$$(M_z)_{c2}=\sum_{nlj\tau}|b_{nlj\tau}|^2(\varphi_2^2(nlj\tau),\mu_z^{\text{ord}}\varphi_2^2(nlj\tau)), \quad (13)$$

since the zero angular momentum part of the core does not contribute to the moment and all nondiagonal terms vanish. It is shown in the Appendix that when an arbitrary number of nucleons in the same l, j, τ subshell couple to a state with total angular momentum two and maximum projection, the resulting moment is

$$(\varphi_2^2(nlj\tau),\mu_z^{\text{ord}}\varphi_2^2(nlj\tau))=(2/j)(M_z)_{lj\tau}, \quad (14)$$

independent of whether the core is constructed from nucleons or holes. Consequently the core moment implied by (3) and (4) is given by

$$(M_z)_{c2}=\sum_{nlj\tau}|b_{nlj\tau}|^2\frac{2}{j}(M_z)_{lj\tau}. \quad (15)$$

Equation (15) is just the weighted average of the quantity $2(M_z)_{lj\tau}/j$. It is shown in the appendix that when an arbitrary number of nucleons in one subshell (n,l,j,τ) and an arbitrary number of nucleons in another subshell (n',l',j',τ') each separately couple to states with the same angular momentum J_I, the two states then coupling to an over-all core angular momentum of two, the magnetic moment is given by the expression

$$\frac{1}{j}(M_z)_{lj\tau}+\frac{1}{j'}(M_z)_{l'j'\tau'}, \quad (16)$$

which is the average of the moments that would result if nucleons from each subshell alone constituted the $J=2$ part of the core for half the time occupied by the combination. Now, the relative probabilities with which the various subshells appear in such combinations would be expected to be in the same ratios as the relative probabilities that these subshells alone constitute the $J=2$ part of the core. If one makes this assumption, the average moment of the core, given by Eq. (15), is unaffected by the inclusion of these particular more complicated couplings.

4. LONGITUDINAL EXCHANGE MOMENT CONTRIBUTION

The longitudinal exchange moment operator[5] is given as

$$\mu_z^{\text{ex}}=\frac{ie}{2\hbar c}\sum_{\pi=1}^{Z}\sum_{\nu=Z+1}^{A}V_{\text{ex}}(r_{\pi\nu})(\mathbf{r}_\pi\times\mathbf{r}_\nu)_z P_{\pi\nu}, \quad (17)$$

where V_{ex} describes that part of the two-body charge exchange potential which is spin-independent, while $P_{\pi\nu}$ interchanges the spatial coordinates of the πth proton and νth proton. The longitudinal exchange moment contribution to the magnetic moment is the expectation value of this operator for that state in which the z-component of angular momentum is maximum, and will be given by the same expression as Eq. (9) if μ_z^{ord} is replaced by μ_z^{ex}. A detailed investigation, similar to that required in the preceding section, shows that the only nonvanishing cross terms occur between states in which a single nucleon or hole is shifted from one subshell to another. Because μ_z^{ex} is a component of a vector operator, the angular momenta of the two states involved must either be equal or differ by ±1;

$$\text{(a)}\quad j'=j\quad\text{or (b)}\quad j'=j\pm1. \quad (18)$$

The case (a), in which $j'=j$, can arise only when $l'=l\pm1$, and this possibility is removed by parity considerations. If an odd number of nucleons change parity, as will happen in this case, the parity of the entire nuclear wave function is changed, in violation of the requirement that this shall be a good quantum number. This leaves the four possibilities subsumed under (b); namely

(1) $j'=j+1$, $l'=l$, $\quad j=l-1/2$, $j'=l+1/2$,

(2) $j'=j+1$, $l'=l+2$, $j=l+1/2$, $j'=l'-1/2=l+3/2$,

(3) $j'=j-1$, $l'=l$, $\quad j=l+1/2$, $j'=l-1/2$,

(4) $j'=j-1$, $l'=l-2$, $j=l-1/2$, $j'=l'+1/2=l-3/2$.

Now, if the interaction of the odd nucleon with the $J=2$ part of the core is neglected (an approximation which is expected to be good, provided that the number of nucleons involved in this part of the core is small compared to the total number of core nucleons), then the possibilities (2) and (4) of (b) are eliminated. This follows from the fact that the operator (17) is spin-independent; the spin coordinates of the odd nucleon can be eliminated from the matrix elements, each matrix element being decomposed into two terms, both of which are matrix elements of a vector ($J=1$) operator between states having total angular momentum l and $l\pm2$ and, as such, vanish.[18]

[18] See reference 17, p. 60.

Consequently, the nonvanishing cross terms occur only between states in which a single odd nucleon or hole is shifted from a $j=l+\frac{1}{2}$ subshell to the respective $j=l-\frac{1}{2}$ subshell, or *vice versa*. The surviving terms of the expectation value of the longitudinal exchange moment operator (17) are, therefore,

$$M_z^{ex}=|\alpha|^2(M_z^{ex})_{shell}+|\beta|^2\sum_{nlj}|a_{nlj}|^2\sum_{m=-2}^{+2}|\langle j2J-mm|j2JJ\rangle|^2$$
$$\times(P\psi_{nlj}{}^{J-m}(o)\Phi_2{}^m(c)\chi_0{}^0(c'),\ \mu_z{}^{ex}\psi_{nlj}{}^{J-m}(o)\Phi_2{}^m(c)\chi_0{}^0(c'))+2|\beta|^2\,\mathrm{Re}\sum_{nl}{}'\bar{a}_{nll+\frac{1}{2}}a_{nll-\frac{1}{2}}$$
$$\times\sum_{m,m'=-2}^{+2}\langle l+\tfrac{1}{2}2J-mm|l+\tfrac{1}{2}2JJ\rangle^*\langle l-\tfrac{1}{2}2J-m'm'|l-\tfrac{1}{2}2JJ\rangle$$
$$\times(P\psi_{nll+\frac{1}{2}}{}^{J-m}(o)\Phi_2{}^m(c)\chi_0{}^0(c'),\ \mu_z{}^{ex}\psi_{nll-\frac{1}{2}}{}^{J-m'}(o)\Phi_2{}^{m'}(c)\chi_0{}^0(c')),\quad(18)$$

where the indicated summations are to be taken over the same subshells as the corresponding sums in Eq. (11). Neglecting the interactions between the odd nucleon and the $J=2$ part of the core and between the protons and neutrons which contribute to this part of the core (on the assumption that there are relatively few interacting pairs of this type as compared to the many interacting pairs between the odd nucleon and the $J=2$ part of the core, on the one hand, and the $J=0$ part of the core, on the other hand) (18) becomes, with the help of Eq. (10)

$$M_z^{ex}=|\alpha|^2(M_z^{ex})_{shell}+|\beta|^2\sum_{nlj}|a_{nlj}|^2\sum_{m=-2}^{+2}|\langle j2J-mm|j2JJ\rangle|^2\left\{\frac{J-m}{j}(M_z^{ex})_{nljr}+\frac{m}{2}(M_z^{ex})_{c2}\right\}$$
$$+2|\beta|^2\,\mathrm{Re}\sum_{nl}{}'\bar{a}_{nll+\frac{1}{2}}a_{nll-\frac{1}{2}}\langle l+\tfrac{1}{2}2J-mm|l+\tfrac{1}{2}2JJ\rangle^*\langle l-\tfrac{1}{2}2J-mm|l-\tfrac{1}{2}2JJ\rangle$$
$$\times(P\psi_{nll+\frac{1}{2}}{}^{J-m}(o)\chi_0{}^0(c'),\ \mu_z{}^{ex}\psi_{nll-\frac{1}{2}}{}^{J-m}(o)\chi_0{}^0(c')).\quad(19)$$

Here, $(M_z^{ex})_{nljr}$ is the exchange moment due to a single nucleon or hole with quantum numbers n, l, j, τ interacting with the $J=0$ part of the core, while $(M_z^{ex})_{c2}$ is the contribution due to the $J=2$ part of the core interacting with the $J=0$ part of the core.

$$(M_z^{ex})_{nljr}=(P\psi_{nljr}{}^{J-m}(o)\chi_0{}^0(c'),\ \mu_z{}^{ex}\psi_{nljr}{}^{J-m}(o)\chi_0{}^0(c')),\quad(20)$$

$$(M_z^{ex})_{c2}=(P\Phi_2{}^2(c)\chi_0{}^0(c'),\ \mu_z{}^{ex}\Phi_2{}^2(c)\chi_0{}^0(c')).\quad(21)$$

By making use of Eqs. (3), (4), and (10), and neglecting the interactions of the particles c with each other, (21) reduces to

$$(M_z^{ex})_{c2}=\sum_{nljr}|b_{nljr}|^2\frac{2}{j}(M_z^{ex})_{nljr}.\quad(22)$$

As in the case of the ordinary core moment, this result will also hold if the more complicated couplings are included in which an arbitrary number of nucleons in one subshell and an arbitrary number of nucleons in another subshell each couple separately to states with the same angular momentum J_I, the two states then coupling to give an over-all core angular momentum of $J=2$, again provided that the relative probabilities that the various subshells appear in such combinations are in the same ratios as the relative probabilities that these subshells alone constitute the $J=2$ part of the core.

Finally, it was shown, in a previous paper,[9] that for the heavier nuclei, the longitudinal exchange contribution to the moment of a single nucleon interacting with a $J=0$ core which also has $L=0$ (a condition which certainly holds if the $J=0$ part of the core consists of complete l-shells) can be expressed approximately in the form

$$(M_z^{ex})_{nljr}=C_\tau D\langle l_z\rangle_{lj},\quad(23)$$

where $C_p=0.3$ for a proton and $C_n=-0.25$ for a neutron, which to the extent that the approximation is valid, is independent of n and depends only on the orbital and total angular momentum of that nucleon. D gives the fraction of the spin-independent part of the neutron-proton force that is charge exchange in nature. The evaluation of the cross-term contributions of Eq. (19) can be effected in the same manner as in the appendix of the above mentioned reference to give

$$(P\psi_{nll+\frac{1}{2}\tau}{}^{J-m}(o)\chi_0{}^0(c'),\ \mu_z{}^{ex}\psi_{nll-\frac{1}{2}\tau}{}^{J-m}(o)\chi_0{}^0(c'))$$
$$=C_\tau D[(l+\tfrac{1}{2})^2-(J-m)^2]^{\frac{1}{2}}/(2l+1).\quad(24)$$

5. RESULTS AND CONCLUSIONS

It will be noted that for each term in the ordinary moment contribution (11), (12), (15), there is a corresponding term in the exchange moment contribution (19), (22), (24). The total nuclear moment can then

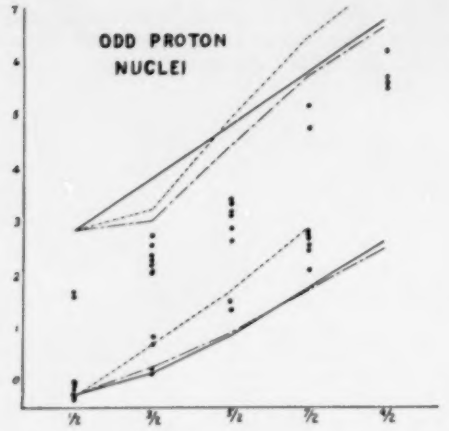

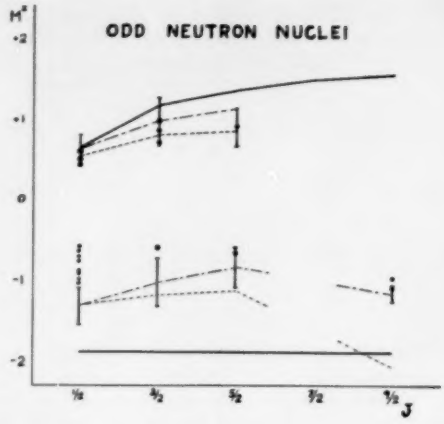

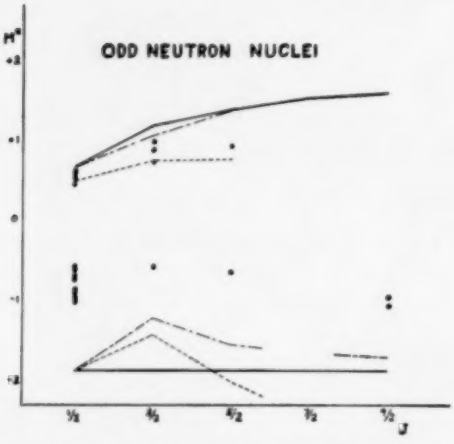

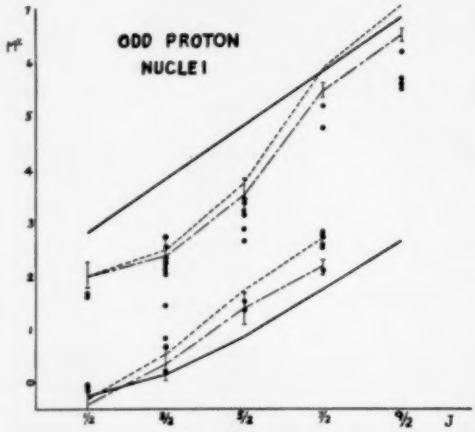

FIG. 1. The magnetic moments, in nuclear Bohr magnetons, of odd-A nuclei with $A>40$ which do not consist of a single particle or hole outside a doubly magic core are plotted against the nuclear angular momentum J. The heavy black lines indicate the shell-model moments and the dashed lines give the moments that follow from the Foldy-Milford model. The coefficients for the latter were taken from Milford[19] for the case in which only zero and one $J=2$ phonon core excitations were considered and the angular momentum of the odd nucleon was held constant at the shell-model assignment. The Foldy-Milford moments corrected for the exchange contributions are indicated by the dotted lines.

FIG. 2. The magnetic moments, in nuclear Bohr magnetons, of odd-A nuclei with $A>40$ which do not consist of a single particle or hole outside a doubly magic core are plotted against the nuclear angular momentum J. The heavy black lines indicate the shell-model moments and the dashed lines give the average of the ordinary moments (averaged over all cases, for each l, j, which correspond to the nuclei observed in each category) that result when the shell-model state is given 50 percent weight and the remaining 50 percent is equally distributed over all allowed alternate states. The vertical lines indicate the maximum deviations that could result, with this weight assignment, from the cross-term contributions. When corrected for the exchange contributions, the average moments are shifted to the positions shown by the dotted lines.

be written in the form

$$M_z^{\rm tot}=M_z^{\rm ord}+M_z^{\rm ex}=|\alpha|^2(M_z^{\rm ord}+M_z^{\rm ex})_{nlj\tau_z}$$
$$+|\beta|^2\left\{\sum_{nlj}|a_{nlj}|^2\sum_{m=-2}^{+2}|\langle j2J-mm|j2JJ\rangle|^2\right.$$
$$\times\left[\frac{J-m}{j}(M_z^{\rm ord}+M_z^{\rm ex})_{nlj\tau}+\frac{m}{2}(M_z^{\rm ord}+M_z^{\rm ex})_{c2}\right]$$
$$\left.+2\,\mathrm{Re}\sum_{nl}{}'a_{nll+\frac{1}{2}}a_{nll-\frac{1}{2}}A_{lJ}(g_{l\tau}-g_{s\tau}+C_\tau D)\right\},\quad(25)$$

where

$$(M_z^{\rm ord}+M_z^{\rm ex})_{c2}=\sum_{nlj\tau}|b_{nlj\tau}|^2\frac{2}{j}(M_z^{\rm ord}+M_z^{\rm ex})_{nlj\tau},$$
$$(M_z^{\rm ord}+M_z^{\rm ex})_{nlj\tau}=(g_{l\tau}+C_\tau D)\langle l_z\rangle_{lj}+g_{s\tau}\langle s_z\rangle_{lj}.\quad(26)$$

It is therefore apparent that the longitudinal exchange contribution to the moment can be expressed as a correction to the single particle orbital g-factor of the ordinary moment which may be regarded as being due

TABLE I. The magnetic moments of odd-A nuclei with $A>40$ which do not consist of a single nucleon or hole outside a doubly magic core are here listed in nuclear Bohr magnetons. M_{exp} and M_{shell} are the experimental and shell model moments respectively. M^{ord} and M^{tot} give the moments that follow from the model described in the text without and with the exchange contribution.

		$j=l+1/2$						$j=l-1/2$			
J	Element	M_{exp}	M_{shell}	M^{ord}	M^{tot}	J	Element	M_{exp}	M_{shell}	M^{ord}	M^{tot}
					Odd-proton nuclei						
1/2	Tl^{203}	1.61	2.79	1.97	1.99	1/2	Y^{89}	−0.14	−0.26	−0.46	−0.39
	Tl^{205}	1.63	2.79	1.97	1.99		Ag^{107}	−0.11	−0.26	−0.40	−0.31
							Ag^{109}	−0.13	−0.26	−0.40	−0.31
3/2	Cu^{63}	2.23	3.79	1.92	1.96						
	Cu^{65}	2.39	3.79	1.92	1.96	3/2	Cl^{35}	0.82	0.13	0.47	0.64
	Ga^{69}	2.02	3.79	2.41	2.52		Cl^{37}	0.68	0.13	0.74	0.99
	Ga^{71}	2.56	3.79	2.41	2.52		K^{41}	0.22	0.13	−0.09	0.02
	As^{75}	1.44	3.79	2.41	2.52		Au^{197}	0.20	0.13	0.26	0.44
	Br^{79}	2.11	3.79	2.41	2.52						
	Br^{81}	2.27	3.79	2.41	2.52	5/2	Rb^{85}	1.35	0.86	1.28	1.57
	Rb^{87}	2.75	3.79	2.90	3.08		Eu^{153}	1.5	0.86	1.51	1.82
5/2	Sb^{121}	3.34	4.79	3.32	3.49	7/2	Cs^{133}	2.58	1.72	2.10	2.56
	Re^{185}	3.14	4.79	3.47	3.72		Cs^{135}	2.73	1.72	2.10	2.56
	Re^{187}	3.18	4.79	3.47	3.72		Cs^{137}	2.84	1.72	2.43	3.08
	Eu^{151}	3.4	4.79	3.47	3.72		La^{139}	2.78	1.72	2.43	3.08
	I^{127}	2.81	4.79	3.58	3.83		Lu^{175}	2.6	1.72	1.96	2.41
	I^{129}	2.62	4.79	3.58	3.83		Ta^{181}	2.1	1.72	1.96	2.41
7/2	Sc^{45}	4.75	5.79	5.06	5.42						
	V^{51}	5.14	5.79	5.79	6.24						
9/2	Nb^{93}	6.17	6.79	6.55	7.11						
	Tc^{99}	5.68	6.79	6.55	7.11						
	In^{113}	5.50	6.79	6.39	6.91						
	In^{115}	5.51	6.79	6.39	6.91						
					Odd-neutron nuclei						
1/2	Cd^{111}	−0.60	−1.91	−1.33	−1.34	1/2	Hg^{199}	0.50	0.64	0.62	0.53
	Cd^{113}	−0.62	−1.91	−1.33	−1.34		Pt^{195}	0.61	0.64	0.62	0.53
	Sn^{115}	−0.92	−1.91	−1.28	−1.28		Yb^{171}	0.45	0.64	0.62	0.53
	Sn^{117}	−1.00	−1.91	−1.28	−1.28						
	Sn^{119}	−1.05	−1.91	−1.28	−1.28	3/2	Xe^{131}	0.7	1.15	0.94	0.72
	Xe^{129}	−0.77	−1.91	−1.32	−1.33		Ba^{135}	0.84	1.15	0.94	0.72
	Te^{123}	−0.73	−1.91	−1.32	−1.33		Ba^{137}	0.96	1.15	1.09	0.92
	Te^{125}	−0.88	−1.91	−1.32	−1.33						
						5/2	Zn^{67}	0.9	1.36	1.14	0.85
3/2	Hg^{201}	−0.60	−1.91	−1.05	−1.20						
5/2	Yb^{173}	−0.65	−1.91	−0.85	−1.14						
9/2	Kr^{83}	−0.97	−1.91	−1.60	−2.22						
	Sr^{87}	−1.1	−1.91	−1.40	−1.93						

to the promimity of nuclear matter.[9] This result holds over an even wider range of states than those expressible in the form (1)–(4) whenever cross terms can be neglected. It then holds as long as the nuclear state can be expanded as a linear combination of products of single particle wave functions with relatively few nucleons not coupled to $L=0$, $J=0$, for then the total magnetic moment is just a linear combination of the $(M_s^{ord}+M_s^{ex})_{nljr}$, and by the second equation of (26), the conclusion is obvious. Even in a liquid drop core model of the nucleus, therefore, the orbital g-factor may, if D, the fraction of the nuclear force which is charge exchange in nature, is roughly taken as 0.5, be written as

$$g_{lp}=1+C_pD\simeq 1.15,$$
$$g_{ln}=C_nD\simeq -0.13. \tag{27}$$

Since the excited part of the core contains approximately equal numbers of protons and neutrons, the exchange contributions of neutrons and protons to the core moment effectively cancel each other, leaving only the ordinary core moment. The remaining exchange contribution (to the odd-nucleon moment) increases the moments of odd-proton nuclei and decreases the moments of odd-neutron nuclei.

Figure 1 shows the magnetic moments that result from the Foldy-Milford model in which the total angular momentum of the odd nucleon does not change in the interaction with the excited core. The coefficients are taken from Milford[10] for the case in which only one angular-momentum-2 phonon is excited on the core

[10] F. J. Milford, Phys. Rev. 93, 1297 (1954).

TABLE II. The magnetic moments of nuclei which consist of one particle or hole outside a doubly magic core are given in nuclear Bohr magnetons. The experimental moments, the shell-model moments, and the moments corrected for the exchange contribution, M_{tot}, are listed.

Element	Shell-model state	M_{exp}	M_{shell}	M^{tot}
K^{39}	$d_{3/2}$	0.39	0.13	0.40
Bi^{209}	$h_{9/2}$	4.04	2.63	3.37
Pb^{207}	$p_{1/2}$	0.59	0.64	0.56

surface. The moments corrected for the exchange contribution are also shown.

Milford estimates that the lowest excited core state corresponds to an excitation energy of about 2.25 Mev for a medium-sized nucleus. For this same nucleus, the higher-energy odd-nucleon states within the same shell do not differ by much more than this, so it is likely that the odd nucleon contributes appreciably from all allowable states within the same shell for which $J-2\leq j\leq J+2$. In this direction, calculations were made assigning 50 percent probability to the shell-model state and equal probability to all allowed alternate states for those nuclei which do not consist of a single nucleon outside of a doubly magic core. These results, with cross terms neglected, are listed in Table I. They include many different cases, depending on the particular neutron and proton shells being filled, and since not much significance can be attached to the rather small differences in the moments that arise from the different cases owing to the roughness of the model, only the average moments (averaged over all combinations of neutron and proton shells, for each j, l, τ which correspond to the actual combinations represented by the appropriate nuclei) are plotted in Fig. 2. It is worth mentioning, however, that the larger deviations of the calculated moments from the average of calculated moments are due to the inability of either neutrons or protons to contribute, in a given nucleus, to the core moment, as happens when the even-type nucleons form a complete shell, or the odd-type nucleons number one more or less than a complete shell. In such cases, it is found that the experimental moments deviate from the average experimental moments in the same direction in 12 cases and in the opposite direction in only 4 cases. Thus, even this rough model follows, to some extent, the fluctuations of the observed moments. Figure 2 also shows the average moments corrected for the exchange contribution and indicates the maximum possible cross-term contribution that could result from this model with the given weight assignment. If this is to be taken as an indication, it is seen that the cross-term contributions are, at worst, small, but not insignificant. The calculated moments give poor agreement in only the $f_{7/2}$ and $g_{9/2}$ cases. The first shortcoming may be taken as an indication that the 21–28 shell, which consists of $f_{7/2}$ particles only, is not widely separated in energy from adjacent states and that there are contributions from these states. The second shortcoming is due to the fact that the $g_{9/2}$ subshell has opposite parity from the rest of the subshells in its shell. This would lead one to suspect a contribution from the $g_{7/2}$ subshell, the rather small deviations of the observed moments from the Schmidt curves being an indication that this contribution is rather small.

For those nuclei which consist of a single nucleon outside of a doubly magic core, it is assumed that the lowest-lying excited states will have energies too high to be appreciably excited. For these nuclei (K^{39}, Bi^{209}, and Pb^{207}), the shell-model state must have nearly unit amplitude, and, as a result, there should be very little contribution to the magnetic moment from any modification of the nuclear model. For these, Table II lists the observed moments, the shell model moments and the shell model moments corrected for the exchange contribution. It is apparent that the exchange contribution reasonably accounts for the moments of these nuclei. As a matter of fact, the exchange contribution to the moment of Bi^{209} is too small by an amount of 0.67 to account for the observed moment. This amount must be due to a small admixture of alternate states, and the contribution should be, and is, a little smaller (on account of the larger energy separation) than the deviations of the $g_{9/2}$ odd proton nuclei, which must be also due to excitation of states outside the shell in question.

APPENDIX I

Let $\varphi^M(nlj; J_c)$ describe the state in which an arbitrary number of nucleons in the n, l, j subshell couple to a state with angular momentum J_c (which need not be 2) and projection M. This state can be written in terms of the individual particle states:

$$\varphi^M(nlj; J_c)=\sum_q C_q \Pi_i \psi_{nljm(q_i)}(\mathbf{r}_i\sigma_i), \tag{28}$$

where

$$\textstyle\sum_i m(q_i)=M \text{ for all } q, \ \sum_q |C_q|^2=1. \tag{29}$$

Here, the summation over q runs over all possible combinations of different values of m which add up to M, while i runs over all nucleons involved in the coupling. Since they are identical, they all have the same $g_{l\tau}$ and $g_{s\tau}$, so that

$$\begin{aligned} M^s &= g_{l\tau}(\varphi, \textstyle\sum_i l_{zi}\varphi)+g_{s\tau}(\varphi, \sum_i s_{zi}\varphi) \\ &= \sum_q |C_q|^2 \sum_i \{g_{l\tau}(\psi_{nlj\tau}{}^{m(q_i)}(i), l_{zi}\psi_{nlj\tau}{}^{m(q_i)}(i)) \\ &\qquad + g_{s\tau}(\psi_{nlj\tau}{}^{m(q_i)}(i), s_{zi}\psi_{nlj\tau}{}^{m(q_i)}(i))\}. \end{aligned} \tag{30}$$

However,

$$\begin{aligned} &\left(\psi_{nlj\tau}{}^{m(q_i)}, \begin{bmatrix} l_z \\ s_z \end{bmatrix}\psi_{nlj\tau}{}^{m(q_i)}\right) \\ &\qquad = \frac{m(q_i)}{j}\left(\psi_{nlj\tau}{}^{j}, \begin{bmatrix} l_z \\ s_z \end{bmatrix}\psi_{nlj\tau}{}^{j}\right), \end{aligned} \tag{31}$$

so that

$$M_s=(\psi_{nljT}{}^j,[g_{lT}l_s+g_{sT}S_s]\psi_{nljT}{}^j)\sum_q|C_q|^2\sum_i\frac{m(q_i)}{j},$$

and, finally,

$$M_s=(M/j)(M_s)_{nljT}. \tag{32}$$

APPENDIX II

Let an arbitrary number of nucleons in the $nljT$ subshell couple to a state with angular momentum J and an arbitrary number of nucleons from the $n'l'j'T'$ subshell couple to a state with angular momentum J', and let these two states couple together to angular momentum 2 with maximum projection:

$$\Phi_2{}^2=\sum_M a_M\varphi_J{}^M(1)\varphi_{J'}{}^{2-M}(2), \tag{33}$$

where 1 and 2 refer to the coordinates of the nucleons in the respective subshells, and the a_M are the Clebsch-Gordon coefficients. The states $\varphi_J{}^M$ and $\varphi_{J'}{}^M$ are of the form described in Appendix I, with the quantum numbers describing the subshell suppressed. Since only diagonal terms of the expectation value of the moment operator survive,

$$M_s=\sum_M|a_M|^2[(\varphi_J{}^M(1),\mu_{s1}\varphi_J{}^M(1))+(\varphi_{J'}{}^{2-M}(2),\mu_{s2}\varphi_{J'}{}^{2-M}(2))]. \tag{34}$$

Using Eq. (10) and realizing that

$$\sum_M|a_M|^2M=\langle J_{s1}\rangle,\ \sum_M|a_M|^2(2-M)=\langle J_{s2}\rangle,$$

(34) yields, using the results of the previous Appendix:

$$M_s=\frac{\langle J_{s1}\rangle}{j}(M_s)_{nljT}+\frac{\langle J_{s2}\rangle}{j'}(M_s)_{n'l'j'T'}. \tag{35}$$

If $J=J'$, then $\langle J_{s1}\rangle=\langle J_{s2}\rangle=1$, giving the result (16).

PHYSICAL REVIEW VOLUME 99, NUMBER 3 AUGUST 1, 1955

Elastic Photoproduction of π^0 Mesons in Helium and (γ,n) Reaction on Helium at High Energies*

GERARD DESAUSSURE AND L. S. OSBORNE
Laboratory for Nuclear Science, Massachusetts Institute of Technology, Cambridge, Massachusetts

(Received March 17, 1955)

The "elastic" photoproduction of π^0 mesons in helium has been measured as a function of center-of-mass angle for gamma-ray energies from 170 Mev to 340 Mev. The total cross section shows a maximum around 270-Mev excitation energy and the angular distribution at 300-Mev peaks around 65° in the center-of-mass system. An attempt has been made to interpret the results in terms of the differential cross section for photoproduction of π^0 mesons in hydrogen, and to obtain (from the amount of interference of the waves emitted by the four nucleons) a value for the "mean radius" of the alpha particle and the relative phase of π^0 emission from proton and neutron.

The photodisintegration reaction $\gamma+He^4\rightarrow He^3+n$ has also been investigated. The angular distribution of the He^3 recoil nuclei is found to be proportional to $\sin^2\theta$ for excitation energies between 40 Mev and 120 Mev.

I. INTRODUCTION

BY "elastic" photoproduction of π^0 mesons in helium, we mean the process in which the helium nucleus is not disintegrated, i.e., the process $\gamma+He^4\rightarrow He^4+\pi^0$.

The photoproduction of π^0 mesons on hydrogen has been investigated by many researchers.[1–4] Other authors have also observed the elastic photoproduction of π^0 mesons in deuterium[5,6] and helium.[7,8] The group at the University of Illinois has compared the elastic and inelastic processes at different energies and found that the elastic process was still relatively important at an excitation energy of 190 Mev. They also find a ratio of production of π^0 mesons per nucleon in hydrogen and helium of about one. The purpose of this experiment was to measure the angular distribution, excitation curve, and total cross section for elastic photoproduction of π^0 mesons in helium. These are strongly affected by interference effects of the meson waves emitted by the four nucleons. The shapes of the angular distribution and the excitation curve depend on the mean distance between the nucleon and the data on those curves can be analyzed so as to obtain a "mean radius" of the alpha particle. The relative efficiency for elastic photoproduction of mesons, of the helium nucleus, and of the proton depends further on the relative phase of

* This work has been supported in part by the joint program of the U. S. Atomic Energy Commission and the Office of Naval Research.

[1] Panofsky, Steinberger, and Steller, Phys. Rev. **86**, 180 (1952).
[2] A. Silverman and M. Stearns, Phys. Rev. **88**, 1225 (1952).
[3] G. Cocconi and A. Silverman, Phys. Rev. **88**, 1230 (1952).
[4] Goldschmidt-Clermont, Osborne, and Scott, Phys. Rev. **89**, 329 (1953); Phys. Rev. **97**, 188 (1955).
[5] DeWire, Silverman, and Wolfe, Phys. Rev. **92**, 520 (1953); Phys. Rev. **94**, 756 (1954).
[6] H. L. Davis and D. R. Corson, Phys. Rev. **94**, 756 (1954).
[7] G. DeSaussure and L. S. Osborne, Phys. Rev. **94**, 756 (1954).
[8] Goldwasser, Koester, and Mills, Phys. Rev. **95**, 1692 (1954).

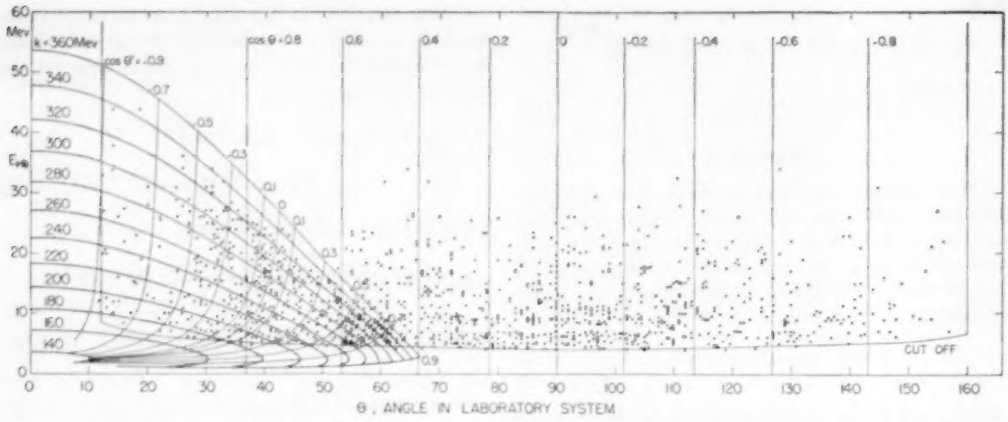

FIG. 1. Plot of events for last high-energy run. Each dot represents a recoil helium nucleus plotted with respect to its angle in the laboratory system and its energy determined from the total range. The superimposed lines give the energy of the photon responsible and the cosine of the meson center-of-mass angle. The points occurring outside this plot are mainly He^3 recoils from the photodisintegration process. The vertical lines are at equal $\cos\theta$ intervals in the laboratory system. The cutoff gives a lower limit of observable tracks because of absorption in the gas or shadowing of the collimator.

meson emission by neutrons and by protons. This phase thus also can be obtained from the experimental data.

II. EXPERIMENTAL PROCEDURE

The experimental data were acquired in three runs. The experimental procedure is very similar to the one described by Goldschmidt-Clermont *et al.*[4] The gamma-ray beam from the Massachusetts Institute of Technology electron-synchrotron was passed through a helium tank and nuclear plates were placed around the beam to record the recoil nuclei from the various meson production and disintegration processes. The electron beam was accelerated to an energy of 350 Mev (calibrated by magnetic field measurement) and then made to strike a 0.06-inch tungsten wire. The resulting x-ray beam has an angular spread of about 0.3°. It was passed through a defining lead collimator so as to have a rectangular cross section of 0.5×1 inch at the position of the plate holder. The beam entered the helium tank through a 1/64 inch aluminum window and left through a 1/16 inch aluminum window. Two four-inch walls screened the plates from particles coming from the windows. The helium tank comprised four sections bolted together through large vacuum-tight flanges. A small "darkroom" was built where the two last sections join, and the plates were introduced in the tank from that point. The plates were mounted on an aluminum plate holder which was slipped into the center of the tank. The tank and collimators were optically aligned with respect to the beam, and this alignment checked with an x-ray picture. The plates were then inserted into the tank and the tank evacuated. After two helium gas flushings, the tank was filled with pure (medical) helium at a pressure of one atmosphere. Impurities in the tank were smaller than 0.5 percent by volume. The total intensity of the beam was monitored by a thick-walled ionization chamber down-stream. This chamber was later calibrated with respect to a portable ion chamber, which had been calibrated at the Cornell synchrotron[4] and the University of Illinois betatron.[4]

The main problem of this experiment was to differentiate those recoil nuclei associated with the elastic photoproduction process from those arising from different photodisintegration processes. For this purpose, it was necessary to be able to discriminate between singly and doubly charged particles. Ilford GO nuclear plates were found to be best suited for this discrimination. The plates were under-developed by the method described by the Bruxelles group[9] (hot stage of $\frac{1}{2}$ hr at 15°C).

Various tests were made to check this discrimination: Some plates were exposed to the neutron flux near the Massachusetts Institute of Technology cyclotron. When under-developed, proton tracks were barely visible, while those alpha tracks connected with Thorium stars were still clear. About a hundred tracks were grain counted near the end of their range. Those tracks could be divided into two groups: some tracks, barely visible, had between 20 and 50 grains in the last 70 microns, others had between 70 and 130 grains for the same remaining range. Finally, by counting the number of grains *versus* the remaining range for one alpha track, one can predict the number of grains for the last 70 microns of other tracks,[10] this number turns out to be 20 for protons and 40 for tritium. It was not found

[9] Dilworth, Occhialini, Vermaesen, and Bonetti, Bull. centre phys. nucléaire univ. libre Bruxelles, Nos. 13a and 13b (1950).
[10] Lattes, Occhialini, and Powell, Proc. Phys. Soc. (London) **61**, 173 (1948).

possible to discriminate between single He^4 and He^3 tracks.

Plates of 100μ and 400μ were disposed in the collimator with one edge parallel to the direction of the beam and in such a way that the particles would come from the beam into the plates at a grazing angle (maximum dip of 40°). About 2000 tracks were scanned, and for each track the dip, the angle with the beam, and the total range were measured. The range measured was corrected to take into account the gas traversed by the particle before reaching the plate, and from this corrected range, the energy was deduced.

III. DATA

A surface of about 20 cm^2 of emulsion was scanned. All helium tracks stopping in the emulsion were recorded on a plot similar to Fig. 1. In this plot each track is represented by a dot, its abscissa corresponding to the angle it makes with the beam (in the laboratory system), its ordinate corresponding to its energy (as calculated from its range). These helium recoil tracks may arise from the Compton photoeffect on the helium nucleus, from photodisintegration, or from elastic or inelastic π-meson production, i.e., they may arise from one of the following reactions[11]:

(a) $\gamma+He^4\rightarrow He^4+\gamma$,

(b) $\gamma+He^4\rightarrow He^3+n$,

(c) $\gamma+He^4\rightarrow\pi+He^3+$nucleon,

(d) $\gamma+He^4\rightarrow\pi^0+He^4$.

We have grounds to assume that the nuclear Compton effect has a relatively small cross section: this cross section should be of the order or smaller than the Thompson cross section (2×10^{-31} cm^2). Experimental evidence seems to indicate even a much smaller value.[12] (The cross sections for photodisintegration or for photoproduction of π mesons are of the order of 10^{-28} cm^2.) In the inelastic photoproduction of π mesons, the He^3 nucleus will acquire very little recoil. It is not possible to predict exactly the dynamical variables involved in this three-body process. If one assumes either that the He^3 "sits by" the reaction, or that the three outgoing particles share the energy in such a way as to have the largest phase space available, the He^3 nucleus will acquire at most a recoil energy of 5 to 10 Mev, and will usually be stopped in the gas between the beam and the plates. The problem remains to separate the photodisintegration from the elastic photoproduction processes. These are two-body processes in which an exact relation can be calculated between the angle of emission and the recoil energy (for a specified gamma-ray energy). The diagram in Fig. 1 represents the cosine of the angle in the center-of-mass system of the emitted π meson and the energy of the gamma rays relative to the angle and energy in the laboratory system of the recoil helium nucleus, for the elastic photoproduction reaction. The tracks represented by points outside the diagram are associated with the photodisintegration process. Those inside the diagram may be associated with the photodisintegration or the elastic photoproduction processes. The kinematics of the photodisintegration process shows that all those recoil He^3 nuclei with energies less than 40 Mev must be associated with gamma rays of energies less than 150 Mev. Thus, a special low-energy run was made to study the angular distribution of the He^3 recoil nuclei from the photodisintegration of helium at gamma-ray energies below 150 Mev. This run was performed in exactly the same arrangement as the high-energy run, but with a maximum gamma-ray energy of the synchrotron beam of 160 Mev. The tracks of this run have been represented on a graph similar to the one of Fig. 1.

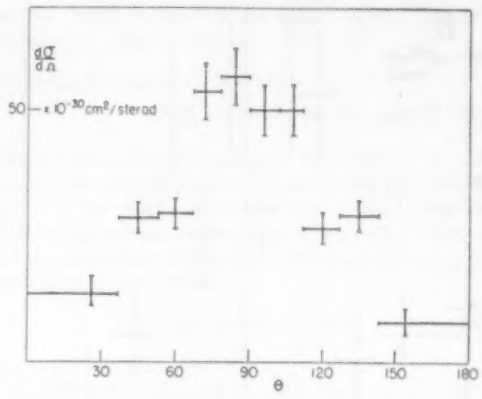

FIG. 2. Angular distribution in the laboratory system of recoil helium tracks from the reaction $\gamma+He^4\rightarrow He^3+n$. This is an average over excitation energies from 36 Mev to 84 Mev.

The angular distribution of He^3 recoil tracks of energies between 5 and 30 Mev is shown in Fig. 2 and Fig. 3. Figure 2 shows the angular distribution of He^3 from the reaction $\gamma+He^4\rightarrow He^3+n$ for excitation energies between 36 Mev and 84 Mev. Figure 3 shows the same curve for excitation energies from 84 to 132 Mev. These two curves have been made by using the data of the low-energy run and that of the high-energy run for large angles. They show that the background is nearly proportional to $\sin^2\theta$ in the laboratory system. Namely, if the background is assumed to be of the form $A\sin^2\theta+B\cos\theta+C$, then the constants that best fit the experimental points are given in the following table, in units of 10^{-30} cm^2/sterad.

E_γ	A	B	C
36 Mev–84 Mev	47.2±5	9.3 ±10	2.7±2.5
84 Mev–132 Mev	12.8±1	4.22± 6	1.5±1

[11] We have assumed that there is no bound state of the He^4 nucleus. Hornyak, Lauritsen, and Morrison, Revs. Modern Phys. 22, 291 (1950).

[12] Pugh, Frisch, and Gomez, Phys. Rev. 95, 590 (1954).

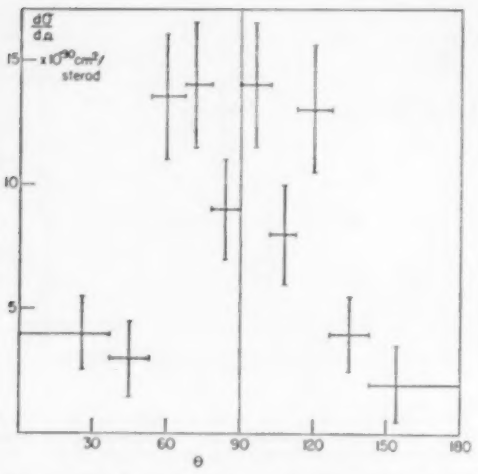

FIG. 3. Angular distribution in the laboratory system of recoil helium tracks from the reaction $\gamma+He^4 \rightarrow He^3+n$. This is an average over excitation energies from 84 Mev to 132 Mev.

Similar results have been found for the reaction[13] $He^4(\gamma,p)H^3$, and there are theoretical reasons to assume a $\sin^2\theta$ distribution: It is reasonable that the main contribution to the $He^4(\gamma,n)He^3$ reaction is due to an electric dipole interaction.[14] To conserve parity and angular momentum, the neutron must be emitted in a P-wave. This, when averaged over polarization of the gamma ray, leads to a $\sin^2\theta$ distribution in the center-of-mass system. The retardation factor for the He^3 and the motion of the center-of-mass are small corrections which should favor the forward angles. These two effects are small due to the large mass of the He^3 nucleus. This may explain why they are not observed in the experimental results. Calculations by Flowers and Mandl[14] and by Gum and Irving[14] give a value for the cross section of the reaction $\gamma+He^4 \rightarrow He^3+n$ around 40 Mev which correspond approximately to the value 0.5×10^{-27} cm^2 found in this experiment. Fuller[13] finds experimentally a somewhat lower value (0.1×10^{-27} cm^2).

IV. THE RESULTS

The angular distribution of He^3 recoils from the $He^4(\gamma,n)He^3$ process is shown in Fig. 2 for low excitation energy and in Fig. 3 for high excitation energy. The excitation function of this process is shown in Fig. 4.

The differential cross section for elastic photoproduction of neutral π mesons, averaged over an energy interval from 280 Mev to 340 Mev, in the center-of-mass system, is shown in Fig. 5. The large statistical errors quoted come from the fact that a large background must be subtracted from the observed distribution.

Figure 6 shows the differential cross section for elastic photoproduction at 90° in the center-of-mass system.

V. DISCUSSION

It is interesting to compare the cross section for elastic photoproduction of mesons on helium with the cross section for photoproduction of neutral mesons in hydrogen. There have been many calculations of the elastic photoproduction of π mesons in deuterium. Those were done under the impulse approximation.[15] The validity of the approximation for the helium case is very questionable for the following reasons: (1) The distance between nucleons can hardly be considered as large compared to the radius of interaction; (2) the

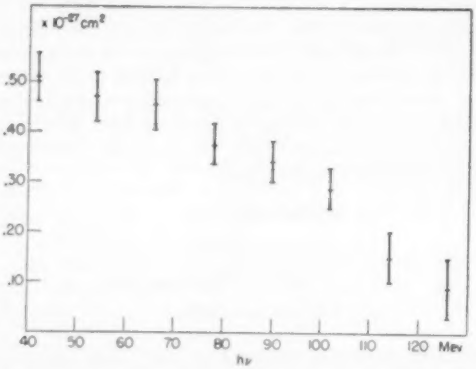

FIG. 4. The total cross section for the reaction $\gamma+He^4 \rightarrow He^3+n$. The total cross section has been calculated from the experimental cross section between 60° and 160° by assuming an angular distribution proportional to $\sin^2\theta$ throughout the energy spectrum (see text).

multiple scattering should not be completely neglected; and (3) the strong nuclear forces binding the nucleus may modify the characters of the nucleons. However, the impulse approximation may allow at least a qualitative interpretation of the results.[16] Under the impulse approximation, the cross section for elastic photoproduction of mesons on helium can be written:

$$(d\sigma/d\Omega')_{\pi_0}=\tfrac{1}{2}\left|\int\psi_a^*[T_p(1)+T_p(2)+T_n(3)+T_n(4)]\psi_a d\tau\right|^2[\gamma\kappa/(2\pi)^2], \quad (1)$$

where

$$(d\sigma/d\Omega')_{\text{proton}}=\tfrac{1}{2}|T|^2[\gamma\kappa/(2\pi)^2],$$

[13] T. S. Benedict and W. M. Woodward, Phys. Rev. **83**, 1269 (1951); E. R. Gaerttner and M. L. Yeater, Phys. Rev. **83**, 146 (1951); E. G. Fuller and M. Weiner, Phys. Rev. **83**, 202 (1951); E. G. Fuller, Phys. Rev. **96**, 1306 (1954).

[14] B. H. Flowers and F. Mandl, Proc. Roy. Soc. (London) **A206**, 131 (1951); I. C. Gum and I. Irving, Phil. Mag. **42**, 1353 (1951).

[15] G. F. Chew and H. W. Lewis, Phys. Rev. **84**, 779 (1951); Heckrotte, Henrich, and Lepore, Phys. Rev. **85**, 490 (1952); N. C. Francis and R. E. Marshak, Phys. Rev. **85**, 496 (1952); N. C. Francis, Phys. Rev. **89**, 766 (1953).

[16] A similar calculation by Y. Yamaguchi at the University of Illinois has just been reported to the authors. (Dr. B. T. Feld, private communication.)

T_p and T_n represent the interaction matrices for photoproduction on protons and neutrons, respectively, and ψ_α, the wave function of the helium nucleus. The neutral meson photoproduction amplitudes on neutrons and protons have been measured to be about the same magnitude[3,17]; however, they may differ by a phase factor δ. The T matrices may be expressed in terms of the spin $\boldsymbol{\sigma}$ of the nucleon:

$$T=\mathbf{K}\cdot\boldsymbol{\sigma}+L. \tag{2}$$

Since both the initial and the final states of the helium nucleus have spin zero, there can be no spin flip and

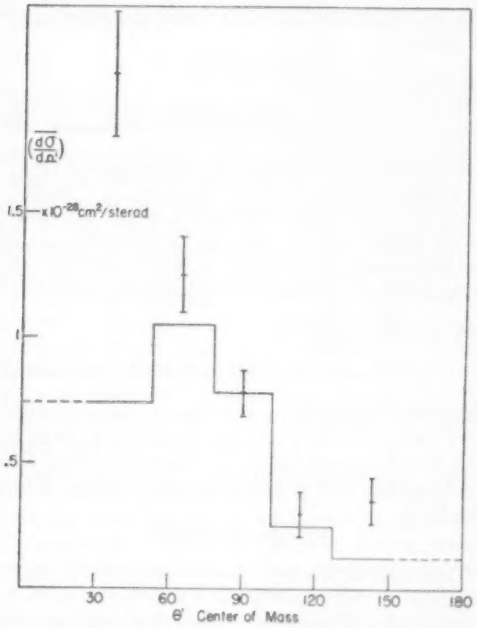

FIG. 5. Angular distribution of π^0 mesons from the reaction $\gamma+He^4\rightarrow He^4+\pi^0$, in the center-of-mass system of the reaction. Averaged from $\gamma=280$ Mev to $\gamma=340$ Mev. The points represent the cross section divided by $\sin^2\theta'$.

formula (1) may be rewritten:

$$(d\sigma/d\Omega')_{He}=16[\tfrac{1}{2}(1+\cos\delta)]\times\tfrac{1}{2}|L|^2|F(\mathbf{K})|^2[\gamma\kappa/(2\pi)^2], \tag{3}$$

$$F(\mathbf{K})=\int|\psi_\alpha|^2e^{i\mathbf{K}\cdot\mathbf{r}_i}d\tau. \tag{4}$$

Here $\mathbf{K}=\boldsymbol{\gamma}-\boldsymbol{\kappa}$, where $\boldsymbol{\gamma}$ and $\boldsymbol{\kappa}$ are the momenta of the photon and of the meson, $\mathbf{r}_i$ is the coordinate of one of the nucleons, and the integration has to be performed over all four nucleons. In order to investigate the behavior of the form factor (4), we assume for each nucleon an $\exp(-r^2/R^2)$ distribution law, where R is a sort of "mean radius" of the alpha nucleus. The expression (4) reduces then to

$$F(K)=\exp[-\tfrac{1}{4}(KR)^2]=\exp[-\tfrac{1}{4}R^2(\kappa^2+\gamma^2-2\kappa\gamma\cos\theta')], \tag{5}$$

where γ and κ are the energy of the incoming photon and the momentum of the outgoing meson (in units of $mc^2=1$). For dipole production, the term $|L|$ has an angular dependence proportional to $\boldsymbol{\kappa}\cdot[\boldsymbol{\gamma}\times\boldsymbol{\varepsilon}]$, where $\boldsymbol{\varepsilon}$ is the polarization vector. This term is proportional to $\sin\theta'$, thus we may write

$$\tfrac{1}{2}|L|^2[\gamma\kappa/(2\pi)^2]=Q_L\sin^2\theta', \tag{6}$$

where Q_L is independent of θ'.

Equations (3), (5), and (6) show that

$$\ln[(d\sigma/d\Omega')_{He}/\sin^2\theta']=\text{const}+\gamma\kappa R^2\cos\theta'. \tag{7}$$

In Fig. 7 are plotted values of $\ln[(d\sigma/d\Omega')_{He}/\sin^2\theta']$ for different values of $\cos\theta'$. The results correspond to a mean excitation energy of 300 Mev; at this energy, $\gamma\kappa=4.05$. The experimental points are consistent, within statistical errors, with a law like (7). The best fit of the experimental points give a value for the mean radius[18] $R=(0.76\pm0.10)\times10^{-13}$ cm corresponding to a rms value $R=(0.93\pm0.12)\times10^{-13}$ cm. [The error is only the statistical error on the determination of (7).] Multiple scattering would give an angular distribution that was less peaked. We might expect that our measurement is a lower limit on the real radius.

There is an independent way to obtain a value for the "mean radius" R: It is known that at low energies at least, the cross section for production of π^0 mesons on protons increases as $\gamma\kappa^2$. Thus, using Eqs. (3) and (5), one finds for the differential cross section at 90°:

$$(d\sigma[90°]/d\Omega')_{He}=\text{const}\,\gamma\kappa^2\exp[-\tfrac{1}{2}R^2(\gamma^2+\kappa^2)]. \tag{8}$$

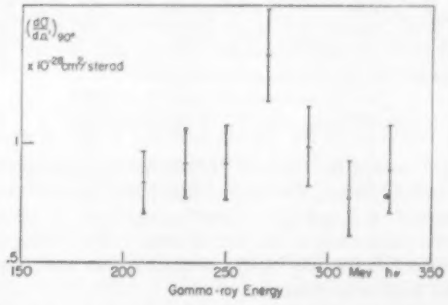

FIG. 6. Differential cross section for the reaction $\gamma+He^4\rightarrow He^4+\pi^0$ at 90° in the center-of-mass system of the reaction as a function of excitation energy.

[17] Jakobson, Schulz, and White, Phys. Rev. **91**, 695 (1953).

[18] Hofstadter, McAllister, and Wiener, Phys. Rev. **96**, 854 (1954), give a rms value $R=1.4(\pm0.2)\times10^{-13}$ cm. Their rms radius is taken with respect to charge. It is an experimental determination of R by electron scattering.

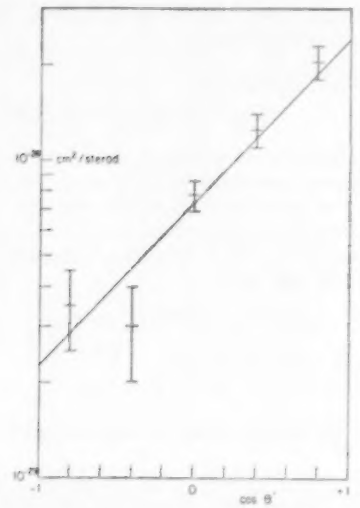

FIG. 7. Plot of the logarithm of points of Fig. 6, as a function of the cosine of the angle in the center-of-mass system. For a certain energy, the slope of the line is proportional to the spread of the radius of the alpha nucleus (see text).

The derivative with respect to energy of expression (8) should equal zero at the excitation energy at which the experimental cross section at 90° goes through a maximum. It is seen on Fig. 6 that this maximum occurs at 270±10 Mev. This gives a new value[18] of $R=(1.15\pm0.2)\times10^{-13}$ cm, corresponding to a rms value $R=(1.41\pm0.2)\times10^{-13}$ cm. From Eq. (3) and the experimental data, it is possible to obtain a value for the phase factor δ by which the photoproduction amplitude on protons and neutrons may differ. This is done by comparing the absolute value of the cross section for elastic photoproduction of mesons in helium with the one for photoproduction of neutral mesons in hydrogen. However, the $|L|^2$ term entering in Eq. (3) does not represent the total cross section on the free proton, but only that part which is spin-dependent.[19] From Eq. (2) one obtains for the cross section on the proton:

$$(d\sigma/d\Omega')_{\text{proton}}=\tfrac{1}{2}\{|K|^2+|L|^2\}[\gamma\kappa/(2\pi)^2], \quad (9)$$

and to obtain the value of $|L|^2$ from the experimental data on hydrogen, one needs a theory giving the relative values of $|K|^2$ and $|L|^2$. Chew[20] worked out the photomeson production in the cut-off theory. He obtains the following expression for the neutral meson production cross section on protons:

$$(d\sigma/d\Omega')_{\text{proton}}=A\{|m_1-e_2|^2\cos^2\theta' + [\tfrac{1}{2}|m_1+e_2|^2+2|m_1|^2]\sin^2\theta'\}, \quad (10)$$

where A does not depend on the angle; m_1 and e_2 are constants given in the reference. The term

$$Q_L=A\cdot2|m_1|^2 \quad (11)$$

is the spin-independent term. From (10) and (11), it is easy to obtain

$$Q_L=[4|m_1|^2/4|m_1|^2+|m_1+e_2|^2] \times(d\sigma[90°]/d\Omega')_{\text{proton}}, \quad (12)$$

where $(d\sigma[90°]/d\Omega')$ is the differential cross section at 90°. It is easy to see that in the forward direction, the form factor (5) is almost unity. If in formula (12) we take $|m_1|=0.58$ and $|e_2|=0.18$, values given by Chew,[20] we obtain

$$\lim_{\theta'\to0}\{(d\sigma/d\Omega')_{\text{He}}/\sin^2\theta'\} =11.2[(1+\cos\delta)/2](d\sigma[90°]/d\Omega')_{\text{proton}}. \quad (13)$$

If in formula (12) we neglect $|e_2|$ with respect to $|m_1|$,[21] we obtain a factor of 12.8 instead of 11.2 in (13). From (13), the angular distribution of $(d\sigma/d\Omega')_{\text{He}}$ at a certain energy and the value of $(d\sigma[90°]/d\Omega')_{\text{proton}}$ at that same energy, it is possible to obtain a value for the phase factor. At 300-Mev excitation energy, we obtain

$$\lim_{\theta'\to0}\{(d\sigma/d\Omega')_{\text{He}}/\sin^2\theta'\} =(2.39\pm0.29)\times10^{-28}\ \text{cm}^2/\text{sterad}.$$

This gives, if we neglect e_2 with respect to m_1, $\cos\delta=0.97\pm0.11$ or, if we use the values of m_1 and e_2 given by Chew[20] and favored by the experimental work,[4] $\cos\delta=1.12\pm0.13$. This is consistent with a phase difference $\delta=0$.

VI. CONCLUSIONS

There is no satisfactory theory to interpret the results obtained by this experiment: those results must be interpreted in a qualitative way. They indicate constructive interference in the contributions of protons and neutrons to the elastic photoproduction of π mesons in helium. The results also indicate a strong interference of the contributions of the four nucleons to the elastic photoproduction process, even at large emission angles of the mesons. This can be understood if the four nucleons are very closely bound.

ACKNOWLEDGMENTS

The authors are indebted to Dr. B. T. Feld and Dr. S. Drell for many helpful discussions on the interpretation of the results of this experiment.

One of them (Gerard deSaussure) is also especially indebted to Dr. Y. Goldschmidt-Clermont and Dr. D. M. Ritson who initiated him into the techniques of the nuclear emulsions.

[18] W. Thirring, Helv. Phys. Acta **27**, 515 (1954).
[19] G. F. Chew, Phys. Rev. **95**, 1669 (1954).
[21] B. T. Feld (private communication).

Multiple Scattering Corrections in $\pi^{\pm}$ Deuteron Scattering*

S. D. DRELL AND L. VERLET
Department of Physics and Laboratory for Nuclear Science, Massachusetts Institute of Technology, Cambridge, Massachusetts
(Received March 9, 1955)

Multiple-scattering corrections to the impulse approximation are calculated for the scattering of $\pi^{\pm}$ mesons by deuterons. These corrections are model-dependent since the scattered wave propagates off the energy shell between the first and last scatterings whereas experimental scattering phase shifts are available only for elastic scattering. Various assumptions are made concerning the off-the-energy-shell behavior of the scattering amplitudes and the double-scattering approximation is analyzed for meson energies of 45 Mev and 169 Mev. The results are tabulated and are found to be sensitive to the different scattering models. The cross sections at 169 Mev were calculated with both the Fermi and Bethe solutions for the meson-nucleon scattering phase shifts and are in close agreement. It thus does not seem to be feasible to use $\pi^{\pm}-D$ scattering as a means of distinguishing between these two solutions.

I. INTRODUCTION

THE impulse approximation provides a straightforward phenomenological approach to the analysis of the scattering of π mesons by deuterons or heavier nuclei. In this approximation the nucleons are considered to scatter as free particles which have the same momentum distribution as the initially bound nucleons. It is thus possible to characterize the scattering purely in terms of the experimentally observed phase shifts for π-nucleon scattering and in terms of the nuclear momentum distribution. Corrections to the impulse approximation arise due to the effect of the binding force during the scattering, the diminution in amplitude of the incident wave in crossing the nucleus, and the multiple-scattering effects, as discussed by Chew, Wick, Ashkin, and Goldberger.[1-3]

This note considers the multiple-scattering corrections to the impulse approximation in the calculation of the scattering cross sections of $\pi^{\pm}$ mesons by deuterons. In consequence of the small deuteron binding energy and of the fact that the deuteron consists of but two nucleons, it is expected that multiple-scattering corrections will be the only ones of importance for incident π mesons of kinetic energies greater than ≈ 50 Mev.

The motivation of this work derives from the experimental feasibility of measuring $\pi^{\pm}$ deuteron scattering cross sections, and from the theoretical interest in testing the accuracy of the impulse approximation and in finding the dominant features of the multiple-scattering correction.

To a certain extent this correction is model-dependent since the scattered wave propagates off the energy shell between the first and last scatterings, whereas experimental scattering phase shifts are available only for elastic scattering (on the energy shell). Various assumptions concerning the off-energy-shell behavior of the scattering amplitude are made in order to test the sensitivity of the results to specific models. In particular, a point-scattering model has been discussed earlier by Chew and Wick[1] and by Brueckner[4] and will be considered within the framework of our results.

II. OUTLINE AND RESULTS

We describe here the approximation and results of these calculations.

Firstly, we neglect the binding and motions of the sources during the scattering, and use the Hulthén wave function to describe the deuteron. *Secondly*, we neglect the possibility of absorption of the meson by the deuteron. *Thirdly*, we treat only the double-scattering corrections. In principle it is possible to retain the higher-order scattering corrections with more complicated algebra to take into account the different scattering phase shifts for various isotopic spin and angular momentum states. However, we expect that the main multiple-scattering corrections arise from the double scattering so that this procedure should yield the qualitative features of these corrections. *Fourthly*, we consider scattering of the meson by a nucleon to occur only in the six states ($S_{\frac{1}{2}}$, $P_{\frac{1}{2}}$, and $P_{\frac{3}{2}}$; isotopic spin $=\frac{1}{2}$ and $\frac{3}{2}$) which have been used in the analysis of π-hydrogen cross sections.

Now the experiments on π-nucleon scattering furnish information on the elastic scattering in the form of a scattering amplitude,

$$f(\mathbf{k},\mathbf{k}_0)=k^{-1}(\alpha+\beta\mathbf{k}\cdot\mathbf{k}_0-i\gamma\boldsymbol{\sigma}\cdot\mathbf{k}_0\times\mathbf{k}), \tag{1}$$

where $\mathbf{k}_0$ and $\mathbf{k}$ are respectively the momenta of the ingoing and outgoing particles, with $k=k_0$; $\boldsymbol{\sigma}$ is the 2×2 Pauli spin matrix for the nucleon; and we write

$$\alpha=\eta, \quad \beta k^2=\eta^-+2\eta^+, \quad \gamma k^2=\eta^--\eta^+, \tag{2}$$

where η, η^+, and η^-, refer respectively to the angular momentum states S, $P_{\frac{1}{2}}$, and $P_{\frac{3}{2}}$. Further, the η's are operators in isotopic space expressing scattering in states of isotopic spin $\frac{3}{2}$ and $\frac{1}{2}$. They appear in the general form for the α, βk^2, γk^2, of the type

$$\eta=\eta'+\mathbf{t}\cdot\boldsymbol{\tau}\eta'', \tag{3}$$

* This work was supported in part by the Office of Naval Research and the U. S. Atomic Energy Commission.

[1] G. Chew and G. Wick, Phys. Rev. **85**, 636 (1952).
[2] J. Ashkin and G. Wick, Phys. Rev. **86**, 686 (1952).
[3] G. Chew and M. Goldberger, Phys. Rev. **87**, 778 (1952).
[4] K. Brueckner, Phys. Rev. **89**, 834 (1953); Phys. Rev. **90**, 715 (1953).

where $\boldsymbol{\tau}$ is the isotopic spin of the nucleon and $\mathbf{t}$ that of the meson.

In treating the multiple-scattering problem we must go beyond the experimentally available η's given previously and construct specific models to describe the scattering of the meson which propagates (virtually) off the energy shell after scattering by the first nucleon and prior to scattering by the second one. That is, we must assume a form for the scattering amplitude for a meson which is scattered by one nucleon off the energy shell from an initial state $\mathbf{k}_0$ to an intermediate state of momentum $\mathbf{q}$, with $q \neq k_0$, before the second nucleon scatters it back to a final state $\mathbf{k}$, with $k=k_0$.

We may assume that the form of Eq. (1), with α, β, and γ dependent upon the momenta of the incident pion only, is valid even for scattering off the energy shell. This case, studied by Brueckner[4] for point sources, corresponds to the use of a singular propagator for the intermediate meson wave of the form $g_0=\exp(ikR)/kR$, with $\mathbf{R}=\mathbf{r}_1-\mathbf{r}_2$ the distance between the two scattering sources. It predicts large scattering amplitudes for scatterings far off the energy shell which lead to virtual intermediate mesons of high momentum. Thereby it attaches great importance to the region of quite small separation between the nucleons where the above approximations may be poor.

To get around this difficulty we can suppose that the scattering amplitude smoothes out for large momenta. This would result physically for scattering by sources of finite extent. It is possible to achieve this effect by considering scattering from a separable potential such as studied by Wentzel,[5] Blatt,[6] Goldberger,[7] and Yamaguchi.[8] In this method we approximate the Schrödinger equation describing the scattering of a particle by a potential, by replacing the wave function which appears in the interaction term by its average over the potential. With this approximation the scattering problem reduces to quadratures. For each nucleon we choose the potential to be a square well of fixed radius, with the depths for S and P states so adjusted as to reproduce the experimental results for the pion-nucleon scattering. With these assumptions we find that when the sources don't overlap, the intermediate wave propagates the same way as for point sources, i.e., $g_0=\exp(ikR)/kR$. When the sources overlap, however, the propagation factor depends on the well parameters, but remains finite. Its detailed variation has but a very slight effect on the cross sections averaged over the Hulthén function.

A third possible model of the momentum variation of the scattering amplitude considers only scattering on the energy shell in the intermediate state. In this approximation the intermediate wave propagates as $g_0=i\sin(kR)/kR$. Since this form of the propagator is finite and smooth for $kR<1$, it doesn't matter whether the sources are assumed to be of zero or of finite extent.

The aforementioned three models give vastly different momentum dependences for the off-the-energy-shell scattering amplitudes and provide a comparison basis for an understanding of the significance of our results. We discuss the predictions of these models for S-wave scattering from two spinless sources in the following paragraph. Our aims are to exhibit the method of obtaining the cross sections with a minimum of algebra, to compare the predictions of the different models, and to analyze the double-scattering approximation. Numerical calculations are presented in paragraph IV, for the actual case of $\pi^{\pm}-D$ scattering at energies of 45 and 169 Mev.

To summarize in brief our results: at 45 Mev the double-scattering correction to the elastic cross section $\pi^{\pm}+D \rightarrow D+\pi^{\pm}$, is of the order of 10 percent or less and is model-dependent. At 169 Mev the same correction for forward scattering depends on the model, but for backward scattering, it is fairly independent of the assumptions made and leads to a 30 percent reduction of the cross sections. For the total cross sections (elastic, inelastic, and absorption) as deduced from the imaginary part of the scattering amplitude in the forward direction, the correction is of the order of 10 percent or less and is quite model-dependent.

Finally, we have considered the possibility of using the $\pi^{\pm}+D \rightarrow D+\pi^{\pm}$ reaction as a means of selecting between the various sets of phase shifts for the π-nucleon cross sections as proposed by Fermi and by Bethe. In view of the uncertainties involved in this calculation, no such distinction can be drawn.

III. S-WAVE SCATTERING BY TWO IDENTICAL SOURCES

Before discussing the physical pion-deuteron scattering problem, we analyze in this section the S-wave scattering by two spinless identical sources. We aim thus to illustrate the methods of this work with a minimum of algebraic complications, to compare the predictions of the various models discussed in the previous paragraph, and to analyze the double-scattering approximation.

Chew and Goldberger[3] have explicitly written the double-scattering term in Eq. (29a) of their paper. It is simply rederived in Appendix A. For two identical sources[9] separated by a distance R, we have the following expression for the elastic (single plus double) scattering of a meson wave with initial wave number $\mathbf{k}_0$ and final wave number $\mathbf{k}$:

$$f(\mathbf{k},\mathbf{k}_0)=f_1(\mathbf{k},\mathbf{k}_0)+f_2(\mathbf{k},\mathbf{k}_0)+\frac{4\pi}{(2\pi)^3}\int\frac{d^3\mathbf{k}}{q^2-k^2-i\epsilon}$$
$$\times\{f_1(\mathbf{k},\mathbf{q})f_2(\mathbf{q},\mathbf{k}_0)+f_2(\mathbf{k},\mathbf{q})f_1(\mathbf{q},\mathbf{k}_0)\}, \quad (4)$$

[5] A. Wentzel, Helv. Phys. Acta **15**, 111 (1942).
[6] J. M. Blatt, Phys. Rev. **72**, 466 (1947).
[7] M. Goldberger, Phys. Rev. **84**, 929 (1951).
[8] S. Yamaguchi, Phys. Rev. **95**, 1628 (1954).

[9] The limitation to identical sources is not necessary.

where $f_i(\mathbf{k},\mathbf{q})$ represents the scattering amplitude for scattering by the ith source from $\mathbf{q}$ to $\mathbf{k}$ and

$$f_2(\mathbf{k},\mathbf{q})=e^{i(\mathbf{q}-\mathbf{k})\cdot\mathbf{R}}f_1(\mathbf{k},\mathbf{q}). \tag{5}$$

Equation (4) exhibits explicitly the sum over the intermediate "off-the-energy-shell" momenta in the double-scattering sum. If we assume for S scattering that $f_1(\mathbf{k},\mathbf{q})$ is a function of the incident energy only and is independent of $\mathbf{q}$, i.e., $f_1=\alpha(k)/k$, then, using Eq. (5), we have directly:

$$f_I(\mathbf{k},\mathbf{k}_0)=\frac{\alpha}{k}\Big(e^{-i(\mathbf{k}_0-\mathbf{k})\cdot\mathbf{R}/2}+e^{i(\mathbf{k}_0-\mathbf{k})\cdot\mathbf{R}/2} +\alpha\frac{e^{ikR}}{kR}(e^{i(\mathbf{k}_0+\mathbf{k})\cdot\mathbf{R}/2}+e^{-i(\mathbf{k}_0+\mathbf{k})\cdot\mathbf{R}/2})\Big). \tag{6}$$

With this model of the scattering amplitude and with the approximation of only single and double scattering, the region of close coincidence of the two scattering sources is falsified badly, since the scattering amplitude diverges as $R\to 0$. Actually, we have for $R=0$ scattering from a source of double the strength of the individual scattering sources. The effect on the scattering amplitude of doubling the source strength is, of course, model-dependent except in the limit where the Born approximation is valid, and the scattering amplitude is also doubled. We can avoid this divergence as $R\to 0$ by summing up directly all of the triple and higher-order scattering effects. As shown, in Appendix A, it is possible to effect this sum for constant $f_1(\mathbf{q},\mathbf{k})$, with the result that the scattering amplitude becomes

$$f_{M\,I}(\mathbf{k},\mathbf{k}_0)=[1-\alpha^2(e^{ikR}/kR)^2]^{-1}f_I(\mathbf{k},\mathbf{k}_0), \tag{7}$$

as deduced by Chew and Wick[1] and Brueckner.[4] We see here that the interference among the multiple-scattered waves leads to the prediction that the scattering amplitude decreases linearly with R, vanishing as $R\to 0$. This again falsifies badly the region of close coincidence of the two sources as discussed above. Equations (6) and (7) indicate the dangers concomitant with the assumption of constant off-the-energy-shell scattering amplitudes as applied to any problem for which the region $kR<1$ is of importance. That this region is of importance in the analysis of the multiple-scattering corrections for π^+-D scattering is seen in Fig. 3 and Table II of reference 4. The main multiple-scattering correction there comes from the region $kR<1$.

We discuss now alternate models which predict widely different behaviors for the scattering amplitude due to two sources near one another. As an extreme assumption we might postulate in Eq. (4) that the individual amplitudes $f_i(\mathbf{k},\mathbf{q})$ vanish for scattering off the energy shell. We then have, since the principal value contribution to the sum in Eq. (4) is omitted according to this assumption,

$$f_{II}(\mathbf{k},\mathbf{k}_0)=\frac{\alpha}{k}\Big(e^{-i(\mathbf{k}_0-\mathbf{k})\cdot\mathbf{R}/2}+e^{i(\mathbf{k}_0-\mathbf{k})\cdot\mathbf{R}/2} +\alpha\frac{i\sin kR}{kR}(e^{i(\mathbf{k}_0+\mathbf{k})\cdot\mathbf{R}/2}+e^{-i(\mathbf{k}_0+\mathbf{k})\cdot\mathbf{R}/2})\Big). \tag{8}$$

The intermediate propagator $g_0=i(\sin kR)/kR$ is non-singular according to this model and yields a reasonable scattering amplitude in the $R\to 0$ limit. Thus we see by Eq. (8) that in this limit of doubled source strength, the scattering amplitude becomes $2[\alpha(k)/k][1+i\alpha(k)]$. With this assumption of no scattering off the energy shell, one can also sum up the multiple-scattering effects, obtaining in analogy with Eq. (7),

$$f_{M\,II}(\mathbf{k},\mathbf{k}_0)=[1+\alpha^2(\sin kR/kR)^2]^{-1}f_{II}(\mathbf{k},\mathbf{k}_0). \tag{9}$$

A less extreme model based on the assumption of a separable potential also admits exact multiple-scattering solutions. According to this model, the Schrödinger equation for the scattering of a wave by a spherical potential λU is replaced by the inhomogeneous equation

$$(\Delta+k^2)\psi(\mathbf{r})=\lambda U(r)\bar{\psi}, \tag{10}$$

where $\bar{\psi}=\int\psi(\mathbf{r})U(r)d^3\mathbf{r}$, with $U(r)$ normalized to unit volume, denotes the wave function averaged over the potential. The solution of this equation corresponding to outgoing scattered waves reads

$$\psi(\mathbf{r})=e^{i\mathbf{k}_0\cdot\mathbf{r}}-\frac{\lambda}{4\pi}\bar{\psi}\int\frac{\exp ik|\mathbf{r}-\mathbf{r}'|}{|\mathbf{r}-\mathbf{r}'|}U(r')d^3\mathbf{r}'.$$

Averaging over the source, we obtain:

$$\bar{\psi}=\langle\varphi(\mathbf{k}_0)\rangle_{Av}-\lambda\bar{\psi}G,$$

with the defining relations

$$\langle\varphi(\mathbf{k}_0)\rangle_{Av}=\int\exp(i\mathbf{k}_0\cdot\mathbf{r})U(r)d^3\mathbf{r},$$

and

$$G=(4\pi)^{-1}\int\int\frac{\exp ik|\mathbf{r}-\mathbf{r}'|}{k|\mathbf{r}-\mathbf{r}'|}U(r)U(r')d^3\mathbf{r}d^3\mathbf{r}'.$$

The scattering amplitude is, accordingly,

$$f_1(\mathbf{k},\mathbf{k}_0)=-(\lambda/4\pi)\bar{\psi}\langle\varphi(-\mathbf{k})\rangle_{Av}=-(\lambda/4\pi)(1+\lambda G)^{-1}\times\langle\varphi(\mathbf{k}_0)\rangle_{Av}\langle\varphi(-\mathbf{k})\rangle_{Av}\equiv\alpha/k, \tag{11}$$

Extending this development to two sources, we replace Eq. (10) by

$$(\Delta+k^2)\psi(\mathbf{r})=\lambda(U_1\bar{\psi}_{(1)}+U_2\bar{\psi}_{(2)}),$$

with

$$\bar{\psi}_{(i)}\equiv\int\psi(\mathbf{r})U_i(\mathbf{r})d^3\mathbf{r}.$$

The corresponding scattering solution reads

$$\psi(\mathbf{r})=e^{i\mathbf{k}_0\cdot\mathbf{r}}-\frac{\lambda}{4\pi}\int\frac{\exp ik|\mathbf{r}-\mathbf{r}'|}{|\mathbf{r}-\mathbf{r}'|}(U_1\psi_{(1)}+U_2\psi_{(2)}).$$

Averaging over the two sources individually, we obtain coupled equations for $\psi_{(1)}$ and $\psi_{(2)}$ which can be solved directly to give the scattering amplitude due to two identical sources. The result of this calculation is

$$f_{M\ III}(\mathbf{k},\mathbf{k}_0)=(\alpha/k)(1-\alpha^2W^2)^{-1}(e^{-i(\mathbf{k}_0-\mathbf{k})\cdot\mathbf{R}/2}+e^{i(\mathbf{k}_0-\mathbf{k})\cdot\mathbf{R}/2}+\alpha W(e^{i(\mathbf{k}_0+\mathbf{k})\cdot\mathbf{R}/2}+e^{-i(\mathbf{k}_0+\mathbf{k})\cdot\mathbf{R}/2})), \tag{12}$$

where

$$W=\frac{\int\int\frac{\exp(ik|\mathbf{r}-\mathbf{r}'|)}{k|\mathbf{r}-\mathbf{r}'|}U_1(\mathbf{r})U_2(\mathbf{r}')d^3\mathbf{r}d^3\mathbf{r}'}{\left(\int\exp(i\mathbf{k}_0\cdot\mathbf{r})U_1(\mathbf{r})d^3\mathbf{r}\right)\left(\int\exp(-i\mathbf{k}\cdot\mathbf{r})U_1(\mathbf{r})d^3\mathbf{r}\right)}, \tag{13}$$

and α is as in Eq. (11). The factor $(1-\alpha^2W^2)$ in the denominator represents all the multiple scattering contributions beyond single and double scattering. For spherical potentials $U_i(\mathbf{r})$ of arbitrary radial profile, Eq. (13) integrates directly to

$$W=e^{ikR}/kR \tag{14}$$

in the case that the separation, R, between the sources is sufficiently large so that they have no common region of overlap. Equation (14) is valid for all values of R in the limit of point sources, in which case Eq. (12) reduces to the previously discussed case of Brueckner. If we assume a square well of radius a for the potentials $U_i(\mathbf{r})$, Eq. (14) is valid for $R\geq 2a$. For $R<2a$, the value of W is dependent on the assumed shape of $U_i(\mathbf{r})$ and can be readily calculated. In the approximation $ka<1$, W reduces simply for $R=0$ to

$$W=6/5ak+i+O(ak). \tag{15}$$

The results of the separable potential model expressed by Eqs. (12)–(15) can be readily applied for various assumed well radii in order to provide a quantitative study of the approach to the point-scattering behavior of Eq. (7).

The physically interesting case corresponds to an average of the above scattering amplitudes over the relative space distribution of the two particles in a bound system. In particular, we may consider the deuteron case. The quantities of interest are thus, for the differential elastic scattering cross section,

$$\sigma(\mathbf{k},\mathbf{k}_0)=\left|\int d^3\mathbf{R}\psi_D^*(R)f_{(R)}(\mathbf{k},\mathbf{k}_0)\psi_D(R)\right|^2, \tag{16}$$

and for the total cross section

$$\sigma_{\text{Tot}}=(4\pi/k)\times\text{Im}\left(\int d^3\mathbf{R}\psi_D^*(R)f_{(R)}(\mathbf{k}_0,\mathbf{k}_0)\psi_D(R)\right). \tag{17}$$

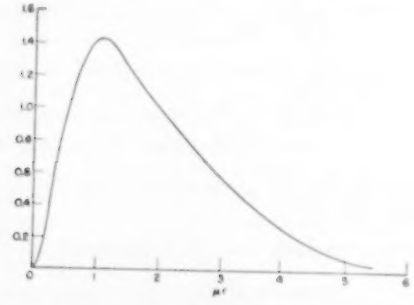

FIG. 1. The deuteron radial distribution, $r^2|\psi_D(r)|^2$, according to the Hulthén function, in arbitrary units.

For the deuteron wave function $\psi_D(R)$ we use the Hulthén function. As illustrated in Fig. 1, the radial density $(R^2|\psi_D(R)|^2)$ cuts down contributions from the $\mu R<\frac{1}{2}$ region. Thus, for[10] $k/\mu\gtrsim 2$ (π-meson kinetic energies >300 Mev, we expect the multiple-scattering corrections to the impulse approximation to be small, and the presence or absence of the singularity in the intermediate-wave propagator to be unimportant in the discussion of the forward elastic scattering or of the total cross section. However, backward elastic scattering will be quite sensitive to the small-distance behavior (or large-momentum components) of both the propagators and of the wave function. This is readily understood since backward scattering results in a large transfer of momentum to the deuteron. This large transfer can be effected only when the two nucleons are in close coincidence in the case that the deuteron remains bound. Thus the probability of finding the two nucleons near one another as well as the behavior of the intermediate-wave propagator for small distances are of decisive importance. In this case, we expect important multiple-scattering corrections to the impulse approximation as well as considerable dependence on the specific form used for the intermediate-wave propagator.

On the other hand, for $k/\mu\lesssim 1$, the entire range of μR values is sensitive to the choice of wave propagator, and we may expect results to be sensitive to the model employed. We also anticipate appreciable multiple-scattering corrections to the impulse approximation in this case for large scattering phase shifts.

[10] $\mu^{-1}=1.4\times10^{-13}$ cm is the meson Compton wavelength in units of $\hbar=c=1$.

The validity of the foregoing remarks has been confirmed in a series of calculations designed primarily to test the reliability of using the double-scattering term alone as a measure of the multiple-scattering corrections. For the three different models discussed previously, we have computed total and differential elastic cross sections according to Eqs. (16) and (17) for two identical S-wave scattering sources with a relative spatial distribution given by the Hulthén wave function for the deuteron:

$$\psi_D(R)=\left(\frac{\alpha+\beta}{\alpha-\beta}\right)\left(\frac{\alpha\beta}{2\pi(\alpha+\beta)}\right)^{\frac{1}{2}}(e^{-\alpha R}-e^{-\beta R})/R,$$

with $\beta/\alpha=6.35$ and $\alpha=2.31\times10^{13}$ cm^{-1}, and have considered incident meson wave numbers of $k/\mu=1$ and 2.2, and individual scattering phase shifts of $\delta=30°$ and 45°; $a=\exp(i\delta)\sin\delta$. The pertinent results of this study are:

(1) The multiple-scattering corrections are acutely model-dependent when they are at all important.

(2) The *double*-scattering approximation fails to reproduce the *multiple*-scattering results only when applied to Model I [Eqs. (6) and (7)] with the singular propagator. In this case, the presence of the singularity in Eq. (6) at $R=0$ introduces a large specious contribution from the region of close coincidence of the scattering sources, $kR<1$.

We fix these statements with a set of numbers: for backward elastic scattering with $k/\mu=2.2$ and $\delta=45°$, Model I [Eq. (7)] gives a decrease from the impulse approximation by a factor of four; Model II [Eq. (9)], by a factor of two; and Model III [Eqs. (12) and (13)] by a factor of three for source radii $a=1/2\mu$. The results for Models II and III are unchanged in the double-scattering approximation, whereas the reduction factor for model I changes from four to two.

Finally, we note from the equations obtained in this section:

(1) In general there may be appreciable multiple-scattering corrections to the impulse approximation for large individual-particle scattering phase shifts in the case where the magnitude of the scattering length $|a/k|$ is comparable with a mean or average spacing R between scattering sources; i.e., $|a/k|$ must be small compared with the mean spacing between the scatterers if multiple scattering is to be safely neglected. This condition reduces to the requirement of small phase shifts, $|a|<1$, for large-angle elastic scattering since two nucleons must be within a distance $(1/k)<R$ of each other in order to accept a momentum transfer of order k.

(2) The double (as well as all even) scattering contributions are most important for scattering in the backward direction because the double-scattered waves are in phase whatever the relative orientation of the two sources.

IV. CALCULATION OF THE CROSS SECTIONS

We consider now $\pi^{\pm}$-deuteron scattering, using the experimentally observed phase shifts for pion-proton scattering together with the assumption of charge independence. We consider only the double-scattering corrections since the algebra of the spin and isotopic spin matrices becomes rather complicated. The double-scattering calculations which we have carried through for the S-wave scattering cases discussed above indicate the qualitative reliability for usch an approximation.

For this calculation we introduce Eqs. (1) and (5) into Eq. (4), obtaining

$$\begin{aligned}kf(\mathbf{k},\mathbf{k}_0)=&\big[e^{-i(\mathbf{k}_0-\mathbf{k})\cdot\mathbf{R}/2}(\alpha_1+\beta_1\mathbf{k}\cdot\mathbf{k}_0-i\gamma_1\boldsymbol{\sigma}_1\cdot\mathbf{k}_0\times\mathbf{k})\\&+e^{-i(\mathbf{k}_0+\mathbf{k})\cdot\mathbf{R}/2}(\alpha_2+i\beta_2\mathbf{k}\cdot\boldsymbol{\nabla}_R+\gamma_2\boldsymbol{\sigma}_2\cdot\boldsymbol{\nabla}_R\times\mathbf{k})\\&\times(\alpha_1+i\beta_1\mathbf{k}_0\cdot\boldsymbol{\nabla}_R+\gamma_1\boldsymbol{\sigma}_1\cdot\mathbf{k}_0\times\boldsymbol{\nabla}_R)g_0(kR)\big]\\&+(\text{same expression with } 1\leftrightarrow2,\text{ and } R\leftrightarrow-R).\end{aligned}\tag{18}$$

Different forms can be introduced for the propagator $g_0(kR)$ corresponding to the various models discussed previously. If we introduce Eq. (3) and project onto the isotopic spin singlet state which represents the deuteron, we have, for example,

$$\langle\pi^{\pm},D|\,2\alpha'+\alpha''(\boldsymbol{\tau}_1+\boldsymbol{\tau}_2)\cdot\mathbf{t}\,|\pi^{\pm},D\rangle=2\alpha'.\tag{19}$$

Finally, after averaging over the orientations of R we obtain the general formula for the scattering amplitude. As it is very voluminous, we shall write it in the Appendix, along with the particular cases $f(R;k;0)$ and $f(R;k;\pi/2)$. We present here the formula for $f(R;k;\pi)$ which is the simplest one:

$$\begin{aligned}f(R;k;\pi)=(2/k)\Big[&(\alpha'-\beta'k^2)\sin(kR)/kR\\&+(\alpha'^2-2\alpha''^2)g_0(kR)-\frac{k^4}{3}(\beta'^2-2\beta''^2)g_0(kR)\\&-\frac{k^4}{3}(\gamma'^2-2\gamma''^2)(\boldsymbol{\sigma}_1\times\mathbf{k}_0)\cdot(\boldsymbol{\sigma}_2\times\mathbf{k}_0)g_0(kR)\Big]\\&\equiv a_\pi+(b_\pi/k^2)(\boldsymbol{\sigma}_1\times\mathbf{k}_0)\cdot(\boldsymbol{\sigma}_2\times\mathbf{k}_0).\end{aligned}\tag{20}$$

The cross section follows then when we project f onto the deuteron triplet spin state and take its absolute square:

$$\sigma(R;k;\pi)=|a_\pi|^2+(4/3)|b_\pi|^2+\tfrac{2}{3}(a_\pi b_\pi^*+a_\pi^* b_\pi).$$

Explicit numerical calculations have been carried through for energies of the impinging pion: $E_{\text{lab}}=45$ Mev corresponding to $k=0.75\mu$, and $E_{\text{lab}}=169$ Mev corresponding to $k=1.46\mu$. The corresponding pion-nucleon phase shifts are collected in Table I. At 45 Mev, we extrapolated the Steinberger[11] results. At 169 Mev we

[11] Bodansky, Sachs, and Steinberger, Phys. Rev. **93**, 1367 (1954).

TABLE I. The phase shifts used in the numerical calculations For $E_{lab}=169$ Mev, corresponding to $k=1.46\mu$, we give the two sets proposed by Fermi and by Bethe. For $E_{lab}=45$ Mev, corresponding to $k=0.75\mu$, we have extrapolated the phase shifts from Steinberger's experiments at 65 Mev, assuming that the S and P phase shifts are proportional to k and k^3, respectively. We use the usual notation for the phase shifts, with the first index representing twice the isotopic spin and the second one, twice the angular momentum for the P states.

	δ_S	δ_P	δ_{33}	δ_{31}	δ_{13}	δ_{11}
$k=0.75\mu$	$-5.3°$	$9.4°$	$5.8°$	0	0	0
$k=1.46\mu$ (Fermi)	$-42°$	$7°$	$48°$	$14°$	0	0
$k=1.46\mu$ (Bethe)	$-4°$	$7°$	$64°$	0	0	0

used both the Fermi[12] and Bethe[13] determinations of the phase shifts.

As stated before, the integration over R was carried out numerically using the Hulthén wave function for the deuteron. The differential elastic cross sections for $\theta=0$, $\pi/2$, and π, and the total cross sections were calculated for the different scattering models discussed in the previous section. The results are summarized in Table II for $E=45$ Mev and in Table III for $E=169$ Mev.

V. CONCLUSIONS

From this study we conclude that a phenomenological calculation of the multiple-scattering correction to the $\pi^{\pm}-D$ scattering can only lead in general to uncertain results. This is due to our lack of knowledge of the off-the-energy-shell amplitudes for which we must introduce specific models. Different models lead to multiple-scattering corrections which have in common only their orders of magnitude.

Since the phase shifts for pion-nucleon scattering are relatively small at pion kinetic energies of 45 Mev, the multiple scattering corrections as exhibited in Table II are of minor importance. However, the phase shifts are large at 169 Mev and the scattering lengths are comparable to the characteristic deuteron size, so that appreciable corrections result from multiple scattering effects. As we see in Table III, these corrections are sensitive to assumptions made concerning the off-the-energy-shell behavior of the scattering amplitudes. They are most important for backward scattering, in which case the double-scattered waves are in phase as discussed previously. However, backward elastic scattering is quite sensitive to the small distance behavior of the deuteron wave function since the large momentum transfer can be effected best when the neutron and proton are in close coincidence. Since the deuteron wave function in this region is both unknown and in itself sensitive to the nuclear force, an interpretation of experimental results on backward elastic scattering must remain to a large extent ambiguous. On the other hand, in that it does depend both on the deuteron wave function and on the scattering amplitudes in a very sensitive manner, backward elastic $\pi^{\pm}-D$ scattering may serve as a critical test of future meson theories.

TABLE II. The double scattering corrections are presented in this table for $E_{lab}=45$ Mev according to Model II and Model III with the two choices of square-well radii corresponding to $a=0.25/\mu$ and $a=0.50/\mu$. Model I, corresponding to $a\to 0$ in Model III, was omitted in these calculations because of unreliability of the double-scattering approximation as discussed in the text.

$k=0.75\mu$ $E_{lab}=45$ Mev	Single scattering	Ratio of the corrected scattering to the single scattering for: Model II	Model III with radius $a=0.25/\mu$	Model III with radius $a=0.50/\mu$
$\sigma(0)$	2.35 mb/sterad	0.99	1.04	1.04
$\sigma(\pi/2)$	0.29 mb/sterad	0.93	1.1	1.05
$\sigma(\pi)$	1.25 mb/sterad	0.97	1.2	1.1
σ_{tot}	25. mb	0.88	0.92	0.94

TABLE III. The double-scattering corrections for $E_{lab}=169$ Mev. The smallness of the cross section at $\pi/2$ is a consequence of near cancellation in the single-scattering calculation. The double-scattering corrections can therefore be relatively very important. However, the smallness of the cross section at $\pi/2$ makes their experimental determination all the more difficult.

$k=1.46\mu$, $E_{lab}=169$ Mev	Single scattering	Ratio of the corrected scattering to the single scattering for: Model II	Model III with radius $a=0.25/\mu$	Model III with radius $a=0.50/\mu$
$\sigma(0)$ (Fermi)	53 mb/sterad	0.89	1.04	0.95
$\sigma(0)$ (Bethe)	55 mb/sterad	0.89	1.07	0.98
$\sigma(\pi/2)$ (Fermi)	0.10 mb/sterad	0.45	1.5	
$\sigma(\pi)$ (Fermi)	5.2 mb/sterad	0.68	0.68	0.63
$\sigma(\pi)$ (Bethe)	5.5 mb/sterad	0.67	0.67	0.57
σ_{tot} (Fermi)	250 mb	0.95	1.01	1.05
σ_{tot} (Bethe)	250 mb	0.97	1.03	1.09

The total cross sections as calculated in Table III can be compared with the experimental results of Ashkin[14] and collaborators. For positive mesons of energy 162 ± 12 Mev they observed a total cross section of 217 ± 14 mb. The predictions of the impulse approximation at 169 Mev is 250 mb and the multiple scattering corrections are calculated to be less than 10 percent. In view of the theoretical and experimental uncertainties, and of the fact that the data were obtained for a broad spread of meson energies in a region of rapidly varying cross section, little more can be inferred from this result than that there is a satisfactory qualitative agreement between the calculated and observed cross sections.

In his analysis of the experiments of Arase, Goldhaber, and Goldhaber[15] on $\pi^{-}-D$ elastic scattering at 140 Mev, Green[16] has pointed out an additional un-

[12] Fermi, Glicksman, Martin, and Nagle, Phys. Rev. **92**, 161 (1953); Fermi, Metropolis, and Alei, Phys. Rev. **95**, 1581 (1954).
[13] de Hoffman, Metropolis, Alei, and Bethe, Phys. Rev. **95**, 1586 (1954).
[14] Ashkin, Blaser, Feiner, Gorman, and Stern, Phys. Rev. **96**, 1109 (1954).
[15] Arase, Goldhaber, and Goldhaber, Phys. Rev. **90**, 160 (1953). See also D. E. Nagle, Phys. Rev. **97**, 480 (1955).
[16] T. Green, Phys. Rev. **90**, 161 (1953).

certainty which the application of the impulse approximation introduces: scattering amplitudes with the momentum energy relations which apply in meson-nucleon collisions are used in the meson-deuteron case for which there are different kinematical conditions. This difference is especially important in this energy region near the resonance where the cross section is rapidly varying with energy.

Finally we note from our results in Table III that it does not seem feasible to use $\pi^{\pm}-D$ scattering experiments alone as a means of distinguishing between the predictions of the Fermi and Bethe sets of meson-nucleon scattering phase shifts since the multiple-scattering corrections are pretty much the same in both cases.

ACKNOWLEDGMENTS

One of us (L. V.) wishes to acknowledge the French "Relations Culturelles" and the C.E.A. of Saclay for financial support.

APPENDIX A

We exhibit in this paragraph a brief deduction of the amplitudes for double and multiple S-scattering from two scattering sources. Writing and formally solving the Schrödinger equation for the case of scattering from a single source described by potential V (in units of $2m/\hbar^2$), we have

$$\begin{aligned}(E-H_0)\psi &= V_1\psi,\\ \psi &= \varphi+GV_1\psi=\varphi+GV_1(1-GV_1)^{-1}\varphi,\end{aligned} \tag{1a}$$

where $\varphi=\exp(i\mathbf{k}_0\cdot\mathbf{r})$ represents the incident wave, ψ the eigensolution, and $G\equiv(E-H_0)^{-1}$ the integral operator for scattering used by Lippman and Schwinger,[17] with the contour at the singularity chosen to satisfy the scattering boundary conditions. In terms of the Green function $g(\mathbf{r};\mathbf{r}')$, we write

$$(Gf)_r=-\int d^3\mathbf{r}'g(\mathbf{r};\mathbf{r}')f(\mathbf{r}'). \tag{2a}$$

The elastic scattering amplitude in this case is given by

$$-(4\pi)^{-1}\langle\mathbf{k}|V_1(1-GV_1)^{-1}|\mathbf{k}_0\rangle=f_1(\mathbf{k},\mathbf{k}_0). \tag{3a}$$

For two sources, Eq. (1a) becomes

$$\psi=\varphi+G(V_1+V_2)[1-G(V_1+V_2)]^{-1}\varphi. \tag{4a}$$

We wish now to express the scattering amplitude from the two sources as given in Eq. (4a) in terms of the scattering amplitudes of the individual sources, Eq. (3a). That is, we shall manipulate the right member of Eq. (4a) into combinations of the form in Eq. (3a). Defining

$$a_i\equiv V_i(1-GV_i)^{-1} \quad \text{for} \quad i=1,2,$$

we find

$$\begin{aligned}&GV_1[1-G(V_1+V_2)]^{-1}\\ &\quad=Ga_1+Ga_1Ga_2+Ga_1Ga_2GV_1[1-G(V_1+V_2)]^{-1}\\ &\quad=(1-Ga_1Ga_2)^{-1}(Ga_1+Ga_1Ga_2).\end{aligned}$$

This gives us then the multiple-scattering expression,

$$\begin{aligned}\psi=\varphi&+(1-Ga_1Ga_2)^{-1}(Ga_1+Ga_1Ga_2)\varphi\\ &+(1-Ga_2Ga_1)^{-1}(Ga_2+Ga_2Ga_1)\varphi,\end{aligned} \tag{5a}$$

in terms of the scattering amplitudes from the individual sources. If we keep only the single- and double-scattering terms, Eq. (5a) approximates to

$$\begin{aligned}\psi_D&=\varphi+G(a_1+a_2+a_1Ga_2+a_2Ga_1)\varphi\\ &=\varphi+G[V_1(1-GV_1)^{-1}+V_2(1-GV_2)^{-1}\\ &\quad+V_1(1-GV_1)^{-1}GV_2(1-GV_2)^{-1}\\ &\quad+V_2(1-GV_2)^{-1}GV_1(1-GV_1)^{-1}]\varphi,\end{aligned}$$

which together with defining Eqs. (2a) and (3a) gives Eq. (4) of the text for the scattering of waves with wave number k which solve the Helmholtz wave equation with Green's function

$$g(\mathbf{r};\mathbf{r}')=(2\pi)^{-3}\int d^3\mathbf{q}\frac{\exp i\mathbf{q}\cdot(\mathbf{r}-\mathbf{r}')}{q^2-k^2-i\epsilon}. \tag{6a}$$

In Eq. (6a), the small negative imaginary term is appended in the denominator to define the contour corresponding to outgoing waves scattered from the source.

The multiple scattering can be handled in Eq. (5a) with the assumption of constant scattering amplitudes as follows. Consider a contribution from the denominator expansion,

$$Ga_1Ga_2Ga_1\varphi.$$

Using Eqs. (2a) and (6a), we have

$$\begin{aligned}&Ga_1Ga_2Ga_1\varphi\\ &=Ga_1\left(\frac{4\pi}{(2\pi)^3}\right)^2\int\frac{d^3\mathbf{q}}{q^2-k^2-i\epsilon}\int\frac{d^3\mathbf{q}'}{q'^2-k^2-i\epsilon}e^{i\mathbf{q}'\cdot\mathbf{r}'}\\ &\quad\times\langle\mathbf{q}|a_2|\mathbf{q}'\rangle\langle\mathbf{q}'|a_1|\mathbf{k}_0\rangle.\end{aligned} \tag{7a}$$

We next note the relation

$$\begin{aligned}\langle\mathbf{q}|a_2|\mathbf{q}'\rangle&\equiv\int d^3\mathbf{r}\exp[i(\mathbf{q}'-\mathbf{q})\cdot\mathbf{r}]a_2(\mathbf{r})\\ &=e^{i(\mathbf{q}'-\mathbf{q})\cdot\mathbf{R}}\langle\mathbf{q}|a_1|\mathbf{q}'\rangle,\end{aligned} \tag{8a}$$

with R introduced as the separation between the two scattering sources. Introducing Eq. (8a) into (7a) and making use of the above assumption that $-(4\pi)^{-1}\times\langle\mathbf{q}|a_1|\mathbf{q}'\rangle\equiv f_1$ is independent of $\mathbf{q}$ and $\mathbf{q}'$, we obtain

$$Ga_1Ga_2Ga_1\varphi=Ga_1e^{i\mathbf{q}\cdot\mathbf{r}'}(e^{ikR}/R)^2f_1^3, \tag{9a}$$

which is equivalent to $(e^{ikR}/R)^2f_1^2Ga_1\varphi$ with our as-

[17] B. A. Lippman and J. Schwinger, Phys. Rev. **79**, 469 (1950).

sumptions. Equation (9a) leads immediately to the result expressed in the text by Eq. (7).

APPENDIX B

In this appendix we write the formula for $f(R,k,\theta)$, $f(R,k,0)$, and $f(R,k,\pi/2)$, which were too cumbersome to be introduced in the text.

$$f(R,k,\theta)=\frac{2}{k}\Big\{\Big(\alpha'+\beta'\mathbf{k}\cdot\mathbf{k}_0-i\gamma'\frac{\boldsymbol{\sigma}_1+\boldsymbol{\sigma}_2}{2}\cdot\mathbf{k}_0\times\mathbf{k}\Big)j_0(z)$$

$$+(\alpha''^2-2\alpha'''^2)j_0(y)g_0(x)+\Big(2(\alpha'\beta'-2\alpha''\beta'')\mathbf{k}_0\cdot\mathbf{l}$$

$$-i(\alpha'\gamma'-2\alpha''\gamma'')\frac{\boldsymbol{\sigma}_1+\boldsymbol{\sigma}_2}{2}\cdot\mathbf{k}_0\times\mathbf{k}\Big)\frac{k}{l}j_1(y)g_1(x)$$

$$+\big[(\beta''^2-2\beta'''^2)\mathbf{k}\cdot\mathbf{k}_0-i(\beta'\gamma'-2\beta''\gamma'')(\boldsymbol{\sigma}_1+\boldsymbol{\sigma}_2)\cdot\mathbf{k}_0\times\mathbf{k}$$

$$+\tfrac{1}{2}(\gamma''^2-2\gamma'''^2)(\boldsymbol{\sigma}_1\times\mathbf{k}\cdot\boldsymbol{\sigma}_2\times\mathbf{k}_0+\boldsymbol{\sigma}_1\times\mathbf{k}_0\cdot\boldsymbol{\sigma}_2\times\mathbf{k})\big]$$

$$\times k^2\Big(\frac{g_1(x)}{x}j_0(y)-g_2(x)\frac{j_1(y)}{y}\Big)+\Big((\beta''^2-2\beta'''^2)\mathbf{k}_0\cdot\mathbf{l}$$

$$-i(\beta'\gamma'-2\beta''\gamma'')\frac{\boldsymbol{\sigma}_1+\boldsymbol{\sigma}_2}{2}\cdot\mathbf{k}_0\times\mathbf{k}\,(\mathbf{k}_0\cdot\mathbf{l}/l^2)-(\gamma''^2-2\gamma'''^2)$$

$$\times\frac{(\boldsymbol{\sigma}_1\cdot\mathbf{k}_0\times\mathbf{k})(\boldsymbol{\sigma}_2\cdot\mathbf{k}_0\times\mathbf{k})}{4l^2}\Big)\times k^2g_2(x)j_2(y)\Big\}, \quad (1b)$$

where $x\equiv kR$; $y\equiv lR$; $\mathbf{l}\equiv(\mathbf{k}_0+\mathbf{k})/2$; $z\equiv|\mathbf{k}_0-\mathbf{k}|R/2$; $j_l(z)$ is the spherical Bessel function of order l, with $j_0(z)\equiv\sin z/z$; $g_0(x)$ is one of the propagators discussed in the text, and $g_1(x)\equiv-g_0'(x)$; $g_2(x)\equiv-x[g_1(x)/x]'$.

$$f(R,k,0)=(2/k)\{\alpha'+\beta'k^2+(\alpha''^2-2\alpha'''^2)j_0(x)g_0(x)$$
$$+2(\alpha'\beta'-2\alpha''\beta'')k^2j_1(x)g_1(x)+(\beta''^2-2\beta'''^2)k^4$$
$$\times[g_1(x)j_0(x)-g_2(x)j_1(x)+xg_2(x)j_2(x)]/x$$
$$+(\gamma''^2-2\gamma'''^2)\boldsymbol{\sigma}_1\times\mathbf{k}_0\cdot\boldsymbol{\sigma}_2\times\mathbf{k}_0k^2[g_1(x)j_0(x)$$
$$-g_2(x)j_1(x)]/x\}\equiv a_0+b_0\boldsymbol{\sigma}_1\times\mathbf{k}_0\cdot\boldsymbol{\sigma}_2\times\mathbf{k}_0/k^2. \quad (2b)$$

$$f(R,k,\pi/2)=\frac{2}{k}\Big\{\Big(\alpha'-i\gamma'k^2\frac{\boldsymbol{\sigma}_1+\boldsymbol{\sigma}_2}{2}\cdot\mathbf{n}\Big)j_0(u)$$
$$+(\alpha''^2-2\alpha'''^2)g_0(x)j_0(u)+[2(\alpha'\beta'-2\alpha''\beta'')$$
$$-i(\alpha'\gamma'-2\alpha''\gamma'')(\boldsymbol{\sigma}_1+\boldsymbol{\sigma}_2)\cdot\mathbf{n}]kg_1(x)j_1(u)/\sqrt{2}$$
$$+[-i(\beta'\gamma'-2\beta''\gamma'')(\boldsymbol{\sigma}_1+\boldsymbol{\sigma}_2)\cdot\mathbf{n}k^2$$
$$+(\gamma''^2-2\gamma'''^2)(\boldsymbol{\sigma}_1\times\mathbf{k}\cdot\boldsymbol{\sigma}_2\times\mathbf{k}_0+\boldsymbol{\sigma}_1\times\mathbf{k}_0\cdot\boldsymbol{\sigma}_2\times\mathbf{k})/2]$$
$$\times k^2[j_0(u)g_1(x)/x-g_2(x)j_1(u)/u]+[(\beta''^2-2\beta'''^2)$$
$$-i(\beta'\gamma'-2\beta''\gamma'')(\boldsymbol{\sigma}_1+\boldsymbol{\sigma}_2)\cdot\mathbf{n}-(\gamma''^2-2\gamma'''^2)\boldsymbol{\sigma}_1\cdot\mathbf{n}\boldsymbol{\sigma}_2\cdot\mathbf{n}]$$
$$\times k^4g_2(x)j_2(u)/2\Big\}\equiv a_{\pi/2}+b_{\pi/2}(\boldsymbol{\sigma}_1+\boldsymbol{\sigma}_2)\cdot\mathbf{n}$$
$$+c_{\pi/2}(\boldsymbol{\sigma}_1\times\mathbf{k}\cdot\boldsymbol{\sigma}_2\times\mathbf{k}_0+\boldsymbol{\sigma}_1\times\mathbf{k}_0\cdot\boldsymbol{\sigma}_2\times\mathbf{k})/k^2$$
$$+d_{\pi/2}\boldsymbol{\sigma}_1\cdot\mathbf{n}\boldsymbol{\sigma}_2\cdot\mathbf{n}, \quad (3b)$$

where $\mathbf{k}_0\times\mathbf{k}=k^2\mathbf{n}$ and $u\equiv x/2^{\frac{1}{2}}$. The cross sections are deduced as in the text and reduce to

$$\sigma(R;k;0)=|a_0|^2+(4/3)|b_0|^2+\tfrac{2}{3}(a_0^*b_0+a_0b_0^*); \quad (4b)$$

$$\sigma(R;k;\pi/2)=|a_{\pi/2}|^2+(8/3)|b_{\pi/2}|^2+(8/3)|c_{\pi/2}|^2$$
$$+|d_{\pi/2}|^2+\tfrac{1}{3}(a_{\pi/2}^*d_{\pi/2}+a_{\pi/2}d_{\pi/2}^*). \quad (5b)$$

The constants in (4b) and (5b) are defined in (2b) and (3b). The total cross section is expressed by Eq. (17) in the text and requires evaluation of the spin sum:

$$\langle\pi^\pm,D|a_0+b_0\boldsymbol{\sigma}_1\times\mathbf{k}_0\cdot\boldsymbol{\sigma}_2\times\mathbf{k}_0/k^2|\pi^\pm,D\rangle=a_0+\tfrac{2}{3}b_0. \quad (6b)$$

Attenuation Cross Sections for 860-Mev Protons*

FRANCIS F. CHEN,† CHRISTOPHER P. LEAVITT, AND ANATOLE M. SHAPIRO‡
Brookhaven National Laboratory, Upton, New York
(Received April 29, 1955)

Integral angular distributions of 860-Mev protons scattered by Be, C, Al, Cu, Sn, and Pb nuclei have been measured in a transmission experiment in which the half-angle subtended at the absorber by the detector was varied from 1.5° to 20°. A counter telescope technique employing plastic scintillation counters and a fast-coincidence circuit was used. From the cross sections measured with poor geometry it is possible to deduce the inelastic cross section for the heavy elements and, less unambiguously, also for the light elements. Agreement with 1.4-Bev neutron data from a concurrent experiment is good. Total cross sections could not be obtained for the heavy elements because of Coulomb effects, but for the light elements rough estimates could be made. The data are consistent with an interpretation in terms of the "optical" model of the nucleus with constant nuclear density. If the nucleon-nucleon cross section at this energy is taken to be 45 mb, these measurements yield a nuclear absorption constant K of 0.56×10^{13} cm^{-1} and a nuclear radius of the form $R=(1.25\pm0.02)A^{\frac{1}{3}}\times10^{-13}$ cm.

1. INTRODUCTION

HIGH-ENERGY experiments on the scattering of various particles by complex nuclei have in recent years yielded information on the size of the nucleus and the gross features of the interior, when analyzed in the light of the transparent model of the nucleus, in which the nuclear potential is given both a real and complex part. When the number of phase shifts is so large that an exact phase shift analysis is impractical, it has been customary to use the classical, or WKB, approximation or its analog in geometrical optics. In connection with the problem of electron scattering, Molière[1] has given the basic formulas in this approximation for scattering by an arbitrary potential. The "optical" model, however, first became popular after the publication of the paper of Fernbach, Serber, and Taylor,[2] in which the formulas were applied to the particular case of neutrons scattered by a uniform, spherical nucleus with a complex index of refraction. Although many theorists use the term "optical model" in the general sense of a nuclear potential which does not depend on the coordinates of the individual nucleons, in this paper the term will be used to denote the case in which the nucleus is assumed to be a uniform sphere with a complex index of refraction, and reflection and refraction at the surface are neglected.

Numerous experiments indicating nuclear transparency have been performed with neutrons up to 280 Mev at Berkeley and Harwell. These experiments, which have been briefly summarized by Nedzel,[3] have been explained satisfactorily by the optical model.[4]

Comparatively few experiments have been done with protons. At the time the present work was begun, there had been only three: a measurement of the differential elastic cross sections at 340 Mev by Richardson *et al.*,[5] one of the inelastic (or the so-called absorption) cross sections σ_a at 185, 240, and 305 Mev by Hicks and Kirschbaum,[6] and one of the total cross sections σ_t for light elements up to C at 408 Mev by Marshall *et al.*[7] Since that time σ_a has been measured for 134-Mev protons by Cassels and Lawson[8] and for 290-Mev protons by Millburn *et al.*[9] De Carvalho[10] has recently determined σ_t for light elements at 208 and 315 Mev.

Since the customary approximation of neglecting reflection and refraction at the surface of the nucleus improves with decreasing wavelength of the incident particles, experiments at higher energies should be comparatively free from the defects of the calculational procedure. Recently, Nedzel[3] has extended measurements of the total neutron cross sections to 410 Mev. Since the completion of the Brookhaven Cosmotron, it has been possible to perform experiments in the Bev region. The present experiment extends the proton cross sections to 860 Mev, which was at the time the highest energy available at the Cosmotron in an external proton beam of appreciable intensity. Concurrently, a neutron experiment was undertaken by Coor and others[11] at a mean energy of approximately 1.4 Bev. In their experiment the energy was determined from the width of the diffraction pattern, and therefore was not independent of the optical model.

The main advantage of using protons lies in the possibility of having a monoenergetic beam of known

* Research performed under the auspices of the U. S. Atomic Energy Commission.
† Now at Project Matterhorn, P. O. Box 451, Princeton, New Jersey.
‡ Now at the Department of Physics, Harvard University, Cambridge 38, Massachusetts.
[1] G. Molière, Z. Naturforsch. **2a**, 133 (1947).
[2] Fernbach, Serber, and Taylor, Phys. Rev. **75**, 1352 (1949).
[3] V. A. Nedzel, Phys. Rev. **94**, 174 (1954).
[4] T. B. Taylor, Phys. Rev. **92**, 831 (1953).
[5] Richardson, Ball, Leith, and Moyer, Phys. Rev. **86**, 29 (1952).
[6] D. A. Hicks and A. J. Kirschbaum, Livermore Report MTA-28, 1952 (unpublished).
[7] Marshall, Marshall, and Nedzel, Phys. Rev. **91**, 767 (1953).
[8] J. M. Cassels and J. D. Lawson, Proc. Phys. Soc. (London) **67A**, II, 125 (1954).
[9] Millburn, Birnbaum, Crandall, and Schecter, Phys. Rev. **95**, 1268 (1954).
[10] H. G. de Carvalho, Phys. Rev. **96**, 398 (1954).
[11] Coor, Hill, Hornyak, Smith, and Snow, Phys. Rev. **98**, 1369 (1955).

energy and energy spread. The complications introduced by an inefficient detector are also avoided. Moreover, it is in theory possible to determine the inelastic cross section accurately by absorbing out the low-energy secondaries. Protons, however, have several disadvantages resulting from the Coulomb field: the beam suffers ionization loss in the counters and the absorber, and is decollimated by multiple scattering. Moreover, at small angles Rutherford scattering interferes with diffraction scattering, making a determination of σ_t, i.e., the total cross section exclusive of Coulomb scattering, very difficult except for elements of low Z. It is for these reasons that most of the proton experiments have been designed to measure σ_a, and most of the neutron experiments to measure σ_t.

The purpose of the present experiment was to make a preliminary survey of the proton-nucleus cross sections at as high an energy as practicable in order to ascertain the applicability of the optical model at very high energies and to compare with the neutron-nucleus cross sections of Coor *et al.*[11] working with neutrons of a high but ill-defined energy. Moreover, since the free p-p cross section was observed[12] to increase between 300 and 800 Mev, it would be interesting to see whether the nuclear opacity increased correspondingly. With the assumption of a known nucleon-nucleon cross section one could determine the nuclear radius R and the absorption constant in nuclear matter K from the values of σ_a. If both σ_a and σ_t could be measured, one could see whether or not the mean real potential in the nucleus remained at the low value of 13 Mev which it seemed to have around 300 Mev.

For this study, six elements were chosen whose mass numbers (with the exception of C) are evenly spaced in units of $A^{\frac{1}{3}}$: Be, C, Al, Cu, Sn, and Pb. At 860 Mev the protons have a reduced wavelength of 1.28×10^{-14} cm; thus the number of phase shifts ($\sim kR$) varies from $\sim$20 for Be to $\sim$60 for Pb.

2. EXPERIMENTAL METHOD

A differential cross section measurement would be a more sensitive test of the transparent nucleus model than a transmission experiment, but the beam intensity available was far below that required for differential measurements. The low counting rate, together with the heavy demand for Cosmotron time, has moreover necessitated the use of thick absorbers and a rather large beam diameter. These compromises introduce such difficulties as loss of beam by multiple Coulomb scattering in the absorber, double diffraction scatterings, and ill-defined geometry. The success of the experiment as a preliminary survey therefore depends on the assumption that the cross sections will not be greatly affected by these effects if rough corrections are made for them. A detailed discussion of errors and corrections will be given in Sec. 6.

[11] Shapiro, Leavitt, and Chen, Phys. Rev. **95**, 663 (1954).

The experimental arrangement is shown in Fig. 1. Use was made of a beam emerging from a 6-in. thick Be target in the east straight section of the Cosmotron at an angle of 32° to the circulating beam direction. This angle is the minimum angle at which the various particles scattered or created at the target could emerge without passing through the field of the Cosmotron magnet. The particles passed through a $\frac{1}{4}$-in. thick portion of the aluminum vacuum chamber wall and entered a lead collimator of 3 in. circular aperture placed in the 8-ft thick concrete shield. The collimated beam was then analyzed by a magnet, and particles of approximately 1500 Mev/c momentum were deflected 11.9° into a counter telescope. The counters were mounted on a U-beam extending 25 ft from the magnet.

The acceleration cycle of the Cosmotron occupied about 0.9 sec and was repeated every 5 sec. By turning off the rf acceleration voltage slowly at the end of the cycle, the 2.2-Bev protons could be made to strike the target over a period of some 50 milliseconds. This "spreading out" of the beam greatly reduced the instantaneous counting rate.

The 860-Mev beam incident on the absorbers was defined by three $2\frac{1}{2}$-in. diameter plastic scintillation counters in triple coincidence. The absorber was placed behind counter 3, and the transmitted beam was measured by a 6-in. diameter counter (No. 4) in quadruple coincidence with the other three. In order to gain as much information as possible from attenuation measurements, counter 4 was placed at various distances behind the absorber. An integral angular distribution curve was thus obtained.

If θ is the half-angle subtended by counter 4 at the center of the absorber, Nx is the number of atoms per cm^2 in the absorber (N being the number of atoms per cm^3 and x the thickness in cm), and $1/r=I/I_0$ is the observed transmission, then the apparent cross section at subtended half-angle θ is given by

$$\sigma_0(\theta)=(Nx)^{-1}\ln r(\theta). \tag{1}$$

This is the cross section for all interactions removing beam protons from the solid angle Ω defined by θ, minus the cross section for production of secondaries detectable by counter 4.

In theory, with suitable corrections and extrapolations, one can obtain σ_a from the poor geometry measurements and σ_t from those at good geometry. The principal problem in the determination of σ_a is the elimination of charged secondaries from the last counter. While at lower energies[6] this can be accomplished by placing additional absorbers in front of the last counter to remove inelastically scattered charged particles, at 860 Mev this method was found to be impracticable.

The determination of σ_t is complicated by the interference of Rutherford scattering with the diffraction scattering. If Rutherford scattering is appreciable only at angles small compared with the angle of the first diffraction minimum, a considerable portion of the

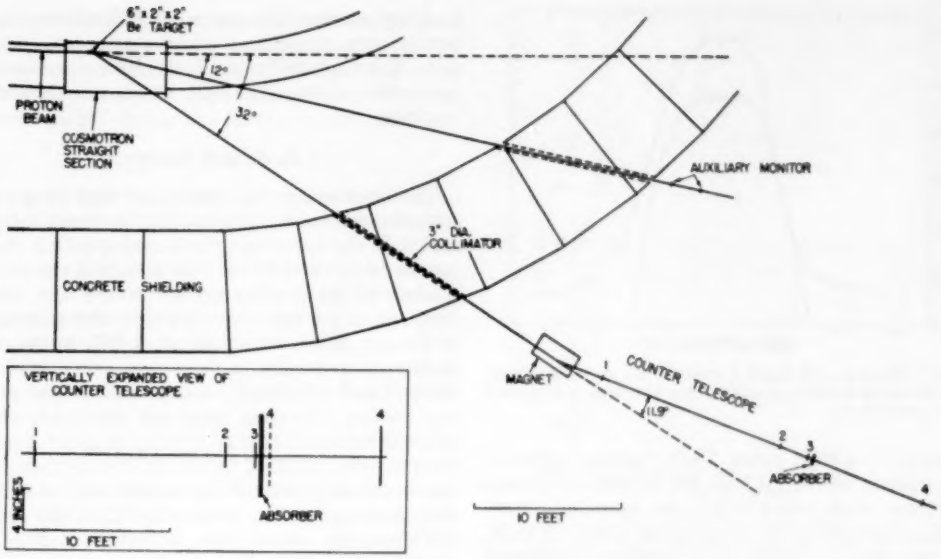

FIG. 1. Experimental arrangement.

primary maximum in the diffraction pattern can be observed. This was the case for the light elements at 315 Mev.[10] The situation becomes worse at higher momenta, however, since the diffraction angle decreases as $1/kR \sim 1/p$, while the angle for a given value of the Coulomb cross section decreases more slowly, as $1/(p\beta)^4$.

3. EQUIPMENT

A. Counters

Counters 1, 2, and 3 were 2½-in. diam disks, ½ in. thick, of plastic scintillator obtained commercially. Each counter was viewed edgewise by two matched 1P21 photomultipliers, whose outputs were connected in parallel. Counter 4 was a 6-in. disk of plastic viewed by three photomultipliers symmetrically placed. Most of the data were taken with counter 4*A*, which was homemade by compression molding of powdered polystyrene activated with terphenyl. Since this counter was not perfectly transparent, its pulses were nonuniform in size and smaller than those of the other counters. Toward the end of the experimental work it was possible to obtain commercially 6 in. plastic scintillators of good quality. Counter 4*B*, made with one of these, produced much larger pulses uniformly over the entire surface. The datum points taken with counters 4*A* and 4*B* have been plotted separately on the graphs (Figs. 10–15).

B. Electronics

Negative pulses from the anodes of the photomultipliers were amplified by Hewlett-Packard distributed amplifiers and clipped to 3×10^{-9} sec in length by 18-in. delay lines. The pulses then entered two identical coincidence circuits, one forming triple coincidences for the incident beam, and the other, quadruple coincidences for the transmitted beam. The outputs of the coincidence circuits were fed into cathode followers, and then to one of two identical amplifier, discriminator, and gating circuits. The uniform pulses of 10^{-7}-sec width from these circuits were then transmitted to the scalers.

The coincidence circuits were of a type designed by Garwin,[13] modified along the lines of a distributed amplifier by Madansky.[14] These circuits were designed to form up to sixfold coincidences without pairing. The resolving time of the counters plus coincidence circuits was tested by delaying or advancing the pulses from one counter by changing the cable length between the counter and the coincidence circuit. Figure 2 shows typical cable curves of counting rate *versus* cable difference. The half-width of the peaks indicates a resolving time of approximately 7×10^{-9} sec.

The discriminator was an EFP-60 secondary-emission tube, whose grid bias was adjusted to set the discrimination level. Plateau curves of counting rate *vs* bias voltage were flat over 1.2 volts, with a total variation of 5% over the whole plateau. In practice, the bias was held constant to 0.05 volt. A gating circuit cut off the EFP-60 except for a period of 80 msec at the end of the acceleration cycle of the Cosmotron.

The fast scalers were Hewlett-Packard 10-megacycle scalers capable of resolving three pulses in 0.2 μsec

[13] R. Garwin, Rev. Sci. Instr. **21**, 569 (1950).
[14] L. Madansky (private communication).

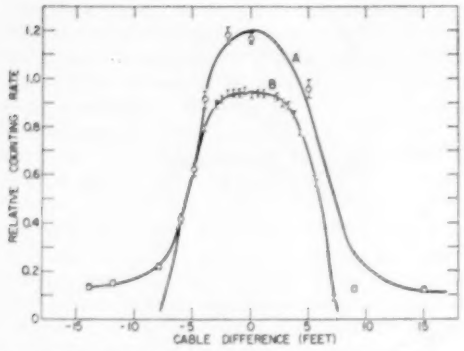

FIG. 2. Typical cable-length curves. Curves *A* and *B* indicate the variation of fourfold coincidence rate with delay in counters 1 and 4, respectively.

produced by a triple pulser. Under running conditions the counting rate varied from 100 to 1000 per Cosmotron pulse, which lasted 30–80 msec. Assuming a maximum average rate of 3×10^4 per second during the pulse, one sees that the scalers could handle a considerable amount of beam bunching. The dead time of the entire apparatus was found to be 2.2×10^{-7} sec.

An auxiliary monitor (see Fig. 1) consisting of two counters in coincidence and a separate system of electronics was placed in another beam. This was used to check that fluctuations in counting rate were real and not caused by instrumental failure. It was also needed in the measurement of beam contamination.

C. Magnet and Absorbers

The analyzing magnet had rectangular 36 in.×18 in. pole pieces with a 6-in. gap. The field was about 10^4 gauss producing a deflection of 11.9° for 870-Mev protons. The absorbers were all 8 in.×8 in. in area, with various thicknesses for each element.

4. AUXILIARY MEASUREMENTS

A. Beam Contamination

The analyzing magnet removed all particles from the beam except protons, mesons, and positrons of momentum approximately 1500 Mev/*c*. The number of heavy mesons, muons, and positrons of this momentum in the 32° beam is estimated to be negligibly small compared to the number of π^+ mesons. We therefore consider the contamination to consist essentially of positive pions. Since the proton and meson velocities are too similar at this momentum to distinguish them by time of flight, and since the protons had too long a range to be absorbed out without greatly attenuating the mesons, determination of the beam contamination was made by an indirect method. The magnet polarity was reversed, and the negative particles of the same momentum, which could only be pions (plus any electrons and muons present), were counted relative to the auxiliary monitor. This rate was 0.15% of the positive particle rate. Assuming a positive to negative meson ratio of not greater[15] than 3, this gave a meson contamination of less than ½%, which was completely negligible.

B. Proton Energy

The beam energy was determined both by a range measurement and by the method of a current-carrying wire.[16] In the latter case the incoming proton energy was found to be 867 Mev. The energy of the protons incident on the absorber was 859 Mev, 8 Mev having been lost in the first three counters. The uncertainty in the wire measurement was about 1%. In the other measurement, a range curve in copper was taken and differentiated graphically, taking nuclear interactions into account. The mean range was 360 g/cm², with a half-width at half maximum of about 30 g/cm². A range-energy curve, prepared by Dr. R. Sternheimer, using the experimental values[17] at 340 Mev and an integration of an energy loss formula including the density and Čerenkov effects, gave an energy of 840 Mev corresponding to this range. Consideration of such effects as straggling and multiple scattering failed to produce closer agreement with the wire measurement.

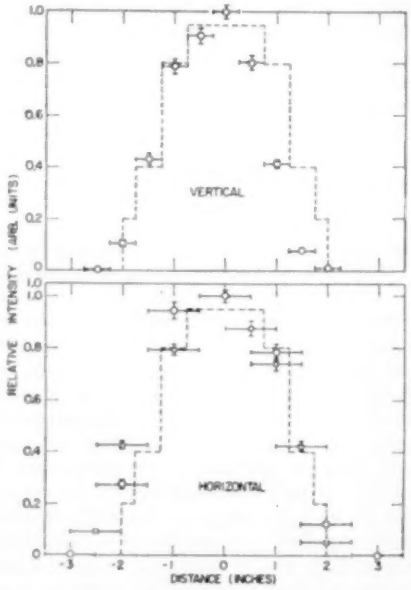

FIG. 3. Distribution of the beam defined by the first three counters. The size of the probe counter is indicated by the horizontal limits. The dotted curve is the axially symmetric step function used to approximate both the horizontal and vertical distributions.

[15] L. C. L. Yuan and S. J. Lindenbaum, Phys. Rev. **93**, 1431 (1954) and private communication.
[16] DeWire, Ashkin, and Beach, Phys. Rev. **83**, 505 (1951).
[17] C. J. Bakker and E. Segrè, Phys. Rev. **81**, 489 (1951).

Since the latter method was believed to be more reliable, the energy of the incident protons in this experiment was taken to be 860±50 Mev, half-width at half-maximum. The mean energy in the absorber varied from 857 to 825 Mev for the samples used.

C. Beam Distribution

Owing to imperfect collimation and to scattering by the counters, the beam incident on the absorber was not uniformly distributed over a circle 2½ in. in diameter. For the purpose of calculating the multiple scattering correction, it was necessary to measure this distribution. This was accomplished by counting at different positions with a small (1 in.×½ in.) counter in quadrupule coincidence with counters 1, 2, and 3. No appreciable divergence of the beam was found; the lateral distribution is shown in Fig. 3.

D. Efficiency of Counter 4

Because of scattering by the defining counters and by the air, the "efficiency," or ratio of quadruples to triples without absorber, was always less than 97%. However, for any particular geometry the efficiency was always smaller for counter 4*A* than for counter 4*B*, indicating that one or both of these counters was not 100% efficient over its entire surface. Since the subtended angle θ would be affected by a nonuniform sensitivity, this was measured with a small probe counter. Counter 4*B* was found to be essentially 100% efficient; the result for counter 4*A* is shown in Fig. 4.

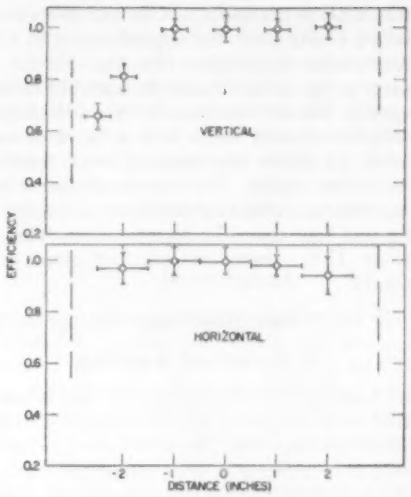

FIG. 4. Uniformity of counter 4*A*. The variation of efficiency is shown along the vertical and horizontal diameters. The difference between these arises from the location of the phototubes. The dotted lines indicate the edge of the counter.

E. Accidental Coincidences

Since the instantaneous counting rates were unknown, the rate of accidentals could not be calculated but had to be measured. This is usually done by displacing one counter at a time or delaying its pulses. One is then faced with the problem of combining these partial accidental rates. Moreover, in a collimated beam in which a large fraction of the counting rate is due to true beam particles this method overestimates the accidental rate: with one counter displaced or its pulses delayed, a beam particle can give rise to an accidental count which under normal conditions would be a true coincidence. In the present experiment "accidental" runs were frequently taken by adding 20 feet of cable to counter 4. Fortunately, the resolving time was such that this rate was usually below 0.6% of the normal rate and could be neglected even if the true accidental rate was somewhat different. Therefore, an accurate calculation of the accidental rate was not necessary. The uncertainty introduced will be discussed later. With the magnet off the background was less than 0.05% of the normal triples rate.

5. EXPERIMENTAL PROCEDURE

The line of centers of counters 1, 2, and 3 was adjusted to maximize the coincidence counting rate. That this line lay along a proton trajectory was confirmed by the current-carrying wire method. The cable lengths between the counters and the coincidence circuits were set at the center of the cable curve (Fig. 2), and plateau curves were taken on each of the two circuits counting triple and quadruple coincidences by varying the discriminator on one circuit and using the other as a monitor. That the discriminator voltage was set at the middle of its plateau and that the cable length curve was flat-topped was checked at the beginning of each day's run. For a given geometry, the "efficiency" remained constant from day to day and served as a convenient check on the stability of the electronics, since every other run was a "zero" run (without absorber). The failure of almost any component in the electronics would have affected the efficiency. Throughout the experiment the magnet current, discriminator voltage, and accidental coincidence rate were frequently checked.

For each element, points were taken at various geometries from $\theta=1.5°$ to $\theta=20°$. For some elements, various thicknesses of absorber were used. Each point was based on a run (approximately 50 000 counts in the triples) with the absorber in, and a "zero" run with the absorber out. The zero run was taken immediately before or after the absorber run, or both. In computing the transmissions, only the zero run taken for each point was used, in order to eliminate the effects of slow drifts in the apparatus; all the zero runs for each geometry were *not* averaged. Some of the points were repeated during the course of the experiment, sometimes after a lapse of several months. The spread of these repeated points was consistent with the statistical errors.

Because of the uncertainty in the multiple scattering correction arising from the approximation of a step-function beam distribution (see Fig. 3), the good geometry points for the heavier elements had extremely large errors. In order to reduce the error on these points, additional runs were taken with a beam of smaller diameter, for which the assumed beam distribution would be less critical. This was accomplished by replacing counter 3 with a counter $1\frac{1}{4}$ in. in diameter and taking runs four times the normal length. The points with the $1\frac{1}{4}$-in. beam are indicated separately on Figs. 9–14.

6. CORRECTIONS AND ERRORS

A. Rutherford Scattering

The Coulomb field of the nucleus affects both the inelastic cross section σ_a and the angular distribution of diffraction scattering. The effect on σ_a is merely to decrease it by a factor α, since the proton trajectories will be bent away from the nucleus by the Coulomb field. α is approximately $1-2eV_c/(p\beta c)$, where V_c is the Coulomb potential at the nuclear surface and p and βc are the momentum and velocity of the incident particle. In this experiment, the heaviest element was Pb, for which this correction was less than about 2%. No Coulomb correction was made in σ_a, and the experimental error was increased to cover this omission.

Interference between Rutherford scattering and elastic nuclear scattering can be estimated by computing the respective scattering amplitudes $f_c(\theta)$ and $f_n(\theta)$. The former was calculated from the Rutherford formula for a charged sphere of radius R:

$$f_c(\theta)=\frac{Ze^2}{2p\beta c}\frac{1}{\sin^2(\theta/2)}\frac{1}{1+[kR\sin(\theta/2)]^2}; \qquad (2)$$

and the latter was approximated by the optical model formula for neutrons (see Eq. (10)). If one requires that $2|f_c||f_n|$ be less than $0.1|f_n|^2$, then Coulomb interference can be neglected only at angles $>5°$ for Be (whose first diffraction minimum is at 11°) and $>7.5°$ for Pb (which corresponds to the third diffraction maximum). For the heavy elements, therefore, one cannot speak of a "total" cross section; the angular distributions are greatly affected by the Coulomb field, and Rutherford scattering cannot be treated as a correction. The theoretical curves shown in the graphs include Coulomb scattering and will be discussed further in Sec. 7.

B. Multiple Scattering Correction

The loss of particles from the transmitted beam by multiple Coulomb scattering in the absorber will give rise to an apparent cross section

$$\sigma_m=-(1/Nx)\ln F, \qquad (3)$$

where Nx is the number of atoms per cm² in the absorber, and $1-F$ is the fraction of the beam lost by multiple scattering; that is, the observed transmission is FI/I_0 instead of I/I_0.

The evaluation of F is made difficult by such factors as the relatively wide beam and the nonuniformity of counter 4*A*. If the beam were extremely narrow, the particles emerging from the absorber would have a gaussian distribution in the deflection angle, and this gaussian can easily be integrated over the solid angle subtended by counter 4. In the case of a wide beam, however, particles off the axis of the beam will have gaussians centered about different points in the cross section of the beam, and there must be an additional integration over the beam distribution. Moreover, after traversing a thick absorber, the beam will have been spread out in space as well as in angle. In connection with this problem we have been fortunate in having the assistance of Dr. R. M. Sternheimer. Sternheimer's results[18] are in the form of curves of F as a function of the parameters r_0 and ρ_0, where ρ_0 is the radius of a uniform circular beam in units of the radius of counter 4, and r_0 is a function of the rms scattering angle and the geometrical arrangement. Since in this case the beam was not uniform, it was necessary to approximate the beam distribution by a superposition of four uniform beams of different radii and intensities. The assumed distribution is shown in Fig. 3. For each experimental point, r_0 was computed using radiation lengths given by Rossi,[19] $F(\rho_0)$ was found for each ρ_0 from Sternheimer's curves, and F was obtained by averaging the four $F(\rho_0)$'s, with appropriate weights.

The resulting σ_m depends critically on the value assumed for the effective radius $\mathfrak{R}$ of counter 4. For counter 4*B*, $\mathfrak{R}$ was quite close to its physical dimension of 3 in.; for counter 4*A*, $\mathfrak{R}$ was somewhat smaller, owing to the inefficiency of this counter (see Fig. 5).

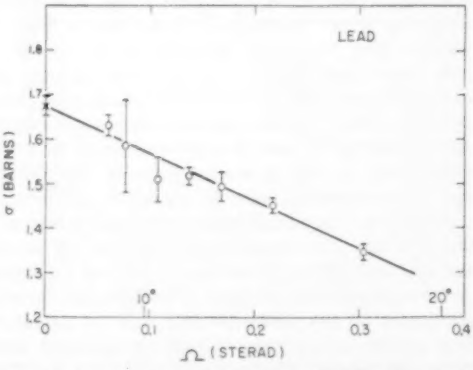

FIG. 5. Poor geometry cross sections for Pb, corrected for residual diffraction scattering, plotted against solid angle subtended by the detector. The inelastic cross section σ_a found by straight-line extrapolation to $\Omega=0$ is shown by the cross.

[18] R. M. Sternheimer, Rev. Sci. Instr. **25**, 1070 (1954).
[19] B. Rossi, *High Energy Particles* (Prentice-Hall, Inc., New York, 1952), p. 55.

A value for $\mathfrak{R}$ was obtained by comparing cross sections measured with counters 4*A* and 4*B* at good geometries, where the cross section changes rapidly with angle because of multiple scattering. These cross sections fell on a smooth curve if the subtended angle for counter 4*A* was computed with $\mathfrak{R}=2.65$ in., which is a reasonable value in view of Fig. 4. Thus counter 4*A* was assigned an effective radius of 2.65 in. for the purposes of computing θ and σ_m. The error in σ_m was estimated roughly, taking into account the error in computing F, the uncertainty in $\mathfrak{R}$ for counter 4*A*, and the uncertainty in the beam distribution.

It was hoped that the variation of the measured cross sections with absorber thickness would provide a check on the accuracy of the multiple scattering correction, since, to a first approximation, the absorber thickness should affect only σ_m. However, it was discovered that the calculated value of σ_m for thick absorbers was too large to bring the corrected cross sections into agreement with the corrected thin absorber measurements. This discrepancy was attributed to the lack of a well-defined geometry in the experiment, and to the inaccuracy of some of the assumptions, such as the one implicit in Eq. (3) that diffracted particles will be lost in the same proportion as noninteracting particles. Because of the uncertainty in this correction whenever it is large, no experimental points for which F was less than 0.9 were used.

Even with this restriction, the errors in the remaining good and intermediate geometry points for the heavy elements were extremely large. One could not hope to reduce σ_m by reducing the absorber thickness by, say, a factor of 4, since the increase in $1/Nx$ in Eq. (3) is sufficient to compensate for the decrease in F. However, one could reduce the error in σ_m by reducing the beam diameter, thereby considerably decreasing the uncertainty in the assumed beam distribution. For this reason, some points were remeasured using a $1\frac{1}{4}$ in. diameter beam, as previously mentioned.

C. Charged Secondaries

Since, as discussed earlier, it was not possible experimentally to eliminate from the transmitted beam charged products of interactions emitted in the forward direction, the data taken at poor geometries had to be corrected for the effects of charged secondaries. The manner in which these were taken into account will be discussed in Sec. 7.

D. Accidental Coincidences

To compute a correction for accidental coincidences would be difficult because the accidental rate (a) is hard to measure, as was mentioned before, and (b) fluctuates with variations in the beam intensity and beam bunching. To provide a rough estimate of the maximum effect on σ of neglecting to correct for accidentals we have used the probably conservative measurements mentioned in Sec. 4E, to set an upper limit of 0.0075 for the ratio of accidental to triples rates. In the extreme case where the accidental rate is unaffected by the insertion of the absorber, the effect on σ would be $\Delta\sigma=0.0075(\Gamma-1)/\Gamma Nx$, where Γ is the ratio of the transmission without absorber to that with absorber. This error is partly systematic and partly statistical. It was calculated for each datum point and, for simplicity, was combined with the other errors as if it were a random error.

E. Beam Spread

Because of the non-negligible diameter of the beam the observed angular distribution will be a superposition of diffraction patterns centered on different points in the beam cross section. The effect will be to increase $\sigma(\theta)$ for intermediate angles and to leave $\sigma(\theta)$ unchanged in the limits of both good and poor geometry. The problem of computing the correction is similar to that of finding the multiple scattering correction. Sternheimer[18] has pointed out that the same curves for F could be used if the diffraction pattern is replaced by the Gaussian

$$\tfrac{1}{4}k^2R^2\exp[-\tfrac{1}{4}(kR\theta)^2](\cong[J_1(kR\theta)/\theta]^2),$$

which closely approximates the optical model pattern in the first maximum. Here R is the nuclear radius, k the propagation constant, and J_1 the first-order Bessel function. Then the error $\Delta\sigma$ introduced in $\sigma(\theta)$ is given roughly by $\Delta\sigma\cong-\sigma_d[F(r_0,0)-F(r_0,\rho_0)]$, where σ_d is the total diffraction cross section, and r_0 is given by $2/kR\theta$. For the $2\frac{1}{2}$-in. diameter beam, this yields a maximum correction of $\sim5\%$, occurring for θ somewhere near the first diffraction minimum. However, the points taken with the $1\frac{1}{4}$-in. diameter beam, for which $\Delta\sigma$ should have been much smaller, did not seem, within the statistical accuracy, to be systematically lower. Because of the difficulty of computing the correction accurately, no correction was made. The points taken at intermediate geometries, therefore, are not necessarily a good indication of the shape of the integral angular distribution.

F. Double-Diffraction Scattering

The use of thick absorbers introduces the possibility that an elastically scattered particle will undergo one or more additional scatterings before leaving the absorber. For the absorbers used, the probability of double scattering is at most 10 or 15% of that of single scattering. The effect on the angular distribution is merely to "smear out" and widen the diffraction pattern slightly since the doubly scattered particles have a distribution which is essentially the convolution of the diffraction pattern by itself. The correction in $\sigma(\theta)$ was estimated to be small and has been neglected.

TABLE I. The attenuation cross sections σ_0 measured with different experimental arrangements, values of the major correction, and the corrected cross sections σ. x is the nominal thickness of absorber, ϵ_s the statistical standard deviation, σ_m the multiple scattering correction, and θ the half-angle subtended by the rear counter.

Element	θ (deg)	Beam diam (in.)	Counter 4	x (in.)	σ_0 (mb)	ϵ_s (mb)	σ_m (mb)	σ (barns)
Pb	2.90	2½	A	0.2	4064	68	1600±900	2.5 ±0.9
	4.40	2½	A	0.2	2374	59	280±240	2.10 ±0.25
	5.1	1¼	B	2	2389	32	450±60	1.94 ±0.07
	5.33	2½	A	0.2	2255	70	100±130	2.16 ±0.15
	6.00	1¼	B	0.2	1838	88	0±0	1.90 ±0.04
	6.2	1¼	B	2	2067	31	143±36	
	6.75	2½	A	0.2	2059	68	0±0	2.06 ±0.07
	7.0	2½	A	2	2091	14	420±170	1.67 ±0.17
	7.9	2½	B	2	1875	11	173±45	1.70 ±0.05
	7.9	1¼	B	2	1834	28	19±15	1.82 ±0.03
	8.9	2½	A	2	1868	17	180±100	1.69 ±0.10
	10.6	2½	A	2	1687	16	90±70	1.59 ±0.07
	10.6	2½	A	0.2	1606	71	0±0	1.61 ±0.07
	11.9	2½	B	2	1623	12	25±16	1.60 ±0.02
	13.3	2½	A	2	1547	16	45±36	1.50 ±0.04
	13.3	2½	A	0.2	1693	54	0±0	1.69 ±0.06
	15.0	2½	B	2	1506	20	7±12	1.49 ±0.02
	15.1	2½	A	2	1499	15	19±16	
	15.0	1¼	B	2	1595	27	0±0	1.60 ±0.03
	17.9	2½	A	2	1401	15	5±8	1.40 ±0.02
Sn	1.51	2½	A	0.25	5660	110	3500±1300	2.2 ±1.3
	1.99	2½	A	0.25	3523	90	1440±790	1.8 ±0.5
	1.99	2½	A	0.5	3812	57	2210±730	
	2.90	2½	A	0.25	2052	75	330±260	1.73 ±0.27
	2.90	2½	A	0.5	2062	43	640±360	1.43 ±0.36
	3.29	1¼	B	0.5	1572	63	9±9	1.56 ±0.06
	4.35	2½	A	0.5	1492	28	120±100	1.38 ±0.10
	4.5	2½	A	2	1561	16	390±160	1.18 ±0.16
	5.0	1¼	B	0.5	1352	53	0±0	1.35 ±0.05
	5.36	2½	A	0.5	1371	28	39±42	1.33 ±0.05
	5.5	2½	A	2	1393	15	200±80	1.19 ±0.09
	6.1	1¼	B	0.5	1253	39	0±0	1.25 ±0.04
	6.8	2½	A	0.5	1275	25	0±0	1.28 ±0.03
	7.0	2½	A	2	1267	14	80±57	1.19 ±0.06
	7.7	1¼	B	0.5	972	99	0±0	0.97 ±0.10
	10.6	2½	A	0.5	1137	31	0±0	1.14 ±0.03
	10.7	2½	A	2	1054	14	10±10	1.04 ±0.02
	14.2	2½	A	2	1015	10	0±0	1.02 ±0.01
	17.9	2½	A	2	941	12	0±0	0.94 ±0.01
Cu	1.71	2½	B	0.5	2407	26	880±120	1.53 ±0.12
	3.32	1¼	B	1.5	1115	16	58±18	1.057 ±0.025
	4.5	2½	A	1.5	1018	10	104±57	0.915 ±0.058
	5.1	1¼	B	1.5	909	15	2±2	0.907 ±0.016
	5.5	2½	A	1.5	924	9	52±33	0.872 ±0.035
	6.2	1¼	B	1.5	858	14	0±0	0.858 ±0.015
	6.9	2½	A	1.5	840	9	18±15	0.822 ±0.018
	7.9	1¼	B	1.5	818	13	0±0	0.818 ±0.014
	7.9	2½	B	1.5	788	9	3±3	0.785 ±0.010
	9.8	2½	A	1.5	742	8	1±3	0.741 ±0.010
	11.1	2½	B	1.5	712	8	0±0	0.712 ±0.009
	12.7	2½	A	1.5	683	8	0±0	0.683 ±0.009
	17.9	2½	A	1.5	588	7	0±0	0.588 ±0.008
Al	1.75	1¼	B	4	813	9	110±17	0.704 ±0.020
	2.31	1¼	B	4	665	9	19±8	0.646 ±0.013
	3.0	2½	A	4	648	6	50±28	0.599 ±0.029
	3.4	1¼	B	4	593	9	1±1	0.592 ±0.010
	4.7	2½	A	4	523	5	8±7	0.515 ±0.009
	5.3	2½	B	4	497	5	5±5	0.492 ±0.008
	5.3	1¼	B	4	489	8	0±0	0.489 ±0.009
	5.7	2½	A	4	486	5	3±3	0.483 ±0.007
	6.5	1¼	B	4	440	7	0±0	0.440 ±0.007
	7.4	2½	A	4	439	4	0±0	0.439 ±0.005
	8.3	1¼	B	4	437	7	0±0	0.437 ±0.008
	8.4	2½	B	4	426	4	0±0	0.426 ±0.005
	9.8	2½	A	4	394	4	0±0	0.394 ±0.005
	11.1	2½	B	4	381	4	0±0	0.381 ±0.004
	13.0	2½	A	4	358	4	0±0	0.358 ±0.005
	17.9	2½	A	4	292	4	0±0	0.292 ±0.004

TABLE I.—*Continued.*

Element	θ (deg)	Beam diam (in.)	Counter 4	x (in.)	σ_0 (mb)	ϵ_s (mb)	σ_m (mb)	σ (barns)
C	1.52	2½	A	1	422.9	19.3	13±12	
	1.53	2½	A	2	418.2	6.7	30±22	
	1.53	2½	A	3	414.5	5.1	44±25	0.381 ±0.011
	1.54	2½	A	4	423.4	3.3	54±26	
	1.56	2½	A	6	426.2	3.2	69±25	
	2.04	2½	A	4	384.8	3.4	20±13	0.365 ±0.014
	3.0	2½	A	4	332.8	3.7	3.3±3.2	0.330 ±0.005
	4.7	2½	A	4	289.4	3.0	0±0	0.2894±0.0035
	5.7	2½	A	4	266.3	2.8	0±0	0.2663±0.0033
	7.4	2½	A	4	246.9	2.9	0±0	0.2469±0.0034
	8.4	2½	B	4	242.0	1.8	0±0	0.2420±0.0025
	10.6	2½	A	4	209.0	2.6	0±0	0.2090±0.0030
	11.1	2½	B	4	212.5	2.9	0±0	0.2125±0.0033
	14.2	2½	A	4	179.5	2.4	0±0	0.1795±0.0027
	20.0	2½	B	4	143.3	1.7	0±0	0.1433±0.0020
Be	1.53	2½	A	2	311.3	4.4	10±9	
	1.54	2½	A	4	317.3	2.5	21±12	0.296 ±0.007
	1.56	2½	A	6	315.7	1.9	29±13	
	2.04	2½	A	4	289.0	2.4	7±6	0.282 ±0.006
	3.0	2½	A	4	261.3	2.2	0.6±1.1	0.2607±0.0030
	4.7	2½	A	4	236.8	2.1	0±0	0.2368±0.0026
	5.7	2½	A	4	217.7	2.1	0±0	0.2177±0.0025
	7.4	2½	A	4	201.7	2.0	0±0	0.2017±0.0024
	11.0	2½	B	4	172.5	2.4	0±0	0.1725±0.0027
	13.0	2½	A	4	153.9	1.9	0±0	0.1539±0.0022
	20.0	2½	B	4	117.6	1.2	0±0	0.1176±0.0014

G. Statistics and Other Errors

The standard deviation due to counting statistics was computed from the formula

$$\frac{\epsilon(\Gamma)}{\Gamma}=\left[\frac{1}{Q}-\frac{1}{T}+\frac{1}{Q_0}-\frac{1}{T_0}\right]^{\frac{1}{2}}, \tag{4}$$

where T and Q are the number of triple and quadruple coincidences with absorber, T_0 and Q_0 are the corresponding numbers without absorber, and $\Gamma\equiv TQ_0/QT_0$ is the ratio of the transmission in the "zero" run to that in the "absorber" run. In view of Eq. (1), the statistical standard deviation in $\sigma(\theta)$ is

$$\epsilon_s(\sigma)=(1/Nx)[\epsilon(\Gamma)/\Gamma]. \tag{5}$$

In plotting the cross sections against θ, one should use that angle at which the mean solid angle $\bar{\Omega}$ is subtended. However, the use of the geometrical center of the absorber in computing θ introduces a negligibly small error. The diffraction pattern was slightly smeared out by the energy spread of the beam, but this effect was small compared with the geometrical effect of the absorber thickness.

The absorber thicknesses were known to within 2%. The magnet current was held constant to 1%. The error due to discriminator bias drift and the slope of the plateau was less than 0.2%; this was small compared to the statistical error. As mentioned previously, the beam contamination was completely negligible. The error caused by the dead time of the apparatus was small, since only one count in 150 would be missed at a maximum counting rate of 3×10^4 sec^{-1}.

7. RESULTS AND COMPARISON WITH THEORY

A. Determination of σ_a

The observed cross sections $\sigma_0(\theta)$ are shown in Table I together with values of the multiple scattering correction and the corrected cross sections $\sigma(\theta)$. In Table I, A is the atomic number; θ is the half-angle, in degrees, subtended by counter 4 at the center of the absorber; x is the nominal absorber thickness in inches; ϵ_s is the statistical counting error; and σ_m is the correction for multiple scattering. The diameter of the beam and the counter ($4A$ or $4B$) used as counter 4 (see Sec. 3) are also shown. The values of θ were computed using 2.65 in. for the radius of counter $4A$ and 3.00 in. for that of counter $4B$. Runs taken at different times under identical conditions have been combined. Points for which the multiple scattering correction was large ($F<0.9$) have been omitted. The error in σ includes (a) the statistical standard deviation, (b) the error in σ_m and (c) the error due to the neglect of accidentals.

From the data in Table I, one can hope to obtain (a) the inelastic cross sections σ_a from the poor geometry points and (b) the total cross sections $\sigma_t(=\sigma_a+\sigma_d)$ from the good geometry points. The cross sections at large angles are appreciably affected by the presence of charged secondaries in the solid angle subtended by the back counter since, as discussed earlier, it was not possible experimentally to eliminate these secondaries from the transmitted beam. The effect of these particles is to cause the apparent cross sections to decrease with increasing subtended angle even beyond those angles for which elastic processes should have an effect. To

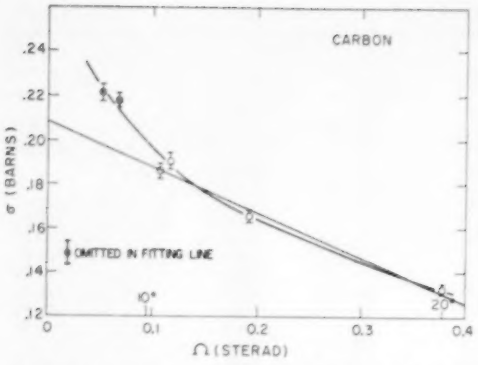

FIG. 6. Poor geometry cross sections for C, corrected for residual diffraction scattering, plotted against solid angle subtended by the detector. Although the points may lie on a curve such as that shown, a least squares line has been drawn, omitting the two lowest angle points as discussed in the text.

obtain the actual inelastic cross sections σ_a, it was thus necessary to extrapolate the values of the cross section measured at various solid angles to zero solid angle, using those points for which the elastic contribution is either negligible or small enough to be easily corrected for.

In performing this extrapolation we have made the assumption that the distribution of secondaries within the angles considered ($\leq 20°$) is substantially isotropic so that the apparent cross section will vary linearly with subtended solid angle. The poor geometry cross sections, corrected where necessary for the small fraction of σ_d still present, were plotted against Ω and a least-squares straight line was drawn through the points. The intercept of this line at $\Omega=0$ was taken to be σ_a. An example of such an extrapolation is shown in Fig. 5. In computing the correction for residual diffraction, σ_d was found from the neutron optical model formula using values of k_1, K, and R determined in a preliminary analysis of the data, and the approximate angular distribution [Eq. (10)] was used. No points were used for which this correction exceeded $0.1\sigma_a$ and an error of 10% was arbitrarily assigned to this correction.

This method of determining σ_a was satisfactory for the heavy elements, including Al, since for these elements the points used for extrapolation were consistent with a straight line. For C and Be, however, the extrapolation becomes somewhat uncertain because the diffraction scattering extends to larger angles and because the secondaries may be bunched forward and no longer as nearly isotropic in the angular interval considered. If one plots the corrected poor geometry cross sections against Ω as before, the points do not lie on a straight line, as shown for C in Fig. 6. If the curvature were due entirely to nonisotropic secondaries an estimate of σ_a could be obtained by a more or less conjectural extrapolation of the curve to $\Omega=0$. There are several reasons, however, for treating this curvature as spurious and omitting the points at small angles. These include errors such as caused by the neglect of the correction for the finite width of the beam (the correction being largest for light elements and intermediate geometries), errors in the computed residual diffraction scattering (the uncertainty is large for many of the points, Eq. (10) not being as good an approximation for light elements as for heavy ones), or even inaccuracy of the optical model itself when applied to small nuclei. Accordingly, points lying within the (calculated) first diffraction minimum were omitted in making the extrapolation. This procedure was actually followed for all the elements, but only for C and Be did it limit seriously the number of points available for extrapolation, since for the heavy elements only the smallest angles were affected, and there were a considerable number of points lying in a straight line outside the first minimum. As will be apparent, this treatment yields values of σ_a which are in remarkably good agreement with the optical model with constant nuclear density. One must remember, however, that the C and Be data do not necessarily contribute to a demonstration of the validity of the optical model; these data can merely be interpreted in such a way as to be consistent with the optical model.

The values of σ_a found in this manner are given in Table II. The error quoted includes (a) the error in the intercept given by the least-squares method, (b) an estimate of the error due to finite beam diameter, (c) the error in neglecting the factor $1-2eV_c/(p\beta c)$ due to the Coulomb field, and (d) an estimate of the uncertainty in the validity of the extrapolation. The last factor imparts a comparatively large error to the Be and C cross sections.

B. Theoretical Curves and Formulas

In the optical model of the transparent nucleus, the nucleus is regarded as a uniform sphere of radius R

TABLE II. Optical model parameters derived from the data. The primes on σ_t and σ_d indicate that they are upper limits.

Element	$A^{\frac{1}{3}}$	σ_a (barns)	σ_t' (barns)	σ_d' (barns)	R (10^{-13} cm)	K (10^{13} cm^{-1})	$\sigma_a/\pi R^2$
Pb	5.92	1.68 ±0.04	···	···	7.42±0.10	0.55	0.97
Sn	4.91	1.11 ±0.03	···	···	6.07±0.09	0.57	0.96
Cu	3.99	0.728±0.017	···	···	4.98±0.07	0.55	0.94
Al	3.00	0.394±0.010	0.75 ±0.05	0.36 ±0.05	3.75±0.06	0.55	0.89
C	2.29	0.209±0.022	0.405±0.023	0.196±0.032	2.81±0.21	0.58	0.84
Be	2.08	0.169±0.015	0.316±0.016	0.147±0.022	2.56±0.18	0.57	0.82

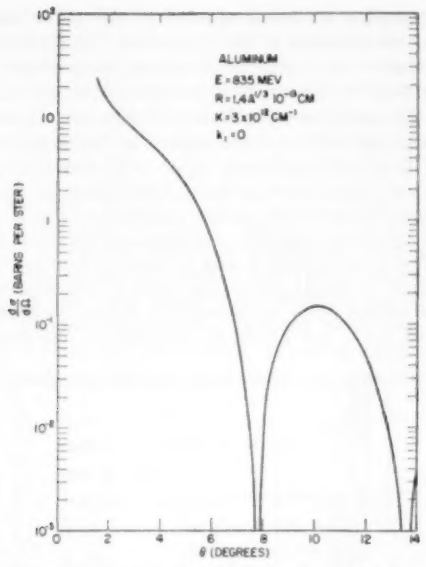

FIG. 7. Example of a diffraction pattern, calculated by the WKB formula of Gatha and Riddell, for the scattering of protons by Al.

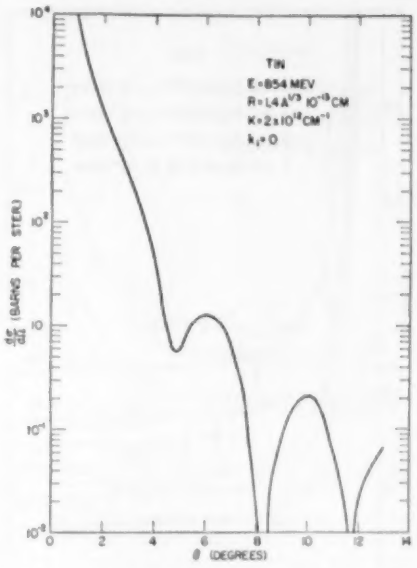

FIG. 8. Example of a diffraction pattern, calculated by the WKB formula of Gatha and Riddell, for the scattering of protons by Sn.

with a complex index of refraction

$$n=1+k_1/k_0+iK/2k_0, \tag{6}$$

where k_0 is the wave number of the incident particle outside the nucleus, $k=k_0+k_1+iK/2$ is the propagation constant inside the nucleus, and K is the absorption constant in nuclear matter, given by

$$K=3A\bar{\sigma}/4\pi R^3. \tag{7}$$

Here $\bar{\sigma}$ is the average nucleon-nucleon cross section inside the nucleus.

For the case of neutrons, the resulting expressions for σ_a and σ_d are well known.[2]

$$\sigma_a=\pi R^2\left\{1-\frac{1}{2K^2R^2}[1-e^{-2KR}(1+2KR)]\right\}. \tag{8}$$

For $k_1=0$, σ_d simplifies to

$$\sigma_d=\pi R^2\left\{1+\frac{1}{2K^2R^2}[8e^{-KR}(1+KR) -e^{-2KR}(1+2KR)-7]\right\}. \tag{9}$$

The expression for $f(\theta)$ cannot be integrated analytically, but in the limit $KR\to\infty$ it approaches the formula for a cylindrical nucleus. Thus for large opacity the differential cross section can be approximated by

$$\frac{d\sigma(\theta)}{d\Omega}=\frac{\sigma_d}{\pi}\frac{J_1^2(k_0R\sin\theta)}{\sin^2\theta}. \tag{10}$$

In order to compute the angular distribution for proton scattering in which the Coulomb field cannot be neglected, one can extend the neutron model to the case in which the potential consists of a square well plus a screened Coulomb field. Assuming a uniform charge density in the nucleus, the potential is then

$$\begin{aligned} V(r)&=V_1+iV_2+Ze^2(3R^2-r^2)/2R^3, && r<R,\\ &=(Ze^2/r)\exp(-r/a), && r>R. \end{aligned} \tag{11}$$

For convenience we have used a formula given by Gatha and Riddell[20] for scattering by a complex square well potential plus an unscreened Coulomb field in the WKB approximation. These authors used an expression, given by Schiff,[21] for scattering by a modified Coulomb potential; and the nuclear phase shifts were computed from Langer's formula.[22] In applying this formula to the present case of a large number of phase shifts, we have replaced the sum over the phase shifts δ_l with an integral over l, making l a continuous variable by approximating $P_l(\cos\theta)$ by $J_0[(l+\frac{1}{2})\theta]$. Angular distributions were computed numerically for two or three values of K and R, with $k_1=0$, for each element. Examples of these curves are shown in Figs. 7 and 8. The integral angular distributions, shown with the experimental data in Figs. 9–14, were then calculated in the following manner. To find $\sigma(\theta)$ for each K and R,

[20] K. M. Gatha and R. J. Riddell, Phys. Rev. 86, 1035 (1952).
[21] L. I. Schiff, *Quantum Mechanics* (McGraw-Hill Book Company, Inc., New York, 1949), p. 120.
[22] N. F. Mott and H. S. W. Massey, *The Theory of Atomic Collisions* (Oxford University Press, London, 1949), p. 127.

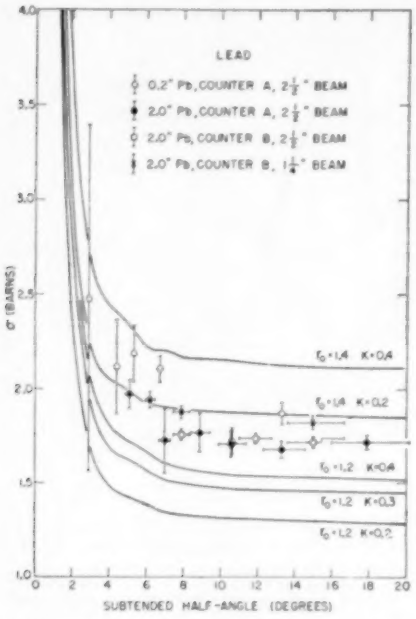

FIG. 9. Attenuation cross sections for Pb measured at various geometries. Points taken with different absorber thicknesses, different beam diameters, and counter $4A$ or $4B$ (see text) are shown. The cross sections have been corrected for multiple scattering and charged secondaries. The indicated errors include estimates of the uncertainty of the corrections. The horizontal limits indicate the total range of angles included, due to the thickness of the absorber; these are not errors in θ. Also shown are theoretical curves computed for various values of the absorption constant K, in units of 10^{13} cm^{-1}, and of r_0, the nuclear radius in units of $A^{\frac{1}{3}}\times10^{-13}$ cm, with $k_1=0$.

the corresponding proton curve for $d\sigma/d\Omega$ was integrated numerically over solid angle from $\Omega(\theta)$ out to the first minimum which was unaffected by the Coulomb field. For the integration from this minimum to $\theta=\pi$, the approximate expression Eq. (10) was used, with σ_d given by Eq. (9). Finally, to this was added σ_a found for the given K and R from Eq. (8), which is independent of the Coulomb field.

C. Integral Angular Distribution

In order to compare the data of Table I with theoretical curves of the integral angular distributions, one must compute a further correction $\delta_s(\theta)$ for detection of secondaries and apply it to the values of $\sigma(\theta)$ in Table I. This correction is easily found from the graphs (see Fig. 5) used for the extrapolation to determine σ_a; $\delta_s(\theta)$ is simply the difference between the ordinates at 0 and at $\Omega(\theta)$ of the least-squares straight line.

The correction δ_s was also computed by an alternate procedure making use of the angular distribution of secondaries from 114 stars found by Widgoff *et al.*[22] in photographic emulsions exposed to the 1-Bev circulating proton beam of the Cosmotron. The fraction of the stars with a gray or minimum track within an angle θ of the forward direction was plotted against θ, and the correction was calculated from a smooth curve through the points and was applied to that part of $\sigma(\theta)$ due to inelastic collisions. When $\sigma(\theta)$ was corrected this way, the integral angular distribution for heavy elements became level at large angles at a value of σ in good agreement with the values of σ_a in Table II. This method of computing δ_s was not expected to be valid for light elements, since the stars in the emulsions arose mainly from collisions with heavy nuclei and, indeed, the C and Be curves corrected by this method

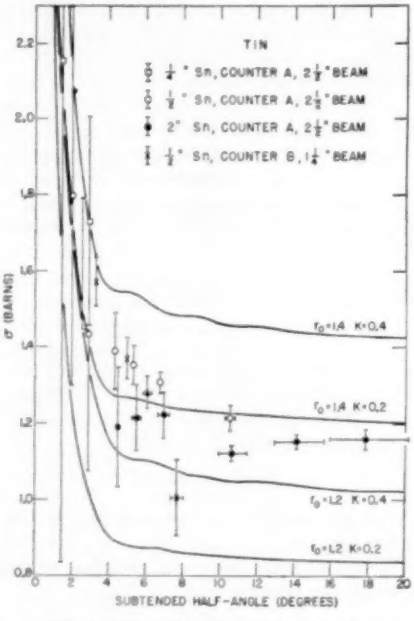

FIG. 10. Attenuation cross sections for Sn. See caption under Fig. 10.

did not level off at large angles. The former method was therefore used for determining this correction.

The data of Table I for Pb, Sn, Cu, and Al, with the effect of secondaries subtracted, are plotted in Figs. 9–12. In Figs. 13 and 14, the data for C and Be are presented without this correction, since the uncertainty in fitting the points (see Fig. 6) to a unique straight line prevented a reliable evaluation of δ_s. The theoretical curves discussed above for various values of the optical parameters are also shown on the graphs. The physical limits of the absorbers are indicated as limits on θ; these are not to be construed as the standard deviations in θ.

As can be seen from Figs. 9–14 the computed theoretical curves do not fit the experimental points well at

[22] Widgoff, Leavitt, Shapiro, Smith, and Swartz (private communication).

all angles. In all cases the measured cross sections seem to level off with increasing θ more gradually than the theoretical curves for $k_1=0$. This is particularly noticeable in Cu (Fig. 11), where both ends of the experimental curve seem to have the proper slope, but the middle is considerably more rounded. The assumption of a large k_1 will increase σ_d relative to σ_a, but not enough, since the opacity is high. A diffuse nuclear edge would smooth out the ripples in $\sigma(\theta)$, but not change its general shape. The assumption of a spin-orbit term in the interaction[24] also does not alter the shape of the curve sufficiently. However, this effect may be purely instrumental, since the corrections due to finite beam size and multiple diffraction scattering, which we have neglected, are largest in the intermediate-

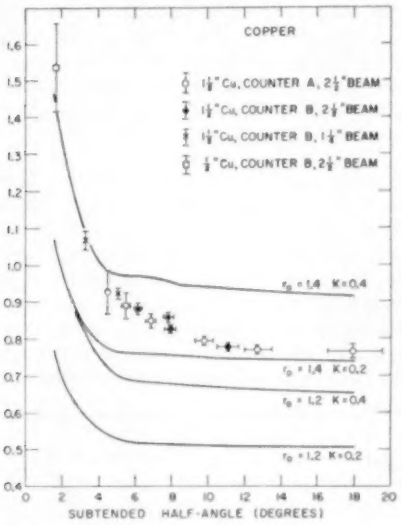
COPPER
1½" Cu, COUNTER A, 2½" BEAM
1½" Cu, COUNTER B, 2½" BEAM
1½" Cu, COUNTER B, 1½" BEAM
½" Cu, COUNTER B, 2½" BEAM
r_0 = 1.4 K=0.4
r_0 = 1.4 K=0.2
r_0 = 1.2 K=0.4
r_0 = 1.2 K=0.2
SUBTENDED HALF-ANGLE (DEGREES)

FIG. 11. Attenuation cross sections for Cu. See caption under Fig. 10.

angle region; and at least part of the discrepancy probably arises from these causes.

In C and Be (Figs. 13 and 14), the observed angular distributions may depart from the theoretical curves at large angles to an extent which cannot be ascribed to the detection of secondaries. There is thus perhaps an indication that the optical model with the above assumptions does not predict the correct angular distribution for light elements. Indeed, there has already been evidence[5] at 340 Mev that C does not have a diffraction minimum at the expected angle. Perhaps the assumption of a rounded potential well, as has been suggested by several authors,[25] or a theory which treats

[24] Snow, Sternheimer, and Yang, Phys. Rev. **94**, 1073 (1954).

[25] R. Jastrow and J. E. Roberts, Phys. Rev. **85**, 757 (1952) and private communication; R. D. Woods and D. S. Saxon, Phys. Rev. **95**, 577 (1954); R. W. Williams, Phys. Rev. **98**, 1387 (1955).

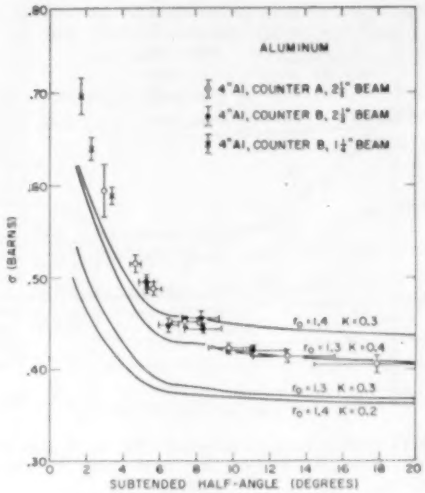

FIG. 12. Attenuation cross sections for Al. See caption under Fig. 10.

directly the nucleon-nucleon interactions, would give a better fit with the data.

D. Determination of σ_t

The determination of $\sigma_t(=\sigma_a+\sigma_d)$ was impossible for Pb, Sn, and Cu because of the effects of multiple Coulomb scattering in the measurements at good geometries; moreover, the purely nuclear diffraction

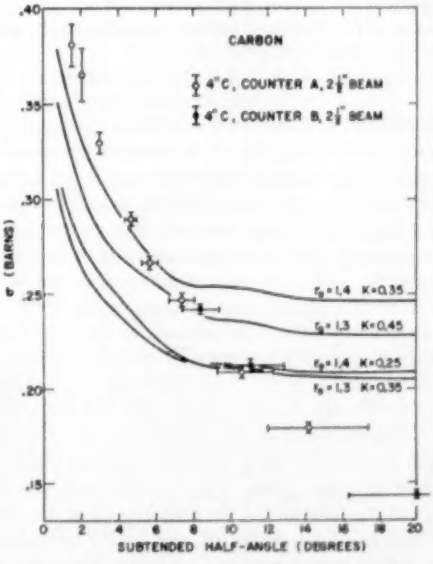

FIG. 13. Attenuation cross sections for C. See caption under Fig. 10. Here no correction has been made for charged secondaries.

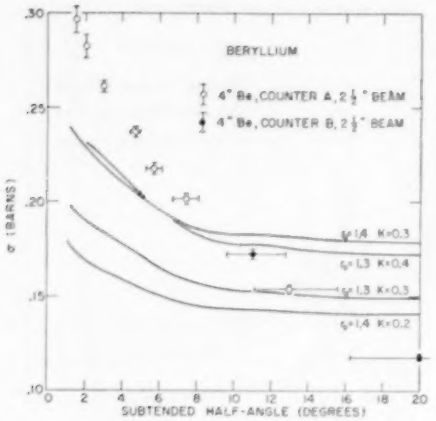

FIG. 14. Attenuation cross sections for Be. See caption under Fig. 10. Here no correction has been made for charged secondaries.

cross section σ_d is undefined where Rutherford scattering is large over the major part of the diffraction pattern. For Al, C, and Be, however, one can obtain a rough estimate of σ_t by approximately subtracting out the Rutherford scattering and extrapolating $\sigma(\theta)$ to 0°. If Eq. (10) is integrated over solid angle to find the integral angular distribution $\sigma_n(\theta)$ for neutrons, the resulting function is approximately linear in θ in the region between $0.1\theta_m$ and $0.7\theta_m$, where θ_m is the angle of the first diffraction minimum. The cross sections in this region can therefore be plotted against θ and extrapolated to 0° by a least-squares straight line. The intercept at $\theta=0°$ will, of course, overestimate σ_t, since the actual curve is rounded off near 0°.

For the purpose of making this extrapolation, the data of Table I for the light elements were further corrected. Rutherford scattering was subtracted from each datum point by using Eq. (2) to compute the contribution $\sigma_c(\theta)$ to the integrated cross section at each angle. The interference term was neglected, and an additional error $[2\sigma_c(\theta)\sigma_n(\theta)]^{\frac{1}{2}}$ was assigned to each point, this being an upper limit to the possible size of this term. Because the points for each element happened to lie very close to a straight line, the size of the errors did not appreciably affect the position of the line drawn through the points but merely determined the error in the extrapolated value. Thus weighting the points in such an arbitrary manner fortuitously had little effect on σ_t. The values of σ_t and $\sigma_d(=\sigma_t-\sigma_a)$ found in this manner are listed in Table II. These numbers should be regarded as upper limits. They overestimate the true cross sections because (a) the rounding off of the curve $\sigma_n(\theta)$ near $\theta=0°$ was neglected, and (b) the interference term, which was neglected, probably increased the measured $\sigma(\theta)$, as one can ascertain by comparing $\sigma_n(\theta)+\sigma_c(\theta)$ with the theoretical curves in Figs. 9–14, which were computed with interference taken into account.

E. Determination of Optical Parameters

To show the consistency of the data with an interpretation in terms of the optical model, we must compute the parameters K, R, and k_1. Since at most only two quantities, σ_a and σ_d, have been measured for each element, we must make an assumption about one of the three parameters. K and R are related by Eq. (7) and σ_a is uniquely determined by these two parameters in Eq. (8). One can, therefore, either assume an $r_0(R=r_0A^{\frac{1}{3}}\times10^{-13}$ cm) and obtain a value for $\bar{\sigma}$, or assume $\bar{\sigma}$ and derive R. The latter alternative was chosen, since recent electromagnetic measurements of nuclear radii have thrown doubt on the earlier values of r_0, and since $\bar{\sigma}$ should be close to the free nucleon-nucleon cross section. The effects of the exclusion principle are estimated to be small at this energy. The value chosen for $\bar{\sigma}$ was 45 mb, an average between the 43 mb measured for the n-p cross section by Coor *et al.*[11] and the 48 mb measured for the p-p cross section by the authors.[12] With this assumption, R is uniquely determined by σ_a. The values of R are shown in Table II, together with the corresponding values of K. The errors quoted include an estimate of the uncertainty in $\bar{\sigma}$, (±2 mb) which has but a small effect on R, particularly in the heavy elements. The graph of R *vs* $A^{\frac{1}{3}}$, Fig. 15, is a straight line through the origin, indicating the consistency of the data with an interpretation in terms of the optical model with constant nuclear density. There is no indication of a finite intercept due

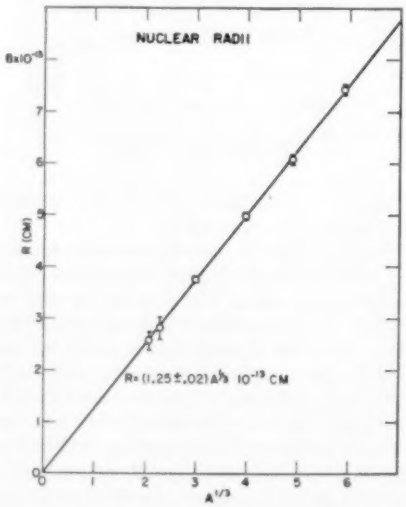

FIG. 15. Nuclear radii, computed according to the optical model from σ_a and an assumed $\bar{\sigma}$ of 45 mb, plotted against $A^{\frac{1}{3}}$. The points lie on a straight line $R=(1.25\pm0.02)A^{\frac{1}{3}}\times10^{-13}$ cm, indicating constant nuclear density. The corresponding value of K is 0.56×10^{13} cm^{-1}.

to the range of nuclear forces. The slope of the line yields an r_0 of 1.25 ± 0.02, corresponding to a K of $(0.56\pm0.03)\times10^{13}$ cm^{-1}, where the error in K does *not* include the uncertainty in $\bar{\sigma}$. The upper limits for σ_d can be used to find an upper limit for k_1/K, using the curves given by Bethe and Wilson[26] for $\sigma_d/\pi R^2$ as a function of $\sigma_a/\pi R^2$ for various values of k_1/K. The result is $k_1/K \lesssim 0.4$ for Al and $\lesssim 0.5$ for C and Be, corresponding to a maximum real well-depth V_1 of about 50 Mev.

8. CONCLUSION AND COMPARISON WITH OTHER DATA

The nuclear cross sections measured in this experiment are consistent with an interpretation in terms of the optical model of a transparent nucleus, with $K=0.56\times10^{13}$ cm^{-1}, $R=(1.25\pm0.02)A^{\frac{1}{3}}\times10^{-13}$ cm, and a nonvanishing value of k_1, although it is probable that the data for light elements would be better fitted by a more elaborate model. The inelastic and total cross sections determined from the data are shown in Fig. 16, together with high-energy cross sections measured by other authors. It is seen that both σ_a and σ_t are rising at very high energies, corresponding to the measured increase in σ_{p-p}[12] and σ_{n-p}.[11] The present measurements of σ_a fit well on these curves; but the values of σ_t, which are upper limits, are too high, as expected. The value of about 0.5 for k_1/K found from these values of σ_t is in agreement with the value found by Coor *et al.*[11] for Be and C but is somewhat higher than their average value of 0.3 for all the elements. The above values of r_0 and K are in good agreement with other data at high energies: Coor *et al.*[11] give $r_0=1.28$, $K=0.48$ (in units of 10^{13} cm^{-1}) for 1.4-Bev neutrons; Nedzel[3] finds $r_0=1.23$, $K=0.51$ for 410-Mev neutrons; deCarvalho[10] finds $r_0=1.23$, $K=0.5$ for 315-Mev protons; and Gatha and Riddell[20] fit the 340-Mev proton data[5] with $r_0=1.25$, $K=0.30$. These values for r_0 are considerably lower than the values around 1.4 found from low-energy data and are more in agreement with recent determinations of the size of the nuclear charge distribution.[27]

The values of σ_a determined in this experiment are also consistent with an optical model in which the nucleus has a constant central density plus a diffuse boundary. In particular the data have been compared with such a model constructed by Williams,[25] in which the shape of the nuclear density distribution is obtained from the results of the high-energy electron scattering experiments of Hofstadter *et al.*,[27] and the absolute size is determined from the high-energy neutron cross sections of Coor *et al.*[11] The data of the present experiment fit this model very well. It does appear that the nuclear force size of medium to heavy nuclei, as determined by high-energy neutron and proton cross section measurements is about 5% larger than the charge distribution size.

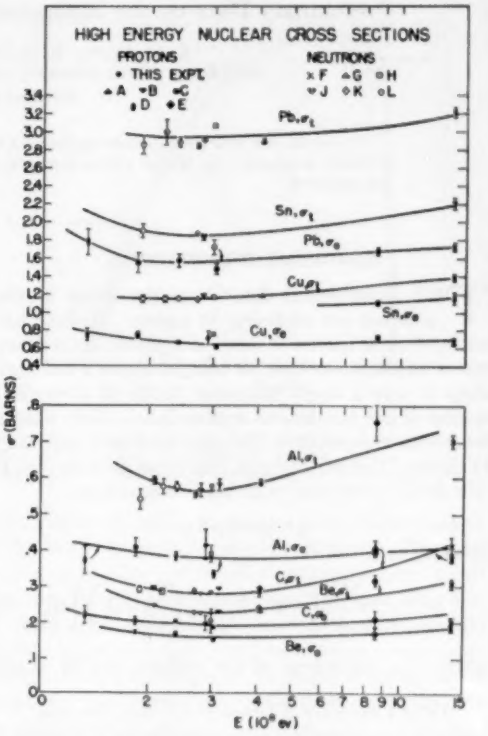

FIG. 16. Nuclear absorption and total cross sections at high energies, plotted as functions of energy. Cross sections for protons are indicated by solid points; cross sections for neutrons, by open points. This compilation is complete only above 200 Mev. References: *A*—reference 7; *B*—reference 10; *C*—reference 7; *D*—reference 8; *E*—reference 9; *F*—reference 11; *G*—reference 3; *H*—W. P. Ball, University of California Radiation Laboratory Report UCRL-1938 (unpublished); *J*—Fox, Leith, Wouters, and MacKenzie, Phys. Rev. **80**, 23 (1950); *K*—J. DeJuren, Phys. Rev. **80**, 27 (1950); *L*—J. DeJuren and B. J. Moyer, Phys. Rev. **81**, 919 (1951).

9. ACKNOWLEDGMENTS

The authors wish to acknowledge the continued interest of Dr. G. B. Collins and are particularly indebted to Dr. R. M. Sternheimer for his assistance in numerous phases of the analysis of the results. We have profited from stimulating conversations with Dr. G. A. Snow, Dr. R. Serber, and Dr. R. Jastrow. The cooperation of the operating crew of the Cosmotron was greatly appreciated.

[26] H. A. Bethe and R. R. Wilson, Phys. Rev. **83**, 690 (1951).
[27] V. L. Fitch and J. Rainwater, Phys. Rev. **92**, 789 (1953); Hofstadter, Hahn, Knudsen, and McIntyre, Phys. Rev. **95**, 512 (1954); Pidd, Hammer, and Raka, Phys. Rev. **92**, 436 (1953).

Preliminary Data on the Measurement of the $\mu^+ - \beta^+$ Decay Spectrum*

K. M. Crowe, R. H. Helm, and G. W. Tautfest
High-Energy Physics Laboratory, Stanford University, Stanford, California
(Received April 14, 1955)

The results of a preliminary nature on the $\mu-\beta$ decay spectrum are given. The data are consistent with a theory as proposed by Michel with a parameter $\rho=0.50\pm0.10$. The background and systematic errors are discussed.

HISTORICAL INTRODUCTION

THE experimental data[1–11] on the decay of the μ meson are confusing at present. Michel[12] has analyzed these spectra in terms of a generalized β decay where he has shown that for energies above a few Mev there is only a single-parameter family of theoretical spectra if the interaction representation obeys simple invariance requirements. The data have been analyzed[13] in terms of this parameter ρ, which can go from 0 to 1. The decay is assumed to go via two neutrinos,

$$\mu^+ \rightarrow \beta^+ + \nu + \nu,$$

in which case

$$N(E)dE \propto \frac{4E^2}{W^4}\left[3(W-E)+2\rho\left(\frac{4}{3}E-W\right)\right]dE, \quad (1)$$

where E is the energy of the positron and W is the upper-energy cutoff; $W=52.71\pm0.07$ Mev.[14,15] The present status is shown in Table I.

TABLE I. Summary of data on $\mu^+-\beta^+$ decay spectrum.

	ρ value	Method	Experimenter	Reference
1	0.23[a]	Spiral orbit spectrometer	Sagane, Gardner, Hubbard	2
2	0.41 ± 0.13	Photographic emulsions	Bramson and Havens	3
3	0.43 ± 0.15 (150 events)[a]	Cloud chamber	Lagarrique	5
4	0.26 ± 0.26	Cloud chamber	Hubbard	6
5	0.50 ± 0.13	Cloud chamber	Vilain and Williams	7
6	$0.23^{+0.03}_{-0.05}$	Spiral orbit spectrometer	Sagane, Dudziak, Vedder	8
7	...	Cloud chamber	Harrison *et al.*	9
8	0.6 ± 0.10	Cloud chamber ($\mu^- \rightarrow \beta^-$)	Lederman and Sargent	10
9	0.72 (42 events)	Photographic emulsions	Mabboux-Stromberg	11

[a] Using new value of muon mass ($W=52.7$).

In view of the interest in the analysis of the β decay of the muon, we present a brief account of an experiment in progress and give our preliminary β spectrum.

APPARATUS AND PROCEDURE

Figures 1 and 2 show the experimental apparatus. The analyzed and collimated electron beam of approximately 400 Mev is from the Stanford Mark III linear electron accelerator. The beam is $\frac{3}{8}$ to $\frac{1}{2}$ in. in diameter; beam current is 5×10^9 electrons per pulse measured by a secondary-emission monitor.[16] The beam strikes a lead radiator 0.065-in. thick; the x-radiation and electrons pass through a target of lithium 1-in.$\times$1-in.$\times$2-in. long. Low-energy mesons produced in the lithium come to rest with relatively uniform density in the target. The positive pions decay to muons, which also stop and decay into positrons with the characteristic 2.2-μsec mean life. The positrons which leave the target at 90° to the beam enter the vacuum chamber of a double-focusing magnetic spectrometer.[17]

After magnetic analysis, the positrons are detected by making a fast coincidence between two $\frac{1}{8}$-in. thick scintillation counters, $1\frac{7}{8}$ in. by $1\frac{1}{2}$ in., spaced two inches apart, with time resolution 5×10^{-8} sec. This output is then placed into a delayed-coincidence gear

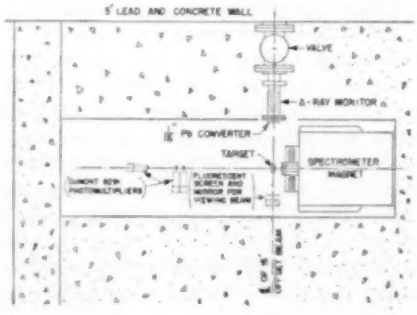

FIG. 1. Top view of experimental arrangement.

* The research reported here was supported by the joint program of the Office of Naval Research and the U. S. Atomic Energy Commission.

[1] Leighton, Anderson, and Seriff, Phys. Rev. **75**, 1432 (1949).
[2] Sagane, Gardner, and Hubbard, Phys. Rev. **82**, 557 (1951).
[3] H. Bramson and W. Havens, Phys. Rev. **83**, 861 (1951); **88**, 304 (1952).
[4] A. Lagarrique and C. Peyrou, J. phys. radium **12**, 848 (1951).
[5] A. Lagarrique, Compt. rend. **234**, 2060 (1952); and private communication.
[6] H. Hubbard, University of California Radiation Laboratory Report No. 1623 (unpublished).
[7] J. H. Vilain and R. W. Williams, Phys. Rev. **92**, 1586 (1953); **94**, 1011 (1954).
[8] Sagane, Dudziak, and Vedder, Phys. Rev. **95**, 863 (1954).
[9] Harrison, Cowan, and Reins, Nucleonics **12**, No. 3, 44 (1954).
[10] L. M. Lederman and C. R. Sargent (private communication to R. Sagane).
[11] C. Mabboux-Stromberg, Ann. phys. **9**, 441 (1954).
[12] L. Michel, Proc. Phys. Soc. (London) **A63**, 514 (1950).
[13] H. J. Bramson, Phys. Rev. **98**, 1187(A) (1955).
[14] Birnbaum, Smith, and Barkas, Phys. Rev. **91**, 765 (1953).
[15] K. M. Crowe and R. H. Phillips, Phys. Rev. **96**, 470 (1954).
[16] G. W. Tautfest and H. R. Fechter, Rev. Sci. Instr. **26**, 229 (1955).
[17] Snyder, Rubin, Fowler, and Lauritsen, Rev. Sci. Instr. **21**, 852 (1950).

which allows counting after the beam pulse. This equipment was built for pion-production experiments[18] by C. Newton, W. S. C. Williams, J. A. Narud, G. Masek, and W. K. H. Panofsky. The gates where counts are recorded are arranged as follows: Gate No. I opens 2.2 μsec after the beam pulse and remains open for 2.2 μsec; gate No. II opens 4.4 μsec after the beam pulse and remains open for 4.4 μsec.

Figure 3 shows the spectrum obtained by varying the current in the spectrometer magnet windings. The maximum magnetic field is approximately 4500 gauss. The curves plotted are the folds of our resolution into various theoretical spectra. The normalization of the folded theoretical curves to the data is arbitrary.

The resolving power of the system is made up of two major parts: (1) The energy loss of the positrons leaving the target; and (2) the finite heights of the target source and the detector crystal. (The shapes of these resolutions are shown in Fig. 4.)

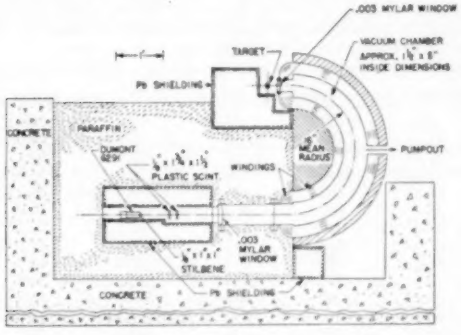

FIG. 2. Side view showing magnet section and counter location.

ANALYSIS OF DATA

The data as shown in Fig. 3 have been corrected for background and the variation in efficiency arising from the constant momentum resolution of the spectrometer. This causes a yield proportional to E times the spectrum which gives approximately an E^3 variation for the yield from Eq. (1). This imposes extremely low background conditions on the study of the low-energy portion of the spectrum.

Our background is of two types: (1) Pions of low energy also leave the target, pass through the spectrometer, and can stop in the first or second counter, depending on their range. These decay and some of the positrons will cause real coincidences with the proper period, the number depending on the solid angle of one counter relative to the other. We have varied this solid angle by a factor of ten by substituting a 1-in.×1-in. ×$\frac{1}{8}$-in. counter six inches behind the original second counter as indicated in Fig. 2. Results are shown in Fig. 5. There is no discernible change within rather poor

[18] Panofsky, Newton, and Yodh, Phys. Rev. **98**, 751 (1955).

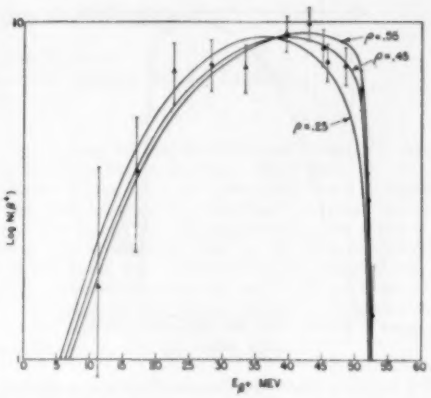

FIG. 3. Data on μ decay obtained with 1-in. by 1-in. lithium target 2-in. long in primary beam direction. Solid curves are obtained by folding the theoretical spectra into our resolution. The vertical normalization of the data to the curves is arbitrary.

statistics in the region of the end point and we believe this effect to be negligible in either geometry. The pions that stop in other places will also produce a real signal indistinguishable from the assumed process. This also is checked by substituting a carbon target which will have a larger real signal relative to those events compared to lithium because of the larger stopping power of carbon. We observe no significant change in the data in the low-energy region.

(2) The second type of delayed background is extremely puzzling. There is a background of neutron-

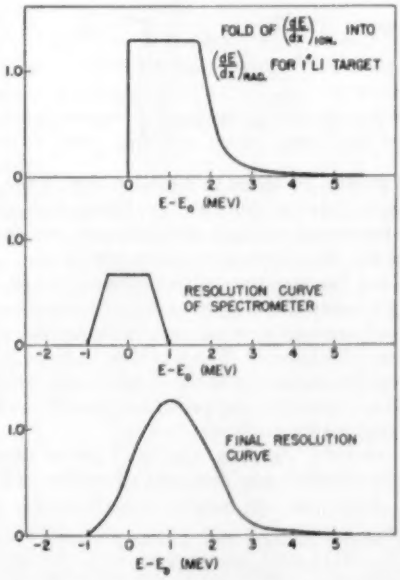

FIG. 4. Resolution curves for 1-in. lithium target.

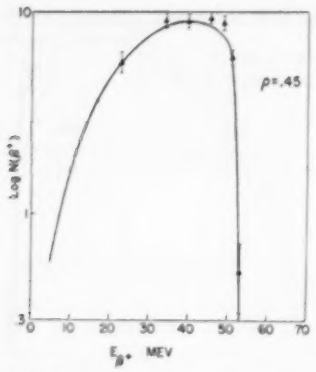

FIG. 5. Lithium data with (improved) counter geometry, without correction for long-period background.

induced counts which is present with no field; this appears to be small. At low-energy settings we find our counts are several times larger than the real signal and we notice that the decay period is not that of the real signal. These events are real coincidences from the lithium target, and they vary slowly with field and do not occur for reversed polarity. In the figures we have used the decay-period information to subtract off the false counts due to any effect with a long decay period (of the order of or greater than 40 μsec). Table II shows the treatment of the data assuming that the background has a period $\tau_B=20\tau_\beta$. Then, if S_β and B are the magnitudes of the μ-decay signal and the background, respectively, and C_I and C_II are the counts in the two delayed gates, we have

$$C_\text{I}=S_\beta\int_0^{t_\text{I}} e^{-t/\tau_\beta}\,dt+B\int_0^{t_\text{I}} e^{-t/\tau_B}\,dt, \qquad (2)$$

$$C_\text{II}=S_\beta\int_{t_\text{I}}^{t_\text{II}} e^{-t/\tau_\beta}\,dt+B\int_{t_\text{I}}^{t_\text{II}} e^{-t/\tau_B}\,dt. \qquad (3)$$

Above 30 Mev, the entire background is small and does not vary with field within statistics. Although the status of the low-energy points is unsatisfactory, the evaluation of the data does not necessarily involve these points and the detector system (with additional 6-in. spacing between counters) used to check the other real pion effect does not show an appreciable amount of the long-period background. This is evident in Fig. 5, where we have plotted the sum of the counts in the two gates without correction for long-period background (we have subtracted out the target-out counts).

We conclude, therefore, that with better detector geometry the effect may disappear altogether, and that making the subtraction described above is the better (although poor) alternative to getting a better detection geometry. Unfortunately, an accident in the form of an electrical fire made necessary the complete rewinding of the spectrometer magnet. Consequently, it will not be possible to obtain any further experimental data for several months from this writing.

RESULTS

The data show a very sharp upper end resolved to four percent at half-maximum. The end point at present is calibrated only very crudely (approximately two-percent error).

We conclude from the data that the spectrum obtained is consistent with a β-coupling characterized by a 'Michel' parameter of $\rho=0.50\pm0.07$, where the error is based upon statistics alone. Combining the systematic errors of about the same size we obtain $\rho=0.50\pm0.10$.

TABLE II. Correction to data for long-period background. Columns C_I and C_II are the counts in the two delayed gates; S_β and B are the signal and background computed using Eqs. (2) and (3), with $t_\text{I}=\tau_\beta$ and $t_\text{II}=2.4\tau_\beta$.

E (Mev)	C_I	C_II	S_β	B
7.9	32	47	−9.5	38.7
11.3	50	56	16.9	40.0
17.0	71	61	57.8	35.1
22.6	123	78	150.6	28.3
28.3	153	91	198.1	28.1
33.9	181	109	232.2	34.9
39.6	232	116	340.7	16.7
43.0	267	132	394.8	17.5
45.2	266	155	350.6	45.2
46.3	242	137	326.2	36.4
48.6	242	133	333.6	31.8
50.9	216	119	297.2	28.6
52.0	112	67	144.2	21.0
52.6	66	50	66.0	24.7
53.7	25	19	24.9	9.5

We find it entirely impossible to devise any mechanism to change our resolution or efficiency or background in the region of most significance (40–50 Mev) to alter these conclusions significantly. However, we must admit that the same remark applies to most of the other experiments with which we do not agree. In particular, the latest result of Sagane *et al.*[8] seems to be extremely accurate and the result entirely different. We are grateful to Dr. Sagane for informing us of his progress and for suggesting many checks which we hope to perform in the future.

ACKNOWLEDGMENTS

We should like to thank all those who contributed to the attainment of the high current density of the external beam of the Mark III linear accelerator.

Nuclear Internal Momentum Distributions*

JOHN M. WILCOX AND BURTON J. MOYER
Radiation Laboratory, Department of Physics, University of California, Berkeley, California

(Received February 28, 1955)

The nuclear internal momentum distributions of protons in light nuclei have been studied with the 340-Mev scattered proton beam from the synchrocyclotron. The two protons from a quasi-elastic scattering event are detected in coincidence, and the energy of one of them is magnetically analyzed. In the limit of the impulse approximation, conservation of energy and momentum can be employed to solve for the momentum of the struck proton. The best fit to the experimental data for beryllium was obtained with a Gaussian momentum density distribution with a $1/e$ value of about 20 Mev. Fermi (rectangular) and Chew-Goldberger distributions did not fit so well. Qualitative differences were observed between lithium, beryllium, and boron. The observed lithium spectrum was interpreted as being caused by two types of protons in lithium; two core protons that have a large momentum distribution and a third proton that has a rather low kinetic energy. This speculation was supported by the shape of the observed lithium spectrum, and by the relative yields from lithium, beryllium, and deuterium. The spectrum observed from beryllium indicated that the protons in beryllium have a larger momentum than the protons in the lighter elements studied. There were some indications that the fifth proton in boron may behave similarly to the third proton in lithium.

I. INTRODUCTION

ONE of the basic properties of the atomic nucleus is the momentum distribution with which the neutrons and protons are moving inside the nucleus. If the correct nuclear spatial wave function were known, then by a fundamental quantum-mechanical principle we could obtain the momentum-density distribution as follows.

If $\psi(\mathbf{r})$ is the solution of the Schrödinger equation, then the wave function in momentum space $\phi(k)$ can be found by a Fourier transform[1]

$$\phi(\mathbf{k})=\frac{1}{(2\pi)^{\frac{3}{2}}}\int_{\infty}e^{-i\mathbf{k}\cdot\mathbf{r}}\psi(\mathbf{r})d\mathbf{r},$$

where the momentum $p=\hbar k$, and $2\pi\hbar$ is Planck's quantum of action. Then the probability that the momentum lies between $\hbar k$ and $\hbar(k+dk)$ is[2]

$$P(k)dk=C|\phi(k)|^2dk,$$

where C is a normalizing coefficient. This gives a measure of the fractional occupancy of the phase states; if we wish to know the number of nucleons with given momenta we must multiply by the volume of phase space available, which is proportional to $4\pi p^2dp$. In the absence of a correct nuclear spatial wave function, it has not been possible to obtain information on momentum distributions in this manner. However, any wave functions which may be proposed in the future should be able to correctly predict the observed momentum distribution.

On the basis of a statistical gas model of the nucleus, Fermi was able to predict a momentum distribution. The nucleus is considered as a gas of neutrons and protons which is confined to a volume $\Omega=(4/3)\pi R^3$, where the nuclear radius $R=1.5\times10^{-13}A^{\frac{1}{3}}$ cm, and A is the mass number. At ordinary nuclear excitation energies of about 10 Mev the particles will occupy the lowest available states, for—owing to the close confinement of the particles—the energy-level spectrum has widely spaced levels. Following Fermi,[3] we have for the number N of states of momentum less than $p_{\max}$ of a proton confined to a volume Ω:

$$N=2[4\pi p^3{}_{\max}\Omega/3(2\pi\hbar)^3],$$

where the factor of two takes account of the two possible orientations of a particle with spin $\frac{1}{2}$. At complete degeneracy the number of states is just equal to the number of protons, and if we assume further that $Z=A/2$ and insert the above value for Ω, we get

$$p_{\max}=(3\pi^2)^{\frac{1}{3}}\hbar\left(\frac{A}{2(4\pi/3)(1.5\times10^{-13}A^{\frac{1}{3}})^3}\right)^{\frac{1}{3}}$$

$$=1.05\times10^{-14}\text{ cgs units},$$

which corresponds to a kinetic energy of 21 Mev. Thus the statistical gas model predicts that all momentum states are occupied up to a maximum corresponding to about 21 Mev, and that states above this are not occupied.

For the deuteron we do have available a fairly reliable wave function, namely the Hulthén wave function $(e^{-\alpha r}-e^{-\beta r})/r$, where $(\alpha\hbar)^2=$(nucleon mass)·(deuteron binding energy) and $\beta/\alpha=7$. This function[4] is a close approximation to the numerical solution of the Schrödinger equation using the Yukawa potential. The value $\beta/\alpha=7$ is obtained from the effective range theory of Blatt and Jackson.[5] The Fourier transform of the Hulthén wave function is proportional to

$$\left|\frac{1}{\alpha^2\hbar^2+p^2}-\frac{1}{\beta^2\hbar^2+p^2}\right|^2.$$

Thus this distribution can be used as a check on the

* This work was supported by the U. S. Atomic Energy Commission.

[1] D. Bohm, *Quantum Theory* (Prentice-Hall, Inc., New York, 1951), p. 77.

[2] See reference 1, p. 95.

[3] Fermi, Orear, Rosenfeld, and Schluter, *Nuclear Physics* (University of Chicago Press, Chicago, 1950), p. 159.

[4] G. F. Chew, Phys. Rev. **74**, 815 (1948).

[5] J. Blatt and J. D. Jackson, Phys. Rev. **76**, 18 (1949).

experimental procedure. Unfortunately there is no clear evidence for the validity of this distribution for high momenta.

Serber[6] has used the Hulthén momentum distribution to explain the angular and energy distributions observed by Helmholz *et al.*[7] when 190-Mev deuterons are incident on various target nuclei. We consider an interaction in which the proton of the deuteron collides with a target nucleus, while the neutron does not. The neutron would continue forward with half the energy of the deuteron, except for its internal momentum with respect to the deuteron. The components of this momentum parallel to the beam direction will add to or subtract from the beam momentum of the neutron (which is half the momentum of the original deuteron) to change the energy of the emerging neutron, while the transverse components of the internal momentum will contribute to the observed angular spread of the neutrons.

The reverse of the above "stripping" process has been observed by Hadley and York,[8] who have found deuterons and tritons produced by bombardment of various targets with 90-Mev neutrons. Since their distribution is peaked in the forward direction, and they have an energy approximately equal to that of the incident neutron, the observed deuterons could not be low energy evaporation[9] particles. If the incident neutron finds a partner proton in the target nucleus moving with a momentum such that their relative momentum forms a state of the deuteron, then the neutron can "pick up" the proton and emerge as a deuteron. This process obviously involves the momentum distribution of the struck nucleus, as well as that of the deuteron. Chew and Goldberger[10] have explained the observed distribution of deuterons, postulating a momentum distribution for carbon which fits the data. This distribution is equal to

$$\alpha/[\pi^2(\alpha^2+p^2)^2],$$

where α is a momentum corresponding to a nucleon energy of 18 Mev. Selove[11] has observed pick-up deuterons at various angles using 95-Mev protons. Pick-up deuterons from various target nuclei have also been observed at small angles to the beam by Bratenahl,[12] using protons of energies from 95 Mev to 138 Mev. Heidman[13] has been able to fit York's data with an excited Fermi gas distribution with a temperature of 9 Mev. However, unless calculation and experiment are quite precise this will be indistinguishable from a gaussian distribution.

Internal momentum distributions have a profound effect on the production of mesons from nuclei; in fact, meson production from complex nuclei tends to give more information about the structure of the nucleus than about interactions of mesons. The threshold bombarding energy can be lowered considerably, since the bombarding nucleon may encounter a target nucleon that is moving toward it with considerable momentum, which will increase the energy available in the center-of-mass system. Thus free nucleon-nucleon production of π mesons[14] requires 290 Mev, while in nuclei π mesons can be produced by incident nucleons having energies as low as 180 Mev. This effect was first predicted by McMillan and Teller.[15] A complete discussion of nucleonic production of π mesons in complex nuclei has been given by Henley and Huddlestone[16] and by Henley,[17] using several momentum distributions. The distribution used affects the production threshold, excitation function, and the energy spectrum and angular distribution of the produced mesons as compared with those resulting from collisions with free nucleons used as targets. For 340-Mev protons incident, the cross section at 90° depends markedly on the nucleon momentum distribution, while at 0° the effect is not as great. This can be accounted for as follows. The produced mesons are observed[18] at energies up to about 80 Mev. At 90°, the meson spectrum in free nucleon-nucleon collisions is cut off at about 9 Mev by energy-momentum conservation. Hence the form chosen for the momentum distribution, which broadens the spectrum to 80 Mev, has considerable effect. At 0°, however, the free-nucleon cutoff does not occur until about 70 Mev, so that the influence of the momentum distribution is less significant. Henley used a gaussian distribution with a $1/e$ value of 19.3 Mev, a 0°K Fermi degenerate gas model, and a modified Chew-Goldberger distribution. The Chew-Goldberger distribution mentioned above was found to have too many high-momentum components, and also has an infinite average energy. Therefore Henley suggested a modified Chew-Goldberger distribution of the form

$$[(\alpha^2+p^2)^2(\beta^2+p^2)^2]^{-1},$$

where $\beta=2.5\alpha$. This has an average energy of 48.1 Mev and still fits York's data fairly well. Nevertheless Henley found that the best fit to the experimental data was obtained from the Gaussian distribution with $1/e$ value of 19.3 Mev. Somewhat similar calculations have been performed by Block, Passman, and Havens[19] for the Columbia cyclotron energy of 380 Mev; they found the best fit to be given with the original Chew-Goldberger distribution. In some later work,[20] however, they have used a gaussian distribution with a $1/e$ value of 14 Mev.

[6] R. Serber, Phys. Rev. **72**, 1008 (1947).
[7] Helmholz, McMillan, and Sewell, Phys. Rev. **72**, 1003 (1947).
[8] J. Hadley and H. F. York, Phys. Rev. **80**, 345 (1950).
[9] N. Bohr, Nature **137**, 344 (1936).
[10] G. F. Chew and M. L. Goldberger, Phys. Rev. **77**, 470 (1950).
[11] W. Selove, Phys. Rev. **92**, 1328 (1953).
[12] A. Bratenahl and B. J. Moyer, Phys. Rev. **92**, 538(A) (1953).
[13] J. Heidman, Phys. Rev. **80**, 171 (1950).
[14] R. E. Marshak, *Meson Physics* (McGraw-Hill Book Company, Inc., New York, 1952), p. 72.
[15] W. McMillan and E. Teller, Phys. Rev. **72**, 1 (1947).
[16] E. Henley and R. Huddlestone, Phys. Rev. **82**, 754 (1951).
[17] E. M. Henley, Phys. Rev. **85**, 204 (1952).
[18] C. Richman and H. A. Wilcox, Phys. Rev. **78**, 496 (1950).
[19] Block, Passman and Havens, Phys. Rev. **83**, 167 (1951).
[20] Block, Passman and Havens, Phys. Rev. **88**, 1239 (1952).

High-energy scattering experiments also provide a powerful means for studying internal momentum distributions. When 340-Mev protons are incident on a hydrogen target, the scattered protons at a given angle have a unique energy, since this is a two-body collision with the struck proton at rest. Nonrelativistically this energy is just $E_0 \cos^2\theta$, where E_0 is the incident energy and θ is the angle of observation. If the struck proton is moving inside a nucleus instead of being a free particle, the observations are somewhat different. Instead of a sharp peak, the energy spectrum is smeared out, owing to the motion of the struck proton. The faster it is moving the greater is the spread in the observed energy. Also the peak of the distribution is decreased in energy, since the binding energy of the proton knocked out and the excitation energy of the residual nucleus must be supplied by the incident proton.

Chamberlain and Segrè[21] have bombarded lithium with 340-Mev protons, and studied the pairs of protons emitted in coincidence as a function of the angle between the two protons. Their data could be fitted by a Fermi gas momentum distribution with a maximum energy of 20 Mev. They found a peak in counting rate when the angle between their two counters corresponded to that for free nucleon-nucleon scattering. This is important evidence for the nucleon-nucleon nature of these scattering processes in light nuclei.

Cladis[22] has made a more direct measurement of internal momenta. When a 340-Mev proton is incident on a nucleus, it is reasonable to think of a nucleon-nucleon collision instead of a nucleon-nucleus collision, since the De Broglie wavelength of the incident proton is comparable with the internucleon spacing in nuclei. Cladis has proposed the name "quasi-elastic scattering" for this type of event, since the process is inelastic in that a rearrangement of the nucleus is brought about, but elastic in the sense that a nucleon-nucleon collision occurs in the nucleus that resembles the scattering of nucleons by free target nucleons. Cladis observed the momentum distribution of single protons quasi-elastically scattered from carbon at 40°, and deduced the nuclear internal momentum distribution with the aid of an equation developed by Wolff,[23] which gives the energy spectrum of the nucleons scattered at a given angle as an integral over the nucleon momentum distributions. Cladis found the best fit to be a Gaussian distribution with a $1/e$ value of 16 Mev, but concluded that any Gaussian with a $1/e$ value between 14 and 19 Mev would not be inconsistent with the experimental results.

It is clear that if both protons emerging from a collision can be detected in coincidence, together with momentum analysis of one of the protons, the event has been more explicitly defined. In this case, conservation of energy and momentum can be used, at least in the limit of the impulse approximation[24–26] to definitely fix the momentum of the struck nucleon. In the present experiment the momentum distributions of protons quasi-elastically scattered from protons in various light elements have been observed under conditions that detect both particles emerging from the collision.

Chew and Wick[25] have given the following criteria for the validity of the impulse approximation:

(I) The incident particle never interacts strongly with two constituents of the system at the same time.

(II) The amplitude of the incident wave falling on each constituent (nucleon) is nearly the same as if that constituent were alone.

(III) The binding forces between the constituents of the system are negligible during the decisive phase of the collision, when the incident particle interacts strongly with the system.

For the case under consideration, we have:

(I) The wavelength of the incident 340-Mev proton is $\lambda = 0.22 \times 10^{-13}$ cm, while $2r_0 = 2.8 \times 10^{-13}$ cm. Thus, the wavelength of the incoming proton is smaller than the diameter of the nuclear volume for light elements, and it is reasonable to consider nucleon-nucleon collisions.

(II) The mean free path for high-energy nucleons in nuclear matter is of the order of 4×10^{-13} cm,[27,28] which is greater than the above diameter of nuclear volume. Thus the attenuation in passing through a light nucleus should not be too great.

(III) The kinetic energies with which particles emerge from collisions in this experiment are in the region of 150 Mev, whereas the nuclear binding energy is of the order of 10 Mev, and the nuclear potential energy is of the order of 30 Mev. Thus, the energy during collision is much larger than the nuclear binding energies.

II. EXPERIMENTAL METHOD

The experiment is done with the scattered external beam of the 184-inch synchrocyclotron, which gives a 15–20 μsec pulse of 340-Mev protons, with a repetition rate of 60 per second. The equipment is set up in the experimental area called the cave. A vertical section including the incident proton beam is shown in Fig. 1.

A. Target

The target is required to be a parallelogram by two considerations. First, the width presented to the spectrometer must be as narrow as possible in order to

[21] O. Chamberlain and E. Segrè, Phys. Rev. **87**, 81 (1952).
[22] J. B. Cladis, thesis, University of California Radiation Laboratory Report UCRL-1621 (unpublished), and Cladis, Hess, and Moyer, Phys. Rev. **87**, 425 (1952).
[23] P. A. Wolff, thesis, University of California Radiation Laboratory Report UCRL-1410 (unpublished).
[24] G. F. Chew, Phys. Rev. **80**, 196 (1950).
[25] G. F. Chew and G. C. Wick, Phys. Rev. **85**, 636 (1952).
[26] G. F. Chew and M. L. Goldberger, Phys. Rev. **87**, 778 (1952).
[27] A. J. Kirschbaum, thesis, University of California Radiation Laboratory Report UCRL-1967 (unpublished).
[28] Fernbach, Serber, and Taylor, Phys. Rev. **75**, 1352 (1949).

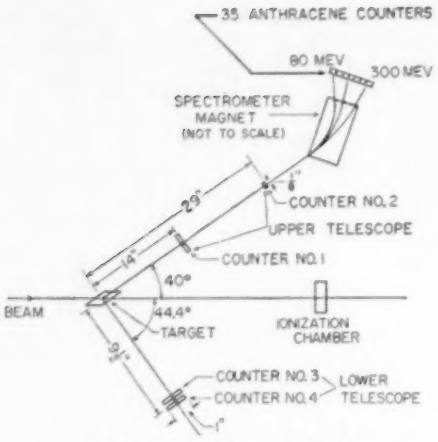

FIG. 1. Section through plane of collision.

preserve good energy resolution, and second, the length of target through which the protons must pass after a scattering event must be as small as possible in order to reduce energy losses in the target. Hydrogen and deuterium were observed in the form of CH_2 and CD_2, with an appropriate subtraction being made for the effect of the carbon. A very thin coating of aluminum was evaporated in a vacuum on the lithium target to protect it from contamination in the air. The boron target was sintered into the proper shape. A one-mil aluminum foil was needed to hold it together.

B. Counter Telescopes

The two protons emerging from a collision are detected in coincidence by two counter telescopes, consisting of *trans*-stilbene crystals viewed by 1P21 photomultiplier tubes. It is desirable that protons pass through the upper telescope without deviation, so that they will enter the energy spectrometer in the proper direction. Therefore, the thickness of these crystals that the protons pass through was one-eighth of an inch. Counter No. 2 defines the path of particles into the spectrometer; therefore, its width (measured in the plane of collision) must be made as narrow as possible, consistent with an adequate counting rate. Counters No. 3 and No. 4 are made thicker, since small-angle scattering does not matter. Counter No. 4 defines the path of particles detected by the lower telescope. It is a rectangle one inch long in the plane of collision and two inches long perpendicular to this plane.

Since crystal counters No. 1 and No. 2 are made very thin to avoid multiple scattering, the protons lose a small amount of energy in passing through, and thus an efficient light-collecting system must be employed. Each crystal is viewed from both ends by 1P21 photomultiplier tubes, with an aluminum housing of the size of the photocathodes to permit maximum light collection.

C. Energy Spectrometer

1. Description.—The momentum of the upper proton is measured with a bending magnet and a row of 35 anthracene counters, viewed by 931A or 1P21 photomultiplier tubes. The scattered beam emerges into the cave in the form of a line approximately one-sixteenth inch wide, which is tilted at 13 degrees from the horizontal, as shown in Fig. 2. It was desired to have this line serve as a line source for the spectrometer, i.e., the pole faces of the magnet should be perpendicular to it. Thus it was necessary to build a steel stand to hold the seven-ton magnet six feet above the floor, tilted at an angle of 13 degrees. The target holder was fastened to this stand, and the base for the 35 anthracene crystals was also permanently attached, making it possible to do all aligning and calibrations outside the cave. For a run the whole assembly was lifted into the cave with the overhead crane.

2. Resolving Power of Particle Spectrometer.—The resolving power of the spectrometer depends on (1) the target width considered as a slit, (2) the width of telescope counter No. 2, (3) the widths of the 35 anthracene crystals, (4) the energy loss of protons in the targets, and (5) the small-angle scattering in telescope counter No. 2. The over-all resolving power of the spectrometer is obtained by "folding" together the widths due to each of the above factors. This process has been described in detail in a previous report.[22] The spectrometer resolution can be checked experimentally at the energy corresponding to scattering from a hydrogen target. Such protons are monoenergetic, and the shape and width of the observed spectrum represents the resolution of the equipment. This was approximately 20 Mev (full width at half-height) for this experiment (see Fig. 4).

3. Nature of Scattered Particles Detected.—Mesons

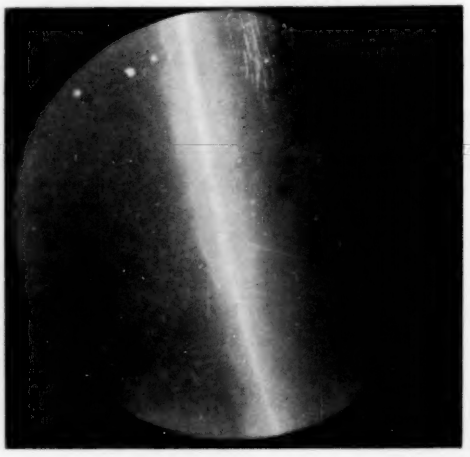

FIG. 2. Scattered proton beam.

will not reach even the lowest energy channel unless they have an energy greater than 300 Mev. The number of deuterons and alpha particles entering the spectrometer had been measured (without demanding correlated particles) by Hess with an absorber technique[29] and found to be less than five percent. When a correlated particle technique is used the deuteron and alpha-particle contamination is greatly reduced below this figure, since the angular correlation demanded by this experiment greatly favors protons. It is therefore assumed that all particles with which we are here involved are protons.

D. Electronics

A block diagram of the electronics is shown in Fig. 3. Signals from the 1P21 photomultipliers that view the crystals in the telescopes go through an adder-and-shaping circuit to a coincidence circuit[30] which, with these shaped pulses, operates with a resolving time of 5×10^{-9} sec. Signals from the 35 counters in the spectrometer are amplified and trip a one-shot multivibrator which in turn actuates a mechanical counter. The output of the coincidence circuit is counted on a scaler, and also makes a 0.4 μsec gate which turns on the 35-channel amplifiers.

E. Monitor

An argon-filled ionization chamber was used to monitor the beam current to which the target was exposed. The scattering of the beam by the various targets introduces a negligible error in the monitor readings.

III. EXPERIMENTAL PROCEDURE

The exact height of the line distribution of the scattered proton beam is first determined with a photographic film. Since this height drifts slightly from time to time, owing to unknown causes, it is necessary to shoot a film every few hours during the run. With the beam at a fixed level, plateaus are obtained of telescope coincidences per monitor as a function of photomultiplier voltage and of linear amplifier gain. The time at which the coincidence gate is sent out to the 35-channel amplifiers is then varied to achieve the optimum counting rate.

Two types of accidentals may occur: (1) in the telescope quadruple coincidence circuit, (2) between a 35-channel counter and the telescope gate. Both types can be measured by changing the beam level. The second type can also be measured by inserting a 2 μsec delay in the telescope gates sent out to the 35-channel amplifiers, so that the gate could not coincide with a real pulse. Results of these two methods are in agreement.

[29] W. N. Hess (private communication).
[30] R. Madey and K. Bandtel, Rev. Sci. Instr. (to be published); University of California Radiation Laboratory Report UCRL-1880 (unpublished).

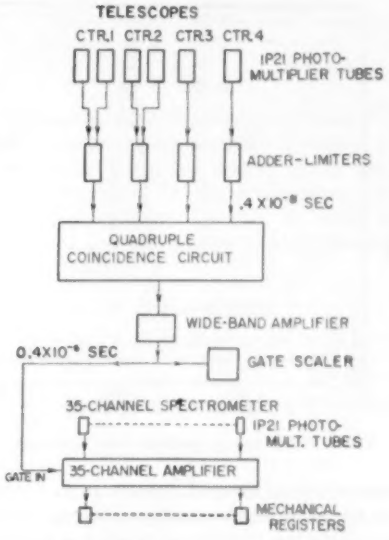

FIG. 3. Block diagram of electronics.

The following data are recorded for each run: (1) number of gates, (2) the integrated beam, (3) the time interval, and (4) the readings of the 35 registers. Repeated runs on various targets are made in sequence to minimize the effects of long-term drifts. The beam intensity is kept constant so that there is a constant proportion of accidentals for a given target.

IV. ANALYSIS OF DATA

A. Subtraction of Accidentals

The spectrum obtained from the 35 registers must be corrected for the two types of accidental counts mentioned above. The greatest number of counts resulting from telescope accidentals may be expected when one proton passes through the top telescope and another particle, which is not a companion proton from the same collision, passes through the bottom telescope. Thus the channel counts arising from this type of accidental gate should have a spectrum similar to that obtained by gating the 35 amplifiers by the upper telescope only. This accidental spectrum is subtracted out. The remaining spectrum is made by true correlated proton gates, but there are still accidentals between the 35 channel pulses and the gates. This accidental spectrum is determined by delaying the gates by 2 μsec as described in the aforementioned, and subtracted out.

B. Channel Efficiencies

Each of the 35 channel counters has a different energy width for accepting protons, ranging from 15 Mev at the high-energy end to 2.2 Mev at the low end. Thus, the counts in each channel must be divided by its energy width to give a true number of counts per

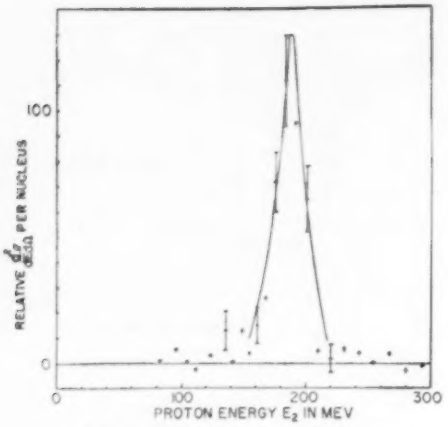

FIG. 4. Proton energy spectrum from hydrogen.

unit energy interval. Several channels at the low energy end are added together to make the energy widths at all parts of the spectrometer more nearly uniform.

The spectrum thus obtained includes the effects of the finite size of the telescope counters and the spectrometer resolution. These effects must be folded into a theoretical momentum distribution before it can be compared with the data.

C. Kinematics of Process

The relation between a value of the target proton momentum and the momentum of an observed proton was calculated from relativistic conservation of energy and momentum. (See Appendix.) The binding energy of the nuclear proton and an estimated excitation energy of 10 Mev for the residual nucleus were added into the conservation-of-energy equation. It must be observed that this experiment compels the struck nucleon to be moving in a well-defined direction. Consider the upper telescope to be a point counter, with the bottom telescope subtending a finite solid angle Ω_5. Then for nuclear protons of energy E_5, only those moving within a fixed solid angle Ω_5 can be counted. Furthermore, the size of Ω_5 depends on the energy E_5 of the nuclear proton. When its energy approaches zero, it is similar to a proton at rest, and every proton in the upper telescope resulting from a collision has its partner detected in the lower telescope. If, on the other hand, the energy E_5 of the nuclear proton is very large, only those protons which were moving within a small cone of solid angle Ω_5 are counted. The value of Ω_5 corresponding to each value of E_5 was computed numerically, as explained in the Appendix. Thus, an assumed momentum distribution must first be multiplied by this solid-angle efficiency factor. The distribution is then corrected for the finite widths of the telescope counters. (See Appendix.) Finally, the resolution of the spectrometer is folded in. The resulting spectrum can then be compared with the experimental data.

The point involved in the discussion of the solid angle Ω_5 may be clearer if we consider a simple analogy. Consider the collision of two nonrelativistic particles of equal mass which are to be detected after the collision by point counters 90° apart. There is a definite restriction on the angle with which the struck particle was moving before the collision, since conservation of energy and momentum will require that before the collision the struck particle had to be moving perpendicularly to the incident particle. This same general type of effect carries over into the more complex problem considered in this experiment.

V. RESULTS

A. Hydrogen

The spectrum obtained from hydrogen is shown in Fig. 4. This is an experimental check of the resolution of the spectrometer, since protons scattered from hydrogen at a fixed angle are monoenergetic. The full width at half height is about 20 Mev, which agrees with the value calculated from the above spectrometer resolution theory. The solid curve is only to guide the eye but is consistent with the resolution curve generated out of the parameter widths mentioned in Sec. II-C-2. The errors shown in all curves are standard deviations.

B. Deuterium

The spectrum obtained from deuterium is shown in Fig. 5. This isotope was observed in order to check the experimental method used, since its momentum distribution is fairly well known.[21] The solid curve was

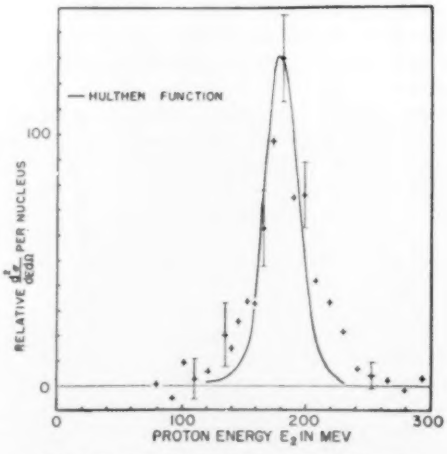

FIG. 5. Proton energy spectrum from deuterium.

[21] This is given by the square of the Fourier transform of the Hulthén wave function $(e^{-\alpha r}-e^{-\beta r})/r$, where $\beta=7\alpha$ and $(\alpha\hbar)^2$ = (nucleon mass)·(deuteron binding energy). This distribution is proportional to

$$\left[\frac{1}{\alpha^2\hbar^2+p^2}-\frac{1}{\beta^2\hbar^2+p^2}\right]^2.$$

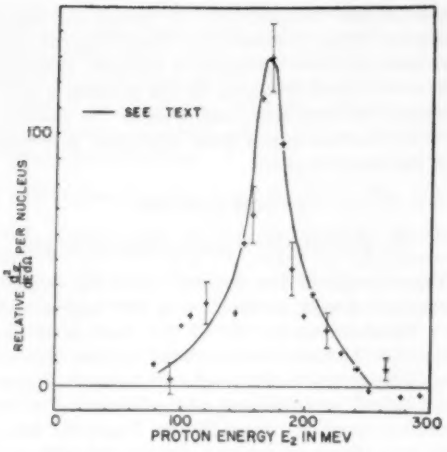

FIG. 6. Proton energy spectrum from lithium.

computed from this distribution by the method outlined previously. Since this curve lies inside the experimental points at its edges, the simple wave function used here does not lead to enough high-momentum components. However, the experimental errors due to subtraction of the carbon spectrum and accidentals are large in this region, since the experiment was not designed to view a narrow distribution such as that from the deuteron.

C. Lithium

The spectrum obtained from lithium is shown in Fig. 6. The shape is rather similar to that obtained from the deuteron. The narrow peak in the center may be due to the unpaired protons having lower kinetic energy than the two paired protons. The peak occurs at an energy 12 Mev lower than the hydrogen peak. The binding energy of the proton knocked out of the lithium (10 Mev) and the excitation energy given to the recoil nucleus (estimated to be 10 Mev) must be given up by the two recoiling protons. Thus we could expect the peak to be shifted by approximately the observed amount. The solid curve is explained in Sec. VI-B.

D. Beryllium

The spectrum obtained from beryllium is shown in Figs. 7 and 8. The best fit is obtained from a Gaussian momentum distribution with a $1/e$ value of about 20 Mev, although—as shown in Fig. 7—Gaussians with $1/e$ values of 16 and 25 Mev can fit the data. The Gaussian distributions are too low at the high-energy tail, but this is the region where the impulse approximation is less valid, and also the errors from subtraction of the background become large. Curves obtained from a degenerate Fermi gas distribution (square distribution) are shown in Fig. 8, with Fermi energies of 15 and 25 Mev. These do not fit as well as the Gaussian. Figure 8 also shows a Chew-Goldberger[10] distribution,[22] which appears to be too narrow.

E. Boron

The spectrum obtained from boron is shown in Fig. 9. The solid curve is to guide the eye to the boron points, while the dashed curve is a best fit to the beryllium points, for comparison. The distribution is more peaked than that of beryllium; this may be owing to the presence of an unpaired proton which is moving with lower kinetic energy.

F. Relative Yield

The relative yield per nuclear proton was as follows:

	Observed	Calculated
Hydrogen	100	100 (assigned)
Deuteron	36	33.6
Lithium	13.3	
Beryllium	4.4	6.5
Boron	5.1	

In order to obtain an adequate counting rate with good spectrometer energy resolution, it was necessary to use targets of varying dimensions. The spatial distribution of the proton beam varies considerably (Fig. 2). Therefore the above observed yields can be considered to indicate only the general trends involved.

The observed relative yield provides a good check on the internal consistency of the experiment. As explained previously, each value of the struck-proton

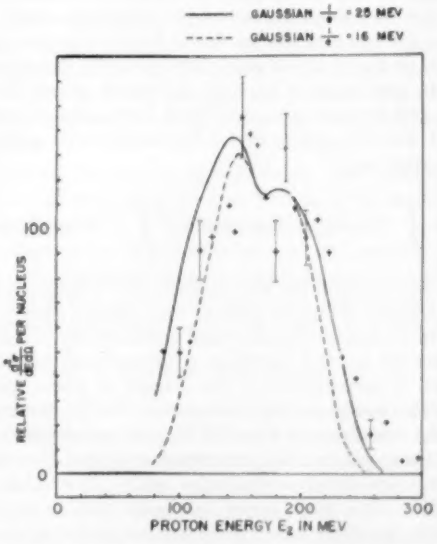

FIG. 7. Proton energy spectrum from beryllium (Gaussian).

[22] The Chew-Goldberger momentum density distribution is

$$N(p) = (\text{const}) \cdot a/(a^2+p^2)^3,$$

where p is the nucleon momentum and a is a momentum corresponding to a nucleon energy of 18 Mev.

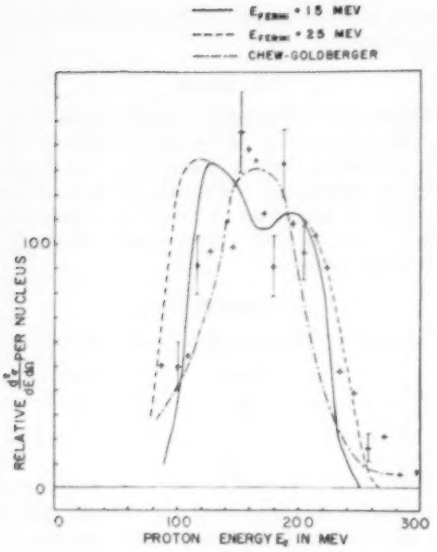

FIG. 8. Proton energy spectrum from beryllium (E_{Fermi}).

momentum has associated with it a definite solid angle Ω_b within which the struck proton must have been moving before the collision, in order that the correlated protons emerging from the collision can be seen by the counters. These solid angles have been computed for deuterium and beryllium. If we now calculate an average solid angle for each element, then the ratios of these average solid angles should be just equal to the ratios of the observed yield. For hydrogen, the appropriate solid angle is 4π, since the struck proton is at rest and hence has no directional limitations imposed on it. For the complex nuclei, the average solid angle is computed as

$$\bar{\Omega}_b = \int_0^\infty [\Omega_b(E_b)] N(E_b) \sqrt{E_b} dE_b \Big/ \int_0^\infty N(E_b) \sqrt{E_b} dE_b;$$

i.e., each value of the solid angle $\Omega_b(E_b)$ is weighted by the number of nuclear protons that have an energy of E_b. In the above formula $N(E_b)$ is the density of states of energy E_b, and $(\sqrt{E})dE$ is proportional to p^2dp, which is proportional to the volume of phase space available to a particle of momentum p. For the deuteron $N(E_b)$ was obtained from the Hulthén wave function, and for beryllium $N(E_b)$ was obtained from a Gaussian momentum density distribution with a $1/e$ value of 16 Mev. This check turned out quite well, as can be seen in the above table. When comparing the observed and calculated yields for beryllium, one should remember that there is a certain fraction of double collisions in beryllium—that is, where one of the correlated protons emerging from a collision suffers a further nucleon-nucleon collision in the same nucleus. These events are not counted, since in general the angular correlation of the protons is lost. Wolff[22] has calculated that one-half of the collisions of 340-Mev protons on carbon will be of this type. If one assumes a loss of one-third for beryllium, and reduces the calculated yield by this amount, a good agreement is obtained with the observed yield.

VI. CONCLUSIONS

A. Quantitative Results from Beryllium

This experiment has indicated that the beryllium momentum-density distribution is best approximated by a Gaussian function with a $1/e$ value of 15 to 25 Mev, with the best value of about 20 Mev. This is in good agreement with the results for carbon of Henley[17] and Cladis.[22] In examining nucleonic production of π mesons in complex nuclei, Henley found the best fit with a Gaussian momentum distribution with a $1/e$ value of 19.3 Mev. With the nucleon scattering experiment previously described, Cladis found the best fit to be a Gaussian distribution with a $1/e$ value of 16 Mev. The Chew-Goldberger[10] distribution, which was used by these authors to explain the production of deuterons by the pickup process, gave a poorer fit in this experiment the Gaussian. The completely degenerate Fermi distribution (rectangular curve) gave the poorest fit of all. An excited Fermi distribution, however, will resemble a Gaussian within the accuracy of this experiment.

As pointed out in Sec. IV-C, the experimental efficiency for observing nuclear protons having a large momentum is much less than the efficiency for ob-

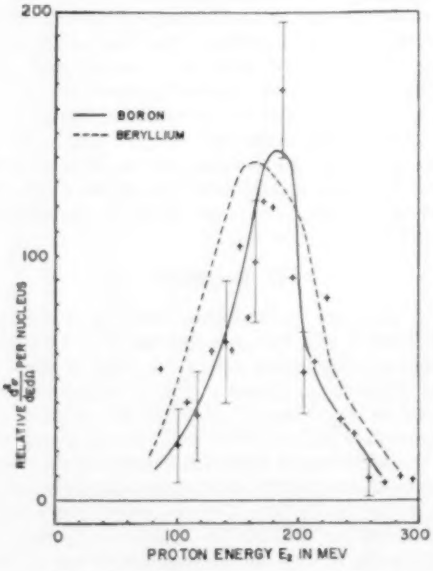

FIG. 9. Proton energy spectrum from boron.

serving nuclear protons having a small momentum. Thus very high momentum values contribute very little, and the results are not statistically significant. The results given here do not disagree with the paper of Selove,[11] who finds from studying a pickup process that there is a very high energy tail to the internal momentum distributions.

B. Qualitative Results from H, D, Li, Be, and B

The narrow peak of the experimental spectrum obtained from hydrogen establishes the spectrometer resolution. The observed curve from the deuteron is only slightly wider, as would be expected, because the binding energy is only 2.2 Mev. It is well known that the deuteron spends more than half the time outside the potential well. In the exterior region (which is classically forbidden), the wave function has the form $\psi = Ae^{-\alpha r}/r$, where $\alpha = (2MB/\hbar^2)^{-\frac{1}{2}}$, M = nucleon mass, B = binding energy, and A is a constant. The expectation value of the kinetic energy in the exterior region then is B.

Owing to the difficulties in working with a helium target, no spectrum was obtained from helium; however, since the alpha particle is a tightly bound, stable structure, one might expect a considerable average kinetic energy.

The lithium spectrum consists of a broad base with a peak at the center which is very similar to the peak observed from the deuteron. In lithium we could postulate two types of protons: two protons with considerable average kinetic energy which belong to the "core" of the nucleus, and a third proton which has considerably less momentum, comparable, in fact, to that of the proton in the deuteron. This hypothesis has been compared with the experimental data in two ways, first by comparing the relative yields from the deuteron, lithium, and beryllium, and secondly by predicting the shape of the observed lithium spectrum by using the spectra from the deuteron and beryllium.

The reason that the relative-yield data are significant is that the efficiency of detection of collisions depends on the energy of the struck proton, as has been explained previously. Thus the slowly moving proton in the deuteron has a large probability of being counted, because of the large solid angle Ω_b associated with it, as explained in IV-C, while the more energetic protons in beryllium are counted with a lower efficiency. If we assume that the two "core" protons in lithium are moving similarly to the protons in beryllium, and thus are counted at the beryllium rate, and that the third proton is being counted at the deuteron rate, we can predict a yield (per nuclear proton) from lithium on the basis of the yield of 36 from the deuteron and 4.4 from beryllium. The calculated lithium yield of 14.9 is consistent with the observed yield of 13.3.

The shape of the lithium spectrum can now be predicted from the shapes of the deuteron and beryllium spectra. If we normalize all these spectra on the basis of the observed yields (i.e., the area under the curve is proportional to the yield), and then add twice the beryllium spectrum (representing the two lithium "core" protons) to the deuteron spectrum (representing the single lithium proton outside the core) we get the predicted spectrum for lithium. The curve obtained in this manner is the solid line drawn in Fig. 6, and is seen to be in good agreement with most of the experimental points.

All the current nuclear models, including Maria Mayer's very successful shell model,[23] put the third proton in lithium in a p state of orbital angular momentum, since the two lowest-energy S states available (spin up and spin down) have already been occupied by the two "core" protons. The binding energy of the last proton in Li^7 is 10.1 Mev, but its average kinetic energy is just a few Mev; therefore this proton would not be like that in the deuteron and would not be expected to spend much time in the region exterior to the potential well.

The spectrum obtained from beryllium was considerably broader than that from lithium. As explained above, the beryllium spectrum has been fitted by assuming a Gaussian momentum-density distribution for all the protons in beryllium with a $1/e$ value of about 20 Mev. To the extent that the alpha-particle model is valid, and that Be^9 is composed of two alpha subgroups plus an extra neutron, it is reasonable to assume that all the protons in beryllium have similar momentum distributions.

The spectrum observed from boron was in general similar to that from beryllium, except that it is somewhat narrower. This could be explained on grounds that the fifth proton in boron is somewhat like the third proton in lithium discussed above. Since this proton is one of five, the percentage effect would be smaller.

Because the binding energy for the "last" proton in Li^6 is distinctly different from that in Li^7 it would be very desirable to employ separated isotopes in this investigation; and a similar remark can apply to B^{10} and B^{11}. The smallness of available targets of isotopic purity in elemental form makes it unreasonable to pursue this refinement under the present techniques.

ACKNOWLEDGMENTS

Wilmot Hess worked with the experiment in the early stages, and George Merkel has helped in the final runs and interpretation of the data. Many valuable theoretical discussions were held with Warren Heckrotte, Robert Karplus, and Malvin Ruderman. Wilson Frank and Kenneth Bandtel gave invaluable assistance with the fast-coincidence gear. Finally, thanks are due James Vale, Lloyd Houser, and the members of the cyclotron crew.

[23] M. G. Mayer, Phys. Rev. 78, 16 (1950).

APPENDIX

Kinematics (See Fig. 10)

The analysis begins with the four relativistic equations which express conservation of energy and momentum:

Conservation of energy:

$$\gamma_1 m + M = \gamma_2 m + \gamma_3 m + \gamma_4 M': \quad (1)$$

Conservation of Z momentum (incident particle enters along Z axis):

$$m\alpha_1 = m\alpha_2 \cos\theta_2 + m\alpha_3 \cos\theta_3 + M'\alpha_4 \cos\theta_4. \quad (2)$$

Conservation of X momentum:

$$O = m\alpha_2 \sin\theta_2 \cos\phi_2 + m\alpha_3 \sin\theta_3 \cos\phi_3 + M'\alpha_4 \sin\theta_4 \cos\phi_4. \quad (3)$$

Conservation of Y momentum:

$$O = m\alpha_2 \sin\theta_2 \sin\phi_2 + m\alpha_3 \sin\theta_3 \cos\phi_3 + M'\alpha_4 \sin\theta_4 \sin\phi_4, \quad (4)$$

where m = mass of proton, M = mass of struck nucleus, M' = mass of recoiling nucleus $+\epsilon/c^2$, ϵ = excitation energy of recoiling nucleus, $\gamma = 1 +$ (kinetic energy)/(rest mass energy), and $\alpha = (\gamma^2 - 1)^{\frac{1}{2}}$. Note that $m\alpha$ represents momentum.

We can first show that the momentum of the struck nucleon is completely determined by the quantities measured experimentally. Before the collision occurs all parameters are known, since the nucleus is at rest and the direction and energy of the incident beam proton are known. After the collision the energy and direction of proton number 2 and the direction of proton number 3 are measured. Thus there remain four unknown quantities: the energy of proton number 3 and the energy and direction (two angular variables) of the recoil nucleus. The four equations involving conservation of energy and momentum are then sufficient to completely define the collision.

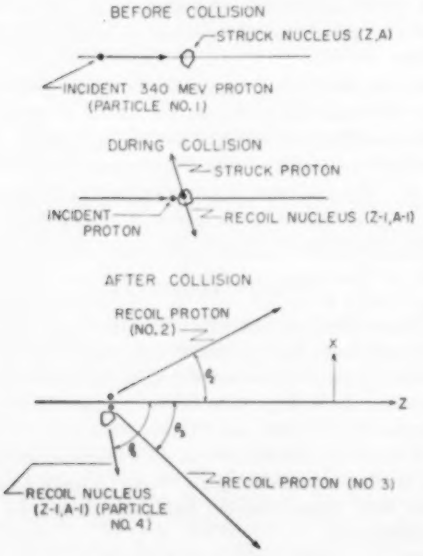

FIG. 10. Kinematics of collision.

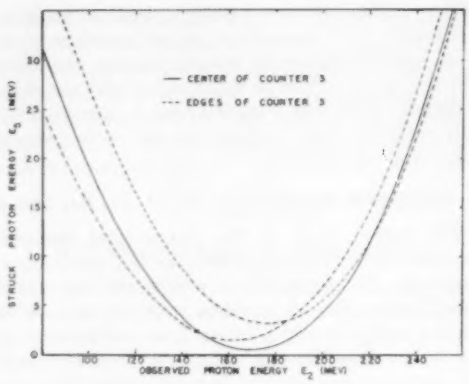

FIG. 11. E_3 *vs* E_2 for beryllium.

Since the nucleus was originally at rest, the struck nucleon must have been moving with momentum equal and opposite to that of the recoiling nucleus. The energy of a proton having the same momentum as the recoiling nucleus is designated E_3.

The solid angle Ω_3 in which the struck nucleon must be moving is calculated numerically. The equations of motion are first solved for the emerging protons passing through the centers of the telescope counters, and then for the emerging protons passing through the corners of telescope counter No. 3. Telescope counter No. 2 is assumed to be a point counter, since its dimensions are an order of magnitude smaller than counter No. 3. Thus the extreme directions of struck nucleon momentum are determined, and the solid angle Ω_3 is defined. The calculations are repeated for a range of values of struck proton momentum, and Ω_3 is determined as a function of E_3.

The proton-proton differential scattering cross section is approximately independent of energy and angle in the c.m. system at these energies. However, since the struck proton is moving, the transformation of solid angle from the c.m. system to the laboratory system will change slightly from event to event. This change has been calculated numerically and found to amount to less than 5 percent.

In general a particle with momentum p has available phase space proportional to p^2dp, or $(\sqrt{E})dE$, since $p^2 = 2ME$. However, for this problem the available phase space is only a fraction of the total, namely $(\Omega_3/4\pi)(\sqrt{E_3})dE_3$. Thus the number of detectable collisions produced by nuclear protons moving with an energy between E_3 and $E_3 + dE_3$ will be proportional to $N(E_3)(\Omega_3/4\pi)(\sqrt{E_3})dE_3$, where $N(E_3)$ is the energy distribution of the nuclear protons. These collisions

will result in scattered protons in telescope counter number 2 having a small range in values of E_2. Thus each value of E_b results in a distribution of protons about a particular value of E_2. The observed spectrum $N(E_2)$ can be obtained by graphical addition of the contributions from all values of E_b.

Figure 11 shows the relationship between the struck proton energy E_b and the observed proton energy E_2 for beryllium. The solid curve is for the case of a proton going through the center of telescope counter number 3, while the dashed curves represent protons which go through the sides of telescope counter number 3. Thus this figure indicates the effects of the finite size of this counter. It should be noted that a given value of E_2 on the left-hand half of the curve ($E_2<170$ Mev) corresponds to a rather wide range in values of E_b, whereas a given value of E_2 on the right-hand half of the curve ($E_2>170$ Mev) corresponds to a smaller range in values of E_b. Thus for a flat-topped momentum distribution such as the Fermi (rectangular), contributions from many values of E_b will add up at a particular value of E_2 to produce the characteristic double-peaked curves. However, in the somewhat narrower Chew-Goldberger distribution this effect is largely washed out.

It should be further noted that each value of E_b corresponds to two values of E_2. Thus the information comes in twice, i.e., either the left half or the right half of the experimental curves would determine the nuclear momentum distribution. The agreement of the experimental points with both halves of the calculated curves thus gives a measure of the internal consistency of the experiment.

The nuclear momentum distribution is assumed to be isotropic.

PHYSICAL REVIEW VOLUME 99, NUMBER 3 AUGUST 1, 1955

Diffusion Cloud-Chamber Study of Very Slow Mesons.* II. Beta Decay of the Muon

C. P. SARGENT,† M. RINEHART, L. M. LEDERMAN, AND K. C. ROGERS
Department of Physics, Columbia University, New York, New York

(Received April 8, 1955)

The spectrum of electrons arising from the decay of the negative mu meson has been determined. The muons are arrested in the gas of a high-pressure hydrogen-filled diffusion cloud chamber. The momenta of the decay electrons are determined from their curvature in a magnetic field of 7750 gauss. The spectrum of 415 electrons has been analyzed according to the theory of Michel. The shape parameter, ρ, is found to be 0.64 ± 0.10. The significance of this result in terms of the beta interaction is discussed.

A. INTRODUCTION

THE determination of the spectrum of electrons which are produced by the decay of the muon is one of the most honored problems in particle physics.[1–10] Some of the difficulties in arriving at definite conclusions from the mass of data are discussed by Williams.[9] One of the principal difficulties is the generally poor resolution that has been used. The earlier data were not accompanied by detailed discussions of the resolution of the respective techniques. The lack of resolution was principally due to radiation losses of the decay electrons in the material used to arrest the muons.

The present experiment employs the gas of a hydrogen-filled diffusion cloud chamber working at a pressure of 19 atmospheres, to stop negative muons and to observe the momentum of the decay electrons. The experimental arrangement has already been reported.[11] In addition to the negligible radiation and ionization losses, the lack of dead mass allows an examination of the entire spectrum. This virtue eliminates the necessity of arbitrarily normalizing the data.

B. EXPERIMENTAL CONSIDERATIONS

Negative mesons from the 60-Mev pion beam of the Nevis cyclotron are moderated and allowed to enter the diffusion chamber, where a small fraction of pions and muons spiral to rest in the gas (see Fig. 1). Muon endings are scanned for associated decay-electrons. Momenta of the electrons are determined from curvature and angle measurements and from the value of the magnet field ($\bar{H}=7750$ gauss) at the time of the event.

Because of the finite depth of the sensitive layer, the visible path length of roughly half of the decay electrons is so short that their inclusion in the data would seriously impair momentum resolution. The mesons decay from Bohr orbits, and hence any criterion which requires that the electrons be emitted within some

* This research was supported in part by the joint program of the Office of Naval Research and the U. S. Atomic Energy Commission.

† Now at Laboratory for Nuclear Science, Massachusetts Institute of Technology, Cambridge, Massachusetts.

[1] R. Thompson, Phys. Rev. **74**, 490 (1948).
[2] J. Steinberger, Phys. Rev. **75**, 1136 (1948).
[3] Leighton, Anderson, and Seriff, Phys. Rev. **75**, 1432 (1949).
[4] A. Lagarrique and C. Reyrou, Compt. rend. **233**, 478 (1951).
[5] Davies, Lock, and Muirhead, Phil. Mag. **40**, 1250 (1949).
[6] Sagane, Gardner, and Hubbard, Phys. Rev. **82**, 557 (1951).
[7] H. Bramson and W. Havens, Phys. Rev. **88**, 304 (1952).
[8] R. Levisetti and G. Tomasini, Nuovo cimento **8**, 12 (1951).
[9] J. Vilain and R. Williams, Phys. Rev. **94**, 1011 (1954).
[10] Sagane, Dudziak, and Vedder, Phys. Rev. **95**, 863 (1954).

[11] Sargent, Cornelius, Rinehart, Lederman, and Rogers, Phys. Rev. **98**, 1349 (1955); referred to as I.

FIG. 1. Diffusion cloud-chamber photograph of the decay of a negative muon.

specified solid angle with respect to any direction in space will not bias the momentum spectrum. A dip angle *versus* height relation constituted the criterion for acceptance of decay events for measurement. For example, an electron starting at the top of the sensitive layer was required to be moving down with a dip angle of less than 48°: $0<\tan\alpha<1.1$. Few of the accepted tracks were shorter than 8 cm. The average electron track was 12 cm in length. In the 15–50 Mev/c momentum range, the curvature of an 8-cm track in a magnetic field of 7750 gauss was measurable to about 5 percent. The error varies inversely as the square of the projected track length.

A monochromatic electron beam of appropriate momentum for investigating resolution was not available. However, one may assign a reasonably good estimate of the momentum uncertainty to each momentum measurement. The distribution of such uncertainties determines a momentum resolution function. Appendix I describes the momentum measurement procedure, the uncertainties involved in the measurements and the determination of the resolution functions.

C. EXPERIMENTAL RESULTS

Figure 2 represents the distribution of 415 decay electrons. The number of events per unit momentum interval is plotted against electron momentum. The horizontal bar attached to each point indicates the momentum interval Δp, used to determine the point. The intervals are chosen sufficiently small that no significant error is made in placing the point at the center of the interval, if one assumes the spectrum to be a smoothly varying function of momentum. The vertical bar attached to each point is a measure of the statistical reliability of the point. It extends $(\Delta N+1)^{\frac{1}{2}}/\Delta p$ from the point, where ΔN is the number of events in the electron momentum interval Δp.

The curves above the momentum scale in Fig. 2 are resolution functions at 20 and 50 Mev/c. The resolution function at momentum p represents the distribution of momenta which would be observed from a monochromatic source of electrons with momentum p. These are determined by the method of Appendix I. The resolution function at momentum p turns out to have a width at half maximum given by $R=(0.066\pm0.020)p$. Figure 3 illustrates the results of improving the resolution by a more stringent set of criteria. These further limit the solid angle for acceptable tracks. The resulting tracks are less steeply inclined to the horizontal and are longer. This division of the data is useful in studying the propagation of resolution errors.

D. ANALYSIS OF DECAY SPECTRUM

The reaction being observed has been interpreted as following the scheme:

$$\mu^-\rightarrow e^-+\nu+\nu. \qquad (1)$$

The theory of this reaction has been developed by Tiomno, Wheeler and Rau[12] and by Michel.[13] The reaction (1) is a weak interaction of four spin-$\frac{1}{2}$ particles and is treated in the same way as the nuclear beta decay interaction. Michel's results are given to excellent approximation by the spectral distribution:

$$P(x)=4x^2[3(1-x)+\tfrac{2}{3}\rho(4x-3)], \qquad (2)$$

where $P(x)dx$ is the probability per unit time for the decay at rest of a muon producing an electron with momentum between p and $p+dp$, $x=p/W$, and W is one-half the muon rest mass. The parameter ρ is a function of the interaction coupling constants and, in Michel's theory, may have values between 0 and 1. Experimental examination of the electron spectrum can then determine but the single parameter ρ.

The right side of Eq. (2) must be modified before it

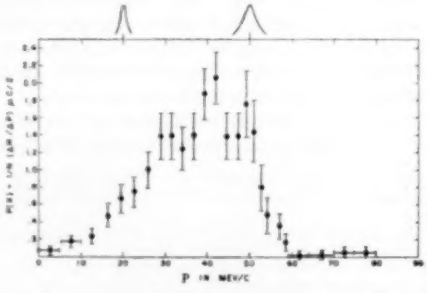

FIG. 2. Spectrum of electrons from muon decay. A total of 415 events were used. The "poor" resolution curves are given above the spectrum at 20 and 50 Mev.

[12] Tiomno, Wheeler, and Rau, Revs. Modern Phys. **21**, 144 (1949).

[13] L. Michel, Nature **163**, 959 (1949); thesis, Paris, 1950 (unpublished); Proc. Phys. Soc. (London) **A63**, 514 (1950).

is compared with experiment. The negative mesons are not at rest when they decay. From a study of stars made by stopped pions and muons,[14] we have established that 35 ± 15 percent of the muons decay from the K shells of mesonic oxygen, nitrogen or carbon which constitute a 0.4 percent impurity in the gas. The remainder decay from the K shell of mesonic hydrogen. The large fraction decaying from the impurity arises from the long lifetime of mesonic hydrogen and the large cross section for collisions in which the muon is transferred to the impurity. Porter and Primakoff[15] have calculated the expected spectrum shape for a meson decaying from a $1s$ orbit about a nucleus of charge Z.

Their result, $P'(x)$ for $Z<10$, is essentially represented by smearing $P(x)$ with a bell-shaped resolution function $R_1(\sigma,x)$ which has a width at half-maximum $\sigma=\alpha(Z/2)x$, $\alpha=1/137$. Thus

$$P'(x)=\int_0^\infty R_1(\sigma, x-y)P(y)dy. \tag{3}$$

Actually, the equations of reference 15 were used to compute $P'(x)$.

The second modification is the experimental resolution function $R_2(x)$ (Appendix I). Thus,

$$P''(x)=\int_0^\infty R_2(x-y)P'(y)dy. \tag{4}$$

This is much more important than R_1. $P''(x)$ is plotted in Fig. 4 for $\rho=0$, $\frac{1}{4}$, $\frac{1}{2}$, $\frac{3}{4}$, and 1 along with the experimental points.

It is necessary to see whether the data are adequately represented by a curve with some value of ρ and, if such is the case, to define a measure of the reliability of the empirically determined ρ. Assuming the data to

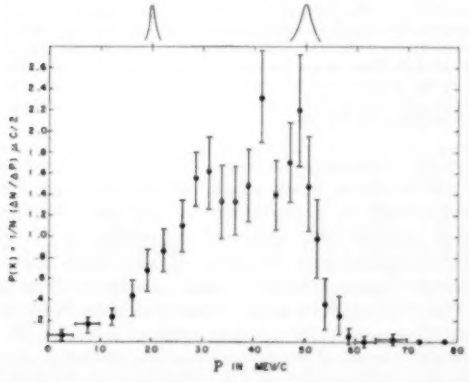

FIG. 3. Spectrum of electrons using "good" resolution. This spectrum includes 282 events which survive the more restrictive criteria designed to yield longer, flatter tracks.

[14] C. P. Sargent, thesis, Columbia University, 1954 (unpublished).

[15] C. E. Porter and H. Primakoff, Phys. Rev. 83, 849 (1951).

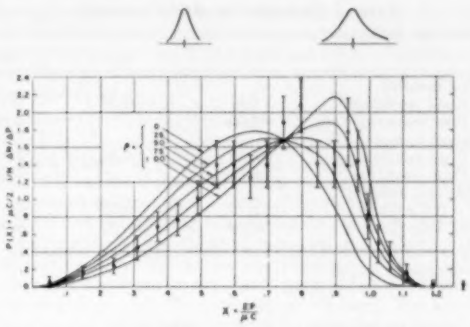

FIG. 4. Theoretical spectra for muon decay. The Michel curves for $\rho=0$, 0.25, 0.50, 0.75, and 1.00 are folded with the experimental resolution of Fig. 2. The poor resolution experimental points are also shown.

represent an unbiased sampling of the μ-electron decay spectrum, there remain five sources of error to consider in comparing theory with experiment.

(i) The uncertainty in the vertical position of the points in Fig. 2 which result from the finite number of events observed in a given momentum interval.

(ii) The uncertainty in the horizontal position of the points which results from conversion of radius of curvature measured in reprojection to electron momentum. The conversion goes via a "momentum scale factor" denoted by H. The uncertainty ΔH in H arises from a lack of precise knowledge of the magnetic field and from imperfect reprojection. Since the field is known to 1.0 percent and the fiduciary mark spacing is reproduced in reprojection to 0.5 percent, $\Delta H/H=0.011$.

(iii) The uncertainty, both vertical and horizontal, in the position of the points which result from a lack of knowledge of $W=\mu/2$. We take $\mu=207.0\pm1.0$ and $\Delta W/W=0.005$. The analysis assumes that two zero-rest-mass neutrinos are emitted in the decay.

(iv) The uncertainty in the position of the curves which results from lack of precise knowledge of the half-width R and the shape S of the momentum resolution function. We find $\Delta R/R\approx0.35$ for the data of Fig. 2. In order to minimize this effect, we have also computed ρ from the better resolution data of Fig. 3. In this way, statistics are traded for resolution in order to uncover any possible large systematic effects which could arise from finite resolution.

The simplest method of obtaining the shape parameter, ρ, from the data is by the method of moments.[16] This method, although statistically not efficient, gives the propagation of various errors quite simply.

Table I summarizes the results of various estimates based on moments. Only the major uncertainties are displayed here.

In Table I, $\Delta\rho_H$ is the contribution to the uncertainty $\Delta\rho$ due to the horizontal scale error ΔH. $\Delta\rho_e$ is the

[16] The ith moment is $\bar{X}_i=\int_0^\infty x^i\rho(x)dx$.

TABLE I. Determination of ρ by moments.

	ρ	$\Delta\rho_H$	$\Delta\rho_s$
First moment			
Good resolution[a]	0.67	+0.05	0.11
Poor resolution[b]	0.60		0.09
Second moment			
Good resolution	0.68	+0.06	0.11
Poor resolution	0.64		0.09
Split first moment			
$0 \leq x \leq 0.75$	0.72	−0.03	0.19
$0.75 \leq x \leq \infty$	0.69	+0.02	0.18

[a] 282 events; see Fig. 3.
[b] 415 events; see Fig. 2.

statistical standard deviation. The split moment is designed to uncover a systematic error in the scale H.

To use the data more efficiently, a least squares analysis has been performed in order to determine ρ and to test the theoretical shape with the best value of ρ determined. To do this, the sum

$$M=\sum_i \frac{[N_{\text{obs}}(x_i)-N_{\text{Michel}}(\rho,x_i)]^2}{N_{\text{obs}}(x_i)}$$

has been evaluated for each of the five curves of Fig. 4. The results are plotted for the poor resolution data in Fig. 5. The curve is fitted by a parabola and the minimum thus determined. The result is:

$$\rho=0.64\pm0.09 \text{ (standard deviation)}.$$

The various confidence levels are indicated on the graph.

The minimum value of $\chi^2[=M(\rho=0.64)]$ is 18 for 18 intervals and one parameter. This agrees well with the statistically expected average chi square which is 16.

Finally, it is necessary to investigate the sensitivity of ρ to the uncertainties ΔH, ΔW, ΔR, ΔS, and ΔF. This is accomplished by varying the indicated parameters by given amounts, which changes the position of either the points or the curves of Fig. 4, and then recalculating ρ.

The results are:

$$\Delta\rho_H=|+3.5\Delta H/H|=3.5\times0.011=0.039,$$
$$\Delta\rho_W=|-2.8\Delta W/W|=2.8\times0.005=0.014,$$
$$\Delta\rho_R=4.4\times10^{-2}\Delta R/R=0.044\times0.35=0.015.$$

If S is Gaussian, ρ is changed by less than 0.005; if $F=1$ (all mesons decay from oxygen) ρ is changed by less than 0.01. The sensitivity of ρ to improvement of the resolution is indicated in Table I and in a comparison of Figs. 2 and 3. The results show that the resolution curve of Fig. 1 contains an undetected "tail" which probably accounts for the events between 65 and 80 Mev.[17] The origin of this tail probably arises from track distortions, not observed in zero field studies which are carried out on flat tracks. The results of Table I indicate that no large error is introduced by the unknown and possibly asymmetric tail in the resolution function.

Combining all uncertainties, we find

$$\rho=0.64\pm0.10 \text{ (standard deviation)}.$$

TABLE II. Beta interaction coupling constants.[a]

Correspondence:	Identical neutrinos $p_{\text{RCE}}\to n_{\text{RCE}}$	Identical neutrinos $p_{\text{RCE}}\to\mu_{\text{RCE}}$	Distinguishable neutrinos $p_{\text{RCE}}\to n_{\text{RCE}}$	Distinguishable neutrinos $p_{\text{RCE}}\to\mu_{\text{RCE}}$
g_p/g_t	+0.5±0.5	+0.5±0.5	+4.5±0.5	+4.5+0.5
g_a/g_t	negative	positive	positive	negative

[a] See reference 19 for notation.

E. DISCUSSION

There has been disagreement between values of ρ obtained by different experiments. Vilain and Williams have examined the decay spectrum of positive muons with an expansion cloud chamber and have found $\rho=0.50\pm0.12$, a value which agrees both with the present work on negative muon decay and with the earlier photographic emulsion measurements of the positive spectrum by Bramson, Havens, and Seifert. However Sagane obtains for positive muons the result $\rho=0.23^{+0.03}_{-0.05}$. The latter result has stimulated an exhaustive search for possible systematic errors. For example, the same set of pictures has yielded a mass measurement for the π^- meson which is about 1 percent below the best value.[11] In addition, several long muon tracks were used to obtain the muon mass by residual

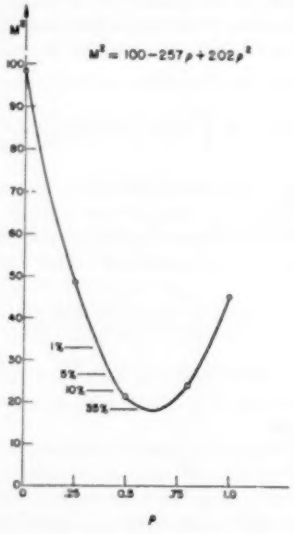

FIG. 5. Chi-square minimum method of estimated ρ from the data of Fig. 2. The probability that chi-square exceeds the value given by the ordinate is also indicated [from H. Cramer, *Mathematical Methods of Statistics* (Princeton University Press, Princeton, 1951)]. Momentum intervals with statistics of fewer than 10 events were pooled to obtain a total of 18 intervals. The number of degrees of freedom for the normalized distribution with one parameter is 16.

[17] The possibility of competing events, e.g., $\mu^-+O^{16}\to(O^{16})^*+\epsilon^-$ contributing to this tail has been ruled out by a recent experiment of Steinberger, Wolfe, and Lokanathan (private communication).

range in hydrogen vs curvature. Also, $\pi^+ \rightarrow \mu^+$ decays at rest were studied. These serve as an independent and overall calibration of the horizontal scale to better than 3 percent. No other sources of error have been discovered. There is of course the (remote) possibility that the spectra of positive and negative muons are different.[18] Before the present results can be applied to a determination of the beta-decay coupling constants, they must be corrected for radiative effects. The inner bremsstrahlung contribution has been computed by Lenard.[19] Nonradiative corrections of the same order have recently been examined.[20] We have estimated that these effects would increase ρ by approximately 0.04. Thus the value of ρ obtained from this experiment is 0.68 ± 0.11, where the error has been increased to allow for the uncertainty in the radiative corrections. Michel and Wightman[21] have discussed the implications of the knowledge of ρ on the beta-decay coupling constants, assuming the usual connections between Fermi interactions. The muon decay spectrum shape may be used to give some information as to the importance of the pseudoscalar component and as to the relative sign of the scalar and tensor interactions. This information is beset by ambiguities of (1) the distinguishability or indistinguishability of the neutrinos in Eq. (1) and (2) the correspondence of the four Fermi particles in nuclear beta decay ($pn\epsilon\nu$) to those in muon decay ($\nu\mu\epsilon\nu$, $\mu\nu\epsilon\nu$, etc.). The acceptable solutions are listed in Table II. The input data are: $|g_s/g_t| = 0.85 \pm 0.13$, $\sigma = 2^8 B/(\mu^5 \tau_\mu \log 2) = 1.22 \pm 0.05$, $\rho = 0.68 \pm 0.11$.[22]

The authors wish to thank Dr. L. Michel, O. Kofoed-Hansen, and J. Steinberger for helpful conversations on this problem.

APPENDIX

A. Angle Measurements

The bottom of the diffusion chamber contains a black glass disk upon which is scribed a grid of fiduciary lines. In measurement the image of the grid is projected onto a rear surface screen at unity magnification. It is generally possible to reproduce all fiduciary dimensions to one part in two hundred.

The camera lens axes are 10 inches apart and intersect the black glass normally. The lenses are 133.5 cm above the glass. The three-dimensional information required for analytical reconstruction of events in space is knowledge of the height z of points on a track above the black glass. Let View A be the reprojection of the picture taken by the camera whose lens axis intersects the black glass at A, with a corresponding definition of View B. Let the displacement of View A of a point on a track from a line DE, perpendicular to AB, be d_A cm, and that in View B be d_B. Then the height z in cm above the black glass of the point on the track is related to $d = d_A - d_B$ by: $z = 131.0d/(25.40+d)$. 131.0 appears in the numerator instead of 133.5 as a result of the effect introduced by the 2.5-inch thick top glass of the chamber. The dip angle of a track is the angle between the tangent to the track and a horizontal plane. z_1 and z_2 are the heights above the black glass of two points 1 and 2 on a track and s is the projected arc length between 1 and 2 as measured in, say, View A. $\Delta z = z_2 - z_1$. Then approximately,

$$\tan\alpha = (\Delta z/s)[1 + (z_1+z_2)/2\times 131.0) + (\Delta z'/s)(b/131.0)],$$

where b cm is the distance, measured in the direction tangent to the track from A to the point on the track halfway between 1 and 2. b is positive if the track is going up as one proceeds along it away from A. If one used View B, s and b would in general be different, but the resulting $\tan\alpha$ should be the same. The first correction term is a magnification correction on z, reflecting the fact that when the reprojection magnification is adjusted to be correct for distances on the black glass projected distances between points above the glass appear too large. The second correction term is the conical reprojection correction to first order in $(\tan\alpha)/131.0$. The above expression for $\tan\alpha$ is adequate for this experiment. Δz may ordinarily be measured to 0.15 cm.

B. Momentum Measurements

A singly charged particle with momentum p and dip angle α moving in a uniform vertical magnetic field of H kilogauss traverses a right circular helix characterized by pitch angle α and radius ρ. P in Mev/c is related to ρ and α by $p = 0.3H\rho/\cos\alpha$, where ρ is measured in cm. Ordinarily in this work $5 \text{ cm} < \rho < 60$ cm and ρ', apparent ρ, is satisfactorily measured by fitting a ruled circular template to the reprojected track. ρ and ρ' are related by

$$\rho = \rho'\left[1 - \frac{z}{131.0} - \frac{2b\tan\alpha}{131.0} + (3b^2 + \tfrac{1}{3}a^2)\tan^2\alpha/(131)^2\right].$$

The symbols have the same meaning and the corrections the same origin as in the expression for $\tan\alpha$. ρ' has reference to the radius of curvature of the reprojected track at a single point, z is the height of that point above the black glass, and a is the distance to the appropriate fiduciary mark measured perpendicular to the track. In the measurement of the μ-decay spectrum the median correction of ρ corresponding to the last term was 0.2 percent. The equation is correct through terms of the second order of cloud-chamber dimensions modulated by $\tan\alpha$ and divided by 131 cm. The use of a finite length of track to measure ρ implies an additional correction of first order in $|\tan\alpha|$, a correction which becomes increasingly important as ρ becomes smaller. For ρ sufficiently small it makes the template method of measurement inappropriate.

The multiple-scattering uncertainty may be calculated. The possible magnitude of photographic and reprojection distortion effects has been checked by photographing ruled templates and has been found to be determined essentially only by the fidelity with which one can reproduce in reprojection the correct relative position of the fiduciary marks. With moderate care, the uncertainty in momentum due to this effect is a small fraction of a percent.

On occasion, the magnetic field was reduced to 120 gauss and the absorber external to the chamber was removed. Most of the particles then photographed would be mesons with a most probable energy of about 65 Mev, or momentum of about 150 Mev/c. Some mesons with decidedly lower momentum and occasional protons and electrons would also be present. The small residual field serves to identify low-momentum tracks whose multiple scattering would otherwise be interpreted as distortion.

The results of this series of photographs lead to the conclusion that for long, flat tracks the turbulence-induced radii of curvature are probably greater than 100 meters.

C. Momentum-Resolution of the μ-Decay Spectrum

The visible length of most of the decay electron tracks is less than 15 cm. For such short tracks the measurement error in the radius of curvature ρ is larger than 1 percent and it makes the major contribution to the total uncertainty of the momentum

[18] W. Panofsky, at the Fifth Annual Rochester Conference on High Energy Physics, presented results of K. Crowe at Stanford on positive muons which indicate a value of $\rho = 0.55 \pm 0.1$. See also Crowe, Helm, and Tautfest, Phys. Rev. (to be published).

[19] A. Lenard, Phys. Rev. **90**, 968 (1953).

[20] R. Finkelstein and R. Behrends, Phys. Rev. **97**, 568 (1955).

[21] L. Michel and A. Wightman, Phys. Rev. **93**, 354 (1954).

[22] J. B. Gerhart, Phys. Rev. **95**, 288 (1954); O. Kofoed-Hansen and A. Winther, Phys. Rev. **86**, 428 (1952) and O. Kofoed-Hansen (private communication).

measurement. In order to assign a standard error to each momentum measurement an estimate of the measurement error was made for each event.

The resolution function $R_2(p,p')$ represents the probability per unit momentum interval of observing electrons with momentum p' if the actual momentum of all electrons is p. If $Q(\sigma)$ represents the probability distribution function of standard momentum errors for all events with momenta roughly equal to p, then an estimate of $R(p,p')$ is:

$$R_2(p,p')=\frac{1}{2\pi}\int_0^\infty Q(\sigma)\exp[-(p-p')^2/2\sigma^2]d\sigma.$$

$R_2(p,p')$ was found for $p=20$ and 50 Mev/c by using events with momenta between 15 and 25, 45 and 55 Mev/c respectively to find $Q(\sigma)$. The resolution functions for $p=20$ and 50 Mev/c are shown on Fig. 2 for all events and on Fig. 3 for the more restricted data.

For the two values of p, the shapes of $R(p,p')$ are very closely identical and the half-widths are nearly proportional to p. The uncertainty in the value of the resolution width is quite large (perhaps of the order of 35 percent) because of the arbitrary nature of the assignment of standard measurement errors to the individual events.

PHYSICAL REVIEW VOLUME 99, NUMBER 3 AUGUST 1, 1955

Asymmetry in High-Energy p-n-p Double Charge-Exchange Scattering*

HUGH BRADNER AND ROBERT E. DONALDSON
Radiation Laboratory, University of California, Berkeley, California

(Received April 4, 1955)

Asymmetries have been observed in double charge-exchange p-n-p scattering from carbon and tantalum. High-energy protons striking a first target gave charge-exchange neutrons. These neutrons were collimated and allowed to strike a second target. The final proton fluxes to the right and left were then counted. The asymmetries are zero at small scattering angles, and increase with angle up to 45° in the laboratory system. The maximum asymmetry observed was 10.4±2.1% for carbon with the first and second scattering angles equal to 45° (lab). Evidence is given for a large n-p charge-exchange polarization from carbon bombarded with 170-Mev neutrons.

INTRODUCTION

POTENTIAL models using tensor forces or spin-orbit coupling have been found[1,2] to give better fit to the experimental n-p angular distribution[3] than those using only central forces. Wolfenstein[4] predicted that the presence of these noncentral forces should give rise to an asymmetry in a double-scattering experiment. The azimuthal asymmetry of a double charge-exchange (p-n-p) scattering has been investigated by Wouters[5] and others,[6-8] with results of the order of a few percent. These asymmetries are much smaller than those obtained by double-proton scattering.[9]

In the experiment presented here, small but experimentally significant asymmetries have been observed in (p-n-p) scattering from carbon and tantalum targets.

This experiment is an extension of Wouters's experiment, with some modification, to elements of higher atomic number. A target was bombarded by the circulating proton beam of the 184-inch cyclotron and the ejected neutrons were collimated and allowed to strike a second target. The right and left fluxes of protons from the second target were then counted.

* This work was performed under the auspices of the U. S. Atomic Energy Commission.

[1] R. S. Christian and E. W. Hart, Phys. Rev. **77**, 441 (1950).
[2] K. M. Case and A. Pais, Phys. Rev. **80**, 203 (1950).
[3] Kelly, Leith, Segrè, and Wiegand, Phys. Rev. **79**, 96 (1950).
[4] L. Wolfenstein, Phys. Rev. **76**, 541 (1949).
[5] L. F. Wouters, Phys. Rev. **84**, 1069 (1951).
[6] J. M. Dickson and D. C. Salter, Proc. Phys. Soc. (London) **A66**, 721 (1953).
[7] Hillman, Culler, and Ramsey, Phys. Rev. **95**, 463 (1954).
[8] Roberts, Tinlot, and Hafner, Phys. Rev. **95**, 1099 (1954).
[9] Chamberlain, Segrè, Tripp, Wiegand, and Ypsilantis, Phys. Rev. **93**, 1430 (1954).

APPARATUS

Experimental Arrangement

Figure 1 shows the experimental arrangement for the p-n-p scattering. The first scattering occurred inside the cyclotron vacuum tank. It was possible to place the first target at each of the following positions: (a) inside the dee in such a position that the observed neutrons came off at an angle of 45° to the right of the circulating proton beam, (b) on the "main probe" in such a position that the observed neutrons came off at 0° to the proton beam (this position provided an unpolarized neutron beam), and (c) on an adjustable probe in such a position that the observed neutrons came off at any desired angle between 0° and 45° to the left of the beam.

TABLE I. Asymmetries measured for carbon and tantalum targets for various angles and rejection energies. The errors are probable errors and include only counting statistics.

First and second target material	First scattering angle	Counter angle ±6°	Bombarding energy (Mev)	Energy of rejection (Mev)	$\epsilon=\frac{L-R}{L+R}$ (percent)
C	17°	25°	190	45	0.4±0.4
C	17	25	190	75	1.9±0.8
C	17	25	190	110	0.5±1.9
C	30	45	225	85	8.7±2.2
C	35	35	245	90	5.2±2.0
C	45	45	340	45	4.3±1.2
C	45	45	340	85	10.4±2.1
C	45	45	340	110	10.5±2.5
Ta	17	25	190	45	1.0±0.5
Ta	17	25	190	85	−1.0±0.3
Ta[a]	45	45	340	45	2.2±2.5
Ta[a]	45	45	340	85	6.0±2.2
Ta[a]	45°	45°	340	110	4.5±2.5

[a] These values are an average of a 45° left and 45° right first scatter.

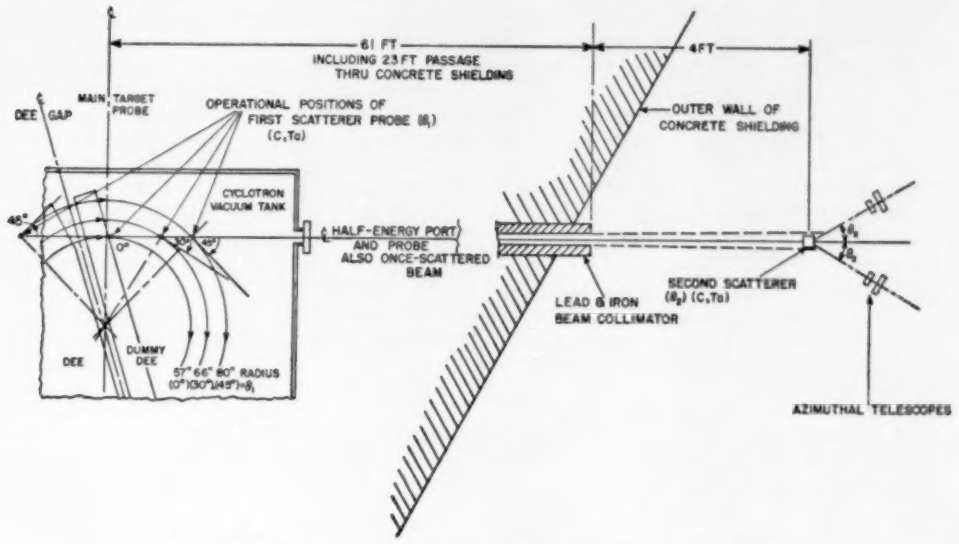

FIG. 1. Schematic layout of p-n-p polarization experiment (scale not uniform).

The maximum proton beam energy was 340 Mev. In the approximation of nonrelativistic nucleon-nucleon collisions between protons of the beam and target nucleons at rest, one sees from the geometry that the energy of the neutrons is a constant, independent of the scattering angle. There is, of course, a variation in energy of the ejected neutrons because of the internal momentum distribution inside the target nucleus. As the momentum of the bombarding protons changes with a change of scattering angle, this variation in energy is a function of the scattering angle.

The second target was placed in the collimated neutron beam. The fluxes of protons to the right and left of the axis of the neutron beam were measured simultaneously by means of two counter telescopes.

Targets, Counters, and Electronics

Targets of carbon and tantalum were used. The first and second tantalum targets were both of 10 g/cm² thickness. The first and second carbon targets were 4.1 g/cm² and 1.5 g/cm², respectively. The solid angle subtended by the second target from the first target was 2×10^{-4} steradian.

The right and left counter telescopes were made as nearly identical as possible. The counters were all liquid scintillators with dimensions of 2 by 2 by ¼ inches for the front and 3.5 by 3 by 0.75 inches for the rear counters. The solid angle subtended by the counter telescopes from the second target was 0.04 steradian. The counter photomultipliers were adequately shielded from stray fields by means of soft iron and μ metal.

Crystal diode double-coincidence circuits with diode clamps were used for both telescopes. Each circuit had a resolution time of 10^{-8} sec.

The plateaus of the coincidence counting rates with respect to the photomultiplier high voltages were located by raising the voltages until the coincidence counting rate for a pair of counters remained constant when the voltage of either counter was lowered by 100 volts. In addition, all counters were supplied by the same high-voltage source to help avoid false asymmetry due to high-voltage drifts.

PROCEDURE

With the first target in the 0° position, the second target and the collimators were aligned by means of a telescope situated about 75 feet from the first target. This defined the axis of the scattered neutron beam. The counter telescopes were then placed in the plane of the first scattering at approximately equal angles to the right and left of the axis of the neutron beam.

With the unpolarized (0°) neutron beam in use, the counting rates in the right and left telescopes, with background subtracted, were equalized by small adjustments in the detector angles. The backgrounds, which were of the order of 10%, were determined by counting with the second target removed. The above adjustments were always within the limits of the estimated error of about 0.3° in the original positioning. This procedure had the effect of eliminating false asymmetries due to small differences in solid angle and counter efficiencies between the right and left telescopes. The counters were then left fixed throughout the run, and all angle changes were made by moving the first scatterer (situated inside the cyclotron).

Counting rates were then obtained for both a 45° left and a 45° right first scatter. Asymmetries of the same magnitude but opposite sign, obtained for right and

left first scatterings, provided a check on the alignment. With the second-scattering angles held constant, asymmetries were then measured for various first-scattering angles.

Some runs were made with copper absorbers placed between the first and second counters of each telescope. This absorber determined the minimum proton energy accepted. In this manner asymmetries were measured as a function of a "rejection energy."

RESULTS

The observed asymmetry e in a double scattering experiment can be defined by the equation $e=(L-R)/(L+R)$, where L and R are the counting rates observed at equal scattering angles to the left and right of the first scattered beam.

Table I shows the asymmetries observed from tantalum and carbon targets at various angles and rejection energies. The errors quoted are probable errors and include only counting statistics. To determine one source of error due to misalignment, the internal targets were displaced perpendicular to the beam by an amount equal to the estimated error of positioning, about $\frac{1}{16}$ in. This displacement gave a change of asymmetry of less than 1%.

CONCLUSIONS

The azimuthal asymmetries for a double charge-exchange scattering from carbon and tantalum are small and in general agreement with previous investigations.[5,6-8]

As might be expected from the Fermi gas model, no significant difference was found between carbon and tantalum. The asymmetries show an increase with angle up to 45° (lab).

The relatively high asymmetry at 45° (lab) is not consistent with the Serber potential (50% exchange). This potential gives no odd angular momentum states, and predicts an asymmetric distribution about 45°.[10]

The subsequent measurement of the p-n quasi-elastic polarization using a proton beam of known polarization[11,12] allows an estimate to be made of the n-p charge exchange polarization for carbon bombarded by 170-Mev neutrons. The p-n quasi-elastic polarization for 315-Mev incident protons is, from Chamberlain *et al.*,[13] $P_1=-16\%\pm2\%$. Ignoring the energy difference, we can apply this polarization to the p-n-p asymmetry for a 45°–45° (lab) scattering through the relation $e=P_1P_2$, where P_1 is the polarization in the first scattering and $P_2=P_2(E,\theta)$ is the polarization in the second scattering. A polarization is obtained for 170-Mev neutrons scattered at 45° equal to $P_2(170, 45)=-64\%\pm15\%$. The same procedure can be applied to the 30°–45° and the 35°–35° p-n-p asymmetries. Using the p-n polarization at 285 Mev given in the following paper, and again ignoring the energy difference between the p-n and p-n-p initial energies, we obtain the polarizations $P_2(170, 45)=-43\%\pm9\%$ and $P_2(170, 35)=-29\%\pm12\%$. The errors quoted are all probable errors and the angular resolution for the second scattering was 12°. The energy extrapolation used in these calculations is quite doubtful; there is some evidence, however, for a large n-p charge-exchange polarization at a neutron energy of 170 Mev and angles near 45° (lab).

It should be noted that because of the internal momentum distribution of the nucleons in the target, the angles at which the asymmetries are measured actually correspond to averages over a distribution of nucleon-nucleon collision angles.

[10] D. Swanson, Phys. Rev. **89**, 749 (1953).
[11] Chamberlain, Donaldson, Segrè, Tripp, Wiegand, and Ypsilantis, Phys. Rev. **95**, 580 (1954).
[12] R. E. Donaldson and H. Bradner, following paper [Phys. Rev. **99**, 892 (1955)].
[13] Chamberlain (private communication).

PHYSICAL REVIEW VOLUME 99, NUMBER 3 AUGUST 1, 1955

Asymmetry in p-n and p-p Scattering from Targets Bombarded with 285-Mev Polarized Protons*

ROBERT E. DONALDSON AND HUGH BRADNER
University of California, Radiation Laboratory, Berkeley, California
(Received April 4, 1955)

Asymmetries in neutron and proton production have been observed in the quasi-elastic scattering of 285-Mev, 65±4% polarized protons by carbon, lithium, and beryllium targets. The neutrons and protons were counted in coincidence with the associated scattered protons. The quasi-elastic neutron data are not antisymmetric about 90° cm. The proton asymmetries are much smaller than the asymmetries from a free hydrogen target.

INTRODUCTION

IN the preceding paper, results on double charge-exchange asymmetry were presented. This paper gives the results of a different approach to the n-p polarization problem and also the p-p polarization problem.

With certain restrictions,[1] the left-right asymmetry of the counting rate of neutrons in a p-n collision can be

* This work was done under the auspices of the U. S. Atomic Energy Commission.

[1] H. Bradner and R. Donaldson, Phys. Rev. **95**, 1701 (1954).

expressed by

$$\epsilon=(L-R)/(L+R)=P_pP_{pn},$$

where ϵ is the asymmetry, L and R are the neutron counting rates at equal angles to the left and right, P_p is the polarization of the incident proton beam, and P_{pn} is the polarization which would occur in a p-n collision in which the initial nucleons were unpolarized. In this experiment the polarized proton beam developed by Chamberlain *et al.*[2] was used as the first scattered beam. Neutrons and protons ejected from the second target were then counted in coincidence with the scattered protons (quasi-elastic coincidence).

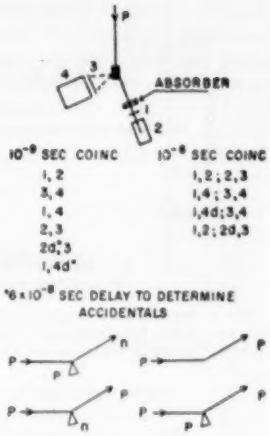

FIG. 1. Experimental setup showing counter arrangement and events recorded. Solid angle subtended by the 1, 2 counter was approximately 0.2×10^{-2} to 0.8×10^{-2} steradian; that of 3, 4 was approximately 0.03 to 0.3 steradian.

APPARATUS

Experimental Arrangement

The polarized proton beam was obtained by scattering the internal proton beam of the 184-inch cyclotron on a Be target, and by bringing this beam out into the experimental area by the method described in reference 2. This beam has a polarization of 65.0 ± 4 percent, an energy of 285 ± 15 Mev, and a flux of approximately 10^5 protons per second entering the bombardment area.

Counters and Targets

Figure 1 shows the general arrangement of the target and counters in the bombardment area.

The counters were all plastic scintillators. Counters 1 and 3 were rectangular in shape, 3 by 3 by 0.25 in., and 6.5 by 6.5 by $\frac{7}{16}$ in., respectively. Counters 2 and 4 were cylindrical, 2 in. diam by 7 in. long, and 5.5 in. diam by 4 in. long, respectively. The angle between telescopes 1, 2 and 3, 4 was kept at 85° in the laboratory system. This angle is the approximate relativistic nucleon-nucleon scattering angle. The distances between the second scatterer and the telescopes were altered for different angles of observation in order to obtain an optimum ratio of counting rate to background. The solid angle subtended by the 1, 2 telescope was varied between 0.2×10^{-2} and 0.8×10^{-2} steradian, and that subtended by the 3, 4 telescope was varied between 0.03 and 0.3 steradian. The counter phototubes were surrounded by soft iron and μ metal to shield against stray magnetic fields. It was shown that the shielding eliminated any effect of the magnetic field on the photomultipliers.

The targets were thin slabs, of vertical dimension greater than that of the incident beam. The thin dimension was oriented perpendicular to the incident beam in order to allow the scattered particles to get out of the target. The targets had the following composition and dimensions: carbon, $1\frac{1}{16}$ by $\frac{11}{16}$ by 9 in.; beryllium, 2 by $\frac{5}{16}$ by 4 in.; lithium, 3 by 0.25 by 3 in.

[2] Chamberlain, Segrè, Tripp, Wiegand, and Ypsilantis, Phys. Rev. **93**, 1430 (1954).

Electronics

Figure 1 shows the coincidences demanded from the four counters. The output of each of the four counter photomultipliers was amplified by distributed amplifiers and then split into two channels. The signals from the first of the two channels (from each of the four counters) were mixed directly into fast-coincidence circuits of 10^{-8}-sec resolution in the four possible combinations of pairs. The signals from the other channel were further amplified and fed into two 10^{-8}-sec coincidence circuits with outputs 4 and 2 delayed in time by one rf cycle (6×10^{-8} sec). The delayed circuits gave a simultaneous measurement of accidental events. The outputs of the 10^{-8}-sec coincidence circuits were then amplified by linear amplifiers, shaped by variable gates, and mixed appropriately (see Fig. 1) into coincidence circuits of 10^{-6}-sec resolution time.

PROCEDURE

The position of the beam was found by means of x-ray film, and the target was then placed in the center of the beam. Photographs were taken periodically to monitor possible changes in the beam position. All the counter angles were measured with a transit centered at the target position. The estimated angular error was of the order of 0.1°, and intentional misalignments of this amount gave errors in asymmetry of less than 1%.

The plateaus of the counters were located by raising the photomultiplier voltages until the coincidence counting rate for a pair of counters remained a constant when the output pulses from either counter were attenuated by a factor of two.

The incident beam was monitored by an argon-filled ionization chamber.

An absorber that rejected protons of energy less than $0.7E_0\cos^2\theta$ was placed in front of Counter 1, where E_0 was the energy of the polarized proton beam and θ was

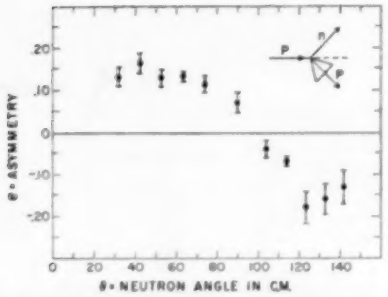

FIG. 2. Asymmetry e plotted as a function of the center-of-mass neutron angle for proton-neutron quasi-elastic scattering in carbon. The errors shown include only counting statistics.

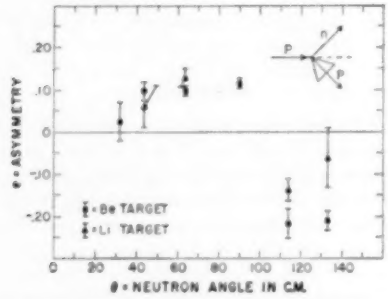

FIG. 3. Asymmetry e plotted as a function of the center-of-mass neutron angle for proton-neutron quasi-elastic scattering in lithium and beryllium. The errors shown include only counting statistics.

the angle of the 1, 2 telescope. This absorber reduced the accidental singles rate in Counter 1 and increased the efficiency for counting fast protons by increasing their pulse heights. The proton-proton coincidence counting rate was found to be independent of this absorber; thus no quasi-elastic events were excluded by the absorber. The value $0.7E_0\cos^2\theta$ was chosen in order to measure separately the proton asymmetry obtained without using the recoil particle in coincidence, and to compare with the results of a similar experiment by Chamberlain *et al.*[2] The observed asymmetries agreed with those observed by Chamberlain, within the statistical errors. When absorbers of greater thickness than the proton range were placed in front of Counter 1, the remaining counting rate decreased by the amount expected from nuclear attenuation alone, thus indicating that neutrons were being counted.

Background counts were determined by removing the target.

RESULTS

Figure 1 shows the events measured. Figures 2 and 3 show the asymmetries observed for neutrons from carbon, lithium, and beryllium. It should be noted that for center-of-mass angles greater than 90° the neutrons were defined by the telescope with poor angular resolution.

Figures 4 and 5 show the p-p quasi-elastic asymmetries obtained for carbon, lithium, and beryllium.

The polarization can be calculated by the relation $e=0.65P_{pn}$.

The p-n asymmetries for Li, Be, and C are not antisymmetric about 90° cm. All three curves show positive asymmetries at this angle. There is indication that asymmetries in the backward direction are greater than in the forward direction.

The p-p quasi-elastic polarization is considerably smaller at all angles than the p-hydrogen polarization.[2]

A similar p-n experiment has been done by Chamberlain *et al.*,[3] with a liquid deuterium target. The n-p polarization they obtain from deuterium agrees, within statistics, with our results from carbon.

ACKNOWLEDGMENTS

The authors are indebted to Dr. Edward Teller, who initiated the experiments, Dr. Luis W. Alvarez for continued support and advice during the experiments, and Dr. Louis Wouters, who furnished equipment that

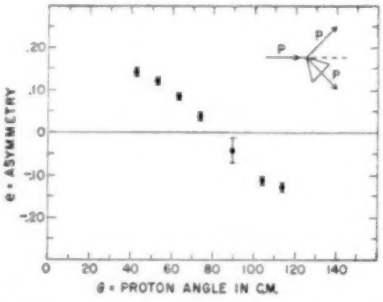

FIG. 4. Asymmetry e plotted as a function of the center-of-mass proton angle for the proton-proton quasi-elastic scattering in carbon. The errors shown include only counting statistics.

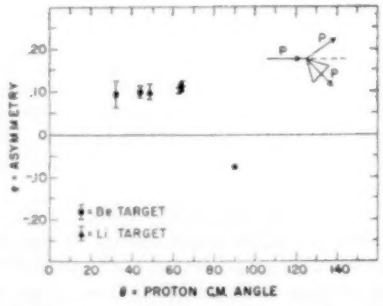

FIG. 5. Asymmetry e plotted as a function of the center-of-mass proton angle for the proton-proton quasi-elastic scattering in lithium and beryllium. The errors shown include only counting statistics.

[3] Chamberlain, Donaldson, Segrè, Tripp, Wiegand, and Ypsilantis, Phys. Rev. **95**, 850 (1954).

he was constructing for a p-n-p experiment. They are deeply indebted to Mr. Richard Blumberg, Dr. Frank Crawford, Jr., Miss Claire E. Johnson, Mr. H. Brook Knowles, Mr. Vern Ogren, and Dr. M. Lynn Stevenson for assistance during the experiments, and Dr. Warren Heckrotte, Dr. Malvin Ruderman, Dr. Stephen Tamor, and Dr. Lincoln Wolfenstein for interesting discussions on polarization. The authors also wish to thank James Vale and the 184-inch cyclotron crew for their cooperation during the bombardments.

PHYSICAL REVIEW VOLUME 99, NUMBER 3 AUGUST 1, 1955

Proton-Proton Scattering in Nuclear Emulsions at 432 Mev*

S. K. Kao† and A. F. Clark‡
Carnegie Institute of Technology, Pittsburgh, Pennsylvania
(Received January 6, 1955; revised manuscript received April 25, 1955)

High-energy protons from the unpolarized external beam of the Carnegie Institute of Technology cyclotron were sent through Ilford *G5* nuclear emulsions of the normal and 4× gelatin types. The emulsions were area-scanned for *V*-shaped stars representing events of elastic collisions of the incident protons with hydrogen nuclei in the emulsions. These events were identified through angular measurements. With known densities of hydrogen atoms in the emulsions, the differential cross sections of proton-proton elastic scattering were calculated. The result is consistent with counter measurements.

SINCE the advent of high-energy machines in various laboratories, proton-proton scattering experiments have been among the first group performed because of the fundamental importance of studying nucleon-nucleon interactions. The present work was performed to verify counter techniques applied in the energy region of 440 Mev. In the present work, we use the hydrogen atoms of the gelatin in nuclear emulsions as the target for the high-energy proton beam and study the angular distribution of the elastic collisions identified by means of angular measurements. The advantages of this method are: (1) the complete event, incoming and both scattered protons are recorded simultaneously; with energy discrimination and ability to recheck everything; (2) relative differential cross sections are independent of errors in monitoring; (3) it is possible to observe events to as low an angle as 5°; (4) the ratio of the background to the elastic events is relatively low. On the other hand, the chief disadvantages are the low statistics for the amount of work involved and the uncertainty in the personal error of missing events during scanning.

Photographic plates 1 in. by 3 in. with 200 micron Ilford *G5* emulsions of normal and 4× gelatin types were exposed to the external proton beam of the Carnegie Institute of Technology cyclotron. The plates subtended an angle of 0.2° from the collimator hole and were area-scanned for events corresponding to the elastic scattering of protons from hydrogen nuclei in the emulsion. The technique has the advantage of positive identification of events and the disadvantage of requiring excessive time to obtain good statistics.

Between 1 and 4×10^6 protons per cm^2 passed through the plates parallel to the supporting glass and perpendicular to the long edges of the plates. With these exposures, some events were missed when both of the proton tracks had low grain densities (cases close to symmetrical scattering) or when their scattering planes made large angles (ϕ) with the field of view in the microscope. Therefore, we do not include in our data events near the symmetrical scattering angles and limit ourselves to small azimuthal angles (ϕ). From the point of view of identifying events from the background, it is also necessary to limit ourselves to small ϕ because space angles can be measured more accurately and there is less distortion of tracks during shrinkage.

In order to eliminate the contribution of background events, i.e., quasi-elastic collisions of incident protons with the nuclear protons of elements in the emulsion other than hydrogen, we set the following stringent criteria for an elastic collision event:

(1) The tracks must have the proper grain densities (energy discrimination).

(2) The three tracks must be coplanar, i.e., the azimuthal angles ϕ of the two scattered tracks must be within 2° of each other (coplanarity).

(3) The space angle between the scattered proton tracks must agree with the calculated angle within 1° (correct space angle).

As θ (the scattering angle in the center-of-mass system) decreases below 20°, the angular tolerances were increased by a factor of two because of the difficulty in measuring the ϕ of the forward (high-energy) track due to the small projected angle and the inaccuracy in measuring the low-energy dark track due to distortion and scattering in the emulsion. When such

* Work supported in part by the U. S. Atomic Energy Commission.
† Submitted in partial fulfillment of the requirements for the degree of Doctor of Philosophy at Carnegie Institute of Technology.
‡ Now at University of California Radiation Laboratory, Livermore, California.

TABLE I. Number of events, and from these the differential cross sections, in various angular regions.

θ limits	16.2°	36.9°	53.1°	66.4°
$1-\cos\theta$ limits	0.04 0.20	0.40	0.60	
Fraction of solid angle in the forward hemisphere	0.16	0.20	0.20	
Limiting ϕ	30°	30°	30°	
Number of events	18	19	21	
Mean $d\sigma/d\Omega$ in mb/sterad	4.5±1.1	3.6±0.8	3.9±0.9	
Mean $d\sigma/d\Omega$ in mb/sterad from counter data[a,b]	4.0±0.1	3.7±0.1	3.5±0.1	

[a] See reference 1.
[b] See reference 2.

a track stops in the emulsion, the range becomes a reliable check.

The mean proton energy in the plates is 432±8 Mev (including the uncertainty and spread of the peak energy).[1,2] The differential cross sections were calculated on the basis of mean free path from the total length of incident tracks through a volume of emulsion with a known number of atoms of hydrogen.

The main errors are governed by the statistics and the efficiency of scanning. Our estimate of the latter, based on extensive rescanning, gives an efficiency of 97±3 percent.

RESULTS

Three groups of data were obtained.

The first group consists of 58 elastic events in normal emulsion; 50 satisfy the stringent criteria for elastic events and 8 fall inside the doubled tolerances allowed for small-angle scattering. The upper limit for θ is chosen at 66.4° because of low scanning efficiency at large angles. Also a higher quasi-elastic background is expected above this angle from a theoretical estimate. The lower limit for θ is chosen at 16.2° because the scanning efficiency decreases when the low-energy protons tracks are short and angular measurements of thick tracks are not too reliable.

The number of events in each angular region are added up and listed in Table I which also gives the differential cross sections deduced from these numbers. The corresponding average cross sections obtained by the counter group are also listed.[1,2]

In the same volume and angular region, we found 15 quasi-elastic events within 5° of the correct space angle and 5° of the coplanarity, which implies a background of 2 percent in the region of acceptance randomly distributed.

The second group of data is concerned with further work to find small angle events, chiefly with diluted (4×) emulsions which have four times as much gelatin as normal *G*5 emulsions. Because of the low grain densities we limit ourselves to θ less than 44.4°. The grain densities of the low-energy tracks are already quite small in the region of θ between 36.9° and 44.4°; thus, we limit ϕ to 20°, which corresponds to 35° in normal emulsion and is therefore close to our former limit of 30°. At the smaller angles, we allow ourselves a higher limit in ϕ up to 50°, because the tracks are sufficiently dark to be seen and the lower distortion permits reliable measurements.

Table II shows the total number of events in each angular region and the differential cross sections. The

TABLE II. Number of events and the deduced differential cross sections at small angles.

θ limits	16.2°	25.8°	36.9°	44.4°
$1-\cos\theta$ limits	0.04 0.10	0.20	0.30	
Fraction of solid angle in the forward hemisphere	0.06	0.10	0.10	
Limiting ϕ	50°	30°	20°	
Number of events	22	30	12	
Mean $d\sigma/d\Omega$ in mb/sterad	4.6±1.0	5.4±1.0	3.2±0.9	
Mean $d\sigma/d\Omega$ in mb/sterad from counter data[a,b]	4.1±0.1	3.9±0.1	3.7±0.1	

[a] See reference 1.
[b] See reference 2.

cross section in the region $0.1<1-\cos\theta<0.2$ is less than two probable errors above the counter result.

A third group of six events was found during part of the scanning of the second group. These events lie between 5° and 16.2°. The choice of a lower limit of 5° assumes that tracks with ranges more than 10 microns are seen. Because of the shortness of the tracks ending in the emulsion we choose 40° as the upper limit for ϕ. These 6 events represent a cross section of 4mb/sterad, which is more compatible with destructive than constructive Coulomb interference.[3,4]

ACKNOWLEDGMENTS

We are indebted to J. Morrison and R. Reiter for aid in scanning a portion of the plates, and to the proton counter group[1,2] of the Carnegie Institute of Technology cyclotron for the use of their equipment and for their help during the exposure of the plates. Finally, we wish to thank Professor J. Ashkin and Professor L. Wolfenstein for enlightening discussions.

[1] Sutton, Fields, Fox, Kane, Mott, and Stallwood, Phys. Rev. **95**, 663 (1954).
[2] Sutton, Fields, Fox, Kane, Mott, and Stallwood, Phys. Rev. **97**, 783 (1955).
[3] D. Fischer and G. Goldhaber, Phys. Rev. **95**, 1350 (1954).
[4] Chamberlain, Pettengill, Segrè and Wiegand, Phys. Rev. **95**, 1348 (1954).

K-Series X-Rays from π-Mesonic Atoms*†

M. Camac, A. D. McGuire,‡ J. B. Platt, and H. J. Schulte§
University of Rochester, Rochester, New York

(Received April 28, 1955)

The K-series x-rays from the π-mesonic Be, B, C, N, and O atoms have been studied. In each case measurements have been made of the $2p$-$1s$ quantum energy, and of the fraction of stopped pions which give rise to K-series x-rays (the "K-series yield"). The yields are: Be, 18.8±1.7%; B, 13.6±1.5%; C, 9.5±1.0%; N, 4.5±0.5%; O, 3.4±0.4%. The decrease in yield with increasing Z is attributed to nuclear absorption of the pion from the $2p$ state. The $2p$-$1s$ quantum energies are: Be, 43±3.5 kev; B, 68±3.5 kev; C, 92±7.5 kev; N, 132±2.5 kev; O, 163.8±2.7 kev. The expected energy in the case of oxygen, if only electromagnetic interactions are important, is 176.0 kev; the difference is presumably due to a pion-nucleus interaction which is repulsive in the $1s$ state.

I. INTRODUCTION

THE formation of a mesonic atom as a step in the absorption process for negative mesons has been postulated for some time, and evidence for the existence of such atoms has been obtained both with cosmic ray[1–3] and machine produced[4–6] mesons. We have observed the K-series x-rays from the π-mesonic Be, B, C, N, and O atoms. In each case we have measured the quantum energy, and have determined the fraction of the stopped pions which give rise to radiative transitions to the mesonic $2s$ level.

The sequence of events from the stopping of a negative meson in condensed matter to the absorption of the meson by a nucleus has been considered in detail by several authors.[7] A pion is first bound to a particular nucleus in a quantum state characterized by large values of the principal and orbital quantum numbers ($n, l \sim 16$). The cascade process to lower energy states can occur through Auger[8] or radiative[9] transitions. The Auger effect predominates, in the low-Z elements considered here, for transitions between states of $n \geq 3$. Then radiative transitions become important, and nuclear capture competes with radiation in depleting these states of low quantum number.

Our determination of the fraction of stopped pions which give rise to the $2p$-$1s$ radiative transition (the $2p$-$1s$ "quantum yield") thus measures the nuclear capture probability for pions in the $2p$ state. We shall discuss the limits of validity of this measurement below. The branching ratio is expected to have a Z^3 dependence, since the radiative transition probability varies as Z^4 and the nuclear absorption probability varies as Z^5. (There are Z protons in the nucleus and the fraction of the time the $2p$ pion spends in the nucleus varies as Z^5.) Messiah and Marshak[10] predict the branching ratio to be $0.2Z^3$, and our results are consistent with this prediction.

The measured quantum energies are in all cases within 10% of the energies predicted by assuming electromagnetic interactions only between the pion and the nucleus. For nitrogen and oxygen, however, the measured $K\alpha$ quantum energies are less than the predicted values by 2% and 7% respectively. We believe these differences are significant. They pre-

* This research was assisted by the U. S. Atomic Energy Commission.

† Based in part on theses submitted by A.D. McGuire and H. J. Schulte to the Graduate School of the University of Rochester in partial fulfillment of the requirements for the degree of Doctor of Philosophy.

‡ Now at the University of Minnesota, Minneapolis, Minnesota.
§ Now at Los Alamos Scientific Laboratory, Los Alamos, New Mexico.

[1] Experimental evidence for radiative transitions in μ-mesonic atoms: W. Y. Chang, Revs. Modern Phys. **21**, 166 (1949); E. P. Hincks, Phys. Rev. **81**, 313 (1951); A. Farfarman and M. H. Shamos, Phys. Rev. **87**, 219 (1952); G. G. Harris and T. J. B. Shanley, Phys. Rev. **89**, 983 (1953); F. D. S. Butement, Phil. Mag. **44**, 208 (1953); W. Y. Chang, Phys. Rev. **95**, 1288 (1954).

[2] Experimental evidence for μ-mesonic Auger transitions: Cosyns, Dilworth, Occhialini, and Schoenberg, Proc. Phys. Soc. (London) **A62**, 801 (1949); C. Franzinetti, Phil. Mag. **41**, 86 (1950); W. F. Fry, Phys. Rev. **79**, 893 (1950); A. Bonetti and G. Tomasini, Nuovo cimento **8**, 693 (1951); Groetzinger, Leder, and Ribe, Phys. Rev. **81**, 626 (1951).

[3] Experimental evidence for π-mesonic Auger transitions: Menon, Muirhead, and Rochat, Phil. Mag. **41**, 583 (1950).

[4] Experimental evidence for radiative transitions in π-mesonic atoms: Camac, McGuire, Platt, and Schulte, Phys. Rev. **88**, 134 (1952); Schulte, Platt, and Camac, Phys. Rev. **89**, 905 (1953); Camac, Platt, and Schulte, Phys. Rev. **89**, 905 (1953); Stearns, DeBenedetti, Stearns, and Leipuner, Phys. Rev. **93**, 1123 (1954); McGuire, Camac, Halbert, and Platt, Phys. Rev. **95**, 625 (1954); Sterns, Sterns, Leipuner, and DeBenedetti, Phys. Rev. **95**, 625 (1954); Sterns, Sterns, DeBenedetti, and Leipuner, Phys. Rev. **95**, 1353 (1954); Sterns, Sterns, DeBenedetti, and Leipuner, Phys. Rev. **96**, 804 (1954); Sterns, Sterns, DeBenedetti, and Leipuner, Phys. Rev. **97**, 240 (1955).

[5] Experimental evidence for radiative transitions in μ-mesonic atoms: V. Fitch and J. Rainwater, Phys. Rev. **92**, 789 (1953); Sterns, DeBenedetti, Sterns, and Leipuner, Phys. Rev. **93**, 1123 (1954); Koslov, Fitch, and Rainwater, Phys. Rev. **95**, 291 (1954); **95**, 625 (1954).

[6] Experimental evidence for μ-mesonic Auger transitions: H. Morinaga and W. F. Fry, Nuovo cimento **10**, 308 (1953); W. F. Fry, Nuovo cimento **10**, 490 (1953).

[7] R. E. Marshak, *Meson Physics* (McGraw-Hill Book Company, Inc., New York, 1952), Chap. 5. Marshak gives a summary of the original papers and many references. References on the problem of meson capture not listed by Marshak include: R. Huby, Phil. Mag. **40**, 685 (1949); R. L. Rosenberg, Phil. Mag. **40**, 759 (1949).

[8] E. H. S. Burhop, *The Auger Effect* (Cambridge University Press, Cambridge, 1952), Chap. 7. G. R. Burbridge and A. H. de Borde, Phys. Rev. **89**, 189 (1953); B. L. Joffe and I. Ya. Pomeranchuk, Zhur. Eksptl. Teort. Fiz. **23**, No. 1 (7), 123-4 (1952); A. H. de Borde, Proc. Phys. Soc. (London) **A67**, 57 (1954).

[9] H. A. Bethe, *Handbuch der Physik* (Verlag Julius Springer, Berlin, 1933), second edition, Vol. **24**, Part 1, 440.

[10] A. M. L. Messiah and R. E. Marshak, Phys. Rev. **88**, 678 (1952).

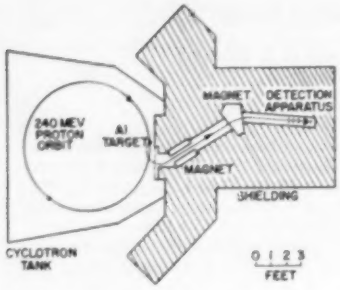

FIG. 1. Experimental arrangement in cyclotron room.

sumably indicate a meson-nuclear interaction which is repulsive for a meson in the 1*s* state.[11]

II. EXPERIMENTAL METHOD

The experiment arrangement is shown in Fig. 1. Pions were produced in an aluminum target in the University of Rochester 240-Mev synchrocyclotron. Negative pions of approximately 50-Mev energy were deflected and focused by the fringing field of the cyclotron magnet and by a separate external magnet. The π-meson beam was defined by the 6-in. horizontal and 3-in. vertical entrance aperture of the secondary magnet and by the 1½-in. diameter of the meson telescope. Identification of the particles as pions was by their magnetic rigidity and range in aluminum.

X-Ray Detection Apparatus

The detection apparatus is shown schematically in Fig. 2. All detectors, except counter 5 were plastic scintillators. This apparatus was used both (1) for taking range measurements and determining the particle composition of the meson beam, and (2) for observing mesonic x-rays. A threefold telescope (counters 1, 2, and 3) defined the incoming pion beam. An aluminum step wedge between counters 2 and 3 was adjusted so that the pions stopped in a block of low-Z material inserted between counters 3 and 4. (We shall call the block the "stopper".) Counters 4 and 6 were used in anticoincidence. Counter 4 rejected events in which

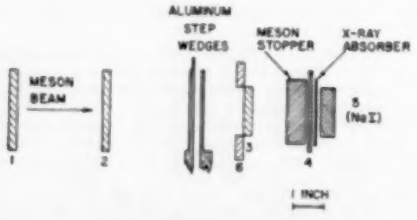

FIG. 2. Detection apparatus.

[11] Deser, Goldberger, Baumann, and Thirring, Phys. Rev. **96**, 774 (1954).

charged particles went completely through the meson stopper. Counter 6 was a 3 in.×3 in. plastic counter with a 1.5-in. diameter hole in the center. It rejected events in which a pion outside the beam defined by counter 3 gave rise to a count in 3 by a secondary process.

The x-ray detector, counter 5, was a cylindrical NaI(Tl) crystal of 1½ in. diameter enclosed in a moisture-proof container[12] and mounted on the photocathode of a DuMont type 7292 photomultiplier. Its thickness was equal to several mean free paths for the x-rays under study.

A block diagram of the coincidence circuit is shown in Fig. 3. The resolving time of the coincidence system

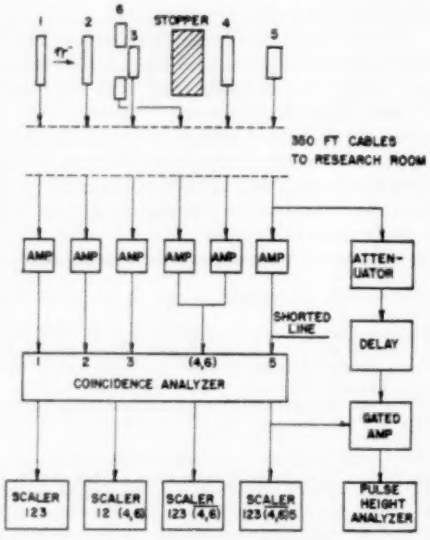

FIG. 3. Simplified block diagram of the electronic equipment. Coincidence inputs to scalers shown here are those used while recording mesonic x-ray spectra. Other coincidence combinations could be selected for other purposes.

was about 5×10^{-8} sec. Events causing the coincidence, anticoincidence combination $1\text{–}2\text{–}3\text{–}\bar{4}\text{–}5\text{–}\bar{6}$ opened the 0.5-microsecond gate of the gated amplifier. The amplitude spectrum of the pulses in counter 5 which occurred in time coincidence with the above type of event was measured on the 24-channel pulse-height analyzer. Energy calibration of the system was established by means of x-rays from artificial radioactive sources.

Because of the large amount of background radiation and the high detection efficiency of the NaI crystal, approximately five feet of brass were required as shielding between the cyclotron and the x-ray detector. The purpose of the shielding was to attenuate fast particles (mainly neutrons) originating in the cyclotron.

[12] C. J. Borkowski and R. L. Clark, Rev. Sci. Instr. **24**, 1046 (1953).

In addition the detector was surrounded in all directions except that of the incident pion beam, by several additional feet of brass, lead, and concrete to attenuate secondary neutrons and gamma rays which scattered about the cyclotron building. Under operating conditions, a typical background counting rate of events in which more than 20 kev of energy was lost to the NaI crystal was 3×10^4/sec during the time the proton beam irradiated the target. At such background counting rates the random coincidence rate of 1–2–3–$\bar{4}$–5 events (the bar denotes anticoincidence) was negligible, and the probability of detecting an unwanted event in an arbitrary opening of the 0.5-μsec gate was also negligible ($\sim10^{-3}$). We nevertheless observed broadening of the x-ray pulse height spectra if the background substantially exceeded this value. We believe the important time constant in this connection is the recovery time of the NaI crystal from the occurrence of a high-energy event to the time at which this event contributes a negligible fluctuation ($\ll$20 kev) from the average light output from the crystal.

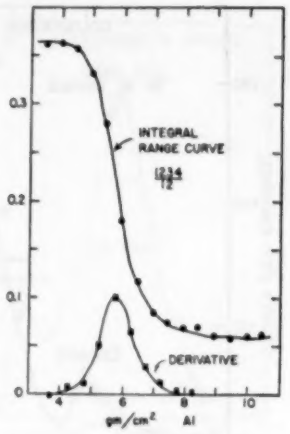

FIG. 4. Typical integral range curve and its derivative, taken with meson stopper in place.

Range Measurements

Integral range curves were taken by plotting the number of coincidence events 1–2–3–4 as a function of the thickness of aluminum between counters 2 and 3, using the number of 1–2 coincidence events as a monitor. The thickness of aluminum was varied in steps of $\frac{1}{2}$ g/cm². This procedure then yields the number of incident particles which penetrate the entire length of the telescope. An integral range curve and its derivative are shown in Fig. 4. The mean range corresponds to an initial energy of 51.5 Mev. The width of the derivative is consistent with a spread in the incident energy of about 1 Mev.

Differential range curves were obtained by plotting the combination 1–2–3–$\bar{4}$ *versus* aluminum thickness, again using 1–2 coincidence events as the monitor. An event 1–2–3–$\bar{4}$ represents a meson stopping in either the stopper or counter 3. Figure 5 shows typical differential range curves taken with and without the meson stopper in place. The peak in the lower curve of Fig. 5, taken with the stopper removed, represents particles stopping in counter 3. The ordinate of the stopper in-out difference curve represents particles stopping in the stopper only; the width indicates the thickness of the stopper in equivalent range in aluminum.

The beam contamination consists primarily of muons and electrons that originate in the vicinity of the target and have the acceptable magnetic rigidity. A determination of the range of the particles of identical magnetic rigidity should suffice to identify the components of the beam. For 51.5-Mev pions, muons of the same momentum should have 62-Mev energy and a a range of 18 g/cm² of Al; electrons should have 130-Mev energy and a range of over 20 g/cm² of Al. In addition, some pions undergo decay in flight after magnetic analysis. The decay muons whose paths are parallel or antiparallel to the pion trajectory also may contaminate the beam. Each of these components has been identified in range measurements and checked by specific ionization measurements in a thin NaI crystal.

In addition to the above contamination of the pion beam, we have also found x-ray evidence for muons with the same range as the pions. In the experiments reported here, these muons are mainly due to $\pi-\mu$ decays in the counter telescope after the pions lose most of their energy. Calculations show that roughly 0.5% of the pions should undergo such decay. Muons with the same range as 51-Mev pions may also arise from pions of lower energy that decay in the fringing field of the cyclotron. These muons enter the secondary

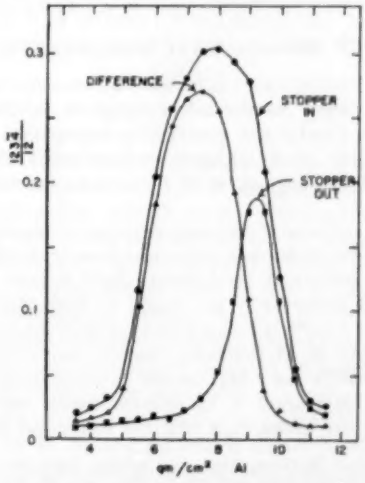

FIG. 5. Typical differential range curves taken with and without the meson stopper in place. The difference between the two is also shown.

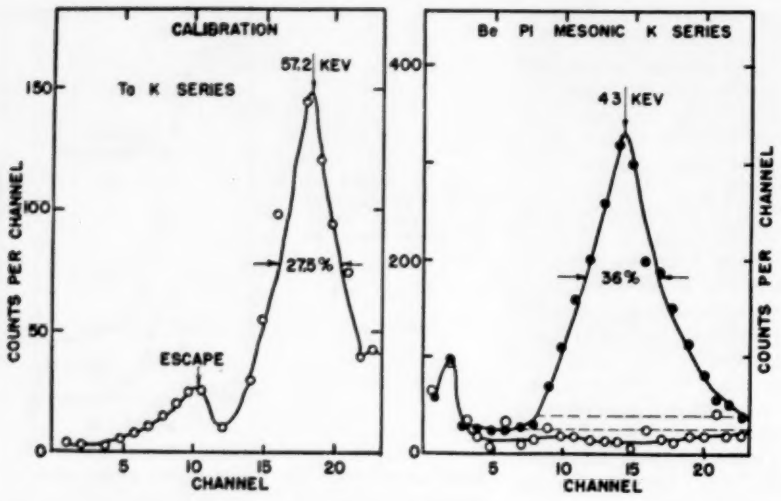

FIG. 6. Beryllium K-series π-mesonic x-ray spectrum and tantalum K-fluorescence calibration spectrum. The lower curve of the Be data was taken with a 0.022-in. Pb absorber in front of the x-ray detector.

magnet at different angles than the pions but a fraction may still be focused in the detection apparatus.

Since the μ-mesonic x-ray yield is large, compared to a π-mesonic x-ray yield of a few percent for oxygen, the μ-mesonic x-rays serve as a sensitive indication of the μ contamination of the stopping particles. The fraction of the stopped particles which give rise to μ-mesonic x-rays, assuming a 100% yield for muons, is measured to be about 1% (see Fig. 9). In work reported earlier,[13] the energy resolution of the NaI scintillation spectrometer was not sufficient to separate the π and μ contribution and no correction was made to the data for the μ contamination of the beam of the correct range. We now believe that our previously published oxygen yield was substantially in error for this reason.

III. MESONIC X-RAY MEASUREMENTS

The materials used as meson stoppers were beryllium metal, boron metal, carbon (graphite or CH_2), hydrazine (N_2H_4) and water. The stoppers were all of nearly the same thickness as that indicated in the differential range curve of Fig. 5; i.e., approximately 2.5 g/cm².

The response of the x-ray detector to monoenergetic x-rays was determined with x-rays from artifically radioactive sources. A low-intensity Hg^{203} source[14] was deposited permanently on counter 4. Both the 279-kev nuclear γ ray[15] following β decay of Hg^{203} and the 72.1-K x-rays of Tl (following internal conversion) were observed in the x-ray counter in coincidence with β pulses in counter 4. Calibration curves were taken during the meson runs with the equipment in all respects in the same condition as when mesonic x-rays were being observed, except that the cyclotron was turned off, and the gated amplifier was triggered with β rather than meson events.

Identification of the observed radiation as mesonic x-rays rests on the following: The pulse-height spectrum of pulses in the x-ray detector in coincidence with mesons stopping in the stopper displayed a maximum in each case within 10% of the energy predicted for the mesonic K x-ray for the element of the stopper. By introduction of metal foils between the meson stopper and the detector, it was established that the peaks in the spectra yielded the expected[16] x-ray absorption curves. Such a foil is shown in Fig. 2 as "x-ray absorber."

Beryllium

Figure 6 shows the pulse-height spectrum of pulses in counter 5 in coincidence with π^- mesons stopping in beryllium. The callibration curve of Fig. 6 was obtained during the beryllium runs the same amplifier gain, so that the abscissae of the two curves are identical. The zero of energy is in channel 1. The calibration curve is that of the fluorescent radiation from Ta emitted when x-rays from the Hg^{203} source were absorbed in a thin Ta foil placed in the "x-ray absorber" position (Fig. 2). The familiar escape peak[17] is seen in the calibration curve.

The predicted instrumental width for the spectrum of a monochromatic x-ray line at the π-mesonic Be $K\alpha$ energy, extrapolating the observed width at the calibration energy by use of an $E^{-\frac{1}{2}}$ energy dependence, is 31%. The observed width is 36% The discrepancy may be

[13] Camac, McGuire, Platt, and Schulte, Phys. Rev. **88**, 134 (1952); Camac, Platt, and Schulte, Phys. Rev. **89**, 905 (1953).
[14] Purchased from Oak Ridge National Laboratory.
[15] Hollander, Perlman, and Seaborg, Revs. Modern Phys. **25**, 469 (1953).
[16] A. H. Compton and S. K. Allison, *X-Rays in Theory and Experiment* (D. Van Nostrand Company, Inc., New York, 1935), Appendix 9.
[17] P. Axel, Rev. Sci. Instr. **25**, 391 (1954).

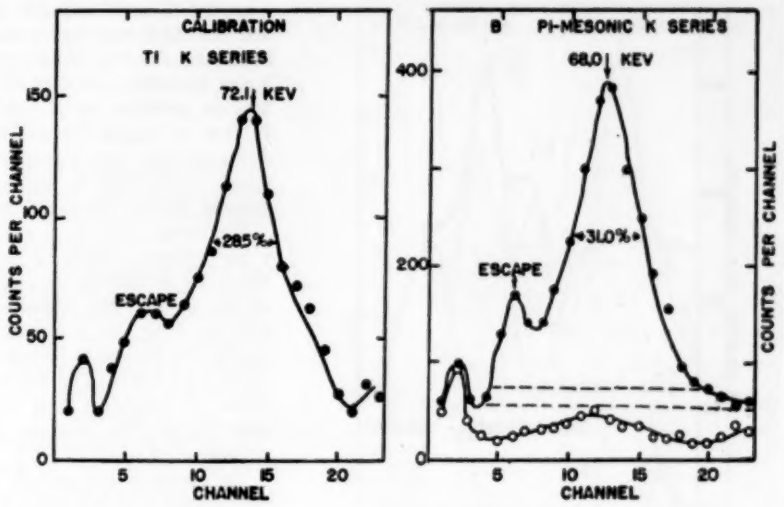

FIG. 7. Boron K-series π-mesonic x-ray spectrum and thallium K x-ray calibration spectrum. The lower curve of the B data was taken with a 0.050-in. W absorber in front of the x-ray detector.

due to the presence of x-rays from higher transitions, or Compton broadening by the stopper and background broadening. We adopt the interpretation that the observed Be π-mesonic x-ray spectrum consists of $K\alpha$ radiation with possible radiation from $K\beta$ and higher transitions, in unknown relative intensities. The measured energy of the peak of the Be spectrum is 43 ± 3.5 kev. The weighted average energy of the Ta K calibration spectrum was taken to be 57.2 kev.

To aid in the determination of the background to be subtracted in determination of the mesonic x-ray yield, a run was made with a 0.022-in. thick Pb absorber in place for the same number of stopped mesons as in the upper curve. The true background must lie above the lower curve since the Pb absorber must remove some of the background in addition to absorbing the mesonic x-rays. The true background was assumed to lie between the dashed lines shown. Uncertainty in the knowledge of the background to be subtracted constitutes the dominant error in the yield measurement.

Boron

In the boron mesonic x-ray spectrum of Fig. 7 it was determined that the energy threshold of the amplifier gate was sufficiently low not to distort the shape of the escape peak associated with the boron mesonic x-rays. This procedure insures that all of the main peak was above threshold. The calibration for boron was established with the Tl K x-rays from the Hg^{203} source. The abscissas of the curves are identical, the zero of energy being in channel 4 in this case. In both curves, the escape peaks appear in the predicted channels. Using 72.1 kev as the energy of the peak in the calibration curve leads to a value of 68.0 kev for the peak of the boron mesonic x-ray curve.

The width of the boron mesonic x-ray curve predicted from the width of the calibration curve is 29.4%, while 31.0% is observed. This observed width is not consistent with an intensity of the π-mesonic $K\beta$ line of more than 25% of that of the $K\alpha$ even if no other source of line broadening were present. The interpretation adopted is that the $K\alpha$ line represents at least 75% of the intensity of the boron π-mesonic K series, and that the observed energy of the boron $\pi K\alpha$ line is 68 ± 3.5 kev.

The lower curve of Fig. 7 was taken with a 0.050-in. thick tungsten absorber in order to estimate the background. Some evidence of tungsten fluorescence can be seen in the lower curve. The true background was assumed to lie between the two dashed lines shown.

Carbon

For carbon, no difference in mesonic x-ray yield was found from graphite and from CH_2 stoppers, which supports the assumption that hydrogen present in chemical combination plays a negligible role in the formation of the mesonic atom.[7] The spectrum (not shown) from carbon appears considerably broader than predicted from the calibration curves. The excess width of this spectrum is attributed to drift in gain of an amplifier during the taking of the data, and to a higher background counting rate in the x-ray detector. The cyclotron was intentionally operated at higher beam level than optimum for best resolution in order to speed the taking of data. Speculation as to the relative intensity of the $K\alpha$ and $K\beta$ lines in carbon on the basis of the observed line widths does not seem profitable. Within the experimental accuracy, the peak in the carbon mesonic x-ray spectrum appears at the energy predicted for the $K\alpha$ lines.

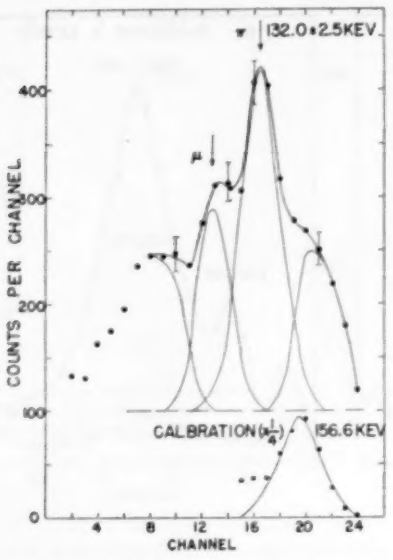

FIG. 8. Nitrogen K-series mesonic x-ray spectrum and calibration. The arrow marked π locates the center of the observed $K\alpha\pi$ x-ray peak. The one marked μ is placed at the predicted $\mu K\alpha$ x-ray energy. The dashed line indicates the background level assumed for the yield calculation. Zero energy is in channel zero.

Nitrogen

The pulse-height spectrum obtained for the nitrogen K-series mesonic x-rays is shown in Fig. 8. The background is much more prominent than with lower-Z elements, because the higher quantum energy requires a thicker NaI crystal and hence more sensitive volume for detection of stray radiation. In addition, the x-ray yield is less than for lower-Z elements.

The higher quantum energy (approximately 132 kev) permits increased resolution, and contributions are apparent from $3p$-$1s$ and higher radiative transitions. This component appears at an energy of approximately 163 kev. One also sees a component at 103 kev attributed to nitrogen μ-mesonic x-rays from the muon contamination in the beam. The observed spectrum was resolved into components of the same line shape as the calibration spectrum, and upper and lower limits on the background were again established with the aid of a thick absorber. We find that $80\pm5\%$ of the π-mesonic K-series radiation appears in the $2p$-$1s$ line, and that $3p$-$1s$ and higher transitions account for the remaining $20\pm5\%$. None of the observed $3p$-$1s$ and higher transition intensity can be attributed to simultaneous collection of K- and L-series quanta, since 0.016 in. of copper foil was used to filter the x-rays. The μ-mesonic x-ray intensity is consistent with 1.5% muon contribution to the stopped particles, if one assumes that all muons give K x-rays.

The energy calibration was established with a Cd^{111} γ ray[15] taken to have an energy of 171.2 kev. Since this γ ray is followed by a delayed γ ray, it was convenient to delay the calibration signal for coincidence, and the delay line attenuated the calibration signal by a known amount to correspond to a quantum energy of 156.8 ± 1.5 Kev. The width of the nitrogen mesonic $2p$-$1s$ line, predicted from calibration, is 23% of the peak energy. The observed spectrum resolves into a component of width $22\pm2\%$.

The energy of the nitrogen π-mesonic $K\alpha$ x-ray line is measured to be 132.2 ± 2.5 kev.

Oxygen

The pulse-height spectrum resulting from pions stopping in water is shown in Fig. 9. Resolution into components has been done in the same manner as that described above for nitrogen, except that a small component at $\sim$100 kev has been added. Such a component is expected from the mesonic carbon K x-rays, due to pions stopping in the last telescope crystal; one can estimate this contribution. The μ x-ray peak at 132 kev, and the peak due to $K\beta$ and higher transitions at 210 kev, are again evident. The full width at half-maximum of the observed $K\alpha$ line is $20\pm2\%$, in agreement with the calibration curve. The calibration was again established with the 171.2 kev Cd^{111} γ ray, attenuated to correspond to a quantum energy of 156.8 ± 1.5 kev. In plotting the calibration spectrum of Fig. 9 a correction has been made for this attenuation. The energy of the O $K\alpha$ line is measured to be 163.8 ± 2.7 kev. The relative intensities of the K-series radiations are $K\alpha$: $79\%\pm9\%$; $K\beta$ and higher transitions: $21\%\pm6\%$.

Determination of Yields

The fraction of stopped pions that yield K-series mesonic x-rays is plotted as a function of the atomic

TABLE I. Quantities used in calculation of K yields, and total K-series yields.

Element	Number of x-ray counts N_x	Number of stopped mesons N_π	Escape correction E	Scattering and absorption correction K	Efficiency-solid angle product ϵ	Total K-series yield Y
Be	1915±170	1.04×10^5	0.83	0.93	0.131	0.188±0.017
B	2535±270	1.47×10^5	1.00	1.07	0.111	0.136±0.015
C	1105±120	1.02×10^5	1.00	1.03	0.101	0.095±0.010
N	1420±150	2.95×10^5	1.00	0.97	0.112	0.045±0.005
O	3280±360	9.99×10^5	1.00	0.94	0.100	0.034±0.004

number of the stopper in Fig. 10. These yields were calculated from the formula

$$Y=\frac{N_x}{N_\pi \epsilon E K}-C_\mu,$$

where Y is the yield. The remaining symbols are defined and their determination from experimental data is discussed below. Table I lists the values of these quantities obtained in our experiments.

N_x is the number of observed x-rays, obtained by determining the total area under the appropriate peak in the pulse height spectrum, and subtracting the background assigned by the methods previously discussed. In all cases, uncertainty in the assignment of background is the dominant error. For Be, B, and C this summation includes both π- and μ-mesonic x-rays.

E is a correction required in the case of Be to take account of x-rays collected by the counter but undetected because of escape of the fluorescent iodine quantum. E is computed from the graph of Axel.[17] For the other elements the "escape peak" fell within the range of detection and the summation included these events.

C_μ is the contribution to the observed yield from μ-mesonic x-rays. This quantity was experimentally determined in the case of oxygen, where it is appreciable compared to the π-mesonic x-ray yield and where the two peaks can be resolved; C_μ in this case is 0.009. The same value was assumed to be appropriate for Be, B, and C. In the case of nitrogen the two peaks were resolved and this correction was not made.

N_π is the number of stopped pions. It is determined by counting the coincidence events 1-2-3-4-6 and multiplying by the fraction of beam particles which come to rest in the stopper as determined from the differential range curves. This fraction was usually about 0.86.

ϵ is the probability that an x-ray quantum originating in the stopper would be detected by the counter if no matter intervened between the point of origin and the counter. ϵ was computed by determining the counter efficiency-solid angle product for a number of source points within the stopper, and then taking the weighted average of such results over the volume in which the mesons stopped. The details of this calculation are given elsewhere.[18]

K is the correction required for Compton scattering and photoelectric absorption of x-rays in the matter around the source point and the counter; that is, the meson stopper, anticoincidence counter 4, any metal foils used as x-ray filters, and the aluminum shell housing the NaI crystal. K was calculated from the known cross sections for absorption and scattering, using a mechanical model to perform the spatial integrations over differential scattering cross sections. This result was checked at quantum energies of 32 kev (Cs^{137}) and 72 kev (Hg^{203}) by measurement with an "analog". A point source of the radioisotope was placed in the desired source position with respect to the x-ray counter, and the relative counting rates were found with the source (1) bare, and (2) surrounded by material of the same electron density, shape and position relative to the counter as that used during mesonic x-ray runs. For both methods a number of source

[18] A. D. McGuire, thesis, University of Rochester, 1954 (unpublished).

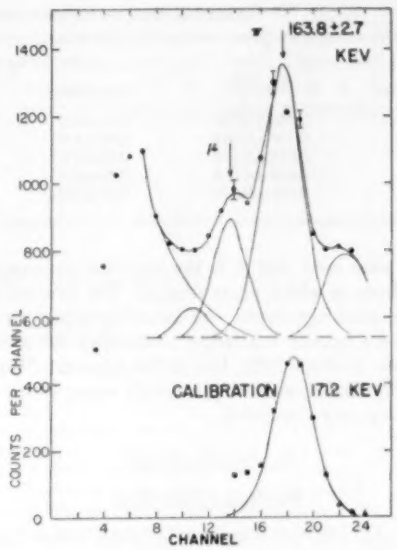

FIG. 9. Oxygen K-series mesonic x-ray spectrum and calibration. The arrow marked π locates the center of the observed $K\alpha\pi$ x-ray peak. The one marked μ is placed at the predicted $\mu K\alpha$ x-ray energy. The dashed line indicates the background level assumed for the yield calculation. The small peak near channel 11 is the expected contribution due to carbon π x-rays from mesons stopping in counter 3. Zero energy is in channel zero.

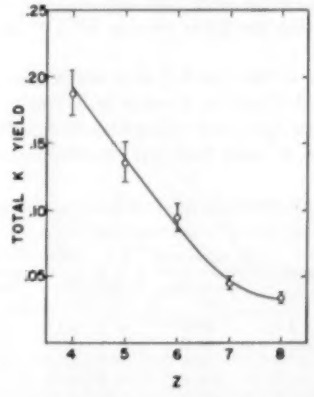

FIG. 10. Total K-series yield vs Z.

TABLE II. Data on radiative and absorption probabilities for pions in $2p$ state.

Element	$K\alpha$ yield $Y_{2p\text{-}1s}$	Population of $2p$ level P_{2p}		Ratio of absorption to radiation probability W_a/W_r		
		Upper limit	Lower limit	Upper	Lower	Predicted
Be	0.150±0.016	0.80±0.05		4.3±0.7		3.2
B	0.109±0.014	0.80±0.05		6.3±1.0		5.0
C	0.076±0.009	0.80±0.05	0.18±0.06	9.5±1.4	2.4±1.1	7.2
N	0.040±0.008	0.80±0.05	0.25±0.06	19±4	5.2±2.0	9.8
O	0.031±0.010	0.80±0.05	0.34±0.03	25±10	9.9±4.8	12.8

points were used, and K is the weighted average over the volume in which pions stopped. The two methods were in good agreement; we found by either method that the Compton scattering probability for a single quantum is about 20%, but in the aggregate, for our geometry, the in-scattering is nearly equal to the out-scattering plus absorption.

IV. CONCLUSIONS

Nuclear Absorption

The yields of the π-mesonic K-series x-rays furnish information on the pion absorption rate by the nucleus from the $2p$ state. Consider the $2p$-$1s$ mesonic x-ray. In order to emit this x-ray the pion must first reach the $2p$ level; let P_{2p} be the probability that a stopped pion reaches the $2p$ state. The pion then makes the radiative transition to the $1s$ state or else undergoes nuclear absorption from the $2p$ state; let the probability per second for these processes be W_r and W_a respectively. (The probability of an Auger transition or of π-μ decay is negligible.) Hence

$$Y_{2p\text{-}1s}=P_{2p}W_r/(W_a+W_r),$$

and

$$W_a=W_r\{(P_{2p}/Y_{2p\text{-}1s})-1\}.$$

Since the mesonic atom is hydrogen-like, W_r is readily evaluated: $W_r=1.75\times10^{11}Z^4\ \text{sec}^{-1}$. $Y_{2p\text{-}1s}$ is measured directly in this experiment for nitrogen and oxygen, and for the other three elements it is reasonable to assume that the $2p$-$1s$ yield is 80% of the total K yield.

P_{2p} can only be bounded with our present information. Since 20% of the K-series radiation is observed to come from $3p$-$1s$ and higher transitions, P_{2p} cannot exceed 0.80. A lower limit can be obtained from the L-series yields given in the following paper,[19] at least in the cases of O, N, and C, since mesons yielding L-series radiation must occupy the $2p$ state (or the $2s$ state, but it is much more probable that a meson initially in a $3p$ or higher p state radiates to the $1s$ level). Table II lists the upper and lower limits obtained for the ratio W_a/W_r, together with the values of this quantity predicted by Messiah and Marshak.[10]

TABLE III. Observed and predicted $2p$-$1s$ quantum energies.

Element	Observed energy kev	Predicted from electromagnetic interactions kev	Energy difference	
			Observed kev	Predicted by Deser *et al.* kev
Be	43 ±3.5	43.9	− 1 ±3.5	− 1.85
B	68 ±3.5	68.8	− 1 ±3.5	− 4.2
C	92 ±7.5	99.1	− 7 ±7.5	− 5.6
N	132 ±2.5	134.9	− 2.7±2.5	−10.4
O	163.8±2.7	176.0	−12.2±2.7	−17.7

Quantum Energies

The measured energies of the mesonic $K\alpha$ x-rays ($2p$-$1s$ transitions) are given in Table III for the five elements reported here. We list in the same table the predicted x-ray energies assuming electromagnetic effects only. These predicted values are found by solution of the Klein-Gordon equation for the hydrogenic (point nucleus) meson-nucleus system, and the use of these solutions in first-order perturbation calculations to find the corrections required for the finite extent of the nucleus and the polarization of the vacuum. These calculations have been performed by Grunstra and are described in detail elsewhere[20]; his methods are essentially similar to those used by the Columbia and the Carnegie groups.[21]

Differences between the observed and the predicted quantum energies are presumably due to a non-electromagnetic interaction between the pion and the nucleus. Such an effect is expected because of the pion-nucleon interaction. Estimates have recently been made by Deser, *et al.*[11] of the energy shift of the $1s$ level resulting from the pion-nucleon interaction. These estimates make use of the pion-nucleon scattering lengths given by Orear[22] and assume that the scattering lengths of the nucleons in the nucleus are additive.

We include in Table III a comparison of the observed energy shifts with those predicted by Deser *et al.* We find, as does the Carnegie group, some evidence for a nonelectromagnetic interaction.

[19] Camac, Halbert, and Platt, following paper [Phys. Rev. **99**, 905 (1955)].

[20] B. R. Grunstra, thesis, University of Rochester, 1954 (unpublished).

[21] Specifically, these calculations assume a pion mass of $272.7m_e$; the nucleus a sphere of uniform charge density and radius $1.2\times10^{-13}A^{\frac{1}{3}}$ cm; and no energy shift due to polarization of the nuclear charge. Grunstra estimates that this last effect, if present, does not change these quoted energies by more than 0.5%.

[22] J. Orear, Phys. Rev. **96**, 176 (1954).

ACKNOWLEDGMENTS

We are indebted to Dr. Messiah and Dr. Marshak for theoretical guidance, as we are to Dr. Kroll of Columbia University and to Professor Wentzel of Chicago. This research has been a group effort, and we are grateful to the members of our group, not primarily concerned with the work reported here, for many suggestions and much help. These men are Dr. M. L. Halbert and E. K. Gatchell, B. R. Grunstra, W. B. Johnson, P. P. Kane, and M. E. Nordberg, Jr.

PHYSICAL REVIEW VOLUME 99, NUMBER 3 AUGUST 1, 1955

L-Series X-Rays from π-Mesonic Atoms*†

M. Camac, M. L. Halbert, and J. B. Platt
University of Rochester, Rochester, New York

(Received April 28, 1955)

The yields of the L-series x-ray lines from π-mesonic atoms have been measured for fourteen elements between $Z=6$ and 26. The total yield rises from 18% at carbon to a maximum of about 70% in the vicinity of aluminum, and then decreases. This decrease is caused primarily by nuclear absorption of pions from the $3d$ state; the $3d\rightarrow 2p$ yield determinations thus measure the nuclear absorption rate from the $3d$ state. The low-Z drop-off is predicted qualitatively by theoretical calculations of the meson cascade scheme. The observed relative intensities of the different L-series emission lines are substantially independent of Z in the range $6\leq Z\leq 16$. The $3d\rightarrow 2p$ transition energies are consistent with electromagnetically predicted values within the experimental error of 3 to 5% for $Z\leq 28$.

I. INTRODUCTION

THE x-ray emission lines from pi-mesonic atoms of light nuclei have been studied by Sterns, DeBenedetti, Stearns and Leipuner[1] and by Camac, McGuire, Platt, and Schulte.[2,3] Using the same equipment and similar techniques as the latter group we have measured the yield and the relative intensities of the L series for the elements $Z=6$ to 17 inclusive (except $Z=10$) and also $Z=20$, 22, and 26. These data furnish information on the competition between the $3d\rightarrow 2p$ radiative transition and the nuclear absorption of pions from the $3d$ state, and also on the cascade scheme of the mesonic atom. We have obtained energy measurements of the $3d\rightarrow 2p$ transitions for some of these elements, providing additional information on the specific pion-nucleus interaction.

The formation of the mesonic atom and details of the experimental procedure are described in the preceding article.[3] We proceed here with a discussion of the L-series data.

II. EXPERIMENTAL DATA

To illustrate the important features of the L-series data, we discuss in detail spectra obtained from several elements. We have chosen the spectra of oxygen, aluminum, and iron, shown in Figs. 1, 3, and 4. The vertical scales have been adjusted so that each spectrum is normalized to the same number of stopped mesons as the no-absorber spectrum for that element. The bars shown represent the standard deviation in a representative point.

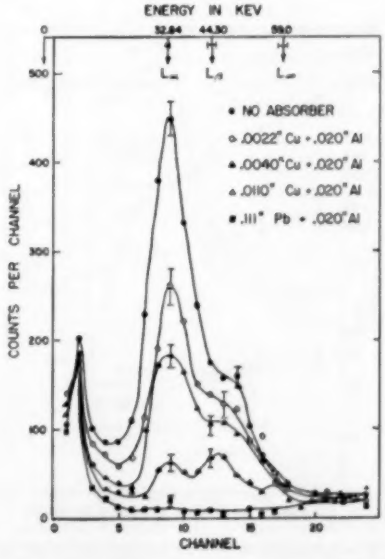

FIG. 1. Oxygen L series. Each spectrum was taken with the indicated x-ray absorber placed in front of the x-ray detector. The energy scale was determined by independent calibration with radioisotopes.

* This research was assisted by the U. S. Atomic Energy Commission.

† Based on a thesis submitted by M. L. Halbert to the Graduate School of the University of Rochester in partial fulfillment of the requirements for the degree of Doctor of Philosophy.

[1] Stearns, DeBenedetti, Stearns, and Leipuner, Phys. Rev. **93**, 1123 (1954).

[2] Camac, McGuire, Platt, and Schulte, Phys. Rev. **88**, 134 (1952); McGuire, Camac, Halbert, and Platt, Phys. Rev. **95**, 625 (1954).

[3] Camac, McGuire, Platt, and Schulte, preceding paper [Phys. Rev. **99**, 897 (1955)].

1. Oxygen, $Z=8$

Figure 1 shows spectra of photons observed in time coincidence with mesons stopping in a sample (H_2O) containing oxygen. These spectra were obtained with a NaI(Tl) scintillation counter and a 24-channel pulse-height analyzer and with the indicated x-ray absorbers between the H_2O sample and the x-ray detector. The energy scale shown was determined by independent calibration with the Ba x-rays from a Cs^{137} source. The arrows marking the predicted $L\alpha(3\rightarrow2)$ and $L\beta(4\rightarrow2)$ transition energies were located using the $3d\rightarrow2p$ and $4d\rightarrow2p$ energies calculated as described below in Sec. VI.

Above the L-series limit there are essentially no counts above the curve taken with the 0.111-inch lead absorber, which is practically opaque to x-rays of these energies. This plus the agreement of the observed with the predicted peak position we take as evidence that the main peak is the oxygen $L\alpha$ line. The existence of $L\beta$ and higher transitions is suggested by the structure of the high-energy side of the main peak in the no-absorber curve and is confirmed by the other spectra—the higher energy transitions are clearly attenuated less readily than the $L\alpha$ line. Each spectrum was separated into $L\alpha$, $L\beta$, and higher transitions. After subtraction of the 0.111-in. Pb background and correction for the 0.020-in. aluminum plate used to support the absorbers, the areas of the separated lines were plotted on semilogarithmic paper as a function of thickness of copper (Fig. 2). The lines on the graph, which seem to fit the points well, have slopes equal to the x-ray absorption coefficients in copper[4] at the predicted transition energies.

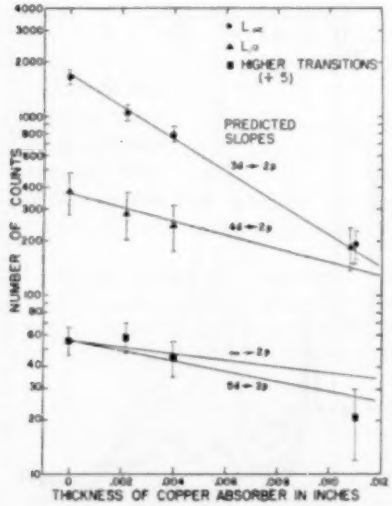

FIG. 2. Semilogarithmic plot of oxygen absorption data. The points are based on the spectra of Fig. 1; the lines are determined by the x-ray absorption coefficients at the various transition energies as given by Compton and Allison. To eliminate crowding, the data for the transitions higher than $L\beta$ have been divided by 5, and the 0.0110 in. point for $L\beta$ has been plotted at 0.0108 in.

The relative intensities of the various transitions obtained from the graph have to be corrected for absorption in the meson stopper. The lower-energy lines are attenuated more than the higher-energy transitions, making the latter appear more prominent in the spectra.

The peak in channel 2 cannot be due to low-energy x-rays because the opaque-absorber curve also shows it. The peak is instrumental, caused by nonlinearity in the the first three channels.

2. Aluminum, $Z=13$

In addition to the $L\beta$ and higher transitions, the aluminum L series (Fig. 3) shows structure on the low-energy side of the main peak as well. The iodine escape peak[5] for the $L\alpha$ line should be centered on channel 7; this accounts for the broadening of the main peak. The counts in the lower channels are probably due to the $n\rightarrow3$ radiative transitions (M series). These become increasingly important as Z increases. However, the spectrum does not give an accurate measure of the M-series intensity because the energy threshold for x-ray detection was not low enough to include all of the M series.

The energy scale was determined by using the 72.1-kev Tl x-rays from an Hg^{203} source.

3. Iron, $Z=26$

The striking features of the iron L series (Fig. 4), namely the prominence of the M series and the relative smallness of the $L\alpha$ line, are typical of the L spectra of the elements of $Z\geqq17$. An accurate determination of the L yield is therefore very difficult. The drop below channel 5 is due to electronic cut-off. The energy scale was determined with the 279-kev nuclear γ ray from an Hg^{203} source.

An absorber substantially opaque to the x-rays in this energy region was not used because it would have been inconveniently thick. Instead, we made use of a 0.030-in. tungsten absorber which should remove about 30% of the $L\alpha$ quanta. Dropping this curve in the vicinity of channel 15 by another 70% below the no-absorber spectrum gives an equivalent of the opaque-absorber curve. The dashed line suggests the result of such an operation. We believe the dashed line gives an absolute upper limit to the area of the peak. A lower limit which is probably closer to the true value is obtained by drawing a line under the observed peak which is tangent to the spectrum outside the region of the peak. In either case, the no-absorber spectrum is then poised above a substantial background, larger than that under the low-Z spectra because a much

[4] A. H. Compton and S. K. Allison, *X-Rays in Theory and Experiment* (D. Van Nostrand Company, Inc., New York, 1935), second edition, Appendix 9.

[5] P. Axel, Rev. Sci. Instr. **25**, 391 (1954).

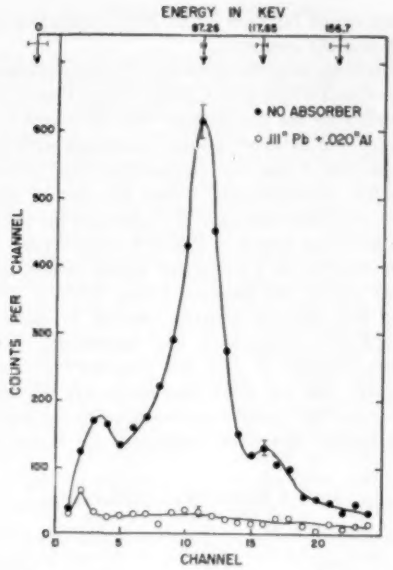

FIG. 3. Aluminum L series. Each spectrum was taken with the indicated x-ray absorber placed in front of the x-ray detector. The energy scale was determined by independent calibration with radioisotopes.

thicker NaI crystal had to be used for a reasonable detection efficiency at these energies.

III. CALCULATION OF YIELDS

We define the yield as the fraction of pions coming to rest in the stopper which give a mesonic x-ray of the desired type. In evaluating the L-series yields the problems encountered are somewhat different from those in the K-series case. We computed the L yields from a formula similar to that previously[3] used:

$$Y=\frac{N_x}{N_\pi \epsilon p^* EK},$$

where N_x is the number of x-rays, N_π is the number of stopped pions, ϵ is the over-all efficiency of the x-ray detector (including the solid angle for detection), p^* is the effective photofraction, E is the escape correction, and K is the correction factor for photoabsorption and scattering. These quantities are discussed below.

Most of the factors in the formula are energy-dependent and vary appreciably over the energy range spanned by the L series. This necessitates computing the yield for each line of the L series separately. In practice, however, only the $L\alpha$ and $L\beta$ were treated separately; the higher transitions, because they cannot be individually resolved, were lumped together and the correction factors calculated for some energy between the $5\rightarrow 2$ and $\infty\rightarrow 2$ transition energies. The problems encountered in the L-yield calculations also differed from those met with in the K yields in that absorption of the L x-rays in a given stopper was more serious because L quanta are of much lower energy.

N_π, the observed number of stop events, included particles stopping in counter 3 as well as the stopper; the range curves tell what fraction actually came to rest in the stopper, usually between 85 and 95%. Large-angle scatterings in the stopper could have caused false stop events, but we have estimated that these constituted no more than a small fraction of a percent of the total. From the oxygen K spectra we learned that about 1% of the stopped particles give a μ x-ray.[3] We assumed the same is true for the L data and accordingly multiplied the number of stopped particles by 0.99 to arrive at the number of stopped pions. The 1% of the stopped particles which are muons make a negligible contribution to the L yield.

We used Teflon plastic (CF_2) and CCl_4 stoppers for the fluorine and chlorine data and assumed that these elements capture mesons in proportion to Z.[6] In a rough check of this "Z-law" we found that the number of carbon x-rays from CF_2 was 0.21 ± 0.11 of that from graphite, which is consistent with the Z-law prediction of 0.25.

N_x, the number of x-rays, was difficult to evaluate because of uncertainties in background and in how one

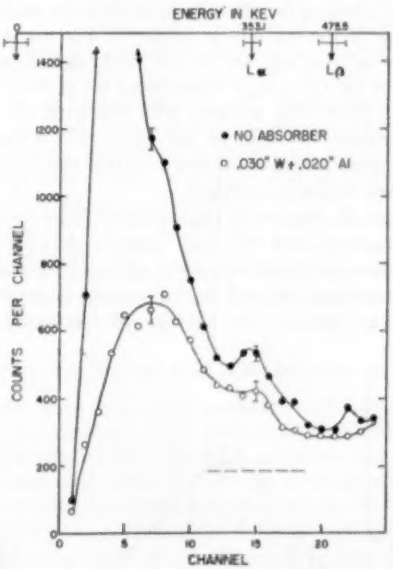

FIG. 4. Iron L series. Each spectrum was taken with the indicated x-ray absorber placed in front of the x-ray detector. The energy scale was determined by independent calibration with radioisotopes. The dashed line under the $L\alpha$ peak represents a lower limit to the background in that region. It was extrapolated from the observed attenuation of the 0.030 in. tungsten absorber.

[6] R. E. Marshak, *Meson Physics* (McGraw-Hill Book Company, Inc., New York, 1952), p. 170.

separates the individual lines of the L series. The curves taken with absorbers opaque or partially opaque to the L series determine only a lower limit to the background because any undesired γ rays of the same energy as the mesonic x-rays are also attenuated. The background counts are in time coincidence with stopped mesons. They probably result from stars following nuclear absorption of the pions. For $Z \leq 16$ the no-absorber curves approach the opaque-absorber curves in the regions where there are no mesonic x-rays (see Figs. 1 and 3), and we have taken the difference between the two as the observed number of x-rays.

For the elements $Z \geqq 17$, we could obtain only approximate upper and lower limits on the $L\alpha$ areas because of the presence of x-rays from the M series and the large background. The upper limit corresponds to identifying as the background the opaque-absorber spectrum (or its equivalent constructed from a partial-absorber curve as described above), and the lower limit to using only the area of the bump on the no-absorber spectrum at the $L\alpha$ energy. The treatment of the $L\beta$ and higher transitions was complicated even more by simultaneous detection of M and L quanta emitted in succession by a mesonic atom. Absorption evidence in the $Z=20$ spectrum is consistent with the apparent $L\beta$ peak being almost completely composed of pulses caused by detection of $L\alpha$ and $M\alpha$ quanta together; after correction for $M\alpha$ quanta we find the relative intensity of the $L\beta$ line is $7\% \pm 5\%$. For elements of $Z \geqq 20$ we have assumed for the yield calculations that none of the $L\beta$ or higher transitions are genuine; these counts have been grouped with the main $L\alpha$ peak. Fortunately the error in the total yield because of these uncertainties is far less than that due to the uncertainty in the background.

ϵ, the efficiency-solid angle product for x-ray detection averaged over the x-ray "source," was calculated by numerical integration, using the total γ-ray absorption coefficient in NaI at the energy of interest as given by White.[7] The average efficiency-solid angle product varied between 5 and 20%, depending on the energy and the geometry.

Corrections must be made for the x-ray interactions in the crystal which give a pulse smaller than that corresponding to the full energy. We calculated for our geometry the ratio p^* of the photopeak area to the area of the Compton continuum plus photopeak ("effective photo-fraction") from the data of Maeder, Müller, and Wintersteiger.[8] We corrected the separated L-line areas for escape of iodine K x-rays using Axel's calculations.[5] K is a correction factor needed because (a) not all of the mesonic x-rays initially directed toward the detector actually reached it—some were absorbed or scattered by the intervening material (stopper, counter 4, and the "window" of the NaI container), and (b) some mesonic x-rays not initially directed toward the detector were scattered into it by this material. We have estimated the factor K by supplementary experiments in which we measured the transmission of analogs of the stopper, counter 4, and the window for photons of various energies from radioisotope sources. For one set of $Z=6$ spectra the factor K for the $L\alpha$ line was only about 33%; above 40 kev it was always greater than 80%.

For most elements studied several independent sets of spectra were taken, often months apart; the yields calculated from these independent runs agree well. The final results listed in Table I are weighted averages of these separate determinations. The fractional errors are large for $Z=6$ and 7 because of uncertainty in the transmission factor K. For the other elements uncertainty in the L areas of the spectra is the most important. The purely statistical error is of relatively little significance.

TABLE I. Final results for total L-series yields and relative intensities.

Z	Total yield	$L\alpha$	$L\beta$	Higher transitions
6	0.18±0.06	0.79±0.28	0.13±0.03	0.08±0.02
7	0.25 0.06	0.73 0.14	0.17 0.05	0.10 0.03
8	0.34 0.03	0.70 0.10	0.17 0.05	0.13 0.03
9	0.37 0.09	0.78 0.13	0.16 0.07	0.13 0.03
11	0.64 0.05	0.78 0.07	0.12 0.03	0.10 0.03
12	0.50 0.04	0.79 0.10	0.13 0.04	0.08 0.01
13	0.68 0.06	0.77 0.08	0.12 0.04	0.11 0.01
14	0.75 0.11	0.75 0.08	0.15 0.03	0.10 0.03
15	0.52 0.14	0.73 0.13	0.13 0.03	0.14 0.03
16	0.59 0.14	0.73 0.08	0.13 0.05	0.14 0.03
17	$0.46^{+0.08}_{-0.18}$			
20	$0.31^{+0.08}_{-0.07}$			
22	$0.16^{+0.17}_{-0.08}$			
26	$0.12^{+0.26}_{-0.04}$			

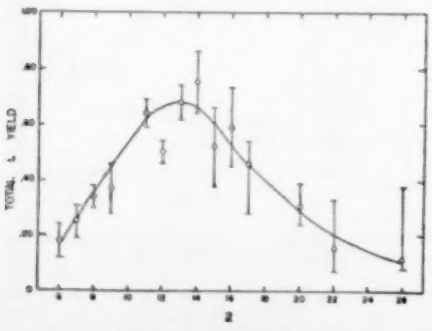

FIG. 5. Total L yield vs Z.

[7] G. R. White, National Bureau of Standards Report 1003, 1952 (unpublished).

[8] Maeder, Müller, and Wintersteiger, Helv. Phys. Acta **27**, 3 (1954).

IV. RELATIVE INTENSITIES

In Fig. 5 are plotted the total yield results of Table I. A smooth curve has been drawn through the points to emphasize the general trend. The point for $Z=12$ lies further off the curve than the estimated experimental error allows, but we feel this may be due to some accidental error. The error bars shown for $Z<17$ are the rms sums of the estimated errors in the various factors in the yield formula. For $Z\geq 17$ the errors introduced by background subtraction dominate. We believe the subtraction method used to determine the lower limit is closer to the correct procedure than that used for the upper limit and we have indicated with open circles our best estimate of the true yield value.

Measurements of the relative L yield have been published by the Carnegie group.[1] Allowing for the difference in the way background is subtracted (their procedure is equivalent to the method we used to find a lower limit on the areas), our results agree with theirs.

By relative intensity of a certain L transition we mean the number of such transitions occurring divided by the total number of all L transitions occurring. The relative intensities for the elements $Z\leq 16$ are also listed in Table I. We have mentioned that $L\beta$ and higher transitions appear to be unimportant in the $Z\geq 17$ elements; this is to be expected, for when the $n\rightarrow 3$ transitions go radiatively rather than by Auger emission a meson is more likely to be brought into the circular Bohr orbits. However, the experimental evidence is not reliable enough to allow us to assign these elements relative intensities for Table I.

V. NUCLEAR ABSORPTION FROM THE $3d$ STATE

A meson entering the $3d$ state will leave in either of two ways: (1) by a $3d\rightarrow 2p$ radiative transition ($L\alpha$), or (2) by direct nuclear absorption. (Auger transitions are unimportant for any elements we have studied; π-μ decay is also unimportant.) We denote the probability that a stopped meson enters the $3d$ state by P_{3d}, the $3d\rightarrow 2p$ radiative transition probability by W_r, and the probability of nuclear absorption by W_a. The yield $Y_{3d\rightarrow 2p}$ of $L\alpha$ quanta (not the total L yield) is thus given by

$$Y_{3d\rightarrow 2p}=P_{3d}W_r/(W_r+W_a).$$

We attribute the observed decrease in L yield at high Z to a more rapid increase with Z of W_a compared to W_r. This is theoretically expected from the following rough argument: Assuming hydrogen-like wave functions apply, $W_r\sim Z^4$ and $W_a\sim Z^8$; the latter dependence arises from multiplying the probability density near the origin for a d-state meson ($\sim Z^7$) by the number of particles in the nucleus which can absorb the meson ($\sim Z$).

We have plotted $1/Y_{3d\rightarrow 2p}$ against Z for $Z\geq 11$ in Fig. 6. Solving the previous equation for W_a/W_r, we find

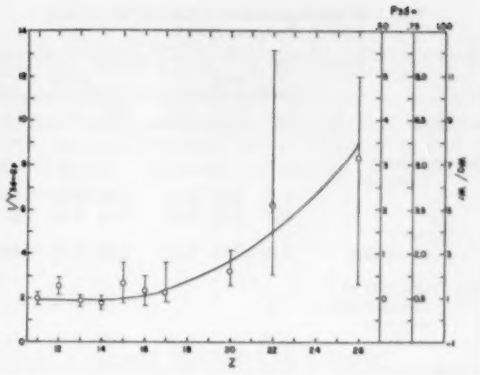

FIG. 6. Plot of $1/Y_{3d\rightarrow 2p}$ vs Z. The right-hand scales give the value of W_a/W_r implied by the data for three choices of P_{3d}.

$$W_a/W_r=(P_{3d}/Y_{3d\rightarrow 2p})-1.$$

Use of the right-hand scales of Fig. 6 performs this transformation automatically for three choices of P_{3d}. This parameter may depend on Z. P_{3d} can never be more than unity, and it cannot be much less than 0.5 for $Z=11$, 13, and 14 since W_a/W_r cannot become negative. The data for Z from 11 to 16 (except for $Z=12$) is consistent with $W_a/W_r=0$ if $P_{3d}\sim 0.5$; P_{3d} cannot be larger than 0.75 for these elements because of the observed relative intensity of the higher order transitions. On the other hand, the reduced relative intensity of the $L\beta$ and higher transitions for elements of $Z\geq 20$ would imply that P_{3d} may be closer to 1 for these elements. The uncertainty in P_{3d} and in $L\alpha$ yield unfortunately make the data useful only for order-of-magnitude estimates of W_a/W_r. This is particularly true of $Z=26$, the most interesting element since it has the highest Z of any on which we have made yield measurements. For $Z=26$ W_a/W_r can be made to vary from 0.3 to 11.0 depending on the choice of assumptions.

VI. CASCADE SCHEME

If one knew the initial quantum states in which pions are captured in mesonic atoms, he could in principle predict the subsequent radiative and Auger transitions, and hence predict the quantum yield if only electromagnetic effects are important. Deviations from these predicted intensities would then give a direct determination of the competition from nuclear absorption. The distribution of pions following capture in states of high quantum numbers is not known; however one can assume various plausible distributions and attempt these yield predictions. We are currently making a study of these cascade schemes and expect to publish detailed results later; however some qualitative results may be of interest here.

TABLE II. Principal results of cascade calculations $Z=8$ and $Z=13$.

	$Z=8$ Population in $n=7$: equal	$2l+1$	l^2	$Z=13$ Population in $n=7$: equal	$2l+1$	l^2
(a) Relative intensity of						
$L\alpha$	0.54	0.63	0.71	0.53	0.62	0.71
$L\beta$	0.26	0.24	0.21	0.18	0.18	0.17
higher transitions	0.20	0.13	0.08	0.29	0.20	0.12
(b) Probability of L emission per meson in $n=7$	0.34	0.53	0.67	0.49	0.68	0.80

We have calculated tables of all important [i.e., $(n_1,l_1)\rightarrow(n_2,\ l_1\pm1)$] radiative and Auger[9,10] transition probabilities in oxygen ($Z=8$) and aluminum ($Z=13$) π-mesonic atoms for $n_1\leqq7$. These are based on the tabulations by Bethe[11] and Slack[12] of the radiative transition probabilities in the hydrogen atom, and a table provided by Dr. de Borde[13] of Auger rates assuming the electronic K and L shells are full. In these elements, for $n>7$, by far the most likely mechanism for meson energy loss is an Auger transition for which $\Delta n=-1$. Starting with various distributions of mesons in the $n=7$ states of these elements, their cascade down through the energy levels has been followed by use of these tables, noting the probability of radiative $n\rightarrow2$ transitions (L series). It was assumed that any meson entering an s state is removed from the cascade by nuclear absorption. Absorption from $l>0$ states was not taken into account.

Results of these calculations are given in Table II. The meson distribution in the various angular momentum states of $n=7$ were assumed to be weighted as l^2, $2l+1$, or equal weighting for each l.

The calculations of L-emission probability qualitatively predict a decrease in total L yield as Z changes from $Z=13$ to $Z=8$. This is observed experimentally. Detailed examination of the cascades shows that this is due to a greater tendency for mesons in oxygen atoms to bypass the $n=2$ states. The observed factor of two in total yield between the two elements is reproduced poorly by all of the $n=7$ populations, particullary the l^2 distribution. More detailed conclusions from comparison with experiment are unsafe because this calculated emission probability is not the same as the yield, but we can say that a uniform $n=7$ population for $Z=13$ appears to be ruled out since it gives an L-emission probability substantially less than the observed yield.

TABLE III. Observed and predicted $L\alpha$ transition energies and differences between observed and predicted energies, in kev.

Z	Observed	Predicted	Observed minus predicted
17	145± 8	149.8	−5± 8
22	251 6	252.2	−1± 6
26	357 14	353.1	+4±14
28	411 12	410.2	+1±12

The experimental data on $L\alpha$ relative intensity implies that an l^2 population is required in both elements. This in turn would imply an initial capture distribution even more sharply peaked toward large l values since for large n and l Auger transitions of the type $(n,l)\rightarrow(n-1,\ l-1)$ predominate, tending to preserve the initial l-distribution of the high l states above $n=7$.

VII. ENERGY MEASUREMENTS

Any deviation of the measured $3d\rightarrow2p$ transition energy from the energy predicted for this transition taking into account all significant electromagnetic effects should be due principally to shift of the $2p$ level caused by the specific pion-nucleus interaction. We have calculated the expected $3d\rightarrow2p$ energies using the Klein-Gordon solution for a point charge, corrected for reduced mass, vacuum polarization, finite extent of the nucleus, and nuclear polarization according to methods outlined by Grunstra[14] in his calculations of the $2p\rightarrow1s$ energies. The pion mass was taken as 273 electron masses; adjustment to the recent value[15] of 272.7 may be made by reducing the predicted energies by about 0.1%.

Measurements of the $L\alpha$ energy were made by comparison of the mesonic x-ray spectra with spectra of photons of known energy from radioisotopes, taken in alternate runs in the same geometry. The 279.2±0.2 kev[16] nuclear γ ray following β decay of Hg^{203} was the reference for the $Z=17$, 22 and 26 spectra; the 411.770 ±0.036 kev[17] γ ray following decay of Au^{198} was used for $Z=28$. Table III presents the results for these elements only. Any shift occurring should be more pronounced at high Z, but all observed energies agree with the predictions within the experimental error. The error is due principally to uncertainty in location of the center of the $L\alpha$ peak because of limited resolution and uncertain background.

[9] G. R. Burbidge and A. H. de Borde, Phys. Rev. **89**, 189 (1953).
[10] A. H. de Borde, Proc. Phys. Soc. (London) **A67**, 57 (1954).
[11] H. A. Bethe, *Handbuch der Physik* (Verlag Julius Springer, Berlin, 1933), second edition, Vol. **24**, Part 1, p. 444.
[12] F. G. Slack, table included at end of article by L. R. Maxwell, Phys. Rev. **38**, 1664 (1931).
[13] A. H. de Borde (private communication).
[14] B. R. Grunstra, thesis, University of Rochester, 1954 (unpublished).
[15] K. M. Crowe and R. H. Phillips, Phys. Rev. **96**, 470 (1954).
[16] A. H. Wapstra *et al.*, Proceedings of the 1954 Glasgow Conference, Pergamon Press, 1955.
[17] Muller, Hoyt, Klein, and DuMond, Phys. Rev. **88**, 775 (1952).

Fortunately it was on nickel ($Z=28$), the highest-Z element studied, that we could make the most precise energy measurement (partly because the calibration energy was practically equal to the $L\alpha$ energy). Attributing all the shift to the $2p$ level, we can say that the energy of the $2p$ state of $Z=28$ is affected by the specific pion-nucleus interaction no more than 12 kev, or 1.6%.

VIII. ACKNOWLEDGMENTS

The valuable assistance of E. K. Gatchell, B. R. Grunstra, W. B. Johnson, A. D. McGuire, and P. P. Kane in taking data, of E. C. Halbert and M. E. Mandl in performing calculations, and of the cyclotron crew, the shop personnel, and the engineering staff of the 130-inch Cyclotron Laboratory is gratefully acknowledged.

PHYSICAL REVIEW VOLUME 99, NUMBER 3 AUGUST 1, 1955

Energy of Electrons or Photons from Their Cascade Showers in Copper*

W. E. HAZEN
Ecole Polytechnique, Paris, France
(Received April 4, 1955)

The photographs obtained by the Ecole Polytechnique cloud-chamber group have been used for the study of cascade showers in copper plates produced by electrons of known momentum. The best constant for obtaining primary energy from the total number of track segments is given. The uncertainty in primary energy as determined by this method is found from the experimentally observed distributions. The results are applied to the interpretation of the heavy S-particle observed at the Massachusetts Institute of Technology.

1. INTRODUCTION

THE main interest in photon-electron cascade showers stems from their use as a tool. In the case of air showers, for example, one uses the theoretical results to estimate the energies of the incident primaries. In the case of particle interactions, one uses the shower-producing property as a qualitative means of identification of electrons or photons and tries to determine the energy from the size of the shower. Here we are dealing with showers in solids, in general, and, in the case of multiplate cloud chambers, the plate material is usually such that the available calculations are not very useful. The Monte-Carlo method[1] gives a better approximation than calculations but it is severely limited by the difficulty of handling the scattering problem. Thus, one must return to purely experimental results and use the theory for a guide or for minor corrections.

D'Andlau[2] has made a detailed study of the showers at particular depths with electron primaries of known energies. Among other things these results enable one to know the probability of mistaking an electron for a heavier particle when observing the penetrating power.

In the study of the radiation emitted by S-particles in multiplate cloud chambers, one is frequently faced with the question of estimating the energy of the initiators of electron-photon cascades.[3] Again, one must turn to experimental results. Previous work utilized π^0 mesons from nuclear disintegrations[3,4] but the statistics were not adequate to allow determination of a probability distribution.

The photographs of nuclear disintegrations obtained by the Ecole Polytechnique group[5] with their double cloud-chamber arrangement give the opportunity to observe the production of cascade showers by electrons of known momentum. Thus, one can observe the showers produced by electrons of known energy and from these data one can deduce the probability distribution in initiating energy for a shower of given size.

2. METHOD

(a) Selection of Data

The photographs of the lower chamber, which contained copper plates of one-centimeter thickness, were scanned for individual cascade showers. Showers that were selected were sufficiently distant from other events so that possible confusion with other radiation would only lead to uncertainties small compared with the inherent statistical uncertainty. The corresponding photographs of the upper chamber were inspected for cases in which the initiating particle could be identified unambiguously. Correspondence between tracks in the upper chamber and showers in the lower chamber could be determined to within ~1 cm on the reprojection table of the laboratory. Since multiple scattering and

* This study was made while on leave from the University of Michigan as a Fulbright research scholar.

[1] R. R. Wilson, Phys. Rev. **86**, 261 (1952).

[2] C. A. D'Andlau, Nuovo cimento **12**, 859 (1954).

[3] Bridge, Courant, DeStaebler, and Rossi, Phys. Rev. **95**, 1101 (1954); H. Courant, Phys. Rev. **94**, 797(A) (1954).

[4] P. A. Bender, thesis, Washington University, St. Louis, Missouri, 1955 (unpublished).

[5] Gregory, Lagarrigue, Leprince-Ringuet, Muller, and Peyrou, Nuovo cimento **11**, 292 (1954).

inelastic scattering contributed uncertainties of the order of 1 or 2 centimeters, depending on the energy, it was unnecessary to use a more accurate method for checking correspondence. The electronic radiation in the upper chamber originated from the π^0 component of the penetrating showers that were generated in material above the top chamber. Thus, in general, a cascade of electrons, positrons, and photons, accompanied by mesons and protons, emerged from the material above the chamber. In the selected events, the axis of the cascade shower was inclined toward the right or left. Therefore, the gamma rays were expected to be well separated from the electron or positron that was bent downward by the magnetic field and passed into the bottom chamber. Since the multiplicity of particles in the upper chamber was usually rather low, there was a consequent low probability of mistaking the identity of the initiator of the shower in the lower chamber. The major cause of uncertainty was the multiple scattering in the bottom wall of the upper chamber. However, since the scattering material constituted 0.25 radiation units at a distance of 40 cm above the bottom chamber, the rms lateral displacement would only be $300/E_0$ (Mev) in centimeters at the bottom chamber. Also, the direction of the shower axis was usually well enough defined to allow a check on correct identification. For example, a γ ray from the generator would have quite a different direction from that of an electron or positron because of the deflection of the charged particles in the magnetic field.

The shower parameter that is expected to have the smallest fluctuations for a given primary energy (E_0) is the total track length of electron secondaries (l). The primary energy is determined from $E_0=(dE/dx)l$, where (dE/dx) is the average rate of energy loss of the cascade particles. Fluctuations are then due only to variations in the distribution of differential track length from event to event. These fluctuations have little effect on the calculated value of E_0 since (dE/dx) is not strongly dependent on the differential track length distribution. However, in a multiplate chamber, most of the energy dissipation is inside the plates. One determines the track length in a plate by taking the mean of the number of tracks entering and leaving the plate[6]; the true track length within the plate fluctuates widely about this "observed" value because of the stepwise nature of the changes in number and because of the effects of scattering. For example, if we choose a simple model, neglecting scattering, in which it is equally likely that a track entering a plate stops at any depth in the plate and a track leaving a plate originates at any depth, the probable error in each element of "measured" track length is $t/2$ (where t is the plate thickness). Consequently the probable error in total track length determined by observation of N segments would be $l/2\sqrt{N}$. If scattering were included in the model, the probable error per element would be increased and we might expect a probable error of the order $l/\sqrt{N}$. Thus the *a priori* expectation is that E_0 might be determined with an accuracy of about $E_0/\sqrt{N}$. In general, other methods for determining E_0, such as the number of particles at the maximum, must involve greater uncertainty. It can be shown that there is negligible gain in averaging E_0 determined from N with E_0 determined from other parameters such as the number of particles at the maximum.

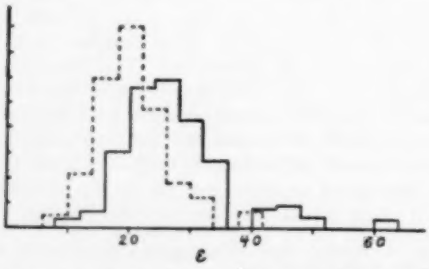

FIG. 1. The distributions in ϵ for two ranges of E_0. The dotted distribution is for $100<E_0<300$; the solid is for $E_0>500$.

TABLE I. Energy per track segment, $\epsilon=E_0/N$.

E range	100 to 200	200 to 300	300 to 500	>500
Number of events	33	25	30	28
Average ϵ	21.0	20.3	26.5	26.7
Average ϵ	20.4		27.8	
$0.67\Delta\epsilon_{rms}$	4.0		6.0	
Average N	10		20	
Expected statistical P.E.	4.3		4.8	

There was a significant probability for loss of energy by radiation by an electron as it traversed the bottom and associated material of the top chamber. The angle of departure of the photon from the path of its parent electron is small (the effect at the bottom chamber is an rms displacement of only $100/E_0$ cm) but the electron is deflected in the fringing magnetic field. The deflection in the fringing field depends on the fraction of energy (f) lost by the electron. When the fractional energy loss by the electron is too large for a given E_0, the electron will arrive at a point too far from the expected point of arrival to be considered as a satisfactory identification between primary and shower. On the

[6] All track segments were counted, including those that might represent back scatterings and those of electrons that scattered noticeably in the gas. The latter may represent less track length in copper than higher energy electrons because they will not penetrate far into the next plate. On the other hand, they have scattered more in the plate from which they emerge and therefore represent more than average path length in the plate of emergence. Consequently, they were given equal weight with higher energy electrons. Back-scattered segments represent less track length in copper than other segments and therefore should be given lower statistical weight, in principle. However, they are not numerous and their identification is difficult in most cases.

other hand, if f is sufficiently small for a given E_0, and E_0 sufficiently large, not only will the electron arrive sufficiently near to the predicted point for satisfactory identification of its shower, but also the photon will arrive sufficiently close to the electron so that the showers are considered as one. A quantitative treatment shows that the region of the f and E_0 plane in which data might be incorrectly interpreted is exceedingly small, affecting no events of $E_0>240$ Mev and giving a maximum uncertainty at $E_0=120$ Mev. At the latter energy, 25 percent of the events might have 20% error, the other events $<20\%$.

(b) Analysis

There are two questions that we seek to answer: what is the best value that we can obtain for the energy (E_0) of a shower initiator; and what is the probability distribution in E_0 for a given observed shower? As noted above, the total track length (l) as measured by the observed track segments above and below the plates gives the best measure of E_0, i.e., $E_0=(dE/dx)l=\epsilon_0 l$, where ϵ_0 is the critical energy and l is measured in radiation units.[7] If n_i represents the number of track segments above the ith plate, $l=K\sum n_i t$, where t is the plate thickness and K is a proportionality constant which, as we noted earlier, is probably >1 because of scattering etc. in the plates. Letting $N=\sum n_i$, we have

$$E_0=K\epsilon_0 tN=\epsilon N, \tag{1}$$

where ϵ is the average energy dissipation in a plate per observed track segment. Thus, we wish to determine the best value for ϵ in order to answer the first question at the beginning of the paragraph. Since scattering is a decreasing function of electron energy and the mean energy of the electrons in the shower is a slowly increasing function of E_0, we expect K (and ϵ) to be a slowly decreasing function of E_0. Thus a possible energy dependence of ϵ should be sought.

The second question, that of the distribution in E_0 for a given N, can be answered by selecting showers in narrow bands of N values, correcting all observed values of E_0 to the equivalent values for the average N, and analyzing the resultant E_0 distribution.

3. RESULTS

(a) Determination of $\epsilon(=E_0/N)$

The data were divided into E_0 groups, since one expects ϵ to depend on E_0, as noted above. Each datum for $E_0<500$ Mev was given a weight E_0, on the assumption that the main uncertainty derives from the statistical variation in the number of track segments N. The average value of N is proportional to E_0, since ϵ does not vary appreciably with E_0, as we shall see later. For $E_0>500$, the uncertainty in momentum measurement becomes comparable with the statistical uncertainty. Therefore these events were weighted equally.

[7] See, B. Rossi, *High Energy Particles* (Prentice-Hall, Inc., New York, 1952) for the information on shower theory that is assumed.

TABLE II. E_0 distributions for a given observed N.

N	5 to 7	8 to 10	11 to 15	16 to 22
Number of events	16	22	26	22
Average N	6.2	9.2	12.9	19.4
Average E	162	265	290	542
$0.67\Delta E_{\text{rms}}/E_{\text{av}}$	37%	28	16	23
$0.67/N^{\frac{1}{2}}$	27%	22	19	15

The results for the four selected energy ranges are shown in Table I. Since no rapid variation of $\bar{\epsilon}$ with E_0 is apparent, the distributions were examined in terms of only two E_0 groups, 100 to 300 Mev and greater than 300 Mev. These distributions are displayed in Fig. 1, and the corresponding parameters are given in Table I. An effective $\bar{N}$ was estimated for each group of data and we see that the breadths of the observed distributions are about what we expect from the statistical fluctuations in N alone. The two values of $\bar{\epsilon}$ differ more than the probable errors of their means. However, since one expects an energy dependence in the opposite direction [see Sec. 2(b)], it is probably most reasonable to assume that we have a fluctuation effect. Therefore, the overall mean of 24 ± 3 is the best value to use for all E_0 from 100 to 1000 Mev.

(b) Uncertainty in E_0

In order to determine the distribution in E_0 for a given N with reasonable accuracy, it was desirable to combine data for neighboring values of N. This grouping is indicated in Table II. Each E_0 was multiplied by $\bar{N}/N$, where $\bar{N}$ is the mean value for each group, and each event was weighted according to the relative frequency of occurrance of events of energy E_0 in the entire body of data.

The results are presented in Table II, where the observed probable errors are compared with the probable error deriving from statistical variations in N. Since the number of events in each group is small, the uncertainty in the probable error is large for any particular group. However, we can combine the results from the four groups if we make some kind of assumption concerning the dependence of the true probable error on shower size. For example, the first approximation would be that the probable error is simply a constant factor times the statistical probable error. We then find that the average factor is 1.25, i.e., that the average ratio of observed to statistical error is 1.25. This sort of result was anticipated from the theory [Sec. 2(b)], namely, that the fluctuations would correspond approximately to the statistics of N events.

4. CONCLUSIONS

(a) Determination of E_0

For showers at normal incidence in assemblies of one centimeter copper plates, the best value for the energy of the shower initiator is given by $E_0=24.N$ (Mev), where N is the total number of track segments in the shower. If asymmetric effects of particle scattering for inclined showers are neglected, we should expect to have, from (1), $E_0=[36(\epsilon_0/20)t/\cos\theta].N$, where ϵ_0 and t are the critical energy and plate thickness (radiation units), and θ the angle of incidence. We have here assumed that scattering effects have the same fractional effect for all materials and hence the validity of the above equation is limited to elements with Z near copper.

The probable error in E_0, when E_0 is determined by this method, is about $[0.15^2+(0.67\times1.25)^2/N]^{\frac{1}{2}}$, where the first term is a pessimistic estimate of the uncertainty in ϵ and the second term depends on the statistical uncertainty deriving from the finite number of track segments.

In cases where the observable longitudinal (or lateral) development is limited by geometry, only a lower limit to E_0 can be established within reasonable limits (the limits given above). If the shower leaves the chamber before an apparent maximum occurs, one might determine a lower energy limit by using the size of a shower at its maximum as a parameter. However, there is no real gain in information since one must then accept the large uncertainty deriving from the large statistical fluctuations in the size of showers at a given depth. Therefore, a lower energy limit based on total number of observed segments will give the narrowest limits for E_0.

(b) Comparison with Shower Theory

The observed track length in copper is found to be $E_0/36$ radiation units from the present data whereas the total track length is approximately $E_0/\epsilon_0=E_0/20$ from consideration of conservation of energy. Thus, only 0.55 of the track length is detected with this technique. Presumably, the major loss is due to scattering within the plates at low energies and we can assume a sharp low energy cut-off as a first approximation. Richards and Nordheim[6] find that 0.55 of the track length is generated by electrons while their energy $>0.3\epsilon_0$ in air or $0.4\epsilon_0$ in lead. These figures are for energies lower than the validity of the detailed track length calculations, but, since the lengths for $E=0$ are known from conservation of energy, only reasonable interpolations are involved in obtaining $0.3\epsilon_0$ and $0.4\epsilon_0$. Thus, for copper, we estimate $0.35\epsilon_0$ ($=7$ Mev) for the equivalent cutoff. This is a physically reasonable figure since electrons of this energy or less scatter with rms angles of the order unity in distances <0.1 radiation unit, with the result that their path lengths in the plates are much longer than inferred from the method of observation.

(c) Results in Lead

During the early stages of their experiment[4] the Ecole Polytechnique group had alternate lead and carbon plates in the lower chamber. A survey of these photographs yielded nine suitable events with correlated electron primaries and electron cascades. The lead plates (7 mm) were 1.22 radiation units thick and the carbon plates (15 mm) 0.09 radiation unit. The collision loss in these carbon plates is about equal to the critical energy in lead.

Only the segments above the lead plates were counted since it is easier to make an approximate correction for the carbon than to try to establish its effect in detail. The result is $\epsilon=50$ Mev per track segment or $\epsilon=40$ Mev/segment for plates of unit thickness. A first-order correction for the carbon plates, taking only collision loss into account and using calculated track lengths in lead,[6] gives 25 Mev/segment for lead plates of unit thickness. This result agrees with a study by Bender of showers produced by π^0 mesons.[4]

(d) Application to the Heavy S-Particle of MIT[5]

If we make a calculation for the total energy of the initiators of the cascade showers that appear to be due to the decay or capture of the heavy particle observed and discussed by MIT, we find $\sum E_0=1630$ Mev, in agreement with the determination of the MIT group. This is a minimum in the sense that momentum is not conserved, as noted by the MIT group, and that two of the showers probably leave the chamber before all their energy is dissipated. As a result of the present work, we can add that the probable error, deriving from a pessimistic estimate of the uncertainty in the constant ϵ and the observed fluctuations in N is about 20%. Thus it seems quite unlikely that the mass energy of the S-particle was as low as 500 Mev, if one assumes that it was a decay event.

5. ACKNOWLEDGMENTS

The data for this analysis were taken from photographs obtained by the cloud-chamber team of the Ecole Polytechnique for their studies of V and S particles. I am deeply grateful to them and to the laboratory director, Professor Leprince-Ringuet, for their generous aid and hospitality.

Radiative τ-Meson Decay

R. H. DALITZ
Institute for Advanced Study, Princeton, New Jersey

(Received April 25, 1955)

The characteristics of the decay process $\tau^{\pm}\to\pi^{\pm}+\pi^{+}+\pi^{-}+\gamma$ are considered. For a pseudoscalar τ-meson, the probability $R(k)$, relative to the 3π-decay, for emission of a photon of energy k Mev or greater is found to be 1.06×10^{-3} for $k=10$ and 1.1×10^{-4} for $k=30$. Quite similar values are obtained for other spin values compatible with the τ-meson decay data. Branching ratios for other decay processes are briefly discussed and it is suggested that the absence of the decay mode $\pi^{\pm}+\gamma$ or $\pi^{\pm}+e^{+}+e^{-}$ may provide some evidence against a nonzero τ-meson spin. Competing decay processes involving a neutrino are not considered.

AN interesting K-meson decay event has recently been reported by Daniels and Pal,[1] in which the observed decay products were three pions of total kinetic energy 46.1 (±2.2) Mev and total momentum 32.1 (±2.7) Mev/c. The most natural interpretation of this event in terms of known particles is that it represents a radiative decay of the τ-meson,

$$\tau^{+}\to\pi^{+}+\pi^{+}+\pi^{-}+\gamma, \tag{1}$$

in which [if one assumes a Q-value[2] of 74.3 (±0.3) Mev for the τ-meson] the energy of the emitted photon was 30.2 (±1.5) Mev. In this note, the characteristics of this alternative mode of decay will be discussed for several possible τ-meson spin values. Several other τ-meson decay processes which involve the electromagnetic field will also be briefly considered.

The emission of such an accompanying photon in τ-meson decay may arise either (a) as radiation from the pions emitted in the 3π-decay of the τ-meson, by the process of "internal bremsstrahlung," or (b) as a decay mode proceeding through distinct channels, a "direct emission" process, which will generally depend on details of the τ-meson structure. These two mechanisms will be coherent, of course, and their amplitudes will interfere in the total probability. They are represented graphically in Fig. 1.

In process (a), the three pions have been emitted and are penetrating the centrifugal barriers appropriate to the spin j and parity w of the τ-meson when the photon is emitted. For photons of long wavelength, the volume concerned in this emission process may be very considerable and the corresponding matrix element may therefore be very large. This is the dominant process in the emission of low-frequency photons, and it is the classical "internal bremsstrahlung" process, well known in beta-decay[3] and in the $\pi-\mu$ decay.[4] Clearly it is dependent on matrix elements (actually off-diagonal in energy) for the 3π-decay process and its probability may be predicted, to a sufficient approximation, from a knowledge of the matrix elements for the normal 3π-decay.

FIG. 1. Diagrams for radiative τ-meson decay.

The amplitude for process (a) may be obtained classically, and for this purpose the following representation of the 3π-decay is adequate. Up to time $t=0$, the τ-meson is at rest at the origin O; suddenly, at $t=0$, three pions, two positive and one negative, begin to move out from O and continue thereafter to move uniformly with momenta $(\mathbf{p}_1,\mathbf{p}_2,\mathbf{p}_3)$ respectively. The probability amplitude for this pion configuration will be denoted by G. Now it is well known[5] that the amplitude for emission of a photon by a particle of charge e which suddenly begins to move with constant momentum $\mathbf{p}$ [and energy $\omega=(\mu^2+p^2)^{\frac{1}{2}}$], is given by

$$\int d\sigma\int_0^{\infty}dt\,e\frac{\mathbf{p}\cdot\boldsymbol{\epsilon}}{\omega}\delta\left(\mathbf{r}-\frac{t}{\omega}\mathbf{p}\right)e^{i(kr-\mathbf{k}\cdot\mathbf{r})}=e\frac{\mathbf{p}\cdot\boldsymbol{\epsilon}}{\omega k-\mathbf{p}\cdot\mathbf{k}}, \tag{2}$$

since the current density $j(\mathbf{r},t)$ is

$$\mathbf{j}(\mathbf{r},t)=e\frac{\mathbf{p}}{\omega}\delta_3\left(\mathbf{r}-\mathbf{p}\frac{t}{\omega}\right),\quad t>0$$
$$=0,\qquad t<0$$

In Eq. (2) $\mathbf{k}$, $\boldsymbol{\epsilon}$ are the momentum and the polarization vectors of the photon. For the present, the nonrelativistic approximation will be made, so that the retardation term $\mathbf{p}\cdot\mathbf{k}$ may be neglected in (2) and ω replaced by the pion mass μ. The inclusion of relativistic effects will be discussed in Appendix A. For the τ-meson decay, the amplitude for the internal bremsstrahlung process is then obtained by adding the separate amplitudes for each pion to give[6]

$$-e\frac{(\mathbf{p}_3-\mathbf{p}_1-\mathbf{p}_2)}{\mu k}G. \tag{3}$$

[1] R. R. Daniels and Y. Pal, Proc. Inst. Acad. Sci. **40**, 114 (1954).
[2] Amaldi, Baroni, Cortini, Franzinetti, and Manfredini, Nuovo cimento **12**, Supplement 2, 181 (1954).
[3] C. S. W. Chang and D. Falkoff, Phys. Rev. **76**, 365 (1949).
[4] H. Primakoff, Phys. Rev. **84**, 1255 (1951); and W. C. Fry, Phys. Rev. **91**, 130 (1951).
[5] Since it is the pion momenta before photon emission which appear in G, the inclusion of the photon recoil would replace $(3^{\frac{1}{2}}$,

For the three-pion system, it is convenient to introduce internal coordinates

$$\mathbf{p}=\mathbf{p}_3-\tfrac{1}{2}(\mathbf{p}_1+\mathbf{p}_2), \quad \mathbf{q}=\tfrac{1}{2}\sqrt{3}(\mathbf{p}_1-\mathbf{p}_2). \tag{4}$$

For a τ-meson initially at rest ($\mathbf{p}_1+\mathbf{p}_2+\mathbf{p}_3+\mathbf{k}=0$), (3) then becomes

$$-e\frac{(4\mathbf{p}+\mathbf{k})\cdot\boldsymbol{\epsilon}}{\mu k}G=-\frac{4e}{3}\frac{\mathbf{p}\cdot\boldsymbol{\epsilon}}{\mu k}G, \tag{5}$$

since ϵ is perpendicular to the photon direction. The energy equation for the system is now

$$\frac{1}{3\mu}(p^2+q^2)+k+\frac{k^2}{6\mu}=E, \tag{6}$$

where $E=M_\tau-3\mu$ is the energy release in the decay.

For spin (0−), it will be shown below that the amplitude for the direct emission process is unlikely to be appreciable in comparison with (5). For this case then, using the coordinates (4) and summing over photon polarizations, the probability per unit time for the decay mode (1) is given by

$$P(3\pi+\gamma)=\frac{16\alpha}{9}\int G^2\frac{p^2\sin^2\theta}{\mu^2k^2}\frac{2\pi}{k}\frac{d_3k\,d_3p\,d_3q}{(2\pi)^6}\times\left(\frac{2}{3\mu\sqrt{3}}\right)^3 2\pi\delta\left(\frac{p^2+q^2}{3\mu}-\Delta\right), \tag{7}$$

where θ is the angle between $\mathbf{p}$ and $\mathbf{k}$, and

$$\Delta=E-k-(k^2/6\mu) \tag{8}$$

is the energy left to the three pions in their barycentric system. For comparison the probability per unit time for the 3π-decay is

$$P(3\pi)=\int G^2\frac{d_3q\,d_3p}{(2\pi)^3}\left(\frac{2}{3\mu\sqrt{3}}\right)^3 2\pi\delta\left(\frac{p^2+q^2}{3\mu}-E\right), \tag{9}$$

with the value $\pi G^2E^2/3\sqrt{3}$. For given k, the average value of p^2 is $3\mu\Delta/2$, and the relative probability of photon emission is then

$$\frac{P(3\pi+\gamma)}{P(3\pi)}=\frac{16}{9}\frac{\alpha}{\pi}\frac{\Delta^3}{\mu E^2}\frac{dk}{k}, \tag{10}$$

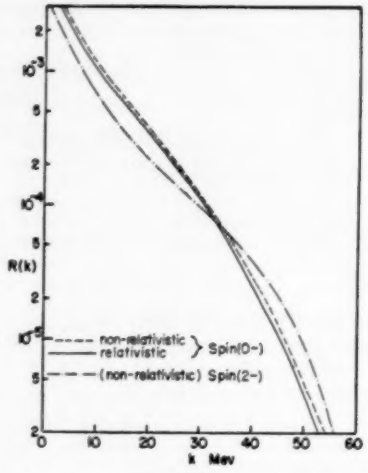

FIG. 2. The probability $R(k)$ for emission of a photon exceeding k Mev.

the maximum photon energy being $(9\mu^2+6\mu E)^{\frac{1}{2}}-3\mu \simeq 69$ Mev. This probability falls off rapidly with increasing k for two reasons, (i) the volume of phase space available to the final pions decreases quadratically with the energy left them by the outgoing photon, and (ii) the photon emission is proportional to the square of the current of the final system and hence to the final energy of the pions. According to (10), the branching ratio for emission of a photon $k>10$ Mev has the value 1.2×10^{-3}, and for a photon $k>30$ Mev, 1.2×10^{-4}, relative to the 3π-decay. The inclusion of the relativistic and retardation terms results in surprisingly little change in these figures, although the pion momenta are always of order μ. For both cases, the probability $R(k)$ for emission of a photon exceeding k Mev is plotted in Fig. 2.

Hence this classical process can account adequately for this one example of Daniels and Pal. The probability that one radiative decay event with photon exceeding 30 Mev should occur among the ~80 τ-meson decays now observed is about 1%, not an unreasonable chance. The probability for less energetic photons is rather greater, but the expected number of events with $k>1$ Mev is still only 0.50. Also, below about 5 Mev, the efficiency of detection of photon emission drops off rapidly, owing to technical difficulties in plate measurements—there has been considerable variation in the reported Q-values and it has often not been possible to establish coplanarity to better than several degrees. It should be added here that the detailed configuration of this event is not in conflict with this classical interpretation. According to expression (7), the photon emission has a $\sin^2\theta$ distribution: the observed angle θ is close to 130°. For given photon energy k, expression (7) indicates that the emission is more probable the greater the magnitude of p, i.e., the greater the pion current: the

---

by

$$-e\boldsymbol{\epsilon}\cdot\left[p_3G(p+k,q)-p_1G\left(p-\tfrac{1}{2}k,q+\frac{\sqrt{3}}{2}k\right)-p_2G\left(p-\tfrac{1}{2}k,q-\frac{\sqrt{3}}{2}k\right)\right]\Big/\mu k$$
$$=-e\left[\boldsymbol{\epsilon}\cdot p\left(2G(p+k,q)+G\left(p-\tfrac{1}{2}k,q+\frac{\sqrt{3}}{2}k\right)+G\left(p-\tfrac{1}{2}k,q-\frac{\sqrt{3}}{2}k\right)\right)-\sqrt{3}\,\boldsymbol{\epsilon}\cdot q\left(G\left(p-\tfrac{1}{2}k,q+\frac{\sqrt{3}}{2}k\right)-G\left(p-\tfrac{1}{2}k,q-\frac{\sqrt{3}}{2}k\right)\right)\right]\Big/3\mu k.$$

However, since the photon momentum is generally somewhat smaller than p or q, this modification will generally be found unimportant.

observed value of p is 95% of the maximum value permissible for the observed k.

The "direct emission" process (b) may be regarded as an electromagnetic transition from the initial τ-meson state (j,w) of the system to final states of various angular momenta J and parities W which then break up into three outgoing pions. Since the photons emitted in this process have wavelength long compared with the τ-meson radius R (which we will assume to be $R\approx\hbar/M_\tau c$), only the lowest multipoles allowed by angular momentum and parity conservation will be effective. The three outgoing pions are then left to penetrate the centrifugal barriers appropriate to the state (J,W) and the amplitude for this may be estimated from considerations of barrier penetrability and angular momentum conservation, as described elsewhere.[6] However it will be found below that, for the cases of interest (even spin j and odd parity w), the structure-dependent multipole terms of the direct process are not generally important, because (a) they contain an additional factor $kR(\lesssim\frac{1}{8})$ and (b) the significant photon momenta are less than the corresponding pion momenta—photons of the highest possible energies are always improbable owing to the rapid decrease of the available phase space and of barrier penetrability with the decreasing energy left to the pions. For spin $j=0$, all direct emission terms are especially unfavoured since the only permissible photon emissions (zero-zero transitions being forbidden) lead to states $J>0$, in which the barriers against 3π-emission greatly exceed those in the initial state $j=0$.

In the limit of low frequencies, only the amplitude for electric dipole emission can be nonvanishing and, in fact, its value in this limit may be obtained from the value of G, the amplitude for the normal 3π-decay process, by gauge invariance arguments. For zero frequency, the external potential is uniform and may be removed by a gauge transformation whose effect is to replace each particle momentum $\mathbf{p}_i$ by $\mathbf{p}_i-e_i\mathbf{A}$. The amplitude $G_A(\mathbf{p},\mathbf{q},\mathbf{X})$ for the 3π-decay in the presence of an external potential is then given by $G(\mathbf{p}+2e\mathbf{A},\ \mathbf{q},\ \mathbf{X}-e\mathbf{A})$, $\mathbf{X}$ being the total momentum of the pion system. The zero-frequency matrix element for the direct emission process is then given by the linear term in the expansion of G_A in powers of $e\mathbf{A}$. This is discussed further in Appendix B. For spin $(0-)$ this leads to an amplitude

$$2e\lambda R^2G\mathbf{p}\cdot\boldsymbol{\epsilon}, \tag{11}$$

where λ is a constant (of order unity) which depends on a derivative of G off the energy shell. This term is generally negligible compared with (5)—a value $\lambda\sim1$ changes the above value of R(30 Mev) only by $\sim5\%$. Assuming spin $j=0$, an accurate value of $P(3\pi+\gamma)/P(3\pi)$ would determine λ and thereby give new information on the $(\tau\to3\pi)$ matrix element. For higher spin values, it may be shown that this gauge-dependent amplitude may be obtained, to a good approximation, simply by the explicit replacement $\mathbf{p}\to\mathbf{p}+2e\mathbf{A}$ in the expression for G—here this direct-emission amplitude is independent of the τ-meson structure except through the normal 3π-amplitude G.

All other direct emission amplitudes must be gauge-invariant and therefore depend only on the field $\mathbf{E}(k)(=k\boldsymbol{\epsilon})$ or $\mathbf{H}(k)(=\mathbf{k}\times\boldsymbol{\epsilon})$ of the photon, according as the transition is electric or magnetic. Following the methods used in the discussion of the τ-meson decay,[6] the form of these amplitudes may readily be written down, particularly for the simplest (and most important) transitions. For 2^l-pole photon emission $(l=j-J)$, from state (j,w) to state (J,W), this amplitude will be a sum of the symmetric, traceless tensors of rank j which are linear in $\mathbf{E}(k)$ or $\mathbf{H}(k)$ (according as the emission is electric or magnetic) and which have $(l-1)$ factors $\mathbf{k}$, the remaining factors consisting of either (i), if $W=(-1)^{J+1}$, an even number $(2n$, say) of factors q, the last $(J-2n)$ factors being $\mathbf{p}$, or (ii), if $W=(-1)^J$, then one factor $\mathbf{p}\times\mathbf{q}$, an odd number $(2n-1)$ of factors $\mathbf{q}$, the remaining $(J-2n)$ factors being $\mathbf{p}$. The state $(J=1,\ W=-1)$ may be omitted, as the barriers against dissociation into three pions are then especially high[7]—in fact, for given J, 3π-emission is more difficult from state $W=(-1)^J$ than from a state $W=(-1)^{J+1}$ and the states (ii) above are not usually important. The coefficients of the various tensors (i) above contain a factor R^{J+1}—their momentum variation may be neglected. A complete expression will not be written out here but the above remarks will be illustrated by discussion of the case $(2-)$. The present statistics[8] on 3π-decay of the τ-meson suggest strongly that the spin j is even and the parity odd, so that this is the simplest case of nonzero spin which need be considered.

For spin $(2-)$, the amplitude G for 3π-decay is given by

$$G=[AT_{ij}(\mathbf{p},\mathbf{p})+BT_{ij}(\mathbf{q},\mathbf{q})]R^2, \tag{12}$$

where the symmetric, traceless, second-rank tensor $(x_iy_j+x_jy_i-\frac{2}{3}\mathbf{x}\cdot\mathbf{y}\delta_{ij})$ has been denoted by $T_{ij}(\mathbf{x},\mathbf{y})$. The present data on the energy correlations between pions in τ-meson decay requires that $|A|\sim|B|$ and that A and B should differ in phase by $\sim\pi/2$. The

[6] R. H. Dalitz, Phil. Mag. **44**, 1068 (1953) and Phys. Rev. **94**, 1046 (1954); E. Fabri, Nuovo cimento **11**, 479 (1954).

[7] The case of spin $(1-)$ is an exceptional one among low-spin values, A 3π-disintegration is very much unfavored because the relative motion of the like pions and the motion of the unlike pion relative to them must each carry two units of angular momentum, and therefore face large centrifugal barriers. E. Fabri and B. F. Touschek [Nuovo cimento **11**, 96 (1954)] have pointed out that these barriers may contribute a factor $\sim10^{-10}$ to the partial lifetime for 3π-decay and that this alone could account for the long observed τ-meson lifetime if all other competing processes were also strongly forbidden. However if the long life arises only from barrier effects, it is not easily understood why other processes for which the barriers are much less should not proceed rapidly—even if the 2π-decay is partially forbidden by some weak selection rule, the decay mode $2\pi+\gamma$ should proceed rapidly. In fact, even $3\pi+\gamma$ decay should proceed more rapidly than 3π-decay, by an $M1$ direct emission to the $(0-)$ state.

[8] R. H. Dalitz, Proceedings of the Fifth Rochester Conference, February, 1955 (to be published). A more detailed report is in preparation.

internal bremsstrahlung amplitude may now be written down, using the expression of reference 5 and the amplitude (12). The gauge-dependent $E1$ matrix element is now

$$4R^2AT_{ij}(\boldsymbol{\varepsilon},\mathbf{p}). \tag{13}$$

The only two gauge-invariant transitions to be considered are an $E1$ emission leading to $J=(1+)$ with amplitude

$$\rho AR^3T_{ij}(\mathbf{E},\mathbf{p})=\rho A(kR)T_{ij}(\boldsymbol{\varepsilon},\mathbf{p})R^2,$$

and an $E2$ emission leading to $J=(0-)$ with amplitude

$$\eta AR^3T_{ij}(\mathbf{E},\mathbf{k})=\eta A(kR)T_{ij}(\boldsymbol{\varepsilon},\mathbf{k})R^2.$$

Unless ρ or η are rather large, neither of these terms will contribute significantly to $P(3\pi+\gamma)$—for example, the η^2 term in the probability will increase $R(30)$ only in the proportion $0.002\eta^2$. Finally, with $B=iA$ and keeping only appreciable terms,

$$\frac{P(3\pi+\gamma)}{P(3\pi)}=\frac{16\alpha}{9\pi}\left|\left(\frac{\Delta}{k}\right)^2-2\frac{\Delta}{k}+4\right|\frac{\Delta^2kdk}{\mu E^4}. \tag{14}$$

That expressions (14) and (10) agree for very soft photons reflects the fact that the matrix element G used in each case reproduces the important features of the observed distributions in the 3π-decay. The form of the spectrum (14) is not greatly different from that predicted for zero spin—$R(30)$ is now 0.98×10^{-4} and $R(10)$ is 6.3×10^{-4}—the function $R(k)$ corresponding to (14) is plotted in Fig. 2.

It is also of interest to discuss on similar lines some further decay processes possible for the τ-meson. A model is necessary for the estimation of their branching ratios, and here we shall assume simply that all these processes are determined by a common "weak link" in the sequence of virtual processes between τ-meson and the final state. For order of magnitude estimates, it is unnecessary to specify the nature of this "weak link" in detail but, for example, it may be that the Λ^0-decay provides the basic weak process, so that

$$\tau^+\rightarrow\bar{\Lambda}^0+p\rightarrow\bar{p}+\pi^++p\rightarrow \text{ final decay products.} \tag{15}$$

Certainly the decay processes of the K-mesons and the hyperons must be linked together through their joint coupling with nucleons, but the situation may well be more complicated than this. With this fairly general model, the probability of a particular decay process may now be estimated from considerations of angular momentum conservation, barrier penetrability, and the volume of phase space allowable to the final particles, and will depend on the mass and radius of the τ-meson and on the coupling strength of the weak link. Such estimates will clearly be uncertain by numerical factors of order unity.

For spin $j\neq0$, the process

$$\tau^+\rightarrow\pi^++\gamma \tag{16}$$

would be rather rapid, owing to the large energy release. For spin $(2-)$ the matrix element has the form $gRT_{ij}(\mathbf{E},\mathbf{k})$, leading to decay probability $16\pi\alpha g^2(kR)^2k^2/M$ per unit time. Assuming $g\sim A$ [Eq. (12)], the branching ratio is

$$\frac{P(\pi+\gamma)}{P(3\pi)}\sim6\left(\frac{k}{E}\right)^4\frac{k}{M}\frac{1}{(\mu R)^2}\sim24. \tag{17}$$

This ratio is typical of the higher spin values. The absence of evidence for the decay process (16) from multiplate cloud-chamber studies is at present an important difficulty in the assumption of a nonzero τ-meson spin, although this could result if g/A were rather small (<0.1).

For $j=0$, the zero-zero transition (16) is, of course, completely forbidden. However, the internal pair conversion process

$$\tau^+\rightarrow\pi^++e^++e^- \tag{18}$$

is possible for all spin values. In plates, this process would be readily identified, whereas there are known to be a number of K-meson decays which lead to one relativistic charged particle and with which an event (16) may be confused. For spin $j\neq0$, process (18) results from internal conversion due to the transverse field produced in the decay and, as in the π^0-decay, the pair produced would be closely collimated opposite the direction of the pion. The internal conversion coefficient is 0.90×10^{-2}, so that the branching ratio $P(\pi+e^++e^-)/P(3\pi)$ would be ~0.2 for spin $(2-)$. The absence of this process in plates at present requires $g/A<\frac{1}{4}$ if the τ-meson has spin $(2-)$. For $j=(0-)$, the virtual electromagnetic field is spherically symmetric (and therefore longitudinal) and the pairs produced are wide angle pairs with angular separation $\sim(1+\cos\theta)d(\cos\theta)$. The coupling with the electric field will have the form $CR\mathbf{k}\cdot\mathbf{E}(k)$ and the branching ratio is then rather small, being $3\alpha^2(\mu R)^2(C/A)^2(M-\omega)^5/\mu^4\omega\sim5\times10^{-5}(C/A)^2$.

The further decay mode

$$\tau^+\rightarrow\pi^++\pi^0+\gamma \tag{19}$$

may occur by a direct emission process. The phase space available is 5.4 times that for the 3π-decay. For spin $(0-)$, this process will proceed by $M1$ photon emission to a $(1-)$ state which then breaks up to two pions. Owing to the increased barriers in the final state, the matrix element $\sigma R^2\mathbf{q}\cdot\mathbf{H}(k)$ is rather small and the relative probability for this mode is reduced to a value $(\mu R)^4\,10^{-2}\sim10^{-4}$ for $\sigma\sim G$. For spin $(2-)$, the most important matrix element is $\eta R^2T_{ij}(\mathbf{H}(k),\mathbf{q})$ and the relative probability to 3π-decay is close to $\sim4\%$.

Other decay processes leading to final states which include neutrinos may also occur but the estimation of their probabilities will require far more detailed assumptions than are needed above—these processes will not be discussed here.

Hence, for a pseudoscalar τ-meson, it would be readily understood for the dominant decay mode (excluding

neutrino processes) to be 3π-decay. The next probable decay process is then the radiative 3π-decay and it is not unreasonable to observe one such event at the present stage. For higher spin values compatible with the 3π-decay statistics, it would be natural to expect the $(\pi+\gamma)$ decay to compete favorably with 3π-decay—the absence of evidence for this decay process or for the related internal conversion process (18) may provide some argument against nonzero spin values for the τ-meson as data on the decay processes accumulate.

In conclusion, I am pleased to thank Dr. M. Gell-Mann for a discussion concerning these questions. I am also much indebted to Dr. B. Peters for early information concerning the radiative τ-meson decay event observed by the Bombay group.

APPENDIX A. RELATIVISTIC CALCULATION OF THE INTERNAL BREMSSTRAHLUNG

In the simple discussion of internal bremsstrahlung given above, retardation terms and other relativistic effects were neglected. However the retardation terms are not generally small compared with the terms retained. In discussing these relativistic terms here, it proves most direct to carry the calculation through in a completely relativistic way.

Using the covariant notation for the various graphs of type (a), the probability for emission of a photon k and pions of four-momenta p_1, p_2, p_3 is given by

$$\Sigma_\nu M_\nu^2(2\pi)^4\delta_4(p_1+p_2+p_3+k-P)\times\frac{d_3p_1}{(2\pi)^3\omega_1}\frac{d_3p_2}{(2\pi)^3\omega_2}\frac{d_3p_3}{(2\pi)^3\omega_3}\frac{d_3k}{(2\pi)^3k}, \quad \text{(A1)}$$

where P is the four-momentum of the τ-meson and M_μ is given by

$$M_\nu=eG\left(\frac{P_\nu}{P\cdot k}-\frac{p_{1\nu}}{p_1\cdot k}-\frac{p_{2\nu}}{p_2\cdot k}+\frac{p_{3\nu}}{p_3\cdot k}\right). \quad \text{(A2)}$$

In this expression the scalar products are four-dimensional and G denotes the amplitude for emission of the three pions, assumed independent of the momenta.

Observations on the photon would naturally be made for τ-mesons at rest, whereas the integration over the pion configurations is most readily carried through in the c.m. system of the three pions. Hence, for fixed photon momentum k, we transfer to the pion c.m. system. In this system the photon has four-momentum $(K_0,\mathbf{K})$ where $\mathbf{K}=\mathbf{k}[M/(M-2k)]^{\frac{1}{2}}$ and $K_0=K$. The τ-meson four-momentum $(P_0,\mathbf{P})$ is given by $P_0=(M^2+K^2)^{\frac{1}{2}}$, $\mathbf{P}=\mathbf{K}$, where M denotes the τ-meson mass, and the pion momenta will be denoted by $\mathbf{q}_1$, $\mathbf{q}_2$ and $\mathbf{q}_3$. Since the volume elements of (A1) are invariant, the probability expression becomes

$$\frac{1}{(2\pi)^4}\Sigma_\nu M_\nu^2\delta_3(\mathbf{q}_1+\mathbf{q}_2+\mathbf{q}_3)\delta(\omega_1+\omega_2+\omega_3-E_k)\times\frac{d_3q_1}{\omega_1}\frac{d_3q_2}{\omega_2}\frac{d_3q_3}{\omega_3}\frac{d_3k}{k}, \quad \text{(A3)}$$

where $E_k=(M^2-2Mk)^{\frac{1}{2}}$ and, now,

$$\Sigma_\nu M_\nu^2=\frac{M-2k}{M}\left[\frac{M^2}{(P\cdot k)^2}+\frac{\mu^2}{(q_1\cdot k)^2}+\frac{\mu^2}{(q_2\cdot k)^2}+\frac{\mu^2}{(q_3\cdot k)^2}-\frac{2P\cdot q_1}{(P\cdot k)(q_1\cdot k)}-\frac{2P\cdot q_2}{(P\cdot k)(q_2\cdot k)}+\frac{2P\cdot q_3}{(P\cdot k)(q_3\cdot k)}+\frac{2q_1\cdot q_2}{(q_1\cdot k)(q_2\cdot k)}-\frac{2q_2\cdot q_3}{(q_2\cdot k)(q_3\cdot k)}-\frac{2q_3\cdot q_1}{(q_3\cdot k)(q_1\cdot k)}\right]. \quad \text{(A4)}$$

Now in the integrations to be carried out there is complete symmetry between q_1, q_2 and q_3, so we may replace (A4) by

$$\frac{M-2k}{M}\left[\frac{M^2}{k^2(M-2k)}+\frac{3\mu^2}{(q_3\cdot k)^2}-\frac{2P\cdot q_3}{(P\cdot k)(q_3\cdot k)}-\frac{2q_1\cdot q_2}{(q_1\cdot k)(q_2\cdot k)}\right]. \quad \text{(A5)}$$

To carry through the integrations over q_1, q_2, a four-dimensional notation is very convenient. The q_1, q_2 phase-space volumes may be written

$$\frac{d_3q_1}{\omega_1}\frac{d_3q_2}{\omega_2}=4\delta(q_1^2-\mu^2)\delta(q_2^2-\mu^2)d_4q_1d_4q_2=\delta(Q\cdot R)\delta(Q^2+R^2-4\mu^2)d_4Qd_4R, \quad \text{(A6)}$$

where $Q=q_1+q_2$, $R=q_1-q_2$. The δ-functions of (A3) imply that Q is $(E_k-\omega_3,-\mathbf{q}_3)$ and only the R integration is left. With the following two integrals,

$$\int\delta(Q\cdot R)\delta(Q^2+R^2-4\mu^2)d_4R=2\pi\left(\frac{Q^2-4\mu^2}{Q^2}\right)^{\frac{1}{2}},$$

$$\int\frac{Q^2-R^2}{(Q\cdot k)^2-(R\cdot k)^2}\delta(Q\cdot R)\delta(Q^2+R^2-4\mu^2)d_4R=\frac{4\pi(Q^2-2\mu^2)}{(Q\cdot k)^2}\arctan\left(\frac{Q^2-4\mu^2}{Q^2}\right)^{\frac{1}{2}}.$$

Integration over directions of $\mathbf{q}_3$ and $\mathbf{k}$ may then be carried through to give the final result

$$P(3\pi+\gamma)=2G^2\frac{2\alpha}{\pi}\left(1-\frac{2k}{M}\right)\Phi(k)\frac{dk}{k}, \quad \text{(A7)}$$

where

$$\Phi(k)=\int\left\{q[1+x^2(k)]\operatorname{arctanh}x(k)+x(k)\omega\operatorname{arctanh}\frac{q}{\omega}-2qx(k)\right\}d\omega, \quad \text{(A8)}$$

and $x(k)=\{(E_k^2-2\omega E_k-3\mu^2)/(E_k^2-2\omega E_k+\mu^2)\}^{\frac{1}{2}}$.

Similarly $P(3\pi)$ is given by

$$P(3\pi)=2G^2\int qx(0)d\omega, \tag{A9}$$

with the value $0.153G^2\mu^2$, assuming an energy release of 74.3 Mev in τ-meson decay. The integral

$$R(k)=\int_k^{k_{max}} P(3\pi+\gamma)/P(3\pi)$$

is plotted in Fig. 2 as function of k (Mev)—the value $R(30)$ is now 1.1×10^{-4}, $R(10)$ being 1.06×10^{-3}.

APPENDIX B. MATRIX ELEMENTS FOR $E1$ TRANSITIONS

In covariant notation, the (off-diagonal) matrix element for 3π-decay of a spin j τ-meson may be denoted by $N_{\alpha\beta}\cdots(P,p,q)$, where $N_{\alpha\beta}\cdots$ has j suffices and P, p, q are four-momenta defined by

$$\begin{aligned} P&=p_1+p_2+p_3,\\ p&=p_3-\tfrac{1}{2}(p_1+p_2),\\ q&=\tfrac{1}{2}\sqrt{3}(p_1-p_2), \end{aligned} \tag{B1}$$

where p_3 and p_1, p_2 refer to the unlike and like pions respectively. The matrix element $N_{\alpha\beta}\cdots$ is a symmetrical, traceless tensor of rank j, which satisfies also

$$P_\alpha N_{\alpha\beta}\cdots=0. \tag{B2}$$

In the c.m. system, $P=(M_\tau,0,0,0)$ so that only completely space-like components of $N_{\alpha\beta}\cdots$ are then nonzero. $N_{\alpha\beta}\cdots$ therefore has just $(2j+1)$ independent components.

If this decay process proceeds in the presence of a weak field $A_\nu(k)$, there will be a first-order addition to the above matrix element, which we denote by $N_{\alpha\beta\cdots,\nu}(P,p,q;k)A_\nu(k)$. In particular, the matrix element for emission of a photon of polarization vector ϵ_ν together with the three pions is then given by $\epsilon_\nu N_{\alpha\beta\cdots,\nu}$. For frequencies $kR\ll1$, this matrix element will vary only little with k if it approaches a nonzero limit as $k\to0$. This zero-frequency limit gives the matrix element for the electric dipole transition, with errors of order (kR) for nonzero k. When $k=0$, the external field $A_\nu(k)$ is a constant field a_ν, say, which can be removed by a gauge transformation. This transformation replaces $N_{\alpha\beta}\cdots(P,p,q)$ by

$$N_{\alpha\beta}\cdots(P-ea,\ p+2ea,\ q), \tag{B3}$$

so that the required $E1$ matrix element (at zero frequency) is

$$\epsilon_\nu N_{\alpha\beta\cdots,\nu}=e\epsilon_\nu\left(2\frac{\partial N_{\alpha\beta}\cdots}{\partial p_\nu}-\frac{\partial N_{\alpha\beta}\cdots}{\partial P_\nu}\right). \tag{B4}$$

After these differentiations, relationships between p, q and P which are effective on the energy shell may then be substituted. Two cases will be considered: (a) *spin 0*. Expanding N in powers of pR and qR gives

$$N=A\left(\frac{P^2}{M^2}\right)+\frac{P\cdot p}{M}RB\left(\frac{P^2}{M^2}\right)+p^2R^2C\left(\frac{P^2}{M^2}\right)+q^2R^2D\left(\frac{P^2}{M^2}\right)+\cdots, \tag{B5}$$

where terms of order $(\mu R)^2$ are omitted, and then

$$N_\nu=e\left[-\frac{2P_\nu}{M^2}\left(A'+B'\frac{P\cdot p}{M}R+\cdots\right)-\frac{B}{M}p_\nu R+2B\frac{P_\nu}{M}R+2Cp_\nu R^2+\cdots\right].$$

In c.m. system, the only part of this appropriate for transverse polarizations is

$$\epsilon_\nu N_\nu=e\mathbf{p}\cdot\boldsymbol{\epsilon}R^2\left(2C-\frac{B}{MR}\right), \tag{B6}$$

where the coefficient is evaluated on the energy shell in the τ-meson rest system. (b) *spin 1*. The form of N_α is given by

$$N_\alpha=(P^2p_\alpha-P\cdot pP_\alpha)(R/M^2)\phi(P^2,P\cdot p,\cdots). \tag{B7}$$

It will be clear that, in calculating (B4), the terms coming from will be of order $(pR)^2$ relative to the main terms, and we will therefore neglect them to find

$$N_{\alpha,\nu}=(-2P_\nu p_\alpha+p_\nu P_\alpha-2P_\nu P_\alpha+\delta_{\alpha\nu}(2P^2+P\cdot p))\frac{R}{M^2}\phi+\cdots. \tag{B8}$$

Only space-like components are relevant in c.m. system and then

$$\epsilon_\nu N_{\alpha,\nu}=2\epsilon_\alpha\left(1-\frac{\omega}{2M}\right)R\phi(P^2=M^2,0,0\cdots). \tag{B9}$$

For consistency the term $\omega/2M$ should also be neglected, to give the result $2\phi R\boldsymbol{\epsilon}$ for this matrix element.

This result (B9) is typical of nonzero spin values and it will readily be seen that generally the dominant term of the zero-frequency $E1$ matrix element is obtained simply by the explicit replacement $p\to p+2eA$ in the matrix element for 3π-decay.

Multiple Meson Production Theories Applied to Cosmic-Ray Showers

OSMAN EL-MOFTY AND MOHAMED EL-NADI
University of Cario, Giza, Egypt
(Received March 11, 1955)

The multiple production theories are discussed from the point of view of multiplicity of produced mesons, and of their angular and radial distributions. Assuming that each π^0 meson produces a shower core, these theories are applied to the analysis of previous experiments on the structure of cosmic-ray showers. The analysis favors Fermi's theory with high anisotropy of angular distribution and it was found necessary to assume that only a small fraction of the energy in the original collision goes into the meson production.

INTRODUCTION

THE establishment of the fact that the primary cosmic radiation does not contain any appreciable number of electrons[1] demanded an explanation for the origin of the soft component of the cosmic rays, especially the extensive air showers. A theory was suggested[2] that these showers have their origin in nucleon-nucleon collisions in the upper atmosphere, with the production of both charged and neutral mesons. The decay of the neutral mesons, each into two γ-ray photons, will then start the cascades. This led experimental investigators to look for multiplicities in the shower cores corresponding to the multiplicities in the produced mesons.

Experiments performed in the last few years[3-6] have indicated a density distribution near the axis of the shower, which is considerably flatter than that predicted by the Molière theory.[7] This flattening of the distribution can be interpreted as an indication of the presence of multiple cores[8] in the shower. It was also pointed out that it is practically impossible to resolve the individual cores of a shower in air, since the half-radius of each core is much larger than the separation between the cores.

A different approach to the problem was suggested,[9] in which the individual cores can be resolved by using water as absorber. A shower, initiated by a single particle, which extends several meters in air, will shrink to a few centimeters after reaching equilibrium in water. The resolution and detection of these cores was carried out[10] by the use of fast ionization chambers under water. In this experiment, two ionization chambers were biased to detect twenty particles or more, so that it could be assumed that only shower cores were detected. Two decoherence curves were obtained at two depths under water, indicating coincidences between shower cores. The results of this experiment make it possible to study the production of mesons responsible for these cores, which leads to the study of the existing theories of multiple meson production for comparison with the available data. The aim of this work is to discuss these theories, the meson distributions they predict, and then calculate the expected decoherence curves for comparison with the experiment.[10]

CALCULATIONS

In the multiple theories of meson production it is assumed that a high-energy collision between two nucleons result in the production of a number N of mesons. On the average, one third of this number will be short-lived neutral mesons (π^0), each of which decays in flight into two γ-ray photons, starting the electron-photon cascades. The angle between the two photons can be easily calculated from the energy-momentum considerations of the decay. These decaying π^0 mesons, however, will have an angular distribution around the axis of the event as they receive a side momentum component during the production. The different theories give different angular distributions for these mesons. The existing theories of multiple meson production are those of Lewis, Oppenheimer, and Wouthuysen[2] (referred to as L.O.W.), Heisenberg, and Fermi.[11,12] The first two theories are fairly similar as regards the angular distributions, and so we will discuss only the L.O.W. and the Fermi theories.

L. O. W. Theory

Mesons are assumed to be pseudoscalar (with pseudovector coupling) and only a fraction K of the energy of the incident nucleon is carried by the emitted mesons. Rigorous calculations by Fukuda and Takeda[13] give for the multiplicity N the expression:

$$N=(2fK/\pi\mu_0)^4\bar{E}^4, \tag{1}$$

where f is the coupling constant, $\bar{E}$ the energy of the incident nucleon in the center-of-mass (c.m.) system, and μ_0 the rest energy of the π^0 meson. As regards the

[1] R. I. Hulsizer and B. Rossi, Phys. Rev. **73**, 1402 (1948).
[2] Lewis, Oppenheimer, and Wouthuysen, Phys. Rev. **73**, 127 (1948).
[3] R. W. Williams, Phys. Rev. **74**, 1689 (1948).
[4] W. E. Hazen, Phys. Rev. **85**, 455 (1952).
[5] Hazen, Williams, and Randall, Phys. Rev. **93**, 578 (1954).
[6] K. Sitte and D. L. Stierwalt, Phys. Rev. **94**, 988 (1954).
[7] G. Molière, *Cosmic Radiation*, edited by W. Heisenberg (Dover Publication, New York, 1946).
[8] J. M. Blatt, Phys. Rev. **75**, 1584 (1944).
[9] W. B. Fretter and J. Ise, Jr., Phys. Rev. **78**, 92 (1950).
[10] O. El-Mofty, Phys. Rev. **92**, 461 (1953).
[11] W. Heisenberg, Nature **164**, 65 (1949); Z. Physik **126**, 569 (1949); Naturwiss. **39**, 69 (1952).
[12] E. Fermi, Progr. Theoret. Phys. **5**, 570 (1951).
[13] H. Fukuda and G. Takeda, Progr. Theoret. Phys. **5**, 957 (1950); H. W. Lewis, Revs. Modern Phys. **24**, 241 (1952).

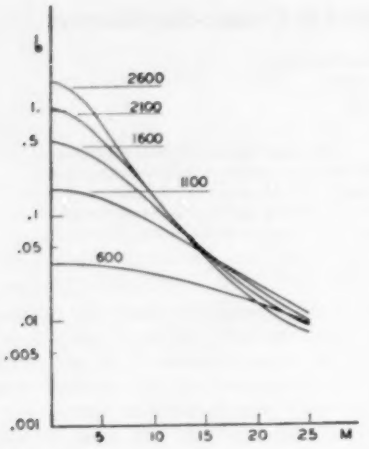

FIG. 1. The radial distribution of cores around the axis of the shower according to the L.O.W. theory, for different values of primary energies. The density σ is in numbers per square meter, and the distance in meters.

angular distribution, it gives a spherically symmetrical distribution in the c.m. system.

An interpretation of the fraction K was given by Heisenberg,[14] who considered K to be proportional to the integral of the overlapping original meson potentials surrounding the two nucleons. For energies occuring in cosmic rays, a value of about 0.1 was given for K. This value was supported experimentally by Hopper *et al.*[15] If one takes for the coupling constant f the value 3 as given by Fukuda,[16] Eq. (1) becomes

$$N=0.88\gamma^{\frac{1}{4}}, \tag{2}$$

where γ is now the energy of the incoming nucleon in the lab system in units of its rest energy.

The angular distribution in the lab system can be obtained by a Lorentz transformation from the c.m. spherically symmetrical distribution. If $F(\tilde{\theta},\gamma_0)d\tilde{\omega}d\gamma_0$ is the number of mesons emitted in the c.m. system between the solid angle $\tilde{\omega}$ (defined by the angle $\tilde{\theta}$) and $\tilde{\omega}+d\tilde{\omega}$, and having energies between γ_0 and $\gamma_0+d\gamma_0$, then the c.m. distribution can be represented by[17]

$$F(\tilde{\theta},\gamma_0)d\tilde{\omega}d\gamma_0=(N/4\pi)\delta(\gamma_0-\gamma_0')d\tilde{\omega}d\gamma_0, \tag{3}$$

where γ_0' is the common energy of the mesons. The transformation to the lab system can be effected to give the distribution $N(\theta)$ in the solid angle defined by θ and $\theta+d\theta$.[17] Let $\sigma(\theta)$ be defined by

$$\int_0^{\pi}\sigma(\theta)d\theta=N. \tag{4}$$

From the expression for $N(\theta)$ and from the fact that at the high energies considered, the ratio of the velocities of the nucleons and mesons in the c.m. system is very nearly equal to one, an expression for $\sigma(\theta)$ can be obtained[18]:

$$\sigma(\theta)d\theta=\frac{2N\gamma\alpha}{\cos^2\theta(\alpha^2+1)^2}d\theta, \tag{5}$$

where $\alpha=\gamma\tan\theta$.

The angles θ involved in these energetic events are very small, so that $\cos\theta$ can be taken equal to one and $\alpha=\gamma\theta$ in (5). If the production of the mesons take place at a height L in the upper atmosphere, and if each of the neutral mesons defines a core in the shower, then a radial distribution function of the cores can be deduced in a plane perpendicular to the direction of the primary particle:

$$\sigma=\frac{N\gamma^2}{3\pi L^2[\gamma^2(r^2/L^2)+1]^3}, \tag{6}$$

where σ is the density of cores at a distance r from the axis, and $N=3\int\sigma 2\pi r dr$. Numerical calculations for $\sigma(\theta)$ and σ were performed and curves were plotted[18] for different values of γ. The curves for σ are shown in Fig. 1.

In the above discussion, the angle between the two photons produced by the decay of the π^0 was neglected. This is possible because of the following considerations: The total angular spread for the mesons, e.g., in the L.O.W. theory, is of the order $\theta=3/\gamma$.[17] The most

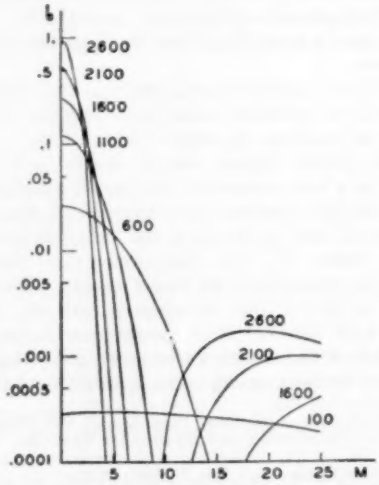

FIG. 2. The radial distribution of cores around the axis of the shower, according to Fermi's theory (for $n=4$), for different values of primary energies. The density σ is in numbers per square meter, and the distance in meters.

[14] W. Heisenberg, *Kosmische Strahlung* (Springer-Verlag, Berlin, 1953).
[15] Hopper, Biswas, and Darby, Phys. Rev. **84**, 457 (1951).
[16] H. Fukuda, Phys. Rev. **89**, 842 (1953).
[17] R. E. Marshak, *Meson Physics* (McGraw-Hill Book Company, Inc., New York, 1952). (Marshak's notation and treatment are followed in the present discussion.)
[18] O. El-Mofty and M. El-Nadi, Proc. Math. Phys. Soc. (Egypt) (to be published, 1955).

probable value for the angle between the two photons in the decay process is equal to $\varphi=2/\gamma_0$.[19] By Lorentz transformation from the c.m. to the lab system, we get

$$\gamma_0=\bar{\gamma}_0\bar{\gamma}+(\bar{\gamma}_0^2-1)^{\frac{1}{2}}\bar{\gamma}\cos\bar{\theta};$$

the angle φ can be expressed as

$$\varphi=\frac{2}{\bar{\gamma}_0\bar{\gamma}+(\bar{\gamma}_0^2-1)^{\frac{1}{2}}\bar{\gamma}\cos\bar{\theta}}\leqq\frac{2}{\bar{\gamma}_0\bar{\gamma}}\ll\theta.$$

Fermi's Theory

The picture given in Fermi's theory is that the angular distribution in the c.m. system is not in general spherically symmetric. It follows a $\cos^{2n}\bar{\theta}$ law, depending on the value of the impact parameter. This means that in an event n can take any of the values 1, 2, etc., which will determine the angular distribution. A transformation to the lab system gives the following result[17,18]:

$$N=\int\sigma(\theta)d\theta=\int\frac{(2n+1)N\bar{\gamma}\alpha(\alpha^2-1)^{2n}}{\cos^2\theta(\alpha^2+1)^{2n+2}}d\theta.$$

The radial distribution function for the shower cores will then be

$$\sigma=\frac{N\bar{\gamma}^2(2n+1)(\bar{\gamma}^2r^2/L^2-1)^{2n}}{6\pi L^2(\bar{\gamma}^2r^2/L^2+1)^{2n+1}}. \tag{7}$$

The multiplicity is related to the available energy in the c.m. system by: $N=1.34(2\bar{\gamma})^{\frac{1}{4}}$. $\sigma(\theta)$ and σ for $n=1$ and $n=2$ for different values of $\bar{\gamma}$ were calculated and plotted.[18] The curves for σ are shown in Fig. 2 for the case $n=4$. The case of $n=0$ corresponds to an isotropic distribution in the c.m. system. In the curves for σ, the value $L=16$ km was chosen on the assumption that the primary events occur after the primary particle had traversed one tenth of the atmosphere, so that the calculations can be compared with observations at mountain altitude[10] (elevation 2765 meters).

Decoherence Curves

It is now desired to consider the predictions based on the above theories with reference to the results of the above mentioned experiment. In this experiment two ionization chambers of area $A=0.087$ m^2 each were used. It was arranged such that they record at least 20 particle each. Coincidence rate was taken for different separations and at two depths in water 185 and 274 cm. The separations ranged from 87 cm to 645 cm. From the characteristic lateral dimensions of the shower under water and from the bias placed on the detector, it was assumed that the experiment was detecting coincidences between cores hitting the two chambers.

Let r_1 and r_2 be the distances of the two chambers from a shower axis intersecting the plane of the chambers. For a density distribution of cores σ in the shower, of multiplicity of cores η ($\eta=N/3$). The probability of a coincidence will be

$$(1-e^{-A\sigma(\eta,r_1)})(1-e^{-A\sigma(\eta,r_2)}).$$

If the frequency of these showers vary with η, according to some integral spectrum $f(\eta)$, the total counting rate of the arrangement will be for any separation of the chambers:

$$W=\int_{\eta_0}^{\infty}f(\eta)d\eta\iint_{\Sigma}(1-e^{-A\sigma(\eta,r_1)})(1-e^{-A\sigma(\eta,r_2)})d\Sigma. \tag{8}$$

The integral over $d\Sigma$ implies that the integration is to be carried out for all possible positions of the shower axis in the horizontal plane, with respect to the chambers.

Let I denote the integral:

$$I=\iint_{\Sigma}(1-e^{-A\sigma(\eta,r_1)})(1-e^{-A\sigma(\eta,r_2)})d\Sigma. \tag{9}$$

Since σ is represented graphically for different values of $\bar{\gamma}$, the integral I can be calculated for each of these energies. This was carried out numerically as follows: The horizontal plane of the chambers was divided into small squares. For a particular separation S between the two chambers, the center of each square was specified by its distances r_1 and r_2 from the two chambers. The corresponding values of σ were obtained, and the integrand of (9) evaluated. Contributions from all the squares were then added to give I for particular showers of primary energy $\bar{\gamma}$ and a particular separation S. The integral (8) can now be written as

$$W=\int_{\eta_0}^{\infty}f(\eta)I(\eta)d\eta. \tag{10}$$

TABLE I. The energies $\bar{\gamma}$ of the incoming particles used in the numerical calculations (in the c.m. system in units of rest mass of the nucleon), and the corresponding values of E, the energy in the lab system (in units of 10^{14} ev).

$\bar{\gamma}$ (in units of Mc^2)	600	1100	1600	2100	2600
$E(10^{14}$ ev)	6.7	22.7	48	91	130

TABLE II. Minimum values of energies, in the lab system (both in Bev and in units of nucleon rest energy), of the incoming nucleons which are capable of developing showers and maintaining at least 20 electrons at the indicated depths.

Depth below surface of water, in cm	Rad. units from production level	Energies Bev (lab. syst.)	γ_2 units of Mc^2
185	22	840	6.2×10^8
274	24.5	4000	2.9×10^9

[19] B. Rossi, *High Energy Particles* (Prentice-Hall Inc., New York, 1952).

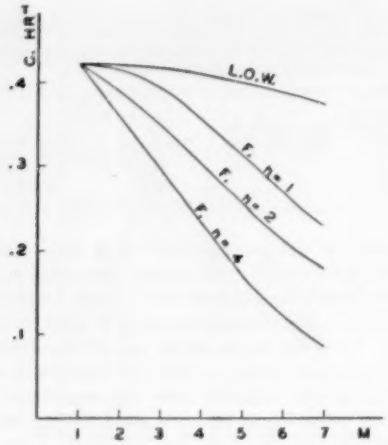

FIG. 3. Decoherence curves, calculated according to the L.O.W. and Fermi theories ($n=1,2,4$), normalized at a distance of one meter.

The energy range considered was divided into intervals of $\bar{\gamma}$, corresponding to the primary energies (in the lab system), shown in Table I. Each of the values of $\bar{\gamma}$ defines a particular value for the integrand in (10). The frequency spectrum $f(\eta)$ is taken to correspond to the energy-frequency spectrum: $f(E)=\text{const}\cdot E^{-2.67}$. By adding the contributions from the different energies, the value of W for the particular separation S is obtained.

In evaluating the limits of the integral I, two factors were considered: (1) the value of σ drops below detectable values, which means that most of the mesons produced are collimated within a specified cone, (2) the energy of the mesons produced at an angle larger than a certain value will not be enough for the core to contain (the detectable) twenty particles at the level of the chambers. This limiting value of the energy was obtained from the Rossi curves.[19] Both limiting values of the energy at the two depths 185 cm and 274 cm in water are shown in Table II. Using these values of γ_0 with different values of $\bar{\gamma}$ in the Lorentz transformation equation, $\gamma_0=\gamma_0\bar{\gamma}-(\gamma_0^2-1)^{\frac{1}{2}}(\bar{\gamma}^2-1)^{\frac{1}{2}}\cos\theta$, a limiting value $\theta(=r/L)$ is obtained. The limit on r is thus determined by the smaller of the values implied by the above two factors.

In determining the limits of the integral over η, the lower limit is that which corresponds to the values of γ_0 in Table II. The upper limit was taken as that corresponding to $\bar{\gamma}=2850$, as the contributions due to higher energies are small enough to be neglected because of the drop in the frequency spectrum.

RESULTS AND DISCUSSIONS

In calculating the decoherence curves by the above method, it was observed that the higher the collimation of the mesons produced, the steeper is the resulting decoherence curves. The L.O.W. theory gives a very flat decoherence curve as can be shown in Fig. 3. The curves based on Fermi's theory are also shown in the figure. The comparison shows clearly that the higher collimation (corresponding to larger values of n) results in steeper decoherence curves. To get agreement with experimental points,[10] values of $n=4$ or higher were found necessary (Fig. 5). It was also noticed during the calculations that most of the contribution to the decoherence curve comes from the lower energies considered; the contribution of the higher energies is reduced because of the form of the energy spectrum of the primary particles.

It is now desired to consider the effect of the absorber on the decoherence curve. The effect of the absorber (water) is to raise the lower limit of the energy (or multiplicity η) integral in Eq. (10). These considerations are directly related to the question of the fraction of the energy carried away by the mesons produced. The value of this fraction affects the separation between the two decoherences curves for the two depths. In the literature discussing Fermi's theory, no mention of the fraction of the available energy in the c.m. system (K) is found. If one takes $K=1$, the two decoherence curves for the different depths were found not to be separated enough to fit the experimental points. Thus, it seemed reasonable to introduce smaller values of K. It is expected that the value of K, in a given event, depends on the impact parameter. This was discussed in detail by Heisenberg,[14] who gave the relation: $K=e^{-b/R}$, where R is the radius of the collision volume and b the impact parameter. If we take the usually adopted median value $R/\sqrt{2}$ for b, we get $K\simeq 0.5$. Introducing now K into Fermi's theory, we get for N:

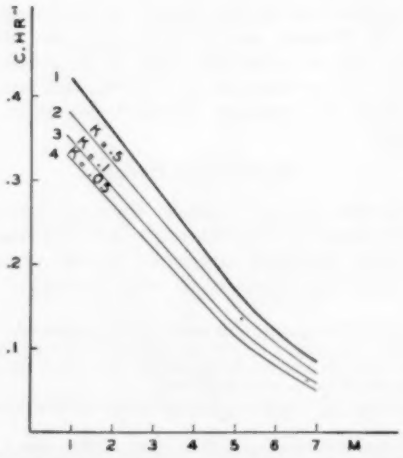

FIG. 4. Decoherence curves calculated according to Fermi's theory ($n=4$). Curve 1, for depth 185 cm of water, represents all values of K (by normalization at a distance of one meter). Curves 2, 3, and 4, for depths 274 cm of water, represent the indicated values of K.

$N=1.34(2K\gamma)^{\frac{1}{4}}$; but since, from the conservation of energy, $2K(\gamma-1)=(\mu_0/M)N\gamma_0$, and $\gamma_0\simeq 2\gamma_0\gamma$, we get:

$$\gamma_0=14K^{\frac{1}{3}}\gamma^{\frac{1}{3}}.$$

The above equation gives the effect of the value of K on the energy cutoff in Eq. (10). It was found, however, that $K=0.5$ was still unsatisfactory when compared with the experimental points. Lower values of K were assumed and the corresponding decoherence curves at the two depths were calculated. These curves are shown in Fig. 4. It was found that values of $K=0.05$ or less give a satisfactory fit with the experimental results. This small value of the energy available for the meson production is supported by the work of Hazen *et al.*[20] In their discussion of the spread of the air showers with reference to their energies, they found that in an average collision, treated according to the Fermi model, if the spread of the shower agrees with experiment, too much energy will be given to the shower.

The curves that fitted the experimental points reasonably are shown in Fig. 5, together with the experimental points. These curves were calculated for the parameters $n=4$ and $K=0.05$. All the decoherence curves were normalized such that, the curve at the smaller depth takes the value of 0.42 count per hour at a separation of one meter. This value was chosen by inspection to give the best fit with the experimental points.

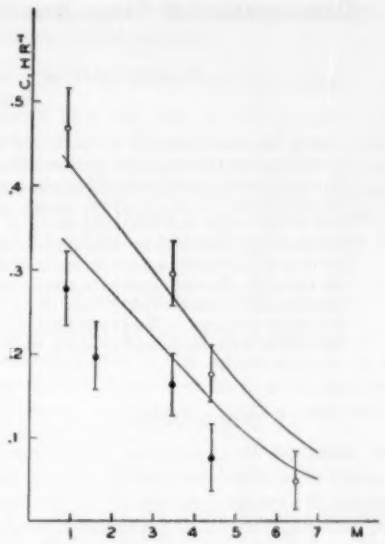

FIG. 5. Calculated decoherence curves for Fermi's theory ($n=4$, $K=0.05$) at the two depths 185 and 274 cm of water. Experimental points are also shown.

CONCLUSIONS

This analysis shows decisively the differences between the existing theories. While it was shown earlier[10] that the Molière distribution does not fit the experimental results on air showers, the present analysis shows clearly that the multiple-production theories give a reasonable agreement. The calculations based on the L.O.W. theory do not fit the experimental results. Agreement is obtained with Fermi's theory with high anisotropy in the angular distribution of the mesons produced in the c.m. system. It was necessary to introduce an inelasticity factor K in Fermi's theory, as the fraction of the energy given to the mesons. Best agreement was obtained with $K=0.05$.

[20] Hazen, Heineman, and Lennox, Phys. Rev. **86**, 198 (1952).

Consequences of Gauge Invariance for Electromagnetic Transitions. II*

R. H. Capps†
Department of Physics, University of Wisconsin, Madison, Wisconsin
(Received March 7, 1955)

Some theorems developed by Sachs and Austern, regarding the electromagnetic properties of gauge-invariant Schrödinger systems, are generalized so that they may be applied to any gauge-invariant, bound system of particles which is describable by a normalizable state vector. In particular, the following theorems are established: (1) At low photon energy, purely electric radiative or absorptive transitions will depend only on the initial and final state vector of the matter system, and on the energy change (the Siegert theorem). (2) f-sum rules are obtained for electric multipole radiation of arbitrary order, and are expressed in terms of the electromagnetic interactions of the system. (3) If the static moments of the particle system are neglected, the cross section for gamma-ray scattering will depend on the fourth or higher power of the photon energy in the low energy limit. Theorem (3) shows that the energy-independent term in the transition amplitude computed by Sachs and Foldy for the scattering of gamma rays from nucleons, occurs because the nucleon state vector used in their work is not normalizable.

I. INTRODUCTION

THE observed electromagnetic transitions of a system of particles may provide a useful tool for investigating the charge structure of the system. For example, such experiments as photomeson production from nucleons and the scattering of high-energy gamma rays from nucleons may reveal important information concerning the charged mesonic structure of the nucleon.

Many properties of electromagnetic transitions are common to a large class of particle systems. In so far as possible, it is worthwhile to delineate these properties before studying the details of the electromagnetic transitions of a particular system. Sachs and Austern[1] have demonstrated that, for any system of particles satisfying a Schrödinger equation, the requirement that the Hamiltonian be gauge-invariant imposes significant limitations on the cross section for photon scattering, and on the lifetimes for radiative transitions. In particular they show that if the static moments of the particle system are neglected, the photon scattering cross section is proportional to the fourth power of the photon energy in the low energy limit. They also show that the Siegert theorem concerning radiative transitions, and the f-sum rules for electric multipole radiation are consequences of gauge invariance.

The purpose of the present work is to examine the applicability of the theorems of I to certain particle systems not described by a nonrelativistic Schrödinger equation. It has been found possible to generalize these theorems to a quite broad class of particle systems. This class includes the system consisting of nucleons in interaction with several types of meson fields. The theorems are independent of the form of the Hamiltonian provided a condition of gauge invariance is satisfied. It is necessary, however, to impose the requirements that the initial and final wave functions be normalizable, and that there exists a complete set of normalizable stationary states of the particle system. It has been assumed here, as it was in I, that the electromagnetic interactions may be treated as a weak perturbation.

II. SOME IMPLICATIONS OF GAUGE INVARIANCE

Let the Hamiltonian for a system of particles in interaction with the electromagnetic field be given by $\mathcal{H}=\mathcal{H}_{em}+H$, where $\mathcal{H}_{em}$ is the Hamiltonian of the free electromagnetic field, and $H=H(\mathbf{A})$ is the Hamiltonian of the particle system, including its interaction with the electromagnetic field described by the vector potential $\mathbf{A}$. The requirement of gauge invariance may be stated as follows:

$$e^{iD}H(\mathbf{A})e^{-iD}=H(\mathbf{A}+\text{grad}G), \tag{1}$$

where

$$D=(1/\hbar c)\int d^3r G(\mathbf{r})\rho(\mathbf{r}). \tag{2}$$

The operator $\rho(\mathbf{r})$ is the charge density operator for the particle system and $G(\mathbf{r})$ is a gauge function, which may be any electromagnetic field operator that commutes with $\mathbf{A}$. Equation (2) is a generalization of the condition used in I and is equivalent to the usual statement that the Hamiltonian of the matter field is invariant under the simultaneous gauge transformation of the matter field operators and the electromagnetic field operators.

Because of the small size of the coupling constant, the electromagnetic interaction may usually be treated as a small perturbation. Therefore it is convenient to expand Eq. (1) in powers of $\mathbf{A}$ and grad G. Following the procedure of I, we write $H(\mathbf{A}+\text{grad}\,G)$ as a series of terms involving increasing powers of $(\mathbf{A}+\text{grad}\,G)$,

$$H(\mathbf{A}+\text{grad}\,G)=H_0+H_1(\mathbf{A}+\text{grad}\,G)+H_2(\mathbf{A}+\text{grad}\,G)+\cdots. \tag{3}$$

On the other hand, the left-hand side of Eq. (1) may

* Supported in part by the U. S. Atomic Energy Commission and in part by the Wisconsin Alumni Research Foundation.
† National Science Foundation Predoctoral Fellow.
[1] R. G. Sachs and N. Austern, Phys. Rev. **81**, 705 (1951). Hereafter, this paper will be referred to as I. Equations in this paper will be referred to as Eq. (I-1), etc.

be expanded in a series of commutators,

$$e^{iD}H(\mathbf{A})e^{-iD}=H(\mathbf{A})+i[D,H(\mathbf{A})]+\tfrac{1}{2}i^2[D,[D,H(\mathbf{A})]]+\cdots. \quad (4)$$

Since Eq. (1) is a formal identity, we may equate the terms of Eqs. (3) and (4) which are of the same order in the electric charge:

$$H_1(\mathbf{A}+\text{grad } G)=H_1(\mathbf{A})+i[D,H_0], \quad (5a)$$

$$H_2(\mathbf{A}+\text{grad } G)=H_2(\mathbf{A})+i[D,H_1(\mathbf{A})]+\tfrac{1}{2}i^2[D,[D,H_0]], \quad (5b)$$

and so on. These equations express necessary conditions on the form of the Hamiltonian and lead to information concerning several types of gamma-ray processes.

It will be convenient to write the vector potential of the radiation field as a sum of two terms:

$$\mathbf{A}(\mathbf{r})=\text{grad } G'+\mathbf{A}', \quad (6)$$

where $\mathbf{A}'$ is that part of $\mathbf{A}(\mathbf{r})$ which cannot be written as a gradient. To make this separation, we write $\mathbf{A}(\mathbf{r})$ in the form:

$$\mathbf{A}(\mathbf{r})=\sum_{\omega u}(2\pi\hbar c/\omega V)^{\frac{1}{2}}\mathbf{u}\exp(i\boldsymbol{\omega}\cdot\mathbf{r})(A_{\omega u}+A^*_{-\omega u}), \quad (7)$$

where $A^*_{\omega u}$ and $A_{\omega u}$ are the creation operator and annihilation operator for a photon of momentum $\hbar\boldsymbol{\omega}$ and polarization in the direction of the unit vector $\mathbf{u}$, and V is the volume of an enclosure used for normalization of the photon waves. The separation of Eq. (6) then corresponds to writing $\mathbf{u}\exp(i\boldsymbol{\omega}\cdot\mathbf{r})$ in the form,

$$\mathbf{u}\exp(i\boldsymbol{\omega}\cdot\mathbf{r})=\text{grad}\left[(\mathbf{u}\cdot\mathbf{r})\int_0^1 dy\exp(iy\boldsymbol{\omega}\cdot\mathbf{r})\right]+i[(\mathbf{u}\times\boldsymbol{\omega})\times\mathbf{r}]\int_0^1 ydy\exp(iy\boldsymbol{\omega}\cdot\mathbf{r}). \quad (8)$$

In the long wavelength limit the matrix elements of grad G' and $\mathbf{A}'$ correspond to the usual definition of electric and magnetic multipole moments, respectively.[2] Therefore we shall refer to grad G' as the electric part of $\mathbf{A}$, and $\mathbf{A}'$ as the magnetic part.

The operator G' in Eq. (6) may now be interpreted as a gauge function and Eqs. (5a) and (5b) may be rewritten with $\mathbf{A}'$ and G' substituted for $\mathbf{A}$ and G.

$$H_1(\mathbf{A})=H_1(\mathbf{A}')+i[D',H_0], \quad (9a)$$

$$H_2(\mathbf{A})=H_2(\mathbf{A}')+i[D',H_1(\mathbf{A})]+\tfrac{1}{2}i^2[D',[D',H_0]], \quad (9b)$$

where D' is given by

$$D'=(1/\hbar c)\int d^3rG'(\mathbf{r})\rho(\mathbf{r}). \quad (10)$$

Equations (9a) and (9b) represent the conditions of gauge invariance in the form we shall use in discussing one and two photon processes.

[2] J. G. Brennan and R. G. Sachs, Phys. Rev. **88**, 824 (1952).

III. SINGLE-PHOTON PROCESSES

Equation (9a) will now be used to show that, for processes involving the emission or absorption of a single, low-energy photon by a matter system, the transition probabilities for purely electric processes will not depend on the details of the electromagnetic interactions. The transition probability for a single photon process is

$$w=(2\pi/\hbar)\rho(E)\,|T|^2,$$

where $\rho(E)$ is the density of final states, and T, the transition amplitude, is the matrix element of $H_1(\mathbf{A})$ between the initial and final states of the particle and photon system. By using Eq. (9a), we may write the transition amplitude in the form,

$$T=\{H_1(\mathbf{A}')+i[D',H_0]\}_{\beta\alpha}, \quad (11)$$

where α and β signify the initial and final states respectively, of the particle and photon system.

It will be convenient to write Eq. (11) in terms of matrix elements between states of the particle system only. In the following discussion, the Greek subscripts α and β will always refer to states of the particle system plus the photon system, while Roman subscripts a and b will refer to the corresponding states of the particle system only.

For the sake of definiteness, we consider the case of photon absorption. Then the only term of Eq. (7) contributing to the transition amplitude is the term containing the annihilation operator $A_{\omega_a u_a}$, where $\hbar\boldsymbol{\omega}_a$ and $\mathbf{u}_a$ are the momentum and polarization of the incident photon. Hence, when Eq. (7) is used to write an explicit expression for the transition amplitude, both D' and $H_1(\mathbf{A}')$ may be replaced as follows:

$$D'\rightarrow d^-\omega_a^{-\frac{1}{2}}A_{\omega_a u_a},$$

$$H_1(\mathbf{A}')\rightarrow h^-\omega_a^{\frac{1}{2}}A_{\omega_a u_a}.$$

The particle operators d^- and h^- depend parametrically on $\boldsymbol{\omega}_a$ and $\mathbf{u}_a$ and, as can be seen from Eqs. (6), (7), and (8), are independent of photon energy in the low energy limit. Equation (11) may now be written in terms of the operators d^- and h^-.

$$T=\{\omega_a^{\frac{1}{2}}h^-+i\omega_a^{-\frac{1}{2}}[d^-,H_0]\}_{ba}, \quad (12)$$

where the Roman indices a and b refer to the initial and final states of the particle system alone.

Since attention will be limited to electric transitions in the long-wavelength limit, just the second term of Eq. (12) is to be considered. This may be rewritten in the form,

$$i\hbar c\omega_a^{-\frac{1}{2}}d^-_{bd}\omega_{db}, \quad (13)$$

if use is made of the general relation,

$$[O,H_0]_{ba}=\hbar c\omega_{ba}O_{ba}, \quad (14)$$

where O is an arbitrary particle operator and $\hbar c\omega_{ab} = E_a - E_b$, the difference in the energies of the particle states labeled a and b. Note here that we are working in the representation in which H_0 is diagonal.

In order to discuss the properties of electric transitions, the operator d^- will be written in terms of the charge density operator and the quantum numbers of the absorbed proton. The operator G' may be expressed in the form

$$G'(\mathbf{r}) = \sum_{\omega\alpha}(A_{\omega\alpha} + A^*_{-\omega\alpha})\omega^{-\frac{1}{2}} f(\omega,\mathbf{u},\mathbf{r}). \quad (15)$$

Then, from Eq. (10) and the definition of d^-, we find

$$d^- = (1/\hbar c)\int d^3r\rho(\mathbf{r}) f(\omega_\alpha,\mathbf{u}_\alpha,\mathbf{r}). \quad (16)$$

The function f may be obtained explicitly from Eqs. (6), (7), and (8). Thus it can be seen from Eq. (16) that the form of the operator d^- does not depend on the nature of the interaction of the matter system with the electromagnetic field. It is clear that this result also applies to the case of photon emission. Hence, at long wavelengths, for processes which are purely electric, the transition probability for the emission or absorption of a single photon depends only on the initial and final wave functions of the particle system, and on the energy change. This result is a generalization of the Siegert theorem.[3]

The derivation in I of the f-sum rules for electromagnetic radiation may be generalized in a similar fashion to the type of system considered here. The generalization is straightforward and the results obtained may be expressed in the form of Eq. (I-35).

IV. APPLICATION TO PHOTOPION PRODUCTION

The results of Sec. III may be applied to the problem of photopion production from hydrogen. Unfortunately, application of the Siegert theorem is strictly valid only in the limit of infinite photon wavelength, while the wavelength in this case must be less than the pion Compton wavelength. However the fact that the pion proper field of a proton seems to be concentrated at distances of the order of the nucleon Compton wavelength[4] indicates that the long-wavelength approximation may be fairly good for the case of the photoproduction of a single pion at an energy not too far from threshold. Thus the Siegert theorem may be applicable to this case.

The long-wavelength approximation to the photopion production problem is quite simple. In the expansion of the vector potential, Eq. (7), $\mathbf{u}\exp(i\omega\cdot\mathbf{r})$ may be replaced by $\mathbf{u}=\text{grad}\,(\mathbf{u}\cdot\mathbf{r})$. The transition is of electric dipole order, and the transition amplitude is given by Eq. (13). If the operator d^- is written in the form of Eq. (16), the function f is, in this case,

$$f(\omega_\alpha,\mathbf{u}_\alpha,\mathbf{r}) = (2\pi\hbar c)^{\frac{1}{2}}(\mathbf{u}_\alpha\cdot\mathbf{r}). \quad (17)$$

Hence the transition amplitude is given by

$$T = i(2\pi\hbar c/\omega_\alpha V)^{\frac{1}{2}}\omega_{ab}\left[\int d^3r\rho(\mathbf{r})(\mathbf{u}_\alpha\cdot\mathbf{r})\right]_{bc}. \quad (18)$$

Since $\rho(\mathbf{r})$ is the charge density operator of the system, this result shows that the transition amplitude is simply related to the matrix element of the static dipole moment between the two states of the nucleon-pion system.

The usefulness of the f-sum rules for the photopion production is more doubtful, since the sum rules may be used to obtain integrated cross sections only when the cross section is small for small photon wavelengths. However, the photopion cross section is large at energies considerably above threshold.

Nevertheless, it is interesting to compare the f-sum rule for electric dipole absorption by protons, to the corresponding rule for absorption by atoms. In making this comparison, it is assumed that the dominant mechanism for photon absorption by protons is that of pion emission, and that the proton ground-state wave function may be written as a sum of terms, each involving a spin $\frac{1}{2}$, i-spin $\frac{1}{2}$, nonrecoiling core particle, surrounded by zero, one, or two charged pions. It is further assumed that any contribution to the operator $H_2(\mathbf{A})$ resulting from the core particle-pion interaction may be neglected.[5]

If these assumptions are made, the electric dipole f-sum rule for the proton may be written in the following form:

$$\int \sigma_0 dE = 2\pi^2 e^2\{\textstyle\sum_k k_0^{-1} f_1^*(\mathbf{k}) f_1(\mathbf{k})$$

$$+2\,\text{Re}[f_0 \textstyle\sum_k k_0^{-1} f_2(\mathbf{k}, -\mathbf{k})]\} + \text{terms in } f_2^2, \quad (19)$$

where the symbols have the following meanings: the integral $\int\sigma_0 dE$ represents the integral over photon energy of the total electric dipole absorption cross section, the complex number f_0 is the amplitude of the zero pion state in the proton ground-state wave function, $f_1(\mathbf{k})$ is the amplitude of the state describing one positive pion of momentum $\hbar\mathbf{k}$ and $f_2(\mathbf{k},\mathbf{k}')$ is the amplitude of the state describing two pions, a positive pion of momentum $\hbar\mathbf{k}$, and a negative pion of momentum $\hbar\mathbf{k}'$.

The corresponding sum rule for absorption by an atom may be written

$$\int \sigma_0 dE = (2\pi^2 e^2\hbar/mc)Z. \quad (20)$$

[3] R. G. Sachs, *Nuclear Theory* (Addison-Wesley Press, Cambridge, 1953), p. 243.

[4] See, for example, G. F. Chew, Phys. Rev. **95**, 1669 (1954); R. G. Sachs, Phys. Rev. **95**, 1065 (1954).

[5] In this derivation, the f-sum rule is written in terms of the interaction $H_2(\mathbf{A})$. See Eq. (I-35).

The first terms in Eq. (19) and Eq. (20) are closely related. The quantity $\sum_s |f_1(\mathbf{k})|^2(1/\hbar c k_0)$ represents the probability for the presence of a single pion in the proton wave function, divided by an average energy of the pion. The atomic sum rule is obtained if this quantity is replaced, in the first term of Eq. (19), by (Z/mc^2), the number of electrons in the atom divided by the electron rest energy.

On the other hand the second term in Eq. (19) represents interference between the zero and the two pion states. There is no atomic analog to such a term.

V. THE SCATTERING OF GAMMA RAYS

Equations (9a) and (9b) may be used to predict several properties of the cross section for the scattering of gamma rays by particle systems in the limit of small photon energy. The treatment to be given here is a generalization and extension of that of I.

The differential cross section is given by the expression $d\sigma/d\Omega=(\omega V/2\pi\hbar c)^2 d\Omega|T|^2$, in which T, the transition amplitude, is the sum of two terms $T=T'+T''$, where T' arises from the direct scattering by the second-order interaction $H_2(\mathbf{A})$, while T'' is due to the first-order interaction $H_1(\mathbf{A})$, which contributes in the second order of the perturbation theory. Using Eqs. (9), we write

$$T'=\{H_2(\mathbf{A}')+i[D',H_1(\mathbf{A}')] +\tfrac{1}{2}i^2[D',[D',H_0]]\}_{\beta\alpha}, \quad (21a)$$

$$T''=\sum_\eta \frac{\{H_1(\mathbf{A}')+i[D',H_0]\}_{\beta\eta}\{H_1(\mathbf{A}')+i[D',H_0]\}_{\eta\alpha}}{E_\alpha-E_\eta}. \quad (21b)$$

Here, the index α refers to the initial state of the entire system, the scattering system plus the initial photon. Similarly, β refers to the final state of the entire system and η to intermediate states. As in Sec. III, Greek subscripts will always refer to states of the entire system, and italic subscripts will refer to the particle system only.

It will be convenient to write Eqs. (21a) and (21b) in terms of matrix elements between states of the particle system only. In order to accomplish this, we first note that since $H_1(\mathbf{A}')$ and D' are linear in the photon annihilation and creation operators, they may be written as,

$$H_1(\mathbf{A}')=H_1{}^+(\mathbf{A}')+H_1{}^-(\mathbf{A}'), \quad D'=D'^++D'^-,$$

where $H_1{}^+$ and D'^+ contain only those terms of Eq. (7) involving creation operators, and $H_1{}^-$ and D'^- contain only those terms involving annihilation operators. The operators $H_1{}^-$ and D'^- always annihilate the incident photon; hence, the only contribution from Eq. (7) to a matrix element of $H_1{}^-$ or D'^- arises from the term having the polarization $\mathbf{u}_a$ and the momentum $\hbar\omega_a$ of the incident photon. Similarly, matrix elements of $H_1{}^+$ and D'^+ contain just the term relating to the polarization $\mathbf{u}_\beta$ and momentum $\hbar\omega_\beta$ of the scattered photon. Therefore, when Eq. (7) is used to obtain explicit expressions for D'^-, D'^+, $H_1{}^-$, or $H_1{}^+$, they may again be replaced as follows:

$$D'^- \to d^-\omega_a{}^{-\frac{1}{2}}A_{\omega_a u_a},$$
$$D'^+ \to d^+\omega_\beta{}^{-\frac{1}{2}}A^*_{\omega_\beta u_\beta},$$
$$H_1{}^-(\mathbf{A}') \to h^-\omega_a{}^{\frac{1}{2}}A_{\omega_a u_a},$$
$$H_1{}^+(\mathbf{A}') \to h^+\omega_\beta{}^{\frac{1}{2}}A^*_{\omega_\beta u_\beta}.$$

The quantities d^- and h^- are operators of the particle system which depend parametrically on the momentum and polarization of the incident photon. Similarly, d^+ and h^+ are particle operators which depend parametrically on the momentum and polarization of the scattered photon.

An important property of the four operators d^-, d^+, h^-, and h^+, which will be used below, is their independence of the energy of the photon in the low-energy limit. This can be seen from Eqs. (6), (7), and (8) by noting that grad G' depends on ω to the power $\omega^{-\frac{1}{2}}$ while $H_1(\mathbf{A}')$ depends on ω to the power $\omega^{\frac{1}{2}}$. The extra power of ω in the magnetic term arises from the factor $[(\mathbf{u}\times\boldsymbol{\omega})\times\mathbf{r}]$ in the magnetic part of Eq. (8).

With the aid of this notation, Eqs. (21) may be written in terms of the particle operators d^-, d^+, h^-, and h^+.

$$T'=\{i\omega_\beta{}^{\frac{1}{2}}\omega_\alpha{}^{-\frac{1}{2}}[d^-,h^+]+i\omega_\alpha{}^{\frac{1}{2}}\omega_\beta{}^{-\frac{1}{2}}[d^+,h^-] +\tfrac{1}{2}i^2\omega_\alpha{}^{-\frac{1}{2}}\omega_\beta{}^{-\frac{1}{2}}[d^+,[d^-,H_0]] +\tfrac{1}{2}i^2\omega_\alpha{}^{-\frac{1}{2}}\omega_\beta{}^{-\frac{1}{2}}[d^-,[d^+,H_0]]\}_{ba} +\text{terms in } H_2(\mathbf{A}'), \quad (22a)$$

$$T''=-\sum_n\left\{\frac{(\omega_a{}^{\frac{1}{2}}h^-+i\omega_a{}^{-\frac{1}{2}}[d^-,H_0])_{bn}(\omega_b{}^{\frac{1}{2}}h^++i\omega_b{}^{-\frac{1}{2}}[d^+,H_0])_{na}}{\hbar c(\omega_{na}+\omega_\beta)} +\frac{(\omega_\beta{}^{\frac{1}{2}}h^++i\omega_\beta{}^{-\frac{1}{2}}[d^+,H_0])_{bn}(\omega_a{}^{\frac{1}{2}}h^-+i\omega_a{}^{-\frac{1}{2}}[d^-,H_0])_{na}}{\hbar c(\omega_{na}-\omega_a)}\right\}. \quad (22b)$$

Equation (22b) has been written as a sum of two terms, the first referring to intermediate states containing two photons, the second referring to zero photon intermediate states. The indices a, b, and n refers to the initial, final, and intermediate states of the particle system, respectively. The quantities $\hbar c\omega_a$ and $\hbar c\omega_\beta$ are

the energies of the initial and scattered photons respectively, and $\hbar c\omega_{na}$ is the energy difference between the particle states n and a.

We now turn our attention to the long-wavelength limit in order to show that if the scattering from the static moments of the particle system is neglected, and if the minimum energy of excitation of the system is finite, then the transition amplitude will depend on the photon energy to the first or higher power.[6] It will be necessary to assume that the ground state of the system is described by a state vector which is normalized in the internal variables.

In the following discussion each term of T' or T'' will be expressed as a sum over intermediate states of the products of matrix elements of two operators. In all such sums the contribution from intermediate states which represent the particle system in its ground state will be neglected. This is equivalent to neglecting the scattering from the static moments of the system. In order to indicate that only scattering through excited states is being included in the discussion, the symbols T, T', and T'' will be replaced by T_e, T_e', and T_e''. In computing a cross section, of course, the terms in the transition amplitude which depend on the static moments must be added to T_e to obtain the complete transition amplitude.

At long wavelength, the energy of recoil is small compared to the energy of the incident photon. Therefore, the recoil energy of the particle system will be neglected, and it will be assumed that the incident and scattered photon have the same energy, $\hbar c\omega$.

If the excitation energies, ω_{na}, of the excited states of the particle system are all greater than some finite quantity, then we may expand the energy denominators of T_e'' in powers of ω/ω_{an} in order to study the low energy limit of the cross section. Upon making this expansion, we see from Eqs. (22a) and (22b) that there are three types of terms which could contribute to T_e to a power of ω lower than the first:

(*A*) The purely electric part of T_e', and the purely electric part of T_e'' which arises in the zero order of the expansion of the denominators. These terms are proportional to ω^{-1} as ω approaches zero.

(*B*) The electric-magnetic cross terms of T_e' and zero order electric-magnetic cross terms of T_e'', which are independent of photon energy in the zero energy limit.

(*C*) The first-order electric term of T_e'', which are independent of energy in the zero energy limit.

The purely magnetic part of T_e' is not written out explicitly in Eq. (22a). However, because of the factor ω^{-1} in Eq. (7), and the factor $[(\mathbf{u}\times\boldsymbol{\omega})\times\mathbf{r}]$ in Eq. (8), the purely magnetic part of T_e' must be proportional to the first or higher power of ω at low energy.

The three types of term, *A*, *B*, and *C* will now be examined.

Type A

The zero-order electric terms of T_e'' cancel identically against the electric terms of T_e'. The proof, which makes use of Eq. (14) and the closure property of the intermediate states labelled by n, is identical with that given in I.

Type B

We use Eqs. (22b) and (14) to write the electric-magnetic cross terms of T_e'' as

$$i\sum_n\left\{\frac{h^-{}_{bn}d^+{}_{na}-d^-{}_{bn}h^+{}_{na}}{1+(\omega/\omega_{ba})}+\frac{h^+{}_{bn}d^-{}_{na}-d^+{}_{bn}h^-{}_{na}}{1-(\omega/\omega_{ba})}\right\}. \tag{23a}$$

The electric-magnetic cross terms of T_e' are seen from Eq. (22a) to be

$$i\{[d^-,h^+]+[d^+,h^-]\}_{ba}. \tag{23b}$$

It can be seen from the closure property of the intermediate states n that the zero-order terms of the expression, Eq. (23a) (i.e., for $\omega/\omega_{na}=0$) cancel identically against the expression, Eq. (23b).

Type C

By making use of Eqs. (22b) and (14), we may write the purely electric terms of T_e'' in the form

$$\frac{\hbar c}{\omega}\sum_n\left\{\frac{d^-{}_{bn}d^+{}_{na}(-\omega_{na}{}^2)}{\omega_{na}+\omega}+\frac{d^+{}_{bn}d^-{}_{na}(-\omega_{na}{}^2)}{\omega_{na}-\omega}\right\}. \tag{24}$$

The terms which arise in the first order of the expansion of the denominators may be written

$$\hbar c\sum_n\{d^-{}_{bn}d^+{}_{na}-d^+{}_{bn}d^-{}_{na}\}=\hbar c[d^-,d^+]_{ba}. \tag{25}$$

The function G' in Eq. (6) can be expressed in the form of Eq. (15). Then as can be seen from Eq. (10) and the definitions of d^- and d^+, the commutator $[d^-,d^+]_{ba}$ becomes

$$(1/\hbar c)^2\int\int d^3r\,d^3r'\,f(\boldsymbol{\omega}_\alpha,\mathbf{u}_\alpha,\mathbf{r})f(-\boldsymbol{\omega}_\beta,\mathbf{u}_\beta,\mathbf{r}')\times[\rho(\mathbf{r}),\rho(\mathbf{r}')]_{ba}. \tag{26}$$

The commutator $[\rho(\mathbf{r}),\rho(\mathbf{r}')]$ must vanish for all values of $\mathbf{r}$ and $\mathbf{r}'$; therefore the first-order electric terms of T_e'' cancel.

This completes the proof that in the limit of zero photon energy, T_e depends on ω to the first or higher power. It should be emphasized that these results depend on the assumption that the particle system is

[6] This theorem has been independently proved, by quite different methods, for the case of a scattering system consisting of a spin one-half particle in interaction with various kinds of meson fields, by F. Low [Phys. Rev. **96**, 1428 (1954)] and by M. Gell-Mann and M. Goldberger [Phys. Rev. **96**, 1433 (1954)]. These authors show that if the transition amplitude for the scattering of a photon from a spin one-half particle is expanded in powers of the energy, the first two terms (of orders ω^{-1} and ω^0) depend only on the charge, mass, and intrinsic and anomalous static magnetic moments of the particle.

described by a normalizable state vector. An example of a calculation using non-normalizable state vectors which violates the above theorem is the work of Sachs and Foldy.[7] These authors calculate the cross section for the scattering of gamma rays from nucleons using nonrelativistic, no-recoil, weak coupling, pseudoscalar meson theory. The state vector representing the nucleon ground state in their calculation is not normalizable in the meson variables. Because of this lack of normalizability, their calculated transition amplitude contains a term [the $\boldsymbol{\sigma}\cdot\mathbf{u}\times\mathbf{u}'$ term in Eq. (20) of reference 4], which results from scattering through excited states of the nucleon, and which is independent of photon energy in the low-energy limit. Therefore, this term violates the above stated theorem. In the following paper, the procedure of Sachs and Foldy is modified in a manner which insures that the state vectors are normalizable, and the cross section is recalculated. The transition amplitude calculated by this procedure no longer contains this energy-independent term.

[7] R. G. Sachs and L. L. Foldy, Phys. Rev. **80**, 824 (1950).

VI. ACKNOWLEDGMENTS

This problem was suggested by R. G. Sachs, who contributed valuable advice during the couse of the work. Several suggestions by W. G. Holladay were helpful in proving the theorem of Sec. V.

PHYSICAL REVIEW VOLUME 99, NUMBER 3 AUGUST 1, 1955

Electromagnetic Properties of the Nucleon in a Finite Source Theory*

R. H. Capps,† and W. G. Holladay†‡
Department of Physics, University of Wisconsin, Madison, Wisconsin
(Received March 7, 1955)

Some electromagnetic properties of nucleons are investigated under the assumption that the nucleon consists of a spin one-half core particle in interaction with the pion field through a gauge-invariant, nonrelativistic, pseudoscalar, finite source interaction. Recoil of the nucleon core is neglected and the weak coupling approximation is used. A method is presented for making the finite source interaction between two particle fields gauge-invariant by introducing filaments of current in the region of the source function. The theoretical contributions of interaction currents to the magnetic moments of the proton and neutron are calculated and found to be small compared to the observed anomalous moments and of the opposite sign. The model is used to calculate, in the limit of zero source size, the total and differential cross sections for scattering of gamma rays from nucleons. The results, which are presented graphically, are found to be in accord with the conditions imposed on a finite theory in the preceding paper. They are compared to the results obtained by Sachs and Foldy on the basis of a point-source theory.

I. INTRODUCTION

THE recent discoveries[1] of heavy mesons and hyperons indicate that it is entirely possible that the nucleon core which emits and absorbs pions, instead of being simple, may be structured, i.e., composed of two or more of the "new" particles, one or more of which may carry the source of the pion field. A complete theory of the nucleon would have to incorporate the details of the structured core and would then depend on the nature of the particles which compose this structure.

However, in many processes involving low-energy pions and photons, the complicated details of the source may not be important and therefore it may be possible to account for the important effects of the core structure by introducing a smooth source function into the interaction between the pion field and its source. This means that the annihilation and creation of pions are not limited to a mathematical point in space, but can occur over a small but finite region, the size of which is determined by the dimensions of the source function.

The notion of the extended source has already been introduced,[2] not for the physical reasons just stated, but for the formal advantage that the extended source possesses in regard to circumventing the well-known divergence difficulties that are encountered in the point source theory. An important result of the introduction of the extended source is that high-momentum pions are quenched, so that the state vector of the pion-nucleon system, which was not normalizable in the point-source theory, can now be normalized. The advantage of working with normalizable state vectors has been emphasized in the preceding paper, in which many of the results depend on this property.

* Supported in part by the U. S. Atomic Energy Commission, and in part by the Wisconsin Alumni Research Foundation.
† National Science Foundation Predoctoral Fellow.
‡ Now at Vanderbilt University, Nashville, Tennessee.
[1] For up-to-date reviews of these matters see: L. Leprince-Ringuet, Ann. Rev. Nuc. Sci. **3**, 39 (1953); Many authors, Proc. Roy. Soc. (London) **A221**, 277–420, (1954); Proceedings of the Fourth Rochester Conference (University of Rochester Press, Rochester, 1954).

[2] W. Pauli and S. M. Dancoff, Phys. Rev. **62**, 85 (1942). W. Pauli, *Meson Theory of Nuclear Forces* (Interscience Publishers, Inc., New York, 1946).

It is clear, then, that certain advantages accrue with the advent of the extended source, but on the other hand, the extended source theory raises new problems of its own. As generally applied, this theory is not Lorentz-covariant. But this fact causes no great concern here since the point of view is taken that the extended source theory is not supposed to be a fundamentally rigorous theory but a way to avoid the complicated details of the nucleon core, a procedure which, it is hoped, has validity at least in low-energy processes.

Furthermore, there is the question of making the theory gauge-invariant when the interaction of the pion-nucleon system with photons is considered. As pointed out by Blair *et al.*,[3] the essential difficulty lies in the fact that in the present form of the extended source theory, the pion is created or absorbed at some particular point inside the source, whereas the entire spread-out nucleon changes from a neutron to a proton or *vice versa*, a process which violates the continuity equation of charge and current density. One of the important features of the present paper is the delineation of the manner in which an extended source, pion-nucleon interaction may be made gauge-invariant. The procedure involves the introduction of filaments of current within the source so that the continuity equation is satisfied everywhere. These filaments of current are not to be construed as accurately representing the physical situation inside the source, but merely as some sort of approximation to the actual currents that presumably exist there. Nevertheless, some physical consequences of these "pseudocurrents" are presented. Consideration is given to a peculiar effect that arises from the virtual photons generated by these currents. The contribution of these currents to the nucleon magnetic moments is deduced and found to be zero for the simplest possible kind of filaments, namely, straight lines of current emanating radially from the origin. However, a contribution to the magnetic moment[4] remains from the interaction current that arises in the gradient-type coupling. This effect is found to be small and in the opposite direction to the observed anomalies.

Attention is then given to the implications of the static, gradient-type, extended-source interaction for the differential and total cross sections for the scattering of γ rays by protons and neutrons. The point source in the pion-nucleon interaction employed in the calculation of this process by Sachs and Foldy[5] is replaced by a finite source and the cross sections recalculated. The SF result for the low-energy expression of the transition amplitude contains a spin-dependent term which is independent of the photon frequency. This violates the theorem of Sec. V of the preceding paper, a result which depends on the fact that the point-source theory of SF leads to non-normalizable state vectors. The violation is found not to occur in the normalizable, extended-source theory, even in the limit as the source size is allowed to approach zero. The numerical results given here are obtained in this limiting case, so that the finite source is used here only as a convergence procedure. It does not represent a physical smearing out of the core particle.

Two other modifications of the procedure used in SF are made. First, the absorptive part of the scattering, omitted by SF, is included. Second, the pion-nucleon coupling constant is obtained from experiments performed since the publication of SF. The discussion of the γ-ray scattering problem in the present paper is an amplification of some remarks published previously.[6]

II. GAUGE INVARIANCE OF THE INTERACTION

The Hamiltonian of a static pion field interacting with an infinitely heavy source can be separated into two parts:

$$H=H_f+H',$$

where H_f is the total energy of the free pion field,[7] and H' is the interaction energy between the pions and the source. For pseudoscalar pions interacting in a charge symmetric way with an extended, spin $\frac{1}{2}$, isotopic spin $\frac{1}{2}$ source, a rather commonly used[2] expression for H' is

$$H'=(4\pi)^{\frac{1}{2}}(gc/\mu)\int d^3\mathbf{r}\, f(\mathbf{r})\tau_+\boldsymbol{\sigma}\cdot\nabla\varphi(\mathbf{r})+\text{h.c.}, \quad (1)$$

where g is the coupling constant in units of electric charge, μ the reciprocal pion Compton wavelength, $f(\mathbf{r})$ the spherically symmetric source function normalized so that $\int f(\mathbf{r})d^3\mathbf{r}=1$, $\varphi(\mathbf{r})$ a component of the charged pion field which creates a negative or absorbs a positive pion, and $\tau_+=\frac{1}{2}(\tau_1+i\tau_2)$ is an isotopic spin operator which converts a neutral into a positively charged source. Only charged pions have been included in H', since the major concern here is the behavior of the system in the presence of an electromagnetic field, with which neutral pions presumably have no direct interaction.

The importance of introducing an electromagnetic field into the Hamiltonian in such a way as to satisfy the condition of gauge invariance has been emphasized in the preceding paper. If $H(\mathbf{A})$ designates the matter Hamiltonian modified to take into account the interaction of matter with photons, the gauge condition of the preceding paper becomes, for the particular Hamiltonian under consideration,

$$e^{iD}H(\mathbf{A})e^{-iD}=e^{iD}[H_f(\mathbf{A})+H'(\mathbf{A})]e^{-iD}$$
$$=H_f(\mathbf{A}+\text{grad}\, G)+H'(\mathbf{A}+\text{grad}\, G), \quad (2)$$

[3] Blair, Chew, Friedman, and Salzman (privately circulated report, 1952).

[4] No consideration is given in this paper to the magnetic moments that derive from the conventional pion convection currents.

[5] R. G. Sachs and L. L. Foldy, Phys. Rev. **80**, 824 (1950). Hereinafter, this paper will be referred to by the symbol SF. Numbered equations in SF will be referred to as Eq. (SF-1), etc.

[6] R. H. Capps and R. G. Sachs, Phys. Rev. **96**, 540 (1954).

[7] For the form of H_f, see Wentzel, *Quantum Theory of Fields* (Interscience Publishers, Inc., New York, 1949), p. 49.

in which $G(\mathbf{r})$ is a guage function which may be any electromagnetic field operator that commutes with $\mathbf{A}$. The expression for D is

$$D=(1/\hbar c)\int[\rho_\pi(\mathbf{r})+\tfrac{1}{2}(1+\tau_3)e\delta(\mathbf{r})]G(\mathbf{r})d^3r, \quad (3)$$

where $\rho_\pi(\mathbf{r})$ is the charge density operator for the pion field. The second term in Eq. (3) is concerned with the charge on the source.

It is of interest to determine the form of $H(\mathbf{A})$ satisfying Eq. (2). The H_f part can be made gauge-invariant by the well-known prescription,[8] of replacing each grad φ and grad φ^* by $[\text{grad}-(ie/\hbar c)\mathbf{A}]\varphi$ and $[\text{grad}+(ie/\hbar c)\mathbf{A}]\varphi^*$, respectively. However, because of the presence of the extended source, H' modified only in this way does not satisfy the gauge condition, but requires an additional factor which[9] can assume the form

$$\exp\left[\pm(ie/\hbar c)\int_0^r A_s ds\right], \quad (4)$$

the argument of the exponential being a line integral of the vector potential from the origin to the point in the source where the pions are created or absorbed. The proper modification of H' in the presence of an electromagnetic field then is

$$H'(\mathbf{A})=(4\pi)^{\frac{1}{2}}(gc/\mu)\int d^3r\Big\{f(\mathbf{r})\tau_+ \times\exp\left[(-ie/\hbar c)\int_0^r A_s ds\right]\boldsymbol{\sigma}\cdot[\nabla-(ie/\hbar c)\mathbf{A}]\varphi\Big\}+\text{h.c.} \quad (5)$$

The fact that this expression for $H'(\mathbf{A})$ satisfies Eq. (2) with D given by Eq. (3) follows from the statements

$$e^{iD}\tau_\pm e^{-iD}=\tau_\pm\exp[(\pm ie/\hbar c)G(0)], \quad (6)$$

$$e^{iD}\{\boldsymbol{\sigma}\cdot[\nabla-(ie/\hbar c)\mathbf{A}]\varphi\}e^{-iD}=\exp[(-ie/\hbar c)G(\mathbf{r})]\times\boldsymbol{\sigma}\cdot[\nabla-(ie/\hbar c)(\mathbf{A}+\text{grad}\,G)]\varphi(\mathbf{r}). \quad (7)$$

Just as the extended source is a phenomenological device to make a complex system susceptible to calculations yielding finite results, so the exponential of the vector potential in $H'(\mathbf{A})$ is a convenient means of preserving the gauge invariance of the theory, i.e., the effect of the exponential is to replace the presumably complicated current distribution inside the source by a more simple current distribution, which nevertheless keeps the continuity equation of charge and current density satisfied. Indeed, the physical effect of this added factor is best seen through an examination of the current distribution that it produces.

Since the small currents produced by external fields are of no interest, the part of the current independent of the electromagnetic field is desired. When $H_1'(\mathbf{A})$, the term in $H'(\mathbf{A})$ linear in $\mathbf{A}$, is cast into the form

$$H_1'(\mathbf{A})=-c^{-1}\int\mathbf{j}_{\text{int}}\cdot\mathbf{A}d^3r, \quad (8)$$

the relevant current density can be identified as the quantity which is denoted by $\mathbf{j}_{\text{int}}$ in the expression.

The current defined in this way satisfies Maxwell's equations, and is referred to as the interaction current, since it arises from the special form of the interaction H'. To obtain the part of $H'(\mathbf{A})$ linear in $\mathbf{A}$, the exponential in Eq. (5) is expanded and the linear terms are found to be

$$H_1'(\mathbf{A})=-(4\pi)^{\frac{1}{2}}(ige/\mu\hbar)\int d^3r f(r)\times\left[\left(\int_0^r A_s ds\right)(\tau_+\boldsymbol{\sigma}\cdot\nabla\varphi-\tau_-\boldsymbol{\sigma}\cdot\nabla\varphi^*)+(\tau_+\boldsymbol{\sigma}\cdot\mathbf{A}\varphi-\tau_-\boldsymbol{\sigma}\cdot\mathbf{A}\varphi^*)\right]. \quad (9)$$

Now the arbitrary line integral from the origin to the point $\mathbf{r}$ may be rewritten in the form,

$$\int_0^r A_s ds=\int_0^r\left[d\mathbf{s}\cdot\int d^3\mathbf{r}'\mathbf{A}(\mathbf{r}')\delta(\mathbf{r}'-\mathbf{s})\right], \quad (10)$$

where $\mathbf{s}$ represents a vector to the point on the line and $d\mathbf{s}$ is an infinitesimal vector tangent to the line at the endpoint of the vector $\mathbf{s}$.

Then

$$H_1'(\mathbf{A})=-(4\pi)^{\frac{1}{2}}(ige/\mu\hbar)\int d^3r'\Big(\mathbf{A}(\mathbf{r}')\cdot\int d^3r f(r)\times\Big\{\Big[\int_0^r d\mathbf{s}\delta(\mathbf{r}'-\mathbf{s})\Big][\tau_+\boldsymbol{\sigma}\cdot\nabla\varphi(\mathbf{r})-\tau_-\boldsymbol{\sigma}\cdot\nabla\varphi^*(\mathbf{r})]+\boldsymbol{\sigma}\delta(\mathbf{r}'-\mathbf{r})[\tau_+\varphi(\mathbf{r})-\tau_-\varphi^*(\mathbf{r})]\Big\}\Big). \quad (11)$$

Comparison with Eq. (8) shows that the current is

$$\mathbf{j}_{\text{int}}(\mathbf{r}')=(4\pi)^{\frac{1}{2}}(igec/\mu\hbar)\int d^3r f(r)\Big\{\Big[\int_0^r d\mathbf{s}\delta(\mathbf{r}'-\mathbf{s})\Big]\times[\tau_+\boldsymbol{\sigma}\cdot\nabla\varphi(\mathbf{r})-\tau_-\boldsymbol{\sigma}\cdot\nabla\varphi^*(\mathbf{r})]+\boldsymbol{\sigma}\delta(\mathbf{r}'-\mathbf{r})[\tau_+\varphi(\mathbf{r})-\tau_-\varphi^*(\mathbf{r})]\Big\}. \quad (12)$$

[8] See reference 7, p. 66.

[9] This form was suggested to the authors by R. G. Sachs. Compare R. G. Sachs, Phys. Rev. **74**, 433 (1948). Factors of this kind were also considered by Peierls and Chretien with regard to nonlocal interactions in field theory, R. Peierls and M. Chretien, Proc. Roy. Soc. (London) **A233**, 468 (1954). See also C. Bloch, Kgl. Danske Videnskab Selskab, Mat.-fys Medd. **27**, 8 (1952).

This is just the current that comes from $H'(\mathbf{A})$, no consideration having been given to current that arises from $H_f(\mathbf{A})$. The first part of the expression, Eq. (12), derives from the exponential term in Eq. (5) and can be interpreted as a line of current[10] flowing between the origin and the point in the source where the pions are created or destroyed. Once again the phenomenological nature of this current should be pointed out. It doubtless does not correctly represent the current distribution within the source and has been inserted for the sake of keeping inviolate the law of conservation of electric charge within the source. The second term in Eq. (12) is the well-known current given previously by Pauli and Dancoff.[2]

III. UNIQUENESS OF THE ELECTROMAGNETIC INTERACTION

In the absence of an electromagnetic field, the form of a linear, charge-symmetric, static interaction of pseudoscalar pions with an infinitely heavy, extended, spin $\frac{1}{2}$, isotopic spin $\frac{1}{2}$ source is given uniquely by Eq. (1). An alternative expression[3] is

$$H'_{\rm alt}=(4\pi)^{\frac{1}{2}}(g\hbar c/\mu)\int d^3r F(r)\tau_+\varphi(\mathbf{r})\boldsymbol{\sigma}\cdot\mathbf{r}+\text{h.c.}, \quad (13)$$

but $H'_{\rm alt}$ can be obtained from H' by an integration by parts of the latter expression, which shows that $H'=H'_{\rm alt}$ if

$$F(r)=(1/r)(df/dr).$$

In the presence of an electromagnetic field, however, $H'_{\rm alt}(A)$, which has the gauge invariant form,

$$H'_{\rm alt}(A)=(4\pi)^{\frac{1}{2}}(g\hbar c/\mu)\int d^3r\left\{F(r)\tau_+\varphi(\mathbf{r})\boldsymbol{\sigma}\cdot\mathbf{r}\times\exp\left[(-ie/\hbar c)\int_0^r A_s ds\right]\right\}+\text{h.c.}, \quad (14)$$

is not equivalent to $H'(\mathbf{A})$. This can be seen by an integration by parts of $H'(\mathbf{A})$, which gives

$$H'(\mathbf{A})=-(4\pi)^{\frac{1}{2}}(g\hbar c/\mu)\int d^3r\left\{\tau_+\varphi(\mathbf{r})\boldsymbol{\sigma}\cdot\left[(\mathbf{r}/r)(df/dr)+(ie/\hbar c)f(r)\left(\mathbf{A}-\text{grad}\int_0^r A_s ds\right)\right]\times\exp\left[(-ie/\hbar c)\int_0^r A_s ds\right]\right\}+\text{h.c.} \quad (15)$$

For purposes of simplification, the line integral is taken along a straight line. Then

$$\boldsymbol{\sigma}\cdot\nabla\int_0^r A_s ds=\boldsymbol{\sigma}\cdot\nabla\int_0^1 d\alpha[\mathbf{r}\cdot\mathbf{A}(\alpha\mathbf{r})]=\boldsymbol{\sigma}\cdot\left\{\mathbf{A}(\mathbf{r})+\int_0^1 d\alpha[\mathbf{r}\times\text{curl}\mathbf{A}(\alpha\mathbf{r})]\right\}, \quad (16)$$

whereupon

$$H'(\mathbf{A})=-(4\pi)^{\frac{1}{2}}(g\hbar c/\mu)\int d^3r\left\{\boldsymbol{\sigma}\cdot\left[(\mathbf{r}/r)(df/dr)-(ie/\hbar c)f(r)\int_0^1\mathbf{r}\times\text{curl}\mathbf{A}(\alpha\mathbf{r})d\alpha\right]\exp\left[(-ie/\hbar c)\times\int_0^1\mathbf{A}(\alpha\mathbf{r})\cdot\mathbf{r}d\alpha\right]\tau_+\varphi(\mathbf{r})\right\}+\text{h.c.} \quad (17)$$

The nonequivalence of $H'(\mathbf{A})$ and $H'_{\rm alt}(\mathbf{A})$ then resides in the presence of the term in $H'(\mathbf{A})$ containing curl$\mathbf{A}$. Whether or not such a term exists must be decided by experiment.

Any linear combination of $H'(\mathbf{A})$ and $H'_{\rm alt}(\mathbf{A})$ will satisfy the conditions of gauge invariance. This is a manifestation of the fact that any term of the form $H(\text{curl}\mathbf{A})$ that satisfies the condition $[\rho,H(\text{curl}\mathbf{A})]=0$, where ρ is the charge density operator for the matter system, may be added to a gauge-invariant Hamiltonian without destroying gauge invariance.

IV. VIRTUAL PHOTONS

Assuming for the moment that $H'(\mathbf{A})$ does give a correct account of the current distribution within the source, let us investigate some of its electromagnetic consequences. First we consider the effects of virtual photons produced by the vector potential in the exponential factor of $H'(\mathbf{A})$. Usually such photons, arising from the interaction of charged particles with the electromagnetic field, cause self-energy divergences such as that encountered, for instance, in the $A^2\varphi^2$ term of the gauge invariant form of H_f.

In contrast to this relatively simple A^2 dependence, arbitrarily high powers of $\mathbf{A}$ are present in the exponential under study, so that the divergence arises here in a quite complicated manner. If all virtual photons are included in a calculation, every matrix element of $H'(\mathbf{A})$ will include a factor of $e^{-\infty}$, which will cause the matrix elements to vanish.[11] This can be seen in the following way. Suppose, for the sake of simplicity, that the line integral is taken along a straight line; then an expansion of the vector potential into plane waves

[10] A filament of current of a very similar nature has been introduced by Adams in connection with nuclear exchange currents. E. N. Adams II, Phys. Rev. **81**, 1 (1951). See also R. K. Osborn and L. L. Foldy, Phys. Rev. **79**, 795 (1950).

[11] This point has been observed by Heitler and communicated to us by W. Thirring. See also R. Peierls and M. Chretien, Proc. Roy. Soc. (London) **A223**, 468 (1954).

yields

$$\exp\left[(\pm ie/\hbar c)\mathbf{r}\cdot\int_0^1 A(\alpha\mathbf{r})d\alpha\right]$$

$$=\exp\left\{(\pm ie/\hbar c)(\hbar c2\pi/V)^{\frac{1}{2}}\sum_{\omega,u}\left[(A_{\omega,u}+A^*_{-\omega,u})\times\omega^{-1}\mathbf{u}\cdot\mathbf{r}\int_0^1\exp(i\boldsymbol{\omega}\cdot\boldsymbol{\alpha}\mathbf{r})d\alpha\right]\right\}, \quad (18)$$

in which $\mathbf{u}$ is the photon polarization, $\boldsymbol{\omega}$ is its wave vector, A and A^* are photon creation and annihilation operators, and V is the volume of an enclosure used for normalization of the photon waves. The effect of the virtual photons can be isolated by arranging the terms in Eq. (18) in such a way that the annihilation operators act first. To accomplish this, use is made of the theorem[12] for two operators, a and b, whose commutator is a c-number,

$$\exp(a+b)=(\exp a)(\exp\tfrac{1}{2}[b,a])(\exp b). \quad (19)$$

If a is identified with the A^* part and b with the A part of the expression, Eq. (18), this expression may be written in the form of the right side of Eq. (19). If the sum over the two directions of polarization is carried out, the terms corresponding to $\exp(\frac{1}{2}[b,a])$ may be written in the following form,

$$\exp\left((-e^2/4\pi\hbar c)\int_{-1}^1 dx\left\{(1-x^2)\int_0^\infty\rho(2/\rho x)^2\times[\sin^2(\rho x/2)]d\rho\right\}\right), \quad (20)$$

where $\rho=\omega r$. The integral over ρ in this expression diverges logarithmically at infinity causing $H'(\mathbf{A})$ to vanish.

Of course, one way to circumvent this predicament in calculations involving real photon processes is to ignore the effect of virtual photons altogether, i.e., replace the expression, Eq. (20) by one. Perhaps a more physically meaningful approach to the removal of the divergence under study is to note that, for extremely short wavelengths, the details of the structure of the source would become important. The consideration of such details would not be consistent with the notion that the complexities of the source could be replaced by the smooth source function $f(r)$. Therefore, the photon wavelengths should be smaller that the dimensions of the source and thus should be limited by the condition

$$\omega r\leqq 1. \quad (21)$$

[12] Harold T. Davis, *The Theory of Linear Operators* (Principia Press, Inc., Bloomington, 1936), p. 198.

Application of this condition limits the integration over ρ in the expression, Eq. (20) to the range $0\leqq\rho\leqq 1$, and Eq. (20) now becomes $\exp(-e^2/6\pi\hbar c)$. This expression is very nearly unity and the vanishing of $H'(\mathbf{A})$ no longer occurs. It is concluded that the formally gauge invariant expression Eq. (5) for $H'(\mathbf{A})$ can be employed in a perturbation calculation of electromagnetic processes for which the condition Eq. (21) is satisfied.

V. MAGNETIC MOMENTS

Having given consideration to the effect of virtual photons, we now investigate some of the implications of $H'(\mathbf{A})$ with regard to real photon processes. Attention will first be given to the contribution of $H'(\mathbf{A})$ to the static nucleon magnetic moments. The moment will be calculated to lowest order in g, i.e., to order g^3. The magnetic moment operator is defined by

$$M_z(\text{int})=\tfrac{1}{2}c^{-1}\int d^3r'[\mathbf{r}'\times\mathbf{j}_{\text{int}}(\mathbf{r}')]_z, \quad (22)$$

where $\mathbf{j}_{\text{int}}(\mathbf{r}')$ is the interaction current density. The insertion of Eq. (12) for the current density yields

$$M_z(\text{int})=(i\pi^{-1}ge/\mu\hbar)\int\int d^3r'd^3r f(r)\mathbf{i}_z\cdot\left(\mathbf{r}'\times\left\{\left[\int_0^r d\mathbf{s}\delta(\mathbf{r}'-\mathbf{s})\right]\times[\tau_+\boldsymbol{\sigma}\cdot\nabla\varphi(\mathbf{r})-\tau_-\boldsymbol{\sigma}\cdot\nabla\varphi^*(\mathbf{r})]+\boldsymbol{\sigma}\delta(\mathbf{r}'-\mathbf{r})[\tau_+\varphi(\mathbf{r})-\tau_-\varphi^*(\mathbf{r})]\right\}\right), \quad (23)$$

where $\mathbf{i}_z$ denotes a unit vector in the positive z direction.

Note that $M_z(\text{int})$ changes sign under the mirror operation in charge space, the operation which reflects the i-spin space through a plane containing the z axis, i.e., $M_z(\text{int})\leftrightarrow -M_z(\text{int})$ when $\tau_+\leftrightarrow\tau_-$, $\varphi\leftrightarrow\varphi^*$ and $\tau_z\leftrightarrow-\tau_z$. But under the assumption that the interaction between mesons and nucleons is charge symmetric, this operation changes a neutron state to a proton state and *vice versa*. Consequently, the expectation value $\langle M_z(\text{int})\rangle$ is equal in magnitude but opposite in sign for the proton as compared to the neutron. Thus, the mirror theorem of Sachs,[13] concerning the sum of neutron and proton moments, is not affected by any contribution from these interaction currents.

To obtain an idea of the size of $\langle M_z(\text{int})\rangle$, we consider the simplest form of $M_z(\text{int})$, which corresponds to choosing the path of the line integral to be a straight

[13] R. G. Sachs, Phys. Rev. **87**, 1100 (1952).

line. Then,

$$M_z(\text{int})=(i\pi^{\frac{1}{2}}ge/\mu\hbar)\int\int d^3\mathbf{r}'d^3\mathbf{r}\,f(r)\mathbf{i}_z\cdot\Big(\mathbf{r}'\times\Big\{\Big[\mathbf{r}\int_0^1\delta(\mathbf{r}'-\alpha\mathbf{r})d\alpha\Big]\times[\tau_+\boldsymbol{\sigma}\cdot\nabla\varphi(\mathbf{r})-\tau_-\boldsymbol{\sigma}\cdot\nabla\varphi^*(\mathbf{r})]+\boldsymbol{\sigma}\delta(\mathbf{r}'-\mathbf{r})[\tau_+\varphi(\mathbf{r})-\tau_-\varphi^*(\mathbf{r})]\Big\}\Big). \quad (24)$$

Because of the factor $\delta(\mathbf{r}'-\alpha\mathbf{r})$, $\mathbf{r}'$ and $\mathbf{r}$ are always parallel and $\mathbf{r}'\times\mathbf{r}$ vanishes. This result is simply a manifestation of our particular choice of the path of integration, which constrains the line current to flow radially, whereas a circulating current is required to produce a magnetic moment. Thus, the contribution to the magnetic moment of the phenomenological line current has been made zero, so that

$$M_z(\text{int})=(i\pi^{\frac{1}{2}}ge/\mu\hbar)\times\int d^3r[f(r)(\mathbf{r}\times\boldsymbol{\sigma})_z(\tau_+\varphi-\tau_-\varphi^*)], \quad (25)$$

which is the result that would be obtained[2] even if the line currents or the exponential factor had not been introduced.

To find $\langle M_z\rangle$ to order g^2, the ground-state eigenfunction of H to order g is needed. This eigenfunction for a nucleon with spin up is, to the required order

$$\Phi=\Phi\{0\}+\Phi\{1\}=\Phi\{0,\sigma_z=1,\tau_z=\pm1\}+\sum_{\substack{k,\text{ spin,}\\ \text{isotopic spin}}}\frac{\langle\Phi\{\mathbf{k},\sigma_z,\tau_z\}|H'|\Phi\{0,\sigma_z=1,\tau_z=1\}\rangle\times\Phi\{\mathbf{k},\sigma_z\tau_z\}}{-\hbar c(\mu^2+k^2)^{\frac{1}{2}}}, \quad (26)$$

where $\Phi\{0,\sigma_z=1,\tau_z=\pm1\}$ is the functional describing the state with no pions present, namely, just the core of the nucleon, with $\tau_z=\pm1$ referring to the positive and neutral cores respectively. Similarly, $\Phi(\mathbf{k},\sigma_z\tau_z)$ represents the core surrounded by one pion in a state of momentum $\hbar\mathbf{k}$. Since the calculation is carried out in momentum space, we record the operators H' and $M_z(\text{int})$ in that representation

$$H'=i(gc/\mu)(2\pi\hbar/cV)^{\frac{1}{2}}\sum_{\mathbf{k}}\{f(k)\boldsymbol{\sigma}\cdot\mathbf{k}(\mu^2+k^2)^{-\frac{1}{4}}\times[(a_{\mathbf{k}}+b_{-\mathbf{k}}^*)\tau_+-(a_{-\mathbf{k}}^*+b_{\mathbf{k}})\tau_-]\}, \quad (27)$$

$$M_z(\text{int})=-(ge/\mu)(\pi/2\hbar cV)^{\frac{1}{2}}\sum_{\mathbf{k}}\{(k^{-1}df/dk)\times(\mu^2+k^2)^{-\frac{1}{4}}(\mathbf{i}_z\cdot\boldsymbol{\sigma}\times\mathbf{k})\times[(a_{\mathbf{k}}+b_{-\mathbf{k}}^*)\tau_+-(a_{-\mathbf{k}}^*+b_{\mathbf{k}})\tau_-]\}, \quad (28)$$

where $a_{\mathbf{k}}$ and $a_{\mathbf{k}}^*$ are the annihilation and creation operator's for positive mesons and the b's refer similarly to negative mesons. The function $f(k)$ is the Fourier transform of the spherically symmetric source function $f(r)$. Then,

$$\langle M_z(\text{int})\rangle=\langle\Phi|M_z|\Phi\rangle=\mp\frac{g^2e}{3\pi\hbar c\mu^2}\int_0^\infty dk f^2(k)\frac{d}{dk}\Big(\frac{k^3}{\mu^2+k^2}\Big), \quad (29)$$

the negative sign referring to the proton and the positive to the neutron. The fact that the integral is always positive for any real function $f(k)$ leads to the conclusion that $\langle M_z(\text{int})\rangle$ gives a magnetic moment anomaly opposite to that observed.[14]

The magnitude of the anomaly depends on the particular form of $f(k)$. For the choice

$$f(k)=1,\quad k\leqq K,\qquad =0,\quad k>K, \quad (30)$$

then

$$\langle M_z(\text{int})\rangle_z=\mp(g^2e/3\pi\hbar c\mu^2)K^3(\mu^2+K^2)^{-\frac{1}{2}}. \quad (31)$$

If the cut-off momentum is large, i.e.,

$$K^2\gg\mu^2, \quad (32)$$

then

$$\langle M_z(\text{int})\rangle=\mp(2g^2/3\pi\hbar c)(MK/\mu^2)(e/2M), \quad (33)$$

where M is the reciprocal nucleon Compton wavelength. Now $\langle M_z(\text{int})\rangle$ may be expressed in terms of the probability P_1^c that a charged pion is present in the nucleon. This quantity is given by

$$P_1^c=\langle\Phi(1)|\Phi(1)\rangle,$$

where $\Phi(1)$ is given by Eq. (26). Then,

$$P_1^c=(g^2/\pi\hbar c\mu^2)\int_0^\infty dk[f^2(k)k^4(\mu^2+k^2)^{-\frac{1}{2}}], \quad (35)$$

and if the conditions, Eqs. (30) and (32), are used,

$$P_1^c=(g^2/\hbar c)(1/2\pi)(K^2/\mu^2), \quad (36)$$

whence

$$\langle M_z\rangle=\mp P_1^c(4M/3K), \quad (37)$$

in units of the nuclear magneton. In order to obtain specific numbers, suppose $K=M$ and[13] $P_1^c=10\%$, then $\langle M_z\rangle\approx\mp0.13$ nuclear magnetons, where again the $\mp$ refers to the proton or neutron, respectively. This number is rather small compared with the observed anomalies of 1.78 nuclear magnetons for the proton and -1.91 for the neutron.

Under the same assumptions that have characterized this calculation based on $H'(\mathbf{A})$, the interaction $H'_{\text{alt}}(\mathbf{A})$ would give no contribution to the magnetic moment. Furthermore, in view of the smallness of the effect derived from $H'(\mathbf{A})$ and in view of the fact that the sign is given incorrectly, the magnetic moment data provide little evidence which can be used to make a choice between different linear combinations of $H'(\mathbf{A})$ and $H'_{\text{alt}}(\mathbf{A})$.

[14] This conclusion is drawn by Blair *et al.*, in reference 3.

VI. SCATTERING OF LOW-ENERGY PHOTONS BY NUCLEONS

Sachs and Foldy[5] have given an expression for the cross section for the scattering of gamma rays from nucleons, calculated on the basis of nonrelativistic, no-recoil, point-source theory. The spin-dependent term in their final expression for the transition amplitude is independent of frequency at low frequency. This is a direct contradiction of the theorem in Sec. V of the preceding paper, namely that the transition amplitude should contain no constant term arising from excitation of the nucleon.

The reason for this contradiction can best be seen by examining the method of approximate stationary states used in SF and described in Appendix I of that paper. The approximate stationary states of the nucleon were derived from weak-coupling pseudoscalar meson theory, with neglect of recoil, by use of the following interaction between the nucleon core particle and the pion field.

$$H'=(4\pi)^{\frac{1}{2}}(gc/\mu)\int d^3r[\delta(\mathbf{r})\tau_+\boldsymbol{\sigma}\cdot\nabla\varphi(\mathbf{r})]+\text{h.c.} \quad (38)$$

In the presence of an electromagnetic field, H' was modified by replacing the gradient operator by the operator $[\nabla-(ie/\hbar c)\mathbf{A}]$. Therefore, $H'(\mathbf{A})$ satisfied the condition of gauge invariance, Eq. (2). However, the state vectors derived from Eq. (38) were not normalizable; hence, it is not surprising that the theorem of the preceding paper does not apply to the cross section derived in this manner.

In the present paper, the form of the interaction between the core particle and pions has been modified in such a way as to insure that the state vectors are normalizable. The delta function in the interaction, Eq. (38), has been replaced by a source function with a finite range. The source function $f(r)$ is required to be spherically symmetric and to satisfy the following two additional requirements:

$$\int f(r)d^3r=1, \quad (39a)$$

and

$$rf(r) \text{ nonsingular.} \quad (39b)$$

The method of approximate stationary states is then used to study the low-energy behavior of the spin-dependent term in the transition amplitude. The approximate stationary states calculated from the modified interaction are normalizable.

In the presence of an electromagnetic field, the interaction term in the Hamiltonian is assumed to have the form of Eq. (5). In this calculation, as in the calculation of SF, the only contribution to the spin-dependent term in the transition amplitude arises in the second order of the perturbation theory, through the intermediate states of the type denoted in SF by β and γ. A β state is a state whose zero-order term corresponds to one free meson in addition to the core particle, while the zero-order term of a γ state represents two free mesons and the core.

There are now three terms in the Hamiltonian which are linear in the vector potential, and hence can make a second-order contribution to the transition amplitude:

$$H_s=(iec/\hbar)\int d^3r[\tau_+\mathbf{A}(\mathbf{r})\cdot\varphi^*(\mathbf{r})\nabla\varphi(\mathbf{r})]+\text{h.c.}, \quad (40a)$$

$$H_{sg}=-i(4\pi)^{\frac{1}{2}}(eg/\hbar\mu)\int d^3r[\tau_+f(r)\boldsymbol{\sigma}\cdot\mathbf{A}\varphi]+\text{h.c.}, \quad (40b)$$

$$H'_{sg}=-i(4\pi)^{\frac{1}{2}}(eg/\hbar\mu)\int d^3r\left[\tau_+f(r)\left(\int_0^r A_s ds\right)\times\boldsymbol{\sigma}\cdot\nabla\varphi\right]+\text{h.c.} \quad (40c)$$

The interactions H_s and H_{sg} are analogous to the interactions H_s and H_{sg} of SF. The interaction H'_{sg} arises from the exponential term $\exp[-(ie/\hbar c)\int_0^r A_s ds]$ in Eq. (5). Although H'_{sg} is zero if $f(r)$ is replaced by a delta function, its influence on the transition amplitude will not vanish in the limit as $f(r)$ collapses to a delta function.

The only spin dependent terms in the transition amplitude which are independent of energy at low energy arise in the long-wavelength electric-dipole approximation, so we shall confine our attention to these terms here. In the electric dipole approximation, the transition amplitude does not depend on the choice of the path of integration in the line integral, $\int_0^r A_s ds$. This follows from the facts that in this approximation, the function $\mathbf{u}\exp(i\boldsymbol{\omega}\cdot\mathbf{r})$ is replaced by $\mathbf{u}$, and the integral $\int_0^r u_s ds=\mathbf{u}\cdot\mathbf{r}$ is independent of the path of integration.

In the electric-dipole approximation, the spin dependent terms in the transition amplitude may be written as a series of integrals:

$$\frac{4ie^2g^2}{\mu^2V\hbar c\omega}(\boldsymbol{\sigma}\cdot\mathbf{u}'\times\mathbf{u})\left\{\int_0^\infty dk\left[\frac{\omega}{k_0^2-\omega^2}\left(\frac{4}{3}\frac{k^4}{k_0^4}f^2(k)-\frac{k^3}{k_0}f^2(k)-\frac{2}{3}\frac{k^3}{k_0}f(k)\frac{df}{dk}\right)\right]-\int_0^\infty dk\left(\frac{1}{3}\frac{\omega}{k_0^2-\omega^2}\frac{k^4}{k_0^4}f^2(k)\right)\right\}, \quad (41)$$

where V is the volume of an enclosure introduced for purposes of normalization, the unit vectors $\mathbf{u}$ and $\mathbf{u}'$ denote the polarization directions of the initial and final photon, the symbol ω represents the magnitude of the wave vector of the incident or final photon, and k_0 is defined by the relation $k_0^2=\mu^2+k^2$. The function $f(k)$ is the Fourier transform of the source function $f(r)$,

which is spherically symmetric in both r space and k space, i.e.,

$$f(k)=(2/\pi)^{\frac{1}{2}}k^{-1}\int_0^\infty r f(r)\sin kr dr. \quad (42)$$

The first integral in Eq. (41) results from a sum over intermediate states of type β, while the second integral results from a sum over γ states. The term containing $f(k)df/dk$ involves the two interactions, H_{ω} and H'_{ω}. No other term of Eq. (41) involves H'_{ω}.

When the source function satisfies the requirement of Eq. (39b), its Fourier transform $f(k)$ must decrease at least as fast as k^{-2} as k approaches infinity. Thus, both integrals of Eq. (41) are convergent.

Since we are interested in the energy independent portion of these integrals, we expand in powers of (ω^2/k_0^2) and retain only the constant term. Then the frequency independent term in the transition amplitude can be written in the form

$$\frac{4ie^2g^2}{\mu^2V\hbar c}(\boldsymbol{\sigma}\cdot\mathbf{u}'\times\mathbf{u})\int_0^\infty dk\frac{d}{dk}\left[-\frac{1}{3}\frac{k^3}{k_0^3}f^2(k)\right]. \quad (43)$$

The function $(k^3/k_0^3)f^2$ vanishes at both limits, hence it is clear that this term, Eq. (43), vanishes. Thus the use of the finite source has removed the term of SF which contradicted the theorem of the previous paper.

It is interesting to compare Eq. (41) with the corresponding equation which occurs in SF in order to see how the disparity arises. The SF equation can be deduced easily from Eq. (41) by setting $f^2(k)$ equal to one. The result is[15]

$$\frac{4ie^2g^2}{\mu^2V\hbar c}(\boldsymbol{\sigma}\cdot\mathbf{u}'\times\mathbf{u})\left[\int_0^\infty\frac{1}{k_0^2-\omega^2}\left(\frac{4}{3}\frac{k^4}{k_0^3}-\frac{k^2}{k_0}\right)dk\right.$$
$$\left.-\frac{1}{3}\int_0^\infty\frac{k^3}{(k_0^2-\omega^2)k_0^3}dk\right]. \quad (44)$$

Each of these integrals is divergent, but in order that a finite result be obtained, the sum of the integrals was replaced by the integral of the sum of the integrands. The resulting integral is convergent, but leads to a result which does not vanish at zero energy.

One might have expected that the finite source procedure, in the limit as the range of the source function becomes zero, would lead to the same results as the point source procedure. But this is not the case. In this limit, the terms in Eq. (41) involving $f^2(k)$ do lead to the point source results obtained in SF, but the term involving $f(df/dk)$, which resulted from the inclusion of the exponential $\exp[-(ie/\hbar c)\int_0^s A_s ds]$ in $H'(\mathbf{A})$, leads to a finite result of proper magnitude and sign to cancel the result of SF at zero energy. Thus the condition of gauge invariance in the finite source plays a direct role in the cancellation, even in the limit as the source range approaches zero.

[15] This result can also be deduced from Eq. (SF-8), by setting $\omega=0$ in such combinations as $\mathbf{k}-\boldsymbol{\omega}$ and carrying out the angular part of the integrals in the spin dependent term.

VII. CROSS SECTION AS A FUNCTION OF ENERGY

If the meson-nucleon interaction used in SF is replaced by an interaction of the form given by Eq. (5), the transition amplitude for the scattering of gamma rays from nucleons may be recalculated. If the incident and scattered gamma rays have wavelengths long compared with the range of the source function in the meson-nucleon interaction, the calculated transition amplitude should not be sensitive to the form of the source function. In the present calculation, the transition amplitude and the cross section will be evaluated in the limit as the range of the source function approaches zero; hence they will be completely independent of the form of the source function. Thus, the finite source is used here only as a device for insuring that the wave function be normalizable, and that the integrals occurring in the transition amplitude converge. As in SF, the transition amplitude is calculated here only to lowest order in $e^2/\hbar c$. The integrals in the expression for the transition amplitude have been evaluated by expanding the angular dependent denominators in the integrands in powers of the parameter $\eta=2\omega k/(k^2+\mu^2+\omega^2)$. The results are computed to order η^2 in this expansion.

It has been found that at all energies, the transition amplitude calculated using the finite source procedure differs from the corresponding quantity in SF by only one additive, energy-independent term. The proof of this statement and the explicit expression for the transition amplitude are given in Appendix A.

In addition to including this constant term, a further correction to the transition amplitude obtained by SF must be made for energies above pion production threshold. Because of the possibility of pion production, the transition amplitude at these energies contains an absorptive part, in addition to the dispersive part which is present at all energies. In SF, the absorptive part was omitted, but it is included in the present calculation. The correction involves only those integrals of the transition amplitude whose integrands contain poles, and it is to be made by integrating each such integral along a path beneath the pole, rather than by replacing the integral by its principal part, as was done in SF.

The correction has a profound effect on the energy dependence of the cross section, as can be seen by comparing the calculated cross section for scattering from neutrons, Fig. 1, with the corresponding cross section shown in Figs. SF-2. The neutron cross section of SF rises to a peak at meson production threshold, then decreases again while the corrected cross section continues to increase.

The proton cross section consists of three terms, an energy independent term resulting from Thomson scattering from the proton as a whole, a term propor-

tional to g^4 resulting from Rayleigh scattering from the meson cloud and a g^2 term from the interference between Thomson and mesonic scattering. The neutron cross section is equal to the g^4 term in the proton cross section.

In order to obtain numerical results, one may assign a value to g^2 by comparing some experimental result to the corresponding prediction of weak coupling, pseudoscalar meson theory. In SF, the experimental result used for this purpose was the nearly zero binding energy to the ^1S state of the deuteron. Since the publication of SF, the low-energy cross section for the photoproduction of positive pions from protons has been measured.[16,17] Since photomeson production is a phenomenon closely related to the scattering of gamma rays, the positive pion production cross section will be used here to fix g^2. The value of $(g^2/\hbar c)$ is taken to be 0.116.[18]

With this choice of g^2 the mesonic scattering term and the interference term in the proton cross sections are of the order of magnitude of the Thomson cross section, at energies in the range 100–200 Mev. Because of this fact, the total cross section and angular distribution for the proton are sensitive to a change in the coupling constant. For example, at a center-of-mass energy of 139 Mev the differential cross section is greater at 180° than at 0° by a factor of 1.8. However, if the coupling constant were multiplied by a factor of 1.7, the cross section would be nearly the same as 0°

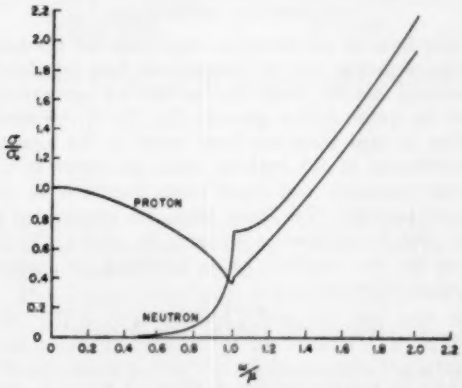

FIG. 1. Calculated total cross sections, in units of the Thomson cross section σ_0, for scattering of gamma rays from neutrons and protons. The quantity ω/μ is the photon energy in units of the pion mass.

[16] G. Bernardini and E. L. Goldwasser, Phys. Rev. **95**, 857 (1954).

[17] G. S. Janes and W. L. Kraushaar, Phys. Rev. **93**, 900 (1954); Jenkins, Luckey, Palfrey, and Wilson, Phys. Rev. **95**, 179 (1954).

[18] This value was taken from an analysis of low-energy photomeson production data by G. Bernardini and E. L. Goldwasser (private communication). The constant f^2 in the work is related to g^2 by $(g^2/\hbar c)=2f^2$. After the numerical work presented here had been completed, Bernardini and Goldwasser, refernce 7, revised their estimate of f^2 to the value 0.066.

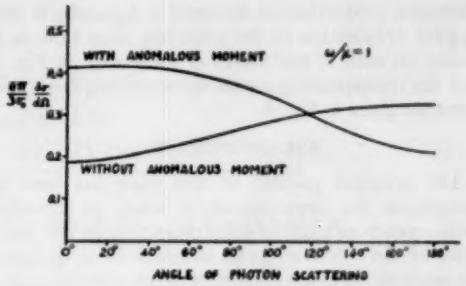

FIG. 2. Calculated differential cross section at 140 Mev center-of-mass energy for the scattering of gamma rays from protons, showing the effect of scattering from the proton anomalous moment.

as at 180°, and at still higher values of the coupling constant, forward scattering would predominate.

At present there are no experimental data available concerning the cross section for the scattering of gamma rays from hydrogen. It seems likely that when experiments are performed in the energy range 100–150 Mev, the results will reveal deviations from the Thomson cross section which will serve to check the present model. A reasonable procedure would be to fit the coupling constant g^2 to the observed total cross section, and use the observed angular distribution and energy dependence to check the model. If the measured cross section were significantly smaller than the Thomson cross section, the results presented here would not be meaningful, since recoil terms and terms of higher order in $(g^2/\hbar c)$ would then be important.

Up to this point, it has been assumed that the meson currents are responsible for the anomalous magnetic moments. If one assumes that the anomalous moment is to be associated with the core, the effect of the anomalous moment on the proton cross section can be approximated by introducing into the Hamiltonian an interaction of the form

$$-(\lambda e\hbar/2\mu c)(\boldsymbol{\sigma}\cdot\mathrm{curl}\mathbf{A}), \tag{45}$$

where λ is the anomalous moment measured in nuclear magnetons. This leads to an additional term in the transition amplitude which has the form

$$(\lambda^2\pi e^2\hbar^2/M^2c^2V)[i\boldsymbol{\sigma}\cdot(\mathbf{v}'\times\mathbf{u}')\times(\mathbf{v}\times\mathbf{u})], \tag{46}$$

where $\mathbf{v}=(\boldsymbol{\omega}/\omega)$ and $\mathbf{v}'=(\boldsymbol{\omega}'/\omega')$. Although this is a term of the same order as recoil effects, it makes an appreciable contribution to the cross section because of the large value of the anomalous moment. The contribution to the angular distribution is shown, at the energy $(\omega/\mu)=1$, in Fig. 2.

The results, when the anomalous moment contribution is not included, are presented in Figs. 1, 3, and 4. Figure 1 shows the total cross section for the proton and neutron as a function of energy. The cusps which appear in these curves at the threshold energy for

photopion production are discussed in Appendix B. The angular distribution of the scattering from protons is shown for each of five values of the energy in Fig. 3, and the corresponding curves for scattering from neutrons are given in Fig. 4.

VIII. CONCLUSION

The principal purpose of this work has been to investigate the consequences of using an extended meson source as a convergence procedure for the treatment of the electromagnetic interactions of nucleons. To establish the gauge invariance of the extended source theory, it has been necessary to introduce filaments of current within the source. Some physical consequences resulting from the presence of these currents have been deduced.

The nucleon magnetic moments are not affected when a simple choice is made for the form of the current filaments. However, the effect of the currents on the γ-ray scattering by nucleons is more profound. The anomalous term (which violates the gauge-invariance theorem of the preceding paper) found by Sachs and Foldy in their point-source theory does not occur in this calculation. In fact, the only effect of using the finite-source procedure of Sec. VI, where the source size is taken to be arbitrarily small, is the cancellation of this one anomalous term, a very interesting point in view of the many divergent integrals that appeared in the SF calculation. Furthermore, the results of Sec. VI do not depend on the choice of the path of integration in the line integral $\int_0^r A_\mu ds$. Thus, this particular method of obtaining gauge invariant results introduces no spurious effects.

Although the cross section for the scattering of γ rays by nucleons has been considered here only in the weak-coupling approximation, the usefulness of the concept of a pion-nucleon interaction of finite range is not limited to weak coupling calculations. In any calculation where a finite source interaction is used, the exponential term provides a convenient method of preserving gauge invariance. Furthermore, if the results of any calculation are finite in the limit as the source size approaches zero, they should not differ appreciably from the results corresponding to a fixed source size, provided this fixed distance is small compared to the wavelength of the radiation under consideration.

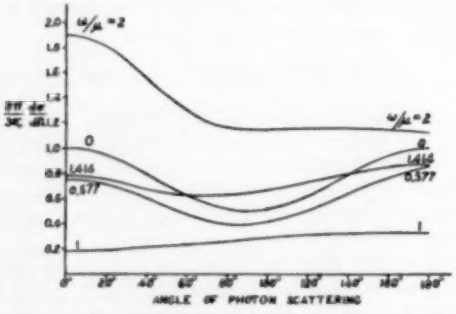

FIG. 3. Calculated differential cross sections for scattering of gamma rays from protons. The quantity ω/μ is the photon energy in units of the pion mass.

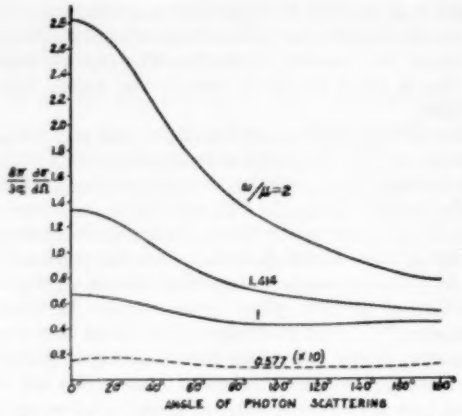

FIG. 4. Calculated differential cross sections for scattering of gamma rays from neutrons.

The calculation of the gamma-ray scattering was performed by direct use of the detailed tables of their work kindly provided by Professor Sachs and Professor Foldy. Many valuable discussions were had with Professor Sachs concerning the material of this article.

APPENDIX A. CALCULATION OF THE TRANSITION AMPLITUDE

The form of the transition amplitude for the scattering of gamma rays by nucleons has been calculated, assuming that the interaction between the core particle and the meson field is given by Eq. (5). If this interaction is used there are three terms in the internal Hamiltonian of the nucleon which are linear in the vector potential, and three terms quadratic in the vector potential. The linear terms are enumerated in Eq. (40). In addition to the term H_{ee} of Eq. (SF-4), there are two quadratic terms involving the integral $\int_0^r A_\mu ds$. They are:

$$H_{eeq}=-(4\pi)^{\frac{1}{2}}(e^2g/\hbar\mu)\int d^3r\left[\tau_+ f(r)\boldsymbol{\sigma}\cdot\mathbf{A}(\mathbf{r})\varphi(\mathbf{r})\times\left(\int_0^r A_\mu ds\right)\right]+\text{h.c.}, \quad \text{(A1)}$$

$$H'_{eeq}=-(4\pi)^{\frac{1}{2}}(e^2g/2\hbar\mu)\int d^3r\left[\tau_+ f(r)\boldsymbol{\sigma}\cdot\nabla\varphi(\mathbf{r})\times\left(\int_0^r A_\mu ds\right)^2\right]+\text{h.c.} \quad \text{(A2)}$$

The transition amplitude T for the scattering of electromagnetic radiation from protons may then be written in the following form, correct to order $(g^2/\hbar c)$

and (μ/M), but not including terms of order $(g^2/\hbar c)\times(\mu/M)$.

$$T=T_a+T_b, \tag{A.3}$$

$$\begin{aligned}
T_a=&(2\pi\hbar e^2/Mc\omega V)(\mathbf{u}\cdot\mathbf{u}')+(e^2g^2/\pi\hbar c\omega V\mu^2)\int d^3k\Bigg(\Bigg\{\frac{(\mathbf{u}\cdot\mathbf{u}')(\mathbf{k}-\boldsymbol{\omega}')\cdot(\mathbf{k}-\boldsymbol{\omega})}{(\mathbf{k}-\boldsymbol{\omega})_0^2(\mathbf{k}-\boldsymbol{\omega}')_0^2}\\
&-\frac{1}{k_0^2-\omega^2}\Bigg[4\frac{(\mathbf{u}\cdot\mathbf{k})(\mathbf{u}'\cdot\mathbf{k})(\mathbf{k}-\boldsymbol{\omega})\cdot(\mathbf{k}-\boldsymbol{\omega}')}{(\mathbf{k}-\boldsymbol{\omega})_0^2(\mathbf{k}-\boldsymbol{\omega}')_0^2}-2\frac{(\mathbf{u}'\cdot\mathbf{k})\mathbf{u}\cdot(\mathbf{k}-\boldsymbol{\omega}')}{(\mathbf{k}-\boldsymbol{\omega}')_0^2}-2\frac{(\mathbf{u}\cdot\mathbf{k})\mathbf{u}'\cdot(\mathbf{k}-\boldsymbol{\omega})}{(\mathbf{k}-\boldsymbol{\omega})_0^2}+(\mathbf{u}\cdot\mathbf{u}')\Bigg]\\
&-\frac{i\omega}{k_0(k_0^2-\omega^2)}\Bigg[4\frac{(\mathbf{u}\cdot\mathbf{k})(\mathbf{u}'\cdot\mathbf{k})\boldsymbol{\sigma}\cdot(\mathbf{k}-\boldsymbol{\omega}')\times(\mathbf{k}-\boldsymbol{\omega})}{(\mathbf{k}-\boldsymbol{\omega})_0^2(\mathbf{k}-\boldsymbol{\omega}')_0^2}-2\frac{(\mathbf{u}'\cdot\mathbf{k})\boldsymbol{\sigma}\cdot(\mathbf{k}-\boldsymbol{\omega}')\times\mathbf{u}}{(\mathbf{k}-\boldsymbol{\omega}')_0^2}+2\frac{(\mathbf{u}\cdot\mathbf{k})\boldsymbol{\sigma}\cdot(\mathbf{k}-\boldsymbol{\omega})\times\mathbf{u}'}{(\mathbf{k}-\boldsymbol{\omega})_0^2}+\boldsymbol{\sigma}\cdot\mathbf{u}'\times\mathbf{u}\Bigg]\Bigg\}\\
&\times f(|\mathbf{k}-\boldsymbol{\omega}|)f(|\mathbf{k}-\boldsymbol{\omega}'|)+\frac{2i\omega}{k_0^2}\Bigg[\frac{1}{(\mathbf{k}-\boldsymbol{\omega}')_0}\frac{(\mathbf{u}'\cdot\mathbf{k})(\boldsymbol{\sigma}\cdot\mathbf{u}\times\mathbf{k})}{[k_0+(\mathbf{k}-\boldsymbol{\omega}')_0]^2-\omega^2}-\frac{1}{(\mathbf{k}-\boldsymbol{\omega})_0}\frac{(\mathbf{u}\cdot\mathbf{k})(\boldsymbol{\sigma}\cdot\mathbf{u}'\times\mathbf{k})}{[k_0+(\mathbf{k}-\boldsymbol{\omega})_0]^2-\omega^2}\Bigg]\\
&\times f(k)f(|\mathbf{k}-\boldsymbol{\omega}-\boldsymbol{\omega}'|)+4i\omega\frac{(\mathbf{u}'\cdot\mathbf{k})(\mathbf{u}\cdot\mathbf{k})\boldsymbol{\sigma}\cdot(\mathbf{k}-\boldsymbol{\omega}')\times(\mathbf{k}-\boldsymbol{\omega})}{k_0[(\mathbf{k}-\boldsymbol{\omega})_0^2-(\mathbf{k}-\boldsymbol{\omega}')_0^2]}\Bigg[\frac{1}{(\mathbf{k}-\boldsymbol{\omega})_0^2}\frac{1}{\omega^2-[k_0+(\mathbf{k}-\boldsymbol{\omega}')_0]^2}\\
&-\frac{1}{(\mathbf{k}-\boldsymbol{\omega}')_0^2}\frac{1}{\omega^2-[k_0+(\mathbf{k}-\boldsymbol{\omega}')_0]^2}\Bigg]f(|\mathbf{k}-\boldsymbol{\omega}|)f(|\mathbf{k}-\boldsymbol{\omega}'|)\Bigg),
\end{aligned} \tag{A4}$$

$$\begin{aligned}
T_b=&(e^2g^2/\pi\hbar c\omega V\mu^2)\int d^3k\Bigg\{\frac{(\mathbf{k}\cdot\mathbf{u}')f(k)\eta_{\omega u}(\mathbf{k}-\boldsymbol{\omega}')}{k_0^2}+\frac{(\mathbf{k}\cdot\mathbf{u})f(k)\eta_{\omega' u'}(\mathbf{k}-\boldsymbol{\omega})}{k_0^2}-\frac{k^2f(k)\eta'(\mathbf{k})}{k_0^2}\\
&-\frac{1}{k_0^2-\omega^2}\Bigg[2\frac{(\mathbf{u}'\cdot\mathbf{k})(k^2-\mathbf{k}\cdot\boldsymbol{\omega}')f(|\mathbf{k}-\boldsymbol{\omega}'|)\eta_{-\omega u}(\mathbf{k})}{(\mathbf{k}-\boldsymbol{\omega}')_0^2}+2\frac{(\mathbf{u}\cdot\mathbf{k})(k^2-\mathbf{k}\cdot\boldsymbol{\omega})f(|\mathbf{k}-\boldsymbol{\omega}|)\eta_{-\omega' u'}(\mathbf{k})}{(\mathbf{k}-\boldsymbol{\omega})_0^2}\\
&-(\mathbf{u}'\cdot\mathbf{k})f(|\mathbf{k}-\boldsymbol{\omega}'|)\eta_{-\omega u}(\mathbf{k})-(\mathbf{u}\cdot\mathbf{k})f(|\mathbf{k}-\boldsymbol{\omega}|)\eta_{-\omega' u'}(\mathbf{k})+k^2\eta_{-\omega u}(\mathbf{k})\eta_{-\omega' u'}(\mathbf{k})\Bigg]\\
&-\frac{i\omega}{k_0(k_0^2-\omega^2)}\Bigg[-2\frac{(\mathbf{u}'\cdot\mathbf{k})(\boldsymbol{\sigma}\cdot\boldsymbol{\omega}'\times\mathbf{k})f(|\mathbf{k}-\boldsymbol{\omega}'|)\eta_{-\omega u}(\mathbf{k})}{(\mathbf{k}-\boldsymbol{\omega}')_0^2}+2\frac{(\mathbf{u}\cdot\mathbf{k})(\boldsymbol{\sigma}\cdot\boldsymbol{\omega}\times\mathbf{k})f(|\mathbf{k}-\boldsymbol{\omega}|)\eta_{-\omega' u'}(\mathbf{k})}{(\mathbf{k}-\boldsymbol{\omega})_0^2}\\
&-(\boldsymbol{\sigma}\cdot\mathbf{u}'\times\mathbf{k})f(|\mathbf{k}-\boldsymbol{\omega}'|)\eta_{-\omega u}(\mathbf{k})-(\boldsymbol{\sigma}\cdot\mathbf{k}\times\mathbf{u})f(|\mathbf{k}-\boldsymbol{\omega}|)\eta_{-\omega' u'}(\mathbf{k})\Bigg]+\frac{2i\omega}{k_0^2}\Bigg[-\frac{(\mathbf{u}'\cdot\mathbf{k})(\boldsymbol{\sigma}\cdot\boldsymbol{\omega}'\times\mathbf{k})f(k)\eta_{\omega u}(\boldsymbol{\omega}'-\mathbf{k})}{(\mathbf{k}-\boldsymbol{\omega}')_0\{[k_0+(\mathbf{k}-\boldsymbol{\omega}')_0]^2-\omega^2\}}\\
&+\frac{(\mathbf{u}\cdot\mathbf{k})(\boldsymbol{\sigma}\cdot\boldsymbol{\omega}\times\mathbf{k})f(k)\eta_{\omega' u'}(\boldsymbol{\omega}-\mathbf{k})}{(\mathbf{k}\cdot\boldsymbol{\omega})_0\{[k_0+(\mathbf{k}-\boldsymbol{\omega})_0]^2-\omega^2\}}\Bigg]\Bigg\}.
\end{aligned} \tag{A5}$$

The transition amplitude for the scattering from neutrons differs from the above expression only in that the first term of T_a is absent.

The corresponding result obtained by SF is given in Eq. (SF-8). The symbol T_a denotes that part of T which does not involve the line integral $\int_0^r A_s ds$, while T_b denotes the part of T which does involve this integral. The functions $\eta_{\omega u}(\mathbf{k})$ and $\eta'(\mathbf{k})$ are related to $\int_0^r A_s ds$; if the path of integration in this integral is taken to be a straight line, η and η' are the Fourier transforms of the functions

$$\eta_{\omega u}(\mathbf{r})=-if(r)(\mathbf{u}\cdot\mathbf{r})\int_0^1\exp(i\boldsymbol{\omega}\cdot\alpha\mathbf{r})d\alpha,$$

$$\eta'(\mathbf{r})=-f(r)(\mathbf{u}\cdot\mathbf{r})(\mathbf{u}'\cdot\mathbf{r})\Bigg[\int_0^1\exp(i\boldsymbol{\omega}\cdot\alpha\mathbf{r})d\alpha\Bigg]\times\Bigg[\int_0^1\exp(i\boldsymbol{\omega}'\cdot\alpha'\mathbf{r})d\alpha'\Bigg].$$

It can be shown that $f(k)$, $\eta_{\omega u}(\mathbf{k})$, and $\eta'(\mathbf{k})$ are all real functions. The symbol $(\mathbf{k}-\boldsymbol{\omega})_0$ in Eqs. (A4) and (A5) denotes $[\mu^2+(\mathbf{k}-\boldsymbol{\omega})^2]^{\frac{1}{2}}$.

If the integration over $\mathbf{k}$ space in Eq. (A4) is carried out, and then the range of the source function is allowed to approach zero, the resulting expression for T_a will become equal to the transition amplitude of SF, Eq. (SF-8). It will now be shown that if this procedure is carried out for Eq. (A-5), the resulting expression will reduce to one energy-independent term, the term mentioned in Sec. VI.

In the following argument, use is made of several properties of the source function. To satisfy the condition Eq. (39a), we write $f(r)$ in the form $f(r)=R^{-3}g(r/R)$, where R represents the range of the source function. The Fourier transform of $f(r)$ is then a function of the product (kR), i.e., $f(k)=\varphi(kR)$. Since $f(r)$ has the property, Eq. (39b), $\varphi(kR)$ must

vanish at least as fast as $(kR)^{-2}$ as (kR) approaches infinity. Hence, all derivatives of $\varphi(kR)$ with respect to (kR) must also vanish at least as fast as $(kR)^{-2}$.

It is convenient to expand the exponential in the functions $\eta_{\omega u}(\mathbf{r})$ and $\eta'(\mathbf{r})$ in power series, i.e.,

$$(\mathbf{u}\cdot\mathbf{r})\int_0^1 \exp(i\omega\cdot\alpha\mathbf{r})d\alpha=(\mathbf{u}\cdot\mathbf{r})+i(\mathbf{u}\cdot\mathbf{r})(\omega\cdot\mathbf{r})+\cdots. \tag{A6}$$

By making use of this expansion, $\eta'_{\omega u}(\mathbf{r})$ and $\eta'(\mathbf{r})$ may be written as sums of terms, each term depending on r to the first or higher power. Hence, $\eta_{\omega u}(\mathbf{k})$ may be written as a sum of terms in the form

$$G_n(\mathbf{u},\mathbf{k})R(R\omega)^{n-1}\varphi^{(n)}(kR), \tag{A7}$$

where G_n is some function independent of R and ω; the exponent n is a positive integer and $\varphi^{(n)}$ represents the nth derivative of the source function $\varphi(kR)$ with respect to (kR). Similarly, $\eta'(\mathbf{k})$ may be written as a sum of terms of the form,

$$G_n(\mathbf{u},\mathbf{u}',\mathbf{k})R^2(R\omega)^{n-2}\varphi^{(n)}(kR). \tag{A8}$$

Thus, T_b may be written as a sum over n and n' of terms of the following form

$$R^\nu\int d^3k[F_{nn'}(k_0,\mathbf{k},\omega,\boldsymbol{\sigma},\mathbf{u},\mathbf{u}')\varphi^{(n)}(k'R)\varphi^{(n')}(k''R), \tag{A9}$$

where the new symbols have the following meanings: The function F_{nn} is bounded in $\mathbf{k}$ and independent of R; the symbols n and n' represent non-negative integers, and the exponent $\nu=n+n'$ is a positive integer. The variable k', or the variable k'', represents some one of the following five quantities, in each of the various terms to be considered: k, $|\mathbf{k}\pm\boldsymbol{\omega}|$, $|\mathbf{k}\pm\boldsymbol{\omega}'|$.

It is convenient to express the integral over all k-space in Eq. (A9) as a sum of integrals over two regions, i.e.,

$$R^\nu\left(\int_0^K d^3kF_{nn'}\varphi^{(n)}\varphi^{(n')}+\int_K^\infty d^3kF_{nn'}\varphi^{(n)}\varphi^{(n')}\right). \tag{A10}$$

The first includes the region in k-space inside a sphere of arbitrary radius K; the second region includes the space outside this sphere.

Since ν is greater than zero, it is clear that the first integral in Eq. (A10) does not contribute to the transition amplitude, as R approaches zero. Thus, we need consider only the second integral. If K is chosen very large compared with μ and ω, k_0 may be set equal to k, and all terms may be expanded in powers of (ω/k). The angular integrations may then be carried out, and thus T_b may be written as a sum (over n, n', and m) of terms of the following nature:

$$R^\nu\omega^m\int_K^\infty dk[F_{nn'm}(k,\boldsymbol{\sigma},\mathbf{u},\mathbf{u}')\varphi^{(n)}(kR)\varphi^{(n')}(kR)]. \tag{A11}$$

Examination of Eq. (A5) leads to the conclusion that $m\geqq-1$. The theorem in Sec. V of the preceding paper tells us that the terms of T_b with $m=0$ and $m=-1$ must have the proper magnitude and angular dependence to cancel the ω^0 and ω^{-1} terms in T_a. In Sec. VI, this was demonstrated for the ω^0 terms. The ω^{-1} terms have been calculated for an arbitrary value of R and the result is in agreement with the theorem, namely the ω^{-1} terms of T_b cancel against the ω^{-1} terms of T_a. In the limit as R approaches zero, the ω^{-1} terms of T_a and T_b separately vanish.

A simple dimensional argument may now be used to demonstrate that all terms in Eq. (A11) corresponding to $m\geqq1$ will vanish as R approaches zero. The combination $\omega^mR^\nu\int_K^\infty dkF_{nn'm}(k,\boldsymbol{\sigma},\mathbf{u},\mathbf{u}')$ must be dimensionless. Hence, $F_{nn'm}$ must be of the form $F_{nn'm}=k^{\nu-m-1}Q_{nn'm}(\boldsymbol{\sigma},\mathbf{u},\mathbf{u}')$, since k is the only dimensional variable in F. Thus Eq. (A11) may be written in the form

$$\omega^mR^\nu Q_{nn'm}(\boldsymbol{\sigma},\mathbf{u},\mathbf{u}')\int_K^\infty dk[k^{\nu-m-1}\varphi^{(n)}(kR)\varphi^{(n')}(kR)]. \tag{A12}$$

Examination of Eqs. (A5), (A7), and (A8) reveals that $m\geqq\nu-3$ or $\nu-m-1\leqq2$. Since $\varphi^{(n)}$ vanishes at least as fast as k^{-2} as k approaches infinity, the integral in Eq. (A12) is therefore always convergent for finite R. If the integral is written in the form of an integral over the variable (kR), then it can be seen that the resulting combination,

$$R^m\int_{KR}^\infty d(kR)[\varphi^{(n)}(kR)\varphi^{(n')}(kR)(kR)^{\nu-m-1}], \tag{A13}$$

vanishes in the limit as R approaches zero if the integer m is positive. This completes the proof that T differs from the T of SF by only one term. This term was discussed in Section VI, and found to be equal to

$$-(8ie^2g^2/3\mu^2V\hbar c)(\boldsymbol{\sigma}\cdot\mathbf{u}'\times\mathbf{u})\times\int_0^\infty dk[(k^3/k_0^3)f(k)df/dk]=(4ie^2g^2/3\mu^2V\hbar c)(\boldsymbol{\sigma}\cdot\mathbf{u}'\times\mathbf{u}). \tag{A14}$$

This result does not depend on the choice of the path of integration in the line integral $\int_0^r A_s ds$ because in the limit as the source size R approaches zero, the only nonvanishing terms of T_b are terms which would arise in the electric dipole approximation and, as discussed in Sec. VI, in the electric dipole approximation the integral is independent of the path of integration for any value of R.

APPENDIX B. CUSPS IN THE TOTAL CROSS SECTIONS

The discontinuity in the energy derivative of the total scattering cross section at photopion production threshold is a very general phenomenon; similar discontinuities occur in many cross sections. The appearance of such cusps in nuclear cross sections has been discussed by Wigner.[19]

[19] E. P. Wigner, Phys. Rev. **73**, 1002 (1948). The fact that cusps probably would appear in the present work was first suggested to the authors by Professor Wigner.

The existence of discontinuities of this type will be demonstrated for a general class of scattering problems. We consider the collision of two particles denoted by A and B, at such an energy that only two reaction channels are open, corresponding to elastic scattering, and to the production of two other particles, C and D, which have a greater total rest mass than the particles A and B. One of the incident particles may be a photon. It is assumed that the particles $C+D$ may be produced in an S state, so that the cross section near threshold for this process has the $(E-E_t)^{\frac{1}{2}}$ energy dependence characteristic of an S state. For simplicity it is also assumed that the particles are all spinless, though this assumption is not necessary for the validity of the conclusions.

The elastic scattering cross section is related to the cross section for production of the particles $C+D$ by the condition that the scattering matrix U be unitary. That part of the U matrix corresponding to zero angular momentum is a two-by-two matrix; the two elements of the first row may be written as

$$U_{AB,AB}=e^{i\delta}(1-r^2)^{\frac{1}{2}}; \quad U_{AB,CD}=ire^{i\rho}, \qquad \text{(B1)}$$

where r, δ, and ρ are real functions of energy. The sum of the absolute squares of the two elements has been set equal to one to satisfy the requirement of unitarity. If the matrix $\mathcal{T}$ is defined to be the matrix equation $U-1=-i\mathcal{T}$, the two S-wave cross sections are related to the corresponding matrix elements of $\mathcal{T}$ by the equation $\sigma_{if}=(\pi/k_i^2)|\mathcal{T}_{if}|^2$ where i and f refer to the initial and final states, respectively, and k_i is the relative momentum in the initial state. If the quantity r^2 of Eq. (B1) is small, $\mathcal{T}_{AB,AB}$ may be expanded in powers of r^2 and written in the form,

$$\mathcal{T}_{AB,AB}=-(\sin\delta)(1-\tfrac{1}{2}r^2+\cdots)+i[(\cos\delta)(1-\tfrac{1}{2}r^2+\cdots)-1]. \qquad \text{(B2a)}$$

At an energy slightly above the threshold for the production of the state $C+D$, $\sigma_{AB,CD}=(\pi/k_{AB}^2)r^2$ is proportional to $\omega^{\frac{1}{2}}$, where $\omega=E-E_t$, E_t being the threshold energy. Thus, r^2 will be small near threshold and will be given by $r^2=a^2\omega^{\frac{1}{2}}$ where a^2 is a positive constant. Then it can be seen from Eq. (B2a) that, in general, both the real and imaginary parts of $\mathcal{T}_{AB,AB}$ contain terms of order $\omega^{\frac{1}{2}}$.

It has been shown by Eden[20] that, for a very general class of scattering problems, the elastic scattering U-matrix element is an analytic function of energy which has a branch point at $E=E_t$, and that the assumption that the particles interact through their retarded fields may be used to specify the proper path of analytic continuation around the branch point. In the case considered here the continuation must be in the region corresponding to a positive imaginary part of E. Thus from the form of $\mathcal{T}_{AB,AB}$ above threshold, Eq. (B2a), we may deduce that its form just below threshold must be given by[21]

$$\mathcal{T}_{AB,AB}=-\sin\delta+\tfrac{1}{2}(\cos\delta)a^2|\omega|^{\frac{1}{2}}+i[\cos\delta-1+\tfrac{1}{2}(\sin\delta)a^2|\omega|^{\frac{1}{2}}]. \qquad \text{(B2b)}$$

Hence, to order $r^2=a^2\omega^{\frac{1}{2}}$, the zero angular momentum part of the total scattering cross section may be written, in the neighborhood of threshold,

$\omega>0$;

$$\sigma_{AB,AB}=C^2[2-2\cos\delta-a^2\omega^{\frac{1}{2}}+(\cos\delta)a^2\omega^{\frac{1}{2}}], \qquad \text{(B3a)}$$

$\omega<0$;

$$\sigma_{AB,AB}=C^2[2-2\cos\delta-(\sin\delta)a^2|\omega|^{\frac{1}{2}}]. \qquad \text{(B3b)}$$

where C^2 is a positive constant. Therefore, the energy derivative of the elastic scattering cross section will, in general, become infinite as the energy approaches threshold from both above and below.

The discussion of the preceding paragraphs may be applied to the cross sections calculated in Sec. VII if particle A is identified with a gamma ray, particles B and C with nucleons, and D with a charged pion. Although this case is slightly complicated by the spins of the particles, the argument is fundamentally the same. Since pions may be photoproduced into S states, the unitarity of the U matrix implies that part of the elastic scattering cross section (that part which results from the scattering of a photon wave of odd parity and angular momentum $\frac{1}{2}$) may be written in the form of Eqs. (B3a) and (B3b) at energies close to photopion threshold.

In Sec. VII only the term of lowest order in the electric charge was calculated. If the quantities a^2 and δ, corresponding to the gamma-ray nucleon-pion problem are expanded in powers of e^2, the lowest order term of each will be proportional to e^2, i.e., $a^2\propto e^2$; $\delta\propto e^2$. To order e^2 Eqs. (B2a) and (B2b) may then be written

$$\omega>0; \quad \mathcal{T}_{\gamma N,\gamma N}=-\delta-\tfrac{1}{2}ia^2\omega^{\frac{1}{2}}, \qquad \text{(B4a)}$$

$$\omega<0; \quad \mathcal{T}_{\gamma N,\gamma N}=-\delta+\tfrac{1}{2}a^2|\omega|^{\frac{1}{2}}. \qquad \text{(B4b)}$$

Hence, Eqs. (B3a) and (B3b) become, to order e^4

$$\omega>0; \quad \sigma_{\gamma N,\gamma N}=C^2\delta^2, \qquad \text{(B5a)}$$

$$\omega<0; \quad \sigma_{\gamma N,\gamma N}=C^2(\delta^2-\delta a^2|\omega|^{\frac{1}{2}}). \qquad \text{(B5b)}$$

Thus, in this case, there is no term in $\sigma_{\gamma N,\gamma N}$ proportional to $|\omega|^{\frac{1}{2}}$ above threshold, but there is such a term below threshold. By making use of the tables prepared by Sachs and Foldy, the cross sections calculated in Sec. VII have been expanded in powers of $|\omega|^{\frac{1}{2}}$, for energies just below pion production threshold. The results to order $|\omega|$ are, for the proton case $\sigma/\sigma_0=0.40-0.89|\omega/\mu|^{\frac{1}{2}}+5.4|\omega/\mu|$, and for the neutron case, $\sigma/\sigma_0=0.71-3.1|\omega/\mu|^{\frac{1}{2}}+6.9|\omega/\mu|$, where σ_0 is the Thomson cross section, and μ is the rest energy of the pion.

[20] R. J. Eden, Proc. Roy. Soc. (London) **A210**, 388 (1952).

[21] The function δ cannot contain a part proportional to a half-odd-integral power of $|\omega|$. This follows from the requirement that the U matrix be unitary below threshold, together with fact that $U_{AB,AB}$ is analytic with a branch point at threshold.

Feynman Amplitudes and Strong-Coupling Pion Theory

HIRONARI MIYAZAWA*
Institute for Nuclear Studies, University of Chicago, Chicago, Illinois
(Received March 21, 1955)

By a method proposed by Gell-Mann and Goldberger for the treatment of the pion-nucleon problem, the case of strong pseudoscalar coupling is studied. Contributions from the closed loops in Feynman diagrams are neglected, though virtual nucleon pair creations are otherwise taken into account. The nucleon recoil turns out to be a small perturbation in the strong-coupling approximation. The theory is not covariant and no attempt is made to renormalize the divergent quantities. Divergent integrals are cut off arbitrarily.

The main P-wave interaction is spin-independent although the next order term is the usual spin-dependent interaction. Magnetic moments of the nucleons are not in agreement with experiments. Nucleons have isobaric states with negative excitation energies. The implication of these states is discussed. The isobaric state plays a role as an intermediate state in pion-nucleon scattering and explains the inequality of the two S-phase shifts.

I. INTRODUCTION

A STRONG coupling theory is applied for the case of pseudoscalar coupling. In treating the pseudoscalar coupling, one is confronted with the vacuum fluctuation and hole theoretical subtraction since in this case nucleon pair creation is very important. This makes the application of the strong-coupling theory a difficult task. Wentzel[1] used the one-particle form of the Dirac equation without considering the vacuum fluctuation. This formulation is correct at least up to the first order of approximation in the pair creation since he used the second-order equation. In a previous paper[2] the lattice space method was used which is simple to do and easy to understand, but which is by no means a good approximation.

In this paper another method is employed. One way of treating a problem in a hole theoretical manner is to use the so-called Feynman amplitudes.[3] In this theory, one does not consider a state, say a one nucleon state $1\rangle$, absolutely, but always relative to a comparison state $0\rangle$, which is usually taken to be the actual vacuum state.[4] Thus instead of obtaining the eigenenergy E_1 of a one-nucleon state, we look for the difference $E=E_1-E_0$ of E_1 and the vacuum energy E_0, and instead of asking the probability of finding n pions in the state $1\rangle$, we consider the probability of finding n pions more (or less) than are to be found in the vacuum. In this way the use of the Feynman amplitudes automatically subtracts the vacuum fluctuation which is irrelevant to our problem.

Gell-Mann and Goldberger[5] showed that if one neglects the effect of closed loops in Feynman diagrams, the Schrödinger equation for the one-nucleon problem becomes so simple that one can handle it even by the strong-coupling theory. The omission of the closed loops is certainly wrong since the probability of pair creation is very large in the pseudoscalar coupling case. However, it is not unreasonable to assume that the chief effect of the closed loops is merely to change the mechanical mass of the pion into its experimental mass. Thus we use the experimental mass of the pion μ instead of its mechanical mass and omit closed loops. It is almost impossible to formulate this approximation in a Schrödinger wave function. It is only possible in Feynman's 4-dimensional form. It is hard to estimate what is the error introduced by this approximation. However, this drawback can be compensated for by the simplicity of our equation. Needless to say, all effects of nucleon pair creation are included if it is represented by a single nucleon line in the Feynman diagram.

The interaction between pions which arises via closed loops of nucleons is not included in this theory. One must add a ϕ^4 term if one wishes to improve the calculations.

In the next section we shall briefly derive the Gell-Mann and Goldberger equation which has not been published in detail.

II. GELL-MANN-GOLDBERGER EQUATION

For the sake of simplicity, the neutral, rather than the more involved charge symmetric, $ps-ps$ theory will be considered in this section. A system containing a single nucleon and an arbitrary number of pions may be described by a set of Feynman amplitudes $\psi^n(x; y_1,y_2,\cdots,y_n)$ of finding the nucleon at x, and finding n pions at $y_1, \cdots, y_n$ respectively. It is more convenient to consider energy-momentum space, in which the $\psi^n(x; y_1,\cdots,y_n)$ is transformed into $\psi^n(p; k_1,\cdots,k_n)$. Furthermore, p can be eliminated by means of the conservation of the total momentum P.

$$p=P-\sum k_i. \tag{1}$$

If the contributions from the closed loops are neglected,

* On leave of absence from the University of Tokyo, Tokyo, Japan.
[1] G. Wentzel, Phys. Rev. **92**, 173 (1953).
[2] H. Miyazawa, Phys. Rev. **97**, 1399 (1955).
[3] M. Gell-Mann and F. Low, Phys. Rev. **84**, 350 (1951); M. Gell-Mann and M. L. Goldberger, Phys. Rev. **87**, 218 (1952); K. Nishijima, Progr. Theoret. Phys. (Japan) **10**, 549 (1953); P. T. Matthews and A. Salam, Proc. Roy. Soc. (London) **A221**, 128 (1953); E. Freeze, Z. Naturforsch. **8a**, 776 (1953); F. Coester, Phys. Rev. **95**, 1318 (1954).
[4] This is a four-dimensional version of Dyson's new Tamm-Dancoff method. F. J. Dyson, Phys. Rev. **90**, 994 (1953); **91**, 421 (1953).
[5] M. Gell-Mann and M. L. Goldberger, reference 3.

these ψ^n are seen to satisfy the equation[6]

$$\psi^n(k_1,\cdots,k_n)=\frac{1}{i\gamma(P-\sum k)+m}ig\gamma_5 \times\left[\frac{i}{(2\pi)^4}\int\psi^{n+1}(k,k_1,\cdots,k_n)d^4k -\sum\frac{1}{k_1^2+\mu^2}\psi^{n-1}(k_2,\cdots,k_n)\right], \quad (2)$$

where m is the mechanical mass of the nucleon. In deriving this equation it is assumed that no incoming or outgoing pion is present. The connection between this wave function ψ^n and the quantities in the Heisenberg representation is given by[3]

$$\begin{aligned}\psi^n(x;y_1,\cdots,y_n)&=\langle 0|P(\psi(x)\phi(y_1)\cdots\phi(y_n))|1\rangle-\tfrac{1}{2}\sum\Delta_F(y_1-y_2)\\&\times\langle 0|P(\psi(x)\phi(y_3)\cdots\phi(y_n))|1\rangle\\&+\tfrac{1}{4}\sum\Delta_F(y_1-y_2)\Delta_F(y_3-y_4)\\&\times\langle 0|P(\psi(x)\phi(y_5)\cdots\phi(y_n))|1\rangle-\cdots, \quad (3)\end{aligned}$$

where $1\rangle$ is the one nucleon state in question and $0\rangle$ is the vacuum state. P in (1) is P_1-P_0 where P_1 and P_0 are the energy momenta of the states $1\rangle$ and $0\rangle$, respectively.

Multiplying by $\beta[i\gamma(P-\sum k)+m]$ on both sides of (1), we have

$$E\psi^n=[\sum k_0+\alpha(P-\sum k)+m\beta]\psi^n +g\rho_2\left[\frac{i}{(2\pi)^4}\int\psi^{n+1}d^4k-\sum\frac{1}{k_1^2+\mu^2}\psi^{n-1}\right]. \quad (4)$$

This equation determines the energy E of the system. However, in order that (4) be an eigenvalue problem, we must impose some boundary condition at the boundary of the 4-dimensional space, or in momentum space we must specify the behavior of the poles of $\psi^n(k)$. If we solve (2) by the iteration method, we see that every pole of $\psi^n(k)$ has the form of

$$\frac{P}{k_0-a}\pm i\pi\delta(k_0-a)=\frac{1}{k_0-a\mp i\epsilon}. \quad (5)$$

We shall assume that, in general, every pole of ψ^n has the form (5). In the Appendix, it is shown that with this boundary condition, the eigenvalue E is real, and we can define the norm of the wave function. The sign of $i\epsilon$ in (5) must be determined from the physical conditions of the problem under consideration. In the integral Eq. (2), the sign of $i\epsilon$ at every pole is fixed. However, in the differential form (4) the sign is not determined. It can easily be seen that $-i\epsilon$ at every pole corresponds to the single-particle theory as originally proposed by Dirac, which does not take into account the occupation of negative energy states.

Equation (4) is not self-adjoint, but we can make it so by the transformation:

$$\psi^n(k_1,\cdots,k_n)\rightarrow(n!)^{\frac{1}{2}}(-i)^{n/2}(2\pi)^{2n} \times(k_1^2+\mu^2)^{-\frac{1}{4}}\cdots(k_n^2+\mu^2)^{-\frac{1}{4}}\psi^n.$$

The new ψ^n satisfy the equation:

$$E\psi^n=[\sum k_0+\alpha(P-\sum k)+m\beta]\psi^n +\frac{g\rho_2}{(2\pi)^2}\left[\int\left(\frac{-i}{k^2+\mu^2}\right)^{\frac{1}{2}}(n+1)^{\frac{1}{2}}\psi^{n+1}(k,k_1,\cdots,k_n) +\frac{1}{n^{\frac{1}{2}}}\sum\left(\frac{-i}{k_1^2+\mu^2}\right)^{\frac{1}{2}}\psi^{n-1}(k_2,\cdots,k_n)\right]. \quad (6)$$

This equation is written in Fock's form. This can also be written in terms of occupation numbers and creation and annihilation operators. Thus,

$$E\Psi(\cdots,n_k,\cdots) =\left[\int k_0C_k^*C_k\,dk+\alpha\left(P-\int kC_k^*C_k\,dk\right) +m\beta+g\rho_2\int G(k)(C_k^*+C_k)\,dk\right]\Psi, \quad (7)$$

where

$$G(k)=\frac{1}{(2\pi)^2}\left(\frac{-i}{k^2+\mu^2}\right)^{\frac{1}{2}}.$$

This equation was derived by Gell-Mann and Goldberger. n_k, C_k and C_k^* are labeled by a 4-dimensional vector k and can be said to be the number of pions with momentum k, etc. C_k and C_k^* satisfy the 4-dimensional version of the usual commutation relations:

$$[C_k,C_{k'}^*]=\delta^4(k-k').$$

Equation (7) is similar to that of the single particle form of the Dirac equation. The first term on the right-hand side represents the total energy of the pions, and the second term represents the recoil of the nucleon due to the emitted pions. However, this Hamiltonian differs from the usual one in two respects. First, the integral over k now extends over all 4-dimensional k-space and is not confined to the surface $k_0^2=k^2+\mu^2$. This is because we are using a space-time approach rather than the conventional 3-dimensional theory. The second difference is the occurrence of minus particles having negative energy.[4] That is, the total energy of the pions can assume a negative value since the integral over k_0 ranges

[6] The ψ^n used in (2) is $[i^n/(2\pi)^{4n}]\psi^n$. This transformation proved convenient.

from $-\infty$ to $+\infty$. This comes from the fact that we are considering the state 1⟩ relative to 0⟩. The apparent pion energy in the Hamiltonian (7) is actually the difference between the pion energies of 1⟩ and 0⟩. Thus for instance a pion of positive energy in (7) means that the pion is present in the state 1⟩ but is not present in 0⟩, and a pion of negative energy means that the pion is missing in 1⟩ although it was present in 0⟩. The concept of one pion is, however, quite different from the usual one in this theory.

Instead of using C_k and C_k^*, (7) can also be written in the following form:

$$E\Psi=\left[\tfrac{1}{2}\int(k_0-\alpha k)(p_k^2+q_k^2)dk+\alpha P+m\beta+g\rho_2\int R(k)q_k dk\right]\Psi, \quad (8)$$

with

$$R(k)=\frac{1}{(2\pi)^2}\left(\frac{-2i}{k^2+\mu^2}\right)^{\frac{1}{2}}, \quad i[p_k,q_{k'}]=\delta(k-k').$$

We note that this equation is general and also applicable for unbound states such as scattering of pions if the boundary conditions are suitably modified.

III. STRONG-COUPLING APPROXIMATION. CLASSICAL SOLUTIONS

Having found the suitable equation to handle, we now proceed to the strong-coupling approximation. This approximation consists in first obtaining a classical equilibrium position with respect to the potential energy by omitting the kinetic energy, and then introducing harmonic oscillations about this point. By the potential energy we mean that part of the Hamiltonian which is described by the variables entering the interaction Hamiltonian. Thus in (8) we omit terms containing p_k and obtain the equilibrium position by the variation principle

$$\delta\left[\tfrac{1}{2}\int(k_0-\alpha k)q_k^2dk+m\beta+g\rho_2\int R(k)q_k dk\right]=0. \quad (9)$$

Here the total momentum P is set equal to zero since we are dealing with the center of mass system. Furthermore, the total momentum of the pions $\frac{1}{2}\int kq^2dk$ must vanish since no incoming or outgoing pions are present and our solution must be symmetric in space. In the first step we diagonalize the Dirac matrices to get

$$\delta\left\{\tfrac{1}{2}\int k_0q^2dk\pm\left[m^2+g^2\left(\int Rq_k dk\right)^2\right]^{\frac{1}{2}}\right\}=0. \quad (10)$$

For the moment we take the $+$ sign in front of the square root. The equation becomes

$$k_0q+\frac{g^2\int Rqdk\cdot R}{\left[m^2+g^2\left(\int Rqdk\right)^2\right]^{\frac{1}{2}}}=0, \quad (11)$$

which shows that q must be of the form

$$q=CR/(k_0-i\epsilon), \quad (12^-)$$

or

$$q=CR/(k_0+i\epsilon). \quad (12^+)$$

By the boundary condition the k_0 in the denominator is accompanied by $\pm i\epsilon$, the sign of which will be specified later. Defining

$$\int\frac{R^2}{k_0\mp i\epsilon}dk=\pm\frac{1}{(2\pi)^3}\int\frac{d^3k}{k^2+\mu^2}\equiv\pm N,$$

(11) can be written as

$$C\pm\frac{Cg^2N}{(m^2+g^2C^2N^2)^{\frac{1}{2}}}=0. \quad (13)$$

If we take the $+$ sign, which corresponds to $-i\epsilon$ in (12), we have only one solution, namely, $C=0$. For the $-$ sign, there are two cases. For small values of g^2, (13) has only one solution $C=0$, but for large values of g^2, we have another solution

$$C^2=g^2-m^2/g^2N^2\equiv C_0^2, \quad \text{if} \quad g^2>m/N. \quad (14)$$

This equilibrium position is stable although (12^+) and (14) correspond to a maximum of the potential energy. For if one expands p_k and q_k in terms of a complete set of functions with (12^+) as the first member,

$$p_k=\frac{1}{A}\frac{R}{k_0+i\epsilon}p_1+\sum_{i=2}^{\infty}\varphi_i(k)p_i,$$

$$q_k=\frac{R}{k_0+i\epsilon}q_1+\sum_{i=2}^{\infty}\varphi_i(k)q_i, \quad A=\int\frac{R^2}{(k_0+i\epsilon)^2}dk>0,$$

then p_1 and q_1 are canonical conjugate and we have for the Hamiltonian

$$H=-\frac{N}{2A}p_1^2+U(q_1)+\cdots,$$

where $U(q_1)$ is the potential energy described by q_1. Thus for the coordinate 1 the kinetic energy is negative and a maximum of the potential energy with respect to q_1 corresponds to a stable position. The point $C=0$ is, however, unstable. We shall immediately see that the solution (14) is compatible with the hole theory, so we must take $+i\epsilon$ in (12) representing the static field

around the nucleon. The energy is given by

$$E=\frac{g^2N}{2}+\frac{m^2}{2g^2N}\equiv M. \tag{15}$$

So far we have taken the + sign in front of the square root in (10). If we take the − sign, we have a different solution

$$q=\frac{C_0R}{k_0-i\epsilon},\quad E=-M=-\frac{g^2N}{2}-\frac{m^2}{2g^2N}. \tag{16}$$

This negative level is of course not observable. The meaning of this state is clear if we go back to the expression (3). The solution (16) corresponds to the case in which 0⟩ is not the vacuum, but the state of one antinucleon and 1⟩ is the vacuum state. Since we did not use the fact that 0⟩ is the vacuum state, the state of the lowest eigenvalue, such a solution is necessarily included in Eq. (10), and it must be rejected as unobservable from physical considerations. It must be remembered, however, that although levels like (16) are not real ones, they must be included in order to make solutions complete. In other words, such unphysical states must be included in the intermediate states, as we are familiar with in the case of Compton scattering, where the negative states play a definite role.

The method used here is rather strange for us and not easily understood, so it would be instructive to see the relation of our solution to the usual wave functions. As we can see easily, for the proper field (12^-), the pion energy is $-\frac{1}{2}C_0^2N$. The fact that this is minus means that some pion field is present in the vacuum but is absent in the state 1⟩. We first consider the vacuum state in the Schrödinger wave function. The vacuum is, according to Dirac, filled with nucleons in negative-energy states. A nucleon in a negative-energy state can make a transition to a positive-energy state and back to a negative-energy state by emitting or absorbing pions. In this case there is no exclusion principle in the intermediate state, at least in lower order approximations, since positive-energy states are all vacant. Thus we need not bother about the exclusion or subtraction in solving the behavior of the nucleon in a negative-energy state.

The Hamiltonian is

$$H=\tfrac{1}{2}\int[\pi^2+(\nabla\phi)^2+\mu^2\phi^2]d^3x+\alpha P+m\beta+g\rho_x\phi(X),$$

$$i[P_i,X_j]=\delta_{ij},\quad i[\pi(x),\phi(x')]=\delta^3(x-x'),$$

or by making a transformation

$$A\to UAU^{-1},\quad U=\exp\left[-iX\int\pi\nabla\phi d^3x\right],$$

$$H=\tfrac{1}{2}\int[\pi^2+(\nabla\phi)^2+\mu^2\phi^2]dx+\alpha\left(P+\int\pi\nabla\phi d^3x\right)+m\beta+g\rho_x\phi(0).$$

This can also be written in momentum space as

$$H=\tfrac{1}{2}\int(p_k^2+\omega_k^2q_k^2)d^3k+\alpha(P+\mathfrak{P})+m\beta+\frac{g\rho_x}{(2\pi)^{\frac{3}{2}}}\int q_k d^3k,$$

where ω_k^2 is $k^2+\mu^2$ and the integral extends over all three dimensional k-space. P is now a constant of the motion and can be put equal to zero if we take the particle to have zero total momentum. $\mathfrak{P}$ means the total momentum of the pion but does not contribute in determining the static proper field. The equation to determine the classical equilibrium position is

$$\delta\left\{\tfrac{1}{2}\int\omega_k^2q_k^2d\mathbf{k}-\left[m^2+\frac{g^2}{(2\pi)^3}\left(\int qd\mathbf{k}\right)^2\right]^{\frac{1}{2}}\right\}=0,$$

or

$$\omega^2q-\frac{g^2}{(2\pi)^3}\frac{\int qd\mathbf{k}}{\left\{m^2+[g^2/(2\pi)^3]\left(\int qd\mathbf{k}\right)^2\right\}^{\frac{1}{2}}}=0. \tag{17}$$

Here the negative sign was chosen in front of the square root since we are dealing with a nucleon of negative energy. q has the form

$$q=C/\omega_k^2$$

and

$$\frac{1}{(2\pi)^3}\int qd\mathbf{k}=\frac{C}{(2\pi)^3}\int\frac{d\mathbf{k}}{k^2+\mu^2}=CN.$$

Substituting this integral into (17), we see that C is just the same as (14) and the energy is given by

$$E_0=-\frac{g^2N}{2}-\frac{m^2}{2g^2N}.$$

In a one-particle state, on the other hand, a nucleon in a positive energy state can make no transition since all negative energy states are already occupied. At the same time the nucleon at rest in the negative energy state can no longer make transition since the corresponding positive energy state is occupied. Thus there is no transition at all in this case and

$$E_1=0.$$

The observable mass,

$$E=E_1-E_0=\frac{g^2N}{2}+\frac{m^2}{2g^2N}=M,$$

is equal to what we have found in (15). In this way we can establish the correspondence between the usual theory and the present theory, and we see that the solution (12^-), (14), and (15) is in accord with hole-theoretical considerations.

So far only the particle at rest has been considered. It is easy to obtain the classical solution for a particle moving with momentum $\mathbf{P}$. In (9) we add a term $\boldsymbol{\alpha}\mathbf{P}$ and solve the equation. Some care must be taken in evaluating the divergent integrals in order to preserve Lorentz invariance. This can be attained by putting

$$\int \frac{R^2}{k_0+\mathbf{v}\mathbf{k}+i\epsilon}dk=\frac{1}{(1-v^2)^{\frac{1}{2}}}\int \frac{R^2}{k_0+i\epsilon}dk=-\frac{N}{(1-v^2)^{\frac{1}{2}}},$$

$$\int \frac{(k_0,\mathbf{k})R^2}{(k_0+\mathbf{v}\mathbf{k}+i\epsilon)^2}dk=-\frac{(1,-\mathbf{v})}{(1-v^2)^{\frac{1}{2}}}N.$$

The solution is

$$q=C'R/(k_0+\mathbf{v}\mathbf{k}),\quad C'=C_0/\gamma,$$
$$\gamma=(1-v^2)^{-\frac{1}{2}},\qquad \mathbf{v}=\mathbf{P}/M,$$
$$E=\gamma M=(P^2+M^2)^{\frac{1}{2}}.$$

These relations are completely relativistically invariant.

IV. QUANTUM THEORY OF STRONG COUPLING

Turning back to the quantum mechanical problem, we now want to introduce small oscillations around the equilibrium position we have found.

The Hamiltonian with which we start is

$$H=\tfrac{1}{2}\int(k_0-\alpha k)(p_k^2+q_k^2)dk+\alpha P+m\beta+g\rho_2\int Rqdk.$$

According to the prescription of Sec. III, we first diagonalize the terms containing β and ρ_2. Under the canonical transformation[7]

$$A\to UAU^{-1},$$

with

$$U=\exp\left[-\frac{i\rho_1}{2}\tan^{-1}\frac{g\int Rqdk}{m}\right],$$

the Hamiltonian takes the form

$$H\to H'=\tfrac{1}{2}\int(k_0-\alpha k)(p^2+q^2)dk+\frac{mg}{4}\int R(\rho_1k_0-\sigma k)\times\left\{P,\frac{1}{m^2+g^2\left(\int Rqdk\right)^2}\right\}dk+\beta\left[m^2+g^2\left(\int Rqdk\right)^2\right]^{\frac{1}{2}}+\alpha P,$$

where $\{\ ,\ \}$ means anticommutator. Then we shift the origin of q to the equilibrium position (12) so that no linear term appears in the Hamiltonian.

$$A\to VAV^{-1},$$

$$V=\exp\left(iC_0\int\frac{Rp}{k_0+i\beta\epsilon}dk\right)=\exp iC_0\left[P\int\frac{Rp}{k_0}dk-i\beta\pi\int\delta(k_0)Rpdk\right],\quad(18)$$

where $P\int$ means the principal part of the integral. The Hamiltonian is transformed into

$$H''=\tfrac{1}{2}\int(k_0-\alpha k)(p^2+q^2)dk+\alpha P+\beta\left(\frac{g^2N}{2}+\frac{m^2}{2g^2N}\right)-\frac{m}{2g^2N^2}\int(\sigma k-\rho_1k_0)Rpdk+\frac{m^2}{2g^4N^2}\left(\int Rqdk\right)^2-C_0\alpha\int\frac{Rk}{k_0}qdk.\quad(19)$$

In the second line, the q appearing in the denominators is neglected since q is supposed to be smaller than the static field (12). ρ_1 is changed by the transformation since V contains β, but this change is not important up to the approximations we need.

The Hamiltonian (19) has the form of a nucleon with mass

$$\frac{g^2N}{2}+\frac{m^2}{2g^2N}=M,$$

and a pseudoscalar pion field interacting through the interaction Hamiltonian given by the second and third lines of (19). The interactions on the second line contain the coupling constant g in the denominators of their coefficients, and thus the diagonalization can be carried out in the inverse power series in the coupling constant. We need not carry this through since these interactions are very familiar to us. The first term is the pseudovector coupling but with a different coefficient from the usual one. The second term is the pion pair term which causes the scattering of S-wave pions. If the static field C_0 is small, namely if $g^2\approx m/N$, this pair term is almost equal to the usual expression $(g^2/2m)\phi^2$. However, for large g^2, this term becomes very small compared with $(g^2/2M)\phi^2$. This fact corresponds to the conclusion of several authors[8] that the inclusion of higher order effects suppresses the virtual nucleon pair creation and thus the pion pair term. At the same time, however, the coefficient of the pseudovector coupling is suppressed also. This is natural since in the pseudoscalar coupling theory, the pseudovector coupling appears through the virtual

[7] L. L. Foldy, Phys. Rev. **84**, 168 (1951).

[8] S. D. Drell and E. M. Henley, Phys. Rev. **88**, 1053 (1952); Brueckner, Gell-Mann, and Goldberger, Phys. Rev. **90**, 476 (1953).

nucleon pairs. After the renormalization of the coupling constant, the suppression of the pion pair term will not be so significant.

The interaction represented by the third line of (19) is proportional to C_0 which is roughly equal to g. However, since this term is multiplied by ρ_1 which couples levels spaced by $\sim Ng^2$, this term can also be treated as a perturbation and the solution can be expanded in a power series of $1/g^2$. When we apply a transformation to eliminate this term, the first term thus obtained is

$$\frac{C_0^2}{2M}\left(\int \frac{k}{k_0} R p dk\right)^2,$$

which gives scattering or double emission or absorption of P-wave pions. For the case of large g^2, since both C_0^2 and M are proportional to g^2, this term is independent of g^2 and is very large compared with the pseudovector coupling term. The scattering of P-wave pions is now almost spin independent.

We did not take into account the other of the two equilibria

$$q=\pm C_0 R/k_0.$$

However, up to the approximation we discussed above, the actual wave function is merely a linear combination of the two oscillations, one around $q=+C_0R/k_0$ and the other around $q=-C_0R/k_0$. The nucleon level is a doublet, corresponding to the symmetrical and antisymmetrical combinations, but the spacing is negligibly small. In calculating higher order approximations, the effect of the other oscillation does come into play. The expectation value of q evaluated over the correct wave function is zero. Thus there is no inconsistency in the fact that q is a pseudoscalar quantity and yet has a nonvanishing static field.

V. SYMMETRICAL THEORY

The treatment of the symmetrical theory goes along the same pattern as for the neutral case. The generalization of Eq. (8) to the symmetrical case is obvious. Each field operator has three components with suffixes $\sigma=1, 2, 3$, and the Hamiltonian is given by

$$H=\tfrac{1}{2}\sum\int (k_0-\alpha k)(p_{k\sigma}^2+q_{k\sigma}^2)dk + \alpha P+m\beta+g\rho_3\sum\tau_\sigma\int Rq_{k\sigma}dk. \quad (20)$$

Vectors in the isotopic spin space are represented by bold-face letters in the following.

In the same way as in Sec. III, we can see that the static field is given by

$$\mathbf{q}=\frac{C_0 R}{k_0\pm i\epsilon}\mathbf{e}, \quad e^2=1, \quad (21)$$

where e_ρ is the direction cosine of the quantity $\int Rq_\rho dk$ and $+i\epsilon(-i\epsilon)$ corresponds to the positive (negative) energy solution. The static field (21) has the character of a symmetrical top with a finite moment of isotopic inertia, and this system has excited states corresponding to higher isotopic momenta as we shall see.

To split the pion field into bound and unbound parts, we follow the method of Pauli and Dancoff.[9] We write

$$\mathbf{q}=\frac{R}{k_0}\mathbf{Q}+\mathbf{q}', \qquad \int R\mathbf{q}'dk=0,$$
$$\mathbf{p}=-\frac{R}{N}\mathbf{P}+\mathbf{p}', \quad \int\frac{R}{k_0}\mathbf{p}'dk=0, \quad (22)$$

where

$$\mathbf{Q}=-\frac{1}{N}\int R\mathbf{q}dk, \quad \mathbf{P}=\int\frac{R}{k_0}\mathbf{p}dk.$$

To avoid unnecessary complications, $+i\epsilon$ is omitted in these equations. It is understood that k_0 is always accompanied by $+i\epsilon$ when we are dealing with positive-energy states. If we are dealing with negative-energy states, we take $-i\epsilon$ instead.[10] The commutation relations are given by

$$i[P_\rho, Q_\sigma]=\delta_{\rho\sigma},$$
$$i[p_\rho'(k), q_\sigma'(k')]=\delta_{\rho\sigma}[\delta(k-k')+R(k)R(k')/Nk_0']. \quad (23)$$

With these new variables, the Hamiltonian becomes

$$H=-\tfrac{1}{2}N\mathbf{Q}^2+m\beta-gN\rho_2\tau\mathbf{Q}+\tfrac{1}{2}\int(k_0-\alpha k)(\mathbf{p}'^2+\mathbf{q}'^2)dk - \frac{\mathbf{P}}{N}\int(k_0-\alpha k)R\mathbf{p}'dk-\alpha\mathbf{Q}\int\frac{k}{k_0}R\mathbf{q}'dk.$$

Introducing a unit vector[11]

$$\mathbf{e}=(\sin\alpha\cos\beta, \sin\alpha\sin\beta, \cos\alpha)$$

in the direction of $\mathbf{Q}$. $\mathbf{Q}$ and $\mathbf{P}$ can be written in the following way:

$$\mathbf{Q}=Q\mathbf{e},$$
$$\mathbf{P}=P\mathbf{e}+\mathbf{L}\times\mathbf{e}/Q,$$

where L is the isotopic angular momentum of the bound field,

$$\mathbf{L}=\mathbf{Q}\times\mathbf{P}.$$

[9] W. Pauli and S. M. Dancoff, Phys. Rev. **62**, 85 (1942).

[10] Actually this $\pm$ sign is a q-number quantity which turns out to be equal to β appearing in (25). So there appear additional terms due to the noncommutativity of this β with ρ_1. However, it can be shown that these quantities are of higher order in $1/g^2$ and no error is introduced up to the desired order by taking this $\pm$ sign as a c-number. To see this clearly, we must proceed in a different way by diagonalizing the last two terms in (20) before we split $\mathbf{p}$ and $\mathbf{q}$ into parts. However, this method is rather complicated and was not employed here.

[11] For the detail of the treatment of this rotator see R. Serber and S. M. Dancoff, Phys. Rev. **63**, 145 (1943), and H. Miyazawa, reference 2.

P and Q are scalar but $\mathbf{e}$ is a pseudoscalar quantity under space reflection. Q is assumed to be positive.

Performing a rotation by the unitary transformation

$$A\rightarrow SAS^{-1},\qquad S=\exp(\tfrac{1}{2}i\alpha\tau_2)\exp(\tfrac{1}{2}i\beta\tau_3), \tag{24}$$

and then performing the Foldy transformation[4]

$$A\rightarrow UAU^{-1},\qquad U=\exp[-\tfrac{1}{2}i\tau_2\rho_1\tan^{-1}(gNQ/m)], \tag{24'}$$

the Hamiltonian becomes

$$\begin{aligned}H=&-\tfrac{1}{2}NQ^2+\beta(m^2+g^2N^2Q^2)^{\frac{1}{2}}\\&+\tfrac{1}{2}\int(k_0-\alpha k)(\mathbf{p}'^2+\mathbf{q}'^2)dk\\&-\frac{P}{N}\int(k_0-\alpha k)R(\mathbf{p}'\mathbf{e})dk\\&-\frac{\mathbf{L}'\times\mathbf{e}}{QN}\int(k_0-\alpha k)R\mathbf{p}'dk\\&+\frac{\tau_3}{2N}\frac{g^2mN}{m^2+g^2N^2Q^2}\int(\sigma k-\rho_1k_0)R(\mathbf{p}'\mathbf{e})dk\\&-Q\int\frac{R}{k_0}(\alpha k)(\mathbf{q}'\mathbf{e})dk,\end{aligned} \tag{25}$$

where

$$\mathbf{L}'=US\mathbf{L}S^{-1}U^{-1},$$

and β is $+1$ since we are dealing with positive energy states. The potential energy is stationary at $Q=C_0$ where C_0 is given by (14). We shift the origin of Q so that no linear term appears:

$$Q=C_0+Q'. \tag{26}$$

Q' is supposed to be small compared with C_0. The first two terms in H become

$$\frac{g^2N}{2}+\frac{m^2}{2g^2N}-\frac{N}{2}\frac{C_0^2}{g^2}Q'^2.$$

In the other terms Q can be replaced by C_0 since Q' is small. Finally we want to eliminate the term in (25) which is linear in L' and p'. This can be achieved by a transformation with the unitary operator

$$V=\exp\frac{i\eta}{C_0}\mathbf{L}'\times\mathbf{e}\int\frac{R\mathbf{q}'}{k_0^2}dk,\quad\frac{1}{\eta}=\int\frac{R^2}{k_0^3}dk=-\frac{1}{2\pi\mu}, \tag{27}$$

by which

$$\begin{aligned}\tfrac{1}{2}\int k_0\mathbf{p}'^2dk-\frac{\mathbf{L}'\times\mathbf{e}}{NC_0}\int Rk_0\mathbf{p}'dk\rightarrow&\tfrac{1}{2}\\&\times\int k_0\mathbf{p}'^2dk+\tfrac{1}{2}\frac{\eta\mathbf{L}'^2}{C_0^2}+\cdots.\end{aligned} \tag{28}$$

The eigenvalues of L'^2 can be obtained[11] by transforming back by the operator S of (24). Thus

$$S^{-1}\mathbf{L}'^2S=\mathbf{L}^2+\lambda(\mathbf{L}\cdot\boldsymbol{\tau})+c,$$

where

$$\lambda=1-(m/g^2N)$$

and c is an additive constant. λ is zero if C_0 is zero and is equal to unity if the coupling is very strong. The eigenvalues are given by

$$\iota(\iota+1)+\lambda[I(I+1)-\iota(\iota+1)]+c', \tag{29}$$

where $I=\frac{1}{2},\ \frac{3}{2},\ \cdots$ is the total isotopic angular momentum of the system and $\iota=0,\ 1,\ \cdots$ is the isotopic angular momentum of the bound pion field. The ground state is given by $(I=\frac{1}{2},\ \iota=0)$ and the first excited state is $(I=\frac{1}{2},\ \iota=1)$, the second excited state is $(I=\frac{3}{2},\ \iota=1)$ and so on. The eigenfunctions are given by combinations of the spherical harmonic $Y_\iota^m(\alpha,\beta)$ representing the bound pion field and the isotopic spin functions $p(\tau_3=1)$ and $n(\tau_3=-1)$ of the nucleon. Especially for the ground state, that is, for proton and neutron, the eigenfunctions are

$$pY_0,\ nY_0.$$

Other quantities in the Hamiltonian are not changed by the transformation by S^{-1} except τ_3 in front of the pseudoscalar coupling. τ_3 is changed back to $\boldsymbol{\tau}\mathbf{e}$.

The final Hamiltonian is

$$\begin{aligned}H=&\frac{g^2N}{2}+\frac{m^2}{2g^2N}-\tfrac{1}{4}\frac{\mu}{C_0^2/4\pi}[\mathbf{L}^2+\lambda(\mathbf{L}\cdot\boldsymbol{\tau})+c]\\&-\frac{NC_0^2}{2g^2}Q'^2+\tfrac{1}{2}\int(k_0-\alpha k)(\mathbf{p}'^2+\mathbf{q}'^2)dk\\&-\frac{P}{N}\int(k_0-\alpha k)R\mathbf{p}'\mathbf{e}dk\\&+\frac{m}{2g^2N^2}\int(\sigma k-\rho_1k_0)R(\mathbf{p}'\mathbf{e})(\boldsymbol{\tau}\mathbf{e})dk\\&+\frac{C_0^2}{2M}\left(\int\frac{Rk}{k_0}(\mathbf{q}'\mathbf{e})dk\right)^2,\end{aligned} \tag{30}$$

where the last term comes from the last term of (25) after the elimination of α. Neglected terms are quantities of higher order in $1/g^2$.

The first two terms represent the mass of the nucleon. The next is the isobar energy. Terms described by P', Q', p' and q' describe the free pions, distorted by the presence of the nucleon, as we shall see in Sec. VII. Quantities multiplied by α describe the recoil effect of the nucleon.

The pseudovector coupling induces a transition from $\iota=0$ to $\iota=2$ states as well as to $\iota=0$. For the ordinary

transition, $\iota=0$ to $\iota=0$,

$$\int Y_0^* e_\rho e_\sigma Y_0 \sin\alpha d\alpha d\beta = \tfrac{4}{3}\delta_{\rho\sigma},$$

so that $(\mathbf{p}'\mathbf{e})(\boldsymbol{\tau}\mathbf{e})$ can be replaced by

$$\tfrac{1}{3}(\boldsymbol{\tau}\mathbf{p}'),$$

the familiar symmetrical coupling except for the coefficient.

The last term gives a scattering of P-wave pions. Its coefficient is, in the limit of strong coupling, independent of g^2 and very much larger than the pseudovector coupling term. For the elastic scattering, $\iota=0$ to $\iota=0$, this term gives scattering independent of spin and isotopic spin. This fact is quite contrary to our experience and is the main objection against this theory. That is, the coupling cannot be very strong. If the coupling is not so large, namely if C_0 is small, the pseudovector coupling term explains the behavior of P-waves.

The pion pair term is included in the Q'^2 term and is not apparent in (27). The scattering of S-wave pions will be described in Sec. VII.

We have to investigate the validity of the various approximations introduced. First, Q' is neglected as compared with the static field C_0. Thus C_0 must be very much larger than the amplitude of the zero point oscillation of Q. That is,

$$C_0^2 \gg \langle Q'^2\rangle_{Av} = \frac{1}{N^2}\left\langle\left(\int R\mathbf{q}dk\right)^2\right\rangle_{Av} = \frac{3}{2N^2}\int R^2 dk$$

$$= \frac{3}{2N^2}\frac{1}{(2\pi)^3}\int \frac{d^3k}{(k^2+\mu^2)^4} = \frac{3N'}{2N^2}.$$

Since N' and N^2 are of the same order of magnitude, we have

$$C_0^2 \gg 1.$$

A second approximation is introduced when applying the transformation (27). The right-hand side of (28) is actually an infinite series. In order that the neglected terms be small, it is necessary that

$$\frac{\eta^2}{C_0^2}\left\langle\left(\int \frac{R}{k_0^3}\mathbf{q}'dk\right)^2\right\rangle_{Av} = \frac{\eta^2}{2C_0^2}\int \frac{R^2}{k_0^4}dk \approx \frac{1}{C_0^2} \ll 1.$$

Thus we see that the condition for the strong coupling approximation to hold is given by

$$C_0^2 = g^2 - (m^2/g^2N^2) \gg 1. \tag{31}$$

In this case, that is, if $g^2 \gg 1$, interactions with coefficients involving g in their denominators can be treated as perturbations.

VI. INTERPRETATION OF NEGATIVE EXCITED LEVELS. NUCLEON ISOBARS

The isobar energy, given by the third term of (30), is negative, which means that excited states of nucleons have masses smaller than the proton mass. Of course this must not happen in nature because nucleons are stable particles and do not decay into lighter particles. So these levels are false ones which do not correspond to real particles. We must see why these states occur and what they correspond to in the usual Schrödinger wave function.

The isobar energy is negative because the kinetic energy corresponding to the proper field (21) with $+i\epsilon$ is negative. The excitation of this negative rotator results in the negative excited levels. Or more simply we can understand it in the following way. The scattering of pions by a nucleon occurs through the transition of the nucleon into a negative energy state. The interaction potential is positive, irrespective of the charge or the energy of the pion. For the usual pions this means a repulsive force. However, for minus pions having negative energy, this is an attractive force. The minus pions, therefore, tend to stick to the nucleon thus forming the bound state with negative binding energy.

These spurious solutions are inevitable to the Gell-Mann–Goldberger equation as well as to all theories using a comparison state. They must be rejected by a physical consideration rather than by a mathematical condition. These arise from the fact that no condition is imposed which assures that the comparison state $0\rangle$ is the vacuum. The energy which appears as an eigenvalue of our equation is the difference E_1-E_0 of the eigenenergies of any two states $1\rangle$ and $0\rangle$ provided that the state $1\rangle$ has one more nucleon[12] than $0\rangle$. Let the eigenvalues for the zero nucleon state be $E_0^{(0)}$, $E_0^{(1)}$, $\cdots$ of which $E_0^{(0)}$ is the energy of the vacuum. Then all the values

$$E_1 - E_0^{(0)} = M, \quad E_1 - E_0^{(1)} = M - (E_0^{(1)} - E_0^{(0)}), \quad \cdots$$

appear as eigenvalues of our equation. It was shown[2] that the zero nucleon state has excited states with spectrum

$$\text{const}\cdot I(I+1), \quad I=0, 1, \cdots. \tag{32}$$

The occurrence of negative excited levels is, therefore, quite natural in the strong-coupling theory.

Of course this difficulty does not happen in the usual perturbation theory using the S-matrix. For if $0\rangle$ is the free vacuum in the remote past, it remains the vacuum, the lowest energy state, during the adiabatic switching on of the interaction. However, it does happen in any treatment other than the perturbation method.

These spurious levels, although not observable as particles, give contributions in a reaction as intermediate states. To see this clearly, let us introduce lattice points in space. Each lattice point in the vacuum

[12] By the number of nucleons we mean the number of nucleons minus the number of antinucleons, which is a constant of motion.

has excited states. Let the first excitation energy be Δ ($=E_0^{(1)}-E_0^{(0)}$). Consider the scattering of a particle with energy ω by one lattice point s. The scattering occurs through these excited states and the matrix element is given by

$$M_{(s)}=\frac{H_{fI}^{(s)}H_{Ii}^{(s)}}{\omega-\Delta}+\frac{H_{fI}^{(s)}H_{Ii}^{(s)}}{-\omega-\Delta},$$

where i, I, and f indicate the initial, intermediate and final states respectively. This scattering amplitude is coherent with these from other lattice points and in the total amplitude

$$M=\sum_s M_{(s)}, \tag{33}$$

the sideward scattering interferes to zero and only forward scattering remains. Thus the net effect is a change of the particle energy or the self-energy of the particle due to the vacuum fluctuation.

Now suppose that a single nucleon is present at the point $s=0$. At this point the level $E_0^{(1)}$ is absent and the amplitude $M_{(0)}$ is not present in the sum (33). The amplitude is now

$$M-M_{(0)}=-M_{(0)}, \tag{34}$$

except for the effect of the self-energy. This is the scattering amplitude of the particle by the nucleon. (34) can be rewritten in the following way:

$$-M_{(0)}=-\frac{H^{(0)}H^{(0)}}{\omega-\Delta}+\frac{H^{(0)}H^{(0)}}{\omega+\Delta}=\frac{H^{(0)}H^{(0)}}{-\omega-(-\Delta)}+\frac{H^{(0)}H^{(0)}}{\omega-(-\Delta)}.$$

The right-hand side of this equation is equivalent to the amplitude of the particle scattered through a level with excitation energy $-\Delta$. Thus we see that a level with a negative excitation energy corresponds in the conventional theory to a level which was present in the vacuum but is absent in a one-nucleon state. The levels (32) of the lattice point in the vacuum are no longer present at the position of the nucleon. Thus they must appear, with the sign reversed, as excitation energies in our theory.

The correspondence between the present theory and the conventional theory is not complete, however, since the levels (29) we found are a little different from the negative of (32). Moreover, in the lattice space method we had positive excited states in one-nucleon states also, but now we have no levels with positive energy. These differences come from the neglect of closed loops in this theory. If we had treated all nucleon pairs correctly, we would have all levels corresponding to (32) and also positive levels. However, in the present theory only such nucleon pairs are taken into account which are present in the vacuum but are forbidden in a one nucleon state by the presence of the nucleon. In the vacuum four transitions are possible, namely creation of pairs $(p\bar{p})$, $(p\bar{n})$, $(n\bar{p})$, and $(n\bar{n})$, while in a one proton state 1), only the latter two are allowed to occur. The net difference between 1) and 0) is, therefore, that transitions vacuum$\rightarrow(p\bar{p})$, $(p\bar{n})$ are missing in 1) compared with 0). What we have calculated is the whole consequence of these transitions with the minus sign, however, because they are missing. It can be seen that the excited states of the nucleon with positive excitation found in the lattice space method are due to the closed loops which we did not take into account here.

In spite of these differences, both theories give similar results for the scattering of S-wave pions by a nucleon as we shall see in Sec. VII.

Some comments on the neglect of closed loops in the Feynman diagrams are necessary. We saw that the vacuum or pions have excited states. This fact contradicts with our assumption that pions travel in space according to the free-propagation function Δ_F, which means that pions do not have any structure at all. However, the situation is not so bad as it may appear. The Feynman method, even after the omission of closed loops, correctly takes into account such nucleon pair creations which are forbidden by the presence of the nucleon. Thus the essential part of the pair creation is taken into account in our equation. Again consider the lattice space method. At the point $s=0$, where the nucleon is, the effect of vacuum fluctuation is taken into account.[12] At other lattice points pair creation is replaced by the substitution $\mu_0\rightarrow\mu$. This approximation certainly becomes wrong if the coupling between lattice points becomes large. For instance, the freezing of the vacuum[2] does not occur in the present method.

VII. SCATTERING OF S-WAVE PIONS

The second line in (30),

$$H_0=\tfrac{1}{2}\int k_0(\mathbf{p}'^2+\mathbf{q}'^2)dk-\frac{NC_0^2}{2g^2}Q'^2-\frac{P}{N}\int Rk_0\mathbf{p}'\mathbf{e}dk, \tag{35}$$

represents unbound pions which are distorted by the nucleon. Terms involving α are omitted since these describe the small effect caused by the recoil of the nucleon. $\mathbf{p}'$ and $\mathbf{q}'$ satisfy the commutation relation (23). Introducing new variables,

$$\begin{aligned}\mathbf{q}''&=\mathbf{q}'+Q'\mathbf{e}\frac{R}{k_0}=\mathbf{q}-\frac{C_0R}{k_0}\mathbf{e},\\ \mathbf{p}''&=\mathbf{p}'-\frac{P}{N}\mathbf{e}R=\mathbf{p}-\frac{R}{N}\frac{\mathbf{L}\times\mathbf{e}}{C_0},\end{aligned} \tag{36}$$

the Hamiltonian (35) can be written in a simple form

$$H_0=\tfrac{1}{2}\int k_0(\mathbf{p}''^2+\mathbf{q}''^2)dk+\frac{m^2}{2g^4N^2}\left(\int R\mathbf{q}''dk\right)^2. \tag{37}$$

[12] Even at this point, pair creation of nucleons with both spins antiparallel to the nucleon is omitted since no Pauli principle operates between them.

However, $\mathbf{p}''$ and $\mathbf{q}''$ are not canonically conjugate because the bound pion field is subtracted. From (23) and (36), they satisfy

$$i[p_\alpha''(k),q_\beta''(k')]=\delta_{\alpha\beta}\delta(k-k')+\frac{R(k)R(k')}{Nk_0'}(\delta_{\alpha\beta}-e_\alpha e_\beta).$$

Because of this incompleteness of $\mathbf{p}''$ and $\mathbf{q}''$, the unbound pions are distorted. Another scattering is induced by the second term of (37), which is the damped pair term. Since this term is very small, it can be safely omitted in the following.

It is more convenient to use canonical variables instead. Again we introduce another pair of variables p''' and q''' and put

$$p_\alpha''=p_\alpha''', \quad q_\alpha''=q_\alpha'''+\frac{R\Lambda_{\alpha\beta}}{Nk_0}\int Rq_\beta'''dk,$$

where

$$\Lambda_{\alpha\beta}=\delta_{\alpha\beta}-e_\alpha e_\beta,$$

and

$$i[p_\alpha'''(k),q_\beta'''(k')]=\delta_{\alpha\beta}\delta(k-k').$$

With these new variables, the Hamiltonian becomes

$$H_0=\tfrac{1}{2}\int k_0(\mathbf{p}'''^2+\mathbf{q}'''^2)dk + \frac{\Lambda_{\alpha\beta}}{2N}\int Rq_\alpha'''dk\int Rq_\beta'''dk. \quad (38)$$

The second term describes the scattering of pions. If the coupling is so strong that the isobar separation is small compared with the kinetic energy of pions, all components of $\mathbf{e}$ commute with all other parts of the Hamiltonian and can be treated as c-numbers. In this case (38) is diagonalized in terms of normal modes each representing incoming and outgoing scattered waves. On the other hand, if the isobar separation is extremely large,[14] we must solve the problem in the subspace $\epsilon=0$, the state of minimum isobar energy. This problem can be solved easily by using the Tamm-Dancoff approximation, namely by assuming that the wave functions containing more than two pions are negligible. In calculating the phase shifts we note that (38) is equivalent to the three-dimensional Hamiltonian,

$$H_0=H_\pi+\frac{\Lambda_{\alpha\beta}}{2N}\phi_\alpha(0)\phi_\beta(0), \quad (39)$$

where H_π means the Hamiltonian of free pions. The Schrödinger equation is

$$(-E+\omega_k)F_I(k)+\int dk'(kI|V|k'I)F_I(k')=0, \quad (40)$$

where E is the incident energy including mass, I is the total isotopic angular momentum of the system, V is the interaction Hamiltonian and $\omega_k^2=k^2+\mu^2$. The matrix element of V is the same for both $I=\frac{1}{2}$ and $\frac{3}{2}$ and

$$(kI|V|k'I)=\frac{1}{6N}\frac{1}{(\omega_k\omega_{k'})^{\frac{1}{2}}}, \quad I=\tfrac{1}{2},\tfrac{3}{2}.$$

From this we obtain the phase shift:

$$\tan\delta_I=-\frac{(1/4\pi)k_E}{3N+\dfrac{P}{2(2\pi)^2}\displaystyle\int\frac{d^3k}{\omega(\omega-E)}}, \quad (41)$$

$$k_E^2=E^2-\mu^2.$$

This phase shift is independent of the isotopic angular momentum. This fact is characteristic for the strong-coupling theory.

If the isobar energy is of the same order of magnitude as that of the incoming pion, then the scattering through the isobar level is very important. The first excited state has isotopic spin $\frac{1}{2}$ and parity opposite to the ground state. Let its excitation energy be $-\Delta$. We assume that other excited levels are so far away that they contribute little to the scattering.

The effect of this level can be included by means of the Born approximation. The scattering matrix has the form

$$T_I=\lambda_I\frac{B(k)B(k')}{\Delta-\omega_k}+\mu_I\frac{B(k)B(k')}{\Delta+\omega_k}, \quad I=\tfrac{1}{2},\tfrac{3}{2}. \quad (42)$$

The matrix element for a transition to or from the isobar state can be calculated by pushing the approximation a step further. λ_I and μ_I are dependent on the total isotopic angular momentum of the state and can be determined, apart from the common factor, from the invariance property in isotopic space:

$$\lambda_{\frac{1}{2}}=-1, \quad \mu_{\frac{1}{2}}=3,$$
$$\lambda_{\frac{3}{2}}=2, \quad \mu_{\frac{3}{2}}=0.$$

If Δ is not very large compared with ω, the first term in (42) dominates over the second term. T is positive for $I=\frac{3}{2}$ and negative for $I=\frac{1}{2}$ state. Thus this isobar state gives an additional repulsive effect on $\frac{3}{2}$-waves, but an attractive force on $\frac{1}{2}$-waves. If this attractive force overcomes the repulsive effect due to the diffraction scattering, the phase shift α_1 becomes positive as required by experiments. The phase shift α_3 for the $\frac{3}{2}$ state is always negative.

This qualitative behavior of phase shifts is the same as that predicted by the theory using the lattice space method, although the isobars in both theories are rather different. When ω_k becomes equal to Δ, the first denominator in (42) vanishes. In this case the first Born approximation is wrong and we must take into account

[14] This is the case when the coupling constant is small. In this case, terms of higher order in $1/g$ which were neglected in the above calculation are no longer small. The argument of this section is, therefore, not of quantitative, but of qualitative, nature.

the damping effect. The behavior of this pole must properly be defined[15] in such a way that no real excitation to an isobaric state occurs in the scattering process.[16]

VIII. MAGNETIC MOMENTS OF THE NUCLEONS

The sum of the proton and neutron magnetic moments, measured in nuclear magnetons, can be expressed by a formula[17]

$$\mu_p+\mu_n=(M/m)\langle\beta\rangle\langle\sigma_z\rangle,$$

if the recoil of the nucleon is small. The expectation values can be calculated out separately since P-wave and S-wave pions are independent and no correlation exists between β and σ_z. The calculation of $\langle\sigma_z\rangle$ has been carried out by Sachs[18] and will not be done here. We note that $\langle\sigma_z\rangle$ is smaller than unity.

The expectation value of β can easily be evaluated. By the transformation (24′), β is changed into

$$\beta\to\frac{1}{(m^2+Q^2g^2N^2)^{\frac{1}{2}}}(m\beta-gNQ\tau_3\rho_2).$$

After the transformation we put $\beta=1$, $\rho_2=0$, and substitute for Q by its static value C_0. We obtain

$$\langle\beta\rangle=m/g^2N.$$

The mass of the nucleon M is given by the first two terms of (30), and thus

$$\nu\equiv(M/m)\langle\beta\rangle=\tfrac{1}{2}[1+(m/g^2N)^2].$$

This ν is unity for $C_0=0$, and is one-half in the limit of strong coupling. In the latter case

$$\mu_p+\mu_n<\nu=0.5.$$

The experimental value for $\mu_p+\mu_n$ is 0.88. Thus this is another evidence that the coupling cannot be very strong.

IX. CONCLUSIONS

The approximation employed in this paper is valid when the coupling is large and solutions can be expanded in the power series in $1/g^2$. However, there are many evidences that the coupling cannot be very strong. The mass of the proton, $(Ng^2/2)+(m^2/2Ng^2)$ must be equal to the observed mass M. Thus unless N, which is of the order of the cut-off-momentum, is very small compared with M, g^2 cannot be very large. Furthermore, if the coupling is very strong, (1) the P-wave interaction becomes spin-independent, (2) $\mu_p+\mu_n$ becomes too small, and (3) the isobar separation becomes too small.

Nevertheless, the strong-coupling approximation is of theoretical interest since it gives entirely different results from that of the weak-coupling approximation, and we can at least qualitatively understand the effect of higher order processes. Especially the behavior of the S-phase shifts can be explained by the introduction of a negative isobar with isotopic spin $\frac{1}{2}$.

The theory is not covariant. There appears linear (instead of logarithmic) divergences and the mass of the nucleon does not become zero when the mechanical mass tends to zero. These difficulties arise from the asymmetrical treatment of space and time, especially from the neglect of nucleon recoil in the static approximation. They must be remedied in a more refined treatment.

ACKNOWLEDGMENTS

The author wishes to thank Professor M. L. Goldberger and Professor M. Gell-Mann for information from their unpublished work and for several discussions. He is also much indebted to Professor G. Wentzel, Dr. S. Cohen, and Mr. P. Murphy for their helpful comments.

APPENDIX. TOMONAGA APPROXIMATION

The equation with which we work is

$$E\psi^n=D_n\psi^n+g\rho_2\left[\frac{i}{(2\pi)^4}\int\psi^{n+1}dk-\sum\frac{1}{k_l^2+\mu^2}\psi^{n-1}\right], \quad \text{(A1)}$$

with

$$D_n=\sum k_0+\alpha(P-\sum k)+m\beta,$$

or

$$E\Psi=H\Psi, \quad \text{(A2)}$$

where Ψ stands for a column with components $\psi^0,\psi^1,\cdots$. Equation (A1) can be expressed in a variational form as

$$\delta E=0, \quad E=(\Phi H\Psi)/(\Phi\Psi),$$

where Φ satisfies the adjoint equation

$$E\Phi=\Phi H, \quad \text{(A3)}$$

or

$$E\phi^n(k_1,\cdots,k_n)=\phi^nD_n+g\left[\frac{i}{(2\pi)^4}\frac{1}{n}\sum\phi^{n-1}(k_2,\cdots,k_n)-(n+1)\int\frac{dk}{k^2+\mu^2}\phi^{n+1}(k,k_1,\cdots,k_n)\right]\rho_2.$$

This equation is of course not independent of (A1). In fact by putting

$$\phi^n=\Lambda_n\chi^n,$$

$$\Lambda_n=\frac{1}{n!}\frac{(-i)^n}{(2\pi)^{4n}}(k_1^2+\mu^2)\cdots(k_n^2+\mu^2),$$

we have

$$E\chi^n=\chi^nD_n+g\left[\frac{i}{(2\pi)^4}\int\chi^{n+1}dk-\sum\frac{1}{k_l^2+\mu^2}\chi^{n-1}\right]\rho_2, \quad \text{(A4)}$$

[15] F. J. Dyson, Phys. Rev. **91**, 421 (1953); A. Klein, Phys. Rev. **95**, 1676 (1954).

[16] The creation of minus particles which is energetically possible, must also be excluded.

[17] H. Miyazawa, Phys. Rev. **97**, 1413 (1955).

[18] R. G. Sachs, Phys. Rev. **87**, 1100 (1952).

or taking its Hermitian conjugate,

$$E\chi^{n\dagger}=D_n\chi^{n\dagger}+g\rho_2\left[\frac{-i}{(2\pi)^4}\int\chi^{n+1\dagger}dk-\sum\frac{1}{k_1^2+\mu^2}\chi^{n-1\dagger}\right]. \quad \text{(A5)}$$

This equation is identical with (A1) except the change of sign of i in front of the integral sign.

In Sec. II we imposed a boundary condition that every pole of ψ^n should have the form (5). It can be shown that if we change the sign of $i\epsilon$ at every pole of ψ^n, the resulting $\psi^{n\prime}$ satisfies Eq. (A5). This can be seen by observing that $\int\psi^{n\prime}dk$ is equal to $-\int\psi^n dk$ when ϵ tends to zero after integration. Thus

$$\chi^n=\psi^{n\prime\dagger},$$

and

$$\phi^n=\Lambda_n\psi^{n\prime\dagger}.$$

The norm of Ψ,

$$(\Phi\Psi)=\sum\int\phi^n\psi^n d^nk=\sum\frac{1}{n!}\left(\frac{-i}{(2\pi)^4}\right)^n\times\int\psi^{n\prime\dagger}\pi(k^2+\mu^2)\psi^n d^nk,$$

is seen to be real and positive. For the sake of simplicity, consider the term of $n=1$:

$$\frac{-i}{(2\pi)^4}\int\psi^{1\prime\dagger}(k)(k^2+\mu^2)\psi^1(k)d^3kdk_0. \quad \text{(A6)}$$

The result of integration over k_0 is $2\pi i$ times the sum of residues of

$$\frac{1}{(2\pi)^3}\int\psi^{1\prime\dagger}(k)(k^2+\mu^2)\psi^1(k)d^3k\Big|_{\epsilon=0}. \quad \text{(A7)}$$

Since $\psi^{1\prime\dagger}$, in the limit of vanishing ϵ, is the hermitian conjugate of ψ^1, the residues are all real. Thus we see that (A6) is a real quantity. In the case of general n, integration over the zeroth component of k_i produces a factor i. These cancel the $(-i)^n$ factor in the coefficient, leaving the whole term real.

In the same way we can prove the realness of

$$(\Phi H\Psi)=(\Psi'^{\dagger}\Lambda H\Psi),$$

where Λ is a diagonal matrix with Λ_n as its element. Thus the realness of every eigenvalue E is proved, provided that ψ^n satisfies the boundary condition (5).

The variational equation is

$$\delta E=0, \quad E=(\Phi H\Psi)/(\Phi\Psi)=(\Psi'^{\dagger}\Lambda H\Psi)/(\Psi'^{\dagger}\Lambda\Psi). \quad \text{(A8)}$$

If the Dirac matrices α, β, and ρ_2 are c-numbers, Eq. (A1) is separable and can be solved by putting

$$\psi^n(k_1,\cdots,k_n)=(C_n/n!)\prod\psi(k_i). \quad \text{(A9)}$$

We assume, according to Tomonaga, that the Hartree-type wave function (A9) is a good approximation even in the case where α, β, and ρ_2 are actual matrices. In this case C_n is a Dirac spinor and C_n and $\psi(k)$ are to be determined by the variational principle. The norm of ψ is fixed to unity,[19]

$$\frac{-i}{(2\pi)^4}\int\psi^{*\prime}(k)(k^2+\mu^2)\psi(k)dk=1. \quad \text{(A10)}$$

Then

$$(\Phi\Psi)=\sum C_n{}^*C_n,$$

where

$$(\Phi H\Psi)=\langle k_0\rangle\sum nC_n{}^*C_n+m\sum C_n{}^*\beta C_n+\eta g\sum\left[(n+1)^{\frac{1}{2}}C_n{}^*\rho_2C_{n+1}+\frac{1}{n^{\frac{1}{2}}}C_n\rho_2C_{n-1}\right],$$

$$\langle k_0\rangle=\frac{-i}{(2\pi)^4}\int\psi^n(k)k_0(k^2+\mu^2)\psi(k)dk,$$

and

$$\eta=\frac{-i}{(2\pi)^4}\int\psi(k)dk.$$

The Schrödinger equation for C_n is

$$(n\langle k_0\rangle+m\beta)C_n+\eta g\rho_2\left[(n+1)^{\frac{1}{2}}C_{n+1}+\frac{1}{n^{\frac{1}{2}}}C_{n-1}\right]=EC_n. \quad \text{(A11)}$$

The equation to determine ψ can be obtained by varying ψ under the condition (A10),

$$2\langle n\rangle k_0(k^2+\mu^2)\psi(k)+\langle V\rangle=\lambda(k^2+\mu^2)\psi(k), \quad \text{(A12)}$$

where

$$\langle n\rangle=\sum nC_n{}^*C_n/\sum C_n{}^*C_n,$$

$$\langle V\rangle=g\sum\left[(n+1)^{\frac{1}{2}}C_n{}^*\rho_2C_{n+1}+\frac{1}{n^{\frac{1}{2}}}C_n\rho_2C_{n-1}\right]\Big/\sum C_n{}^*C_n,$$

and λ is a Lagrangian multiplier. Thus

$$\psi(k)=\frac{\langle V\rangle}{2\langle n\rangle}\frac{1}{k_0-\lambda'}\frac{1}{k^2+\mu^2}. \quad \text{(A13)}$$

where λ' is given in terms of $\langle V\rangle/\langle n\rangle$ by the normalization requirement (A10).

Equation (A11) can be solved in both weak and strong coupling limits.

[19] Sometimes the integral $[-i/(2\pi)^4]\int\psi^{*\prime}(k^2+\mu^2)\psi dk$ is negative ($=-C^2$). In this case we normalize ψ by multiplying by i/C, where this i is assumed to change its sign under the prime operation.

In the weak coupling case, the Ansatz (A9) is exact since only wave functions ψ^0, $\psi^1(k)$ are involved. This can also be verified directly. Up to order g^2, (A11) gives energy value

$$E=m+\frac{\eta^2 g^2}{2m-\langle k_0\rangle}. \tag{A14}$$

From this we have

$$\frac{\langle V\rangle}{2\langle n\rangle}=\frac{\partial E/\partial\eta}{2\partial E/\partial\langle k_0\rangle}=\frac{2m-\langle k_0\rangle}{\eta}\equiv C. \tag{A15}$$

It is easy to see that

$$\psi=C\frac{1}{(2m-k_0-i\epsilon)(k^2+\mu^2)} \tag{A16}$$

satisfies the normalization condition (A10) and therefore is the solution of the variational Eq. (A12). For if we calculate $\langle k_0\rangle$ and η with the wave function (A16) and put them into (A15), we have the relation

$$\frac{1}{C^2}=\frac{-i}{(2\pi)^4}\int\frac{dk}{(2m-k_0)^2(k^2+\mu^2)},$$

which is the normalization condition for (A15).

In this case, the energy (A14) is

$$E=m+\frac{\eta}{C}g^2=m-\frac{g^2}{(2\pi)^4}\int\frac{dk}{(2m-k_0)(k^2+\mu^2)}$$
$$=m+\frac{g^2}{2(2\pi)^3}\int\frac{d^3k}{(2m+\omega)\omega},$$

which is equal to that obtained from (A1) by the perturbation method (neglecting, however, recoil momentum).

In the strong-coupling case, it is convenient to transform (A11) into the form

$$\left[\frac{\langle k_0\rangle}{2}(p^2+q^2)+m\beta+\sqrt{2}\eta g\rho_2 q\right]\Psi=E\Psi,$$
$$i[p,q]=1.$$

The classical solution is obtained by omitting the p^2 term. The energy is given by

$$E=-\frac{\eta^2 g^2}{\langle k_0\rangle}-\frac{1}{4}\frac{\langle k_0\rangle m^2}{\eta^2 g^2},\quad(\langle k_0\rangle<0). \tag{A17}$$

Equations (A13) and (A10) can be satisfied by

$$\psi(k)=\gamma\frac{1}{(k_0+i\epsilon)(k^2+\mu^2)}, \tag{A18}$$

where γ is the normalizing constant. Since, in this case,

$$\langle k_0\rangle=\frac{-\gamma^2 i}{(2\pi)^4}\int\frac{dk}{k_0(k^2+\mu^2)}=-\frac{\gamma^2 N}{2},$$

$$\eta=-\frac{\gamma N}{2},\quad\text{and}\quad\frac{\langle V\rangle}{2\langle n\rangle}=\frac{\partial E/\partial\eta}{\partial E/\partial\langle k_0\rangle}=\frac{\langle k_0\rangle}{\eta}=\gamma,$$

then (A13) with $\lambda'=0$ is the correctly normalized function. The energy is

$$E=\frac{g^2 N}{2}+\frac{m^2}{2g^2 N},$$

which is equal to (15).

In the limiting cases, the Tomonaga Ansatz (A9) agrees with the weak and strong coupling theories. The Tomonaga approximation links continuously between the weak and strong coupling theories. λ' in (A13) continuously varies from $2m-i\epsilon$ in the weak coupling limit to $-i\epsilon$ in the strong coupling limit.

In order to calculate the expectation value of some quantity Q, we use the following principle. Let the change of eigenvalue caused by adding λQ (λ: constant) to the Hamiltonian be $\Delta E(\lambda)$. Then the expectation value of Q is given by

$$\langle Q\rangle=\left.\frac{\partial\Delta E(\lambda)}{\partial\lambda}\right|_{\lambda=0}.$$

Now if we add λQ to the original Hamiltonian, the corresponding Hamiltonian H of (A2) will get an additional term Q' (for instance if Q is $\int\psi^* O\psi d^3x$, Q' is simply O). The change in the energy caused by this additional term, to first order in λ, is

$$(\Phi\lambda Q'\Psi)/(\Phi\Psi),$$

since (A8) is a stationary expression. Thus

$$\langle Q\rangle=(\Phi Q'\Psi)/(\Phi\Psi).$$

This method of evaluating expectation values can be applied to any four-dimensional theory, for instance, the Bethe-Salpeter formulation of the two-body problem.

Pion-Nucleon Scattering at High Energies*

A. N. MITRA†
Laboratory of Nuclear Studies, Cornell University, Ithaca, New York
(Received April 28, 1955)

The pseudoscalar theory in the Tamm-Dancoff approximation is applied to high-energy pion-nucleon scattering with a view to explaining the observed maximum in π^--p scattering around 1 Bev as a resonant interaction. The integral equation is solved for the $D_{\frac{3}{2}}$ state of $T=\frac{1}{2}$ which is attractive. The various singularities in the kernel and the wave function are taken into account in a semianalytical fashion. A short derivation is given of the complex intefral equation which takes the effects of meson production into account, and it is solved in an approximate manner.

It is found that, contrary to the original expectation of a resonant interaction, the increase of $D_{\frac{3}{2},\frac{3}{2}}$ phase shift over the Born approximation is not large. Also the effects of meson production are not found to be very significant over the energy range 1 Bev to 2 Bev. This last is contrary to the observations in this energy range.

1. INTRODUCTION

THE early Brookhaven experiments on the total cross section for π^--p scattering indicated a maximum near 1 Bev (laboratory system) in addition to the (now famous) maximum around 200 Mev which had been observed before. The latter one had been successfully explained by means of the Tamm-Dancoff (T.D.) approximation in pseudoscalar theory,[1] as a resonant interaction in the state $P_{\frac{3}{2},\frac{3}{2}}$ ($J=\frac{3}{2}$, $T=\frac{3}{2}$) of the meson-nucleon system. The success of the T.D. approximation encouraged the belief that a similar explanation of the maximum around 1 Bev might not be unreasonable.

The basis for this expectation was, of course, somewhat weaker than in the case of the first maximum around 200 Mev. Firstly, the data were rather few (and not too accurate), so that any detailed analysis (of the type carried out for the "low"-energy case) had not been feasible in this region. Thus the interpretation of the high-energy region had to be based on rather general considerations instead of more positive experimental facts (which were available in the "low"-energy case). Secondly, the maximum around 1 Bev was believed to be much broader[2] than that around 200 Mev. Still it was thought worthwhile carrying out an investigation similar to Dyson's for this case as well.

The interesting feature of this "second" maximum is that it occurs only in the π^--p cross section, unlike the previous case where both the π^+-p and π^--p cross sections showed maxima at the same energy (~200 Mev); no maximum in (π^+-p) scattering has been observed in the region of 1 Bev.[3] Thus a possible explanation of the "second" maximum would require an isotopic spin state $T=\frac{1}{2}$, rather than $T=\frac{3}{2}$, since the latter would contribute mostly to π^+-p scattering. Now the most important feature of the T.D. method (as has been clearly shown by Dyson's work) is that it considerably enhances the Born approximation phase shift for attractive states and reduces it for repulsive states. Hence, in order to interpret the second maximum as a one-meson resonance, one has to look for some state of $T=\frac{1}{2}$ which has an attractive interaction. Now it can be shown generally[1,4] that for $T=\frac{1}{2}$, the states of $j=2n+\frac{1}{2}$ (where 'n' is an integer) have an attractive interaction, while for $T=\frac{3}{2}$ it is the states $j=2n-\frac{1}{2}$ which are attractive.

Among the states $j=2n+\frac{1}{2}$, the states $j=\frac{1}{2}$ occupy a special position because only in these states can the meson be absorbed by the nucleon *before* the latter emits one. As a result, these states exhibit self-energy effects due to the possibility of successive emission and reabsorption of a meson by the nucleon, in the framework of the T.D. formalism. Consequently these states require a special renormalization which has been treated by Dalitz and Dyson.[5] On account of these special features these states are not expected to be strongly attractive. (Moreover, their j- value is much too small to account for the magnitude of the cross section at the observed maximum.) This leaves as the first strongly attractive states those of $j=5/2$. At an energy as high as 1 Bev, it is reasonable to consider states of such high j; indeed the large cross section observed around 1 Bev (~50 mb) requires a j at least as high as this.

Now for a given j, the state with $l=j-\frac{1}{2}$ has always the stronger interaction; for $l=j+\frac{1}{2}$ the interaction begins to be important only in the relativistic region (but cannot exceed the former). So one may expect the $D_{\frac{3}{2}}$ state to be the more important one, rather than $F_{\frac{5}{2}}$. For the same reason one would not expect important effects from the $D_{\frac{5}{2}}$ state of $T=\frac{3}{2}$ (which would,

* Based on a thesis submitted in partial fulfillment of the requirements for the degree of Doctor of Philosophy at Cornell University.

† Now at the Department of Physics, University of Delhi, Delhi, India.

[1] Dyson, Ross, Salpeter, Schweber, Sundaresan, Visscher, and Bethe, Phys. Rev. **95**, 1644 (1954); referred to as A.

[2] This was the situation in January, 1954 when this calculation was undertaken. Recently, more accurate data have appeared which indicate that the curve drops fairly sharply on the high-energy side.

[3] The more recent data indicate that there is a *minimum* in the (π^+-p) cross section somewhat below 1 Bev.

[4] Bethe, DeHoffman, and Schweber, *Mesons and Fields* (Row, Peterson and Company, Evanston, 1955), Vol. 2.

[5] R. H. Dalitz and F. J. Dyson, Phys. Rev. **99**, 301 (1955).

moreover, contribute predominantly to π^+-p scattering).

Having thus decided on this choice of the state to be considered, we shall take the paper of Dyson *et al.*[1] as basic and freely use the various equations and formulas of this paper with the same notation as far as possible.

2. NECESSARY FORMALISM

From Eqs. (23), (27), and (27a) of A, we find that the wave function $f(p)$ of the $D_{\frac{3}{2}\frac{3}{2}}$ state satisfies the equation:

$$f(p)=2\lambda\int_0^\infty \frac{s^2}{(E_p\omega_p E_s\omega_s)^{\frac{1}{2}}}L_1(p,s)\times\left[\delta(E-E_s-\omega_s)+P\frac{f(s)}{E-E_s-\omega_s}\right], \quad (1)$$

where

$$\lambda=G^2/(16\pi^2), \quad (2)$$

and

$$L_1(p,s)=-\tfrac{1}{3}[(E_p+M)\{(A-2M)K_2(C)+(E-M)K_2(B)\}+sp(E_s+M)^{-1}\times\{AK_2(C)+(E+M)K_3(B)\}]. \quad (3)$$

The other symbols are as defined in A. $f(p)$ is related to the phase shift according to the equation:

$$\tan\delta=-\pi f(k). \quad (4)$$

It is somewhat more convenient to work in terms of the quantities $f_1(p)$ and x defined as follows:

$$f_1(p)=(E_p\omega_p)^{\frac{1}{2}}f(p), \quad (5)$$

$$x=E_s+\omega_s-E. \quad (6)$$

The transformations (5) and (6) bring (1) into the form:

$$f_1(p)=f_B(p)+\lambda\int L(p,s)f_1(s)(ds/x), \quad (7)$$

where

$$L(p,s)=-2s(E_s+\omega_s)^{-1}L_1(p,s), \quad (8)$$

$$f_B(p)=-\lambda(E_k\omega_k)^{\frac{1}{2}}L(p,k), \quad (9)$$

$$\tan\delta=-\pi(E_k\omega_k)^{-\frac{1}{2}}f_1(k). \quad (10)$$

The quantities $f_1(s)$ and $L(p,s)$ should now be regarded as functions of x rather than s. This has the advantage that the singularity at $x=0$ can be evaluated very simply in a semianalytical manner, without introducing any complexities elsewhere.

So far, the Eqs. (1) or (7) do not take account of the possibility of meson production. However, if the total energy of the system is sufficiently large, the latter process becomes energetically possible (threshold energy in the c.m. system being only $E=M+2\mu$), and its importance increases with energy. Since the energies to be considered are rather large ($\gtrsim$1 Bev), it is expected that these reactive processes will play an important part, and their effects should therefore be taken into account.

The Eq. (15) of A (before angular integration) suggests the modification necessary for including meson production effects. We find that one of the terms in the kernel (corresponding to the (1,2) state) involves an energy denominator $E-E_{p+s}-\omega_p-\omega_s$ which can vanish only for $E\gtrsim M+2\mu$. Now in Eq. (A15), the integral is evaluated as a principal value, representing standing waves. To include the effects of meson production, we should now add an *outgoing* two-meson wave to the one-meson equation (A15) through the modification:

$$P\frac{1}{E_1}\longrightarrow\lim_{\epsilon\to 0}\frac{1}{E_1+i\epsilon}=P\frac{1}{E_1}+i\pi\delta(E_1), \quad (11)$$

where

$$E_1=E-\omega_s-\omega_p-E_{p+s}, \quad (11a)$$

and $\epsilon>0$. The kernel therefore becomes a complex function of p and s, and in place of (1), we now have a *complex* integral equation of the form:

$$f(p)+i\phi(p)=2\lambda\int_0^\infty s^2ds(E_s\omega_sE_p\omega_p)^{-\frac{1}{2}}\{L_1(p,s)+iL_2(p,s)\}\times\left[\delta(E-\omega_s-E_s)+P\frac{1}{E-E_s-\omega_s}\{f(s)+i\phi(s)\}\right]. \quad (12)$$

The evaluation of $L_2(p,s)$ may be carried out by noting that, according to (11), the quantities $K_n(C)$ in (3) [see Eq. (A22)] are changed into

$$K_n(C)+i\pi(2ps)^{-1}P_n[(c^2-1-r^2)/2r], \quad (13)$$

where the P_n's are the usual Legendre polynomials. It may be noted that the above modification does not change the B-terms in (3). Thus we have:

$$L_2(p,s)=-\pi(ps)^{-1}[(E_p+M)(A-2M)P_2(y)+spA(E_s+M)^{-1}P_3(y)], \quad (14)$$

where

$$y=(c^2-1-r^2)/2r. \quad (15)$$

The important property of $L_2(p,s)$ is that it is zero unless $E=\omega_p+\omega_s+E_{p+s}$ as may be seen from the appearance of the δ function in (11). This condition cannot be satisfied for real values of θ (angle between $\mathbf{p}$ and $\mathbf{s}$) unless *both* p and s are *less* than k in magnitude. In particular, $L_2(p,s)$ vanishes on and above the energy the energy shell (*i.e.*, when $p\gtrsim k$ or $s\gtrsim k$ or both).

Transformation of (12) according to (5) and (6) leads finally to the equation:

$$f_1(p)+i\phi_1(p)=f_B(p)+\lambda\int\{L(p,s)+iL'(p,s)\}[f_1(s)+i\phi_1(s)](dx/x), \quad (16)$$

where

$$L+iL'=-2s(E_s+\omega_s)^{-1}(L_1+iL_2). \quad (17)$$

The quantity $f_B(p)$ in (16) is purely real and is given as before by (9), since $L'(p,k)=0$ (from what has been said in the last paragraph).

The complex phase shift $\delta+i\eta$ is now given by:

$$\tan(\delta+i\eta)=-\pi(E_k\omega_k)^{-\frac{1}{2}}[f_1(k)+i\phi_1(k)]=A+iB. \quad (18)$$

The contributions of a particular state (j,T) to the total cross sections (elastic and inelastic) are[6]

$$\sigma_{el}(j,T)=\pi\lambda^2(j+\tfrac{1}{2})|\exp(2i\delta-2\eta)-1|^2, \quad (19a)$$

$$\sigma_{in}(j,T)=\pi\lambda^2(j+\tfrac{1}{2})[1-\exp(-4\eta)]. \quad (19b)$$

In terms of the quantities A and B of (18), the cross sections are easily seen to be:

$$\sigma_{el}(j,T)=2\pi\lambda^2(2j+1)(A^2+B^2)[(1+B)^2+A^2]^{-1}, \quad (20a)$$

$$\sigma_{in}(j,T)=2\pi\lambda^2(2j+1)B[(1+B)^2+A^2]^{-1}. \quad (20b)$$

For the state $T=\frac{1}{2}$, the contributions to (π^-p) scattering are finally given by:

$$\begin{aligned}\sigma_{el}(\pi^-p)&=\tfrac{2}{3}\sigma_{el}(j,\tfrac{1}{2}),\\ \sigma_{in}(\pi^-p)&=\tfrac{2}{3}\sigma_{in}(j,\tfrac{1}{2}).\end{aligned} \quad (21)$$

3. KERNEL OF THE INTEGRAL EQUATION

The solution of the complex integral equation (16) is an extremely complicated process, since it appears in a coupled form when the real and imaginary parts are separated out. It is more feasible first to solve the real equation (7) (which does not take account of meson production) and then to use this solution as a basis for the more general case of (16). Even for the simpler case of (7) a completely analytical solution is virtually impossible, and a semi-analytical approach seems to be the most that can be done. For this purpose, it is useful first to discuss some of the important features of the kernel $L(p,s)$. $L(p,s)$ contains the various functions $K_n(b)$ and $K_n(C)$ which have been defined in A. It is useful to express these functions in terms of the parameters u and v defined by:

$$u=r/(1+b), \quad v=r/(1+c); \quad (22)$$

where

$$c=C/\bar{E}, \quad b=B/\bar{E}; \quad (22a)$$

$$\bar{E}=\tfrac{1}{2}[E(p+s)+E(p-s)]; \quad (22b)$$

$$C=\omega_p+\omega_s-E, \quad r=sp/\bar{E}^2. \quad (22c)$$

Thus, explicitly,

$$v=sp/\bar{E}(\bar{E}+C)=\{E(p+s)-E(p-s)\}/\{E(p+s)+E(p-s)-2C\}. \quad (22d)$$

A similar expression holds for u. We now have the following expressions for the K_n-functions:

$$K_0(C)=\tfrac{1}{2}(sp)^{-1}\ln[(1+v)/(1-v)]; \quad (23a)$$

$$K_1(C)=yK_0(C)+\tfrac{1}{2}(1-c)/sp; \quad (23b)$$

$$K_2(C)=\tfrac{3}{4}yK_1(C)+\tfrac{1}{4}c/\bar{E}^2-\tfrac{1}{2}K_0(C); \quad (23c)$$

$$K_3(C)=(5/3)yK_2(C)-\tfrac{2}{3}K_1(C)-\tfrac{1}{6}cr/\bar{E}^2. \quad (23d)$$

Exactly similar expressions hold for $K_n(B)$.

For small values of u and v, the logarithmic terms $\ln[(1+v)/(1-v)]$ and $\ln[(1+u)/(1-u)]$ can be expanded in ascending powers of these parameters and a certain number of terms may be retained, depending on the accuracy needed. On the other hand, for $|v|$ or $|u|\geq\frac{1}{4}$, the closed forms are more suitable for numerical work.

The asymptotic behavior of the kernel can be obtained by expanding in powers of $(p_</p_>)$ (where $p_<$ and $p_>$ are respectively the smaller and larger of p and s). Following the procedure of Bethe and others,[7] one has the following asymptotic form of $L(p,s)$, for the case of $j=l+\frac{1}{2}$:

$$L(p,s)\approx\tfrac{1}{2}ps^{-1}[H_{j-\frac{1}{2}}(p/s)+H_{j+\frac{1}{2}}(p/s)], \quad (s>p); \quad (24)$$

where

$$H_n(x)=\ln(1+x)-x+\tfrac{1}{2}x^2-\cdots+(-1)^nx^n/n. \quad (24a)$$

Retaining the most important terms in the expansion of $H_n(x)$ for $|x|<1$, one finds that (24) reduces to the following expression $(l=2)$:

$$L(p,s)\approx 38/405(p/s)^3+O(p/s)^4. \quad (24b)$$

Using (24), one can derive the asymptotic behavior of $f_1(p)$, assuming $f_1(p)\to p^{-n}$, $(n>0)$, and substituting in (7) to determine n in terms of λ. This relation is given by[4]:

$$\begin{aligned}-\lambda/Q'=&\frac{1}{n(1-n)}\left[\frac{\pi}{\sin\pi n}-\frac{1}{n(1-n)}+2\right]\\&+2\sum_{k=1}^{j-\frac{1}{2}}(-1)^k\left[\frac{1}{k^2-n^2}+\frac{1}{k^2-(1-n)^2}\right]\\&+(-1)^{j+\frac{1}{2}}\left[\frac{1}{(j+\frac{1}{2})^2-n^2}\right.\\&\left.+\frac{1}{(j+\frac{1}{2})^2-(1-n)^2}\right].\end{aligned} \quad (25)$$

Using the argument of Bethe *et al.*,[4] one can derive from (25) an upper limit λ_0 on the value of λ, from the requirement of square integrability of the wave function which demands that $n>\frac{1}{2}$. This "critical" coupling constant $(4\pi\lambda_0)$ is obtained by putting $n=\frac{1}{2}$ in (25) (limit of normalizability) and using the values of

[6] J. M. Blatt and V. F. Weisskopf, *Theoretical Nuclear Physics* (John Wiley and Sons, Inc., 1952), Chap. 8.

[7] Dalitz, Sundaresan, and Bethe, Proc. Cambridge Phil. Soc. (to be published).

$j=5/2$ and $Q'=-1$. This gives finally:

$$4\pi\lambda_0=G_0^2/(4\pi)=176.8. \tag{25a}$$

It may be noted from the expressions (23) that the functions $K_n(C)$ are real as long as $|v|<1$, diverge logarithmically when $v=\pm 1$, and become complex when $|v|>1$.[6] Thus the imaginary part of the kernel vanishes except when $|v|>1$. This gives a simple criterion for the existence of the imaginary part. For the energies we shall consider, $|u|$ is always less than unity, so that $K_n(B)$ is always real. Moreover, for the real equation (7), $\ln x_1$ is replaced by $\ln|x_1|$, where $x_1=(1+v)/(1-v)$.

Since $|v|>1$ makes the kernel complex this condition must be equivalent to the possibility of simultaneous production of two mesons, of momenta $\mathbf{p}$ and $\mathbf{s}$, with conservation of energy. Such production is possible if, for *some* relative direction of $\mathbf{p}$ and $\mathbf{s}$, the energy conservation equation [see (11)],

$$E(\mathbf{p}+\mathbf{s})+\omega_s+\omega_p=E, \tag{26}$$

can be fulfilled. This is obviously the case if, for the given p and s,

$$E(p-s)+C\leqslant 0\leqslant E(p+s)+C, \tag{26a}$$

where C is defined in (22c). But according to the definition (22d) of v, $v=\pm 1$ means that

$$E(p\mp s)+C=E(p\mp s)+\omega_p+\omega_s-E=0. \tag{27}$$

This equation is clearly equivalent to the two limiting cases of Eq. (26a). It can then easily be shown that the energy equation (26a) can indeed be fulfilled if and only if $|v|\geqslant 1$.

The region in which the kernel is complex is then the one between the two curves in the $p-s$ plane defined by Eq. (27), with the $-$ and $+$ signs in $E(p\mp s)$ respectively; they are plotted in Fig. 1 for the case $k=1.0M$.

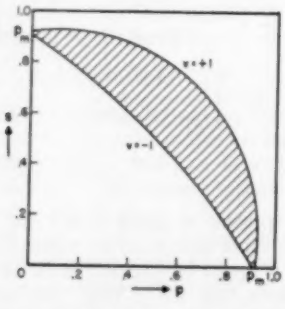

FIG. 1. The curves $v=\pm 1$; the shaded portion between the curves is the region of meson production.

[6] This follows from the relation:
$\ln[(1+v)/(1-v)]=\ln|(v+1)/(v-1)|+i\pi$, for $|v|>1$.

If p is kept fixed and s varied, then for $s=0$ we have

$$\bar{E}+C=E(p)+\omega(p)+\mu-E. \tag{28}$$

Production of an additional meson s together with p is only possible if the expression (28) is negative which will only be the case if $p<p_{\max}$, where $p_{\max}$ is defined by:

$$E(p_{\max})+\omega(p_{\max})+\mu=E, \tag{28a}$$

and is always somewhat smaller than k.

The nature of the kernel is quite different according as $p\leqslant$ or $>p_{\max}$. For $p\leqslant p_{\max}$, v can vary from $-\infty$ to $+\infty$, so that the $K_n(c)$ functions have logarithmic singularities. Thus for such values of p the kernel is expected to show rather large variations as a function of s. On the other hand, for $p>p_{\max}$, $|v|$ is less than unity for all s, so that the kernel is expected to be a smooth function.

The quantity $L(p,s)$ was first tabulated numerically by programming it for the Card-Programmed-Computer

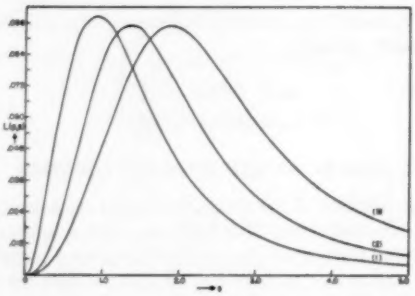

FIG. 2. The function $L(p,s)$ as a function of s, when $p>p_{\max}$ and $k=1.0M$. Curves (1), (2), and (3) correspond respectively to $p=1.0M$, $p=1.4M$ and $p=2.0M$.

(C.P.C.) situated at the Cornell Computing Center. Two different initial C.M. momenta, $k=0.7M$ and $k=1.0M$ were considered. These correspond respectively to 1.135-Bev and 2.128-Bev meson kinetic energies in the laboratory system. For each of these two energies, the kernel was programmed as a function of the "variable" s and the "parameter" p. Use of two different "instruction fields" greatly facilitated the programming for $|v|>\frac{1}{4}$ and $|v|\leqslant\frac{1}{4}$ respectively. The regions where the kernel was expected to show rather marked variations (according to the previous paragraph) were given due weights by taking smaller intervals of s and p for them. For the asymptotic region (large s) the behavior of the kernel, as given by (24a) was taken as a rough indication of the maximum value of s needed for a given p, with the specification that the least tabulated value of $L(p,s)$ (for given p) should be about 1% of its maximum value.

Some typical curves are shown in Figs. 2 and 3. For $p>p_{\max}$, Fig. 2 shows that the kernels are indeed smooth functions of s, with fairly well-defined maxima

at roughly $s=\phi$. There is a tendency for these peaks to be somewhat broader as ϕ is increased.

Figure 3 shows that for $\phi<\phi_{max}$, the kernel has logarithmic singularities. There is a fairly deep minimum in between these singularities. The signularities shift towards the left as ϕ is increased, and finally disappear at $\phi=\phi_{max}$.

4. SOLUTION OF THE REAL EQUATION

For a solution of the integral equation (7), it was necessary first to transform it into a set of linear simultaneous equations in suitable parameters representing the wave function. Because of the presence of various singularities it was thought somewhat more convenient (and probably safer) to use a semianalytical approach by fitting simple functions of the appropriate type to the numerical data representing the kernel, instead of taking only those discrete points at which the kernel had been tabulated. This procedure permitted the integrations over singular regions to be carried out in a relatively simple way. It is particularly useful for $\phi<\phi_{max}$, though not so much for $\phi>\phi_{max}$. However, since the procedure of curve fitting turned out to be very much simpler for $\phi>\phi_{max}$, it was decided to adopt the same procedure throughout.

As already noted, it was found convenient to work in terms of $x(=E_s+\omega_s-E)$ rather than s. This makes the integration over the singularity at $x=0$ a fairly trivial matter.

Since it was not possible to represent $L(\phi,s)$ by a single function of x over its entire range (without sacrificing a considerable amount of accuracy), the latter was broken up into several suitable intervals in each of which the kernel could be represented accurately by simple functions of 'x'. It was expected that the number of intervals should increase with k in order to achieve the same degree of accuracy; therefore it was decided to take 4 intervals for $k=0.7M$, and 6 for $k=1.0M$.

The wave function $f_1(\phi)$ could be conveniently represented in the *corresponding* intervals by means of simple analytic functions of a similar type. As regards the *shape* of $f_1(\phi)$, the function $L(\phi,k)$ (which is just the Born approximation $f_B(\phi)$, apart from the factor $-\lambda(E_k\omega_k)^{\frac{1}{2}}$, was taken as a rough indication. The assumption of similarity between $L(\phi,k)$ and $f_1(\phi)$ is probably not unreasonable at moderate energies, but may not be valid for larger ones. However, as long as the number of parameters used to represent $f_1(\phi)$ is reasonably large, the assumption of a particular shape (like the one mentioned above) should not make any important difference, especially since $f_1(\phi)$ cannot have any unphysical singularity (being a wave function). For $\phi>\phi_{max}$ it was found that the functions $L(\phi,s)$ as well as $L(s,k)$ could be represented very accuractely

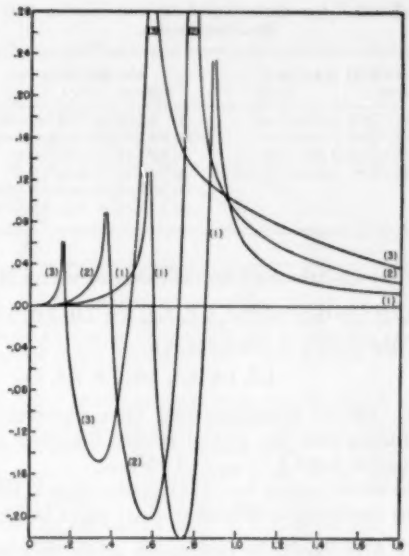

FIG. 3. $L(\phi,s)$ as a function of s when $\phi<\phi_{max}$ and $k=1.0M$. Curves (1), (2), and (3) corresponding respectively to $\phi=0.4M$, $\phi=0.6M$ and $\phi=0.8M$.

by simple quadratic functions of x for moderate values of s and by functions of the type

$$f_1(s)=\alpha/x+\beta/x^2+\gamma/x^3 \tag{29}$$

in the asymptotic region. This conclusion was thoroughly checked for all the values of $L(\phi,s)$ $(\phi>\phi_{max})$ which had been tabulated. This gave a basis for the choice of functions needed to represent $f_1(s)$.

As for $\phi<\phi_{max}$, there were some additional complications on account of the appearance of logarithmic singularities in $L(\phi,s)$ at the values of s corresponding to $v=\pm1$. To take these features into account, it was necessary to use functions which would have the correct singular behavior of $L(\phi,s)$ at the appropriate places. With some trial and error it was found that $L(\phi,s)$ and $(\phi<\phi_{max})$ could be represented in the neighborhoods of $v=1$ and $v=-1$ in the form:

$$L(\phi,s)=a+bx+cx^2+(Bx+Cx^2)\ln|1+\alpha x|, \tag{30}$$

α being so chosen that the function would diverge logarithmically at the value of x corresponding to $v=+1$ or $v=-1$ as the case might be. A term like $A\ln|1+\alpha x|$ was not considered in (30) in order to avoid integrals involving Spence functions. The function (30) was thoroughly checked to give the correct shape of $L(\phi,s)$ near the singularities and the addition of a term like $A\ln|1+\alpha x|$ was not found to improve the fit in any significant way.

TABLE I. Representations of the wave function $f_1(s)$ as a function of x.

$k=0.7M$ (1.135 Bev) Interval	$f_1(s)$	$k=1.0M$ (2.128 Bev) Interval	$f_1(s)$
(1) $0\leqslant x\leqslant 0.5$	$a_1+b_1x+c_1x^2$	(1) $0\leqslant x\leqslant 0.4$	$a_2+b_2x+c_2x^2$
(2) $0.5\leqslant x\leqslant 0.9$	$a+bx+cx^2$	(2) $0.4\leqslant x\leqslant 0.8$	$a_1+b_1x+c_1x^2$
(3) $0.9\leqslant x\leqslant 1.5$	$\alpha+\beta x+\gamma x^2$	(3) $0.8\leqslant x\leqslant 1.2$	$a+bx+cx^2$
(4) $1.5\leqslant x\leqslant \infty$	$\alpha_1/x+\beta_1/x^2+\gamma_1/x^3$.	(4) $1.2\leqslant x\leqslant 1.7$	$\alpha+\beta x+\gamma x^2$
		(5) $1.7\leqslant x\leqslant 2.5$	$\alpha_1/x+\beta_1/x^2+\gamma_1/x^3$
		(6) $2.5\leqslant x\leqslant \infty$	$\alpha_2/x+\beta_2/x^2+\gamma_2/x^3$.

$L(p,s)$ was tabulated for the following values of p:

$$k=0.7M: p=0.2,\ 0.5,\ 0.7,\ 0.9,\ 1.2,\ 1.5,\ 2.0,\ 3.0;$$
$$k=1.0M: p=0.2,\ 0.4,\ 0.6,\ 0.8,\ 1.0,\ 1.2,\ 1.4,\ 1.7,\ 2.0,\ 2.5,\ 3.5,\ 5.0. \tag{31}$$

The various functions were then represented in accordance with the general scheme described above for the two cases $p<p_{\max}$ and $p>p_{\max}$.

The wave function $f_1(s)$ was represented as in Table I. The continuity conditions on $f_1(s)$ are as follows:

(1) $f_1(s)$ should be continuous at the junction of two successive intervals;

(2) $f_1(s)$ should vanish at $s=0$ (since both $f_B(p)$ and $L(p,s)$ vanish at $p=0$).

These conditions reduce the number of independent parameters in Table I to 8 and 12 respectively and these are just the number of "data" represented by (31).

The integral equation (7) was converted into a set of linear equations in the parameters representing $f_1(s)$ by carrying out the integrations with the help of (29), (30) and Table I, in a straightforward way. These equations were then solved for two different values of λ, corresponding to $G^2/(4\pi)=15$ and 10π. The results for the phase shifts so obtained are summed up in Table II below, which also includes $\tan\delta_B$.

Table II shows that the percentage increase in the phase shift over the Born approximation is small even for $G^2/(4\pi)$ as large as 10π. The quantity $\tan\delta_B$ was calculated for intermediate energies $k=0.8M$ and $k=0.9M$ as well.

Figure 4, which exhibits $(\pi\lambda)^{-1}\tan\delta_B=L(k,k)$ (independent of λ) as a function of k, shows that the quantity is strictly monotonic in k. This behavior of $L(k,k)$, together with the fact that the percentage increase of the phase shift over the Born approximation is not large, suggests strongly that the exact phase shift also increases monotomically in the entire range from $k=0.7M$ to $k=1.0M$, rather than, for example, passing through a maximum at some intermediate energy. In view of this result it was not thought necessary to calculate the exact $\tan\delta$ for the intermediate energies, but its value was obtained by a simple interpolation formula assuming that $\tan\delta/\tan\delta_B$ is linear[9] in k. The curves for $(\pi\lambda)^{-1}\tan\delta$ which are drawn in Fig. 4 are thus based on the equation $\tan\delta=\tan\delta_B(a+bk)$.

TABLE II. Calculated phase shifts.

$k=0.7M$ (1.135 Bev)			$k=1.0M$ (2.128 Bev)		
$G^2/4\pi$	$\tan\delta$	$\tan\delta_B$	$\tan\delta$	$\tan\delta_B$	$(\tan\delta)_{\text{mod}}$
15	0.1961	0.1777	0.3762	0.3722	0.4075
10π	0.5032	0.3676	1.1164	0.7700	1.5380

The wave functions obtained from a solution of the simultaneous equations are shown in Figs. 5 and 6 for the two cases $k=0.7M$ and $k=1.0M$ respectively. The quantity actually plotted is $g(s)=-\lambda^{-1}(E_k\omega_k)^{-1}f_1(s)$. The corresponding quantity in the Born approximation (also shown) is $g_B(s)=L(s,k)$, independent of λ. This allows a direct comparison of the percentage change in the wave function for different values of λ.

Figure 5 shows that for the lower energy ($k=0.7M$) the effect of the integral equation is to increase the peak and to push the entire wave function somewhat towards higher momenta. This only means that the region of s above the energy shell plays a more important part than the Born approximation form indicates. Apart from this feature, $f_1(s)$ seems to be similar in shape to $f_B(s)$. The behavior is qualitatively the same for both the coupling constants; only the effect is more pronounced for the larger one.

The situation seems to be qualitatively different, however, for the case $k=1.0M$, as one sees from Fig. 6. Here the exact function $g(s)$ has sharp oscillations below the energy shell which are not present in $g_B(s)$. This seems to contrast sharply with the situation encountered for $k=0.7M$, where no such oscillations are perceptible. The behavior is again qualitatively similar for the two coupling constants.

It appears that the oscillations in $g(s)$ in Fig. 6 may be due to the peculiar shape of $L(p,s)$ for $p<p_{\max}$, as may be seen from Fig. 3. The importance of this region apparently increases with energy (see Figs. 5 and 6).

An explanation of these oscillations was attempted by looking for the second Born approximation which is given by:

$$f_B^{(2)}(p)=\lambda\int L(p,s)f_B(s)(ds/s). \tag{32}$$

It was expected that if the Born approximation were not too inaccurate, this quantity should approximately represent the difference between $f_1(s)$ and $f_B(s)$, and hence show large oscillations in the appropriate region. The quantitative evaluation of the integral (32) did indicate oscillations in this quantity below the energy shell, but they were found to be too small to account for the actual difference between $f_1(s)$ and $f_B(s)$. Apparently, Born approximation is too inadequate. The solution of the integral equation apparently amplifies the oscillations to a large extent (and also shifts the wave function generally to the right).

[9] This approximation is justified since the percentage increase over $\tan\delta_B$ is small, i.e., the phase shifts are far from resonance.

As regards the lower energy ($k=0.7M$), such oscillations should exist in principle, but since the region of $p<p_{\max}$ is much less important in this case, than for $k=1.0M$, they are probably too small to be detected.

5. THE COMPLEX INTEGRAL EQUATION

So far, we have considered the solution of the integral equation by neglecting the reactive effects arising from the possibility of meson production. To take these effects into account, we have to turn to the more general equation (16) which may be written as:

$$f_1(p)=f_B(p)+\lambda\int\{L(p,s)f_1(s)-L'(p,s)\phi_1(s)\}(dx/x), \quad (33)$$

$$\phi_1(p)=\lambda\int L'(p,s)f_1(s)(dx/x)+\lambda\int L(p,s)\phi_1(s)(dx/x). \quad (34)$$

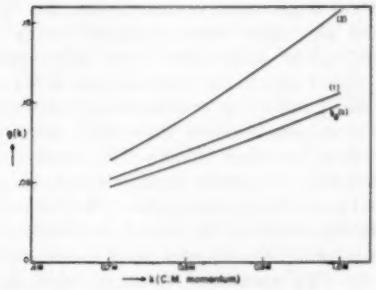

FIG. 4. The quantity $g(k)=(\pi\lambda)^{-1}\tan\delta$ as a function of k. The curves (1) and (2) correspond respectively to the values 15 and 10π for the coupling constant. $g_B(k)=L(k,k)$ is the corresponding quantity in the Born approximztion.

The coupling of these equations makes their general solution a very laborious task. If, however, we neglect the last term on the right-hand side of (33), the simplification will be considerable, since the equations will be decoupled. There are two main arguments in support of this approximation. Firstly, the quantity $L'(p,s)$ vanishes identically for $p>p_{\max}$, so that for such values of p, the Eq. (33) reduces exactly to (7). Now a considerable contribution to the solution of the integral equation comes from the region of high momenta. In fact, Figs. 5 and 6 indicate that the wave function is considerably enhanced for $p\gtrsim k$ and reduced for $p<k$, as compared with the Born approximation. Our approximation is, in fact, exact in the region from which we expect most of the contribution to the integral equation.

Secondly, it has been noted that even in the region of $p<p_{\max}$, $L'(p,s)$ can be nonzero only in a narrow strip of the $p-s$ plane, between the singularities of any of the curves of Fig. 3. Thus if $L(p,s)$ and $L'(p,s)$ are

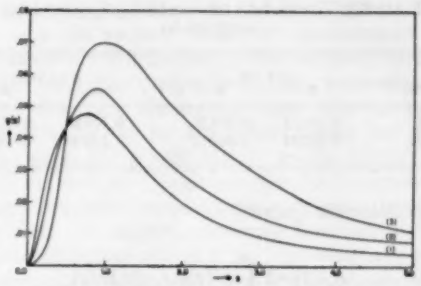

FIG. 5. The function $g(s)=-\lambda(E_k\omega_k)^{-1}f_1(s)$, for the case $k=0.7M$. Curve (1) corresponds to the Born approximation $g_B(s)=L(s,k)$. Curves (2) and (3) are for the two coupling constants of 15 and 10π respectively.

of the same orders of magnitude (in the region where L' exists) and if the same is true for $f_1(s)$ and $\phi_1(s)$, the contribution from the second term $\int L'\phi_1(dx/x)$ in the integral of (33) is expected to be small, compared with that from the first term $\int Lf_1(dx/x)$.[10]

Both the arguments tend to emphasize the importance of the term $\int Lf_1(dx/x)$ compared with $\int L'\phi_1\times(dx/x)$ in the entire two-dimensional domain of p and s. We may therefore feel confident that our approximation will not affect the solution seriously.

With the approximation, (33) is identical with (7) and its solution can be taken over from Sec. 4. Thus in Eq. (34), the first term on the right is a known quantity, and may serve as the "inhomogeneous" term of the integral equation for $\phi_1(s)$. Moreover, the "homogeneous" part of (34) is identical with that of (7), except that $\phi_1(s)$ replaces $f_1(s)$. Thus all the results of Sec. 4 can be used quantitatively if similar assumptions are made about $\phi_1(s)$ as for $f_1(s)$.[11] All that is needed is

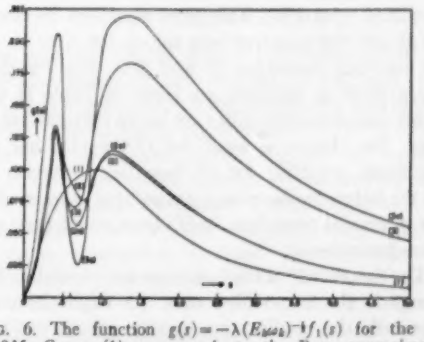

FIG. 6. The function $g(s)=-\lambda(E_k\omega_k)^{-1}f_1(s)$ for the case $k=1.0M$. Curve (1) corresponds to the Born approximation $g_B(s)=L(s,k)$. Curves (2) and (3) correspond respectively to the solutions for the two coupling constants 15 and 10π. Curves (2a) and (3a) represent modifications of (2) and (3) when the effects of meson production are taken into account.

[10] These considerations need modification near "resonance" where the relative magnitudes of $\int Lf_1(dx/x)$ and $\int L'\phi_1(dx/x)$ play a more important part than implied here. [For details, see M. Nelkin, Cornell thesis, 1955 (unpublished).]

[11] Mathematically, this simplification stems from the equality of the Green function for both the equations.

TABLE III. Values of $A+iB=-\pi(E_{\mathbf{k}}\omega_k)^{-\frac{1}{2}}[f_1(k)+i\phi_1(k)]=\tan(\delta+i\eta)$.

$G^2/4\pi$	$k=0.7M$ A	$k=0.7M$ B	$k=1.0M$ A	$k=1.0M$ B
15	0.19613	0.00425	0.39638	0.05566
10π	0.50324	0.06816	1.23990	0.60517

to evaluate the quantity:

$$\phi_B(p)=\lambda\int L'(p,s)f_1(s)(ds/s), \tag{35}$$

which plays the role of $f_B(p)$ in (7). This can be obtained by simple quadrature with $f_1(s)$ and $L'(p,s)$ (which is defined by (14) and (17)). From (26), we can deduce immediately that the parameter $y=(s^2-1-r^2)/(2r)$ is simply equal to $\cos\theta$, where θ is the angle between $\mathbf{p}$ and $\mathbf{s}$. Thus y should lie between -1 and $+1$ for real values of θ.

Solution of Eq. (34) in a straightforward manner gave results for the complex phase shift (defined by (18)), which are listed in Table III. A comparison of the relative magnitudes of A and B shows that the latter increases fairly rapidly with energy and coupling constant. These figures serve to give a general idea of the relative importance of the effects of meson production at these energies, as predicted by the T.D. method.

For a discussion of the validity of our "decoupling" approximation, it is enough to confine our attention to $k=1.0M$, since Table III shows already that the approximation is quite good for the lower energy.

An iterative procedure was employed to check the approximation. The last term of (33) was evaluated on the basis of the solution for $\phi_1(s)$ as obtained from the simplified equations. This term was then included in $f_B(p)$ and the equation was solved for $f_1(s)$ for both the coupling constants 15 and 10π. The "modified" phase shifts so obtained are listed in Table II which shows that these quantities are larger than the previous ones. The change is small for $G^2/4\pi=15$, but quite significant ($\sim 20\%$) for $G^2/4\pi=10\pi$. However, even for the latter, the increase is not so large as to invalidate the interation procedure itself; (one might need a few more interations).

The "modified" wave functions are plotted in Fig. 6 alongside the unmodified ones. As might have been expected, the modification mostly affects the region *below* the energy shell, at least for the lower coupling constant. The effect is of course much more pronounced for the larger coupling constant, where even the region above the energy shell is significantly affected. The general tendency is to increase the importance of the region above the energy shell, indicating a somewhat stronger interaction than the real integral equation alone implies.

6. DISCUSSION OF THE RESULTS

The significant feature of the results derived in the previous sections is the total absence of any resonance over a wide range of energies and coupling constants. If the maximum in the π^--p cross section near 1 Bev were indeed due to a one-meson resonance, the value $\delta\approx 90°$ should have occurred at an energy somewhat higher than 1 Bev,[12] and the range of energies considered here would have been sufficient to locate such a point. On the contrary, the results obtained in the previous sections strongly suggest that the phase shift for the $D_{\frac{3}{2},\frac{3}{2}}$ state increases monotonically over a wide range of energies and coupling constants, without ever reaching 90°.

As shown in the introduction, the state chosen for the purpose of the present investigation seemed the most plausible one theoretically as a one-meson resonant state. It is unlikely that any other *single* meson state of the π-p system will give any better results of the type desired. Thus we are forced to conclude that it is apparently not possible to explain the second maximum in terms of single meson resonant states like $P_{\frac{3}{2},\frac{3}{2}}$.

If the $D_{\frac{3}{2},\frac{3}{2}}$ state were considered as an *isolated* problem, $G^2/4\pi$ could have been taken arbitrarily large, subject only to the condition that $G^2/4\pi<G_0^2/4\pi$ [Eq. (25a)], and it is quite conceivable that a resonance would have been obtained for a fairly large value of $G^2/4\pi$ (but less than 176.8). The more important consideration, on the other hand, is how far the coupling constant so obtained is compatible with other conditions.

Increasing evidence has been accumulating in favor of the value $G^2/4\pi\approx 15$, ever since it was determined from the $P_{\frac{3}{2},\frac{3}{2}}$ resonance.[1] A considerable theoretical basis for the interpretation of experimental results in terms of the coupling constant has been provided by a theorem of Kroll and Ruderman[13] and the recent theory of Low.[14] These questions are discussed in detail in Bethe's forthcoming book. It now appears that even a value of 20 for the coupling constant is too high, and we are certainly not justified in considering any value greater than 10π.

For a direct comparison of the experimental results with the theory, we have evaluated the cross sections [using the formulas (20) and (21)] which are described in Table IV.

TABLE IV. Theoretical cross sections in mb.

	$k=0.7M$ (lab energy $=1.135$ Bev) $G^2/4\pi=15$	$k=0.7M$ (lab energy $=1.135$ Bev) $G^2/4\pi=10\pi$	$k=1.0M$ (lab energy $=2.128$ Bev) $G^2/4\pi=15$	$k=1.0M$ (lab energy $=2.128$ Bev) $G^2/4\pi=10\pi$
$\sigma_{01}(\pi^-p)$	0.834	4.196	1.400	5.166
$\sigma_{10}(\pi^-p)$	0.092	1.108	0.4866	1.635

[12] This is because of the factor λ^3 in the cross section.
[13] N. M. Kroll and M. Ruderman, Phys. Rev. **93**, 233 (1954).
[14] F. Low, Rochester Conference Proceedings, 1955 (unpublished).

TABLE V. Experimental cross sections.

Process ($\pi^-+p\to$)	Cross sections (mb) 1.0 Bev	1.5 Bev
1. Diffraction scattering	14	7
2. Elastic (large angle)	5	2
3. Inelastic processes	28–33	26

The experimental curves for the total cross sections[14,15] show a maximum of about 50 mb at 1 Bev in π^--p scattering. The π^+-p scattering at this energy is about 30 mb. From this one estimates the $T=\frac{3}{2}$ contribution to π^--p scattering to be 10 mb. This leaves about 40 mb to be explained by the state $T=\frac{1}{2}$. Unfortunately the values given in Table IV are much too small to account for this magnitude.

It may be worthwhile analyzing this large discrepancy in terms of elastic and inelastic contributions. According to Table IV, the reactive cross section is rather small compared with the elastic contribution, though the former increases with energy. However, even at $k=1.0M$, the ratio σ_{in}/σ_{el} is only $\sim\frac{1}{3}$. The various contributions to the cross sections estimated from the experiments of Walker,[16] Piccioni,[17] and others are given in Table V.

Comparison of these figures with those in Table IV shows that the discrepancy is very much larger for the inelastic processes than for elastic ones. The calculated ratio σ_{in}/σ_{el} is too small to account for the observed ratio of $\sim$1 at 1 Bev and $\sim$2 at 1.5 Bev.

It may be noted from Table V that most of the contribution to the elastic events comes from diffraction scattering (confined to small angles). The large angle scatterings are mostly inelastic. Now a large number of angular momentum states make comparable contributions to diffraction scattering, so that even large l-values are important for this process. On the other hand, we have assumed only one l value ($l=2$), so that this process has not been adequately treated in our theory.

It has been suggested by the Brookhaven group that a possible explanation may be based on a two-meson interaction. As the experiments indicate, the cross section for the production of a meson increases very rapidly with energy. If the total available energy is shared in comparable amounts by the various particles concerned, the conditions may be such that around 1 Bev, one or both the mesons are in a resonant $P_{1,1}$ state with the nucleon. Walker's[16] measurements of the momentum distributions of the scattered mesons at 1 Bev and 1.5 Bev, respectively, throw some valuable light on this point. His analysis shows only one peak (at $p\sim350$ Mev/c) for the 1-Bev mesons and two distinct peaks (at $p\sim300$ Mev/c, $p\sim600$ Mev/c) for the 1.5-Bev mesons. This gives support to the argument that at 1 Bev, both the mesons are at the same resonant state with the nucleon. Assuming therefore a $P_{1,1}$ resonance, it follows that at 1 Bev, one essentially gets the *square* of the enhancement factor which comes from the $P_{1,1}$ state, and this is probably enough to explain the large magnitude of the cross section at 1 Bev.

One difficulty about this explanation is that there is no simple reason why this enhancement will affect only the $T=\frac{1}{2}$ state and not $T=\frac{3}{2}$. According to Ross,[18] the $P_{1,1}$ state might still account for the peak at 1 Bev, but only if the subsequent scatterings of *both* the mesons by the nucleon are important.

An explanation which avoids the enhancement in the $T=\frac{3}{2}$ state has been recently proposed by Dyson.[19] According to him, a "particle" with a strong interaction with the nucleon is probably formed when the π-meson strikes the target. This particle which is assumed to have a mass of about $1000m_e$ and an isotopic spin $T=0$ decays into two π mesons with an unobservably short lifetime. This picture can explain why the $T=\frac{1}{2}$ scattering can be very large in several angular momentum states simultaneously, without affecting the $T=\frac{3}{2}$ state. It may be noted in this connection that a calculation performed some time ago[20] indicated an attractive interaction between two mesons in a state $T=0$. It is therefore suggested that a more detailed study of this interaction may prove useful in this connection.

ACKNOWLEDGMENTS

The author is deeply indebted to Professor H. A. Bethe who suggested this problem to him and who gave constant guidance and encouragement throughout the work. The author is also indebted to Dr. M. Ross for valuable discussions, to Dr. Piccioni for sending some of the experimental data on π^--p scattering, and to Mr. R. Lesser of the Cornell Computing Center for his assistance in carrying out the computations. Finally, a scholarship awarded by the Ministry of Education, Government of India is gratefully acknowledged.

[15] O. Piccioni (private communication).
[16] W. Walker, Proceedings of the Fifth Annual Rochester Conference on High Energy Physics, 1955 (to be published).
[17] O. Piccioni, Proceedings of the Fifth Annual Rochester Conference on High Energy Physics, 1955 (to be published).
[18] M. Ross (private communication).
[19] F. J. Dyson (private communication); I am grateful to Professor Dyson for permission to mention his idea in this paper.
[20] A. N. Mitra and F. J. Dyson, Phys. Rev. **90**, 372(A) (1953).

Electromagnetic Properties of the Deuteron. I. Charge Density and Quadrupole Moment*

JEREMY BERNSTEIN AND ABRAHAM KLEIN†‡
Harvard University, Cambridge, Massachusetts

(Received April 27, 1955)

The Tamm-Dancoff method is applied to the calculation of the electrostatic properties of the deuteron. The state vector is assumed to contain amplitudes for at most two mesons in the field, but the possible presence of nucleon-antinucleon pairs is ignored. A formula applicable to the calculation of any multipole moment is derived and used to compute the leading exchange corrections, of order g^3 and g^4, respectively, to the usual expression for the quadrupole moment. For a suitably chosen hard-core wave function the ratio of successive terms is about one tenth, and the g^3 term is itself only a few percent of the total effect.

I. INTRODUCTION

IN this paper we shall present a Tamm-Dancoff calculation of the mesonic contributions to the charge density and quadrupole moment of the deuteron in which we shall explicitly include the presence of as many as two mesons in the field. We have chosen to do a Tamm-Dancoff calculation, despite the well-known difficulties in properly taking into account nucleon "self" effects, for two reasons. Firstly, the method can be used to give a reasonable account of the low-energy properties of the two-nucleon system.[1] The finite explicitly two-body contributions arising from the equal times reduction of the covariant equation are also given by our formalism.[2-4] The effects of self-interactions, the treatment of which requires a covariant formalism, are logically separable from the exchange terms treated in this work and will be discussed in a future paper.

Our decision to calculate charge density effects rather than magnetic moments rests on the oft-noted fact that the expressions for charge density phenomena, like the quadrupole moment, are less sensitive than the magnetic effects in a given order to the behavior of the wave function in the region of interaction. The validity of our approach rests upon the rapid convergence of the effects calculated; it is, therefore, a satisfactory result of our work that the one-meson exchange effects amount to a few percent while the two-meson effects are about a tenth as much.

The heart of the calculation consists in determining the effective one-meson and two-meson charge density operators associated with the nucleon current.[5] In Sec. II, we develop the formal apparatus for doing this and discuss the relationship between the charge density operator and the protons probability density. In Sec. III, we present the quadrupole moment formulas and the numerical evaluation of these with appropriately chosen wave functions. In Sec. IV, we discuss the more general aspects of our results; in the appendices, recoil effects are discussed and the Tamm-Dancoff approach as used in this paper is related to the method of canonical transformations and to the covariant two-body equation.

II. FORMALISM

In principle, all of the information about the static electromagnetic effects in the two-nucleon system can be obtained from the Schrödinger equation:

$$(H^0+H'+H^{e1})\Phi=W\Phi, \tag{1}$$

where

$$H^{e1}=-e\int d\mathbf{x}\bar{\psi}(\mathbf{x})\tfrac{1}{2}(1+\tau_3)\gamma_\mu A_\mu{}^e(\mathbf{x})\psi(\mathbf{x}), \tag{2a}$$

and

$$H'=-g\int d\mathbf{x}\bar{\psi}(\mathbf{x})\gamma_5\tau_i\psi(\mathbf{x})\phi_i(\mathbf{x}). \tag{2b}$$

Here $\bar{\psi}$ and ψ are the usual nucleon field operators, and $A_\mu{}^e$ is an external electromagnetic field.

Our program is to obtain explicit expressions for the electromagnetic and nuclear energies defined by Eq. (1) after Φ has been expanded in a basis of free-particle

* A preliminary account of this work was presented at the Washington meeting of the American Physical Society, April, 1954 [Phys. Rev. **95**, 655(A) (1954)].

† Harvard Society of Fellows.

‡ Now at the Department of Physics, University of Pennsylvania, Philadelphia, Pennsylvania.

[1] K. Brueckner and K. M. Watson, Phys. Rev. **92**, 1023 (1953).

[2] For a treatment of electromagnetic effects with the covariant equation, including recoil effects but not radiative corrections, see S. Deser, Phys. Rev. **92**, 1542 (1953). The very large (of the order of 50%) mesonic correction which Deser finds in order eg^2 is due partly to his taking the asymptotic form of the deuteron wave function seriously down to the origin and partly to an incorrect coordinate-space reduction of his energy operator. Our treatment also differs from his in the treatment of recoil effects. See Appendix B for a discussion of this point.

[3] Another interesting and quite different calculation has been given by F. Villars, Phys. Rev. **86**, 476 (1952) who uses covariant perturbation theory (canonical transformations) to estimate the mesonic effects on the deuteron moments. He finds that the quadrupole effect is of the order of a few percent and in his approach is given entirely by terms which have a vanishing adiabatic limit. One evident drawback with using canonical transformations, as pointed out by Villars himself, is that the potential to which it leads will not bind the deuteron [M. M. Lévy, Phys. Rev. **84**, 441 (1951)] and hence it is not quite consistent to evaluate the expressions with a phenomenological wave function based on two nucleon binding. The essentials of this approach are described in Appendix C.

[4] A. Sessler, Phys. Rev. **96**, 793 (1954) has given a calculation of charge density effects to order eg^2 which is quite similar to our work. We are pleased to acknowledge an informative correspondence with Dr. Sessler. See also I. Sato and K. Itabashi, Progr. Theoret. Phys. (Japan) **12**, 100 (1954).

[5] The meson current effects depend on the nucleon coordinates via the antisymmetric operator $(\tau_1\times\tau_2)$ and hence, as has often been remarked, yield vanishing expectation values for any two-nucleon state.

states. Then, in the spirit of ordinary perturbation theory, we shall evaluate the exchange contributions to the electrostatic energy with the solution of Eq. (1) taken in the absence of the external field, A_μ^e.

In the expansion of the state vector, using a free-particle basis, we shall restrict ourselves to the form

$$\Phi = a_0\Phi_0 + a_1\Phi_1 + a_2\Phi_2, \tag{3}$$

where the Φ_i are the solutions of the free-particle Schrödinger equation involving two nucleons and i mesons, and the a_i are the amplitudes for the ith meson state. We have omitted all nucleon-pair amplitudes.[6] The relations among the a_i can be determined by a variational principle. Thus, if

$$W = (\Phi,\ (H_0+H^I)\Phi)/(\Phi,\Phi), \tag{4}$$

where H^I is the total interaction Hamiltonian, then putting Eq. (3) into Eq. (4) we see at once that

$$\begin{aligned} W(a_0,a_1,a_2) = [&|a_0|^2\epsilon_0 + |a_1|^2\epsilon_1 + |a_2|^2\epsilon_2 \\ &+ |a_0|^2 H_{00}{}^I + |a_1|^2 H_{11}{}^I + |a_2|^2 H_{22}{}^I \\ &+ a_0^* a_1 H_{01}{}^I + a_1^* a_0 H_{10}{}^I \\ &+ a_1^* a_2 H_{12}{}^I + a_2^* a_1 H_{21}{}^I] \\ &\times [|a_0|^2 + |a_1|^2 + |a_2|^2]^{-1}, \end{aligned} \tag{5}$$

integrations over momentum variables being understood and where the ϵ_i are free-particle kinetic energies. The correct choice of the a_i is given by the condition

$$\partial W/\partial a_i = 0, \tag{6}$$

and hence

$$\begin{aligned} (W-\epsilon_0 - H_{00}{}^I)a_0 &= H_{01}{}^I a_1, \\ (W-\epsilon_1 - H_{11}{}^I)a_1 &= H_{10}{}^I a_0 + H_{12}{}^I a_2, \\ (W-\epsilon_2 - H_{22}{}^I)a_2 &= H_{21}{}^I a_1. \end{aligned} \tag{7}$$

By carrying out a formal elimination of the other a_i in terms of a_0 we obtain the following integral equation,

$$\begin{aligned} &(W-\epsilon_0 - H_{00}{}^{e1})a_0 \\ &= [H_{01}{}'(W-H^0-H^{e1})^{-1}H_{10}{}' \\ &\quad + H_{01}{}'(W-H^0-H^{e1})^{-1}H_{12}{}'(W-H^0-H^{e1})^{-1} \\ &\qquad \times H_{21}{}'(W-H^0-H^{e1})^{-1}H_{10}{}']a_0. \end{aligned} \tag{8}$$

Since the physical consequences of the theory cannot depend upon how Φ is normalized, we set $\|a_0\| = 1$. Hence upon expanding the electromagnetic effects to first order and taking the scalar product of Eq. (8) with a_0, we find

$$W = \langle H^0\rangle + \langle V'(W)\rangle + \langle V^{e1}(W)\rangle, \tag{9}$$

[6] The justification of the neglect is twofold: quite generally, the work of many authors [for example, see A. Klein, Phys. Rev. **95**, 1061 (1954) where references to previous literature are given] indicates that pair effects associated completely with the nuclear interaction are in fact suppressed. On the other hand, those effects in which the pair is either created or annihilated by the external field and thus not necessarily suppressed [see, N. M. Kroll and M. Ruderman, Phys. Rev. **93**, 233 (1954)] give smaller contributions to the electrostatic effects than the leading terms by the ratio of meson to nucleon mass.

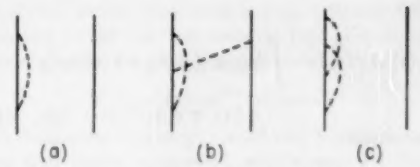

FIG. 1. Diagrams for parts of $\langle V'\rangle$ which involve self-interactions. Solid lines represent nucleons, dashed lines are mesons, and the sense of time can be taken as running up the page.

where, with $G_0 = (W-H^0)^{-1}$, we have

$$\begin{aligned} \langle V'(W)\rangle = &\langle H_{01}{}'G_0H_{10}{}'\rangle \\ &+ \langle H_{01}{}'G_0H_{12}{}'G_0H_{21}{}'G_0H_{10}{}'\rangle, \end{aligned} \tag{10a}$$

and

$$\begin{aligned} \langle V^{e1}(W)\rangle = &\langle H_{00}{}^{e1}\rangle + \langle H_{01}{}'G_0H_{11}{}^{e1}G_0H_{10}{}'\rangle \\ &+ \langle H_{01}{}'G_0H_{12}{}'G_0H_{22}{}^{e1}G_0H_{21}{}'G_0H_{10}{}'\rangle \\ &+ \langle H_{01}{}'G_0H_{11}{}^{e1}G_0H_{12}{}'G_0H_{21}{}'G_0H_{10}{}'\rangle \\ &+ \langle H_{01}{}'G_0H_{12}{}'G_0H_{21}{}'G_0H_{11}{}^{e1}G_0H_{10}{}'\rangle. \end{aligned} \tag{10b}$$

Of course, Eqs. (10a) and (10b) contain many divergent contributions. Typical samples of these are indicated in Fig. 1 and in Fig. 2. Since estimates of such effects with the present model are necessarily cruder than that of the finite contributions, we shall not attempt to give them here. However, since these terms are easily recognized, we can split them off and lump them together as $S(W)$ leaving a finite residue which we call $\langle V'(W)\rangle_c$ and $\langle V^{e1}(W)\rangle_c$. Hence Eq. (9) becomes

$$\begin{aligned} W = &\langle H^0\rangle + \langle V'(W)\rangle_c + \langle V^{e1}(W)\rangle_c \\ &+ \langle S'(W)\rangle + \langle S^{e1}(W)\rangle. \end{aligned} \tag{11}$$

We now turn to the essential business of extracting the two-body electrostatic moments from Eq. (11) and learning what effect the $\langle S(W)\rangle$ have upon these. To this end, we recall that the electrostatic energy of the two-body system in the presence of an external potential $A_0^e(\mathbf{r})$ can always be written in the form,

$$\int \langle \rho_{op}(\mathbf{r})\rangle A_0^e(\mathbf{r})d\mathbf{r}, \tag{12}$$

where $\rho_{op}(\mathbf{r})$ is the effective charge density operator which will include the effects which arise from meson exchange. We may expand $A_0^e(\mathbf{r})$, about the center of mass of the system, taken at $\mathbf{r}=0$, and thus obtain the

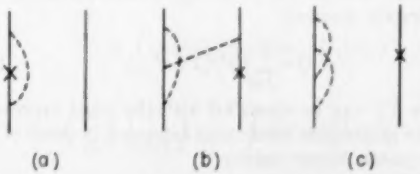

FIG. 2. Diagrams for parts of $\langle V^{e1}\rangle$ which involve self-interactions. The notation is the same as in Fig. 1 with the addition of a cross to indicate an interaction with the external field.

equation

$$\int\langle\rho_{op}(\mathbf{r})\rangle A_0{}^e(\mathbf{r})d\mathbf{r}=\int\langle\rho_{op}(\mathbf{r})\rangle[A_0{}^e|_0+\mathbf{r}\cdot\boldsymbol{\nabla}A_0{}^e|_0+\tfrac{1}{2}\mathbf{r}\mathbf{r}:\boldsymbol{\nabla}\boldsymbol{\nabla}A_0{}^e|_0+\cdots]d\mathbf{r}, \quad (13)$$

or symbolically,

$$\langle V^{e1}(W)\rangle=\sum_i\langle V_i{}^{e1}(W)\rangle\lambda_i, \quad (14)$$

where

$$\lambda_i=(i!)^{-1}(\partial_x+\partial_y+\partial_z)^i A_0{}^e(\mathbf{r})|_0. \quad (15)$$

One can then define the 2^ith static moment tensor by means of the terms contained in $\partial W/\partial\lambda_i|_{\lambda=0}$. However, using Eq. (11), one obtains

$$\partial W/\partial\lambda_i|_0=[\langle\partial V'(W)/\partial W\rangle_c\partial W/\partial\lambda_i]_{\lambda=0}+[\langle\partial S'(W)/\partial W\rangle\partial W/\partial\lambda_i]_{\lambda=0}+[\langle V_i{}^{e1}(W)\rangle_c]_{\lambda=0}+[\langle S_i{}^{e1}(W)\rangle]_{\lambda=0} \quad (16)$$

or, again understanding the limit $\lambda_i=0$,

$$\partial W/\partial\lambda_i=[\langle V_i{}^{e1}(W)\rangle_c+\langle S_i{}^{e1}(W)\rangle]\times[1-\langle\partial S'/\partial W\rangle-\langle\partial V'/\partial W\rangle_c]^{-1}. \quad (17)$$

On the other hand, the electrostatic energy must also be given by

$$(\Phi,H^{e1}\Phi)/(\Phi,\Phi), \quad (18)$$

and if we expand Φ and H^{e1} and remember that $\|a_0\|=1$, we learn that

$$\partial W/\partial\lambda_i=[\langle V_i{}^{e1}\rangle_c+\langle S_i{}^{e1}\rangle]\times\left[1+\sum_{i=1}^{\infty}\int|a(\mathbf{p}_1,\mathbf{p}_2,\mathbf{k}_1,\cdots\mathbf{k}_i)|^2\times d\mathbf{p}_1d\mathbf{p}_2d\mathbf{k}_1\cdots d\mathbf{k}_i\right]^{-1}. \quad (19)$$

Since the $\int|a(\mathbf{p}_1,\mathbf{p}_2,\mathbf{k}_1,\cdots\mathbf{k}_i)|^2$ are the relative probabilities for finding i mesons in the field, we are thus led to the theorem[7]:

$$\sum_{i=1}^{\infty}\int|a(\mathbf{p}_1,\mathbf{p}_2,\mathbf{k}_1,\cdots\mathbf{k}_i)|^2d\mathbf{p}_1d\mathbf{p}_2d\mathbf{k}_1,\cdots d\mathbf{k}_i=-\langle\partial S'/\partial W\rangle-\langle\partial V'/\partial W\rangle_c\equiv P. \quad (20)$$

However, as can be seen from Eq. (12b), $\langle V_i{}^{e1}\rangle_c$ is itself, in the general case, an infinite series in g^2. Thus if we choose $\lambda_i=(2!)^{-1}(\partial_x+\partial_y+\partial_z)^2A_0{}^e$ we are led in the standard way to the following infinite series for the quadrupole moment,

$$Q=\sum_{J=0}^{\infty}\langle Q^J\rangle[1+P]^{-1}, \quad (21)$$

where $\langle Q^0\rangle$ can be identified with the usual expression for the quadrupole moment as expressed in terms of the bare proton charge density.

[7] See also remarks by A. Klein, Proceedings of the Fourth Annual Rochester Conference (University of Rochester Press, Rochester, 1954), p. 44.

Until now we have been dealing with P and $\langle S^{e1}(W)\rangle$ as if they were perfectly finite. However, under the assumption that in a properly renormalized theory P would be small compared to unity, we would expand $[1+P]^{-1}$ and hence note the additivity of *all* self-effects to those arising from exchange interaction. Leaving it at that, we shall henceforth devote ourselves solely to interaction effects.

In ordinary quantum mechanics one defines the charge density in terms of the probability density of the proton coordinate and the quadrupole moment in terms of this charge density. In our calculation, however, the probability density of the proton in momentum space can be taken as

$$\rho(\mathbf{p}_1)=\sum_{i=0}^{\infty}\int|a(\mathbf{p}_1,\mathbf{p}_2,\mathbf{k}_1,\cdots\mathbf{k}_i)|^2d\mathbf{p}_2d\mathbf{k}_1,\cdots d\mathbf{k}_i, \quad (22)$$

from which it follows that the sum in Eq. (21) has the form

$$\sum_{J=0}^{\infty}\langle Q^J\rangle=\int\rho(\mathbf{r})r^2\times(3\cos^2\theta-1)d\mathbf{r}, \quad (23)$$

where $\rho(\mathbf{r})$ is the Fourier transform of Eq. (22). For the remainder of this section we illustrate how $\rho(\mathbf{r})$ may be computed directly from the nuclear interaction, in a manner analogous to the use of Eq. (20).

To this end, we shall consider in parallel the expressions in momentum space arising from Figs. 3(a) and 3(b). Inserting the details of the coupling we may write as the contribution to the energy from Fig. 3(a)

$$\frac{g^2}{(2\pi)^3}\int\frac{d\mathbf{p}_1d\mathbf{p}_2d\mathbf{k}}{2\omega(\mathbf{k})}a^*(\mathbf{p}_1-\mathbf{k},\mathbf{p}_2+\mathbf{k})\times\langle\gamma_0\gamma_5\rangle_1\boldsymbol{\tau}_1\cdot\boldsymbol{\tau}_2\langle\gamma_0\gamma_5\rangle_2\times[W-\epsilon(\mathbf{p}_1-\mathbf{k})-\epsilon(\mathbf{p}_2)-\omega(\mathbf{k})]^{-1}a(\mathbf{p}_1,\mathbf{p}_2), \quad (24a)$$

where $\langle\ \rangle$ means that we are to take the matrix element of the enclosed Dirac operator between free spinors. From Fig. 3(b) we have

$$\frac{eg^2}{(2\pi)^3}\int\frac{d\mathbf{p}_1d\mathbf{p}_2d\mathbf{k}d\mathbf{q}}{2\omega(\mathbf{k})}a^*(\mathbf{p}_1-\mathbf{k}+\mathbf{q},\mathbf{p}_2+\mathbf{k})\times\langle A_0{}^e(\mathbf{q})\Lambda_+(\mathbf{p}_1-\mathbf{k})\gamma_0\gamma_5\rangle_1\times\boldsymbol{\tau}_1\cdot\boldsymbol{\tau}_2\langle\gamma_0\gamma_5\rangle_2\{[W-\epsilon(\mathbf{p}_1-\mathbf{k}+\mathbf{q})-\epsilon(\mathbf{p}_2)-\omega(\mathbf{k})]\times[W-\epsilon(\mathbf{p}_1-\mathbf{k})-\epsilon(\mathbf{p}_2)-\omega(\mathbf{k})]\}^{-1}a(\mathbf{p}_1,\mathbf{p}_2). \quad (24b)$$

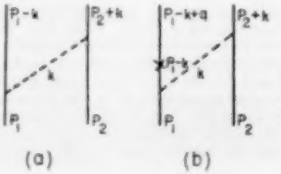

FIG. 3. Contributions to $\langle V^e\rangle_c$ and to $\langle V^{e1}\rangle_c$ in the order of g^2 and eg^2 respectively.

If in Eq. (23b) we perform the same expansion as in Eq. (15), then the contribution to the quadrupole energy is obtained by replacing $-A_0{}^e(\mathbf{q})$ by

$$\tfrac{1}{2}\sum_{i,j}(\partial^2/\partial q_i\partial q_j)\delta(\mathbf{q})\partial_i\partial_j A_0{}^e|_0. \tag{25}$$

It is also useful at this stage to introduce center of momentum and relative coordinates in the amplitudes in Eq. (23) which is done under the approximation that the deuteron is unperturbed, i.e., we write typically

$$a(\mathbf{p}_1,\mathbf{p}_2)=\delta(\mathbf{P})a(\mathbf{p})(2\pi)^{\frac{1}{2}}V^{-\frac{1}{2}}, \tag{26}$$

where

$$\mathbf{P}=\mathbf{p}_1+\mathbf{p}_2,\quad \mathbf{P}=\tfrac{1}{2}(\mathbf{p}_1-\mathbf{p}_2), \tag{27}$$

and V is the system volume. An integration by parts, then, transfers the δ function differentiations on to the other functions of q in Eq. (23b). We shall show in Appendix A that the only term arising from this process which has a nonvanishing adiabatic limit has the form

$$-\frac{eg^2}{(2\pi)^3}\int[\tfrac{1}{4}(\partial^2/\partial p_i\partial p_j)a^*(\mathbf{p}-\mathbf{k})]\times\langle\gamma_0\gamma_5\rangle_1\boldsymbol{\tau}_1\cdot\boldsymbol{\tau}_2\langle\gamma_0\gamma_5\rangle_2[2\omega(\mathbf{k})]^{-1}\times[W-\epsilon(\mathbf{p}-\mathbf{k})-\epsilon(\mathbf{p})-\omega(\mathbf{k})]^{-2}\times a(\mathbf{p})\partial_i\partial_j A_0{}^e|_0 d\mathbf{p}d\mathbf{k}. \tag{28}$$

One need only compare Eq. (28) with Eq. (24a) to understand that in the limit contemplated, $\rho(\mathbf{r})$ is given by $-\partial V'(\mathbf{r})/\partial W$, where the last quantity is the adiabatic limit of the energy derivative of the interaction. Hence, it is sufficient to give the formulas for $\partial V'/\partial W$, from which both the normalization P and the moment terms can be computed.

III. RESULTS

We write the expressions for $\partial V'/\partial W$ at the stage after the spin-matrix elements have been reduced to large components and the adiabatic limit taken. We are then led to a local operator in coordinate space which has the form

$$-\partial V_1'(\mathbf{r})/\partial W=\left(\frac{g}{2M}\right)^2\frac{1}{(2\pi)^3}\int d\mathbf{k}e^{i\mathbf{k}\cdot\mathbf{r}}\frac{\boldsymbol{\sigma}_1\cdot\mathbf{k}\boldsymbol{\sigma}_2\cdot\mathbf{k}}{\omega^2}\boldsymbol{\tau}_1\cdot\boldsymbol{\tau}_2, \tag{29}$$

$$\begin{aligned}-\partial V_2'(\mathbf{r})/\partial W&=\left(\frac{g}{2M}\right)^4\frac{1}{(2\pi)^6}\int\frac{d\mathbf{k}_1d\mathbf{k}_2}{4\omega_1\omega_2}e^{i(\mathbf{k}_1+\mathbf{k}_2)\cdot\mathbf{r}}\\&\times\{[6(\mathbf{k}_1\cdot\mathbf{k}_2)^2+4(\boldsymbol{\tau}_1\cdot\boldsymbol{\tau}_2)(\boldsymbol{\sigma}_1\cdot\mathbf{k}_1\times\mathbf{k}_2)(\boldsymbol{\sigma}_2\cdot\mathbf{k}_1\times\mathbf{k}_2)]\\&\times[4(\omega_1^2\omega_2)^{-1}+(\omega_1\omega_2)^{-2}]\\&+[2(\boldsymbol{\tau}_1\cdot\boldsymbol{\tau}_2)(\mathbf{k}_1\cdot\mathbf{k}_2)^2+3(\boldsymbol{\sigma}_1\cdot\mathbf{k}_1\times\mathbf{k}_2)(\boldsymbol{\sigma}_2\cdot\mathbf{k}_1\times\mathbf{k}_2)]\\&\times[8(\omega_1^2\omega_2)^{-1}-2(\omega_1\omega_2)^{-2}\\&\quad-4(\omega_1\omega_2)^{-1}(\omega_1+\omega_2)^{-2}]\}.\end{aligned} \tag{30}$$

All of the Fourier transforms in Eqs. (29) and (30) are standard except the last term of Eq. (27) which we evaluate under the assumption that

$$4[\omega_1\omega_2(\omega_1+\omega_2)^2]^{-1}\cong(\omega_1\omega_2)^{-2} \tag{31}$$

over the momentum range considered. Setting $x=\mu r$, we then find (with $\boldsymbol{\tau}_1\cdot\boldsymbol{\tau}_2=-3$ and $\boldsymbol{\sigma}_1\cdot\boldsymbol{\sigma}_2=+1$ for the deuteron),

$$\begin{aligned}-\partial V_1'(r)/\partial W&=(g^2/4\pi)(\mu/2M)^2(2/\pi)\\&\times\{[K_0(x)-K_1(x)/x]\\&+S_{12}[K_0(x)+2K_1(x)/x]\},\end{aligned} \tag{32}$$

$$\begin{aligned}-\partial V_2'(r)/\partial W&=(g^2/4\pi)^2(\mu/2M)^4\\&\times\{(2/\pi)^2[(43/2)(K_1(x)/x)^2\\&+19K_0(x)(K_1(x)/x)+6(K_0(x))^2]\\&-(e^{-2x}/x^4)[3x^3+2x^2+8x+4]\}\\&-S_{12}(2/\pi)^2[7(K_1(x)/x)^2+(7/2)K_0(x)(K_1(x)/x)]\\&\quad-S_{13}(e^{-2x}/x^4)[2x^2+5x+4]\}.\end{aligned} \tag{33}$$

In terms of the standard expression for the deuteron ground state, which we identify with a_0,

$$\psi(\mathbf{r})=(4\pi)^{-\frac{1}{2}}r^{-1}[u(r)+2^{-\frac{1}{2}}w(r)S_{12}]\chi_{1,1}, \tag{34}$$

we obtain by means of Eqs. (32) and (33) the following contributions to the quadrupole moment, separated according to order in g^2 and orbital angular momentum state:

$$Q_{1S}=\frac{g^2}{4\pi}\frac{2}{\pi}\left(\frac{1}{2M}\right)^2\frac{1}{5}\times\int dru^2(r)x^2[K_0(x)+2K_1(x)/x], \tag{35}$$

$$Q_{1S-D}=-\frac{g^2}{4\pi}\frac{2}{\pi}\left(\frac{1}{2M}\right)^2\frac{1}{5\sqrt{2}}\times\int druwx^2[K_0(x)+5K_1(x)/x], \tag{36}$$

$$Q_{1D}=\frac{g^2}{4\pi}\frac{2}{\pi}\left(\frac{1}{2M}\right)^2\frac{1}{20}\times\int dru^2x^2[5K_0(x)+13K_1(x)/x], \tag{37}$$

$$\begin{aligned}Q_{2S}=-\left(\frac{g^2}{4\pi}\right)^2\left(\frac{\mu}{2M}\right)^4\frac{1}{\mu^2}\frac{1}{5}\int dru^2(r)x^2\{(2/\pi)^2\\\times[7(K_1(x)/x)^2+(7/2)K_0(x)K_1(x)/x]\\+(e^{-2x}/x^4)[2x^2+5x+4]\},\end{aligned} \tag{38}$$

$$Q_{2S-D}=\left(\frac{g^2}{4\pi}\right)^2\left(\frac{\mu}{2M}\right)^4\frac{1}{\mu^2}\frac{1}{5\sqrt{2}}\int dr u w x^2\Big\{\left(\frac{2}{\pi}\right)^2 \times[(71/2)(K_1(x)/x)^2+12K_0(x)(K_1(x)/x) +6(K_0(x))^2]+(e^{-2x}/x^4) \times[-3x^3+2x^2+2x+4]\Big\}, \quad (39)$$

$$Q_{2D}=-\left(\frac{g^2}{4\pi}\right)^2\left(\frac{\mu}{2M}\right)^4\frac{1}{\mu^2}\frac{1}{20}\int dr w^2 x^2\Big\{\left(\frac{2}{\pi}\right)^2 \times[(127/2)(K_1(x)/x)^2-2K_0(x)(K_1(x)/x) +6(K_0(x))^2]+(e^{-2x}/x^4) \times[-3x^3+10x^2+22x+20]\Big\}. \quad (40)$$

We must also record the normalization terms arising from $-\langle\partial V'/\partial W\rangle_{c_1}$

$$N_{1S}=\left(\frac{g^2}{4\pi}\right)\left(\frac{2}{\pi}\right)\left(\frac{\mu}{2M}\right)^2\int dr w^2(K_0-K_1/x), \quad (41)$$

$$N_{1S-D}=\left(\frac{g^2}{4\pi}\right)\left(\frac{2}{\pi}\right)\left(\frac{\mu}{2M}\right)^2 4\sqrt{2} \times\int dr w(K_0+2K_1/x), \quad (42)$$

$$N_{1D}=-\frac{g^2}{4\pi}\left(\frac{2}{\pi}\right)\left(\frac{\mu}{2M}\right)^2\int dr w^2(K_0+5K_1/x), \quad (43)$$

and in fourth order

$$N_{2S}=\left(\frac{g^2}{4\pi}\right)^2\left(\frac{\mu}{2M}\right)^4\int dr w^2\Big\{\left(\frac{2}{\pi}\right)^2 \times[(43/2)(K_1/x)^2+19K_0(K_1/x)+6K_0^2] +(e^{-2x}/x^4)[3x^3+2x^2+8x+4]\Big\}, \quad (44)$$

$$N_{2S-D}=-\left(\frac{g^2}{4\pi}\right)^2\left(\frac{\mu}{2M}\right)^4 4\sqrt{2}\int dr w w\Big\{\left(\frac{2}{\pi}\right)^2 \times[7(K_1/x)^2-(7/2)K_0K_1/x] +(e^{-2x}/x^4)[2x^2+5x+4]\Big\}, \quad (45)$$

$$N_{2D}=\left(\frac{g^2}{4\pi}\right)^2\left(\frac{\mu}{2M}\right)^4\int dr w^2\Big\{\left(\frac{2}{\pi}\right)^2 \times[(71/2)(K_1/x)^2+12K_0(K_1/x)+6K_0^2] +(e^{-2x}/x^4)[-3x^3+2x^2+2x+4]\Big\}. \quad (46)$$

It will be noticed that the operators in Eqs. (44), (45), and (46) are too singular to permit the integrations to be performed down to the origin. Hence, in performing the numerical evaluation of our theory we made use of a phenomenological wave function based on a hard core, which gives a good fit to the bound-state data.[8] The results are given in Table I. We have chosen $(g^2/4\pi)=10$, even though the experimental evidence indicates a slightly larger constant, in order to facilitate comparison with previous work.[2,4] The g^2 terms, which are perfectly convergent at the origin, have, for comparison's sake, been calculated using a Hulthén wave function. One should keep in mind when considering our meson correction terms that the measured Deuteron moment is 2.73×10^{-27} cm^2.

If, from Eq. (21) we take as the total mesonic correction to the quadrupole moment,

$$\Delta Q_{\text{tot}}=\langle Q^1\rangle+\langle Q^2\rangle-Q(P_1+P_2), \quad (47)$$

then from Table I, $\Delta Q_{\text{tot}}=-0.539\times10^{-28}$ cm^2, which is the order of two percent of the measured moment.

IV. FINAL REMARKS

As in all treatments of the two-nucleon problem which make use of the adiabatic approximation, the validity of the results depends upon the justification of the use of the hard-core wave function. With this proviso, however, it appears that the Tamm-Dancoff method provides a means of computing mesonic contributions to charge density effects which is rapidly convergent. In fact, the rate of convergence for these effects, as shown in Table I, is considerably more favorable than that for the nuclear potential itself, since the second moment of $\partial V'/\partial W$ is less singular in the interaction region than V' itself.

TABLE I. Numerical results for quadrupole moment and normalization integrals. The coupling constant $g^2/4\pi$ has been chosen equal to 10.

Wave function	Order	Quadrupole moment ($\times10^{28}$ cm^2)	Normalization integrals ($\times10^2$)
Core: $S-S$	eg^2	0.974	−0.289
$S-D$		−0.435	5.136
$D-D$		0.115	−0.778
Hulthén $S-S$	eg^2	1.177	−3.797
$S-D$		...	...
$D-D$		...	...
Core: $S-S$	eg^4	−0.270	0.742
$S-D$		−0.050	−0.395
$D-D$		0.350	0.176
Core:	Total eg^2	0.636	4.069
	Total eg^4	0.028	0.523

[8] J. M. Blatt and M. H. Kalos, Phys. Rev. **92**, 1563 (1953). We are grateful to Dr. Kalos for giving us the use of his wave function tables and to Dr. Sessler for correspondence relevant to the numerical integrals performed.

It is to be noted that the same techniques employed in calculating the quadrupole moment can be used to estimate the deuteron charge density radius. Here, mesonic contributions may play a role in the interpretation of high-energy electron-deuteron scattering experiments when these become accurate enough to give a precision measurement of this quantity. One may also employ the formalism of the paper for transition problems where meson currents play the dominant role at high energies (over 100 Mev). Such work is in progress.

APPENDIX A. RELATION OF CHARGE DENSITY TO QUADRUPOLE MOMENT

In this Appendix, we shall present the details upon which the remarks following Eq. (22) of the text are based.

To this end we consider in detail Eq. $(24b)_1$ with the substitutions indicated in Eqs. (25), (26), and (27), and with all irrelevant multiplicative factors omitted, as follows:

$$\int d\mathbf{P}d\mathbf{p}d\mathbf{k}d\mathbf{q}\delta(\mathbf{P}+\mathbf{q})a^*(\mathbf{p}-\mathbf{k}+\tfrac{1}{2}\mathbf{q})$$

$$\times[u^*(\mathbf{p}+\tfrac{1}{2}\mathbf{P}-\mathbf{k}+\mathbf{q})\Lambda_+(\mathbf{p}+\tfrac{1}{2}\mathbf{P}-\mathbf{k})$$

$$\times\gamma_0\gamma_\delta u(\mathbf{p}+\tfrac{1}{2}\mathbf{P})]_1[u^*(\tfrac{1}{2}\mathbf{P}-\mathbf{p}+\mathbf{k})\gamma_0\gamma_\delta u(\tfrac{1}{2}\mathbf{P}-\mathbf{p})]_2$$

$$\times a(\mathbf{p})\delta(\mathbf{P})\partial^2/\partial q_\epsilon\partial q_\beta\delta(\mathbf{q})\partial_\epsilon\partial_\beta A_0{}^e|_0$$

$$\times\{\omega(\mathbf{k})[W-\epsilon(\mathbf{p}+\tfrac{1}{2}\mathbf{P}-\mathbf{k})-\epsilon(\tfrac{1}{2}\mathbf{P}-\mathbf{p})-\omega(\mathbf{k})]$$

$$\times[W-\epsilon(\mathbf{p}+\tfrac{1}{2}\mathbf{P}-\mathbf{k}+\mathbf{q})-\epsilon(\tfrac{1}{2}\mathbf{P}-\mathbf{p})-\omega(\mathbf{k})]\}^{-1}. \quad (A.1)$$

At this stage one performs an integration by parts with respect to q. One then has four classes of terms to consider. There are terms in which one or more derivatives acts on $\delta(\mathbf{P}+\mathbf{q})$. All of these vanish quite independently of the adiabatic limit since on the one hand single derivatives give rise to vanishing odd integrals and the double derivatives when integrated pick out only the trace of $\partial_\epsilon\partial_\beta A_0{}^e|_0$, which vanishes since there are no sources of the external field in the nucleus. Next, there are the terms in which one or more derivatives act on an energy denominator. These can all be shown to have vanishing adiabatic limits and represent recoil corrections not evaluated explicitly in the text. The derivatives acting on the spinor $u^*(\mathbf{p}_1-\mathbf{k}+\mathbf{q})$ also give rise to recoil terms dropped in the adiabatic limit.

Hence, we are left with the term in which both derivatives act on the amplitude $a(\mathbf{p}-\mathbf{k}+\frac{1}{2}\mathbf{q})$, Eq. (28) of the text. Transforming this term to coordinate space will readily convince the reader that this is the contribution to the quadrupole energy defined as in Eq. (23). The structure of Eq. (A.1) is general enough to indicate that the argument will go through similarly to any order in g^2. We therefore conclude that in the adiabatic limit it is correct to compute charge density effects from $\partial V'/\partial W$, as we have done.

APPENDIX B. RECOIL CORRECTIONS

The problem of the treatment of nuclear recoil in our work has two aspects. There is the problem of defining a suitable nuclear interaction from which the amplitude $a(\mathbf{p}_1,\mathbf{p}_2)$ is to be computed. In this connection we have adopted the attitude that Eq. (10) has been solved with sufficient accuracy so that $a(\mathbf{p}_1,\mathbf{p}_2)$ actually contains the significant facets of the nuclear motion in intermediate states. There is also the occurrence of recoil effects in the exchange operators themselves. Here we have uniformly employed the adiabatic approximation in order to facilitate our numerical computations. Thus all energy denominators of the form

$$W-\epsilon(\mathbf{p})-\epsilon(\mathbf{p}')-\omega(\mathbf{k}), \quad (B.1)$$

occurring in $\partial V'/\partial W$, have been set equal to $-\omega(\mathbf{k})$. This has been done under the assumption that

$$[W-\epsilon(\mathbf{p})-\epsilon(\mathbf{p}')]/\omega(\mathbf{k})\ll 1, \quad (B.2)$$

and since in the deuteron this ratio is of order μ/M, we do not expect modifications of the effective exchange operators based on the inclusion of recoil terms to make substantial alterations in our results.

However, another entirely different approach to recoil terms can be given in the Tamm-Dancoff formalism along the lines of what Deser[2] has done for the covariant equation. In this approach one assumes that the static nuclear potential binds the deuteron, i.e., one solves Eq. (10) of the text in the adiabatic limit, and then one adds both the electromagnetic field and the "recoil potential" as perturbations on the system. If one now applies perturbation theory, it is evident that cross terms between the velocity dependent potential and the electromagnetic field will make a contribution to the exchange moment energies. It is interesting to follow this idea through in detail in our formalism since we shall succeed then in making connection with Deser's results.

To this end we consider a typical contribution to V' as given, for example, by Eq. (23a) of the text, with the structure,

$$\frac{g^2}{(2\pi)^3}\frac{\langle\gamma_0\gamma_\delta\rangle_1\tau_1\cdot\tau_2\langle\gamma_0\gamma_\delta\rangle_2}{2\omega(\mathbf{k})[W-\epsilon(\mathbf{p}'-\mathbf{k})-\epsilon(\mathbf{p})-\omega(\mathbf{k})]}. \quad (B.3)$$

In order to separate the recoil effects in Eq. (B.3) we write

$$[W-\epsilon(\mathbf{p}'-\mathbf{k})-\epsilon(\mathbf{p})-\omega(\mathbf{k})]^{-1}$$
$$=-\omega^{-1}+[W-\epsilon(\mathbf{p}'-\mathbf{k})-\epsilon(\mathbf{p})]$$
$$\times\{\omega[W-\epsilon(\mathbf{p}'-\mathbf{k})-\epsilon(\mathbf{p})-\omega]\}^{-1}. \quad (B.4)$$

Thus by the "recoil potential," V_r', we shall mean all contributions to V' such as Eq. (B.3) with the nucleon energy denominators replaced by expressions like the *last* term of Eq. (B.4).

By standard second-order perturbation theory the eg^2 contribution to the electrostatic energy due to V_r' and

$A_0^e(q)$ is given by

$$\Delta W=\sum_n \frac{\langle 0|V_r'|n\rangle\langle n|V^{el}|0\rangle+\langle 0|V^{el}|n\rangle\langle n|V_r'|0\rangle}{W_0-W_n}. \quad \text{(B.5)}$$

Here, W_0 refers to the unperturbed deuteron energy and the summation is over continuum states of the two nucleon system. In order to get a manageable expression for Eq. (B.5) we shall ignore interactions in intermediate states and write for the continuum wave functions indexed by momentum variables,

$$\begin{aligned}\phi_n(\mathbf{p}_1,\mathbf{p}_2)&=\phi_{\mathbf{p}',\mathbf{p}''}(\mathbf{p}_1\mathbf{p}_2)\\&=u(\mathbf{p}')u(\mathbf{p}'')\delta(\mathbf{p}_1-\mathbf{p}')\delta(\mathbf{p}_2-\mathbf{p}''),\end{aligned} \quad \text{(B.6)}$$

where the $u(\mathbf{p})$ are free-particle spinors. If we put in the details we obtain as a typical contribution to Eq. (B.5),

$$\begin{aligned}&\frac{eg^2}{(2\pi)^9}\int\frac{d\mathbf{p}_1d\mathbf{p}_2d\mathbf{k}d\mathbf{q}}{2[\omega(\mathbf{k})]^2}a_0^*(\mathbf{p}_1,\mathbf{p}_2+\mathbf{q})\langle\gamma_\sigma\gamma_5\tau_i\rangle_1\\&\times\langle A_0^e(\mathbf{q})\Lambda_+(\mathbf{p}_2)\gamma_\sigma\gamma_5\tau_i\rangle_2 a_0(\mathbf{p}_1-\mathbf{k},\mathbf{p}_2+\mathbf{k})\\&\times\Bigg[\frac{W-\epsilon(\mathbf{p}_1)-\epsilon(\mathbf{p}_2+\mathbf{k})}{[W-\epsilon(\mathbf{p}_1)-\epsilon(\mathbf{p}_2)][W-\epsilon(\mathbf{p}_1)-\epsilon(\mathbf{p}_2+\mathbf{k})-\omega(\mathbf{k})]}\\&+\frac{W-\epsilon(\mathbf{p}_1-\mathbf{k})-\epsilon(\mathbf{p}_2)}{[W-\epsilon(\mathbf{p}_1)-\epsilon(\mathbf{p}_2)][W-\epsilon(\mathbf{p}_1-\mathbf{k})-\epsilon(\mathbf{p}_2)-\omega(\mathbf{k})]}\Bigg],\end{aligned} \quad \text{(B.7)}$$

to which must be added three terms of similar structure. The subscript zero on $a_0(\mathbf{p}_1,\mathbf{p}_2)$ means that these amplitudes are solutions of Eq. (10) of the text *after* the adiabatic limit has been taken in the interaction kernel.

If in Eq. (B.7) we were to set all ratios of the form

$$[W-\epsilon(\mathbf{p})-\epsilon(\mathbf{p}')]/[W-\epsilon(\mathbf{p}'')-\epsilon(\mathbf{p}''')]=1 \quad \text{(B.8)}$$

and take the adiabatic limit, Eq. (B.7) would become at once,

$$\begin{aligned}&\frac{-2eg^2}{(2\pi)^9}\int\frac{d\mathbf{p}_1d\mathbf{p}_2d\mathbf{k}d\mathbf{q}}{2\omega^3}\{a_0^*(\mathbf{p}_1,\mathbf{p}_2+\mathbf{q})\\&\times\langle\gamma_\sigma\gamma_5\tau_i\rangle_1\langle A_0^e(\mathbf{q})\Lambda_+(\mathbf{p}_2)\gamma_\sigma\gamma_5\tau_i\rangle_2\\&\times a_0(\mathbf{p}_1-\mathbf{k},\mathbf{p}_2+\mathbf{k})+\cdots\}.\end{aligned} \quad \text{(B.9)}$$

To Eq. (B.9) we add the electrostatic exchange energy computed directly from the adiabatic nuclear potential, i.e., terms of the form

$$\begin{aligned}&\frac{eg^2}{(2\pi)^9}\int\frac{d\mathbf{p}_1d\mathbf{p}_2d\mathbf{k}d\mathbf{q}}{2\omega^3}\{a_0^*(\mathbf{p}_1,\mathbf{p}_2+\mathbf{q})\\&\times\langle\gamma_\sigma\gamma_5\tau_i\rangle_1\langle A_0^e(\mathbf{q})\Lambda_+(\mathbf{p}_2)\gamma_\sigma\gamma_5\tau_i\rangle_2\\&\times a_0(\mathbf{p}_1-\mathbf{k},\mathbf{p}_2+\mathbf{k})+\cdots\}.\end{aligned} \quad \text{(B.10)}$$

The principal point to notice is that the structure of Eq. (B.9) is identical to that of Eq. (B.10), and differs from it only by a factor of -2. If these two equations are now added together, we get as a total expression of the eg^2 electromagnetic energy exactly Eq. (21) of Deser's paper.[2] Hence, the burden of this appendix has been to show under what conditions Deser's covariant calculation and the three-dimensional configuration-space approach reduce to each other, the transitions having been made only by means of the two unverified assumptions contained in Eqs. (B.6) and (B.8).

APPENDIX C. METHOD OF CANONICAL TRANSFORMATIONS

In this Appendix, we want to explore the question of the existence of exchange effects in the method of canonical transformations. Thus we consider the Schrödinger equation,

$$(H^0+H'+H^{el})\Phi=W\Phi, \quad \text{(C.1)}$$

where H^0 is the free-meson Hamiltonian,

$$\begin{aligned}H'=-g\sum_k\sum_i(2V\omega_k)^{-\frac{1}{2}}\tau_\lambda^{(i)}(\gamma_\sigma\gamma_5)^{(i)}e^{i\mathbf{k}\cdot\mathbf{x}_i}\\\times(a_{k\lambda}+a_{-k\lambda}^\dagger),\end{aligned} \quad \text{(C.2)}$$

and

$$H^{el}=-e\sum_i(\gamma_\sigma\gamma_\mu)^{(i)}A_\mu(x_i)\tfrac{1}{2}(1+\tau_3^{(i)}), \quad \text{(C.3)}$$

that is, we ignore nucleon recoil in intermediate states *ab initio*. Equation (C.1) is then transformed by means of a sequence of canonical transformations designed to uncouple components of Φ belonging to different numbers of mesons. The first of these is chosen according to the equation

$$[S^{(1)},H^0]=-H', \quad \text{(C.4)}$$

and is given by

$$\begin{aligned}S^{(1)}=g\sum_k\sum_i(2V\omega_k^3)^{-\frac{1}{2}}\tau_\lambda^{(i)}(\gamma_\sigma\gamma_5)^{(i)}e^{i\mathbf{k}\cdot\mathbf{x}_i}\\\times(a_{k\lambda}-a_{-k\lambda}^\dagger).\end{aligned} \quad \text{(C.5)}$$

The electromagnetic effects to this order are then evaluated by taking the expectation value of

$$\exp(S^{(1)})H^{el}\exp(-S^{(1)}) \quad \text{(C.6)}$$

in the two-nucleon, no-meson amplitude. However, $S^{(1)}$ has the very special property that it can be written as a sum of commuting operators belonging to distinct nucleons, i.e.,

$$S^{(1)}=S_1^{(1)}+S_2^{(1)}, \quad \text{(C.7)}$$

and

$$[S_1^{(1)},S_2^{(1)}]=0. \quad \text{(C.8)}$$

Hence Eq. (C.6) can be written

$$\exp(S_2^{(1)})\exp(S_1^{(1)})H^{el}\exp(-S_1^{(1)})\exp(-S_2^{(1)}). \quad \text{(C.9)}$$

However,

$$H^{el}=\sum_i H_i^{el}, \tag{C.10}$$

with

$$[H_i^{el},S_j^{(1)}]=0, \quad i\neq j. \tag{C.11}$$

It is now evident from Eq. (C.9) that Eq. (C.6) contains no exchange terms. In agreement with Villars,[3] we would have to include nucleon recoil to obtain a nonvanishing result to this order.

If we now construct the next term in the sequence of canonical transformations it can be shown that no decompositions of the form of Eqs. (C.7) and (C.9) is possible. Hence, there are adiabatic exchange effects in the theory, but they are at least of order eg^4.

PHYSICAL REVIEW VOLUME 99, NUMBER 3 AUGUST 1, 1955

Neutron-Electron Interaction

GEORGE SALZMAN*
Physics Department, University of Illinois, Urbana, Illinois
(Received March 21, 1955)

The effective neutron-electron interaction is calculated with the cut-off pseudoscalar meson theory and neglect of nucleon recoil. Values of -7.1 and -8.6 kev are obtained for the meson contribution with two different shapes for the cut-off function. The nucleon contribution is ambiguous in the cut-off theory since the shape of the core charge is undetermined. It is shown that if the no recoil theory with cutoff is interpreted to be the limit, as the nucleon mass becomes infinite, of a relativistic theory with a cutoff, then the contribution of the anomalous magnetic moment (or Foldy) term is not contained in our calculation. Since the Foldy term alone accounts for the major part of the experimental interaction, the sum of pion and nucleon charge contributions in this theory, if correct, should be at most of the order of a few hundred ev, or an order of magnitude less than the pion part. Finally, a brief calculation is made to illustrate the fact that, if spread out in a plausible way, the nucleon core charge could effect the needed cancellation.

1. INTRODUCTION

RECENT experiments at Brookhaven[1] give $-eV_0=-3.86\pm0.37$ kev for the effective neutron-electron interaction energy, where the effective potential V_0 is assigned a radius equal to the classical electron radius, and $-e$ is the electron charge. Although the weak coupling approximation to relativistic pseudoscalar meson theory with pseudoscalar coupling is in qualitative agreement[2] with this value if the coupling constant is fitted with the neutron anomalous magnetic moment μ_N, this theory must be considered unreliable because of its inability[3] to give simultaneously the experimental ratio of μ_N/μ_P, where μ_P is the proton anomalous magnetic moment. The neutron-electron interaction and the neutron anomalous magnetic moment are closely related; one involves the interaction of a slow neutron with a static electric field, the other with a static magnetic field.

Our approach to the nucleon meson problem is related to that of Sachs,[4] who also neglects nucleon recoil. The two treatments differ in that here a specific interaction is assumed, whereas his more general analysis is independent of such details. For the present purposes however, a more important difference lies in our belief that a theory without nucleon recoil should explain only the "large components" part of the neutron-electron interaction. The parameters of this theory were thus fitted to a set of data which is not equivalent to the set of data used by Sachs.

These facts, and recent efforts to describe nucleon meson phenomena by a no recoil cut-off pseudoscalar meson theory,[5,6] make it of interest to examine the neutron-electron interaction in this theory, because it gives the nucleon anomalous magnetic moments fairly well[6,7] without having any adjustable parameters. The parameters were previously determined in pion-nucleon scattering and photomeson production calculations. The mesonic part of the electrostatic neutron-electron interaction is as well defined in this theory as are the nucleon anomalous magnetic moments.

In Sec. 2, the approximation is described and the usual expression for $-eV_0$ is obtained [Eq. (2)]. In Sec. 3, the meson charge density surrounding the neutron is calculated by second-order perturbation theory, and shown to be negative definite independent of the choice of cut-off function. It then follows that the mesonic contribution to $-eV_0$ is negative. This is intuitively expected from a picture of the neutron dissociating according to $N\rightleftharpoons P+\pi^-$. In Sec. 4, an expression for the pion contribution to $-eV_0$ is obtained [Eq. (9)] which applies for the particular meson

* Now at the University of Rochester, Rochester, New York.
[1] Hughes, Harvey, Goldberg, and Stafne, Phys. Rev. **90**, 497 (1953).
[2] B. Fried, Phys. Rev. **88**, 1142 (1952). References are given here to earlier calculations.
[3] L. Foldy, Phys. Rev. **87**, 675 (1952); **87**, 693 (1952).
[4] R. Sachs, Phys. Rev. **87**, 1100 (1952); **95**, 1065 (1954).
[5] G. Chew, Phys. Rev. **94**, 1748 (1954); **94**, 1755 (1954).
[6] G. Chew, Phys. Rev. **95**, 1669 (1954).
[7] M. Friedman, Phys. Rev. **97**, 1123 (1955).

nucleon interaction assumed. Given a cut-off function, this expression, which involves a single one-dimensional integral, can be evaluated. This is done in Sec. 5 for a Gaussian cutoff and for a Yukawa-transform cutoff. In Sec. 6, it is shown that this calculation does not include the anomalous magnetic moment (or Foldy) term,[8] provided the no recoil theory with cutoff is given the specified interpretation. In Sec. 7 we conclude that our answer should be 7–8 kev closer to zero. Reliance on recoil corrections is argued against, and the ability of a static, distributed core charge to correct the answer is mentioned. Finally, the effect of spreading out the core charge in a particular simple way is briefly examined, and shown capable of leading to the correct value.

2. STATIC APPROXIMATION

The nucleon is assumed to be permanently at rest (no recoil) and the electron is scattered from an initial state of small momentum $\mathbf{k}_i$.[9] Because the electron is moving slowly it is affected only by the electric field of the nucleon-meson system. This field is assumed to be static. The scattering matrix element is then

$$S_{fi}=\left(\psi_f(\mathbf{r}_e),\,(-e)\int d\mathbf{r}\frac{\rho(\mathbf{r})}{|\mathbf{r}-\mathbf{r}_e|}\psi_i(\mathbf{r}_e)\right), \tag{1}$$

where $\psi_i(\mathbf{r}_e)$ and $\psi_f(\mathbf{r}_e)$ are the initial and final state electron wave functions, $\rho(\mathbf{r})$ is the charge density of the physical neutron [core charge $\rho_c(\mathbf{r})$ plus meson charge $\rho_\pi(\mathbf{r})$], $d\mathbf{r}$ is the volume element $dx\,dy\,dz$, and $|\mathbf{r}-\mathbf{r}_e|$ is the length of the vector $(\mathbf{r}-\mathbf{r}_e)$.

The effective interaction potential V_0 is conventionally defined by equating the above expression for S_{fi} to

$$(\psi_f(\mathbf{r}_e),\,(-e)V(\mathbf{r}_e)\psi_i(\mathbf{r}_e)),$$

where

$$V(\mathbf{r}_e)=V_0 \text{ for } r_e<r_0=e^2/m$$
$$=0 \text{ otherwise,}$$

and m is the rest mass of an electron. Assuming that

$$\psi_i(\mathbf{r}_e)=V^{-\frac{1}{2}}\exp(i\mathbf{k}_i\cdot\mathbf{r}_e) \text{ and } \psi_f(\mathbf{r}_e)=V^{-\frac{1}{2}}\exp(i\mathbf{k}_f\cdot\mathbf{r}_e),$$

where V is the quantization volume, we obtain, for the limiting case of very small K:

$$-eV_0=\frac{-3e}{4\pi r_0^3}\int d\mathbf{r}_e\int d\mathbf{r}\frac{\rho(\mathbf{r})}{|\mathbf{r}-\mathbf{r}_e|}e^{-i\mathbf{K}\cdot\mathbf{r}_e},$$

where $\mathbf{K}=\mathbf{k}_f-\mathbf{k}_i$. If $\rho(\mathbf{r})$ is assumed to be spherically symmetric, and to approach zero quickly enough as $r\to\infty$, it is easy to show that for very small K,

$$-eV_0=(e/2r_0^3)\int d\mathbf{r}r^2\rho(r), \tag{2}$$

and

$$(-eV_0)_\pi=(e/2r_0^3)\int d\mathbf{r}r^2\rho_\pi(r). \tag{3}$$

If the core charge is concentrated at small values of r, then $-eV_0\approx(-eV_0)_\pi$. To evaluate (3) we need $\rho_\pi(\mathbf{r})$.

As is known, the neutron-electron interaction may also be expressed in terms of an effective radius. If one discusses the meson and core contributions separately, it is appropriate to define an effective radius for the pions by

$$\langle r_\pi\rangle_{\text{rms}}=\left[\int d\mathbf{r}r^2\rho_\pi(r)\Big/\int d\mathbf{r}\rho_\pi(r)\right]^{\frac{1}{2}}$$

and to characterize the mesonic contribution by the value of $\langle r_\pi\rangle_{\text{rms}}$.

3. MESON CHARGE DENSITY

The meson charge density $\rho_\pi(\mathbf{r})$ is the expectation value

$$\rho_\pi(\mathbf{r})=\langle\Psi_N|\rho_{\pi[\text{op}]}(\mathbf{r})|\Psi_N\rangle, \tag{4}$$

where the meson charge density operator is[10]

$$\rho_{\pi[\text{op}]}(\mathbf{r})=ie(\pi^*\phi^*-\pi\phi)$$

and Ψ_N is the state vector of the physical neutron. Our approach is to calculate Ψ_N correct to second order in the meson-nucleon coupling constant using time independent perturbation theory with the perturbing hamiltonian density,[6] for a single nucleon at $\mathbf{r}_N$,

$$\mathcal{H}'(\mathbf{r})=(4\pi)^{\frac{1}{2}}(f/\mu)\sum_{\lambda=1}^{3}\tau_\lambda s(\mathbf{r}-\mathbf{r}_N)\boldsymbol{\sigma}\cdot\boldsymbol{\nabla}_r\phi_\lambda(\mathbf{r}), \tag{5}$$

where f is the unrationalized symmetric coupling constant, μ^{-1} is the meson compton wavelength, τ_λ is the nucleon isotopic spin operator, $s(\mathbf{r}-\mathbf{r}_N)$ is the "source" function that prescribes the points $\mathbf{r}$ at which mesons may be created and annihilated by the nucleon, $\boldsymbol{\sigma}$ is the nucleon spin operator, and $\phi_\lambda(\mathbf{r})$ are the operators of the meson fields (π^-,π^0,π^+). With only a single fixed nucleon the origin is taken at the nucleon and the coordinate $\mathbf{r}_N$ will not appear. However, mesons with relativistic velocities are not excluded.

An equivalent calculation could have been done using time dependent scattering theory, with virtual mesons created and annihilated by the meson electron interaction,

$$(-e)\int d\mathbf{r}\frac{\rho_{\pi[\text{op}]}(\mathbf{r})}{|\mathbf{r}-\mathbf{r}_e|}.$$

Each method of calculation leads to the same result if carried to order e^2f^2.

The perturbation theory calculation of the state vector Ψ_N is straightforward. When this result for Ψ_N

[8] L. Foldy, Phys. Rev. **83**, 688 (1951).
[9] The "natural" units $\hbar=c=1$ are used.
[10] G. Wentzel, *Quantum Theory of Fields* (Interscience Publishers, Inc., New York, 1949).

is substituted into Eq. (4) the following expression is obtained for the mesonic charge, correct to order f^3:

$$\rho_\pi(\mathbf{r})=\frac{-4e}{(2\pi)^5}\left(\frac{f}{\mu}\right)^2\int d\mathbf{k}\int d\mathbf{k}' \times\frac{v(k)v(k')\boldsymbol{\sigma}\cdot\mathbf{k}\boldsymbol{\sigma}\cdot\mathbf{k}'}{(\omega+\omega')\omega\omega'}e^{i(\mathbf{k}-\mathbf{k}')\cdot\mathbf{r}}. \quad (6)$$

Here $\omega=(\mu^2+k^2)^{\frac{1}{2}}$, $\omega'=(\mu^2+k'^2)^{\frac{1}{2}}$ and the cutoff function $v(k)$, defined by

$$v(\mathbf{k})=\int d\mathbf{r}s(\mathbf{r})\exp(i\mathbf{k}\cdot\mathbf{r}), \quad (7)$$

is a function of the length of $\mathbf{k}$ because $s(\mathbf{r})$ is assumed to be spherically symmetric. Equation (6) may be manipulated into a form in which the spherical symmetry of $\rho_\pi(\mathbf{r})$ is manifest, namely

$$\rho_\pi(\mathbf{r})=\frac{-4e}{(2\pi)^5}\left(\frac{f}{\mu}\right)^2\int d\mathbf{k}\int d\mathbf{k}' \times\frac{v(k)v(k')\mathbf{k}\cdot\boldsymbol{\varepsilon}(\mathbf{r})\mathbf{k}'\cdot\boldsymbol{\varepsilon}(\mathbf{r})}{(\omega+\omega')\omega\omega'}e^{i(\mathbf{k}-\mathbf{k}')\cdot\mathbf{r}}, \quad (8)$$

where $\boldsymbol{\varepsilon}(\mathbf{r})=\mathbf{r}/r$.

Before using (8) to evaluate the integral in (3), it is interesting to see that $\rho_\pi(\mathbf{r})$ is negative definite, for all $\mathbf{r}$ and for all choices of $v(k)$. Using the fact that

$$\frac{1}{\omega+\omega'}=\int_0^\infty d\xi e^{-\xi(\omega+\omega')},$$

Eq. (8) may be rewritten as

$$\rho_\pi(\mathbf{r})=\frac{-4e}{(2\pi)^5}\left(\frac{f}{\mu}\right)^2\int_0^\infty d\xi\left[\int d\mathbf{k}\frac{v(k)\mathbf{k}\cdot\boldsymbol{\varepsilon}(\mathbf{r})}{\omega}e^{i\mathbf{k}\cdot\mathbf{r}-\xi\omega}\right] \times\left[\int d\mathbf{k}'\frac{v(k')\mathbf{k}'\cdot\boldsymbol{\varepsilon}(\mathbf{r})}{\omega'}e^{-i\mathbf{k}'\cdot\mathbf{r}-\xi\omega'}\right].$$

Since $v(k)\mathbf{k}/\omega$ is an odd function, it follows that

$$\rho_\pi(\mathbf{r})=\frac{-4e}{(2\pi)^5}\left(\frac{f}{\mu}\right)^2\int_0^\infty d\xi \times\left[\int d\mathbf{k}\frac{v(k)}{\omega}\mathbf{k}\cdot\boldsymbol{\varepsilon}(\mathbf{r})e^{-\xi\omega}\sin(\mathbf{k}\cdot\mathbf{r})\right]^2.$$

Since the expression in the square bracket is real its square is non-negative and the final integration over ξ must give a positive function of $\mathbf{r}$, whatever the choice of $v(k)$. It is clear from Eq. (3) that since $\rho_\pi(\mathbf{r})<0$, $(-eV_0)_\pi$ is negative.

4. INTERACTION ENERGY

Substitution of (8) into (3) gives

$$(-eV_0)_\pi=\frac{-2e^2}{(2\pi)^5r_0^3}\left(\frac{f}{\mu}\right)^2\int d\mathbf{r}r^2\int d\mathbf{k}\int d\mathbf{k}' \times\frac{v(k)v(k')}{(\omega+\omega')\omega\omega'}\mathbf{k}\cdot\boldsymbol{\varepsilon}(\mathbf{r})\mathbf{k}'\cdot\boldsymbol{\varepsilon}(\mathbf{r})e^{i(\mathbf{k}-\mathbf{k}')\cdot\mathbf{r}}.$$

By doing the $\mathbf{r}$ integration first, this becomes

$$(-eV_0)_\pi=\frac{e^2}{2\pi^2r_0^3}\left(\frac{f}{\mu}\right)^2\int d\mathbf{k}\int d\mathbf{k}' \times\frac{v(k)v(k')}{(\omega+\omega')\omega\omega'}\mathbf{k}\mathbf{k}'\cdot\cdot\nabla_k\nabla_k\delta(\mathbf{k}-\mathbf{k}'),$$

where $\cdot\cdot$ means the dyadic inner product. By two partial integrations, and use of the δ function in doing the $\mathbf{k}'$ integration, we get

$$(-eV_0)_\pi=\frac{e^2}{2\pi^2r_0^3}\left(\frac{f}{\mu}\right)^2\int d\mathbf{k} \times\left[\nabla_k\nabla_k\cdot\cdot\frac{v(k)v(k')}{(\omega+\omega')\omega\omega'}\mathbf{k}\mathbf{k}'\right]_{\mathbf{k}'=\mathbf{k}}.$$

Straightforward calculation, which uses the spherical symmetry of $v(k)$, and partial integration of the term involving d^2v/dk^2, leads to

$$(-eV_0)_\pi=\frac{-e^2}{2\pi r_0^3}\left(\frac{f}{\mu}\right)^2J, \qquad J=\int_0^\infty dk\frac{k^4}{\omega^3}\left[2\omega^4\left(\frac{dv}{dk}\right)^2+5(3\omega^2-2k^2)v^2\right]. \quad (9)$$

5. EVALUATION OF $(-eV_0)_\pi$ FOR PARTICULAR CUT-OFF FUNCTIONS

For the case of a square cutoff, namely

$$v(k)=1 \text{ for } k<k_{\max},$$
$$=0 \text{ otherwise},$$

the determination of the coupling constant f^2 and of $k_{\max}$ is discussed by Chew.[8] The values that he obtains are 0.058 and 5.6μ respectively.[11] Since the integral J of Eq. (9) involves dv/dk, a square cutoff is unsatisfactory. In fact, as the limiting case of a square cutoff is approached, $J\to\infty$. However, the square cutoff is not to be taken too seriously because it implies that $s(r)$ is negative for some values of r, and we assume that $s(r)$ is nowhere negative.

For sample calculations, we chose for cutoffs the

[11] Recent work indicates that these values are likely to be increased slightly, but this will not alter any of the conclusions in the present paper.

relatively short-tailed Gaussian:

$$v(k)=A\exp(-k^2/B^2),$$

and the relatively long-tailed Yukawa-transform:

$$v(k)=C/[1+(k^2/D^2)].$$

To evaluate the constants A and C, we note from Eq. (7) that $v(0)=\int d\mathbf{r}s(\mathbf{r})$, and since $s(\mathbf{r})$ is assumed normalized so that this integral equals 1, it follows that $A=C=1$. The constants B and D are determined by requiring that a certain important integral which arises in the meson-nucleon scattering problem have the same value when evaluated with these cutoffs as when evaluated with the already determined square cutoff. This requirement leads to the values $B=5.6\sqrt{2}\mu$ and $D=5.6\mu$. Numerical integration with each of these cutoffs gives $J=7.20$ and $J=5.98$ respectively. Note that J is the sum of two positive terms. With the Gaussian cutoff the dv/dk term contributes 19 percent as much as the v term, with the Yukawa transform cutoff it contributes 11 percent as much. With a pion mass $m_\pi=273m$,

$$\frac{-e^2}{2\pi r_0^3}\left(\frac{f}{\mu}\right)^2=-1.20\text{ kev},$$

and this gives for $(-eV_0)_\pi$, and for $\langle r_\pi\rangle_{\text{rms}}$ the values shown in the table in Sec. 7.

6. RELATIVISTIC CONTRIBUTIONS TO $-eV_0$

The average of the two values of $(-eV_0)_\pi$ is -7.9 kev, about twice the experimental value. In this section, we show that if the no recoil theory with cutoff is interpreted to be the limit, as the nucleon mass becomes infinite, of a relativistic theory with a cutoff, then our calculation does not include the Foldy term. Addition of this term to our answer gives a result roughly three times as great as the experimental value.

We need the fact, derived in the Appendix, that the scattering matrix element that describes the elastic scattering of a nucleon, or any Dirac particle, by an external unquantized electromagnetic field, may be written, correct to first order in the electromagnetic field,

$$S^a{}_{fi}=-i\int dx\bar{u}_2e^{-ip_2x}\sum_{n=0}^{\infty}(-i)$$

$$\times\left[\epsilon_n\Box^n\gamma_\mu A_\mu+\tfrac{1}{2}\mu_n\Box^n\gamma_\mu\gamma_\nu\left(\frac{\partial A_\mu}{\partial x_\nu}-\frac{\partial A_\nu}{\partial x_\mu}\right)\right]u_1e^{ip_1x},\quad(10)$$

where x stands for $\mathbf{r}$ and t, dx is the space-time volume element, p_1 and p_2 are the initial and final four momenta of the nucleon, γ_μ are the Dirac matrices, $A_\mu(x)$ are the electromagnetic potentials, the summation convention applies to Greek subscripts, $\Box$ is the D'Alembertian operator, u_1 and $\bar{u}_2[=u_2^*\beta]$ are the Dirac spinors for the initial and final nucleons, $px=p_\mu x_\mu=\mathbf{p}\cdot\mathbf{r}-Et$, and ϵ_n and μ_n are invariant constants which depend only on the particular kind of Dirac particle being scattered, and are independent of the nature of the electromagnetic field responsible for the scattering. The D'Alembertian operators act only on the x dependence of the electromagnetic potentials. u_2^* is the Hermitian adjoint of u_2, and u_1 and $\bar{u}_2$ satisfy the equations

$$\begin{aligned}(\gamma_\mu p_{1\mu}-im_N)u_1&=0,\\(p_{2\mu}\bar{u}_2\gamma_\mu-im_N\bar{u}_2)&=0,\end{aligned}\qquad(11)$$

where m_N is the rest mass of the nucleon.

The validity of Eq. (10) was conjectured by Foldy,[12] who, in his work on the electromagnetic properties of Dirac particles, derived an analogous[13] result by means independent of the S-matrix formalism. That such a result exists was pointed out to the author by F. Low, whose help in establishing the proof is gratefully acknowledged.

The coefficients ϵ_n and μ_n are the "same" ones introduced by Foldy[12] to characterize the electromagnetic properties of Dirac particles. He discusses their meaning in detail, and they will not be further discussed here, except to mention that ϵ_0 and μ_0 are the static charge and static anomalous magnetic moment respectively, of the Dirac particle under consideration.

Equation (10) is a consequence of (a) the relativistic and gauge invariance of the scattering formalism, (b) the fact that we consider only those Feynman graphs which have two external nucleon lines and in which the electromagnetic field acts at exactly one vertex, and (c) the assumption that the nucleon four-current (to first order in A) is an analytic function of the four-momentum transfer in the neighborhood of zero transfer. It is therefore independent of the details of the meson-nucleon interaction, and of the presence or absence of interactions with heavier mesons.

For the neutron-electron problem, note that $\epsilon_0=0$. Then, writing μ_N for μ_0, and remembering that $\partial A_\mu/\partial x_\nu$ is of order $\Delta p_\nu=p_{2\nu}-p_{1\nu}$, we have from Eq. (10), correct to order $(\Delta p)^2$,

$$S^a{}_{fi}=-i\int dx e^{-i\Delta px}(-\bar{i})\bar{u}_2$$

$$\times\left[\epsilon_1\Box\gamma_\mu A_\mu+\tfrac{1}{2}\mu_N\gamma_\mu\gamma_\nu\left(\frac{\partial A_\mu}{\partial x_\nu}-\frac{\partial A_\nu}{\partial x_\mu}\right)\right]u_1.$$

If A_μ is the potential for a fixed Coulomb scattering center, then this reduces, when the time integration is

[12] L. Foldy, Phys. Rev. **87**, 688 (1952).

[13] Our Eq. (10) is the counterpart of Eq. (4) of reference (10). The two equations differ in that we believe the factor $\frac{1}{2}$ just preceding μ_n is necessary if μ_0 is to be the static anomalous magnetic moment.

performed, to

$$S^e_{fi}=-2\pi\delta(E_2-E_1)\int d\tau e^{-i\Delta\mathbf{p}\cdot\mathbf{r}}u_2^*\times[\epsilon_1\nabla^2A_4+\mu_N\gamma_j\partial A_4/\partial x_j]u_1,$$

where the index j is summed from 1 to 3. If the effective interaction potential is introduced in a manner analogous to that used in Sec. 2, it is not hard to show that

$$-eV_0=\frac{3}{4\pi r_0^3}\int d\tau e^{-i\Delta\mathbf{p}\cdot\mathbf{r}}(-i)u_2^*\times[\epsilon_1\nabla^2A_4+\mu_N\gamma_j\partial A_4/\partial x_j]u_1. \quad (12)$$

Note that

$$\gamma_j=\begin{pmatrix}0 & -i\sigma_j\\ i\sigma_j & 0\end{pmatrix},\quad u_n=N_n\begin{pmatrix}\chi_n\\ \dfrac{\boldsymbol{\sigma}\cdot\mathbf{p}_n}{E_n+m_N}\chi_n\end{pmatrix},$$

where the σ_j are the 2×2 Pauli spin matrices, n may assume the values 1 and 2, χ_1 and χ_2 are the initial and final nucleon spin states, and N_n is the normalization constant. The ϵ_1 term in (12) connects large to large spinor components, and for the case that $\chi_1=\chi_2$, $u_2^*u_1\approx1$ if the momenta $\mathbf{p}_1$ and $\mathbf{p}_2$ are small.

If now we consider the no recoil theory with cutoff to be the limit, as m_N becomes infinite, of a relativistic theory with a cutoff, then our calculation of $-eV_0$ should be the limit, as $m_N\to\infty$, of the value for $-eV_0$ given by Eq. (12). But in this limit the μ_N term in (12) vanishes, provided that μ_N remains finite. However, with a cutoff to suppress high-momentum virtual mesons, we can be very sure that μ_N will remain finite. Thus, our calculation does not include the μ_N term, if this interpretation is correct.

Taking the limit, Eq. (12) becomes, when we replace A_4 by $i(-e/r)$, take $\chi_1=\chi_2$, and do the integration,

$$-eV_0=\frac{3e}{r_0^3}\lim_{m_N=\infty}\epsilon_1.$$

Comparison of this with Eq. (2) shows that

$$\lim_{m_N=\infty}\epsilon_1=-\frac{1}{6}\int d\tau r^2\rho(r),$$

i.e., that it is the no recoil limit of ϵ_1 which is proportional to the second moment of the charge distribution.

7. CONCLUSIONS

The Foldy term alone accounts for -4.1 kev of the value of $-eV_0$. Since the experimental value is, to two significant figures, -3.9 ± 0.4 kev, it follows that all contributions other than that of the Foldy term should add up to a value between about -0.2 and $+0.6$ kev. Our calculation, with corrections, should thus give an answer of the order of a few hundred ev.

One correction that should be made is the inclusion of higher order mesonic effects, which can be expected to alter the meson charge distribution around the core. Although nucleon recoil would act to spread out the core charge, which is essentially positive, and thus improve our value of $-eV_0$, it is the absence of recoil in Chew's theory which provides the correct μ_N/μ_P ratio. A further difficulty involved in taking recoil into account, though not a difficulty of principle, is that terms which vanish in the limit of no recoil are present in both the Foldy and the ϵ_1 parts of $-eV_0$, and one would need to pick out just the non-Foldy part of the recoil terms.

A different possibility is to drop the assumption that the core charge is concentrated at a point. If the core charge were spread out appropriately, one could obtain any desired positive value for $\int d\tau r^2\rho_c(r)$, and thus agree with the experimental value of $-eV_0$. We have calculated the core contribution under the assumption that the core charge density is proportional to the source function,

$$\rho_c(r)=Ces(r),$$

where C is the proportionality constant. The zero charge of the physical neutron leads immediately to the result that C is the total meson charge, in units of $-e$. It is easy to show that

$$(-eV_0)_c=C\frac{e^2}{2r_0^3}[\nabla_k^2v(k)]_{k=0}.$$

To evaluate C, it is convenient to use the form of $\rho_\tau(r)$ given in Eq. (6). This leads to the expression

$$C=-\frac{2}{\pi}\left(\frac{f}{\mu}\right)^2\int_0^\infty dk\frac{k^4v^2}{\omega^3},$$

which is just the probability of the one charged meson state to second order in f. Numerical calculation gives:

	Gaussian cutoff	Yukawa-transform cutoff
C	0.50	0.50
$(-eV_0)_c$	+3.1 kev	+6.2 kev
$(-eV_0)_\tau$	−8.6 kev	−7.1 kev
$(-eV_0)_{c+\tau}$	−5.5 kev	−0.9 kev
$\langle r_\tau\rangle_{\rm rms}$	7.3×10^{-14} cm	6.7×10^{-14} cm

The low value obtained for $(-eV_0)_{c+\tau}$ with the Yukawa-transform cutoff may seem a bit surprising at first, since one might expect the meson cloud to be characterized by μ^{-1}, the meson Compton wavelength, which would imply that the nucleon core charge could not reasonably be expected to be far enough out to eliminate the attractive force. However, in this theory the meson cloud is roughly characterized by $k_{\rm max}^{-1}$, and with $k_{\rm max}=5.6\mu$, this is only 1.2 times the nucleon Compton wavelength. Thus a static distribution of the core charge over a region characterized by the nucleon

Compton wavelength could easily provide the needed correction.

I am much indebted to Professor Chew for his suggestion of an continued interest in this problem, and to Professor Low for valuable discussions.

8. APPENDIX

Equation (10) may be derived as follows. Consider a relativistic field theory for nucleons, mesons of various kinds, and an external electromagnetic field, described in the Schrödinger representation by a Hamiltonian density:

$$\mathcal{H}(\mathbf{r})=\mathcal{H}_0(\mathbf{r})+\mathcal{H}_I(\mathbf{r}), \quad \mathcal{H}_I(\mathbf{r})=\mathcal{H}'(\mathbf{r})+\mathcal{H}^e(\mathbf{r}).$$

Free, noninteracting nucleons and mesons are described by $\mathcal{H}_0(\mathbf{r})$, meson nucleon interactions by $\mathcal{H}'(\mathbf{r})$, and electromagnetic interactions by $\mathcal{H}^e(\mathbf{r})$. The scattering operator, in the interaction representation, is

$$S=1+\sum_{n=1}^{\infty}\frac{(-i)^n}{n!}\int dx_1\cdots dx_n P[\mathcal{H}_I(x_1)\cdots\mathcal{H}_I(x_n)],$$

where P is Dyson's time ordering operator.[14] If $\mathcal{H}'(x)+\mathcal{H}^e(x)$ is substituted for $\mathcal{H}_I(x)$ in the above, one obtains

$$S=1+\sum_{n=1}^{\infty}\frac{(-i)^n}{n!}\int dx_1\cdots dx_n P[\mathcal{H}'(x_1)\cdots\mathcal{H}'(x_n)]$$
$$+(-i)\sum_{n=1}^{\infty}\frac{(-i)^{n-1}}{(n-1)!}\int dx_1\cdots dx_n$$
$$\times P[\mathcal{H}^e(x_1)\mathcal{H}'(x_2)\cdots\mathcal{H}'(x_n)]+\cdots,$$

where the $+\cdots$ represents terms of higher order in $\mathcal{H}^e$. The terms without $\mathcal{H}^e$ are unrelated to electromagnetic interactions, and are of no interest in this discussion. The part of S linear in $A(x)$, which we call S^e, is wholly contained in the sum of terms linear in $\mathcal{H}^e$.

The part of $\mathcal{H}^e$ linear in $A(x)$ may be written as $v_\mu(x)A_\mu(x)$, where $v(x)$ is a four vector operator which in general contains creation and annihilation operators for mesons and nucleons. Then, since $A_\mu(x)$ commutes with all the operators in the P bracket, we can write

$$S^e=-i\sum_{n=1}^{\infty}\frac{(-i)^{n-1}}{(n-1)!}\int dx_1\cdots dx_n$$
$$\times P[v_\mu(x_1)\mathcal{H}'(x_2)\cdots\mathcal{H}'(x_n)]A_\mu(x_1),$$

or

$$S^e=-i\int dx[-j_\mu(x)A_\mu(x)],$$

where

$$j_\mu(x)=-v_\mu(x)-\sum_{n=2}^{\infty}\frac{(-i)^{n-1}}{(n-1)!}\int dx_2\cdots dx_n$$
$$\times P[v_\mu(x)\mathcal{H}'(x_2)\cdots\mathcal{H}'(x_n)].$$

[14] F. Dyson, Phys. Rev. **75**, 486 (1949).

It follows immediately from the invariance of S^e under an arbitrary gauge transformation that $j(x)$ does satisfy the conservation equation $\partial j_\mu(x)/\partial x_\mu=0$.

Now consider matrix elements

$$S^e{}_{fi}=\left(\Psi_2,\,-i\int dx[-j_\mu(x)A_\mu(x)]\Psi_1\right),$$

where Ψ_1 and Ψ_2 are the initial and final states of the nucleon field, there being one nucleon with four momentum p_1 in state Ψ_1, and one with four momentum p_2 in state Ψ_2. Thus

$$S^e{}_{fi}=-i\int dx(\Psi_2,\,-j_\mu(x)\Psi_1)A_\mu(x). \tag{A1}$$

The next step is to determine the most general form of $(\Psi_2,j_\mu(x)\Psi_1)$ which can occur in (A1). Each of the terms in the sum comprising $j_\mu(x)$ may be written as a sum of normally ordered terms[15] with all annihilation operators at the right and all creation operators at the left. Only those terms with exactly one nucleon annihilator and one nucleon creator can contribute to $(\Psi_2,j_\mu(x)\Psi_1)$. Each such term will introduce a factor $\bar{u}_2\exp(-ip_2x_j)$ at the left and a factor $u_1\exp(ip_1x_k)$ at the right, where x_j and x_k may vary from term to term, and each must be chosen from among $x, x_2, \cdots, x_n$ in the nth term. If all the space time integrations other than that over x are carried out, these lead to four-momentum conservation at each "intermediate" vertex. In order that the final integration over x insures, as it must, four-momentum conservation for the entire process, it is necessary that the x dependence of $(\Psi_2,j_\mu(x)\Psi_1)$ be of the form

$$(\Psi_2,j_\mu(x)\Psi_1)=\bar{u}_2j_\mu u_1\exp(-i\Delta px), \tag{A2}$$

where j is a four-vector independent of x.

Note that the right-hand side of (A2) can be written in the form $(\Psi_2,\bar{\psi}(x)j_\mu\psi(x)\Psi_1)$, where $\psi(x)$ and $\bar{\psi}(x)$ are the field operators for the nucleons, just as though the initial and final nucleons were annihilated and created at the same point x at which $A_\mu(x)$ acts.

In order to determine j_μ, we observe that the only quantities available from which to construct it are p_1, p_2, and γ_μ. Applying the charge current conservation condition to (A2), we get

$$\bar{u}_2j_\mu u_1\Delta p_\mu=0. \tag{A3}$$

Using these conditions and also Eqs. (11), it can be shown that the most general form of the four vector j in Eq. (A2) is

$$j_\mu=i[\epsilon\gamma_\mu+\tfrac{1}{2}i\mu\gamma_{\mu\nu}\Delta p_\nu], \tag{A4}$$

where ϵ and μ are invariant functions, and are independent of x, and $\gamma_{\mu\nu}=\gamma_\mu\gamma_\nu-\gamma_\nu\gamma_\mu$. Other terms can be reduced to linear combinations of these two. Equations

[15] G. Wick, Phys. Rev. **80**, 268 (1950).

(A1), (A2), and (A4) imply

$$S^c_{fi}=-i\int dx e^{-(\Delta p)x}\bar{u}_2(-i)\times(e\gamma_\mu+\tfrac{1}{2}i\mu\gamma_\mu\Delta p_\nu)u_1A_\mu(x), \quad \text{(A5)}$$

which may also be written as,

$$S^c_{fi}=-i\int dx e^{-(\Delta p)x}\bar{u}_2(-i)\times\left(e\gamma_\mu A_\mu+\tfrac{1}{2}\mu\gamma_\mu\gamma_\nu\left(\frac{\partial A_\mu}{\partial x_\nu}-\frac{\partial A_\nu}{\partial x_\mu}\right)\right)u_1.$$

The invariant functions ϵ and μ must depend only on the invariants that can be formed from p_1 and p_2, which are $(m_N)^2$ and $(\Delta p)^2$. This, together with the assumption on the analyticity of j in the neighborhood of $\Delta p_\mu=0$, implies that we may write

$$\epsilon=\epsilon_0-\epsilon_1(\Delta p)^2+\epsilon_2(\Delta p)^4-\cdots,$$
$$\mu=\mu_0-\mu_1(\Delta p)^2+\mu_2(\Delta p)^4-\cdots.$$

If these expressions for ϵ and μ are subsittuted into the last equation, one readily obtains Eq. (10).

PHYSICAL REVIEW VOLUME 99, NUMBER 3 AUGUST 1, 1955

Causality Conditions and Dispersion Relations. I. Boson Fields*

MARVIN L. GOLDBERGER
Institute for Nuclear Studies and Department of Physics, University of Chicago, Chicago, Illinois
(Received April 7, 1955)

The dispersion relations of Kramers and Kronig as generalized for charged and neutral Bose particles with finite rest mass are derived in a new way using the formalism of quantum field theory. The alternative forms of dispersion relations obtained by making various assumptions on the high-frequency limit of total cross sections are used to obtain information about the high-frequency behavior of the total cross section for the scattering of γ rays by electrons.

1. INTRODUCTION

IN two recent papers,[1] a discussion has been given of the derivation of the Kramers-Kronig dispersion relation for photon propagation from the standpoint of quantum field theory. It was shown in the first of these papers (GGT) that the relation followed from the "causality requirement" that the commutator of two vector potential operators taken at space-like points shall vanish. The derivation was based on the use of perturbation theory and a quite restrictive form of interaction between matter and electromagnetic fields. These two limitations were removed in the second paper (G). Another problem treated in GGT was the dispersion relation for Bose particles with mass. Only a very idealized situation was considered and the discussion was very involved and not very satisfactory. In addition, some erroneous and misleading statements were made in connection with the results. One of the purposes of the present work is to give a simplified and more satisfactory derivation of the generalized dispersion relations for particles with mass based on a general formulation analogous to that used in G.

In Sec. 2, we shall discuss the scattering of bosons with finite mass by a matter system, the exact nature of which is unimportant. We shall use no specific theory to specify the interaction in detail. Only the usual assumptions of quantum field theory necessary for the definition of an S-matrix are used. Section 3 contains a discussion of the results and a comparison with the work of GGT.

We shall confine our attention in this paper to the scattering of bosons. There are a number of novel features involved in the fermion scattering problem and these will be treated in a separate paper which is being prepared in collaboration with Dr. R. Oehme. We remark only that the dispersion relations derived here do not seem to hold in the case of fermion-fermion scattering processes.

2. DERIVATION OF DISPERSION RELATIONS

We consider the scattering of particles of mass μ, described by a real boson field $\phi_\alpha(x)$, by a matter system, the exact nature of which need not be specified too closely. (We shall assume, however, that it is distinguishable from the projectile field. The difficulties which arise in the case of identical particle scattering will be discussed in Sec. 3.) The index α may designate an internal degree of freedom of the boson field, such as isotopic spin, polarization, etc. The Heisenberg equation of motion for ϕ_α will be taken to be

$$(\mu^2-\Box^2)\phi_\alpha(x)=j_\alpha(x), \quad (2.1)$$

where the "current," $j_\alpha(x)$, will be assumed to depend, perhaps, on $\phi_\alpha(x)$, but on $\dot{\phi}_\alpha(x)$. (To avoid the latter we do not carry out explicit wave function renormaliza-

* Supported in part by a grant from the U. S. Atomic Energy Commission.
[1] Gell-Mann, Goldberger, and Thirring, Phys. Rev. **95**, 1612 (1954); M. L. Goldberger, Phys. Rev. **97**, 508 (1955).

tion; if the above assumption is not correct, or if one wants to do the renormalization at this point, it is simple to generalize the derivations.[2] We assume that ϕ_α is an Hermitian operator. We shall furthermore demand that

$$[j_\alpha(x),j_\beta(y)]=0, \quad (x-y)^2>0, \tag{2.2}$$

which follows from Eq. (2.1) and the requirement that the commutator of two ϕ's taken at space-like points shall vanish. This is our causality condition.

A typical physical situation which could be described by our formalism is the scattering of symmetrical pseudoscalar mesons by nucleons in which case the index α refers to the isotopic spin of the meson field. In the conventional theory, $j_\alpha(x)$ is given by

$$j_\alpha(x)=-ig\bar{\psi}\gamma_5\tau_\alpha\psi+\delta\mu^2\phi_\alpha-\lambda(\phi_\beta\phi_\beta)\phi_\alpha, \tag{2.3}$$

where we have explicitly included the mass and meson-meson interaction renormalizations.

We now calculate the Feynman matrix element for the process in which a particle of four-momentum q, index β, is scattered into a particle of four-momentum k, index α, while the matter system goes from p,λ to p',λ'. The labels λ,λ' mean all quantum numbers beside the four-momenta, p,p' needed to characterize the matter system. This matrix element is given, just as in G, by

$$\mathfrak{F}_{\alpha\beta}(k,q;p'\lambda',p\lambda)=i\int d^4x\int d^4y e^{-ik\cdot x+iq\cdot y}$$
$$\times(\mu^2-\Box_x)(\mu^2-\Box_y)\langle p'\lambda'|(\phi_\alpha(x)\phi_\beta(y))_+|p\lambda\rangle, \tag{2.4}$$

where $(\phi_\alpha(x)\phi_\beta(y))_+$ stands for the familiar P-bracket of $\phi_\alpha(x)$ and $\phi_\beta(y)$. For real particles, $k^2=q^2=-\mu^2$. Carrying out the operations indicated in (2.4), we obtain

$$\mathfrak{F}_{\alpha\beta}(k,q;p'\lambda',p\lambda)=i\int d^4x\int d^4y e^{-ik\cdot x+iq\cdot y}$$
$$\times\langle p'\lambda'|(j_\alpha(x),j_\beta(y))_+-\delta(x_0-y_0)$$
$$\times[j_\alpha(x),\phi_\beta(y)]|p\lambda\rangle. \tag{2.5}$$

It is convenient at this point to assume that

$$j_\alpha(x)=e^{-iP\cdot x}j_\alpha(0)e^{iP\cdot x}, \tag{2.6}$$

where P is the total momentum operator. [It is sufficient to assume that only the time dependence of j_α is given by a relation like (2.6) but the algebra is simplified by the assumption of full translational invariance.] Using Eq. (2.6), we may easily separate from Eq. (2.5) a factor of $(2\pi)^4\delta(p'+k-p-q)$ which expresses the over-all energy momentum conservation. Calling the coefficient of this factor $F_{\alpha\beta}(k,q;p'\lambda',p\lambda)$, we have

$$F_{\alpha\beta}(k,q;p'\lambda',p\lambda)=i\int d^4x e^{-ik\cdot x}\langle p'\lambda'|(j_\alpha(x)j_\beta(0))_+$$
$$-\delta(x_0)[j_\alpha(x),\phi_\beta(0)]|p\lambda\rangle, \tag{2.7}$$

where we must remember the restriction $p'+k=p+q$. We specialize now to the case of forward, but not necessarily coherent scattering, i.e., we put $p'=p$, $q=k$, but allow α and β as well as λ' and λ to be distinct. We write then[3]

$$F_{\alpha\beta}(k;\lambda',\lambda)=i\int d^4x e^{-ik\cdot x}\langle p\lambda'|(j_\alpha(x)j_\beta(0))_+$$
$$-\delta(x_0)[j_\alpha(x),j_\beta(0)]|p\lambda\rangle. \tag{2.8}[4]$$

The state $|p\lambda\rangle$ of the matter system will be assumed to be stable. Under this circumstance we may define a quantity $M_{\alpha\beta}(k;\lambda',\lambda)$ which is fundamentally simpler than $F_{\alpha\beta}(k;\lambda',\lambda)$ and which contains all the same information:

$$M_{\alpha\beta}(k;\lambda',\lambda)\equiv i\int d^4x e^{-ik\cdot x}\langle p\lambda'|\eta(x)[j_\alpha(x),j_\beta(0)]$$
$$-\delta(x_0)[j_\alpha(x),\phi_\beta(0)]|p\lambda\rangle, \tag{2.9}$$

where $\eta(x)$ is the step function, zero for $x_0<0$, unity for $x_0>0$. The relation between $F_{\alpha\beta}(k;\lambda',\lambda)$ and $M_{\alpha\beta}(k;\lambda'\lambda)$ is as follows: If the two quantities be written as a sum of a dispersive and an absorptive part, where the division is made according to whether real or virtual intermediate states are involved, one finds

$$\begin{aligned}F_{\alpha\beta}(k;\lambda',\lambda)&=D_{\alpha\beta}(k;\lambda',\lambda)+i\epsilon(k_0)A_{\alpha\beta}(k;\lambda',\lambda),\\ M_{\alpha\beta}(k;\lambda',\lambda)&=D_{\alpha\beta}(k;\lambda',\lambda)+iA_{\alpha\beta}(k;\lambda',\lambda).\end{aligned} \tag{2.10}$$

Thus, for positive frequencies, k_0, the two quantities are identical, but the absorptive parts differ in sign for negative frequencies. [See the corresponding discussion in GGT, Eqs. (3.12), (3.14), (3.15), (3.16). The notation has been changed slightly: $A\rightarrow\epsilon(k_0)A$.] It should be noted that the quantities D and A are not necessarily real. The great advantage of Eq. (2.9) over Eq. (2.8) for our purposes is that the quantity $\eta(x)[j_\alpha(x),j_\beta(0)]$ is a truly retarded function which vanishes not only for $x_0<0$ but also for $x_\mu^2>0$, according to our causality requirement, Eq. (2.2). As we shall see shortly, this is the key to the whole derivation.

It is convenient at this point to choose a definite Lorentz frame in which to evaluate the quantities

[2] Wave function renormalization must, of course, be carried out in practice eventually. All of the relations to be derived are homogeneous in the scattering amplitude and a multiplicative factor is of no consequence.

[3] The dependence on the momentum p will be suppressed.

[4] We have defined the forward scattering amplitude as the limit of the amplitude for nonforward scattering, as is usually done. Our final formula, however, contains terms which in an actual computation should consequently be dropped, namely, essentially vacuum fluctuation terms in which the state of the matter system is unchanged. We must subtract from the matrix element in Eq. (2.8) $\delta_{\lambda'\lambda}$ times the vacuum expectation value of the same operator. This causes no modification of any of our subsequent results, and to save space we shall not write it explicitly. The author is indebted to Professor Y. Nambu for this observation.

appearing in Eq. (2.10). Since both $F_{\alpha\beta}(k;\lambda',\lambda)$ and $M_{\alpha\beta}(k;\lambda',\lambda)$ are effectively invariants, this entails no loss of generality. We shall choose the system in which $\mathbf{p}$ is zero, the laboratory system. The particular advantage of this system for us is that the k dependence of our quantities F and M is explicitly exhibited in the factor $\exp(-ik\cdot x)$. We may also assume then that the states $|p\lambda\rangle$ has a definite parity.

We wish now to break $M_{\alpha\beta}(k;\lambda',\lambda)$ into its dispersive and absorptive parts and then eventually each of these into parts which are even and odd under interchange of α and β. These operations are facilitated by the observations that

$$M_{\alpha\beta}(\mathbf{k},\omega;\lambda',\lambda)=M_{\alpha\beta}(-\mathbf{k},\omega;\lambda',\lambda), \tag{2.11a}$$

$$\langle p\lambda'|[j_\alpha(-x),j_\beta(0)]|p\lambda\rangle = \langle p\lambda'|[j_\alpha(0),j_\beta(x)]|p\lambda\rangle, \tag{2.11b}$$

where we have written $k_0=\omega$, and, of course, we have $\omega^2=\mathbf{k}^2+\mu^2$. The proof of these statements is elementary: Eq. (2.11a) follows from the observation that the behavior of ϕ_α (and hence of j_α) under reflections is, with $\mathbf{P}$ the parity operator, $\mathbf{P}\phi_\alpha(\mathbf{x},x_0)\mathbf{P}^{-1}=\pm\phi_\alpha(-\mathbf{x},x_0)$, and that $\mathbf{P}|p\lambda\rangle=\exp(i\chi)|p\lambda\rangle$, χ real. Equation (2.11b) follows trivially from the assumed translational invariance, Eq. (2.6). We see from Eq. (2.11a) that $M_{\alpha\beta}(\mathbf{k},\omega;\lambda',\lambda)$ must be an even function of $\mathbf{k}$ and, thus, the $\exp(-i\mathbf{k}\cdot\mathbf{x})$ in Eq. (2.9) may be replaced by $\cos(\mathbf{k}\cdot\mathbf{x})$. The same is true for $F_{\alpha\beta}(\mathbf{k},\omega;\lambda',\lambda)$. These quantities then effectively depend on $\mathbf{k}$ through $\mathbf{k}^2=\omega^2-\mu^2$ and we shall henceforth regard them as functions of ω only. There appear to be no branch points at $\omega=\pm\mu$, although if there were, they would cause no trouble. Finally, we note the very important relation

$$M_{\alpha\beta}(-\omega;\lambda',\lambda)=[M_{\alpha\beta}(\omega;\lambda,\lambda')]^*. \tag{2.11c}$$

If we regard $M_{\alpha\beta}$ as a matrix in the λ',λ labels, we may say that changing ω to $-\omega$ causes $M_{\alpha\beta}$ to go into its Hermitian conjugate. It should be noted that the Feynman amplitude $F_{\alpha\beta}(\omega;\lambda',\lambda)$ *does not* satisfy Eq. (2.11c).

The dispersive and absorptive parts of $M_{\alpha\beta}(\omega;\lambda',\lambda)$ are given, respectively, by

$$D_{\alpha\beta}(\omega;\lambda',\lambda)=\frac{i}{2}\int d^4x e^{i\omega x_0} \times\cos(\mathbf{k}\cdot\mathbf{x})\langle p\lambda'|\epsilon(x)[j_\alpha(x),j_\beta(0)] -2\delta(x_0)[j_\alpha(x),\phi_\beta(0)]|p\lambda\rangle \tag{2.12}$$

and

$$A_{\alpha\beta}(\omega;\lambda',\lambda)=\frac{1}{2}\int d^4x e^{i\omega x_0} \times\cos(\mathbf{k}\cdot\mathbf{x})\langle p\lambda'|[j_\alpha(x),j_\beta(0)]|p\lambda\rangle, \tag{2.13}$$

where we have merely written $\eta(x)=[1+\epsilon(x)]/2$. Now in all conventional theories, the second term in Eq. (2.12) is independent of ω, since the equal time commutator always leads to a factor of $\delta(\mathbf{x})$; furthermore, it is inevitably symmetric in α and β. We shall assume for simplicity that this circumstance always obtains for the remainder of the discussion. Let us separate Eq. (2.12) and Eq. (2.13) into parts which are symmetric and antisymmetric under interchange of α and β. With the understanding that the matrix element between the states $|p\lambda'\rangle$ and $|p\lambda\rangle$ will be eventually formed we may write, using Eq. (2.11b),

$$[j_\alpha(x),j_\beta(0)]=K_{\alpha\beta}^{(-)}(x)+K_{\alpha\beta}^{(+)}(x), \tag{2.14}$$

where

$$\begin{aligned}K_{\alpha\beta}^{(-)}(x)&=\tfrac{1}{2}\{[j_\alpha(x),j_\beta(0)]-[j_\alpha(0),j_\beta(x)]\},\\ K_{\alpha\beta}^{(+)}(x)&=\tfrac{1}{2}\{[j_\alpha(x),j_\beta(0)]+[j_\alpha(0),j_\beta(x)]\}.\end{aligned} \tag{2.15}$$

Note that $K_{\alpha\beta}^{(-)}(x)$ is an odd function of x whereas $K_{\alpha\beta}^{(+)}(x)$ is even. Furthermore,

$$\begin{aligned}K_{\alpha\beta}^{(-)}(x)&=K_{\beta\alpha}^{(-)}(x),\\ K_{\alpha\beta}^{(+)}(x)&=-K_{\beta\alpha}^{(+)}(x).\end{aligned} \tag{2.16}$$

By using Eqs. (2.15) and (2.16), the separation of Eqs. (2.12) and (2.13) into symmetric and antisymmetric parts is easily carried out. We write

$$D_{\alpha\beta}(\omega;\lambda',\lambda)=D_{\alpha\beta}^{(1)}(\omega;\lambda',\lambda)+iD_{\alpha\beta}^{(2)}(\omega;\lambda',\lambda), \tag{2.17}$$

$$A_{\alpha\beta}(\omega;\lambda',\lambda)=A_{\alpha\beta}^{(1)}(\omega;\lambda',\lambda)+iA_{\alpha\beta}^{(2)}(\omega;\lambda',\lambda), \tag{2.18}$$

where

$$D_{\alpha\beta}^{(1)}(\omega;\lambda',\lambda)=\frac{i}{2}\int d^4x\cos\mathbf{k}\cdot\mathbf{x} \times\cos\omega x_0\langle p\lambda'|\epsilon(x)K_{\alpha\beta}^{(-)}(x) -2\delta(x_0)[j_\alpha(x),\phi_\beta(0)]|p\lambda\rangle, \tag{2.19}$$

$$D_{\alpha\beta}^{(2)}(\omega;\lambda',\lambda)=\frac{i}{2}\int d^4x\cos\mathbf{k}\cdot\mathbf{x} \times\sin\omega x_0\langle p\lambda'|\epsilon(x)K_{\alpha\beta}^{(+)}(x)|p\lambda\rangle, \tag{2.20}$$

$$A_{\alpha\beta}^{(1)}(\omega;\lambda',\lambda)=\frac{i}{2}\int d^4x\cos\mathbf{k}\cdot\mathbf{x} \times\sin\omega x_0\langle p\lambda'|K_{\alpha\beta}^{(-)}(x)|p\lambda\rangle, \tag{2.21}$$

$$A_{\alpha\beta}^{(2)}(\omega;\lambda',\lambda)=-\frac{i}{2}\int d^4x\cos\mathbf{k}\cdot\mathbf{x} \times\cos\omega x_0\langle p\lambda'|K_{\alpha\beta}^{(+)}(x)|p\lambda\rangle. \tag{2.22}$$

By construction, the quantities labeled with superscript 1 are symmetric in α and β, while those labeled 2 are antisymmetric. All four quantities are hermitian matrices in the λ', λ space. Note that regarded as functions of the frequency, ω, $D^{(1)}$ and $A^{(2)}$ are even functions whereas $D^{(2)}$ and $A^{(1)}$ are odd. If $\lambda'=\lambda$, all four quantities are real. Finally, we see that the integrations over x_0 may be restricted to positive values only.

There is one further step which must be taken before we proceed to the derivation of the dispersion relations.

We must investigate the nature of whatever singularities might be expected for real values of ω for the function $A_{\alpha\beta}(\omega;\lambda',\lambda)$. To simplify the writing, we will not at this point separate A into its two parts as we did previously. We simply expand the matrix element in Eq. (2.13) into a complete set of states for the interacting systems and obtain, after carrying out the x_0 integration,

$$A_{\alpha\beta}(\omega;\lambda',\lambda)=\pi\sum_n[f_{\alpha\beta}(\omega,n;\lambda',\lambda)\delta(E_p-E_n+\omega) -f_{\alpha\beta}^*(\omega,n;\lambda,\lambda')\delta(E_p-E_n-\omega)], \quad (2.23)$$

where

$$f_{\alpha\beta}(\omega,n;\lambda',\lambda)=\int d^3x e^{-i\mathbf{k}\cdot\mathbf{x}} \times\langle p\lambda'|j_\alpha(\mathbf{x})|n\rangle\langle n|j_\beta(0)|p\lambda\rangle. \quad (2.24)$$

We note that unless there are discrete bound states of energy $E_n=E_p+\mu-B_n$, $B_n>0$, $A_{\alpha\beta}(\omega;\lambda',\lambda)$ is zero for $|\omega|<\mu$. This point was overlooked in GGT and was pointed out to the author by F. Low and Y. Nambu, independently. It has been further discussed by Karplus and Ruderman in a recent paper.[5] It is clear from Eq. (2.23) that there will be branch points for values of $|\omega|>\mu$ corresponding to the thresholds for real reactions.

Consider now the quantity $I_{\alpha\beta}(\omega,\omega_0;\lambda',\lambda)$ defined by

$$I_{\alpha\beta}(\omega,\omega_0;\lambda',\lambda)\equiv\frac{\omega^2-\omega_0^2}{\pi}\int_{-\infty}^{\infty}d\omega' \times\frac{A_{\alpha\beta}^{(1)}(\omega';\lambda',\lambda)+iA_{\alpha\beta}^{(2)}(\omega';\lambda',\lambda)}{(\omega'-\omega_0)(\omega'^2-\omega^2)}. \quad (2.25)$$

The integrations over the singularities are to be taken in sense of Cauchy principal values and the branch points mentioned above are to be detoured by small semicircles into the upper half plane. From the nature of the ω dependence in the neighborhood of any such threshold point, it is clear that as the semicircles are shrunk to zero, they make no contribution to the integral. The only role played by the branch points is to determine the phase of $A_{\alpha\beta}(\omega';\lambda',\lambda)$ on either side of them. The frequencies ω, ω_0 are arbitrary, but we shall take them to be greater than or equal to μ. We shall now substitute for $A_{\alpha\beta}(\omega';\lambda',\lambda)$ its value as given by Eqs. (2.18), (2.21), and (2.22), and *interchange the order of integration*. Recall now that the space-time integrations in these expressions for the absorptive parts extend over the interior and surface of the future light cone. As long as $x_0>|\mathbf{x}|$, the proposed interchange may be probably justified without too great difficulty, since the contributions to $A_{\alpha\beta}(\omega';\lambda',\lambda)$ from these regions approach zero for large ω. (This assumes that the quantities $\langle p\lambda'|K_{\alpha\beta}^{(\pm)}(x)|p\lambda\rangle$ are reasonably well behaved, which is an assumption which underlies all field theoretic calculations. If this is so, then since $x_0>|\mathbf{x}|$, we always have an oscillatory integrand which will make the integral go to zero as $|\omega|\to\infty$.) The contributions from the light cone itself cannot be neglected since we must be prepared for very singular behavior of our matrix element, such as being proportional to $\delta(x^2)$ or even derivatives thereof. It is, of course, the high-frequency behavior which will be determined from the matrix elements on the light cone, and we must assume that we have supplied a sufficient number of inverse powers of ω to make our procedure legitimate. We shall return to this point later in the discussion.

If the above outlined steps are carried out, we obtain,

$$I_{\alpha\beta}(\omega,\omega_0;\lambda',\lambda)=i\int_0^\infty dx_0\int d^3x \times[\langle p\lambda'|K_{\alpha\beta}^{(-)}(x)|p\lambda\rangle J^{(1)}(x;\omega,\omega_0) +\langle p\lambda'|K_{\alpha\beta}^{(+)}(x)|p\lambda\rangle iJ^{(2)}(x;\omega,\omega_0)], \quad (2.26)$$

where

$$J^{(1)}(x;\omega,\omega_0)=\frac{\omega^2-\omega_0^2}{\pi}\int_{-\infty}^{\infty}d\omega'\frac{\omega'\sin\omega' x_0\cos\mathbf{k}'\cdot\mathbf{x}}{(\omega'^2-\omega_0^2)(\omega'^2-\omega^2)}, \quad (2.27)$$

$$J^{(2)}(x;\omega,\omega_0)=-\frac{\omega^2-\omega_0^2}{\pi}\int_{-\infty}^{\infty}d\omega' \times\frac{\cos\omega' x_0\cos\mathbf{k}'\cdot\mathbf{x}}{(\omega'^2-\omega_0^2)(\omega'^2-\omega^2)}. \quad (2.28)$$

These integrals may be evaluated by elementary contour integration following the replacement of $\sin\omega x_0$ by $-i\exp(i\omega x_0)$ and $\cos\omega x_0$ by $\exp(i\omega x_0)$, since for $x_0>|\mathbf{x}|$, these factors dominate the integrands, and even for $x_0=|\mathbf{x}|$, $\exp(i\omega x_0)\cos\mathbf{k}'\cdot x$ is bounded, and we have supplied enough inverse powers of ω that the usual infinite semicircle in the upper half ω plane makes no contribution. We obtain then

$$J^{(1)}(x;\omega,\omega_0)=\cos\omega x_0\cos\mathbf{k}\cdot\mathbf{x}-\cos\omega_0 x_0\cos\mathbf{k}_0\cdot\mathbf{x}, \quad (2.29)$$

$$J^{(2)}(x;\omega,\omega_0)=(\omega_0/\omega)\sin\omega x_0\cos\mathbf{k}\cdot\mathbf{x} -\sin\omega_0 x_0\cos\mathbf{k}_0\cdot\mathbf{x}. \quad (2.30)$$

Substituting these equations into Eq. (2.26) and comparing with Eqs. (2.19) and (2.20), we find

$$I_{\alpha\beta}(\omega,\omega_0;\lambda',\lambda)=D_{\alpha\beta}^{(1)}(\omega;\lambda',\lambda)-D_{\alpha\beta}^{(1)}(\omega_0;\lambda',\lambda) +i[(\omega_0/\omega)D_{\alpha\beta}^{(2)}(\omega;\lambda',\lambda)-D_{\alpha\beta}^{(2)}(\omega_0;\lambda',\lambda)], \quad (2.31)$$

where we have assumed that the second term in Eq. (2.19) is a constant, independent of frequency. Since the quantities with superscript 1 (2) are symmetric (antisymmetric) under interchange of α and β, we may separate Eq. (2.31) into two distinct parts:

$$D_{\alpha\beta}^{(1)}(\omega;\lambda',\lambda)-D_{\alpha\beta}^{(1)}(\omega_0;\lambda',\lambda) =\frac{2(\omega^2-\omega_0^2)}{\pi}\int_0^\infty d\omega'\omega'\frac{A_{\alpha\beta}^{(1)}(\omega';\lambda',\lambda)}{(\omega'^2-\omega_0^2)(\omega'^2-\omega^2)}, \quad (2.32)$$

$$D_{\alpha\beta}^{(2)}(\omega;\lambda',\lambda)-\frac{\omega}{\omega_0}D_{\alpha\beta}^{(2)}(\omega_0;\lambda',\lambda) =\frac{2\omega(\omega^2-\omega_0^2)}{\pi}\int_0^\infty d\omega'\frac{A_{\alpha\beta}^{(2)}(\omega';\lambda',\lambda)}{(\omega'^2-\omega_0^2)(\omega'^2-\omega^2)}. \quad (2.33)$$

[5] R. Karplus and M. Ruderman, Phys. Rev. **98**, 771 (1955).

We have used the fact that $A_{\alpha\beta}^{(1)}$ is an even function of ω while $A_{\alpha\beta}^{(2)}$ is odd in rewriting the definition of $I_{\alpha\beta}$, Eq. (2.25). These are the generalized dispersion relations appropriate for particles with mass. They correspond to Eqs. (5.13) of GGT, and in fact coincide with them in the limit $\mu \to 0$.

Our final task is to express the integrals appearing in Eqs. (2.32) and (2.33) in terms of physical quantities in so far as it is possible. We recall that our fundamental quantity, $M_{\alpha\beta}(\omega;\lambda',\lambda)$, becomes identical with the Feynman matrix element, $F_{\alpha\beta}(\omega;\lambda',\lambda)$, for $\omega>0$. The relation between this quantity and the true forward scattering amplitude for elastic scattering, $T_{\alpha\beta}(\omega;\lambda',\lambda)$, in general depends the choice of a Lorentz frame. For any two particle scattering process, $T_{\alpha\beta}(\omega;\lambda',\lambda)=F_{\alpha\beta}(\omega';\lambda',\lambda)$ for the laboratory system in which the target is initially at rest, to within a constant factor.[6] In virtue of the fact that $T_{\alpha\beta}(\omega;\lambda',\lambda)/|\mathbf{k}|$ is an invariant we may easily convert our forward scattering amplitudes to the center-of-mass system: $[T_{\alpha\beta}]_{\text{lab}} = (W/M)[T_{\alpha\beta}]_{\text{c.m.}}$, where W is the total energy in the center-of-mass frame and M is the mass of the target. We know also that for $\omega>\mu$, the absorptive parts of $T_{\alpha\beta}$ are related to what we may loosely refer to as total cross sections by the so-called optical theorem. In general only the portion $A_{\alpha\beta}^{(1)}(\omega;\lambda,\lambda)$ which is symmetric in α and β is related to a true physical cross section but under some circumstances $A_{\alpha\beta}^{(2)}(\omega;\lambda,\lambda)$ may also be so identified. For the energy interval $0\leq\omega<\mu$, we shall use the expression Eq. (2.23) for $A_{\alpha\beta}(\omega;\lambda',\lambda)$, appropriately broken into its symmetric and antisymmetric parts:

$$A_{\alpha\beta}^{(1)}(\omega;\lambda',\lambda)=\pi\sum_n\{f_{\alpha\beta}^{(+)}(\omega,n;\lambda',\lambda)\delta(E_p-E_n+\omega) - f_{\alpha\beta}^{(+)*}(\omega,n;\lambda',\lambda)\delta(E_p-E_n-\omega)\}, \tag{2.34}$$

$$A_{\alpha\beta}^{(2)}(\omega;\lambda',\lambda)=\pi\sum_n\{f_{\alpha\beta}^{(-)}(\omega,n;\lambda',\lambda)\delta(E_p-E_n+\omega) + f_{\alpha\beta}^{(-)*}(\omega,n;\lambda',\lambda)\delta(E_p-E_n-\omega)\},$$

where

$$f_{\alpha\beta}^{(+)}(\omega,n;\lambda',\lambda) =[f_{\alpha\beta}(\omega,n;\lambda'\lambda)+f_{\beta\alpha}(\omega,n;\lambda',\lambda)]/2, \tag{2.35}$$

$$f_{\alpha\beta}^{(-)}(\omega,n;\lambda',\lambda) =[f_{\alpha\beta}(\omega,n;\lambda',\lambda)-f_{\beta\alpha}(\omega,n;\lambda',\lambda)]/2i.$$

We now write Eqs. (2.32) and (2.33) in terms of total cross sections and bound state contributions by using for $A_{\alpha\beta}^{(1)}$ and $A_{\alpha\beta}^{(2)}$ the above expressions for $0<\omega<\mu$ and for $\omega>\mu$, we define two "cross sections," $\sigma_{\alpha\beta}^{(1)}(\omega,\lambda)$ and $\sigma_{\alpha\beta}^{(2)}(\omega,\lambda)$, by

$$\sigma_{\alpha\beta}^{(1)}(\omega;\lambda)=(4\pi/k)A_{\alpha\beta}^{(1)}(\omega;\lambda,\lambda), \tag{2.36}$$

$$\sigma_{\alpha\beta}^{(2)}(\omega;\lambda)=(4\pi/k)A_{\alpha\beta}^{(2)}(\omega;\lambda,\lambda). \tag{2.37}$$

We have set $\lambda'=\lambda$, for it is only when one has not changed the state of the scatterer that one has the coherence necessary for the optical theorem to hold. We have also written $|\mathbf{k}|=k$, $k^2=\omega^2-\mu^2$. It is convenient to introduce the wave number as the variable of integration and we find, using the same letter to designate now fundtions of k as we had previously used for functions of ω, the results

$$D_{\alpha\beta}^{(1)}(k;\lambda)-D_{\alpha\beta}^{(1)}(k_0;\lambda)=\frac{k^2}{2\pi^2}\int_0^\infty dk'\frac{\sigma_{\alpha\beta}^{(1)}(k';\lambda)}{k'^2-k^2} -\frac{k_0^2}{2\pi^2}\int_0^\infty dk'\frac{\sigma_{\alpha\beta}^{(1)}(k';\lambda)}{k'^2-k_0^2}+2\sum_n(E_n-E_p)\cdot \times f_{\alpha\beta}^{(+)}(E_n-E_p,n;\lambda)\left[\frac{1}{(E_n-E_p)^2-k^2-\mu^2} -\frac{1}{(E_n-E_p)^2-k_0^2-\mu^2}\right], \tag{2.38}$$

$$D_{\alpha\beta}^{(2)}(k;\lambda)-\frac{\omega}{\omega_0}D_{\alpha\beta}^{(2)}(k_0;\lambda)=\frac{\omega k^2}{2\pi^2}\int_0^\infty\frac{dk'}{\omega'}\frac{\sigma_{\alpha\beta}^{(2)}(k';\lambda)}{k'^2-k^2} -\frac{\omega k_0^2}{2\pi^2}\int_0^\infty\frac{dk'}{\omega'}\frac{\sigma_{\alpha\beta}^{(2)}(k';\lambda)}{k'^2-k_0^2}+2\omega\sum_n f_{\alpha\beta}^{(-)}(E_n-E_p,n;\lambda) \times\left[\frac{1}{(E_n-E_p)^2-k^2-\mu^2}-\frac{1}{(E_n-E_p)^2-k_0^2-\mu^2}\right]. \tag{2.39}$$

The sums extend over those states $|n\rangle$ for which $E_n-E_p\leq\mu$.[7] The most natural reference energy is $k_0=0$, in which case our formulas take their final form:

$$D_{\alpha\beta}^{(1)}(k;\lambda)-D_{\alpha\beta}^{(1)}(0;\lambda)=\frac{k^2}{2\pi^2}\int_0^\infty dk'\frac{\sigma_{\alpha\beta}^{(1)}(k';\lambda)}{k'^2-k^2} +2\sum_n(E_n-E_p)f_{\alpha\beta}^{(+)}(E_n-E_p,n;\lambda) \times\left[\frac{1}{(E_n-E_p)^2-k^2-\mu^2}-\frac{1}{(E_n-E_p)^2-\mu^2}\right], \tag{2.40}$$

$$D_{\alpha\beta}^{(2)}(k;\lambda)-\frac{\omega}{\mu}D_{\alpha\beta}^{(2)}(0;\lambda)=\frac{k^2\omega}{2\pi^2}\int_0^\infty\frac{dk'}{\omega'}\frac{\sigma_{\alpha\beta}^{(2)}(k')}{k'^2-k^2} +2\omega\sum_n f_{\alpha\beta}^{(-)}(E_n-E_p,n;\lambda) \times\left[\frac{1}{(E_n-E_p)^2-k^2-\mu^2}-\frac{1}{(E_n-E_p)^2-\mu^2}\right]. \tag{2.41}$$

[6] In meson-nucleon scattering, for example, $F_{\alpha\beta}=4\pi T_{\alpha\beta}$ if we use Heaviside units for the meson field; with Gaussian units, $F_{\alpha\beta}=T_{\alpha\beta}$.

[7] We have included in the bound state contribution only terms arising from the singularities associated with the first δ function Eq. (2.34). These correspond to true discrete bound states of energy $M<E_n<M+\mu$. It is also possible for the argument of the second δ function to vanish and in fact in the case of meson-nucleon scattering it is only this second δ function which makes a "bound state" contribution. It is not a true bound state, of course; however when the energy of the meson is continued below the rest energy, and the state $|n\rangle$ corresponds to a one-nucleon state, we indeed find a singularity in the scattering amplitude. This point is discussed in the paper on meson-nucleon scattering which immediately follows this one.

A typical application of these generalized Kramers-Kronig relations is to the problem of meson nucleon scattering. We shall treat this case in detail in a separate paper, so at this time we merely mention the physical significance of $D^{(1)}$, $D^{(2)}$, $\sigma^{(1)}$ and $\sigma^{(2)}$: $D^{(1)}(D^{(2)})$ is one half the sum (difference) of the dispersive forward amplitudes for π^-+p and π^++p (ordinary) scattering and consequently $\sigma^{(1)}(\sigma^{(2)})$ is one half the sum (difference) of the total $\pi^{(-)}$ and $\pi^{(+)}$ cross sections for all processes. These results follow from the fact that the total forward scattering amplitude, regarded as a matrix in nucleon charge space, may be written as

$$T_{\alpha\beta}(\omega)=\delta_{\alpha\beta}T^{(1)}(\omega)+i\epsilon_{\alpha\beta\gamma}\tau_\gamma T^{(2)}(\omega), \quad (2.42)$$

assuming, of course, symmetrical theory, and

$$T^{(j)}(\omega)=D^{(j)}(\omega)+i\epsilon(\omega)A^j(\omega), \quad j=1,2. \quad (2.43)$$

There is a bound state corresponding to the neutron whose contribution may be calculated from meson theory almost exactly (to within terms of order $(\mu/M)^2$); numerically, it is a very important effect.

3. DISCUSSION AND COMPARISON WITH GGT

The actual simplicity of the derivation of the generalized dispersion relations, Eqs. (2.40) and (2.41) has probably been obscured by the algebraic details. For this reason it is perhaps worthwhile to summarize the procedure. We first observed that the Feynman matrix element describing the scattering event could be replaced by a quantity which was the Fourier transform of a function which vanished everywhere except inside the future light cone. This new quantity was divided into two parts one of which satisfied the relation $M^{(1)}(-\omega;\lambda)=[M^{(1)}(\omega;\lambda)]^*$ and the other satisfied $M^{(2)}(-\omega;\lambda)=-[M^{(2)}(\omega;\lambda)]^*$.[8] An integral operation, Eq. (2.25), was applied to the absorptive part of $M^{(1)}+iM^{(2)}$ and the two dispersion relations (2.32) and (2.33) emerged. The remainder of the task was to express these results in terms of physical quantities. There are, however, a number of points concerning the final relations which should be discussed further.

The reason for the special role played by the forward scattering amplitude would appear to be the fact that the entire k-dependence, as given, say, by Eq. (2.9) occurs in the explicit $\exp(-ik\cdot x)$, whereas if $p'\neq p$, but instead $p'=p+q-k$, the k dependence becomes much more complicated. In this connection, it should be noted that the dispersion relations which we have derived cannot necessarily be expected to hold without modification for identical particle scattering processes, since the forward amplitude for such events is a linear combination of forward and backward scatterings for nonidentical particles and the backward amplitude does not satisfy the normal relations. This point will be taken up in more detail in connection with fermion-fermion scattering in another paper. The problem of finding dispersion relations for other than forward scattering is being studied further.

In this paper we avoided explicit mention of the behavior of the forward scattering amplitude or rather our quantity $M_{\alpha\beta}(\omega;\lambda',\lambda)$, in the complex ω plane. The use of complex variable theory does not appear to add anything to our understanding, although it is certainly true that a sufficient condition for the existence of our general dispersion relations is that $M_{\alpha\beta}(\omega;\lambda',\lambda)$ be the boundary value of a function which is analytic in the upper half plane, together with certain boundedness requirements. Our "boundedness requirement" had to do with the legitimacy of the interchanging of certain orders of integration. Because of the fact that principal value integrals are rather singular, the conventional theorems on such matters are not immediately applicable. However reference to our integral operation, Eq. (2.25), shows that at the point where the operation is really singular, namely if $\omega=\omega_0$, we have the factor $(\omega^2-\omega_0^2)$ in front which is then zero, and thus the singularity is removed. The remaining troublesome point that is involved is the behavior of the scattering amplitude for large frequencies. That this is indeed the case was borne out by examples in which the results of the two orders of integration were compared. Our particular form of the dispersion relations, Eqs. (2.40) and (2.41) would appear to be valid provided $\sigma_{\alpha\beta}^{(1)}(\omega;\lambda)/\omega$ and $\sigma_{\alpha\beta}^{(2)}(\omega;\lambda)/\omega^2$ tend to zero for $\omega\to\infty$. The behavior of scattering amplitudes at high energies is of central importance in field theory and it should be clearly recognized that the precise form of any dispersion relation depends on this (unknown) high-energy behavior. Violations of the dispersion relations as given might perhaps be interpreted as an error in the assumed behavior, although it is certainly possible that it means that our original causality requirement, Eq. (2.2), has perhaps broken down at small distances.

It is interesting to see what happens if we make our high-frequency assumption more stringent. For simplicity we confine our remarks to the completely coherent amplitude, i.e., $\alpha=\beta,\lambda',\lambda$, and assume that there are no bound states. Further, assume that the second (and usually constant) term in Eq. (2.9) is absent. A physical model which satisfies these conditions is provided by ordinary quantum electrodynamics. We shall assume that $\int^\infty d\omega\sigma_{\alpha\alpha}^{(1)}(\omega;\lambda)$ is bounded, i.e., $\omega\sigma_{\alpha\alpha}^{(1)}(\omega;\lambda)\to 0$ as $\omega\to\infty$. Under these circumstances we may consider, instead of Eq. (2.25), a quantity $I_{\alpha\alpha'}$, defined by

$$I_{\alpha\alpha'}(\omega;\omega_0;\lambda)\equiv\frac{\omega^2-\omega_0^2}{\pi}\int_{-\infty}^{\infty}d\omega'\frac{\omega'^2A_{\alpha\alpha}^{(1)}(\omega';\lambda)}{(\omega'^2-\omega_0^2)(\omega'^2-\omega^2)}. \quad (3.1)$$

[8] Note that it is M, rather than the Feynman amplitude (which is essentially the same as the scattering amplitude) which has these simple properties and which is the fundamental quantity for our purposes.

This quantity is evaluated, as before, with the result

$$I_{aa}'(\omega,\omega_0;\lambda)=\omega^2 D_{aa}^{(1)}(\omega;\lambda)-\omega_0^2 D_{aa}^{(1)}(\omega_0;\lambda_0), \quad (3.2)$$

and following the same steps which led to Eqs. (2.40) and (2.41), we find

$$D_{aa}^{(1)}(k;\lambda)-\frac{\mu^2}{\omega^2}D_{aa}^{(1)}(0;\lambda)-\frac{1}{2\pi^2}\frac{k^2}{\omega^2}\int_0^\infty dk\sigma_{aa}^{(1)}(k;\lambda)$$
$$=\frac{k^2}{2\pi^2}\int_0^\infty dk'\frac{\sigma_{aa}^{(1)}(k;\lambda)}{k'^2-k^2}. \quad (3.3)$$

Evidently, if (3.3) is valid, so is (2.40) and comparison of the two shows that

$$D_{aa}^{(1)}(0;\lambda)=\frac{1}{2\pi^2}\int_0^\infty dk\sigma_{aa}^{(1)}(k;\lambda). \quad (3.4)$$

Consider now the scattering of photons by free electrons. We know that $D_{aa}^{(1)}(0;\lambda)=-e^2/m$, where e and m are the physical charge and mass of the electron. Thus, Eq. (3.4) cannot be satisfied and we must conclude that the assumed existence of $\int^\infty dk\sigma_{aa}^{(1)}(k;\lambda)$ is incorrect. All indications from perturbation theory lead one to believe that the integral diverges, nevertheless it is interesting that a rigorous demonstration of the fact may be given. It should be noted that although we have proved that Eq. (3.3) is not applicable in quantum electrodynamics, we have not established the correctness of Eq. (2.40).

Before concluding, we must make a few remarks on the relation between the results of the present paper and those of GGT. For the case of photon scattering, they are identical. However, for the case of particles with mass, aside from the bound states which were assumed absent by them, their formula, namely,

$$D_{aa}^{(1)}(\omega;\lambda)-D_{aa}^{(1)}(\omega=0;\lambda)$$
$$=\frac{2\omega^2}{\pi}\int_0^\infty d\omega'\frac{A_{aa}^{(1)}(\omega';\lambda)}{\omega'(\omega'^2-\omega^2)}, \quad (3.5)$$

corresponds to choosing the ω_0 of the previous section equal to zero, instead of μ, as we have done. As has been remarked earlier, if there are no bound states, the lower limit of the integral should be set equal to μ. Then, changing to the wave number as variable, we may rewrite Eq. (3.5) as

$$D_{aa}^{(1)}(k;\lambda)-D_{aa}^{(1)}(k^2=-\mu^2;\lambda)$$
$$=\frac{k^2}{2\pi^2}\int_0^\infty dk'\frac{\sigma_{aa}^{(1)}(k')}{k'^2-k^2}+\frac{\mu^2}{2\pi^2}\int_0^\infty dk'\frac{\sigma_{aa}^{(1)}(k')}{k'^2+\mu^2}, \quad (3.6)$$

which perhaps illustrates more clearly the choice of $\omega_0=0$ as reference energy.

The derivation of the dispersion relations which we have given here is based on the formalism of present day quantum field theory. It would appear, however, to make use only of the essentially minimal features of the theory, which we would abandon only with extreme reluctance, such as Lorentz invariance, and the concept of the S-matrix. If one were to assume that our condition on the vanishing of the commutator of the currents at space like points were too stringent, and instead should be replaced by the requirement of vanishing for space-like separations greater than a certain fundamental length, the dispersion relations would be modified in an essential manner. We shall not discuss these modifications here, but merely remark that there are complications similar to those which arise when one considers the scattering amplitudes for individual angular momenta.

ACKNOWLEDGMENTS

The derivation presented here is one whose existence was conjectured by Dr. M. Gell-Mann and the author several years ago and various aspects of this early work with Dr. Gell-Mann appear throughout the paper. The author is also indebted to Professor Y. Nambu and to Dr. H. Miyazawa and Dr. R. Oehme for many very helpful suggestions.

Note added in proof.—It has been pointed out to the author by Professor R. Karplus (private communication) that in the derivation of the dispersion relation, Eq. (3.3), we have effectively assumed that not only does $\sigma_{aa}^{(1)}(k)$ go to zero faster than $1/k$ for large k, but also that $D_{aa}(k)$ also approaches zero. This may be seen by comparing Eq. (3.4) with the limit as k goes to infinity of Eq. (2.40), dropping the bound states. We cannot, however, exclude the possibility of $D_{aa}^{(1)}(k,\lambda)$ approaching a constant in which case there need be no contradiction, since $D_{aa}^{(1)}(0)-D_{aa}^{(1)}(\infty)$ may be positive and equal to the right-hand side of Eq. (3.4). It is the author's opinion that this is not the case and that the conclusion drawn in the text is correct.

Application of Dispersion Relations to Pion-Nucleon Scattering*

M. L. GOLDBERGER, H. MIYAZAWA, AND R. OEHME
Institute for Nuclear Studies, University of Chicago, Chicago, Illinois
(Received April 20, 1955)

The generalized Kramers-Kronig dispersion relations for charged bosons are used to treat the problem of pion-nucleon scattering. The complications associated with the charge of the pions are discussed. The importance of a "bound state" corresponding to the neutron is emphasized and its constrbution to the scattering amplitude is computed rigorously, assuming only that pions are pseudoscalar and that the interaction with nucleons is charge-independent. The connection between our exact dispersion relations and the approximate equations for pion-nucleon scattering given by Low is discussed. A rigorous effective-range relation is derived.

1. INTRODUCTION

IN the preceding paper,[1] a new derivation of dispersion relations of the Kramers-Kronig type has been given which is of sufficient generality that the problem of the scattering of charged pions by nucleons may be treated. In the present paper we wish to specialize the results of I to this case and cast them into a form suitable for comparison with experiment. The application of dispersion relations to pion-nucleon scattering was first suggested by R. Karplus and M. Ruderman (preprint, January, 1955). Their results, however, could not be applied to the description of the scattering of charged pions by protons. In view of the importance of this tool in the analysis of experimental data, it was felt worth while to discuss the problem in detail.

In Sec. 2, we shall give the explicit formulas appropriate for the description of the scattering of positive and negative pions by protons. There appears in these dispersion relations a term corresponding to a rather unusual bound state, the neutron, whose contribution may be expressed in terms of the strength of the pion-nucleon interaction. In Sec. 3, the results will be discussed and the connection between our work and that of Low[2] will be developed.

2. DISPERSION RELATIONS FOR PION-NUCLEON SCATTERING

The general dispersion relations given in I must now be written explicitly for the case of pion-nucleon scattering. Regarded as a matrix in nucleon isotopic spin space, the forward-scattering amplitude describing the scattering of a meson with isotopic spin index β into one with isotopic spin index α ($\alpha, \beta = 1, 2, 3$) may be written as

$$T_{\alpha\beta}(\omega) = \delta_{\alpha\beta} T^{(1)}(\omega) + \tfrac{1}{2}[\tau_\alpha, \tau_\beta] T^{(2)}(\omega), \qquad (2.1)$$

where ω is the total meson energy in the laboratory system and we have assumed charge independence. Both $T^{(1)}$ and $T^{(2)}$ have a dispersive and an absorptive part:

$$T^{(j)}(\omega) = D^{(j)}(\omega) + i\epsilon(\omega) A^{(j)}(\omega), \quad j = 1,2. \qquad (2.2)$$

We have introduced the factor $\epsilon(\omega)$ in order that our notation coincide with that of I. We consider here only positive energies, so it is of no importance. In place of the representation we have been using it is convenient to introduce the amplitudes for pure isotopic spin states, namely

$$\begin{aligned} T^{\frac{1}{2}}(\omega) &= T^{(1)}(\omega) - T^{(2)}(\omega), \\ T^{\frac{3}{2}}(\omega) &= T^{(1)}(\omega) + 2T^{(2)}(\omega). \end{aligned} \qquad (2.3)$$

We have assumed that the nucleon charge state does not change and we shall assume that it is a proton. It follows immediately from Eq. (2.3) that

$$\begin{aligned} T^{(1)}(\omega) &= \tfrac{1}{2}[T_-(\omega) + T_+(\omega)], \\ T^{(2)}(\omega) &= \tfrac{1}{2}[T_-(\omega) - T_+(\omega)], \end{aligned} \qquad (2.4)$$

where $T_\pm(\omega)$ are the forward amplitudes for the coherent scattering of $\pi^\pm$ mesons by protons, i.e., $\pi^+ \to \pi^+$, $\pi^- \to \pi^-$. We note that the four quantities $D^{(j)}$ and $A^{(j)}$ are real since the nucleon charge is not changed. [See discussion following I-(2.22).] Thus $D^{(j)}$ and $A^{(j)}$ are respectively the real and imaginary parts of the forward scattering amplitudes defined by Eq. (2.4). Since we have our simple dispersion relations [I-(2.40), I-(2.41)] only for the quantities $D^{(j)}$ and $A^{(j)}$, it is evident that neither the pure isotopic spin amplitudes nor the charged meson amplitudes satisfy them separately. The mathematical reason is, of course, that these more physical amplitudes have no simple behavior of evenness or oddness when $\omega \to -\omega$. We shall return to this point later in the discussion.

We now write the dispersion relations for $T^{(1)}$ and $T^{(2)}$ in the following form:

$$\tfrac{1}{2}[D_-(\omega) + D_+(\omega)] - \tfrac{1}{2}[D_-(\mu) + D_+(\mu)] = \frac{2(\omega^2 - \mu^2)}{\pi} \int_0^\infty d\omega' \frac{\omega' \tfrac{1}{2}[A_-(\omega') + A_+(\omega')]}{(\omega'^2 - \mu^2)(\omega'^2 - \omega^2)}, \qquad (2.5)$$

$$\tfrac{1}{2}[D_-(\omega) - D_+(\omega)] - \frac{\omega}{\mu} \tfrac{1}{2}[D_-(\mu) - D_+(\mu)] = \frac{2\omega(\omega^2 - \mu^2)}{\pi} \int_0^\infty d\omega' \frac{\tfrac{1}{2}[A_-(\omega) - A_+(\omega')]}{(\omega'^2 - \mu^2)(\omega'^2 - \omega^2)}. \qquad (2.6)$$

* Supported in part by a grant from the U. S. Atomic Energy Commission.

[1] M. L. Goldberger, preceding paper [Phys. Rev. **99**, 979 (1955)]; hereafter referred to as I.

[2] F. E. Low, Phys. Rev. **97**, 1392 (1955).

These are just Eqs. I-(2.32) and I-(2.33), with $\omega_0=\mu$. We have introduced the obvious notation $T_\pm(\omega)=D_\pm(\omega)+i\epsilon(\omega)A_\pm(\omega)$. Recall that the integrations over the singularities are to be carried out in the sense of Cauchy principal values. All quantities appearing in Eqs. (2.5) and (2.6) are to be computed in the laboratory system in which the proton is initially at rest.

For the region of integration extending from μ to ∞, we have the relations

$$\sigma_\pm(\omega)=(4\pi/k)A_\pm(\omega), \tag{2.7}$$

where $k=(\omega^2-\mu^2)^{\frac{1}{2}}$ and $\sigma_\pm(\omega)$ are the total cross sections for all processes originating from positive or negative pions incident upon a proton. In the integration region $0\leq\omega<\mu$, there is a contribution from a "bound state" corresponding to an intermediate state consisting of a neutron. This may be computed almost exactly from meson theory.

To find the bound state contribution we write out the amplitudes $A_\pm(\omega)$ as sums over a complete set of states, following I-(2.23), modified of course approximately to describe our charged-meson amplitudes:

$$A_\pm(\omega)=\pi\sum_{n,\,p_n=k}\{|\langle n|j_\pm(0)|p\rangle|^2\delta(E_p-E_n+\omega) - |\langle n|j_\mp(0)|p\rangle|^2\delta(E_p-E_n-\omega)\}, \tag{2.8}$$

where $j_\pm(x)$ are the "currents" associated with the charged meson fields, defined by

$$\begin{aligned}(\mu^2-\Box^2)\phi(x)&=j_-(x),\\ (\mu^2-\Box^2)\phi^*(x)&=j_+(x),\end{aligned} \tag{2.9}$$

and the connection between ϕ, ϕ^*, and the ϕ_a of I is

$$\begin{aligned}\phi&=(\phi_1-i\phi_2)/\sqrt{2},\\ \phi^*&=(\phi_1+i\phi_2)/\sqrt{2}.\end{aligned} \tag{2.10}$$

It is evident that the only states $|n\rangle$ which can possibly contribute to an integral over ω in the region $0\leq\omega<\mu$ are those corresponding to a single nucleon state. For all others, even though we allow ω to be less than μ (or $k^2=\omega^2-\mu^2<0$) and consequently $E_n=(M_n^2+k^2)^{\frac{1}{2}}<M_n$, where M_n is the total rest mass of the states $|n\rangle$, the δ functions can never vanish. For the positive values of ω to which we have restricted ourself, only the second term in (2.8) can contribute and in particular, if $|p\rangle$ represents a proton state, by charge conservation only $\langle n|j_-(0)|p\rangle$ is different from zero, corresponding to the emission of a π^+ meson by a proton leading to a neutron state. The "energy" of this state is $E_n=M-\mu^2/2M$, corresponding to $\omega=\mu^2/2M$ and $k^2=-\mu^2+(\mu^2/2M)^2$. Consequently only $A_+(\omega)$ exhibits the δ function singularity for $0<\omega<\mu$.

Since the state $|n\rangle$ represents a single nucleon state the required matrix element in (2.8) may be expressed in terms of the vertex operator Γ_5 corresponding to the emission of a virtual positive meson by a proton leading to a neutron. According to Low,[2] we have to within terms of order $(\mu/M)^2$ the result

$$\langle n|j_-(0)|p\rangle=-ig\sqrt{2}\boldsymbol{\sigma}\cdot\mathbf{k}/2M, \tag{2.11}$$

and thus

$$A_+(\omega)=-2\pi g^2\frac{k^2}{(2M)^2}\delta\left(\omega-\frac{\mu^2}{2M}\right),\quad 0<\omega<\mu. \tag{2.12}$$

In these equations, g is the renormalized coupling constant of the symmetrical pseudoscalar theory (in Gaussian units, with $\hbar=c=1$) and M is the nucleon mass. Note that we always maintain the relation $k^2=\omega^2-\mu^2$, even when $\omega<\mu$. In other words, our scattering amplitudes are to be expressed entirely in terms of ω and then continued from $\omega>\mu$ to $\omega<\mu$. We observe that for $\omega>\mu$, only the first term in Eq. (2.8) contributes to $A_+(\omega)$, and it is a positive contribution, and as a result of the fact that $k^2=\omega^2-\mu^2=+(\mu^2/2M)^2-\mu^2$, $A_+(\omega)$ is also positive for $\omega<\mu$. The contribution of this neutron state to the real part of the forward amplitudes is numerically very important.

We now substitute Eqs. (2.7) and (2.12) into Eqs. (2.5) and (2.6) and also change the variables from energy to wave number. We find then, using the same letters to designate functions of k that had been used for functions of ω, the results

$$\tfrac{1}{2}[D_-(k)+D_+(k)]-\tfrac{1}{2}[D_-(0)+D_+(0)]=\frac{k^2}{4\pi^2}\int_0^\infty dk' \times\frac{\sigma_-(k')+\sigma_+(k')}{k'^2-k^2}+2f^2\frac{k^2}{\omega^2-(\mu^2/2M)^2}\frac{1}{2M}, \tag{2.13}$$

$$\tfrac{1}{2}[D_-(k)-D_+(k)]-\frac{\omega}{\mu}\tfrac{1}{2}[D_-(0)-D_+(0)]=\frac{k^2\omega}{4\pi^2}\int_0^\infty\frac{dk'}{\omega'} \times\frac{\sigma_-(k')-\sigma_+(k')}{k'^2-k^2}-2f^2\frac{k^2}{\omega^2-(\mu^2/2M)^2}\frac{\omega}{\mu}\frac{1}{\mu}. \tag{2.14}$$

We have introduced the small coupling constant $f=\mu g/2M$ characteristic of the pseudovector interaction. The energy dependence of the bound state term is exact, however the coefficient, $2f^2$, as we have remarked before, is accurate only to terms of order $(\mu/M)^2$. The final form of the dispersion relations for the individual amplitudes $D_\pm(k)$ is obtained by combining Eqs. (2.13) and (2.14):

$$D_+(k)-\frac{1}{2}\left(1+\frac{\omega}{\mu}\right)D_+(0)-\frac{1}{2}\left(1-\frac{\omega}{\mu}\right)D_-(0) =\frac{k^2}{4\pi^2}\int_\mu^\infty\frac{d\omega'}{k'}\left[\frac{\sigma_+(\omega')}{\omega'-\omega}+\frac{\sigma_-(\omega')}{\omega'+\omega}\right]+\frac{2f^2}{\mu^2}\frac{k^2}{\omega-\mu^2/2M}, \tag{2.15}$$

$$D_-(k)-\frac{1}{2}\left(1+\frac{\omega}{\mu}\right)D_-(0)-\frac{1}{2}\left(1-\frac{\omega}{\mu}\right)D_+(0) =\frac{k^2}{4\pi^2}\int_\mu^\infty\frac{d\omega'}{k'}\left[\frac{\sigma_-(\omega')}{\omega'-\omega}+\frac{\sigma_+(\omega')}{\omega'+\omega}\right]-\frac{2f^2}{\mu^2}\frac{k^2}{\omega+\mu^2/2M}. \tag{2.16}$$

[2] See reference 2, Eq. (3.8). It is worth noting that the form of this matrix element is essentially independent of any details of the pion-nucleon interaction, although we have used the terminology of the usual γ_5 theory, and depends only on parity and angular momentum considerations. It affords a definition of the coupling constant which measures the strength of the interaction.

We have reverted to the original variable, ω', in the integrals, although the wave number is more convenient for numerical evaluation.

3. DISCUSSION

The final forms of the dispersion relations, Eqs. (2.15) and (2.16), for the real part of the scattering amplitudes, $D_\pm(k)$, are quite different from what one obtains by naively applying a dispersion relation such as Eq. (2.15) to the individual amplitudes for the scattering of positive and negative pions. We should perhaps note that this is the correct procedure for the case of π^0 scattering. The underlying physical reason for the profound difference between the scattering of neutral and charged pions seems to be that in making the continuation of the scattering amplitudes to negative frequencies, the charge of the beam must be changed. Thus only the symmetric and antisymmetric combinations of amplitudes which we have considered have simple properties when we continue them to negative frequencies. It may in fact be shown that if we define two quantities $M_\pm(\omega)$ by the relations

$$M_\pm(\omega)\equiv D_\pm(\omega)+iA_\pm(\omega), \tag{3.1}$$

which coincide with $T_\pm(\omega)$ for $\omega>0$, that

$$M_\pm(\omega)=M_\mp^*(-\omega). \tag{3.2}$$

As was shown in I, it is the M's for which the dispersion relations, strictly speaking, hold, and it is this fact that leads to our fundamental relations Eqs. (2.5) and (2.6). In the case of neutral pions, because the π^0 is its own charge conjugate we have

$$M_0(\omega)=M_0^*(-\omega), \tag{3.3}$$

and consequently the appropriate dispersion relation is

$$D_0(\omega)-D_0(\mu)=\frac{2(\omega^2-\mu^2)}{\pi}\int_0^\infty d\omega'\omega'\frac{A_0(\omega')}{(\omega'^2-\omega^2)(\omega'^2-\mu^2)}. \tag{3.4}$$

Our expressions for the amplitudes $D_\pm(k)$, Eqs. (2.15) and (2.16) bear a striking resemblance to the equations for pion-nucleon scattering recently proposed by Low. In fact, if one assumes that scattering occurs only in p-states and further considers the limit $M\to\infty$, and replaces our exact total cross sections by the total *elastic* cross sections, one gets two combinations of Low's three integral equations for the phase shifts.[3] We can obtain only those which do not involve spin flips, because there is no spin flip in the forward direction.[4] Our expressions are of course much more general although they are not equations for the determination of the complete scattering amplitudes.

We may also provide the exact form of the effective range relations which have been suggested by Chew and Low[5] by expanding the integrals in Eqs. (2.15) and (2.16) in powers of ω. This must be done with some care because of the singular nature of principal value integrals; however, the leading term is trivially obtained simply by setting ω equal to zero. Calling the left-hand sides of Eqs. (2.15) and (2.16) $L_\pm(k)$, we have the rigorous effective range relations

$$\left(\omega\mp\frac{\mu^2}{2M}\right)\frac{L_\pm(k^2)}{k^2}=\pm\frac{2f^2}{\mu^2}+\frac{(\omega\mp\mu^2/2M)}{4\pi^2}\int_\mu^\infty\frac{d\omega'}{k'}\frac{\sigma_+(\omega')+\sigma_-(\omega')}{\omega'}+\cdots. \tag{3.5}$$

Note that the effective range, r_s, defined by

$$r_s=\frac{\mu^2}{4\pi}\int_\mu^\infty\frac{d\omega'}{k'}\frac{\sigma_+(\omega')+\sigma_-(\omega')}{\omega'}, \tag{3.6}$$

is a positive quantity.

Note added in proof.—An interesting sum rule may be obtained by dividing Eq. (2.14) by ω and passing to the limit of $\omega\to\infty$. Within the framework of the assumptions already made in deriving the dispersion relations it can be shown that the difference $[D_-(\omega)-D(\omega)]/\omega$ either approaches a constant or goes to zero as $1/\omega^2$. Calling the quantity $\Delta(\omega)$, we have the result

$$\Delta(\mu)-\Delta(\infty)=\frac{4f^2}{\mu^2}+\frac{1}{2\pi^2}\int_\mu^\infty\frac{d\omega}{k}[\sigma_-(\omega)-\sigma_+(\omega)]. \tag{3.7}$$

Using the value of f^2 given by reference 5, namely 0.081, and the experimental data on the total cross sections one finds $\Delta(\mu)-\Delta(\infty)=0.18/\mu^3$ which is precisely the value given by Orear[6] for $\Delta(\mu)=2[a_1-a_3]/3\mu$. Thus to within the present experimental accuracy, we may conclude that $\Delta(\infty)=0$. We have not as yet been able to prove theoretically that $\Delta(\infty)$ must be zero, but it would not be unreasonable. If true, Eq. (3.7) then provides us with a sum rule relating the difference of the s-wave scattering lengths to the coupling constant and the total cross sections.

The results obtained in this paper have been applied to the phase-shift analysis of pion-nucleon scattering data by H. L. Anderson, W. Davidon, and U. Kruse. This work will be published shortly.

[4] *Note added in proof.*—It has been shown by one of us (R. O.) and independently by W. Thirring (private communication) that the spin flip equations may also be deduced from the causality considerations of the preceding paper by studying the derivative of the scattering amplitude with respect to angle, evaluated in the forward direction.

[5] G. F. Chew and F. E. Low, Fifth Annual Rochester Conference on High-Energy Nuclear Physics, 1955 (to be published).

[6] J. Orear, Phys. Rev. **96**, 176 (1954).

Quasi-Bound States of the Pion-Nucleon System in the Lowest Tamm-Dancoff Approximation*

B. P. NIGAM† AND H. P. NOYES
University of Rochester, Rochester, New York

(Received April 15, 1955)

The question is asked whether the lowest order Tamm-Dancoff equation, which agrees with the observed p-state meson-nucleon scattering for $G^2/4\pi \sim 15$, leads to a quasi-bound state of high angular momentum capable of being identified with the Λ^0 particle. Both a static potential approximation and an approximate form of the integral equation indicate that values of $G^2/4\pi$ of the order of several hundred would be required to give sufficient binding. Although the results are not quantitatively reliable, the authors feel they indicate that either the T-D approximation is inadequate for this problem or that the Λ^0 particle cannot be a quasi-bound state of the pion-nucleon system.

INTRODUCTION

THE work of Dyson *et al.*[1] and Fubini[2] has shown that reasonable agreement with the observed scattering in the $I=3/2$ p-states of the pion-nucleon system can be obtained by using the lowest order (unrenormalized) Tamm-Dancoff approximation to the covariant pseudoscalar meson theory with pseudoscalar coupling. It is therefore of interest to see whether other experimental results can be explained in the same way. Since the Λ^0 particle is known to decay to a pion and a proton with a lifetime of about 3×10^{-10} sec, and an energy of 37 Mev,[3] and a strong short-range force between meson and proton capable of overcoming the centrifugal repulsion could easily lead to a quasi-bound state of high angular momentum with these properties, an attempt is made here to see if the lowest Tamm-Dancoff approximation leads to such a state. This model for the Λ^0, first proposed by Fermi and Feynman,[4] allows for copious production of Λ^0's, even though their lifetime is long, since in energetic pion-nucleon collisions it is possible to radiate most of the energy as pions, leaving one pion trapped in the quasi-bound state of high angular momentum. The model presupposes that it can be shown that there are no quasi-bound states of lower energy and angular momentum, since decay to these states by electromagnetic radiation would be rapid.

The problem has been attacked by two different sets of approximations, which lead to qualitatively similar conclusions. First the energy-dependent interaction is reduced to a static potential in coordinate space by using approximations similar to those employed by Arnowitt and Deser,[5] who approached the same problem via the covariant Green's function[6] for the system. It is found that in order to obtain binding, a coupling parameter $G^2/4\pi$ of the order of several hundred is required, which would not only invalidate the T-D approximation, but also disagrees with the value of about 15 which explains the scattering data.[1] The discrepancy with the more reasonable values of 9.0 and 13.5 obtained by Arnowitt and Deser is explicable, since their potential approximation still includes negative frequency components not present in the Tamm-Dancoff equation, and which on elimination yield a potential varying at short distances something like $1/r^2$ and capable of overriding the centrifugal repulsion.

Since there is little reason to trust a static potential approximation to the Tamm-Dancoff equation, an attempt was made to solve the integral equation in momentum space, using the approximation successfully employed by Lévy and Marshak[7] for states of lower angular momentum. If the energy eigenvalue is taken to be complex, the equation for the imaginary part determines the lifetime, while the equation for the real part determines $G^2/4\pi$, given the energy of the decay. Although the approximation used cannot be trusted quantitatively, it is argued that the qualitative features of the interaction are preserved. In this approximation, it proves to be impossible to find a decaying state for $I=3/2$, and for $I=1/2$ the quasi-bound solution seems to require a complex $G^2/4\pi$. In both cases, however, it is found that, as in the static approximation, values of $G^2/4\pi$ of the order of several hundred are indicated.

STATIC POTENTIAL APPROXIMATION

The lowest order Tamm-Dancoff equation for the pion-nucleon system can be derived directly from the Hamiltonian form of the pseudoscalar meson theory with pseudoscalar coupling,[1] or can be obtained by taking the adiabatic limit of the covariant two body equation in the usual manner,[8] iterating once, and

* This work was supported in part by the U. S. Atomic Energy Commission.

† Government of India Scholar on leave from Delhi University, Delhi, India. Based on work submitted in partial fulfillment of requirements of Ph.D. degree.

[1] Dyson, Ross, Salpeter, Schweber, Sundaresan, Visscher, and Bethe, Phys. Rev. **95**, 1644 (1954).

[2] S. Fubini, Nuovo cimento **10**, 564 (1953).

[3] See, for example Thompson, Burwell, Huggett, and Kazmark, Phys. Rev. **95**, 1526 (1954).

[4] E. Fermi and R. P. Feynman (unpublished).

[5] R. Arnowitt and S. Deser, Phys. Rev. **92**, 1061 (1953).

[6] J. Schwinger, Proc. Nat. Acad. Sci. (U. S.) **37**, 452, 455 (1951).

[7] M. M. Lévy and R. E. Marshak, Nuovo cimento **11**, 366 (1954).

[8] E. E. Salpeter and H. A. Bethe, Phys. Rev. **84**, 1232 (1951); M. M. Lévy, Phys. Rev. **88**, 72 (1952).

projecting out the positive frequency components of *both*[9] meson and nucleon. As is well known, there is a difficulty in using this theory for states of isotopic spin one-half, because in some of these states an isolated nucleon can be present part of the time and the integral equation then corresponds to adding up an infinite series of divergent self-energy effects even though the matrix elements in the kernel are themselves finite. However, for the present problem, we are concerned only with states of total angular momentum greater than one-half, so that an isolated nucleon can never appear, and none of these divergences occur. For these states the lowest order Tamm-Dancoff is then simply[10]

$$[W-E(p)-\omega(p)]g_\alpha(\mathbf{p})$$
$$=-\frac{G^2}{16\pi^3}\Lambda_+(\mathbf{p})Q_{\alpha\delta}'\int d^3s\frac{M^2}{[E(p)\omega(p)E(s)\omega(s)]^{\frac{1}{2}}}$$
$$\times\left\{-\frac{\Lambda_-(\mathbf{p}+\mathbf{s})}{W-E(\mathbf{p}+\mathbf{s})-\omega(p)-\omega(s)}\right.$$
$$\left.+\frac{\Lambda_+(\mathbf{p}+\mathbf{s})}{W-E(\mathbf{p}+\mathbf{s})-E(p)-E(s)}\right\}g_\delta(\mathbf{s}),\quad(1)$$

where

$$\Lambda_\pm(\mathbf{p})=[H(\mathbf{p})+E(\mathbf{p})]/[\pm 2E(\mathbf{p})].$$

We have found that the same equation holds in the "New Tamm-Dancoff"[11] approach provided only finite graphs are retained. Consequently the only effect of renormalization to order $G^2/4\pi$ would be to replace the masses occurring on the left-hand side of the equation by momentum-dependent factors; the possible effects of this replacement will not be considered in what follows.[12]

In order to obtain a static potential approximation to Eq. (1), it is necessary to assume that the interaction is adiabatic, that is that the nucleon in the intermediate state is transmitted instantaneously, but that otherwise the nucleon and meson may be treated as nonrelativistic. The adiabatic approximation thus requires us to leave $E(\mathbf{p}+\mathbf{s})$, the energy of the intermediate nucleon, untouched while approximating the energies of the states of momentum $\mathbf{p}$ and $\mathbf{s}$ by the actual energy of the system, that is $E(p)+\omega(p)\approx W\approx E(s)+\omega(s)$. The two terms in the kernel then combine to give

$$\{H(\mathbf{p}+\mathbf{s})-[W-E(p)-E(s)]\}$$
$$\div\{[E(\mathbf{p}+\mathbf{s})]^2-[W-E(p)-E(s)]^2\}.$$

If we now make a second nonrelativistic approximation, namely that $E(p)\approx E(s)\approx M+[MQ/(M+\mu)]$, where $MQ/(M+\mu)$ is that fraction of the total kinetic energy Q which is carried by the nucleon, the equation becomes

$$[W-E(p)-\omega(p)]g_\alpha(\mathbf{p})=Q_{\alpha\delta}'\frac{G^2}{(2\pi)^3}\frac{1}{2\omega(p)}\int d^3s$$
$$\times\frac{\boldsymbol{\alpha}\cdot(\mathbf{p}+\mathbf{s})+\beta M-W(M-\mu)/(M+\mu)}{(\mathbf{p}+\mathbf{s})^2+M^2-[W(M-\mu)/(M+\mu)]^2}g_\delta(\mathbf{s}),\quad(2)$$

where this equation agrees with the adiabatic limit of the covariant two-body equation[5] when written out for the positive frequency component $g_\alpha(p)$ to order $G^2/4\pi$.

After multiplying Eq. (2) by $[(W^2-M^2+\mu^2)/2W+\omega(p)][W+E(p)-\omega(p)]/2W$, it is transformed to coordinate space, dropping a term

$$\int[\exp(i\mathbf{p}\cdot\mathbf{r})]/\omega(p)=\frac{4\pi}{r}\frac{d}{dr}K_0(\mu r)$$

compared to $\int\exp(i\mathbf{p}\cdot\mathbf{r})=(2\pi)^3\delta(\mathbf{r})$. The large and small components can be separated in the usual way, giving for the large component the equation

$$d^2u(r)/dr^2+2\mu'[Q-V_1(r)-V_2(r)]u(r)=0,$$

where

$$V_1(r)=(J-\tfrac{1}{2})(J+\tfrac{1}{2})/2\mu' r^2,$$
$$V_2(r)=(-1)^{J-\frac{1}{2}}(Q'/2)(G^2/4\pi)(1/2\mu')$$
$$\times[(W+M-\mu)/2W]\left(M-\frac{M-\mu}{M+\mu}W\right)e^{-\rho r}/r,$$
$$2\mu'=(W+M+\mu)(W+M-\mu)(W-M+\mu)/4W^2,$$
$$\rho=\left[M^2-\left(\frac{M-\mu}{M+\mu}W\right)^2\right]^{\frac{1}{2}},\quad W=M+\mu+Q.$$

Since $Q'=2$ for isotopic spin $3/2$ and $Q'=-1$ for isotopic spin $1/2$, the potential $V_2^{(r)}$ is attractive in the former case for $J=3/2, 7/2, 11/2, \cdots$ and in the latter for $J=5/2, 9/2, 13/2, \cdots$.

Although this equation could be solved exactly, a rough approximation shows clearly this is scarcely worth the effort. The first part of this approximation is to replace the Yukawa potential $V_2(r)$ by a square well of range $1/\rho$ and depth given by $\bar{V}_2$, where $\int_0^\infty V_2(r)r^2dr=\bar{V}_2\int_0^{1/\rho}r^2dr$; the centrifugal repulsion is retained outside this range, but replaced by a constant repulsive potential inside $1/\rho$ whose value $\bar{V}_1$ is given by $\bar{V}_1\int_0^{1/\rho}r^2dr=\int_0^{1/\rho}V_1(r)r^2dr$. The problem is then readily handled by the WKB approximation, and for a

[9] If one does not follow this prescription, as given for example in S. Deser and P. C. Martin, Phys. Rev. **90**, 1075 (1953), and instead projects only the positive frequency components of the nucleon, the resulting equation contains terms other than those given by the noncovariant approach even to order $G^2/4\pi$.

[10] See reference 1, Eq. (13) and also for notation. We use $W=M+\mu+Q$ for the total energy of the system rather than E.

[11] F. J. Dyson, Phys. Rev. **90**, 994 (1953); and **91**, 1543 (1953).

[12] W. M. Visscher [Phys. Rev. **96**, 788 (1954)] has shown that renormalization introduces a pole in the equation which he is unable to interpret physically and which casts doubt on the whole T.D. approach. In any case, we are motivated here by the agreement with experiment obtained by the unrenormalized equation and ask simply if the A^0 particle can be explained within the same framework.

given Q-value both lifetime and coupling constant are determined, selected values being given in Table I. The approximations leading to these results are so crude, and the results so sensitive to the precise value of ρ, that close agreement with the experimental values of $Q=37$ Mev and $\tau=3\times10^{-10}$ second is hardly to be expected. However, Dyson *et al.*[1] obtained agreement with the p-wave scattering for a value of $G^2/4\pi$ slightly greater than 15, while the values of several hundred indicated in Table I would invalidate the whole Tamm-Dancoff approach. We interpret these results as an indication that for reasonable values of $G^2/4\pi$ this theory does not give sufficient binding to form long-lived states of high angular momentum.

This result is in striking contrast to that of Arnowitt and Deser[5] who find, after making a similar potential approximation to the adiabatic limit of the covariant two-body equation, metastable states with orbital angular momentum $l=5$ of $Q\sim40$ Mev and $\tau\sim2\times10^{-10}$ second using a coupling constant $G^2/4\pi$ of either 9.0 or 13.5. It is true that the approximations we have used underestimate the potential strength by dropping a p dependence in the numerator, whereas Arnowitt and Deser overestimate their potential by the approximation $\int d^3p[M/E(p)]\exp(i\mathbf{p}\cdot\mathbf{r})\approx(2\pi)^3\delta(\mathbf{r})$, but this could not account for so large a discrepancy. The essential difference is that in their result the potential approximation still couples in states of negative frequency. They replace Yukawa potentials by square wells and decouple these equations, which gives an additional $1/r$ potential in their final equation (again approximated by a square well in their calculation). Thus a more exact treatment would presumably give an interaction varying something like $1/r^2$ at the origin, and it is not surprising that this attractive term can overcome the centrifugal repulsion for reasonable values of $G^2/4\pi$. Hence it is clear that their result comes about precisely because they retain the negative frequency components which are absent in the Tamm-Dancoff treatment.

APPROXIMATE SOLUTION OF THE INTEGRAL EQUATION

Since there is no particularly good reason to believe that the static potential approximation does justice to the interaction we are considering, an attempt was also made to solve the integral equation directly. That is, W is treated as a complex eigenvalue, $W=M+\mu+Q-i\lambda$, $\lambda>0$ whose imaginary part is related to the lifetime by $\tau=\hbar/2\lambda$. By a series of approximations, the kernel is factored and, for an assumed value of Q, the imaginary part of the equation determines λ while the real part determines $G^2/4\pi$. Although the approximations used can at best lead to only qualitative results, these results reinforce the conclusion drawn from the potential approximation that this equation does not give sufficient binding to form a metastable state of high angular momentum.

TABLE I. Numerical results in the static potential approximation.

I	Q(Mev)	J	$2\mu'$	ρ	$G^2/4\pi$	τ(sec)
3/2	35	11/2	$0.28497M$	$0.47921M$	147.9	2.1×10^{-11}
	25	11/2	$0.27822M$	$0.49341M$	142.5	2.1×10^{-10}
1/2	35	9/2	$0.28497M$	$0.47921M$	203.3	8.6×10^{-16}
	35	13/2	$0.28497M$	$0.47921M$	406.4	6.7×10^{-8}
	60	13/2	$0.30144M$	$0.44099M$	450.3	5.3×10^{-10}

The angular and spin dependence in Eq. (1) can be separated in a straightforward manner [see, e.g. reference 1, Eq. (23)] and the kernal of the resulting one-dimensional integral equation depends on quantities of the form

$$\int_{1-r}^{1+r}[z/(b+z)]P_l[(z^2-1-r^2)/2r]dz,$$

where $r=4ps/[E(p+s)+E(p-s)]^2$. In order to obtain manageable expressions, these quantities are expanded as functions of rx/R, where $x=(z^2-1-r^2)/2r$ and $R=1+r^2$; this expansion parameter is always less than $1/2$ and only approaches this value in the region where both p and s are very nearly equal and both much larger than M, so this expansion is reasonably good in the region of the interest. This expansion leads, ultimately, to the following equation:

$$[W-E(p)-\omega(p)]g(p)=\eta\int_0^\infty ds\frac{s^2[M+E(p)]}{E(p)\omega(p)\bar{E}R^{\frac{1}{2}}}\times\left\{\left(\frac{r}{R}\right)^l I_{l,l}\left[\frac{A^-}{C}A_l(p,s;\gamma)+\frac{W-M}{B}A_l(p,s;\beta)\right]+\frac{ps}{[M+E(p)][M+E(s)]}\left(\frac{r}{R}\right)^{l\pm1}I_{l\pm1,l\pm1}\times\left[\frac{A^+}{C}A_{l\pm1}(p,s;\gamma)+\frac{W+M}{B}A_{l\pm1}(p,s;\beta)\right]\right\}g(s),\tag{4}$$

where the various quantities entering this expression are given in Appendix I, including explicit expressions for $A_l(p,s;\beta)$ for $0\leq l\leq11$ neglecting terms of order $(r/R)^2$ and higher.

This approximation is still insufficient to make the equation tractable, so the approximation procedure of Lévy and Marshak[7] is used. This consists of replacing either p or s by a constant momentum p_1 in those terms [such as $E(p+s)$] which do not factor. Provided $p_1\lesssim M$ the approximation $p=p_1$ is good except in the region where both $s\lesssim M$ and $p\gg M$, while $s=p_1$ is a good approximation except in the region where both $p\lesssim M$ and $s\gg M$. Consequently we can divide the wave function into two parts at some value of p of the order

of a few M, which we label p_0, and take

$$\begin{aligned} p&=p_1, \quad 0<p<p_0, \quad 0<s<\infty, \\ s&=p_1, \quad p_0<p<\infty, \quad 0<s<p_0, \end{aligned} \tag{5}$$

while retaining the unfactored kernel in the region where both s and p are greater than p_0. This is still a reasonable approximation to the original equation for a judicious choice of p_0 and p_1. Specifically, for $J=l+1/2$, in which case the term containing $I_{l\pm1,\,l\pm1}$ in Eq. (4) can be dropped, this approximation gives us

$$\begin{aligned} 0<p<p_0\colon\ \phi_1(p)&=\eta_l\int_0^{p_0} M_1(p)N_1(s,p_1)\phi_1(s)ds \\ &\quad+\eta_l\int_{p_0}^{\infty} M_1(p)N_1(s,p_1)\phi_2(s)ds \\ &=\eta_l d_1(p_1,p_0)M_1(p) \\ p_0<p<\infty\colon\ \phi_2(p)&=\eta_l\int_0^{p_0} M_2(p,p_1)N_2(s)\phi_1(s)ds \\ &\quad+\eta_l\int_{p_0}^{\infty} K(p,s)\phi_2(s)ds \\ &=\eta_l d_2(p_1,p_0)M_2(p,p_1) \\ &\quad+\eta_l\int_{p_0}^{\infty} K(p,s)\phi_2(s)ds, \end{aligned} \tag{6}$$

where the notation is defined in Appendix I. If we now iterate the equation once and eliminate constants d_1 and d_2, we arrive at the eigenvalue equation:

$$\begin{aligned} 1=\eta_l\int_0^{p_0} M_1(s)N_1(s,p_1)ds+\eta_l^2\Big[\int_0^{p_0} M_1(p)N_2(p)dp\Big] \\ \times\Big[\int_{p_0}^{\infty} N_1(p,p_1)\Big\{M_2(p,p_1) \\ +\eta_l\int_{p_0}^{\infty} K(p,s)M_2(s,p_1)ds\Big\}dp\Big]. \end{aligned} \tag{7}$$

As is shown in Appendix II, it is possible to use the asymptotic form of $K(p,s)$ to demonstrate that for finite p_0 the contribution of the term proportional to η_l^2 is negligible, so that we are left with the eigenvalue equation

$$1=\eta_l\int_0^{p_0} M_1(s)N_1(s,p_1)ds. \tag{8}$$

TABLE II. Numerical results for $J=l+1/2$ ($M=\hbar=c=1$).

l	p_1	p_0	L_{11}	L_{12}	L_{13}	$G^2/4\pi$	λ
11	0.103375M	3.0M	66.24	−53.92	-3.2226×10^{-14}	~760	no solution
	0.103375M	4.0M	134.40	−87.56	-3.226×10^{-14}	~374	no solution
7	1.05M	3.0M	4.2356	−2.4689	-3.8989×10^{-15}	~600	no solution

This is equivalent to replacing p by p_1 in Eq. (4) in $\bar{E}$, R, and the terms inside the [ ], eliminating $g(p)$, and cutting off the integral at p_0.

On examination of Eq. (8), it is found that the integral depends logarithmically on the cutoff p_0. This divergence has been artificially introduced by the failure of our approximation of replacing p by p_1 in the region where p is large. We have just proved, however, that the contribution from this region to the eigenvalue equation is, in fact, negligible. Therefore, an appropriate choice of both p_0 and p_1 must give a valid approximation to the original equation. We have already seen that we must choose $p_1<M$ and p_0 of the order of a few M, so what is done below is to solve the equation for a few appropriate choices. In order to justify a particular choice quantitatively it would be necessary to iterate the resulting wave function and show that the correction is small. However, the results of our particular choices, which should reveal the qualitative nature of the solution, are so completely negative, that it did not appear worth while to attempt such an iteration to obtain more quantitative results.

In order for our eigenvalue to give a lifetime of the order of 10^{-10} second, λ must be of the order of $10^{-15}M$, so Eq. (8) can be expanded in powers of λ and the real and imaginary parts separated giving

$$\begin{aligned} 1&=\eta_l L_{11}(E;\,p_1,p_0)=\frac{Q'}{8\pi}\frac{G^2}{4\pi}-I_{l,l}L_{11}, \\ \lambda&=-L_{12}(E;\,p_1)/L_{12}(E;\,p_1,p_0), \end{aligned} \tag{9}$$

where the integrals L_{11}, L_{12}, and L_{13} are defined in Appendix III. A rough estimate shows that for $p_1=k=0.103375$, $l\sim11$ should give $\lambda\sim10^{-15}M$, so the numerical work was carried out for this case. The results are given in Table II. Since L_{11} is positive, only isotopic spin 3/2 gives a real $G^2/4\pi$. (If l were even only isotopic spin 1/2 would lead to a real $G^2/4\pi$.) Since $I_{11,11}=512/2028117=2.52\times10^{-4}$, values of $G^2/4\pi$ of the order of several hundred are required, as given in the table. In addition, both L_{12} and L_{13} are negative, so that, although λ was assumed positive (corresponding to a decaying state), we find a negative value; in other words

TABLE III. Numerical results for $J=l-1/2$ ($M=\hbar=c=1$). The values of L_{11}, L_{12}, and L_{13} are the same as given in Table II.

	$l=11$		$l=7$
	$p_0=3.0$	$p_0=4.0$	$p_0=3.0$
L_{21}	19.33	34.54	1.1441
L_{22}	−15.50	−22.75	−0.68049
L_{23}	-1.607×10^{-14}		-1.9443×10^{-15}
M_{11}	−116.78	−277.96	−8.4880
M_{12}	93.46	166.99	4.8410
M_{13}	-3.2172×10^{-14}		5.6457×10^{-15}
M_{21}	−33.19	−67.11	−2.2743
M_{22}	27.06	43.54	1.3207
M_{23}	-1.6043×10^{-14}		2.8153×10^{-15}

TABLE IV. Final numerical equations for $J=l-1/2$.

l	p_1	p_0	Equation (10)	Equation (11)
11	k	$3.0M$	$7.8\times10^{-6}\eta^2+8.0\times10^{-4}\eta+1=0$	$\lambda(\eta+94.1) = -6.8\times10^{-15}(\eta+6.8)$
11	k	$4.0M$	$7.7\times10^{-6}\eta^2+1.5\times10^{-3}\eta+1=0$	$\lambda(\eta+18.1) = -3.5\times10^{-15}(\eta+2.0)$
7	$1.05M$	$3.0M$	$4.1\times10^{-6}\eta^2+3.2\times10^{-3}\eta+1=0$	$\lambda(\eta+321.0)=-2.1\times10^{-14}(\eta+92.3)$

the equations do not possess a solution for any sign of λ. If we were to take l even, A and consequently both L_{12} and L_{13} change sign, so that there are also no decaying states for $J=l+1/2$ and $I=1/2$.

The equations for $J=l-1/2$ are more complicated, since both the term in $I_{l,l}$ and $I_{l-1,l-1}$ must be retained. However, the same approximations lead, eventually, to the two eigenvalue equations

$$1-\eta_{l-1}M_{21}=\eta_l[L_{11}+\eta_{l-1}(L_{21}M_{11}-L_{11}M_{21}+L_{13}M_{23}-L_{23}M_{13})], \quad (10)$$

and

$$(\eta_{l-1}/\eta_l)(\lambda M_{22}+M_{23})=-\lambda L_{12}-L_{13}-\eta_{l-1}\{\lambda(L_{21}M_{12}+L_{22}M_{11}-L_{11}M_{22}-L_{12}M_{21})+(L_{21}M_{13}+L_{22}M_{11}-L_{11}M_{23}-L_{13}M_{21})\}. \quad (11)$$

The definitions of the integrals are given in Appendix III and their numerical values for particular cases in Table III. For the various cases indicated in Table III, the resulting numerical equations (10) and (11) for η and λ are given in Table IV. For the case $l=11$, $p_1=k=0.103375M$, $p_0=3.0M$ we see that in order for λ to be positive, η must be negative (that is, the isotopic spin is $1/2$) and lie between 6.8 and 94.1 in absolute value. The value of $G^2/4\pi$ required to give $\lambda\sim10^{-15}M$ is about 450. But the quadratic equation for η indicates still higher v. lues. Unfortunately the solutions to this quadratic are complex, so that again the equations are inconsistent. If the cutoff is increased to $4.0M$, the value of $G^2/4\pi$ required to give $\lambda\sim10^{-15}M$ comes down to about 125, but Eq. (10) still has a complex solution. If we take $l=7$, $p_1=1.05M$ and $p_0=3.0M$, the limits for λ to be greater than zero are that the absolute value of η lie between 92.3 and 321.0, corresponding to a fantastically high coupling constant. Again Eq. (10) is inconsistent in that it give complex roots.

CONCLUSION

We feel that it is indicated by these calculations that the lowest order Tamm-Dancoff equation does not give sufficient binding in states of high angular momentum to lead to a quasi-bound state capable of being identified with the Λ^0 particle, if the value of $G^2/4\pi$ indicated by the p-state scattering calculations[1] is approximately correct. The much larger coupling parameter found above would make it virtually certain that the Tamm-Dancoff approximation could not be employed in any case. Since it may well be, as Pais and others[12] have suggested, that the long-lived hyperons are evidence for a new fundamental interaction or new symmetry principle, this negative result may indicate that there are, in fact, no long-lived excited states of the meson-nucleon system. Conversely, if there are such states, the lowest Tamm-Dancoff approximation, which agrees fairly well with the observed p-state scattering, appears to be incapable of predicting them.

ACKNOWLEDGMENT

We are indebted to Professor R. E. Marshak for originally suggesting this problem and for many stimulating discussions. Professor M. M. Lévy was actively concerned with the final stages of the work on the integral equation, and his advice and help were most useful. One of us (B.P.N.) is indebted to the Government of India for the award of the Central States Scholarship.

APPENDIX I

The quantities appearing in Eq. (4) are defined as follows.

$$A^{\pm}=E(p)+\omega(p)+E(s)+\omega(s)\pm M-W=B+C\pm M+W,$$

$$B=E(p)+E(s)-W, \qquad C=\omega(p)+\omega(s)-W,$$

$$2\bar{E}=E(p+s)+E(p-s), \qquad r=ps/\bar{E}^2, \qquad R=1+r^2,$$

$$\beta=R^{\frac{1}{2}}/(R^{\frac{1}{2}}+B/E), \qquad \gamma=R^{\frac{1}{2}}/(R^{\frac{1}{2}}+C/\bar{E}).$$

$$I_{n,m}=\int_{-1}^{1}z^nP_m(z)dz=\frac{2^{m+1}n!(\frac{1}{2}n+\frac{1}{2}m)!}{(\frac{1}{2}n-\frac{1}{2}m)!(n+m+1)!} \quad \text{when } n-m \text{ is even and positive}$$

$$=0 \text{ otherwise,}$$

$$I_{m,m}=\frac{2^{m+1}(m!)^2}{(2m+1)!},$$

$$\eta=(Q'/8\pi)(G^2/4\pi).$$

[12] A. Pais, Physica **19**, 869 (1953); M. Gell-Mann, Phys. Rev. **92**, 833 (1953); D. C. Peaslee, Phys. Rev. **86**, 127 (1952); M. M. Lévy and R. E. Marshak, Proceedings Padua Conference, 1954 Suppl. al 12, ser. 9 del Nuovo Cimento p. 253 (1954). M. Gell-Mann and A. Pais, Proc. Intnatl. Phys. Conf., Glasgow, 1954 (to be published).

The explicit expressions for $A_l(p,s;\beta)$ or $A_l(p,s;\gamma)$ are

$$A_0(p,s;\gamma)=(1-\gamma)+O(r/R)^2+\cdots.$$

$$A_1(p,s;\gamma)=(-1+\gamma^2)+O(r/R)^2+\cdots.$$

$$A_2(p,s;\gamma)=\{\tfrac{3}{2}-(\tfrac{1}{2}\gamma^2+\gamma^3)\}+O(r/R)^2+\cdots.$$

$$A_3(p,s;\gamma)=\{-5/2+(\tfrac{1}{2}\gamma^2+\gamma^3+\gamma^4)\}+O(r/R)^2+\cdots.$$

$$A_4(p,s;\gamma)=\left\{\frac{35}{8}-\left(\frac{5}{8}\gamma^2+\frac{5}{4}\gamma^3+\frac{3}{2}\gamma^4+\gamma^5\right)\right\}+O\left(\frac{r}{R}\right)^2+\cdots.$$

$$A_5(p,s;\gamma)=\left\{-\frac{63}{8}+\left(\frac{7}{8}\gamma^2+\frac{7}{4}\gamma^3+\frac{9}{4}\gamma^4+2\gamma^5+\gamma^6\right)\right\}+O\left(\frac{r}{R}\right)^2+\cdots.$$

$$A_6(p,s;\gamma)=\left\{\frac{231}{16}-\left(\frac{21}{16}\gamma^2+\frac{21}{8}\gamma^3+\frac{7}{2}\gamma^4+\frac{7}{2}\gamma^5+\frac{5}{2}\gamma^6+\gamma^7\right)\right\}+O\left(\frac{r}{R}\right)^2+\cdots.$$

$$A_7(p,s;\gamma)=\left\{-\frac{429}{16}+\left(\frac{33}{16}\gamma^2+\frac{33}{8}\gamma^3+\frac{45}{8}\gamma^4+6\gamma^5+5\gamma^6+3\gamma^7+\gamma^8\right)\right\}+O\left(\frac{r}{R}\right)^2+\cdots.$$

$$A_8(p,s;\gamma)=\left\{\frac{6435}{128}-\left(\frac{429}{128}\gamma^2+\frac{429}{64}\gamma^3+\frac{297}{32}\gamma^4+\frac{165}{16}\gamma^5+\frac{75}{8}\gamma^6+\frac{27}{4}\gamma^7+\frac{7}{2}\gamma^8+\gamma^9\right)\right\}+O\left(\frac{r}{R}\right)^2+\cdots.$$

$$A_9(p,s;\gamma)=\left\{-\frac{12155}{128}+\left(\frac{715}{128}\gamma^2+\frac{715}{64}\gamma^3+\frac{1001}{64}\gamma^4+\frac{143}{8}\gamma^5+\frac{275}{16}\gamma^6+\frac{55}{4}\gamma^7+\frac{35}{4}\gamma^8+4\gamma^9+\gamma^{10}\right)\right\}+O\left(\frac{r}{R}\right)^2+\cdots.$$

$$A_{10}(p,s;\gamma)=\left\{\frac{46189}{256}-\left(\frac{2431}{256}\gamma^2+\frac{2431}{128}\gamma^3+\frac{429}{16}\gamma^4+\frac{1001}{32}\gamma^5+\frac{1001}{32}\gamma^6\right.\right.$$
$$\left.\left.+\frac{429}{16}\gamma^7+\frac{77}{4}\gamma^8+11\gamma^9+\frac{9}{2}\gamma^{10}+\gamma^{11}\right)\right\}+O\left(\frac{r}{R}\right)^2+\cdots.$$

$$A_{11}(p,s;\gamma)=\left\{-\frac{88179}{256}+\left(\frac{4199}{256}\gamma^2+\frac{4199}{128}\gamma^3+\frac{596}{128}\gamma^4+\frac{7072}{128}\gamma^5+\frac{6552}{128}\gamma^7\right.\right.$$
$$\left.\left.+\frac{7280}{128}\gamma^6+\frac{5096}{128}\gamma^8+\frac{3328}{128}\gamma^9+\frac{27}{2}\gamma^{10}+5\gamma^{11}+\gamma^{12}\right)\right\}+O\left(\frac{r}{R}\right)^2+\cdots.$$

The quantities appearing in Eq. (6) are defined as follows:

$$\eta_l=\eta I_{l,l}=\left(\frac{Q'}{8\pi}\right)\left(\frac{G^2}{4\pi}\right)I_{l,l},$$

$$M_1(p)=p^l[M+E(p)]/E(p)\omega(p)[W-E(p)-\omega(p)],$$

$$N_1(p_1,s)=s^{l+2}\alpha_l^-(p_1,s;W)/(R^{\frac{1}{2}}\bar{E})^{2l+1},$$

$$M_2(p,p_1)=p^l[M+E(p)]\alpha_l^-(p,p_1;W)/E(p)\omega(p)[W-E(p)-\omega(p)](R^{\frac{1}{2}}\bar{E})^{2l+1},$$

$$N_2(s)=s^{l+2},$$

$$K(p,s)=M_1(p)N_1(p,s)=M_2(p,s)N_2(s),$$

$$\alpha_l^{\pm}(p,s;W)=\frac{A^{\pm}}{C}A_l(p,s;\gamma)+\frac{(W\pm M)}{B}A_l(p,s;\beta).$$

APPENDIX II

The term to be estimated is

$$\eta_l^2\left[\int_0^{p_0} M_1(p)N_2(p)dp\right]\left[\int_{p_0}^{\infty} N_1(p_1,p)\left\{M_2(p,p_1)+\eta_l\int_0^{\infty}K(p,s)M_2(s,p_1)ds\right\}dp\right]. \tag{II-1}$$

For $p\gg M$, we have $M_1\sim p^{l-2}$, $N_1\sim A/p^{l-1}$, $M_2\sim A/p^{l+3}$, $N_2\sim p^{l+2}$, where A is the asymptotic numerical value of A_l and is independent of p. Then

$$\int_{p_0}^{\infty}K(p,s)M_2(s,p_1)\sim\frac{A^2}{p^{l+3}}\ln\frac{p}{p_0}+\frac{A^2}{(2l+1)p^{l+3}}, \tag{II-2}$$

where we have used the fact that in this region $ps/\bar{E}^2$ behaves like the lesser of (p,s) divided by the greater of (p,s). For p_0 finite, the entire contribution from (II-1) is therefore

$$\frac{\eta_l^2A^2}{(2l+1)^2}(1+2\eta_lA/2l+1),$$

provided only p_0 is finite, and since η_lA is quite small for reasonable values of $G^2/4\pi$, this term is negligible compared to the leading term in Eq. (7).

APPENDIX III

The quantities [L's and M's] appearing in Eqs. (9)–(11) are defined as follows.

$$L_{11}(E,\lambda;p_1,p_0)=\int_0^{p_0}dp(I_{R\gamma 1}+I_{R\beta 1}),$$

$$L_{12}(E\lambda;p_1,p_0)=\int_0^{p_0}dp\{I(p,\gamma_1)+I(p,\beta_1)\}+\left\{\int_0^{k-\epsilon_1}+\int_{k+\epsilon_1}^{p_0}\frac{I_{R\gamma 1}}{E-E(p)-\omega(p)}dp\right\}$$
$$-\int_0^{p_0}dp\frac{I_{R\gamma 1}}{C}+\left\{\int_0^{k-\epsilon_1}+\int_{k+\epsilon_1}^{p_0}\frac{I_{R\beta 1}}{E-E(p)-\omega(p)}dp\right\}-\int_0^{p_0}dp\frac{I_{R\beta 1}}{r},$$

$$L_{13}(E,\lambda;p_1)=\lambda\int_{k-\epsilon_1}^{k+\epsilon_1}dp\frac{I_{R\gamma 1}+I_{R\beta 1}}{E-E(p)-\omega(p)}\approx\pi\frac{E(k)\omega(k)}{k[E(k)+\omega(k)]}K_1(p_1,k)\left\{\frac{A^-}{C}A_l(p_1,p;\gamma_1)+\frac{E-M}{B}A_l(p_1,p;\beta_1)\right\}_{p=k},$$

$$I_{R\gamma 1}=K_2(p,p_1)\frac{C}{C^2+\lambda^2}A^-A_l(p_1,p;\gamma_1);\quad I_{R\beta 1}=K_2(p,p_1)\frac{B}{B^2+\lambda^2}(E-M)A_l(p_1,p;\beta_1),$$

$$I(p,\gamma_1)=K_2(p,p_1)\frac{C}{C^2+\lambda^2}\left\{A_l(p_1,p;\gamma_1)-\frac{A^-}{C+\bar{E}R^l}\gamma_1\frac{\partial}{\partial\gamma_1}A_l(p_1,p;\gamma_1)\right\},$$

$$I(p,\beta_1)=-K_2(p,p_1)\frac{B}{B^2+\lambda^2}\left\{A_l(p_1,p;\beta_1)+\frac{E-M}{B+\bar{E}R^l}\beta_1\frac{\partial}{\partial\beta_1}A_l(p_1,p;\beta_1)\right\},$$

$$K_1(p,p_1)=\frac{[M+E(p)]}{E(p)\omega(p)}\left(\frac{p}{\bar{E}R^l}\right)^{2l+1};\quad K_2(p,p_1)=K_1(p,p_1)\frac{E-E(p)-\omega(p)}{[E-E(p)-\omega(p)]^2+\lambda^2},$$

where in the expression for $A^{\pm}$, B, C, $\bar{E}$, and R, the variable $s=p_1$, and W is to be replaced by E wherever it occurs, k is defined by the relation $E=E(k)+\omega(k)$ and ϵ_1 is very small but $\gg\lambda$. L_{21}, etc., are defined exactly the same except that they have a factor $M+E(p)$ more in the denominators. M_{11}, etc., follow from the definition of L_{11}, etc., if the replacements

$$K_1\to K_3=p\frac{p^{2l+1}}{E(p)(\omega p)(\bar{E}R^l)^{2l-1}},$$

$A^-\to A^+$, $E-M\to E+M$, and $l\to l-1$ are made. M_{21}, etc., bear the same relation to M_{11}, etc., as L_{21} to L_{11}, etc.

Phase Shift Formulas for Nucleon-Nucleon Scattering*

S. COURTENAY WRIGHT
Institute for Nuclear Studies, University of Chicago, Chicago, Illinois
(Received February 10, 1955)

An explicit formula for the scattering spin matrix in terms of phase shifts and mixing parameters is derived for the case of nucleon-nucleon scattering. The treatment is nonrelativistic and assumes that charge independence is valid.

DALITZ and Wolfenstein and Ashkin[1] have shown how the results of any nucleon-nucleon scattering experiment may be predicted if the scattering matrix M, operating in the spin space of the nucleons, is known. They limited the form of M by certain invariance conditions to

$$M=BS+C(\boldsymbol{\sigma}_1+\boldsymbol{\sigma}_2)\cdot\mathbf{n}+D(\boldsymbol{\sigma}_1-\boldsymbol{\sigma}_2)\cdot\mathbf{n}+N(\boldsymbol{\sigma}_1\cdot\mathbf{n})(\boldsymbol{\sigma}_2\cdot\mathbf{n})T+\tfrac{1}{2}G[(\boldsymbol{\sigma}_1\cdot\mathbf{k})(\boldsymbol{\sigma}_2\cdot\mathbf{k})+(\boldsymbol{\sigma}_1\cdot\mathbf{p})(\boldsymbol{\sigma}_2\cdot\mathbf{p})]T+\tfrac{1}{2}H[(\boldsymbol{\sigma}_1\cdot\mathbf{k})(\boldsymbol{\sigma}_2\cdot\mathbf{k})-(\boldsymbol{\sigma}_1\cdot\mathbf{p})(\boldsymbol{\sigma}_2\cdot\mathbf{p})]T, \quad (1)$$

where B, C, D, N, G, H are energy-dependent functions of the c.m. scattering angle θ. S and T are singlet and triplet projection operators; $\mathbf{n}$, $\mathbf{k}$, $\mathbf{p}$ are unit vectors directed along $\mathbf{k}_i\times\mathbf{k}_f$, $\mathbf{k}_f-\mathbf{k}_i$, and $\mathbf{k}_i+\mathbf{k}_f$ respectively, where $\mathbf{k}_i$ and $\mathbf{k}_f$ are the initial and final c.m. momenta of one of the particles.

The D term changes the symmetry of the initial spin function and will be absent when the exclusion principle forbids singlet-triplet transitions, i.e., in p-p scattering and n-p scattering if isotopic spin is conserved.

In the absence of a satisfactory theory of nuclear forces the primary object of nucleon scattering experiments is to estimate the phase shifts (δ) and mixing parameters (ϵ) of those partial waves responsible for the scattering. Recently Wolfenstein[2] has related the results of certain triple scattering experiments to simple bilinear combinations of the B, C, G, H, N and their complex conjugates. These relations form a most convenient basis for the phase shift analysis if the explicit dependence of the B, C, G, H, N on θ, the δ's and the ϵ's can be found. This analysis could proceed as follows: For an arbitrary choice of δ's and ϵ's a digital computer is coded to first find the complex numbers B, C, G, H, N for the angles θ at which the experiments have been carried out, then to combine these complex numbers according to the Wolfenstein formulas and compute for all the observables O the least-squares sum $\chi=\sum_i[O_{\text{obs}}{}^i-O_{\text{calc}}{}^i)^2/\sigma_i]$. The procedure is repeated with a different choice of δ's and ϵ's until the minimum or minima of χ are found. The direct derivation of the form of M which follows is in the style of Lepore[3] who treated the equivalent problem for scattering of a spin $\frac{1}{2}$ particle by a spinless particle.

The wave describing the system in p-p scattering is

$$\psi(\mathbf{r})\sim(1-E)e^{i\mathbf{k}_i\cdot r+i\alpha\ln(kr-\mathbf{k}_i\cdot r)}\cdot\chi(1,2)+\frac{e^{ikr-i\alpha\ln 2kr}}{r}M\chi(1,2), \quad (2)$$

where $\alpha=e^2/\hbar v$, E is the particle exchange operator, $\chi(1,2)$ is the product of the two incident proton spin functions, and M is the scattering spin matrix. To find M, first expand the incident wave in terms of the eigenfunctions of the constants of the motion: $\mathbf{J}^2$, parity, and spin symmetry. Then construct the scattered wave according to the standard S-matrix prescription.[4] If the operator form of the projection operators which occur is retained, the M matrix may be easily identified in the scattered wave, namely,

$$M=\frac{(1+E)}{2ik}\{\sum_l(S^l-1)(2l+1)P_l\}\Lambda_s+\frac{(1-E)}{2ik}\Big\{(S_1{}^0-1)3\Lambda_0{}^1P_1+\sum_l(S_l{}^l-1)(2l+1)\Lambda_l{}^lP_l+\sum_l\Big[(S_{11}{}^{l+1}-1)(2l+1)\Lambda_{l+1}{}^lP_l+(S_{22}{}^{l+1}-1)\times(2l+5)\Lambda_{l+1}{}^{l+2}P_{l+2}+\frac{S_{12}{}^{l+1}}{[(l+1)(l+2)]^{\frac{1}{2}}}\times\Big((2l+1)\Lambda_{l+1}{}^l[(l+1)-(2l+3)(1-\epsilon_z{}^2)]P_l+(2l+5)\times\Lambda_{l+1}{}^{l+2}[(l+2)-(2l+3)(1-\epsilon_z{}^2)]P_{l+2}\Big)\Big]\Big\}\Lambda_s.$$

Here $\Lambda_s(\Lambda_s)$ are singlet (triplet) projection operators; $\Lambda_J{}^l$ projects states of total angular momentum J out

* This work supported by joint contract of the Office of Naval Research and the U. S. Atomic Energy Commission.
[1] R. H. Dalitz, Proc. Phys. Soc. (London) **A65**, 175 (1952); L. Wolfenstein and J. Ashkin, Phys. Rev. **85**, 947 (1952).
[2] L. Wolfenstein Phys. Rev. **96**, 1654 (1954).
[3] J. V. Lepore, Phys. Rev. **79**, 137 (1950).
[4] J. M. Blatt and L. C. Biedenharn, Revs. Modern Phys. **24**, 258 (1952).

of $P_\alpha(1,2)$.

$$\Lambda_{l+1}{}^l=\frac{\lambda^2+(l+2)\lambda+l+1}{(l+1)(2l+1)},\quad \Lambda_l{}^l=-\frac{\lambda^2+\lambda-l(l+1)}{l(l+1)},$$

$$\Lambda_{l-1}{}^l=\frac{\lambda^2-(l-1)\lambda-l}{l(2l+1)},$$

$$\lambda=\mathbf{l}\cdot\boldsymbol{\varepsilon},\quad \mathbf{l}=\mathbf{r}\times\mathbf{p}/\hbar,\quad \boldsymbol{\varepsilon}=\tfrac{1}{2}(\boldsymbol{\sigma}_1+\boldsymbol{\sigma}_2),\quad \text{with}\quad \boldsymbol{\sigma}_1\cdot\boldsymbol{\sigma}_2=1.$$

The elements of the S matrix are written S^J and $S_l{}^J$ for nondegenerate singlet and triplet states respectively. $S_{ij}{}^{l+1}$ is the submatrix of S referring to the two degenerate triplet states with $J=l+1$ and parity $(-1)^l$. The coefficient of the $S_{12}{}^{l+1}$ term depends on $\langle J_z\rangle$ unlike the invariant S matrix. This is the origin of the $\boldsymbol{\varepsilon}_z{}^2$ term in the last summand. To put M in the form (1), carry out the spatial operations in the $\Lambda_J{}^l P_l$ terms and then reduce all expressions to at most a bilinear dependence on the components of $\boldsymbol{\varepsilon}$. This last operation is facilitated if the formula,

$$(\mathbf{A}\cdot\boldsymbol{\varepsilon})(\mathbf{B}\cdot\boldsymbol{\varepsilon})(\mathbf{C}\cdot\boldsymbol{\varepsilon})=i(\mathbf{A}\times\mathbf{B}\cdot\boldsymbol{\varepsilon})(\mathbf{C}\cdot\boldsymbol{\varepsilon})+i(\mathbf{A}\cdot\boldsymbol{\varepsilon})(\mathbf{B}\times\mathbf{C}\cdot\boldsymbol{\varepsilon})+\mathbf{A}\cdot(\mathbf{B}\cdot\boldsymbol{\varepsilon})\mathbf{C}-i\mathbf{A}\cdot\mathbf{B}\times\mathbf{C},$$

is used. $\mathbf{A}$, $\mathbf{B}$, $\mathbf{C}$ need only commute with $\boldsymbol{\varepsilon}$. This formula follows from the identities for a spin-one operator $\boldsymbol{\varepsilon}$, namely

$$\boldsymbol{\varepsilon}_z{}^3=\boldsymbol{\varepsilon}_z,\quad (\boldsymbol{\varepsilon}_z\pm i\boldsymbol{\varepsilon}_y)^3=0,\quad (\boldsymbol{\varepsilon}_z\mp 1)(\boldsymbol{\varepsilon}_z\pm i\boldsymbol{\varepsilon}_y)^2=0.$$

The final expressions for B, C, N, H, and $G-N$ are

$$B=-\frac{\alpha}{2k}e^{2i\eta_0}[\mathcal{S}+\mathcal{C}]+\frac{1}{ik}\sum_{\text{even } l}e^{2i\eta_l}\alpha_{l,0}{}^N(2l+1)P_l,$$

$$C=\frac{\sin\theta}{4k}\left\{\sum_{\text{odd } l}\left[\beta_1{}^{l+1}\frac{(2l+3)}{l+1}P_l'-\beta_2{}^{l+1}\frac{(2l+3)}{l+2}P_{l+2}'-\alpha_{l,1}{}^N e^{2i\eta_l}\frac{(2l+1)}{l(l+1)}P_l'\right]-\alpha_{0,1}{}^N e^{2i\eta_1}\right\},$$

$$N=-\frac{\alpha}{2k}e^{2i\eta_0}[\mathcal{S}-\mathcal{C}]+\frac{1}{2ik}\left\{\sum_{\text{odd } l}\left[\beta_1{}^{l+1}\left(2(l+1)P_l-\frac{\mu P_l'}{l+1}\right)+\beta_2{}^{l+1}\left(2(l+2)P_{l+2}-\frac{\mu P_{l+2}'}{l+2}\right)\right.\right.$$
$$\left.\left.-\frac{\beta_3{}^{l+1}}{[(l+1)(l+2)]^{\frac{1}{2}}}P_{l+1}'+e^{2i\eta_l}\alpha_{l,1}{}^N\frac{(2l+1)}{l(l+1)}\mu P_l'\right]+\alpha_{0,1}{}^N e^{2i\eta_1}P_1\right\},$$

$$H=\frac{1}{2ik}\left\{\sum_{\text{odd } l}\left[\beta_1{}^{l+1}\frac{P_l'}{l+1}+\beta_2{}^{l+1}\frac{P_{l+2}'}{l+2}+\frac{\beta_3{}^{l+1}}{[(l+1)(l+2)]^{\frac{1}{2}}}(\mu P_{l+1}'-2(l+2)(l+1)P_{l+1})\right.\right.$$
$$\left.\left.-e^{2i\eta_l}\alpha_{l,1}{}^N\frac{2l+1}{l(l+1)}P_l'\right]+\alpha_{0,1}{}^N e^{2i\eta_1}\right\},$$

$$G-N=-\frac{\alpha}{2k}e^{2i\eta_0}[\mathcal{S}-\mathcal{C}]+\frac{1}{ik}\left\{\sum_{\text{odd } l}\left[\beta_1{}^{l+1}\left(P_l+\frac{\mu P_l'}{l+1}\right)+\beta_2{}^{l+1}\left(-P_{l+2}+\frac{\mu P_{l+2}'}{l+2}\right)\right.\right.$$
$$\left.\left.+\frac{\beta_3{}^{l+1}}{[(l+1)(l+2)]^{\frac{1}{2}}}P_{l+1}'+e^{2i\eta_l}\alpha_{l,1}{}^N(2l+1)\left(P_l-\frac{\mu P_l'}{l(l+1)}\right)\right]\right\},$$

where $P_l'=dP_l/d\mu$, $\mu=\cos\theta$, and P_l is the legendre polynomial of order l.

$$e^{2i\eta_l}=\Gamma(l+1+i\alpha)/\Gamma(l+1-i\alpha),$$
$$\alpha_{J,1}{}^N e^{2i\eta_l}=e^{2i\delta_J}-e^{2i\eta_l},$$

where δ_J is the phase shift for triplet states of orbital and total angular momentum l and J respectively. $\alpha_{L,0}{}^N e^{2i\eta_l}$ is the corresponding quantity for singlet states.

$$\beta_1{}^J=(\exp(2i\delta_J{}^1)-\exp(2i\eta_l))\cos^2\epsilon_J+(\exp(2i\delta_J{}^2)-\exp(2i\eta_l))\sin^2\epsilon_J,$$
$$\beta_2{}^J=(\exp(2i\delta_J{}^1)-\exp(2i\eta_{l+2}))\sin^2\epsilon_J+(\exp(2i\delta_J{}^2)-\exp(2i\eta_{l+2}))\cos^2\epsilon_J,$$
$$\beta_3{}^J=(\exp(2i\delta_J{}^1)-\exp(2i\delta_J{}^2))\sin 2\epsilon_J.$$

Here $\delta_J{}^1$ and $\delta_J{}^2$ are the two eigen phase shifts of the triplet states with angular momentum J and parity $(-1)^l$ and ϵ_J is the mixing parameter.[4] The separation of nuclear and Coulomb phase shifts has no physical significance if mixing occurs, because a mixture of states of different orbital angular momentum cannot have a pure Coulomb phase shift. The separation is made here so that the slowly convergent Coulomb series can be replaced by the usual Rutherford scattering amplitude.

$$\mathcal{S}=[\sin^2(\theta/2)]^{-1}\exp[-i\alpha\ln\sin^2(\theta/2)],$$
$$\mathcal{C}=[\cos^2(\theta/2)]^{-1}\exp[-i\alpha\ln\cos^2(\theta/2)].$$

The formulas apply to neutron proton scattering if $\alpha=e^2/\hbar v$ is put equal to zero, the sums are extended

over all l save for the absent $^2S_0$ state, and charge independence is valid. In this case, it is useful to write the formulas in terms of $\beta_1^J+\beta_2^J$, $\beta_1^J-\beta_2^J$, and β_3^J because the last two have the same complex phase.

It is interesting to note the connection between this derivation of M and the limitation placed on M by its invariance under time reversal.[1] Terms in $(\boldsymbol{\sigma}_1-\boldsymbol{\sigma}_2)\cdot\mathbf{n}$ and $\boldsymbol{\sigma}_1\times\boldsymbol{\sigma}_2\cdot\mathbf{n}$ do not occur here because change of spin symmetry is forbidden by the assumed charge independence of the interaction. The term in $(\boldsymbol{\sigma}_1\cdot\mathbf{k})(\boldsymbol{\sigma}_2\cdot\mathbf{p})+(\boldsymbol{\sigma}_1\cdot\mathbf{p})(\boldsymbol{\sigma}_2\cdot\mathbf{k})$ disappears only because of the symmetric nature of the S matrix. This property of the S matrix can be proved by the invariance of S under time reversal.

The formulas have been checked against those derived by Stapp[5] by a different technique up to f waves with mixing but without Coulomb phase shifts and against Breit and Ehrman[6] formula for $2\,\mathrm{Re}(C^*B)$ without mixing. This work was started after some illuminating discussions the author had with Professor E. Segrè and Professor O. Chamberlain about the analysis of proton-proton scattering experiments.

[5] H. P. Stapp (private communication).
[6] G. Breit and J. B. Ehrman, Phys. Rev. **96**, 805 (1954).

PHYSICAL REVIEW VOLUME 99, NUMBER 3 AUGUST 1, 1955

Low-Energy Theorems for Renormalizable Field Theories

ABRAHAM KLEIN*†
Harvard University, Cambridge, Massachusetts
(Received April 27, 1955)

A general method is described whereby the low-energy behavior of collision processes can be investigated systematically. The basic procedure is the construction of the renormalized Green's functions for the participating particles in the presence of external sources. For processes involving the collision of a boson with a fermion,—photon scattering, meson scattering, and photoproduction of mesons—one requires the propagation function of a nucleon in the presence of external electromagnetic and meson fields, as well as the propagator for a meson in an electromagnetic field. The rather direct relation of these functions to the various transition matrices is derived. The possible forms of the Green's functions are limited by the principles of Lorentz, gauge, and charge conjugation invariance. Their detailed structure is determined in part by the requirement that they describe particles of known mass, charge, magnetic moment, and mesic coupling constant. These conditions are sufficient to imply a number of theorems. For example, it is shown that the amplitude for photon-proton scattering is given correctly up to terms of first order in the photon energy by a Born approximation calculation, if one assigns to the proton its experimental charge and magnetic moment. If one includes the meson-nucleon coupling constant in this set of parameters, then perturbation theory is also valid for the leading terms in a momentum-energy expansion of the P-wave in meson-nucleon scattering, the S- and P-waves associated with the nucleon current in photomeson production, and the entire meson current for the same process.

The methods employed to establish the theorems are extended in order to provide a phenomenological framework for the description of the experiments for energies low enough so that the expansions in boson energy are still valid, but for which the deviations from the theorems are of practical significance. Thus, it is suggested that for the description of photon scattering one should attribute an electric and a magnetic polarizability to the nucleon. The description of the P-wave in meson-nucleon scattering also requires the introduction of two additional parameters. From the manner in which these enter the scattering amplitude, it can be concluded that the phase shift in the state of angular momentum and isotopic spin 3/2 is enhanced compared to its Born value, if only the phase shifts in the other states deviate in the opposite direction. Finally, parameters are introduced to describe the S-wave in meson-scattering, and the basis for a phenomenological description of photoproduction is indicated.

I. INTRODUCTION

CONSIDERABLE attention has been devoted recently to the investigation of the low-energy limit of field theories which can be renormalized. In particular, the study of the simplest processes involving the collision of a boson with a fermion—photon scattering,[1] photoproduction of mesons,[2] and scattering of mesons[3]—has yielded a number of theorems which have proved of considerable utility in the interpretation of experiment. For the phenomena involving mesons, the theorems have been of special value in pointing to suitable experiments for measuring the meson-nucleon coupling constant.[2]

In order to investigate the threshold behavior of scattering or production matrices, one expands these, in effect, in power series in the four-momenta of the bosons. One then observes that one or more of the leading powers is of the same form as its Born approximation, expressed, however, in terms of the experimental charge, magnetic moment, and mesic coupling constant of the fermion. The purpose of this note is to report a systematic procedure for the construction of such theorems; in the course of the discussion we shall rederive the results that are already known,[1–3] as well

* Society of Fellows.
† Now at the Department of Physics, University of Pennsylvania, Philadelphia, Pennsylvania.
[1] The zero-frequency limit was first treated in full generality by W. Thirring, Phil. Mag. **41**, 1193 (1950), the amplitude to first order in the frequency by F. E. Low, Phys. Rev. **96**, 1428 (1954) and by M. Gell-Mann and M. L. Goldberger, Phys. Rev. **96**, 1433 (1954).
[2] N. M. Kroll and M. A. Ruderman, Phys. Rev. **93**, 233 (1954).
[3] Deser, Goldberger, and Thirring, Phys. Rev. **94**, 711 (1954).

as a number of additional theorems on photomeson production and meson-nucleon scattering.[4]

The physical properties of a nucleon which underlie these results are most clearly subsumed in the structure of its Green's function in the presence of external boson sources.[5] The rather direct relation of this quantity to the transition amplitudes is derived in Sec. II. The basic physical information at our disposal, to be fitted naturally into a framework that satisfies the requirements of Lorentz, gauge, and charge conjugation invariance, is twofold. First, we know the form and analytic properties of the field-independent part of the renormalized Green's function, G, for four-momenta in the neighborhood of the free-nucleon mass shell. Second, we can insist that the propagator describe a particle with the correct experimental electric and mesic charge and magnetic moment, a condition imposed on the terms of G which are linear in the boson sources. The role of the requirement that we deal with a renormalizable theory is merely that the above statements have a meaning, after a suitable scale change, if necessary, for the various functions of the theory.

It is perhaps worth emphasizing that the true significance of the theorems is that they provide a means of measuring parameters which are logically defined by other experiments. Thus, the charge and magnetic moment of the proton is measured, in principle, in the scattering of the proton by a weak, slowly varying external electromagnetic field, weak enough so that only effects linear in the field need be considered and sufficiently slowly varying so that any space-time variation of the *field-strengths* may be neglected. Again, the meson-nucleon coupling constant—in the sense in which the term will be used in this paper[6]—is measured by the scattering of a nucleon by a weak, slowly varying meson field. Because of the pseudoscalar nature of the meson, the coupling constant so defined is more the analog of the magnetic moment than of the charge, since there is no scattering to first order in the field from a uniform meson field.[7] If we notice the formal identity between the scattering and production phenomena to be considered and the dependence of the scattering of the fermion on terms of second order in the external boson fields, then the theorems may be given an alternative statement. It is that the matrix elements which determine the scattering of a fermion by a weak, slowly varying field also determine—with exceptions to be noted below—the scattering by somewhat stronger but still slowly varying fields.

We have divided the detailed considerations according to phenomena. Section III, which treats of γ-ray scattering, contains the proof that the scattering amplitude for this process is correctly given up to terms of first order in the frequency of the photon by the Born approximation computed for a nucleon with given charge and Pauli moment.[1] We actually construct the Green's function in greater detail than is required for the proof of the theorem. Thus, we are in a position to specify the number of additional parameters required to determine the scattering amplitude to the second power of the photon momentum. It is suggested that it should be possible to understand experiments up to energies somewhat below the threshold for meson production by assigning to the proton (approximately) constant electric and magnetic polarizabilities in addition to its charge and magnetic moment. The interpretation of existing experiments[8] in terms of single nucleon scattering cross sections is not sufficiently certain to allow a real test of this hypothesis.

In Sec. IV, it is shown that the P-wave in meson-nucleon scattering is given by Born approximation except for relative corrections which vanish as *both* the momentum and mass of the meson go to zero. That there is no analogous theorem for the S-wave is merely a consequence of the fact that the coupling constant taken as fundamental in the discussion is the strength for the emission of a meson into a P state.[6,7] The S-wave near threshold is determined by two parameters,[9] the coefficients of the S-wave terms which are independent of and linear respectively in the energy of the meson. The first deviation from the Born amplitude for the P-wave can also be expressed in terms of two parameters. Since there are three independent P-wave phase shifts ($\alpha_{31}=\alpha_{13}$ in the approximation which neglects nucleon recoil[9]), it is then possible to derive a single relation among them. One qualitative statement of this relation is that if α_{11} and α_{13} are reduced compared to their Born values, then α_{33} is necessarily enhanced. Comparison with experiment yields values for these parameters by no means small compared to the coupling constant, although this is easily understood in terms of the resonance in the scattering.

Three theorems on photomeson production are established in Sec. V. The S-wave theorem for the nucleon current leading to charged meson production (Kroll-Ruderman theorem)[2] is shown to be a direct consequence of the definition of the mesonic coupling constant and of gauge invariance. It is then demonstrated that the P-wave production from the nucleon is given near threshold by the Born approximation computed with the actual meson-nucleon coupling

[4] The new results to be established in this paper concerning the P-wave in meson scattering and the P-wave and meson current effects in photoproduction have been established by independent methods by F. E. Low, to whom the author is indebted for illuminating discussions.

[5] In the treatment of photoproduction we also require the Green's function of a meson in an external electromagnetic field.

[6] The alternative definition proposed by Deser, Thirring, and Goldberger, reference 3, in terms of meson scattering at zero energy is less closely related to the original Yukawa hypothesis. In the absence of a satisfactory dynamical theory, however, one can only remark that this definition is of use in the correlation of a different class of phenomena than those considered in this paper.

[7] This is, of course, equivalent to the observation that the emission of a single pseudoscalar meson is into a P state.

[8] Pugh, Frisch, and Gomez, Phys. Rev. **95**, 590 (1954).

[9] We use the notation of Fermi for the S and P phase shifts, Anderson, Fermi, Martin, and Nagle, Phys. Rev. **91**, 155 (1953).

constant and magnetic moment. Thirdly, a similar statement is established for the contribution of the meson current which involves the charge and the coupling constant. The latter contribution contains all angular momenta for the meson and multipoles for the photon because of a retardation factor for the motion of the meson. The deviations from these theorems can also be considered. In the present instance, however, it leads only to a type of analysis which has essentially been exploited in the literature;[10] we have therefore been content with noting the general forms of the correction terms.

II. EXPRESSION FOR SCATTERING AMPLITUDE

We shall derive the scattering amplitude for a boson-fermion collision, taking as a representative case that of photon scattering. As is well known, the transition amplitude from a given state of the system at some initial time to another state at a later time is determined by a suitably expressed matrix element of the Green's function for the system taken between those states. The S matrix is defined as the amplitude for going from a free-particle state in the remote past to another such state in the remote future.[11] For the example chosen, the S matrix is given by the expression

$$\begin{aligned}&(p'\sigma', k'\mu|S|p\sigma, k\nu)\\&\quad=-(\lim x_{10},\ \xi_{10}\to+\infty\ ;\ x_{20},\ \xi_{20}\to-\infty)\\&\quad\times\int d\mathbf{x}_1 d\xi_1 d\mathbf{x}_2 d\xi_2\ (p'\sigma', k'|x_1,\xi_1)_\alpha\\&\quad\times\tfrac{1}{2}i(\overleftarrow{\partial}/\partial\xi_{10}+\partial/\overrightarrow{\partial}\xi_{10})G_{\alpha\beta,\mu\nu}(x_1,x_2;\xi_1,\xi_2)\\&\qquad\times\tfrac{1}{2}i(\overleftarrow{\partial}/\partial\xi_{20}+\partial/\overrightarrow{\partial}\xi_{20})(x_2,\xi_2|p\sigma,k)_\beta.\end{aligned}\tag{1}$$

Here $p\sigma$, $p'\sigma'$ are four-momentum and spin variables specifying initial and final nucleon states, $k\nu$, $k'\mu$, are the corresponding momentum and vector component variables of the photon. The amplitude $(x,\xi|p\sigma,k)_\beta$ is the initial state of the combined system:

$$(x,\xi|p\sigma,k)_\beta=(x|p\sigma)_\beta\,(\xi|k),\tag{2}$$

$$(x|p\sigma)=\left[\frac{1}{(2\pi)^3}\frac{(p^2+m^2)}{m^2}\right]^{\frac{1}{2}}e^{ipx}u_\beta(p\sigma),\tag{3}$$

$$(\xi|k)=[(2\pi)^3 2k_0]^{-\frac{1}{2}}e^{ik\xi},\tag{4}$$

and

$$(p\sigma,k|x,\xi)_\beta=[(x,\xi|p\sigma,k)^\dagger\gamma_0]_\beta,\tag{5}$$

where γ_0 is the usual Dirac matrix and the four-momenta are those of free particles. The Green's function of the photon-nucleon system is defined by the relation[12]

$$\begin{aligned}&G_{\alpha\beta,\mu\nu}(x_1,x_2;\xi_1,\xi_2)\\&\quad=-\langle(\psi_\alpha(x_1)\bar\psi_\beta(x_2)A_\mu(\xi_1)A_\nu(\xi_2))_+\rangle\epsilon(x_1-x_2)\\&\quad=G_+(x_1,x_2)_{\alpha\beta}\mathcal{G}_+(\xi_1,\xi_2)_{\mu\nu}\\&\qquad-i\delta^2G_+(x_1,x_2)_{\alpha\beta}/\delta J_\mu(\xi_1)\delta J_\nu(\xi_2)|_{J=0},\end{aligned}\tag{6}$$

with $J_\mu(\xi)$ standing for the external current which is usefully assumed to be coupled to the electromagnetic field.

To transform Eq. (1), consider the first term of Eq. (6). Since $x_{10}>x_{20}$, we can write

$$\begin{aligned}G_+(x_1,x_2)_{\alpha\beta}&=i\langle0|\psi_\alpha(x_1)\bar\psi_\beta(x_2)|0\rangle\\&=i\textstyle\sum_n e^{iP_n(x_1-x_2)}\langle0|\psi_\alpha(0)|n\rangle\langle n|\bar\psi_\beta(0)|0\rangle,\end{aligned}\tag{7}$$

where the sum is over all states of unit "charge," and P_n is the four-momentum of the state n,

$$P_n=(\mathbf{p},E_n(p)=(p^2+m_n^2)^{\frac{1}{2}}).$$

Among the allowed values of m_n, there is the isolated lowest point $m_n=m$, the mass of a nucleon. Separating the contribution from this state from all the others, we may write according to the theory of renormalization[13]

$$\begin{aligned}&G_+(x_1,x_2)_{\alpha\beta}\\&=\frac{i}{(2\pi)^3}Z_2\sum_\sigma\int d\mathbf{p}\exp[i\mathbf{p}(\mathbf{x}_1-\mathbf{x}_2)-iE(\mathbf{p})(x_{10}-x_{20})]\\&\qquad\times\langle0|\psi_\alpha(0)|\mathbf{p}\sigma\rangle\langle\mathbf{p}\sigma|\bar\psi_\beta(0)|0\rangle+\cdots,\end{aligned}\tag{8}$$

where $\cdots$ indicates the contribution from higher mass states and the matrix element $\langle0|\psi_\alpha(0)|\mathbf{p}\sigma\rangle$ is now understood to be finite and a solution of the free particle Dirac equation for a real nucleon. From Eq. (8) combined with Eqs. (3) and (5), we then obtain the the relation:

$$\begin{aligned}&\lim(x_{10}\to\infty)\int d\mathbf{x}_1(\mathbf{p}\sigma|x_1)_\alpha G_+(x_1,x_2)_{\alpha\beta}\\&\qquad=i(2\pi)^{-\frac{1}{2}}e^{-ipx_2}\bar u_\beta(p\sigma)Z_2.\end{aligned}\tag{9}$$

Equation (9) is true in the sense that all terms which oscillate with infinite rapidity are to be equated to zero, the limiting procedure of Eq. (1) being understood in that sense. We have also required the normalization condition

$$\bar u_\alpha(p\sigma)u_\alpha(p,\sigma')=\delta_{\sigma\sigma'}m/E(\mathbf{p}).\tag{10}$$

For the photon propagator $\mathcal{G}_+(\xi_1,\xi_2)_{\mu\nu}$, there are

[10] For example, see M. Gell-Mann and K. M. Watson, Ann. Rev. Nuc. Sci. **4**, 219 (1954).

[11] These states are most conveniently considered to describe particles with their experimental masses.

[12] The completely analagous case of the meson-nucleon system has been studied by S. Deser and P. C. Martin, Phys. Rev. **90**, 1072 (1953). For the notation see J. Schwinger, Proc. Natl. Acad. Sci. U.S. **37**, 452 (1951).

[13] F. J. Dyson, Phys. Rev. **85**, 1736 (1949).

similar expressions. From the equation $(\xi_{10}>\xi_{20})$

$$\mathcal{G}_+(\xi_1,\xi_2)_{\mu\nu} = \frac{i}{(2\pi)^3}Z_3\sum_\lambda\int\frac{d\mathbf{k}}{2k_0}\exp[i\mathbf{k}\cdot(\xi_1-\xi_2)-ik_0(\xi_{10}-\xi_{20})] \times\langle 0|A_\mu(0)|k\lambda\rangle\langle k\lambda|A_\nu(0)|0\rangle+\cdots, \quad (11)$$

we conclude the relation

$$\lim(\xi_{10}\to\infty)\int d\xi_1(k|\xi_1) \times\tfrac{1}{2}i(\overleftarrow{\partial}/\partial\xi_{10}+\overrightarrow{\partial}/\partial\xi_{10})\mathcal{G}_+(\xi_1,\xi_2)_{\mu\nu} = i[(2\pi)^3 2k_0]^{-\frac{1}{2}}e^{-ik\xi_2}\delta_{\mu\nu}Z_3. \quad (12)$$

Applying Eqs. (9), (12) and corresponding expressions for the limit $(x_{20},\xi_{20}\to-\infty)$, to the second term of Eq. (6) as well as to the first, we obtain for Eq. (1) the more immediately useful equation:

$$\begin{aligned}&(p'\sigma',k'\mu|S|p\sigma,k\nu)\\ &=Z_2Z_2\delta_{\sigma\sigma'}\delta_{\mu\nu}\delta(\mathbf{p}'-\mathbf{p})\delta(\mathbf{k}'-\mathbf{k})+\frac{iZ_2^2Z_3^2}{(2k_0'2k_0)^{\frac{1}{2}}(2\pi)^6}\\ &\times\int d^4\xi'd^4x'd^4\xi d^4x e^{-ip'x'}e^{-ik'\xi'}\bar{u}(p'\sigma')\\ &\times\mathcal{G}_+^{-1}(\xi',\xi'')_{\mu\rho}G_+^{-1}(x',x'')\delta^2G_+(x'',x''')/\\ &\quad\delta J_\rho(\xi'')\delta J_\epsilon(\xi''')|_{J=0}\\ &\times G_+^{-1}(x''',x)\mathcal{G}_+^{-1}(\xi''',\xi)_{\epsilon\nu}u(p\sigma)e^{ipx}e^{ik\xi}, \quad (13)\end{aligned}$$

where summation or integration over repeated variables is understood. Several additional observations are required before Eq. (13) is transformed into final working form. First, we note that we must divide by the product Z_2Z_3 to obtain a unitary and indeed finite S matrix. Second, we make a change of variables from the external current to the external electromagnetic potential according to the expression[14] (in which vector indices have been suppressed):

$$\delta^2G/\delta J(\xi)\delta J(\xi') = Z_3(\delta^2G/\delta A_c(\xi'')\delta A_c(\xi''')) \times\mathcal{G}_+^{(0)}(\xi'',\xi)\mathcal{G}_+^{(0)}(\xi''',\xi'), \quad (14)$$

since A_c and J are related by the expression

$$A_c(\xi)=Z_3^{\frac{1}{2}}\mathcal{G}_+^{(0)}(\xi\xi')J(\xi'), \quad (15)$$

involving the uncoupled photon Green's function $\mathcal{G}_+^{(0)}$. We next note the validity of the equation

$$\int d^4\xi'e^{-ik'\xi'}\mathcal{G}_+^{-1}(\xi',\xi'')\mathcal{G}_+^{(0)}(\xi'',\xi''')\varphi(\xi''') = Z_3^{-1}\int d^4\xi'e^{-ik'\xi'}\varphi(\xi'), \quad (16)$$

for k' the four-momentum of a real photon and $\varphi(\xi)$ any function of ξ. Finally, we introduce into Eq. (13) the convergent Green's function, G_c, where[15]

$$G=Z_2G_c. \quad (17)$$

By the use of Eqs. (14)–(17) and the accompanying remarks, we are now in a position to state a convergent expression for the S matrix for photon-proton scattering,[16] conveniently expressed in terms of a transition matrix T, where

$$\begin{aligned}&\delta(p'+k'-p-k)(p'\sigma',k'\mu|T|p\sigma,k\nu)\\ &=-\frac{e^2}{(2\pi)^4}\int d^4\xi'd^4x'd^4\xi d^4x e^{-ip'x'}e^{-ik'\xi'}\bar{u}(p'\sigma')\\ &\times(x'|G^{-1}\delta^2G/\delta(eA_\mu(\xi))\delta(eA_\nu(\xi'))|_{A=0}G^{-1}|x)\\ &\times u(p\sigma)e^{ipx}e^{ik\xi}, \quad (18)\end{aligned}$$

and T is then related to S according to the equation

$$\begin{aligned}&(p'\sigma',k'\mu|S|p\sigma,k\nu)\\ &=\delta_{\sigma\sigma'}\delta_{\mu\nu}\delta(\mathbf{p}'-\mathbf{p})\delta(\mathbf{k}'-\mathbf{k})-2\pi i\delta(p'+k'-p-k)\\ &\times[(2\pi)^3 2k_0'2k_0]^{-\frac{1}{2}}(p'\sigma',k'\mu|T|p\sigma,k\nu). \quad (19)\end{aligned}$$

In Eq. (18) e is the renormalized charge of the proton.

Before proceeding to the proofs of the photon scattering theorems, it is perhaps worthwhile to exemplify the use of Eq. (18) by deriving the Born approximation scattering for a fermion with a charge but no anomalous moment. For the Green's function in the external field, we then take

$$G(x,x'[A])=(x|G[A]|x') =\left(x\left|\left\{\int d^4\xi[\gamma(\xi)(p-eA(\xi))]+m\right\}^{-1}\right|x'\right). \quad (20)$$

The significance of the notation is expressed by the equations

$$(x|\gamma(\xi)|x')=\gamma\delta(\xi-x)\delta(x-x'), \quad (21)$$

$$\int\gamma(\xi)d\xi=\gamma, \quad (22)$$

[14] In Eqs. (14) and (15), $A_c(\xi)$ is the renormalized external field, whereas $J(\xi)$ is the unrenormalized current. Consistency between the definition (compare reference 12) $\mathcal{G}_+=\delta(A)/\delta J$ and the renormalization scheme, $\mathcal{G}_+=Z_3\mathcal{G}_{+c}$, $\langle A\rangle=Z_3^{\frac{1}{2}}\langle A\rangle_c$, requires the renormalization $J=Z_3^{-\frac{1}{2}}J_c$.

[15] The renormalization succeeds formally if we assume this relation to obtain even in the presence of the electromagnetic field. The scale factors in Eq. (13) then disappear without any necessity of mentioning vertex renormalization. The proof of equivalence to the more usual statements is easily carried through.

[16] In what follows we discard the subscripts $+$ and c, since except briefly at the start of Sec. V, we shall be dealing exclusively with convergent propagation functions of the indicated type.

with p the ordinary four-momentum operator. It then follows directly that

$$G^{-1}\delta G[A]/\delta(eA_\mu(\xi))\delta(eA_\nu(\xi'))\,|_{A=0}G^{-1}$$
$$=\gamma_\mu(\xi)(\gamma p+m)^{-1}\gamma_\nu(\xi')+\gamma_\nu(\xi')(\gamma p+m)^{-1}\gamma_\mu(\xi), \quad (23)$$

which yields in turn the following form for Eq. (18):

$$(p'\sigma', k'\mu\,|\,T\,|\,p\sigma, k\nu)$$
$$=-e^2\bar{u}(p'\sigma')\{\gamma_\mu[\gamma(p+k)+m]^{-1}\gamma_\nu$$
$$+\gamma_\nu[\gamma(p-k')+m]^{-1}\gamma_\mu\}u(p\sigma), \quad (24)$$

wherein it is understood that

$$p'+k'=p+k. \quad (25)$$

We have here illustrated and wish further to emphasize the point, which is fundamental to our further discussion, that in any consideration of the second variational derivative of $G[A]$, only that part of it which has a second-order pole on the free-particle energy shell, that is a factor of $G[0]$ standing both on the right and the left, contributes anything to the scattering. Otherwise the factors of

$$\int G^{-1}(x', x[0])e^{ipx}d^4xu(p\sigma), \quad (26)$$

whose vanishing assert the free particle character of initial and final nucleon states, dominate the situation.

III. PHOTON SCATTERING

We require the structure of the Green's function in the presence of an external electromagnetic field. It is instructive to begin our considerations with the zero-field propagator, since this suffices to obtain the zero frequency limit of the scattering. We thus consider the structure

$$G^{-1}(p;[0])=(\gamma p+m)[1+(2m)^{-1}(\gamma p+m)\mathfrak{F}_1(p^2/m^2)$$
$$+(2m)^{-2}(\gamma p+m)^2\mathfrak{F}_2(p^2/m^2)], \quad (27)$$

as determined by the dual requirements of Lorentz invariance and the condition that

$$G^{-1}(p;[0])(\gamma p+m)^{-1}u(p)=u(p), \quad (28)$$

when $u(p)$ itself satisfies

$$(\gamma p+m)u(p)=0. \quad (29)$$

Equation (28) prescribes the singularity of G itself for four-momenta satisfying $p^2+m^2=0$. It follows that $\mathfrak{F}_1$ and $\mathfrak{F}_2$ are analytic functions of their argument in this neighborhood.[17] As a consequence, if we expand G itself about the point $\gamma p+m=0$, we obtain

$$G(p;[0])=(\gamma p+m)^{-1}+(2m)^{-1}\mathfrak{F}_1(0)$$
$$+(2m)^{-2}(\gamma p+m)\mathfrak{F}_2(0)+\cdots$$
$$=(\gamma p+m)^{-1}+\Delta G(\gamma p), \quad (30)$$

with ΔG again analytic in the domain of interest.

Now to obtain the scattering which is independent of the boson momenta, we can ignore any explicit dependence of $G[A]$ on the field strengths or their derivatives, since for such a dependence we have, for example, the relation

$$\frac{\delta G}{\delta A_\mu(\xi)}=\int\frac{\delta G}{\delta F_{\lambda\rho}(\xi')}\frac{\delta F_{\lambda\rho}(\xi')}{\delta A_\mu(\xi)}$$
$$=\int\frac{\delta G}{\delta F_{\lambda\rho}(\xi')}(\delta_{\mu\rho}\partial_\lambda'-\delta_{\lambda\mu}\partial_\rho')\delta(\xi'-\xi), \quad (31)$$

and each derivative with respect to the photon coordinates leads to a factor of the photon momentum upon insertion into Eq. (18). We therefore require only the explicit dependence on the electromagnetic potential, and the form in which this may occur is restricted by the principle of gauge invariance to the combination $\Pi_\mu=p_\mu-eA_\mu$; more explicitly this means the combination

$$\Pi_\mu=p_\mu-e\int d^4\xi\mathbf{1}(\xi)A_\mu(\xi), \quad (32)$$

with the understanding that $\gamma\mathbf{1}(\xi)=\gamma(\xi)$. But Eq. (30) now tells us that $\Delta G(\gamma\Pi)$ is an analytic function of $\gamma\Pi$ so that its derivatives can contribute nothing to any scattering process. Our result is thus that the Green's function, G_1, effective for zero energy scattering is[18]

$$G_1(p;[A])=(\gamma\Pi+m)^{-1}. \quad (33)$$

To extend our considerations, we must now include in the Green's function its explicit dependence on electromagnetic field strengths. It is generally true, however, quite independent of the expansion in the photon momentum, that we may ignore any dependence on the external current, $J_\mu(\xi)$, since this is zero for a real photon; that is, $J_\mu(\xi)=-\Box^2A_\mu(\xi)$ contributes, after computation of the variational derivative, a factor k^2 or k'^2 both of which vanish. Again, we require the dependence on the field strengths themselves in a very restricted sense, for G need be correct only to the second order of the field. Moreover, terms which depend on the square of the field strength will contribute to the scattering first to the second order in the frequency.

To see these arguments in more detail, we consider the problem of constructing invariants which are linear in $F_{\mu\nu}$. We shall be guided in part by the requirements

[17] This will certainly be the case if we exclude virtual interactions with quanta of vanishing rest mass.

[18] The subscript 1 on G_1 will be used to denote that part of the Green's function effective for scattering throughout the varying contexts of this paper.

of charge conjugation invariance, which can be stated in the convenient form

$$CG^{-1}(p,[-A])^{T}C^{-1}=G^{-1}(p,[A]), \qquad (34)$$

where C is the charge conjugating matrix and the operation of transposition is to be applied to all variables of the nucleon, remembering that $p^{T}=-p$. For the formation of the required invariants, we have at our disposal the linearly independent Dirac matrices and the vector Π_μ. A systematic consideration then shows that essentially the only combination that satisfies Eq. (34) is $\sigma_{\mu\nu}F_{\mu\nu}=\sigma F$; all other possibilities are simply expressible as multiple commutators and anticommutators of $\gamma\Pi$ with σF. To the first order in the field then, it is correct to write the series

$$\begin{aligned}G^{-1}(\Pi,[A])=&\gamma\Pi+m-\tfrac{1}{2}\mu'\sigma F+(2m)^{-1}(\gamma\Pi+m)^{2}\mathfrak{F}_1+\cdots\\&+\tfrac{1}{2}(2m)^{-1}\{\gamma\Pi+m,\sigma F\}\mathfrak{M}_1\\&+\tfrac{1}{4}(2m)^{-2}\{\gamma\Pi+m,\{\gamma\Pi+m,\sigma F\}\}\mathfrak{M}_{21}\\&+\tfrac{1}{4}(2m)^{-2}[\gamma\Pi+m,[\gamma\Pi+m,\sigma F]]\mathfrak{M}_{22}+\cdots \qquad (35)\end{aligned}$$

in terms of the additional set of parameters $\mathfrak{M}_1,\mathfrak{M}_{21},\cdots$, and μ'. The latter can be correctly identified as the anomalous magnetic moment of the nucleon if we compute from Eq. (35) the scattering of the nucleon to first order in the field, as given by the expression

$$\begin{aligned}&\delta(p'-p-k)(p'\sigma'|\,T_\mu\,|p\sigma)\\&=-\frac{e}{(2\pi)^4}\int d^4x'd^4xd^4\xi e^{-ip'x'}e^{ipx}e^{ik\xi}\bar{u}(p'\sigma')\\&\qquad\times(x'|\,\delta G^{-1}/\delta eA_\mu(\xi)\,|_{A=0}\,|x)u(p\sigma)\\&=\delta(p'-p-k)\bar{u}(p'\sigma')\{\gamma_\mu+i(\mu'/e)k_\lambda\sigma_{\lambda\mu}\}u(p\sigma)\\&=\delta(p'-p-k)\bar{u}(p'\sigma')\{[(2p+k)_\mu/2m]\\&\qquad+(i/e)k_\lambda\sigma_{\lambda\mu}(\mu'+e/2m)\}u(p\sigma). \qquad (36)\end{aligned}$$

Equation (35) suffices to compute the scattering to first order in the frequency, since any terms of second order in the field not already contained therein are by the requirements of gauge invariance proportional to the square of the field tensor. Indeed, we wish to establish the theorem that to first order in k, the scattering is correctly described by the Green's function

$$G_1=[\gamma\Pi+m-\tfrac{1}{2}\mu'\sigma F]^{-1}. \qquad (37)$$

To see this most clearly, we consider a trivial analytic continuation of the series, Eq. (35), obtained by choosing as independent operators G_1^{-1} and σF, rather than $\gamma\Pi+m$ and σF. The numerical values of $\mathfrak{M}_1,\cdots$ will then be altered, but without changing notation, the new series reads

$$\begin{aligned}G^{-1}(\Pi,[A])=&G_1^{-1}+G_1^{-2}(2m)^{-1}\mathfrak{F}_1+\cdots\\&+\tfrac{1}{2}(2m)^{-1}\{G_1^{-1},\sigma F\}\mathfrak{M}_1+\cdots. \qquad (38)\end{aligned}$$

Inverting and expanding about G_1, we obtain[19]

$$\begin{aligned}G(\Pi,[A])=&G_1+(2m)^{-1}\mathfrak{F}_1+\cdots\\&+\{G_1,(2m)^{-1}\tfrac{1}{2}\sigma F\}\mathfrak{M}_1+\cdots. \qquad (39)\end{aligned}$$

The theorem now follows from the observations that when we compute the second derivative of G at the point $A=0$, the terms involving the coefficients $\mathfrak{F}$ are, as before, analytic on the free-particle energy shell, whereas the new contributions involving the coefficients $\mathfrak{M}$ exhibit at most a pole of the first order. Indeed, the representative terms exhibited in Eq. (38) are the most singular members of their respective classes.

The actual form of the T matrix of Eq. (18) computed to first order in k by means of the G_1 of Eq. (37) and expressed as the scalar product of a Pauli spin operator with initial and final polarization vectors is[1]

$$\begin{aligned}\mathbf{e}'\cdot\mathbf{T}\cdot\mathbf{e}=&(e^2/m)\mathbf{e}'\cdot\mathbf{e}-(ie/2m)\mu'2k_0\boldsymbol{\sigma}\cdot(\mathbf{e}'\times\mathbf{e})\\&+(ie/2m)\mu k_0[(\mathbf{n}\cdot\mathbf{e}')(\boldsymbol{\sigma}\cdot\mathbf{n}\times\mathbf{e})+(\boldsymbol{\sigma}\cdot\mathbf{n})(\mathbf{n}\cdot\mathbf{e}\times\mathbf{e}')\\&-(\mathbf{n}'\cdot\mathbf{e})(\boldsymbol{\sigma}\cdot\mathbf{n}'\times\mathbf{e}')-(\boldsymbol{\sigma}\cdot\mathbf{n}')(\mathbf{n}'\cdot\mathbf{e}'\times\mathbf{e})]\\&+2i\mu^2k_0\boldsymbol{\sigma}\cdot(\mathbf{n}'\times\mathbf{e}')\cdot(\mathbf{n}\times\mathbf{e}). \qquad (40)\end{aligned}$$

Here $\mathbf{n}$ and $\mathbf{n}'$ are unit vectors in the direction of the incident wave and in the direction of observation respectively, and μ is the total magnetic moment. The differential cross section for unpolarized particles to which Eq. (40) gives rise, may be written as

$$\begin{aligned}d\sigma/d\Omega=&(e^4/m^2)\tfrac{1}{2}(1+\cos^2\theta)+k^2[6\mu^4+(\mu^2e^2/m^2)\\&-(\mu e^2/m^3)+\tfrac{3}{8}(e^4/m^4)]\\&+k^2\cos\theta[-8\mu^3(e/m)+2\mu^2(e^2/m^2)]\\&+k^2\cos^2\theta[-2\mu^4+3\mu^2(e^2/m^2)\\&-\mu(e^2/m^3)-\tfrac{1}{8}(e^4/m^4)]. \qquad (41)\end{aligned}$$

In Eq. (41), we have returned to unrationalized units in which e^2 is the fine structure constant. It should be remarked that for γ rays with energy of 100 Mev or more scattered from protons, the magnetic terms are of the same order of magnitude as the Thomson cross section, the main contribution arising from the isotropic terms which is proportional to the forth power of the total magnetic moment.

Equation (41) is not yet accurate enough to be compared with experiment even in the energy range for which a frequency expansion of the scattering amplitude might be expected to have approximate validity, the region below the threshold for meson production, since there are additional contributions to the cross section of second order in the photon energy. These come about as a result of interference between spin

[19] The structure of the Green's function, Eq. (39), could have been inferred equally well by considering the proton to be situated in a weak uniform magnetic field, in which it is still possible to prescribe energy values, as determined by the singularities of G_1. The term depending on $\mathfrak{M}_1$ is then associated with the first order change in the wave functions.

independent terms in the scattering amplitude, of second order in the photon frequency, and the Thomson amplitude. The terms in question may be divided conveniently into two classes. There are first those which are contained in the Green's function, G, itself.[20] The leading effect on the cross section is, at most, proportional to μ^2 and therefore should be small compared to the magnetic scattering. In any case, such additions can be readily calculated although, for reasons to be stated below, we shall not take the trouble.

More important, undoubtedly, are the effects of the transition of the nucleon to excited states after absorption of the incident photon, the Rayleigh scattering. For energies below the threshold for meson production, we may expect to obtain an approximate description of this scattering by adding to the Green's function of Eq. (38) members which are quadratic in the electromagnetic field strengths.

We require only such terms as have nonvanishing matrix elements between solutions of the free-particle Dirac equation and, further, remain linearly independent when such matrix elements are computed. There are in fact only three such forms, which may be taken conveniently as $F_{\mu\nu}^2$, $(\gamma_\mu \Pi_\nu/m)F_{\mu\lambda}F_{\nu\lambda}$, and $\gamma_5 F_{\mu\nu}F_{\mu\nu}^*$, where $F_{\mu\nu}^*$ is the tensor dual to $F_{\mu\nu}$. Of these, the last is effectively of third order in the frequency, the second proportional to E^2, and the first to H^2-E^2. For a nonrelativistic description, therefore, it is sufficient to consider the addition to G^{-1} of the terms

$$-\tfrac{1}{2}\alpha E^2-\tfrac{1}{2}\beta H^2, \tag{42}$$

which yield the not unexpected result that the Rayleigh scattering should be describable by means of an electric and magnetic polarizability, α and β respectively.

For a model which includes Thomson but omits magnetic scattering, we then obtain the scattering amplitude:

$$\mathbf{e}'\cdot\mathbf{T}\cdot\mathbf{e}=(e^2/m)\mathbf{e}'\cdot\mathbf{e}-\alpha k_0{}^3\mathbf{e}'\cdot\mathbf{e}+\beta k_0{}^3(\mathbf{n}\times\mathbf{e})\cdot(\mathbf{n}'\times\mathbf{e}'), \tag{43}$$

and a cross section

$$d\sigma/d\Omega=[(e^2/m)-\alpha k^2]^2\tfrac{1}{2}(1+\cos^2\theta) -2[(e^2/m)-\alpha k^2]\beta k^2\cos\theta+\beta^2 k^4\tfrac{1}{2}(1+\cos^2\theta). \tag{44}$$

The characteristics of Eq. (44) are suited to fit the one existing experiment[8] with the not surprising values for α and β,[21]

$$\alpha\sim\beta\sim(e^2/mm_\pi{}^3), \tag{45}$$

to within a factor of two, with m_π the mass of the π meson. We hesitate to draw any conclusions from this circumstance since the interpretation of the experimental results in terms of individual nucleon scattering cross sections is subject to considerable doubt, especially in view of the fact that no deviation from Thomson scattering was detected for heavy nuclei.

[20] In this sense our method of calculation has greater generality than a direct momentum expansion of the scattering amplitude.

[21] The values of α and β in Eq. (44) justify the neglect of the additional contributions of order k^3 arising directly from G_1.

IV. MESON-NUCLEON SCATTERING

In direct analogy with Eq. (18), the formula for the renormalized transition amplitude is given by the equation[22]

$$(p'\sigma', q'j|T|p\sigma, qi) =-\frac{g^2}{(2\pi)^4}\int d^4x'd^4\xi'd^4xd^4\xi e^{-ip'x'}e^{-ik'\xi'}\bar{u}(p'\sigma') \times(x'|G^{-1}\delta^2G/\delta(g\phi_i(\xi))\delta(g\phi_j(\xi'))|_{\phi=0}G^{-1}|x) \times u(p\sigma)e^{ipx}e^{ik\xi}. \tag{46}$$

Here $\phi_i(\xi)$ is the external meson field, i and j the isotopic indices of incident and emergent meson.

We proceed immediately to the construction of the Green's function, $G(p, [\phi])$. If we consider first terms linear in ϕ, we have at our disposal besides the principle of Lorentz invariance, the property corresponding to charge conjugation invariance, as expressed by the condition

$$CG^{-1}(p, [-\phi])^TC^{-1}=G^{-1}(p, [\phi]), \tag{47}$$

where C has the same effect on the Dirac matrices as in the electromagnetic case, and in addition for the isotopic matrices τ_i,

$$C\tau_iC^{-1}=-\tau_i. \tag{48}$$

Again, there is really only one invariant independent of γp, that is, the quantity $\gamma_5\boldsymbol{\tau}\cdot\boldsymbol{\phi}$, all other invariants being expressible as multiple commutators and anticommutators of the two operators. For example, we have the relation

$$\{\gamma p, \gamma_5\boldsymbol{\tau}\cdot\boldsymbol{\phi}\}=i\gamma_5\gamma_\mu\partial_\mu\boldsymbol{\tau}\cdot\boldsymbol{\phi}. \tag{49}$$

It is important to remark that in the choice of a fundamental coupling term to define the constant g, we have at our disposal either $-g\gamma_5\boldsymbol{\tau}\cdot\boldsymbol{\phi}$, or $i(g/2m)\gamma_5\gamma_\mu\partial_\mu\boldsymbol{\tau}\cdot\boldsymbol{\phi}$, since both lead to the same scattering of the nucleon by ϕ to the first order in the momentum transfer.[23] As will become clear gradually, it is convenient to choose the latter form.[24]

Employing the effective Green's function G_1,

$$G_1=[\gamma p+m+i(g/2m)\gamma_5\gamma_\mu\partial_\mu\boldsymbol{\tau}\cdot\boldsymbol{\phi}]^{-1}, \tag{50}$$

[22] The symmetry of Eq. (46) in the meson field variables immediately establishes the relation

$$(p'\sigma', q'j|T|p\sigma, qi)=(p'\sigma', -qi|T|p\sigma, -q'j).$$

There was, of course, a similar relation in the case of photon scattering.

[23] We recall that $\bar{u}(p)\gamma_5u(p)=0$.

[24] It is perhaps well to emphasize that this choice has absolutely nothing to do with the fundamental dynamics of the meson-nucleon system.

which will be the subject of a theorem, the expansion to first order in ϕ analogous to Eq. (38) can be expressed as

$$G^{-1}(p,[\phi])=G_1^{-1}+G_1^{-2}(2m)^{-1}\mathfrak{F}_1+\cdots +\tfrac{1}{2}\{G_1^{-1},\gamma_5\boldsymbol{\tau}\cdot\boldsymbol{\phi}\}\mathfrak{C}_1+\cdots \quad (51)$$

of which we are assured that only the first term contributes anything to the scattering. Indeed, the insertion of Eq. (50) into Eq. (46) yields the Born approximation for the P wave of order (q^2/ω), where ω is the meson energy, whereas the S wave behaves as ω^2. If we admit, provisionally, the result that any other P wave in the theory must behave as q^2, we should then have established the validity of the Born approximation to the P wave in the limit as $\omega\to 0$. On the other hand, we shall see that there may be S waves in the theory of zero and first order in ω.

To verify these last assertions, we must consider those contributions to G which are second order in ϕ and no more than first order in the derivatives of each of the fields.[25] A systematic procedure for generating those forms which have nonvanishing and linearly independent matrix elements between free-particle nucleon states is to transform the quantities $\boldsymbol{\tau}\cdot\boldsymbol{\phi}(\gamma\Pi)^n\boldsymbol{\tau}\cdot\boldsymbol{\phi}$, $n=0, 1\cdots$ by commuting the factors $\gamma\Pi$ to the outside where they can be replaced by $-m$. By this means we find five independent forms, conveniently expressed as $\boldsymbol{\phi}^2$, $\gamma_\mu\boldsymbol{\tau}\cdot\boldsymbol{\phi}\times\partial_\mu\boldsymbol{\phi}$, $(\partial_\mu\phi_i)^2$, $\sigma_{\mu\nu}\boldsymbol{\tau}\cdot(\partial_\mu\boldsymbol{\phi}\times\partial_\nu\boldsymbol{\phi})$, and $\{\gamma_\mu\Pi_\nu, \partial_\mu\phi_i\partial_\nu\phi_i\}$. By carrying out the reduction to the nonrelativistic limit, separating S and P wave effects, we find that the S wave up to first order in the meson energy can be represented by adding to G^{-1} the forms

$$\rho_1(g^2/2m)\phi^2+\rho_2(g/2m)^2\boldsymbol{\tau}\cdot\boldsymbol{\phi}\times(\partial\boldsymbol{\phi}/\partial t), \quad (52)$$

whereas the leading P waves are of the form

$$-\lambda_1[g^2/(2m)^3]\nabla\boldsymbol{\phi}\cdot\nabla\boldsymbol{\phi}+\lambda_2[g^2/(2m)^3] \times\epsilon_{\gamma\alpha\beta}\sigma_\gamma\boldsymbol{\tau}\cdot\nabla_\alpha\boldsymbol{\phi}\times\nabla_\beta\boldsymbol{\phi}, \quad (53)$$

where $\epsilon_{\gamma\alpha\beta}$ represents the three-dimensional Levi-Civita tensor density. Equations (52) and (53) provide the justification for the conclusion of a theorem for the P wave, although not for the S wave.

If the parameters ρ_1, ρ_2, λ_1, and λ_2 were all of order unity, it would betoken the validity of the Born approximation for pseudoscalar theory with pseudoscalar coupling, at least in the low-energy region. To understand this, one need only recall the form of the Hamiltonian for this theory which results from the Dyson or Foldy transformations.[26] To see to what extent the actual circumstances differ from this simple one, it is instructive to compare with experiment the phase shifts obtained from a Green's function constructed from Eqs. (50), (52), and (53). Turning first to the P waves, we obtain by a straightforward calculation, the following formula for the transition amplitude, expressed as an operator in isotopic and ordinary spin space,

$$(q'j|T|qi)=-(g/2m)^2\{\tau_j\tau_i[\boldsymbol{\sigma}\cdot\mathbf{q}\boldsymbol{\sigma}\cdot\mathbf{q}'/-\omega(\mathbf{q})] +\tau_i\tau_j[\boldsymbol{\sigma}\cdot\mathbf{q}\boldsymbol{\sigma}\cdot\mathbf{q}'/\omega(q')]\}-2\lambda_1[g^2/(2m)^3]\mathbf{q}\cdot\mathbf{q}'\delta_{ij} +2\lambda_2[g^2/(2m)^3]\epsilon_{jik}\tau_k\boldsymbol{\sigma}\cdot\mathbf{q}'\times\mathbf{q}. \quad (54)$$

If we decompose the scattering into the separate channels labeled by values of total isotopic spin and angular momentum, we obtain for the phase shifts, in the approximation in which $e^{i\delta}\sin\delta\cong\delta$, the formulas

$$\begin{aligned}
\alpha_{33}&=(4/3)(g^2/4\pi)(\mu/2m)^2\eta^3(\mu/\omega)\times[1+\tfrac{1}{4}(\omega/m)(\lambda_1+\lambda_2)],\\
\alpha_{31}=\alpha_{13}&=-(2/3)(g^2/4\pi)(\mu/2m)^2\eta^3(\mu/\omega)\times[1-\tfrac{1}{4}(\omega/m)(\lambda_1-2\lambda_2)],\\
\alpha_{11}&=-(8/3)(g^2/4\pi)(\mu/2m)^2\eta^3(\mu/\omega)\times[1-\tfrac{1}{4}(\omega/m)(\lambda_1+4\lambda_2)].
\end{aligned} \quad (55)$$

Here μ is rest mass of the meson and $\eta=q/\mu$. From Eq. (55), we can derive the interesting result that if $\alpha_{31}=\alpha_{13}$ and α_{11} are reduced compared to their Born approximation values, then α_{33} is enhanced relative to its perturbation theoretic value. This is a consequence of the fact $\lambda_1+\lambda_2$ necessarily lies between $\lambda_1-2\lambda_2$ and $\lambda_1+4\lambda_2$, both of which are positive, by hypothesis. Under the same assumptions, λ_1, itself, is necessarily positive. It is perhaps worth emphasizing that this result holds for the nonrelativistic limit of the relativistic theory and is independent of the actual dynamics of the meson-nucleon system.

Of the P-wave phase shifts only α_{33} is known with any accuracy. For meson energies below 100 Mev, roughly, it is represented by the formula[27]

$$\alpha_{33}=0.235\eta^3. \quad (56)$$

To obtain the order of magnitude of $\lambda_1+\lambda_2$ from Eqs. (55), we shall set $\omega\cong\mu$ and assume that[28]

$$(g^2/4\pi)(\mu/2m)^2=0.081.$$

We then find

$$\lambda_1+\lambda_2\cong 4.8M/\mu, \quad (57)$$

a result that hardly inspires confidence in the validity of the energy expansion.[29] Actually, if we look upon Eqs. (55) as the linear approximation to resonance and antiresonance formulas, then Eq. (57) predicts a reso-

[25] Thus, a form such as $\phi\cdot\Box^2\phi$ is of no interest in the present discussion.

[26] F. J. Dyson, Phys. Rev. **73**, 929 (1948); Berger, Foldy, and Osborn, Phys. Rev. **87**, 106 (1952).

[27] H. A. Bethe and F. de Hoffman, Phys. Rev. **95**, 1100 (1954); J. Orear, Phys. Rev. **96**, 176 (1954).

[28] Value quoted at the Fifth Annual Rochester Conference (to be published) by G. Chew and F. E. Low, based on fit to data using an effective range formula. The S wave in photoproduction yields the somewhat smaller value of 0.066. See G. Bernadini and E. L. Goldwasser, Phys. Rev. **95**, 857 (1954).

[29] This value justified, however, the neglect of the corrections to the Born approximation that can be obtained directly from G_1.

nance at much too low an energy compared with experiment. It almost certainly determines that the other phase shifts change sign compared to their Born values if we take Eqs. (55) seriously for these also. This means that Eqs. (55) have at most a qualitative validity even in the extreme low-energy region.

We conclude this section by comparing with experiment the S wave represented in Eq. (52). We first record the scattering amplitude

$$(q'j|T|qi)=\rho_1(g^2/m)\delta_{ij}-\rho_2(g/\partial m)^2 \times i\epsilon_{jik}\tau_k[\omega(\mathbf{q})+\omega(\mathbf{q}')], \quad (58)$$

from which we obtain directly the phase shifts for isotopic spin $\frac{3}{2}$ and $\frac{1}{2}$,

$$\begin{aligned}\alpha_3&=-\rho_1(g^2/4\pi)(\mu/M)\eta-\tfrac{1}{2}\rho_2(g^2/4\pi)(\mu\omega/m^2)\eta,\\ \alpha_1&=-\rho_1(g^2/4\pi)(\mu/M)\eta+\rho_2(g^2/4\pi)(\mu\omega/m^2)\eta.\end{aligned} \quad (59)$$

There is perhaps still some question as to whether the S phase shifts behave strictly linearly with momentum near zero energy. For the sake of illustration only, we shall favor such advocacy and select the phase shifts of Orear,[27]

$$\alpha_3=-0.11\eta, \quad \alpha_1=0.16\eta. \quad (60)$$

We then find that

$$\rho_1\cong 0.01, \quad \rho_2\cong 0.56, \quad (61)$$

a rather dramatic expression of the difficulty of the problem of constructing a dynamical theory of the S wave.

V. PHOTO-MESON PRODUCTION

Since it is our aim to display a formula for the transition amplitude in which the contribution of the meson current alone is separated from the remainder, we must alter somewhat the procedure followed subsequent to Eq. (13). Let $\mathcal{G}_p$ be the photon propagation function and $\mathcal{G}_M$ that for the meson. Let us further suppose that the renormalization constants Z_2 and Z_3 have the same significance as in Sec. II and that Z_5 is the constant that renormalizes $\mathcal{G}_M$. For the *renormalized* transition matrix, it then is a straightforward matter to derive the expression, analogous to Eq. (13),

$$\begin{aligned}&\delta(p'+q'-p-k)(p'\sigma'\tau', q'j|T|p\sigma\tau, k\mu)\\ &=-\frac{Z_2Z_3^{\frac{1}{2}}Z_5^{\frac{1}{2}}}{(2\pi)^4}\int d^4\eta'd^4x'd^4\xi d^4x\bar{u}(p'\sigma'\tau')e^{-ip'x'}\\ &\times e^{-iq'\eta'}\mathcal{G}_M^{-1}(\eta'\eta'')_{jl}G^{-1}(x',x'')\\ &\times\delta^2G(x'',x''')/\delta K_l(\eta'')\delta J_s(\xi'')|_dG^{-1}(x''',x)\\ &\times\mathcal{G}_p^{-1}(\xi'',\xi)_{sr}u(p\sigma\tau)e^{ipx}e^{ik\xi},\end{aligned} \quad (62)$$

wherein K is the external source of the meson field, and we have included the charge degree of freedom in designating variables for the nucleon. The various propagation functions remain to be renormalized. It is convenient to change variables from K, J to $\langle\phi\rangle$, $\langle A\rangle$, the vacuum matrix elements of the *quantized* fields.[30] In carrying out this transformation, it is well to remember that K and J each depend on *both* matrix elements. We thus find, suppressing indices, and recalling the definitions

$$\mathcal{G}_p=\delta\langle A\rangle/\delta J, \quad \mathcal{G}_M=\delta\langle\phi\rangle/\delta K, \quad (63)$$

that

$$\begin{aligned}&(\delta/\delta J)(\delta G/\delta K)\\ &=\mathcal{G}_M[\delta^2G/\delta\langle\phi\rangle\delta\langle A\rangle]\mathcal{G}_p+(\delta\mathcal{G}_M/\delta\langle A\rangle)(\delta\mathcal{G}/\delta\langle\phi\rangle)\mathcal{G}_p\\ &\quad+\mathcal{G}_M[\delta^2G/\delta\langle\phi\rangle\delta\langle\phi\rangle](\delta\langle\phi\rangle/\delta J)\\ &\quad+(\delta\mathcal{G}_M/\delta\langle\phi\rangle)(\delta G/\delta\langle\phi\rangle)(\delta\langle\phi\rangle/\delta J)\\ &\qquad+(\delta/\delta J)[(\delta\langle A\rangle/\delta K)(\delta G/\delta\langle A\rangle)].\end{aligned} \quad (64)$$

When Eq. (64) is inserted into Eq. (62), only the first two terms survive in virtue of the observation that

$$\begin{aligned}&\int d^4\eta'e^{-iq'\eta'}\mathcal{G}_M^{-1}(\eta',\eta'')\delta\langle A\rangle/\delta K(\eta'')\\ &\qquad=\int d^4\xi(\delta\langle\phi\rangle/\delta J(\xi'))\mathcal{G}_p^{-1}(\xi'\xi)e^{ik\xi}=0,\end{aligned} \quad (65)$$

since the functions $(\delta\langle A\rangle/\delta K)=\delta\langle\phi\rangle/\delta J$ are nonsingular. The renormalization goes through smoothly if first we remember Eq. (17), and second we recall the relations

$$\begin{aligned}\langle A\rangle&=Z_3^{\frac{1}{2}}A+O_1(\Box^2)A+Q_1(\Box^2-\mu^2)\phi,\\ \langle\phi\rangle&=Z_5^{\frac{1}{2}}\phi+Q_2(\Box^2-\mu^2)\phi+O_2(\Box^2)A,\end{aligned} \quad (66)$$

where A and ϕ are the prescribed fields and the operators O and Q possess the property

$$O(0)=Q(0)=0. \quad (67)$$

Since it is only the latter value of the operators that enters Eq. (62), the renormalization constants cancel out and we obtain finally the desired formula:

$$\begin{aligned}&\delta(p'+q'-p-k)(p'\sigma'\tau', q'j|T|p\sigma\tau, k\mu)\\ &=-\frac{eg}{(2\pi)^4}\int d^4\eta'd^4x'd^4\xi d^4xe^{-ip'x'}e^{-iq'\eta'}\bar{u}(p'\sigma',\tau')\\ &\times\{(x'|G^{-1}\delta^2G/\delta g\phi_j(\eta')\delta eA_\mu(\xi)G^{-1}|x)\\ &-(x'|\mathcal{G}_M^{-1}(\eta',\eta'')\delta\mathcal{G}_M(\eta'',\eta''')/\delta eA_\mu(\xi)\\ &\times\delta G^{-1}/\delta g\phi_l(\eta''')|x)\}_{A=\phi=0}u(p\sigma\tau)e^{ipx}e^{ik\xi},\end{aligned} \quad (68)$$

which is understood to be expressed completely in terms of finite propagation functions. Of the two terms of Eq. (68), the first has the same structure as encountered in the previous sections, and will be considered below. We turn now to the second term, which describes the effect of the meson current.

The general form of the renormalized meson propa-

[30] See J. Schwinger, reference 12.

gator in the zero-field limit is given by the expression:

$$\mathcal{G}_M^{-1}(q,[0]) = (q^2+\mu^2)\{[1+(q^2+\mu^2)/m^2]\mathcal{K}(q^2/m^2)\}, \quad (69)$$

where q is the meson-momentum operator and $\mathcal{K}(q^2/m^2)$ is an analytic function of its variable. The dependence of $\mathcal{G}_M$ on the electromagnetic potential is given by the replacement

$$q \to q - eA. \quad (70)$$

To construct invariants depending explicitly on the field strengths and currents, we have at our disposal solely the vector q_μ. The only invariants permissible in a power series expansion are then of the form $(\Box^2)^n q_\mu J_\mu$, for integral n, and such terms can contribute nothing to processes involving real photons. In the present instance, therefore, it suffices to assume the relation

$$\mathcal{G}_M^{-1}(q,[A])=\mathcal{G}_M^{-1}(q-eA,[0]). \quad (71)$$

The combination that occurs in Eq. (68) can now be evaluated using Eqs. (69) and (71) as follows:

$$\mathcal{G}_M^{-1}(\delta\mathcal{G}_M/\delta eA_\mu)\,|_0 = -(\delta\mathcal{G}_M^{-1}/\delta eA_\mu)\,|_0\mathcal{G}_M = 2q_\mu[1+O(q^2/m^2)](q^2+\mu^2)^{-1}[1+O(q^2/m^2)]. \quad (72)$$

Consequently, the relative correction to the Born approximation is of the second order of smallness in q. Likewise, the matrix element for the emission of a meson, $\delta G^{-1}/\delta(g\phi)$, taken between free-particle states is by definition given by its Born approximation with relative corrections once again of the second order. Taken together, these statements constitute a proof that the contribution to photoproduction arising from the meson current is given correctly to the leading order in the boson momenta by perturbation theory, with the relative corrections as specified.[21] The actual form of the transition amplitude for charged production is

$$(q'\pm|T_M|k\mu) \cong -ie\sqrt{2}(g/2m)\frac{\boldsymbol{\sigma}\cdot(\mathbf{k}-\mathbf{q})}{\mathbf{k}\cdot\mathbf{q}-k_0\omega(\mathbf{q})}(q-k)_\mu, \quad (73)$$

wherein the isotopic matrix element has already been evaluated [compare Eq. (79) below].

We turn finally to the consideration of the nucleon current, for which we assert that the leading contributions to both the S and P wave are contained in the Green's function (which ignores the neutron-proton mass difference)

$$G_1^{-1}(p,[A],[\phi]) = \gamma[p-e\tfrac{1}{2}(1+\tau_3)A]+m-\tfrac{1}{2}\mu_p'\sigma F\tfrac{1}{2}(1+\tau_3) -\tfrac{1}{2}\mu_n'\sigma F\tfrac{1}{2}(1-\tau_3)+i(g/2m)\gamma_5\gamma_\mu\partial_\mu\boldsymbol{\tau}\cdot\boldsymbol{\phi} +(eg/2m)\gamma_5\gamma_\mu A_\mu\tfrac{1}{2}[\tau_3,\boldsymbol{\tau}\cdot\boldsymbol{\phi}]. \quad (74)$$

[21] The corrections to the meson current are actually only one order smaller, when one takes into account the nucleon current.

Here μ_p' and μ_n' are anomalous moments of proton and neutron respectively. The familiar last term of Eq. (74) is a consequence of the requirements of gauge invariance for the interaction of charged mesons with the electromagnetic field, as expressed by the replacement

$$\partial_\mu\delta_{ij} \to \partial_\mu\delta_{ij} - ieA_\mu(\mathcal{T}_3)_{ij}, \quad (75)$$

where $\mathcal{T}_3$ is the matrix

$$\mathcal{T}_3=\begin{bmatrix}0 & -i & 0\\ i & 0 & 0\\ 0 & 0 & 0\end{bmatrix}. \quad (76)$$

It follows that

$$\tau_s(\mathcal{T}_3)_{ij}\phi_j=\tfrac{1}{2}[\tau_3,\boldsymbol{\tau}\cdot\boldsymbol{\phi}]. \quad (77)$$

Alternatively we could have remarked that

$$\partial_\mu\boldsymbol{\tau}\cdot\boldsymbol{\phi}=-i[p_\mu,\boldsymbol{\tau}\cdot\boldsymbol{\phi}]\to\partial_\mu\boldsymbol{\tau}\cdot\boldsymbol{\phi} -ie\tfrac{1}{2}[(1+\tau_3)A_\mu,\boldsymbol{\tau}\cdot\boldsymbol{\phi}]. \quad (78)$$

Either Eqs. (75)–(77) or Eq. (78) reminds us of the existence of the last term in Eq. (74).

Now this term contributes to charged photo-meson production an S wave which is energy independent. We have only to observe that there is no other energy-independent S wave in the theory to complete the proof of the Kroll-Ruderman theorems. Direct computation establishes that the remainder of G_1 contributes an S wave which is linear in the photon (or meson) energy. Any other S wave must appear in G^{-1} as a term bilinear in A,ϕ and will be at least first order in the photon energy, according to the requirements of gauge invariance. Such a term will be exhibited below.

To separate photoproduction processes according to the charge of the meson produced, we introduce the usual definitions

$$\phi=-(2)^{-\frac{1}{2}}(\phi_1+i\phi_2),\quad \phi^*=(2)^{-\frac{1}{2}}(\phi_1-i\phi_2),$$
$$\tau_+=\tfrac{1}{2}(\tau_1+i\tau_2),\quad \tau_-=\tfrac{1}{2}(\tau_1-i\tau_2). \quad (79)$$

Up to terms of first order in the meson energy, G_1 yields for positive and negative meson production, from protons and neutrons respectively,

$$\mathbf{T}_\pm\cdot\mathbf{e}=\sqrt{2}(eg/2m)i\boldsymbol{\sigma}\cdot\mathbf{e}\{1\mp[\omega(q)/2m]\}. \quad (80)$$

Equation (80) predicts a threshold yield of negative to positive mesons:

$$\sigma(-)/\sigma(+)\cong(1+2\mu/m)=1.3, \quad (81)$$

not in essential disagreement with experiment.[22]

As the final theorem of this paper, we have the statement that except for relative corrections which vanish as $\omega\to 0$, the P wave is given by Born approximation computed for a nucleon characterized by its experimental charge, magnetic moment, and mesic

[22] Sands, Teasdale, and Walker, Phys. Rev. **95**, 592 (1954).

coupling constant, that is, by the Green's function G_1. By analogy with the meson scattering case, G_1 generates a P wave of order (kq/ω), whereas any other P wave in the theory behaves at least as kq.

We may record here for convenience the leading P-wave terms for positive production from protons, negative production from neutrons, and neutral production from protons, respectively:

$$\mathbf{T}_+\cdot\mathbf{e}=\sqrt{2}\frac{g}{2m}\left[\mu_n\frac{(\boldsymbol{\sigma}\cdot\mathbf{k}\times\mathbf{e})(\boldsymbol{\sigma}\cdot\mathbf{q})}{\omega}-\mu_p\frac{(\boldsymbol{\sigma}\cdot\mathbf{q})(\boldsymbol{\sigma}\cdot\mathbf{k}\times\mathbf{e})}{k_0}\right], \quad (82)$$

$$\mathbf{T}_-\cdot\mathbf{e}=\sqrt{2}\frac{g}{2m}\left[\mu_n\frac{(\boldsymbol{\sigma}\cdot\mathbf{q})(\boldsymbol{\sigma}\cdot\mathbf{k}\times\mathbf{e})}{k_0}-\mu_p\frac{(\boldsymbol{\sigma}\cdot\mathbf{k}\times\mathbf{e})(\boldsymbol{\sigma}\cdot\mathbf{q})}{\omega}\right], \quad (83)$$

$$\mathbf{T}_0\cdot\mathbf{e}=\frac{g}{2m}\mu_p\left[\frac{(\boldsymbol{\sigma}\cdot\mathbf{q})(\boldsymbol{\sigma}\cdot\mathbf{k}\times\mathbf{e})}{k_0}-\frac{(\boldsymbol{\sigma}\cdot\mathbf{k}\times\mathbf{e})(\boldsymbol{\sigma}\cdot\mathbf{q})}{\omega}\right], \quad (84)$$

in terms of the total magnetic moments of proton and neutron.

As with the processes of photon and meson scattering, our methods provide a basis for the phenomenological treatment of photoproduction as long as the experimental behavior of the cross section is "normal," that is, as long as the S wave goes linearly and the P wave cubically with the meson momentum. We prefer not to enter into the details of a numerical analysis since such an analysis would not differ substantially from considerations that have already been recorded in the literature.[10] We shall, conclude this work, however, by providing the framework for such an analysis, at the same time essentially filling in the details of proofs given in the foregoing.

It is amusing to remark first that in the formation of invariants bilinear in A, ϕ we are *not* constrained to terms which are explicitly gauge-invariant. Thus a term in G^{-1} of the form $(2m)^{-1}i\gamma_5\gamma_\mu\Box^2\partial_\mu\boldsymbol{\tau}\cdot\boldsymbol{\phi}$, not hitherto considered, gives rise by the considerations of gauge invariance discussed in connection with Eq. (78) and preceding equations, to an additional term of the form

$$[e/(2m)^3]\gamma_5\gamma_\mu\tfrac{1}{2}[\tau_3,\tau_i][A_\mu\Box^2+\tfrac{1}{2}(\Box^2A_\mu)+2A_\lambda\partial_\lambda\partial_\mu+(\partial_\lambda A_\mu)\partial_\lambda+(\partial_\mu A_\lambda)\partial_\lambda]\phi_i, \quad (85)$$

of which the first three members essentially describe electric dipole absorption with emission of charged mesons into an S state and the last two members electric quadrupole absorption with emission in a P state; both effects are quadratic in the energy-momentum vectors of the bosons.

Turning to forms that are explicitly gauge invariant, we have three possible types of isotopic dependence, $\boldsymbol{\tau}\cdot\boldsymbol{\phi}$, $(\boldsymbol{\tau}\times\boldsymbol{\phi})_3$, and ϕ_3. If Φ stands for a linear combination of these, the permissible, independent Dirac invariants at most of second order in the momenta are four in number, $\gamma_5\Phi\sigma F$, $\gamma_5\gamma_\lambda\partial_\mu\Phi F_{\mu\lambda}$, $\{\gamma_5\gamma_\mu\partial_\mu\Phi,\sigma F\}$, and $\{\gamma_5\Pi_\mu\gamma_\Lambda\gamma_\rho,\partial_\mu\Phi F_{\lambda\rho}\}$. Passing to the nonrelativistic limit, we obtain as the leading S wave $\Phi\boldsymbol{\sigma}\cdot\mathbf{E}$, representing electric dipole absorption, and as the leading P waves $\nabla\Phi\cdot\mathbf{H}$ and $\boldsymbol{\sigma}\cdot\nabla\Phi\times\mathbf{H}$, giving magnetic dipole absorption. To obtain additional electric quadrupole absorption beyond that contained in Eq. (82) we must include terms of still one higher power in the energy of the photon. We have therefore verified the assertions about the minimal energy-momentum dependence of the invariants bilinear in electromagnetic and meson fields.

ACKNOWLEDGMENTS

The author is deeply indebted to Professor Julian Schwinger for inculcating in him many of the ideas contained in this paper.

Constraints in Covariant Field Theories. II*

JAMES L. ANDERSON
Department of Physics, University of Maryland, College Park, Maryland
(Received April 18, 1955)

In this paper we analyze the difficulties which occur when one attempts to quantize a theory such as electrodynamics or the general theory of relativity. Because of the invariance properties of theories of this type all of the canonical variables of the theory are not independent of one another but rather there exists certain algebraic relations between them called constraints. These constraints plus the Hamiltonian, in the unquantized version of the theory, constitute a function group. It is proved that there exists at least one ordering of factors in the quantized theory for which this is also true. From this fact we conclude that it is possible, at least formally, to construct a quantum version of the theories under consideration and that the quantum version will possess the same invariance properties as the corresponding unquantized theory.

I. INTRODUCTION

IF one attempts to cast a field theory, like electrodynamics or gravitation, into a canonical form, one is faced with the following difficulty; it is generally impossible to express the "velocities" (first time derivatives of the field variables) uniquely in terms of the momenta. Rather, one finds that the momenta, together with the field variables canonically conjugate to them, satisfy certain algebraic relations which are free of the velocities. As has been previously pointed out,[1] these identities, which we shall refer to as constraints, occur in any theory which is invariant with respect to a group of transformations, an element of which is specified by one or more continuous functions of x, y, z, t. The gauge group of electromagnetic theory and the group of continuous coordinate transformations are examples of such groups of transformations.

In spite of this apparent difficulty it has been possible to develop a Hamiltonian formalism for theories of the type mentioned above.[2] The role played by the constraints in such a formalism has been investigated, as far as the classical theory is concerned, in I. There it was found that, in addition to the primary constraints, there exist secondary constraints which must be satisfied if the primary constraints are to remain satisfied at all future times. We were able to show that the number of these secondary constraints is finite (usually equal to the number of primary constraints) and that, together with the Hamiltonian of the theory, they form a function group.[3] This last property of the constraints is absolutely necessary if all the constraints are to be satisfied simultaneously and remain satisfied in the course of time.

The proof of the above statements were obtained by noting that the constraints, being constants of the motion, when multiplied by an appropriate number of arbitrary functions of x, y, z, t, and added, serve as generators for invariant canonical transformations. In particular we showed in I that the invariant transformations so generated are nothing but those which led originally to the existence of the constraints. Here the argument rested upon the fact that one was able to set up an isomorphism between elements of the abstract group associated with our group of invariant transformations in the Lagrangian formalism and a subgroup of contact transformations in the Hamiltonian formalism.

Since the arguments contained in I were based on the Lagrangian formalism, they cannot be taken over directly when we attempt to quantize our theory.[4] The difficulty is compounded by the fact that, since our quantum theory must necessarily start from a Hamiltonian formalism, we have none of the simple methods of the Lagrangian formalism available to us for investigating the invariance properties of our theory. If we knew, for instance, that in the quantum theory the constraints, together with the Hamiltonian, also formed a function group[5] with the same commutation properties as the corresponding classical group, the proof of invariance would be essentially completed. Conversely, if we could prove the invariance of the quantum theory independently, i.e., without using the properties of the constraints, we would be able to conclude that the constraints plus Hamiltonian indeed do form a function group. These last assertions follow from the fact that in the quantum form of the theory we can also use the constraints to generate the invariant transformations. If, then, there is an isomorphism

* Supported by the Office of Naval Research. Part of the material reported here appears in the author's thesis presented to the Graduate Faculty of Syracuse University in partial fulfillment of the requirements for the Doctor of Philosophy degree.

[1] J. L. Anderson and P. G. Bergmann, Phys. Rev. **83**, 1018 (1951), referred to as I.

[2] Robert H. Penfield, Phys. Rev. **89**, 737 (1951). For an alternate approach see P. A. M. Dirac, Can. J. Math. **2**, 129 (1950).

[3] A function group is defined as a set of functions of the canonical variables with the property that the Poisson bracket of any two members of the set is again a member of the set.

[4] At the present moment we know of no method of quantization, based on the Lagrangian formalism, which is generally applicable to the types of theories under consideration. The methods of Lagrangian quantization which do exist are applicable only to essentially linear theories.

[5] The definition of function group in the quantum theory is the same as in the classical theory, except that commutators replace Poisson brackets. In what follows we shall use the word commutation in the group theoretical sense, i.e., classically the commutator of two elements of a function group corresponds to forming their Poisson bracket; quantum mechanically it corresponds to actually forming their commutator.

between members of the quantum function group and the corresponding classical group, we can conclude that there is also an isomorphism between the generators of the corresponding invariant transformations. This isomorphism is enough to insure that the quantum theory has the same invariant properties as the corresponding classical theory.

The usual procedure for determining whether the constraints plus Hamiltonian form a function group is by direct calculation. This is the method used in the electromagnetic theory where, for example, the constraints take on an extremely simple form.[6] However, in any essentially nonlinear theory such as gravitation, direct calculation becomes, at best, exceedingly involved. Furthermore, for most purposes, we do not need to know the structure of the function group, but merely that it does exist. Thus such computations become unnecessary in the face of an existence proof. In addition, there is another difficulty which one encounters in attempting to proceed by direct calculation. In any quantum-mechanical expression there is always an ambiguity in the ordering of factors. It is not evident that two different orderings of factors in the constraints would not produce markedly different results, i.e., the constraints when ordered one way would form a function group while ordered in another way they would not. Hence a calculation which showed the constraints not to form a function group could never be considered conclusive proof of an inconsistency since some other ordering might well produce the opposite results.

We shall examine these difficulties in some detail. In particular, we shall prove that in the quantum version of the theory there exists at least one ordering of factors for which the constraints plus Hamiltonian form a function group possessing the same commutation properties as the corresponding classical group. Hence we can conclude that the quantum theory has the same transformation properties as the corresponding classical theory. The proof consists essentially in showing that, classically, there exists a canonical transformation which reduces all of the constraint equations to the form

$$\pi^\xi(x)=0, \quad \xi=1, 2, \cdots, n, \tag{1}$$

where $\pi^\xi(x)$ are the momenta canonically conjugate to the "constraint" variables $\phi_\xi(x)$ and n is the total number of constraints and is assumed to be less than N, the total number of field variables.

Once in this form, it is evident that upon quantization the constraints will still form a function group among themselves. Further, we can prove in a simple manner that the commutator of a constraint and the Hamiltonian is again at most a constraint. Finally, since we never explicitly obtain the canonical transformation which reduces the constraints to the form given in (1) we must discuss to what extent it is possible to introduce a norm for our state vectors when the constraints have their original form.

[6] See Wentzel, *Quantum Theory of Fields* (Interscience Publishers, Inc., New York, 1949), p. 116.

II. REDUCTION OF CONSTRAINTS

In this section we will prove that there exists a canonical transformation which will reduce the elements of a function group to an equal number of momenta in the new variables introduced by the transformation. Let us denote the elements of our function group by $f^\xi(\phi_A,\pi^A)$. They have the following properties:

$$f^\xi=0, \tag{2a}$$

$$\dot{f}^\xi=\Gamma^\xi{}_\sigma f^\sigma, \tag{2b}$$

$$(f^\xi,f^\eta)=\Delta^{\xi\eta}{}_\lambda f^\lambda, \tag{2c}$$

where (f^ξ,f^η) is the Poisson bracket[7] of f^ξ and f^η and where the Γ's and Δ's are determined by actually carrying out the indicated operations and may be complicated functions of the ϕ's and π's. It is our task to show that there exists a canonical transformation such that, in terms of the new variables, the constraints assume the simple form (1). To this end let us consider for a moment the Hamilton-Jacobi equation of the theory.

We look for a quantity $S(\phi_A,\bar{\pi}^A;t)$ which will serve as the generator of a canonical transformation[8] for which the new Hamiltonian of the theory vanishes outright. As in the case of a discrete number of variables we have that

$$\pi^A(x)=\delta S/\delta\phi_A(x), \tag{3}$$

and hence, the Hamilton-Jacobi equation becomes

$$H(\phi_A, \delta S/\delta\phi_A)+\partial S/\partial t=0, \tag{4}$$

where $H(\phi_A,\pi^A)$ is the integrated Hamiltonian density of the theory. In addition to (4), S must of course satisfy Eq. (2a), i.e.,

$$f^\xi(\phi_A, \delta S/\delta\phi_A)=0. \tag{5}$$

In order that this system of equations [(4), (5)] have solutions, it is necessary that the Poisson bracket between any two of them, considering $\delta S/\delta\phi_A$ as the momentum canonically conjugate to ϕ_A, must vanish at least modulo the constraints themselves. This condition is satisfied providing the constraints fulfill requirements (2). Whether or not (4) and (5) actually possess solutions is another matter. We can only assume that we are working with a sensible theory and that they do indeed possess solutions.

Since, as has been assumed, Eqs. (4) and (5) possess solutions, it must be possible to append to them an additional system of $N-n$ equations of the form

$$f^i(\phi_A, \delta S/\delta\phi_A)=g^i(x), \quad i=n+1, \cdots, N, \tag{6}$$

[7] See Appendix I for a definition of functional differentiation and Poisson bracket as they appear in this paper.

[8] See Appendix II for a brief discussion of canonical transformations in field theory.

where the $g^i(x)$ are arbitrary functions of position only. (The f^i of course must have vanishing Poisson brackets with the Hamiltonian and with the constraints modulo the constrains.) The reason for the existence of these last equations is the following: Eqs. (5) represent a number of conditions on the possible initial dependence of S on its ∞^N arguments, the $\phi_A(x)$ However, since there are only ∞^n of them we need an additional ∞^{N-n} equations of the form (6) to completely specify S as a function of its arguments. The arbitrary functions $g^i(x)$ can be considered as initial condition for the problem. Putting it another way, if we form the generalized Pfaffian

$$\delta S=\frac{\partial S}{\partial t}\delta t+\int\frac{\delta S}{\delta\phi_A(x)}\delta\phi_A(x)d^3x,$$

then we can use Eqs. (4) and (5) to determine $\partial S/\partial t$ and n of the $\delta S/\delta\phi_A$. The remaining $N-n$ quantities $\delta S/\delta\phi_A$ must come from some additional equations like (6).[9]

Having established the existence of Eqs. (6), we now assert that it is possible to solve the system (5) and (6), for the $\delta S/\delta\phi_A$ in terms of the ϕ_A and g^i. This assertion can be shown in the following manner: We consider a solution of the system (4), (5), and (6) and form

$$\delta S/\delta\phi_A=\mathfrak{D}^A(\phi_A,g^i). \tag{7}$$

When substituted in (5) and (6), Eqs. (7) must satisfy them identically and hence, considered as equations for S, they are equivalent to (5) and (6). Conversely, we must be able to solve (5) and (6) for the $\delta S/\delta\phi_A$ and obtain equations of the form given in (7).

Since we are able to solve the total system (5) and (6) for the $\delta S/\delta\phi_A$ we can of course solve the subsystem (5) for n of the $\delta S/\delta\phi_A$ in terms of the ϕ_A and remaining $N-n$ quantities $\delta S/\delta\phi_A$, i.e., there must exist a system of equations of the form

$$\delta S/\delta\phi_t=\Lambda^t(\phi_A,\ \delta S/\delta\phi^i), \tag{8}$$

which are in every respect equivalent to the set (5). That such solutions actually exist can be seen as follows: Eqs. (5) and (6) together possess solutions provided that the Jacobian

$$J\left(\frac{f^t,f^i}{\delta S/\delta\phi_A}\right)\neq 0. \tag{9}$$

Similarly, the set (5) will possess solutions of the form (8) provided that at least one Jacobian

$$J\left(\frac{f^t}{\delta S/\delta\phi_n}\right) \tag{10}$$

does not vanish. But this must be the case since the left side of (9) can be expanded as a linear combination of these Jacobians. Since the right side of (9) is nonzero, we conclude that not all of the Jacobian's (10) can vanish. Hence we conclude that solutions of the form (8) really do exist.

From the standpoint of the Hamilton-Jacobi theory then, Eqs. (8) are those which would result if our constraints had the form

$$\pi^t-\Lambda^t(\phi_A,\pi^i)=0. \tag{11}$$

Thus we conclude that it is always possible to bring any system of constraints, which satisfy the requirements (2), into the form (11).

Once having established the result given by (11), we are in a position to construct a canonical transformation which will reduce the constraints further to the form (1). Indeed, consider the canonical transformation generated by the functional

$$C=\int\phi_t(x)\bar{\pi}^t(x)d^3x+S(\phi_A,\bar{\pi}^i), \tag{12}$$

where we have made the identification

$$g^i(x)=\bar{\pi}^i(x). \tag{13}$$

We have the following transformations:

$$\pi^t(x)=\delta C/\delta\phi_t(x)=\bar{\pi}^t(x)+\delta S/\delta\phi_t(x), \tag{14a}$$

$$\pi^i(x)=\delta C/\delta\phi_i(x)=\delta S/\delta\phi_i(x), \tag{14b}$$

$$\bar{\phi}_t(x)=\delta C/\delta\bar{\pi}^t(x)=\phi_t(x), \tag{14c}$$

$$\bar{\phi}_i(x)=\delta C/\delta\bar{\pi}^i(x)=-\delta S/\delta\bar{\pi}^i(x). \tag{14d}$$

Now, since S satisfies (8), we can rewrite (14b) as

$$\pi^t-\Lambda^t(\phi_A,\ \delta S/\delta\phi_i)=\bar{\pi}^t \tag{15}$$

or substituting from (12b) we have finally that

$$\pi^t-\Lambda^t(\phi_A,\pi^i)=\bar{\pi}^t, \tag{16}$$

and since (11) holds, we have

$$\bar{\pi}^t=0$$

as our constraints in terms of the new variables. Thus we have succeeded in finding a canonical transformation which reduces all of the constraints to the form given in (1). Furthermore, since the proof does not depend upon which of the infinity of Hamiltonians (which differ from each other by terms which are linear in the primary constraints) we choose, it is applicable in all coordinate systems.[10] Unfortunately in most cases of interest, the field equations are of such a complicated nature that it is extremely difficult to actually construct the generating functional which accomplishes this reduction. As we shall see, this is not a serious defect in the theory since for all practical purposes we never

[9] The actual method for arriving at the form of Eqs. (6) is very complicated. For our purposes we need only know that they exist.

[10] See I for a detailed analysis of the relation between choice of coordinates and choice of Hamiltonian. By coordinates we mean the mode of description of our theory. Thus that in general relativity a choice of coordinates corresponds to actually making a choice of space-time coordinates while in electromagnetic theory it corresponds to choosing a particular gauge.

really need know the explicit form of the generating function; we need know only that such a generating function exists.

III. QUANTIZATION

With the foregoing material in hand, we shall proceed to "quantize" our theory. This we do in the usual manner, i.e., we now treat the field variables as operators, postulate commutation relations for them, introduce a Hamiltonian for the theory and assume a Schrödinger equation. The Hamiltonian which we choose will be the one corresponding to the set of field variables for which the constraints have the form (1).

As is usual in such theories, the existence of constraints complicates the process of quantization by placing restrictions on the possible states which can describe our system. Generally, a state is represented by a vector in a linear vector space for which all operators of the theory are defined. In particular, we do not require in this "big" space that the constraints be satisfied. If we wish to obtain a theory which is equivalent to the original one (where the constraints are satisfied), then we must limit the possible states of the "big" space to those which are eigenvectors of the constraints with eigenvalue 0, i.e., we choose only those states for which

$$\pi^t(x)\,|\,,t\rangle=0. \tag{17}$$

The subspace of the "big" space defined by those vectors which satisfy (17) then forms the space of all possible state vectors which can describe our system.

To complete our scheme of quantization, we must define a norm in our subspace of allowable states.[11] Now, it is a well-known fact that canonical variables, *viz.*, variables having a commutation relation of the form

$$[q,p]=ih$$

cannot have normalizable eigenstates. Hence it follows that we can only normalize the allowed state vectors over the variables not canonically conjugate to the π^t. That this indeed must be the case can be seen in another way. Since the π^A have as commutation relations with their canonical field variables

$$[\phi_A(x),\pi^B(x')]=ih\delta_A{}^B\delta(x-x'),$$

we can introduce a representation in which we associate with ϕ_A the operator "multiplication by ϕ_A" and with π^A the operator $ih\mathfrak{d}/\mathfrak{d}\phi_A$. The state vectors are then functionals of the $\phi_A(x)$. Equation (17) then reads

$$ih\frac{\mathfrak{d}}{\mathfrak{d}\phi_t(x)}\,|\,\phi_A,t\rangle=0. \tag{18}$$

In other words, the allowable state vectors are those which are independent of $\phi_t(x)$, the field variables canonically conjugate the constraint momenta $\pi^t(x)$. If we were to attempt to normalize our state functionals by integrating over $\phi_t(x)$ as well as over the remaining field variables, we would obtain an infinite result. There would be nothing in the integral which would go to zero fast enough as $\phi_t(x)$ approached infinitely large values. In quantum electrodynamics this situation is reflected in the fact that we cannot normalize our state functionals over the scalar and longitudinal parts of the field.[12]

A corollary of the above result is that only those operators which do not depend upon the ϕ_t and π^t can have meaningful matrix elements. This corollary follows from the fact that a matrix element is a c-number. If the allowable state functionals do not depend upon the ϕ_t and if we do not normalize with respect to them, the matrix element of an operator which does depend upon either ϕ_t or π^t will still be an operator as far as these variables are concerned. The requirement that physically meaningful quantities do not depend upon the ϕ_t and π^t can be expressed mathematically by saying that we only make use of those quantities which commute with a linear combination of the constraints.[13]

Once we have quantized our theory as outlined above we are free to carry out unitary transformations on the canonical variables. In particular there will exist a series of unitary transformations which will carry us back to the original set of variables[14] where the primary constraints have the form given in (2). That such transformations do exist follows from the fact that to every canonical transformation in the classical theory there corresponds at least one unitary transformation in the quantum theory. The unitary transformations envisioned here correspond to the canonical transformations which are the inverse of the ones employed to reduce the constraints to the form (1).

The reason for returning, in the quantum theory, to our original set of variables is that, as mentioned previously, it is extremely difficult to construct the actual transformations which reduce our constraints to the form (1). The transformations were performed in the first place so that we would be able to prove certain theorems in the quantum theory. For instance, we now can state that there exists some ordering of factors for which all constraints commute with each other (modulo

[11] The problem of treating the norm in a theory with constraints was discussed by P. G. Bergmann at the International Congress of Mathematics in Cambridge, Massachusetts in 1950. (American Mathematical Society, Providence, 1952.) See the report of this Conference for an abstract of his talk.

[12] S. N. Gupta, Proc. Phys. Soc. (London) **A63**, 681 (1950) and I. Bleuler, Helv. Phys. Acta. **23**, 567 (1950) have introduced into quantum electrodynamics a method whereby one can normalize the allowable state functionals over all four components of the potential. The extension of such methods to our problems is still under investigation by the author.

[13] For a more thoroughgoing analysis of this problem see P. G. Bergmann and Ralph Schiller, Phys. Rev. **89**, 4 (1953).

[14] The fact that classically we had essentially to divide through the secondary constraints by functions of the constraint variables will occasion no difficulty. Since the secondary constraints are independent of any constraint momenta we can, even in the quantum version of the theory, multiply the reduced secondary constraints by functionals of the constraint variables without regard to order of factors.

the constraints themselves). The statement is of course trivially true when the constraints have the form (1). However, the relationship between constraints is invariant under either a unitary or a canonical transformation. Therefore, the statement is true also for the quantum form of the original theory. In fact, one can assert that there is an isomorphism between the group of constraints in the classical theory and in the quantum theory.

One can also prove that the constraints all commute with the Hamiltonian (again modulo the constraints). This is certainly true in the original form of the classical theory, as was proven in I. It is therefore true also in the transformed classical theory. Furthermore, since the commutator of a constraint and the Hamiltonian is again at most a constraint, the Hamiltonian can depend upon the constraint variables through terms of the form $c_f\pi^f$, where the c_f are arbitrary functions of the independent variables and possibly of the field variables.

When we go to quantize the theory, the Hamiltonian will again depend on the constraint variables through terms of the form mentioned above. We can conclude therefore that also in the quantum theory, at least in terms of the new variables, the constraints all commute with the Hamiltonian, modulo the constraints. This relationship, however, is unaffected by a unitary transformation. Therefore, it is also true as far as the old variables are concerned. Thus we can assert that in the quantum form of the theory the constraints, together with the Hamiltonian form a function group.

The problem of the normalization of the allowable state functions is not so easily solved when we return to the old variables. Since we can normalize our states in the transformed system of variables, we should be able to normalize our states in the old system, for normalization is invariant under a unitary transformation. The actual prescription to be used has not been worked out in general and will probably depend to a large extent upon the method of solution employed. We can assert, from our previous results, that the allowable states are eigenvectors of the constraints with eigenvalue zero and that the only physically meaningful quantities are those which commute with the constraints.

IV. INVARIANCE OF THE THEORY

We will conclude our discussion by demonstrating that the quantized theory is invariant with respect to the same group of transformations as the corresponding classical theory. This demonstration is accomplished by showing that to every element of our abstract group there corresponds a unitary transformation in the quantum version of the theory. To proceed with the proof, we recall that in I we proved the existence of an isomorphism between elements of the abstract group and a subset of canonical transformations in the Hamiltonian formalism. These particular canonical transformations, of course, formed a group in the sense that the commutator of any two generators was again a generator. In fact the relation was such that if C_1 is the generator corresponding to the infinitesimal transformation $\bar{\delta}_1\phi_A$ while C_2 is the generator corresponding to the infinitesimal transformation $\bar{\delta}_2\phi_A$, then

$$C_f=[C_1,C_2]$$

is the generator corresponding to the transformation

$$\bar{\delta}_1(\bar{\delta}_2\phi_A)-\bar{\delta}_2(\bar{\delta}_1\phi_A).$$

Finally it was shown in I that the generator of an invariant transformation could be written as a linear combination of the constraints, with the coefficients of the constraints being directly related to the description of the group.

In the last section we proved that the constraints, together with the Hamiltonian, form a function group which is isomorphic to the function group formed by the constraints and Hamiltonian in the classical theory. Again, within the quantum theory we can construct generators of infinitesimal unitary transformations by forming linear combinations of the constraints. From the results of the previous section, we can conclude that these unitary transformations will be isomorphic to the group of invariant infinitesimal canonical transformations in the classical theory. Hence there will exist an isomorphism between a subgroup of unitary transformations in the quantum theory and our abstract group. This, however, is enough to prove invariance of the quantum theory. Certainly the commutation relations are invariant under a unitary transformation. In addition, the change in the Hamiltonian as a function of its arguments is given by

$$\delta' H=i\hbar\partial C/\partial t+[H,C],$$

and as we have already shown in I it can be at most a linear combination of the primary constraints. Therefore, in the subspace in which the constraints are satisfied, the Schrödinger equation or the Heisenberg equations of motion will remain unchanged in form in the face of a unitary transformation generated by a linear combination of constraints, i.e., an invariant transformation. Finally, any method of normalization which we prescribe will remain unchanged under our unitary transformation and hence, once normalized, will remain normalized.

V. SUMMARY

In this paper, we have discussed some of the problems arising from an attempt to quantize a theory like electrodynamics or general relativity. Complications resulted from the existence of constraints which are always found in such theories. One was faced with the problem of deciding whether or not there existed an ordering of factors such that these constraints plus Hamiltonian formed a function group in the quantum

theory. It was found that such an ordering does indeed exist and furthermore that the function group in the quantum theory is isomorphic to the corresponding function group in the classical theory. This last result allowed us to prove, in a very simple manner, the invariance of the quantized theory. Finally we showed that it was possible to normalize the state vectors of our theory, although we did not prescribe any particular method of doing so.

From the aforementioned results one can conclude that it is indeed possible to set up, in an invariant fashion, a consistent scheme for quantizing theories possessing constraints. We are, however, in no better position than before when it comes to actually using this formalism for practical calculations. Indeed, except for electrodynamics, most theories of the type considered are highly nonlinear. Furthermore, this nonlinearity is usually essential to the theory. (In the general theory of relativity, it is responsible for the motion of singularities in the field.) Therefore we do not have available to us the usual perturbation techniques. Nor would it help matters too much if we did. We know that, in any perturbation scheme, infinities are bound to occur. To remove these infinities one must put the theory into a manifestly invariant form. However, as we have seen, the theories considered here are inherently incapable of being cast in this form. In order to set up the Hamiltonian one must choose a particular reference frame, *viz.*, gauge or coordinate condition, and this immediately spoils the manifest invariance of the theory.

It is evident that one must develop new and more powerful tools of analysis if one is to carry through the quantization of a theory like the gravitational theory of general relativity. In spite of these difficulties we can be assured that, at least on the formal level, theories with constraints are capable of quantization.

The author would like to express his thanks to Dr. Peter Bergmann for having suggested this problem and for the many interesting discussions which took place during the course of the investigation.

APPENDIX I

The functional derivative as employed in this paper is defined through the following equation:

$$\delta F(\phi_A,\pi^A)=\int\left\{\frac{\delta F}{\delta\phi_A(x)}\delta\phi_A(x)+\frac{\delta F}{\delta\pi^A(x)}\delta\pi^A(x)\right\}d^3x, \quad \text{(A)}$$

where $F(\phi_A,\pi^A)$ is some arbitrary functional and may either be a point to point functional such as the energy density or an integrated functional, such as the total field. In employing the definition one calculates δF by expanding $F(\phi_A+\delta\phi_A,\pi^A+\delta\pi^A)$ in a Taylor series about ϕ_A and π^A and then subtracting $F(\phi_A,\pi^A)$. The coefficient of $\delta\phi_A(x)$ is then, by the foregoing definition, just $\delta S/\delta\phi_A$ and similarly for the coefficient of $\delta\pi^A(x)$.

As an example, consider the functional

$$I=\int\Im(\phi_A,\pi^A)d^3x,$$

where $\Im$ may depend upon ϕ_A and π^A through gradient terms. Then

$$\delta I=\int\delta\Im(\phi_A,\pi^A)d^3x$$

$$=\int\left\{\frac{\partial\Im}{\partial\phi_A(x)}\delta\phi_A(x)+\frac{\partial\Im}{\partial\phi_{A,r}(x)}\delta\phi_{A,r}(x)+\frac{\delta\Im}{\delta\pi^A(x)}\delta\pi^A(x)+\frac{\delta\Im}{\delta\pi^A{}_{,r}(x)}\delta\pi^A{}_{,r}(x)\right\}d^3x,$$

where $\phi_{A,r}=\partial\phi_A/\partial x^r$. Integrating by parts, we see that

$$\delta I=\int\left\{\left[\frac{\partial\Im}{\partial\phi_A(x)}-\left(\frac{\partial\Im}{\partial\phi_{A,r}(x)}\right)_{,r}\right]\delta\phi_A(x)+\left[\frac{\partial\Im}{\partial\pi_A(x)}-\left(\frac{\partial\Im}{\partial\pi^A{}_{,r}(x)}\right)_{,r}\right]\delta\pi^A(x)\right\}.$$

Comparing with (A), we see thus that

$$\frac{\delta I}{\delta\phi_A(x)}=\frac{\partial\Im}{\partial\phi_A(x)}-\left(\frac{\partial\Im}{\partial\phi_{A,r}(x)}\right)_{,r},$$

and similarly for $\delta\Im/\delta\pi^A(x)$. We see in the special case that I is an integrated point-functional, that the functional derivative is identical with the variational derivative employed by Wentzel. As a further example, consider the point-functional

$$F=\phi_B(y).$$

We can write F as

$$F=\int\phi_A(x)\delta_B{}^A\delta(x-y)d^3x,$$

then

$$\delta F=\int\delta\phi_A(x)\delta_B{}^A\delta(x-y)d^3x,$$

and again comparing with (A) we have

$$\frac{\delta\phi_B(y)}{\delta\phi_A(x)}=\delta_B{}^A\delta(x-y).$$

Actually, our definition is quite analogous to the equation

$$\delta f(x^i)=\sum_i\frac{\partial f}{\partial x_i}\delta x^i,$$

which one uses in the case of a finite number of variables. In the case of functionals the variables x play

the role of indicies while the $\phi_A(x)$ are the independent variables of our theory. The chief advantage to using functional derivatives as defined in (A) instead of the variational derivative is that functional differentiation is commutative, while variational differentiation is not.

By keeping in mind the idea that the space variables are really indices, we can, by analogy, define a Poisson bracket between two functionals F and G as

$$(F,G)\equiv\int\left\{\frac{\delta F}{\delta\phi_A(x)}\frac{\delta G}{\delta\pi^A(x)}-\frac{\delta G}{\delta\phi_A(x)}\frac{\delta F}{\delta\pi^A(x)}\right\}d^3x. \quad \text{(B)}$$

APPENDIX II

A canonical transformation from variables ϕ_A, π^A to $\bar{\phi}_A$, $\bar{\pi}^A$ can be generated by the generating functional $C(\phi_A,\bar{\pi}^A)$ by requiring that

$$\pi^A(x)=\delta C/\delta\phi_A(x), \quad \bar{\phi}_A(x)=\delta C/\delta\bar{\pi}^A(x), \qquad H'=H+\partial C/\partial t. \quad \text{(C)}$$

It can be shown by direct calculation that the transformation (C) preserves Poisson bracket relations and the canonical form of the equations of motion.

PHYSICAL REVIEW VOLUME 99, NUMBER 3 AUGUST 1, 1955

Multiple Bremsstrahlung

SURAJ N. GUPTA
Department of Physics, Purdue University, Lafayette, Indiana

(Received April 18, 1955)

The cross section for the multiple production of photons in bremsstrahlung at high energies is calculated, and it is shown that the probability for multiple bremsstrahlung is quite small compared with that for the ordinary bremsstrahlung even in the very high energy region of cosmic rays.

The general problem of multiple photon production is further discussed, and it appears that even at high energies the probability for multiple photon production is appreciable only in the following two cases: (1) an energetic charged particle is deflected through an angle, which is large compared with the ratio of its rest energy and its total energy; (2) an energetic charged particle is annihilated, captured or converted into a neutral particle.

1. INTRODUCTION

THE Bethe-Heitler[1,2] formula for bremsstrahlung is one of the most widely used results in the study of cosmic rays. Therefore, various types of corrections to this formula have been investigated from time to time.[3] In this paper, we shall consider the possibility of multiple photon production in bremsstrahlung to see how far the Bethe-Heitler formula is adequate to describe the emission of photons and energy loss of electrons at very high energies. It would also be interesting to see whether there is a reasonable possibility of directly observing the multiple bremsstrahlung in cosmic rays.

Recently, the author[4] has investigated the multiple production of photons in the electron-positron annihilation, and it has been found that the probability for the production of several photons in this process becomes appreciable at high energies, which are available in cosmic rays. But, we shall see that the probability for multiple bremsstrahlung is quite small at all energies of experimental interest. The reason for this difference in the two cases will be discussed in this paper. We shall also further discuss the general problem of multiple photon production to see under what conditions such processes are most likely to occur.

It seems to us convenient to represent the ordinary bremsstrahlung process as

$$e^- \overset{N}{\longrightarrow} e^-+\gamma,$$

where $\overset{N}{\longrightarrow}$ indicates that the above process can take place only in the presence of a nucleus. We can then represent a bremsstrahlung process involving the multiple production of n photons as

$$e^- \overset{N}{\longrightarrow} e^-+n\gamma.$$

2. MATRIX ELEMENT FOR DOUBLE BREMSSTRAHLUNG

In the presence of an external electromagnetic field, we can write Dyson's S matrix[5] as

$$S_n=(1/n!)(-i/c\hbar)^n\int dx'\cdots\int dx^{(n)} \times P[H(x'),\cdots,H(x^{(n)})], \quad (1)$$

with

$$H=-ie\bar{\psi}\gamma_\mu\psi(A_\mu+A_{\mu,ex}), \quad (2)$$

[1] H. A. Bethe and W. Heitler, Proc. Roy. Soc. (London) **A146**, 83 (1934).
[2] H. A. Bethe, Proc. Cambridge Phil. Soc. **30**, 524 (1934).
[3] For the latest work on this subject, see H. A. Bethe and L. C. Maximon, Phys. Rev. **93**, 768 (1954), and Davies, Bethe, and Maximon, Phys. Rev. **93**, 788 (1954).
[4] S. N. Gupta, Phys. Rev. **98**, 1502 (1955).
[5] F. J. Dyson, Phys. Rev. **75**, 486, 1736 (1949).

where $A_{\mu,ex}$ denotes the external field. If this external field is due to a heavy nucleus of charge Ze at the origin, then we have

$$A_{i,ex}(x)=0,$$
$$A_{0,ex}(x)=(Ze/V)\sum_{\mathbf{q}} e^{i\mathbf{q}\cdot\mathbf{x}}(1/\mathbf{q}^2), \tag{3}$$

where V is the volume of a large cubical box within which the interacting fields have been confined.

Following Dyson's treatment, we can write the S matrix element for double bremsstrahlung as

$$S_3=(e/c\hbar)^3\int dx\int dx'\int dx''A_{\mu,ex}(x)A_\nu(x')A_\lambda(x'')$$
$$\times[\bar\psi(x)\gamma_\mu S_F(x-x')\gamma_\nu S_F(x-x'')\gamma_\lambda\psi(x'')$$
$$+\bar\psi(x')\gamma_\nu S_F(x'-x)\gamma_\mu S_F(x-x'')\gamma_\lambda\psi(x'')$$
$$+\bar\psi(x')\gamma_\nu S_F(x'-x'')\gamma_\lambda S_F(x''-x)\gamma_\mu\psi(x)], \tag{4}$$

where the various terms in (4) represent the contribution of the Feynman diagrams shown in Fig. 1. We also put

$$\psi(x)=V^{-\frac{1}{2}}a_r(\mathbf{k})u_r(\mathbf{k})e^{ikx},$$
$$\bar\psi(x')=\sum_{\mathbf{k}',s}V^{-\frac{1}{2}}a_s^*(\mathbf{k}')\bar u_s(\mathbf{k}')e^{-ik'x'},$$
$$\mathbf{A}(x')=\sum_{\mathbf{q}',\sigma'}V^{-\frac{1}{2}}(c\hbar/2q_0')^{\frac{1}{2}}\mathbf{e}'a_{\sigma'}^*(\mathbf{q}')e^{-iq'x'},$$
$$\mathbf{A}(x'')=\sum_{\mathbf{q}'',\sigma''}V^{-\frac{1}{2}}(c\hbar/2q_0'')^{\frac{1}{2}}\mathbf{e}''a_{\sigma''}^*(\mathbf{q}'')e^{-iq''x''}, \tag{5}$$
$$S_F(x-x')=\lim_{\epsilon\to+0}(2\pi)^{-4}\int dp e^{ip(x-x')}\frac{ip\gamma-\kappa}{p^2+\kappa^2-i\epsilon},$$

where k and k' are the propagation four vectors for the initial and the final electrons respectively, q' and q'' are the propagation four vectors for the two photons, and other quantities have the usual meaning. Substituting (3) and (5) in (4), we obtain

$$S_3=V^{-3}\sum_{\mathbf{q}}\sum_{\mathbf{q}',\sigma'}\sum_{\mathbf{q}'',\sigma''}\sum_{\mathbf{k}',s}\int dx e^{i(\mathbf{q}\cdot\mathbf{x}}e^{ix(k-k'-q'-q'')}K, \tag{6}$$

where

$$K=\frac{iZe^4}{(c\hbar)^2}\frac{1}{(4q_0'q_0'')^{\frac{1}{2}}}\frac{1}{|\mathbf{k}-\mathbf{k}'-\mathbf{q}'-\mathbf{q}''|^2}$$
$$\times\Big[\bar u_s(\mathbf{k}')\gamma_4\frac{i(k-q'-q'')\gamma-\kappa}{(k-q'-q'')^2+\kappa^2}(\boldsymbol{\gamma}\cdot\mathbf{e}')$$
$$\times\frac{i(k-q'')\gamma-\kappa}{(k-q'')^2+\kappa^2}(\boldsymbol{\gamma}\cdot\mathbf{e}'')u_r(\mathbf{k})+\bar u_s(\mathbf{k}')(\boldsymbol{\gamma}\cdot\mathbf{e}')$$
$$\times\frac{i(k'+q')\gamma-\kappa}{(k'+q')^2+\kappa^2}\gamma_4\frac{i(k-q'')\gamma-\kappa}{(k-q'')^2+\kappa^2}(\boldsymbol{\gamma}\cdot\mathbf{e}'')u_r(\mathbf{k})$$
$$+\bar u_s(\mathbf{k}')(\boldsymbol{\gamma}\cdot\mathbf{e}')\frac{i(k'+q')\gamma-\kappa}{(k'+q')^2+\kappa^2}(\boldsymbol{\gamma}\cdot\mathbf{e}'')$$
$$\times\frac{i(k'+q'+q'')\gamma-\kappa}{(k'+q'+q'')^2+\kappa^2}\gamma_4u_r(\mathbf{k})\Big]. \tag{7}$$

FIG. 1. Feynmann diagrams for double bremsstrahlung.

We shall now consider the extreme relativistic case, i.e., we shall take $k_0\gg\kappa$. We shall also assume that the major contribution to the cross section for the process under consideration arises from those values of q_0' and q_0'', which are small compared with k_0. We can then simplify the denominators and the numerators in (7) as

$$(k'+q'+q'')^2+\kappa^2=2k'q'+2k'q'',$$
$$(k-q'-q'')^2+\kappa^2=-2kq'-2kq''; \tag{8}$$
$$[i(k-q')\gamma-\kappa](\boldsymbol{\gamma}\cdot\mathbf{e}')u_r(\mathbf{k})=2i(\mathbf{k}\cdot\mathbf{e}')u_r(\mathbf{k}),$$
$$\bar u_s(\mathbf{k}')(\boldsymbol{\gamma}\cdot\mathbf{e}')[i(k'+q')\gamma-\kappa]=\bar u_s(\mathbf{k}')2i(\mathbf{k}'\cdot\mathbf{e}'),\ \text{etc.} \tag{9}$$

Therefore, we can express (7) as

$$K=\frac{-iZe^4}{2(c\hbar)^2}\frac{1}{(q_0'q_0'')^{\frac{1}{2}}}\frac{1}{|\mathbf{k}-\mathbf{k}'-\mathbf{q}'-\mathbf{q}''|^2}[\bar u_s(\mathbf{k}')\gamma_4u_r(\mathbf{k})]$$
$$\times\Big[\frac{(\mathbf{k}\cdot\mathbf{e}')(\mathbf{k}\cdot\mathbf{e}'')}{(kq'+kq'')(kq'')}-\frac{(\mathbf{k}'\cdot\mathbf{e}')(\mathbf{k}\cdot\mathbf{e}'')}{(k'q')(kq'')}$$
$$+\frac{(\mathbf{k}'\cdot\mathbf{e}')(\mathbf{k}'\cdot\mathbf{e}'')}{(k'q')(k'q'+k'q'')}\Big]. \tag{10}$$

But, due to the indistinguishability of photons in the same state, we have to write (6) as

$$S_3=V^{-3}\sum_{\mathbf{q}}\sum_{\mathbf{q}',\mathbf{q}''}{}'\sum_{\sigma',\sigma''}\sum_{\mathbf{k}',s}\int dx e^{i\mathbf{q}\cdot\mathbf{x}}$$
$$\times e^{ix(k-k'-q'-q'')}(K+K'), \tag{11}$$

where K' is obtained from K by interchanging the roles of the photons $\mathbf{q}'$ and $\mathbf{q}''$, and $\sum'_{\mathbf{q}',\mathbf{q}''}$ denotes summation over all values of $\mathbf{q}'$ and $\mathbf{q}''$ such that each physically different state occurs only once. It then follows from (10) that

$$K+K'=\frac{-iZe^4}{2(c\hbar)^2}\frac{1}{(q_0'q_0'')^{\frac{1}{2}}}\frac{1}{|\mathbf{k}-\mathbf{k}'-\mathbf{q}'-\mathbf{q}''|^2}$$
$$\times[\bar u_s(\mathbf{k}')\gamma_4u_r(\mathbf{k})][(\mathbf{k}\cdot\mathbf{e}')/(kq')-(\mathbf{k}'\cdot\mathbf{e}')/(k'q')]$$
$$\times[(\mathbf{k}\cdot\mathbf{e}'')/(kq'')-(\mathbf{k}'\cdot\mathbf{e}'')/(k'q'')]. \tag{12}$$

Let us now denote the angle between $\mathbf{k}$ and $\mathbf{k}'$ as γ. Further, let the angles made by $\mathbf{q}'$ with $\mathbf{k}$ and $\mathbf{k}'$ be denoted as α' and β', respectively, and the angles made by $\mathbf{q}''$ with $\mathbf{k}$ and $\mathbf{k}'$ be denoted as α'' and β'' respectively. Since it is evident from the denominators in (12) that the major contribution to the cross section arises from small values of the above angles, we can simplify

these denominators as

$$|\mathbf{k}'+\mathbf{q}'+\mathbf{q}''-\mathbf{k}|^2\approx(|\mathbf{k}'|+|\mathbf{q}'|+|\mathbf{q}''|-|\mathbf{k}|)^2+k_0^2\gamma^2$$
$$\approx\kappa^4(q_0'+q_0'')^2/(4k_0^4)+k_0^2\gamma^2, \quad (13)$$

$$kq'=-\tfrac{1}{2}q_0'k_0(\kappa^2/k_0^2+\alpha'^2), \quad \text{etc.}, \quad (14)$$

where we have also made use of the conservation relations

$$\mathbf{k}+\mathbf{q}-\mathbf{k}'-\mathbf{q}'-\mathbf{q}''=0, \quad k_0-k_0'-q_0'-q_0''=0. \quad (15)$$

Using (13) and (14), we can express (12) as

$$K+K'=\frac{-2iZe^4}{(c\hbar)^2}\frac{1}{(q_0'q_0'')^{\frac{1}{2}}}$$
$$\times\frac{1}{[\kappa^4(q_0'+q_0'')^2/(4k_0^4)+k_0^2\gamma^2]}[\bar{u}_s(\mathbf{k}')\gamma_4 u_r(\mathbf{k})]$$
$$\times\left[\frac{(\mathbf{k}\cdot\mathbf{e}')}{k_0(\kappa^2/k_0^2+\alpha'^2)}-\frac{(\mathbf{k}'\cdot\mathbf{e}')}{k_0(\kappa^2/k_0^2+\beta'^2)}\right]$$
$$\times\left[\frac{(\mathbf{k}\cdot\mathbf{e}'')}{k_0(\kappa^2/k_0^2+\alpha''^2)}-\frac{(\mathbf{k}'\cdot\mathbf{e}'')}{k_0(\kappa^2/k_0^2+\beta''^2)}\right]. \quad (16)$$

3. CROSS SECTION FOR DOUBLE BREMSSTRAHLUNG

In order to find the cross section for double bremsstrahlung, we have to square the element (16). Then, averaging over the spin states of the electron in the initial state, summing over the spin states of the electron in the final state, and also summing over the states of polarization of the photons $\mathbf{q}'$ and $\mathbf{q}''$, we get

$$\sum(|K+K'|^2)_{\text{Av}}$$
$$=\frac{4Z^2e^8}{(c\hbar)^4}\frac{1}{(q_0'q_0'')^3}\frac{1}{[\kappa^4(q_0'+q_0'')^2/(4k_0^4)+k_0^2\gamma^2]^2}$$
$$\times\left\{\frac{\alpha'^2}{(\kappa^2/k_0^2+\alpha'^2)^2}+\frac{\beta'^2}{(\kappa^2/k_0^2+\beta'^2)^2}\right.$$
$$\left.-\frac{\alpha'^2+\beta'^2-\gamma^2}{(\kappa^2/k_0^2+\alpha'^2)(\kappa^2/k_0^2+\beta'^2)}\right\}$$
$$\times\left\{\frac{\alpha''^2}{(\kappa^2/k_0^2+\alpha''^2)^2}+\frac{\beta''^2}{(\kappa^2/k_0^2+\beta''^2)^2}\right.$$
$$\left.-\frac{\alpha''^2+\beta''^2-\gamma^2}{(\kappa^2/k_0^2+\alpha''^2)(\kappa^2/k_0^2+\beta''^2)}\right\}. \quad (17)$$

The cross section σ_2 for the process under consideration is related to the quantity (17) as

$$\sigma_2=(1/2!)V^{-2}\sum_{\mathbf{q}'}\sum_{\mathbf{q}''}(2\pi)^{-2}\int d\omega\mathbf{k}'^2$$
$$\times d|\mathbf{k}'|/dk_0'\sum(|K+K'|^2)_{\text{Av}}, \quad (18)$$

where $d\omega$ is an element of solid angle along $\mathbf{k}'$. Putting

$$k_0'=k_0, \quad d|\mathbf{k}'|/dk_0'=1,$$
$$V^{-1}\sum_{\mathbf{q}'}=(2\pi)^{-3}\int d\mathbf{q}', \quad \text{etc.}, \quad (19)$$

we have

$$\sigma_2=(1/2!)(2\pi)^{-3}\int d\mathbf{q}'\int d\mathbf{q}''\int d\omega k_0^2$$
$$\times\sum(|K+K'|^2)_{\text{Av}}. \quad (20)$$

We now choose our coordinate axes in such a way that $\mathbf{k}$ is along the z axis, and $\mathbf{k}'$ lies in the xz plane. Then, we can write the components of $\mathbf{k}$ and $\mathbf{k}'$ as

$$\mathbf{k}=(0, 0, |\mathbf{k}|), \quad \mathbf{k}'=(|\mathbf{k}'|\sin\gamma, 0, |\mathbf{k}'|\cos\gamma). \quad (21)$$

We further assume that the azimuthal angles of $\mathbf{q}'$ and $\mathbf{q}''$ around the z axis are ϕ' and ϕ'' respectively, so that the components of $\mathbf{q}'$ and $\mathbf{q}''$ are

$$\mathbf{q}'=(q_0'\sin\alpha'\cos\phi', q_0'\sin\alpha'\sin\phi', q_0'\cos\alpha'),$$
$$\mathbf{q}''=(q_0''\sin\alpha''\cos\phi'', q_0''\sin\alpha''\sin\phi'', q_0''\cos\alpha''). \quad (22)$$

Since the angles γ, α', β', α'', and β'' have been assumed to be small, it follows that

$$\beta'^2=\alpha'^2+\gamma^2-2\alpha'\gamma\cos\phi',$$
$$\beta''^2=\alpha''^2+\gamma^2-2\alpha''\gamma\cos\phi'', \quad (23)$$

$$\int d\mathbf{q}'=\int dq_0'q_0'^2\int_0^\delta\alpha'd\alpha'\int_0^{2\pi}d\phi',$$
$$\int d\mathbf{q}''=\int dq_0''q_0''^2\int_0^\delta\alpha''d\alpha''\int_0^{2\pi}d\phi'', \quad (24)$$

$$\int d\omega=2\pi\int_0^\delta\gamma d\gamma, \quad (25)$$

where δ represents the upper limit of integration for the angles α', α'', and γ. We can choose any suitable value for this upper limit, provided that δ^2 is large compared with κ^2/k^2 but small compared with 1.

Using (17), (24), and (25), we can express (20) as

$$\sigma_2=\frac{16Z^2}{\pi}\left(\frac{e^2}{4\pi c\hbar}\right)^4\int\frac{dq_0'}{q_0'}\int\frac{dq_0''}{q_0''}\int_0^\delta\gamma d\gamma$$
$$\times\frac{k_0^2}{[\kappa^4(q_0'+q_0'')^2/(4k_0^4)+k_0^2\gamma^2]^2}I'I'', \quad (26)$$

where

$$I'=\frac{1}{2\pi}\int_0^\delta \alpha' d\alpha' \int_0^{2\pi} d\phi' \left\{ \frac{\alpha'^2}{(\kappa^2/k_0^2+\alpha'^2)^2} + \frac{\beta'^2}{(\kappa^2/k_0^2+\beta'^2)^2} - \frac{\alpha'^2+\beta'^2-\gamma^2}{(\kappa^2/k_0^2+\alpha'^2)(\kappa^2/k_0^2+\beta'^2)} \right\}, \quad (27)$$

$$I''=\frac{1}{2\pi}\int_0^\delta \alpha'' d\alpha'' \int_0^{2\pi} d\phi'' \left\{ \frac{\alpha''^2}{(\kappa^2/k_0^2+\alpha''^2)^2} + \frac{\beta''^2}{(\kappa^2/k_0^2+\beta''^2)^2} - \frac{\alpha''^2+\beta''^2-\gamma^2}{(\kappa^2/k_0^2+\alpha''^2)(\kappa^2/k_0^2+\beta''^2)} \right\}. \quad (28)$$

Substituting (23) in (27), and carrying out the integration over the azimuthal angle ϕ', we get

$$I'=\int_0^\delta \alpha' d\alpha' \left\{ \frac{\gamma^2+2\kappa^2/k_0^2}{(\kappa^2/k_0^2+\alpha'^2)[(\kappa^2/k_0^2+\alpha'^2+\gamma^2)^2-4\alpha'^2\gamma^2]^{\frac{1}{2}}} - \frac{\kappa^2}{k_0^2}\frac{(\kappa^2/k_0^2+\alpha'^2+\gamma^2)}{[(\kappa^2/k_0^2+\alpha'^2+\gamma^2)^2-4\alpha'^2\gamma^2]^{\frac{1}{2}}} - \frac{\kappa^2}{k_0^2}\frac{1}{(\kappa^2/k_0^2+\alpha'^2)^2} \right\}. \quad (29)$$

The above integral can be easily evaluated, but the resulting expression is a rather complicated function of γ. However, we find approximately

$$\begin{aligned} I' &= \tfrac{1}{3}k_0^2\gamma^2/\kappa^2 \qquad (\text{for } \gamma^2<4\kappa^2/k_0^2), \\ &= \log(k_0^2\gamma^2/\kappa^2)-1 \quad (\text{for } 4\kappa^2/k_0^2<\gamma^2<\delta^2), \end{aligned} \quad (30)$$

and we also note that $I''=I'$. Hence, substituting (30) in (26), and integrating over γ, we obtain

$$\sigma_2 \approx \frac{7}{4\pi}\frac{16Z^2\alpha^4\hbar^2c^2}{3\mu^2}\int\frac{d\omega'}{\omega'}\int\frac{d\omega''}{\omega''}, \quad (31)$$

with

$$\alpha=e^2/4\pi c\hbar, \quad \mu=\kappa c\hbar, \quad \omega'=q_0'c\hbar, \quad \omega''=q_0''c\hbar, \quad (32)$$

where α is the fine structure constant, μ is the rest energy of the electron, and ω' and ω'' are the energies of the emitted photons.

In order to estimate the influence of screening on double bremsstrahlung, we note that the minimum value of the quantity $|\mathbf{q}|$ appearing in the integral (6) is

$$\begin{aligned} |\mathbf{q}|_{\min} &= |\mathbf{k}|-|\mathbf{k}'|-|\mathbf{q}'|-|\mathbf{q}''| \\ &\approx \tfrac{1}{2}\kappa^2(q_0'+q_0'')/k_0^2, \end{aligned} \quad (33)$$

and we also note that the square of the above quantity appears on the right-hand side of (13). It is well known[6] that roughly the effect of screening is to replace the above minimum value of $|\mathbf{q}|$ by

$$Z^{\frac{1}{3}}\alpha\kappa. \quad (34)$$

Hence, taking into account the effect of screening, we have instead of (26):

$$\sigma_2' \approx \frac{16Z^2}{\pi}\left(\frac{e^2}{4\pi c\hbar}\right)^4 \int\frac{dq_0'}{q_0'}\int\frac{dq_0''}{q_0''}\int_0^\delta \gamma d\gamma \times \frac{k_0^2}{[Z^{\frac{1}{3}}\alpha^2\kappa^2+k_0^2\gamma^2]^2} I'I''. \quad (35)$$

According to the present approximations, the above integral gives the same result as (26), which shows that the effect of screening on double bremsstrahlung at high energies is negligible.

4. DISCUSSION

In the extreme relativistic case, the cross section for the ordinary bremsstrahlung due to an incident electron of energy E is approximately given by[6]

$$\sigma_1=\frac{16Z^2\alpha^3c^2\hbar^2}{3\mu^2}\int\frac{d\omega}{\omega}\log\frac{2E^2}{\mu\omega}, \quad (36)$$

$$\sigma_1'=\frac{16Z^2\alpha^3c^2\hbar^2}{3\mu^2}\int\frac{d\omega}{\omega}\log(183Z^{-\frac{1}{3}}), \quad (37)$$

where σ_1 denotes the cross section without screening, σ_1' denotes the cross section with screening, and ω is the energy of the emitted photon. For a rough estimate, we may take the upper and lower limits of integration for ω as E and μ, respectively, so that we have

$$\sigma_1=\tfrac{1}{2}(16Z^2\alpha^3c^2\hbar^2/3\mu^2)[\log(E/\mu)]^2, \quad (38)$$

$$\sigma_1'=(16Z^2\alpha^3c^2\hbar^2/3\mu^2)\log(E/\mu)\log(183Z^{-\frac{1}{3}}). \quad (39)$$

Choosing the upper and lower limits of integration for ω' and ω'' also in a similar way, we obtain from (31)

$$\sigma_2=(7\alpha/4\pi)(16Z^2\alpha^3c^2\hbar^2/3\mu^2)[\log(E/\mu)]^2. \quad (40)$$

Comparing (40) with (38) and (39), we find that even at $E\approx 10^{14}$ ev the probability for double bremsstrahlung is quite small compared with that for the ordinary bremsstrahlung.

Using the approximations, described in this paper and the earlier one,[4] we can also calculate the cross section for bremsstrahlung involving the production of n photons. The cross section for this process is found to be

$$\sigma_n=\frac{8\pi Z^2\alpha^2}{n!}\left(\frac{2\alpha}{\pi}\right)^n\int\frac{dq_0'}{q_0'}\cdots\int\frac{dq_0^{(n)}}{q_0^{(n)}}\int\gamma d\gamma \times \frac{k_0^2}{[\kappa^4(q_0'+\cdots+q_0^{(n)})^2/(4k_0^4)+k_0^2\gamma^2]^2} I'^n, \quad (41)$$

[6] W. Heitler, *Quantum Theory of Radiation* (Clarendon Press, Oxford, 1954).

where the integral I' is given by (27). Substituting (30) in (41), we can easily see that even at very high energies σ_n rapidly decreases as n increases.

The above situation is quite different from that in the case of the electron-positron annihilation. For, we have already shown[4] that in electron-positron annihilation at high energies multiple production of several photons can easily take place. This difference between the two cases is due to the following reasons: In high energy bremsstrahlung the average angle, through which the electron is deflected, is of the order of μ/E. Further, it follows from the general treatment in Sec. 5 of reference 4 that the photons emitted by an energetic electron mainly lie within a cone of angle μ/E around the direction of motion of the electron. Therefore, in bremsstrahlung the photons emitted by the initial and the final electrons interfere strongly, which greatly reduces the cross section. On the other hand, there is no appreciable interference between the photons emitted by the electron and the positron during their annihilation.

It is interesting to note that if $\gamma \gg \mu/E$, we obtain from (41) and (30)

$$\sigma_n = \frac{8\pi Z^2\alpha^2}{n!}\left(\frac{4\alpha}{\pi}\right)^n \int \frac{dq_0'}{q_0'} \cdots \int \frac{dq_0^{(n)}}{q_0^{(n)}} \int \gamma d\gamma \times \frac{1}{k_0^2\gamma^4}\left(\log\frac{k_0\gamma}{\kappa}\right)^n$$

or

$$\sigma_n = \frac{\sigma_0}{n!}\left(\frac{4\alpha}{\pi}\right)^n \left(\log\frac{E}{\epsilon}\right)^n \left(\log\frac{k_0\gamma}{\kappa}\right)^n, \qquad (42)$$

where σ_0 is the cross section for the radiationless scattering of an electron through an angle γ, and ϵ is the lower limit to the energy of emitted photons. The above result is in agreement with that obtained by following the general treatment in Sec. 5 of reference 4, if we ignore the interference between the photons emitted by the initial and the final electrons. This confirms the fact that if an energetic electron is deflected through an angle, which is large compared with μ/E, there is very little interference between the photons emitted by the initial and the final electrons. In such a case, the probability for multiple photon production is appreciable, but a high-energy bremsstrahlung process with a large deflection of the incident electron is a very rare event.

5. GENERAL REMARKS ON MULTIPLE PHOTON PRODUCTION

The present investigation also throws some light on multiple photon production in nuclear collisions. For, according to the present view, a proton, too, is described by the Dirac equation, and therefore the treatment in Sec. 5 of reference 4 also holds for collisions involving high energy protons. Hence, in high-energy nuclear collisions sometimes multiple photon production is bound to take place along with the production of mesons and other particles. Moreover, a proton possesses an anomalous magnetic moment, which might also appreciably increase the cross section for multiple photon production by protons.

It further follows from the discussion in the preceding section that even at very high energies, the probability for multiple photon production is appreable only if there is no interference between the photons emitted in the initial and the final states. This condition is evidently satisfied in the following two cases: (1) an energetic charged particle is deflected through an angle, which is large compared with μ/E; (2) an energetic charged particle is annihilated, captured or converted into a neutral particle. Therefore, we should specially look for multiple photon production in nuclear collisions under the above conditions.

Radiative Correction to High-Energy Electron Scattering*

HIROSHI SUURA†
Department of Physics, Stanford University, Stanford, California
(Received March 25, 1955)

The one-photon radiative correction to the high-energy electron scattering by a nuclear field is analyzed to all orders of Born approximation for the nuclear potential. The leading term of the fractional decrease of the elastic scattering cross section is shown to be exactly the same as that given by the first Born approximation. A detailed analysis of the effect of the long Coulomb tail on the infrared divergence is made. Also, an analysis is made on the origin of the log$m$ term which appears in the radiative correction.

I. INTRODUCTION AND SUMMARY

THE radiative correction to electron scattering by a nuclear field was calculated by Schwinger[1] in the first Born approximation for the nuclear potential, and to the lowest order in the coupling between the electron and the radiation field. (The phrase "Born approximation" will refer here to the interaction between the electron and the nuclear potential.) In view of recent experiments[2] on the scattering of high-energy electrons by heavy nuclei, it is the purpose of this paper to investigate higher Born approximations of the radiative correction, still including only one-photon processes. According to A, the contribution to the cross section from the radiative correction, $\sigma_{\rm rad}$, is proportional to the first Born elastic scattering cross section, $\sigma_{\rm el}$, so that to order $(Z\alpha)^2$ we have

$$\sigma_{\rm rad} = -\delta\sigma_{\rm el}, \tag{1}$$

with the fractional decrease δ being given asymptotically in the high-energy limit by

$$\delta \sim (4\alpha/\pi)\log[(2p_0\sin\theta/2)/m]\log(p_0/\Delta E), \tag{2}$$

Here, the notation is as follows: α is the fine structure constant, m the electron mass, p_0 the electron energy, θ the scattering angle, and ΔE is the energy resolution associated with the experiment. We use units such that $\hbar=c=1$ throughout. The expression (2) is the leading term of δ in the sense that it is the product of the two logarithms with the large arguments p_0/m and $p_0/\Delta E$, the neglected terms being either linear in these logarithms or constants of order unity depending only on the scattering angle θ. We shall use the symbol $\sim$ for this meaning. We show in this paper that, in the same sense as above, the expression (2) represents the leading term of δ to *all* orders of the Born approximation, so that $\sigma_{\rm el}$ in Eq. (1) now stands for the exact elastic scattering cross section. Since the expression (2) is apparently connected with the infrared divergence, we shall prove the above statement in two steps. First we shall show that the coefficient of the infrared divergence, namely, the coefficient of $\log(\Delta E)$, is exactly given by the same expression as (2) to all orders of Born approximation in the high-energy limit. The second step is to show that no $(\log m)^n$ with $n\geqq 2$ appears in the radiative correction. This will exclude such large terms as $[\log(p_0/m)]^2$ and at the same time will fix the argument of the second logarithm in (2) as $p_0/\Delta E$, since δ should be a function of the three parameters m/p_0, $\Delta E/p_0$ and $\Delta E/m$ in the case of the point Coulomb potential. (We consider large angle scattering, so that $\sin\theta/2$ is of order unity, and we can omit it from consideration in our discussion of the leading term.) If the nuclear charge has an extension of order $1/a$, Eq. (2) will be still true. This is because no term such as $\log(a/p)$ appears in the cross section. If it did, the differential cross section would diverge in the point charge limit $a\to\infty$.

Concerning the first step, the same conclusion has been reached by Newton[3] and also by Jauch and Rohrlich.[4] The essential point of the argument of these authors is that in the inelastic scattering of an electron with emission of a soft photon, the infrared divergence occurs only when the photon is emitted either before or after the potential scatterings (see diagrams A and C of Fig. 1). This follows from a simple inspection of the energy denominators appearing in the integrand of the various processes. It is also physically acceptable, since the electron confined in the scattering region would be more likely to emit hard photons of wavelength shorter than the atomic dimension, rather than soft ones.

However, such an argument applies only for low-energy electrons in a screened potential.[5] For electrons of energy as high as a few hundred Mev the large-angle scattering takes place almost inside the nucleus, and since the energy resolution also increases, we have to deal with relatively high energy "soft photons." In such a case the screening plays no role at all. In the unscreened potential, the electron could emit soft photons in the course of the gradual deflection by the long tail of the Coulomb potential. Therefore, we should expect an infrared divergence also in the processes omitted in the

* Supported by the Office of Scientific Research, Air Research and Development Command.
† On leave of absence from Hiroshima University, Hiroshima, Japan. Now at Cornell University, Ithaca, New York.
[1] J. Schwinger, Phys. Rev. **76**, 790 (1949), referred to as A.
[2] Hofstadter, Fechter, and McIntyre, Phys. Rev. **92**, 978 (1953); Hofstadter, Hahn, Knudsen, and McIntyre, Phys. Rev. **95**, 512 (1954).
[3] R. G. Newton, Phys. Rev. **94**, 1773 (1954).
[4] J. M. Jauch and F. Rohrlich, Helv. Phys. Acta **27**, 613 (1954).
[5] The importance of the screening was noticed by Mittleman in his paper which also reached to Eq. (1) for the nonrelativistic electron in a screened potential. M. H. Mittleman, Phys. Rev. **93**, 453 (1954).

foregoing discussion. Mathematically, this is reflected in the fact that the elastic scattering matrix element between the two virtual states (off-energy-shell matrix element) has a discontinuity on the energy shell, as was noticed by Dalitz.[6] This means that we cannot always neglect the photon momentum in the internal electron propagators between the successive potential scatterings, as was done in references 3 and 4.

In Sec. II, we shall perform the potential integrations of the second Born approximation in the soft photon limit, and separate out the discontinuity term which contributes to the additional infrared divergences. It will be shown that this discontinuity term actually comes from the small momentum transfer by the electron to the external field, either just before or after the emission of the photon, which indicates the effect of the long Coulomb tail. However, these additional infrared divergences cancel out completely, when the contributions from all the possible processes of Bremsstrahlung are added. The same cancellation occurs also for the virtual radiative processes. This cancellation of the additional infrared divergences resulting from the Coulomb tail is quite general, and can be shown to hold to any order of Born approximation and also for any number of soft photons emitted.[7] Thus, we are justified to take only such diagrams as (A) and (C) of Fig. 1 and (A) of Fig. 3, and to set $k=0$ in the internal electron line AB in the consideration of the infrared divergence.

The second step, namely to prove the nonexistence of a term $(\log m)^2$, needs an analysis of the origin of $\log m$,[8] which appears in the first Born approximation. This will be done in Sec. III by a careful examination of the photon momentum integration. It develops that $\log m$ originates from each of the "outer" electron propagators such as XA and BY of diagram (A) of Fig. 3, when the photon momentum is parallel to the incident or outgoing electron momentum. Since for a large-angle scattering the incident and scattered electron momenta are not parallel, and since the poles of the internal electron lines between the potential scatterings do not generally coincide with those of the outer electron lines, we can infer the nonexistence of the higher powers of $\log m$.[9]

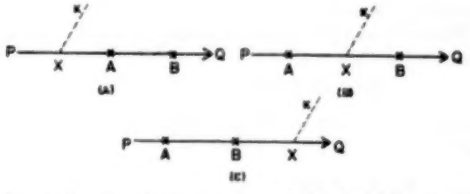

FIG. 1. Feynman diagrams for second order inelastic processes. ———, electron line; - - - - - - -, photon line; ×, external field.

A remark will be necessary about the fact that some methods for treating the infrared divergence, for instance, the method employed in A and the method of assuming a small photon mass, actually give $(\log m)^2$ in some integrals even in the calculation of the first Born approximation. However, such $(\log m)^2$ terms are of a quite fictitious character, since they are shown to originate from the contribution of the soft photon, and hence are bound to cancel in the final expression. The method employed in the present paper, namely, to restrict the photon momentum space by the condition $K \geqq K_{\min}$, has the advantage of giving no fictitious $(\log m)^2$ of the above kind[10] and is suited for the present purpose. The noncovariant character of the method leads to no trouble at all as is seen by the facts that all the methods give the same value for the noninfrared divergent integrals and that we get a unique answer for the radiative correction in the first Born approximation by any method.

A more important point to examine is the effect of the long tail of the Coulomb potential, which has the possibility of giving rise to higher powers of $\log m$ by overlapping the poles of the internal electron lines with those of the outer. This is also checked and the answer is negative.

II. INFRARED DIVERGENCE IN A COULOMB FIELD

For the three possible diagrams of the inelastic scattering in the second order (Fig. 1) we have the following matrix elements in momentum representation:

$$M_A=[ieF/(2K)^{\frac{1}{2}}]\int d\mathbf{l}(\mathbf{l}^2\mathbf{l}'^2)^{-1}\bar{u}_q\gamma_0[i\gamma\cdot(p-k-l)+m]^{-1}\times\gamma_0[i\gamma\cdot(p-k)+m]^{-1}i\gamma\cdot\epsilon u_p, \quad (3)$$

$$M_B=[ieF/(2K)^{\frac{1}{2}}]\int d\mathbf{l}(\mathbf{l}^2\mathbf{l}'^2)^{-1}\bar{u}_q\gamma_0[i\gamma\cdot(p-k-l)+m]^{-1}\times i\gamma\cdot\epsilon[i\gamma\cdot(p-l)+m]^{-1}\gamma_0 u_p, \quad (4)$$

where the momenta l, l', and k satisfy the conditions

$$\mathbf{q}-\mathbf{p}+\mathbf{l}+\mathbf{l}'+\mathbf{k}=0, \quad q_0-p_0+k_0=0, \quad \text{and} \quad k^2=0.$$

M_C is similar to M_A and will not be mentioned here. Here, light-face letters p, q, and k denote the four momenta of the incident electron, the scattered electron

[6] R. H. Dalitz, Proc. Roy. Soc. (London) **A206**, 509 (1951).

[7] Such a Coulomb anomaly has been investigated independently by Newton in his paper on the second Born calculation of the radiative correction to the electron scattering. R. G. Newton, Phys. Rev. **97**, 1162 (1955). His result is essentially the same as that of the present paper, although his calculation is limited to the second order, and the anomaly is treated not as an additional infrared divergence but as a Coulomb divergence.

[8] The pure elastic scattering cross section can be expanded in powers of m. Yennie, Ravenhall, and Wilson, Phys. Rev. **95**, 500 (1954).

[9] The aforementioned paper of Newton gave $(\log m)^2$ in the second Born approximation. However, after the completion of the present work, his result was corrected and it no longer gives a $(\log m)^2$ term. Hence, his result confirms the validity of the general argument presented in this paper. Roger G. Newton, Phys. Rev. **98**, 1514 (1955). See also, Max Chrétien, Phys. Rev. **98**, 1515 (1955).

[10] The invariant minimum momentum method employed in A, has some mathematical difficulty as pointed out by Elton and Robertson. A close analysis shows that the method in A is almost equivalent to assuming a small photon mass. L. R. B. Elton and H. H. Robertson, Proc. Phys. Soc. (London) **A65**, 144 (1952).

and the emitted photon, respectively. l and l' are the momentum transfers at A and B, respectively; bold-face letters will be used for the spatial vectors, and capital letters for their magnitude. Thus, for instance,

$$p=(\mathbf{p};p_0), \quad |\mathbf{p}|=P; \quad l=(\mathbf{l};0), \quad |\mathbf{l}|=L.$$

ϵ denotes the polarization vector of the photon. F represents $F=(2\pi)^4(-Ze^2/2\pi^2)^2$. The other notations will be evident. The second Born elastic scattering matrix element is given by

$$M_{el}=iF\int d\mathbf{l}(\mathbf{l}^2\mathbf{l}'^2)^{-1}\bar{u}_q\gamma_0[i\gamma\cdot(p-l)+m]^{-1}\gamma_0 u_p, \quad (5)$$

with

$$\mathbf{q}-\mathbf{p}+\mathbf{l}+\mathbf{l}'=0, \quad \text{and} \quad q_0-p_0=0.$$

Rationalizing the denominators and neglecting k in the numerator, we get

$$M_A=\frac{ieF}{(2K)^{\frac{1}{2}}}\left(-\frac{p\cdot\epsilon}{p\cdot k}\right)\int d\mathbf{l} \times\frac{\bar{u}_q(2\gamma_0 p_0-i\gamma\cdot l)u_p}{[(k+l)^2-2p\cdot(k+l)]\mathbf{l}^2(\mathbf{l}-\Delta\mathbf{p}+\mathbf{k})^2}, \quad (3')$$

$$M_B=\frac{ieF}{(2K)^{\frac{1}{2}}}\int d\mathbf{l} \times\frac{[2\epsilon\cdot(p-l)]\bar{u}_q(2\gamma_0 p_0-i\gamma\cdot l)u_p}{[(k+l)^2-2p\cdot(k+l)]\times(l^2-2l\cdot p)\mathbf{l}^2(\mathbf{l}-\Delta\mathbf{p}+\mathbf{k})^2}, \quad (4')$$

$$M_{el}=iF\int d\mathbf{l}\frac{\bar{u}_q(2\gamma_0\cdot p_0-i\gamma\cdot l)u_p}{(l^2-2l\cdot p)\mathbf{l}^2(\mathbf{l}-\Delta\mathbf{p})^2}, \quad (5')$$

with

$$\Delta\mathbf{p}=\mathbf{p}-\mathbf{q}, \quad |\Delta\mathbf{p}|=\Delta P=2P\sin(\theta/2) \quad \text{for } M_{el}.$$

In Eq. (4'), we have neglected a noninfrared divergent term

$$\int d\mathbf{l}\frac{\bar{u}_q i\gamma\cdot\epsilon u_p}{[(k+l)^2-2p\cdot(k+l)]\mathbf{l}^2(\mathbf{l}-\Delta\mathbf{p}+\mathbf{k})^2},$$

which is discontinuous but finite in the limit $k\to 0$, as will be seen from Eqs. (6), (9), and (10) below. The potential integrations in (3') and (5') are all reduced to the first two of the following integrals by the change of the integration variable according to $\mathbf{p}-\mathbf{k}-\mathbf{l}\to\mathbf{l}$ for (3') and $\mathbf{p}-\mathbf{l}\to\mathbf{l}$ in (5')

$$(I_0;I_i;I_{ij})=\int d\mathbf{l}(1;l_i;l_il_j) \times[(\mathbf{l}^2-R^2)(\mathbf{l}-\mathbf{p}')^2(\mathbf{l}-\mathbf{q}')^2]^{-1}, \quad (6)$$

with

$$\mathbf{p}'=\mathbf{p}-\mathbf{k}, \quad \mathbf{q}'=\mathbf{q}, \quad R^2=Q^2=P^2-2p_0K+K^2 \quad \text{for } M_A, \quad (7)$$

$$\mathbf{p}'=\mathbf{p}, \quad \mathbf{q}'=\mathbf{q}, \quad R^2=Q^2=P^2 \quad \text{for } M_{el}. \quad (8)$$

[In (5), the pole of the denominator l^2-R^2 is defined by adding a small negative imaginary part, according to Feynman's prescription.[11]] The integrals (6) can be integrated exactly. Although the quantities $\mathbf{p}'$, $\mathbf{q}'$ and R, defined by (7) for M_A, approach the corresponding quantities for M_{el}, (8), in the soft photon limit $k\to 0$, the corresponding values of the integrals do not. In order to see that there is this discontinuity on the energy shell, the integration was made by employing the Yukawa potential $e^{-\lambda r}/r$ instead of the Coulomb potential. The value of the integral (6) as well as its value near the energy shell (8) in the limit $\lambda\to 0$ are listed in the Appendix. The integrals assume the following form near the energy shell:

$$\begin{aligned} I_0&=I_0^{el}+\Delta(f)+\Delta(g),\\ I_i&=I_i^{el}+p_i\Delta(f)+q_i\Delta(g),\\ I_{ij}&=I_{ij}^{el}+p_ip_j\Delta(f)+q_iq_j\Delta(g), \end{aligned} \quad (9)$$

where I_0^{el}, I_i^{el} and I_{ij}^{el} denote the value of the integrals (6) on the energy shell (8), while $\Delta(f)$ is the discontinuity term defined by

$$\Delta(f)=\lim_{\lambda\to 0}\frac{\pi^2}{P\Delta P^2}\left(\tan^{-1}\frac{f}{2\lambda P}+i\log\frac{2\lambda P}{(f^2+4\lambda^2P^2)^{\frac{1}{2}}}\right). \quad (10)$$

Here f and g represent the measure of the distance from the energy shell,

$$f=P'^2-R^2, \quad g=Q'^2-R^2. \quad (11)$$

It is seen from (10) that the value of $\Delta(f)$ depends critically on the relative magnitude of f, g, and λ, which is the origin of the discontinuity. The condition on the magnitude of K for Eq. (9) to hold is

$$K\ll\Delta P, \quad (12)$$

which is necessary and sufficient to replace $\Delta P'=|\mathbf{p}'-\mathbf{q}'|$, P', and Q' by the corresponding quantities ΔP, P, and Q, on the energy shell (8) respectively, everywhere except in f and g.

From (7) and (11), and remembering $q_0+K=p_0$, we have

$$f=-2p\cdot k>0, \quad g=0 \quad \text{for } M_A.$$

Using these values in (9) and (10), we get from (3') and (5')

$$M_A=\frac{ie}{(2K)^{\frac{1}{2}}}\left(-\frac{p\cdot\epsilon}{p\cdot k}\right) \times[-iM_{el}+F(\bar{u}_q 2p_0\gamma_0 u_p)\Delta(-2p\cdot k)]. \quad (13)$$

In just the same way, we have also that

$$M_C=\frac{ie}{(2K)^{\frac{1}{2}}}\left(\frac{q\cdot\epsilon}{q\cdot k}\right) \times[-iM_{el}+F(\bar{u}_q 2p_0\gamma_0 u_p)\Delta(2q\cdot k)]. \quad (14)$$

[11] R. P. Feynman, Phys. Rev. **76**, 749 (1949).

Since the real parts of $\Delta(-2p\cdot k)$ and $\Delta(2q\cdot k)$ are $\pm\pi^2/2P\Delta P^2$, respectively, these terms do actually give the additional infrared divergence.

The evaluation of M_B can be performed as follows. Introducing an auxiliary variable x, we combine the two propagators of (4′) into

$$\int_0^1 dx[l^2-2l\cdot(p-xk)-2xp\cdot k]^{-2}.$$

If we change the integration variable by $\mathbf{p}-\mathbf{l}-x\mathbf{k}\to\mathbf{l}$, we get integrals of the form

$$\int_0^1 dx(\partial/\partial R^2)I_i \quad\text{and}\quad \int_0^1 dx(\partial/\partial R^2)I_{ij},$$

with

$$R^2=P^2-2xp_0K+x^2K^2,$$
$$\mathbf{p}'=\mathbf{p}-x\mathbf{k} \quad\text{and}\quad \mathbf{q}'=\mathbf{q}+(1-x)\mathbf{k},$$

which give from (11)

$$f=-2xp\cdot k \quad\text{and}\quad g=2(1-x)q\cdot k. \tag{15}$$

At $x=0$ and $x=1$, we have $f=0$ and $g=0$, respectively, and the discontinuity at these points gives an infinite integrand when differentiated by R^2. Therefore, only the discontinuity factors $\Delta(f)$ and $\Delta(g)$ in I_i and I_{ij} contribute terms of order $1/K$. Thus, the foregoing integrals reduce to the evaluation of

$$\int_0^1 dx(\partial/\partial R^2)\Delta(f) \quad\text{and}\quad \int_0^1 dx(\partial/\partial R^2)\Delta(g).$$

From (11), (15), and (A-8), we have

$$\begin{aligned}\int_0^1 dx(\partial/\partial R^2)\Delta(f) &= -\int_0^1 dx(\partial/\partial f)\Delta(f)\\ &= \int_0^1 dx(2p\cdot k)^{-1}(\partial/\partial x)\Delta(-2xp\cdot k)\\ &= (2p\cdot k)^{-1}\Delta(-2p\cdot k).\end{aligned} \tag{16}$$

In the same way, we get

$$\int_0^1 dx(\partial/\partial R^2)\Delta(g)=-(2q\cdot k)^{-1}\Delta(2q\cdot k). \tag{17}$$

Equations (16) and (17), together with (6), enable us to write (4′) as

$$\begin{aligned}M_B=&[ieF/(2K)^{\frac{1}{2}}](\bar u_q 2p_0\gamma_0 u_p)\\ &\times[(p\cdot\epsilon/p\cdot k)\Delta(-2p\cdot k)-(q\cdot\epsilon/q\cdot k)\Delta(2q\cdot k)].\end{aligned} \tag{18}$$

Adding (13), (14), and (18), we get

$$\begin{aligned}M_{\text{inel}}&=M_A+M_B+M_C\\ &=-[e/(2K)^{\frac{1}{2}}](p\cdot\epsilon/p\cdot k-q\cdot\epsilon/q\cdot k)M_{\text{el}},\end{aligned} \tag{19}$$

which is equivalent to what we would obtain if we were to take only M_A and M_C and neglect k in the potential integration from the beginning. The same procedure applied to the higher Born approximations is readily shown to give the same expression as above, so that Eq. (18) is the exact expression, so long as the cancellation of the additional infrared divergences always occur, as shown later. The inelastic cross section for the emission of a photon of energy smaller than certain energy ΔE such that $\Delta E\ll\Delta P$ is then

$$\begin{aligned}\sigma_{\text{inel}}=[e^2/(2\pi)^3]\sum_\epsilon \int_{K_{\min}}^{\Delta E} d\mathbf{k}(1/2K)\\ \times(p\cdot\epsilon/p\cdot k-q\cdot\epsilon/q\cdot k)^2\cdot\sigma_{\text{el}}.\end{aligned} \tag{20}$$

Performing the polarization sum and rearranging the terms, we have

$$\begin{aligned}\sigma_{\text{inel}}=(\alpha/2\pi^2)\int_{K_{\min}}^{\Delta E} d\mathbf{k}(1/K)\\ \times[p^2/(p\cdot k)^2-p\cdot q/(p\cdot k)(q\cdot k)]\sigma_{\text{el}}.\end{aligned} \tag{21}$$

We shall next show that the second term of M_A, Eq. (13), stems actually from the small momentum transfer at the point A. This means that in (3′), small $\mathbf{l}$ contributes to $\Delta(-2p\cdot k)$ term, or that in I_0, I_i and I_{ij} defined by (6) the small region around $\mathbf{l}=\mathbf{p}$ gives $\Delta(f)$. In order to see this, we take the difference M_A, (3′), and M_{el}, (5′), and show that this gives $\Delta(-2p\cdot k)$ when integrated over a small region of $\mathbf{l}$ around the origin.

For small $\mathbf{l}$, we may approximate the integrands of (3′) and (5′) as follows:

$$\begin{aligned}\int d\mathbf{l}\to\int d\mathbf{l}2p_0\gamma_0/\{[-2p\cdot(k+l)-i\epsilon]\\ \times(\mathbf{l}^2+\lambda^2)\Delta\mathbf{p}^2\}, \quad(\lambda,\epsilon\to 0),\end{aligned} \tag{22}$$

$$\begin{aligned}\int_{\text{el}} d\mathbf{l}\to\int d\mathbf{l}2p_0\gamma_0/[(-2p\cdot l-i\epsilon)\\ \times(\mathbf{l}^2+\lambda^2)\Delta\mathbf{p}^2], \quad(\lambda,\epsilon\to 0).\end{aligned} \tag{23}$$

Taking the difference and performing the angle integration first, we have

$$\begin{aligned}&\int_A d\mathbf{l}-\int_{\text{el}} d\mathbf{l}\\ &=2\gamma_0 p_0(\pi/P\Delta P^2)\\ &\quad\times\Big\{\int dL(1/L)\log(p\cdot k-PL)/(p\cdot k+PL)\\ &\quad+i\int dL[L/(L^2+\lambda^2)]\\ &\quad\times[\tan^{-1}(2p\cdot k+2PL)/\epsilon-\tan^{-1}2PL/\epsilon]\Big\}.\end{aligned}$$

But the difference of the two inverse tangents in the second term has the value $-\pi$ for $PL<-p\cdot k(>0)$, and vanishes for $PL>-p\cdot k$. Hence the second term gives, when integrated over $[0, -p\cdot k/P]$,

$$(i\pi^2/P\Delta P^2)\log[\lambda P/(-p\cdot k)],$$

which is just equal to the imaginary part of $\Delta(-2p\cdot k)$. The first integrand becomes infinite at $L=-p\cdot k/P$, and decreases as $1/L^2$ for large L. Therefore, the main contribution comes from $L=-p\cdot k/P$. Extending the integration limit to infinity, we get the real part of $\Delta(-2p\cdot k)$:

$$\pi^2/(2P\Delta P^2).$$

This result at the same time justifies the use of approximations (22) and (23). In the same way, we can show that the anomalous term of M_C comes from the small momentum transfer l' at B, and that those of M_B come from small $\mathbf{l}$ at A and small $\mathbf{l}'$ at B.

Once we know that the Coulomb anomalies come from the small momentum transfer just before or after the emission of the photon as in the foregoing, the cancellation can be shown quite generally as follows. For instance, suppose $\mathbf{l}$ is small. By the same approximation made in (22) and (23) the integrand of (3′) and (4′) become

$$M_A:\ 2p_0\gamma_0(2\epsilon\cdot p)/\{[-2p\cdot(k+l)](-2p\cdot k)\mathbf{l}^2\Delta\mathbf{p}^2\},$$
$$M_B:\ 2p_0\gamma_0(2\epsilon\cdot p)/\{[-2p\cdot(k+l)](-2p\cdot l)\mathbf{l}^2\Delta\mathbf{p}^2\}.$$

Combining these two, we have

$$2p_0\gamma_0(-\epsilon\cdot p/p\cdot k)[(-2p\cdot l)\mathbf{l}^2\Delta\mathbf{p}^2]^{-1},$$

which is simply equal to what is obtained by neglecting k in the internal electron line AB of M_A and assuming $\mathbf{l}$ is small.

For the third Born approximation we have four diagrams shown in Fig. 2. Call the momentum transfer at A, B, and C as $\mathbf{l}_1$, $\mathbf{l}_2$, and $\mathbf{l}_3$, respectively. The anomalous terms occur in the following way:

$\mathbf{l}_1$ is small: (A) and (B) have anomalous terms.
$\mathbf{l}_1$ and $\mathbf{l}_2$ is small: (A), (B), and (C) have anomalous terms.
$\mathbf{l}_2$ and $\mathbf{l}_3$ is small: (B), (C), and (D) have anomalous terms.
$\mathbf{l}_3$ is small: (C) and (D) have anomalous terms.

The first and the last cases are just the same as those of the second Born approximation discussed above. In the second case, after making the approximation analogous to (22) in the matrix elements, we combine (A) and (B). It is obvious that we get what is equivalent to neglect of k in the electron line AB of (A). Then, we combine the resulting term with (C). We then get a term which is equivalent to neglect of k in the two electron lines AB and BC of (A).

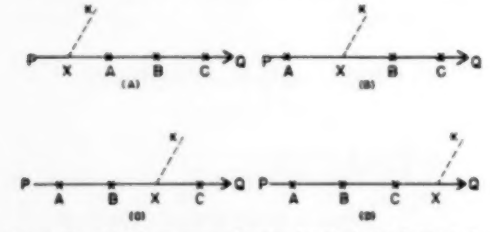

FIG. 2. The third Born approximation for the inelastic scattering.

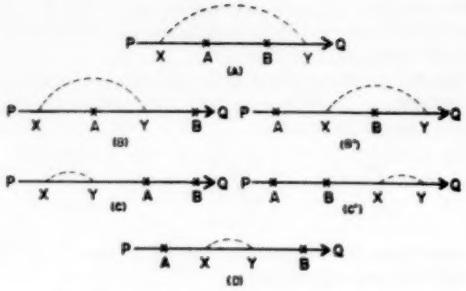

FIG. 3. Virtual photon processes for the second Born approximation.

A similar discussion can readily be made for many photon emissions as well. Thus, we conclude that the cancellation of the additional infrared divergences holds to any order of the Born approximation and also to any number of photons emitted.

Next we shall examine the virtual photon processes. Here we have such processes as are given in Fig. 3. We omit from our consideration the diagrams containing δm and also the vacuum polarization diagrams, because they contain neither an infrared divergence nor $(\log m)^2$. The matrix elements are, for instance,

$$M_{(A)}=-[e^2F/(2\pi)^4]\int d^4k/k^2\int d\mathbf{l}(\mathbf{l}^2\mathbf{l}'^2)^{-1}$$
$$\times\bar{u}_q\gamma_\mu[i\gamma(q-k)+m]^{-1}\gamma_0[i\gamma(p-k-l)+m]^{-1}$$
$$\times\gamma_0[i\gamma(p-k)+m]^{-1}\gamma_\mu u_p; \quad (24)$$

$$M_{(B)}=-[e^2F/(2\pi)^4]\int d^4k/k^2\int d\mathbf{l}(\mathbf{l}^2\mathbf{l}'^2)^{-1}$$
$$\times\bar{u}_q\gamma_0[i\gamma(p-l)+m]^{-1}\gamma_\mu[i\gamma(p-k-l)+m]^{-1}$$
$$\times\gamma_0[i\gamma(p-k)+m]^{-1}\gamma_\mu u_p, \quad (25)$$

$$M_{(D)}=-[e^2F/(2\pi)^4]\int d^4k/k^2\int d\mathbf{l}(\mathbf{l}^2\mathbf{l}'^2)^{-1}$$
$$\times\bar{u}_q\gamma_0[i\gamma(p-l)+m]^{-1}\gamma_\mu$$
$$\times[i\gamma(p-k-l)+m]^{-1}\gamma_\mu[i\gamma(p-l)+m]^{-1}\gamma_0 u_p, \quad (26)$$

with

$$q-p+l+l'=0.$$

We are interested at the moment only in the contribution of the soft photon, so that we integrate over the momentum space defined by

$$K_{\min}<K<\bar{K}(\ll\Delta P). \quad (27)$$

We shall examine these integrals without doing the separation of the ultraviolet divergent term, although they are infrared divergent at the same time.[12] This is justified because the ultraviolet divergent terms of the vertex and self-energy part in diagrams (B), (B'), (C), (C') and (D) are known to cancel with each other from the renormalization theory as a result of $Z_1=Z_2$.[13,14] Then, diagrams (B), (B') and (D), without separation of the ultraviolet divergence, contain no infrared divergence besides those coming from Coulomb anomalies. The exceptional case is diagrams (C) and (C'), where the finite part of the self-energy part drops as a result of the Dirac spinor operating from the left or right, leaving an ultraviolet as well as an infrared divergent term. The treatment of these diagrams is well known.[15] (C) and (C') give

$$M_{(C)}+M_{(C')}=iIM_{el}, \tag{28}$$

where

$$I=-[e^2/(2\pi)^4]\int d^4k(1/k^2)\{\bar{u}_p\gamma_\mu[i\gamma(p-k)+m]^{-1}\times\gamma_\lambda[i\gamma(p-k)+m]^{-1}\gamma_\mu u_p\}/(\bar{u}_p\gamma_\lambda u_p).$$

Performing the k_0 integration and taking only the infrared divergent term we get

$$M_{(C)}+M_{(C')}=-[\alpha/(4\pi^2)]\cdot\int_{K_{\min}}^{\bar{K}}d\mathbf{k}(1/K)\times[p^2/(p\cdot k)^2]M_{el}. \quad (k^2=0) \tag{29}$$

This expression holds of course to any order of Born approximation for such diagrams as (C) and (C'), which have a self-energy part on the extreme right or left.

The potential integrations in $M_{(A)}$, $M_{(B)}$, $M_{(B')}$ and $M_{(D)}$ can be reduced to (6) and the result again contains two discontinuity terms $\Delta(k^2-2k\cdot p)$ and $\Delta(k^2-2k\cdot q)$, which can, however, be shown to cancel out exactly when we add the four matrix elements. Here we shall show this cancellation by the general argument presented before. Assuming k and $\mathbf{l}$ are small, the integrands of (24), (25), and (26) reduce to

$$M_{(A)}:\ -4(p\cdot q)\cdot 2\gamma_0 p_0/\{(-2k\cdot q)(-2k\cdot p)\times[-2p\cdot(k+l)]\mathbf{l}^2\Delta\mathbf{p}^2\}, \tag{30}$$

$$M_{(B)}:\ 4m^2\cdot 2\gamma_0 p_0/\{(-2p\cdot l)(-2k\cdot p)\times[-2p\cdot(k+l)]\mathbf{l}^2\Delta\mathbf{p}^2\}, \tag{31}$$

$$M_{(B')}:\ -4(p\cdot q)2\gamma_0 p_0/\{(-2k\cdot q)(-2p\cdot l)\times[-2p\cdot(k+l)]\mathbf{l}^2\Delta\mathbf{p}^2\}, \tag{32}$$

$$M_{(D)}:\ 4m^2\cdot 2\gamma_0 p_0/\{(-2l\cdot p)^2[-2p\cdot(k+l)]\mathbf{l}^2\Delta\mathbf{p}^2\}. \tag{33}$$

Adding $M_{(B)}$ and $M_{(D)}$, we get

$$4m^2 2\gamma_0 p_0/[(-2l\cdot p)^2(-2p\cdot k)\mathbf{l}^2\Delta\mathbf{p}^2],$$

which is no longer infrared divergent. Adding $M_{(A)}$ and $M_{(B')}$, we have

$$-4(p\cdot q)2\gamma_0 p_0/[(-2k\cdot p)(-2k\cdot q)(-2p\cdot l)\mathbf{l}^2\Delta\mathbf{p}^2],$$

which is equal to what we obtain by putting $k=0$ in the internal propagator of $M_{(A)}$. Thus, we are allowed to take only $M_{(A)}$ and to put $k=0$ always in the internal propagator AB in the consideration of infrared divergence. Therefore, we have

$$M_{(A)}+M_{(B)}+M_{(B')}+M_{(D)}=-ie^2/(2\pi)^4\int d^4k(4p\cdot q)/[k^2\cdot(k^2-2k\cdot p)(k^2-2k\cdot q)]M_{el}. \tag{34}$$

Performing the k_0 integration, we get as the infrared divergent term

$$M_{(A)}+M_{(B)}+M_{(B')}+M_{(D)}=(\alpha/4\pi^2)(p\cdot q)\int_{K_{\min}}^{\bar{K}}d\mathbf{k}(1/K)\times[1/(k\cdot p)(k\cdot q)]M_{el}. \tag{35}$$

From the interference with the pure potential scattering matrix element M_{el}, (35) plus (29) give the following contribution of order α to the cross section,

$$\sigma_{virt}=-(\alpha/2\pi^2)\int_{K_{\min}}^{\bar{K}}d\mathbf{k}(1/K)\times[p^2/(p\cdot k)^2-p\cdot q/(q\cdot k)(p\cdot k)]\sigma_{el}. \tag{36}$$

Adding the inelastic cross section (21), the lower limit $K_{\min}$ cancels out and is replaced by the physically meaningful quantity ΔE. The $\mathbf{k}$ integration can be done easily and gives as a leading term

$$\sigma_{rad}=\sigma_{inel}+\sigma_{virt}\sim-(4\alpha/\pi)\log(\Delta P/m)\log(\bar{K}/\Delta E)\cdot\sigma_{el}. \tag{37}$$

The coefficient of $\log\Delta E$ coincides with that of Eq. (2), which is the required result.

III. EXAMINATION OF $(\log m)^2$

To understand the origin of $\log m$, which does not appear in the pure potential scattering, we shall examine the typical integral

$$\int d^4k[k^2(k^2-2k\cdot p)(k^2-2k\cdot q)]^{-1}, \tag{38}$$

which appeared in Eq. (34), and is also the most important integral in the first Born approximation. Since this is infrared divergent, we have either to restrict the photon momentum space by

$$K\geqq K_{\min} \tag{39}$$

[12] R. Karplus and N. Kroll, Phys. Rev. **77**, 536 (1950).
[13] F. J. Dyson, Phys. Rev. **75**, 1736 (1949).
[14] J. C. Ward, Phys. Rev. **78**, 182 (1950).
[15] See, for instance, F. J. Dyson, "Advanced Quantum Mechanics," Lecture notes at Cornell University, 1951 (unpublished).

as before, or to assume a small photon mass μ, and replace the photon propagator by $1/(k^2+\mu^2)$. Although the former method is noncovariant, it gives the correct answer, as explained later. For our purpose of examining the $\log m$ term, it is convenient to employ it. We perform the k_0 integration first by contour integral. The pole of the photon propagator $1/k^2$ contributes a term

$$(\pi i/4)\int d\mathbf{k}(1/K^3)[1/(p_0-\mathbf{n}\cdot\mathbf{p})][1/(p_0-\mathbf{n}\cdot\mathbf{q})], \quad (40)$$

where $\mathbf{k}=\mathbf{n}K$. The angular integration can be readily done and gives

$$(16\pi/\Delta P^2)\log(\Delta P/m). \quad (p_0\gg m)$$

It is apparent from the form of the integrand that $\log m$ is contributed from $\mathbf{n}\parallel\mathbf{p}$ or $\mathbf{n}\parallel\mathbf{q}$, where one of the denominators becomes

$$p_0-P\approx m^2/2p_0,$$

while the other becomes

$$p_0-\mathbf{p}\cdot\mathbf{q}/P\approx\Delta P^2/2P.$$

The pole of the factor $1/(k^2-2k\cdot p)$ of (38) gives the following contribution after a little manipulation:

$$\frac{\pi i}{4}\int d\mathbf{k}\frac{1}{\mathbf{k}\cdot\Delta\mathbf{p}}\cdot\frac{1}{[(\mathbf{k}-\mathbf{p})^2+m^2]^{\frac{1}{2}}} \cdot\frac{\{\mathbf{k}\cdot\mathbf{p}-p_0^2+p_0[(\mathbf{k}-\mathbf{p})^2+m^2]^{\frac{1}{2}}\}}{K^2[p_0^2-(\mathbf{n}\cdot\mathbf{p})^2]}. \quad (41)$$

Again, this has a denominator $(\mathbf{n}\cdot\mathbf{p})^2-p_0^2$, which becomes small when $\mathbf{k}\parallel\mathbf{p}$ or $\mathbf{k}\parallel-\mathbf{p}$, and gives $\log m$ by angular integration. When especially $\mathbf{k}\approx\mathbf{p}$, the second denominator becomes $\sim m$, but at the same time the numerator of the last factor becomes $-m^2+mp_0$, so that no $(\log m)^2$ can be expected from this additional singularity. (We shall call such factors as $1/[(\mathbf{k}-\mathbf{p})^2+m^2]^{\frac{1}{2}}$ or $1/[K^2p_0^2-(\mathbf{k}\cdot\mathbf{p})^2]$, m-singular, because they become singular when $m\to0$.) The first denominator never vanishes as long as $\mathbf{k}\parallel\mathbf{p}$ except when $\mathbf{k}\approx0$, where the numerator also becomes $\sim2k\cdot p$. The same analysis holds for the third factor $1/(k^2-2k\cdot q)$. Thus, we can expect no $(\log m)^2$ term from the integrals of the type (38). The actual evaluation of the integral (38) can be done more easily by combining the three denominators by the usual perscription, integrating first over k_0 and then integration over k subject to (39). The result is

$$\sim(4i\pi^2/\Delta P^2)\log(\Delta P/m)\log(p_0/K_{\min}). \quad (42)$$

Thus we actually get no term $(\log m)^2$. It will be noticed also that we get exactly the term in Eq. (2) if we substitute the value (42) into Eq. (34).

On the other hand, if we assume the small photon mass μ, the integral (38) becomes

$$\sim(2i\pi^2/\Delta P^2)\log(\Delta P/m) \times[2\log(\Delta P/\mu)-\log(\Delta P/m)], \quad (43)$$

which now contains a $(\log m)^2$ term. But this $(\log m)^2$ is cancelled in the calculation of the first Born approximation by another $(\log m)^2$ in the bremsstrahlung integral which is now, for instance [the second term of (21)],

$$\int_0^{\Delta E}d\mathbf{k}[1/(K^2+\mu^2)][1/(k\cdot p)(k\cdot q)] \sim(8\pi/\Delta P^2)\log(\Delta P/m)[2\log(\Delta E\Delta P/\mu p_0) -\log\Delta P/m], \quad (k^2+\mu^2=0), \quad (44)$$

instead of the noncovariant integral

$$\int_{K_{\min}}^{\Delta E}d\mathbf{k}(1/K)[1/(k\cdot p)(k\cdot q)]\sim(16\pi/\Delta P^2) \times\log(\Delta P/m)\log(\Delta E/K_{\min}), \quad (k^2=0) \quad (45)$$

employed in the evaluation of (37). That the $(\log m)^2$ terms in (43) and (44) come from the contribution of small k will be evident by remarking that the integral

$$\int d^4k\cdot k_\lambda/[k^2\cdot(k^2-2k\cdot p)(k^2-2k\cdot q)]$$

no longer gives $(\log m)^2$ and leads to a unique value by any integration method. Since we have established in Sec. II the exact cancellation of the contribution from the soft photon $K<\Delta E\ll\Delta P$, we conclude that the difference of the two methods, that is solely associated with the soft photon, should cancel in the final answer completely. [Note that (21) and (36) have the same integrand. If we assume a small photon mass μ, we have only to replace the factor $1/K$ by $1/(K^2+\mu^2)^{\frac{1}{2}}$, and $k_0=K$ by $k_0=(K^2+\mu^2)^{\frac{1}{2}}$, and set $K_{\min}=0$, in *both* integrands. This leads to no change in the above conclusion.] In fact, in the case of the first Born approximation, we can show that the two methods give exactly the same answer including the terms of order unity.

It remains to examine the effect of the long Coulomb tail. Let us take as a typical integral $M_{(A)}$, Eq. (24). The integrand is

$$N\{k^2(k^2-2k\cdot p)(k^2-2k\cdot q) \times[(k-p+l)^2+m^2]^{\frac{1}{2}}(\mathbf{l}-\Delta\mathbf{p})^2\}^{-1}, \quad (46)$$

where the numerator N is given by

$$N=\bar u_q\gamma_\mu[-i\gamma(q-k)+m]\gamma_0[-i\gamma(p-k+l)+m]\gamma_0 \times[-i\gamma(p-k)+m]\gamma_\mu u_p. \quad (47)$$

In order to get $(\log m)^2$ in (46), it is clear from the foregoing analysis that the $\mathbf{l}$-integral,

$$\int d\mathbf{l}\{1/[l^2-2l\cdot(p-k)+k^2-2k\cdot p]\} \times(1/\mathbf{l}^2)[1/(\mathbf{l}-\Delta\mathbf{p})^2], \quad (48)$$

must be singular or m-singular at some point near $\mathbf{k}\parallel\mathbf{p}$ or $\mathbf{k}\parallel\mathbf{q}$. In the first denominator of (48) we can expect that the singularity will occur at that point which

satisfies the following two conditions:

$$\mathbf{k}-\mathbf{p}\approx 0, \quad k^2-2k\cdot p\approx 0, \tag{49}$$

because there the first factor of (48) is of order $1/\mathbf{l}^2$, which gives a very high singularity at $\mathbf{l}\approx 0$, together with the potential factor $1/\mathbf{l}^2$ in (48). The condition (49) is equivalent to $k-p\approx 0$. (The symbol $\approx$ allows an error of order $\sim m$.) In the same way we know that when $\mathbf{k}-\mathbf{q}\approx 0$ and $k^2-2k\cdot q\approx 0$, the first factor of (48) becomes of the order $1/(\mathbf{l}-\Delta\mathbf{p})^2$, which again overlaps with the second potential factor of (48). Thus the higher m-singularity, if any, will occur at either

$$k\approx p, \quad \mathbf{l}\approx 0$$

or

$$k\approx q, \quad \mathbf{l}\approx \Delta p, \tag{50}$$

where the singularity of the $\mathbf{l}$-integral overlaps with those of the second or third denominators of (46). The conclusion is readily confirmed by looking at the exact value of the $\mathbf{l}$-integral given by (A-1). For instance, assuming $f, g>0$, (A-1) gives for the real part of the integrals the value

$$\pi^3/[\Delta P(R^2\Delta P^2+f\cdot g)^{\frac{1}{2}}],$$

which is singular at $R^2\approx 0$ and $f\approx 0$ (or $g\approx 0$). Remembering that $R^2=(k_0-p_0)^2-m^2$, $f=k^2-2k\cdot p$ and $g=k^2-2k\cdot q$ for (48), the singular point is equivalent to $k\approx p$ (or $k\approx q$). On the other hand if the integral (48) has one l_i in the numerator, the integral is no longer singular at $k\approx p$, as is readily seen from (A-1) and (A-9). This implies that the singularity at $k\approx p$ occurs because $\mathbf{l}\approx 0$.

However, at the points (50), the numerator (47) is of order $\sim m^3$, which is enough to cancel the m-singularity of the l-integration. Therefore, we get no $(\log m)^2$ from diagram A of Fig. 3.

The integrand of M_B, Eq. (25), is

$$N\{k^2(k^2-2k\cdot p)[(k-p+l)^2+m^2] \times(l^2-2l\cdot p)\mathbf{l}^2(\mathbf{l}-\Delta\mathbf{p})^2\}^{-1}, \tag{51}$$

with

$$N=\bar{u}_q\gamma_0[-i\gamma(p-l)+m]\gamma_\mu[i\gamma(p-k-l)+m]\gamma_0 \times[-i\gamma(p-k)+m]\gamma_\mu u_p. \tag{52}$$

Comparing (51) with (38), it is apparent that (51) cannot give a higher m-singularity than (38), except when $\mathbf{l}\approx 0$. From $\mathbf{l}\approx 0$, the $\mathbf{l}$-integration gives rise to a singular term

$$-(\pi^3/2P\Delta P^2)[1/(k^2-2k\cdot p)].$$

(Incidentally, this was the origin of the additional infrared divergence appearing in $M_{(B)}$.) Inserting this into (51) we get the double pole $(k^2-2k\cdot p)^2=0$, which gives a term of the order $1/m^2$ after k-integration. However, the direct calculation shows that this $1/m^2$ is cancelled by the numerator N, as we should expect. [The matrix element should be expressed as a power series of m/p_0 plus some function of $\log(m/p_0)$.] The $\mathbf{l}$-integration of (51) gives another less singular term of the same order as (48), which is singular only at $k\approx p$. (This comes from an integral that has one power of $\mathbf{l}$ in the numerator.) However, again at $k\approx p$ the numerator (52) becomes of the order $\sim m$, which cancels the singularity.

The same kind of argument applies also for $M_{(B')}$, $M_{(C)}$, $M_{(C')}$, and $M_{(D)}$ and in any case we can exclude the possibility of the appearance of $(\log m)^2$. A more rigorous analysis has been done by integrating first by k_0, then performing the $\mathbf{l}$-integration and finally integrating over $\mathbf{k}$ in the small region around $\mathbf{k}=\mathbf{p}$. The result conforms with the foregoing discussion.

ACKNOWLEDGMENTS

In conclusion, the author wishes to express his sincere thanks to Professor L. I. Schiff for his stimulating discussions throughout the course of this work. The author is indebted to Professor R. P. Feynman for his helpful discussion in a part of Sec. II. Thanks are also due to Dr. D. R. Yennie and Dr. D. G. Ravenhall for their valuable discussions and criticisms.

APPENDIX

The potential integrations were made following the method of Dalitz[6] and Lewis[16] employed for the calculation of the second Born elastic scattering matrix elements. The calculation was made for the Yukawa potential $e^{-\lambda r}/r$, in order to express the results for off-and-on-energy shell matrix elements compactly, and also to exhibit the discontinuity on the energy shell clearly. The necessary integrals for the evaluation of (6) are the following:

$$\begin{aligned} I_0(\mathbf{p}',\mathbf{q}',R^2) &= \int d\mathbf{l}\cdot 1/\{(l^2-R^2-i\epsilon)[(\mathbf{l}-\mathbf{p}')^2+\lambda^2] \times[(\mathbf{l}-\mathbf{q}')^2+\lambda^2]\}, \quad (\epsilon\to 0) \\ &= (i\pi^2/\sqrt{A})\log[(B-iC-iD)/(B-iC+iD)] \\ &= (\pi^2/\sqrt{A})[\tan^{-1}(D+C)/B+\tan^{-1}(D-C)/B] \\ &\quad +(i\pi^2/\sqrt{A})\log\{[B^2+(C+D)^2]/ [B^2+(C-D)^2]\}^{\frac{1}{2}}, \end{aligned} \tag{A-1}$$

where

$$\begin{aligned} A&=R^2\Delta P'^2(\Delta P'^2+4\lambda^2)-\lambda^2(f-g)^2 \\ &\quad +\Delta P'^2(\lambda^2+f)(\lambda^2+g), \\ B&=\lambda(2\lambda^2+f+g)\Delta P'^2; \quad C=R\Delta P'^2(\Delta P'^2+4\lambda^2), \\ D&=\Delta P'^2\sqrt{A}, \end{aligned} \tag{A-2}$$

[16] R. R. Lewis, Jr., thesis, University of Michigan, 1954 (unpublished).

with

$$\Delta P'=|\mathbf{p}'-\mathbf{q}'|, \quad f=P'^2-R^2, \quad \text{and} \quad g=Q'^2-R^2.$$

$$J(\mathbf{p}',R^2)=\int d\mathbf{l}\cdot 1/\{(l^2-R^2-i\epsilon)[(\mathbf{l}-\mathbf{p}')^2+\lambda^2]\}$$
$$=(i\pi^2/P')\log[(\lambda-iR+iP')/(\lambda-iR+iP')]$$
$$=(\pi^2/P')[\tan^{-1}(R+P')/\lambda+\tan^{-1}(P'-R)/\lambda]$$
$$+(\pi^2 i/P')\log\{[\lambda^2+(R+P')^2]/[\lambda^2+(R-P')^2]\}^{\frac{1}{2}}. \quad \text{(A-3)}$$

$$K(\mathbf{p}',\mathbf{q}')=\int d\mathbf{l}\cdot 1/\{[(\mathbf{l}-\mathbf{p}')^2+\lambda^2][(\mathbf{l}-\mathbf{q}')^2+\lambda^2]\}$$
$$=(\pi^2 i/\Delta P')\log[(2\lambda-i\Delta P')/(2\lambda+i\Delta P')]$$
$$=(2\pi^2/\Delta P'^2)\tan^{-1}\Delta P'/\lambda. \quad \text{(A-4)}$$

In all these expressions the argument of the numerator and the denominator of the logarithmic functions must be taken as $[-\pi/2, \pi/2]$.

The value of the integrals depends critically on the relative magnitude of f, g, and λ^2, in the limit $f, g, \lambda^2 \to 0$. Keeping these quantities finite, whenever the relative magnitudes are relevant, the soft photon limit, as well as the unscreened limit, is obtained by replacing P', Q', R^2, and $\Delta P'$ by P, Q, $P^2=Q^2$ and ΔP, respectively, and taking $\lambda \to 0$. The results are

$$I_0(\mathbf{p}',\mathbf{q}',R^2)\approx\frac{\pi^2}{P\Delta P^2}\left[\left(\tan^{-1}\frac{f}{2\lambda P}+\tan^{-1}\frac{g}{2\lambda P}\right)+i\log\frac{4P^2\Delta P^2}{[(f^2+4\lambda^2P^2)(g^2+4\lambda^2P^2)]^{\frac{1}{2}}}\right], \quad \text{(A-5)}$$

$$J(\mathbf{p}',R^2)\approx\frac{\pi^2}{P}\left[\frac{\pi}{2}+i\tan^{-1}\frac{f}{2\lambda P}+i\log\frac{4P^2}{f^2+4\lambda^2P^2}\right],$$

$$K(\mathbf{p}',\mathbf{q}')\approx\pi^2/\Delta P.$$

Separating the terms which remain when $f=g=0$ (on-energy-shell value) and denoting them as I_0^{el}, J^{el} and K^{el}, we get

$$\begin{aligned} I_0(\mathbf{p}',\mathbf{q}',R^2)&\approx I_0^{el}+\Delta(f)+\Delta(g),\\ J(\mathbf{p}',R^2)&\approx J^{el}+\Delta P^2\Delta(f),\\ J(\mathbf{q}',R^2)&\approx J^{el}+\Delta P^2\Delta(g),\\ K(\mathbf{p}',\mathbf{q}')&\approx K^{el}, \end{aligned} \quad \text{(A-6)}$$

where

$$\Delta(f)=\lim_{\lambda\to 0}\frac{\pi^2}{P\Delta P^2}\left(\tan^{-1}\frac{f}{2\lambda P}+i\log\frac{2\lambda P}{(f^2+4\lambda^2P^2)^{\frac{1}{2}}}\right). \quad \text{(A-7)}$$

From this definition, we have, of course,

$$\Delta(0)=0. \quad \text{(A-8)}$$

I_i defined in (6), Sec. II, can be reduced to the linear combination of I_0, J and K, as follows:

$$I_i=\{p_i'/[P'^2Q'^2-(\mathbf{p}'\cdot\mathbf{q}')^2]\}\cdot\{(\mathbf{p}'\cdot\mathbf{q}')J(\mathbf{p}',R^2)-Q'^2J(\mathbf{q}',R^2)+(Q'^2-\mathbf{p}'\cdot\mathbf{q}')K+[R^2(Q'^2-\mathbf{p}'\cdot\mathbf{q}')+p'^2(P'^2-\mathbf{p}'\cdot\mathbf{q}')]I_0\}+(\mathbf{p}'\rightleftarrows\mathbf{q}'). \quad \text{(A-9)}$$

From (A-6) we have, in the soft photon limit,

$$I_i\approx I_i^{el}+p_i\Delta(f)+q_i\Delta(g). \quad \text{(A-10)}$$

In the same way, we get

$$I_{ij}\approx I_{ij}^{el}+p_ip_j\Delta(f)+q_iq_j\Delta(g). \quad \text{(A-11)}$$

Letters to the Editor

PUBLICATION of brief reports of important discoveries in physics may be secured by addressing them to this department. The closing date for this department is five weeks prior to the date of issue. No proof will be sent to the authors. The Board of Editors does not hold itself responsible for the opinions expressed by the correspondents. Communications should not exceed 600 words in length and should be submitted in duplicate.

Elastic Scattering of 5.25-Mev Protons on Nickel and Copper*

D. A. BROMLEY AND N. S. WALL

Department of Physics, University of Rochester, Rochester, New York

(Received June 13, 1955)

THE recent successes of the complex-potential model in fitting the elastic scattering data for low-energy neutrons[1] and higher-energy protons[2] have prompted the study of the elastic scattering of low-energy protons (5.25 Mev). Prior results on copper in this energy range have shown the scattering to be relatively independent of the energy of the incident proton.[3,4]

We have extended these investigations by examining the elastic scattering of 5.25-Mev protons both from copper ($Z=29$) and the adjacent element, nickel ($Z=28$). Our experimental arrangement was such that we were able to take our high-pressure ion chamber detector to sufficiently forward angles to observe a region in which the scattering was purely Coulomb. The results obtained are shown in Figs. 1 and 2. The estimated total error in the absolute value of any point is about 10%, whereas the relative error, as determined from the reproducibility of the angular distribution at different times, is about 5%.

The outstanding, and probably most significant, feature of these results is the marked difference in the general shape of the curves obtained for these adjacent elements. The abundant isotopes of Ni and Cu are Ni^{58} (67.4%), Ni^{60} (26.7%) and Cu^{63} (68%), Cu^{65} (32%). The binding energies of the last proton in the compound nuclei corresponding to the Ni^{58} and Cu^{63} target nuclei are 9.01 and 7.92 Mev respectively.[5] If, as might be expected on the basis of the complex-potential model, the characteristics of the angular distribution depend only on the particular region reached in the compound nucleus, it might be expected that our nickel results should be somewhat similar to the 6.0-Mev data of the Zurich group.[3] The fact that our observations are contrary to this expectation indicates that some other mechanism must be responsible for the difference.

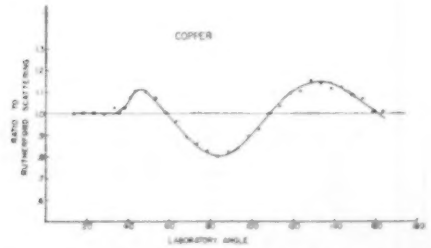

FIG. 1. The differential cross section for the elastic scattering of 5.25-Mev protons on copper plotted as a ratio to the Rutherford differential cross section. The errors are as indicated in the text, and include those due to angular-setting uncertainty. The flat section of the curve at forward angles was normalized to a ratio of 1.

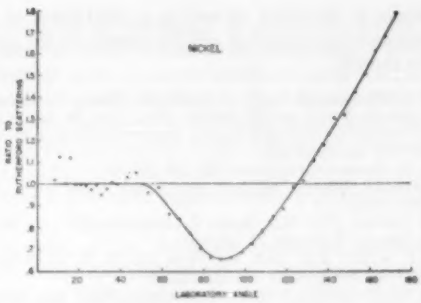

FIG. 2. The differential cross section for the elastic scattering of 5.25-Mev protons on nickel plotted as a ratio of the Rutherford differential cross section. The errors are as indicated in the test, and include those due to angular setting uncertainty. The flat section of the curve at forward angles was normalized to a ratio of 1.

Since both abundant nickel isotopes are even-even they presumably have spin 0 whereas the stable copper isotopes are known to have spin 3/2.[6] The different observed distributions may well reflect this spin difference. It is of course conceivable that since we have bombarded natural targets rather than separated isotopes, we are observing the superposition of two different distributions in each case. This would require, however, that isotopes differing by two neutrons and having the same spin and parity should yield quite different angular distributions.

With the elastically scattered protons we have also observed inelastically scattered groups corresponding to the lowest excited states in the target isotopes which were observed by the Rice Institute group.[7] In agreement with their results we have found that none of the inelastic groups have more than about 12% of the intensity of the elastic group at any angle.[8] We could not resolve groups corresponding to levels of less than about 500-kev excitation, if such exist. Coulomb excitation measurements have failed to show any levels in either nickel or copper below this energy.[9]

The energy dependence of the elastic scattering from these and from neighboring elements, in particular zinc, is being examined in an attempt to understand the phenomenon responsible for the differences in the nickel and copper distributions.

Details of this work as well as a description of our experimental arrangement will be submitted for publication shortly.

* Supported in part by the U. S. Atomic Energy Commission.
[1] Feshbach, Porter, and Weisskopf, Phys. Rev. **96**, 443 (1954).
[2] D. Saxon, Proceedings of the Brookhaven Conference, January 24-26, 1955 (unpublished).
[3] L. M. Goldman, Phys. Rev. **89**, 349 (1953).
[4] Schneider, Martin, Sempert, and Salad, Helv. Phys. Acta **27**, 170 (1954).
[5] N. Feather, Phil. Mag. Suppl. **2**, 141 (1953).
[6] R. Ritschl, Z. Physik **79**, 1 (1932).
[7] J. P. Schiffer *et al.*, Bull. Am. Phys. Soc. **30**, No. 3, 55 (1955).
[8] John Schiffer (private communication).
[9] G. M. Temmer and N. P. Heydenburg, Phys. Rev. **93**, 351 (1954).

Production and Identification of Long-Lived Technetium Isotopes at Masses 97, 98, and 99

G. E. Boyd, J. R. Sites, Q. V. Larson, and C. R. Baldock
Oak Ridge National Laboratory, Oak Ridge, Tennessee
(Received May 23, 1955)

THE properties of the "missing" beta-unstable technetium isotope at mass 98 have recently become of considerable interest; it now appears[1] that the technetium isotopes at masses 97 and 99 are also unstable and decay with half-lives of less than 10^6 years. If, therefore, primordial technetium is detected on the crust of the earth, presumably this will occur because the half-life of Tc^{98} exceeds 10^8 years.

Arguments based on shell theory have suggested[2,3] that the spin of Tc^{98g} may be very high, so that its beta decay can be highly forbidden and occur with an extremely long half-life. On the other hand, because the odd proton in Tc^{98} may be either $g_{9/2}^+$ or $p_{1/2}^-$ and the odd neutron either $d_{5/2}^+$ or $g_{7/2}^+$, application of Nordheim's rules[4] leads to the prediction of either a low-spin (1^+ or 2^-) or a high-spin (4^- or 6^+, 7^+) ground state. Since approximately 1.8 Mev are available for beta disintegration, in the former instance the decay of Tc^{98} should be "allowed" with a half-life of 10 ± 5 minutes. However, exhaustive searches by the senior author for a short-lived Tc^{98} produced by 14-Mev deuteron irradiation[5] of electromagnetically enriched Mo^{98} (95.0%) and separated by rapid chemistry have failed to reveal any hitherto-unassigned technetium activity in this half-life range. Additional attempts to detect a very short-lived Tc^{98} formed by the irradiation of 100 mg quantities of carefully purified fission-product TcO_2 with 80-Mev x-rays[6] were also unsuccessful. It was concluded that it was unlikely that Tc^{98g} possessed a low spin and was short-lived. Alternatively, measurements of the decay of the radiations from numerous other technetium sources for periods as long as seven years indicated that the half-life of Tc^{98} was either extremely long or that, fortuitously, it decayed with a period and radiations nearly identical with one of the previously known technetium activities and hence had been overlooked.

To resolve this possible ambiguity a large piece of molybdenum metal was bombarded with 22-Mev protons from the ORNL 86-inch cyclotron for a time sufficient to produce about 10 μg of Tc^{98}.[7] After 270 days to allow for the complete decay of the shorter-lived technetium isotopes and to reduce the amount of 60-day Tc^{99m} formed, the complete target was processed chemically, and the technetium fraction was separated and purified by anion exchange chromatography. An aliquot was electroplated on an iridium strip which subsequently was heated at 400°C in a stream of hydrogen gas to produce an adherent layer of technetium metal. Approximately one microgram of technetium was present on the iridium strip employed as a filament source in a 60° mass spectrometer of eight-inch radius. Technetium ions produced both by electron bombardment and by thermal ionization appeared at a temperature consistent with that observed in previous analyses on fission product Tc^{99g}. The prominent ions were those at masses 97, 98, and 99 (Fig. 1) with the indicated relative abundances taken from several other measurements. These masses were positively identified by employing ions formed by electron bombardment together with a section of the mass-time dispersion curve. Known ion peaks used were Ir^{++} at 95.5 and 96.5; Pt^{++} at 97, 97.5, and 98; and Rh^+ at 103. A check dispersion curve section was made with thermally produced ions using Sr^+ at 86, 87, and 88 and Rh^+ at 103.

These results appear to be of interest for a number of reasons which may include the following: (a) Weighable quantities of three long-lived technetium isotopes were produced, and technetium 95, 97, and 98 isotopes have been seen on a mass spectrometer for the first

FIG. 1. Mass spectrogram of technetium produced by the irradiation of molybdenum metal with 22-Mev protons.

time. (b) The "missing" isotope, Tc^{98}, has been observed and hence must be long-lived. (c) The occurrence of a long-lived isomer of Tc^{100} seems to be excluded. (d) The relative abundance of the 60-day Tc^{95m} found suggests that as little as 5×10^{-9} g of technetium can be estimated by mass spectrometry.

[1] G. E. Boyd, Phys. Rev. **95**, 113 (1954).
[2] G. E. Boyd, Record Chem. Progr. (Kresge-Hooker Sci. Lib.) **12**, 67 (1951).
[3] E. Segrè, Nuovo cimento **9**, 1008 (1952).
[4] L. W. Nordheim, Revs. Modern Phys. **23**, 322 (1951).
[5] These bombardments were conducted on the 60-inch cyclotron at the Department of Terrestrial Magnetism, Carnegie Institution of Washington. The hospitality and interest of Dr. M. A. Tuve, Dr. P. H. Abelson, and Dr. Dean Cowie are gratefully acknowledged.
[6] Thanks and appreciation are expressed to Dr. S. K. Allison and Dr. B. C. Cook for making the University of Chicago betatron available for these irradiations. These experiments were assisted by J. W. Cobble.
[7] Assistance with the special target problem and with the high-current bombardment was generously afforded by J. A. Martin and F. Green of the Oak Ridge National Laboratory.

Fine Structure in the Photoproton Spectrum of Oxygen

SVEN A. E. JOHANSSON AND BENGT FORKMAN
Department of Physics, University of Lund, Lund, Sweden
(Received May 27, 1955)

IT has been known for some time that the excitation curves for (γ,n) reactions show pronounced breaks.[1,2] These breaks have been explained as due to sharp resonances in the cross-section curves. If this is true, one should expect the energy spectra of the emitted particles to be composed of peaks. In general, the number of peaks would be so great that it would be extremely difficult to resolve them. Under certain conditions, however, the peaks may appear. When the maximum bremsstrahlung energy is set fairly close to the threshold, only a limited number of levels are excited. Furthermore, if the level density of the residual nucleus is low, only transitions to the ground state will be of any importance.

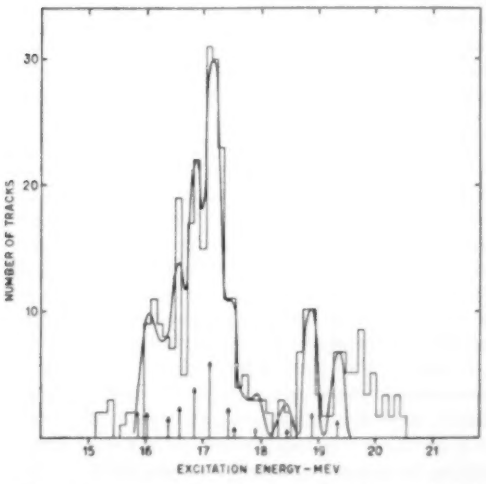

FIG. 1. Histogram showing the energy distribution of photoprotons from oxygen. The curve gives the distribution calculated from the breaks in the (γ,n) activation curve. The arrows indicate the position of the breaks.

In order to test the feasibility of this method, the photoproton spectrum of oxygen was investigated. The maximum bremsstrahlung energy was 21 Mev. The first excited state in N^{15} is at 5.28 Mev;[3] hence the ground-state transitions will be predominant. The proton energy was measured with nuclear plates mounted in a camera filled with oxygen at 2 atmos. The collimated beam from the University of Lund synchrotron was sent through the camera. The proton tracks in the plates were measured in the usual way. Great care was taken to make the energy measurements as accurate as possible. A correction was applied for the energy loss in the gas. There is a certain background from the (n,p) reaction in oxygen. It was determined by blocking the hole in the collimator by a lead cylinder. The background, which has been subtracted from the spectra, amounted to about 20%. The background tracks were all of low energy so that they have very little influence on the photoproton spectrum.

The energy spectrum is shown in Fig. 1 as a histogram. The curve has been obtained in the following way. At the position of each break in the excitation curve[1,2] (shown by arrows in Fig. 1) a peak has been placed. The width of the peaks is determined by the resolution of the experimental arrangement and has been calculated. The height of the peaks has been chosen to give the best possible fit to the histogram. The peaks are then added to give the curve in Fig. 1. The agreement with the measured spectrum is surprisingly good. This agreement strongly supports the assumption of sharp resonances in the cross-section curve. It should perhaps be mentioned that the relative height of the peaks (indicated by the height of the arrows) is about the same as calculated from the breaks, when the shape of the bremsstrahlung spectrum is taken into account.

The proton spectrum gives further information about the character of the photonuclear cross-section curve. The fact that the width of the peaks agrees so closely with the calculated values, sets an upper limit for the width of the resonances. A conservative estimate is 75 kev. Another interesting fact is that the sharp resonances can account for the whole spectrum below 19.5 Mev. Hence there is no continuous component in the cross-section curve. The part above 19.5 Mev may correspond to breaks not seen in the excitation curve or possibly to the onset of a continuous cross-section component. When the angular distribution of the protons is plotted separately for the strongest peaks, in-

formation is obtained about the spin values of the excited states in oxygen.

The present investigation indicates that this method gives considerable information about the levels in an energy interval, several Mev wide, above the (γ,p) threshold. It should be possible to increase the resolution by a factor of 2 or 3. It would then be possible to resolve the peaks with great certainty, especially if the statistics is improved by measuring a great number of tracks.

[1] L. Katz *et al.*, Phys. Rev. **95**, 464 (1954).
[2] Spicer, Penfold, and Goldemberg, Phys. Rev. **95**, 629 (1954). (See also reference 3.)
[3] F. Ajzenberg and T. Lauritsen, Revs. Modern Phys. **27**, 77 (1955).

Size Distribution of Neutron Widths*

D. J. Hughes and J. A. Harvey
Brookhaven National Laboratory, Upton, Long Island, New York
(Received June 16, 1955)

In the program of work carried out with the Brookhaven fast chopper[1] on total cross sections of heavy elements, various regularities have been observed[2] with regard to the widths and spacings of energy levels. In contrast to the near-constancy of Γ_γ ($\sim$20 percent variation from level to level in a given nuclide), the neutron widths were found to have an extremely large variation in size; the reduced neutron widths, Γ_n^0 (given by $\Gamma_n/E_0^{\frac{1}{2}}$ with E_0 the neutron energy at resonance), differed by factors as high as several hundred.

In the work of Harvey *et al.*,[2] in which several hundred neutron widths were measured, it was found that within experimental error the neutron widths had an exponential distribution in size for each nuclide that was investigated. When the number of resonances in a given energy range with widths larger than a given value were plotted as a function of the latter, the resulting distribution was consistent with an exponential distribution, implying that the differential distribution, that is, the number of levels as a function of neutron width, was also exponential. It was difficult to draw any definite conclusion, however, from individual nuclides because the number of levels observed in each case was rather small, of the order of ten levels. In order to investigate the distribution in more detail it is obviously desirable to combine the data from many nuclides to attain greater statistical accuracy.

The combination of data from various nuclides has been accomplished by plotting the reduced neutron widths relative to the average value for each nuclide rather than in terms of actual widths. This process normalizes the distributions for different nuclides so they can be plotted together, but some distortion of the final distribution results because the average neutron widths are not accurately known for individual nuclides.

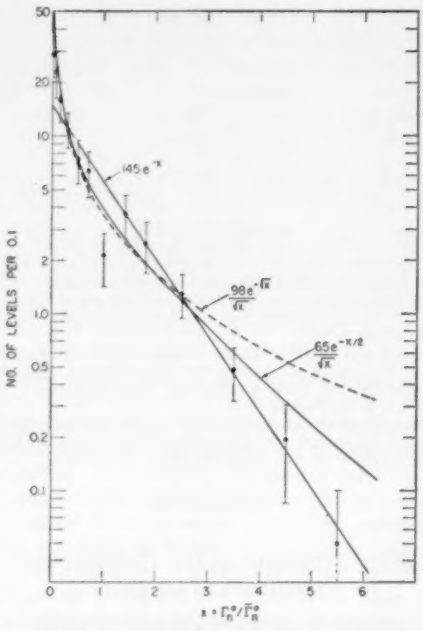

FIG. 1. Distribution (per 0.1 in Δx) of 145 reduced neutron widths relative to the average value for each nuclide. The curves are various suggested distribution laws described in the text.

Fortunately, it is possible to compute the distorting effect rather easily and the experimental points were corrected for it before plotting.

The distortion just described would of course add to a similar one already present in the distribution for the individual nuclides, which is a result of the presence of levels of two spin values. In computing the neutron widths from experimental transmission data the statistical factor, g, was assumed to be $\frac{1}{2}$, except for zero-spin target nuclei, where it is known to be unity. As a result, the distribution obtained for a given nuclide actually consists of two sets of levels, each with a different g value.[3] The spurious curvature in the distribution arising from the uncertainties in $\bar{\Gamma}_n^0$ and in g was computed and the experimental points were corrected before being plotted in Fig. 1. The distortion arising from the error in the average widths is much larger than that arising from the g uncertainty; the total correction is less than 10 percent for $x<3$ but reaches a factor of one half for the highest x value.

In plotting the points of Fig. 1, a careful attempt was also made to investigate other possible experimental distortions of the distribution, particularly the loss of very small levels simply because of their small size, as well as the loss of levels by failure to resolve them at high energy. One method that was used to investigate the failure to observe levels was to determine for each nuclide a neutron energy below which it was felt that

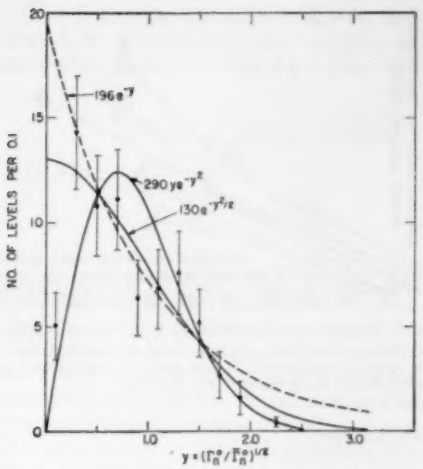

FIG. 2. The data and curves of Fig. 1 plotted as distributions (per 0.1 in Δy) of $y=(\Gamma_n^0/\bar{\Gamma}_n^0)^{\frac{1}{2}}$.

essentially no levels were lost by insufficient resolution, this process involving the plotting of location of levels as a function of energy. The average neutron width was then determined as an arithmetical average for the levels below this limiting energy, and the size distribution of these levels plotted. The process just described was then repeated with an energy limit one half of the value first used and again with an energy limit $1\frac{1}{2}$ times that limit. It was felt that this method would reveal experimental failure to locate levels because the rapid change of resolving power with energy would give in that case distributions that would differ in shape as the energy region covered was varied. The resulting distributions, however, show no significant difference in shape, providing a strong indication that the observed distribution is not strongly affected by missed levels. In addition, direct estimates based on examination of the experimental transmission curves lead to the conclusion that the distribution shape, especially at the small-size limit, is not affected greatly by failure to find levels, the correction being less than the statistical error shown.

Since the neutron width distribution was first found, several theoretical treatments have been made on the possibility of correlating it with nuclear theory. In addition to the exponential distribution,[4] the curved solid line shown in Fig. 1 has been suggested by Porter and Thomas,[5] and the dotted line by Bethe.[6] At large widths, the exponential gives the best fit, whereas at small widths, the other suggestions provide better agreement. Actually, as the square root of the neutron width is a property more closely related to nuclear structure theory[7,8] than the width itself,[9] it is instructive to consider the distribution in size of $(\Gamma_n^0)^{\frac{1}{2}}$. For example, a Gaussian distribution in $(\Gamma_n^0)^{\frac{1}{2}}$ was assumed by Porter and Thomas, whereas the exponential distribution of widths requires a $y\exp(-y^2)$ distribution, where $y=(\Gamma_n^0/\bar{\Gamma}_n^0)^{\frac{1}{2}}$. The experimental points and suggested distributions of Fig. 1 are shown as functions of y, on a linear scale, in Fig. 2. The points of Fig. 2, which can be considered to give more fundamental nuclear data than the width of Fig. 1, do not decide in favor of one distribution definitely but the e^{-y} curve (leading to Bethe's suggested curve of Fig. 1) seems to predict too many small and large values of y. The $y\exp(-y^2)$ curve, corresponding to the simple exponential distribution of neutron widths of Fig. 1, seems as satisfactory as $\exp(-y^2/2)$, although it does not seem to have as firm a theoretical basis (for it implies[4] complex y's).

* Work carried out under contract with U. S. Atomic Energy Commission.

[1] Seidl, Hughes, Palevsky, Levin, Kato, and Sjöstrand, Phys. Rev. **95**, 476 (1954).

[2] Harvey, Hughes, Carter, and Pilcher, Phys. Rev. **99**, 10 (1955).

[3] $\xi=\frac{1}{2}[1\pm 1/(2I+1)]$, with I the spin of the target nucleus.

[4] J. M. C. Scott, Phil. Mag. **45**, 1322 (1954).

[5] C. E. Porter and R. G. Thomas (private communication).

[6] H. A. Bethe (private communication).

[7] J. M. Blatt and V. F. Weisskopf, *Theoretical Nuclear Physics* (John Wiley and Sons, Inc., New York, 1952), Chap. 8.

[8] Lane, Thomas, and Wigner, Phys. Rev. **98**, 693 (1955).

[9] The quantities that are proportional to $(\Gamma_n^0)^{\frac{1}{2}}$ determine the decay probability into different channels, and are variously titled (references 7 and 8) most recently (reference 8) as "reduced-width amplitudes." We prefer not to use this terminology because of possible confusion with the usual use of amplitude as (cross section/4π)$^{\frac{1}{2}}$.

Inelastic Polarization and Nucleon Momentum Distribution*

L. MARSHALL

Institute for Nuclear Studies, The University of Chicago, Chicago, Illinois

(Received May 31, 1955)

INELASTIC $\phi-p$ polarization is similar in angular dependence, but smaller in magnitude than free $\phi-p$ polarization. In particular, at 310 Mev it is about 65 percent[1] of the latter.[2] It may be represented as being the free polarization distorted by the effect of the momentum distribution of the target protons in the nucleus.

We assume here that an incoming 310-Mev proton hits a 20-Mev proton in a 30-Mev potential well. The effective kinetic energies of the colliding protons are, therefore, 340 Mev and 20 Mev. We consider five types of collisions classified in terms of the resultant B of the momenta, $P_1=869$ Mev and $P_2=193$ Mev, of the two colliding protons, and listed in Fig. 1. These are assumed to occur with equal probability in the plane of the two emitted protons.

For each case, the barycentral momentum p and energy w are calculated. To demonstrate the range of

w, we may consider an equivalent collision of a proton of energy E with a proton at rest. For the 5 cases, the equivalent energies are, respectively: (1) 184 Mev, (2) 232 Mev, (3) 344 Mev, (4) 460 Mev, and (5) 504 Mev.

In each case we calculate from w and p the laboratory angle ϕ of the scattered proton as a function of barycentral scattering angle θ and plot it in Fig. 2.

We assume that, in each collision, protons are scattered with a polarization characteristic of a free $p-p$ collision. For purposes of comparison, the energy dependence of the free $p-p$ polarization is temporarily assumed constant, and for each case, using the relationships of Fig. 2, polarization is plotted *versus* ϕ. The new angular dependences resulting from the effect of the momenta of the struck nucleons are shown in Fig. 3.

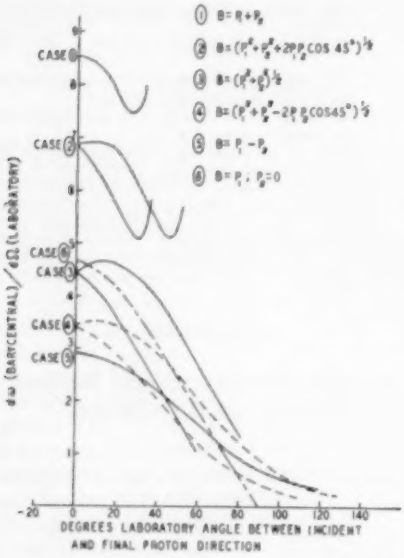

FIG. 1. $d\omega$ (barycentral)/$d\Omega$ (laboratory) *versus* laboratory angle ϕ between incident and final proton.

For cases 1 and 2 the free polarization pattern is squeezed into the forward direction, but for cases 4 and 5 it is considerably broadened.

The polarizations of Fig. 3 must be weighted by the appropriate solid angle factors. These are plotted in Fig. 1. From the calculated kinetic energy of the scattered proton in the laboratory system is subtracted the well depth, 30 Mev, giving the proton energy outside the well. The angle at which the energy reaches zero is the high-angle cutoff, and correspondingly the complement of its barycentral equivalent determines a low-angle cutoff. Namely, if the scattered proton has not enough energy to leave the nucleus, the collision is not recorded in the coincidence measurement.

The average inelastic polarization is computed from

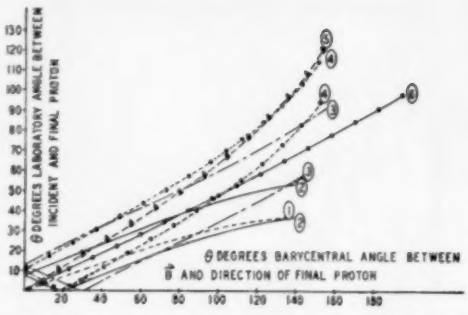
θ DEGREES LABORATORY ANGLE BETWEEN INCIDENT AND FINAL PROTON
θ DEGREES BARYCENTRAL ANGLE BETWEEN B AND DIRECTION OF FINAL PROTON

FIG. 2. Barycentral angle θ between $\mathbf{B}$ and direction of emitted proton *versus* laboratory angle ϕ between incident and final proton direction, calculated for six different orientations of the momenta $\mathbf{P}_1$ and $\mathbf{P}_2$ of the colliding protons.

the relationship:

$$\langle P(\phi)\rangle_{\text{Av}}=\frac{\sum_{i=1}^{5} P_i(\theta,E_i)\dfrac{d\sigma}{d\omega}(\theta,E_i)\dfrac{d\omega}{d\Omega}(\theta,E_i)}{\sum_{i=1}^{5}\dfrac{d\sigma}{d\omega}(\theta,E_i)\dfrac{d\omega}{d\Omega}(\theta,E_i)}.$$

Because $d\sigma/d\omega$ is practically constant against energy and angle, this relation becomes approximately

$$\langle P(\phi)\rangle_{\text{Av}}=\sum_{i=1}^{5} P_i(\phi,E_i)\frac{d\omega}{d\Omega}(\phi,E_i)\Big/\sum_{i=1}^{5}\frac{d\omega}{d\Omega}(\phi,E_i).$$

Now the energy dependence[2,3] of the free $p-p$ polarization $P_i(\phi,E_i)$ must be considered. The maximum polarization is known to be about 20 percent at 150 Mev, about 41 percent at 310 Mev, and about 32 percent at 430 Mev. Lacking further information, we multiply the polarizations in Fig. 3 by the following factors $f(E_i)$: Case (1): 0.70; Case (2): 0.87; Case (3): 1.00; Case (4): 0.70, and Case (5): 0.55.

A further correction factor $v_i(E_i)$ must be applied to take into account the fact that there are more collisions per unit time when the relative momentum is

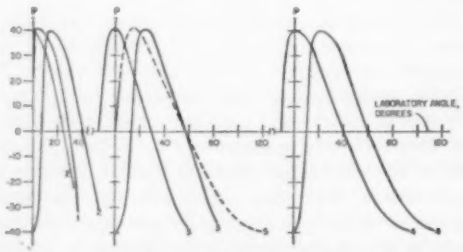

FIG. 3. Polarization *versus* laboratory angle ϕ between incident and final proton, for cases 1 to 5, assuming that the scattered protons resulting from any $p-p$ collision are polarized in the barycentral system of those two protons as if in a free collision.

high; these factors are 0.64, 0.69, 0.82, 0.95, and 1.00 for cases 1 to 5 respectively. Now $\langle P(\phi)\rangle_{\text{av}}$ for the 20-Mev proton gas as a function of ϕ is given by:

$$\langle P(\phi)\rangle_{\text{av}}=\frac{\sum P_i(\phi,E_i)\dfrac{d\omega}{d\Omega}(\phi,E_i)f_i(E_i)v_i(E_i)}{\sum \dfrac{d\omega}{d\Omega}(\phi,E_i)v_i(E_i)}.$$

However, a large fraction of the nucleon gas in a nucleus has low-momentum components. A crude way to take into account its effects is to assume that 70 percent of the nucleons are at rest and 30 percent have 20-Mev kinetic energy in the plane of $\mathbf{P}_1$ and $\mathbf{P}_2$. But in reality the counters used in the coincidence measurement extend above and below such a plane, so that the effective momentum distribution is something between that in a plane and that in three dimensions. Consequently one guesses that a more proper ratio is about 2:1 and with this assumption obtains the calculated inelastic $p-p$ polarizations shown in Fig. 4.

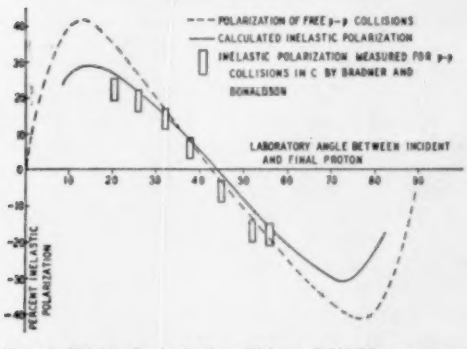
POLARIZATION OF FREE p–p COLLISIONS
CALCULATED INELASTIC POLARIZATION
INELASTIC POLARIZATION MEASURED FOR p-p COLLISIONS IN C BY BRADNER AND DONALDSON
LABORATORY ANGLE BETWEEN INCIDENT AND FINAL PROTON
PERCENT INELASTIC POLARIZATION

FIG. 4. $\langle P(\phi)\rangle_{\text{av}}$ for inelastic collisions of 310-Mev protons on a nucleus for which the probability to find a nucleon of energy 20 Mev is $\frac{1}{2}$ and of 0 Mev is $\frac{1}{2}$ in the plane defined by the incoming momenta, $\mathbf{P}_1$ and $\mathbf{P}_2$. The free $p-p$ polarization at 310 Mev is shown for comparison. The inelastic $p-p$ polarizations measured on carbon by coincidence methods at 285 Mev are indicated.

For comparison, the inelastic $p-p$ polarizations measured in coincidence by Bradner and Donaldson[1] for carbon at 285 Mev are shown plotted.

The experimental data can be fitted at least as well by more sophisticated choices of momentum distributions. The behavior of the inelastic polarization would seem very closely related to this kind of explanation.

* Research supported by a joint program of the Office of Naval Research and the U. S. Atomic Energy Commission.

[1] H. Bradner and R. Donaldson, Phys. Rev. **95**, 1701 (1954).

[2] Chamberlain, Segrè, Tripp, Wiegand, and Ypsilantis, Phys. Rev. **93**, 1430 (1954); Marshall, Marshall, and de Carvalho, Phys. Rev. **93**, 1431 (1954).

[3] J. M. Dickson and D. C. Salter, Nature **173**, 946 (1954); Kane, Stallwood, Sutton, Fields, and Fox, Phys. Rev. **95**, 1694 (1954).

Hyperfine Structure Anomaly in Atomic *P*-States*

CHARLES SCHWARTZ

Department of Physics and Research Laboratory of Electronics, Massachusetts Institute of Technology, Cambridge, Massachusetts

(Received June 10, 1955)

LURIO and Prodell[1] have inferred a value for the hfs anomaly Δ for the two stable isotopes of gallium by comparing their measurements on the atomic $p_{\frac{1}{2}}$ states with the measurements of Daly and Holloway[2] on the $p_{\frac{3}{2}}$ states, assuming that there could be no anomaly in the latter. The purpose of this Letter is to point out that as a result of electronic configuration mixing there can in principle be an hfs anomaly in any atomic state, and to calculate this important effect for Ga. Furthermore, before one can use a measured value of Δ to study the nuclear magnetic structure through the Bohr-Weisskopf[3] (B-W) theory, the contribution to the anomaly of other mechanisms must be subtracted. We arrive at the conclusion that the net B-W effect in Ga appears rather smaller than expected, but that one cannot yet be certain of its precise value.

The hfs anomaly Δ in a particular atomic state is defined as follows:

$$\Delta=\frac{a_1\mu_2}{\mu_1 a_2}-1, \tag{1}$$

where a is the dipole hfs interaction constant measured in that state, μ is the nuclear magnetic moment, and the subscripts 1, 2 refer to two isotopes (2 heavier than 1). Theoretical explanations of Δ will usually depend on some coefficient b which represents the density at the nucleus of the electrons which are responsible for the hfs. Thus only valence electrons with $j=\frac{1}{2}$ are of interest, the value of b for a $p_{\frac{1}{2}}$ electron being smaller than that for an $s_{\frac{1}{2}}$ electron by roughly α^2Z^2.

Now it is well known[4] that in an atomic state nominally described as ^2P_j there is often a noticeable admixture of excited s-electron states contributing to the hfs. For such states we should use an effective value of b given by

$$b_{\text{eff}}=(1-\beta_j)b_{pj}+\beta_j b_s, \tag{2}$$

where β_j, the fractional contribution of s-electrons to the hfs in the particular state ^2P_j, may be calculated from the dipole interaction constants $a_{\frac{1}{2}}$ and $a_{\frac{3}{2}}$ measured in both states of the doublet.[5]

$$\beta_{\frac{1}{2}}=(1-5\theta a_{\frac{3}{2}}/a_{\frac{1}{2}})/(1+5\theta) \tag{3}$$

$$\beta_{\frac{3}{2}}=-(a_{\frac{1}{2}}/a_{\frac{3}{2}})\beta_{\frac{1}{2}}. \tag{4}$$

For Ga, $a_{\frac{3}{2}}/a_{\frac{1}{2}}=7.02$, θ (a relativistic correction factor) $\cong 1.10_5$ so we have $\beta_{\frac{1}{2}}=0.033$, $\beta_{\frac{3}{2}}=-0.23$; the ratio $b_s/b_{p\frac{1}{2}}$ for the coefficients of the B-W theory is 23; so in the $p_{\frac{1}{2}}$ state we have $b_{\text{eff}}=1.7b_{p\frac{1}{2}}$ and in the $p_{\frac{3}{2}}$ state $b_{\text{eff}}=-5.3b_{p\frac{1}{2}}$. We thus have the result that there

should already be a hfs anomaly in the $p_{\frac{1}{2}}$ state, about -3 times that in the $p_{\frac{3}{2}}$ state.

The result of Lurio and Prodell's measurement is

$$a_{\frac{1}{2}}^{69}/a_{\frac{1}{2}}^{71}=0.7870196_8\pm0.0000006,$$

and the earlier measurements of Daly and Holloway on the $p_{\frac{3}{2}}$ state give

$$a_{\frac{3}{2}}^{69}/a_{\frac{3}{2}}^{71}=0.7869949\pm0.0000013,$$

while the new value for the moment ratio given by Rice and Pound[6] is

$$\mu^{69}/\mu^{71}=0.7870147_6\pm0.0000012.$$

From these data, we have the two anomalies

$$\Delta_{\frac{1}{2}}=(6.2\pm2.3)\times10^{-6},$$
$$\Delta_{\frac{3}{2}}=(-25.2\pm3.2)\times10^{-6},$$

and the number given by Lurio and Prodell is

$$\Delta_{\frac{1}{2}}-\Delta_{\frac{3}{2}}=(31.5\pm2.4)\times10^{-6},$$

which is independent of the exact value of the moment ratio. The best check on our interpretation of this data is obtained from the ratio $\Delta_{\frac{1}{2}}/(\Delta_{\frac{1}{2}}-\Delta_{\frac{3}{2}})$ which is (-8.0 ± 1.6), while we predict $-5.3/(1.7+5.3)=-7.6$.

For the purpose of further analysis, the value of $\Delta_{\frac{1}{2}}-\Delta_{\frac{3}{2}}$ is still the most accurately known of these numbers, but we now see that as a result of the mixing s-electrons, this number represents seven times the anomaly that would be produced by a $p_{\frac{1}{2}}$ electron alone. Still, before we can interpret this as the B-W effect in Ga, we must first allow for other effects which can give an hfs anomaly. Crawford and Schawlow[7] have calculated the effect of the changing size of the nuclear charge distribution on the hfs of two isotopes. In Ga, the admixture of s-electrons again magnifies this effect in both states of the doublet, and we have estimated that this contributes about 20×10^{-6} to the difference $\Delta_{\frac{1}{2}}-\Delta_{\frac{3}{2}}$. If this is a correct and complete description of the problem, we are left with a B-W effect for a single $p_{\frac{1}{2}}$ electron of $1/7(31-20)10^{-6}=1.6\times10^{-6}$, while the simple theory predicts $\sim7\times10^{-6}$. (Our calculations use a nuclear charge radius of $1.2A^{\frac{1}{3}}\times10^{-13}$ cm.)

However, this number 1.6×10^{-6} may in fact be off by even a factor of 2 since the Crawford-Schawlow term was calculated using the doubtful assumption that the nuclear charge radius varies as $A^{\frac{1}{3}}$ as one adds two neutrons to Ga^{69}. The quantity $\gamma=(dR/R)(3A/dA)$ (which is usually <1) may, in principle, be deduced from measurements of the spectroscopic isotope shift; but the interpretation of such data in medium-weight atoms depends on the difficult calculation of the specific mass effect.[8] It may be that other observations, such as measurements of x-rays from μ-mesonic atoms of the separated isotopes, could be carried out with sufficient accuracy to give γ.

Still, the question of what other effects—such as second-order hfs proportional to μ^2, nuclear polarizability, etc.—might show up as part of an hfs anomaly greater than about 1×10^{-6} is as yet unanswered and should be the subject of further study.

* This work was supported in part by the Signal Corps; the Office of Scientific Research, Air Research and Development Command; and the Office of Naval Research.

[1] A. Lurio and A. G. Prodell, Bull. Am. Phys. Soc. **30**, No. 3, 13 (1955).

[2] R. T. Daly, Jr., and J. H. Holloway, Phys. Rev. **96**, 539 (1954).

[3] A. Bohr and V. F. Weisskopf, Phys. Rev. **77**, 94 (1950).

[4] E. Fermi and E. Segrè, Z. Physik **82**, 729 (1933).

[5] C. Schwartz, Phys. Rev. **97**, 380 (1955).

[6] M. Rice and R. V. Pound, following Letter [Phys. Rev. **99**, 1036 (1955)].

[7] M. F. Crawford and A. L. Schawlow, Phys. Rev. **76**, 1310 (1949). [The Crawford-Schawlow effect accounts for essentially all of the hfs anomaly observed in thallium: A. Berman, Phys. Rev. **86**, 1005 (1952).] This calculation was first carried out by J. E. Rosenthal and G. Breit, Phys. Rev. **41**, 459 (1932).

[8] Crawford, Gray, Kelley, and Schawlow, Can. J. Phys. **A28**, 138 (1950).

Ratio of the Magnetic Moments of the Stable Gallium Isotopes*

MICHAEL RICE AND R. V. POUND

Department of Physics, Harvard University, Cambridge, Massachusetts

(Received June 10, 1955)

INTERPRETATIONS by Schwartz of recent measurements of the ratios of the hyperfine structure splittings of the gallium isotopes[1] made an improved measurement of the ratio of their magnetic moments desirable. The most accurate value available from published results is derived as the ratio of the ratios of resonant frequencies to that of Na^{23} and is $\mu(Ga^{71})/\mu(Ga^{69})=1.27059\pm0.000023$.[2]

We have made a new determination using the recording oscillating rf spectrometer[3] and a permanent magnet. The sample was a solution of $GaCl_3$ in about 6N HCl. The line widths between points of maximum slope were 440 and 520 cps for Ga^{71} and Ga^{69}, respectively, of which width part appears to be attributable to inhomogeneity of the 6350-gauss static magnetic field. Trial experiments revealed considerably greater line width, and reduced intensity, in solutions of less acidity. The points of zero slope in the lines were determined by recording their derivatives with the spectrometer steadily scanning in frequency, making frequency marks every 20 cps as determined by standard procedures from our quartz crystal standard. The signal-to-noise amplitude ratios, (100:1 and 40:1) allowed determination of the zeroes of the recorded derivative curves to ±2 and ±4 cps.

A slow but reasonably steady drift of the static field, of thermal origin, necessitated alternate observations of each line and interpolation between pairs of measurements of one line to the time of observation of the other. For each direction of frequency scan four observations were made of one line and three of the

other. For scans in the direction of decreasing frequency, the five ratios so determined averaged to 1.2706211 with an average deviation of ±0.0000018, whereas for scans in the other direction the ratios averaged to 1.2706272±0.0000009. The two differ because of the lag introduced by the not negligible integrating time constant in the recording system ($RC=10$ sec in two cascaded stages) compared to the time of passage through the line (4 min for the high-frequency line and 9 min for the low). Assuming this effect to be eliminated in the arithmetic average, the final result is

$$\mu(\mathrm{Ga}^{71})/\mu(\mathrm{Ga}^{69})=1.2706242\pm0.0000020,$$

where the estimated error is larger than the largest average deviation from the mean in the runs for one direction and makes some allowance for residual systematic error. This result is in excellent agreement with Schwartz's prediction from the hfs data.[1]

We are indebted to Dr. R. E. Richards for helpful suggestions regarding chemical aspects of the problem and to Dr. J. W. Meadows for the $GaCl_3$ used.

* Supported in part by the joint program of the Office of Naval Research and the U. S. Atomic Energy Commission.

[1] C. Schwartz, preceding Letter [Phys. Rev. **99**, 1035 (1955)].

[2] H. E. Walchli, Oak Ridge National Laboratory Report ORNL-1775 (unpublished).

[3] G. Watkins and R. V. Pound, Phys. Rev. **82**, 343(A) (1951).

Second Maximum in the Negative Pion Scattering Cross Section

FREEMAN J. DYSON

Institute for Advanced Study, Princeton, New Jersey

(Received May 23, 1955)

THE total cross section for scattering of negative pions by protons[1] has a pronounced second maximum at about 900 Mev. The cross section is about 30 mb at 700 Mev and at 1100 Mev, and rises between these limits to a peak value of about 50 mb. As Yang[2] and others have observed, it is difficult to interpret this maximum as a resonance in a single state of the meson-proton system. First, there is no maximum in the positive pion scattering at this energy, and so the excess scattering must occur in states of total isotopic spin $T=\frac{1}{2}$. Second, the maximum contribution to the total cross section from a state with $T=\frac{1}{2}$ and total angular momentum J is limited by

$$\sigma\leq(4\pi/3)\lambda^2(2J+1)\rho, \tag{1}$$

where λ is the de Broglie wavelength in the center-of-mass system, and ρ is the ratio of elastic to total cross section in the resonant state. Experimentally it appears[3] that $\rho\sim\frac{1}{2}$, so that taking $\sigma=20$ mb and $\lambda=3.45\times10^{-14}$ cm at 900 Mev, Eq. (1) would imply

$$J\geq11/2, \tag{2}$$

which is highly unlikely at this energy. For this and other reasons, it is believed that several angular momentum states with $T=\frac{1}{2}$ must simultaneously give maximum cross sections at 900 Mev, while none of the states with $T=\frac{3}{2}$ does so.

The following simple hypothesis[4] appears to give a qualitative explanation of the facts. Suppose there is a strongly interacting or resonant state of two mesons which collide at a relative momentum of 250 Mev/c. We consider the excess inelastic π^-+p scattering to be a resonant elastic scattering of the incident meson by a meson in the charge cloud around the proton. The second meson is supposed to be "loosely bound" so that the interaction usually results in both mesons escaping from the proton. If the resonant state has $T=0$ it will contribute nothing to π^++p scattering at this energy. The excess scattering will be observed in several angular momentum states of the (π^-+p) system simultaneously.

The maximum excess cross section is given by

$$\sigma=(4\pi/3)\lambda^2(2I+1)F, \tag{3}$$

where I is the angular momentum of the resonant state, $\lambda=7.87\times10^{-14}$ cm is now the de Broglie wavelength in the center-of-mass system of the two mesons, and F is the probability of finding a positive pion in the proton charge cloud. With $\sigma=20$ mb, (3) gives

$$(2I+1)F\geq0.77, \tag{4}$$

which is possible if $I=0$ and is easily to satisfy if $I=2$. [$T=0$ states must have even parity.]

The main predictions on which this hypothesis may be tested are these:

(i) The excess inelastic scattering should lead entirely to outgoing neutrons and not to protons.

(ii) The final states should be $(n+\pi^++\pi^-)$ and $(n+2\pi^0)$ in the ratio 2:1.

(iii) The neutron should be emitted with very low energy in the lab system, 20 Mev being an estimated average value.

The width of the observed maximum is compounded from the natural width of the 2-meson resonance and the momentum distribution of the meson in the charge cloud. On this basis the resonance may be estimated to have a width at half-maximum of 50–100 Mev/c in momentum units. It is not clear, however, whether such an estimate based on an "impulse approximation" has any validity.

[1] Shapiro, Leavitt, and Chen, Phys. Rev. **92**, 1073 (1953); Cool, Madansky, and Piccioni, Phys. Rev. **93**, 637 (1954).

[2] C. N. Yang, Proceedings of the Fifth Annual Rochester Conference (University of Rochester Press, Rochester, to be published).

[3] L. M. Eisberg *et al.*, Phys. Rev. **96**, 797 (1955). These measurements were made at 1.4 Bev. A direct measurement of ρ at 900 Mev is still lacking.

[4] This idea was suggested by O. Piccioni several years ago, before any experiments existed to support it.

Observations on S Particles*

J. Ballam, A. L. Hodson,† and George T. Reynolds
Palmer Physical Laboratory, Princeton University, Princeton, New Jersey
(Received May 26, 1955)

SINCE March, 1954, the Princeton cloud-chamber group has been operating a dual cloud chamber similar to that of the Ecole Polytechnique.[1] The upper or magnet chamber has been described previously.[2] The lower or multiplate chamber has an illuminated region approximately 20 in.×20 in.×7 in. and the illuminated regions of both chambers are separated by 8 in. The material in the lower chamber has been in succession seven ½-in. Pb plates and seven ½-in. Cu plates. More recently, eleven tungsten plates each approximately 0.6 in. thick for a total of 290 g/cm² in the vertical direction have been installed. In this paper it is intended to describe those events in which either the primary or secondary of the S event[3] was observed in both chambers.

We have observed five S events whose primary masses were measurable by a momentum-range method. In one of these the secondary proceeded back into the upper chamber so that its momentum could be ascertained. In one other event the secondary stopped in the lower chamber. In all events the secondary traversed more than 30 g/cm² of copper, and no associated γ's were observed.

In a sixth event the primary was not observed in the upper chamber, but the secondary traveled back through the upper chamber for a distance of 30 cm. The measurements on this event are given in Table I.

To obtain the momentum of the secondary at the point of decay (p^*) one has to assume its mass and then use range-energy relations. Assuming the secondary is a μ meson and using the tables of Aron, Hoffman, and Williams,[4] we obtain $p^*=222\pm4$ Mev/c. Using the corrections to these tables described in the following Letter, we obtain 221 ± 4 Mev/c. On the assumed decay scheme $K_{\mu2}\rightarrow\mu+\nu$ the mass of the primary becomes $915\pm15m_e$ or $912\pm15m_e$, respectively. If, on the other hand, one assumes the secondary is a π meson and analyzes the event as a $\theta^+\rightarrow\pi^++\pi^0$ the secondary momentum becomes 235 ± 4 Mev/c when one uses reference 4, and 234 ± 4 Mev/c corrected, with the primary mass $1065\pm15m_e$ and $1062\pm15m_e$, respectively. This is inconsistent with the assumed decay scheme if the θ has a mass near that of the τ meson.[2,5]

In event number 244–96322, in which both primary and secondary are observed in the upper chamber, the secondary range and total momentum are not so well defined because it is impossible to determine whether or not the secondary traveled through a vertical counter wall of 8.5 g/cm² of Cu placed between the chambers. However, it appears in the upper chamber as a minimum ionizing track of momentum 117 ± 3 Mev/c after traversing a minimum of 51 g/cm² of Cu. The primary mass was measured as $(860_{-90}{}^{+70})m_e$ and it is therefore felt that this event is a well-established $K_{\mu2}$ heavy meson.

TABLE I. Measurements on secondary particle in event 161–48942.

Measured momentum in upper chamber	Range in material between chambers	Range in plates of lower chamber
147 ± 3.5 Mev/c	25.4 ± 1 g/cm² Cu	15.4 ± 1 g/cm² Cu

In event 242–94370 the secondary had a range of 63–83 g/cm² Cu. The masses of the five primaries when one uses reference 4 are (780 ± 90), (900 ± 80), (1080 ± 180), (935 ± 80), and $(860_{-90}{}^{+70})m_e$. The weighted mean of all five is $(891\pm40)m_e$, and for the two cases in which the secondary has a range greater than 50 g/cm² Cu it is $(905_{-80}{}^{+65})m_e$. When corrected for changes in the range-energy curves, these become $(900\pm40)m_e$ and $(914_{-80}{}^{+65})m_e$, respectively. These mass measurements coupled with the well-determined secondary of event 161–48942 are considered as confirming the evidence that the $K_{\mu2}$ has a mass lower than the τ meson, as indicated by the Paris group.[6]

* Supported by the Office of Naval Research and the U. S. Atomic Energy Commission.
† Now at Leeds University, Leeds, England.
[1] Gregory, Lagarrigue, Leprince-Ringuet, Muller, and Peyrou, Nuovo cimento **11**, 292 (1954).
[2] Hodson, Ballam, Arnold, Harris, Rau, Reynolds, and Treiman, Phys. Rev. **96**, 1089 (1954).
[3] S events were first described by the Massachusetts Institute of Technology group, e.g., Bridge, Courant, DeStaebler, and Rossi, Phys. Rev. **91**, 1024 (1953).
[4] Aron, Hoffman, and Williams, U. S. Atomic Energy Commission Report AECU-663 (unpublished).
[5] Bridge, De Staebler, Rossi, and Sreekantan, Nuovo cimento (to be published).
[6] Armenteros, Gregory, Hendel, Lagarrigue, Leprince-Ringuet, Muller, and Peyrou, Nuovo cimento (to be published).

Masses of S Particles*

George T. Reynolds and W. A. Aron
Palmer Physical Laboratory, Princeton University, Princeton, New Jersey
(Received May 26, 1955)

MASS determinations of stopping K-mesons have been reported by several cloud-chamber groups.[1–3] Two methods are available when the so-called double cloud-chamber technique is used. (1) The mass of the K-meson is measured "directly" by a momentum range method. (2) The mass of the K-meson is determined by measuring the range of the charged decay product, assuming the nature of both the charged and neutral decay procucts, and treating the event as a two-body decay. This second method is available also when a single cloud chamber is used, containing plates of suitable stopping material.

During the past few years masses obtained by these two methods have appeared to differ systematically. Both methods require the use of the so-called range-energy curves, and all three groups referred to have used the results of Aron, Hoffman, and Williams.[4] The Paris group has pointed out that an error in the range-energy curves would affect the masses deduced by the two methods described above in opposite senses.

The recent work of several authors[6-8] indicates that for copper and lead, the stopping materials primarily used in the multiplate cloud-chamber experiments, a more suitable value of the mean excitation potential I would be $I=13.0Z$. In particular, the values of Bichsel and Mozley were: for Cu, $12.9Z$; and for Au, $13.1Z$ (corrected for K-shell electron effects, using protons of energy 6 to 18 Mev). When this new value of I is used, the range-energy curves shift in such a way that for a given mass and momentum, the range is increased by 1.6 percent. The several mass values available have been reconsidered on this basis.

The values of the Paris group[1] were as follows:

(a) $906\pm27m_e$ for an average of six events measured by method 1, where the secondary range was such as to require a μ meson, thus indicating a K_μ particle.

(b) $928\pm12m_e$ for an average of 22 events measured by method 1 not necessarily all K_μ's, thus indicating an upper limit to the K_μ mass.

(c) $941\pm11m_e$ determined by method 2 on the basis of nine events.

The value of the M.I.T. group for determination of the mass by method 2 was:

$948\pm15m_e$ based on the best two events of their sample. (This mass was obtained by taking the range reported,[2] using a μ mass of 105.8 Mev, and the curves of reference 4.)

The change in the range-energy curves reported above results in raising masses of method 1 and lowering those of method 2. The new results are then:

Paris:	906 is increased to $915\pm27m_e$,	(method 1)
	928 is increased to $936\pm12m_e$,	(method 1)
	941 is decreased to $934\pm11m_e$,	(method 2)
M.I.T.:	948 is decreased to $941\pm15m_e$.	(method 2)

The Princeton results[3] have been reported, taking into account the effect of the range-energy changes. These results were:

$900\pm40m_e$ for method 1 on the basis of five events,
$912\pm15m_e$ for the backward S.

This result is less sensitive to the range-energy changes than those masses obtained by method 2, due to the fact that a measurement of a residual momentum was possible.

At this time there seems to be no systematic difference between masses obtained by the two methods and no systematic difference among the results of the various groups. Also, it appears that the $K_{\mu 2}$ mass is significantly less than the τ mass. It is also of interest to note that the mass of the $K_{\tau 2}$ reported by the M.I.T. group[2] is changed from 952 to $946\pm12m_e$ by the change in the range-energy results.

Further improvement in the interpretation of the range-energy results is under consideration. This involves the use of more recent improved shell corrections for both the K- and L-shells in the analysis of the experimental stopping-power data and in the calculation of the range-energy relation.

* Supported by the Office of Naval Research and the U. S. Atomic Energy Commission.

[1] Armenteros, Gregory, Hendel, Lagarrigue, Leprince-Ringuet, Muller, and Peyrou, Nuovo cimento (to be published). We are indebted to B. Gregory for helpful discussions on the interpretation of these results, made available prior to publication.

[2] Bridge, DeStaebler, Rossi, and Sreekantan, Nuovo cimento (to be published).

[3] Ballam, Hodson, and Reynolds, preceding Letter [Phys. Rev. 99, 1038 (1955)].

[4] Aron, Hoffman, and Williams, U. S. Atomic Energy Commission Report AECU 663 (unpublished).

[5] N. Bloembergen and P. J. van Heerden, Phys. Rev. 83, 561 (1951).

[6] D. O. Caldwell and J. R. Richardson, Phys. Rev. 94, 79 (1954).

[7] E. L. Hubbard and K. R. MacKenzie, Phys. Rev. 85, 107 (1952).

[8] H. Bichsel and R. F. Mozley, Phys. Rev. 94, 764 (1954). Also, private communication.

Gamma Stability of K-Mesons*

S. B. Treiman and H. W. Wyld, Jr.

Palmer Physical Laboratory, Princeton University, Princeton, New Jersey

(Received May 31, 1955)

ONE of the mysterious, and presumably significant, aspects of the heavy unstable particles is the remarkable clustering of masses in the neighborhood of 900–$1000m_e$.[1] The reasonably well-established decay processes in this mass range are

$$\tau^\pm \to \pi^\pm+\pi^++\pi^-,$$
$$\theta^0 \to \pi^++\pi^-,$$
$$\theta^\pm \to \pi^\pm+\pi^0,$$
$$K_{\mu 2}{}^+ \to \mu^++\nu,$$
$$K_{\mu 2}{}^\pm \to \mu^\pm+2 \text{ neutrals},$$
$$K_{e 2}{}^\pm \to e^\pm+2 \text{ neutrals}.$$

The best-known mass is that of the τ meson ($965.5\pm0.7m_e$)[2]; within the experimental errors this is identical with the mass of the θ^0 meson ($966\pm10m_e$).[3] The masses of the other particles are less well known, but there is some experimental indication that the $K_{\mu 2}{}^+$ mass (estimated value $\sim 940m_e$)[4] is distinctly below that of the τ meson. The estimated lifetimes for the various K-mesons lie in the range 10^{-10} to 10^{-8} sec.

If there exist among this group of K-mesons distinct particles with somewhat different masses, the question arises as to why the heavier members do not decay into the lighter members by photon emission. Since the lifetimes for the normal decay modes are so long, it might be expected that even with small mass differences such processes should compete favorably with the normal decay modes.

For example, even if the θ, τ, and γ are not directly coupled to one another, the θ and τ mesons are presumably strongly coupled to nucleons and pions, as evidenced by their copious production in collisions of these particles; and by the inverse processes they might therefore be expected to be strongly coupled to one another. The same remark holds for any other pair of K-mesons (perhaps $K_{\mu 2}^{+}$ and θ^{+}) which are strongly coupled to nucleons and pions in a similar way. In the "associated production" scheme of Gell-Mann,[5] for example, the θ and τ mesons would be expected to have the same isotopic spin assignments and would therefore be strongly coupled to one another. The situation with regard to the $K_{\mu 2}^{+}$ is much less certain, since there is little evidence regarding its mode of production or other charge states.

At any rate, in the discussion that follows we consider the possibility, still not excluded by experimental evidence, that two or more of the K-mesons are strongly coupled. Within this framework there are still several obvious ways to understand the absence of rapid decay by photon emission, each possibility being of some interest and being subject ultimately to experimental test.

(a) The strongly coupled K-mesons may have very nearly identical masses. This is especially indicated experimentally for the pair θ, τ; but it does not seem to be the case for the pair $K_{\mu 2}^{+}$, τ.

(b) If two particles both have spin zero, the decay of one into the other by single photon emission is of course absolutely forbidden. However, in this case one must also consider the possibilities of double photon decay and decay by the emission of an electron pair (the latter is possible only if both K-mesons have the same parity).[6] A rough estimate of the lifetime for either of these processes gives

$$T\sim\frac{1}{\alpha^2}\frac{R}{c}\left(\frac{\Delta Mc}{\hbar}R\right)^{-7}. \tag{1}$$

Here ΔM is the difference in mass between the two mesons; R is the range of the interaction, which we take to be of the order of a nucleon Compton wavelength, since the decay would likely take place via intermediate states involving particles of nucleonic mass; and $\alpha=1/137$. Taking ΔM even as large as $25m_e$ (the indicated mass difference between the τ- and $K_{\mu 2}^{+}$-mesons) one finds $T\sim 1.5\times 10^{-7}$ sec, which is longer than the lifetimes of the normal decay modes.

TABLE I. Values of $(2l+1)!!(2l-1)!!\left[(\Delta Mc/\hbar)R\right]^{-(2l+1)}$.

l	$\Delta M=10m_e$	$\Delta M=25m_e$
1	1.9×10^{7}	1.2×10^{6}
2	9.5×10^{13}	9.5×10^{10}
3	1.1×10^{19}	1.8×10^{14}

(c) Another mechanism for inhibiting the decay by photon emission would be to assign very different spins to the strongly coupled K-mesons. A rough estimate of the lifetime for a 2^l-pole photon transition between strongly coupled K-mesons gives

$$T_l\sim\frac{1}{\alpha}\frac{R}{c}(2l+1)!!(2l-1)!!\left(\frac{\Delta Mc}{\hbar}R\right)^{-(2l+1)}. \tag{2}$$

The "natural" lifetime $(1/\alpha)(R/c)=9.4\times 10^{-23}$ sec. To effectively forbid the photon decay, the difference in spins of the two K-mesons must be chosen so that the l-dependent factors in Eq. (2) increase the lifetime to something greater than the 10^{-10} to 10^{-8} sec observed lifetimes for the normal decay modes. These factors are tabulated in Table I for two choices of ΔM. We see that even if the mass difference between $\theta^{\pm}$ and $\tau^{\pm}$ is as small as the present experimental error in the θ^0 mass ($\sim 10m_e$), and if both particles do not have spin zero, then the difference in spin must be at least two units. For the pair $K_{\mu 2}^{+}$ and τ^{+}, where as far as we now know the mass difference could be as large as say $25m_e$, the difference in spin would correspondingly have to be at least three units.

* Supported in part by the Office of Naval Research and the U. S. Atomic Energy Commission.

[1] For a general discussion of recent K-meson results, see Proceedings of the Fifth Annual Rochester Conference (University of Rochester Press, to be published).

[2] See Report of the Padua Conference, Nuovo cimento **12**, Suppl. 2 (1954).

[3] Thompson, Burwell, Cohn, Huggett, and Karzmark, Phys. Rev. **95**, 661 (1954).

[4] See the summary by B. Rossi in reference 1.

[5] A summary of the Gell-Mann and Pais theories appears in the Proceedings of the International Physics Conference, Glasgow, 1954 (to be published).

[6] We would like to thank A. Pais and R. Dalitz for pointing out to us the possibilities of double photon and pair emission and for discussions of the estimate in Eq. (1).

Observations on the Charge and Mass Distributions in Nuclei

OSAMU MIYATAKE AND CLARK GOODMAN*

Osaka City University and Osaka University, Osaka, Japan

(Received June 6, 1955)

RECENT measurements[1,2] of electric excitation cross section, σ_{ex}, and energy of first excited states, ΔE, gave different electric quadrupole moments,[1] Q_0, and electric quadrupole transition probabilities, $B(E2)$, using the Bohr-Mottelson theory[3] which

TABLE I. Values of the parameters.

Isotope	ΔE (kev)	β	$\left(\frac{\Delta R}{R}\right)_{\Delta E}$	$Q_0(\Delta E)$ (10^{-24} cm^2)	$Q_0(\sigma_{ex})$ (10^{-24} cm^2)	$\left(\frac{\Delta R_c}{R_c}\right)_{ex}$	$\left(\frac{\Delta R}{R}\right)_{ex}$
Hf^{176}	87	0.610	0.385	22.4	22.1	0.519	0.380
Hf^{178}	91	0.591	0.373	21.8	16.8	0.401	0.292
Hf^{180}	92	0.582	0.367	21.6	16.3	0.388	0.283
W^{182}	101	0.550	0.347	21.1	5.2	0.127	0.091
W^{184}	112	0.518	0.327	19.9	4.5	0.110	0.078
W^{186}	124	0.488	0.308	18.8	4.1	0.099	0.071
Os^{188}	137	0.464	0.293	18.3	...	...	...
Pt^{194}	330	0.289	0.182	11.7	2.4	0.055	0.039
Pt^{196}	360	0.274	0.173	11.2	1.7	0.038	0.027
Pt^{198}	425	0.258	0.162	10.5	1.4	0.032	0.022
Pd^{106}	500	0.388	0.245	6.3	1.3	0.077	0.055
Pd^{108}	425	0.414	0.261	6.9	1.5	0.082	0.059
Pd^{110}	365	0.440	0.278	7.4	1.6	0.090	0.064
Cd^{112}	610	0.336	0.212	5.8	1.1	0.060	0.043
Cd^{114}	545	0.350	0.221	6.2	1.2	0.062	0.044

assumes (1) incompressible and uniformly charged nucleus, and (2) irrotational collective motion.

These differences may result from a difference in mass distribution as compared to charge distribution.[1,2] In fact, as indicated below, the nucleus may contain a protonic core of a symmetry different from that of the nucleus as a whole. We can estimate the latter from the observed ΔE's of even-even nuclei by using

$$\Delta E=(\hbar^2/2\mathcal{I})[I(I+1)],\quad \mathcal{I}=3B\beta^2,\quad B=(3/8\pi)AMR^2,$$
$$\beta=423/A^{5/6}\Delta E^{\frac{1}{2}},\quad (I=2,\ \Delta E \text{ in kev})$$

where B is the mass coefficient, R the mean nuclear radius, and β the deformation parameter. If one uses $R=1.4\times10^{-13}A^{\frac{1}{3}}$ cm, the values of β and $(\Delta R/R)_{\Delta E}=(5/4\pi)^{\frac{1}{2}}\beta$ obtained from the ΔE's are given in columns 3 and 4 of Table I, where ΔR is the elongation of the major axis for an assumed spheroid. The central sections of heavy nuclei would have relative geometries shown schematically in the outer ellipses of Fig. 1.

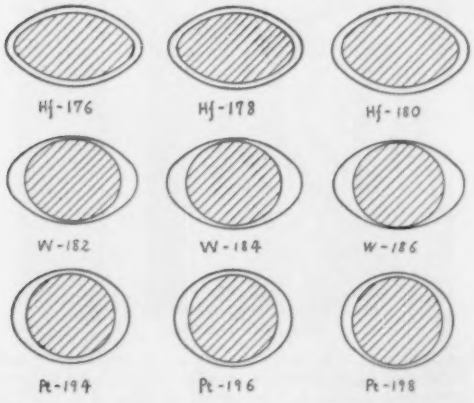

FIG. 1. Schematic central sections of distorted heavy nuclei (outer ellipses) and of distorted proton cores (shaded areas), which are obtained from the first excited energies ΔE and electric excitation cross sections σ_{ex}, respectively.

The values of $Q_0(\Delta E)$, column 5, were obtained by using

$$Q_0=\frac{\rho}{e}\int(3z'^2-r'^2)d\tau'=\frac{2Z}{5}(a^2-b^2),$$

where a and b are the semiaxes of the spheroid, assuming that the protons are uniformly distributed throughout the whole nucleus. These values are to be compared with those in column 6 where $Q_0(\sigma_{ex})$ has been obtained from σ_{ex}. The two sets of values agree for Hf^{176} but the $Q_0(\sigma_{ex})$'s decrease more rapidly than the $Q_0(\Delta E)$'s. For even isotopes of Pd and Cd, the two sets of Q_0's differ by a factor 4 to 5.

$Q_0(\sigma_{ex})$ is indicative of the nuclear charge distribution. From the data of $Q_0(\sigma_{ex})$, values of $(\Delta R/R)_{ex}$, column 8, have been computed by assuming a uniform charge distribution throughout the nucleus, and values of $(\Delta R_c/R_c)_{ex}$ given in column 7 based on a uniform charge distribution in a spheroid of mean radius $R_c=1.18\times10^{-13}A^{\frac{1}{3}}$ cm as suggested by recent experiments.[4] The corresponding proton cores would have central sections shown by the shaded ellipses in Fig. 1. The assumption of $R_c<R$ results in very large asymmetries $(\Delta R_c/R_c)_{ex}$ for the proton cores in the Hf nuclei, but for all other nuclei listed, the asymmetries of the proton cores would be substantially less than the values of $(\Delta R/R)_{\Delta E}$ for the nucleus as a whole. In other words, the proton core becomes spherically symmetric much more rapidly than the nucleus as a whole as the proton number 82 is approached. Such a model implies that the flow of the nuclear matter is not irrotational throughout the nucleus.

It does not seem possible to retain both irrotational flow and uniformity of proton distribution because of the discrepancy between the values of $(\Delta R/R)_{\Delta E}$ and $(\Delta R/R)_{ex}$.

Since $(\Delta R/R)_{\Delta E}\propto(B\Delta E)^{-\frac{1}{2}}$, it can be brought into agreement with $(\Delta R/R)_{ex}$ or $(\Delta R_c/R_c)_{ex}$ by an increase of B above the value $(3/8\pi)AMR^2$ based on an assumed irrotational flow. Also, if it is not necessary that the

flow be irrotational throughout the nucleus, a wide range of values of B becomes possible, some of which are larger than $(3/8\pi)AMR^2$. It is of interest that values of B which make $(\Delta R/R)_{\Delta E}$ nearly equal to $(\Delta R_c/R_c)_{ex}$ are obtained by assuming an extreme model with a spherical proton core of the size estimated above surrounded by a fluid neutron shell. In any event, it appears that the irrotational character of the flow must be abandoned in the B-M theory.

The assistance of the U. S. Educational Commission in Japan in granting a Fulbright Lectureship to one of us (C.G.) is gratefully acknowledged.

* On leave from the Massachusetts Institute of Technology, Cambridge, Massachusetts.

[1] McClelland, Mark, and Goodman, Phys. Rev. **97**, 1191 (1955).
[2] Mark, McClelland, and Goodman, Phys. Rev. **98**, 1245 (1955).
[3] A. Bohr and B. R. Mottelson, Kgl. Danske Videnskab Selskab. Mat.-fys. Medd. **27**, No. 16 (1953).
[4] L. Fitch and J. Rainwater, Phys. Rev. **92**, 789 (1953); L. I. Schiff, Phys. Rev. **92**, 988 (1953).

K-Meson Mass from a K-Hydrogen Scattering Event*

WARREN W. CHUPP, GERSON GOLDHABER, SULAMITH GOLDHABER, WILLIAM R. JOHNSON AND JOSEPH E. LANNUTTI

Radiation Laboratory, Department of Physics, University of California, Berkeley, California

(Received May 19, 1955)

ONE of the basic problems in the classification and understanding of K-mesons is the relation between the various modes of decay ($K_{\tau 2}\equiv\theta^+$, $K_{\mu 2}$, $K_{\mu 3}$, K_{e3}, and τ). There has been much discussion recently[1] on the K-meson mass and to what extent the masses of the various K-mesons (or perhaps just different decay modes) differ from that of the τ meson (965.3 m_e).

In this connection, we want to report here on a K_L^+-particle which underwent a scattering from hydrogen in a nuclear emulsion stack and thus enabled us to obtain a rather good mass measurement. The mass value obtained as the weighted mean of two independent methods is 973 ± 12 m_e.

The emulsion stack (Ilford G.5, 600μ pellicles) was exposed to the focused K^+, beam[2] of the Bevatron in a momentum channel of 411 ± 12 Mev/c (proper time of flight of $\sim10^{-8}$ sec). The incoming track was picked 4 cm after entering the stack on the basis of the expected grain density for K-particles of the appropriate momentum. On following the track, the scattering event (Fig. 1) was found after 5.16 cm of travel in the emulsions.[3] Both of the two outgoing tracks end in the emulsion. One is a proton of 2.427 ± 0.034 mm range (variable-cell-length scattering measurements give a mass of 0.96 ± 0.3 M_p). The other is a K-particle of 32.21 ± 0.54 mm range which emits a secondary on coming to rest. The secondary particle is emitted at a dip angle of 36° and leaves the stack after traversing seven pellicles with a path length of 7.1 mm in the stack. Grain density and blob density measurements have been made on the track of the secondary relative to 280 ± 20 Mev π mesons. (See Table I.) The average values obtained are $g/g_0=1.25\pm0.03$ and $b/b_0=1.17\pm0.03$. These measurements permit us to exclude a τ' meson ($\tau'\rightarrow\pi^++2\pi^0$) almost with certainty as the τ' can give a π^+ meson of energy up to $E_{max}=53.0$ Mev corresponding to a $g/g_0=1.63$ and a $b/b_0=1.37$.[4,5] Our measured values are 13 and 7 times their respective standard deviations from the latter values. The measurements on the scattering event (see Fig. 1) are summarized in Table II. The errors for the angular measurements include observational errors and the effect of multiple scattering. Since all dip angles in the scattering event are smaller than 5°, errors in the dip angle measurements and distortion effects hardly influence the space angle. The maximum deviation of one prong from the plane of the other two is 0.45° which is of the same order as the deviation evaluated from the errors in the

TABLE I. Measurements on the secondary of the scattered K-particle.[a]

Emulsion number	Relative grain density[b] g/g_0	Relative blob density[b] b/b_0
31–12	1.16±0.08	1.03±0.08
31–13	1.19±0.09	1.15±0.09
31–14	1.31±0.09	1.19±0.09
31–15	1.43±0.09	1.33±0.09
31–16	1.38±0.09	1.23±0.09
31–17	1.15±0.07	1.18±0.09
31–18	1.14±0.08	1.16±0.09
Average	1.25±0.03	1.17±0.03

[a] The grain density and blob density measurements were normalized to minimum ionization by comparison with 280±20 Mev π mesons of 1.007 ±0.005 minimum in each emulsion.
[b] These values include a dip correction by the cosine of the dip angle.

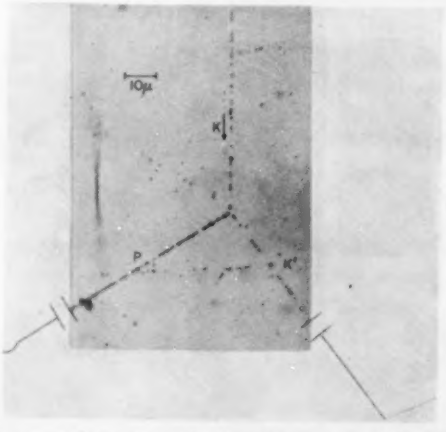

FIG. 1. A photomicrograph of a K-hydrogen scattering event $E_K=102$ Mev. Both outcoming particles come to rest (endings are sketched in) in the emulsion. $R_{K'}=32.21$ mm, $R_p=2.427$ mm (Observer: S. Livingston, Photomicrograph: R. P. Michaelis).

TABLE II. Measurements on the scattering event.

Measurement \ Particle	Incident K-particle	Scattered K-particle (K')	Recoil proton (p)
Dip angle	$+4.78°\pm0.33°$	$-3.85°\pm0.27°$	$-1.04°\pm0.07°$
Projected angle	0°	$38.9°\pm0.18°$	$59.1°\pm0.34°$
Range	···	32.07 ± 0.54 mm	2.427 ± 0.034 mm
Range (corrected for dip)	···	32.21 ± 0.54 mm	2.427 ± 0.034 mm
Space angles (computed)	0°	$38.80°\pm0.2°$	$59.12°\pm0.35°$

measurements. The actual mass determination was carried out by two independent methods.

a. *From the scattered K-particle range and conservation of transverse momentum.*—In this method two sets of the quantity $\beta_{K'}\gamma_{K'}$ are obtained for assumed K-particle mass values. (1) The quantity $R_{K'}/M_K$ is a function of the velocity of the K-particle only. Thus from the measured value of $R_{K'}$ we have obtained a set of values of $\beta_{K'}\gamma_{K'}$ as a function of the mass of the K-particle. (Curve A, Fig. 2.) (2) The momentum of the scattered K-particle ($P_{K'}=289.15\pm1.85$ Mev/c) is determined by transverse momentum balance from the proton momentum ($P_p=211.08\pm0.91$ Mev/c) which has been obtained from the proton range. Using this momentum for the K-particle, another set of values of $\beta_{K'}\gamma_{K'}(=P_{K'}/M_Kc)$ as a function of K-particle mass is calculated. (Curve B, Fig. 2.) The intersection of the bands formed by curves A and B, together with their resoective errors, gives the K-particle mass as $972\pm12\ m_e$.

In passing from ranges to momenta we have used the tables of Barkas and Young[6] which are based on Vigneron's calculations.[7] This method utilizes the range and space angles of both outcoming particles and is principally sensitive to the errors in the range measurements. As two range measurements are used, uncertainties in the range-energy relation and emulsion composition tend to cancel out.

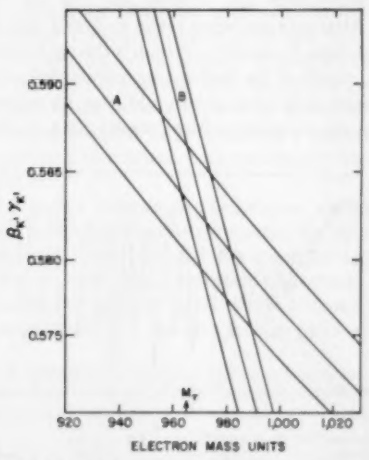

FIG. 2. A plot of $\beta_{K'}\gamma_{K'}$ as a function of K-particle mass. Curve A is based on the scattered K-particle range $R_{K'}=32.21$ mm. Curve B is based on the scattered K-particle momentum $P_{K'}=289.15$ Mev/c which is obtained from the recoil proton range. The intersection of curves A and B together with their error limits defines the K-particle mass as $972\pm12\ m_e$. The mass of the τ meson M_τ is shown for comparison.

b. *From the conservation of energy and momentum in the scattering event.*—In this method the K-particle mass was expressed analytically in terms of the recoil proton energy (from proton range) and the two space angles only. The resulting mass is $984\pm79\ m_e$. The much larger error inherent in this method is mainly due to the very strong dependence on the error in the angular measurement. The agreement between the two mass determinations together with the coplanarity check and the absence of a recoil or electron at the scattering center (Fig. 1) leads us to believe that our interpretation of the event as a K-hydrogen scattering is correct.

We wish to thank Professor E. Segrè for many helpful discussions.

* This work was performed under the auspices of the U. S. Atomic Energy Commission.

[1] See for instance the summary by B. Rossi of the papers presented on this topic in the Proceedings of the Fifth Annual Rochester Conference on High-Energy Physics (University of Rochester Press, Rochester, to be published).

[2] Kerth, Stork, Birge, Haddock, and Whitehead, Bull. Am. Phys. Soc. **30**, No. 3, 41 (1955).

[3] A comparison between the momentum of the incoming particle as obtained from the magnetic momentum selection and from the kinematics of the scattering event affords an additional check on its identity as a K-particle. The incoming particle has a momentum of 411 ± 12 Mev/c as defined by its $H\rho$. After 5.16 cm of travel in the emulsion this momentum is reduced to 316 ± 24 Mev/c in agreement with $P_K=333.71\pm2.1$ Mev/c as obtained from the kinematics of the collision.

[4] R. M. Sternheimer, Phys. Rev. **91**, 256 (1953).

[5] J. R. Fleming and J. J. Lord, Phys. Rev. **92**, 511 (1953). Also J. R. Fleming, M.S. thesis, University of Washington, 1954 (unpublished).

[6] W. H. Barkas and B. M. Young, University of California Radiation Laboratory Report UCRL-2579 (revised) (unpublished).

[7] L. Vigneron, J. physiol. (Paris) **14**, 145 (1952).

Mass Measurement and Excited States of F^{21}†

NELSON JARMIE

University of California, Los Alamos Scientific Laboratory, Los Alamos, New Mexico

(Received May 31, 1955)

NEW masses of the isotopes of light nuclei have been of interest particularly to those working with systematic studies. We wish to report that we have experimentally determined that F^{21} is heavy-particle-stable and has a mass defect of 6.125 ± 0.030 Mev or an atomic mass of 21.005703 ± 0.000025 amu. Alpha particles from the reaction $O^{18}(t,\alpha)N^{15}$ were used for the energy calibration. Excited states of F^{21} are indicated at 0.33, 1.11, 1.84, and 2.16 Mev. Masses used in the calculations were taken from the review article of Ajzenberg and Lauritsen.[1]

This information was obtained from an experiment designed to measure the energy levels of O^{18} by observing alpha particle groups from the reaction $F^{19}(t,\alpha)O^{18}$. Narrow proton groups, presumably from the reaction $F^{19}(t,p)F^{21}$, were observed that did not correspond to any level possible from any of the common contaminants (O, C, N, etc.) or to any level observed in any background run. The groups were obtained by bombarding thin evaporated targets of CaF_2 or PbF_2 with a 1.82-Mev triton beam from one of our 2.5-Mev Van de Graaff accelerators and analyzing the reaction products at 90° with a Cal-Tech type 16-inch double-focusing magnetic spectrometer.

If one plots the masses and half-lives of nuclei differing from F^{21} by one or more alpha particles against the mass number as the abscissa, one gets rough curves with which one might empirically predict the characteristics of F^{21} and other such nuclei. It is of interest that the measured mass of F^{21} is consistent with this curve. The predicted value of the half-life of F^{21} from such considerations is 100 to 200 sec.

A detailed report of this work, verification, and more accurate values of the excited states, and information on O^{18} will be published in the future.

† Work performed under the auspices of the U. S. Atomic Energy Commission.

[1] F. Ajzenberg and T. Lauritsen, Revs. Modern Phys. **27**, 157 (1955).

Elastic Scattering of 48.2-Mev Alpha Particles*

ROBERT E. ELLIS AND LARRY SCHECTER
Radiation Laboratory, University of California, Berkeley, California
(Received May 9, 1955)

IN view of the recent interest in the elastic scattering of alpha particles by heavy nuclei,[1–5] it seems desirable to report the results of investigations that have been under way here for some time.

The angular distributions of 48.2-Mev alpha particles (from the 60-inch cyclotron at Crocker Laboratory in Berkeley) elastically scattered by Au and Ag nuclei have been investigated in considerable detail for angles between 7° and 135° in the laboratory system (Figs. 1 and 2).

The 36-inch scattering chamber[6] was used, and the scattered particles detected by a proportional counter telescope. The long-time reproducibility of data was excellent, so there was no difficulty in normalizing from run to run. The angular resolution is estimated to be ±0.75 degree. No background difficulties were encountered below 90 degrees. At the wider angles the low yields made it difficult to accumulate statistics,

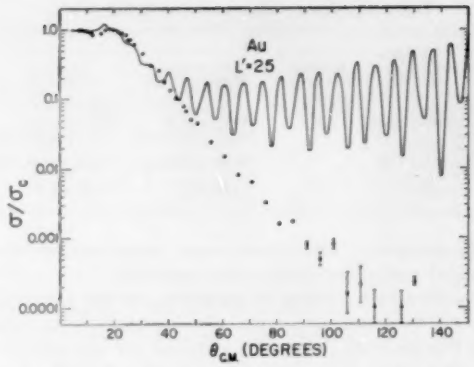

FIG. 1. Angular distribution (relative to Coulomb scattering) of elastically scattered alpha particles from Au. The curve represents the distribution predicted by Blair's sharp cut-off model.

but we feel sure that there is no appreciable rise in the cross sections.

The most striking features in these distributions are the departure from Coulomb scattering by factors of 10^2 to 10^4 at angles beyond 25°, and the structure exhibited in the silver curve between 20° and 60°. According to Blair's model[2] these may be attributed to the effect of collisions by the incident alpha particle with the nucleus. At these energies the incident particles interact strongly with the nucleus in spite of the Coulomb barrier, and it is reasonable to expect that a satisfactory theoretical explanation of these detailed distributions may shed light on the form of the interaction potential. As the figures show, the sharp cut-off model reproduces the general features for forward angles. Attempts are being made to find a satisfactory fit to the data by modifying Blair's theory to include a gradual cutoff of the interaction radius, following the suggestions of Wall *et al.*[4] In addition, an approach is being made using an optical model with a potential

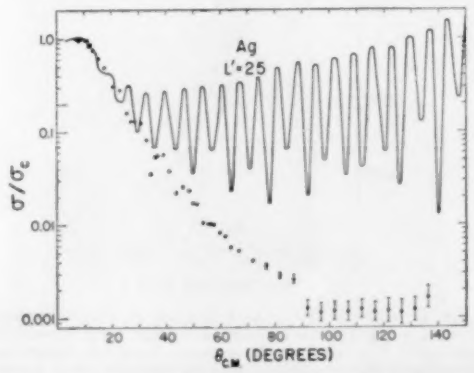

FIG. 2. Angular distribution of (relative to Coulomb scattering) elastically scattered alpha particles from Ag. The curve represents the distribution predicted by Blair's sharp cut-off model.

having real and imaginary parts. The complexity of the analysis has been mitigated by the cooperation of the electronic computing section at the University's Livermore laboratory.

Work is continuing in order to extend the distributions to wider angles, and other targets will be bombarded in order to determine the possible effects of shell structure on the interaction.

* This work was done under the auspices of the U. S. Atomic Energy Commission.

[1] G. W. Farwell and H. E. Wegner, Phys. Rev. **95**, 1212 (1954).
[2] J. S. Blair, Phys. Rev. **95**, 1218 (1954).
[3] K. Izumo, Progr. Theoret. Phys. (Japan) **12**, 549 (1954).
[4] Wall, Rees, and Ford, Phys. Rev. **97**, 726 (1955).
[5] Wegner, Eisberg, and Igo, Bull. Am. Phys. Soc. **30**, No. 3, 40 (1955).
[6] G. E. Fischer, Phys. Rev. **96**, 704 (1954).

Lifetime of the 279-kev Excited State of Tl^{203}

H. DE WAARD
Institute of Physics, The University of Upsala, Upsala, Sweden
(Received June 16, 1955)

A HALF-LIFE of $(1.2\pm0.3)\times10^{-10}$ sec was found for the 279-kev level of Tl^{203} from measurements of delayed coincidences between betas announcing this level and gammas de-exciting it.

For these measurements, an automatically recording "fast-slow" coincidence arrangement was used, in the fast section of which a unit with helical delay line of the type described by Bell *et al.*[1] had been incorporated. Samples of Hg^{203}, mounted on aluminum backings which absorb the electrons, were sandwiched between two stilbene crystals of equal thickness (0.5 cm) and area (1.5 cm^2), each attached to a 1P21 photomultiplier. The crystal at the absorber side detects the gammas in coincidence with betas accepted by the other crystal. Pulse-height selectors in both channels transmit pulses corresponding to electron energies roughly between 75 and 150 kev.

For such low energies, the accuracy of measurements of very short lifetimes is often seriously impaired by instrumental imperfections. In order to reduce the influence of such effects as much as possible, a "self-comparison-comparison" method was adopted in which the centroid shifts of self-comparison pairs of delayed coincidence plots obtained with samples of Hg^{203} were compared with those of a suitable reference source. The self-comparison pairs are obtained by recording first one run and then, after turning the source plus absorber assembly around, another run.

In the present case, thorium B is very suitable as a reference source because the energies of its strongest coincident radiations are not too much different from those of mercury (for Hg^{203}: $E_{\beta\,max}=215$ kev, $E_\gamma=279$ kev; for ThB: $E_{\beta\,max}=340$ kev, $E_\gamma=238$ kev) and because the lifetime of the 238-kev level excited in the decay of ThB is known to be very short: Graham and Bell[2] set an upper limit of 2×10^{-11} sec; Knowles[3] even gives the upper limit as 2×10^{-13} sec. This means that the centroid shift of self-comparison pairs obtained with this source is almost exclusively caused by instrumental effects. The experimental half-life of the 279-kev level of Tl^{203} is therefore given as 0.346 times the difference of the centroid shifts of self-comparison pairs obtained with samples of Hg and ThB.

In the experiments with mercury, unwanted prompt coincidences may occur between x-rays emitted by Tl^{203} nuclei after conversion processes and gammas or conversion electrons. They may also be caused by two successive Compton scatterings. Such coincidences would reduce the centroid shift to a value smaller than the lifetime of the investigated level. From measurements with suitable x-ray or electron absorbers at the appropriate side of the sample it was found, however, that the total contribution of prompt coincidences amounts to only about 8% of the total coincidence counting rate. To account for this effect the measured half-life was increased by 8%.

Combining the measured half-life with experimental conversion data, e.g., those found by Marty,[4] a lifetime $\tau_\gamma=(2.2\pm0.6)\times10^{-10}$ sec for decay by gamma-emission results. There is an appreciable difference between the present result for the lifetime and the value $\tau_\gamma=(5.5\pm1.8)\times10^{-10}$ sec obtained by Barloutaud *et al.*[5] from a measurement of the cross section for Coulomb excitation.

If we assume that the 279-kev transition is 30% magnetic dipole and 70% electric quadrupole, which is in agreement with most measurements,[4,6] partial lifetimes $\tau_\gamma(M1)=(7.2\pm1.3)\times10^{-10}$ sec and $\tau_\gamma(E2)=(3.1\pm0.6)\times10^{-10}$ sec result for these modes of decay. A comparison with Weisskopf's formula shows that the $M1$ transition is retarded by a factor $f=480$. This value of f is of the same magnitude as that found by Graham and Bell[2] and by de Waard and Gerholm[7,8] for a number of $M1$ transitions which according to the shell-model should be l-forbidden ($\Delta l=2$). In this way, the shell model assignments $d_{\frac{3}{2}}$ and $s_{\frac{1}{2}}$ for the 279-kev level and the ground state are confirmed. The $E2$ transition on the other hand is sped up by a factor $F=10$ compared with Weisskopf's estimate. This enhancement is a measure of the part played by collective phenomena. For a nucleus with only one hole in the

TABLE I. Comparative results of lifetime measurements by resonance fluorescence and delayed coincidence methods.

Nucleus	Level (kev)	Lifetime τ_γ in 10^{-10} sec units Res. fluor.	Del. coinc.
Pr^{141}	145	35 ±10[a]	39 ±4[b]
Hg^{199}	411	0.33$\pm$ 0.03[c]	0.15$\pm$0.25[d]
Tl^{203}	279	10 $\pm$ 4[b]	2.2 $\pm$0.6

[a] See reference 10.
[b] See reference 7.
[c] See reference 9.
[d] See reference 11.

closed proton shell ($Z=82$), the value of F appears to be rather large.

A noteworthy discrepancy exists with the value $\tau_\gamma=(10\pm4)\times10^{-10}$ sec found by Metzger[9] from three independent types of nuclear resonance scattering experiments. Of three cases known to the author and given in Table I[7,9-11] where the lifetime of a level has been obtained both from its width by nuclear resonance scattering and directly by the delayed coincidence technique, only in the present case is there such a large difference.

Attempts to find a theoretical explanation for this discrepancy have thus far been unsuccessful. All conditions for the validity of the formula that relates the resonance scattering cross section to the lifetime of the level appear to be fulfilled except that of noncoherence of resonant and other types of scattering. The measured scattering cross section might be reduced by such coherence if the phase angle between resonant and nonresonant (in particular, Rayleigh) scattering is not zero. In the present cases, however, there is spherical symmetry around the nucleus of the great majority of the electrons that participate in Rayleigh scattering, so that this phase angle should be very near zero.

The author is much indebted to Professor Kai Siegbahn for his active interest in this work. Cordial thanks are due to Mr. T. R. Gerholm of this Institute for discussions of the experimental method and to Dr. H. J. Groenewold of the Institute of Physics of The University of Groningen, Netherlands, for his comments on theoretical matters. A stipend of the Netherlands Organization for Pure Research (Z.W.O.) during part of the work is gratefully acknowledged.

[1] Bell, Graham, and Fetch, Can. J. Phys. **30**, 35 (1952). Sincere thanks are due to Dr. R. E. Bell for constructing this coincidence unit and for his useful remarks regarding its use.
[2] R. L. Graham and R. E. Bell, Can. J. Phys. **31**, 377 (1953).
[3] J. W. Knowles, Phys. Rev. **94**, 795 (1954); Ref. card Nucl. Sci. Abstr. No. 43-5-153.
[4] N. Marty, Compt. rend. **240**, 291 (1955).
[5] Barloutaud, Grjebine, and Riou, Compt. rend. **240**, 1207 (1955).
[6] J. B. Swan and R. D. Hill, Australian J. Phys. **6**, 371 (1953).
[7] H. de Waard and T. R. Gerholm, Physica (to be published).
[8] T. R. Gerholm and H. de Waard, Physica (to be published).
[9] F. R. Metzger, Proceedings of the 1954 Glasgow Conference on Nuclear and Meson Physics (Pergamon Press, London, 1955), p. 201; F. R. Metzger and W. B. Todd, Phys. Rev. **95**, 627 (1954).
[10] F. R. Metzger, Bull. Am. Phys. Soc. **30**, No. 3, 13 (1955).
[11] R. L. Graham and R. E. Bell, Phys. Rev. **84**, 380 (1951).

Mesonic Decay of a H_1^4 Nucleus

Ö. Haugerud and S. O. Sörensen
Institute of Physics, University of Oslo, Oslo, Norway
(Received June 15, 1955)

FROM the cosmic-ray laboratory of the University of Bristol[1] an event has recently been reported which could be interpreted as the mesonic decay of a H_1^4 nucleus containing a bound Λ^0 particle in place of a neutron, according to the mode

$$H_1^4 \rightarrow He_2^4+\pi^-+Q(\cong 55 \text{ Mev}).$$

A very similar event has been observed in our laboratory. It was recorded in a stack of stripped Ilford *G*5 emulsions, each 600μ thick, exposed at high altitude by means of free balloons during the Sardinian Expedition, 1953. A photomicrograph of the event is shown in Fig. 1.

From a star, A, of type $6+0p$, is emitted a slow unstable particle B which comes to rest after 50μ and gives rise to a two-prong star C. The prong D is a short black track of range 8.3μ. The other prong E is due to a negative π meson which stops after 37.61 mm and produces a sigma star. The two prongs are colinear within the errors of measurements. Using the range-energy relations calculated by Baroni *et al.*,[2] the kinetic energies and momenta of the He_2^4 nucleus and of the π meson are 2.4 Mev, 134 Mev/c and 52.1 Mev, 131 Mev/c, showing momentum balance between the two tracks within the errors of measurement. These values compare very well with the corresponding ones in the Bristol event: 2.5 Mev, 137 Mev/c and 53.0 Mev, 133 Mev/c, thus strongly supporting the interpretation of the process as a disintegration of an excited H_1^4 fragment.

Using the values 8.5 Mev and 28.3 Mev, respectively, for the binding energies of the H_1^3 and He_2^4, and 36.9 Mev for the Q-value in the disintegration of the Λ^0 particle, we obtain for the binding energy of the Λ^0

FIG. 1. Photomicrograph of the event.

particle in the H_1^4 nucleus:

$$\text{B.E.}(\Lambda^0)=36.9+28.3-8.5-2.4-52.1=2.2 \text{ Mev.}$$

This value is to be considered preliminary due to the uncertainty in the application of range-energy relations for π mesons at high energies.

The authors are indebted to Professor J. Holtsmark and Professor R. Tangen for providing laboratory facilities and to the Royal Norwegian Council for Scientific and Industrial Research for financial support.

[1] "*G*-Stack Collaboration Experiment, 1954." Preliminary report from the Universities of Bristol, Dublin, Genova, Milano, and Padova (unpublished).
[2] G. Baroni *et al.*, Bureau of Standard CERN Bull. No. 9 (unpublished).

Phenomenological Evidence for Polarization of 310-Mev Protons by Elastic Scattering in *G*5 Emulsion*

JEROME I. FRIEDMAN

Institute for Nuclear Studies, The University of Chicago, Chicago, Illinois

(Received May 31, 1955)

THE first measurements[1-4] of polarization of high-energy protons by nuclear scattering caused some discussion as to whether these high polarizations were due to elastic or quasi-free nucleon scattering. At that time, it was suggested by Fermi that a phenomenological test for elasticity could be applied to polarization measurements in nuclear emulsion. The analysis of elastically scattered protons in nuclear emulsion shows them to be highly polarized according to the data presented here. In addition, data are now being collected to measure the polarization due to inelastic scattering.

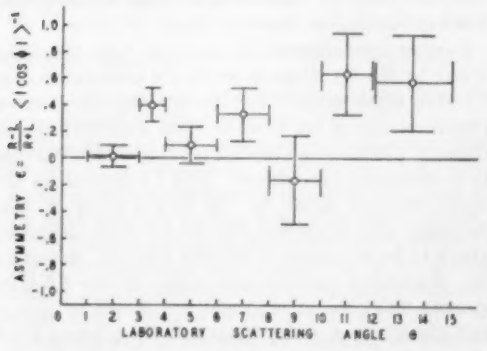

FIG. 1. The asymmetry of 64% polarized protons elastically scattered in *G*5 emulsion. R and L are the number of scatterings to the right and left, ϕ is the azimuthal angle of scattering, and $\langle|\cos\phi|\rangle$ is the average of $|\cos\phi|$ over-all events. The factor $\langle|\cos\phi|\rangle^{-1}$ is present because the data consist of scatterings over a range of ϕ. Also, $\epsilon=P_0P(\theta)$, where P_0 is the polarization of the incoming beam and $P(\theta)$ is the polarization caused by elastic scattering in *G*5 emulsion.

A 64% polarized beam of 310-Mev protons from the University of Chicago synchrocyclotron was scattered in 600μ *G*5 nuclear emulsion. The initial polarization was measured as previously described.[5] The emulsion was scanned along the track for elastic scatterings between 1° and 15°. These appear as kinks in the tracks with no other observable prongs. Recoil nuclei are not observable. The efficiency for finding scatterings down to 2° was nearly 100% The faster technique of area scanning was attempted, but was not found useful because of its low efficiency in detecting this type of event.

Inelastic scatterings in which one or more neutrons come off, in addition to the incident proton, also appear as kinks in the tracks. These had to be rejected or subtracted from the observed elastic scatterings. Events were rejected in which there was an energy loss, as measured by grain counting, greater than that consistent with the statistics, namely ± 30 Mev.

To determine, roughly, what percentage of the remaining scatterings were inelastic, another method was used. An examination was made of all two-prong stars which had one track within 30 Mev of the beam energy and 15° of the beam direction. Proton-proton scatterings were excluded from this group. From the energy of the second prong of each such star, one can estimate, roughly, from evaporation theory, the number of inelastic scatterings included in the data. The subtraction of this number from the total number of elastic scatterings changes the average value of the polarization in the angular interval from 3° to 15° by less than 0.03.

Scatterings in which the recoil nucleus is left intact, but in an excited state, could not be distinguished from true elastic scatterings in this experiment. However, this effect is expected to be relatively small at small angles.

Between 1° and 15°, 471 elastic scatterings were found; 284 of them were between 3° and 15°, where nuclear scattering predominates. More than 80% of the cross section for elastic scattering in *G*5 emulsion is due to silver and bromine. These, however, are fairly similar in terms of diffraction scattering, because their nuclear radii differ only by about 10%.

In Fig. 1, the asymmetry ϵ is shown as a function of the scattering angle. The events are grouped into angular intervals as indicated. The average polarization in the angular region between 3° and 15° is 0.44 ± 0.13. Errors are compounded from statistical error and from an uncertainty in the subtraction of inelastic events which makes less than a 0.01 contribution to the total error.

This experiment gives phenomenological evidence for a high polarization due to elastic scattering, a result in good agreement with previous measurements.[3-6]

Little can be said about the detailed shape of the ϵ vs θ curve because of the large statistical errors.

* Research supported by a joint program of the Office of Naval Research and the U. S. Atomic Energy Commission.

[1] Oxley, Cartwright, and Rouvina, Phys. Rev. **93**, 806 (1954).
[2] Chamberlain, Segrè, Tripp, Wiegand, and Ypsilantis, Phys. Rev. **93**, 1430 (1954).
[3] Marshall, Marshall, and de Carvalho, Phys. Rev. **93**, 1431 (1954).
[4] J. M. Dickson and D. C. Salter, Nature **173**, 946 (1954).
[5] de Carvalho, Marshall, and Marshall, Phys. Rev. **96**, 1081 (1954).
[6] Chamberlain, Segrè, Tripp, Wiegand, and Ypsilantis, Phys. Rev. **95**, 1105 (1954).

New Elements Einsteinium and Fermium, Atomic Numbers 99 and 100

A. Ghiorso, S. G. Thompson, G. H. Higgins, and G. T. Seaborg, *Radiation Laboratory and Department of Chemistry, University of California, Berkeley, California*

M. H. Studier, P. R. Fields, S. M. Fried, H. Diamond, J. F. Mech, G. L. Pyle, J. R. Huizenga, A. Hirsch, and W. M. Manning, *Argonne National Laboratory, Lemont, Illinois*

and

C. I. Browne, H. L. Smith, and R. W. Spence, *Los Alamos Scientific Laboratory, Los Alamos, New Mexico*

(Received June 20, 1955)

THIS communication is a description of the results of experiments performed in December, 1952 and the following months at the University of California Radiation Laboratory (UCRL), Argonne National Laboratory (ANL), and Los Alamos Scientific Laboratory (LASL), which represent the discovery of the elements with the atomic numbers 99 and 100.

The source of the material which was used for the first chemical identification of these elements was the Los Alamos Scientific Laboratory which provided uranium which had been subjected to a very high instantaneous neutron flux in the "Mike" thermonuclear explosion (November, 1952). Initial investigations at ANL showed the presence in this material of the new isotope Pu^{244},[1] and investigations at ANL and LASL showed the presence of Pu^{245} and Am^{245},[2] pointing to the presence of neutron excess isotopes in greater abundance than expected.

This led the UCRL group to look for isotopes of transcalifornium elements in material from the same source. Samples were subjected to chemical procedures to separate the actinide from the lanthanide fraction,[3] tracer Cf^{245} (36-hour, 6.75-Mev alpha particle[4]) was added and a separation of the tripositive actinides was effected using the cation-exchange resin Dowex-50 and elution at 87°C with ammonium citrate solution.[5] These experiments showed the elution in a transcalifornium position of a 6.6-Mev alpha activity and hence proved conclusively that a new (transcalifornium) element had been found. Before the atomic number identification for the newly discovered element was completed (i.e., the correct choice between atomic numbers 99 and 100 had been made) a tentative assignment to "100^{254}" was made and this information was communicated to the ANL and LASL Laboratories. Immediately following this, further ion-exchange elution separations were carried out at both UCRL and ANL resulting in essentially simultaneous identification of the 6.6-Mev alpha activity as belonging to the element with atomic number 99 (i.e., elution in the eka-holmium position). The results of these definitive elution experiments are shown in Fig. 1.

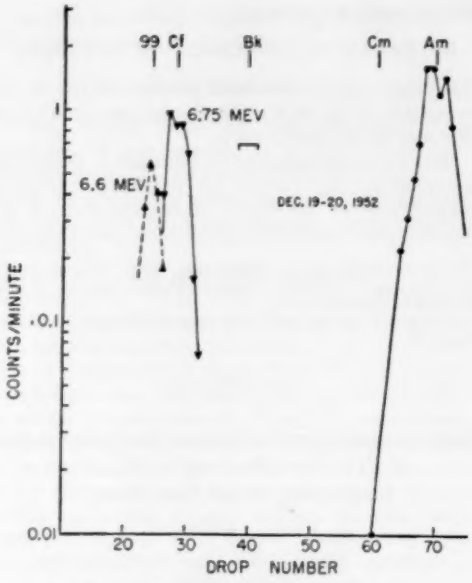

FIG. 1. Elution of element 99 relative to californium (citrate eluant).

Further measurements on material from the same source by the LASL group led to the observation of a 7.1-Mev alpha activity (at an intensity of about 4 percent of that of the 6.6-Mev alpha activity) without chemical identification beyond proving that it was due to a transplutonium element. This 7.1-Mev alpha activity was first shown by the UCRL group in ion-exchange elution experiments of the type described above to be an isotope of element 100 (i.e., elution in the eka-erbium position just ahead of the 6.6-Mev element 99 alpha activity) and was shown to have a half-life of about a day sustained by a longer-lived element 99 parent. This establishment of the isotope responsible for the 7.1-Mev alpha activity as having the atomic number 100 was confirmed in a similar experiment by the ANL group somewhat later. The elution data for the experiments that established this atomic number are shown in Fig. 2. The californium, berkelium,

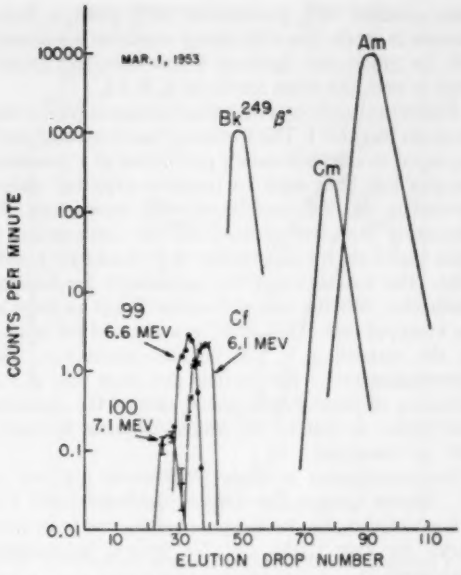

FIG. 2. Elution of element 100 relative to other actinide elements (citrate eluant).

and curium radioactivities will be discussed in a forthcoming publication.

Isotopic assignments which were made as the result of this early work were largely confirmed by the later work on the intense neutron irradiation[6-9] of Pu^{239}. Thus it can be said that the mass number for the 6.6-Mev 99 alpha activity is 253, corresponding to the decay sequence $Cf^{253} \xrightarrow[\sim 20\ day]{\beta^-} 99^{253}$ (~20-day, 6.6-Mev alpha particle), the Cf^{253} originating from the beta decay of U^{253} and daughters. Also, the mass number for the 7.1-Mev 100 alpha activity is 255 corresponding to the decay sequence $99^{255} \xrightarrow[\sim 30\ day]{\beta^-} 100^{255}$ (~16-hour, 7.1-Mev alpha particle), the 99^{255} originating from the beta decay of U^{255} and daughters.

We suggest for the element with the atomic number 99 the name einsteinium (symbol E) after Albert Einstein, and for the element with atomic number 100 the name fermium (symbol Fm), after Enrico Fermi.

The primary acknowledgment is to the personnel of LASL for the design and construction of the thermonuclear (Mike) weapon, which gave rise to the extreme neutron flux required to produce the very heavy nuclides. We wish to thank H. F. Plank for his very able direction of the sampling operation. In addition the ANL group wishes to acknowledge helpful discussions with A. Turkevich and its indebtedness to D. F. Peppard and his group (George Mason, John Maier, and Richard Wallace), who isolated a heavy element fraction. The LASL group wishes to acknowledge its gratitide to R. A. Penneman and personnel of his group for their cooperation and the use of their pulse analyzer. The UCRL group wishes to acknowledge the cooperation of K. Street, Jr., W. W. T. Crane, L. R. Zumwalt, L. B. Werner, N. E. Ballou, and I. J. Russell in providing samples, and to thank N. B. Garden, Rosemary Barrett, and R. A. Glass for active assistance.

[1] Hess, Pyle, Fried, and Ingram (to be published).
[2] Asprey, Browne, Engelkemeir, Fields, Fried, Pyle, Smith, Spence, and Stevens (to be published).
[3] K. Street, Jr., and G. T. Seaborg, J. Am. Chem. Soc. **72**, 2760 (1950).
[4] Ghiorso, Thompson, Street, and Seaborg, Phys. Rev. **81**, 154 (1951).
[5] See, e.g., Thompson, Street, Ghiorso, and Seaborg, Phys. Rev. **80**, 790 (1950).
[6] Thompson, Ghiorso, Harvey, and Choppin, Phys. Rev. **93**, 908 (1954).
[7] Harvey, Thompson, Ghiorso, and Choppin, Phys. Rev. **93**, 1129 (1954).
[8] Studier, Fields, Diamond, Mech, Friedman, Sellers, Pyle, Stevens, Magnusson, and Huizenga, Phys. Rev. **93**, 1428 (1954).
[9] Fields, Studier, Mech, Diamond, Friedman, Magnusson, and Huizenga, Phys. Rev. **94**, 209 (1954).

Multiple Meson Production in Emulsions Exposed to the Bevatron Beam*†

WILLIAM R. JOHNSON

Radiation Laboratory, Department of Physics, University of California, Berkeley, California

(Received May 31, 1955)

MEASUREMENTS have been made on the shower-particle production in nuclear stars formed in 600-micron Ilford G.5 stripped emulsions. Production

TABLE I. Observed and calculated shower-particle multiplicity percentages—Fermi model.

Energy in Bev		n_s	Extension of Fermi's calculations[a]	Experimental observations
3.2		0	20	42
		1	47	28
		2	29	25
		3	4	4
		4	...	1
	Av	$\bar{n}_s$	1.17	0.94±0.09
4.8		0	16	25
		1	41.5	38
		2	35	20
		3	7.5	17
		4	...	0
	Av	$\bar{n}_s$	1.34	1.3±0.11
5.7		0	14	17
		1	38	31
		2	38	30
		3	10	18
		4	...	3
		5	...	1
	Av	$\bar{n}_s$	1.44	1.62±0.11

[a] In the computation of the percentages for each value of n_s the tabulated number represents the shower tracks that would actually be observed, not the number of pions created. The numbers in column 3 for $n_s=2$ include the following production schemes: $pp+-$, $nn++$, $pp+-0$, $nn++0$, and $pn+-0$. (The $+$, $-$, and 0 refer to the charges of the created mesons.)

has been investigated at three beam energies: 3.2, 4.8, and 5.7 Bev. At each energy 114 events that had beam protons for primaries were found by area scanning.

A shower particle is defined as one whose track has a grain density less than 1.4 times minimum.[1] This upper limit of grain density includes tracks of created pions and recoil protons of kinetic energies greater than 80 Mev and 500 Mev, respectively. The assumption is made, as in similar cosmic-ray studies,[1] that the number of emitted pions with energies below 80 Mev is small and is equal, in the first approximation, to the number of emitted protons with energies greater than 500 Mev.

The average values of the numbers of shower and heavy particles, $\bar{n}_s$ and $\bar{N}_h$, are plotted in Fig. 1 and the indicated errors are standard deviations based on the number of tracks recorded. For comparison, results of Camerini *et al.*[1] are dashed lines. There is fair agreement with the cosmic-ray results, but values are somewhat lower. This might be expected because cosmic-ray primaries were an admixture of pions and protons, and a pure proton beam was used in this experiment. The ratio of the amount of energy available for interaction (in the center-of-mass system) with an incoming pion to that available with an incoming proton of the same energy reduces to

$$\frac{W_{\pi\ \mathrm{inc}}}{W_{p\ \mathrm{inc}}} \cong \frac{(1+2\gamma_p)^{\frac{1}{2}}-1}{(2+2\gamma_p)^{\frac{1}{2}}-2},$$

where $\gamma_p = E_p/M_pc^2$.

At an energy of 6 Bev the ratio is 1.65. If a primary beam contains 50% protons and 50% pions, a linear increase in production with energy available is assumed, and the production figure at 6 Bev from this experiment is used, the value found for $\bar{n}_s$ is 2.4.

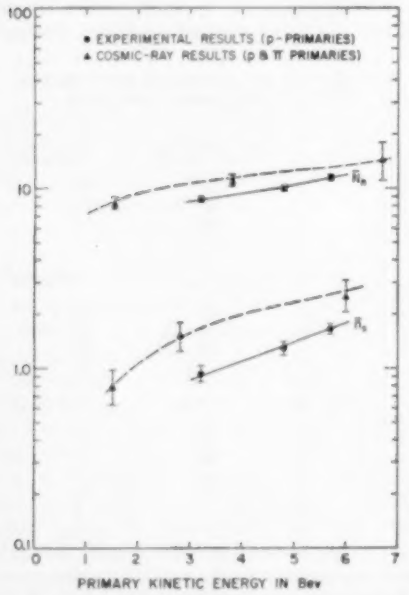

FIG. 1. Comparative plots of the average number of heavy prongs and the average number of shower particles *versus* kinetic energy of primary particles.

Theoretical and observed values of meson production are given in Table I. The statistical model which Fermi[2] employed to calculate meson production at Cosmotron energies has been used to compute expected meson production at the energies of this experiment. In tabulating expected probabilities the assumption is made that there is a like number of $p-n$ and $p-p$ collisions. The model shows fair agreement for average production, but the rate of increase is not as large as the observed rate. This could be accounted for in part by the restriction, $n_s \leq 3$, in the calculations. The observations at 5.7 Bev include five stars with $n_s > 3$. Exclusion of these events would reduce the observed multiplicity to 1.46 ± 0.12, which compares favorably with the computed 1.44.

Acknowledgment is made and thanks are due to Dr. Warren Chupp, Dr. Gerson Goldhaber, and Dr. Sulamith Goldhaber for the use of emulsions from their stacks for this study and for several informative discussions.

* This letter is a summary of some of the results contained in a thesis submitted in partial fulfillment of the requirements for the M.S. degree at the U. S. Naval Postgraduate School, University of California Radiation Laboratory Report UCRL-2979 (unpublished).

† This work was carried out under the auspices of the U. S. Atomic Energy Commission.

[1] Camerini, Davies, Fowler, Franzinetti, Muirhead, Lock, Perkins, and Yekutielli, Phil. Mag. **42**, 1241 (1951).

[2] E. Fermi, Phys. Rev. **92**, 452 (1953); Phys. Rev. **93**, 1434 (1954).

Breakup of Deuterons on H, T, He^3, and He^4†

R. L. HENKEL, J. E. PERRY, JR., AND R. K. SMITH

Los Alamos Scientific Laboratory, University of California, Los Alamos, New Mexico

(Received June 6, 1955)

THE $T(d,n)He^4$ reaction has been the most useful source of monoenergetic neutrons for energies greater than 12 Mev. All measurements of the reaction indicate that monoenergetic neutrons are produced for deuteron bombarding energies below 3.5 Mev. In the deuteron range 2.5 to 5 Mev the 0° yield of neutrons from $T(d,n)He^4$, as measured by a neutron spectrometer,[1] shows a slow monotonic rise with energy. However, recent data taken with a neutron long counter[2] and a U^{238} fission counter, show a copious yield of low-energy neutrons, which increases rapidly as the deuteron energy is raised above 3.7 Mev.

Since the neutrons from the $T(d,n)He^4$ reaction show no corresponding dip above this energy, one hesitates to interpret the low-energy neutrons in terms of an

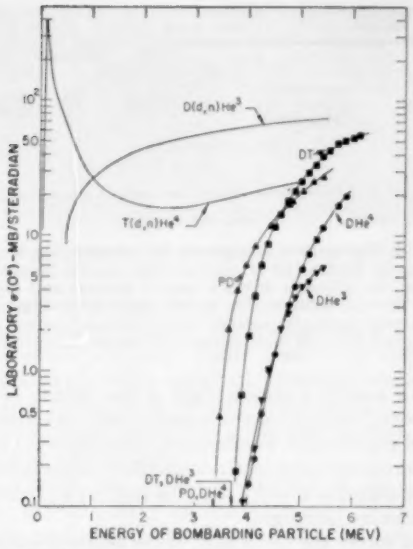

FIG. 1. Laboratory zero-degree cross sections for neutron production *versus* laboratory bombarding energy. The theoretical deuteron breakup thresholds are indicated, together with yields of observed neutrons presumed to occur because of breakup. The standard neutron source cross sections represent, in part, unpublished Los Alamos counter-telescope data taken by Smith, Perry, and Henkel [$D(d,n)He^3$] and Bame, Henkel, and Smith [$T(d,n)He^4$].

excited state of He^4. Rather, the explanation seems to lie in the breakup of the incident deuteron. At a laboratory energy of 3.71 Mev the center-of-mass deuteron energy is equal to its binding energy, 2.225 Mev. Above this energy the deuteron may disintegrate.

As a test of this hypothesis several cases of possible deuteron breakup were investigated. The disintegration thresholds in the laboratory system are given in Table I,[3] together with an indication of whether low-energy[4] neutrons were found. The results are given in Figs. 1 and 2. The cross sections shown therein were measured with a long counter[2] placed in the 0° direction at either one or two meters from the target, and calibrated with a RaBe neutron source. Since no attempt was made to measure the energy distribution or angular distribution of the neutrons, the absolute values of the cross section may be in considerable error.

TABLE I. Disintegration thresholds in the laboratory system.

Reaction	Laboratory threshold energy	Low-energy neutron yield
$D(p,np)H$	$E_p=3.34$ Mev	Yes
$D(d,np)D$	$E_d=4.45$	No*
$T(d,np)T$	$E_d=3.71$	Yes
$He^3(d,np)He^3$	$E_d=3.71$	Yes
$He^4(d,np)He^4$	$E_d=3.34$	Yes

* No low-energy neutrons have been observed for deuteron energies up to 7 Mev.

The *dd* interaction showed no low-energy neutrons. However, a cross section of 5 to 10 mb/steradian for low-energy neutron production could have been missed in the high yield of $D(d,n)He^3$ neutrons. Deuteron breakup is to be expected in the bombardment of heavier elements,[5] but is not apparent in the data of Bonner and Cook[6] in the case of Li^7.

It may be expected[7] that the *S* state of the deuteron would play an important role in the deuteron breakup reactions near threshold, because of the *S* resonance near zero energy. The unobserved yield in the *dd* case might then be explained as the operation of an isotopic spin selection rule[8] which would forbid a transition to such a state in the *dd* reaction but not in the *pd*, *dt*, and dHe^3 reactions. This selection rule would not apply in the *dd* case where both deuterons disintegrate simultaneously (laboratory threshold 8.9 Mev). Although one would expect this rule to operate against breakup in the dHe^4 reaction, low-energy neutrons are actually observed, but with an apparent threshold about 0.4 Mev above the theoretical threshold for breakup (Fig. 2). This fact suggests that the mechanism here may be the stripping reaction $He^4(d,p)He^5$, involving the ground state of He^5. This state[9] is unstable by about 1 Mev to breakup into He^4 and a neutron, and has a width of about 1 Mev. The small energy displacement of the dHe^3 yield above that of the *dt* and *pd* reactions may be due to the additional Coulomb field which is involved.

It should be noted that the breakup neutrons arise from a three-body reaction and hence have a continuum

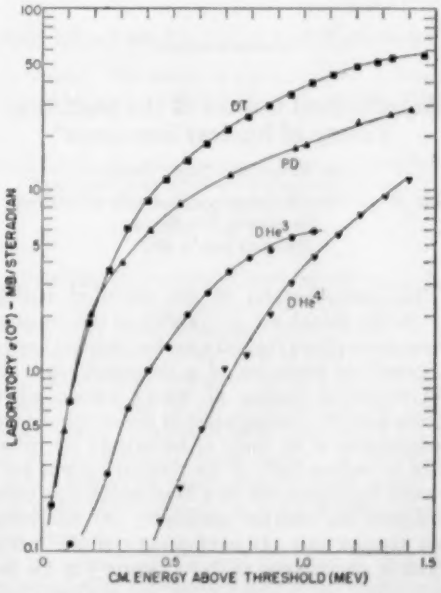

FIG. 2. Laboratory zero-degree cross sections for neutron production *versus* center-of-mass energy above theoretical deuteron breakup threshold.

of energies extending between well-defined limits that can be readily calculated from the collision kinematics. These low-energy neutrons destroy the purity of the neutrons from the $T(d,n)He^4$ reaction. At some high energy (certainly above 8.9 Mev) a similar contamination of the $D(d,n)He^3$ reaction is probable. Thus at high energies it will be necessary to use an associated-particle coincidence technique[10] in order to perform neutron experiments which are sensitive to low-energy neutrons. Unfortunately, such experiments will be complicated and the useful neutron yield will be low when associated-particle coincidence counting is required.

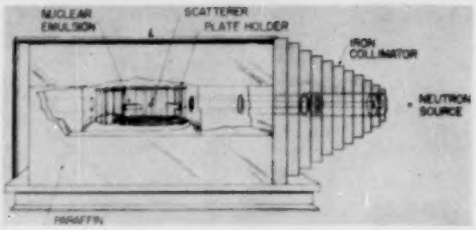

FIG. 1. Experimental arrangement for measuring the spectral and spatial distributions of neutrons from neutron induced reactions. The collimator defines a beam of neutrons only slightly larger than the scatterer. The nuclear plates are arranged with their axes all passing through the center of the scatterer and making angles of 20°—150° with respect to the incident beam direction.

actions provide a sensitive test of the validity of the compound nucleus concept in general and the statistical model in particular. Furthermore, advantages of avoiding the complications of Coulomb effects argue strongly for experiments in which both the incident and emitted particles are uncharged.

The energy spectra of most of the neutrons resulting from nonelastic interactions of 14-Mev neutrons with medium weight and heavy nuclei[3] are in accord with assumptions (1) and (2). However, since these experiments are integral experiments they provide little information with regard to assumptions (3) and (4). To test these assumptions, one can investigate the angular distribution of the nonelastic neutrons.

An experiment was therefore designed to measure the distribution in energy and angle of the neutrons resulting from the incidence of 14-Mev neutrons on various elements. The experimental arrangement is indicated in Fig. 1. Thus far, data have been obtained only on bismuth and even these are preliminary.

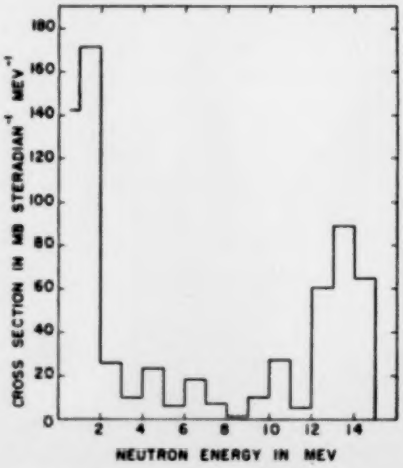

FIG. 2. Cross section for the emission of neutrons vs neutron energy at 30°.

† Work performed under the auspices of the U. S. Atomic Energy Commission.

[1] The proton-recoil neutron spectrometer used in this experiment was a modification of the coincidence-telescope spectrometer described by F. L. Ribe and J. D. Seagrave, Phys. Rev. **94**, 934 (1954).

[2] A. O. Hanson and J. L. McKibben, Phys. Rev. **72**, 673 (1947).

[3] In Table I and in the text where complete reactions are cited, the bombarding particle is that symbol which occurs first inside the parentheses. As an abbreviation in the text and figures the *breakup* reactions are indicated by two symbols, the first being the incident particle and the second the target nucleus.

[4] That the extraneous neutrons have low energy has been directly measured in the two cases *pd* and *di* (miscellaneous unpublished work by the authors). That neutrons from dHe^3 and dHe^4 must have low energy is assumed from their appearance only above a threshold, an argument which also applies to the *pd* and *di* cases.

[5] F. A. Aschenbrenner, Phys. Rev. **98**, 657 (1955).

[6] T. W. Bonner and C. F. Cook, Phys. Rev. **96**, 122 (1954).

[7] R. G. Thomas (private communication).

[8] N. Austern (private communication).

[9] Bashkin, Mooring, and Petree, Phys. Rev. **82**, 378 (1951).

[10] Barschall, Rosen, Taschek, and Williams, Revs. Modern Phys. **24**, 1 (1952).

Experimental Checks of the Statistical Theory of Nuclear Reactions*

LOUIS ROSEN AND LEONA STEWART

Los Alamos Scientific Laboratory, University of California, Los Alamos, New Mexico

(Received June 6, 1955)

THE basic features of the statistical model,[1,2] briefly stated, are (1) validity of the compound nucleus assumptions that (a) a nuclear reaction involves the immediate formation of a compound state with rapid statistical sharing of energy among all the nucleons and (b) disintegration of the compound state is independent of its mode of formation; (2) reduced widths to various levels of the residual nucleus are all the same (this gives rise to a Maxwellian-type energy distribution for emitted particles); (3) interference terms average out; (4) level density of the residual nucleus is proportional to $2j+1$, where j is the level spin.

It has long been recognized that the spatial and spectral distributions of the products of inelastic inter-

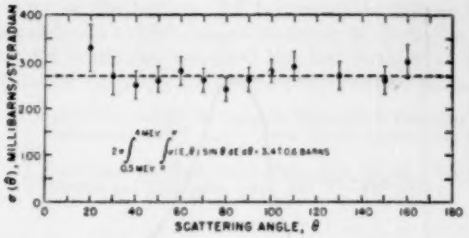

FIG. 3. Angular distribution of neutrons of energy 0.5–4.0 Mev.

Figure 2 shows the kind of information one obtains at each detector position. The high-energy group is due to elastic scattering. Figure 3 shows the angular distribution of the low-energy (0.5–4.0-Mev) neutrons. It is seen that there is not only symmetry about 90° [in accord with feature (3)], but also isotropy [in agreement with feature (4)].[4]

In contrast, the angular distribution of the high-energy (4.0–12.0-Mev) nonelastic neutrons (Fig. 4) is strongly peaked in the forward direction, indicative of nucleon-nucleon interactions. An attractive way of looking at this phenomenon is to invoke the model of Thomas[5] which divides the nucleus into two regions, an inner strong-interaction region and an outer region where the interactions are relatively weak. It is presumably this outer region which is responsible for the noncompound nucleus processes as indicated by the data. The important point, however, is that only ~0.2 barn out of a total inelastic collision cross section of 2.5 barns[6] is associated with neutrons which have spectral and spatial distributions at variance with the above listed assumptions. (Part of the 4–12-Mev neutrons have an isotropic distribution and may represent the tail of the Maxwellian which described the low-energy neutrons.)

In evaluating the validity of the statistical model, one should bear in mind the following additional points: (1) It would appear that energy distributions of low-energy inelastic neutrons and protons may not lead to a reliable estimate of level densities or nuclear "temperatures" because, when energetically possible, the decay of the compound nucleus presumably takes place by the emission of more than one particle. Calculations[7] show that $(n,2n)$ reactions have a marked effect on the apparent nuclear "temperatures" deduced from neutron energy distributions. (2) In experiments involving charged particles,[8] it would appear that the forward-peaked angular distributions which are observed probably account for only a small fraction of the total inelastic cross section. (3) Emission of low-energy protons from heavy nuclei is not necessarily inconsistent with the compound nucleus concept. Such protons may arise when an $(X,2n)$ reaction is energetically forbidden, while an (X,np) reaction is not.

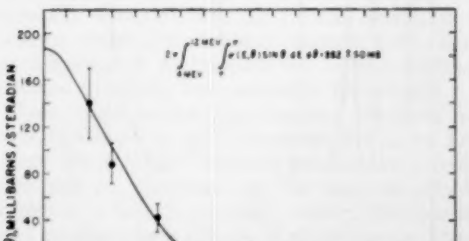

FIG. 4. Angular distribution of neutrons of energy 4.0–12.0 Mev.

* Work performed under the auspices of the U. S. Atomic Energy Commission.

[1] J. M. Blatt and V. F. Weisskopf, *Theoretical Nuclear Physics* (John Wiley and Sons, Inc., New York, 1952), p. 340.
[2] R. G. Thomas, Phys. Rev. **97**, 224 (1955).
[3] E. R. Graves and L. Rosen, Phys. Rev. **89**, 343 (1953).
[4] L. Wolfenstein, Phys. Rev. **82**, 690 (1951); W. Hauser and H. Feshbach, Phys. Rev. **87**, 366 (1952).
[5] R. G. Thomas, Phys. Rev. (to be published); see also Austern, Butler, and McManus, Phys. Rev. **92**, 350 (1953).
[6] E. R. Graves and R. W. Davis, Phys. Rev. **97**, 1205 (1955).
[7] L. Rosen and L. Stewart, Los Alamos Report LA-1560, 1953 (unpublished). (It is shown that the nuclear temperature resulting from emission of the first neutron may be as much as 35% higher than the apparent nuclear temperature as derived from all the neutrons.)
[8] P. C. Gugelot, Phys. Rev. **93**, 425 (1954); B. L. Cohen, Phys. Rev. **98**, 49 (1955); Schrank, Gugelot, and Dayton, Phys. Rev. **96**, 1156 (1954); and R. M. Eisberg and G. J. Igo, Phys. Rev. **93**, 1039 (1954).

Shell Effect on Photonuclear Reactions*

J. GOLDEMBERG, *Departamento de Física, Faculdade de Filosofia, Ciências e Letras, Universidade de São Paulo, São Paulo, Brasil*

AND

J. LEITE LOPES, *Faculdade Nacional de Filosofia, Universidade do Brasil and Centro Brasileiro de Pesquisas Físicas, Rio de Janeiro, Brazil*

(Received May 6, 1955)

A PREVIOUS analysis of some experimental data on photonuclear reactions led the authors[1] to point out that the mean-square displacement of nucleons in the nuclear ground state presents evidence in favor of an alpha-particle structure of nuclei. Although the theoretical basis for this conclusion is not free of criticism—since correlations were neglected in the formula for the harmonic mean energy[2] of photon absorption, which we used—this evidence might be investigated experimentally in a more direct way at higher energies.

On the other hand, the shell structure of nuclei has been revealed, in the energy region of the photonuclear effect, by Nathans and Halpern.[3] Features of different nuclear models are expected to be presented by nuclear

matter. The predominance of one special model over the others depends on the energy and mass number regions and probably on the manner of excitation. It is, therefore, desirable to look for information extracted from experiment and independent, whenever possible, from *a priori* theoretical views and disputable assumptions.

TABLE I. Values of Δ [the difference between the energy at which the (γ,n) cross section is half-maximum and the threshold] for several nuclei.

Element	Z	N	A	Threshold	$E(\frac{1}{2}\sigma_{max})$	Δ(Mev)	Reference
C	6	6	12	18.70	20.6	1.9	a,b
N	7	7	14	10.54	19.3	8.8	c
O	8	8	16	15.60	21.8	6.2	c
Na	11	12	23	12.10	15.4	3.3	a
Mg	12	12	24	16.0	18.2	2.2	d
Al	13	14	27	14.0	17.5	3.5	a
Si	14	14	28	16.9	18.8	1.9	e
P	15	16	31	12.4	16.2	3.8	f
S	16	16	32	15.0	18.0	3.0	g
Cl	17	18	35	13.0	16.8	3.8	h
A	18	20	38	10.5	15.0	4.5	i
K	19	20	39	12.5	17.5	5.0	h
Ca	20	20	40	15.8	18.0	2.2	e
Cr	24	26	50	13.4	16.8	3.4	j
V	23	28	51	10.8	15.5	4.7	j
Mn	25	30	55	10.0	14.5	4.5	a
Fe	26	28	54	11.7	17.7	6.0	k
Co	27	32	59	10.2	15.0	4.8	a
Ni	28	30	58	12.0	15.5	3.5	l
Cu	29	34	63	10.6	14.5	3.9	m
Cu	29	36	65	10.2	14.1	3.9	m
Zn	30	34	64	11.6	14.5	2.9	n
As	33	42	75	10.1	13.0	2.9	a
Br	35	46	81	10.0	14.0	4.0	o
Rb	37	50	87	9.3	14.7	5.4	p
Nb	41	52	93	8.7	14.5	5.8	a
Mo	42	50	92	13.1	15.1	2.1	p
Ag	47	62	109	9.3	13.2	3.9	q
In	49	66	115	9.0	12.5	3.5	a
Sb	51	70	121	9.3	12.4	3.1	m
I	53	74	127	9.1	13.2	4.1	a
La	57	82	139	8.0	12.5	4.5	j
Ta	73	108	181	8.8	11.5	2.7	m
Au	79	118	197	7.9	11.4	4.1	a
Bi	83	126	209	7.4	11.6	4.2	a
U	92	146	238	6.0	9.5	3.5	r

[a] Montalbetti, Katz, and Goldemberg, Phys. Rev. **91**, 659 (1953).
[b] Haslam, Johns, and Horsley, Phys. Rev. **82**, 270 (1951).
[c] Johns, Horsley, Haslam, and Quinton, Phys. Rev. **82**, 856 (1951).
[d] L. Katz and A. G. W. Cameron, Phys. Rev. **84**, 1115 (1951).
[e] Summers-Gill, Haslam, and Katz, Can. J. Phys. **31**, 70 (1953).
[f] L. Katz and A. S. Penfold, Phys. Rev. **81**, 815 (1951).
[g] Haslam, Summers-Gill, and Crosby, Can. J. Phys. **30**, 257 (1952).
[h] O. Borello, Ann. acad. brasil. scienc. (to be published).
[i] McPherson, Pederson, and Katz, Can. J. Phys. **32**, 593 (1954).
[j] J. Goldemberg and L. Katz, Can. J. Phys. **32**, 49 (1953).
[k] E. Silva, Ann. acad. brasil. scienc. (to be published).
[l] Katz, Johns, Baker, Haslam, and Douglas, Phys. Rev. **82**, 271 (1951).
[m] Johns, Katz, Douglas, and Haslam, Phys. Rev. **80**, 1062 (1950).
[n] S. S. Vilaça, Ann. acad. brasil. scienc. (to be published).
[o] Katz, Pease, and Moody, Can. J. Phys. **30**, 476 (1952).
[p] Katz, Baker, and Montalbetti, Can. J. Phys. **31**, 250 (1953).
[q] B. C. Diven and G. Almy, Phys. Rev. **80**, 407 (1950).
[r] R. Nathans and J. Halpern, Phys. Rev. **93**, 437 (1954).

Nathans and Halpern found that the width of the giant resonance, as given by the total neutron yield, is smaller for magic nuclei. This criterion seems to us not very satisfactory since the width might depend on the relative importance of $(\gamma,2n)$ and (γ,np) reactions, and also on the threshold of these reactions. A way to avoid this ambiguity is to plot the energy distance from the threshold for (γ,n) reactions to the first point where the cross section is half-maximum, against A. This quantity Δ gives a measure of the steepness of rise of the (γ,n) cross-section curve as a function of the energy, as shown in Fig. 1. For magic nuclei and neighbors, one expects Δ to be larger than for the others. This is indeed the case, as indicated in Fig. 2 and in Table I, where Δ is plotted against A. The shell structure is clearly exhibited in this curve and the effect is neater for higher mass numbers.

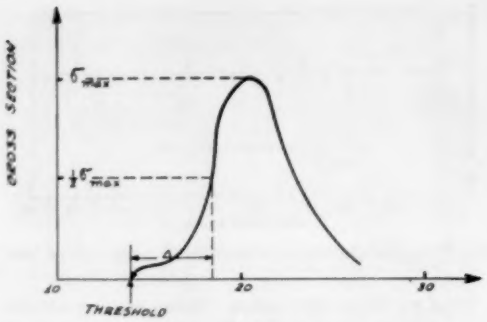

FIG. 1. Definition of Δ.

For very light nuclei, there are marked deviations from the expected curve; this might be accounted for by the fact that for such nuclei the (γ,n) process is not dominant. Thus, whereas carbon, which has a complete subshell, has a low Δ, nitrogen has an anomalously high Δ. Magic nuclei with $N=20$, 28, 82, and 126 show their shell structure very clearly in the graph. At $N=50$, we find an anomaly: Nb ($N=52$), which is not a magic nucleus, shows a value $\Delta=5.8$, although Rb ($N=50$), which is magic, has a $\Delta=5.4$, and Mo ($N=50$), also a magic nucleus, has $\Delta=2.1$. This anomaly suggests that new measurements should be made with these elements.

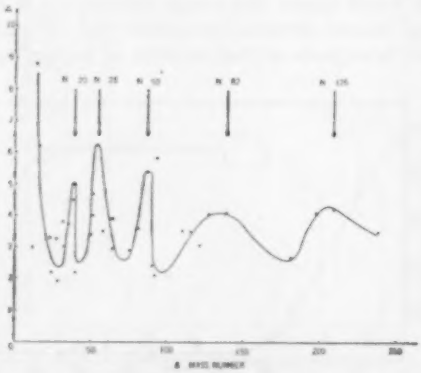

FIG. 2. Δ as a function of A. Magic nuclei are on peaks of the curve.

One of the authors (J.L.L.) wishes to express his appreciation to his colleague Professor M. D. S. Santos for the hospitality extended him last January at the Betatron Laboratory of the University of São Paulo.

* Supported in part by the Conselho Nacional de Pesquisas.
[1] J. Goldemberg and J. Leite Lopes, Nuovo cimento **12**, 817 (1954).
[2] J. S. Levinger and H. A. Bethe, Phys. Rev. **78**, 115 (1950).
[3] R. Nathan and J. Halpern, Phys. Rev. **93**, 437 (1954).

Evidence Against the Existence of 23-Hour V^{53}†

RAYMOND K. SHELINE AND JOSEPH R. WILKINSON, *Department of Chemistry, Florida State University, Tallahassee, Florida*

AND

BRUCE J. DROPESKY AND THEODORE T. SHULL, *Los Alamos Scientific Laboratory, University of California, Los Alamos, New Mexico*

(Received December 6, 1954; revised manuscript received June 17, 1955)

A 23-HOUR activity assigned to V^{53} has been reported[1] to have been produced by the (γ,p) reaction on Cr^{54} and[2] by the (n,p) reaction on Cr^{53}.

Three additional bombardments have been employed to produce this activity for decay scheme studies. In the first attempt, the enriched isotope Cr^{53} was bombarded with fast neutrons produced by 21-Mev protons on beryllium; in the second attempt, enriched Ti^{50} was bombarded with 50-Mev alpha particles. The third attempt employed a fast-neutron bombardment of "spec. pure" normal chromium (9.5% Cr^{53}) in the fast-neutron flux of the Los Alamos Water Boiler. In none of these cases was any 23-hour vanadium activity produced. In view of the extremely favorable conditions for producing this activity, particularly in the alpha-particle bombardment of Ti^{50}, it seems highly probable that there is no 23-hour vanadium activity. The experimental details follow.

Enriched Cr^{53} (Cr^{50}: 0.5%, Cr^{52}: 5.7%, Cr^{53}: 92.1%, Cr^{54}: 1.7%) was bombarded for one hour by the spectrum of neutrons resulting from the bombardment of a thick beryllium target with 21-Mev protons at the Oak Ridge National Laboratory. The vanadium was chemically separated from the Cr and counted in a standard Geiger-Müller counter eighteen hours after the completion of the bombardment. Within counting statistics, no activity was observed in this sample.

"Spec. pure" normal chromium was irradiated for about 13.4 hours in the fast neutron flux of the Los Alamos Water Boiler. Vanadium was chemically separated from the chromium and the vanadium sample counted in a beta proportional counter. This sample had a maximum beta activity of approximately 3 cpm which might be attributed to 23-hour V^{53}. No measurable gamma activity was present. Assuming 5 Mev to be a reasonable value for the effective threshold for the $Cr^{53}(n,p)V^{53}$ reaction and using what is considered to be the approximate value of the flux of neutrons greater than 5 Mev, i.e., 3.6×10^{10} n/cm^2 sec, an approximate limit of the average cross section for this reaction was calculated to be approximately 3.4×10^{-5} millibarn.

Enriched Ti^{50} (Ti^{46}: 2.51%, Ti^{47}: 1.62%, Ti^{48}: 12.23%, Ti^{49}: 3.33%, and Ti^{50}: 80.31%) was bombarded in the external beam of the 60-inch cyclotron of the University of California for 5 hours with 48.5-Mev alpha particles. Vanadium was chemically separated from the titanium and counting of the sample was begun 26 hours after the completion of the bombardment.

Gamma spectra as a function of time were taken on the vanadium separated from the Ti^{50} bombardment and showed peaks at 0.12, 0.52, 1.00, and 1.32 Mev. The peaks at 1.00 Mev and 1.32 Mev agree very closely with the reported values of 0.99 Mev and 1.32 Mev of 16-day V^{48}. The half-life of the 1.00-Mev and 1.32-Mev gamma rays is 16.2 days, which seems to indicate that the gamma rays are definitely those of V^{48}. The peak at 0.52 Mev is very probably due to the positron of V^{48}. The peak at 0.12 Mev agrees with the reported value of 0.12 Mev for V^{49}.

The production of a substantial amount of V^{48} activity by the alpha-particle bombardment of enriched Ti^{50} and the failure to produce any 23-hour V^{53} activity would seem to indicate that the 23-hour V^{53} does not exist, or if it does exist, the cross section for the production of V^{53} by alpha-particle bombardment is extremely small.

We wish to thank Bernard Rossi of the Radiation Laboratory of the University of California and Farno Green and John Martin of the Oak Ridge National Laboratory for the necessary bombardments and the Stable Isotopes Division of the Oak Ridge National Laboratory for the loan of the enriched isotopes.

† This work was supported by the U. S. Atomic Energy Commission.
[1] L. Hsiao and R. B. Duffield, as reported in Hollander, Perlman, and Seaborg, Revs. Modern Phys. **25**, 469 (1953).
[2] R. K. Sheline and J. R. Wilkinson, Phys. Rev. **94**, 729 (1954).

$\pi-\mu$ Decay with an Associated Electron Pair*

W. F. FRY, J. SCHNEPS, G. A. SNOW,† AND M. S. SWAMI

Department of Physics, University of Wisconsin, Madison, Wisconsin

(Received June 15, 1955)

AN interesting $\pi-\mu$ decay has been found in a pellicle stack which was exposed to the Berkeley bevatron. A projection-drawing of the event is shown in Fig. 1. Two minimum-ionizing tracks are observed to originate from the $\pi-\mu$ decay point. The multiple scattering and grain density along these two tracks

clearly indicate that they were produced by electrons. The energy of each of these electrons was found to be 0.6 ± 0.3 Mev from the multiple scattering. The opening angle between the pair of electrons is about 25°.

The range of the μ meson from the π-meson decay is 520 ± 10 microns, which is somewhat less than the normal range[1] (596 microns). A decay electron track (not shown on the figure) is observed from the stopped μ meson. The large amount of multiple scattering along the incident meson track suggests that it stopped before

FIG. 1. A $\pi-\mu$ decay with an associated electron pair is shown in the above projection drawing.

it decayed. Furthermore, the μ meson track is in the same general direction as the π meson track; therefore the short range of the μ meson cannot be explained by assuming that the π meson decayed in flight.

Several $\pi-\mu$ decays have previously been observed by one of the authors[2] and by others[3] in which the μ meson track was unusually short. These events were explained[4] by assuming that a soft photon accompanied the $\pi-\mu$ decay due to the charge acceleration at the time of the decay.

It seems reasonable to interpret the event described in this note in the same way, except that we must further assume the direct production of an electron pair during the $\pi-\mu$ decay. Although the probability for such a process must be very small ($\sim10^{-6}$), the energetics of this event are in agreement with this interpretation. If the masses[5] of the π and μ mesons are taken to be 272.5 m_e and 206 m_e, respectively, the energies of the μ meson and the neutrino are 4.1 and 29.8 Mev, respectively, if the π meson decays from rest. In the event here described, the energy of the μ meson was found from its range to be 3.7 ± 0.15 Mev. If the momentum of the neutrino is assumed to be equal to the vector sum of the μ meson and the electron pair momenta, the energy of the neutrino is found to be 27.8 ± 0.4 Mev. The total kinetic energy release, plus the rest energy of the two electrons, is then $27.8+0.6+0.6+1.0+3.7=33.7\pm0.9$ Mev which is in excellent agreement with the normal decay energy of 33.9 Mev.

The authors are very grateful to Professor E. J. Lofgren and Mr. Roy Kerth for their wholehearted cooperation and help in the exposures.

* Supported in part by the Graduate School from funds supplied by the Wisconsin Alumni Research Foundation.

† On leave of absence from Brookhaven National Laboratory.

[1] W. F. Fry and George R. White, Phys. Rev. **90**, 207 (1953).

[2] W. F. Fry, Phys. Rev. **91**, 130 (1953).

[3] W. H. Barkas, Am. J. Phys. **20**, 5 (1952); Seifert, Bramson, and Havens, Phys. Rev. **86**, 603 (1952); W. Riezler and A. Rudloff, A. Naturforsch. **7a**, 570 (1952).

[4] Nakano, Nishimura, and Yamaguchi, Progr. Theoret. Phys. (Japan) **6**, 1028 (1951); T. Eguchi, Phys. Rev. **85**, 943 (1952); G. E. A. Fialho, Notas de Fisica No. 1 (1952) (unpublished); B. Ioffe and A. Rudick, Doklady Akad. Nauk. U.S.S.R. **82**, No. 3, 359 (1952).

[5] Walter H. Barkas and D. M. Young, University of California Radiation Laboratory Report UCRL-2579, 1954 (unpublished).

Neutron and Proton Distributions in Heavy Nuclei

R. G. P. VOSS AND R. WILSON

Clarendon Laboratory, Oxford, England

(Received June 6, 1955)

RECENTLY it has been suggested by several authors[1–5] that the neutrons in a nucleus may have a larger spatial extension than the protons. In support of this suggestion we have analyzed inelastic cross sections for 134-Mev protons[6] and for 140-Mev neutrons[7] in terms of the optical model, using both a square well[8] and a tapered density distribution.[9] In the case of the former one can calculate the square-well radius R, and in the latter the parameter a, which is related to the radius. The values derived from the proton measurement we have called R_p and a_p re-

TABLE I. Values of the parameters. Both the R's and a's are in units of 10^{-13} cm.

Element	R_n	R_p	a_n	a_p
Pb	7.80 ± 0.05	8.45 ± 0.40	0.78 ± 0.01	0.85 ± 0.05
Cd	6.35 ± 0.05	7.45 ± 0.45	0.785 ± 0.01	0.940 ± 0.06
Cu	5.50 ± 0.05	5.65 ± 0.35	0.83 ± 0.01	0.87 ± 0.07
Al	4.6 ± 0.2	4.25 ± 0.45		
C	3.8 ± 0.4	3.90 ± 0.8		

spectively, and those from the neutron measurement R_n and a_n.

The principle of the argument which follows is that the neutron-proton total cross section at these energies is larger than the proton-proton cross section. Thus the proton inelastic cross sections depend mainly on the radius of the neutron distribution, and the neutron cross sections upon the radius of the proton distribution. This argument only holds at energies below about 400 Mev; at 1 Bev the np and pp cross sections are equal and there should be (and is[9]) no difference in the radii determined from neutron or proton inelastic cross sections.

In the case of the protons, the expression valid for neutrons has been corrected for Coulomb repulsion by the factor $(1-W/E)$, where E is the incident proton energy and $W=Ze^2/R$; this can be justified on a classical impact parameter argument.[6]

For heavy nuclei the absorption coefficient is not very different from πR^2, and the radius so determined is not strongly dependent on the absorption coefficient in nuclear matter, K. For light nuclei this is not so, and it is difficult to obtain reliable values for the nuclear radii.

The absorption coefficient K depends on a mean cross section defined by

$$A\bar{\sigma}_n = Z\alpha_{np}\sigma_{np} + (A-Z)\alpha_{nn}\sigma_{nn}$$

for incoming neutrons, and

$$A\bar{\sigma}_p = Z\alpha_{pp}\sigma_{pp} + (A-Z)\alpha_{np}\sigma_{np}$$

for incoming protons. σ_{np} and $\sigma_{pp}(=\sigma_{nn})$ are the free neutron-proton, proton-proton cross sections, respectively, and the α's are factors which account for the reduction of the free nucleon-nucleon cross sections due to the exclusion principle.

It is seen from Table I that for the heavy elements lead and cadmium R_n is significantly smaller than R_p, and a_n than a_p. Since a direct comparison between similar cross sections is being made, the values of the α's used are not very critical. The values used for lead were $\alpha_{pp}=\alpha_{nn}=0.81$; $\alpha_{np}=\alpha_{pn}=0.67$. Decreasing them reduces the difference between R_n and R_p, or between a_n and a_p, but this difference is still significant even if they are reduced by 10%.

If the assumptions of the optical model are correct, the values of R_n and R_p (or a_n and a_p) deduced from the two sets of cross sections should be equal. We suggest that the discrepancy can be explained by assuming that the radius of the neutron distribution is greater than that of the proton distribution. If σ_{pp} were zero, R_p would be the radius of the neutron distribution and R_n that of the proton distribution. Since σ_{pp} is not zero, the difference between the radii of the two distributions necessary to account for the discrepancy will be slightly larger than the difference between R_n and R_p (or a_n and a_p).

Since inelastic scattering is an incoherent process, the result will not be appreciably influenced by details of the Coulomb phase shifts. Also, since only differences are being discussed, the result is not critically dependent on the range of nuclear forces.

More detailed calculations are in progress, and will be reported later.

[1] L. N. Cooper and W. Tobocman, Phys. Rev. **97**, 243 (1955).
[2] S. D. Drell, Bull. Am. Phys. Soc. **30**, No. 3, 19 (1955).
[3] W. N. Hess and B. J. Moyer, Phys. Rev. **96**, 859 (1954).
[4] M. H. Johnson and E. Teller, Phys. Rev. **93**, 357 (1954).
[5] W. J. Świątecki, Phys. Rev. **98**, 204 (1955).
[6] J. M. Cassels and J. D. Lawson, Proc. Phys. Soc. (London) **A67**, 125 (1954).
[7] R. G. P. Voss and R. Wilson, Physical Society Spring Meeting at Harwell, March, 1955; (to be published); R. G. P. Voss, thesis, Oxford (unpublished).
[8] Fernbach, Serber, and Taylor, Phys. Rev. **75**, 1352 (1949).
[9] R. W. Williams, Phys. Rev. **98**, 1387, 1393 (1955).

Capture of Negative K Mesons*

STANLEY C. FREDEN AND HAROLD K. TICHO
Department of Physics, University of California, Los Angeles, California
(Received June 7, 1955)

NUCLEAR emulsions exposed to a K^- beam of the Berkeley bevatron are being scanned at the University of California at Los Angeles. A polyethylene target was bombarded by 5.7-Bev protons and the magnetically analyzed beam containing particles with momenta of the order of 360 Mev/c was admitted to the stack.

These plates are being scanned near the edges where the beam entered for all particles whose ionization is about 2.3 times minimum and whose angle is within $\pm 5°$ of the direction of the incoming beam. Such particles are then traced to their endings. The mean range of K^- mesons entering the stack is $\simeq$3.7 cm. To date four endings of K^- mesons have been found. The flux of π^- mesons relative to K^- mesons is $\simeq 6\times 10^3$.

In star 3A two particles are emitted. Particle (1) has a range of 700μ and is singly charged. It is most likely a proton of 11 Mev. Particle (2) passes out of the stack after traversing a distance of 28 mm. Measurements of the variation of grain density with residual range indicate that this particle is a proton whose energy is 120 ± 20 Mev.

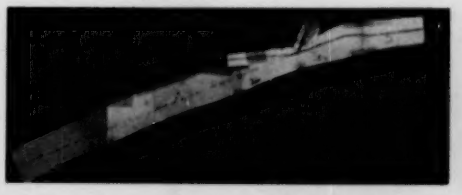

FIG. 1. Photomicrograph of σK^- event No. 11-6. The numbers of the particles refer to those given in Table I.

TABLE I. Summary of K^- meson capture stars.

Event number	Star particle number	Star particles	Energy (Mev)
3*A*	1	Proton	11
	2	Probable proton	120±20
3*I*	1	Proton	120
		Recoil$\simeq 2\mu$	
11–6	1	Proton, deuteron or α-particle	2.5 for proton
	2	Proton	9
	3	Probable proton	135±10
		Recoil$\simeq 2\mu$	
11–4	1	Proton	4
	2	Proton	18
	3	Proton	65

In star 3*I* one particle is emitted. This particle ends in the stack and is identified as a proton of 120 Mev. A visible recoil of $\simeq 2\mu$ accompanies this star.

Star 11–6 is a three-pronged star with a visible recoil of $\simeq 2\mu$. Two of the tracks are evaporation tracks and are probably protons of 2.5 and 9 Mev respectively, although the former could be as heavy as an α particle. The third track passes out of the stack after a distance of 35 mm. This track is consistent with that of a proton of 135±10 Mev. Figure 1 is a photomicrograph of this event.

Similarly, in star 11–4 there are two evaporation tracks which are most likely due to protons of 4 and 18 Mev respectively. Particle (3) from this star is also a proton which stops in the stack and has an energy of 65 Mev.

The data for the four stars listed in the foregoing is summarized in Table I.

Preliminary mass measurements of the four K^- mesons, based on a g *vs* R method, yield a value for each which is consistent with a mass of $1000\pm 80\ m_e$.

The capture stars observed in this investigation do not differ significantly from many σK^- events observed in the cosmic radiation.[1,2] On the other hand, they do not appear to have the characteristic features of the σK^- events reported by Hornbostel and Salant[3] at Brookhaven. Using a bombarding energy of 2.8 Bev and a similar scanning procedure, they found that 11 out of 13 σK^- stars yielded L-mesons, or hyperons, or both. The hyperons decayed after coming to rest or in flight after a few millimeters of range. None of the σK^- stars observed by us emitted L-mesons. While the possibility that the two fast particles emitted in stars 3*A* and 11–6 could be hyperons cannot be ruled out, they together had a moderation time of $\simeq 8\times 10^{-10}$ second in the emulsion without decaying.

We wish to thank Dr. W. H. Barkas for arranging the exposure and Dr. L. Rosen and Dr. G. Frye for the loan of the processed emulsions.

* Sponsored by the Office of Ordnance Research, U. S. Army.

[1] Review article by Dilworth, Occhialini, and Scarsi, Ann. Rev. Nuc. Sci. **4**, 307 (1954).
[2] C. Dilworth *et al.*, Nuovo cimento, Suppl. No. 2, 433 (1954).
[3] J. Hornbostel and E. O. Salant, Phys. Rev. **98**, 218 (1955).